

Structures *in* Fire

Proceedings of the Sixth International Conference

Organized by Michigan State University

Edited by

Venkatesh Kodur
Jean-Marc Franssen



DEStech Publications, Inc.

Structures in Fire

DEStech Publications, Inc.
439 North Duke Street
Lancaster, Pennsylvania 17602 U.S.A.

Copyright © 2010 by DEStech Publications, Inc.
All rights reserved

No part of this publication may be reproduced, stored in a retrieval system, or transmitted, in any form or by any means, electronic, mechanical, photocopying, recording, or otherwise, without the prior written permission of the publisher.

Printed in the United States of America
10 9 8 7 6 5 4 3 2 1

Main entry under title:
Structures in Fire (Proceedings of the Sixth International Conference)

A DEStech Publications book
Bibliography: p.
Includes index p. 1023

ISBN: 978-1-60595-027-3

HOW TO ORDER THIS BOOK

BY PHONE: 1-877-500-4337 or 717-290-1660, 9AM–5PM Eastern Time

BY FAX: 717-509-6100

BY MAIL: Order Department

DEStech Publications, Inc.

439 North Duke Street

Lancaster, PA 17602, U.S.A.

BY CREDIT CARD: American Express, VISA, MasterCard, Discover

BY WWW SITE: <http://www.destechpub.com>

Table of Contents

<i>Preface</i>	xv
<i>Scientific Committee</i>	xvii
<i>Organizing Committee</i>	xviii
<i>Steering Committee</i>	xviii
<i>Acknowledgements</i>	xix

STEEL STRUCTURES

Experimental Investigation of Fundamental Behavior of Steel Members under Fire Loading	3
L. CHOE and A. H. VARMA	
A 3D Numerical Analysis of a Typical Steel Highway Overpass Bridge under a Hydrocarbon Fire	11
I. PAYÁ-ZAFORTEZA and M. E. M. GARLOCK	
Numerical Analysis of the Cross-Sectional Capacity of Structural Steel Members in Fire.	19
M. KNOBLOCH, D. SOMAINI, J. PAULI and M. FONTANA	
Stability Check of Steel Frames Exposed to Fire	27
P. V. REAL, C. COUTO, N. LOPES and J. P. RODRIGUES	
Thermal Response of Steel Columns Exposed to Localized Fires—Numerical Simulation and Comparison with Experimental Results	35
G-Q. LI and C. ZHANG	
Structural and Fire Behaviour of a New Light Gauge Steel Wall System	43
S. GUNALAN and M. MAHENDRAN	

Development of a 3D Co-Rotational Beam-Column Element for Structural Analysis of Steel and Composite Frames Exposed to Fire	51
Q-T. LE, B. ZHAO and M. HJIAJ	
Fire-Induced Progressive Collapse of Steel Structures that have Sustained Localized Damage	59
S. E. QUIEL and S. M. MARJANISHVILI	
Lateral-Torsional Buckling of Carbon Steel and Stainless Steel Beams Subjected to Combined End Moments and Transverse Loads in Case of Fire	67
N. LOPES, P. V. REAL, L. S. DA SILVA and J-M. FRANSEN	
Reliability-Based Capacity Reduction and Fire Load Factors for Design of Steel Members Exposed to Fire	75
S. IQBAL and R. S. HARICHANDRAN	
Temperature of External Column During Fire Test	83
M. PULTAR, Z. SOKOL and F. WALD	
Restrained Steel Beam Behaviour in Case of Fire, Depending on Load Ratio, Performed in Case Study of a Bus Station	91
J. DE LA QUINTANA, J. AURTENETXE, F. MORENTE and S. EGUIA	
Experimental and Numerical Modelling of Cellular Beams with Elongations Openings at Elevated Temperature	98
E. NAILI, A. NADJAI, H. SONG, F. ALI, S. CHOI, B. WONG, I. BURGESS and R. PLANK	
Performance Based Design Approach for Evaluating Fire Resistance of Restrained Steel Beams	106
M. DWAIKAT and V. KODUR	
Load Bearing Capacity of Steel Structures after Fire	114
J. FALKE and H. N. MUSTAFA	
Stress-Based Equations for Predicting the Buckling Capacity of Steel Plates Exposed to Fire	122
S. E. QUIEL and M. E. M. GARLOCK	
A Study of Damage Mechanism of Thick Fireproof Coating for Steel Member Subjected to Monotonic Loading.	130
S.-W. CHEN, J. CHU and G.-Q. LI	
CONCRETE STRUCTURES	
New Regulations for Hollow Core Slabs After Premature Partial Collapse	141
T. VAN OVERBEEK, A. BREUNESE, J. GIJSBERS, K. BOTH, J. MALJAARS and L. NOORDIJK	

Performance in Fire of Fibre Reinforced Polymer Strengthened Concrete Beams Including Embedded Fibre Optic Sensors	149
M. F. GREEN, M. ADELZADEH, T. KHALIFA, R. EEDSON, L. BISBY, N. BÉNICHOU, X. BAO and W. LI	
Fire Performance of Precast Prestressed Concrete Beam with Openings	157
S. BABA, S. MICHIKOSHI, S. SAKAMOTO and T. HIRASHIMA	
Explosive Spalling of Concrete Columns with Steel and Polypropylene Fibres Subjected to Severe Fire.	165
P. DOHERTY, F. ALI and A. NADJAI	
Fire Resistance of a Concrete Box Beam Prestressed by External Tendons	173
S. TATTONI and A. GASPERI	
Behavior of Concrete Columns Subjected to Fire.	181
A. M. B. MARTINS and J. P. C. RODRIGUES	
The Influence of Travelling Fires on the Response of a Concrete Frame.	189
A. LAW, J STERN-GOTTFRIED, M. GILLIE and G. REIN	
Simplified Procedure for Shear Failure Assessment of RC Framed Structures Exposed to Fire	197
R. FARIA, H. F. XAVIER and P. V. REAL	
Modeling the Fire Response of Reinforced Concrete Columns under Biaxial Bending	206
N. RAUT and V. KODUR	
Modelling the Fire Resistance of Prestressed Concrete Floors Using Multi-Spring Connection Elements	216
J-K. MIN, P. MOSS, R. DHAKAL and A. BUCHANAN	
Behaviour of Earthquake Damaged Reinforced Concrete Structures in Fire.	224
A. ERVINE, M. GILLIE and PANKAJ	
Fire Testing of an Earthquake Damaged RC Frame	231
P. BHARGAVA, U. K. SHARMA, Y. SINGH, B. SINGH, A. USMANI J. TORERO, M. GILLIE, PANKAJ, I. MAY and C. S. MANOHAR	
A Simplified Sectional Analysis Approach for RC Elements During Fire Events	239
S. F. EL-FITIANY and M. A. YOUSSEF	
Moment Curvature Relationships for Fire Damaged Reinforced Concrete Sections	247
D. M. S. PHANI PRASAD, V. KUMAR, U. K. SHARMA and P. BHARGAVA	

Experimental Examination of Residual Load Bearing Capacity of RC Beams Heated Up to High Temperature	254
R. KOWALSKI and P. KROL	
Influence of Thermal Elongation of Beams on the Fire Resistance of RC Frames	262
H. F. XAVIER, R. FARIA and P. V. REAL	
Stability of RC Structure Under Non-Uniform Thermal Exposure	270
S. DEENY and T. STRATFORD	
The Fire Performance of Polymer Fibre Reinforced Composite Concrete Slabs	278
D. FOX and T. STRATFORD	
Estimating the Response of Flat Plate Concrete Slab Systems to Fire Exposure	286
M. GHOREISHI, A. BAGCHI and M. A. SULTAN	
Structural Behavior of Reinforced Pre-Compressed Concrete (r.c.) Structures in Fire: Paradigms and Lessons from Experience	294
D. MAXIA, A. PORCU, R. PORCU and S. TATTONI	
Spalling of Normal Strength Concrete Walls in Fire	301
M. GUERRIERI and S. FRAGOMENI	
A Material Model for the Numerical Simulation of High Strength Concrete Columns Subjected to Fire Loading.	312
S. HUISMANN, M. KORZEN and U. SCHNEIDER	
Modeling R/C Columns in Fire According to Different Constitutive Models for Heated Concrete	320
P. BAMONTE AND F. LO MONTE	
Performance of FRP-Strengthened Reinforced Concrete Beams Under Design Fire Exposure	328
A. AHMED and V. KODUR	
COMPOSITE STRUCTURES	
Composite Columns Made of Partially Encased Steel Sections Subjected to Fire.	341
M. KORZEN, J. P. C. RODRIGUES	
Parametrical Study on the Behaviour of Steel and Composite Cellular Beams Under Fire Conditions	349
O. VASSART, C. G. BAILEY, G. BIHINA, M. HAWES, A. NADJAI, C. PEIGNEUX, W. I. SIMMS and J.-M. FRANSSSEN	

Performance of RC Beam to Concrete Filled Steel Tubular (CFST) Column Frames Subjected to Fire	358
L.-H. HAN, W.-H. WANG and H.-X. YU	
Experimental and Analytical Investigations of the Behaviour of Protected Composite Floor Beams with Web Openings in Fire	366
V. Y. B. WONG, I. W. BURGESS and R. J. PLANK	
Influence of Reinforcement Properties on the Failure of Composite Slabs in Fire	374
K. A. CASHELL, A. Y. ELGHAZOULI, B. A. IZZUDDIN	
Collapse Mechanisms of Composite Slab Panels in Fire	382
A. ABU, V. RAMANITRARIVO and I. BURGESS	
Planning for a Large-Scale Fire Test on a Composite Steel-Frame Floor System	390
D. J. PROE and I. R. THOMAS	
Large-Scale Fire Test of Unprotected Cellular Beam Acting in Membrane Action	398
O. VASSART, C. G. BAILEY, M. HAWES, A. NADJAI, W. I. SIMMS, B. ZHAO, T. GERNAY and J.-M. FRANSSSEN	
Experimental and Numerical Investigations of Steel and Concrete Composite Floors Subjected to ISO Fire Condition	407
B. ZHAO and M. ROOSEFID	
Experimental Evaluation of Composite Floor Assemblies Under Fire Loading.	417
E. WELLMAN, A. H. VARMA, R. FIKE, P. PAKALA and V. KODUR	
A Numerical Model for Unbraced Composite Frames in Fire	425
P. SCHAUMANN and O. BAHR	
Fire Resistance of Axially Loaded Slender Concrete Filled Steel Tubular Columns	433
G. S. LEITE, JR., K. A. GOMIDE, A. L. MORENO, JR., and V. P. SILVA	
Performance Based Fire Resistance Design of CFT Columns in a Railway Station	441
C. ZHANG, S.-C. JIANG and G.-Q. LI	
Fire-Resistance Evaluation of Double CFT Columns Under Central Axial Load	449
Y. A. WON, S. H. KIM, S. K. JUNG, K. S. CHUNG and S. M. CHOI	
Fire Endurance Performance of Cellular GFRP Columns with Water-Cooling System.	458
Y. BAI, E. HUGI, C. LUDWIG and T. KELLER	

Influence of Moisture Transport on Fire Resistance of Steel Concrete Composite Slab	466
T. HOZJAN, J. KOLSEK, M. SAJE, I. PLANINC, S. BRATINA and S. SRPCIC	
Numerical Modelling of Membrane Action of Composite Slabs in Fire Situation.	474
C. VULCU, TH. GERNAY, R. ZAHARIA, J. M. FRANSEN	
Fire Test of Composite Floor with Castellated Beams	484
J. BEDNAR, F. WALD and M. STUJBEROVA	
The Slab Panel Method: Design of Composite Floor Systems for Dependable Inelastic Response to Severe Fires	492
G. C. CLIFTON, A. G. GILLIES and N. MAGO	
TIMBER STRUCTURES	
Design Method for the Separating Function of Timber Structures.	503
A. FRANGI, V. SCHLEIFER, M. FONTANA and E. HUGI	
Design Model for Fire Exposed Cross-Laminated Timber	511
J. SCHMID, J. KÖNIG and J. KÖHLER	
Failure Mechanisms of Structural Insulated Panel (SIP) Systems Under Natural Fire Conditions	520
D. HOPKIN, T. LENNON, J. EL-RIMAWI and V. SILBERSCHMIDT	
Fire Resistance of Connections in Timber Structures.	528
P. J. MOSS, T. M. NILSEN, M. FRAGIACOMO and A. H. BUCHANAN	
Design of Timber-Concrete Composite Floors for Fire Resistance. . .	536
J. O'NEILL, D. M. CARRADINE, P. J. MOSS, M. FRAGIACOMO and A. H. BUCHANAN	
Fire Performance of Epoxied Connections in Heavy Timber Structures.	544
R. B. GERARD, D. M. CARRADINE, P. J. MOSS and A. H. BUCHANAN	
Fire Resistance of Wood-Steel-Wood Bolted Timber Connections. . .	552
L. PENG, G. HADJISOPHOCLEOUS, J. MEHAFFEY and M. MOHAMMAD	
Fire Performance of Engineered Versus Traditional Lumber	560
R. BACKSTROM, M. TABADDOR and P. D. GANDHI	
Fire Resistance of Traditional Timber Post and Beam Construction—An Experimental and Modeling Study	568
A. NAKAJIMA, Y. HASEMI, N. YASUI, A. SUZUKI, D. HIRAKURI, Y. SAWANO, K. WATANABE, H. HIRAI, A. OGAWA, M. S. SEKI, M. KOSHIHARA, M. MURAKAMI, T. KIMURA and Y. TAMURA	

Timber Bolted Joints Subjected to High Temperatures.	576
N. D. CORREIA, J. P. C. RODRIGUES and P. D. MORAES	
Post Protection Behaviour of Wooden Wall and Floor Structures Completely Filled with Glass Wool.	584
A. JUST	
Failure Times of Gypsum Boards	593
A. JUST, J. SCHMID and J. KÖNIG	
Using Artificial Neural Networks for Predicting Temperatures in Timber.	602
P. CACHIM	
A Laboratory Study into the Fire Resistance Performance of Structural Insulated Panels (SIPs)	611
D. HOPKIN, T. LENNON, V. SILBERSCHMIDT and J. EL-RIMAWI	
CONNECTIONS	
Improved Details for Fire-Induced Steel Single Plate Shear Connections	621
S. SELAMET and M. E. M. GARLOCK	
Fire Performance of External Semi-Rigid Composite Joints.	629
P. SCHAUMANN, B. ZHAO, O. BAHR and C. RENAUD	
Experimental Investigations and Analytical Model for the Behavior of Grade 8.8 Bolts and Butt Welds Under Heating and Subsequent Cooling.	638
F. HANUS, G. ZILLI and J-M. FRANSEN	
Investigations on the Behavior of Steel Single Plate Beam End Framing Connections in Fire	646
G. HU, E. SCHELL and M. D. ENGELHARDT	
A Simplified Model for Modelling End-Plate Connections in Fire.	654
Z. HUANG	
Testing of Composite Top-and-Seat-and-Web Angle Joints at Ambient and Elevated Temperature	662
Y. ZHEN, T. K. HAI and T. S. KIONG	
Numerical Modelling of HSS Endplate Connections at Elevated Temperatures	671
X. QIANG, F. BIJLAARD, H. KOLSTEIN and L. TWILT	
Experimental Study of Mechanical Properties of High-Strength Bolts After Fire.	679
G.-B. LOU, S. YU and R. WANG	

Finite Element Analyses of Flexible End-Plate Connections Between Steel Beams and Columns at Elevated Temperatures.	687
K. AL-JABRI and F. AL-JAHWARI	
How Connections Affect Global Response.	694
K. ANDERSON and M. GILLIE	
MATERIAL BEHAVIOUR	
Constitutive Equations and Empirical Creep Law of Structural Steel S460 at High Temperatures.	703
R. SCHNEIDER and J. LANGE	
Experimental Study of the Mechanical Properties of Prestressed Steel Wire at Elevated Temperatures.	711
Y. WANG, Z. SHEN and Y. LI	
Influence of Polypropylene Fibres on the Thermal Strain of High Strength Concrete at High Temperatures	719
S. HUISMANN, F. WEISE, B. MENG and U. SCHNEIDER	
Fire Induced Transient Creep Causing Stress Relaxation and Tendon Rupture in Unbonded Post-Tensioned Structures: Experiments and Modeling	727
J. GALES, L. BISBY and C. MACDOUGALL	
Experimental Study of Aging Effects on Insulative Properties of Intumescent Coating for Steel Elements	735
L. WANG, Y. C. WANG and G. Q. LI	
Bond Strength Degradation for Prestressed Steel and Carbon FRP Bars in High-Performance Self-Consolidating Concrete at Elevated Temperatures and in Fire	743
C. MALUK, L. BISBY, G. TERRASI and E. HUGI	
Strain Development of Traditional and Self-Compacting Concrete During Fire.	751
E. ANNEREL and L. TAERWE	
Behaviour at High Temperature of Concretes Prepared with Flint, Quartzite or Limestone Aggregates	759
Z. XING, A.-L. BEAUCOUR, R. HEBERT, A. NOUMOWE and B. LEDESERT	
How the Steel Fibres Improve the Residual Properties of Concrete Subjected to High Temperature	767
P. PLIYA, A.-L. BEAUCOUR and A. NOUMOWÉ	
Experimental Study on Fire Performance and Protection of Building Seismic Rubber Bearings	775
B. WU, L. HAN, F. ZHOU and C. SHEN	

Consideration of Transient Creep in the Eurocode Constitutive Model for Concrete in the Fire Situation.	784
T. GERNAY and J.-M. FRANSSSEN	
Deformation of Concrete Due to Mechanical and Fire Loads	792
E. JENSEN, J. VAN HORN and M. JOSHI	
Physical Properties and Behaviour of High-Performance Concrete at High Temperatures	800
U. SCHNEIDER, M. C. ALONSO, P. PIMIENTA and R. JANSSON	
Permeability of High Performance Concrete at Elevated Temperatures	809
U. SCHNEIDER	
Uni-Axial Behaviour of Confined Fiber Reinforced High Strength Concrete Exposed to Elevated Temperatures	817
K. A. ZAIDI, U. K. SHARMA, P. BHARGAVA and N. M. BHANDARI	
Effect of Heating Method on the Physical Properties of Hybrid Fibre Reinforced High Strength Concrete at High Temperature	826
K. WATANABE and T. HORIGUCHI	
Pore Pressure Measurement Inside Hybrid Fibre-Reinforced High Strength Concrete Under High Temperature Condition	833
M. R. BANGI and T. HORIGUCHI	
The Application of RGB Histogram Analysis of Colour Images as a Method of Assessing the Condition of Concrete in Structures After Fire.	841
I. HAGER	
On High-Temperature Properties of Structural Shotcrete Containing Different Accelerating Agents	848
P. BAMONTE, P. G. GAMBAROVA and A. NAFARIEH	
Proposal for the Model and the Mechanical Properties at High Temperature for High Strength Concrete Mixed with Fiber Cocktail	856
K.-H. PARK, H.-Y. KIM, H.-J. KIM, H. K. JEON and K. S. YOUM	
High-Strength Concrete Reinforced Jute Fiber and Water-Soluble PVA Fiber under High Temperature	864
M. OZAWA and H. MORIMOTO	
A Theoretical Approach for Estimating Mechanical and Electric Properties of Polymers and Polymer-Concrete Mixtures at Elevated Temperatures	872
I. E. SHKOLNIK and H. R. HIZIROGLU	

Fire Behaviour of High Performance Concrete—An Experimental Investigation on Spalling Risk	880
P. PIMIENTA, D. PARDON and J.-C. MINDEGUIA	
Stress-Strain Curves of Steel and Aluminium Exposed to Natural Fires.	890
J. MALJAARS	
Tangent Modulus of ASTM A992 Steel at Elevated Temperatures	900
M. A. MOROVAT, J. LEE, G. HU and M. D. ENGELHARDT	
Behaviour of Galvanized High Strength Grade 10.9 Bolts Under Fire Conditions	908
F. GONZÁLEZ and J. LANGE	
FIRE SAFETY ENGINEERING AND PRACTICE	
Using OpenSees for Structures in Fire	919
A. USMANI, J. ZHANG, J. JIANG, Y. JIANG, KOTSOVINOS, J. ZHANG and I. MAY	
Significance of Common U.S. Construction Details on Fire Resilience of Structural Steel Floor Systems.	927
N. ABOUD, C. MCARTHUR, C. BEYLER, T. FAY and N. IWANKIW	
Structural Response of Unprotected Floor Assemblies in Realistic Residential Fire Scenarios.	935
N. BÉNICHOU, J. Z. SU, A. C. BWALYA, G. D. LOUGHEED, B. C. TABER and P. LEROUX	
Mitigation of Post-Earthquake Fire Risk to Building Structures . . .	943
M. H. YASSIN, A. BAGCHI and V. K. R. KODUR	
The Use of Adiabatic Surface Temperature to Design Structures for Fire Exposure	951
U. WICKSTRÖM, A. ROBBINS and G. BAKER	
Variability of Fire and Concrete Temperatures and the Associated Uncertainty in Structural Behavior	959
E. JENSEN, J. VAN HORN and C. D. EAMON	
Feedback and Knowledge Gaps from a Variety of Structural Fire Engineering Projects	967
F. M. BLOCK, N. A. BUTTERWORTH and M. G. GREEN	
Prediction and Calibration of Fire Resistance of Standard Units . . .	975
T. MOLKENS and L. PYL	
A Simplified Approach for Evaluating Equivalent Fire Resistance Under Design Fire Exposures.	983
P. PAKALA, V. KODUR and M. DWAIKAT	

An Assessment of the Use of Structural Deformation as a Method of Determining Area of Fire Origin	993
A. T. TINSLEY and D. J. ICOVE	
Structures Fire Safety: The Brazilian Research Project.	1001
C. CALIL, JR., V. P. E SILVA, A. L. MORENO, JR. and J. M. NETO	
Overview of the AISC Specification Appendix 4—Structural Design for Fire Conditions	1008
N. IWANKIW and B. R. ELLINGWOOD	
Determining the Moment-Curvature Diagram of Aluminium Cross-Sections in Fire; A Numerical Code and Practical Examples	1015
O. R. VAN DER MEULEN, J. MALJAARS, F. SOETENS and L. TWILT	
<i>Author Index</i>	1023

Preface

The idea of specialized “Structures in Fire” (SiF) workshop series was conceived in late 1990’s and bore fruit in 2000 when the “1st International SiF workshop” was organized in Copenhagen, Denmark. This was followed by 2nd, 3rd and 4th International SiF workshops that were held in Christchurch, New Zealand, Ottawa, Canada and Aveiro, Portugal in 2002, 2004 and 2006 respectively. The objective of these specialized workshops was to provide an opportunity for researchers, practitioners and engineers, specializing in *structural fire engineering* field, to share their research, technology and expertise with their peers at an international forum. The special features of SiF workshop series include high quality presentations, adequate time for presentation and discussion, availability of printed proceedings at the start of conference, single-track session, specific focus on “Structures in Fire” theme and affordable costs for participants. The first four workshops were organized by various research groups under the “SiF” leadership headed by Prof. J.M. Franssen.

Over this period, the SiF forum and workshops have grown in size and stature, with increasing international awareness of its mission and vision. Taking note of this success, SiF members, at the “4th International SiF workshop”, endorsed the elevation of “SiF International workshop” series to “International Conference on SiF” series. In addition, to recognize the growing importance of this forum, a steering committee was formed to oversee the SiF activities and conferences. Under this new framework Nanyang Technological University, Singapore, hosted the “5th International Conference on SiF” in May 2008. Following this, Michigan State University was selected to organize the “6th International Conference on SiF” (SiF’10) in East Lansing, MI, in June 2010.

The response for call for papers for SiF’10 was overwhelming and the SiF steering committee received more than 200 abstracts for this year’s conference. Based on the review of each abstract by at least three reviewers, selected from the scientific committee, the steering committee finalized 123 papers for publication in the conference proceedings. Most of the abstracts were of high quality and not all of them could be included in the program due to limited slots available over three days of the conference. The papers in the proceedings are grouped under:

Steel Structures
Concrete Structures
Composite Structures
Timber Structures
Connections
Material Behavior
Fire Safety Engineering and Practice

The papers contained in the proceedings draw on the experience and special knowledge of academics and the practitioners, both in the public and private sectors, from 29 countries, spread over 5 continents: Asia, Australia, Europe, North America and South America. The efforts of these authors are gratefully acknowledged.

It is hoped that the high quality of the technical papers presented in this proceedings will enable researchers and practitioners to develop greater insight of structural fire engineering, so that safer structures could be designed for fire conditions.

We would like to thank members of the “Scientific Committee” for reviewing the abstracts within an incredibly short period of time. Our sincere appreciation to the “SiF Steering Committee” for organizing the review process and for providing direction to the successful organization of this conference. Special acknowledgement to the “conference secretariat—(Department of Civil and Environmental Engineering at Michigan State University)”, for helping us with the nitty-gritty of organizing a conference. Thanks to generous sponsors for supporting the conference and supporting organizations for promoting the conference among the engineering community. Also, our sincere acknowledgments to Mr. Mahmud Dwaikat, PhD student at MSU, for helping us in putting together this proceedings. Last but not the least, special thanks to all the authors and the participants of the conference for making the “6th International Conference on SiF” a great success.

Venkatesh K.R. Kodur
Chairman
Organizing Committee

Jean-Marc Franssen
Chairman
Scientific Committee



Sixth International Conference Structures in Fire (SiF` 10)

Kellogg Hotel & Conference Center
Michigan State University
East Lansing, MI, USA
2-4 June, 2010



**MICHIGAN STATE
UNIVERSITY**

Scientific Committee

Jean-Marc Franssen, Chair	University of Liege, Belgium
Alexandre Landesmann	Fed. Univ. of Rio de Janeiro, Brazil
Ali Nadjai	The University of Ulster, UK
Andrea Frangi	ETH Zürich, Switzerland
Andy Buchanan	Univ. of Canterbury, New Zealand
Arnoud Breunese	Efectis, Netherlands
Asif Usmani	University of Edinburgh, UK
Bassam Izzuddin	Imperial College, UK
Bin Zhao	CTICM, France
Bo Wu	South China Univ. of Tech., China
Colin Bailey	The University of Manchester, UK
Didier Talamona	Univ. of Newcastle, Australia
Faris Ali	University of Ulster, UK
Florian Block	Buro Happold, UK
Frank Dehn	MFPA, Germany
Frantisek Wald	Czech Tech. Univ. in Prague, Czech
Frederick Mowrer	University of Maryland, USA
Guo Qiang Li	Tongji University, China
Ian Burgess	University of Sheffield, UK
Jim Milke	University of Maryland, USA
Jurgen Konig	SP Tech. Res. Inst., Sweden
Kuldeep Prasad	Nat. Inst. of Stds. & Tech., USA
Linus Lim	Arup Fire, UK
Long Phan	Nat. Inst. of Stds. & Tech., USA
Luc Taerwe	University of Gent, Belgium
Marc Janssens	Southwest Research Institute, USA
Martin Gillie	University of Edinburgh, UK
Olivier Vassart	Arcelor-Mittal, Luxemburg
Paulo Vila Real	University of Avero, Portugal
Peter Moss	Univ. of Canterbury, New Zealand
Peter Schaumann	University of Hannover, Germany
Pietro Gambarova	Politecnico. di Milano, Italy

Stephen Pessiki	Lehigh University, USA
Steve Craft	Forintek, Canada
Takashi Horiguchi	Hokkaido University, Japan
Tan Kang Hai, Philip	Nanyang Tech. Univ., Singapore
Ulrich Schneider	Vienna Univ. of Tech., Austria
Venkatesh Kodur	Michigan State University, USA
Yong C. Wang	The University of Manchester, UK

Organizing Committee

Venkatesh Kodur, Chair	Michigan State University, USA
Amit Varma	Purdue University, USA
Fahim Sadek	Nat. Inst. of Stds. & Tech., USA
Farid Alfawakhiri	Am. Inst. of Steel Const., USA
Luke Bisby	University of Edinburgh, UK
Maria Garlock	Princeton University, USA
Mark Green	Queen's University, Canada
Michael Engelhardt	Univ. of Texas at Austin, USA
Nestor Iwankiw	Hughes Associates, Inc., USA
Ronald Harichandran	Michigan State University, USA
Steve Szoke	Portland Cement Assn., USA

Steering Committee

Jean-Marc Franssen	University of Liege, Belgium
Andy Buchanan	Univ. of Canterbury, New Zealand
Venkatesh Kodur	Michigan State University
Paulo Vila Real	University of Aveiro, Portugal

Acknowledgements



STEEL STRUCTURES

Experimental Investigation of Fundamental Behavior of Steel Members Under Fire Loading

L. CHOE and A. H. VARMA

ABSTRACT

Experimental are being conducted to determine the fundamental behavior of steel columns. Column and beam-column specimens are being tested by subjecting them to combined mechanical and thermal loading. The experimental approaches involves the use of: (a) innovative radiant heating and control equipment to apply thermal loading instead of using a conventional furnace and (b) digital image processing technique incorporated with close-range photogrammetry to measure the deformation and curvature over the heated region. Also, a unique self-reacting test frame was designed by the authors to conduct the column experiments. The measured axial force-moment-curvature-temperature ($P-M-\Phi-T$), axial force-displacement-temperature ($P-\Delta-T$), and axial force-end rotation-temperature ($P-\theta-T$) responses of steel columns were compared with those obtained by 3D finite element analyses.

INTRODUCTION

The standard fire ratings of building components have been obtained experimentally by testing them according to ASTM E119 [1] standard fire test. Standard fire tests of *loaded* columns are, however, extremely difficult and expensive because large axial loads have to be applied along with the elevated temperatures. A handful of column testing furnaces are available in the world. As a result, currently, there is a lack of experimental data regarding the *fundamental behavior* of steel columns at elevated temperatures.

The fundamental behavior can be defined as: the axial force-moment-curvature-temperature ($P-M-\Phi-T$) response of the failure section of steel beam-columns and columns subjected to elevated temperatures simulating fire loading. This knowledge is essential to develop *structural* performance-based design guidelines for steel members in building structures subjected to realistic fire loading events [2]. The

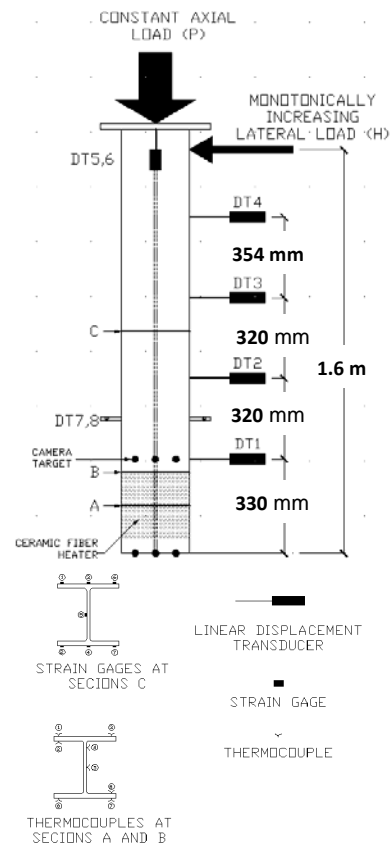
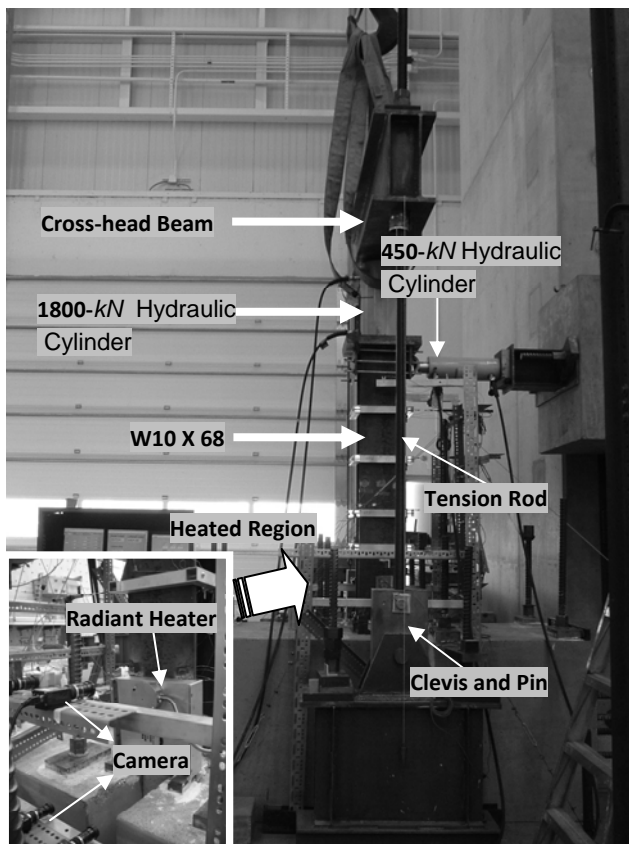
Bowen Laboratory, School of Civil Eng., Purdue University, 1040 South River Road, West Lafayette, IN 47907

behavior of steel building structures under fire loading depends significantly on the elevated temperature performance of the steel members, particularly columns [3].

This paper presents an innovative experimental approach developed and implemented by the authors to investigate the *fundamental behavior* of steel columns subjected to elevated temperatures. The 3D finite element models (3D FEM) were also developed to predict the fire behavior of steel columns and to compare with experimental results.

TEST PROGRAM

The experimental investigations consist of two main parts including steel beam-columns and steel columns under fire loadings. The experimental tests presented herein were intended to examine (1) lateral load-displacement ($F-\Delta$) responses of steel beam-column at elevated temperature, (2) the axial force-moment-curvature-temperature ($P-M-\Phi-T$) behavior of steel beam-columns at base segment (i.e., failure segment), and (3) the stability of steel columns subjected to elevated temperatures.



(a)

(b)

Figure 1. (a) Test Setup and (b) Instrumentation layout for W10 x 68 beam-column tests.

Beam-Column Tests

Figure 1 (a) shows the test frame of beam-column experiments. Test specimens are W10 x 68 cantilever beams (free at the top and fixed at the base). The overall length of specimen from foundation to free end is equal to 2.5 m. Two concrete blocks (914 mm x 914 mm x 914 mm) were designed to clamp the bottom portion of specimen. Test length of specimen was equal to 1.6 m. Steel beam-column specimens were tested at ambient to examine the test setup itself and to compare the behavior with specimens tested at elevated temperatures.

An 1800-kN hydraulic cylinder was used to apply axial loading at the top of specimen. Several preliminary tests were conducted to minimize the eccentricity of load. A 450-kN hydraulic cylinder was used to apply the lateral loading at the top of the specimen. A half-cylinder steel bearing was mounted at the location of lateral force to prevent the local failure of flanges and to allow free rotation of the end. Two 64 mm-diameter tension rods were designed to resist the reaction due to axial load equivalent to 2700 kN. The bottom portion of tension rods were connected to clevis and pin so that they can rotate in the direction of lateral loading without creating undesired restraints.

The digital imaging system developed by Hong [4] was implemented to measure deformations, average strains, and curvature of the heated region. The camera target points were located as shown in Figure 1 (a). The distance between top and bottom rows of target points is equal to 330 mm. The focal length of each camera lens was 75 mm. Digital cameras were also installed perpendicular to the target points such that the effect of lens distortion was negligible on displacement measurement. Digital cameras were programmed to acquire images every second during the experiment.

As shown in Figure 1 (a), a set of cameras took snapshots of the movement of target points and saved them into data acquisition system. The stored images were then post-processed to determine the axial and lateral displacements in real units to compute the average longitudinal strains, curvature, and base rotation of heated region. In the ambient test, displacement data obtained from digital cameras were compared with other voltage-based sensors. The average strain values obtained by the imaging system and strain gages agree reasonably to each other.

Figure 1 (b) shows the instrumentation layout including displacement transducers at various locations along the specimen length. Two rotation transducers were mounted on clevis—pin assemblies. K-type thermocouples were welded to the surfaces of specimen to obtain temperature histories at failure segments. A set of proportional-integral-derivative (PID) controllers was employed to control heaters individually. The pre-determined temperature-time ($T-t$) curve for specimen was programmed to each PID controller so that base segment was heated uniformly. The temperatures of heat generated by heaters were monitored during the test.

The test procedure was conducted as follows: (1) axial load ($P/P_o = 0.3$) was applied at the top of specimen. The load was then held constant throughout the test. (2) Radiant heat was applied to the surface of base segment (i.e., failure segment) using ceramic fiber heaters. Power rates of heaters were controlled and monitored until the average temperature of failure segment reached to 300°C. (3) After the surface temperature of specimen stabilized, the monotonically increasing lateral load was applied near the free end until flexural failure.

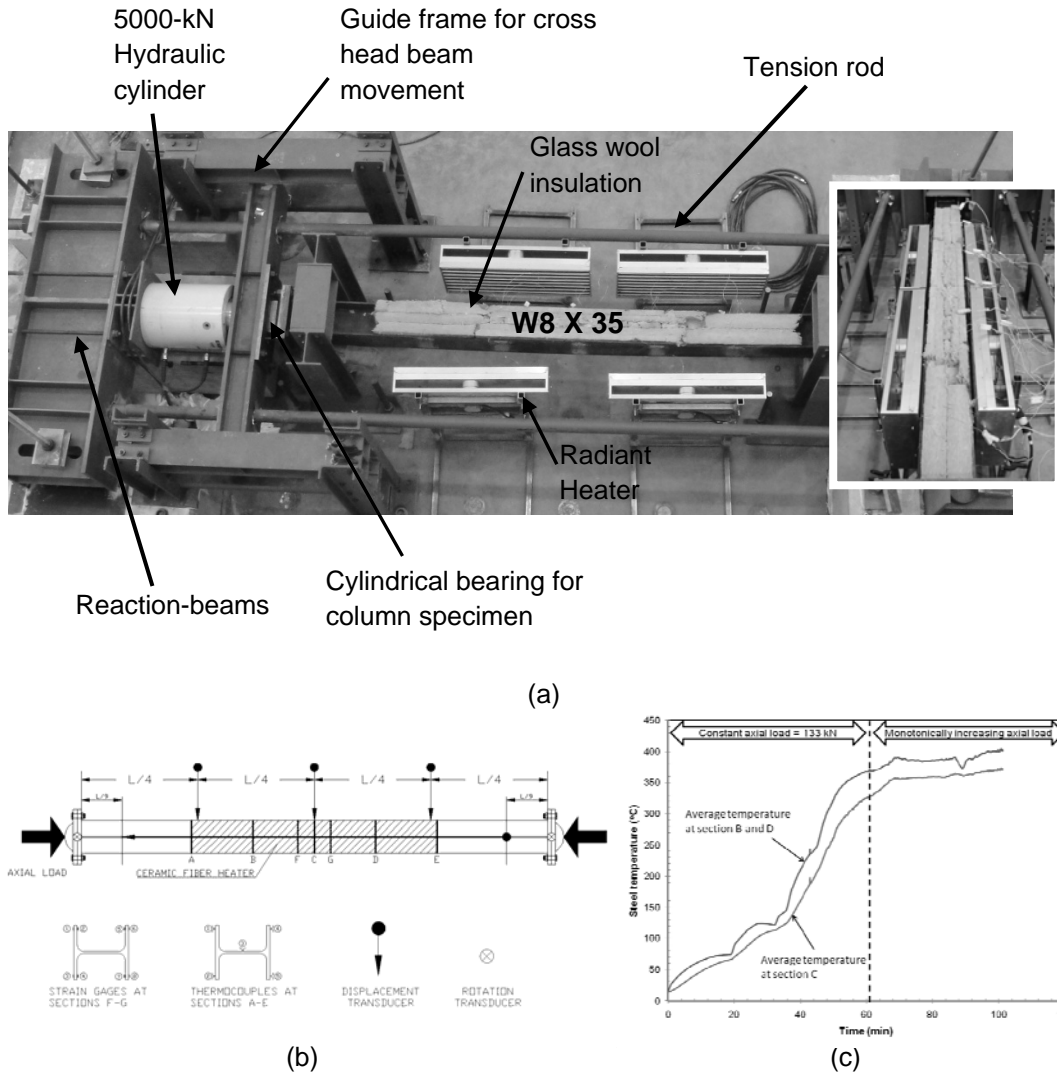


Figure 2. (a) Test Setup, (b) Instrumentation layout, and (c) Temperature-time histories for W8 x 35 column tests.

Column Tests

Figure 2 (a) shows the self-reacting test frame designed and assembled for the column tests. This test frame specially allows conducting the column tests with various parameters and axial load up to 4000 kN . The entire setup was supported by four concrete blocks (1524 mm x 610 mm x 610 mm). Smooth surfaces of steel plates (thickness = 9 mm) and Teflon machine grease were placed on the blocks to minimize the friction between the bottom edges of reaction beams and concrete surfaces. A surveyor's level and hydro-stone paste were utilized when assembling test frame.

A 5000-*kN* hydraulic cylinder was installed for axial loading. Two high strength tension rods (diameter = 76 *mm*) were designed to resist the reaction induced by axial load equivalent to 4000 *kN*. Half-cylinder steel bearings and matching saddles were assembled to reaction-beams to avoid the undesired bending of tension rods. Several preliminary tests were conducted to minimize the eccentricity of load.

The columns were subjected to radiant heat using ceramic fiber heaters with surface dimensions equal to 400 *mm* x 1000 *mm*. The column length subjected to high temperature is equivalent to 2000 *mm*. The adjunct stands were fabricated to allow installing heaters as close as 1 *cm* from each side of specimen. The lateral movement of column caused by axial loading was not interfered by the heaters.

Figure 2 (b) shows the instrumentation layout of column tests. Displacement transducers located along the specimen length were used for ambient tests only. Two rotation transducers were mounted at column ends. K-type thermocouples were welded to the specimen in order to obtain temperature histories of bare steel surfaces as shown in Figure 2 (c). PID controllers were employed to operate heaters individually. Glass wool insulation was placed at the top of steel web at which radiant heat was not directly exposed.

The following test procedure was conducted sequentially: (1) Initial axial load (about 133 *kN*) was applied in order to align the specimen horizontally. Also, strain gages were installed near column mid-section to examine the eccentricity of load. (2) After the initial axial load was maintained by hydraulic controller, the specimen was subjected to thermal loading by using four ceramic fiber radiant heaters. Steel surface temperatures were monitored by PID controllers. (3) After the average temperature was reached to 300 °C, the axial load was applied monotonically until the ultimate strength of column specimen was achieved.

TEST RESULTS

Beam-Column Tests

Test results presented herein show typical comparisons between the fundamental behavior of W10 x 68 specimen tested at ambient temperature and the specimen subjected to steel surface temperature of 300°C. Axial loading ($P/P_o = 0.3$) was imposed and maintained constant throughout the test. When the average temperature of steel surfaces at base segment reached 300°C, lateral load was applied until the lateral displacement was about 160 *mm*. Further investigations of test parameters (e.g., axial load level, geometric and material properties of specimens, steel surface temperature, temperature gradient, and thickness of fireproof) on the behavior of steel beam-columns are currently in progress.

As the applied lateral load increases, the yielding spreads at base segment (i.e., heated region) to form the plastic hinge mechanism. The lateral (u_i) and axial (v_i) displacements of top and bottom of the heated region were measured by the digital imaging system. The average strain ($\epsilon_{avg,j}$) and curvature (Φ) of the failure segment were calculated using u_i and v_i . The flexibility of test setup also caused rigid-body rotation of specimen base. Hence, the measured lateral displacements along the specimen length were adjusted by subtracting the lateral displacement due to base rotation.

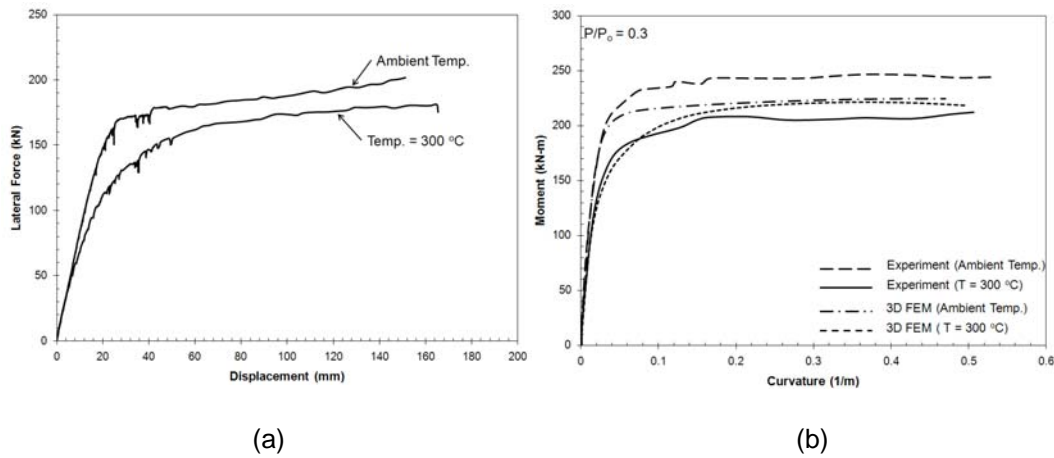


Figure 3. (a) The measured $F-\Delta-T$ response and (b) $M-\Phi-T$ response of W10X68 beam-columns.

Figure 3 (a) shows the typical lateral force-deformation-temperature ($F-\Delta-T$) response of W10 x 68 beam-columns subjected to axial load ($P/P_o = 0.3$) and two different thermal loadings (ambient and $T = 300^\circ\text{C}$). The lateral $F-\Delta$ response is initially linear followed by nonlinearity as the applied lateral load increases. The specimen maintains its lateral load capacity with increasing lateral displacements, while yields occur and spread in the base segment. For elevated temperatures, nonlinear behavior takes place at the earlier stage of loading.

Figure 3 (b) illustrates typical comparisons of moment-curvature-temperature ($M-\Phi-T$) responses of failure segment (i.e., heated region) between 3D FEM models and experiment results. At ambient temperature, the measured flexural stiffness agrees reasonably with the results obtained from 3D FEM. However, plastic moment capacity is higher than that of 3D FEM model. The reasons would be: (1) 3D FEM models assume elastic and perfect plastic (no strain hardening) material properties. (2) There would be the discrepancy between the measured and nominal material properties at ambient temperature used for 3D FEM models.

As the surface temperature increased, flexural stiffness decreased more significantly at the earlier stage of loading. Also, the plastic moment capacity is not extensively affected by the difference between nominal and actual material properties. The comparisons in Figure 3 (b) indicate that the assumed material properties at 300°C compare better with the test specimens than those at ambient. This is probably because the actual material yield stress is greater than 345 MPa at ambient but reduces to the assumed value (i.e., 212 MPa) at $T = 300^\circ\text{C}$.

Column Tests

Test results presented herein shows the comparisons between the fundamental behaviors of a W8 x 35 column tested at ambient temperatures and the specimen subjected to steel surface temperature of 300°C . Further investigations of test parameters (e.g., slenderness ratio, steel temperature, and rotational restraints) are currently in progress.

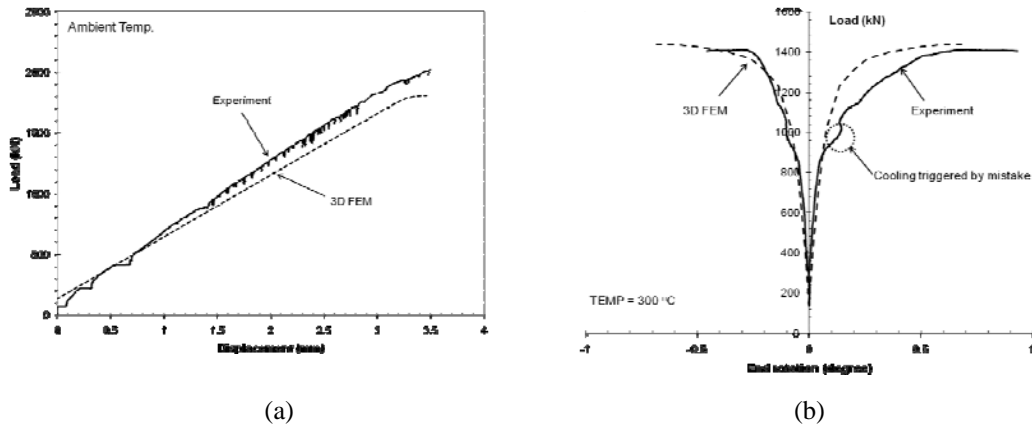


Figure 4. (a) $P - \Delta$ response at ambient and (b) $P - \theta$ response at $T = 300^{\circ}\text{C}$.

Figure 4 (a) shows the comparison between the measured and calculated axial load-displacement ($P-\Delta$) response of W8 x 35 column specimen. The slenderness ratio (L/r) is equal to 67. Note that the direct comparison with $P-\Delta$ response at $T = 300^{\circ}\text{C}$ was not investigated because: (1) the ambient column test was a trial experiment to examine the performance of the self-reacting test frame itself. (2) Developing the layout of displacement transducers to measure the column deformation at elevated temperature is currently in progress.

At ambient, the measured axial stiffness agrees reasonably with the result obtained from 3D FEM. There is a slight discrepancy between the measured and the calculated axial load capacity. The reasons would be: (1) 3D FEM models assume elastic and perfect plastic (no strain hardening) material properties. (2) There would be some discrepancy between the measured and nominal material properties at ambient temperature used for 3D FEM model.

Figure 4 (b) shows the comparison of axial load-end rotation ($P-\theta$) response of a heated W8 x 35 column specimen ($T = 300^{\circ}\text{C}$) between 3D FEM model and experiment results. The solid lines in Figure 4 (b) present the rotations measured at each column end. Positive values indicate the rotation measured near hydraulic cylinder; negative values indicate the rotation measured at far end.

Temperature-dependent steel material properties were used for developing a 3D FEM model as specified in Eurocode [5]. The steel yield strength used in 3D FEM was 400 MPa . The measured and calculated axial load capacity of column at $T = 300^{\circ}\text{C}$ was 1400 kN . The measured $P-\theta$ response agrees reasonably with the results obtained from 3D FEM. The slight discontinuity shown in Figure 4 (b) is due to cooling that was triggered by mistake.

SUMMARY AND CONCLUSION

This paper presented the experimental investigations to determine the fundamental behavior of steel members (beam-columns and columns) at elevated temperature. Further investigations of various test parameters are currently in progress. The experimental approaches included: (a) innovative heating and control equipment to

apply thermal loading instead of using a conventional furnace and (b) digital image processing technique incorporated with close-range photogrammetry to measure deformation and curvature of the heated region. A unique self-reacting test frame was designed to conduct the various column tests with the axial load up to 4000 kN.

The measured fundamental behavior of steel columns including $P-M-\Phi-T$, $P-\Delta-T$, and $P-\theta-T$ were compared to those obtained from 3D FEM models. The experimental results indicate:

- (1) As the steel surface temperature increased, flexural stiffness decreased more significantly at earlier stages of loading. Also, the plastic moment capacity at elevated temperature is less affected by the differences between nominal and actual material properties than at ambient.
- (2) The measured $P-\theta$ response agrees reasonably with the results obtained from 3D FEM when Eurocode steel material properties were used. The $P-\theta$ responses show that the setup was able to conduct column tests while achieving simply supported end conditions.

ACKNOWLEDGMENT

The research presented in this paper was funded by the National Science Foundation (Grant No. CMMI-0825506 and 0601201). The project is titled “Structural Mechanics of Steel columns and Beam-Columns under Fire Loading”. Experimental data, findings, and conclusions or recommendations are those of the authors only.

REFERENCE

1. ASTM Standard E119 (2008). *Standard Methods of Fire Test of Building Construction and Materials*, American Society for Testing and Materials: West Conshohocken, PA, USA.
2. Varma, A. H. and Hong, S. (2007). “Fundamental Behavior of Composite CFT Members under Standard Fire Loading.” *Proceeding of the 2007 Structures Congress*, Long Beach, CA, ASCE, 12 pp.
3. Agarwal, A., Varma, A.H., and Cedeno, G. (2009). “Steel columns under fire loading: Stability behavior and design.” *Proceedings of the Annual Stability Conference*, Structural Stability Council, Phoenix, Arizona, in press, 405–429.
4. Hong, S. (2007). “Fundamental behavior and stability of concrete filled tubes (CFTs) members under fire loading.” Ph.D dissertation, School of Civil Engineering, Purdue University, West Lafayette, IN, May 2007.
5. EN 1993-1-2 (2005). Eurocode 3: Design of Steel Structures, Part 1-2: General Rules—Structural Fire Design, European Committee for Standardization, Brussels, Belgium.

A 3D Numerical Analysis of a Typical Steel Highway Overpass Bridge Under a Hydrocarbon Fire

I. PAYÁ-ZAFORTEZA and M. E. M. GARLOCK

ABSTRACT

Structural fire safety has traditionally focused on buildings and has paid little attention to bridges. This paper aims to develop knowledge on the behavior of steel bridges under fire. It focuses on the study of a simply supported bridge of 12.20 m (40 ft.) span length designed by the Federal Highway Administration of the United States of America. The cross section of the bridge has five steel girders supporting a reinforced concrete slab, the slab not being structurally connected to the girders. A 3D model of the bridge has been built with the commercial software LUSAS using solid elements. The model is submitted to a hydrocarbon design fire that could be caused, for example, by the crash or the overturning of a gasoline tanker. The bridge response to such a fire was studied by varying the following parameters: magnitude of gravity load (dead and live) and the axial restraint (fixed or free). Results show that the times to failure of the bridge are very small (less than 10 minutes in all the cases analyzed) which gives almost no time for the firemen to reach the bridge in case of a fire event. Therefore some protective measures should be undertaken in these kinds of bridges if they are in a fire risk situation and its fire safety wants to be ensured. Furthermore, horizontal displacements of the bridge are big enough to require the consideration of the interaction between the bridge deck and the adjacent span or abutment.

Ignacio Payá-Zaforteza, Ph.D. (corresponding author), Assistant Professor, Instituto de Ciencia y Tecnología del Hormigón (ICITECH), Universidad Politécnica de Valencia, Valencia, 46023 Spain; igpaza@cst.upv.es

Maria E.M. Garlock, Ph.D., Assistant Professor, Department of Civil and Environmental Engineering, Princeton University, Princeton, NJ, 08544, USA; mgarlock@princeton.edu

1. INTRODUCTION

Recent studies on the state-of-the art of bridge fires [1, 2] indicates that bridge fires are a major concern. The occurrence of bridge fires is increasing and these fires can cause collapse (Fig. 1a) or at the very least significant traffic delays, detours, and costly repairs. For example, in April of 2007, a tanker truck overturned and started an intense fire under the I-580, which in 20 minutes resulted in the collapse of two spans of the MacArthur Maze in Oakland, CA, USA [3]. This event cost millions of dollars and almost one month of detours.

Structural fire safety has been traditionally focused on buildings; but the response of fire on bridges will be different for many reasons including:

(1) *Cause of fire*: A literature review indicates that bridge fires are commonly caused by collisions (crashing of gasoline trucks and burning of gasoline in the vicinity of the bridge) or construction (the wood scaffolding or formwork ignites). On the other hand, building fires are commonly caused by accidental ignition of the fuel sources in the compartment. Since the ‘fuel’ is different, the fire “loads” are different.

(2) *Fire loads*: Bridge fires are typically petrol fires, also referred to as hydrocarbon fires, which are much more severe than building fires and are characterized by fast heating rates or high fire intensities. Thus, the bridge fire is likely to be much more intense than typical building fire and can reach very high temperatures within the first few minutes of fire exposure. It therefore poses a severe threat to structural members of the bridge and the transportation system.

(3) *Fire protection*: bridge girders typically have no fire protection whereas buildings have active fire protection (such as sprinklers) and passive fire protection (such as spray fire resistant material);

(4) *Beam depth*: bridge beams are much deeper than common building beams and therefore more susceptible to web buckling. A typical building beam is about 0.30 m (12 in) deep and a bridge girder depth is typically more than three times deeper than that, with about the same web thickness. Thus the bridge girder web is more slender and susceptible to buckling, especially at high temperature. Plate girders are even deeper, generally more than 5 times deeper than building beams.

(5) *Connections*: bridge girders are typically supported by bearing on the bottom flange, whereas in buildings the connection is made through the web and/or the flanges. The boundary conditions of a bridge and building beam are therefore different.



Fig. 1(a): Bridge fire collapse over I-75 Hazel Park, MI (July 15, 2009).



Fig. 1(b): Typical steel girder highway overpass (Route 1, NJ).



Fig. 1(c): Typical simply supported condition (Route 1, NJ).

The objective of this paper is to evaluate the fire response of a simply supported steel highway overpass bridge commonly found in the USA (see Fig 1b and c for example). Previous fire events, such as that shown in Figure 1a, have indicated that these types of bridges are susceptible to fire induced collapse. Our study examines the effects of (1) magnitude of gravity load (dead and live) and (2) the axial restraint (fixed or free) on a W33 (840 mm deep) steel girder subject to a hydrocarbon pool fire: This is the beginning of a research program being developed by the authors with an ultimate goal to improve fire safety of steel bridges subject to fire.

2. PROTOTYPE AND NUMERICAL MODEL

2.1 Prototype

The prototype bridge used in our study is a typical simply supported bridge designed by the Federal Highway Administration (FHWA) of the United States of America based on their standard plans for highway bridges. The bridge spans 12.2 m (40 ft.) and its cross section is shown in Fig. 2. The bridge consists of five hot rolled steel girders of type W33x141. The beams support a reinforced concrete slab 0.2 m (8 inches) deep but the slab is not connected to the girders and, therefore, there is no composite action. Transverse diaphragms are placed at mid span and at the supports to laterally stiffen the bridge deck. The bridge has two expansion joints at its extremities with a width of 3.6 cm. At ambient temperature, material properties correspond to the nominal values for A36 steel (see [4]) and therefore its minimum yield stress is 250 MPa (36 ksi). High temperature material assumptions are discussed later.

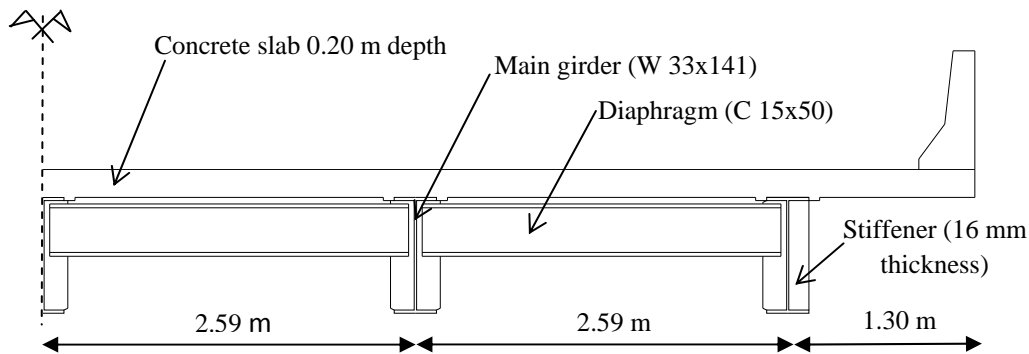


Fig. 2: Half section of the studied bridge near bearing.

2.2 Test Parameters

Our study applies on the full length of the bridge the Eurocode hydrocarbon fire [5], which is defined by the following equation:

$$T = 1080(1 - 0.325e^{-0.167t} - 0.675e^{-2.5t}) + T_0 \quad (1)$$

“ t ” is the time in minutes and “ T_0 ” is the ambient temperature (20°C). It is a fast and hot fire that reaches a temperature of 743°C in one minute for example.

Using this fire load, we examine the response of the bridge varying the following parameters: the magnitude of gravity load (dead and live), and the axial restraint (fixed or free). Table I shows the test matrix where the name of each analysis represents the following nomenclature:

- (1) $0, 1, 2, 3, 4$ – represents the five gravity loading conditions shown in Table I;
- (2) fre, fix – represents the axial restraint (boundary condition) as being free or fixed.

TABLE I. TEST MATRIX OF VARIOUS ANALYSES.

Analysis Name	Gravity Loads	Axial Restraint
<i>0-fre</i>	none	Free
<i>1-fre</i>	G	Free
<i>2-fre</i>	G+0.3Q	Free
<i>3-fre</i>	G+0.5Q	Free
<i>4-fre</i>	G+Q	Free
<i>2-fix</i>	G+0.3Q	Fixed

Dead Loads (G) consider the weight of the tributary area of concrete slab and wearing surface of the deck (22542 N/m) plus the self weight of the girder (2067 N/m). Live loads (Q) consider a uniform load according to AASHTO [6] equal to 10700 N/m of girder. While it may seem unrealistic to consider live loads while the bridge is on fire, in the case of the fire-induced collapse of the bridge shown in Fig. 1(a), cameras have shown cars crossing over the bridge while fire raged below. Our prototype bridge was originally designed to support the HS20-44 truck load of the AASHTO code [6], but no evidence has been found of any truck crossing the bridge while it is on fire. Therefore, this load has not been considered in the analyses. Note that in analysis *0-fre* no gravity load has been applied. This does not correspond to a real possibility but we use it to study the influence of thermal loading alone.

Most of our analyses assume that the girder is free to expand axially since bridges are designed with expansion joints for temperature variations. However, the temperature change in a fire is significantly larger than that due to weather changes and it is realistic to consider that the girder may expand enough to be eventually restrained by the abutments or an adjacent span. We expect that the actual axial restraint of the bridge is somewhere between fixed and free but these analyses capture the upper and lower limits of response.

2.3 Finite Element Model

The numerical study was done with the finite element (FE) software LUSAS [7]. An uncoupled thermo-mechanical analysis is used where in the first phase (the thermal analysis) the heat transfer method provides transient nodal temperatures with respect to time. In the second phase (the structural analysis), the nodal temperatures are read from the thermal analysis and corresponding temperature dependent mechanical material properties are used based on those given in EN 1993-1-2 [8] for steel and EN 1992-1-2 [9] for concrete. It was assumed that

concrete aggregates were calcareous. Note that the convective heat transfer coefficient, h_c , is defined as $50 \text{ W/m}^2\text{K}$ for the hydrocarbon fire per EC1 [5] and not $25 \text{ W/m}^2\text{K}$ as commonly used in other cases.

For the thermal analysis, LUSAS element HF8 was used, which is a three dimensional eight-noded solid field element with one degree of freedom per node. For the structural analysis, LUSAS element HX8M was used, which is a three dimensional eight-noded solid continuum element with three degrees of freedom per node. This element does not suffer from locking due to parasitic shear.

Since the slab is not composite with the girder, the slab was included in the thermal phase of the analysis, but then was “deactivated” in the structural analysis. In this manner, only the thermal impact of the slab was considered (as well as the self imposed weight as described earlier). The fire load was applied to the underside of the girder and slab.

All the gravity loads (with the exception of the self weight of the steel girder) were applied as a uniform pressure acting on the top of the upper flange of the steel girder. The self weight of the girder was automatically generated by the software.

2.3 Mesh discretization

Figure 3 shows the meshes used in the analyses where a roller is drawn at the supports (to represent vertical support with free axial expansion and rotation). This vertical support is provided along a line of nodes on the bottom flange beneath the stiffener. Note that analysis *2-fix* is not properly represented by the boundary conditions shown in Fig 3. In that analysis, the axial expansion is restrained at the point that the horizontal displacement of the roller equals the length of the expansion joint. From that moment on, analysis *2-fix* is axially restrained at all the nodes on the outer cross section. Appropriate boundary conditions were used at midspan (meaning that the midspan had free vertical motion, but it was restrained from rotating and from translating on the longitudinal axis). The mesh was refined near the supports, which was an area of high stress. The model had 6640 solid elements and 9033 nodes. Geometric non linearity was considered using an Eulerian formulation described in [7].

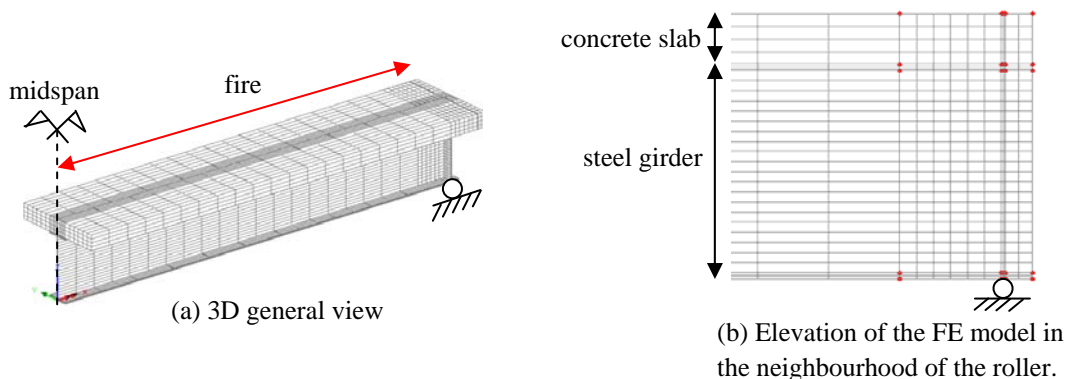


Figure 3. Views of the FE models.

The accuracy and efficiency of the mesh and FE model was checked in the following ways:

(1) Results of stresses and deflections at midspan (due to dead loads) were compared with the theoretical values given by the beam theory and with values found in the original drawings of the bridge. The difference in deflections was 1.7 % whereas difference in stresses was 3 %, which is very small considering that beam theory does not account second order effects nor does it consider the loads as a surface load on the flange, which produces non-uniform stresses on the flanges.

(2) The number of elements in the central area of the beam where the mesh was coarser was multiplied by a factor of 2.5 and the change of both, thermal and structural results was negligible; and

(3) A similar model was created in ABAQUS [10], which yielded similar results.

3. RESULTS AND DISCUSSION

Figure 4 shows the evolution of the temperatures of the steel girder as a function of time. A non-linear thermal gradient appears in the girder, although the temperatures in a big part of the web are uniform. This non-linearity is due to the fact that the bottom flange and the web always have higher temperatures than the upper flange, as this element has one of its sides protected from fire by the RC slab. As a result of this gradient, stresses due to thermal gradients appear even if the structure is statically determinate in relation to its support conditions and even if no dead or live load is applied (analysis *0-fre*).

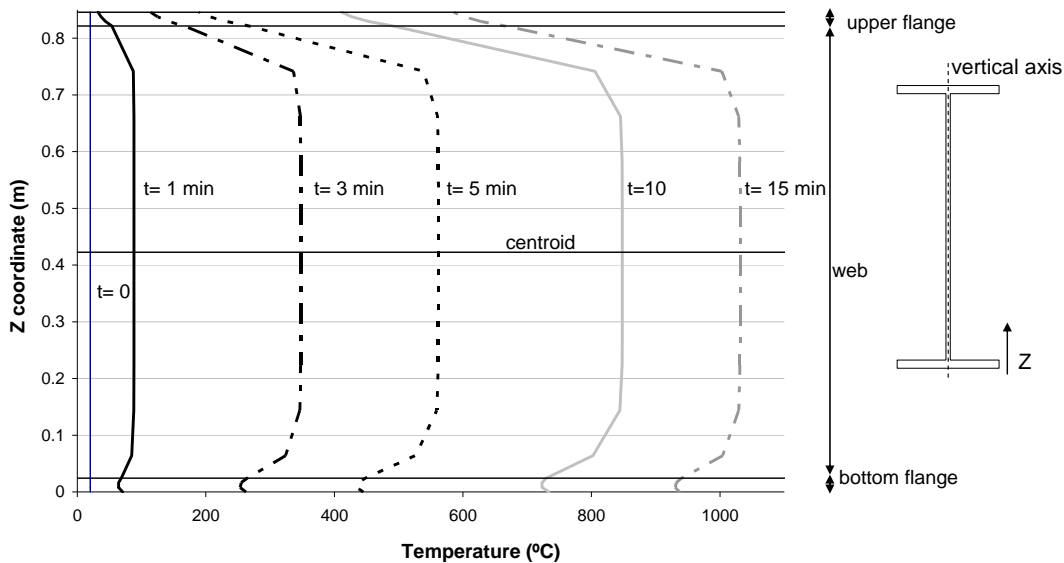


Figure 4. Profile of temperatures along the vertical axis of the girder

Times to failure for each one of the analysis as well as the location of failure, the maximum horizontal displacements and the midspan deflections of the structure are given in Table II. Figure 5 shows the evolution of midspan deflections and Figure 6 displays the collapse mechanisms which are related to the yielding of the bottom flange and the web of the girder. The analysis of these results shows that:

(1) Times to failure are always below 9.5 minutes what gives almost no time for the firemen to reach the bridge location. Therefore, this structural system seems to

be prone to collapse due to fire events and some preventive measures against the fire hazard should be undertaken depending on the fire risk.

(2) The gravity load does not have a remarkable influence on the times to failure. Only the case where the whole live load was applied on the girder showed a significantly lower time, but this loading case is unlikely in a fire situation.

(3) The support condition has an appreciable influence in the mode of failure and the final deflections but not in the time that the bridge can withstand the fire.

(4) Horizontal displacements in the analyses *1-fre* to *4-fre* were much bigger than the expansion joint width (0.036 m). Therefore, the restraint due to the existence of an adjacent girder or abutment should be considered in future studies as it provides a more realistic approach to the problem.

TABLE II. MAIN ANALYSES RESULTS.

Analysis Name	Time to failure (min)	Maximum mid-span deflections (m)	Maximum horizontal displacement (m)	location of failure
<i>1-fre</i>	9.5	0.47	0.25	midspan
<i>2-fre</i>	9	0.43	0.24	midspan
<i>3-fre</i>	8.75	0.39	0.22	midspan
<i>4-fre</i>	8.25	0.39	0.22	midspan
<i>2-fix</i>	8.75	0.18	0.04	roller support

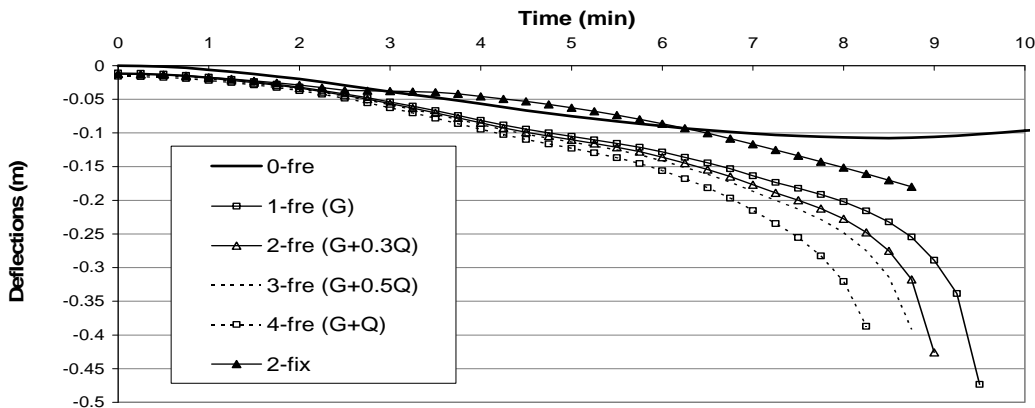


Figure 5. Midspan deflections

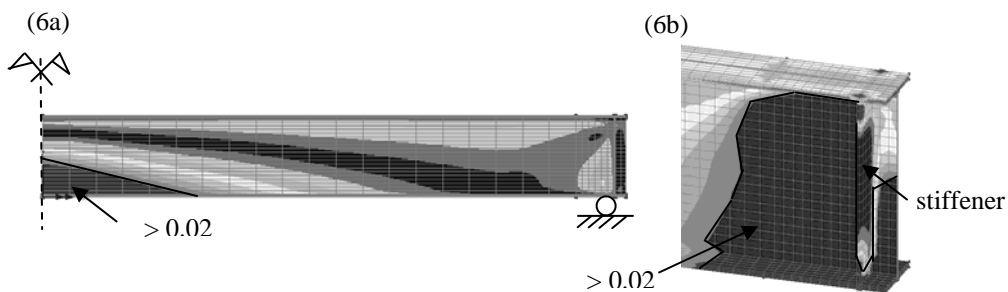


Figure 6. Views of the equivalent strains (ϵ) at the moment of collapse: (6a) mid-span yielding for the *-fre* analyses, (6b) web and bottom yielding near the supports for the *2-fix* analyses. Strains in marked areas are bigger than 0.02.

4. CONCLUSIONS

Bridge fires are a major concern as the occurrence of these events is increasing and the fires can cause the collapse of the structure or, at the very least, significant traffic delays, detours, and costly repairs. This paper studies the effect of a standard hydrocarbon fire on a steel girder bridge under different live loads and support conditions using a FE model developed with the software LUSAS. Numerical results show that the time to failure of the bridge is very small (less than 9.5 minutes in all the cases analyzed). Therefore some protective measures should be undertaken in this kind of bridges if they are in a fire risk situation and its fire safety needs to be ensured.

ACKNOWLEDGEMENTS

Funding for this research has been provided to Mr. Paya-Zaforteza by the Program for Postdoctoral Stays administered by the Spanish Ministry of Education (contract number EX-2008-0669). All opinions, findings, and conclusions expressed in this paper are the authors' and do not necessarily reflect the policies and views of the Princeton University, the Spanish Ministry of Education or the ICITECH. The authors are grateful to Mr. John Roadnight from LUSAS Technical Support for his help and to Mr. Serdar Selamet, graduate student at Princeton University, for his assistance in comparing LUSAS results with the software ABAQUS.

REFERENCES

1. Kodur V., Gu L., Garlock M. E., 2010. "Review and Assessment of Fire Hazard in Bridges", *Proceedings of the TRB Annual Meeting*, Washington D.C. January.
2. Kodur V., Garlock M.E., Gu L., Paya-Zaforteza I. "Fire Hazard in Bridges: Review, Assessment and Repair Strategies"(in prep. for submission to ASCE Journal of Bridge Eng).
3. Astaneh-Asl A., Noble C. R., Son J., Wemhoff A.P., Thomas M.P., and McMichael L.D. (2009) "Fire Protection of Steel Bridges and the Case of the MacArthur Maze Fire Collapse", *Proc. of the ASCE TCLEE Conf.* pp. 1-12
4. American Society for Testing and Materials (ASTM). 2004. *ASTM A6/A6M Standard Specification for Structural Steel (A36-/A36M-04a)*, ASTM, West Conshohocken, PA, USA.
5. European Committee for Standardization (CEN). 2005. *EN 1993-1-2: 2005 Eurocode 3: Design of Steel Structures. Part 1.2 General Rules – Structural Fire Design*, CEN, Brussels.
6. AASHTO, 2009. *LRFD Bridge design specifications*. Washington D.C., USA.
7. FEA Ltd. 2009. *LUSAS Theory Manual*. FEA Ltd., V.14, Surrey, UK.
8. European Committee for Standardization (CEN). 2004. *EN 1992-1-2: 2004 Eurocode 2: Design of Concrete Structures. Part 1.2 General Rules – Structural Fire Design*, CEN, Brussels.
9. European Committee for Standardization (CEN). 2002. *EN 1991-1-2: 2002 Eurocode 1: Actions on structures. Part 1.2 General actions - Actions on structures exposed to fire*, CEN, Brussels.
10. Simulia, 2009. *Abaqus Theory Manual*. Pawtucket, USA.

Numerical Analysis of the Cross-Sectional Capacity of Structural Steel Members in Fire

M. KNOBLOCH, D. SOMAINI, J. PAULI and M. FONTANA

ABSTRACT

A comprehensive research project on the cross-sectional capacity and the overall structural behavior of steel members in fire has been performed at ETH Zürich. The paper analyses the cross-sectional capacity of steel sections subjected to combined axial compression and biaxial bending moments at elevated temperatures considering full section yielding and local buckling effects. The results of a parametric study using the finite element approach are presented as temperature-dependent normalized N - M interaction curves and compared to results using elastic and plastic formulae.

INTRODUCTION

The structural resistance of steel members, in particular columns or beam-columns, is limited by three limit states (and their interaction): First, full section yielding considering axial compression-bending moment interaction, secondly, local/distorsional buckling, and thirdly, overall structural stability (member buckling), especially flexural and lateral-torsional buckling. Several studies focus on the overall structural stability (limit state 3) at elevated temperatures implicitly considering section yielding (limit state 1), e.g. [1]. These studies implicitly assume that short beam-columns without overall buckling effects and cross sections classified as ‘plastic’ (Class 1), ‘compact’ (Class 2) or ‘semi-compact’ (Class 3) at ambient temperature reach their full plastic or elastic capacity respectively without developing local buckling even under fire conditions. Elevated temperatures, however, strongly influence the cross-sectional capacity and the local buckling behavior of steel sections [2]. Due to elevated temperatures in fire, the strength and stiffness of steel decreases, and the stress-strain curve become distinctly nonlinear. The proportional limit is reached for smaller strains than at ambient temperature and very large strains possibly leading to local buckling are required to reach full

Markus Knobloch (corresponding author), PhD.

Diego Somaini, MSc.

Jacqueline Pauli, MSc.

Mario Fontana, Professor, PhD.

ETH Zürich, Institute of Structural Engineering, 8093 Zürich, Switzerland.

plastic capacity, both strongly influencing the cross-sectional capacity and the overall structural behavior of steel members in fire. The cross-sectional capacity at elevated temperatures considering full plastic capacity as well as local instability effects is essential for the fire design of structural steel members. However, a fundamental study on the cross-sectional capacity of common steel sections subjected to axial compression and biaxial bending moments under fire conditions have not been carried out so far.

The yield capacity of steel sections subjected to combined axial load, bending moment, and thermal gradient is analyzed by Garlock/Quiel [3]. Dharma/Tan experimentally [4] and numerically [5] studies the rotational capacity of steel I-beams under fire conditions. The rotational capacity reduces at elevated temperature. An overall concept for the cross section capacity in the elastic-plastic range at ambient temperature without classification is proposed by Kettler [6] based on experimental and numerical calculations. Simplified fire design models based on ambient temperature design models considering temperature-dependent reduction factors, e.g. [7], do not explicitly consider the nonlinear stress-strain relationships of steel at elevated temperatures and disregard local buckling effects of ‘compact’ and ‘semi-compact sections’. These models are easy to use in design practice but have difficulty describing the structural behavior of steel members in fire precisely.

A comprehensive analytical, experimental and numerical study analyzing the cross-sectional capacity of steel sections in axial compression and bending as well as the overall structural behavior of steel members at elevated temperatures in fire has been carried out at ETH Zürich. This paper determines the first (i.e. temperature-dependent yield capacity) and second (i.e. local buckling) limit state of structural steel sections under combined axial compression and biaxial bending moments.

FINITE ELEMENT MODEL

A numerical study using the finite element approach was carried out for analyzing the cross section capacity of steel profiles subjected to fire. The finite element program Abaqus, Rel. 6.9EF was used to numerically determine the cross-sectional capacity of common ‘plastic’, ‘compact’ and ‘semi-compact’ hot-rolled I-/H-sections and hot-finished rectangular hollow sections (RHS). A geometrically and temperature-dependent material nonlinear analysis of the imperfect structure (GTMNIA) was carried out following a linear eigenvalue prediction. The numerical calculations were performed using fully integrated 4-node-shell elements (designated as S4 general purpose linear shell elements of the Abaqus element library). The elements typically had a size of approximately 10x10 mm in the flat parts of the cross sections. A mesh refinement was used for the fillets of the I-/H-sections and the corners of the hollow sections. The corners of the hollow sections were modeled with five shell elements as a quarter of a circle for simplicity (inside radius 0.5t, outside radius 1.5t). The fillet of the I-/H-sections was considered by increasing the thickness of the adjacent flange elements resulting in a coextensive cross section. Rigid beam connections were used for connecting the web and the flanges. Figure 1 shows the modeling of the corners for the rectangular hollow section and the fillets of the I-/H-section in principle.

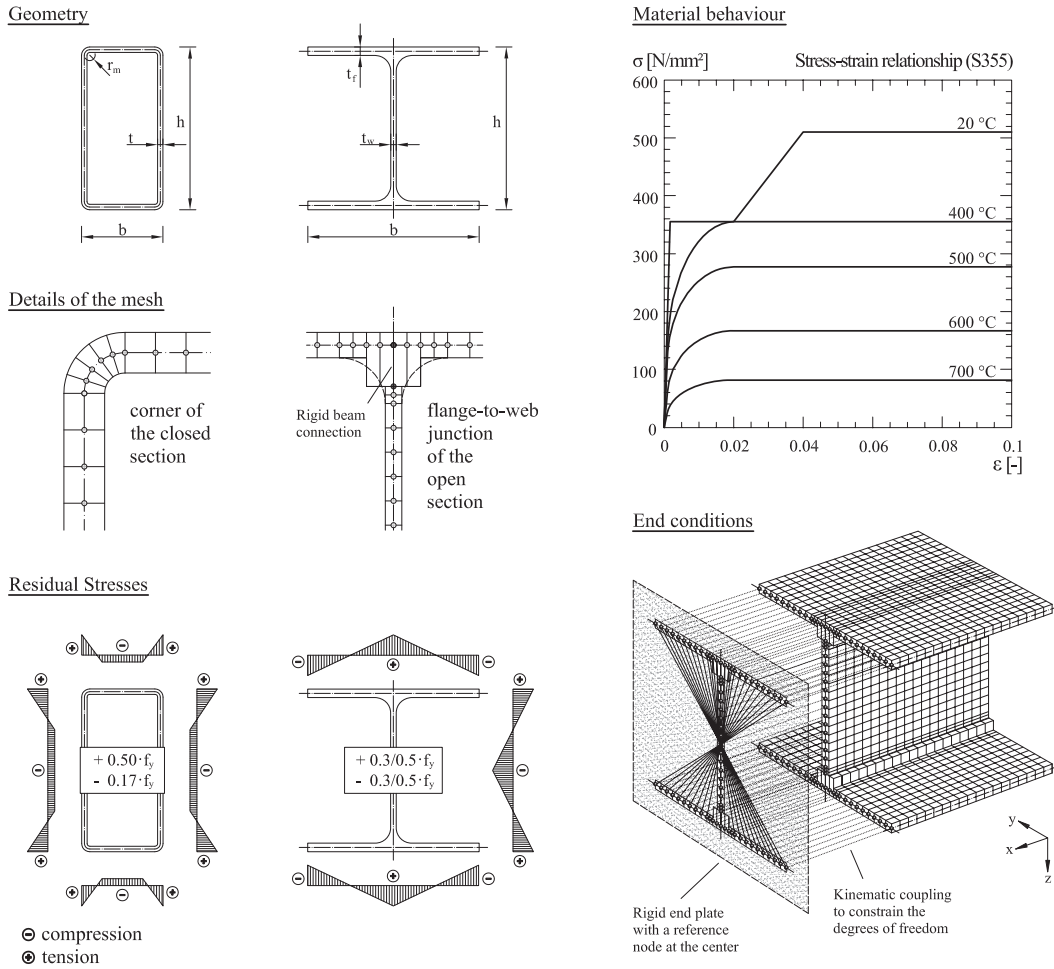


Figure 1. Numerical model. Geometry, temperature-dependent material behavior, residual stresses and details of the end conditions.

The lengths of the specimens was three times the height of the cross section which corresponded to an associated experimental study [8] and was considered sufficiently long to minimize the influence of the end conditions on the local buckling behavior, but suitable short to avoid overall member buckling effects. Fork end boundary conditions with rigid endplate conditions resulting in a perfect warping constrain were used for the calculations. While the bending and torsional deformations are fully separated for elastic problems, coupling effects may occur for plasticity. A common I-/H-profile under combined axial compression and biaxial bending moments reaches its full plastic cross section resistance only if a warping moment exists [9]. In practical applications rather thick endplates are necessary to guaranty the warping moment that is needed to reach the full plastic capacity of the profile [6]. Ideal simply supported boundary conditions for local buckling were realized for both ends of the specimens. Therefore, coupling constraints were used between the profile and the end plates (Fig. 1). The translation and rotation at the ends of the profile were coupled to the associated degrees of freedom of the rigid end plates. However, the rotation about y-axis for the flanges and about the z-axis for the web was not coupled and was therefore free. The axial compression force N and the bending moments about the strong and weak

axis M_y and M_z are applied to the reference points of the rigid end plates positioned at the centroid of the cross sections. Rigid multi-point constraints are used to connect the reference point to the rigid end plates. The numerical study used the temperature-dependent stress-strain relationships for steel grades S235, S355 and S460 according to [7] and [10] for the entire section (including corners of the hollow sections) including strain-hardening effects (Fig. 1).

Both initial local equivalent geometrical imperfections and residual stresses were considered in the numerical study. The first (symmetrical) local buckling eigenmode due to pure compression were scaled to $e_{0,w} = b/200$ for all ratios of axial compression and bending moments, for simplicity. The residual stress pattern corresponded to typical distributions and were considered with a triangular shaped distribution for the I-/H-sections and a linear distribution for the rectangular hollow sections (Fig. 1). The maximum residual stress values were $0.3f_{y,20^\circ\text{C}}$ for IPE sections and $0.5f_{y,20^\circ\text{C}}$ for H-sections and hot-finishes RHS sections.

The numerical parametric study considered steady-state conditions with uniform temperature distributions in the cross sections. The temperatures analyzed were ambient temperature, 400°C , 500°C , 600°C and 700°C , covering the critical steel temperature of the majority of practical situations. Three hot rolled H-sections (HEA 280, HEA 280 and HEB 300), one hot rolled I-section (IPE 300) and one hot finished RHS section (RHS 120*60*4) were considered in the parametric study. The width-to-thickness ratios of the profiles used for the study and the classification for ambient temperate and fire design according to [7] and [10] are given in Table I. The classification for the fire design situation considers a uniform reduction factor for the maximum width-to-thickness ratios of 0.85 [7].

Table I. Width-to-thickness ratios and classification of the cross sections for ambient temperature and fire design according to EN 1993 [7], [10].

Cross section	Width-to-thickness		Classification in pure compression according to EN1993					
	web	flange	Ambient temperature design			Fire design situation		
	b/t	c/t	S235	S355	S460	S235	S355	S460
HEA 200	20.6	7.9	Class 1	Class 2	Class 3	Class 2	Class 3	Class 3
HEA 280	24.5	8.6	Class 1	Class 3	Class 3	Class 3	Class 3	Class 4
HEB 300	18.9	6.2	Class 1	Class 1	Class 1	Class 1	Class 1	Class 3
IPE 300	35.0	5.3	Class 2	Class 4	Class 4	Class 3	Class 4	Class 4
RHS 120*60*4	27.0/12.0	-	Class 1	Class 2	Class 2	Class 1	Class 3	Class 4

The numerical parametric study considered axial compression as well as bending moments about both the strong and weak axes. A uniform bending moment distribution about both axes over the length of the profiles was used for the calculations. The axial load N was applied to the profiles in a first step. The axial load ratio between the axial load and the temperature-dependent plastic resistance N_{pl} , calculated with temperature-dependent so-called effective yield strength reached at 2% strain was 0, 0.15, 0.3, 0.5 and 0.7. The bending moments about the strong and weak axis were applied simultaneously in a second step. The cross section capacity was not limited by maximum strain considerations or deformation criteria, partly leading to very large deformations especially for members predominantly subjected to weak axis bending moments. The finite element model used for the parametric study was verified with the numerical results presented in

[6] for ambient temperature and the stub column furnace test results on rectangular hollow sections presented in [8]. In total 3450 GTMNIA calculations were carried out for the parametric study:

- 5 cross sections: HEA 200, HEA 280, HEB 300, IPE 300, RHS 120·60·4
- 3 steel grades: S235, S355, S460
- 5 temperatures: 20°C, 400°C, 500°C, 600°C and 700°C
- 5 axial load ratios: 0, 0.15, 0.3, 0.5, 0.7
- 75 pure axial load resistances

N- M_y - M_z INTERACTION BEHAVIOR IN FIRE

Normalized axial compression biaxial bending moment interaction curves for cross-sectional capacity were developed from the results of the parametric study. Every interaction curve belongs to a particular cross section, steel temperature and steel grade. The capacities are given relative to their full plastic capacities calculated with the temperature-dependent effective yield strength reached at 2% strain for elevated temperatures and standard yield strength at ambient temperature. Figure 2 shows the normalized N - M_y - (top left), M_y - M_z - (top right) and N - M_z -interaction curves (bottom right) for a HEA 200 profile (steel grade S235) at a temperature of 500°C as an example. A parameter of the M_y - M_z - interaction curves is the ratio N/N_{pl} , between the axial load and the plastic axial resistance. In addition to the bending moments $M_{y,end}$ and $M_{z,end}$ – applied to the ends of the profiles (white dots) – the bending moments $M_{y,mid}$ and $M_{z,mid}$ giving the actual stresses at mid-length and considering second order effects are given (black dots). The member length was chosen very short to avoid member buckling effects. However, the results showed that even for these short members second order effects caused by the deflections were not negligible.

The HEA 200 profile (S235) is classified as a ‘compact’ cross section in pure compression even at elevated temperature. However, the profile did not reach its full plastic axial resistance N_{pl} , due to local buckling effects (Fig 2 top left and bottom right). Local buckling effects additionally influenced the strong axis bending moment capacity. The HEA 200 profile did not reach its full plastic strong axis bending moment capacity at elevated temperature $M_{pl,y}$, even without axial compression (Fig. 2 top right). The axial load affected additionally the bending moment capacity, particularly for high axial load to plastic axial capacity ratios N/N_{pl} . Figure 2 additionally shows the full plastic and elastic interaction curves according to [10] both considering yield strength reached at 2% according to [7]. The comparison of the elastic and plastic interaction curves to the numerical results shows that the use of the yield strength reached at 2% strain lead to unconservative result, particularly for members predominately subjected to axial compression.

Figure 3 exemplarily compares the axial compression biaxial bending moment interaction curves for cross-sectional capacity at ambient temperature (left) and 500°C (right) for HEA 280 (top), HEB 300 (middle) and RHS 120·60·5 (bottom) profiles (steel grade S355). The interaction behavior was strongly affected by the nonlinear stress-strain relationship at elevated temperatures and local buckling

effects. The normalized bending moment resistance about the weak axis (without axial compression) at elevated temperatures was less reduced compared to ambient

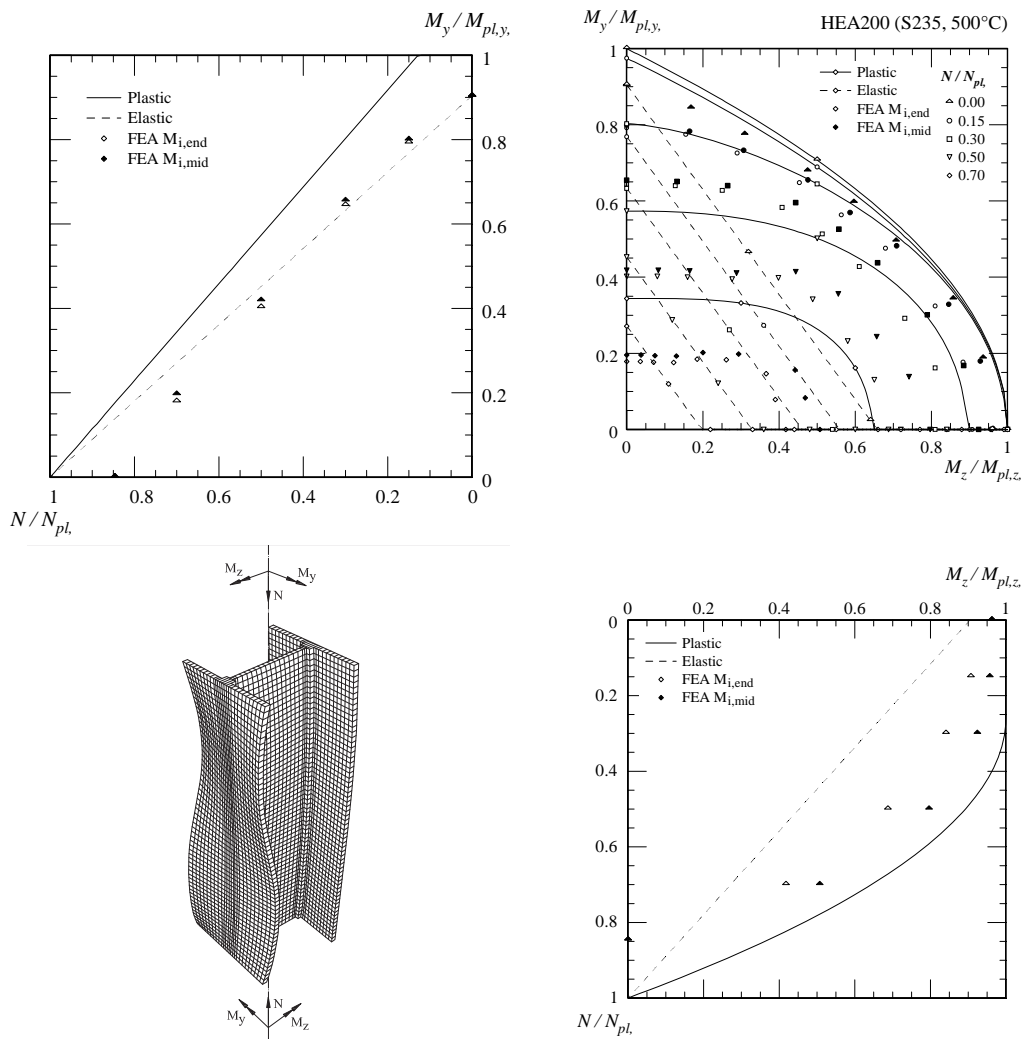


Figure 2. Normalized N - M_y - (top left), M_y - M_z - (top right) and N - M_z - (bottom right) interaction curves for cross-sectional capacity developed from the parametric study (dots) and according to elastic (dashed line) and plastic interaction (continuous line) considering effective yield strength.

temperature than the normalized resistance about the strong axis. Local buckling effects limited the bending moment resistance about the strong axis before reaching the full plastic resistance particularly for sections with relatively large width-to-thickness ratios of the flanges (HEA 280, Fig. 3 top). For ambient temperature, bending moment capacities that are larger than full plastic capacity were possible, in particular for the bending resistance about the weak axis of very stocky sections (HEB 300), due to the consideration of strain hardening effects (Fig. 3 middle).

The temperature-dependent normalized interaction curves developed from the numerical results were used for performing a comparative study of various interaction formulae. Figure 3 again compares the plastic (continuous line) and elastic (dashed line) N - M_y - M_z interaction curves considering the temperature-dependent effective yield strength (even for the elastic curves) according to [7] with the numerical results. The use of the elastic interaction curves led to conservative results, in particular for members predominately subjected to weak axis bending. The use of plastic interaction curves, however, led to unconservative results even

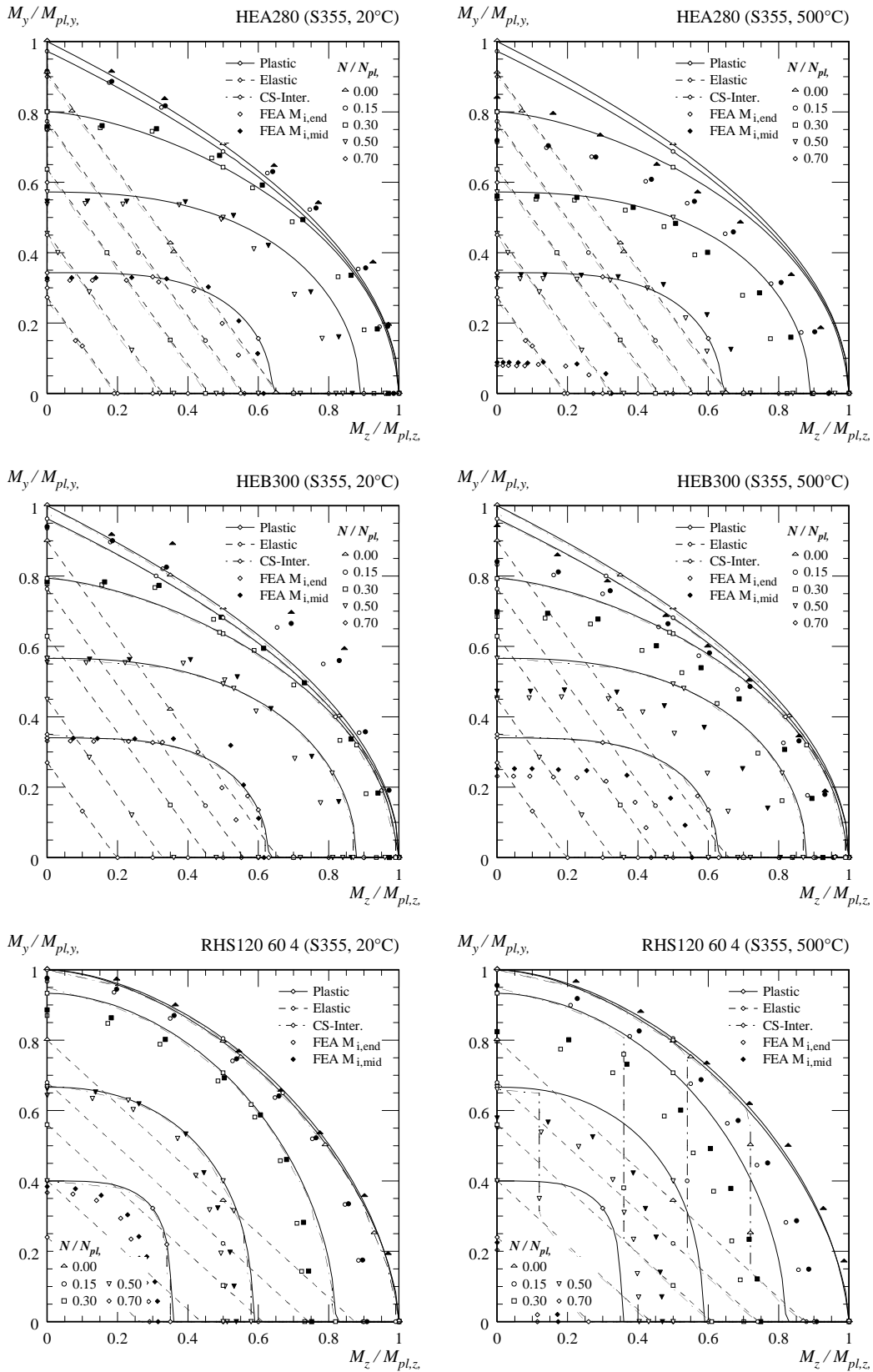


Figure 3. Normalized N - M_y - M_z interaction curves for the cross-sectional capacity of a HEA 280 (top), HEB 300 (middle) and RHS 120 60 4 (bottom) profile at ambient temperature (left) and 500°C (right), steel grade S355. Finite element results (dots) and various interaction formulae (lines).

for very stocky cross sections (e.g. HEB 300), especially for members predominately subjected to axial compression and strong axis bending moments. In addition to the elastic and plastic interaction, Fig. 3 shows the analytical interaction considering the cross-sectional capacity interaction formulae of [10] in conjunction with the effective yield strength and the cross section classification according to [7] (CS-Inter, dash-dotted line). These interaction curves at elevated temperature are identical to the elastic curve for the HEA 280 (S355, Class 3) and to the plastic curve for the HEB 300 (Class 1). For the RHS 120·60·4 (S355), however, the cross-sectional capacity interaction curve (CS-Inter) followed the plastic curve for small and medium N/N_{pl} ratios and large $M_y/M_{y,pl}$ ratios (bending stress distribution of the webs) and dropped down to the elastic curve for increasing $M_z/M_{z,pl}$ ratios due to the increasing uniform stress distribution of the webs. For large axial compression ratios $N/N_{pl} = 0.7$ the cross section was classified as Class 3 and the CS-Interaction curve followed the elastic interaction curve for the entire curve.

CONCLUSIONS

A comprehensive numerical parametric study using the finite element approach on the cross-sectional capacity of structural steel members in combined axial compression and biaxial bending under fire conditions has been carried out. Temperature-dependent normalized N - M interaction curves have been developed from the numerical results. These interaction curves for the cross-sectional capacity considering full plastic capacity (limit state 1) as well as local instability effects (limit state 2) are essential for the fire design of structural steel members. Additionally, the interaction curves constitute an upper limit of the overall structural behavior considering member buckling effects (limit state 3). Therefore, interaction formulae for beam-columns in fire could be limited to the cross-sectional capacity for short beam-columns without member buckling effects.

REFERENCES

1. Knobloch, M., Fontana, M. and Frangi, A. Steel beam-columns subjected to fire, *Steel Construction* 1(1): 51–58 (2008).
2. Knobloch, M. Local Buckling Behavior of Steel Section Subjected to Fire, *Fire Safety Science* 9:1239-1254 (2008).
3. Garlock, M.E.M. and Spencer, S.E. Plastic Axial Load and Moment Interaction Curves for Fire-Exposed Steel Sections with Thermal Gradients, *Journal of Structural Engineering*, 134(6): 874–880 (2008).
4. Dharmaraj, R.B. and Tan, K.-H. Rotational capacity of steel I-beams under fire conditions Part I: Experimental study, *Engineering Structures* 29: 2391–2402 (2007).
5. Dharmaraj, R.B. and Tan, K.-H. Rotational capacity of steel I-beams under fire conditions Part II: Numerical simulations, *Engineering Structures* 29: 24030–2418 (2007).
6. Kettler, M. *Elastic-Plastic Cross-Sectional Resistance of Semi-Compact H- and Hollow Sections*, TU Graz, 2008 [thesis].
7. EN 1993-1-2, Design of steel structures, Part 1-2 General rules – Structural fire design, CEN, 2005.
8. Knobloch, M., Somaini, D., Pauli, J. and Fontana, M. Stability of steel columns subjected to fire, *SDSS'Rio 2010 Stability and Ductility of steel structures 2010*, in press.
9. Kindmann, R. and Frickel, J. *Elastische und plastische Querschnittstragfähigkeit – Grundlagen, Methoden, Berechnungsverfahren, Beispiele*, Ernst & Sohn, Berlin (2002).
10. EN 1993-1-1, Design of steel structures, Part 1-1 General rules and rules for buildings, CEN, 2005.

Stability Check of Steel Frames Exposed to Fire

P. V. REAL, C. COUTO, N. LOPES and J. P. RODRIGUES

ABSTRACT

This paper aims at evaluating the validity of using in fire situation the same procedures used at normal temperature for checking the stability of unbraced steel frames. A comparison is made between simple and advanced calculation models. Based on a parametric study a procedure is proposed for evaluating the buckling lengths of columns in unbraced frames in case of fire.

INTRODUCTION

At normal temperature, where it is necessary to consider the influence of the deformed geometry of the structure (2nd order effects) to verify the stability of columns belonging to a structural framed system, when frame imperfections are considered but member imperfections are not taken into account [1,2], two procedures can be adopted: i) perform a 2nd order analysis including the effects of lateral displacements and check of the member instability with non-sway buckling lengths; and ii) perform a 1st order analysis and check of the member instability with sway buckling lengths. For the first procedure, it should be noted that non-sway effective lengths can be used because no sway will occur in addition to that which causes the second-order effects calculated by a P- second-order analysis. For sake of simplicity, the column length of a member may be taken as its system length, which is safe and suggested by the Eurocode 3 [1] for normal temperature design. In fire situation, Eurocode 3 [3] states that, using simple calculation methods, a global analysis of the frame should be done as for normal temperature and the buckling length of a column for the fire design should generally be determined as for normal temperature design.

However, in the case of a braced frame in which each storey comprises a separate fire compartment with sufficient fire resistance, the buckling length, l_{fi} , of

Paulo Vila Real, Carlos Couto, Nuno Lopes, LABEST—Department of Civil Engineering, Univ of Aveiro, Portugal.

João Paulo Rodrigues, ISISE—Department of Civil Engineering, Univ of Coimbra, Portugal.

a continuous column may be taken as $0,5L$ in an intermediate storey and $0,7L$ in the top storey, where L is the system length in the relevant storey. For unbraced structures no specific guidance is given by the Eurocode. For these cases this paper shows that considering a buckling length of the columns in a sway mode, independently of the 2nd order effects being negligible or not (so-called P- effects), gives good results, for the case of regular multi-storey buildings. Only few studies were made on that subject. Publication no. 159 from Steel Construction Institute [4] proposes for the case of columns in sway frames in fire conditions that the effective slenderness ratio may conservatively be taken as $\bar{\lambda}_\theta = 1.25\bar{\lambda}$ (considering the buckling length equal to the system length) and a publication from ECCS [5] suggests that if a global analysis of the frame is not performed to take account of instability effects at elevated temperature, default critical temperature of 300 °C should be considered, which is too conservative. A global analysis including the instability effects at elevated temperature is rather complex to be used with simple calculation models, therefore simple and safe procedures should be available for design purpose.

The methodology for fire design with simple calculation models consists of evaluating the internal forces in the structure as for normal temperature considering the accidental load combination for fire situation and then check for the fire resistance of each member separately. This was the procedure adopted in this paper where an advanced calculation model [4] was also used for comparison.

ANALYSIS OF AN UNBRACED MULTI-STOREY BUILDING IN FIRE SITUATION

An unbraced steel frame of a three bay – three storey office building shown in Figure 1 has been studied. This frame has been analysed at normal temperature in the publication no. 119 from ECCS [2]. The members are made of hot-rolled profiles of steel grade S235 according to EN 10025 [7].

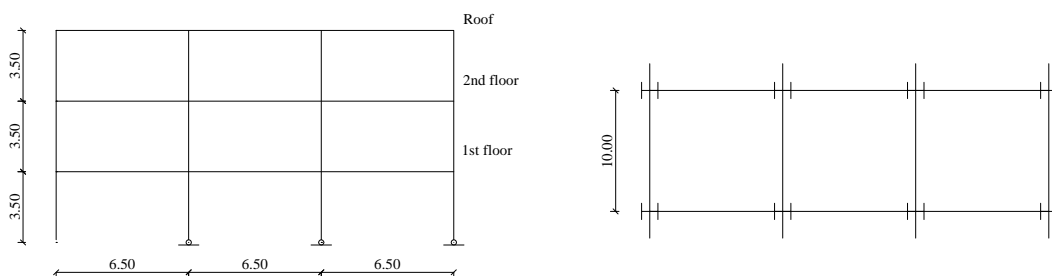


Figure 1. Frame geometry.

The structure is assumed to be braced in the out of plane direction and unbraced in the plane of the frame. Out of plane column buckling is prevented and lateral restraint is assumed to be provided to the beams by the concrete floor and roof slabs. The columns bases at the level of foundation are assumed to be either pinned or fully fixed. The columns are continuous throughout of the full height of the building.

Classification of the frame: sway or non-sway frame

The 2nd order effects may be neglected when the response of the frame to in-plane horizontal forces is so stiff that it is acceptable to neglect any additional forces or moments arising from horizontal displacements of its storeys. At normal temperature the Eurocode 3 states that this condition may be assumed to be fulfilled in an elastic analysis, if the following criterion is satisfied:

$$\alpha_{cr} = \frac{F_{cr}}{F_{Ed}} \geq 10 \quad (1)$$

where α_{cr} is the factor by which the design loading would have to be increased to cause elastic instability in a global mode, F_{cr} is the elastic critical load producing sway instability and F_{Ed} is the sum of the design vertical loads applied to the frame. This factor should be evaluated for each load combination and can be determined either directly with a computer program or analytically, for instance, using the Horne method [8].

The fire situation is classified as an accidental action in EN 1990 "Basis of structural design" [9] and the design effect of actions for the fire situation, $E_{fi,d}$, can be obtained using the accidental load combination given by

$$\sum G_k + \psi_{1,i} \cdot Q_{k,1} + \sum \psi_{2,i} \cdot Q_{k,i} + \sum A_d \quad (2)$$

The basic loading cases shown in Figure 2 are the same adopted in [2].

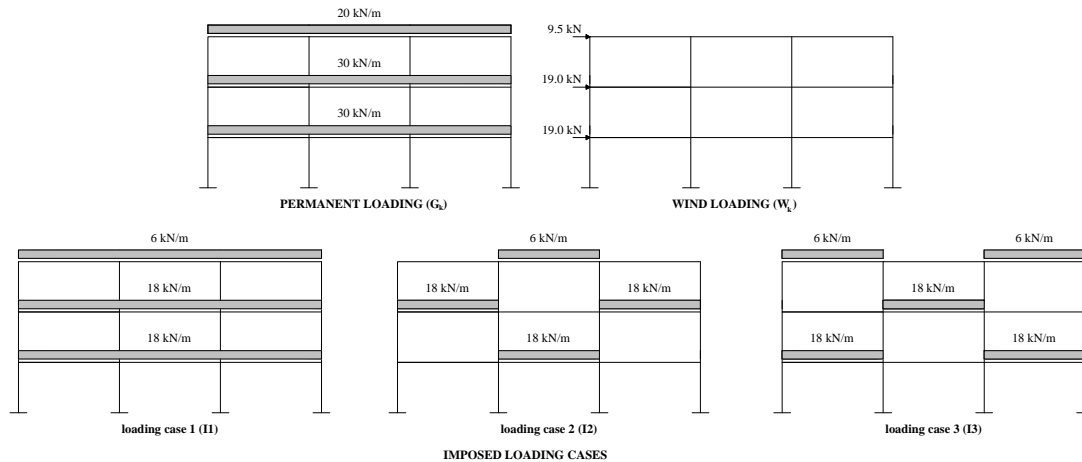


Figure 2. Loading cases.

Load combinations for accidental fire situation are listed in Table I.

TABLE I. LOAD COMBINATION CASES.

Load combination	Accidental Combination
Case 1	$G_k + 0.2W_k$
Case 2	$G_k + 0.5I_1$
Case 3	$G_k + 0.5I_2$
Case 4	$G_k + 0.5I_3$
Case 5	$G_k + 0.2W_k + 0.3I_1$
Case 6	$G_k + 0.2W_k + 0.3I_2$
Case 7	$G_k + 0.2W_k + 0.3I_3$

Frame imperfections due to unavoidable initial out-of-plumb were taken into account prescribing a notional horizontal force that is applied at each story level [1].

Table II shows the value of the horizontal equivalent forces for each load case.

TABLE II. EQUIVALENT HORIZONTAL FORCES.

Basic loading case	Storey	V_{Ed} (kN)	H_{Ed} (kN)
G	Roof	390	1.03
	2nd floor	585	1.54
	1st floor	585	1.54
I_1	Roof	117	0.31
	2nd floor	351	0.92
	1st floor	351	0.92
I_2	Roof	39	0.10
	2nd floor	234	0.62
	1st floor	117	0.31
I_3	Roof	78	0.21
	2nd floor	117	0.31
	1st floor	234	0.62

Table III shows the computed values of the factor cr by which the design loading would have to be increased to cause elastic instability in a global node.

TABLE III. FRAME CLASSIFICATION.

Load combination	Storey	H_{Ed} (mm)	V_{Ed} (kN)	H_{Ed} (kN)	cr	cr,min	Classification
Case 1	Roof	3.7	390.0	2.9	154.68	10.79	Non-sway
	2nd floor	3.5	975.0	8.3	41.81		
	1st floor	2.8	1560.0	13.6	10.79		
Case 2	Roof	1.3	448.5	1.2	-308.26	8.15	Sway
	2nd floor	1.4	1209.0	3.2	41.91		
	1st floor	1.1	1969.5	5.2	8.15		
Case 3	Roof	1.2	409.5	1.1	-230.77	9.04	Sway
	2nd floor	1.2	1111.5	2.9	46.13		
	1st floor	1.0	1755.0	4.6	9.04		
Case 4	Roof	1.2	429.0	1.1	-308.67	9.05	Sway
	2nd floor	1.2	1072.5	2.8	46.18		
	1st floor	1.0	1774.5	4.7	9.05		
Case 5	Roof	3.9	425.1	3.0	146.41	9.30	Sway
	2nd floor	3.7	1115.4	8.6	37.13		
	1st floor	3.0	1805.7	14.3	9.30		
Case 6	Roof	3.8	401.7	3.0	151.71	10.02	Non-sway
	2nd floor	3.6	1056.9	8.5	39.03		
	1st floor	2.9	1677.0	13.9	10.02		
Case 7	Roof	3.8	413.4	3.0	158.37	9.97	Sway
	2nd floor	3.6	1033.5	8.4	39.09		
	1st floor	2.9	1688.7	14.0	9.97		

For the load combination where the condition of Eq. (1) is verified a 1st order analysis is enough. In all the other cases, the equilibrium of the frame should be based on the deformed configuration meaning that a 2nd order analysis must be performed.

Buckling lengths

Part 1.2 of Eurocode 3 states that the buckling length l_{fi} of a column for the fire design situation should be determined as for normal temperature design. It is not clear if it should be used the same procedure but considering the mechanical properties of steel, namely the Young's modulus, at elevated temperature. If elevated temperature should be used, the process is not an easy task for design

purposes. Due to this difficulty, the Wood method [2] at normal temperature has been used in this work to evaluate the buckling length ratio (l_{cr}/L) of the columns. The buckling length at elevated temperature will be considered with the same value as at normal temperature, i.e., $l_{fi} = l_{cr}$. The buckling length of a column in a non-sway or sway mode may be obtained from Figure 3 and Figure 4 respectively, function of the distribution factors η_1 and η_2 , which are given by:

$$\eta_1 = \frac{K_c + K_1}{K_c + K_1 + K_{11} + K_{12}} \quad \eta_2 = \frac{K_c + K_2}{K_c + K_2 + K_{21} + K_{22}}$$

where K_c , K_1 and K_2 are the flexural stiffness coefficients (EI/L) for the adjacent length of columns, and K_{ij} are the effective beam flexural stiffness coefficient. For beams with double curvature $K_{ij} = 1.5 EI/L$ and for the case of single curvature $K_{ij} = 0.5EI/L$.

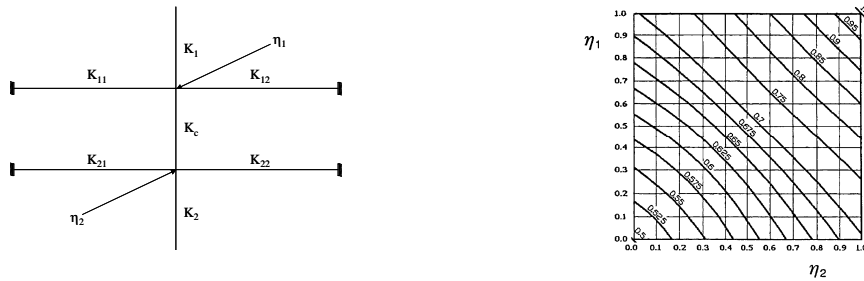


Figure 3. Buckling coefficient l_{cr}/L for non-sway frames.

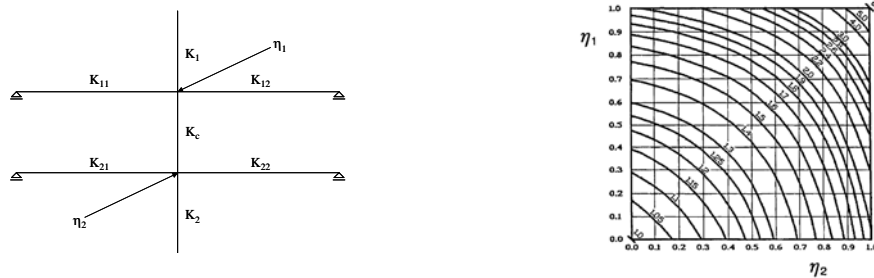


Figure 4. Buckling coefficient l_{cr}/L sway frames.

Fire resistance of the frame

To check the fire resistance of the frame by a simple calculation model, the internal forces were obtained at normal temperature and the column buckling lengths have been obtained according to the following procedures: i) performing a second-order analysis including sway effects and checking of the members instability with non-sway buckling lengths, and ii) performing a first order analysis and checking of the member instability with sway buckling lengths.

The standard fire curve ISO 834 has been used and the results obtained with simple calculation model were compared with the ones obtained with the finite element program SAFIR [6]. Beams were assumed to be heated on three sides and all the columns on four sides.

Simple calculation model

After being obtained the internal forces for the load combinations (see Table I), the fire resistance of all the members of the frame was calculated using the software Elefir-EN [10]. A summary of the results is given in the Tables IV and V for the most unfavourable load combination. These results show that when performing a second-order analysis using non-sway buckling lengths the fire resistance is governed by the collapse of a beam while a column is the critical member if a first order analysis is performed together with sway buckling lengths.

TABLE IV. 2nd ORDER ANALISYS + NON-SWAY BUCKLING LENGHTS.

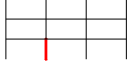
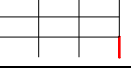
Load combination	Member	Section	N_{Ed} (kN)	M_1 (kN.m)	M_2 (kN.m)	l_{fi}/l	L (m)	cr (°C)	$t_{fi,d}$ (min)
$G_k + 0.5I_1$ (case 2)		HEB 260	-688.19	0.00	-12.14	0.87	3.5	657.57	21.45
$G_k + 0.5I_1$ (case 2)		IPE 360	-26.44	-46.40	-92.78	-	6.5	699.78	20.57

TABLE V. 1st ORDER ANALISYS + SWAY BUCKLING LENGHTS.

Load combination	Member	Section	N_{Ed} (kN)	M_1 (kN.m)	M_2 (kN.m)	l_{fi}/l	L (m)	cr (°C)	$t_{fi,d}$ (min)
$G_k + 0.5I_1$ (case 2)		HEB 220	-298.39	0.00	-29.16	2.33	3.5	578.99	16.77

The fire resistance of $t_{fi,d} = 16.77$ min. is in good agreement with the value obtained with advanced calculation method shown in the next section. This result suggests that for the case of unbraced multi-storey frames in fire situation, the sway buckling length of the columns should be used irrespectively of the sway or non sway behaviour of the structure at normal temperature.

Advanced calculation model

The results obtained with the program SAFIR are summarised in Table VI for the fire scenario and the load case combination considered.

TABLE VI. ADVANCED CALCULATION MODEL RESULTS.

Fire Scenario	Case 1 (min)	Case 2 (min)	Case 3 (min)	Case 4 (min)	Case 5 (min)	Case 6 (min)	Case 7 (min)	$t_{fi,d}$ (min)
	17.63	16.63	17.51	17.46	16.75	17.20	17.12	16.63
	27.95	23.39	23.85	22.72	25.21	25.73	24.55	22.72
	25.12	23.01	24.70	23.01	23.62	25.13	23.61	23.01

A fire resistance of $t_{fi,d} = 16.63$ min has been obtained, being close to the fire resistance obtained with the simple calculation model. Figure 5 shows the bending

diagram and the deformed shape prior to collapse for the fire scenario in which the fire is on the ground floor. From that figure it is clear that a plastic sway mechanism has developed.

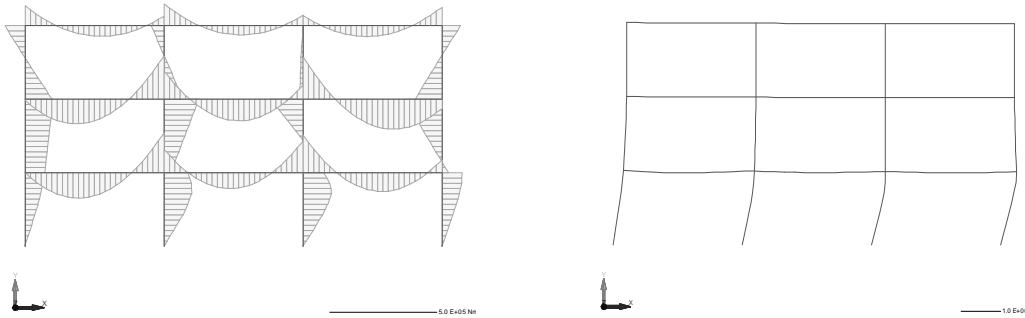


Figure 5. Bending moment and deformed shape (x2) immediately prior to collapse.

PARAMETRIC STUDY

A parametric study has been performed considering several combinations of bays and storeys from 1x1 to 3x3 in a total of 9 unbraced frames. The frames were considered to be pinned or fixed at the supports and the seven load combinations presented in Table I were considered. The results of the parametric study are plotted in Figure 6 showing that the proposal made to consider the sway buckling lengths in the case of unbraced frames is mostly on the safe side when compared with the advanced calculation method.

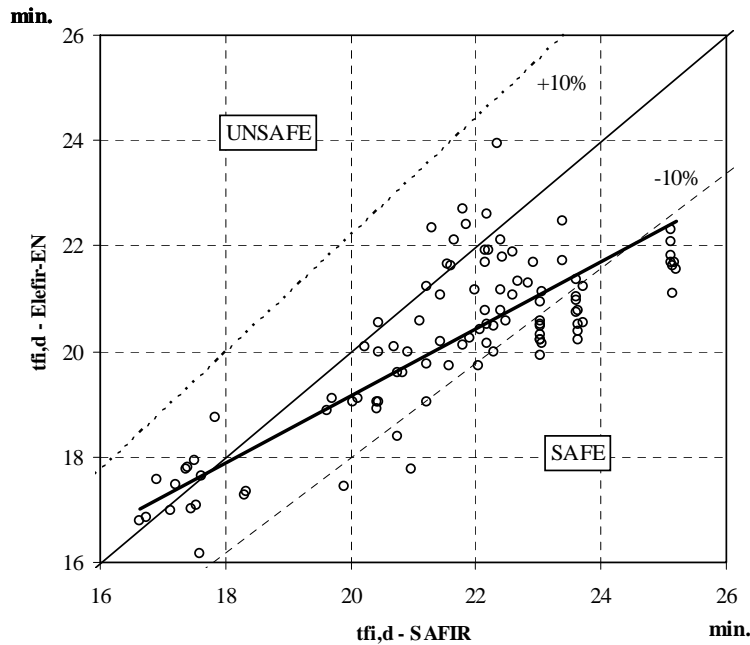


Figure 6. Comparison between the proposed simple calculation models and advanced calculation models.

There are few unsafe results but, as no additional end fixity of the columns, due to the colder members they are connected, is considered, it seems that the proposal

made in this work to adopt the sway buckling length in the case of unbraced frames is acceptable.

CONCLUSIONS

A simplified procedure for the assessment of the fire resistance of unbraced steel structures was proposed in this paper. Part 1.2 of Eurocode 3 does not treat unbraced frames explicitly only stating that in fire situation, using simple calculation methods, a global analysis of the frame should be done as for normal temperature and the buckling length l_{fi} of a column for the fire design should generally be calculated as for normal temperature design. It is however expectable that the buckling length should be increased to take account of instability effects at elevated temperatures. Based on a parametric study it was proposed for unbraced frames in fire situation the use of sway buckling lengths irrespectively of the sway or non sway behaviour of the frame at normal temperature.

REFERENCES

1. EN 1993-1-1, (European standard). *Eurocode 3: Design of steel structures. Part 1.1: General rules and rules for buildings*. CEN (Comité Européen de Normalisation), Brussels, 2005.
2. ECCS. *Rules for Member Stability in EN 1993-1-1: Background documentation and Design Guidelines*. European Convention for Constructional Steelwork. ECCS publication no. 119, Brussels, 2006.
3. EN 1993-1-2, (European standard). *Eurocode 3: Design of steel structures. Part 1.2: Structural fire design*. CEN (Comité Européen de Normalisation), Brussels, 2005.
4. SCI, Steel Construction Institute, *Structural Fire Design to EC3 & EC4, and comparison with BS 5950*. Technical Report, SCI publication no. 159, 1996.
5. ECCS, *European Recommendations for the Fire Safety of Steel Structures*. European Convention for Constructional Steelwork. ECCS, Elsevier, 1983.
6. Franssen J-M, SAFIR, *A Thermal/Structural Program Modelling Structures under Fire*, Engineering Journal, A.I.S.C., Vol 42, No. 3, 143-158, 2005.
7. EN 10025-2, *Hot rolled products of structural steels – Part 2: Technical delivery conditions for non-alloy structural steels*, Nov. 2004.
8. Horne, M. R., *An Approximate Method for Calculating the Elastic Critical Loads of Multistorey Plane Frames*, The Structural Engineer, Vol. 53, no. 6, pp 242, 1975.
9. EN 1990, (European standard). *Eurocode: Basis of Structural Design*,. CEN (Comité Européen de Normalisation), Brussels, 2002.
10. Franssen, J.-M., Vila Real P. M. M., *Fire Design of Steel Structures*, ECCS ed., 2010.

Thermal Response of Steel Columns Exposed to Localized Fires—Numerical Simulation and Comparison with Experimental Results

G.-Q. LI and C. ZHANG

ABSTRACT

The popular CFD code FDS is adopted to predict the thermal behaviors of steel columns exposed to localized fires. Two real localized fire tests (one surrounded fire test that the column is inside the fire source and one adjacent fire test that the column is adjacent to the fire source) are modeled in FDS. The effects of input parameters such as grid size and number of solid angles on the accuracy of the numerical results have been investigated. Experimental results about heat fluxes and temperatures are compared with the numerical results. Good agreements between the predicted and measured results are found in surround fire case, whilst acceptable predictions are given in adjacent fire.

INTRODUCTION

In prescriptive fire codes, steel structures are requested to be protected with thermal insulation, according to the fire resistance requirements of the building components, to ensure fire safety. The fire resistance of building components (with or without protection) is usually determined by standard fire tests which use fully-developed compartment fire environments such as ISO834, ASTM E119 etc., for testing. However, in many buildings like atria, open car parks, airport terminals, etc., large spaces exist. In large spaces flashover is unlikely to happen that the fire hazards to the structural components in those spaces are comparatively low. As a result, it will be too conservative to determine the fire protection of steel members in large spaces by standard fire tests or standard fire based methods.

Alternatively, performance-based method (PBM) has been developed and prompted in many countries. PBM, using the state-of-art knowledge in structural fire engineering (SFE), has its capability of considering fire loads, ventilation and robust mechanical behavior of real structures

Guo-Qiang Li, Professor, College of Civil Engineering, Tongji University, 1239 Siping Road, Shanghai 200092, China

Chao Zhang (corresponding author), PHD student, College of Civil Engineering, Tongji University, 1239 Siping Road, Shanghai 200092, China

in fire condition. To reasonably evaluate the fire resistance of steel structures in large spaces by PBM, the thermal response of steel structures in large space fires should be calculated. Usually, localized fire model is adopted to represent large space fires.

At present, the fire environments in localized fire which are gas temperature distribution, smoke movement, etc., can be determined with little difficulty by plume theory [1], zone models [2-3] and sophisticated CFD models [4-5], as well as by experimental tests [6-7]. However, the heat flux calculation in large space fire is still difficulty, mainly due to the complexity of the calculation of radiation (For convection, it can be simply calculated by applying Newton's law of cooling).

Developed by McGrattan et al. [5] at NIST, the CFD code FDS is very popular in current fire engineering and research fields. Till now, numerous studies have been investigated to assess FDS's ability of modeling fire phenomena [8]. Most of the studies are focused on FDS's capability of simulating fire plume behaviors [9]. However, for FDS's capability of predicting the structural fire engineer concerned thermal response of steel members, little reference is available.

The purpose of this paper is to investigate FDS's capacity of predicting the thermal response of steel columns exposed to localized fires. Kamikawa et al. [10] have experimentally studied the thermal mechanism of steel columns exposed to localized fire. In [10], totally 9 fire tests (5 adjacent and 4 surrounding fire tests) have been considered, where 'adjacent' and 'surrounding' is the location of the fire source to the column. In this paper, two typical tests (one adjacent and one surrounding) in [10] have been 'rebuilt' in FDS. Outputs from FDS which are heat flux and column surface temperature are compared with the experimental results. FDS (version 5) is used in our study. Grid sizes used in the simulation is determined by literature review with referring to our previous work [11]. Good agreements between the numerical and experimental results are found.

THEORETICAL MODELS IN FDS

FDS is a Large-Eddy Simulation (LES) [4] based CFD code, developed in particular for fire related simulations. In FDS the combustion is modeled with a mixture fraction concept and thermal radiation is computed by solving the radiation transport equation for a gray gas using a Finite Volume Method (FVM) on the same grid as the flow solver. The governing equations are approximated on one or more rectilinear grids that obstructions with complex geometries are approximated with groups of prescribed rectangles in FDS. Detail description of the heat transfer models used in FDS is given bellow.

Heat conduction

FDS assumes that solid obstructions consist of multiple layers, with each layer composed of multiple material components. Heat conduction is assumed only in the direction normal to the solid surface. One-dimensional (1D) heat conduction equation for solid temperature $T_s(x,t)$ along normal direction x is given by

$$\rho_s c_s \frac{\partial T_s}{\partial t} = \frac{\partial}{\partial x} k_s \frac{\partial T_s}{\partial x} + \dot{q}_s \quad (1)$$

where k_s and $\rho_s c_s$ are the thermal conductivity and thermal capacity and \dot{q}_s is heat generation contributed by chemical reaction and radiative absorption.

The boundary condition on the front surface of a solid is expressed as

$$-k_s \frac{\partial T_s}{\partial x}(0,t) = \dot{q}_c + \dot{q}_r \quad (2)$$

where \dot{q}_c and \dot{q}_r are convective and radiative heat flux to the surface.

Convection

In an LES calculation, the convective heat flux to the surface is obtained from a combination of natural and forced convection correlations

$$\dot{q}_c = h\Delta T ; \quad h = \max[C|\Delta T|^{1/3}, \frac{k}{L}0.037\text{Re}^{4/5}\text{Pr}^{1/3}] \quad (3)$$

where ΔT is the difference between the wall and the gas temperature (taken as the grid cell abutting the wall), C is the coefficient for natural convection (1.52 for a horizontal surface and 1.31 for a vertical surface) [12], L is a characteristic length related to the size of the physical obstruction, taken to be 1m for most calculations and k is the thermal conductivity of the gas.

Thermal radiation

The radiation transport equation (RTE) for a non-scattering grey gas is

$$\mathbf{s} \cdot \nabla I_\lambda(\mathbf{x}, \mathbf{s}) = \kappa_\lambda(\mathbf{x})[I_b(\mathbf{x}) - I_\lambda(\mathbf{x}, \mathbf{s})] \quad (4)$$

where $I_\lambda(\mathbf{x}, \mathbf{s})$ is the radiation intensity at wavelength λ , $I_b(\mathbf{x})$ is the source term given by the Planck function, \mathbf{s} is the unit normal direction vector and $\kappa_\lambda(\mathbf{x})$ is the spectral absorption coefficient.

In practical simulations the spectral dependence cannot be solved accurately. Instead, a simple wide band model is developed by dividing the radiation spectrum into a relatively small number of bands. The band specific RTE is

$$\mathbf{s} \cdot \nabla I_n(\mathbf{x}, \mathbf{s}) = \kappa_n(\mathbf{x})[I_{b,n}(\mathbf{x}) - I_n(\mathbf{x}, \mathbf{s})], \quad n = 1, 2, \dots, N \quad (5)$$

where I_n is the intensity integrated over the band n and κ_n is the appropriate mean absorption coefficient.

In most large-scale fire scenarios soot is the most important combustion product affecting thermal radiation from the fire and hot smoke. As the radiation spectrum of soot is continuous, it is possible to assume that the gas behaves as a gray medium. The spectral dependence is then lumped into one effective absorption coefficient ($N=1$) and the source term is given by the blackbody radiation intensity. Numerical experiments found that six bands ($N=6$) are usually enough to improve the accuracy for fire application.

The grey or band mean absorption coefficient κ_n is calculated by a narrow band model RADCAL [13] which has been implemented in FDS. To obtain the discretized form of the RTE, the unit sphere is divided into a finite number of the solid angles.

NUMERICAL MODEL

Description of the experiments

Figs. 1a-1b show the experimental setup in [10]. Two 4.5mm thick, 2.50m tall and 0.15m square steel columns were prepared as the specimen. In adjacent fire tests, a 0.50 square

diffusion burner with propane as the fuel was used as the fire source (Fig. 1a). The burner surface was 450mm above the floor. The heat release rate (HRR) was controlled by fuel supply rate to range from 52 to 255kW. In order to investigate into the effectiveness of the isolation of the column from the fire source, burner-column distance L was changed between 0 and 250mm. In surrounding fire tests, eight 0.15m square porous burners were placed around the 0.15m square column to make a 0.45m square burner-column complex (Fig.1b). Total HRR was controlled within the range from 40.5 to 162 kW. Heat flux to the column surfaces were measured by 15mm diameter Schmidt-Boelter heat flux gages and temperature of the column surfaces were measured by K-type thermocouples.

Numerical details

The grid sizes used is one of the most important numerical parameter in CFD dictating its numerical accuracy. The necessary spatial resolution for a proper LES simulation is customary defined in terms of the characteristic diameter of a plume, which is defined as [5],

$$D^* = \left(\frac{\dot{Q}}{\rho_{\infty} c_p T_{\infty} \sqrt{g}} \right)^{2/5} \quad (6)$$

The special resolution R^* of a numerical grid is defined as,

$$R^* = \frac{\Delta x}{D^*} \quad (7)$$

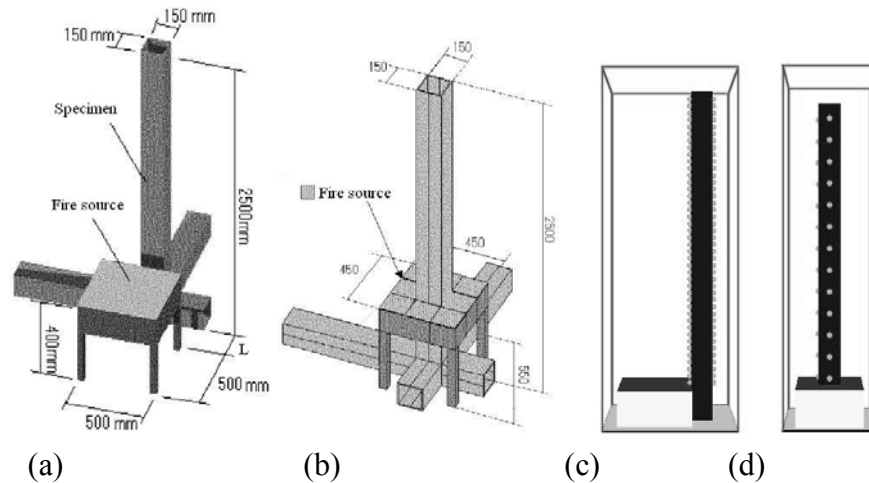


Figure 1. Experimental setup in [10] and the corresponding numerical models.

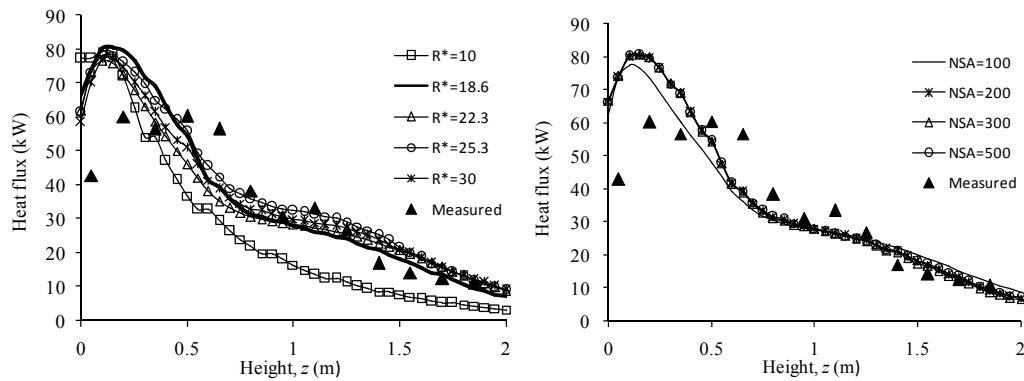


Figure 2. Effect of resolution R^* and number of solid angles (NSA) on the simulation results.

where δx is the characteristic length of a cell for a give grid. The necessary resolution suggested in most studies is between 1/5 and 1/20 [5, 14]. Ma and Quintiere [9] suggested resolution of 1/20 to successfully predict the flame height. Resolution between 1/10 and 1/15 were chosen by [15] to successfully mode atrium fires. Lin et al. [16] suggested $R^*=1/13$ is enough for CFD simulations to resolve the fire characteristics (flame height and thermal radiation). Lin et al. [13] also suggested 500 solid angles (when using gray model to solve RTEs) are enough to predict the radiative heat fluxes emitted from the burners. In [17], 304 solid angles were used for radiation solver to ensure accuracy of the FVM solution. In a previous work [11], resolution of 1/20 is used to give good prediction of heat flux to a ceiling beam above a localized fire.

In present simulations, adjacent fire test with HRR of 255kW, $L=0$ mm, and surrounded fire test with HRR of 81kW are investigated. Fig.1c and Fig.1d show the corresponding numerical models. Dimensions of the computational domains for adjacent and surrounded fire tests are $0.9\text{m} \times 0.7\text{m} \times 2.5\text{m}$ (Fig. 1c) and $0.6\text{m} \times 0.6\text{m} \times 2.4\text{m}$ (Fig.1e). In both models, the grids in all directions are uniform. Resolution of about 1/20 is used in models (For adjacent fire, $R^*=1/18.6$; for surrounded fire model, $R^*=1/23.5$). Grid sensitive tests show that further refinement of the grid size has negligible effect on the simulation results, as shown in Fig.2. After sensitive tests, 300 solid angles are used in the simulations, as shown in Fig.2. The platform for the simulation is the Intel® Core™2 Duo CPU, 3.00GHz, 3.25GB RAM, and with Windows XP. For a model consisted of 100,800 control volumes (the surrounded fire case), It took approximately 110h for the run of 2400s physical time.

RESULTS AND DISSCUSSIONS

Fig. 3 shows comparisons of the FDS predictions and measured results for 81kW surrounded fire case. For heat fluxes to the column surface, the predicted results agree very well with the measured data. For column surface temperatures, the predicted results also agree well with the measured data.

Fig.4 shows the comparisons of the FDS predictions and measured results for 255kW adjacent fire case. The predicted heat fluxes to front surface of the column are acceptable, especially at high elevation z (z is the height above the fire source), as shown in Fig.4a. However, the predicted heat fluxes to side surface divergence significantly to the measured data, as shown in Fig. 4b. At high elevation, the predicted temperatures on front and side surfaces agree well with the measured data, however at low elevation, the divergence between the predicted and measured results reach to 165°C for front surface and 80°C for side surface. For back surface the predicted

temperatures agree very well with the measured data at high elevation, as shown in Fig. 5a. Fig. 5b shows the gas temperature distribution in the cavity of the column.

Those differences between the predicted and measured results could be mainly attributed to the accuracy of the sub-models in FDS. It is well known that the accuracy of combustion and radiation models has a paramount effect on the heat flux prediction. Although FDS provides a reliable flow solver, the mixture fraction combustion model could yield errors as large as 20% as suggested by the code developer [5] and the radiation model cannot solve accurately the radiation equation with grid sizes on the order of centimeter due to the fourth power dependence of radiation on temperature. Furthermore, the 1D conduction model in FDS also influences the accuracy of the predicted column surface temperatures.

CONCLUSIONS

To assess the capacity of FDS in predicting the thermal behavior of steel columns exposed to localized fire, two localized fire tests given by Kamikawa et al. [10] were simulated in FDS. Experimental data about heat fluxes to column surfaces and column surface temperatures were compared with the predicted results. The main conclusions of this work are,

- FDS predicts well the heat fluxes and temperatures along the full length of the column in 81kW surrounded fire. The influence of parameters such as HRR, geometry of the fire source, etc. on the accuracy of numerical results have not been investigated at present due to the long calculation time and limited experimental data. Thus, it's too early to give a general conclusion on FDS's capacity of predicting thermal behavior of steel columns surrounded by fire, however, at least for the investigated case FDS's capacity has been verified.

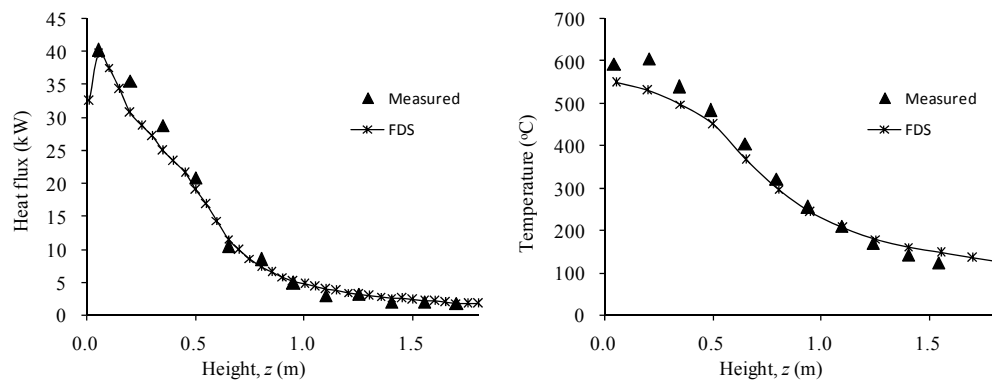
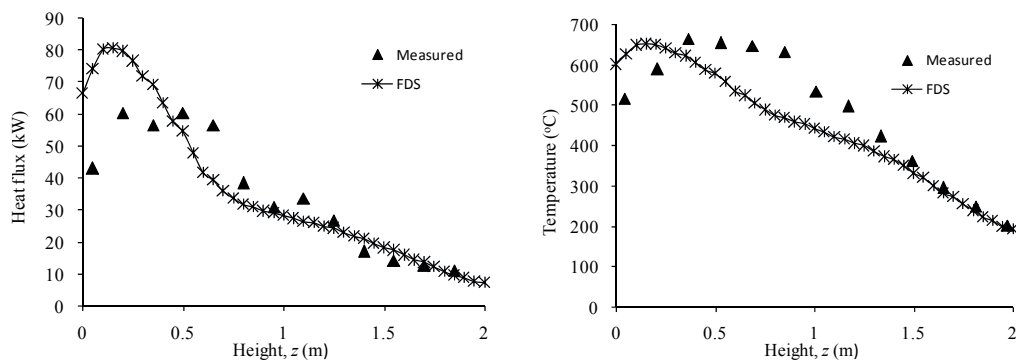


Figure 3. Comparisons of predicted and measured results for surrounded fire case.



(a) Front surface of the column

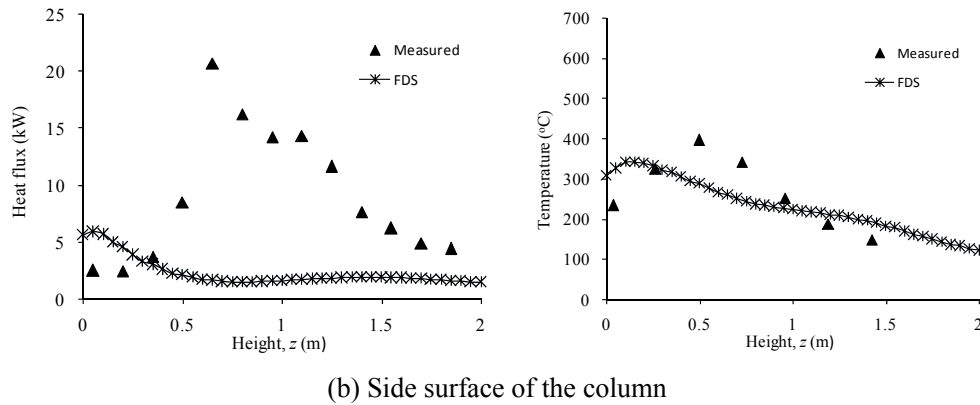


Figure 4. Comparisons of predicted and measured results for adjacent fire case.

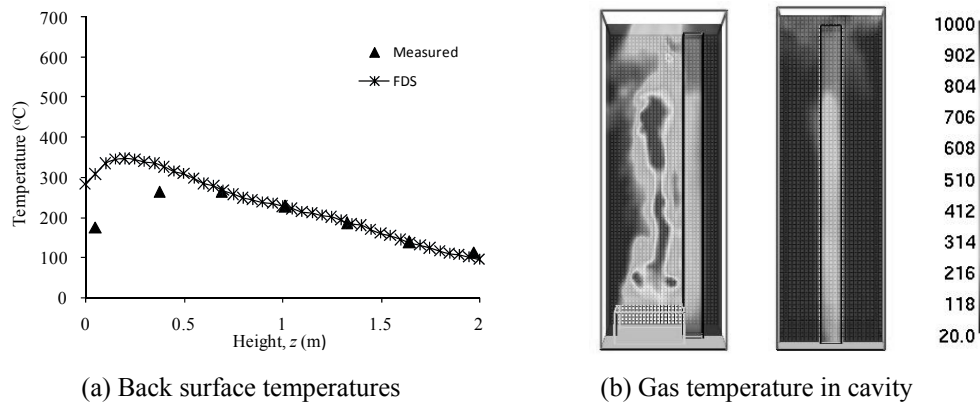


Figure 5. Temperatures on back surface of the column and gas temperature distribution in the cavity of the column in adjacent fire simulation.

- FDS gives acceptable prediction of heat fluxes to front surface of the column, but fails to predict heat fluxes to side surface in 255kW adjacent fire. The predicted column surface temperatures agree with the measured data at high elevation. The large differences between the predicted and measured results at low elevation in adjacent fire should draw special attention by engineer.
- Resolution of about 1/20 and 300 solid angles is enough to predict heat fluxes in localized fire.

REFERENCES

1. G Heskestad. Fire Plumes, flame height, and air entrainment.000 SFPE Handbook 3rd edition, Sec. 2-1, National Fire Protection Association, 2003.
2. J-F Cadorin, D Pintea, J-C Dotreppe, J-M Franssen. A tool to design steel elements submitted to compartment fires – Ozone V2. Part 2: Methodology and application. Fire Safety Journal, 2003;38:429–451.
3. Z Fu, G Hadjisophocleous. A two-zone fire growth and smoke movement model for multi-compartment buildings. Fire Safety Journal, 2000;34:257–85.
4. K B McGrattan, H R Baum, R G Rehm. Large eddy simulations of smoke movement. Fire Safety Journal, 1998:30:161–78.
5. K McGrattan, B Klein, S Hostikka, J Floyd. Fire Dynamics Simulator (Version 5) User’s Guide. NIST Special Publication 1019-5, National Institute of Standards and Technology (NIST), Gaithersburg, Maryland, 2009.

6. C Gutierrez-Montes, E Sanmiguel-Rojas, A Viedma, G Rein. Experimental data and numerical modeling of 1.3 and 2.3 MW fires in a 20m cubic atrium. *Building and Environment*, 2009;44:1827–39.
7. W K Chow, Y Z Li, E Cui, R Huo. Natural smoke filling in atrium with liquid pool fires. *Building and Environment*, 2001;36:121–27.
8. <http://code.google.com/p/fds-smv/source/browse/trunk/FDS/trunk/Validation>
9. T G Ma, J G Quintiere. Numerical simulation of axi-symmetric fire plumes: accuracy and limitations. *Fire Safety Journal*, 2003;38:467-92.
10. D Kamikawa, Y Hasemi, T Wakamatu, K Kagiya. Experimental flame heat transfer and surface temperature correlations for a steel column adjacent to and surrounded by a pool fire. *Proceedings of IFASS 2002*, 2002.
11. Chao Zhang, Guo-qiang Li. Thermal behavior of a steel beam exposed to a localized fire—Numerical simulation and comparison with experimental results. 4th International Conference on Protection of Structures against Hazards, 23-25 October, Beijing, China.
12. JP Holman. *Heat transfer*. 9th ed. New York: McGraw-Hill inc.; 2002.
13. WL Grosshandler. RADCAL: A narrow-band model for radiation calculations in a combustion environment. National Institute of Standard and Technology. NIST Technical Note 1402, 1993.
14. J Dreisbach, K McGrattan. Verification and validation of selected fire models for nuclear power plant applications. In: *Fire dynamics simulator (FDS)*, NUREG-1824 final report, vol. 7. U.S. Nuclear Regulatory Commission, Office of Nuclear Regulatory;2007.
15. C Gutiérrez-Montes, E Sanmiguel-Rojas, A Viedma, G Rein. Experimental data and numerical modeling of 1.3 and 2.3 MW fires in a 20 m cubic atrium. *Building and Environment*, 2009;44:1827–39.
16. CH Lin, YM Ferng, WS Hsu. Investigating the effect of computational grid sizes on the predicted characteristics of thermal radiation for a fire. *Applied Thermal Engineering*, 2009;29:2243–50.
17. S Hostikka, K McGrattan, A Hamins. Numerical modeling of pool fires using LES and Finite Volume Method for radiation. *Fire Safety Science—Proceedings of the 7th international symposium*, pp.383–94.

Structural and Fire Behaviour of a New Light Gauge Steel Wall System

S. GUNALAN and M. MAHENDRAN

ABSTRACT

Fire design is an essential element of the overall design procedure of structural steel members and systems. Conventionally the fire rating of load-bearing stud wall systems made of light gauge steel frames (LSF) is based on approximate prescriptive methods developed on the basis of limited fire tests. This design is limited to standard wall configurations used by the industry. Increased fire rating is provided simply by adding more plasterboards to the stud walls. This is not an acceptable situation as it not only inhibits innovation and structural and cost efficiencies but also casts doubt over the fire safety of LSF stud wall systems. Hence a detailed fire research study into the performance and effectiveness of a recently developed innovative composite panel wall system was undertaken at Queensland University of Technology (QUT) using both full scale fire tests and numerical studies. Experimental results of LSF walls using the new composite panels under axial compression load have shown the improvement in fire performance and fire resistance rating.

This paper presents the results of experimental investigations into the structural and fire behaviour of light gauge steel stud walls protected by the new composite panel. It demonstrates the improvements provided by the new composite panel system in comparison to traditional wall systems. The numerical validation of these test results is also presented in this paper. Numerical analyses were undertaken using the finite element program ABAQUS. Measured temperature profiles of the studs were used in the numerical models and the numerical analysis results were used to calibrate against full scale fire test results.

Gunalan. S, PhD Researcher, Faculty of Built Environment and Engineering, Queensland University of Technology, Brisbane, Australia.

Mahendran. M, Professor, Faculty of Built Environment and Engineering, Queensland University of Technology, Brisbane, Australia.

INTRODUCTION

The commonly used Light Gauge Steel Framing (LSF) load bearing stud wall systems are made of cold-formed thin-walled steel lipped channels. However, under fire conditions, these thin-walled steel sections heat up quickly resulting in fast reduction in their strength and stiffness. Innovative fire protection systems are therefore essential without simply adding on more plasterboards, which is inefficient. According to Feng et al. [1], the cavity insulation was found to be improving the fire resistance of steel stud wall panels. However, in the studies of Kodur and Sultan [2] and Alfawickhari [3], LSF wall assemblies without cavity insulation provided higher fire resistance compared to cavity insulated assemblies. Full scale tests were also undertaken by others [4-6] to investigate the behaviour of stud wall systems. Recently Kolarkar and Mahendran [7] developed a new composite panel system (Figure 1), where the insulation was placed outside the steel frame. They found that the fire resistance of LSF walls improved considerably. However, their study was limited to fire tests with a load ratio of 0.2. Hence a further experimental study was undertaken with higher load ratios and the results were validated using finite element analyses. This paper presents the details of the experimental and numerical studies, which were carried out to investigate the thermal and structural performance of load bearing steel stud wall assemblies using the new composite panel system under different load ratios. Experimental results are presented along with stud failure times, modes and temperatures. Details of the development and validation of the finite element model are also presented.

TEST SPECIMENS

Three test LSF wall specimens were built and tested with 25 mm thick insulation sandwiched between two plasterboards on both sides of the steel wall frame [7]. Table I gives the details of the three full scale load bearing test wall specimens (2400 mm x 2100 mm) used in this study. Four studs of lipped channel sections (90 x 40 x 15 x 1.15 mm) were used at a spacing of 600 mm. These studs were attached to the top and bottom tracks made of unlipped channel sections (92 x 50 x 1.15 mm). All the studs and tracks used were fabricated from galvanized steel sheets having a nominal base metal thickness of 1.15 mm and a minimum specified yield strength of 500 MPa. The plasterboards with a thickness of 16 mm were used, which are manufactured by Boral Plasterboard under the name of Fire-stop [8].

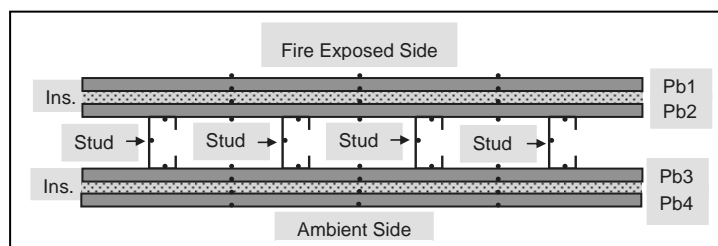


Figure 1. LSF stud walls using the new composite panel. Ins. - Insulation, Pb – Plasterboard.

TABLE I: DETAILS OF TEST SPECIMEN CONFIGURATIONS.

Test	Load Ratio	External Insulation
1	0.2 (15kN/stud)	Glass Fibre
2	0.4 (30kN/stud)	Glass Fibre
3	0.4 (30kN/stud)	Rock Fibre

TEST SET-UP AND PROCEDURE

The loading frame was used to load the individual studs at concentrically using four jacks connected to a single hydraulic pump (see Figure 2). The target load was applied first and maintained throughout the fire test in order to allow the free vertical expansion of the wall. A propane fired gas furnace was used to expose one side of the wall to the standard temperature-time fire curve in accordance with AS1530.4 [9] until failure. Many Linear Variable Displacement Transducers (LVDT) were used in order to measure the out-of-plane movements and axial shortening of the wall specimen during the test. K type thermocouples were used to measure the temperature development across the steel stud walls.

TEST OBSERVATIONS AND RESULTS

All the test wall specimen failures were due to the structural collapse of studs before any insulation or integration failure occurred. From the beginning of the fire test, the wall specimens were observed to be bending towards the furnace. However, near the failure, the lateral deflection of Test Specimens 1 and 2 started to reverse its direction and finally the studs bent outwards and away from the furnace, resulting in the breaking of plasterboards. On the other hand Test Specimen 3 continued to bend until the failure and resulted in failing towards the furnace. The exposed plasterboards were stripped off and the debris removed to expose the frame (see Figure 3). The local buckling waves along the studs were observed and it confirmed the occurrence of local buckling of studs before the ultimate failure.

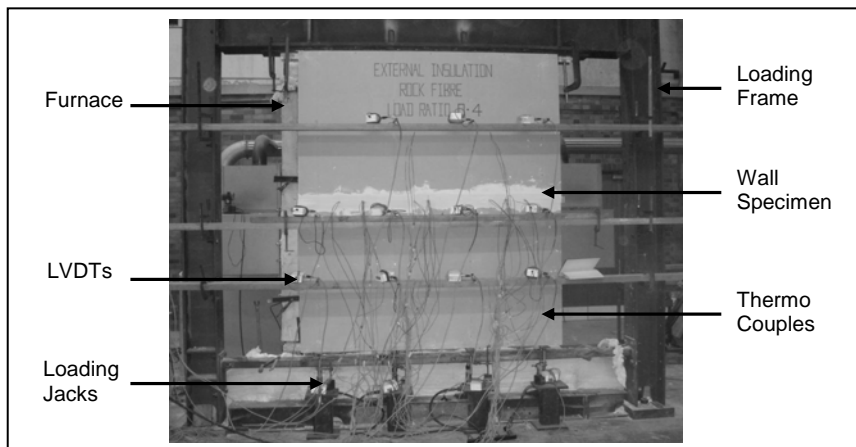


Figure 2. Test Specimen before testing.

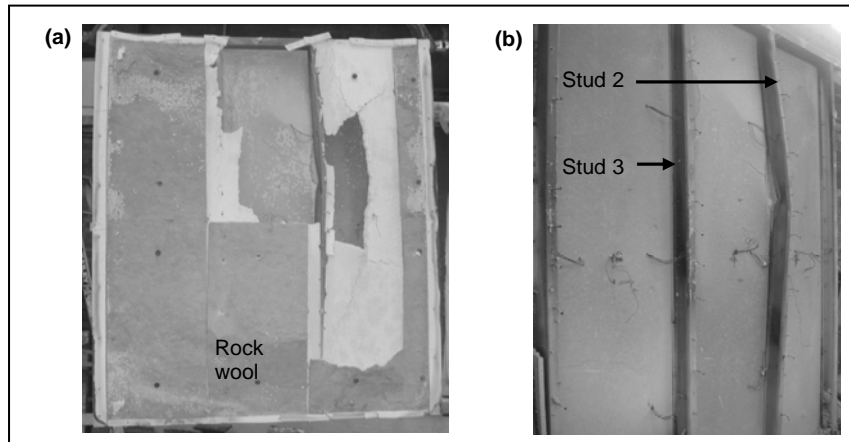


Figure 3. Test Specimen 3 after test: (a) partial collapse of exposed plasterboards, (b) frame after removing debris.

Table II gives the fire resistance ratings (in minutes) of the load bearing LSF wall specimens tested under a constant axial compression load during the fire tests in this study (Tests 1 - 3). It also includes the results of some of the tests conducted by Kolarkar [10] for the purposes of comparison (Tests 1* - 4*). The results confirm the superior performance of LSF walls using external insulation over cavity insulation. For example, Test 1* gave higher fire ratings than Tests 2* and 3*, where the insulation was placed inside the cavity. On the other hand Tests 1 and 4* gave about 20 % increase in fire rating compared to Tests 2* and 3*, respectively at a load ratio of 0.2.

Tests 1 and 2 were identical except for the applied load. The temperature profiles of the studs for Tests 1 and 2 were very similar as expected with a negligibly small time lag. However, the failure temperatures of the studs were higher for Test 1 compared to Test 2 since the first specimen was exposed to a lower applied load.

The only difference between Test Specimens 2 and 3 was the type of insulation used. In Test Specimen 3 rock fibre was used instead of glass fibre as in Test Specimen 2. The temperature profiles across the studs were similar in shape. However, a time delay of 25 minutes was observed between them resulting in increased fire resistance rating for Test Specimen 3. At failure the temperatures across the studs were nearly the same for Test Specimens 2 and 3, since the studs in both tests were stressed to the same level by the applied load of 30 kN.

Stud Temperatures and Failures

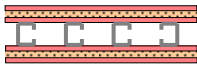
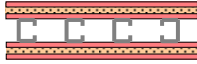
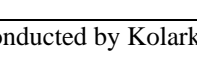
Table III, gives the comparison of the temperature values of the central studs at the end of the test for the current study. In all three tests, the studs that had vertical plasterboard joint was subjected to more heat flow due to the opening up of joints in plasterboards. Hence their temperatures (Stud 3 in Tests 1 and 2, and Stud 2 in Test 3) were higher than those of other studs and thus the wall failure was also influenced and initiated by these studs. The hot flange failure temperatures of these studs were very close to each other (i.e. 554 and 556°C). For these studs the

temperature differences between hot and cold flanges were 168 and 124°C, respectively. This may mean that stud failure was mostly governed by the (maximum) hot flange temperature than the temperature difference between hot and cold flanges. Hence we can conclude that structurally similar wall panels will fail once their studs reach a particular temperature and the fire resistance can be increased only by delaying the maximum temperature in the studs. This was confirmed by the increase in fire resistance time in Test 3, which was achieved by the delay in temperature rise on studs due to the use of better insulation.

Plasterboard Performance

Lateral restraint provided by plasterboard plays a significant role in the design of LSF stud walls. The minimum temperature difference between the faces of plasterboard attached to studs was 500°C until failure. Lateral or torsional buckling failure modes of studs were also not observed in the tests. This may suggest that this plasterboard (Pb2 shown in Figure 1) did not fully calcinate to lose its ability to provide lateral restraint until failure. Hence in the numerical modelling of LSF walls tested in this study, lateral restraint provided by plasterboards could be considered for both (hot side and cold side) flanges of the studs until failure.

TABLE II: STRUCTURAL RESPONSE OF TEST SPECIMENS.

Test	Configuration	Insulation Type	Insulation Location	Load Ratio	Failure Time (min.)
1		Glass Fibre	External	0.2	118
2		Glass Fibre	External	0.4	108
3		Rock Fibre	External	0.4	134
1*		None	-	0.2	111
2*		Glass Fibre	Cavity	0.2	101
3*		Rock Fibre	Cavity	0.2	107
4*		Rock Fibre	External	0.2	136

(*) - Tests conducted by Kolarkar [10]

TABLE III: THERMAL RESPONSE OF TEST SPECIMENS IN THE CURRENT STUDY.

	Test 1		Test 2		Test 3	
	Stud 2	Stud 3	Stud 2	Stud 3	Stud 2	Stud 3
Hot Flange Temperature (°C)	582	664	505	554	556	523
Cold Flange Temperature (°C)	491	490	371	386	432	420

FINITE ELEMENT MODELLING

This section presents the details of the development and validation of finite element models of LSF studs under fire conditions using ABAQUS. Based on past research results, an isolated stud with appropriate loading and boundary conditions was considered to simulate LSF stud walls. In the finite element model of studs, the element type S4R was used with a mesh size of 4mm x 4mm. The load was applied at the geometric centre of the cross-section of the stud while pinned end support conditions were used with translation restraints of the stud at every 300 mm. The lateral restraint provided by the plasterboards was considered for both flanges as per the studies of [6,11,12]. The non-uniform temperature field in the cross-section of a column was simplified by assuming uniform temperatures in the flanges and lips on both the hot and cold sides, and a linear temperature distribution in the web. The material properties were defined as a function of temperature and the temperatures were defined as a boundary condition. The reduction factors for yield stress and elastic modulus were obtained from a previous study at QUT [13].

The initial geometric imperfection values used in the previous studies varied among the past studies. Both local and global initial imperfections were included in [11]. On the other hand an imperfection amplitude value of 1 mm and $L/1000$ were used in the studies of [6] and [12], respectively. However, due to the dominance of thermal bowing the effect of initial imperfection does not have any significant effect on the behaviour of LSF studs at elevated temperature. Hence, a value of $b/150$ was used in this model after considering the modes from the bifurcation buckling analysis of LSF studs at ambient condition. At higher temperatures, the effect of residual stresses is also negligible. Therefore it was neglected in this model as per past researches. The finite element modelling was performed under dynamic condition where the stud was first subjected to pre-determined axial loads and then it was exposed to the measured temperature profiles. Each finite element analysis was performed in eleven steps. The first step was an eigen buckling analysis at ambient condition, in which the buckling modes were obtained and the deformed profile of the lowest buckling mode was used to determine the stud initial imperfection. Nonlinear analyses were then performed for the remaining steps with Riks-off method. In the second step, the load was applied incrementally up to the target level. Temperature was then applied one after the other in the remaining steps to follow the measured temperature profiles until failure.

Validation of Finite Element Models

The accuracy of the developed finite element models was validated using the failure modes, failure time and deformation curves obtained from the full scale fire tests. Table IV confirms the failure time obtained by both experiments and FEA. Figure 4 shows the failure mode of the stud where the local buckling waves and bending about the major axis were observed. The temperature profiles used in the numerical analyses based on fire test results are shown in Figure 5(a). Figures 5(b) and 5(c) show the close agreement of the deflection curves between tests and FEA. The agreement of these curves is very good compared to the previous numerical studies of LSF walls at fire conditions. Further improvements are currently being considered and used in the finite element models reported in this paper.

TABLE IV: FAILURE TIMES FROM EXPERIMENTS AND FINITE ELEMENT ANALYSES.

	Test 1		Test 2		Test 3	
	Stud 2	Stud 3	Stud 2	Stud 3	Stud 2	Stud 3
Failure Time Exp. (min.)	118	118	108	108	134	134
Failure Time FEA (min.)	118	115	107	111	133	136

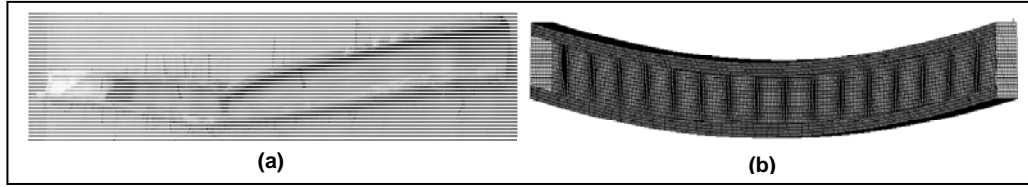


Figure 4. Failure mode of Stud 2 of Test Specimen 3: (a) experiment, (b) FEA.

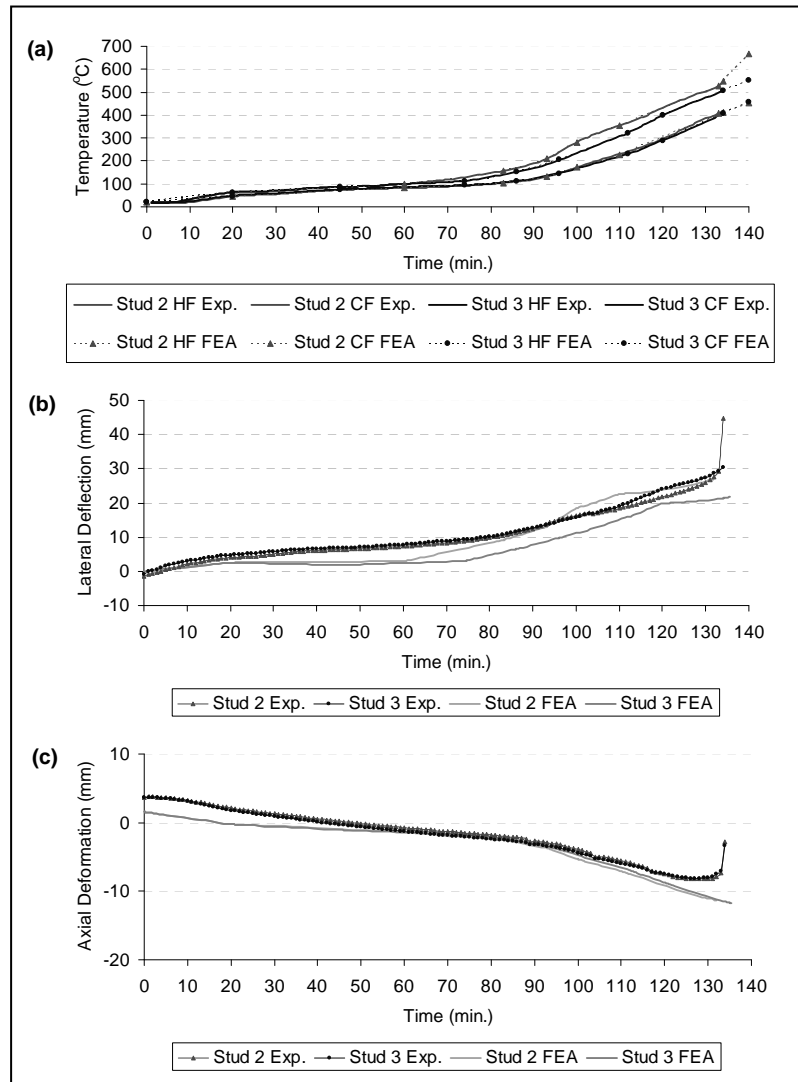


Figure 5. Results of Test Specimen 3: (a) measured and assumed section temperature distributions in numerical simulation, (b) lateral deflection plots obtained from experiment and FEA, (c) axial deformation plots obtained from experiment and FEA. HF - Hot Flange, CF - Cold Flange.

CONCLUSIONS

This paper has described an experimental study of the thermal and structural performance of cold-formed steel stud wall systems used as load-bearing walls. This study has confirmed that the use of external insulation increases the fire resistance of LSF walls significantly even at higher loads. Details of fire tests results are presented and discussed. Also the plasterboard performance and its resistance to provide lateral restraint are discussed. The numerical models were developed and validated to fully understand the improvements offered by the new composite system and to confirm the fire test observations. The use of accurate numerical models as described above allowed the inclusion of various complex thermal and structural effects such as thermal bowing, local buckling and material deterioration at elevated temperatures.

ACKNOWLEDGEMENT

The authors wish to thank Australian Research Council for the financial support to this project through the Discovery Grants Scheme, QUT for providing the required experimental and computing facilities and technical support, and Boral and Fletcher Insulation for providing the required plasterboard and insulation materials. Contributions to fire test results from Prakash Kolarkar are also acknowledged.

REFERENCES

1. Feng, M, Y.C. Wang, and J.M. Davies. 2003. "Thermal performance of cold-formed thin-walled steel panel systems in fire," *Fire Safety Journal* 38, pp. 365-394.
2. Kodur, V.R, and M.A. Sultan. 2001. "Factors governing fire resistance of load-bearing steel stud walls," *Proceeding of 5th AOSFST International Conference*, Newcastle, Australia, pp. 1-2.
3. Alfawakhiri, F. 2001. "Behaviour of cold-formed-steel-framed walls and floors in standard fire resistance tests," PhD Thesis, Carleton University, Ottawa, Ontario, Canada.
4. Gerlich, J.T, P.C.R. Collier and A.H. Buchanan. 1996. "Design of light steel framed walls for fire resistance," *Fire and Materials* 20, pp. 79-96.
5. Feng, M, and Y.C. Wang. 2005. "An experimental study of loaded full-scale cold-formed thin-walled steel structural panels under fire conditions," *Fire Safety Journal* 40, pp. 43-63.
6. Zhao, B, J. Kruppa, C. Renaud, M. O'Connor, E. Mecozzi, W. Apiazu, T. Demarco, P. Karlstrom, U. Jumppanen, O. Kaitila, T. Oksanen, and P. Salmi. 2005. "Calculation rules of lightweight steel sections in fire situations," *Technical steel research*, European Commission.
7. Kolarkar, P.N, and M. Mahendran. 2008. "Thermal performance of plasterboard lined steel stud walls," *Proceeding of 19th International Specialty Conference on Cold-Formed Steel Structures*, St. Louis, Missouri, USA, pp. 517-530.
8. Standards Australia (SA). 1998. AS/NZS 2588, "Gypsum Plasterboard," Sydney, Australia.
9. Standards Australia (SA). AS 1530.4, "Methods for fire tests on building materials, components and structures, Part 4: Fire-resistance tests of elements of building construction," Sydney.
10. Kolarkar, P.N. 2010. "Fire performance of plasterboard lined steel stud walls," PhD Thesis, QUT, Brisbane, Australia, In preparation.
11. Kaitila, O. 2002. "Finite Element Modelling of Cold-formed Steel Members at High Temperatures," Masters Thesis, HUT, Otakaari, Finland.
12. Feng, M, Y.C. Wang, and J.M Davies. 2003. "Axial strength of cold-formed thin-walled steel channels under non-uniform temperatures in fire," *Fire Safety Journal* 38, pp. 679-707.
13. Dolamune Kankanamge, N. 2010. "Structural Behaviour and Design of Cold-formed Steel Beams at Elevated Temperatures," PhD Thesis, QUT, Brisbane, Australia, In preparation.

Development of a 3D Co-Rotational Beam-Column Element for Structural Analysis of Steel and Composite Frames Exposed to Fire

Q.-T. LE, B. ZHAO and M. HJIAJ

ABSTRACT

This paper presents a 3D beam-column finite element including warping effects for the analysis of both steel and composite structures subjected to fire. This beam-column finite element is based on the co-rotational formulation and considers a local Bernoulli fibre element. It possesses seven degrees of freedom at each node and can be used to deal with steel and composite members with arbitrary cross-sections. Another advantage of this element is that the meshing of the cross-section can be arbitrary. Hence, a non-uniform temperature distribution can be considered both along the element length and within the beam cross-section. In addition, the shift of the shear (torsional) centre with respect to temperature variation in the cross section is taken into account. Steel and concrete elasto-plastic models based on recommendations given in the fire section of Eurocode 2 and 3 are considered. The geometrical non-linearity with large displacement is implemented in the model to deal with largely deformed structures in fire situation. The validation of the developed computational model is performed by comparing the model predictions against results obtained with a 3D solid finite element model. It is shown that this model is able to represent accurately the fire behaviour of both steel and composite frames with low computational effort.

INTRODUCTION

Numerical analysis of steel and composite spatial frames exposed to fire requires involve a nonlinear analysis which requires robust numerical tools that perform well in all situations. One efficient way of deriving nonlinear finite elements is to use the element-independent co-rotational algorithm, which was proposed by Rankin and Brogan [1]. This procedure separates the element rigid body motion from its smaller deformational response through the use of a

Quang-Trung LE and Bin ZHAO, CTICM, Espace Technologique, L'orme des Merisiers, Immeuble Apollo, 91193 SAINT-AUBIN, France
Mohammed HJIAJ, Structural Engineering Research Group/LGCGM, INSA de Rennes, 20 Avenue des Buttes de Coësmes, 35043 Rennes Cedex, France
qtrungle@cticm.com, binzhao@cticm.com, mohammed.hjjaj@insa-rennes.fr

reference system which continuously rotates and translates with the element, thus allowing moderate rotation and small strain-displacement relations to be used in the context of arbitrarily large total rotations.

Several authors developed the co-rotational finite element formulations; here we mention the papers of M. A. Crisfield [3,11], Rankin and co-workers [1,2]. Efficient co-rotational beam elements have been proposed by Pacoste, Eriksson and Battini [5-8]. In this paper, the formulation proposed by Battini [7] is adopted as it is applicable to arbitrary cross-section.

For structures subjected to real fire, the temperature distribution within the cross section is never uniform. In order to take into account this feature, a specific numerical model of which theoretical aspects have been proposed by Gruttmann and al. [9,10] and used in [7,8] is adopted. This model is capable of dealing with any cross-section divided into arbitrary meshing.

At material level, the steel and concrete elasto-plastic models are introduced on the basis of the material laws given in the fire section of Eurocode 2 and 3. Due to the non-linear stress-strain relationship, the stress resultants and associated linearizations are obtained by numerical integration over the cross-section. In the present work, the von-Mises yield criterion is adopted for the steel model, whereas two distinct yield criteria are needed for concrete in order to account for behaviour in both tension (Rankine yield surface) and compression (Drucker-Prager criterion). At each integration point, the constitutive equations are solved iteratively by using the radial return-mapping algorithm [11,12] and the consistent elasto-plastic tangent modulus is used for global iteration.

The content of the paper is outlined as follows: In the next section we present the fundamental finite element formulation. In section 3, are presented only the constitutive equations for elasto-plastic concrete material model. The validity of the developed element is demonstrated in Section 4 with several examples. Finally, the conclusions are given in Section 5.

FINITE ELEMENT FORMULATION

Corotational framework for 3D beams

The central idea in the corotational formulation for a two-noded 3D beam is to introduce a local coordinate system which continuously rotates and translates with the element. Then, local deformational displacements \mathbf{d}_l are defined by extracting the rigid body movements from the global displacements \mathbf{d}_g . The local displacements are expressed as functions of the global ones, i.e.

$$\mathbf{d}_l = \mathbf{d}_l(\mathbf{d}_g) \quad (1)$$

Then, \mathbf{d}_l is used to compute the internal force vector \mathbf{f}_l and tangent stiffness matrix \mathbf{K}_l in the local frame. The transformation matrix \mathbf{B} between the local and global displacements is defined by

$$\delta \mathbf{d}_l = \mathbf{B} \delta \mathbf{d}_g \quad (2)$$

and is obtained by differentiation of **Error! Reference source not found.**. The expression of the internal force vector in global coordinates \mathbf{f}_g and the tangent stiffness matrix \mathbf{K}_g in global coordinates can be obtained by equating the internal virtual work in both the global and local systems, i.e.

$$\mathbf{f}_g = \mathbf{B}^T \mathbf{f}_l, \quad \mathbf{K}_g = \mathbf{B}^T \mathbf{K}_l \mathbf{B} + \partial(\mathbf{B}^T \mathbf{f}_l) / \partial \mathbf{d}_g \Big|_{\mathbf{f}_l} \quad (3)$$

Relations (1), (2) and transformations (3) are explained in details in [7].

Local strain definition

The beam strains are based on the Bernoulli kinematic model with torsion-warping deformation [4,10]. Based on these assumptions, the Green-Lagrange strains tensor can be derived and then simplified by neglecting most of the non-linear terms.

Hermitian interpolations are used for the local displacements. Hence, the integration along the beam length is computed with two Gauss points.

Cross-section warping

The warping function $\bar{\omega}(y, z)$ is defined according to the Saint-Venant torsion theory for bars and refers to the centroid. For pure torsion, the variational formulation related to the warping function computation can be expressed as

$$\int_A G_e (\bar{\omega}_{,y} \delta \bar{\omega}_{,y} + \bar{\omega}_{,z} \delta \bar{\omega}_{,z}) dA_e = \int_A G_e (z \delta \bar{\omega}_{,y} - y \delta \bar{\omega}_{,z}) dA_e \quad (4)$$

where G_e is the shear modulus of each fibre element of the cross-section. In the [9,10], linear elasticity is adopted and then the shear moduli are eliminated in both sides of the equation. Although frequently used, this assumption is certainly debatable. In case of fire situation with non-uniform temperature distribution, the shear modulus of the fibre elements of the cross section wouldn't be the same and in consequence can not be eliminated from both sides of the equation. However, its correctness should be checked. In the later examples, the assumption of linear elasticity is still considered.

The above equation is solved numerically using a finite element approach. Isoparametric quadratic plane elements (Serendip family) are used to discretize the cross-section. This means that the coordinates y, z , the unknown warping functions $\bar{\omega}$, and the temperatures t are interpolated within an element using the same Serendip shape functions

$$\begin{aligned} y &= \sum_{i=1}^8 N_i(\xi, \eta) y_i, \quad z = \sum_{i=1}^8 N_i(\xi, \eta) z_i \\ \bar{\omega} &= \sum_{i=1}^8 N_i(\xi, \eta) \bar{\omega}_i, \quad t = \sum_{i=1}^8 N_i(\xi, \eta) t_i \end{aligned} \quad (5)$$

The element stiffness matrix and load vector are obtained as

$$\mathbf{K}_{ij} = \int_A (N_{i,y} N_{j,y} + N_{i,z} N_{j,z}) dA_e, \quad \mathbf{f}_i = \int_A (N_{i,y} z - N_{i,z} y) dA_e \quad (6)$$

Using the isoparametric transformation, the integrations over each element are performed numerically with four Gauss points. After assembly, the system

$$\mathbf{K} \mathbf{u} = \mathbf{f} \quad (7)$$

is solved. This provides the vector \mathbf{u} which contains the nodal values of $\bar{\omega}$. The vector \mathbf{u} is next transformed using

$$\bar{\omega} := \bar{\omega} - \frac{1}{A} \int_A \bar{\omega} dA \quad (8)$$

in order to satisfy the normality condition

$$\int_A \bar{\omega} dA = 0 \quad (9)$$

Hence, the coordinates y, z , the warping functions $\bar{\omega}$, and the temperatures t at the Gauss points are determinate.

Local finite element formulation

The expression of the principal of virtual work can be written as

$$\int_V \delta \boldsymbol{\varepsilon}^T \cdot \boldsymbol{\sigma} dV = \delta \mathbf{d}_l^T \mathbf{f}_l \quad (10)$$

Considering Hermitian interpolations, and after some algebra, the local strain-displacement relations can be rewritten as

$$\delta \boldsymbol{\varepsilon} = \begin{pmatrix} \delta \boldsymbol{\varepsilon}_{xx} \\ 2\delta \boldsymbol{\varepsilon}_{xy} \\ 2\delta \boldsymbol{\varepsilon}_{xz} \end{pmatrix} = \mathbf{HCA} \delta \mathbf{d}_l \quad (11)$$

where \mathbf{C} is a matrix which contains constants and functions of local coordinate x , \mathbf{A} is a matrix which contains constants and functions of initial length of element l_0 , and \mathbf{H} is a matrix which contains local displacements, derivatives of warping function, and local coordinates y, z .

Using Eq. (11), the virtual work (10) can be rewritten as

$$V = \int_V \delta \boldsymbol{\varepsilon}^T \cdot \boldsymbol{\sigma} dV = \delta \mathbf{d}_l^T \int_V \mathbf{A}^T \mathbf{C}^T (\mathbf{H}^T \cdot \boldsymbol{\sigma}) dV = \delta \mathbf{d}_l^T \mathbf{f}_l \quad (12)$$

which gives the expression of the internal force \mathbf{f}_l

$$\mathbf{f}_l = \int_V \mathbf{A}^T \mathbf{C}^T (\mathbf{H}^T \cdot \boldsymbol{\sigma}) dV \quad (13)$$

The local tangent stiffness matrix defined by $\delta \mathbf{f}_l = \mathbf{K}_l \delta \mathbf{d}_l$, can be calculated by differentiation of Eq. (13), which gives

$$\mathbf{K}_l = \mathbf{A}^T \mathbf{C}^T \int_V (\mathbf{H}^T \mathbf{D}_m \mathbf{H} + \mathbf{M}) \mathbf{C} \mathbf{A} dV \quad (14)$$

where \mathbf{D}_m is the consistent elasto-plastic tangent modulus, and \mathbf{M} is the local geometric stiffness matrix which has only three non zero terms

$$\mathbf{M}_{2,2} = \mathbf{M}_{3,3} = \boldsymbol{\sigma}_{xx}, \quad \mathbf{M}_{6,6} = (y^2 + z^2) \boldsymbol{\sigma}_{xx} \quad (15)$$

NON-LINEAR MATERIAL MODEL FOR CONCRETE

In this section, only the elasto-plastic concrete material model is described considering that the material model for steel is much more familiar and its description is not necessary. The Rankine and Drucker-Prager yield functions are respectively

$$\mathbf{F}_t = \frac{\boldsymbol{\pi}^T \boldsymbol{\sigma}}{2} + \frac{(\boldsymbol{\sigma}^T \mathbf{P}_t \boldsymbol{\sigma})^{\frac{1}{2}}}{2} - \sigma_y^t(\kappa_t) \quad (16)$$

$$\mathbf{F}_c = (\boldsymbol{\sigma}^T \mathbf{P}_c \boldsymbol{\sigma})^{\frac{1}{2}} + \beta \boldsymbol{\pi}^T \boldsymbol{\sigma} - (1 - \beta) \sigma_y^c(\kappa_c) \quad (17)$$

where β is a dimensionless constant related to uniaxial and biaxial strength in compression, κ_t and κ_c is the set of internal variables, σ_y^t and σ_y^c are the apparent resistance stress which are function of the internal variables, and the projection matrices \mathbf{P}_t and \mathbf{P}_c and the projection vector $\boldsymbol{\pi}$ are defined by

$$\mathbf{P}_t = \begin{bmatrix} 1 & 0 & 0 \\ 0 & 4 & 0 \\ 0 & 0 & 4 \end{bmatrix} \quad \mathbf{P}_c = \begin{bmatrix} 1 & 0 & 0 \\ 0 & 3 & 0 \\ 0 & 0 & 3 \end{bmatrix} \quad \boldsymbol{\pi} = \begin{pmatrix} 1 \\ 0 \\ 0 \end{pmatrix} \quad (18)$$

An associated flow rule is adopted and fully implicit scheme is used to integrate the flow rule.

VALIDATION OF THE NUMERICAL MODEL

The numerical model has been implemented in FORTRAN. Two examples relative to steel members are presented hereafter.

Cantilever beam of channel-section

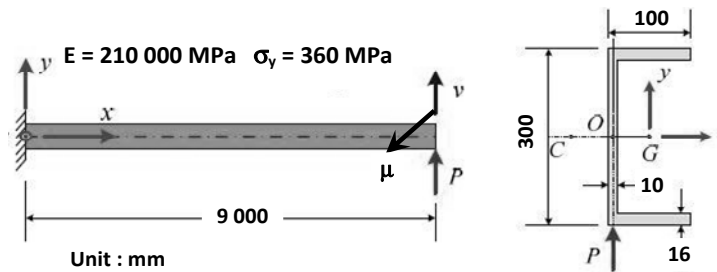


Figure 1. Channel-section beam with cross-section and material data.

As indicated in Figure 1, this example concerns a channel-section beam clamped at one end and subjected to a tip force at the free end. The load is applied at the bottom of the section (see **Figure 1Error! Reference source not found.**). The behaviour of this beam under uniform and non-uniform temperature distributions is investigated. In all cases, the applied load remains constant and equals to 3 kN at elevated temperatures.

The numerical results of our model are obtained with 20 elements and 200 integration points within the cross-section. In parallel, the same beam was also modelled with the computer code ANSYS using solid brick elements in order to investigate the accuracy of the beam element model. In **Error! Reference source not found.** a, b, c, d, e, the vertical and lateral displacements v and u of point O at the cantilever tip are compared between the two models in the cases of room temperature, uniform temperature distribution within the cross-section, temperature gradient along y-axis, temperature gradient along z-axis and temperature gradients along both z and y axis.

It can be seen from above comparison that the two models predict very close results whatever the temperature distribution is in the cross-section even under large displacement (see Figure 3). It shows also that the developed beam element is able to accurately simulate the structural behaviour of slender steel members at elevated temperatures.

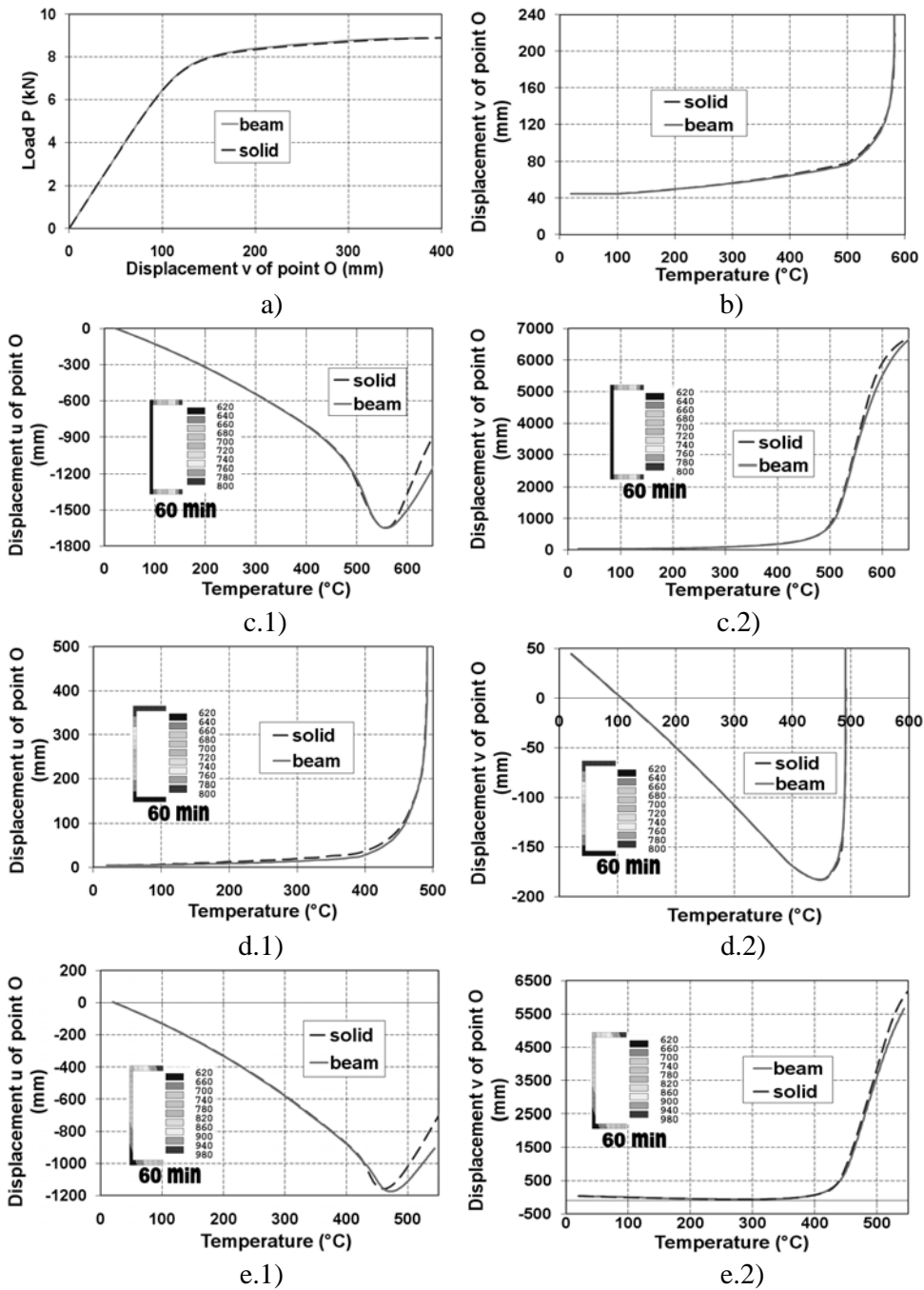


Figure 2. Curves of load-displacement v and temperature-displacements u and v of point O.

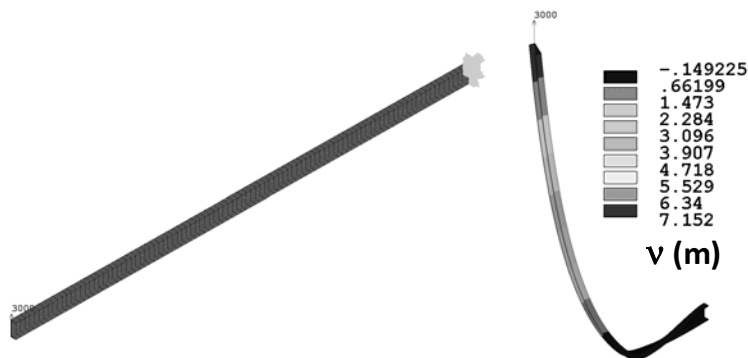
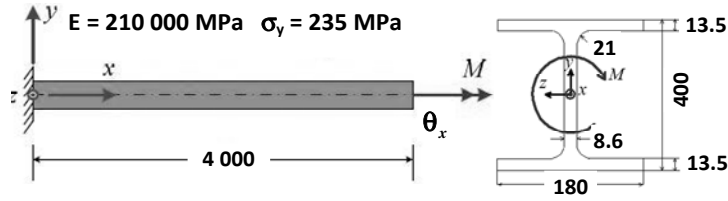


Figure 3. Meshing and deformation of solid element model.

Cantilever beam of I-section



Unit : mm
Figure 4. Cantilever beam of I-section with cross-section and material data.

The non-linear torsion of the I section cantilever beam, depicted in Figure , was investigated considering both uniform and non-uniform temperature distributions. The clamped end of the beam is fully restrained. The value of pure torsion moment is constantly 4.50 kN.m.

The numerical results with our beam element model are obtained using 10 elements and 152 integration points within the cross-section and compared to those obtained with a 3D solid element model. Figure 5 shows respectively the comparisons in the cases of uniform temperature distribution within the cross-section, temperature gradient along z-axis, temperature gradient along y-axis, and the temperature gradient along the both z and y axis. The element and cross-section meshing of the solid model and its deformation are presented in Figure .

It can be found that the two models are close to each other if the rotation remains relatively small. But difference appears once the rotation becomes significant. In fact, the discrepancy is due to the fact that the initial cross-section of the beam according to solid element model was locally distorted and no longer consistent with beam element model which was based on the assumption that the cross section remains planar and undeformed in its own plane. However, this discrepancy has no impact on the fire resistance of steel members because under so important axial rotation, the collapse of steel members will certainly occur.

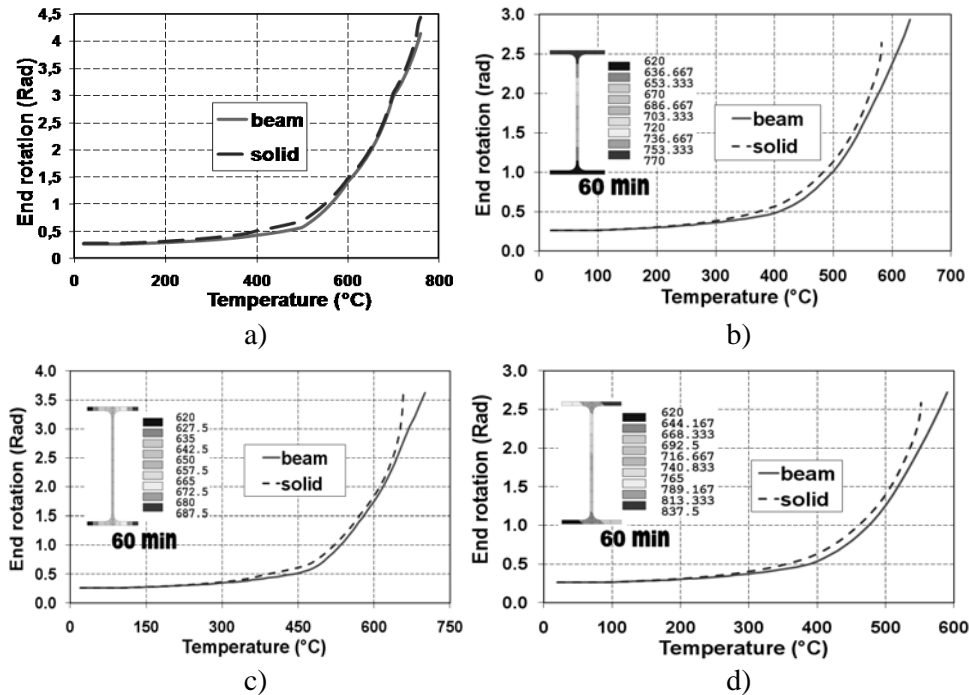


Figure 5. Curves of temperature-end axial rotation of the I-section beam at uniform and non-uniform temperature condition.

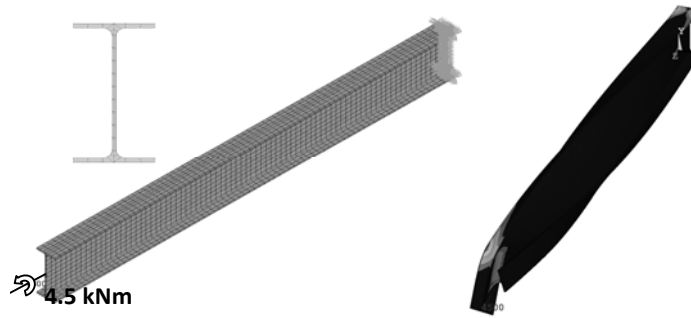


Figure 6. Meshing and deformation of solid element model.

CONCLUSION

The beam finite element developed in this paper is based on a co-rotational formulation for three-dimensional beams with arbitrary cross-section. Each node of the element possesses seven degrees of freedom. The displacement field proposed by Gruttmann and al. [9,10] and repeated in [7,8] was adopted and used to construct a consistent second-order approximation to the Green-Lagrange strains, at the level of the local element frame. Constitutive models based on recommendations of the fire section of Eurocode 2 and 3 are considered.

The presented examples show the validity of the developed beam element applied to geometrical and physical non-linear problems at the both normal temperature and high temperature conditions. A good agreement between the results given by the beam elements and those given by the solid elements is obtained.

REFERENCE

1. C.C. Rankin and F.A. Brogan, An element-independent corotational procedure for the treatment of large rotations, *ASME J. Pressure Vessel Technol.* 108 (1986) 165–174.
2. B. Nour-Omid, C. C. Rankin, Finite rotation analysis and consistent linearization using projectors, *Comput. Methods Appl. Mech. Engrg.* 93 (1991) 353–384.
3. M. A. Crisfield, A consistent co-rotational formulation for non-linear, three-dimensional, beam-elements, *Comput. Methods Appl. Mech. Engrg.* 81 (1990) 131–150.
4. J. C. Simon, L. Vu-Quoc, A geometrically-exact rod model incorporating shear and torsion-warping deformation, *Int. J. for Solids and Structures.* 27 (1991) 371–393.
5. C. Pacoste, A. Eriksson, Beam elements in instability problems, *Comput. Methods Appl. Mech. Engrg.* 144 (1997) 163–197.
6. C. Pacoste, A. Eriksson, Element behaviour in post-critical plane frame analysis, *Comput. Methods Appl. Mech. Engrg.* 125 (1995) 319–343.
7. J. M. Battini, C. Pacoste, Co-rotational beam elements with warping effects in instability problems, *Comput. Methods Appl. Mech. Engrg.* 191 (2002) 1755–1789.
8. J. M. Battini, C. Pacoste, Plastic instability of beam structures using co-rotational elements, *Comput. Methods Appl. Mech. Engrg.* 191 (2002) 5811–5831.
9. F. Gruttmann, R. Sauer and W. Wagner, Shear stresses in prismatic beams with arbitrary cross-sections, *Int. J. Numer. Methods Engrg.* 45 (1999) 865–889.
10. F. Gruttmann, R. Sauer and W. Wagner, Theory and numerics of three-dimensional beams with elasto-plastic material behaviour, *Int. J. Numer. Methods Engrg.* 48 (2000) 1675–1702.
11. M. A. Crisfield, *Non-linear Finite Element Analysis of Solids and Structures, Volume 1: Essentials*, Wiley, Chichester, 1991.
12. J. C. Simo, T. J. R. Hughes, *Computational Inelasticity*, Springer, New York, 1998.

Fire-Induced Progressive Collapse of Steel Structures that have Sustained Localized Damage

S. E. QUIEL and S. M. MARJANISHVILI

ABSTRACT

In current practice, progressive collapse analysis typically includes two types of hazards: the initial hazard that causes the localized damage and the subsequent response of the structure to bridge loads across the damaged areas (analysis referred to as alternate path method). However, little detailed information is available on a third type of hazard such as fire that typically follows the initial hazard. Prolonged exposure of a damaged structure to fire could be detrimental to the short-term stability of that structure and may pose a significant threat to the safe evacuation of building occupants. This paper presents a study of the effects of fire following an extreme event (i.e. blast or impact) that causes failure of one column on the perimeter of a common steel building frame. The approach focuses on a steel structure that is designed to satisfy new US DoD guidelines and assumes that the extreme event not only damages one column but also damages active and passive fire protection in the vicinity of the structural damage. Results of this study include estimates of the time to collapse initiation and a correlation between the level of fire protection and the collapse time. The goal of this study is to raise awareness of potential fire hazards that may follow extreme events and provide recommendations regarding evacuation times for occupants of damaged buildings under fire.

INTRODUCTION

The ability of a structure to resist a disproportionately large collapse due to localized damage (i.e. progressive collapse) has become a topic of increasing concern within the building community in the wake of structural collapses worldwide over the last half century. Design concepts for progressive collapse resistance have been developed for building codes and criteria in response to these events, which include the 1968 collapse at Ronan Point in the UK and the progressive collapse of the Murrah Federal Building resulting from the 1995 Oklahoma City bombing. Even though

Spencer E. Quiel, PhD, Project Engineer, Hinman Consulting Engineers, 225 Reinekers Lane, Suite 250, Alexandria, VA 22314 USA, Email: squiel@hce.com

Shalva M. Marjanishvili, PhD, PE, SE, Technical Director, Hinman Consulting Engineers, One Bush Street, Suite 510, San Francisco, CA 94104 USA, Email: shalva@hce.com

these methodologies have improved the design of structures to resist a collapse disproportionate to the damage sustained during an extreme event, recent structural collapses have highlighted the need for the progressive collapse resistance in structures that have been damaged by an extreme event and experience a subsequent fire resulting from the event. This combination is typically not considered in current progressive collapse design guidance and can be critical to the resistance of a structure to the entirety of an extreme event. The investigation of the collapse of the World Trade Center (WTC) Twin Towers by the NIST concluded that the fire following the aircraft impact and explosion caused the progressive collapse of the damaged structure [2]. As was the case for the Twin Towers, the extreme event can also cause damage to the active and passive fire protection systems, allowing the fire to severely affect the performance of the potentially damaged structure. Steel-framed structures are a concern in this case because they rely heavily on these protection measures, typically more so than concrete structures, to limit the increase of member temperatures and thus prevent further structural degradation.

This study uses a multihazard approach to evaluate the performance of a structure that is damaged by an extreme event and is subsequently subjected to a resulting fire. The prototype used for this study is based on a five-story steel-frame office building recently designed by Hinman Consulting Engineers (hereby referred to as “Hinman”) for progressive collapse resistance according to criteria established by the US Department of Defense (DoD) [1]. The building has a conventional steel-framed design and therefore represents a common example of low-rise office construction. The objective of this study is to evaluate the effectiveness of the design implemented for progressive collapse resistance (which assumes the structure to be at ambient temperature) when the structure is subjected to fire following the emergence of localized damage. Several design scenarios with varying levels of passive fire protection applied to the heated structural elements are considered.

MULTIHAZARD APPROACH

The concept of analyzing structures that have been damaged by an extreme event and experience a subsequent fire has been considered by several but few other researchers. Among those studies are those by Della Corte et al. [3], which examined the performance of a steel moment resisting frame (MRF) under fire after it had sustained permanent deformations due to earthquake loading, and Chen and Liew [4], which evaluated the fire resistance of steel columns that had been damaged by blast. The study presented in this paper takes a similar approach by evaluating the response of a steel building frame that has been explicitly designed to resist progressive collapse to fire once it has been damaged by blast or impact. The multihazard approach used here is also multiphase, as it considers that the structure experiences the following, in order: (1) removal of a few key structural elements via blast or impact, occurring on a time scale of milliseconds; (2) the onset of stable plastic deformations as designed according to the criteria, on a time scale of seconds; and (3) the development of a severe fire near the location of member removal, on a time scale of minutes. The approach focuses on the behavior of the damaged structure once the members targeted for removal have already been removed, and our analyses therefore begin in phase (2) described above. It is assumed that the building sustains no additional structural damage due to the initial extreme event beyond the targeted removed members and that the fire initiates immediately after the onset of stable plastic deformations in the structural frame near the removal location.

PROTOTYPE

The prototype selected for this study is a five-story office building with approximate rectangular dimensions of 310 ft. by 110.5 ft. by 75 ft. (length by width by height) and typical bay dimensions of 30 ft. x 40.25 ft. The framing plan of the building at each floor is shown in Fig. 1. The structural steel frame is composed of wide-flanged steel sections. At each occupied floor, the steel framing supports a 3-in. reinforced lightweight concrete floor slab poured over a 3.5-in. metal deck. Lateral resistance for the steel frame is provided by several perimeter moment resistant frames (MRF's) as well as four eccentrically braced frames in its interior, as shown in Fig. 1. The façade was composed primarily of 7 3/4-in. thick precast concrete panels with cut window openings, with the remainder comprised of a glazed curtainwall system. The building is designed with an automatic sprinkler system as its primary fire protection. Due to its occupancy classification and height, the building code allows for all structural elements beside those supporting elevators or stairwells to have no passive applied fire protection when a sprinkler system (i.e. active fire protection) is installed [5]. This is not uncommon for office buildings of this type, which represent a large portion of the steel-framed low-rise office inventory in the US.

DESIGN OF PROGRESSIVE COLLAPSE RESISTANCE

Progressive collapse occurs when relatively localized damage causes chain of failures eventually leading to the collapse of disproportionately large part of the building. The most recent criteria published by the US DoD (UFC) specify levels of progressive collapse resistance as a function of the building's occupancy and height [1]. According to these classifications, the prototype structure considered for this study was designed for progressive collapse resistance using the alternate path method, in which the structure must bridge across elements that are removed due localized damage. For structural steel frames, the alternate path method according to UFC [1] specifies that the structure be able to bridge over columns that are removed. Column removal is mandated as one at a time in one-story lengths from the structural frame at several plan and elevation locations. When a column is removed, beam-to-beam continuity is assumed to be preserved. The plan locations of column removal required for this prototype included perimeter columns at the middle of a long or short side of the building, a corner, adjacent to a corner, and at any location where building's perimeter geometry changed significantly. In elevation, these columns were removed at the first story above grade, the story above a column splice, the story at mid-height, and the story directly below the roof.

As required by the criteria [1], analysis of each column removal case was performed using a 3-D beam-element model of the entire building frame in SAP2000 [6]. In this model, the floor slabs

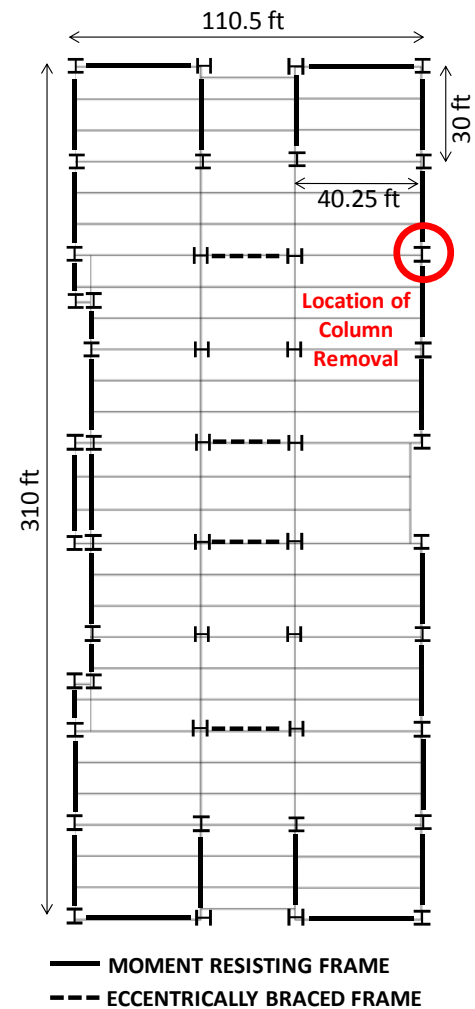


Figure 1. Plan of the prototype building frame, showing the location of column removal.

were represented as a rigid lateral diaphragm. Analysis was performed via the nonlinear dynamic analysis option, in which a time integration procedure is used to account for inertial effects and material and geometric nonlinearities [7]. Gravity and lateral loads were applied according to the following load combination for extreme events: $1.2D + 0.5L + L_{LAT}$, where lateral load L_{LAT} is applied to the perimeter of each floor in one direction and is calculated as 0.2% of the total load acting on that floor. At the start of each analysis, the undamaged structure (i.e. with no columns yet removed) is initialized for gravity and lateral loads. Once equilibrium is reached, the targeted column is then removed and the frame is analyzed until a subsequent state of equilibrium is achieved [8]. According to [1], it is assumed that all elements are at ambient temperature throughout the progressive collapse event.

Criteria for Progressive Collapse Performance

UFC [1] mandates that the performance criteria for the analysis of elements in the damaged frame are divided into two categories according to ASCE 41 [9]: force-controlled and deformation-controlled. Components under high axial load ($P/P_{CL} > 0.5$, where P_{CL} is the lower-bound axial load capacity) are classified as force-controlled. These components must have a demand-to-capacity ratio (DCR) less than unity for both (1) combined axial load and bi-axial bending and (2) shear. Components with low axial load ($P/P_{CL} \leq 0.5$) are classified as deformation-controlled. These components are capable of developing plastic deformations without significant strength degradation. Plastic deformations are assumed to be primarily in flexure and hinge models are derived as recommended in ASCE 41 [9]. Limits of plastic rotation for deformation-controlled steel members are provided in Chapter 5 of ASCE 41 [9].

Results for Progressive Collapse Analysis

This study focuses on the column removal location shown in Fig. 1 (i.e. middle of a perimeter MRF span) at the first floor because this scenario represents one of the most critical cases for the prototype’s progressive collapse resistance. Fig. 2 shows the elevation of this perimeter MRF, which provides nearly all resistance to progressive collapse in this case, both before and after the column removal as calculated by the 3-D SAP2000 model.

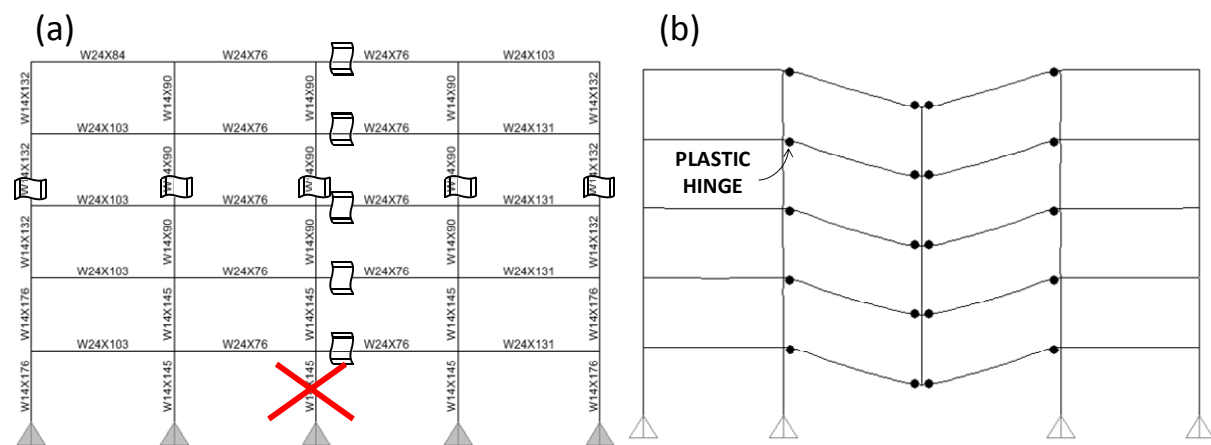


Figure 2. Elevation of the perimeter MRF modeled for progressive collapse: (a) before and (b) after column removal (deformations are shown 5x magnified).

P/P_{CL} for the perimeter girders is low, and therefore the girders bridging over the removed column develop plastic hinges in response to the column removal as shown in Fig. 2(b). The rotation of each hinge complies with plastic rotation limits specified in [9]. P/P_{CL} for the perimeter columns adjacent to the removed column is high, and all of these members have a DCR for axial load and bi-axial bending less than unity. Therefore, the prototype MRF design meets the criteria for progressive collapse resistance according to [1].

This study evaluates the fire resistance of the prototype structure for the column removal scenario illustrated in Fig. 2. It is assumed that the fire will initiate immediately following the onset of stable permanent deformation. Time integration analysis for fire exposure is performed using SAFIR, a software developed at the University of Liege specifically for the analysis of structures under fire [10]. SAFIR uses uncoupled analyses of, first, a thermal model of each member exposed to fire and, second, a structural model of the frame composed of those members. Della Corte et al. [3] implemented a similar two-phase approach in a previous study of a steel MRF structure that was damaged by earthquake and then subjected to fire.

Modeling the Structure

As noted previously, the perimeter MRF provides nearly all of the progressive collapse resistance for the column removal case shown in Fig. 2. Therefore, the structural-fire model of the damaged frame includes only the 2-D portion of the perimeter MRF as shown in Fig. 3. This model conservatively assumes that all load redistribution will take place in the MRF bays above and immediately adjacent to the removed column. Analysis of the 2-D model is much less computationally expensive than a full 3-D analysis of the frame and provides adequate accuracy since the behavior of the interior non-MRF members under fire will have little impact on the structure's progressive collapse resistance.

Three-noded 2-D non-torsional fiber-beam elements are used to represent the structural elements. Each column length is modeled with 15 fiber-beam elements, and each girder is modeled with 30 elements (i.e. roughly a 1-ft. discretization). The same loads and loading initialization used for progressive collapse analysis are also used for structural-fire analysis and the fire starts once the loads are initialized. Before structural time integration analysis of the frame can be performed, a thermal model of each element must be analyzed to obtain its temperature time history. Two-dimensional heat transfer is calculated across the cross-sectional depth of each element, whose cross-sections are discretized into solid thermal elements or "fibers." Each flange is modeled with 96 fibers, and each web is modeled with 48 fibers. The cross-sectional blow-ups in Fig. 3 show that the heated columns are exposed to fire on two sides (facing the fire in the perimeter bay) and the heated girders are exposed on three sides (with their top face shielded by the slab). The unexposed sides of the column are modeled as exposed to ambient temperature. The slab is included in the thermal model of the girder to account for heat transfer between them but not in the structural model of the girder because it will have little effect on the solution [11].

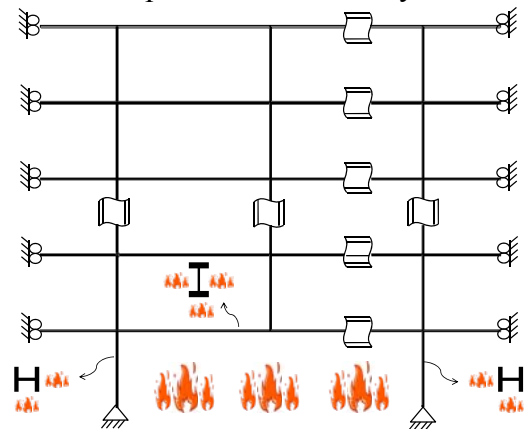


Figure 3. Elevation of the perimeter MRF modeled for structural-fire analysis.

Modeling the Fire

It is likely that the automatic sprinkler system near the location of column removal will also be damaged by the extreme event to the point of inoperability. For the column removal case shown in Fig. 2, it is assumed that the fire following the extreme event will initiate at the location of column removal and will burn in both the adjacent bays at the first floor perimeter, as shown in Fig. 3. It is also assumed that the fire will not spread horizontally or vertically beyond this location, although the study of such scenarios may be warranted in the future. The performance of the interior members under fire is considered to be outside the scope of this study since the perimeter MRF is assumed to provide the resistance to progressive collapse.

The ASTM E119 standard fire curve [12], shown in Fig. 4, is used to represent the fire temperature time history for this study. This curve assumes an initial rapid growth of compartment temperature followed by a gradual temperature increase. The curve does not include a decay phase or consider compartment properties but is rather a conservative curve used to ensure eventual failure by exposing the damaged structure to a prolonged period of high temperature. Structural-fire analysis of the damaged frame for exposure to realistic fire curves, which include a decay phase, will be explored in future research and indicate whether the frame can survive through burnout.

Analysis Cases

Four analysis cases, summarized in Table 1 were used to evaluate the effect of various levels of passive fire protection, applied to the girders and columns, on the performance of the prototype structural-fire model as shown in Fig. 3. The letters in caps denotes member (**G**irder or **C**olumn), the lower case letter denotes fire protection (**p**rotected or **u**nprotected), and the number denotes hourly rating (**1**-hr. or **2**-hrs.) Hourly fire protection ratings were achieved using specified thicknesses of the same spray-on fire resisting material (SFRM) used to protect the members supporting the prototype's elevators and stairwells [13]. For this study, the applied SFRM is assumed to be intact and fully effective on member adjacent to the column removal. Although SFRM is used here simply to obtain an hourly rating, passive fire protection materials that are more resistant to impact or vibration, such as intumescent paint, should be used in practice to provide fire protection to frames designed to resist progressive collapse.

RESULTS

Fig. 4 shows (a) the deflection of the girder above the removed column and (b) axial displacement of the undamaged column at the top of the first floor. As expected, Fig. 4 shows that the rate of girder deflection or column axial displacement decreases with increasing fire protection (i.e. with slower growth of the member's steel temperature). Fig. 4(a) shows that analysis cases GuCu, Gp1Cp1, and Gp2Cp1 experience a sudden increase and similar maximum values of girder deflection when the analyses terminate (i.e. the time at which the frame becomes unstable and fails). The column displacements for these three cases show no such increase in Fig. 4(b), indicating that failure initiated in the girder. Fig. 5(a) shows the final deformed shape of analysis case GuCu (those for Gp1Cp1 and Gp2Cp1 are similar) and confirms this result. For analysis case Gp1Cu, its sudden decrease of column displacement in Fig. 4(b) and its final deformed shape in Fig. 5(b) indicates that failure initiated in the unprotected column. These results are summarized in Table 1.

As expected, Table 1 shows that the GuCu fails after 5 min. of fire exposure due to instability of its rapidly sagging girders above the removed column, providing inadequate time for building egress following the extreme event before the damaged frame collapses. Applying 1 hr. of fire protection to the girder bridging over the removed column, even with columns unprotected (Gp1Cu), provides an additional 25 min. for evacuation. However, the Gp1Cu case experiences a brittle failure of its heated columns, which should be avoided at all possible. Applying 1 hr. of fire protection to both the girder and column in case Gp1Cp1 provides less additional increase in time to failure but switches the mode of failure initiation back to the girder, whose sagging failure is more ductile than the column failure. The Gp2Cp1 case provides over an hour of fire resistance to the ASTM E119 standard fire. This fire protection case provides more time for not only egress but also for firefighting efforts to prevent the frame from reaching this length of fire exposure and collapsing. For exposure to a realistic fire, the damaged frame may also avoid collapse if burnout (i.e. when the fire begins to decay, having consumed most of the available fuel) is achieved within the first hour of fire exposure.

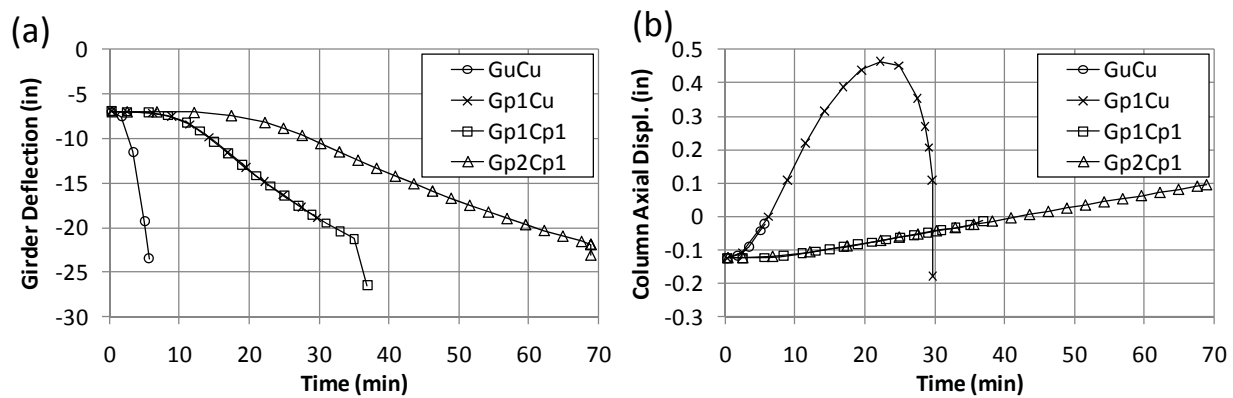


Figure 4. Plots of (a) girder deflection directly above the removed column and (b) axial displacement of the undamaged columns at the top of the first floor.

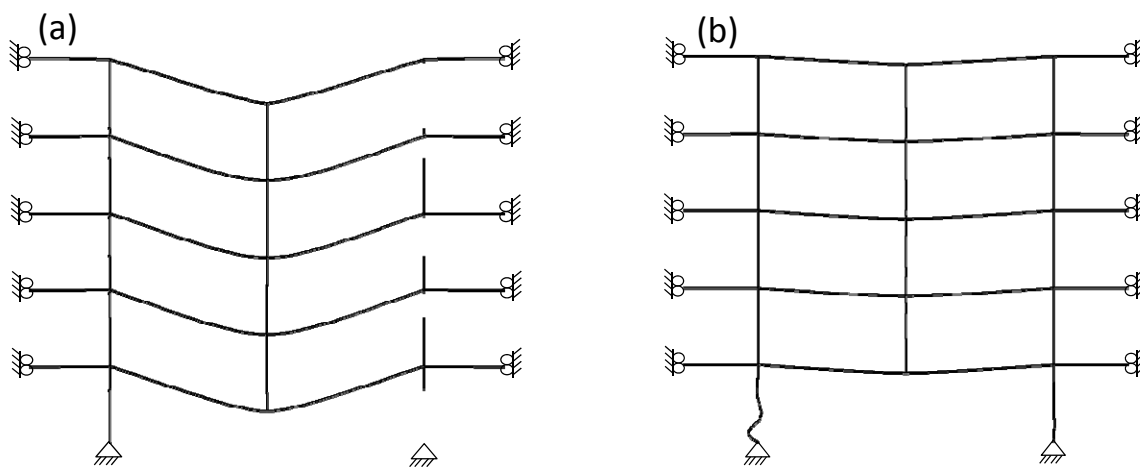


Figure 5. Final deflected shape of analysis case (a) GuCu and (b) Gp1Cu (shown 5x magnified).

TABLE I. SUMMARY OF STRUCTURAL-FIRE ANALYSIS RESULTS.

Analysis Case	Fire Protection		Time to Failure	Increase of Time to Failure Relative to GuCu (As-Built)	Failed Element	Downward Girder Defl. at Failure (in)
	Girder	Column				
GuCu	0 hr	0 hr	5 min	-	Girder	23.44
Gp1Cu	1 hr	0 hr	29 min	4.8	Column	18.93
Gp1Cp1	1 hr	1 hr	36 min	6.2	Girder	26.46
Gp2Cp1	2 hr	1 hr	1 hr 8 min	12.6	Girder	23.06

CONCLUSIONS

This paper presents a study of the effects of fire following an extreme event (such as blast or impact) that causes failure of one column on the perimeter of a prototype steel frame building. This prototype building was designed to comply with the most current DoD/UFC [1] requirements for progressive collapse resistance. The structural-fire analyses conducted in this study demonstrated that when there is no fire protection, the damaged structure remains stable for a duration of only 5 min. When passive fire protection is applied, the structure will remain stable for a duration up to 1 hr. depending on the level of protection. It is clear, based on this study, that fire following an extreme event represents a significant threat to stability of the structure. Hence, further studies are warranted to determine the correlation between fire intensity, passive fire protection rating, ASCE 41 acceptance criteria [9], and collapse time. These correlations have potential as a decision making tool for rescue personnel. Findings in this paper underline the importance of using a multihazard approach in the attempt to reduce risk of progressive collapse and improve structural life safety.

REFERENCES

1. UFC. 2009. "Design of Buildings to Resist Progressive Collapse," *Unified Facilities Criteria (UFC) 4-023-03*, US Department of Defense (DoD), July 14, 2009.
2. NIST. 2005. NIST NCSTAR 1: Final report of the National Construction Safety Team on the collapse of the World Trade Center Twin Towers, National Institute of Standards and Technology (NIST), Gaithersburg, MD.
3. Della Corte, G, Landolfo, R, Mazzolani, FM. 2003. "Post-earthquake fire resistance of moment resisting steel frames," *Fire Safety Journal* 38:593–612.
4. Chen, H, Liew, JYR. 2005. "Explosion and fire analysis of steel frames using mixed element approach," *Journal of Engineering Mechanics* (ASCE) 131(6):606–616.
5. ICC. 2009. 2009 International Building Code, International Code Council (ICC), Country Club Hills, IL.
6. CSI. 2009. SAP2000, Version 12, Integrated Software for Structural Analysis and Design, Analysis Reference Manual, Computers and Structures, Inc. (CSI), Berkeley, CA.
7. Wilson, EL. 2001. Three Dimensional Static and Dynamic Analysis of Structures, A Physical Approach with Emphasis on Earthquake Engineering, Computers and Structures, Inc. (CSI), Berkeley, CA.
8. Clough, RW, Penzien, J. 1993. *Dynamics of Structures, 2nd Edition*, McGraw-Hill, Inc, New York, NY.
9. ASCE. 2007. ASCE/SEI 41-06: Seismic Rehabilitation of Existing Buildings, American Society of Civil Engineers (ASCE), Reston, VA.
10. Franssen, J-M. 2005. "SAFIR: A thermal/structural program for modeling structures under fire." *Engineering Journal* (AISC) 42(3), 143–158.
11. Quiel, SE, Garlock, MEM. 2010. "Parameters for modeling a high-rise steel building frame subject to fire," *Journal of Structural Fire Engineering*, accepted for publication.
12. ASTM (2008). Designation: E119-08a—Standard Test Methods for Fire Tests of Building Construction and Materials. West Conshohocken, PA: American Society for Testing and Materials (ASTM) International.
13. ICC. 2008. ES Report (ESR) 1649, ICC Evaluation Services, Inc., Country Club Hills, IL.

Lateral-Torsional Buckling of Carbon Steel and Stainless Steel Beams Subjected to Combined End Moments and Transverse Loads in Case of Fire

N. LOPES, P. V. REAL, L. S. DA SILVA and J.-M. FRANSSSEN

ABSTRACT

This paper presents a numerical study on the behaviour of carbon steel and stainless steel I-beams subjected to lateral-torsional buckling (LTB) in case of fire. The main motivation for this work is the fact that part 1-2 of Eurocode 3 (EC3) does not take into consideration the beneficial effect, resulting from the reduction of the plastic zones connected with non-uniform bending diagrams along the beam.

Although new formulae for the LTB, that approximate better the real behaviour of steel structural elements in case of fire, have been proposed in previous works, they still do not considered the combination of end moments and transverse loads, as it is stated in part 1-1 of EC3. Therefore, in this paper numerical simulations, of steel beams with combined end moments and transverse loads, are compared with the LTB design curves of EC3, and new correction factors that improve these curves are presented.

INTRODUCTION

Part 1-1 of EC3 [1] presents two design approaches for the evaluation of the LTB of steel beams at ambient temperature: a general method and a method for hot rolled sections or equivalent welded sections.

Based on this last method for hot rolled sections, recent studies by the authors [2-4], using numerical simulations, fitting the methodology usually designated geometrically and materially non-linear imperfect analysis (GMNIA), on the LTB of carbon steel and stainless steel beams at elevated temperatures, have shown that

Nuno Lopes, Paulo Vila Real, LABEST—Department of Civil Engineering, University of Aveiro, Portugal.

Luís Simões da Silva, ISISE—Department of Civil Engineering, University of Coimbra, Portugal.

Jean-Marc Franssen, Structural Engineering, University of Liege, Belgium.

the beam fire design curve from part 1-2 of EC3 [5] is over-conservative for loadings different from the uniform bending.

The LTB curve proposed in the EN 1993-1-2 [5] only takes in consideration the loading type in the determination of the elastic critical moment, not accounting for the additional beneficial effect resulting from the reduction of the plastic zones, directly related to the fact that the bending diagrams are variable along the beam, leading to over-conservative results in beams not subjected to uniform bending diagrams. This influence is already considered in the method for hot rolled or equivalent sections at normal design [1, 6].

Following this acknowledgment, a new approach, similar to this method for normal temperature design [1], was proposed for carbon steel beams in fire situation through the introduction of a factor f affecting the reduction factor for the LTB resistance moment [2].

Part 1-4 of EC3 “Supplementary rules for stainless steels” [7] gives design rules for stainless steel structural elements at room temperature, and only mentions its fire resistance by referring to the fire part of the same Eurocode, (EN 1993-1-2). Although carbon steel and stainless steel have different constitutive laws [3], EC3 states that the structural elements made of these two materials must be checked for its fire resistance using the same formulae. This fact, led to the developing of a proposal for the LTB of stainless steel beams in case of fire, different from the carbon steel formulae. However, for the evaluation of the effect of the loading type, the same factor f , developed for carbon steel beams, revealed to be satisfactorily accurate [3, 4].

These proposals [2-4] did not take into account the case of combined end moments and transverse loads (as it is considered for cold design in part 1-1 of EC3). These loading types will be the main focus of this paper.

Comparisons between numerical results obtained with the program SAFIR [8] (using GMNIA), and the buckling curves from part 1-2 of EC3, for unrestrained carbon steel and stainless steel beams in case of fire, subjected to the combination of transverse loads and end moments, are presented. Finally, based on these comparisons and on a parametric study, new correction factors are proposed for these loading cases.

EC3 FORMULAE FOR THE LTB OF STEEL ELEMENTS

As mentioned before, the procedure adopted by part 1-2 of EC3 [5] for the safety evaluation of stainless steel beams is the same used for carbon steel beams.

Then, according to EN 1993-1-2, the LTB resistant moment for Class 1 and Class 2 cross-sections at high temperatures is given by

$$M_{b,fi,t,Rd} = \chi_{LT,fi} W_{pl,y} k_{y,\theta} \frac{f_y}{\gamma_{M,fi}} \quad (1)$$

where $\chi_{LT,fi}$ is determined by

$$\chi_{LT,fi} = \frac{1}{\phi_{LT,\theta,com} + \sqrt{\phi_{LT,\theta,com}^2 - \bar{\lambda}_{LT,\theta,com}^2}} \quad \text{with} \quad \chi_{LT,fi} \leq 1 \quad (2)$$

being

$$\phi_{LT,\theta,com} = \frac{1}{2} \left(1 + \alpha \bar{\lambda}_{LT,\theta,com} + \bar{\lambda}_{LT,\theta,com}^2 \right) \quad (3)$$

In this expression, the imperfection factor α depends on the steel grade and is determined by the expression:

$$\alpha = 0.65\varepsilon \text{ with } \varepsilon = \sqrt{235 / f_y} \quad (4)$$

Finally, the LTB non-dimensional slenderness at high temperatures $\bar{\lambda}_{LT,\theta,com}$ (or $\bar{\lambda}_{LT,\theta}$, if the temperature field in the cross-section is uniform) is given by

$$\bar{\lambda}_{LT,\theta,com} = \bar{\lambda}_{LT,\theta} = \bar{\lambda}_{LT} \left[\frac{k_{y,\theta}}{k_{E,\theta}} \right]^{0.5} \quad (5)$$

where $k_{y,\theta}$ and $k_{E,\theta}$ are reduction factors for the yield strength and for Young modulus at the steel temperature θ_a

PREVIOUS IMPROVEMENT OF THE PROPOSALS FOR THE LTB

Recent studies by the authors [2- 4], based on numerical simulations of the LTB on carbon steel and stainless steel beams at elevated temperatures, resulted on the proposals of more accurate LTB curves when compared with EC3. In addition, and as mentioned before, the consideration of the beneficial effect of non-uniform bending was also introduced. In this section those previous proposals are presented.

Carbon steel beams

On the proposal for carbon steel beams [2], the influence of the steel grade (S235 to S460), the influence of the cross-sectional slenderness and the influence of the pattern of residual stresses (hot rolled [9] and welded [10] sections) on the LTB under fire conditions is considered.

Equation (4), which defines the imperfection factor at high temperatures α , was rewritten in function of a severity factor η

$$\alpha = \eta \sqrt{235 / f_y} \quad (6)$$

being the severity factor η given in table I.

TABLE I. SEVERITY FACTOR FOR THE LTB OF CARBON STEEL ELEMENTS.

Cross-section	limits	η	
		S235, S275, S355, S420	S460
Rolled I-section	$h/b \leq 2$	0.65	0.70
	$h/b > 2$	0.75	0.80
Welded I-section	$h/b \leq 2$	0.70	0.75
	$h/b > 2$	0.80	0.85
Other cross-sections	-	0.80	0.85

Finally, to take into account the moment distribution between the lateral restrains of members, with Class 1 or 2 cross-sections, the reduction factor $\chi_{LT,fi}$ must be modified as follows:

$$\chi_{LT,fi,mod} = \frac{\chi_{LT,fi}}{f} \quad \text{but} \quad \chi_{LT,fi,mod} \leq 1 \quad (7)$$

where f depends on the loading type.

Initially, the adequacy of part 1-1 [1] proposals for f was tested. The results were better and closer to the numerical values but still remained conservative [2]. Consequently, in order to have better approximations, a new function for f was proposed:

$$f = 1 - 0.5(1 - k_c) \quad (8)$$

where k_c is a correction factor, given in table II, which was established by numerical adjustment to match as closely as possible a representative sample of finite element numerical results.

TABLE II. CORRECTION FACTORS FOR THE LTB IN CASE OF FIRE.

Moment distribution	k_c
$-1 \leq \psi \leq 1$  Distributed load	$0.6 + 0.3\psi + 0.15\psi^2$ but $k_c \geq 1$
 Concentrated load	0.91
	0.79

Figure 1 shows the influence, on the LTB fire design curves, of the consideration of different bending moment diagrams through this factor f .

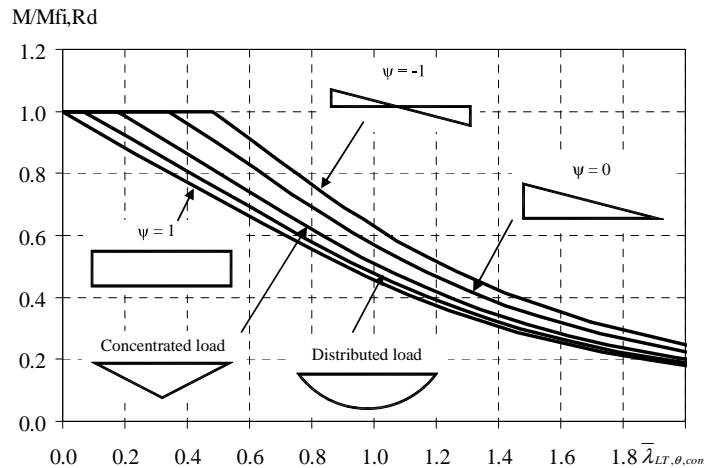


Figure 1. Influence on the LTB design buckling curves of different bending moment diagrams.

Stainless steel beams

On the studies [3] and [4] it was proposed that the design LTB resistance moment, of a laterally unrestrained stainless steel beam with Class 1 or Class 2 in case of fire, should be improved.

In order to consider the different behaviour at high temperatures provided by the different stainless steel grades, the imperfection factor can be written in function of the temperature as:

$$\alpha = \eta \sqrt{\frac{235}{f_y} \frac{E}{210000}} \sqrt{\frac{k_{E,\theta}}{k_{y,\theta}}} \quad (9)$$

The values of factor η to be used with this equation, are given in table III in a linear function of the ratio h/b (h is the depth and b the width of a cross-section).

TABLE III. SEVERITY FACTOR FOR THE LTB OF STAINLESS STEEL ELEMENTS.

	1.4301; 1.4401; 1.4404; 1.4571	1.4462 and 1.4003
η	$0.22 \left(\frac{h}{b} \right) + 0.38$	$0.16 \left(\frac{h}{b} \right) + 0.34$

To consider the loading type, expressions (7) and (8) are used, where the correction factor k_c is given in table II, similar to the one proposed for carbon steel elements in case of fire.

NEW CORRECTION FACTORS FOR COMBINED END MOMENTS AND TRANSVERSE LOADS

As presented in section 3 and mentioned before, these proposals do not take into account the case of combined end moments and transverse loads (see table II).

Therefore, regarding the bending moment variation along the member length, four different loading types were chosen to be studied in this work: i) uniformly distributed load with equal end moments; ii) uniformly distributed load with only one end moment; iii) concentrated load with equal end moments; iv) concentrated load with only one end moment (see figure 2).

In the numerical simulations, the values of the applied end moments were obtained from a plastic analysis of a fixed-end beam and a propped cantilever beam with the corresponded concentrated and distributed loads, as illustrated on figure 2, where the maximum negative bending moment is equal to the maximum positive value (as in EN 1993-1-1). The loads were applied at the cross section shear centre.

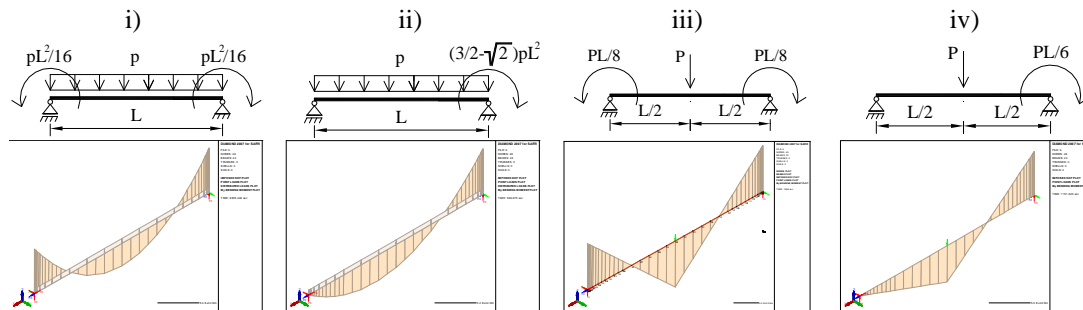


Figure 2. Studied bending moment diagrams.

Table IV shows the complete set of correction factors, proposed in this work, which resulted from the parametric study presented on section 5.

TABLE IV. COMPLETE SET OF CORRECTION FACTORS FOR FIRE SITUATION.

Moment distribution	k_c
$-1 \leq \psi \leq 1$ 	$0.6 + 0.3\psi + 0.15\psi^2$ but $k_c \leq 1$
	0.91
	0.90
	0.91
	0.79
	0.73
	0.75

Note: for others bending diagrams $k_c = 1$.

PARAMETRIC STUDY

Simply supported beams with fork supports were chosen to explore the validity of these beam safety verifications. For the carbon steel it was studied a hot rolled IPE220 of the grade S235. For the stainless steel beams it was also used an IPE220 but in this case it was considered as a welded section of the grade 1.4301 [11, 12]. This section is of Class 1 for both materials. A uniform temperature distribution in the cross-section was used so that comparison between the numerical results and the Eurocode could be made. In this paper, the temperatures chosen were 400, 500, 600 and 700°C, deemed to cover the majority of practical situations. In the numerical simulations, a lateral sinusoidal geometric imperfection with a maximum value of $l/1000$ [13] was considered. For the hot rolled carbon steel sections, a triangular distribution for the residual stresses with a maximum value of $0.3 \times 235\text{MPa}$ [9], was chosen. For the welded sections, the distribution used has the maximum value equal to the yield strength [10]. These two patterns of the residual stresses are depicted in figures 3 and 4.

The following figures present the comparisons between the numerical results obtained with the program SAFIR, the EC3 designated “EN1993-1-2” and the proposal presented in section 4 named “New proposal”, for the carbon steel beams (figure 3) and for the stainless steel beams (figure 4).

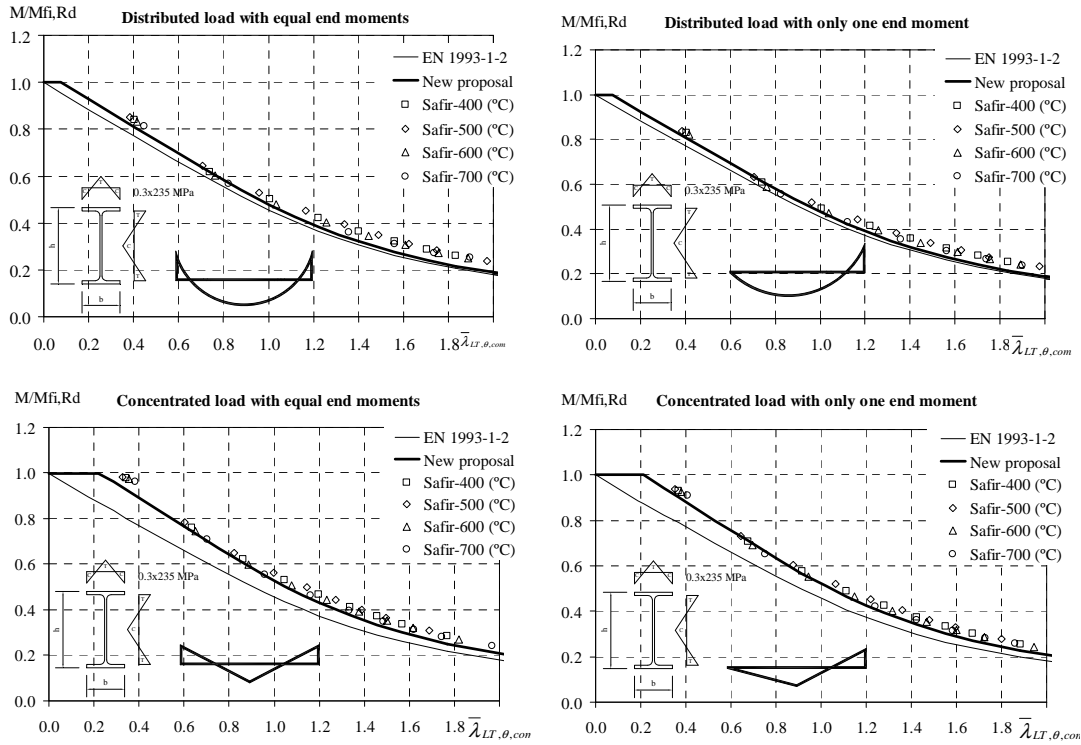


Figure 3. Numerical results for carbon steel beams.

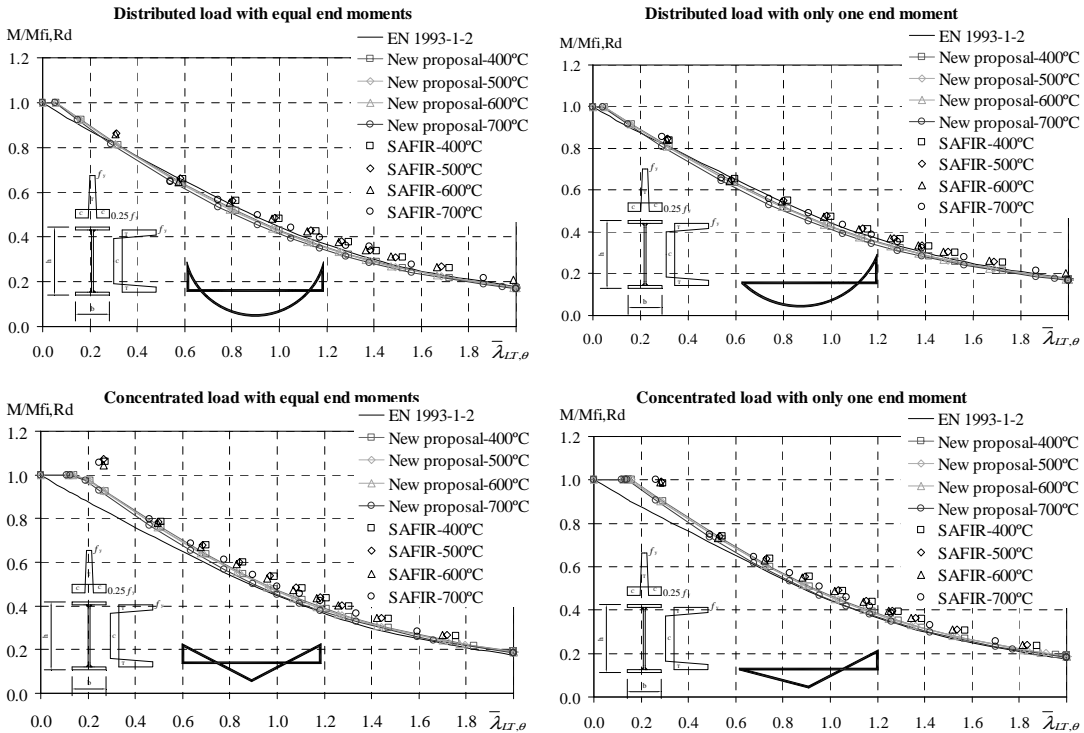


Figure 4. Numerical results for stainless steel beams.

CONCLUSIONS

In this paper an improvement of the recent proposals for the LTB, by the authors, for carbon steel [2] and stainless steel [3, 4] elements, with Class 1 or 2

cross-sections, was presented. This improvement increases the approximation to the real behaviour of steel beams subjected to the combination of transverse loads and end moments in case of fire.

The introduced improvement consists on the consideration of new correction factors, to take into account the reduction of the plastic zones, resulted from the variation of the bending moment diagrams along the beam.

These new corrections factors should be used only when the bending moment diagrams have the maximum negative bending moment value equal to the maximum positive value, as in part 1-1 of EC3 [1].

Although the study presented here only considered one cross-section, these results and proposals are expected to be accurate and safe when other cross-sections are considered, as observed in previous studies [4].

ACKNOWLEDGEMENTS

The authors wish to acknowledge the Calouste Gulbenkian Foundation (Portugal) for its supports through the scholarship given to the first authors.

REFERENCES

1. CEN, *EN 1993-1-1, Eurocode 3, Design of Steel Structures—Part 1-1: General rules and rules for buildings*, Brussels, Belgium, 2005.
2. Vila Real, P.; Lopes, N.; Simões da Silva, L.; Franssen, J.-M. “Parametric analysis of the Lateral-torsional buckling resistance of steel beams in case of fire”, *Fire Safety Journal*, Elsevier, volume 42 / (6-7), pp 416–424, September/October of 2007.
3. Vila Real, P.; Lopes, N.; Simões da Silva, L.; Franssen, J.-M. “Lateral-torsional buckling of stainless steel I-beams in case of fire”, *Journal of Constructional Steel Research*, Elsevier, volume 64 / 11, pp 1302-1309, November of 2008.
4. Lopes, N. “*Behaviour of stainless steel structures in case of fire*”, thesis presented for obtaining the degree of European Doctor of Philosophy in Civil Engineering at the University of Aveiro, May of 2009.
5. CEN, *EN 1993-1-2, Eurocode 3, Design of Steel Structures—Part 1-2: General rules—Structural fire design*, Brussels, Belgium, 2005.
6. Boissonnade, N.; Greiner, R.; Jaspart, J. P. “*Rules for Member Stability in EN1993-1-1 Background documentation and design guidelines*”, ECCS Technical Committee 8 – Stability, 2006.
7. CEN, *EN 1993-1-4, Eurocode 3: Design of steel Structures—Part 1-4: General rules—Supplementary Rules for Stainless steels*, Brussels, Belgium, 2006.
8. Franssen, J.-M., “SAFIR. A Thermal/Structural Program Modelling Structures under Fire”, *Engineering Journal*, AISC, Vol. 42 (3), pp. 143–158, 2005.
9. ECCS, European Convention for Constructional Steelwork. *Ultimate Limit State Calculation of Sway Frames with Rigid Joints*, Technical Committee 8—Structural Stability, Technical Working Group 8.2 – System, first edition, ECCS, 1984.
10. Chen WF, Lui EM. *Stability design of steel frames*, CRC Press, 1991.
11. Gardner L. “The use of stainless steel in structures”, *Progress in Structural Engineering and Materials*, 2005; 7(2), 45–55.
12. Greiner R, Hörmaier I, Ofner R, Kettler M. *Buckling behaviour of stainless steel members under bending*, ECCS Technical Committee 8 – Stability, 2005.
13. CEN, *EN 1090-2. Execution of Steel and aluminium Structures—Part 2: Technical Requirements for the execution of steel structures*, Brussels, Belgium, 2005.

Reliability-Based Capacity Reduction and Fire Load Factors for Design of Steel Members Exposed to Fire

S. IQBAL and R. S. HARICHANDRAN

ABSTRACT

A general reliability-based methodology is proposed for developing capacity reduction and fire load factors for the load and resistance factor design of steel members exposed to fire. The effect of active fire protection systems (e.g., sprinklers, smoke and heat detectors, fire brigade, etc.) in reducing the probability of occurrence of a severe fire is included. The design parameters that significantly affect the fire design of steel members are chosen as random variables, and their statistics are obtained from the literature and the analysis of raw data. Capacity reduction and fire load factors are obtained using the proposed methodology and particular design equations for steel beams and columns. It is shown that capacity reduction and fire load factors should vary for different design situations depending on the presence of active fire protection systems in the building.

INTRODUCTION

Performance-based codes allow use of engineering approaches for fire design of steel members instead of prescriptive approaches that have been commonly used. For example, the 2005 AISC Specifications [1] now allow steel members to be designed against fire using room temperature design specifications and reduced material properties. This fire design approach is described below.

According to the AISC Specifications, the design action (applied axial force, bending moment or shear force, etc.) is determined from the gravity load combination given by

$$w_u = 1.2 D + 0.5 L + 0.2 S + T \quad (1)$$

where, D , L and S are nominal dead, live and snow loads, respectively and T includes loads induced by the fire itself, especially due to restraints preventing thermal expansions.

Shahid Iqbal, Graduate Student, Department of Civil & Environmental Engineering, Michigan State University, East Lansing, MI 48824-1226.

Ronald S. Harichandran, Professor and Chair, Department of Civil & Environmental Engineering, Michigan State University, East Lansing, MI 48824-1226.

The nominal capacity of steel members exposed to fire, $R_{n,f}$, is a function of fabrication parameters, F_i , and reduced material properties, $k_j(T_s)M_j$, and may be written as

$$R_{n,f} = \phi_f f_R (F_1, \dots, F_l, k_1(T_s)M_1, \dots, k_k(T_s)M_k) \quad (2)$$

where ϕ_f is the capacity reduction factor, the F_i are dimensional and sectional properties (e.g., depth of section, cross-sectional area, etc.), and M_j are the material properties at room temperature (e.g., yield strength, etc.). $k_j(T_s)$ are factors that account for reduction in strength and stiffness of steel at elevated temperature, and their values are specified in the AISC Specifications [1].

While the AISC Specifications [1] states that the capacity reduction factors for fire design be the same as those used for room temperature design, the Eurocode 3 [2] suggests that a partial safety factor of 1.0 be used. $R_{n,f}$ given by Eq. (1) is function of steel temperature, T_s , which in turn depends on the design fire. The AISC Specifications [2] and its Commentary [3] suggest that due considerations should be given to the effect of active fire protection systems (e.g., sprinklers) when describing design fires, and the fire load may be reduced up to 60% if reliable sprinklers are present. In a similar vein, reduction in fire load is suggested in Eurocode 1 [4]. However, no substantial work has been done to develop capacity reduction and fire load factors based on rigorous reliability analysis.

A general reliability-based methodology is presented herein for developing capacity reduction and fire load factors for the load and resistance factor design of steel members exposed to fire.

METHODOLOGY TO DEVELOP CAPACITY REDUCTION AND FIRE LOAD FACTORS

Target Probability of Failure and Target Reliability Index

CIB W 14 [5] suggests that the rare occurrence of a severe fire should be taken into account while developing safety factors for fire design. The presence of active fire protection systems such as sprinklers, fire brigade, etc., reduces the probability of occurrence of a severe fire and the probability of failure. Safety factors depend on the selected target reliability index, β_t , which is related to the target probability of failure, and is a relative measure of safety. Therefore, the reduced probability of failure under fire can be accounted for by using a reduced target reliability index.

A detailed methodology for calculating β_t by incorporating the effect of active fire protection systems was presented in the ECSC study [6]. The study also suggested appropriate values for the effectiveness of different active fire protection systems in reducing the probability of occurrence of a severe fire. Using the methodology described in the ECSC study, β_t was estimated for typical fire compartments in U.S. office buildings (ranging in floor areas from 25-500 m²). It was found that it is reasonable to use β_t values ranging from zero to 2.0 for developing capacity reduction and fire load factors.

Performance Function for Reliability Analysis and Statistics of Parameters

Ellingwood [7] showed that the probability of coincidence of a fire with maximum values of live load, roof live load, snow, wind, or earthquake loads is negligible, and a

structure is likely to be loaded to only a fraction of the design load when a fire occurs. The load effect W_f for reliability analysis may then be calculated as

$$W_f = D + L_{apt} \quad (3)$$

where D and L_{apt} are dead and arbitrary-point-in-time live loads, respectively.

The actual capacity of steel members under fire can be obtained by modifying the nominal capacity given by Eq. (2) to

$$R_f = P \cdot f_R(f_1 F_1, \dots, f_l F_l, k_1(t_s T_s) m_1 M_1, \dots, k_k(t_s T_s) m_k M_k) \quad (4)$$

where P = “professional factor” reflecting uncertainties in the assumptions used to determine the capacity from design equations (e.g., use of approximations in place of exact theoretical formulas, assumptions such as perfect elasto-plastic behavior, and a uniform temperature across the section), f_i = random variable that characterizes the uncertainties in “fabrication,” m_j = random variable that characterizes uncertainties in “material properties,” and t_s = random correction factor that accounts for differences between the steel temperature obtained from models and that measured in actual tests. The random variables f_i and m_j are the same as those used for developing LRFD specifications for ambient temperature conditions and their statistics are available in the literature. The statistics of P are specific to each design equation, cannot be generalized, and can be obtained from a comparison between the predicted capacity and test results. The statistics of t_s are characterized in the next subsection.

The capacity, R_f , of steel members given in Eq. (4) is a function of the steel temperature, T_s , which depends on the design fire (time-fire temperature curve). The variation of fire temperature, T_f , with time can be estimated using a suitable mathematical model from the literature. In this study, the Eurocode parametric fire model modified by Feasey and Buchanan [8] is used to estimate the fire temperature under real fire scenarios. In this model, T_f is a function of the opening factor, F_v , fire load, q_t , and thermal absorptivity, b . Once the fire temperature variation with time is known, the temperature of steel members can be estimated through thermal analysis. Most design specifications such as the Eurocode 3 [2] and AISC Specifications [1], allow the steel temperature to be calculated using simple thermal analysis methods such as the lumped heat capacity method. The lumped heat capacity method assumes that the steel section is a lumped mass at uniform temperature. The heat balance differential equation for protected steel members can be written as [8]

$$\frac{dT}{dt} = \left(\frac{F}{V} \right) \left(\frac{k_i}{d_i \rho_s c_s} \right) \left\{ \frac{\rho_s c_s}{\rho_s c_s + 0.5(F/V)d_i \rho_i c_i} \right\} (T_f - T_s) \quad (5)$$

where dT/dt = rate of change of steel temperature, F = surface area of unit length of the member (m^2), V = volume of steel per unit length of the member (m^3), ρ_s = density of steel (kg/m^3), c_s = specific heat of steel ($J/kg.K$), ρ_i = density of insulation (kg/m^3), c_i = specific heat of insulation ($J/kg.K$), d_i = thickness of insulation (m), k_i = thermal conductivity of insulation ($W/m.K$), T_s = steel temperature ($^{\circ}C$), and T_f = fire temperature ($^{\circ}C$). The design parameters in Eq. (5) that significantly affect the fire design of steel members were chosen as random variables, and their means, COV, and distribution types are summarized in Table 1. We analyzed raw experimental data to obtain the statistics of all parameters in Table 1 except for the dead load, arbitrary-point-in-time live load and fire load. The statistics of the dead and arbitrary-point-in-time live loads were reported by Ellingwood [7], and the statistics of the fire load were taken from a survey of U.S. office buildings by Culver [9].

TABLE I. MEAN, COV AND DISTRIBUTION OF FIRE DESIGN PARAMETERS.

Variable	Mean	COV	Distribution
Arbitrary-point-in-time live load, L_{apt}	0.24*nominal	0.6	Gamma
Dead load, D	1.05*nominal	0.10	normal
Fire load, q_f	564 MJ/m ²	0.62	Gumbel
Ratio of floor area to total area, A_f/A_t	0.192	0.23	lognormal
Opening factor, F_v	1*nominal	0.05	normal
Thermal absorptivity of NWC, b_{NWC}	1830 W s ^{0.5} /m ² K	0.09	normal
Thermal absorptivity of LWC, b_{LWC}	640 W s ^{0.5} /m ² K	0.11	normal
Thermal absorptivity of gypsum board, b_g	423.5 W s ^{0.5} /m ² K	0.09	normal
Thermal absorptivity of 50/50 mix of NWC and gypsum board, b_{mix}	1127 W s ^{0.5} /m ² K	0.10	normal
Thickness of insulation, d_i			
(1) spray applied materials	nominal+1/16 inch	0.20	lognormal
(2) gypsum board systems	nominal	0.05	normal
Density of insulation, D_i			
(1) spray applied materials	307 kg/m ³	0.29	normal
(2) gypsum board systems	745 kg/m ³	0.07	lognormal
Thermal conductivity of insulation, k_i			
(1) spray applied materials			
(2) gypsum board systems	0.187 W/m. K	0.24	lognormal
	0.159 W/m. K	0.28	lognormal

The limit state equation for reliability analysis may be written as

$$g(\mathbf{X}) = R_f - W_f \quad (6)$$

where \mathbf{X} denotes a vector containing all the random variables in Eqs. (3) and (4). The probability of failure of a steel element under fire is $p_f = P[g(\mathbf{X}) < 0]$.

Model Error for Steel and Fire Temperatures

The maximum temperature of steel sections estimated using Eq. (5) differs from that measured in actual fire tests. To account for the differences in calculated and measured steel temperatures, the model error was characterized, both for steel beams (three sided exposure) and steel columns (four sided exposure). The experimental temperature of steel elements has been reported by many researchers but most tests were carried out under standard fires instead of real fires, and thus cannot be used to estimate the error arising from the fire models. Kirby et al. [11] carried out a series of nine real fire tests and recorded the temperature of protected and unprotected steel elements. The tests were performed for a range of fire loads (380 – 760 MJ/m² of floor area), for different opening conditions ($F_v = 0.0029 - 0.062 \text{ m}^{1/2}$), and various types of materials were used as compartment boundaries. The model error for the temperature of steel beams, t_{sb} , has a mean of 0.98 and COV of 0.11, and the model error for the temperature of steel columns, t_{sc} , has a mean of 1.05 and COV of 0.13. Both t_{sb} and t_{sc} were best described by the Gumbel distribution.

Derivation of Capacity Reduction and Fire Load Factors

The detailed framework for first-order reliability analysis and the simplified expressions for obtaining the partial safety factors for each design parameter is

described in NBS 577 [12]. For a normally distributed random design parameter, X , the partial safety factor resulting from the first-order reliability method (FORM) is given by [12]

$$\phi_X = \frac{m_X}{X_n} (1 + \alpha_X \beta_t V_X) \quad (7)$$

where m_X , V_X , X_n , and α_X are the mean, COV, nominal value of X and the direction cosine of the “design point,” respectively. All the parameters in Eq. (7) were described earlier except the direction cosine of the design point which is obtained through reliability analysis.

DERIVATION OF CAPACITY REDUCTION AND FIRE LOAD FACTORS FOR SIMPLY SUPPORTED BEAMS AND COLUMNS

Performance Functions for Reliability Analysis

In this section, the bending capacity of simply supported beams given in the AISC Specifications [1] and axial capacity of steel columns given by Takagi and Deierlein [13] are used. Predictions of structural capacity under fire are still relatively new and evolving. With improved understanding of structural behavior under fire, predictive equations may change and future design refinements may be necessary. However, the statistics of random parameters and the methodology described in the previous section are general and may be used for any predictive equations.

The nominal moment capacity of a simply supported, laterally restrained steel beam exposed to fire can be expressed as

$$M_{n,f} = Z_x k_y(T_s) F_y \quad (8)$$

where Z_x = plastic section modulus, F_y = yield strength of steel at room temperature, and $k_y(T_s)$ = yield strength reduction factor that depends on the temperature, T_s , of the steel member.

The actual moment capacity can be obtained by modifying Eq. (8) to

$$M_f = P_b f_z Z_x k_y(t_{sb} T_s) m_{F_y} F_y \quad (9)$$

where f_z is a random variable with a mean = 1.03 and COV = 0.034 that characterizes uncertainty in Z_x [14], m_{F_y} is a random variable with a mean = 1.03 and COV = 0.063 that characterizes uncertainty in F_y [14] and t_{sb} is the model error for steel temperature with the statistics given earlier. The steel temperature, T_s , is a function of many parameters (see Eq. (5)) whose statistics are given in Table 1. P_b is the professional factor (model error) that is characterized in the next subsection. The performance function for reliability analysis of a beam can then be expressed as

$$g(\mathbf{X}) = M_f - M_{a,f} \quad (10)$$

where $M_{a,f}$ is the applied moment under fire that can be expressed in terms of basic random variables as shown in Eq. (3). \mathbf{X} denotes a vector containing all the random design parameters.

Takagi and Deierlein [13] compared the AISC and Eurocode 3 design specifications with finite element simulations for columns exposed to fire. They reported that the AISC Specifications [1] are unconservative at elevated temperatures, particularly for slenderness ratios between 40 and 100 and temperatures above 500°C.

For instance, at 500°C the nominal capacities predicted by the AISC specifications are up to 60% larger than capacities predicted by simulations. On the other hand, the Eurocode 3 column strength equations were within 20% of the simulated results. We used the equations proposed by Takagi and Deierlein [13] in this study, which have a format similar to that of the AISC Specifications and predict strengths similar to the Eurocode 3 [2] columns strength equations (see figure 6 of reference [13]):

$$R_{n,f} = \left\{ 0.42 \sqrt{\frac{k_y(T_s)F_y}{F_e(T_s)}} \right\} A_s k_y(T_s) F_y, \quad F_e(T_s) = \frac{\pi^2 k_E(T_s) E_s}{(KL/r)^2} \quad (11)$$

where $R_{n,f}$ = nominal capacity of column under fire, A_s = cross-sectional area, KL = effective length, r = radius of gyration about the buckling axis, E_s = elastic modulus. $k_E(T_s)$ is the elastic modulus reduction factor that depends on the temperature, T_s . The actual capacity of steel columns under fire can be obtained by modifying the nominal capacity given in Eq. (11) to

$$R_f = P_c \left\{ 0.42 \sqrt{\frac{k_y(t_{sc} T_s) m_{F_y} F_y}{F_e(T_s)}} \right\} f_{A_s} A_s k_y(t_{sc} T_s) m_{F_y} F_y, \quad F_e(T_s) = \frac{\pi^2 k_E(t_{sc} T_s) m_{E_s} E_s}{(KL/f_r r)^2} \quad (12)$$

where f_{A_s} is a random variable with a mean of 1.03 and COV of 0.031 that characterizes uncertainty in A_s [14], f_r is a random variable with a mean of 1.0 and COV of 0.016 that characterizes uncertainty in r [14], m_{E_s} is a random variable with a mean of 1.04 and COV of 0.045 that characterizes uncertainty in E_s [14], and t_{sc} is the model error for steel temperature with the statistics given earlier. P_c is the professional factor (model error) that is characterized in the next subsection. The performance function for reliability analysis of a column can then be expressed by Eq. (6) with W_f being the applied axial load under fire given by Eq. (3).

Professional Factor (Model Error) for Beams and Columns

To account for differences in the measured capacity of a beam in a laboratory and that predicted by Eq. (8), the professional factor, P_b , was characterized using the test results reported by Kruppa [15]. P_b (ratio of measured bending capacity to nominal capacity) has a mean of 0.99 and a COV of 0.11, and is best described by the lognormal distribution.

To account for differences between the axial capacity of column measured in the laboratory and that predicted by Eq. (11), the professional factor, P_c , was characterized using the test results reported by Janss and Minne [16] and Franssen et al. [17]. P_c (ratio of measured to nominal capacity) has a mean of 1.10 and a COV of 0.18, and is best described by the normal distribution.

Reliability Analysis

Ten laterally restrained beams ranging in length from 3 m (10 ft) to 13.7 m (45 ft) with live loads ranging from 2.4 kPa (50 psf) to 4.8 kPa (100 psf), and twenty steel columns having slenderness ratios ranging from 25 to 200 and axial load capacities ranging from 133 kN (30 kips) to 10,675 kN (2400 kips) were selected for the reliability study. The AISC Specifications were used to first design the beams and columns for ambient temperature conditions. The same beams and columns were then

designed for fire exposure ($b = 640 \text{ W/m.K}$ and $F_v = 0.02 \text{ m}^{1/2}$) and the required thickness of insulation to withstand the design fire was determined using the procedure described in the AISC Specifications. As suggested in most codes, a capacity reduction factor of 1.0 was used for the initial design for fire. The beams and columns were assumed to be protected by spray applied fire protection materials and gypsum board, respectively, which is generally the case in the U.S.

The FERUM (Finite Element Reliability Using Matlab) software [18] was used to perform first-order reliability analysis for each design situation (each of the 10 beams and 20 columns). The partial safety factors for each design parameter were obtained through Eq. (7). These individual partial safety factors except for the fire load were then combined into a single capacity reduction factor. Thus 10 different capacity reduction factors (one for each beam) and 20 different capacity reduction factors (one for each column) were obtained. Thereafter, both for beams and columns, a single optimized capacity reduction factor corresponding to dead and live load factors of 1.2 and 0.5, respectively, was obtained using the optimization procedure described in NBS 577 [12] for each β_t value ranging from zero to 2.0. A similar procedure was used to obtain the fire load factors corresponding to each β_t value.

Results

The plot of the capacity reduction factor, ϕ_f , vs. the target reliability index, β_t is shown in Fig. 1. Most codes suggest that $\phi_f = 1.0$ be used. However, $\phi_f = 0.9$ is suggested in the Commentary to the AISC Specifications. Results obtained in this study indicate that the nominal capacity need not be reduced (i.e., $\phi_f = 1.0$) if β_t is less than 1.25, which in turns depends on the effectiveness of active fire protection systems in reducing the probability of occurrence of a severe fire. Since most office buildings in the U.S. are required to have automatic sprinklers, β_t is not likely to exceed 1.25. Therefore, using $\phi_f = 1.0$ is reasonable for most design situations.

The plot of the fire load factor, γ_q , vs. β_t is also shown in Fig. 1. The nominal value of the fire load was taken as the 90th percentile [8]. When β_t is less than 1.42, γ_q is less than 1.0 indicating that the fire load can be reduced as suggested in the Commentary to the AISC Specifications [2], Eurocode 1 [4] and the ECSC study [6].

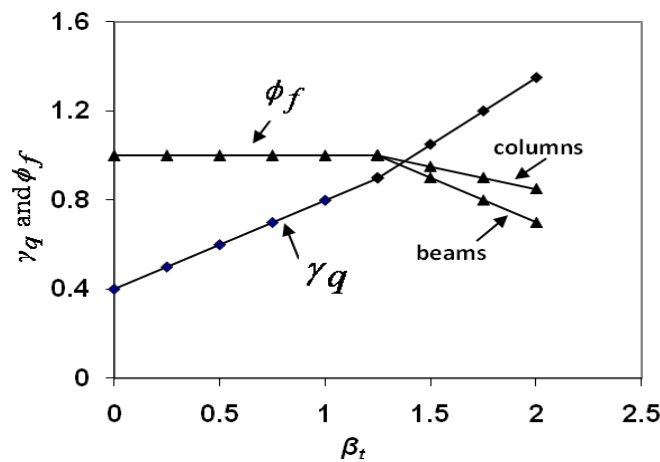


Figure 1. Capacity reduction and fire load factors vs. target reliability index.

CONCLUSIONS

A reliability-based methodology is proposed for developing capacity reduction and fire load factors for the design of steel members exposed to fire. Statistics of a variety of parameters important for the design of steel members under fire were obtained from experimental data reported in the literature. Model errors associated with the thermal models were also characterized based on experimental data. Using the proposed methodology capacity reduction and fire load factors are developed for simply supported beams and columns in U.S. office buildings exposed to fire. It is found that the capacity reduction and fire load factors should not be constant for all design situations as suggested in design specifications, but should vary depending on the presence of active fire protection systems in a building.

REFERENCES

1. AISC. 2005. "Load and Resistance Factor Design Specifications for Structural Steel Buildings." American Institute of Steel Construction, Inc., Chicago, Illinois.
2. EN. 2005. "Eurocode 3: Design of Steel Structures- Part 1-2: General Rules-Structural Fire Design." BS EN 1993-1-2.
3. AISC. 2005. "Commentary on the Load and Resistance Factor Design Specifications for Structural Steel Buildings." American Institute of Steel Construction, Inc., Chicago, Illinois.
4. EN. 2002. "Eurocode 1: Actions on Structures- Part 1-2: General Actions- Actions on Structures Exposed to Fire." BS EN 1991-1-2.
5. CIB W14. 1986. "Design Guide for Structural Fire Safety." *Fire Safety Journal*, 10(2), 81-137.
6. European Coal and Steel Community (ECSC). 2001. Natural Fire Safety Concept, Valorization Project, Product-Structural Dept. ARBED-Research Centre L-4009 ESCH/ALZETTE, Luxembourg.
7. Ellingwood, B. R. 2005. "Load Combination Requirements for Fire-Resistant Structural Design." *Journal of Fire Protection Engineering*, 15(1): 43-61.
8. Buchanan, A. H. 2001. Structural Design For Fire Safety, John Wiley & Sons Ltd., New York.
9. Culver, C. G. 1976. "Survey Results for Fire Loads and Live Loads in Office Buildings." National Bureau of Standards.
10. Kirby, B. R., D. E. Wainman, L. N. Tomlinson, T. R. Kay, and B. N. Peacock. 1994. "Natural Fires in Large Scale Compartments—A British Steel Technical, Fire Research Station Collaborative Project." British Steel Technical.
11. Ellingwood, B., T. V. Galambos, J. G. MacGregor, and C. A. Cornell. 1980. "NBS Special Publication 577: Development of a Probability Based Load Criterion for American National Standard A58." National Bureau of Standards, Ernest Ambler.
12. Takagi, J., and G. G. Deierlein. 2007. "Strength Design Criteria for Steel Members at Elevated Temperatures". *Journal of Constructional Steel Research*, 63(8): 1036-1050.
13. Schmidt, B.J., and F.M. Bartlett. 2002. "Review of Resistance Factors for Steel: Data Collection". *Canadian Journal of Civil Engineering*, 29(1): 98-108.
14. Kruppa, J. 1979. "Collapse Temperature of Steel Structures." *Journal of the Structural Division*, 105(ST9): 1769-1788.
15. Janss, J., and R. Minne. 1981. "Buckling of Steel Columns in Fire Conditions". *Fire Safety Journal*, 4(4): 227-235.
16. Franssen, J. M., D. Talamona, J. Kruppa, and L.G. Cajot. 1988. "Stability of Steel Columns in Case of Fire: Experimental Evaluation". *Journal of Structural Engineering*, 124(2): 158-163.
17. Der Kiureghian, A., T. Haukaas, and K. Fujimura. 2006. "Structural Reliability Software at the University of California, Berkeley". *Structural Safety*, 28(1-2): 44-67.

Temperature of External Column During Fire Test

M. PULTAR, Z. SOKOL and F. WALD

ABSTRACT

The temperature of steel column located outside the fire compartment was studied during fire test in Mokrsko (carried out in September 2008) [1], [2]. The column was placed in front of the compartment window. The measured temperatures were used to validate numerical models of heat transfer. There are two models described: FEM model using software Ansys and software for prediction of column temperature developed at CTU in Prague.

INTRODUCTION

The fire test in Mokrsko was focussed on observation of temperature of the structural elements exposed to natural fire, on the overall behaviour of the structure and behaviour of the structural connections. The building was constructed using three types of floor systems with the beam to column connections partially encased in composite slab. The walls were created from different systems: concrete wall, sandwich panels or cassette sections filled with mineral wool.

The test was performed on building representing a part of one floor of an office building. The size of the building was 12×18 m. The largest part of the floor structure was made from composite steel concrete beams supporting the concrete slab. The slab was cast in corrugated sheets, the total depth of the slab was 120 mm. There were used two types of unprotected steel beams spanning 9 m. One half of the floor was created using Angelina beams made from IPE 270 sections, the final height of the beams was 395 mm. One quarter of the floor structure was created using beams with corrugated web thickness 2,5 mm, the total height of the beams was 500 mm. The beams on the perimeter of the building were made from IPE 400 sections and were protected to fire. The remaining part of the floor structure was made from pre-stressed hollow core concrete panels thickness 320 mm spanning 9 m.

Milan Pultar, RNDr. CSc., Department of Mathematics, Faculty of Civil Engineering, Czech Technical University, Prague, Thákurova 7, 166 29 Praha 6, Czech Republic
Zdeněk Sokol, Ing. Ph.D., Department of Steel and Timber Structures, Faculty of Civil Engineering, Czech Technical University, Prague, Thákurova 7, 166 29 Praha 6, Czech Republic
František Wald, Prof. Ing. CSc., Department of Steel and Timber Structures, Faculty of Civil Engineering, Czech Technical University, Prague, Thákurova 7, 166 29 Praha 6, Czech Republic

There was single fire compartment in the building sized 12×18 m with two openings created in the front wall. The size of each opening was 4×2,40 m, height of the window sill was 0,8 m. The fire load was created from timber cribs 50×50 mm, 1 m long, placed in 50 stacks. There was 35,5 kg of timber per 1m², which represents the fire load density about 620 MJ/m². The measured gas temperature in the compartment is shown on Figure 1.

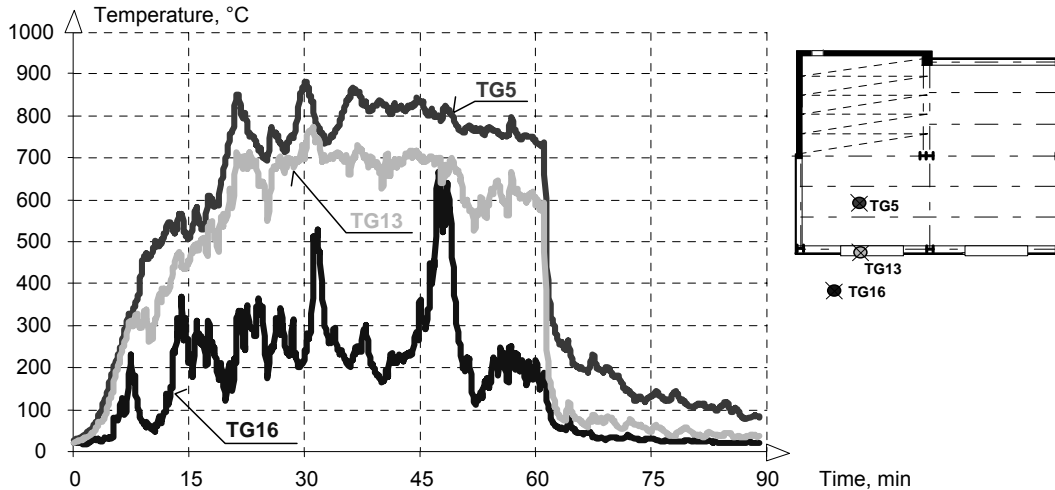


Figure 1. Gas temperatures measured during the fire test, temperature in the compartment TG5, temperature on top of the window TG13, temperature near the column TG16.

MEASURED TEMPERATURE OF THE EXTERNAL COLUMN

The column simulating the external steel structure was installed at a distance 1 m in front of the opening of the fire compartment, see Figure 2. The flanges were parallel to the front wall of the building. The column temperature was measured by 16 thermocouples along its height, see Figure 3 and 4. The temperatures of both flanges of the column section were recorded to investigate non-uniform temperature distribution in the cross section. In addition, the gas temperature near the column was measured by 8 thermocouples. The measured values are presented on Figure 6 - 9.



Figure 2. The building during the fire test, location of the external column.

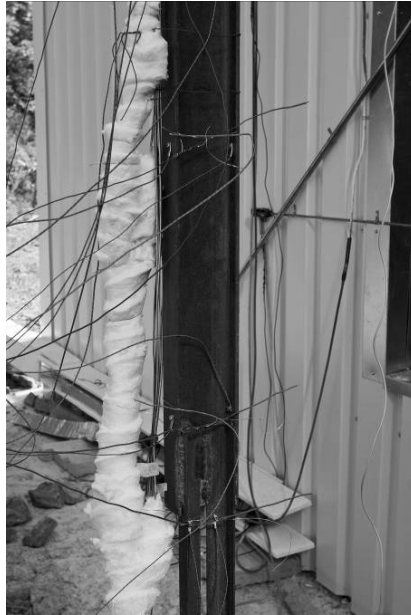


Figure 3. The thermocouples on the external column.

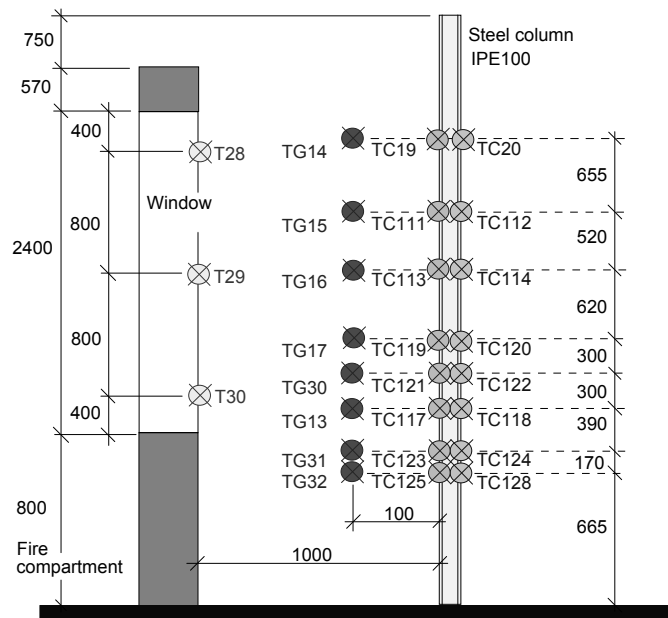


Figure 4. The position of thermocouples on the column.

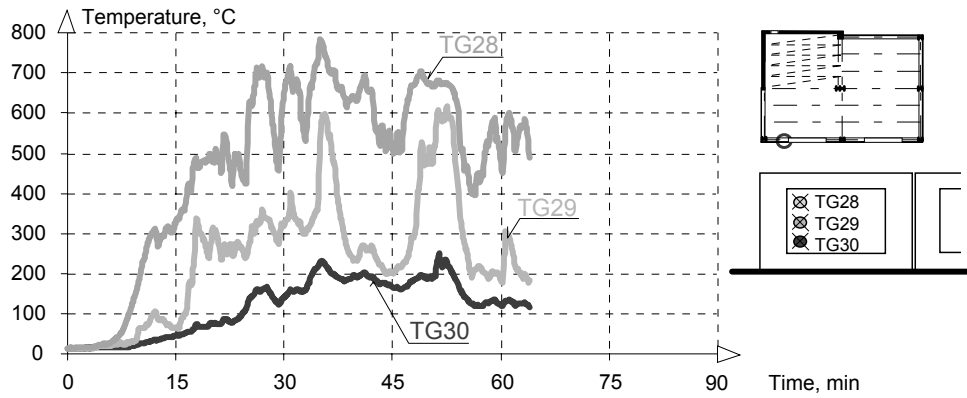


Figure 5. Gas temperature in the window.

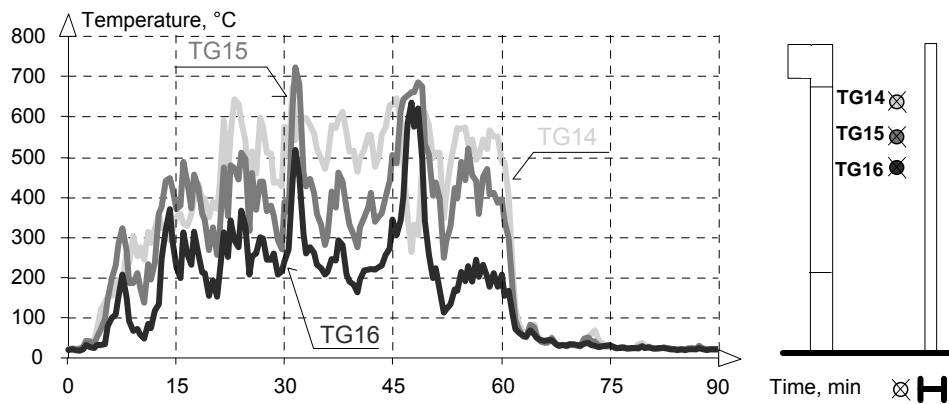


Figure 6. Gas temperature in front of the upper part of the column.

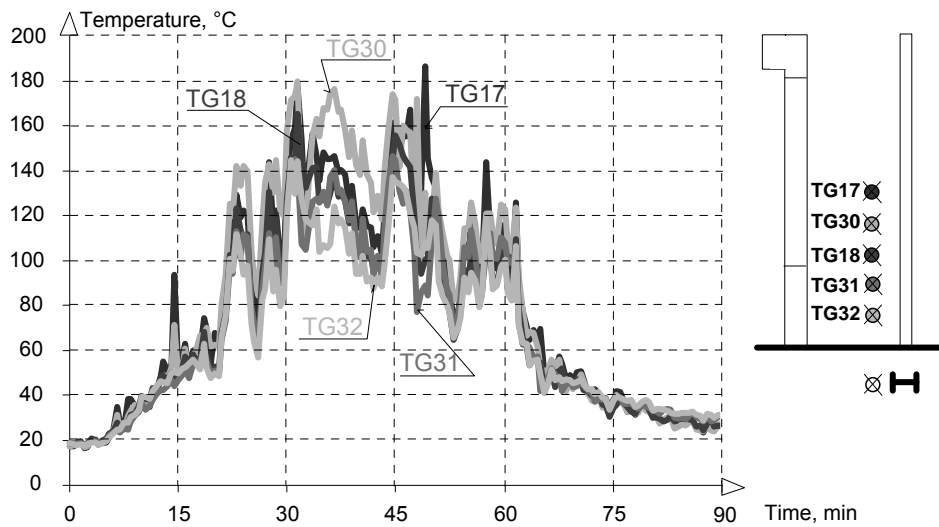


Figure 7. Gas temperature in front of the lower part of the column.

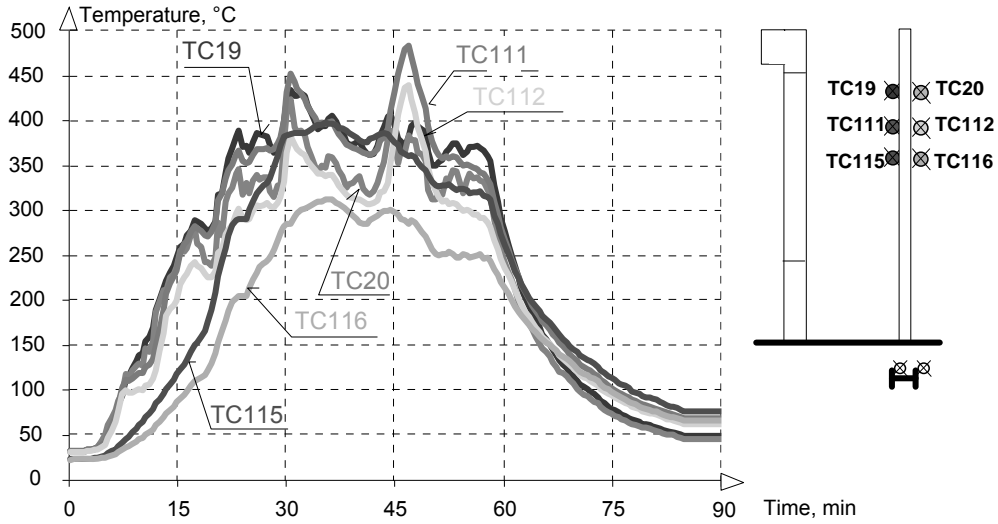


Figure 8. Temperature of the upper part of the external column.

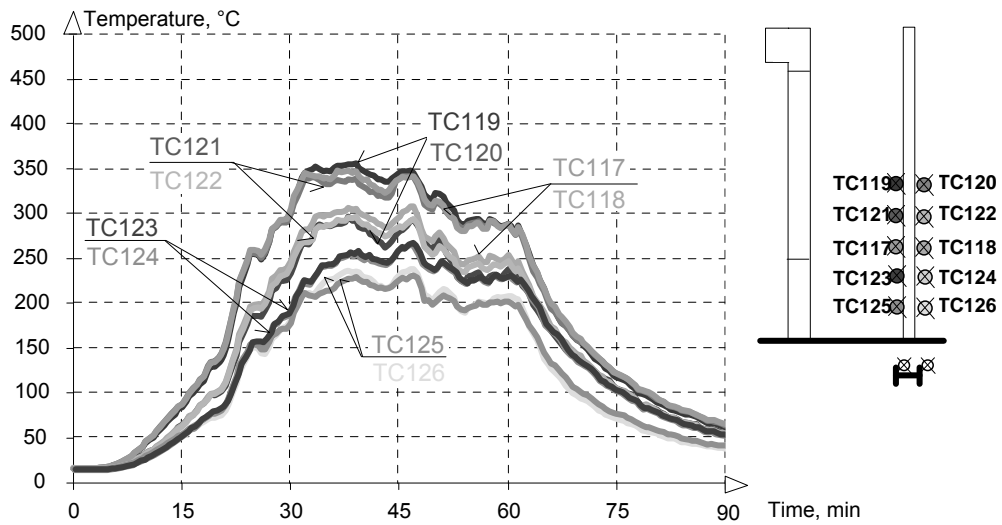


Figure 9. Temperature of the lower part of the external column.

The experiment proved temperature gradient in the column cross-section and along the height. The flange close to the window is directly exposed to radiation and higher temperatures are reached in comparison to the unexposed flange. Significant temperature gradient was observed along the column length as the lower part is exposed to cold air entering the fire compartment but the upper part is exposed to hot gases escaping from the window.

TEMPERATURE PREDICTION USING FINITE ELEMENT MODEL

The temperature of the column was calculated by FEM model using Ansys software. The calculation used 3D model with Solid70 elements for the column and Shell 57 elements for the radiating surface representing the window, see Figure 10. The material properties of steel (non-linear properties for thermal capacity and conductivity) were taken from EN 1993-1-2.

The air temperature used for convective heat flux was taken from the experiment. The radiation from the flames was modeled by radiation from the rectangle representing the window, its temperature was considered equal to the gas temperature inside the fire compartment. Constant temperature was considered in the whole window. The calculated temperatures can be seen on Figure 11.

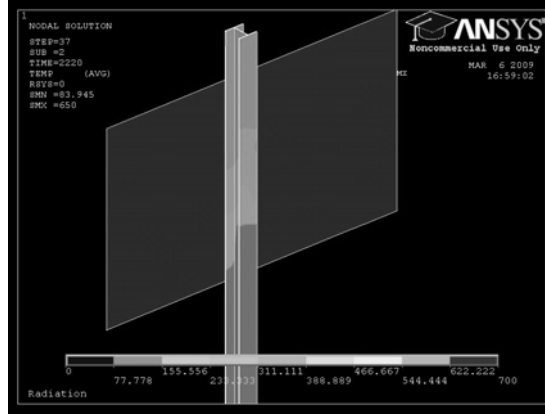


Figure 10. Predicted temperature of the external column at 37 minute.

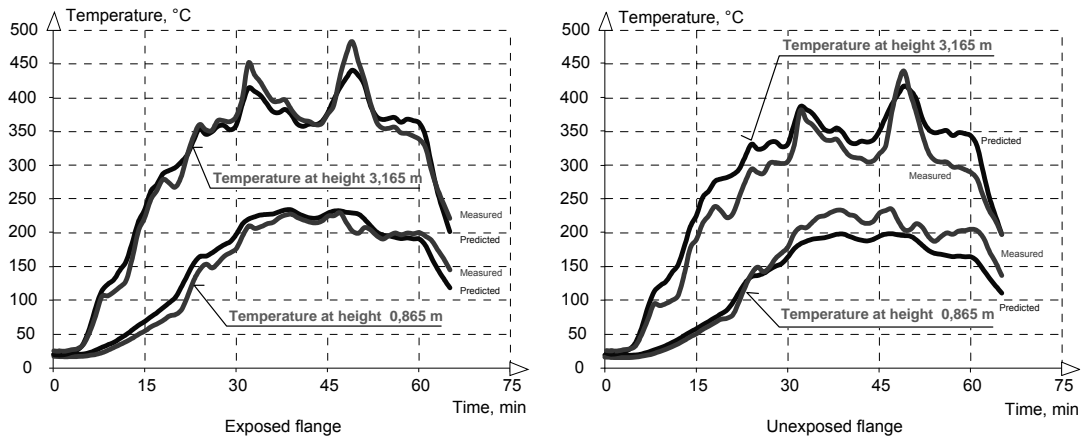


Figure 11. Comparison of predicted and measured temperatures at 37 minute.

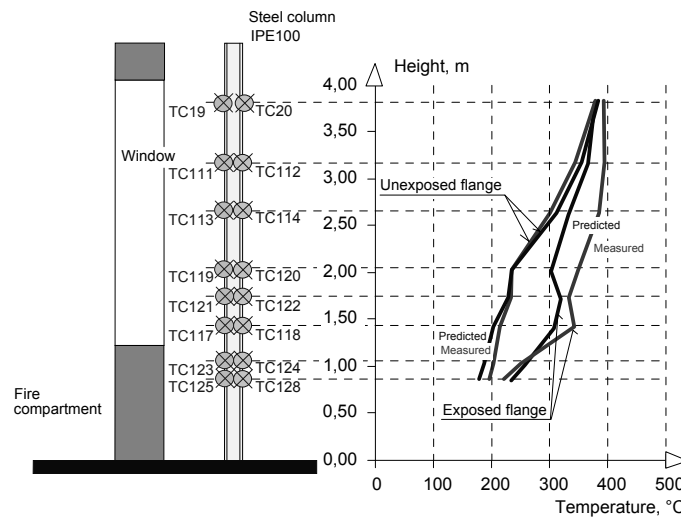


Figure 12. Predicted column temperature along height of the column at 37 minute.

SIMPLIFIED MODEL FOR TEMPERATURE PREDICTION

To simplify the temperature prediction a software enabling the temperature calculation of the column was developed. The input data are the gas temperature near the column and in the fire compartment. The 2D model is based on Stephan-Boltzman law. Temperature increment of each column element is evaluated from the following formula

$$M = \sigma \cdot T^4 \left[W m^{-2} \right], \quad (1)$$

where $\sigma = 5,67051 \cdot 10^{-8} \text{ Wm}^{-2}\text{K}^{-4}$ is Stefan-Boltzmann constant. The heat flux $\Phi_{1,2}$ for two radiating surfaces is given by

$$\Phi_{1,2} = \bar{\varphi}_{1,2} \cdot \bar{S}_1 \frac{\sigma (T_1^4 - T_2^4)}{1 + \bar{\varphi}_{1,2} \left(\frac{1}{\alpha_{e1}} - 1 \right) + \bar{\varphi}_{2,1} \left(\frac{1}{\alpha_{e2}} - 1 \right)}, \quad (2)$$

where T_1 a T_2 is temperature of these surfaces, $\varphi_{1,2}$ and $\varphi_{2,1}$ are configuration factors and $\alpha_{e,1}$ and $\alpha_{e,2}$ are absorptances of these surfaces. This can be simplified to

$$\Phi_{1,2} = \varepsilon_1 S_1 \bar{\varphi}_{1,2} \sigma (T_1^4 - T_2^4), \quad (3)$$

where ε_1 is emissivity of the flames.

The temperature of the column elements can be obtained from the following equation:

$$\begin{aligned} c(T) \rho S \int_{x_1}^{x_2} \frac{\partial T}{\partial t} dx - a S \left(\frac{\partial T}{\partial x}(x_2) - \frac{\partial T}{\partial x}(x_1) \right) - b r (x_2 - x_1) \frac{\partial T}{\partial n} \\ = \sigma w \int_{x_1}^{x_2} (\varphi T_f^4(x) - \varepsilon_1 \varphi(x) T^4(x)) dx \\ + \varepsilon_2 \varphi \int_{x_1}^{x_2} (w(1 - \varphi(x)) + q) (T_z^4 - T^4(x)) dx + \alpha (w + q) \int_{x_1}^{x_2} (T_z - T) dx \end{aligned}, \quad (4)$$

where T is column temperature, T_f temperature of the flames, T_z ambient gas temperature, c specific heat, α thermal conductivity and ρ density of steel, S cross-sectional area of the column, ε_1 emissivity of the fire, ε_2 emissivity of the ambient space, w width of column exposed to the fire, q width of the unexposed part of the column, r length of the boundary and φ is configuration factor defined as

$$\varphi = \int_{S_1} \frac{\cos \theta_1 \cos \theta_2}{\pi r^2} dS_1 \quad (5)$$

and

$$\varphi T_f(x) = \int_{S_1} \frac{\varepsilon_1(y) T_f(y) \cos \theta_1(x, y) \cos \theta_2(x, y)}{\pi r^2} dS_1(y) \quad (6)$$

The nonlinear equation was solved by finite differences method. The equations are solved by Newton's method. The predicted and measured temperatures are compared in Figure 13.

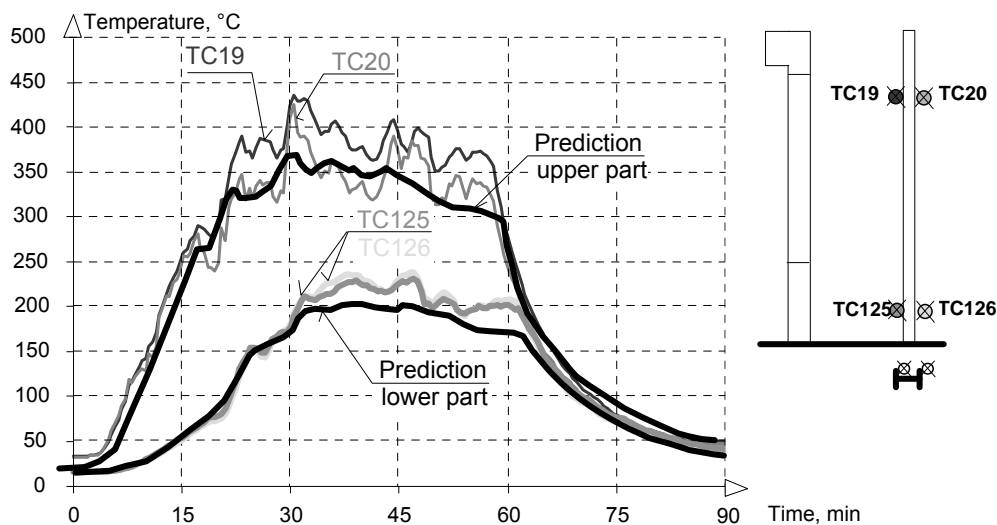


Figure 13. Comparison of measured and calculated temperatures.

CONCLUSION

Two methods for prediction of column temperature located in front of compartment window are described. The finite element model has to be used when thermal gradient in the cross section needs to be calculated. The other method gives only average temperature of the column but the computation time is much shorter. Both models are compared to experimental data obtained during fire test in Mokrsko 2008 and show good accuracy.

ACKNOWLEDGEMENT

This outcome has been achieved with the financial support of the Ministry of Education, Youth and Sports of the Czech Republic, project No. 1M0579, within activities of the CIDEAS research centre.

REFERENCES

1. Wald, F., Chlouba, J., Uhlíř, A., Kallerová, P. and Štujberová, M., "Temperatures During Fire Tests on Structure and its Prediction According to Eurocodes", *Fire Safety Journal*, Vol. 44, No. 1 (2009), p. 135–146.
2. Chlouba, J., Wald, F. and Sokol, Z., "Temperature of Connections During Fire on Steel Framed Building", *International Journal of Steel Structures*, Vol. 9, No. 1, (2009), p. 47–55.
3. Pultar, M. and Wald, F., "Uniform Heating of External Elements During Fire", *Technical Sheets 2008— Part 3*. Praha: CIDEAS-Centrum integrovaného navrhování progresivních stavebních konstrukcí, Vol. 3, (2009), p. 61–62.

Restrained Steel Beam Behaviour in Case of Fire, Depending on Load Ratio, Performed in Case Study of a Bus Station

J. DE LA QUINTANA, J. AURTENETXE, F. MORENTE and S. EGUIA

ABSTRACT

A new bus station infrastructure, in San Sebastian city, in Spain, was seriously compromised by the strict requirements of fire safety regulations, due to the necessity of maintaining its aesthetic appearance, not jeopardizing a beautiful steel structure. The structural system is compounded by several twenty meters long radial beams and an iconic central multi-column.

The infrastructure is a 7,500 m² bus station hall located underground with a 7.2 m maximum height. The steel structure is made of Corten steel and it is compounded by restrained beams connected to columns with a bracing system based on concrete rings.

A comprehensive fire safety engineering study was required, specially focusing on structural analysis, defining and validating an integrated solution based on fire suppression systems. During this study, restrained beams happened to fail before what it was expected. So, a more detailed analysis was developed, because it is normally supposed that restrained steel beams have better fire-resistant capability than isolated steel beams, due to “catenary action”.

When the steel beams reached temperatures below 350°C, a lateral buckling failure happened, before the tension force initiates and catenaria action does not occur.

A real application is presented, in which the length (20m) and properties (hollow section) of steel elements make that the real critical temperature was load ratio dependent, and the results could be considered unsafe if the analysis was developed according to the sound principle appearing in the Eurocodes regarding the verification of the fire resistant of an element as isolate, submitted to an ISO fire curve without considering indirect effects caused by elongations.

Jesús de la Quintana, Head of FSE, Labein—Tecnalia, Department of Fire Safety Engineering, Spain, Derio
Jon Aurtenetxe, Researcher, Labein—Tecnalia, Department of Fire Safety Engineering, Spain, Derio
Fernando Morente, Researcher, Labein—Tecnalia, Department of Fire Safety Engineering, Spain, Derio
Saio Eguia, PhD student, Labein—Tecnalia, Department of Fire Safety Engineering, Spain, Derio

INTRODUCTION

This paper presents a FSE analysis of a new singular bus station, designed with CORTEN steel elements and several concentrically made concrete rings.



Figure 1. The future station.

Due to the necessity of maintaining its aesthetic appearance, the objective of the presented study was to justify the no need of passive protection of the metallic structure. Therefore, an active fire protection system will be validated, providing the structure with the level of security demanded by the regulation.

DESCRIPTION OF SELECTED FIRE SCENARIO

The floor of the buses' docks has a circular shape and a surface of 4780 m². The height is 7.20 m in the central zone and 5 m in the zone outside the "V" shape columns. The lay-out can be appreciated in the figure below.

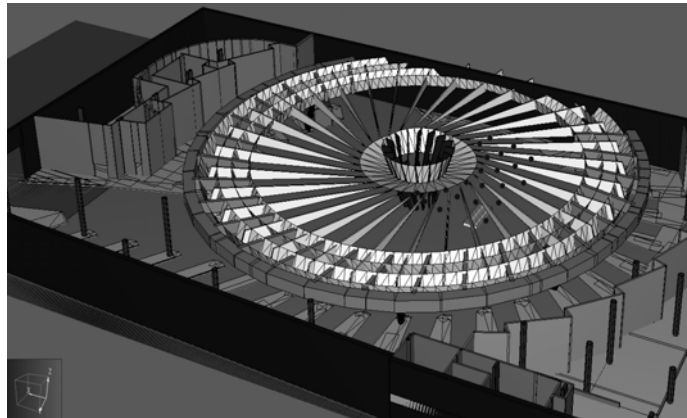


Figure 2. Image of the geometric model.

According the Spanish regulation of automatic water sprinkler systems UNE 12845, the deluge sprinkler system was designed with the following characteristics: 12,5 litros/min·m², simultaneously in an area not smaller than 367,5 m², and a K Factor equal to 115.

The design of the fire scenario was based on a documented real scale test regarding a van (Citroen Jumper) loaded with 18 Euro – pallets and 3 tyres, able of developing a fire power greater than 20 MW.



Figure 3. Images of the real scale test.

During the mentioned tests, the activation of the sprinkler system was hand made when the heat generated inside the van was 7.5 MW approximately. That way, the maximum capacity of the designed sprinkler system to contain and put out the developed fire was verified.

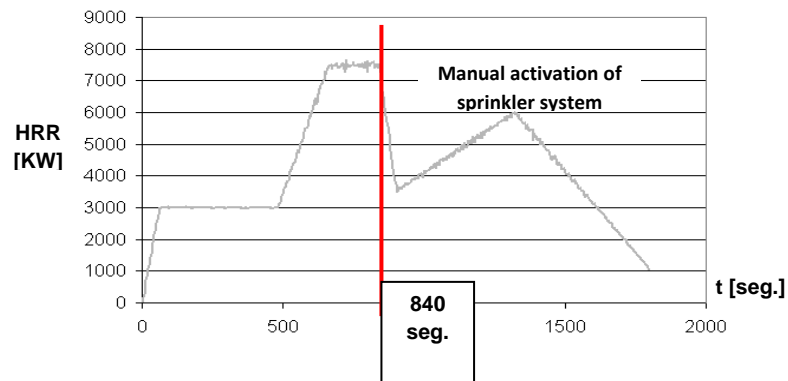


Figure 4. HRR measured in fire tests.

The parabolic design fire curve was built considering a maximum HRR of 7.5 MW with a growing phase conservatively characterized by a $\alpha=100$. A previous detection and sprinkler activation was verified with CFD simulations.

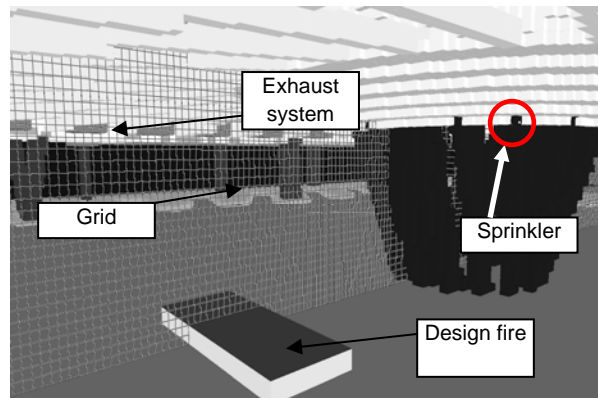


Figure 5. Fire scenario.

THERMAL ANALYSIS OF FIRE EFFECTS

A CFD analysis was developed to study smoke temperatures, considering the effect of the deluge sprinkler system.

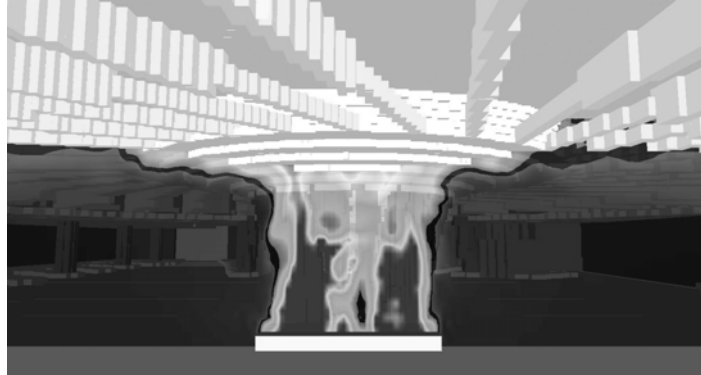


Figure 6. Temperature slice (t=250sec.).

The radiative and convective heat flux were also analyzed to compute steel temperature in the different structural elements. The maximum heat fluxes were 7,53 kw/m² on beams and 28 kw/m² on columns.

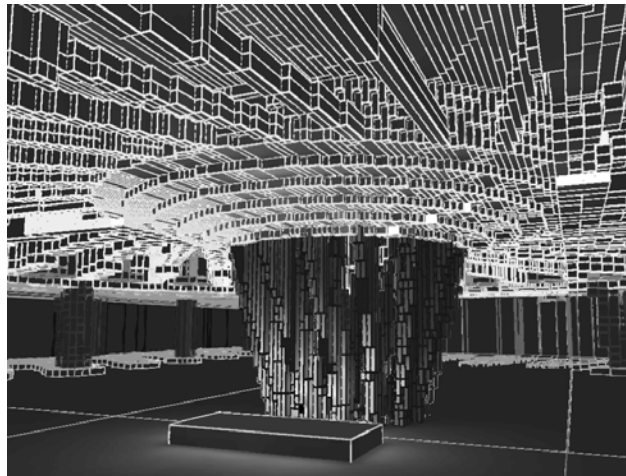


Figure 7. Heat flux slice (t=250sec.).



Figure 10. Tension field in the steel beam

Normally, at the beginning of the fire heating, an internal axial compression force is produced in the restrained beams by thermal expansion. When the temperature surpasses a certain value, the internal axial compression force starts decreasing in the beams, and eventually the compression force vanishes and the tension force is initiated, due to the increase of the deflection of the beams causing a “catenary action”.

But, in the studied case, when the steel beams reached 241°C, a lateral buckling happened, before the tension force initiates and catenary action does not occur. And the critical temperature varies in function of the load ratio,.

These restrained beams happened to fail before what it was expected, so a more detailed analysis was developed.

With the aim of the verification of the FEM strategy, the full scale test made by Guo-Qiang Li and Shi-Xiong Guo, Tongji University (China) [3] was modelled, obtaining a very good agreement with test results. In this case, a better behaviour was obtained for normally used restrained beams in case of fire (5m length), also modifying the load ratio.



Figure 11. Deformed test specimen [3].

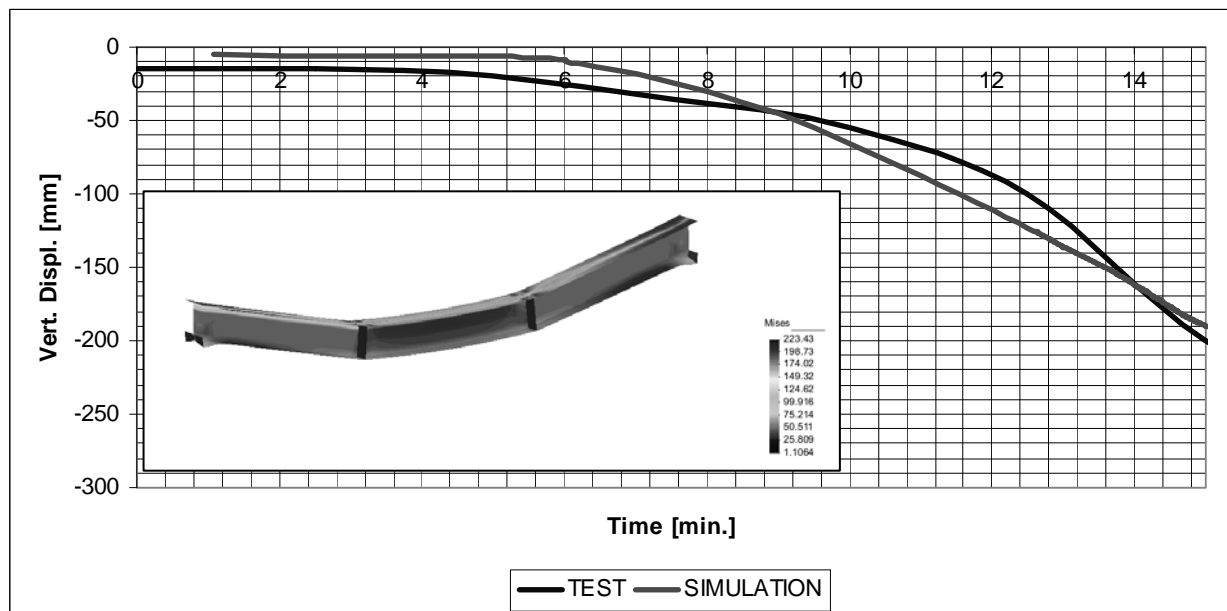


Figure 12. Test and simulation results.

CONCLUSIONS

With a validated FEM strategy, it was found that the sound principle appearing in the Eurocodes regarding the verification of the fire resistant of an element as isolate, without considering indirect effects caused by elongations or beneficial effect of restrained supports, may only obtain safe results in case of normal building structures.

A real application was presented, in which the length (20m) and properties (hollow section) of steel elements make that the critical temperature was load ratio dependent, and the results could be considered unsafe if the analysis was developed as an isolated member submitted to an ISO fire.

REFERENCES

1. P.L. Hinkley, "Smoke and heat venting", *The SFPE Handbook of Fire Protection Engineering*, (1995).
2. Maria E.M. Garlock, Spencer E. Quiel, "Combined Axial load and Moment capacity of fire-exposed beam-columns with thermal gradients", *Structure In Fire 2006, Aveiro, Portugal*, (2006).
3. Guo-Qian Li, Shi-Xiong Guo, "Experiment on restrained steel beams subjected to heating and cooling", *Journal of Constructional Steel Research* 64 (2008) 268–274 (2007).

Experimental and Numerical Modelling of Cellular Beams with Elongations Openings at Elevated Temperature

E. NAILI¹, A. NADJAI¹, H. SONG¹, F. ALI¹, S. CHOI¹, B. WONG²,
I. BURGESS² and R. PLANK²

ABSTRACT

The growing popularity of the use of Cellular steel beams in composite floors comes at the same time as an increasing attention to the fire safety engineering design. The recommendation for their design in fire limit states remains very primitive and this is due to the lack of general research in this area. In fire, the temperature distribution across a composite member is non-uniform, since the web and bottom flange have thin cross-sections and a greater exposed perimeter than the top flange. The deterioration of the material properties of the web will therefore become an important effect on the overall performance of the member in the event of fire.

This work describes an experimental and numerical study at elevated temperatures on the behaviour of full scale composite floor cellular steel beams with elongation openings. A total of three specimens, comprising three different steel geometries and loading conditions were tested at elevated temperatures. All beams were designed for a full shear connection between the steel beam and the composite slab using shear studs.

Finite element models are established with both material and geometrical non-linearity using shell elements and solid brick element to compare the experimental results. This paper will also demonstrate the capability of the developed simple design approach in comparison with numerical modelling, experimental tests and existing design software used by the Steel Construction Institute (SCI).

1. INTRODUCTION

Cellular beams (CBs) are currently being widely used in multi-storey buildings where, as well as reducing the total weight of the steelwork, they help decrease the depth of floors by accommodating pipes, conduits and ducting. They are also used in commercial and industrial buildings, warehouses, and portal frames. CBs produced by modern automated fabrication processes can be competitive for the construction of both floor and roof systems. Their widespread use as structural members has prompted several investigations into their structural behaviour.

¹University of Ulster, School of the Built Environment, FireSERT Block 27, Shore Road, Jordanstown, Belfast, Co Antrim, BT37 0QB

²University of Sheffield, Department of Civil and Structural Engineering Sir Frederick Mappin Building, Mappin Street, Sheffield, S1 3JD

Early studies concentrated on in-plane response in both the elastic [1,2] and plastic [3,4] ranges. Extensive measurements were made of the stress distributions across the cross-section, and these were compared with the predictions of various theoretical studies employing a Vierendeel analogy [5], finite difference techniques [6], various finite element schemes [7], and a complex-variable analytical method [8]. As a result of various series of tests a number of different failure modes have been observed [9-12]. The main failure modes are a Vierendeel collapse mechanism in which plastic hinges form at four locations approximating to “corners” of an opening, buckling of a web-post, and web weld failure. Several collapse mechanisms have been proposed [13-15] and the lateral buckling of the web posts has been analysed.

This paper aims to present the experimental and numerical studies of cellular beams with elongation opening at elevated temperatures which have the potential to provide essential data in several areas currently lacking systematic research. The target of this study comprehends the investigation and the performance under a standard heating regime, the failure mechanisms of cellular beams and temperature distribution through the specimens. The current studies will be followed by a series of well-controlled and instrumented experiments to investigate the influence of load level, slenderness, degree of restraint and heating rate on the restraint forces generated, and on the overall performance of composite cellular beams.

2. FIRE TEST PROGRAMME

The test programme comprehends 3 tests and was carried out on full-scale composite cellular steel beams on composite beams using 3 different geometries. The following types of beams have been tested:

- a) Test-1: Asymmetrical composite cellular beam produced on the basis of UB 356x171x57 as a top tee section and of UB 610x305x179 as a bottom tee section having a finished depth of 555x171/191 ACUB x118kg/M (see Figure1). The dimension of the diameter cells is 375 mm at 600mm centres.
- b) Test-2: Symmetrical composite cellular beam produced on the basis of UB 457x191x74as a top tee section and of UB 457x191x74 as a bottom tee section having a finished depth of 550x191 CUB 74 kg/M (see Figure 2). The dimension of the diameter cells is 335 mm at 600mm centres.
- c) Test-3: Asymmetrical composite cellular beam produced on the basis of UB 356x171x57 as a top tee section and of UB457x191x74 as a bottom tee section having a finished depth of 555x171/191 ACUB x 65.5kg/M (see Figure 3). The dimension of the diameter cells is 375 mm at 600mm centres.

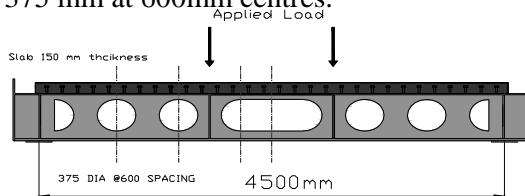


Figure 1. Details of the asymmetrical composite beam-1.

Beam detail:

Top Tee:

Tee depth = 255.0 mm
 Web thickness = 8.1 mm
 Flange width = 172.2 mm
 Flange thickness = 13 mm

Bottom Tee:

Tee depth = 300.0 mm
 Web thickness = 14.1 mm
 Flange width = 307.1 mm
 Flange thickness = 23.6 mm
 375 mm diameter cell at 600 mm

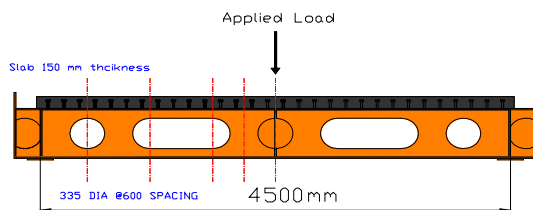
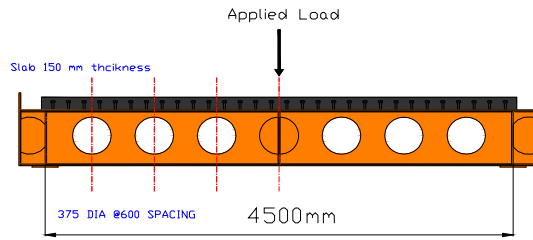


Figure 2. Details of the symmetrical composite beam-2

Beam detail:

Tee depth = 550.0 mm
 Web thickness = 9.0 mm
 Flange width = 190.4 mm
 Flange thickness = 14.5 mm
 335 mm diameter cell at 600 mm centres



Beam detail:

Top Tee:

Tee depth = 255.0 mm

Web thickness = 8.1 mm

Flange width = 172.2 mm

Flange thickness = 13 mm

Bottom Tee:

Tee depth = 300.0 mm

Web thickness = 9.0 mm

Flange width = 190.4 mm

Flange thickness = 14.5 mm

375 mm diameter cell at 600 mm

Figure 3. Details of the asymmetrical composite beam-3

The steel grade of the beams was given as S355. The concrete slabs were nominally 150 mm thick and 1100 mm wide, using normal-weight concrete (Grade 35 N/mm²). The steel deck was of strength 250N/mm², full interaction between the slab and beam was ensured in all specimens by the use of a high density of shear connectors. The beams were tested under one point and two-point loadings; both ends of beams were simply supported. The applied loads during the fire tests were considered equal to 30% of the ultimate load found from the pre-design at cold conditions and by taking into account the previous tests [16] conducted at Ulster University as reference. The three fire tests were carried out under the ISO834 parametric fire curve from the British Standard. Only the lower side of the slab and the steel section were fire-exposed.

TABLE I. FIRE TESTS DURATION AND LOADING APPLIED.

	Test-1	Test-2	Test-3
Loading maintained (kN)	200	150	150
Heating Phase (min)	60	43	50
Ultimate Failure Time (min)	49	39	39

3. INITIAL STUDIES AT AMBIENT TEMPERATURE

The initial studies of specimens that were tested at elevated temperature helped to investigate the behaviour of cellular beams at ambient temperature in order to determinate the ultimate failure loading.

3.1. Finite Element modelling at ambient temperature

Geometrically nonlinear finite element simulations have been carried out using the FEA package DIANA with non-linear material properties in order to simulate the complete behavior of cellular beams at cold conditions and validate how well it can predict the failure load. A curved shell element was used for cellular steel beams. Solid-brick element was used for concrete slab in the analysis to improve the rate of convergence. Full interaction between the cellular steel beam and the concrete slab was assumed in the model due to the high density of shear connectors in the test without the inclusion of the steel decking shape or shear studs. Figure 4 shows the load-deflection- relationship and the ultimate failures load of beam-2.

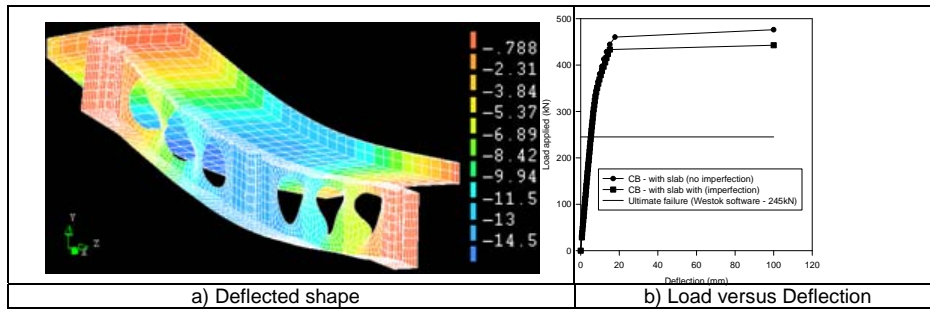


Figure 4. Loading versus Deflection of composite cellular beam-2.

A linear elastic response can be seen in the load deflection curves at the initial loading stage. The first yield occurred at a load level of approximately 382kN, 245kN and 432kN for beam-1, beam-2 and beam-3 respectively (approximately 58%, 54% and 76% of DIANA ultimate failure load respectively). By introducing a web imperfection to the model, the sections failed at a smaller load and the failure mechanism was closer to Vierendeel mechanism and web post buckling as expected. The main ultimate failure of the test-1 and test-2 was Vierendeel bending associated with web-post buckling. For test-3, the web-post buckling occurs as the main failure mode associated also with Vierendeel mechanism. The maximum deflection just before failure was between 10mm and 20mm which should not exceed: span/200 (BS5950-Part 1).

3.2. Initial Design using Westok software

The specimens were pre-designed using Westok software which is based on the SCI documentation for the design of composite cellular beams which gives a linear elastic response. Vierendeel Bending, web post buckling and horizontal shear were considered as the main failure modes of the three specimens. Table II gives Westok/SCI unity factor which is the degree of utilisation of the beam in the failure mode and the ultimate failure load.

TABLE II. WESTOK SOFTWARE RESULTS.

Section	Vierendeel bending	Web post buckling	Horizontal shear	Failure load (kN)
Beam-1	90%	51%	102%	382
Beam-2	102%	35%	44%	245
Beam-3	111%	73%	88%	432

3.3. Simple approach

The simple method proposed by Chung et al [17] to estimate the failure ultimate load of cellular beams considers that the beam alone contributes to the strength of the specimen with the slab just taking into account as a uniform distributed loading along the length of the beam. This method uses simple interaction formula that relates the shear forces, moments and section capacities as follows:

$$\left(\frac{V_{sd}}{V_{o,Rd}} \right)^{2.5} + \left(\frac{M_{sd}}{M_{o,Rd}} \right)^{2.5} \leq 1 \quad (1)$$

V_{sd} applied shear force, $V_{o,Rd}$ shear capacity of cellular section, M_{sd} applied moment, $M_{o,Rd}$ moment capacity of cellular section.

However this method only investigates non-composite beams and the beam-slab acts independently from each other but it may estimates a conservative value for the load carrying capacity. This formula can be used to determinate the moment capacity of the cellular section against Vierendeel mechanism ($M_{vo,Rd}$).

$$M_{vo,Rd} = M_{o,Rd} \cdot \left[1 - \left(\frac{V_{sd}}{V_{o,Rd}} \right)^{2.5} \right]^{0.4} \geq M_{sd} \quad (2)$$

By taken this approach and applying it for the specimens, the properties of the steel profile are given in Table III.

TABLE III. SUMMARY OF BEAM DETAILS AND PROPERTIES.

Section	$M_{o,Rd}$ (kN)	$V_{o,Rd}$ (kN)
Beam-1	756.42	454.33
Beam-2	652.01	412.16
Beam-3	572.34	332.12

3.4. Comparison of simple method with DIANA and Westok software

Table IV shows that both of the pre-design approaches produce the same outcome regardless of the different loading cases. The values found are conservative when compared to DIANA failure load.

TABLE IV. COMPARISON OF THE ULTIMATE FAILURE LOAD RESULTS.

Section	Simple approach (kN)	Westok Software (kN)	DIANA (kN)
Beam-1	380 57%	382 58%	[640;690]
Beam-2	240 53%	245 54%	[430;480]
Beam-3	432 76%	432 76%	[540;600]

4. FIRE TESTS AND RESULTS

4.1. Temperature distribution and deflection

The average temperature distribution along the steel profile in test-2 specimens is shown in Figure 5. The average temperature of top flange is the coldest part of the steel profile with a significant thermal gradient due to the slab on the top and only its bottom part that is exposed to the fire compares to the other parts of the steel section that were fire-exposed on 3 sides.

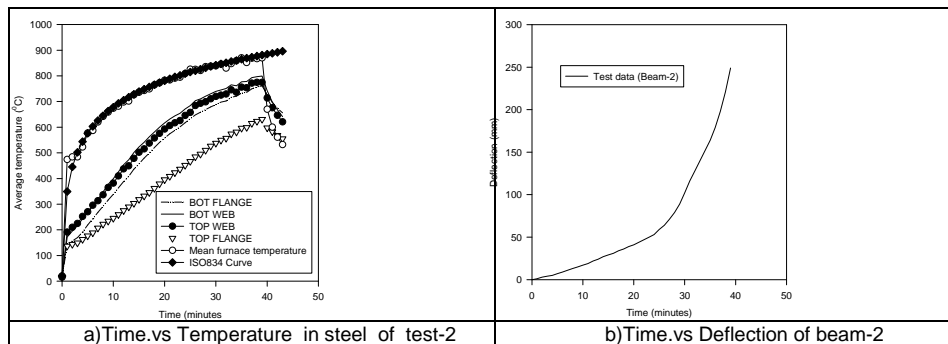


Figure 5. Time.vs Temperature in steel and deflection at mid-span of beam-2.

The maximum temperature values were recorded in the web, reaching up to 795°C in the test-2 after 39 minutes. The beam responds linearly due to the severe rise in temperature until about 15 minutes by which time the furnace temperature has risen to over 730°C. After these points the beam rate of deflection begins to gradually increase due to the deterioration of the beam properties until about 24 minutes when the beam deflection is recorded at furnace temperature around 800°C. Between 20 and 25 min time, beam-2 rate of deflection starts to increase rapidly until the point of failure at 39 minutes by which time the beam have deflected by 249mm at furnace temperature around 870°C. In case of ISO fire, there is no time for significant heat to be conducted through the concrete slab so there is less of a restraining force generated and the deflection rises rapidly. It can be deduced from this that the main reason for failure occurring is due to the loss of the steel strength and stiffness rather than a combined loss of material property in the steel and concrete. Figure 6 shows the results of the fire test1 and test-3.

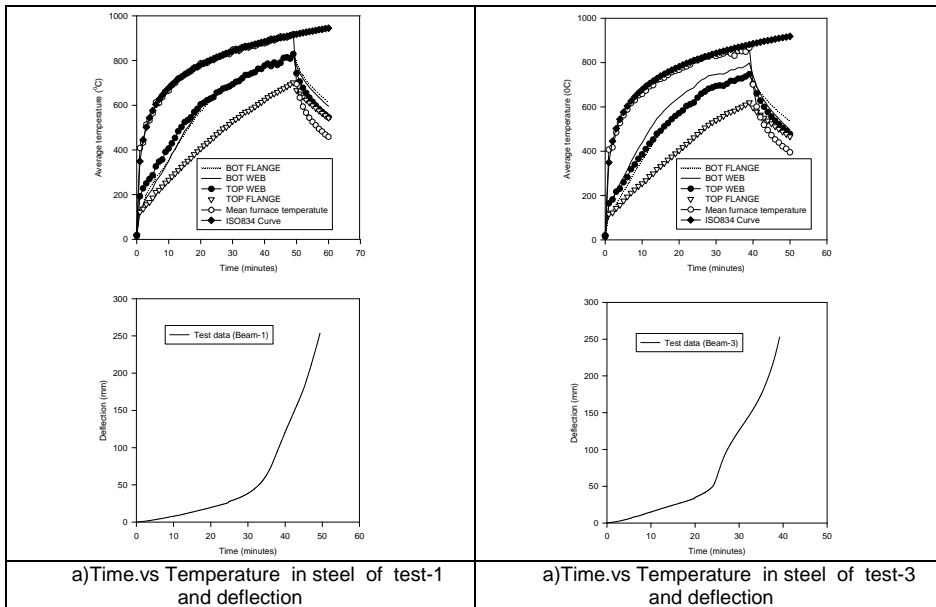


Figure 6. Time vs Temperature in steel and deflection at mid-span of beam-1 & 3.

4.2. Failure mode

All sections of the fire tests fail due to the fact that they lose strength and stiffness due to the rise in temperature.

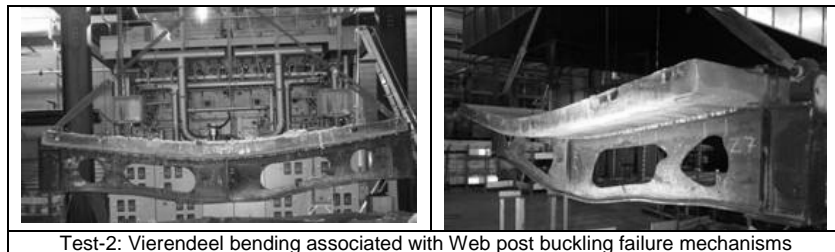


Figure 7. Deformed beam (test-2).

The temperature difference between the top and bottom flange is observed to be greater due to the significant rise in furnace temperature in the case of the ISO fire, but it is not relevant for the web-post buckling. However, buckling of the web posts begins to occur before the final point of failure as the steel beam temperatures are in excess of 600°C at which point the steel has less than half of its design strength and Young’s modulus is reduced to 20%. When the furnace temperature is around 750°C, the Young modulus decreases quicker than the steel strength limit which causes the failure modes. The main failure mode in test-1 and test-2 was the Vierendeel bending associated with the buckling of the web posts of the steel section. The web post buckling was the main failure mode in the test-3.

4. FINITE ELEMENT MODEL FOR FIRE CONDITIONS

The steel beam sections and slab are modelled as the concrete section in the ambient temperature models using the solid-brick element and heating element in order to add a temperature dependent mesh over the top of the structural mesh. In order to simulate the tests as accurately as possible the beams were split into different areas. Different time/temperature curves were introduced to the model according to the average thermocouple reading recorded in the tests for the bottom flange, bottom web, upper web, upper flange, bottom layer of steel decking and concrete slab.

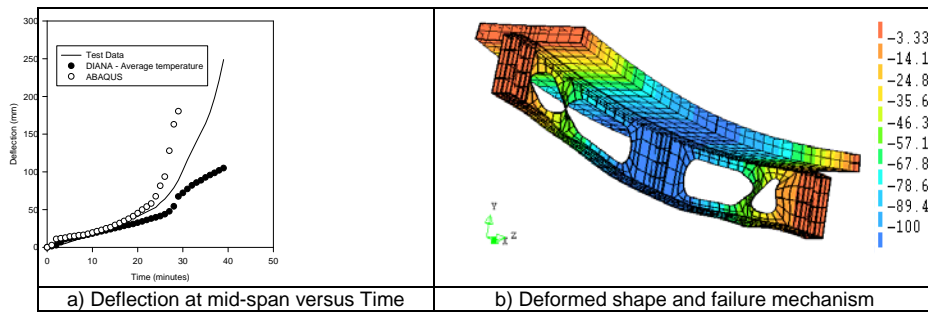


Figure 8. Comparison of DIANA model and test-2.

The failure mode that has taken place in the cellular beam-2 is due to the Vierendeel bending associated with web posts buckling as was seen in the fire test and in the ambient temperature conditions. Figure. 8. a) illustrates a comparison between the experimental test and the existing commercial softwares (DIANA and ABAQUS). The first approach of the numerical modelling seems not to agree well with the experimental fire test in comparison with the failure load. However, a proper calibration of the model is under development to predict better response with the experimental fire test.

6. CONCLUSION

This paper describes an experimental and numerical study of the behaviour of three CBs with with elongation opening at elevated temperature. Veirendeel bending associated with the buckling of the web post were the main failure modes of the composite cellular beam-1 and beam-2 with one and two elongations openings respectively. The beam-3 failed due to the web post buckling and the main reason for this failure is due to the loss of the steel strength and stiffness. The modelling can be extended further and improved in order to predict the

structural behaviour and fire resistance of different specimens. The models can be used for further parametric studies in order to extend the existing fire design rule.

REFERENCES

1. "Properties and strength of castellated beams. Consideration of previous tests", Report D.GE. 71/262, The United Steel Companies Ltd, Swinden Laboratories, Rotherham, (1957).
2. Gibson & Jenkins, *The Structural Engineer*, 35 (12), (1957) pp467-479.
3. Sherbourne, Proc. 2nd Commonwealth Welding Conference, Institute of Welding, London, C2 (1966) pp1-5.
4. Hosain & Speirs, *J. American Welding Society*, Welding Res. Supp., 52 (8), (1973) pp329- 342.
5. Mandel et al., *J. Structural Division, ASCE*, 97 (ST7), (1971) pp1947-1967.
6. Shoukry, *J. American Welding Society*, *Welding Res. Supp.*, 44 (5), (1965) pp231-240.
7. Srimani, & Das, *Computers and Structures*, 9, (1978) pp169-174.
8. Gotoh, *Trans. JSCE*, 7, (1976) pp37-38.
9. Nethercot & Rockey, *The Structural Engineer*, 49 (7), (1971) pp312-330.
10. Nethercot & Traihair, *The Structural Engineer*, 54 (6), (1976) pp197-204.
11. Kerdal & Nethercot, *J. Construct. Steel Research*, 4, (1984) pp295-315.
12. Okubo & Nethercot, *Proc. Instn. Civ. Engrs., Part 2*, (79), (1985) pp533-557.
13. Knowles, *Proc. Instn. Civ. Engrs., Part 1*, 90, (1991) pp521-536.
14. Dougherty, *J. South African Institution of Civil Engineers*, 35 (2), (1993) pp12-20.
15. Zaarour & Redwood, *Journal of Structural Engineering, ASCE*, (1996) pp860-866.
16. Nadjai, A., Vassart, O., Ali, F., Talamona, D., Allam, A. & Hawes M., 'Performance of cellular composite floor beams at elevated temperatures', *Fire Safety Journal*, 42, (2007) pp489-497.
17. Chung, Liu & Ko, Investigation on Vierendeel Mechanism in Steel Beams with Circular Web Openings, 2000
18. SCI, Design of Composite and Non-Composite Cellular Beams, 1994

Performance Based Design Approach for Evaluating Fire Resistance of Restrained Steel Beams

M. DWAIKAT and V. KODUR

ABSTRACT

In this paper, a performance based approach is proposed for fire resistance assessment of simply supported or restrained steel beams. The approach is based on equilibrium and compatibility principles and evaluates fire resistance by applying strength and deflection limiting criteria. The proposed approach takes into consideration various factors governing fire response, including fire scenario, end restraints, connection configuration (location of axial restraint force), thermal gradient, load level, beam geometry, and failure criteria. The validity of the proposed approach is established by comparing predictions from the proposed approach with results obtained through rigorous finite element analysis. The applicability of the proposed approach to practical design situations is illustrated through a numerical example.

Keywords: Fire resistance, axial restraint; rotational restraint; catenary action; elasto-plastic response; fire response.

INTRODUCTION

Restrained beams, when exposed to fire, develop significant restraint forces and these forces can alter the response of the beam. The development of fire induced forces, and gradual softening of steel resulting from high temperature, produce large deflections in the beam. Strength failure occurs in the beam either when the capacity of the connections is exceeded due to large rotations, or when a plastic mechanism develops in the beam after undergoing large deflections.

There have been limited studies on the behavior of restrained beams under fire conditions. Fire resistance tests on axially restrained steel beams revealed the development of significant axial force and large deflections due to restraint [1-3].

Mahmud Dwaikat, Ph.D Candidate, Dept. of Civil & Env. Engineering, Michigan State University, East Lansing, MI (dwaikat1@egr.msu.edu).

Venkatesh Kodur, Professor, Dept. of Civil & Env. Engineering, Michigan State University, East Lansing, MI. (Correspondences: Tel: (+1)(517)353-981, kodur@egr.msu.edu.)

Also, these tests showed that fire response of restrained beams is significantly enhanced by the development of catenary action. Yin and Wang [4] and Wang and Yin [5] developed an analytical method for predicting the fire behavior of restrained steel beams. In this method, an initial deflection profile for the beam is assumed and then the internal fire-induced forces are calculated by differentiating the deflection profile and applying relevant boundary conditions. This makes the method case-specific since the assumed initial deflection profile is a function of the applied load and the boundary conditions of the beam. Further, the proposed method is laborious and requires lengthy calculations and numerical integration.

Current fire resistance provisions in codes and standards for steel structures are based on strength limit state which is indirectly related to critical temperature of steel. However, fire tests and actual fire incidents clearly show that strength limit state in restrained beams is reached after undergoing large deflections. Thus, there is lack of reliable and simple methods for assessing the fire response of restrained steel beams. In this paper a simplified performance-based approach for evaluating fire resistance of restrained steel beams is presented.

RESPONSE OF RESTRAINED BEAMS UNDER FIRE

Beams are primary load carrying members in a steel framed structure, especially in high rise buildings. A restrained steel beam, shown in Fig. 1(a), when exposed to fire, develops significant internal forces (axial force and bending moment) and large deflections due to the effect of restraints and deterioration in properties of steel with increasing temperatures. If the beam (shown in Fig. 1(a)) is laterally braced, and is made of a compact section (i.e. no local buckling), then the beam undergoes three distinct stages, as shown in Fig. 1(b and c) during exposure to fire. In Stage I, elastic response dominates the behavior wherein the beam expands as a result of continuous heating, and compressive axial force and hogging bending moment develop in the beam due to the effect of end-restraints. Fire-induced internal forces and deflections continue to increase until yielding occurs in the beam. Elasto-plastic response dominates the behavior in Stage II, as shown in Fig. 1(b). As steel temperature continues to increase with fire exposure time, softening of steel causes larger deflections and rotations until the first plastic hinge develop in the beam. The plastic hinge, which forms at the location of maximum bending moment in the beam, causes sudden increase in deflection (see Fig.1(c)), which leads to reduction and then reversal of the axial force in the beam from compressive to tensile force. The beam enters a catenary phase in Stage III when the fire-induced compressive axial force vanishes as shown in Fig. 1(b). In the catenary phase, tensile force develops in the beam and the load bearing mechanism gradually shifts from flexural to cable (tensile) until failure occurs by rupture of the beam (or in the connections). When the beam undergoes the above three stages, it is assumed that the connections continue to perform elastically. Therefore, fire-induced forces and rotations in the beam must not exceed the connections capacity.

CURRENT PROVISIONS IN CODES AND STANDARDS

Most of the provisions in codes and standards adopt critical temperature limit state for evaluating fire resistance. The critical temperature (T_{cr}) is defined as the temperature at which *steel* loses 50% of its room-temperature yield strength. The concept of critical temperature continues to be used in codes adopting performance-based approach, such as the Eurocode 3 [6], New Zealand Standards [7], and Japanese Building Code [8], but with slight modification to the definition of T_{cr} in which steel *member* (rather than steel *material*) loses 50% of its room-temperature capacity. Empirical or semi-empirical formulas are provided in these codes to

evaluate the critical temperature. For instance, Eurocode 3, New Zealand and Japanese steel design codes provide the following relations for computing the critical temperature (T_{cr}) of steel beams [6-8]:

$$T_{cr}^{EC3} = 39.19 \ln \left[\frac{1}{0.967 \times r^{3.833}} - 1 \right] + 482 \quad (1)$$

$$T_{cr}^{SNZ} = 905 - 690 \times r \quad (2)$$

$$T_{cr}^{JBC} = 700 - 375 \times r \quad (3)$$

where the load ratio (r) is defined as the ratio between the bending moment (M_o) resulting from reduced load during fire to the room-temperature plastic moment capacity of the steel beam (M_p). Obviously, in these equations (and the like) the influence of restraint conditions and fire is not properly accounted for.

PERFORMANCE-BASED APPROACH

The influence of end restraints on the fire response of a steel beam can be accounted for through a performance based design approach. The derivation of the necessary equations has been presented by the authors elsewhere [9, 10]. In this approach, the fire response of the restrained beam is traced and the failure of the beam is assessed based on performance criteria. By referring to Fig. 1, the transition in the fire response of a restrained beam between elastic and elastoplastic response is marked by the occurrence of yielding (if the beam section is designed to be a compact section and local buckling effect is neglected). Since the restrained beam will experience fire induced axial force ($P(T)$) and bending moment ($M_G(T)$) due to restraint of non uniform thermal expansion, the temperature (T_y) at which yielding occurs can be computed using the following yield P-M interaction equation.

$$\frac{P(T)}{k_y(T)P_y} + \frac{M(T) \mp M_G(T)}{k_y(T)M_y} < 1.0 \quad (4)$$

where P_y and M_y are the room-temperature yield axial and moment capacity of the steel section, respectively. $k_y(T)$ is the temperature-dependent reduction factor for yield strength. Based on this approach the critical value of T_y evaluated at both critical sections (midspan and support sections) is obtained as:

$$T_y = \frac{1 - M_o / M_y - 0.5 F_R \Delta T}{F_A + a_2}, \quad T_y < 600^\circ\text{C} \quad (5)$$

where M_o is the maximum bending moment in the beam due to gravity load. M_y is the yield bending moment at room temperature. ΔT is the thermal gradient between the top and bottom flanges of the section. F_R and F_A are the rotational and axial restraint factors, respectively, and are defined as:

$$F_R = \frac{\alpha E_s}{F_y} \left(\frac{a_1 K_r L / (E_s I)}{2a_1 + K_r L / (E_s I)} \right) \quad \text{and} \quad F_A = \frac{\alpha E_s}{F_y} \left(\frac{a_1 K_a L / (E_s A_s)}{2a_1 + K_a L / (E_s A_s)} \right) \quad (6a \text{ and } 6b)$$

K_a and K_r in Eq. [6] are the axial and rotational restraint stiffnesses, respectively. L , I , A_s are the total length, second moment of area and cross sectional area of the steel beam, respectively. E_s , F_y and α are the room-temperature values of elastic modulus, yield strength and coefficient of thermal expansion of steel, respectively. The coefficients a_1 and a_2 result from the linearization of temperature-dependent reduction factors for yield strength ($k_y(T)$) and elastic modulus ($k_E(T)$), and thus, a_1 and a_2 are dependent on the material model of steel which vary depending on the codes [10]:

- For steel properties as specified in Eurocode 3: $a_1 = 0.6$ and $a_2 = 0.0013$
- For steel properties as specified in ASCE manual: $a_1 = 0.6829$ and $a_2 = 0.0008$

As plasticity spreads throughout the section, the axial compressive force reduces until it reaches zero at temperature T_c as shown in Fig 1(b) and this temperature can be computed using the following relation:

$$T_c = \frac{1}{a_2} \left(1 - \frac{M_o}{M_u} - \frac{M_y}{M_u} \frac{F_R \Delta T}{2} \right) \quad (7)$$

where $M_u = F_u Z_x$ and $M_y = F_y S_x$.

The plastic deflection of the restrained beam at the instant of catenary action ($P = 0$ at $T = T_c$) can be approximated as:

$$\Delta_c = \frac{L}{2} \sqrt{2\alpha(T_c - 20)} \quad (8)$$

Using linear interpolation, as shown in Fig 1, the elasto-plastic deflection between T_y and T_c can be obtained as:

$$\Delta = \Delta_y + \frac{\Delta_c - \Delta_y}{T_c - T_y} (T - T_y), \quad T_y < T < T_c \quad (9)$$

Using Eq. 9, a limiting temperature based on a deflection limiting criterion $\Delta = L_F$ can be obtained as:

$$T_{DLS} = T_y + \frac{(L_F - \Delta_y)(T_c - T_y)}{(\Delta_c - \Delta_y)} \quad (10)$$

where T_{DLS} is steel temperature at deflection limit state, L_F is the deflection limit state and is usually taken as $(1/30 - 1/20)L$. Also, strength failure is assumed to occur at temperature (T_f) where the tensile catenary force in the beam is maximal, and this temperature is computed as:

$$T_f = \frac{T_c T_y F_A + a_1 a_3 (T_c - T_y)}{T_y F_A + a_1 a_4 (T_c - T_y)} \quad (11)$$

where a_3 and a_4 are regression coefficients that are dependent on steel properties:

- For steel properties as specified in Eurocode 3: $a_3 = 1.139$; $a_4 = 0.0013$
- For steel properties as specified in ASCE manual; $a_3 = 1.329$; $a_4 = 0.0014$

It will be shown through a design example that Eqs. 10 and 11 can effectively be used as a performance-based guideline for fire design of restrained beam based on deflection criteria.

VERIFICATION OF THE PROPOSED APPROACH

The proposed approach has been verified by comparing its predictions against results from rigorous finite element analysis carried out using ANSYS (11). The details of the finite element modeling and validation can be found elsewhere [9, 10]. The validation covered a wide range of beams with varying factors, such as end restraint, connection configuration, load level, slenderness, and thermal gradient. Figure 2 compares the results from the proposed approach (Eq. (10)) to results from finite element analysis on beams with different load, restraint and fire exposure conditions. Two deflection criteria were used, $L_F = L/20$ and $L_F = L/30$. These deflection criteria are commonly used in fire tests (10) and are chosen for comparison. As shown in Fig. 2, the approach predicts the temperature at deflection limit state (T_{DLS}) within 10% margin of error.

Comparison to Current Approaches

Predictions from the proposed approach are also compared in Fig. 3 against current code provisions for evaluating critical temperature. Both deflection and strength limit states were applied to evaluate fire resistance. The enhanced fire resistance due to effect of restraint is captured by the proposed approach and is evident in Fig. 3(b), however, restraint effect is not captured by the code provisions.

Design Example

An example is presented here to demonstrate the applicability and rationality of the proposed approach. Step-by step design procedure in analyzing a typical restrained beam under fire is presented below:

PROBLEM

Evaluate the fire resistance of the restrained beam shown in Fig. 1 (a). The beam, which is subjected to maximum bending moment of 285.8 kN.m, has the following characteristics.

- $L = 7000$ mm, Section W24x76 (AISC). Steel; $F_y = 355$ MPa and $F_u = 445$ MPa.
- Load combination under fire $w_f = 70$ kN/m. $K_a = 41.3$ kN/mm and $K_r = 50$ kN.m/milrad. Thermal gradient (ΔT) = 150°C. Contour insulation of 1 inch. (thermal conductivity 0.1 W/m.°C). Assume failure to occur when deflection exceed $L/30$.

RESPONSE PARAMETERS

- Axial and rotational restraint factors:

$$F_A = \frac{\alpha E_s}{F_y} \left(\frac{a_1 K_a L / (E_s A_s)}{2a_1 + K_a L / (E_s A_s)} \right) = \frac{14 \times 10^{-6} \times 2 \times 10^5}{355} \left(\frac{0.6829 \times 0.1}{2 \times 0.6829 + 0.1} \right) = 0.00037$$

$$F_R = \frac{\alpha E_s}{F_y} \left(\frac{a_1 K_r L / (E_s I)}{2a_1 + K_r L / (E_s I)} \right) = \frac{14 \times 10^{-6} \times 2 \times 10^5}{355} \left(\frac{0.6829 \times 2}{2 \times 0.6829 + 2} \right) = 0.0032$$

- Yield and catenary temperatures

$$T_y = \frac{1 - M_o / M_y - 0.5 F_R \Delta T}{F_A + a_2} = \frac{1 - 285.8 / 1023.8 - 0.5 \times 0.0032 \times 150}{0.00037 + 0.0008} = 411^\circ \text{C}$$

$$T_c = \frac{1}{a_2} \left(1 - \frac{M_o}{M_u} - \frac{M_y}{M_u} \frac{F_R \Delta T}{2} \right) = \frac{1}{0.0008} \left(1 - \frac{285.8}{1308.9} - \frac{1023.8}{1308.9} \times \frac{0.0032 \times 150}{2} \right) = 878.8^\circ \text{C}$$

- Deflection at catenary point

$$\Delta_c = \frac{L}{2} \sqrt{2 \times \alpha (T_c - 20)} = \frac{7000}{2} \sqrt{2 \times 14 \times 10^{-6} (878.8 - 20)} = 542 \text{ mm}$$

- Temperature at deflection limit state (neglecting elastic deflection)

$$T_{DLS} = T_y + \frac{L_F (T_c - T_y)}{\Delta_c} = 411 + \frac{(7000/30)(878.8 - 411)}{542} = 612^\circ \text{C}$$

- Temperature at ultimate strength failure

$$T_f = \frac{T_c T_y F_A + a_1 a_3 (T_c - T_y)}{T_y F_A + a_1 a_4 (T_c - T_y)} = \frac{878.8 \times 411 \times 0.00037 + 0.6829 \times 1.329 \times (878.8 - 411)}{411 \times 0.00037 + 0.6829 \times 0.0014 \times (878.8 - 411)} = 931^\circ \text{C}$$

FIRE RESISTANCE USING PROPOSED APPROACH

After computing the limiting temperature (T_{DLS}) based on deflection limit state, the fire resistance duration can be computed using best fit equation (or more elaborate spreadsheet calculation method specified in Eurocode 3). The best fit equation is expressed as:

$$t = 40(T_{lim} - 140) \left[\frac{d_i / k_i}{F/V} \right]^{0.77} \quad (11)$$

where $T_{lim} = T_{DLS}$ or T_f , and d_i is the insulation thickness in m. (0.025m) and k_i is the thermal conductivity of insulation (0.1 W/m. $^\circ$ C), and F/V is the section factor and is equal to 160 m $^{-1}$ for this example under 3-side fire exposure. By substitution into Eq.(11), the fire resistance duration based on deflection limit state is 130 min., and based on strength failure ($T_f = 931^\circ \text{C}$) is 218 min as shown in Fig. 4.

FIRE RESISTANCE USING CODE PROVISIONS

In the current code provisions, the critical temperature is computed based on specified semi-empirical equations. First, the load ratio under fire conditions (r) is computed as: $r = M_o/M_p = 285.8/1308.9 = 0.21$. Second, the critical temperature is computed as per Eqs. 1 through 3:

$$T_{cr}^{EC3} = 717^\circ \text{C}, \quad T_{cr}^{SNZ} = 760^\circ \text{C} \quad \text{and} \quad T_{cr}^{JBC} = 621^\circ \text{C}$$

By substituting into Eq.(11), the following fire resistances are obtained using equations specified in Eurocode 3, New Zealand, and Japanese codes, respectively:

$$t^{EC3} = 160 \text{ min.}, \quad t^{SNZ} = 170 \text{ min.} \quad \text{and} \quad t^{JBC} = 132 \text{ min.}$$

The proposed approach is compared to nonlinear transient finite element analysis of the beam and the result is plotted in Fig. 4. The fire resistances from the finite element analysis (149 and 248 min.) compare well with the conservative values computed from the proposed approach (130 and 218 min) for deflection and strength limit states, respectively.

CONCLUSIONS

Current approaches for fire design of steel structures do not account for the influence of fire induced restraint on the response steel beams. The proposed performance-based design

procedure, which is based on equilibrium and compatibility principles, is capable of evaluating fire resistance of restrained steel beams, and the performance of the restrained beam can be checked under strength or deflection failure criteria. The proposed approach yielded better fire resistance predictions than those predicted by current codes of practice. Thus the proposed approach can be effectively applied for undertaking performance-based fire design of restrained steel beams.

REFERENCES

1. Li, G.Q., He, J.L., and Jiang, S.C. 2000. "Fire-resistant experiment and theoretical calculation of a steel beam," China Civil Engineering Journal, 32 (4):23–26.
2. Liu, T.C.H., Fahad, M.K., Davies, J.M. 2002. "Experimental investigation of behaviour of axially restrained steel beams in fire," J. Constr. Steel Res. 58: 1211-1230.
3. Li, G-Q. and Guo, S-X. 2008. "Experiment on restrained steel beams subjected to heating and cooling," Journal of Constructional Steel Research 64: 268-274.
4. Yin, Y.Z. and Y.C. Wang. 2003. "Numerical simulations of the effects of non-uniform temperature distributions on lateral torsional buckling resistance of steel I-beam," Journal of Constructional Steel Research, 59:1009-1033.
5. Wang, Y.C. and Y.Z. Yin. 2006. "A simplified analysis of catenary action in steel beams in fire and implications on fire resistant design," Steel and Composite Structures, 6(5):367-386.
6. Eurocode 3. 2005. "EN1993-1-2: The European Standard; Part 1-2: General rules - Structural fire design," European Committee for Standardization, Brussels, Belgium.
7. Standards New Zealand. 1997. "Steel Structures Standard. NZS 3404: Part 1 & Part 2". New Zealand, Wellington.
8. Harada, K., Ohmiya, Y, Natori, A. and Nakamichi, A. 2004. "Technical basis on structural fire resistance design in building standards law of Japan," Fire and Materials, 28:323–34.
9. Dwaikat, M.M.S and Kodur, V.K.R. 2009. "A performance-based methodology for fire design of restrained steel beams," Submitted, Computers & Structures Journal.
10. Dwaikat, M.M.S and Kodur, V.K.R. .2009. "An Engineering Approach for Predicting Fire Response of Restrained Steel Beams," Submitted, Journal of Engineering Mechanics, ASCE.
11. ANSYS. 2007. "ANSYS Multiphysics," Version 11.0 SP1 ANSYS Inc., Canonsburg, PA. USA.

FIGURES

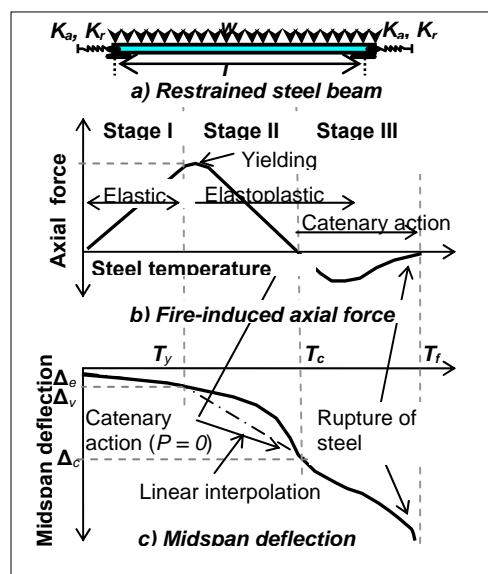
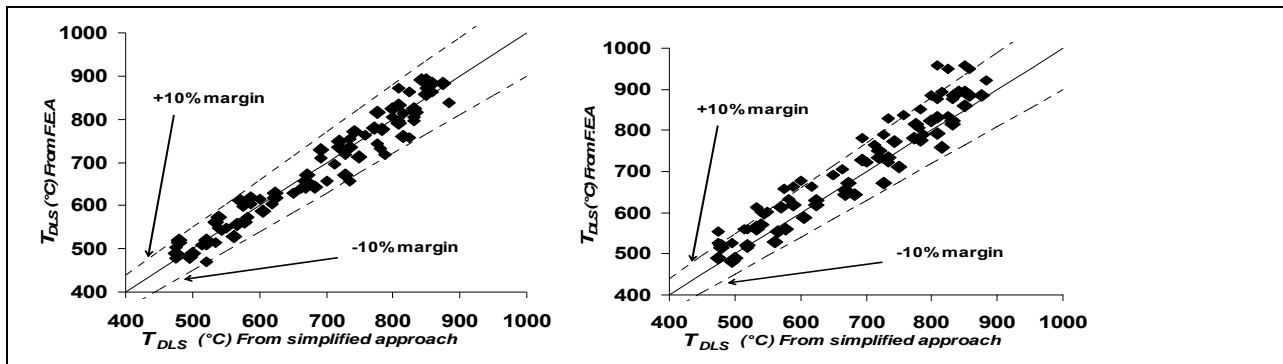


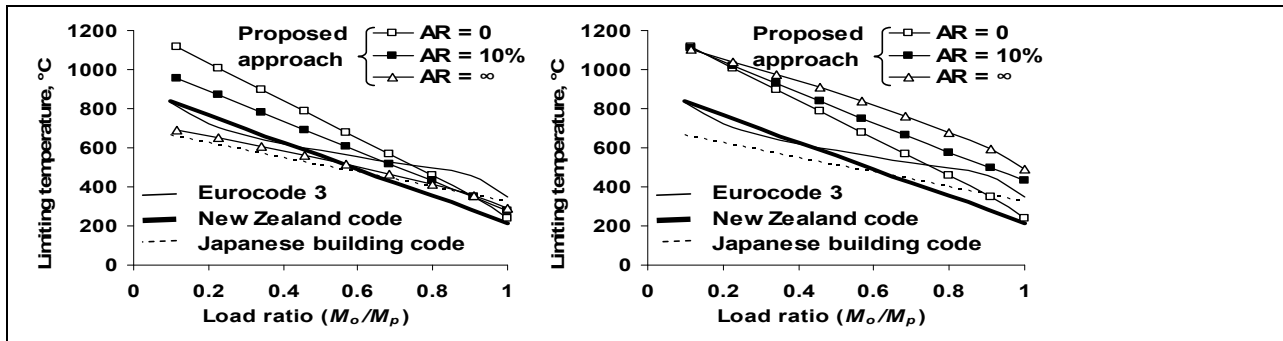
Figure 1. Typical fire response of a restrained steel beam that fails by yielding.



a) Deflection limit state ($L_F = L/20$)

b) Deflection limit state ($L_F = L/30$)

Figure 2. Comparing temperatures at deflection limit state as predicted by finite element analysis and from Eq. 10 for $L_F = L/20$ and $L/30$.



a) Limit state ($L_F = L/20$)

b) Strength failure

Figure 3. Comparing the limiting temperature from proposed approach and from codes and standards (AR : Axial restraint ratio).

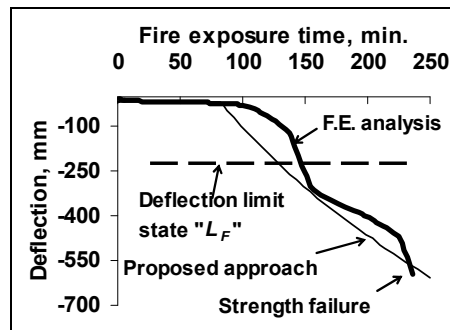


Figure 4. Comparing the proposed approach with finite element analysis of the restrained beam

Load Bearing Capacity of Steel Structures After Fire

J. FALKE and H. N. MUSTAFA

ABSTRACT

The load bearing capacity of steel structures after fire is examined. Considerations and numerical studies, in this work phase, have been made for members under bending. During fire members under restraint experience significant compression forces due to thermal expansion. This leads to residual internal moments and residual deformations. Statically undetermined structures show inelastic load carrying behavior after fire. Residual deformations often are in a range that they can be left without repair or compensated by affordable means of repair. In the planning phase of a building sensitivity to fire can be checked and the structural detailing can be done in a way, that no or little means are necessary to compensate for fire damages, e. g. residual deformations.

INTRODUCTION

Many efforts have been spent on determining the load carrying behavior of steel structures under fire during the heating phase. Much lesser results are given for structures under fire comprising the cooling phase in [1] and [2]. Few results are given for the load bearing behavior and bearing capacity of structures after fire in [3]. Recently the authors have investigated the load bearing capacity of steel structures after fire. Considerations and non-linear numerical studies have been made on members under tension in [4] and bending in this paper. Due to fire considerable residual forces and deformations occur after fire which affect the load bearing behavior and thus the serviceability of steel structures after fire. Numerical studies done permit to better evaluate whether fire damaged structure may be reinstated and reused rather than demolished. Thus, this paper contributes to evaluate and improve sustainability of steel structures.

Prof. Dr.-Ing. J. Falke, University of Siegen, Paul Bonatz Str. 9-11, D-57076 Siegen
Dipl.-Ing. H. N. Mustafa, University of Siegen, Paul Bonatz Str. 9-11, D-57076 Siegen

ASSUMPTIONS AND BASIC REMARKS

ABBREVIATIONS

A	cross sectional area
E, E _θ	modulus of elasticity at room temperature (20° C), at steel temperature θ
L	length of a member
M _{Ed}	design moment
M _{pl,Rd,θ}	design resistance of a bending member at steel temperature θ
N _{pl,Rd,θ}	design resistance of a tension member at steel temperature θ
f _y , f _{y,θ}	yield strength at room temperature (20° C), effective yield strength at steel temperature
g _k	characteristical permanent load
k _{E,θ}	reduction factor for the modulus of elasticity at steel temperature θ [5]
k _{y,θ}	reduction factor for the yield strength at steel temperature θ [5]
p _{Ed}	design load
p _{u,Rd}	design ultimate limit load for permanent situation
p _{u,Rd,fi}	design ultimate limit load for fire situation
q _k	characteristical variable load
w	deformation / deflection in middle span
γ _G	partial safety factor for permanent loads for permanent situation, γ _G = 1.35
γ _{G,fi}	partial safety factor for permanent loads for fire situation, γ _{G,fi} = 1.0
γ _q	partial safety factor for variable loads for permanent situation, γ _p = 1.50
γ _{q,fi}	partial safety factor for variable loads for fire situation, γ _{p,fi} = 1.0
γ _M	partial safety factor for material properties for permanent situation, γ _M = 1.1
γ _{M,fi}	partial safety factor for material properties for fire situation, γ _{M,fi} = 1.0
φ, φ _{pl}	rotation, plastic rotation
θ, max θ	steel temperature, maximum steel temperature reached during a fire [°C]
θ _{cr}	critical steel temperature [°C]
ρ (ρ ^{bf} , ρ ^{af})	degree of utilization (before fire, after fire)
ρ _{cr}	critical degree of utilization

MATERIAL BEHAVIOR

For the numerical studies the temperature dependant functions for yield strength, modulus of elasticity and thermal elongation (appr. 0.000012) as given in [5] have been used. It is noted that mild steel grades show the same yield strength before and after fire [6], whereas fine grain high strength steel grades lose up to 40 % of the yield strength depending on the maximum temperature reached during fire, see figure 1 based on results from [7]. Material behavior in the cooling phase of natural fire is unknown and assumed similar to the heating phase.

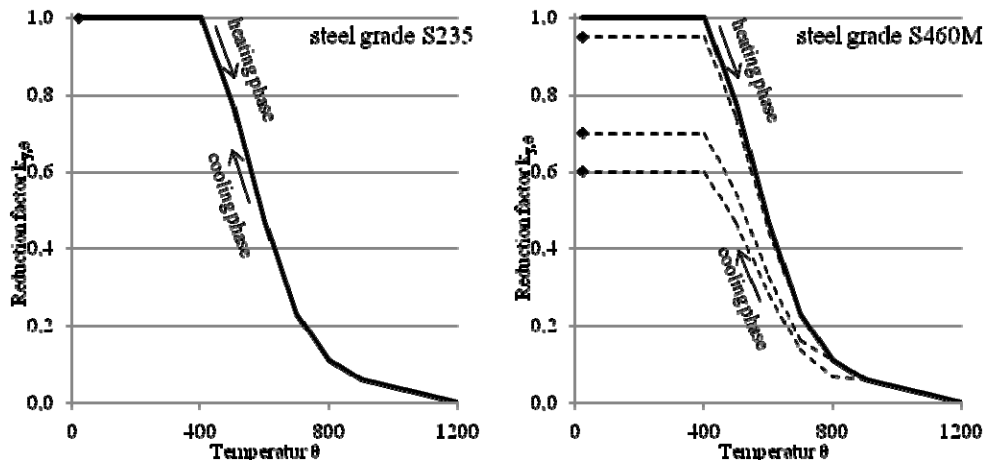


Figure 1. Effective yield strength of mild steel grade (left) and fine grain high strength steel (right).

Load bearing behavior of frames in and after fire is strongly influenced by modulus of elasticity. In material science the modulus of elasticity is correlated with the melting temperature. Only effects on the melting temperature alter the modulus of elasticity.

Some experimental results on the modulus of elasticity after fire are given in [8]. The steel grade S355J2H with determined mechanical properties ($f_y = 529 \text{ N/mm}^2$ and $E = 198000 \text{ N/mm}^2$) was investigated. The results are collated in figure 2. For these numerical studies the modulus of elasticity is assumed to be the same before and after fire.

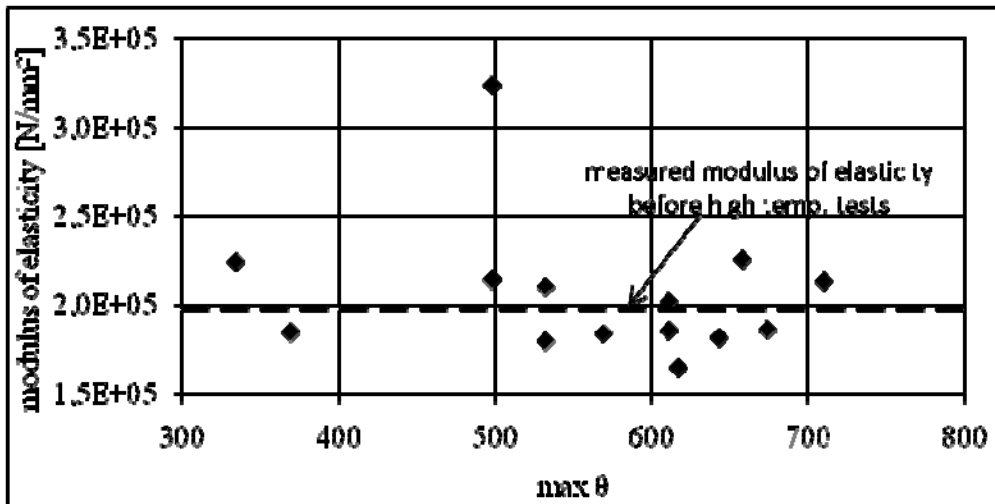


Figure 2. Modulus of elasticity after high temperature tests.

The ultimate strain after fire can decrease down to 16% and is not needed to be considered. Effects of embrittlement are negligible, because structures exposed to natural fire always are cooling down slowly even by using water for fire fighting.

For the numerical studies material non-linear behavior is taken into account by assuming a linearly elastic-ideally plastic stress-strain-relationship.

MEMBER BEHAVIOR

Members are considered to show elastic behavior until the characteristic tension, compressive or bending resistance is reached.

Design resistance of tension and stocky compression members at steel temperature θ is given by

$$N_{pl,Rd,\theta} = \frac{A \cdot f_y \cdot k_{y,\theta}}{\gamma_{M,\bar{n}}} \quad (1)$$

It is independent from geometrical and physical imperfections. Reduction in bearing capacity after fire is proportional to the reduction of yield strength accordingly. As the compression forces occurring during fire are small buckling can be neglected.

Design resistance of bending members at steel temperature θ is given by

$$M_{pl,Rd,\theta} = \frac{W_{pl} \cdot f_y \cdot k_{y,\theta}}{\gamma_{M,\bar{n}}} \quad (2)$$

As local imperfections are influenced by fire, the cross section classification may be different before during and after fire. This effect is neglected for these studies. Also beams are considered to have sufficient laterally restraints, lateral torsion buckling is not considered.

The interaction of normal forces and bending moments is considered as given in [5] by

$$M_{N,pl,Rd,\theta} = M_{pl,Rd,\theta} \cdot \left(1 - \left(\frac{N_{Ed}}{N_{pl,Rd,\theta}} \right)^2 \right) \quad (3)$$

The loads are scaled by

$$m_i = \frac{M_{i,Ed}}{M_{pl,Rd,\bar{n}}^{bf}} \quad (4)$$

to visualize the curves in a suitable format in figure 5 to 8. The function m_s describes the hogging moment and the function m_F describes the maximum moment in field.

FRAME BEHAVIOR

Fire causes high internal forces and moments in statically indeterminate structures, which often reach yield limit. Plastic deformations are irreversible and thus after fire high residual forces are encountered or, already in the cooling phase of a fire, members or connections are overstressed [1]. Due to plastic deformations during fire frame behavior is different before and after fire.

Numerical studies have been done for structures as shown in figure 3. Restraints are given by bracings and being represented in the studies by springs with stiffness of common bracings. It is considered to be representative for structures under bending. Degree of utilization and maximum steel temperature reached during fire $\max \theta$ have been varied. Members are assumed stocky and stability effects are not considered. Second order analysis has been used.

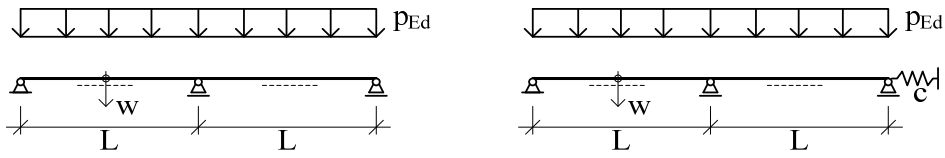


Figure 3. Statical system 1 (left) and 2 (right).

TIME-TEMPERATURE CURVES AND DEGREE OF UTILIZATION

For the numerical studies uniform steel temperature in the whole cross sections and along the length of the members is assumed (steady state conditions). These studies do not require time-temperature curves. For clarification in figure 4 time dependency is shown in principal for steel temperature, loading and resistance.

The degree of utilization ρ is given by:

$$\rho = \frac{p_{Ed}}{p_{u,Rd}} = \frac{1.35 \cdot g_k + 1.5 \cdot q_k}{p_{u,Rd}} \leq 1.0 \quad (5)$$

and

$$\rho^{bf} = \frac{3 \cdot p_{Ed}}{(1.35 + 2 \cdot 1.5) \cdot 1.1 \cdot p_{u,Rd}} \leq 0.63 \quad (6)$$

Taking a ratio variable/permanent loads of 2.0 at room temperature for a common building the degree of utilization under fire loads is $\rho = 0.69$; considering $\gamma_M / \gamma_{M,fi}$ yields $\rho^{bf} = 0.63$. As the yield strength can be different before and after fire this leads to different ultimate limit loads and degrees of utilization, indicated by ^{bf} and ^{af} (e.g.: ρ^{bf} , ρ^{af}) if necessary.

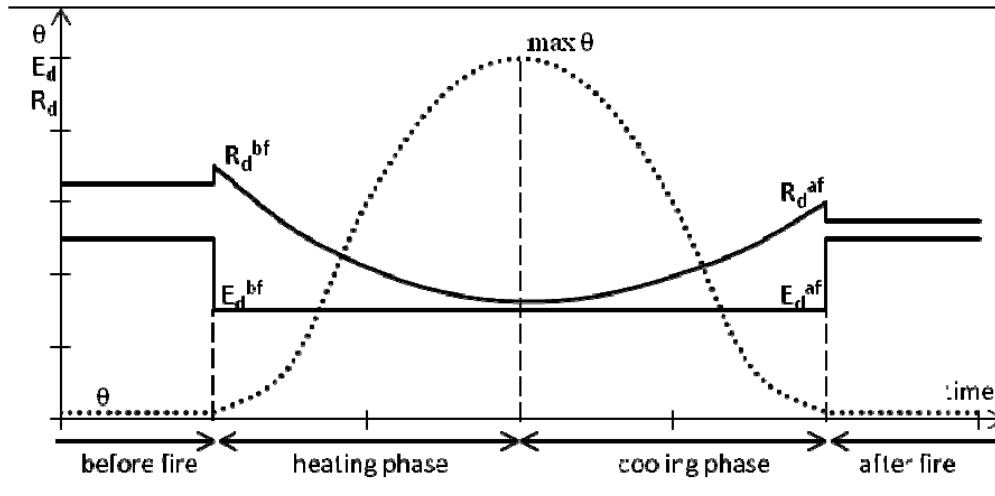


Figure 4. Steel temperature θ , design loading E_d and design resistance R_d in function of time.

LOAD BEARING CAPACITY AFTER FIRE

For room temperature the design ultimate limit load $p_{u,Rd}$ for the statical systems in figure 2 is given by:

$$p_{u,Rd} = 11,66 \cdot \frac{W_{pl} \cdot f_y}{L^2 \cdot \gamma_M} \text{ and } p_{u,Rd,fi} = 11,66 \cdot \frac{W_{pl} \cdot f_y}{L^2 \cdot \gamma_{M,fi}} \quad (7), (8)$$

In a first step internal forces and moments and deformations, occurring during fire situation, have been analysed. Frame analysis is made by using plastic hinge theory. Whenever a cross section is fully plastified, a plastic hinge and a couple of moments $M_{pl,Rd,\theta}$ is introduced in the statical system. Whenever, in the cooling phase, an internal moment in a plastified member is decreasing, the plastic hinge is extracted but the plastic rotation is imposed. The plastic rotation is given by the rotation φ (taken from frame analysis) reached at maximum steel temperature $\max \theta$ minus elastic rotation:

$$\varphi_{pl}(\max \theta) = \varphi(\max \theta) - \int_L \frac{M_p \cdot \bar{M}}{E \cdot I \cdot k_{y,\max \theta}} dx \quad (9)$$

As the normal force does not reach the ultimate limit load there is no plastic strain along the neutral axis and thermal strain and normal force do not affect the rotation; for tension members see [4]. It is noted, that the moment $M_{\varphi,pl}$ induced by the plastic rotation is increasing with decreasing temperature as the modulus of elasticity is increasing.

$$\Delta M_{\varphi,pl} = \frac{3 \cdot (E_{\theta} - E_{\max \theta}) \cdot I \cdot \varphi_{pl}}{L} \quad (10)$$

There is one load-displacement curve for the heating phase but, as the plastic rotation depends on the maximum steel temperature reached during fire, there are innumerable load-displacement curves for the cooling phase.

Reduced yield strengths, after fire lower than before fire, lead to reduced design resistances and thus to lower residual forces, see figures 5 to 6. For the residual moments given in this paper this effect has been neglected, i.e. upper limits are given here.

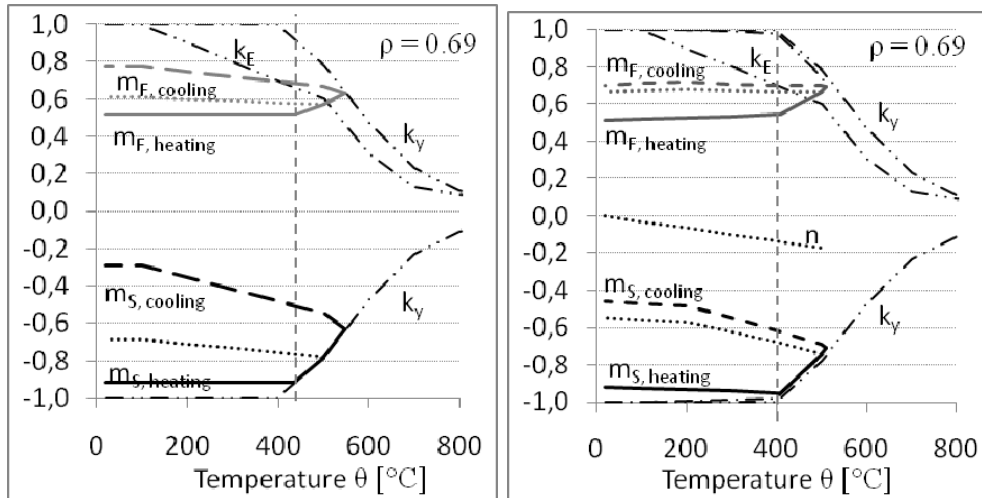


Figure 5. Relative moments for statical system 1 (left) and 2 (right) and $\rho = 0.69$.

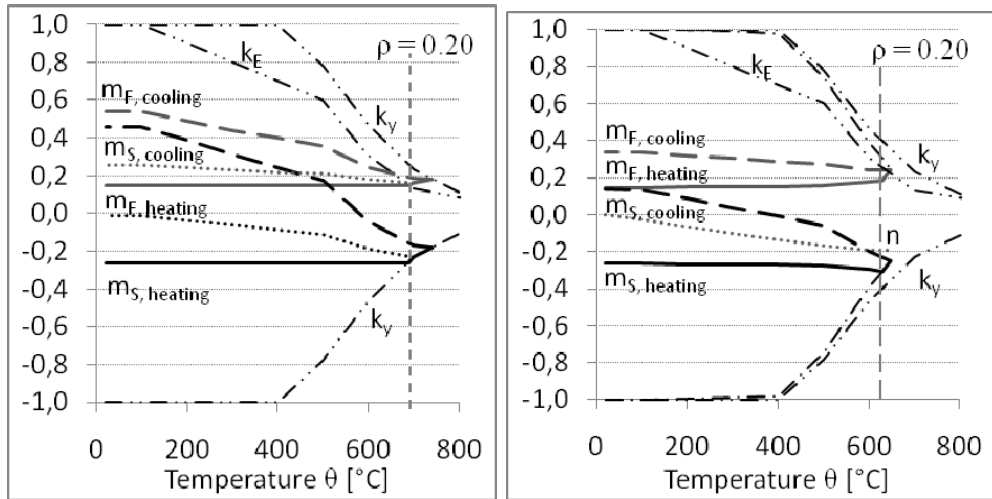


Figure 6: Relative moments for statical system 1 (left) and 2 (right) and $\rho = 0.20$

Using equilibrium conditions residual moments and deformations can be derived from the internal moments of the members. They differ with the maximum steel temperature reached during fire. The residual moments in function of maximum steel temperature reached during fire $\max \theta$ and degree of utilization ρ are given in figure 7. For low maximum steel temperatures and low degrees of utilization the structure remains fully in the elastic range, no residual moments occur. Residual moments and deformations are nonlinear in function of maximum steel temperature and degree of utilization. Lateral torsion buckling effects reduce significantly the residual moments.

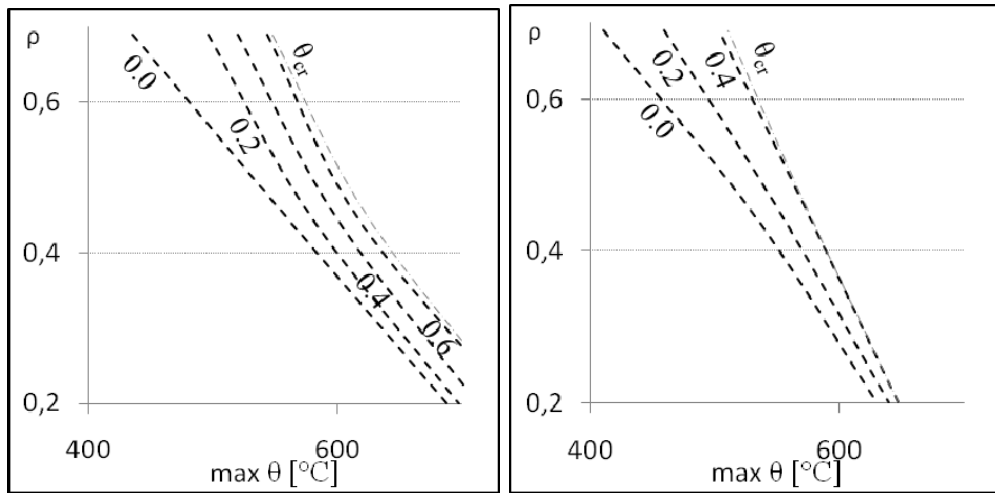


Figure 7: Relative residual moments $m_{s,res}$ for the statical system 1 (left) and 2 (right)

CONCLUSIONS AND FINAL REMARKS

After fire in general residual moments and displacements appear. An elastic frame analysis will not reflect sufficiently the load bearing behavior.

For low maximum temperatures reached in fire no residual displacements appear. For low degrees of utilization residual displacements may reach limit values of serviceability. For high degrees of utilization, structures designed using plastic theory, serviceability limit states are less important and thus residual displacements in general can be left without repair.

Results are based on uniform temperature distribution. For non-uniform temperature distribution residual normal forces and displacements tend to be lesser. The load bearing capacity tends to be unaffected.

REFERENCES

1. C. Roben and M. Gillie: Structural behaviour of multi-storey frames during the cooling phase of a fire. Proceedings of the 5th International Conference on Advances in Steel Structures, Singapore, 2007.
2. P. Wang, G. Li, S. Guo: Effects of the cooling phase of a fire on steel structure. Fire Safety Journal 43 (2008) 451–458.
3. U. Hamme: Zum Gesamttragverhalten stählerner Stabwerke während und nach einer thermisch instationären Beanspruchung. Dissertation, Bergische Universität Wuppertal, 1989.
4. J. Falke and H. N. Mustafa: Contribution to Sustainability in Steel Structures. Proceedings of the 6th international Conference on Advances in Steel Structures, Hong Kong, 2009.
5. EN 1993-1-2 Eurocode 3 Design of steel structures—Part 1-2 General rules—structural fire design. CEN, Brussels, 2005.
6. C. Smith, B. R. Kirby, D. G. Lapwood, K. J. Coole, A. P. Cunningham and R. R. Preston: The Reinstatement of fire damaged steel framed structures. Fire Safety Journal 4 (1) 21–62, 1981.
7. N. Wohlfeil: Werkstoffgesetze von S460 unter Brandeinwirkung und nach Abkühlung. Dissertation, Technische Universität Darmstadt, Darmstadt, 2006.
8. J. Outinen, Olli Kaitila and P. Mäkeläinen: High-Temperature Testing of Structural Steel and Modelling of Structures at Fire Temperatures. Research Report, Helsinki University of Technology, Laboratory of Steel Structures, Publication 23, Espoo, 2001.
9. EN 1991-1-2 Eurocode 1 Actions on structures—Part 1-2 Actions on Structure exposed to fire. CEN, Brussels, 2003.
10. J. A. El-Rimawi, I. W. Burgess and R. J. Plank: The Treatment of Strain Reversal in Structural Members During the Cooling Phase of Fire. J. Construct. Steel Res., Vol. 37, No. 2, pp. 115–135, Elsevier Science Ltd., 1996.
11. J. Falke and H. N. Mustafa: Contribution to Enhance Sustainability of Steel Structures. (to be published)

Stress-Based Equations for Predicting the Buckling Capacity of Steel Plates Exposed to Fire

S. E. QUIEL and M. E. M. GARLOCK

ABSTRACT

Current codes of practice can estimate the reduced capacity of compression members due to local buckling under ambient conditions, but the results of this study indicate that these codes, especially the American one, do not adequately predict the buckling capacity of steel plates at elevated temperatures. This paper proposes new and simple equations to calculate the buckling capacity of steel plates at elevated temperature. The approach modifies existing stress-based methods specified by American (AISC) and European (Eurocode) codes to account for steel material non-linearities at high temperature as well as reductions of strength and stiffness. A parametric study of ultimate plate strength was performed via finite-element analysis to obtain curves describing the relationship of critical stress to plate slenderness. The proposed equations are validated by comparison to these finite element analyses, and comparisons are also made to the AISC and Eurocode predictions.

INTRODUCTION

Local buckling is a concern for structural steel members in compression because they are composed of thin plates, which may buckle before the section reaches its plastic or overall flexural buckling capacity under load and thus reduce its ultimate strength. Under fire conditions, changes in the material properties of steel will affect the local buckling capacity of the plates in a steel cross-section subject to fire and must be accounted for in the design of steel members to resist fire.

The design of steel structures at elevated temperature as specified by AISC's steel construction manual [1] and the Eurocode [2,3] currently uses stress-based methods to calculate the ultimate strength of plates for local buckling in fire-exposed sections. Although the AISC and the Eurocode approaches account for temperature-induced reductions of yield strength and stiffness, each has some limitations in accounting for a non-linear stress-strain relationship at high temperature. These limitations may lead to inaccurate estimations of ultimate strength at elevated temperature depending on the slenderness of the plate. Another publication by the authors [4] provides a detailed literature review of previous research regarding plate buckling at elevated temperature.

Spencer Quiel, Hinman Consulting Engineers, 225 Reinekers Lane, Suite 250, Alexandria, VA 22314 US; Tel.: +1 703 416 6780. Fax: +1 703 836 4423; squiel@hce.com
Maria Garlock, Department of Civil and Environmental Engineering, Princeton University, Princeton, NJ USA; mgarlock@princeton.edu

This paper proposes a new generalized approach to calculate the ultimate strength of steel plates at elevated temperature due to local buckling prior to the onset of plasticity. The approach modifies existing stress-based methods specified by AISC and Eurocode to account for steel material nonlinearities at high temperature as well as reductions of strength and stiffness. A parametric study of ultimate plate strength was performed via finite-element analysis of individual plates to obtain strength curves. Computational analyses considered a wide range of slenderness ratios over a range of temperatures for a variety of boundary conditions and initial imperfections. The proposed method is validated by comparison to these curves, and comparisons are also made to the AISC and Eurocode standards. This approach is believed to be amenable to the current state of practice because its form is similar to existing methods and ultimate strength can be calculated for plates with a wide range of temperature, loading and boundary conditions.

EXISTING APPROACHES

“Stiffened” plate elements are supported on both longitudinal edges parallel to the direction of axial compression loading whereas “unstiffened” plates are supported on only one edge. Elastic buckling of plates at ambient temperature with no initial imperfection is given by Euler’s equation:

$$F_{cr} = \frac{k\pi^2 E}{12(1-\mu^2)(b/t)^2} \quad (1)$$

where k is the buckling coefficient, μ is Poisson’s ratio ($\mu = 0.3$ for steel), E is Young’s modulus, and b/t is the width-to-thickness ratio. Table I shows the stiffened and unstiffened boundary conditions and their corresponding theoretical values of k . The ratio of F_{cr} to yield strength (F_y) can also be conveniently expressed in terms of the non-dimensional slenderness ratio, λ_c :

$$\lambda_c = \sqrt{\frac{F_y}{F_{cr}}} = \sqrt{\frac{12(1-\mu^2)(b/t)^2 F_y}{k\pi^2 E}} \quad (2)$$

Although AISC uses the width-to-thickness ratio b/t in its calculations of ultimate strength, this study will use the non-dimensional slenderness ratio λ_c , as does the Eurocode, in order to derive expressions that are normalized with regard to the buckling coefficient, F_y , and E .

For stiffened elements with uniform stresses, the AISC specifications calculate post-buckling ultimate strength using an effective width, b_e , approach [1]. Another paper by the authors [4] shows how those equations can be rewritten in the following way:

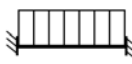
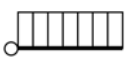
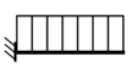
$$\frac{b_e}{b} = \left(\frac{F_{cr}}{F_y} \right)_{plate} = \frac{2}{\lambda_c \sqrt{k}} \left(1 - \frac{0.80}{k\lambda_c} \right) \quad (3)$$

Eurocode uses a similar approach to calculate the post-buckling ultimate strength of stiffened steel plates in compression [3].

For unstiffened elements, AISC specifies an equivalent uniform distribution of average stress over the width of the plate (instead of an equivalent width approach). Our proposed equations, however, will be based on the equivalent width approach, which is used by the Eurocode:

$$\text{For } \lambda_c > 0.748: \quad \frac{b_e}{b} = \left(\frac{F_{cr}}{F_y} \right)_{plate} = \frac{1}{\lambda_c} \left(1 - \frac{0.188}{\lambda_c} \right) \quad (4)$$

TABLE I. PLATE CASES CONSIDERED FOR THIS STUDY.

	Case	Boundary Condition	Buckling coeff., k
Stiffened	1		4.00
	2		6.97
Unstiffened	3		0.425
	4		1.277

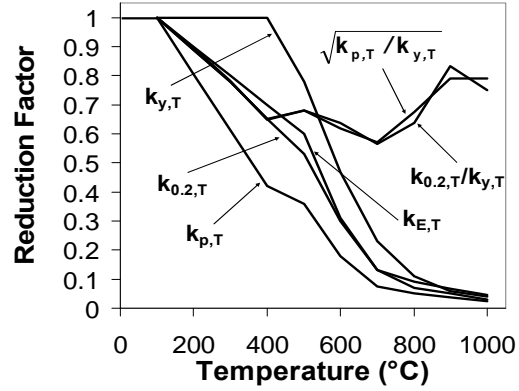


Fig. 1. Temperature-based reduction factors per Eurocode [2].

At elevated temperatures, steel will undergo a reduction of strength and stiffness, and its stress-strain relationship will become increasingly non-linear. Fig. 1 shows a plot of the reduction factors of yield strength ($k_{y,T}$), Young's modulus ($k_{E,T}$), and the proportional limit ($k_{p,T}$) versus temperature according to Eurocode [2]. The current AISC approach for calculating the ultimate buckling strength of steel plates at elevated temperature is the same as that used for ambient temperature design except that temperature-dependent reduction factors are applied to both yield strength and Young's modulus [1]. The non-dimensional slenderness at elevated temperature, $\lambda_{c,T}$, is therefore calculated as:

$$\lambda_{c,T}(AISC) = \sqrt{\frac{F_y k_{y,T}}{F_{cr,T}}} = \sqrt{\frac{12(1-\mu^2)(b/t)^2 F_y k_{y,T}}{k\pi^2 E k_{E,T}}} \quad (5)$$

No further reduction factors are specified for the calculations of effective width, b_e , and therefore also F_{cr}/F_y of the plate (Eq. 3 for example).

Eurocode uses a similar approach for calculating $\lambda_{c,T}$, except that the proof stress at 0.2% plastic strain, $F_{0.2}$, is substituted for yield strength [3]:

$$\lambda_{c,T}(Eurocode) = \sqrt{\frac{F_{0.2} k_{0.2,T}}{F_{cr,T}}} = \sqrt{\frac{12(1-\mu^2)(b/t)^2 F_{0.2} k_{0.2,T}}{k\pi^2 E k_{E,T}}} \quad (6)$$

Fig. 1 shows a plot of reduction factor $k_{0.2,T}$ versus temperature according to Eurocode and it shows that the values are smaller than $k_{y,T}$. The figure also plots $k_{0.2,T}/k_{y,T}$ versus temperature and shows this ratio to be on average about 0.7. Since the maximum stress in the plate is now assumed to be $F_{0.2}$ instead of F_y , Eqs. 3 and 4 are multiplied by $k_{0.2,T}/k_{y,T}$ to obtain values of $(F_{cr}/F_y)_{plate,T}$.

$$\text{Stiffened elements:} \quad \text{For } \lambda_c > 0.673: \quad \left(\frac{F_{cr}}{F_y}\right)_{plate,T} = \left(\frac{k_{0.2,T}}{k_{y,T}}\right) \left(\frac{1}{\lambda_{c,T}}\right) \left(1 - \frac{0.22}{\lambda_{c,T}}\right) \quad (7)$$

$$\text{Unstiffened elements:} \quad \text{For } \lambda_c > 0.748: \quad \left(\frac{F_{cr}}{F_y}\right)_{plate,T} = \left(\frac{k_{0.2,T}}{k_{y,T}}\right) \left(\frac{1}{\lambda_{c,T}}\right) \left(1 - \frac{0.188}{\lambda_{c,T}}\right) \quad (8)$$

COMPARISON OF AISC AND EUROCODE

Fig. 2 shows a comparison of the AISC and Eurocode models for both stiffened and unstiffened plates with pinned boundary conditions and uniform compression at ambient temperature, 300°C, and 600°C. The AISC and Eurocode plots are produced using the theoretical values of k (as shown in Table I). For the stiffened plate, both models produce a nearly identical prediction of ultimate plate strength at ambient temperature. As the steel temperature increases, the Eurocode curves decrease in magnitude according to reduction factor $k_{0.2,T}/k_{y,T}$. The AISC approach, however, does not account for any additional temperature-based reduction beyond the application of reduction factors to λ_c (Eq. 5), and thus its ultimate strength curves vary little with increasing temperature. This will be shown later in this study to be an unconservative prediction.

Fig. 2(b) also shows a similar temperature-slenderness relationship for the unstiffened plate based on the Eurocode and AISC methods. The shape of the ultimate strength curves for each approach is different mainly because Eurocode calculates capacity with an effective width calculation and AISC uses an average stress approximation.

Note that the Eurocode curves for elevated temperature in Fig. 2 experience a sudden discontinuity (cutoff) at $\lambda_{c,T} = 0.673$ for stiffened plates and at $\lambda_{c,T} = 0.748$ for unstiffened plates. This sudden change in predicted strength at elevated temperature is used by Eurocode because the solution of Eqs. 7 and 8 may be discontinuous when $k_{0.2,T}/k_{y,T}$ is less than one. In other words, the maximum value of the solution may never reach a value of $F_{cr}/F_y = 1$ unless a cutoff is enforced, as shown in Fig. 2.

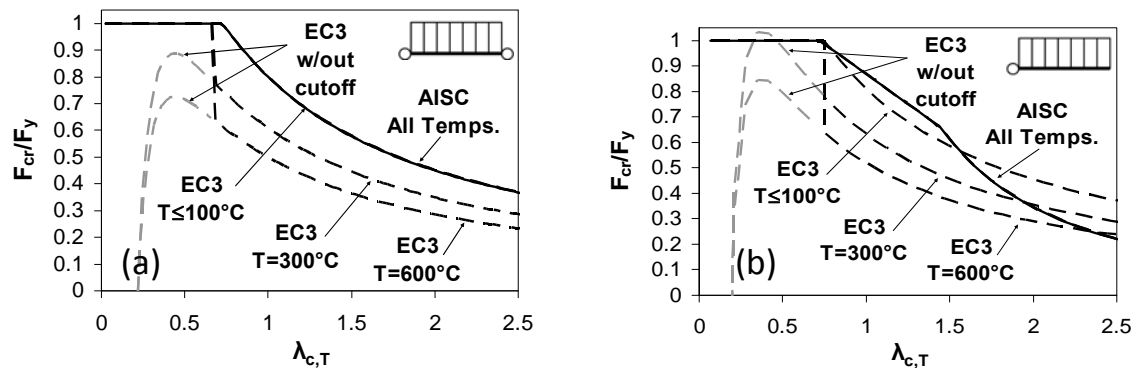


Figure 2. Ultimate strength of (a) stiffened and (b) unstiffened plates according to AISC and Eurocode.

PARAMETRIC COMPUTATIONAL STUDY

A series of computational analyses were conducted to generate ultimate strength curves for thin steel plates under axial compression at elevated temperature. These curves were used to (1) evaluate the accuracy of both the AISC and Eurocode approaches to calculating the ultimate strength of steel plates, and (2) calibrate a new approach that addresses the aforementioned shortcomings of the existing codified approaches.

Non-linear structural analysis of shell-element models representing stiffened and unstiffened plates was performed using SAFIR, a software specifically designed for the analysis of structures exposed to fire [5]. The plates were modeled with a square discretization scaled to 10% of the plate width, b . The length of the modeled plates was scaled according to the aspect ratio of the lowest

buckling mode. Steel material properties at elevated temperature, including a non-linear stress-strain relationship, were based on Eurocode [3].

Table I shows the four boundary condition cases considered for this study. The authors also examined 3 additional cases with linearly varying stresses but these are not discussed in this paper and can be found in [4]. The loaded edges on each end of the plate were modeled as pinned. Lateral and out-of-plane translation of supported edges parallel to the direction of loading was restrained. For each case, a series of analyses was conducted for a range of width-to-thickness ratios over a range of temperatures relevant to design as well as at ambient temperature. In each analysis, shell elements were modeled with uniform temperature, and axial compression loads were linearly increased until the analysis terminated. At this point, the plate had reached either its ultimate local buckling load or its plastic capacity, depending on its slenderness.

Residual stresses were not included in computational shell-element models of stiffened and unstiffened plates in this study since such tends to relax in a fire [6]. The models did include the effects of initial geometric imperfections. Sinusoidal initial imperfections were modeled as having the same wavelength as the lowest buckling mode obtained from linear analysis of the plate at ambient temperature. Based on the results of several studies [7, 8, 9, 10], our analyses consider initial imperfection magnitudes of both $b/200$ and $0.1t$ for comparison.

PROPOSED APPROACH

A new stress-based approach is proposed for calculating the ultimate strength of stiffened and unstiffened steel plates under uniform compression at elevated temperature:

$$\text{For stiffened plates: } \frac{b_e}{b} = \left(\frac{F_{cr}}{F_y} \right)_{plate,T} = \frac{1.41}{\sqrt{\lambda_{c,T}} \sqrt{k}} \sqrt{\frac{k_{p,T}}{k_{y,T}}} \left(1 - \frac{0.96}{k \lambda_{c,T}^{0.5}} \right) < 1 \quad (9)$$

$$\text{For unstiffened plates: } \frac{b_e}{b} = \left(\frac{F_{cr}}{F_y} \right)_{plate,T} = \frac{0.81}{\sqrt{\lambda_{c,T}} \sqrt{k}} \sqrt{\frac{k_{p,T}}{k_{y,T}}} \left(1 - \frac{0.084}{k \lambda_{c,T}^{0.5}} \right) < 1 \quad (10)$$

$\lambda_{c,T}$ is calculated according to Eq. 5 and k accounts for the effects of boundary conditions (see Table I). These expressions calculate ultimate strength using an effective width method similar to those originally proposed by Winter [11] and implemented by AISC and Eurocode. The form of Eqs. 9 and 10 is kept similar to those of codified standards for consistency but includes the temperature-based modification $\sqrt{k_{p,T}/k_{y,T}}$. These new expressions are continuous functions that can be calculated for any ratio of b_e/b less than one, an advantage over the Eurocode equations which include a discontinuity at $\lambda_{c,T} = 0.673$ (for stiffened elements) or 0.748 (for unstiffened elements) to reach $b_e/b = 1$ (see Fig. 2).

The proposed approach includes a similar reduction of ultimate plate strength as that prescribed by Eurocode. A plot of $\sqrt{k_{p,T}/k_{y,T}}$ as a function of temperature in Fig. 1 shows that this proposed reduction factor used in Eqs. 9 and 10 produces a similar reduction of ultimate strength as the $k_{0.2,T}/k_{y,T}$ factor used in Eurocode. The proposed reduction allows the user to avoid using the 0.2% plastic strain concept, which is not used in the AISC specifications for calculating the ultimate strength of plates.

VALIDATION OF PROPOSED APPROACH

Before proceeding to the analysis of plates at elevated temperature, ultimate plate strength at ambient temperature is examined in Fig. 3 for the stiffened and unstiffened (pinned) boundary conditions. Good agreement is seen between the capacity calculated using “proposed” Eqs. 9 and 10 at ambient temperature and (1) the corresponding curves obtained from computational analysis with initial imperfections of $b/200$ and $0.1t$, and (2) the curves calculated according to AISC and Eurocode. Because of this good agreement, these imperfection magnitudes can be used to accurately predict ultimate strength at elevated temperature since they will have similar influence as at ambient temperature [12]. Examination of the $\delta = 0.1t$ and $\delta = b/200$ curves indicate that initial imperfections lead to reductions of buckling strength for intermediate values of λ_c .

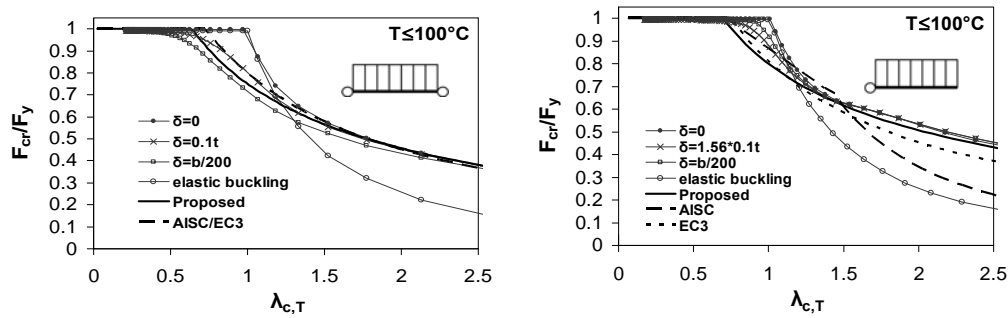


Figure 3. Ultimate strength curves at ambient temperature (i.e. $T \leq 100^\circ\text{C}$) for (left) a stiffened plate and (right) unstiffened plate with pinned ends and uniform compression.

Fig. 4 shows the ultimate plate strength curves for a stiffened plate with *pinned* ends and uniform stress distribution along its width for a three different temperatures. This figure shows good agreement between the proposed approach (Eq. 9) and the computationally obtained ultimate plate strength curves at elevated temperature. The $\sqrt{k_{p,T} / k_{y,T}}$ reduction factor used in Eq. 9 provides an accurate prediction of ultimate strength reduced by temperature-based changes in the material properties of steel. Good agreement is also shown between the proposed approach and the Eurocode model for values of $\lambda_{c,T} > 0.673$. For $\lambda_{c,T} < 0.673$, the proposed approach provides a reasonable prediction of strength whereas the Eurocode model unconservatively predicts that the plate will reach full yield. The proposed approach also delivers a much more accurate prediction of strength at elevated temperature in this case than the curves corresponding to AISC specifications.

Fig. 5 shows the ultimate plate strength curves for an unstiffened plate with *pinned* ends and uniform stress distribution along its width for three temperatures. This figure shows similar agreement between the proposed approach and the computational results at elevated temperature. As with the stiffened elements, the Eurocode model shows reasonable agreement with the proposed approach for $\lambda_{c,T} > 0.748$ and is unconservative for $\lambda_{c,T} < 0.748$ due to the vertical cutoff at $\lambda_{c,T} = 0.748$. At elevated temperature, the AISC prediction becomes increasingly unconservative because it does not include reductions beyond those included in Eq. 5.

Fig 6 shows the ultimate strength curves for a stiffened and unstiffened plate with *fixed* boundary conditions at $T = 700^\circ\text{C}$. The “Proposed” curve is based on Eq. 9 with $k = 6.97$ for the stiffened plate and Eq. 10 with $k = 1.277$ for the unstiffened plate. Good agreement is again shown between the solution of the proposed approach and the computational results. Comparison to the Eurocode and AISC predictions is similar as for pinned boundary conditions.

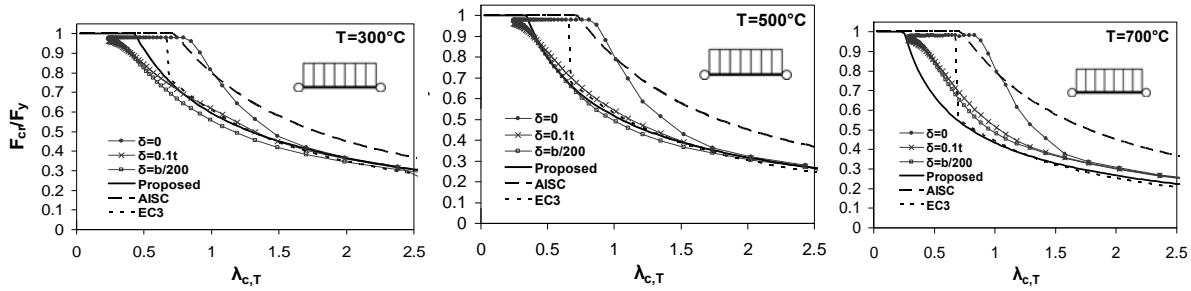


Figure 4. Ultimate strength curves for a stiffened plate with pinned ends at $T = 300^\circ\text{C}$, 500°C , and 700°C .

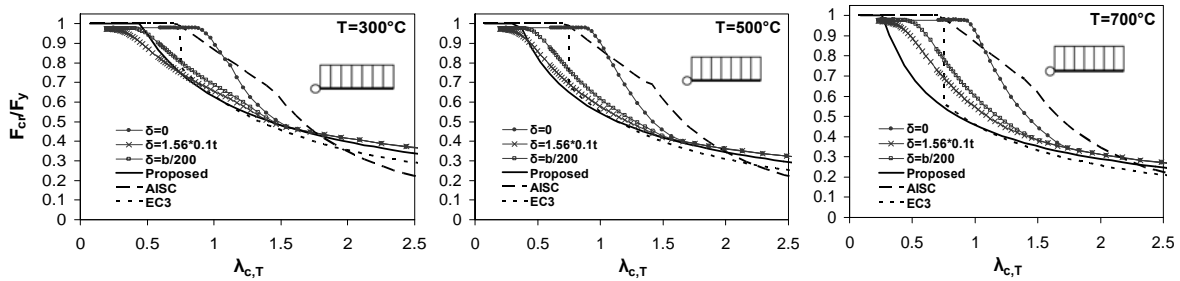


Figure 5. Ultimate strength curves for an unstiffened plate with pinned ends at $T = 300^\circ\text{C}$, 500°C , and 700°C .

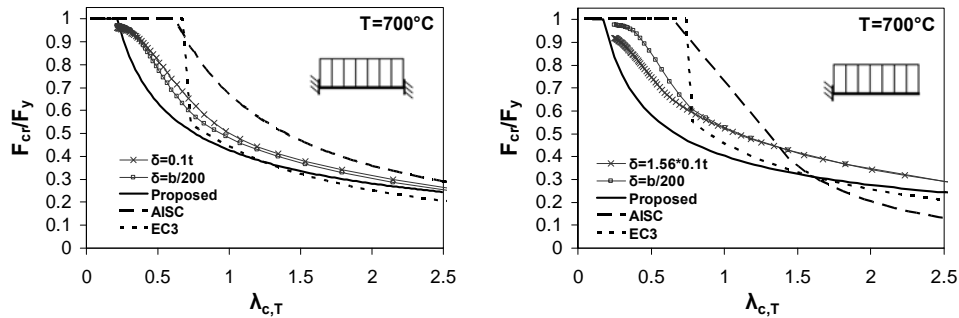


Figure 6. Ultimate strength curves at $T = 700^\circ\text{C}$ for (left) a stiffened plate and (right) unstiffened plate with fixed ends.

CONCLUSIONS

The methods currently available for calculating the local buckling strength of thin steel plates under compression at elevated temperature were evaluated, and a new approach was proposed to address their limitations. The proposed approach was developed via calibration against the results of parametric computational analyses of stiffened and unstiffened steel plates that included initial imperfections as recommended by previous studies by other researchers. For each plate type, the proposed approach used a single continuous function to calculate an effective width over which maximum stress is applied. These expressions used temperature-based reduction factors whose magnitudes were similar to those used by Eurocode to predict the reduction of ultimate plate strength at elevated temperature. The proposed expressions showed good agreement with computational results for a range of temperatures, boundary conditions, and loading scenarios.

Both AISC and Eurocode standards provide similar predictions of ultimate strength as the proposed approach and the computational results for steel plates at ambient temperature. Comparisons of plate buckling strengths at elevated temperature showed that current AISC methods for predicting the ultimate strength of heated plates are unconservative. Eurocode standards provide an accurate prediction of strength for most values of plate slenderness. However, the Eurocode equations are unable to accurately predict strength for some plates with low slenderness because they become discontinuous when temperature-based reduction factors are included. Also, the Eurocode expressions use the 0.2% proof stress as a substitute for yield stress at higher temperatures, a concept not commonly used by North American practice. It is intended that the proposed expressions, which use a similar stress-based approach as the Eurocode but do not include the 0.2% proof stress, be used as an adequate substitute for either standardized approach in design due to its accuracy and simplicity.

ACKNOWLEDGMENTS

The research presented in this paper is based on work that is co-sponsored by the National Science Foundation (NSF) (under grant number CMMI-0652282) and the National Institute of Standards and Technology (NIST) (under grant number 60NANB7D6121). Dr. Quiel's involvement with this research project began while on appointment as a U.S. Department of Homeland Security (DHS) Fellow under the DHS Scholarship and Fellowship Program, which is administered by the Oak Ridge Institute for Science and Education (ORISE) for DHS through an interagency agreement with the U.S. Department of Energy (DOE). ORISE is managed by Oak Ridge Associated Universities under DOE contract number DE-AC05-00OR22750. All opinions, findings, and conclusions expressed in this paper are the authors' and do not necessarily reflect the policies and views of the NSF, NIST, DHS, DOE, or ORISE.

REFERENCES

1. AISC. Steel Construction Manual, Thirteenth Edition. Chicago: American Institute of Steel Construction, 2005.
2. CEN. Eurocode 3: Design of Steel Structures, Part 1.2: General Rules—Structural Fire Design (ENV 1993-1-2:2001). Brussels: European Committee for Standardization, 2001.
3. CEN. Eurocode 3: Design of Steel Structures, Part 1.5: Plated Structural Elements (ENV 1993-1-5:2004). Brussels: European Committee for Standardization, 2004.
4. Quiel, S., Garlock, M. Calculating the buckling strength of steel plates exposed to fire. *Thin-Walled Str* 2010; tentatively accepted for publication.
5. Franssen, J-M. SAFIR: A thermal/structural program for modeling structures under fire. *AISC Eng J* 2005;42:143-158.
6. Tide, RHR. Integrity of structural steel after exposure to fire. *AISC Eng J* 1998;35:26-38.
7. Ala-Outinen, T and Myllymäki, J. The local buckling of RHS members at elevated temperatures. VTT Research Notes 1672. Espoo, Finland: Technical Research Centre of Finland (VTT), 1995.
8. Hancock, GJ. Nonlinear analysis of thin sections in compression. *ASCE J Struct Div* 1981;107:455-471.
9. Kaitila, O. Imperfection sensitivity analysis of lipped channel columns at high temperatures. *J Constr Steel Res* 2002;58:333-351.
10. Feng, M, Wang, YC, Davies, JM. A numerical imperfection sensitivity study of cold-formed thin-walled tubular steel columns at uniform elevated temperatures. *Thin-Walled Str* 2004;42:533-555.
11. Winter, G. Strength of thin steel compression flanges. *ASCE Transactions* 1947;112:527-554.
12. Ranby, A. Structural fire design of thin walled steel sections. *J Constr Steel Res* 1998;46:303-304.

A Study on Damage Mechanism of Thick Fireproof Coating for Steel Member Subjected to Monotonic Loading

S.-W. CHEN, J. CHU and G.-Q. LI

ABSTRACT

Post-earthquake fire is an important issue for buildings in seismic zone, especially for the steel buildings. To evaluate fire resistance of steel buildings after earthquake, one should consider the seismic induced damage to the fire protection of steel member. Thick fireproof painting is one of the most frequently used ways to protect steel members from fire.

In this paper, firstly a series of experiments have been conducted for obtaining the mechanical properties of fireproof material, including compressive strength, tensile strength, normal bonding strength and shear bonding strength between the coating and the steel member. Then, for investigating the damage mechanism of fireproof coating, a series of monotonic loading experiments have been conducted on fireproof coated steel members in compression, or in tension, or in bending. After that, the interlaminar stress analysis has been carried out. From the interlaminar stress analysis and experimental study, damage mechanism of thick fireproof coating when steel member subjected to monotonic loading has been revealed.

Su-wen Chen, PhD, Associate Professor, State Key Laboratory for Disaster Reduction in Civil Engineering, College of Civil Engineering, Tongji University, Shanghai, 200092, P.R. China

Jin Chu, Graduate Student, Dept. of Building Engineering, College of Civil Engineering, Tongji University, Shanghai, 200092, P.R. China

Guo-qiang Li, PhD, Professor, State Key Laboratory for Disaster Reduction in Civil Engineering, College of Civil Engineering, Tongji University, Shanghai, 200092, P.R. China

INTRODUCTION

Steel has been widely used in modern civil engineering because of its advantages. However, fire-resistance of steel is poor. The strength and elastic modulus of steel decrease with the increase of temperature. At 500°C temperature, the yield strength and ultimate strength may drop to half of that at room temperature [1]. Thus it is necessary to take measures to protect steel structures from fire, while the fire protection may be damaged due to earthquake or other actions. To evaluate fire resistance of the steel buildings after earthquake, one should consider the seismic induced damage to the fire protection of steel member. There are few researches in this topic yet [2].

Thick fireproof coating is one of the most frequently used ways to protect steel members from fire. To analyze the seismic induced damage to thick fireproof coating, one needs to know the mechanical properties and bonding performance between the coating and steel member. But there are few researches on the mechanical properties of fireproof coating material till now with only minimum requirements of compressive strength and normal bonding strength for product. For an example, Chinese code GB14907-2002 requires indoor thick fireproof coating for steel structure to meet: the normal bonding strength $\geq 0.04\text{MPa}$, and the compressive strength $\geq 0.3\text{MPa}$ [3].

In this paper, a series of experiments have been conducted on the mechanical properties of thick fireproof coating material, including compressive strength, tensile strength, normal bonding strength and shear bonding strength between the coating and the steel member since these are basic properties for analyzing the damage to the fire proof coating. Then, for investigating the damage mechanism of fireproof coating, a series of experiments have been conducted on fireproof coated steel members in compression, or in tension, or in bending. After that the interlaminar stress analysis has been carried out. From the interlaminar stress analysis and experimental study, damage mechanism of thick fireproof coating when steel member subjected to monotonic loading has been revealed.

MECHANICAL PROPERTY EXPERIMENTS OF THICK FIREPROOF MATERIAL

YC-1 thick fireproof material is used in this experiment. According to the product instruction, weight proportion of interfacial agent is specific interfacial agent : YC-1: water = 1 : 3 : 2.5 and weight proportion of coating is YC-1: water = 1 : 0.86. The specimens would be conserved in room condition for 28 days.

For compressive strength, the specimen preparations and the experiments (Figure 1) are carried out according to chinese code GB14907-2002, with the mode size in 70.7mm x 70.7mm x 70.7mm. The failure mode is shown in Figure1(c).



(a) Specimen (b) Experiment setup (c) Failure mode

Figure 1. Compressive strength experiment.

Then the compressive strength can be calculated as:

$$f_c = \frac{F_c}{A_c} \quad (1)$$

Where, f_c , F_c and A_c are compressive strength (MPa), ultimate load (N) and Compressive area (mm^2), respectively.

For the tensile strength, the specimen can't be clamped directly because the strength of fireproof material is too low. Thus, we designed a new experimental way. The specimen of tensile strength is shown in Figure 2(a) with end section of 90mm x 90mm and mid-section of 50mm x 90 mm, where supposed to be failure location. After 28 days' curing, both ends of the specimen are respectively glued to a steel T-stub with epoxy resins and the experiments would be conducted as Figure 2(b) with the failure mode shown in Figure 2(c).



(a) Specimen (b) Experiment setup (c) Failure mode

Figure 2. Tensile strength experiment.

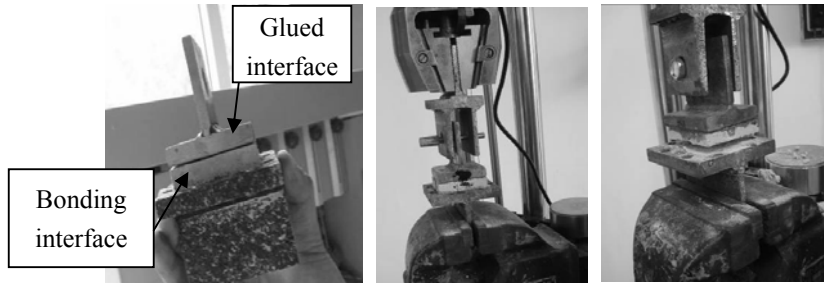
The tensile strength can be calculated as:

$$f_t = \frac{F_t}{A_t} \quad (2)$$

Where, f_t , F_t and A_t are tensile strength (MPa), ultimate load (N) and Tensile area (mm^2), respectively.

For preparing bond strength experimental specimen, firstly interface agent in 2-3mm thickness is painted on steel surface followed by coating painted 12 hours later.

Before loading, the top face would be glued to a steel T-stud with epoxy resins as Figure 3(a). Then, the experiment will be conducted as shown in Figure3(b) with the failure mode shown in Figure 3(c).



(a) Specimen (b) Loading style (c) Failure mode

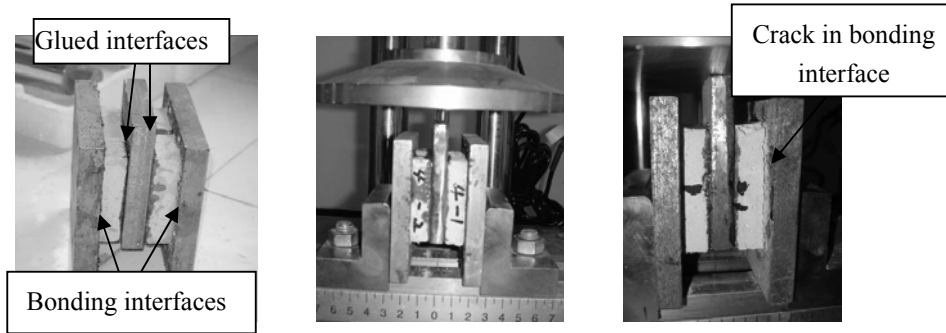
Figure 3. Normal bonding strength experiment.

Then the normal bonding strength can be obtained as:

$$f_n = \frac{F_n}{A_n} \quad (3)$$

Where, f_n , F_n and A_n are normal bonding strength (MPa), ultimate load (N) and normal bonding area (mm²), respectively.

The shear bonding strength specimen and experimental set-up is shown in Figure 4(a) and (b) with the failure mode shown in Figure 4(c).



(a) Specimen (b) Experiment setup (c) Failure mode

Figure 4. shear bonding strength experiment.

The shear bonding strength can be get from:

$$f_s = \frac{F_s}{A_l + A_r} \quad (4)$$

Where, f_s , F_s , A_l and A_r are shear bonding strength (MPa), ultimate load (N), shear bonding areas on the left (mm²) and on the right (mm²), respectively.

The property results of the fireproof coating from the experiments are listed in the Table I, which satisfy the requirements of GB14907-2002.

TABLE I THE PROPERTY RESULTS OF THE FIREPROOF MATERIAL

Density (g/cm ³)	f_c (Mpa)	E_c (MPa)	f_t (Mpa)	f_n (Mpa)	f_s (Mpa)
0.55	0.59	32.43	0.05	0.04	0.07

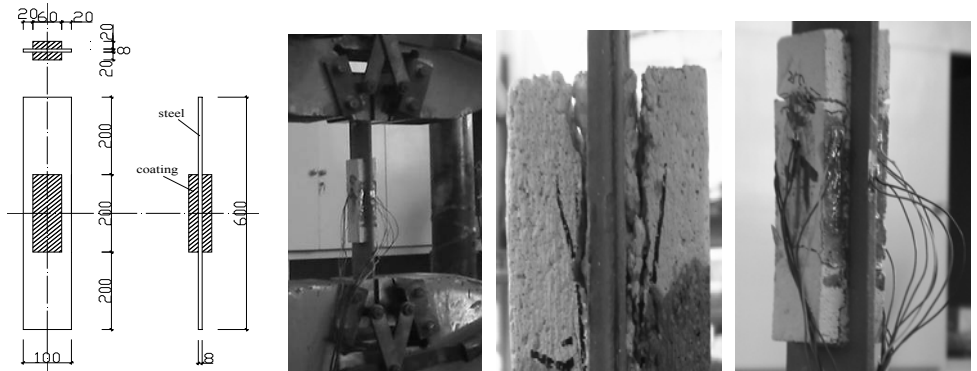
EXPERIMENTS OF FIREPROOF COATED STEEL MEMBERS IN TENSION, IN COMPRESSION OR IN BENDING

For each set of these steel member experiments, four specimens with 20mm-thickness coating are prepared.

For tension experiment, the dimension of specimen is shown in Figure5(a) and the test set-up is shown in Figure5(b). With the loading going on, firstly the interfacial cracks at the ends observed and then detachments(Figure5(c)) followed by the transverse cracks of the coating layers(Figure5(d)). Finally the specimen ruptured into several segments without falling down.

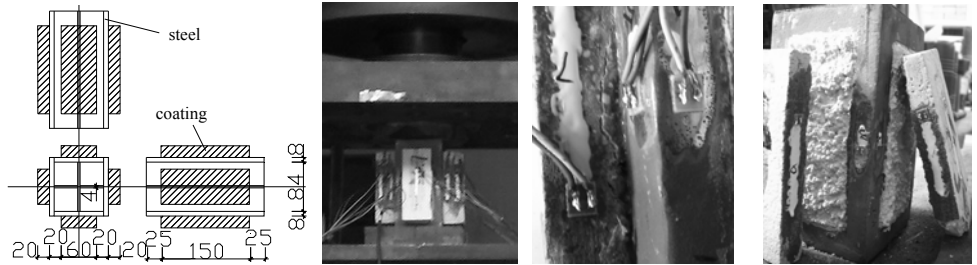
For compression experiment, the specimen is shown in Figure6(a) and the experiment is conducted as Figure6(b). With the loading going on, firstly interfacial cracks appear and develop (Figure6(c)). Finally all the coating layers fell off (Figure6(d)). No damage in the coating itself is observed.

For the bending case, the dimension of the specimen is shown in Figure7(a) and the test is carried out as in Figure7(b). The interfacial cracks at ends both in compression and tension are firstly observed followed by some minor transverse tensile cracks. With the loading going on, more cracks developed and widened especially after the yielding of steel plate. Finally the compression layer crushed at both ends (Figure7(c)) and the tension layer ruptured into several segments (Figure7(d)). The failure mode is shown in Figure7(e).



(a) Specimen (b) Loading set up (c) Detachment (d) Failure mode

Figure 5. Tension experiment



(a) Specimen (b) Loading set up (c) Cracked (d) Fell off

Figure 6. Compression experiment.

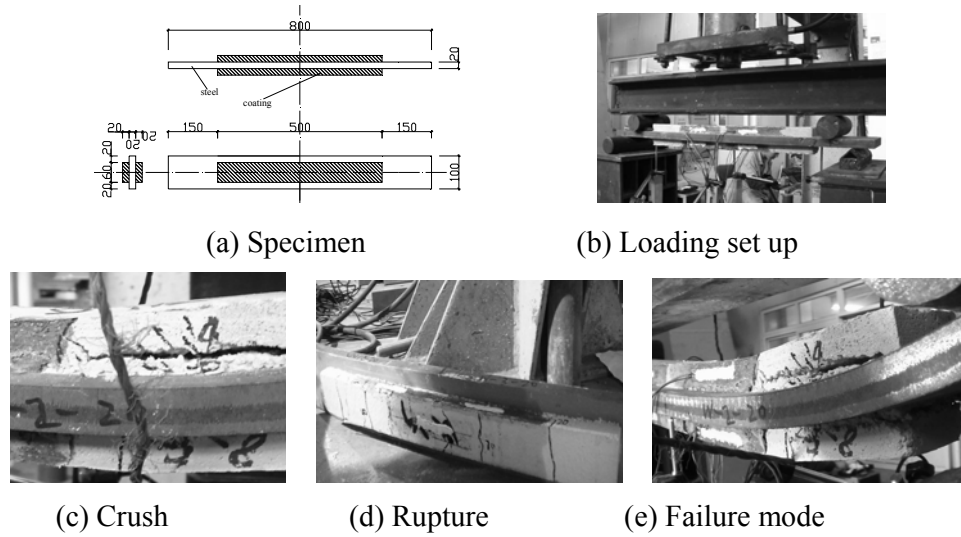


Figure 7. Bending experiment.

INTERLAMINAR STRESS ANALYSIS

To study the damage mechanism of thick fireproof coating, interlaminar stress between the coating and steel is investigated. There are two kinds of interlaminar stress: normal interlaminar stress and shear interlaminar stress. The principle of the interlaminar stress theory is briefly explained as follows[4].

Basic assumptions are adopted herein : 1) Both steel and fireproof coating material are assumed isotropic. 2) The stress is in elastic range. 3) Plane cross-section assumption.

The shear and normal interlaminar stresses are expressed as following:

$$\tau_0 = \sum_{n=1}^{\infty} a_n \sin \frac{n\pi x}{l}, \quad \sigma_0 = \sum_{n=1}^{\infty} b_n \cos \frac{n\pi x}{l} \quad (5)$$

Where a_n and b_n are coefficients to be determined.

When the steel plate is loaded in simple condition, such as in compression, in tension or in bending, analytical resolutions of interlaminar stresses can be obtained considering the equilibrium condition and Minimum Energy Principle[3].

Then, the S.E.Yamada criterion [5] are adopted to analyze the damage of fireproof coating. When s calculated from Eq.(6) is larger than 1, it means the failure happens, otherwise not.

$$\left(\frac{\sigma_0}{f_n} \right)^2 + \left(\frac{\tau_0}{f_s} \right)^2 = s^2 \quad (6)$$

THE DAMAGE MECHANISM OF FIREPROOF COATING

Interlaminar stress analysis is carried out to analyze the aforementioned steel

plate tension experiment as shown in Figure 5. The distributions of the normal and shear interlaminar stresses along the length are shown in Figure 8, in which half length is shown because of symmetry and the origin of the curve is the middle point of the specimen.

From Figure 8(a), the normal interlaminar stress at the end is the maximum along the length, which explains the detachment of coating from the steel plate as shown in Figure 5 (c). From the Figure 8 (b), the shear interlaminar stress peaks in the zone of $l/10 \sim l/5$ away from the end and the normal interlaminar stress at this zone reaches the negative maximum. This may imply that the zone of $l/10 \sim l/5$ from the end may be “danger zone” because s from Eq. (6) may be the largest. This means that the coating in this zone may be fractured, which is demonstrated by Figure 5(d).

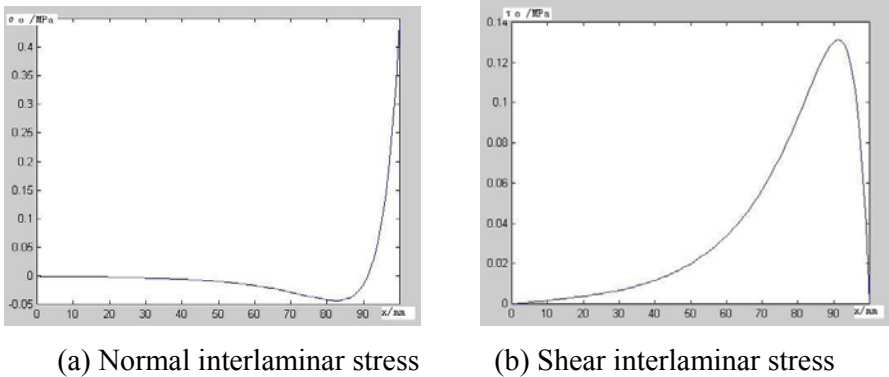


Figure 8. Distributions of interlaminar stresses when steel plate in tension.

When the steel plate is in compression, no damage in the coating itself would occur and the coating would detach from the steel plate and finally fall off because the coating’s compressive strength is much larger than the shear bonding strength and normal bonding strength.

For an example, when the compressive force is 300 kN, the maximum negative normal interlaminar stress and shear interlaminar stress can be calculated as: $\sigma = -0.0137\text{MPa}$, $\tau = 0.0664\text{MPa}$. Substitute them into Eq. (6), we can get $s = 1$, which means the failure of the interface. Nevertheless, the compressive strength of the coating is 0.59MPa and much larger than the interlaminar stress, with no damage in the coating itself. This agrees well with the experimental phenomenon in Figure 6.

For the steel plate in bending as tested in Figure 7, the distributions of the normal and the shear interlaminar stresses along the length are shown in Figure 9. Also only half length is shown because of symmetry and the origin of the curve is the mid-point.

From Figure 9, similar phenomenon is observed with the tension case, the normal interlaminar stress reaches maximum at the end and implies the end interfacial crack. And the peak of the shear interlaminar stress locates in the zone of $l/20 \sim l/10$ from the end and the negative peak of the normal interlaminar stress locates at the same zone, which implies that the zone of $l/20 \sim l/10$ may be dangerous for bending case.

Take the test shown in Figure 7 as an example. When the moment is

1200N.m, the maximum negative normal and maximum shear interlaminar stress can be calculated as: $\sigma=-0.0212\text{MPa}$, $\tau=0.0582\text{MPa}$. Substitute them into Eq. (6), we can get $s^2=0.97<1$ which means no failure at the interface. And the surface tensile stress can be calculated as follows

$$\sigma = \frac{6}{bh_c^2} \frac{E_c I_c}{2E_c I_c + E_s I_s} M = 0.05\text{MPa} \quad (7)$$

Thus, the surface tensile stress reaches the tensile strength, 0.05Mpa from TABLE I, and causes the tensile cracks and even fractures. After the fracture, the interlaminar stress may release. In compressive area, damage won't occur in the coating itself because of high compressive strength but the composited stress s in the danger zone may reach the limit and cause the detachment of the coating layer. This agrees well with the phenomenon as shown in Figure 7.

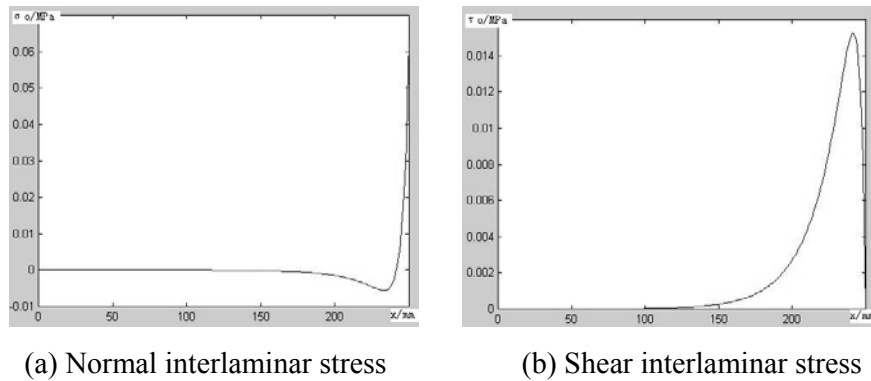


Figure 9. Distribution of interlaminar stresses when steel plate in bending

CONCLUSION

In this paper, the mechanical property experiments of thick fireproof material are firstly introduced and tensile strength, compressive strength, shear and normal bonding strengths are obtained. Then a series of monotonic loading experiments are carried out for fireproof coated steel members when in tension, in compression and in tension and damage mode and development are observed. After that, the interlaminar stress analysis are carried out and well explain the experimental phenomena.

ACKNOWLEDGMENTS

This research was financially supported by National Nature Science Foundation of China through project No. 50808143 and State Key Laboratory for Disaster Reduction in Civil Engineering.

REFERENCES

1. Guo-qiang Li, Lin-hai Han Guo-biao Lou, Shou-chao Jiang. 2006. Fire resistant design for steel structure and steel-concert composite structure, China Architectural Building Press.

2. Wei-Yong Wang,2008,Damage Mechanism of Fire Protection on Steel Columns under Earthquake and Influence of Damage on the Fire : [Ph.D thesis],School of Civil Engineering Tongji University.
3. GB14907-2002, Fire resistive coating for steel structure, People's Republic of China.
4. F.F.Zhang,1993,The interlaminar stress theory of composited material, High Education Press.
5. S.E.Yamada,C.T.Sun,1978, "Analysis of laminated strength and its distribution", J. of Composited materials, Vol 12, July.

CONCRETE STRUCTURES

New Regulations for Hollow Core Slabs After Premature Partial Collapse

T. VAN OVERBEEK, A. BREUNESE, J. GIJSBERS, K. BOTH,
J. MALJAARS and L. NOORDIJK

ABSTRACT

In October 2007, a floor made up of pre-cast prestressed hollow core floor elements suffered early partial collapse during a fire in a carpark of a moderately high new building in Rotterdam, predominantly in use for housing and for limited enterprise.

The damage pattern revealed horizontal cracks through the webs of the hollow core slabs, causing collapse of the underflanges which contain the prestressing strands. As a consequence, the structural integrity of the floor and the entire building was jeopardized.

In 2007, the municipal authorities of Rotterdam commissioned Efectis Nederland to investigate the damage that occurred during the fire. The results of the study strongly recommended further investigation and addressing the observed damage pattern in the assessment and design rules for hollow core slabs.

Based on this conclusion, TNO was commissioned in 2008 by BFBN (Dutch precast industry) to further investigate the incident and whether or not this early partial collapse concerns an omission in the current regulations.

Ton van Overbeek, M.Sc., TNO Built Environment and Geosciences, Van Mourik Broekmanweg 6, 2628 XE, Delft, The Netherlands

Arnoud Breunese, M.Sc., Efectis Nederland, Lange Kleiweg 5, 2288 GH, Rijswijk, The Netherlands

Jan Gijsbers, M.Sc., TNO Built Environment and Geosciences, Van Mourik Broekmanweg 6, 2628 XE, Delft, The Netherlands

Kees Both, Ph.D., Efectis Nederland, Lange Kleiweg 5, 2288 GH, Rijswijk, The Netherlands

Johan Maljaars, Ph.D., TNO Built Environment and Geosciences, Van Mourik Broekmanweg 6, 2628 XE, Delft, The Netherlands

Leander Noordijk, M.Sc., Efectis Nederland, Lange Kleiweg 5, 2288 GH, Rijswijk, The Netherlands

TNO concluded that the structure did meet the requirements stated by the authorities, the fire development did not significantly deviate from the standard fire curve, the damage pattern has been observed more often, and the fire resistance of hollow core slabs in fire tests is often lower than the expected fire resistance based on current regulations. Therefore, TNO concluded that the current regulations contain an omission.

Therefore, additional detailing and design rules for hollow core slabs were advised by BFBN, which are partially based on new rules for hollow core slabs developed by CEN.

This paper addresses the research commissioned by the municipal authorities of Rotterdam, the research commissioned by BFBN and the additional rules advised by BFBN. This includes the fire development and damage to the hollow core slabs in the carpark in Rotterdam, the relevant collapse mechanisms for hollow core slabs in case of fire, their relative importance and respective uncertainties, and the measures taken in the new rules.

DESCRIPTION OF BUILDING

The immediate cause of the investigations presented here is the damage following a fire in the moderately high new building “Harbour Edge” in Rotterdam, The Netherlands. The twelve-storey building is predominantly in use for housing and for limited enterprise and was completed in 2007. The lower part of the building contains a two-storey open car park. The building is presented in figure 1.

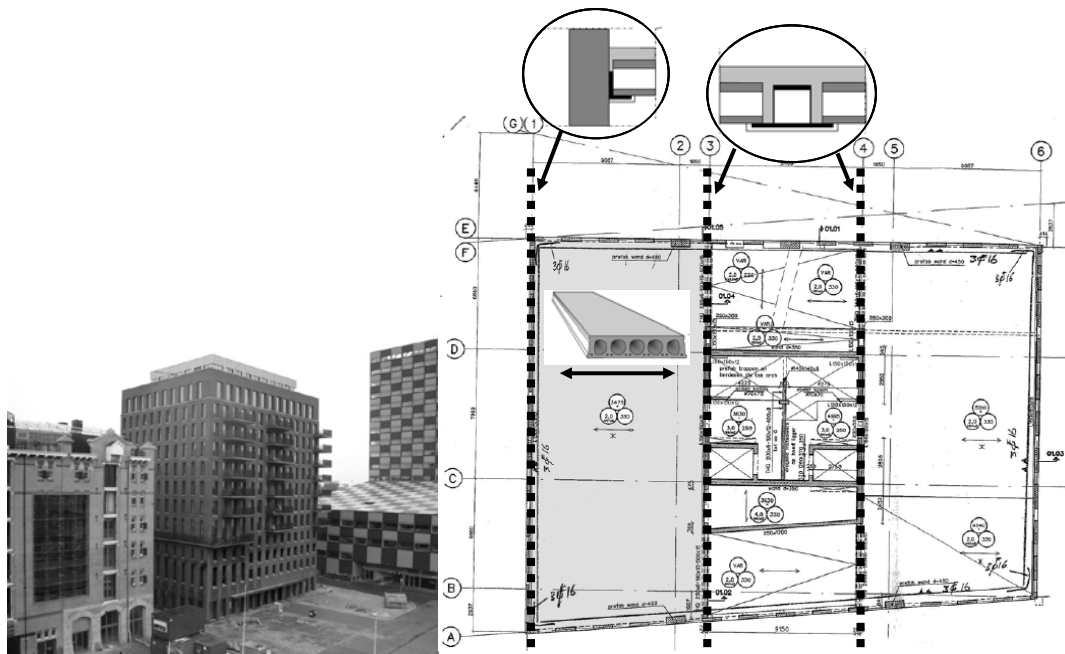


Figure 1. The building “Harbour Edge” in Rotterdam, The Netherlands (Left) and overview of structure in car park (Right) [5].

The building is primarily a concrete structure with a pile foundation. At the fire location the load bearing structure of the floors consists of hollow core slabs with a height of 260 mm, and on top of it a compression layer with a varying thickness of some 70 to 90 mm. The hollow core slabs span a distance of approximately 11 meters and the concrete cover on the pre-stressing strands is approximately 40 mm. These hollow core slabs are supported on steel L-sections that are fixed to the precast concrete building façade (in figure 1, see axes 1 and 6).

On axes 3 and 4 the floors are supported by steel L-sections that are fixed to the walls of the concrete building core, and on THQ-beams that span from the core to the façade. All exposed steel flanges are fire protected.

FIRE AND DAMAGE

On October 1st 2007, one car caught fire on the second floor of the car park. The fire spread to five other cars. About 45 minutes later most of the combustible materials had burnt and the remaining fire was extinguished. See Figure 2.

During the fire, the fire brigade had to withdraw because of the noise of concrete falling down from the ceiling. Their impression was that parts of the hollow core slabs were collapsing. After extinguishing of the fire it appeared that six hollow core slabs had cracked horizontally through the webs, separating the slabs in an upper and lower half (comprising the pre-stressing strands). After extinguishing it was observed that four slabs had completely collapsed, as a consequence of these cracks. In the hours after the fire, two more slabs collapsed.

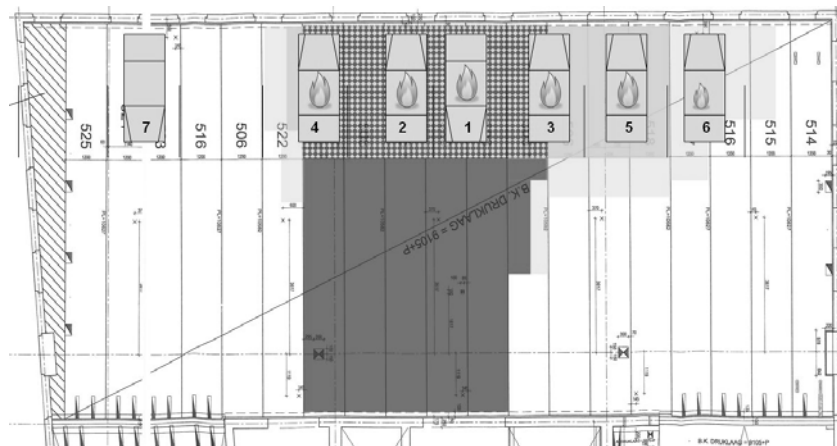


Figure 2. Top view of the car park with the positions of the burned cars Green = spalling of the concrete ceiling, red = hollow core slabs horizontally cracked [5].



Figure 3. Collapsed bottom halves of hollow core slabs (right) and top half of a hollow core slab after the fire (right) [5]

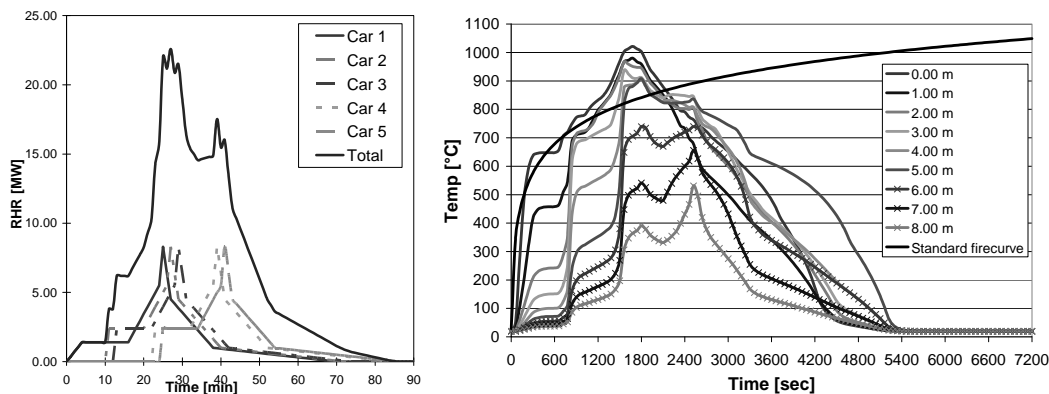


Figure 4. Heat release rate (left) and temperature development on different locations (right) [5].

Based on the damage pattern and observations from fire brigade and eyewitnesses the fire development has been reconstructed. It is assumed that the 2nd and 3rd car were ignited 10 and 12 minutes after the first car, and the 4th and 5th car were ignited 22 and 24 minutes after the first car. The heat release rate and temperature development have been calculated using CaPaFi, that uses the design rules for localised fires as described in Eurocode 4. The calculated heat release rate and temperature development on different locations is shown in figure 4. The temperature development is in the latter figure also compared with the ISO 834 standard fire curve.

BUILDING REGULATIONS

In The Netherlands fire resistance requirements with regard to collapse are related to the main load bearing structure and on the structural parts of whom the collapse leads to an escape route becoming unserviceable. The Dutch Building Decree means by main load bearing structure that part of the building structure of which lacking leads to lacking of structural parts that are not in the immediate vicinity of the lacked component. The fire resistance requirements made in the Building Decree are performance requirements. The main load bearing structure

must be provided with sufficient fire resistance to maintain stability for the design time, under standardised fire circumstances (ISO 834), to the in the Dutch Standards mentioned special load combinations that can occur in case of fire. The required level of performance (design time) varies according to height and purpose. For concrete structures there are two determination methods namely NEN 6069 for experimental determination and NEN 6071 for arithmetical determination. In NEN 6069 and NEN 6071 is not explicitly specified that mechanical stresses due to restrained thermal expansion have to be taken into account. Therefore, in practice this is rarely done. Usually the verification is done by calculation, solely checking bending moment capacity. This comes down to a check of the axis distance of the reinforcement steel or pre-stressing steel relative to the fire exposed surface.

LITERATURE SURVEY

Sponsored by the Dutch precast industry, jointly represented in BFBN, an international literature survey was done into the fire resistance of hollow core slab floors and damage cases in which hollow core slabs (partially) failed during heating or cooling down. Within the literature survey, 32 sources were investigated. A source in this case could be a test report, Ph.D. thesis, article or an e-mail message. More information can be found in the official report that was written for BFBN (only available in Dutch).

From the Ph.D. thesis of Fellingner an analysis of 66 fire tests, carried out before the year 2000, was taken into account. In addition to these tests, Fellingner also performed 25 fire tests. His analysis of the latter tests was also taken into account. The other tests have been analysed based on publications by the laboratories that did the tests. Tests that were not published by the performing test laboratory itself were not taken into account, with a view of objective research.

An overview per failure mode is presented in figure 5 (pie-diagram).

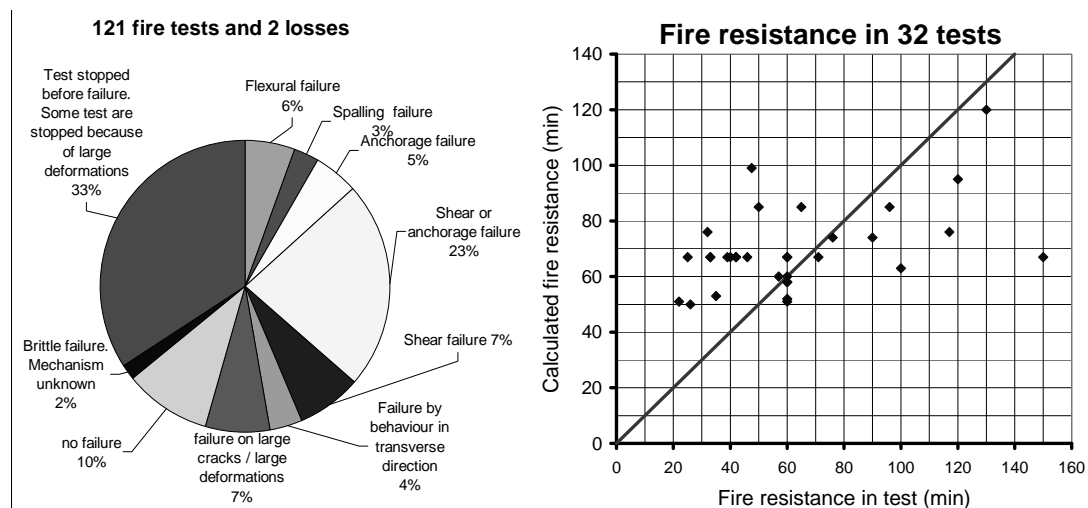


Figure 5: Overview per failure mode (left hand side) and per achieved fire resistance (right hand side) [5].

Figure 5 shows 121 fire tests and 2 fire damages in total. Tests in which the floor was not loaded or loaded more heavily than the theoretical capacity at room temperature have been omitted. The failure mode of each given test has been copied directly from the relevant publication. In cases where the failure mode was not stated, it was determined as far as possible based on the available information. The pie-diagram in figure 5 shows that in many cases the failure mode is not bending moment. It is noted that several tests specifically aimed at other failure modes than bending moment.

For the representation according to fire resistance, 32 tests were selected from the total of 121. Tests with a doubtful test set up and/or execution have not been taken into account. Moreover, the 32 selected tests meet the following criteria:

- The temperature development during the test is sufficiently similar to the ISO 834 fire curve;

- One or more full hollow core slabs were tested;

- The time to failure or end of the test in minutes has been recorded;

- The axis distance of the pre-stressing strands to the exposed surface has been recorded;

- The mechanical loading during the test was greater than nil and less than the capacity at room temperature;

- The test specimen has not been exposed to fire before, either or not with fire protective insulation.

For these 32 tests the fire resistance was calculated according to NEN 6071, based on the axis distance. The calculated and measured fire resistances for each of the 32 fire tests are compared in the diagram on the right hand side in figure 5.

In the tests in figure 5 (right hand side) in one case failure in bending moment occurred. In that case, the measured fire resistance was greater than the calculated fire resistance. In approximately 45% of the fire tests the calculated fire resistance is not achieved in the test.

This shows that the commonly applied method of verification of the bending moment capacity during fire according to NEN 6071, where in fact the axis distance is checked, is not sufficient for determination of the fire resistance of a hollow core slab floor.

The available information shows that horizontal cracking occurs more than once, both in real fire damages and in fire tests. Apart from the geometry of the cross-section of the slab, restrained thermal expansion of the slab seems to be of influence. Also the possible presence of a compressive top layer seems to play a role. Possibly due to the relatively low number of fire tests with restrained thermal expansion, it is not fully clear under which conditions the horizontal cracks do or do not occur.

CONCLUSIONS AND RECOMMENDATIONS

From the observations that:
the applied floor system and manufacturing method and details are not extraordinary
the fire conditions are not significantly different from standard fire conditions
and the fact that horizontal cracks through the webs have been observed in more real fires as well as in fire tests, within a relevant period of time
it is concluded that horizontal cracks through the webs of pre-stressed hollow core slabs, as observed in particular in the actual fire in the car-park in Rotterdam, are not a mere incident but refer to an underlying structural issue.

It should be noted of course that the occurrence of horizontal cracks as meant above, does not imply (premature) collapse of the entire floor system, let alone the complete building, in itself. In Rotterdam, large parts of the floor system did indeed fall down, but the load bearing integrity in the practical investigated case, remained by and large intact.

On the basis of the conclusion that the phenomena described refer to a structural issue, it is highly recommended to further explore possible adaption of practical design rules for hollow core slabs appointed in the (international) building legislation. A convincing argument for this is the fact that the common fire design approach in the Netherlands is based only on the bending moment capacity calculation through a check on reinforcement cover. This evidently does not suffice to cover the phenomena observed in real fires and fire tests.

TEMPORARY DESIGN GUIDANCE

The concrete industry, supported by the parties involved in the Dutch research, advise the parties in the design and construction processes for new projects, to apply a design flow chart as presented below in Table I. Although not all research questions have been answered as yet, and justification and adequate quantitative support is lacking, it is recommended to use the design flow chart at least in the period until further results of research and findings can be presented. In doing so it is believed that an adequate response is formulated and a path towards new design rules is paved to cope with the phenomena observed in the real fire cases and the Rotterdam car park in particular.

TABLE I. DESIGN FLOW CHART FOR NEW PROJECTS, USING
PRE-CAST HOLLOW CORE SLABS [6].

Advised method, depending on fire resistance requirement		Advised method in particular cases
30 min	60 minutes or more	
Calculation method acc. NEN 6071 (bending moment capacity), similar to Eurocode 2 (EN 1992-1-2)	Calculation method acc. NEN 6071 (bending moment capacity), and calculation method for shear capacity acc. Annex G EN 1168 and additional detailing (support)	Measures to limit the temperature development to 400 degC at the exposed concrete surface, in combination with the methods as given for 60 minutes fire resistance or Measures to limit the temperature development to 200 degC at the exposed concrete surface or a risk analysis as indicated in Eurocode 1 (EN 1991-1-7), proving equivalent safety level

REFERENCES

1. Van Overbeek, A.B.M., 2005, "System approach on structural fire safety, Literature Investigation", internal TNO report, 2005-CVB-R0068
2. Van Overbeek, A.B.M. and F. B. J. Gijsbers, "Research into the structural fire behaviour of a hollow core slab as applied in a car park in Rotterdam", TNO report 2007-TNO-1236/C
3. De Feijter, M. P. and A. J. Breunese, "Investigation of the fire in the Lloydstraat car park, Rotterdam", Efectis Report 2007-Efectis-R0984(E)
4. Fellingier, J. H. H., "Shear and anchorage behaviour of fire exposed hollow core slabs", PhD thesis Delft University of Technology, the Netherlands, 2004, ISBN 90-407-2482-2
5. Brekelmans, J. W. P. M., Van Overbeek, A.B.M., Breunese, A. J. and N. P. M. Scholten, "Fire resistance of hollow core slab floors, research results part A", TNO report TNO-034-DTM-2009-00651 (in Dutch), available at www.cobc.nl
6. Pielkenrood, A. P., 2nd interim letter from BFBN, 2009, available at www.cobc.nl

Performance in Fire of Fibre Reinforced Polymer Strengthened Concrete Beams Including Embedded Fibre Optic Sensors

M. F. GREEN, M. ADELZADEH, T. KHALIFA, R. EEDSON,
L. BISBY, N. BÉNICHOU, X. BAO and W. LI

ABSTRACT

Fibre reinforced polymer (FRP) materials are increasingly being applied in many areas of construction, particularly for strengthening of concrete beams. However, concerns associated with fire remain an obstacle to applications of FRP materials in buildings and parking garages due to their susceptibility to degradation at elevated temperatures. For FRP strengthened concrete beams, the bond properties of FRP materials at high temperature are critical. Additionally, in both industrial applications and fire scenarios, sensing may be required at very high temperatures. Such sensing could be used to monitor and control equipment in industrial situations or to provide an emergency management system in a structural fire. Conventional fibre optic sensors (FOS), however, are limited to relatively low temperatures. Thus, this paper also discusses the development of technology for fibre optic sensing at high temperatures. To illustrate the potential application in a structure, two full-scale T-beams (4 m span) are constructed with FOS attached to the internal longitudinal reinforcement. These T-beams are strengthened with external FRP, and fire protection for the FRP is provided by sprayed insulation. These beams will then be exposed to a standard ASTM fire while under sustained loading. This paper also presents an experimental investigation to characterize the bond properties of some currently available FRPs under various loading and thermal regimes ranging from ambient temperature to 200°C. Lap splice tests are conducted under both steady-state and transient temperature conditions, and the results of the two types of testing are compared.

M.F. Green, Professor, Civil Eng., Queen's University, Canada. greenm@civil.queensu.ca
M. Adelzadeh, Ph.D. Student, Civil Eng., Queen's, CA. masoud.adelzadeh@ce.queensu.ca
T. Khalifa, M.Sc. Student, Civil Eng., Queen's, CA. tarek.khalifa@ce.queensu.ca
R. Eedson, M.Sc. Student, Civil Eng., Queen's, CA. reedson@gmail.com
L. A. Bisby, Reader, University of Edinburgh, UK. luke.bisby@ed.ac.uk
N. Bénichou, Senior Research Officer, National Research Council, CA.
Noureddine.Benichou@nrc-cnrc.gc.ca
X. Bao, Professor, University of Ottawa, Ottawa, CA. xbao@science.uottawa.ca
W. Li, Postdoctoral Fellow, University of Ottawa, Ottawa, CA. Wenhai.Li@uottawa.ca

INTRODUCTION

Fibre reinforced polymer (FRP) materials are increasingly being applied in many areas of construction, particularly for strengthening of concrete beams. However, concerns associated with fire remain an obstacle to applications of FRP materials in buildings and parking garages due to their susceptibility to degradation at elevated temperatures [1]. Research is being conducted at Queen's University in conjunction with the National Research Council of Canada (NRC) and industry partners to investigate the effects of fire on such FRP strengthened concrete beams [2]. A major portion of the study involves numerical fire endurance modelling. For such models, the bond properties of FRP materials at high temperature are critical.

Additionally, in both industrial applications and fire scenarios, sensing may be required at very high temperatures. Such sensing could be used to monitor and control equipment in industrial situations or to provide an emergency management system in a structural fire. Conventional fibre optic sensors (FOS), however, are limited to relatively low temperatures. Thus, this paper also discusses the development of technology for fibre optic sensing at high temperatures.

To illustrate the potential application in a structure, two full-scale T-beams (4 m span) are constructed with FOS attached to the internal longitudinal reinforcement. These T-beams are strengthened with external FRP, and fire protection for the FRP is provided by sprayed insulation. These beams will then be exposed to a standard ASTM fire while under sustained loading.

This paper also presents an experimental investigation to characterize the bond properties of some currently available FRPs under various loading and thermal regimes ranging from ambient temperature to 200°C. Lap splice and FRP to concrete bond tests are conducted. Tests are conducted under both steady-state and transient temperature conditions, and the results of the two types of testing are compared and discussed. Results from these tests will also be used to develop analytical models representing the bond behaviour of FRP. Information from these tests will be used in calibrating coupled heat transfer and structural analysis numerical models for FRP strengthened members which are currently being developed at Queen's University.

BACKGROUND & RESEARCH SIGNIFICANCE

Very few studies have considered the fire behaviour of externally bonded FRP strengthened beams. Dearing [3] tested six beams (300mm by 400mm by 5m) where four of them were strengthened with carbon FRP (CFRP) plates and some were insulated with fire resistance boards. The un-insulated beams had a fire endurance of 81 minutes while the insulated beams gave an endurance of 146 minutes. Interestingly the endurance of insulated CFRP plated beam was larger than the un-strengthened reinforced concrete beam. Blontrock [4] tested CFRP plated beams using multiple insulation schemes. During his experiments, when the temperature of FRP reached the glass transition temperature, T_g , the load bearing contribution of FRP was significantly reduced. The glass transition temperature is defined as "the midpoint of the temperature range over which an amorphous material (such as glass or a high polymer) changes from (or to) a brittle, vitreous

state to (or from) a plastic state” [1]. Williams et al. [2] tested two full-scale insulated T-beams and found that beams with sufficient insulation can achieve fire endurance of more than 4 hours.

EXPERIMENTAL PROGRAM

A two-pronged experimental approach is being taken to address the issue of the performance of FRP strengthened concrete beams in fire. Full-scale fire tests are being conducted on T-beams including specialized high temperature fibre optic sensors. To evaluate the material performance of the FRP, extensive small-scale tests are being carried out to determine the effects of high temperature on bond of FRP.

Full-scale tests

Figure 1 shows the construction details of the T-beams including the internal reinforcement and the location of thermocouples and innovative fibre optic sensors. The beams are 3900 mm long and 400 mm deep with a 1220 mm wide flange (150 mm thick) and a 300 mm wide web. The beams are reinforced in flexure with 2-15 mm diameter steel bars (total area of 400 mm²) and in shear with 11 mm diameter stirrups (bar area of 100 mm²). The clear cover to the stirrups is 50 mm giving an effective depth to the flexural reinforcement of 330 mm. The tested 28 day cylinder strength of the concrete was 32 MPa. A Sika CarboDur S812 CFRP plate or 1 layer of Sika Hex 103C sheets (200 mm wide) is planned for flexural strengthening with a 40 mm insulation thickness. The beams will also be strengthened in shear with U-wraps. Table I summarizes the material properties of the FRP.

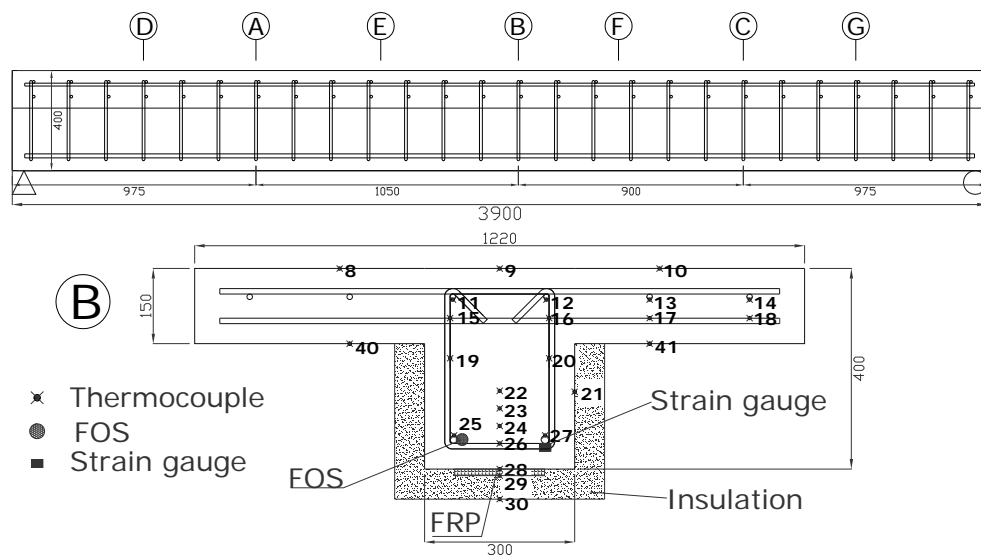


Figure 1. Details of T-beams (dimensions in mm).

TABLE I. MATERIAL PROPERTIES OF FRP.

Type of material	Thickness (mm)	Modulus (GPa)	Strength (MPa)	Ultimate strain (%)	T _g (C)
CarboDur S812 CFRP plate	1.2	165	2800	1.7	150
Sikadur 330 epoxy	—	3.8	30	1.5	60
SikaWrap Hex 103C CFRP sheet	1.0	70.6	849	1.1	60
Sikadur 300 epoxy	—	1.7	55	3.0	60 - 85
Tyfo SCH-41 CFRP sheet	1.0	95.8	968	1.0	75
Tyfo Type S resin	—	3.2	72.4	5.0	75

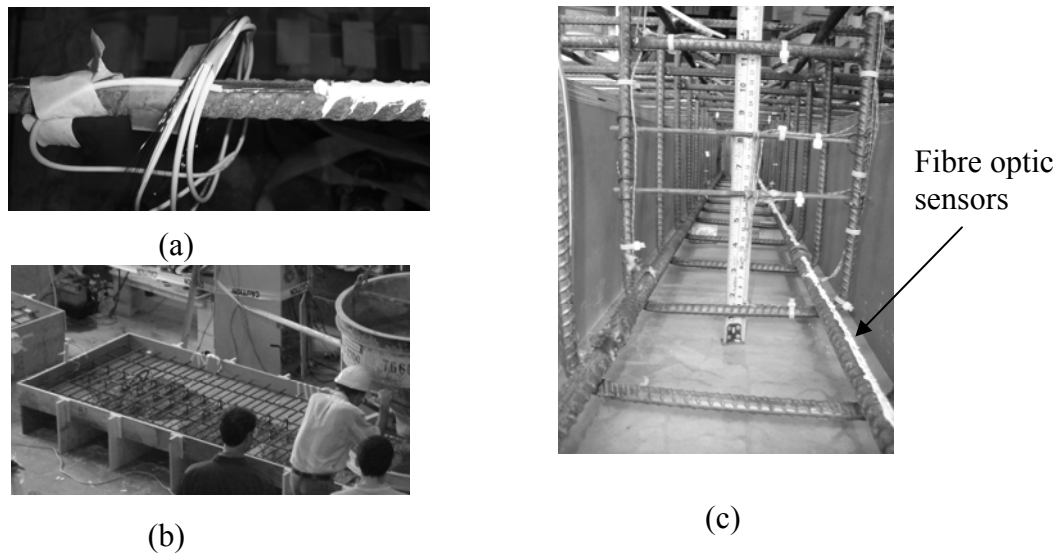


Figure 2. Installation of fibre optic sensors (a) sensors on reinforcing bar (b) construction of beams (c) sensors shown along length of reinforcing bar in reinforcement cage.

The T-beams were also instrumented with specialized high temperature fibre optic sensors as shown in Fig. 2. To protect the fibres from damage, they are attached to reinforcing steel bars as shown in Fig. 2. The high temperature adhesive used to attach the fibre to steel protects the fibres from high alkaline environment of concrete. The distributed fibre-optic sensing system is based on Brillouin scattering. Zeng et.al. [5] used Brillouin-based sensors to measure strain in a reinforced concrete beam with a spatial resolution of 500 mm along a 1.65 m long beam. One of the advantages of Brillouin-based sensors is the capability of measuring temperature and strain simultaneously. Zou et al. [6] have reported temperature and strain measurement resolution of $1.3 \pm ^\circ\text{C}$ and $15 \mu\epsilon$ using this type of fibre optic sensors with a spatial resolution of 150 mm. Recently most of the strain sensing using Brillouin scattering sensor has been based on a standard single mode fibre (SMF28) with acrylate coating, which can sustain maximum strain of 1%-1.5% and

temperature of 80°C and this limitation is insufficient for many monitoring applications. Recently, novel sensing fibre with carbon/polyimide coating has been emerged for applications in harsh environments. This kind of fibre can sustain a maximum strain of up to 4% and temperature as high as 450°C and becomes idea candidate for monitoring applications at high temperatures.

After strengthening and insulating the beams, they will be fire tested at the National Research Council of Canada in the full scale floor furnace. Table II summarizes the predicted strength of these beams using various North American design provisions. Based on these calculations, the applied load during the fire test will be taken as 31.2 kN/m which corresponds to the full service load for the predicted strength according to CSA S806 [7]. The standard ASTM E119 [8] fire curve will be followed during the test.

Bond testing

One of the critical elements in the FRP strengthening system is the bond between the FRP and concrete. To better understand the bond performance at high temperatures and in fire situations, material testing is on-going to quantify the bond performance at high temperature of FRP to FRP through lap-splice specimens and between FRP and concrete.

Figure 3 shows the test configurations for testing the lap-splice and FRP to concrete bond. These tests are conducted in an INSTRON Universal Testing Machine (UTM), shown in Fig. 3(c), which has an integrated, custom designed thermal chamber with an internal dimension of 250 mm (width) by 250 mm (depth) by 300 mm (height) and has a maximum load capacity of 600 kN.

TABLE II. PREDICTED STRENGTH FOR BEAM STRENGTHENED WITH CFRP PLATES.

CarboDur S812			Mr	increase	Mservice D+L	wD=wL	Vf end
			kN.m	%	kN.m	kN/m	kN
ACI 440.2R-08 [1]	Un-strengthened		52.3		37.4	10.3	55.0
	Strengthened	Debonding	70.0	33.7%	50.0	13.8	73.5
		FRP rupture	127.9	144.4%	91.4	25.2	134.5
CSA S806 04 [7]	Un-strengthened		50.2		36.5	10.1	52.8
	Strengthened	Debonding	77.7	54.7%	56.5	15.6	81.6
		FRP rupture	125.5	149.8%	91.2	25.2	131.8
CSA S6 06 [9]	Un-strengthened		53.2		36.7	10.1	55.9
	Strengthened	Debonding	75.7	42.3%	52.2	14.4	79.5
		FRP rupture	128.6	141.8%	88.7	24.5	135.2
Predicted Actual	Un-strengthened		68.1		-	18.8	71.6
	Strengthened		164.5		-	45.4	172.8
	Tension steel yield limit		53.4		-	14.7	56.1

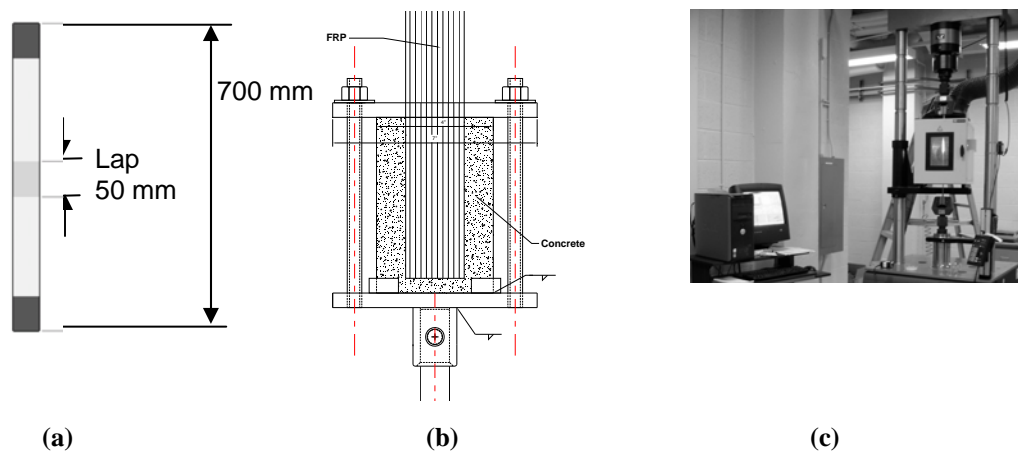


Figure 3. Bond testing configuration (a) Lap-splice (b) FRP to concrete bond (c) test machine.

For the purposes of this paper, results are presented for Fibrwrap SCH-41 Carbon Fibre with Type S resin tested in the lap-splice configuration and in tension. Table I presents the properties of these materials. The FRP to concrete bond tests are still in progress and data are not yet available. Both steady-state and transient temperature tests were conducted. For the steady-state tests, the coupons were exposed to a specified temperature and then loaded to failure. For the transient tests, the FRP specimens were subjected to a specified sustained load for 10 minutes under ambient temperature and then heated at 10°C/min until failure. The specimens were loaded to 10%, 20%, 40%, or 70% of their room temperature lap-splice bond strength. No investigation on the heating and loading rate, both of which may be important, has been conducted thus far.

For all levels of temperature, exposure, and sustained load levels, five identical coupons were tested. This number of coupons was chosen as a reasonable minimum number of samples to allow a meaningful statistical comparison of the different treatments. Even with this relatively small number of coupons for each treatment, approximately 100 tests were conducted for the results presented in this paper.

The tension coupons made using carbon fibre experienced notable strength loss at temperatures of 45°C. The tests reliably suggested that approximately 20% strength was consistently lost after exposure to this temperature. At higher temperatures, beginning at 60°C the coupons maintained about 45% of their average ambient temperature strength and appeared to retain this strength level up until temperatures of 90°C. Beyond, at exposure to 200°C additional strength loss was evident and the coupons retained approximately 34% of their room temperature strength. Tension coupons were also tested in transient conditions. The coupons were loaded to 37% of their ambient temperature ultimate strength and failed at 96°C with a standard deviation of 14°C.

For the lap-splice specimens, CFRP coupons retained approximately 80% of their ambient lap-splice strength at 45°C. However, at exposure to higher temperatures the CFRP lap-splice coupons had virtually no strength in bond at all. The coupons were reduced to 16% strength at 60°C and less than 5% of their strength at exposure to temperatures of 90°C and 200°C. The CFRP coupons held under sustained load failed at temperatures expected based on the constant

temperature tests. The coupons again exhibited a rapid loss of strength at exposure to temperatures above 45°C. This finding is similar to the preliminary work of Gamage et al. [10]. This research will expand significantly on Gamage's work by considering different types of materials and an extensive number of data points to develop statistically relevant material properties.

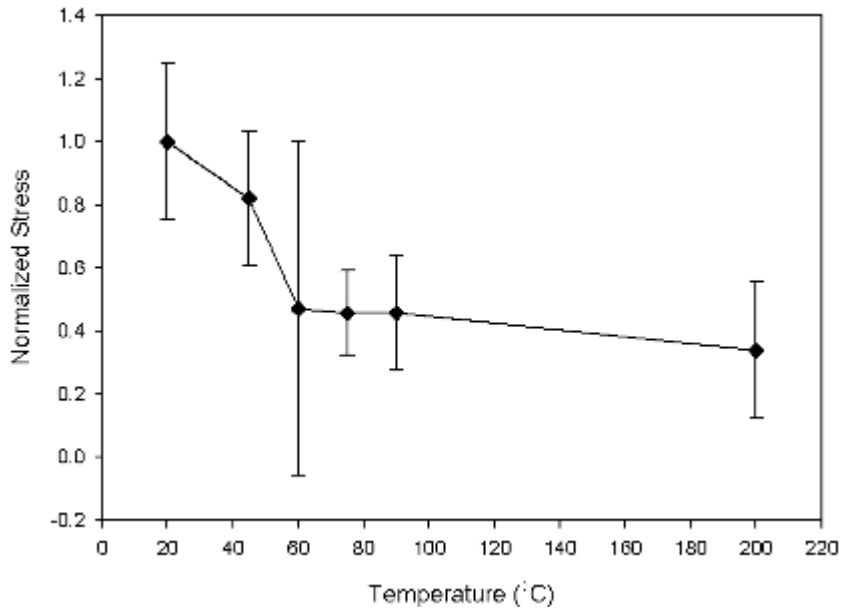


Figure 4. Tensile strength stress of CFRP with S type resin normalized with respect to the room temperature strength.

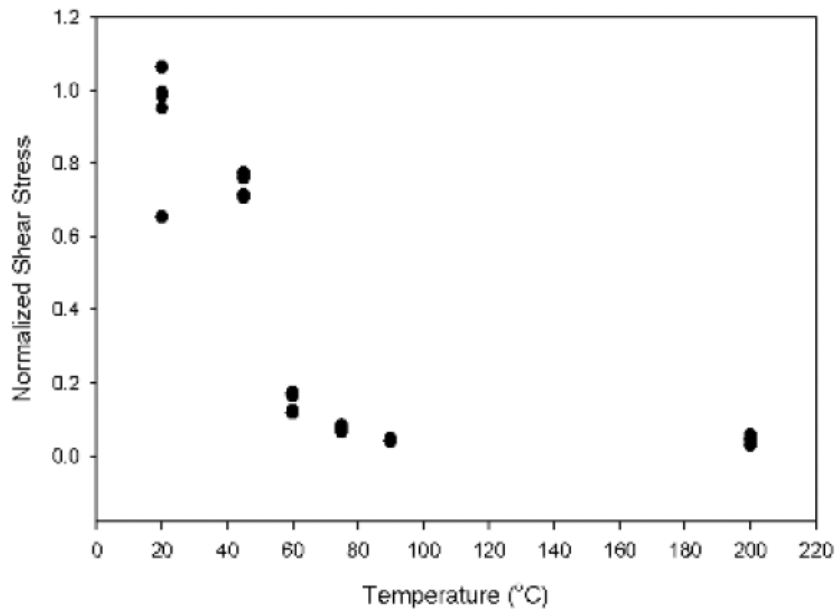


Figure 5. Lap splice bond shear stress of CFRP with S type resin normalized with respect to the room temperature strength.

CONCLUSIONS AND RECOMMENDATIONS

This paper discussed testing to evaluate the fire performance of FRP strengthened concrete beams including the development of technology for fibre optic sensing at high temperatures. This paper also presented tests to characterize the material properties of some currently available FRPs up to 200°C. The CFRP material tested in this paper experienced 55% loss in tensile strength, and 85% loss in FRP lap-splice strength at a temperature of 60°C. Thus, these CFRP materials, with sufficient anchorage, can maintain 40% of their tensile strength at temperatures well in excess of the T_g of their resins. Approximately 90% of the CFRP lap-splice strength was lost at temperatures slightly above T_g . These results should be taken with caution because they represent the most severe possible test of FRP lap-splice strength and are not representative of longer FRP splice lengths used in practice. Thus, more research is required to investigate longer bond lengths and to determine the consequences for member performance in fire.

ACKNOWLEDGEMENTS

The authors are members of the Intelligent Sensing for Innovative Structures Network (ISIS Canada) and wish to acknowledge the support of the Networks of Centres of Excellence Program, the Natural Sciences and Engineering Research Council, the National Research Council of Canada (NRC), Fyfe Co., Fibwrap Installations, Sika Corp., and technical staff at Queen's University and NRC.

REFERENCES

1. ACI, 2008. *ACI 440.2R-08 Guide for the Design and Construction of Externally Bonded FRP Systems for Strengthening Concrete Structures*, American Concrete Institute, Farmington Hills, MI.
2. Williams, B.K., V.K.R. Kodur, M.F. Green, and L.A. Bisby. 2008. "Fire Endurance of FRP Strengthened Concrete T-Beams," *ACI Struct. J.*, 105(1): 60–67.
3. Deuring, M. 1994. "Brandversuche an Nachtraglich Verstarkten Tragern aus Beton," Research Report EMPA No. 148,795, Swiss Federal Laboratories for Materials Testing and Research (EMPA), Dübendorf, Switzerland.
4. Blontrock, H., L. Taerwe, and P. Vandavelde. 2000. "Fire Tests on Concrete Beams Strengthened with Fibre Composite Laminates," in *Third PhD Symposium*, Vienna, Austria, 10 pp.
5. Zeng, X., X. Bao, C. Y. Chhoa, T. W. Bremner, A. W. Brown, M. D. DeMerchant, G. Ferrier, A. L. Kalamkarov, and A. V. Georgiades. 2002. "Strain measurement in a concrete beam by use of the Brillouin-scattering-based distributed fiber sensor with single-mode fibers embedded in glass fiber reinforced polymer rods and bonded to steel reinforcing bars," *Appl. Opt.* 41(24): 5105–5114.
6. Zou, L., X. Bao, V. S. Afshar, and L. Chen, 2004. "Dependence of the Brillouin frequency shift on strain and temperature in a photonic crystal fiber," *Optics letters* 29 (13): 1485–1487.
7. CSA, 2002. *CAN/CSA S806-02 Design and Construction of Building Components with Fibre-Reinforced Polymers*, Canadian Standards Association, Mississauga, ON.
8. ASTM, 2001. *ASTM Test Method E119-01: Standard Methods of Fire Test of Building Construction and Materials*, American Society for Testing and Materials, West Conshohocken, PA.
9. CSA, 2006. *CAN/CSA S6-06 Canadian Highway Bridge Design Code*, Canadian Standards Association, Mississauga, ON.
10. Gamage, J.C.P.H. , M.B. Wong, and R. Al-Mahaidi, 2005. "Performance of CFRP Strengthened Concrete Members under Elevated Temperatures," in *Proceedings of the International Symposium on Bond Behaviour of FRP in Structures (BBFS 2005)*, 7- 9 Dec. Hong Kong, China, pp. 113–118.

Fire Performance of Precast Prestressed Concrete Beam with Openings

S. BABA, S. MICHIKOSHI, S. SAKAMOTO and T. HIRASHIMA

ABSTRACT

Precast prestressed concrete (PCaPC) beams with high-strength rebars and multiple large openings have tremendous potential in architectural applications. They are high in quality, and can realize larger building spaces providing smaller and lighter beams. In Japan, under the current Building Standard Law of Japan aside from conventional prescription-based fire safety regulations, it is now possible for designers to test and to apply new materials and new members on projects if their fire resistance performances are confirmed by tests. Their performances can be evaluated based on fuel loads and fire scenarios calculated room by room. In this regard, the fire test for new pre-stressed precast beams was conducted by the authors for extracting their performances. This paper is intended to provide a summary of the findings obtained from the fire experiment. Three specimens for precast prestressed beams were tested. Test parameters are the level of vertical loading and the quantity of shear reinforcement. All specimens are made of high strength concrete mixed with organic fibers for the prevention of explosive spalling. It was confirmed from the results that PCaPC beams are able to resist the allowable permanent during 3 hours standard fire. In the paper, evaluation method for bending and shear strength of PCaPC beams at high temperature, as well as the results of the fire experiment will be presented. The analytical results showed that the truss analogy model underestimates the shear strength of the beam at opening. It was clarified that not only truss model but also the arch analogy should be considered for evaluating the shear strength of the beam.

Shigeaki Baba, Taisei Corporation, Technology Center, 344-1, Nase-cho, Totsuka-ku, Yokohama, Japan.

Shintaro Michikoshi, Dr., Taisei Corporation, Technology Center, 344-1, Nase-cho, Totsuka-ku, Yokohama, Japan.

Shigehiro Sakamoto, Dr., Taisei Corporation, Technology Center, 344-1, Nase-cho, Totsuka-ku, Yokohama, Japan.

Takeo Hirashima, Dr., Chiba University, Graduate School of Engineering, Department of Architecture, 1-33, Yayoi-cho, Inage-ku, Chiba, Japan.

1.INTRODUCTION

Precast prestressed (PCaPC) concrete beams, using high strength concrete and rebars, and with multiple large openings, have a tremendous potential for use in architectural projects, because they enlarge building space and decrease building weights. They also enable equipment system changed and can be supplied in high quality. Furthermore, these beams use longitudinal deformed bars as pre-stressing bars. This can realize the short depth of the beam section and large diameter of the opening [1]

On the other hand, the PCaPC beam is consisting of high-strength concrete/rebar. From the fire safety perspective, it is known that the failure of high-strength concrete and prestressed members occurs sometimes rapidly due to the explosive spalling of concrete cover exposed to fire [2], [3]. It is generally believed that explosive spalling results from the buildup of internal pressure due to the transformation of water to vapor and from the development of internal stress due to the thermal gradient. Improving concrete strengths requires more cement, whose permeability is low compared with normal concrete. It makes difficult for the concrete to transport vapor and moisture in it. Accordingly, higher vapor pressure and steeper thermal gradient take place close to the surface of concretes with higher strength. Here, it is known that organic fibers in the concrete can mitigate that vapor pressure and the stress by the thermal gradient. To use organic fibers has been one of the solutions for eliminating spalling [4].

The fire performance of prestressed concrete structure was dictated the temperature of prestressing steel according to the required time [2], but there are few data of them, bending and shear strengths at high temperature. The paper provides findings from a series of fire tests on full-scale section beam model. Furthermore, the shear strength of PCaPC beams are discussed.

2.FIRE RESISTANCE TEST

2.1 Test Program

The first objective of the test program is to obtain experimental evidence that the PcaPC beam is design to meet the fire resistance requirements. Concretely, the beam should not collapse up during the equivalent endurance time. In this regard, three PCaPC specimens have actual openings.

The test specifications are listed in Table 1. Elevation and the cross-sectional details are given in Figure 1. Three full-scale section pre-stressed beam specimens with slab are fabricated and tested in this program. The test parameters include the level of vertical loading (48% or 78% of ultimate bending moment at room temperature), quantity of shear reinforcement (0.34% to 1.2% of ratio of shear reinforcement). The specimens consist of PCaPC beam and slab, the PCaPC beams are 865mm high and 290mm width. The slabs are 135mm high and 600mm width. The beams have five openings, whose diameters are about 400mm, with the distance of 1,200mm. All specimens were pre-stressed with the pre-tensioning system. The PCaPC specimens with slab were 7500mm in length, and their spans are 6800mm. The beams are steam treated after setting, for enhancing strength in early age because it is preferable to introduce prestressed force in early age. Moreover, for improving the fire resistance, organic fibers are added in the PCaPC beam concrete.

The compressive strength at the age of the fire test ranged from 106 to 119MPa. Compressive strength were determined on cylinder specimens of 100 x 200mm cured under similar conditions of temperature history expected in the beams during setting. All specimens were dried in the laboratory for five months prior to the fire test. The moisture content as of testing ranged from 2.95 to 3.92 %.

Figure 2 shows the setup of the test for the PCaPC beams subjected to fire. All specimens are simply supported with a support length of 6800mm. Two hydraulic jacks, located 3000mm distance of the supporting points, act the downward force on the beam. The measurements include vertical displacements at the middle of the span and at the supporting points etc., furnace temperatures, temperatures of the concrete throughout the specimen thickness and temperatures of longitudinal and shear reinforcement steel. All measurements are conducted every 30 seconds during the test. The specimens were subjected to the fire temperature history as specified in ISO 834 [5].

TABLE I. Test specifications.

Specimen	Prestressing bar	Prestress Force (kN)	shear reinforcement	shear reinforcement at opening	Acting moment at middle of span M (kN×m)	bending strength M_u^* (in calculation) (kN×m)	PCaPC Beam Concrete		
							M/Mu	Compressive Strength (N/mm ²)	Moisture content (%)
No.1	4-D38 SD685	2655	D13-□-@200 (SD295, Pw=0.42%)	D13-□-@70 (SD295, Pw=1.2%)	1242	2588	0.48	111	3.50
No.2			U12.6-□-@100 (SBPD1275/1420, Pw=0.84%)	U12.6-□-@70 (SBPD1275/1420, Pw=1.2%)				119	3.19
No.3			D13-□-@200 (SD295, Pw=0.42%)	D10-□-@140 (SD295, Pw=0.34%)	2025	0.78	106	3.40	

* $M_u = \Sigma 0.9$ at $o y d = 0.9 \times 1140 \times 2 \times 742 \times (800+900) = 2588\text{kNm}$ (refer to Equation 1)

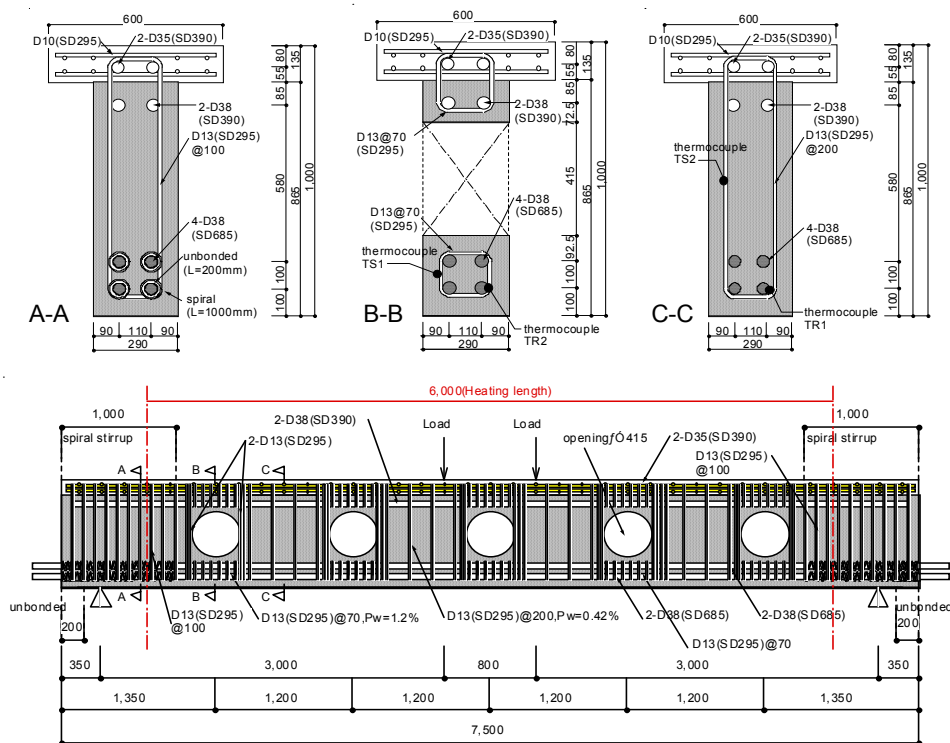


Figure 1. Elevation and cross-section of No.1 beam.

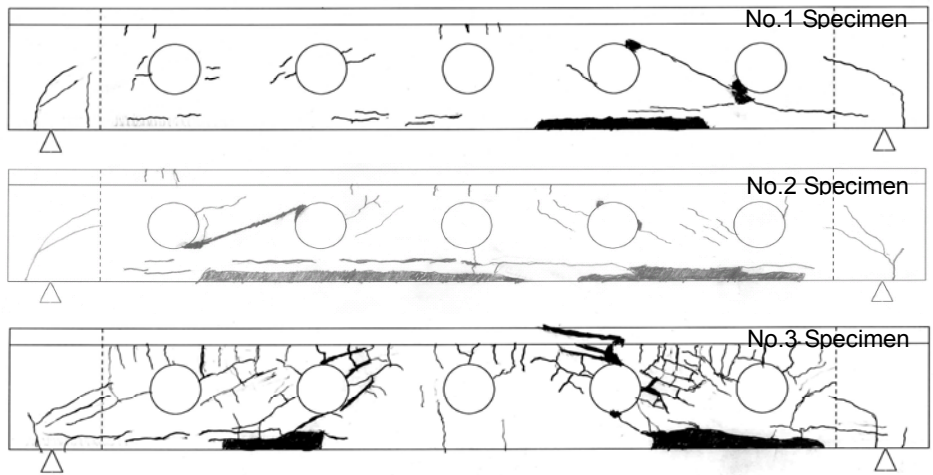


Figure 3. Crack patterns of specimens.

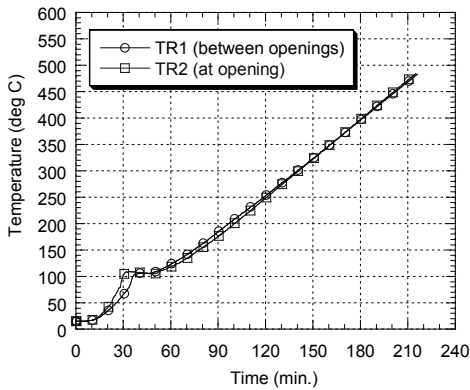


Figure 4. Temperature of Longitudinal Steel (No.1 specimen).

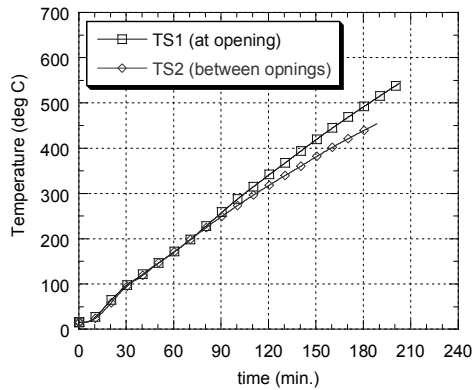


Figure 5. Temperature of shear reinforcement (No.1 specimen).

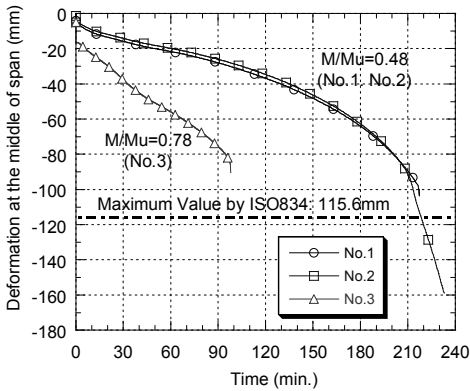


Figure 6. Deflection at the Middle of Span.

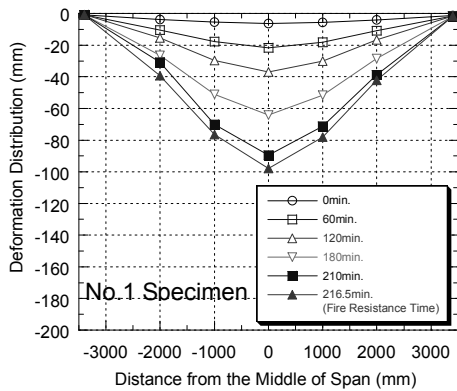


Figure 7. Deformation Distribution.

the earlier stage obviously induced by temperature gradient, (2) slower deflection as the gradient of temperature stabilizes, (3) gradual increase of deformation because of the decrease in bending stiffness with time.

As shown in Figure 6, which compares specimens No.1, No.2 with No.3,

deflection of No.3 specimen is larger than those of No.1 and No.2 specimens, where the external load of No.3 specimen is larger than others. As for No.1 and No.2 specimens, where acting loads were in the same level, showed similar trends of deflection. These two specimens have the same bending stiffness at high temperature.

3. ESTIMATION OF FIRE RESISTANCE

3.1 Methodologies

3.1.1 ULTIMATE BENDING MOMENT

The following assumption yields a simple equation (Equation 1) to estimate the time up for bending failure: If reinforcing / pre-stressing steel reaches yielding before the concrete reaches critical compressive strain, the ultimate bending moment of the member is governed only by the temperature of reinforcing / pre-stressing steel regardless of pre-stressing force.

$$M_u = \sum_{i=1}^N 0.9 \times a_i \times \sigma_y \times d_i \quad (1)$$

where, M_u : ultimate bending moment, N : the number of reinforcing / pre-stressing steel, a_i : cross-section area of reinforcing / pre-stressing steel i , σ_y : yield strength of reinforcing / pre-stressing steel i , d_i : depth to reinforcing / pre-stressing steel i

3.1.2 SHEAR STRENGTH

The following assumption yields an equation (Equation 2) to estimate the time up for the shear failure by truss analogy model, and Equation 3 for the shear failure by arch analogy model. The assumption is that shear reinforcements reach yielding strength at high temperature in the truss model, and longitudinal reinforcement bars reach yielding strength at high temperature in the arch model.

Two models for truss model are considered. One is the model at openings (Figure 8) and another is the model between openings, where the shear strength of the model at opening is the sum of those of upper truss and lower truss (Figure 8). Figure 8 and 9 also illustrate the angle by the arch model with openings and without openings, respectively. The arch model with openings has two arches as shown in Figure 8.

Finally, four models for evaluating shear strength are considered: the truss model at openings and between openings, and the arch model with openings and without openings.

$$Q_t = b \times j_t \times P_w \times c_{wy} \times \cot \phi \quad (2)$$

where, Q_t : shear strength by truss model, b : width of PCaPC beam, j_t : distance between longitudinal reinforcements, c_{wy} : yield strength of shear reinforcement steel, P_w : ratio of shear reinforcement, ϕ : the angle of truss model (here, $\phi = 45^\circ$)

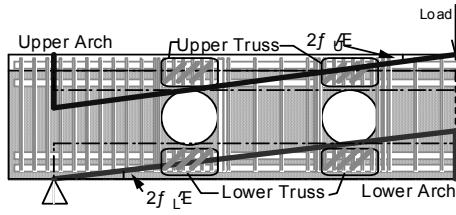


Figure 8. Arch and truss models with openings.

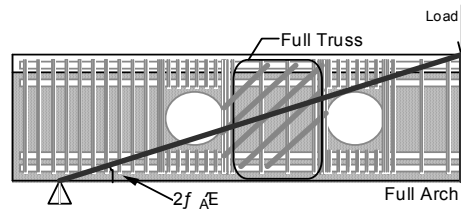


Figure 9. Arch and truss models without openings.

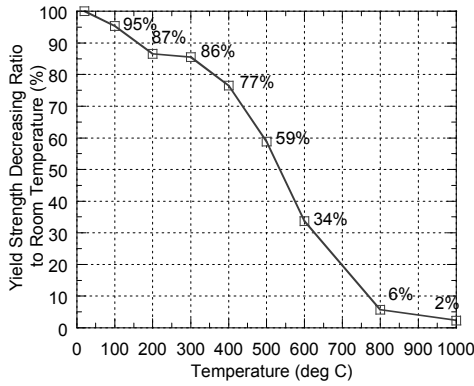


Figure 10. Assumption of Yield Strength of Reinforcing Bar (SD685).

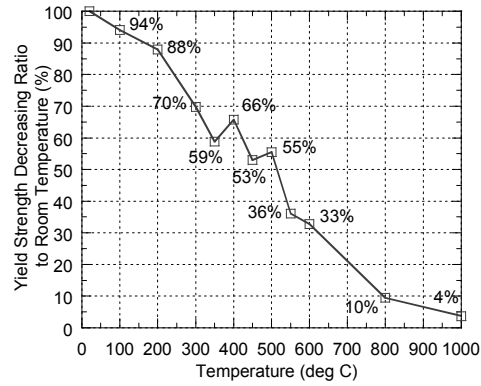


Figure 11. Assumption of Yield Strength of Shear Reinforcement (SD295).

$$Q_a = \sum_{i=1}^N a_i \times \sigma_y \times \tan \theta \quad (3)$$

where, Q_a : shear strength by arch model, θ : the angle of arch model (refer to Figure 8, 9)

3.2 Estimation Results

Figure 10 [6] gives the temperature vs yield strength relationship of reinforcing / pre-stressing steel. Figure 11 [6] gives the temperature vs yield strength relationship of shear reinforcement steel.

Figure 12 exemplifies the time history of ultimate bending moment of All specimens. From the observation of the test and from the collapse time obtained by the test and by the calculation, it can be said that these specimens did not failed by the bending moment. Figures 13 to 15 show the time history of shear strength by truss and arch model. As shown in the figures, the shear strength by truss model at opening [2] is underestimated. Even if the shear strength by the arch model with opening is added, the summed strength is still underestimated. So, the shear strength would be distributed to arch model without at openings. The values of this distribution are 62% (No. 1 specimen), 67% (No. 2 specimen) and 89% (No. 3 specimen). Because this estimated method showed only respective shear strength by truss and by arch analysis, further discussion may have to be done on the combinations of truss and arch analysis.

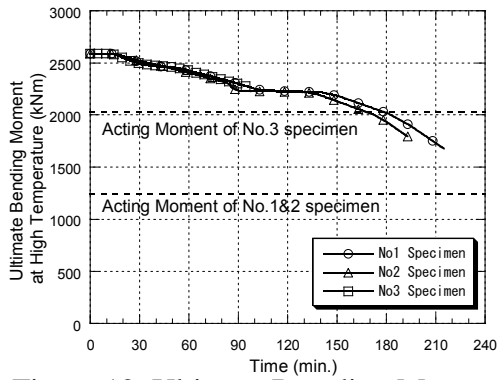


Figure 12. Ultimate Bending Moment.

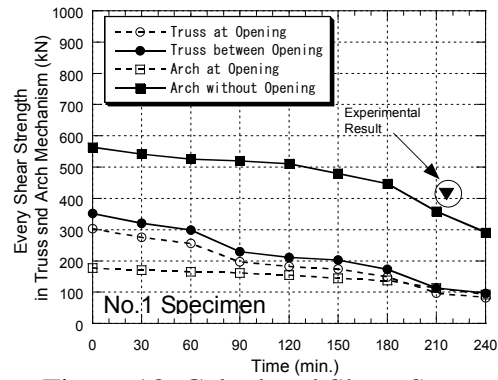


Figure 13. Calculated Shear Strength.

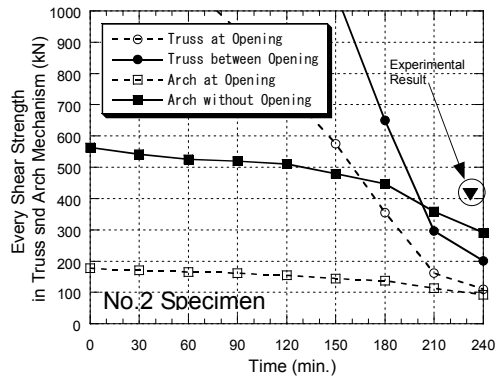


Figure 14. Calculated Shear Strength.

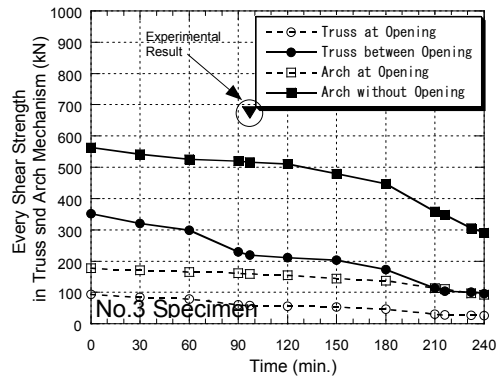


Figure 15. Calculated Shear Strength.

4. CONCLUSIONS

Fire resistance test of PCaPC beams were carried out and their fire resistance performances were clarified. The tests were conducted with specimen of the actual size. It was confirmed that in this specific model the failure patterns of the specimens are shear failure. In addition, the ultimate bending moment and the shear strength by using truss and arch model was estimated. The analytical study should be discussed further on the combinations of truss and arch effect.

5. REFERENCES

1. Kawamoto, S., et al, May 2002. "Structural Performance of Precast Prestressed Concrete Beam with Openings" (in Japanese), Summaries of Technical Papers of Annual Meeting Architectural Institute of Japan, C-2, pp. 949–950.
2. Architectural Institute of Japan, May 2002. "Standard for Structural Design and Construction of Prestressed Concrete Structures" (in Japanese).
3. Saito, H. 1996. "A Explosive Spalling of Prestressed Concrete in Fire" (in Japanese), Bull. of the Fire Prevention Society of Japan, Vol.15, No.2, pp.23–30.
4. e. g., Kuroiwa, S., et al, 2002. "Fire Performance of Reinforced Concrete Columns Using High-Strength Concrete with Polypropylene Fibers", Proceedings of the First fib Congress, Session.11, pp. 129–134.
5. ISO/FDIS 834-1, 1999. "Fire-resistance tests –Elements of building construction-, Part 1 General requirements".
6. Architectural Institute of Japan, Nov., 2003. "Guide Book for Fire-Resistive Performance of Structural Materials" (in Japanese).

Explosive Spalling of Concrete Columns with Steel and Polypropylene Fibres Subjected to Severe Fire

P. DOHERTY, F. ALI and A. NADJAI

ABSTRACT

The exposure of concrete elements to high temperatures during fire can cause major risk to life safety and to the serviceability of a building. One of the main reasons for this is due to concrete spalling which caused by pore pressure and thermal stresses. Previous research has indicated that the inclusion of polypropylene fibres to concrete reduces explosive spalling. However, concrete containing polypropylene fibre can still be vulnerable to explosive spalling during fire. This paper presents the outcomes of a research investigating the effect of using steel fibres in addition to polypropylene fibres to reduce explosive spalling of concrete. The experimental part of this study evaluates the performance of six normal strength columns under a loading ratio = 60% of the design capacity and subjected to severe heating rate higher than ISO 834. The columns were cast using various dosages of steel and polypropylene fibres. Analyses of the main findings included evaluation of the measured concrete temperatures along with axial displacement recordings. The analysis demonstrates a clear assessment of the spalling levels of the various representative specimens. The study also compares the experimental axial displacement with theoretical predictions using DIANA. Conclusions drawn from the study indicate that adding steel fibres along with polypropylene fibres can reduce the degree and severity of spalling if compared with concrete containing polypropylene fibres only. The spalling degree was reduced from 22.03% to 12.41% in best case and from 14.95% to 10.49% in average when steel fibres were used with polypropylene fibres.

INTRODUCTION

One of the most structural damaging and harmful outcomes of concrete exposure to elevated temperatures is the occurrence of concrete spalling. More importantly, spalling exposure inflicts detrimental harm to human life due to its explosive nature. This has been highlighted by several major catastrophes in the last decade. As a result, the fire resistance of normal and high strength concrete remains an important topic within the concrete technology field ⁽¹⁾. Essentially reinforced concrete under ambient conditions has countless advantageous whereas concrete subjected to elevated temperatures generally behaves unfavourably.

In a mere overview, the spalling phenomenon can be defined as the violent removal of concrete layers and shrapnel from the compounds surface when exposed to elevated temperatures. Spalling activities can transpire at various severities however the aforementioned activity is generally of an explosive nature. The causes and factors influencing explosive spalling are somewhat inconsistent and unquantifiable. Various authors ⁽¹⁻⁶⁾ have indicated that w/c ratio, heating rate, strength of concrete matrix, concrete microstructures with low permeability, moisture content and imposed loading all have notable influences on the spalling phenomena. Brittle like matrices such as concrete are susceptible to physical and chemical changes or reactions due to heating. Studies highlight that concrete spalling occurs due to the development of thermal stresses and pore pressure within the concrete microstructure. The pressure development is caused by the transformation of the residing free water within the concrete pores together with the chemically bound moisture into the gaseous phase ⁽²⁾. In the work undertaken by Hertz ⁽³⁾, spalling only occurred under the presence of moisture. Moreover it was indicated that spalling will only occur when the moisture content is above 3–4% by weight. Experimental work conducted by Bian et al ⁽¹⁾ indicated that explosive spalling is likely to occur under temperatures greater than 320 C when the water/cement ratio is equal to that of 0.26. The same research indicated that higher moisture contents produced explosive spalling at a greater frequency while inflicting a greater degree of damage. In addition, published findings state that the thermal expansion of aggregate increases the internal stresses on the concrete matrix causing the development and formation of micro cracks ⁽⁴⁾.

The research community has worked hard with the construction sector to devise new techniques to reduce the occurrence of spalling. Ultimately the development of pore pressure can be alleviated through the use of varies fibres within the concrete matrix ⁽⁵⁾. Fundamentally, the inclusion of polypropylene (PP) fibre has proved to be one of the most advantageous techniques employed to reduce the spalling phenomenon. Moreover experimental studies have indicated that the practical inclusion of PP is the most effective method of passive fire protection ⁽⁶⁾. Introduced at a prescribed dosage, the randomly oriented polymer melts at approximately 160 C creating a network of hallow channels and a much more permeable microstructure compared with that of plain concrete⁽⁷⁾⁽⁸⁾. From existing studies, there is little data presented on the effects of fibre length and dosage on the occurrence of spalling however it is suggested that fibre inclusion at a dosage rate as low as 0.9 kg/m³ can be influential ⁽⁹⁾. It is worth emphasizing that published work highlighted the importance of uniform distribution within the concrete i.e. better distribution is beneficial to reducing the spalling resistance of concrete ⁽¹⁰⁾. Extensive work has been conducted on polymer material yet very few studies have reviewed the influence of hybrid fibre (combination of polypropylene and steel fibre) inclusion therefore the current international knowledge and awareness of hybrid fibre is

limited. Experimental research presented by Chen and Liu ⁽¹¹⁾ indicated that the inclusion of steel fibre along with polypropylene fibre reduced the occurrence of spalling. Essentially steel fibre resists the initiation and expansion of cracks in the concrete while the polypropylene fibre melts to create micro channels in the matrix which alleviates the vapour tension. In fact research indicates that the inclusion of fibres and in particular polypropylene fibres have notable affects on the mechanical properties of concrete both at ambient and elevated temperatures. The respective studies highlight that fibre inclusion does not improve the compressive strength while other research indicates a negative effect on strength ⁽¹⁾⁽¹²⁾.

The objective of the research study is to investigate how the inclusion of PP and steel fibres at various prescribed dosages and combinations would influence the spalling patterns of reinforced concrete columns (RCC) under elevated temperatures. It was hoped that experimental data would provide an overall picture of the columns behaviour particularly with respect to spalling severity, failure time and the method/mode of failure (deformed shape). The detailed fabrication and testing program at the University of Ulster, Fire Research Centre comprised of 6 fire tests on half scale 1800 x 127 x 127mm RC columns under same parameters of loading and heating.

EXPERIMENTAL PROGRAM

Test Specimen Specification

All 6 columns were designed and fabricated with a reinforcement cage which consisted of four 12mm steel longitudinal bars tied with twenty 6mm links as detailed in figure 1. The 5 outermost links at each end were spaced at 60mm to avoid any local failure imposed by loading while the remaining ten were spaced at 120mm centres.

Mix Design and Materials

The research anticipated to produce normal strength concrete with a planned 28 day compressive strength in region of 40–45 N/mm². Three concrete mixes were designed and shown in Table I. Essentially Mix 1 consisted of a plain fibreless mix while Mix 2 contained a combination of steel and polypropylene fibre reinforced concrete. Finally Mix 3 contained a prescribed dosage of polypropylene fibres.

TABLE I. Individual mix proportions for 1 m³.

Ingredients	Mix 1	Mix 2	Mix 3
Water	224	224	224
Cement	440	440	440
Natural concreting sand	800	800	800
Coarse aggregate (10mm)	1000	1000	1000
Steel fibres	-	80	-
Polypropylene fibres	-	3	3

All concrete mixes were produced from standard CEM 1 Class 42.5 N Ordinary Portland cement. Natural concreting sand consisting of fine gain was utilised while 10mm basalt in saturated & surface dried state formed the maximum sized aggregate. The respective fibres utilised were a 100% homopolymer polypropylene (Fibermesh 300 – e3)

and steel (Novocon FE1050). All columns were cured in water for 7 days before being removed. Hereafter the columns were wrapped in plastic with the moisture content maintained between 4.5–7.0 % until furnace testing after 28 days.

Test Methodology

The uniquely designed test rig produced heating rate greater than ISO 834 fire curve using propane burner. Axial loads at 60% of the ultimate design load were imposed laterally via hydraulic rams with loading ratio monitored using load cells. Furthermore displacement values were measured using LVDT's while K type thermocouples measured the surface temperature at three locations along the column. Additionally the gas temperature was collected using an additional thermocouple. All data was independently recorded using data logging software. More extensive test methodology can be obtained in Ali et al ⁽¹³⁾.

EXPERIMENTAL RESULTS

In a mere overview, all 6 columns experienced some unfavourable damage and deterioration with the degree and severity of spalling varying significantly for various column scenarios (see Figure 1). It should be noted that the type and degree of spalling were assessed using criteria previously developed by Ali et al ⁽¹³⁾⁽¹⁴⁾. Table II summarizes the test parameters and measured data. As expected, the control concrete exhibited the worst cases of spalling with degrees of spalling noted to be 22.45 and 15.20% while the combination of steel and polypropylene proved the most effective. This hybrid combination reduced the respective degrees of spalling to 8.57 and 12.41%. During the testing, it was observed that the spalling activity of the plain fibreless concrete was very explosive and violent compared with fibrous samples which were less explosive and only for short durations. Significant deviations in the spalling levels were recorded for the PP samples. The initial polypropylene specimen presented high degrees of spalling which also saw a very unusual spalling pattern take place (spalling of large concrete chunks only in the upper section of column). In addition, the second PP specimen demonstrated minimal levels of spalling. The variation in spalling levels/severities between each case can be attributed to the non homogeneity of concrete. Therefore it is felt that the degree of spalling for the initial PP case should be disregarded since it is deemed out of character with the second case.

TABLE II. Furnace test results.

Ref:	Failure time (mins)	Failure mode	Failure temperature (°C)	Type of Spalling	Degree of Spalling (%)	Moisture Content (%)
C1	40.24	Buckling	918.86	Severe	22.45	6.0
C2	62.00	Buckling	1075.96	Major	15.20	5.5
SPP1	63.00	Shear	1078.12	Minor	12.41	6.9
SPP2	72.85	Shear	1060.09	Minor	8.57	6.8
PP1	50.70	Buckling	1018.18	Severe	22.03	6.3
PP2	69.57	Shear	1058.33	Minor	7.87	5.5



Figure 1. Explosive spalling and columns' failure by buckling and shear.

With respect to axial displacement, all tested columns produced displacement profiles of a similar nature. Initially there was no thermal deflection generated until approximately 380 C of heating. Thereafter the axial displacement increased constantly until reaching a peak value of 6.5 mm at a temperature in the region of a 1000 C. Generally this period of expansion lasted for a duration of approximately 40–60 minutes before the column lost its stability and thus progressed into its runaway condition, consequently failing in a buckling or shearing mode. It can be said that the inclusion of fibres does not influence the trend of thermal expansion development or the maximum value of displacement. The following chapter studies the theoretical estimation of axial displacement and furthermore compares the experimental measurements with numerical prediction.

Effect of Fibres on Concrete Compressive Strength

The fibrous cube samples indicated a decrease in compressive strength compared to the respective control samples. This decrease in residual strength can be principally attributed to the entrainment of air as a result of fibre inclusion. The aforementioned entrainment created a weak porous microstructure which is evident from the results presented in table III.

TABLE III: 7 & 28 day compressive cube results.

Age	Control Mix	Steel + PP Mi	PP Mix
7 Day (N/mm^2)	31.75	25.5	28.5
28 Day (N/mm^2)	42.75	33.25	39.5

THEORETICAL PREDICTION

In addition to the experimental studies, the research aimed to theoretically estimate the trend of axial displacement along with the maximum value. Fundamentally concrete under non ambient conditions will thermally expand. If the axial expansion or elongation is restrained then additional axial forces are created within the column⁽¹⁵⁾⁽¹⁶⁾.

Experimental and numerical comparison

Figure 2 presents a comparison between the experimental findings of the three columns and the FEM calculations using DIANA⁽¹⁷⁾. The model has been developed previously with a more detailed methodology provided in Ali et al⁽¹⁸⁾. It should be highlighted that the model doesn't account for concrete spalling or for the inclusion of fibres in the concrete. The graphical representation demonstrates acceptable agreement with the numerical prediction and the experimental findings. Comparing the percentage difference it can be noted that the combination of steel and polypropylene fibre produced the greatest thermal expansion value of the experimental scenarios, i.e. 13.68 and 9.24% respectively. Ultimately the control samples produced the lowest values for maximum displacement. It can be concluded that the theoretical prediction produces an initial displacement trend which is higher than the experimental findings. The divergence in the results can be attributed to the effect of concrete spalling which has reduced the column section hence affecting the column displacement.

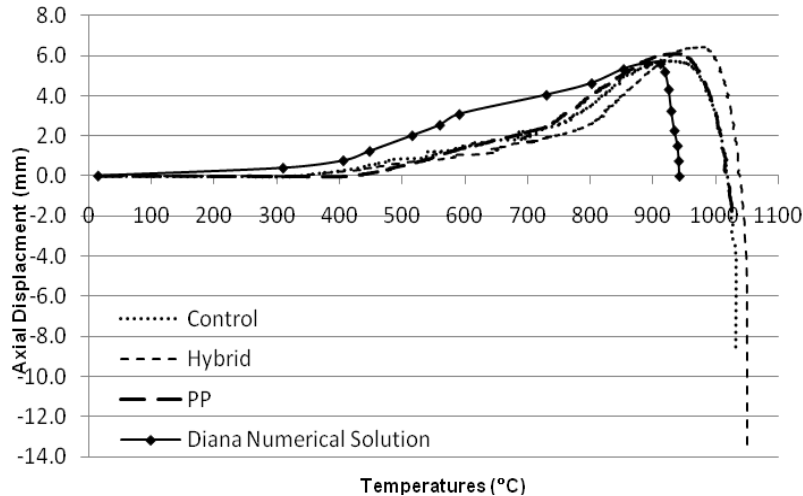


Figure 2. Comparison between experimental results and theoretical estimation.

CONCLUSIONS

1. Cubes containing fibres produced a better mode of failure under compressive failure compared with the fibreless specimens which failed in an explosive and crumbling manner. Concrete containing hybrid or polypropylene fibres produced a 22% and 7.6% compressive strength reduction compared with plain counterpart.

2. The addition of fibres of any type or combination into normal strength concrete delays the time of spalling activity and furthermore reduces the damage under severe heating.
3. The control specimens exhibited severe spalling with large fragments of concrete shrapnel being removed thus recording degrees of spalling in the region of 15.20 – 22.45%. Moreover it was observed that the spalling activity was very explosive and violent compared with the fibre reinforced specimens.
4. The combination of PP and steel fibre (hybrid) exhibited the best performance for spalling reduction. The hybrid fibre reduced the spalling activity to minor non explosive occurrence with the degree of spalling between 8.57–12.41% of the initial column weight. It is believed that this reduction can be attributed to the steel fibre resisting the initiation and expansion of cracks in the concrete matrix while the melting action of the polypropylene fibre created micro channels in the concrete mass which alleviated vapour tension.
5. The presence of polypropylene fibres demonstrated reasonable spalling protection by reducing its occurrence, decreasing the severity (not as explosive) and increasing the overall fire resistance. The degree of spalling was noted as 7.87 and 22.03%.
6. It is worth emphasizing that explosive spalling only occurred when the column specimens were expanding. In effect, no spalling activity was recorded in the contraction phase.
7. From visual observation, it was noticed that spalling only occurred on the trowelled face of the specimens with only minor surface cracks becoming visible on the remaining surfaces. In effect this can be attributed to the particular finishing action which created a less permeable surface with fewer voids and imperfections than the column surface produced from the mould surface thus inducing a greater development of pore pressure.

REFERENCES

1. Effect of various moisture contents, variety and dosage of fibres on explosive spalling and residual compressive strength of high performance concrete subjected to high temperatures. **Song-Hua Bian, Gai-Fei Peng et al.** Switzerland : Trans Tech Publications, 2006, Key Engineering Materials , Vols. 302 - 303, pp. 618–623.
2. Pore pressure and explosive spalling in concrete. **Long T, Phan.** s.l. : Rilem, 2008, Materials and structures , Vol. 41, pp. 1623–1632.
3. Limits of spalling of fire - exposed concrete. **Hertz, K.D.** 2003, s.l. : Elsevier, 2002, Fire Safety Journal , Vol. 38, pp. 103–116 .
4. Effects of elevated temperatures on properties of concrete. **Arioz, Omer.** s.l. : Elsevier Ltd, 2007, Fire Safety Journal , Vol. 42, pp. 516–522.
5. Passive fire protection of concrete structures. **Khoury, G.A.** SB3, s.l. : ICE, 2008, Structures & Buildings, Vol. 161, pp. 135–145.
6. Optimum dosage of PP fibre for the spalling control of high strength reinforced concrete columns. **S.H., Yoo, S.W., Shin and Kim, I. K.** Switzerland : Trans Tech Publications, 2007, Key Engineering Materials , Vols. 348 - 349, pp. 621–624.
7. Effects of porosity and fracture toughness on explosive spalling of concrete. **Dita Matesova, Zbynek Kersner.** s.l. : ZTUREK RSI and Woodhead Publ, 2006, Brittle Matrix Composites 8.
8. Effects of polypropylene fibres on the properties of high strength concretes. **Aulia, T.B.** 2002, Lacer No. 7 , pp. 43–59.

9. High temperature behaviour of HPC with polypropylene fibres from spalling to microstructure. **P. Kalifa, G. Chene, C. Galle.** s.l. : Pergamon, 2001, Cement and concrete research , Vol. 31, pp. 1487–1495.
10. Effect of exposure to elevated temperature on polypropylene fibre reinforced concrete. **Z. Bayasi, M.A. Dhaheri.** 1, 2002, Materials Journal , Vol. 99, pp. 22–26.
11. Residual strength of hybrid fibre reinforced high strength concrete after exposure to high temperature. **Chen, B. and Liu, J.** s.l. : Pergamon , 2004, Cement and Concrete Research , Vol. 34, pp. 1065–1069.
12. Improvement of residual compressive strength and spalling resistance of high strength CR columns subjected to fire. **Cheon-Goo Han, Min-Cheol Han, Young-Sun Heo.** s.l. : Construction and Building materials , 2008, Vol. 23, pp. 107–116.
13. Explosive spalling of high strength concrete columns in fire. **Ali, F.A.** 3, s.l. : Thomas Telford , 2001, Magazine of concrete research, Vol. 53, pp. 197–204.
14. Is high strength concrete more susceptible to explosive spalling than normal strength concrete in fire? **Ali, Faris.** s.l. : John Wiley & Sons, 2002, Fire and Materials , Vol. 26, pp. 127–130 .
15. Calculation of forces generated in restrained concrete columns subjected to fire. **Ali, F., et al.** 2, s.l. : Baywood Publishing Co., 2003, J. Applied fire science , Vol. 12, pp. 125–135 .
16. Calculation of axial forces generated in restrained pin ended steel columns subjected to high temperatures. **Ali, F.A., O' Connor, D.J.** 4, s.l. : Baywood Publishing Co., 1997, J. Applied fire science , Vol. 6, pp. 383–394.
17. **Research, TNO Building and Construction.** DIANA Finite Element Analysis. User Manuals. s.l. : Delft, 2008.
18. Numerical and experimental investigation of the behaviour of high strength concrete columns in fire. **F.Ali, A.Nadjai and S. Choi.** January 2010, Journal of Engineering Structures .
19. Tunnel concretes under fire: Part 1 - Explosive spalling. **Khoury, G.A.** s.l. : Tunnels and Tunnelling, 2006, Concrete , pp. 62–65.

Fire Resistance of a Concrete Box Beam Prestressed by External Tendons

S. TATTONI¹ and A. GASPERI²

ABSTRACT

The paper deals with analytical and experimental results concerning the behavior of a prestressed concrete box beam subjected to fire. The concrete box beam is prestressed by tendons positioned inside the box beam, but outside the concrete (unbounded). The main goals of the research is to find out how the temperature increases in the external tendons in case of fire.

The results of some numerical analysis are reported concerning the box beam subjected to ISO Standard Fire. According to these results the temperature of the tendons, inside the concrete box beam, increases slowly and remains under critical level for more then three hours.

The theoretical results have been validated by an experimental test on a portion of a modified concrete box beam, smaller than the real one, but equivalent to the real box beam as regards the temperature values during fire. During the test, the temperature of the tendon remains under 150 °C for more the 180 minutes.

The experimental results confirm the possibility to reach high fire resistance in a box beam prestressed by unbounded internal tendons.

FOREWORD

In the paper the behavior of a prestressed concrete box beam subjected to fire is illustrated.

The box beam is made of concrete and is prestressed by high strength steel external tendons i.e. by tendons positioned inside the box beam, but outside the concrete (unbounded).

The beam is precast and has been designed as a simple supported main beam for the roofing structure of industrial buildings of large span (30 – 40 m). The main dimensions of the concrete cross section of the beam are illustrated in Figure 1. Note that the tendons are not illustrated.

The main goal of this study is to find out which values of temperature the volume inside the box beam reaches in case of fire, considering that external tendons are located inside this volume.

¹Professor of Structural Engineering, Cagliari University, via Marengo 2, 08123 Cagliari (CA)—Italy

²Consultant Engineer, viale dello Zodiaco, 72, 41126 Modena (MO)—Italy

The values of the temperature in the external tendons are essential for the evaluation of the strength of the beam in case of fire.

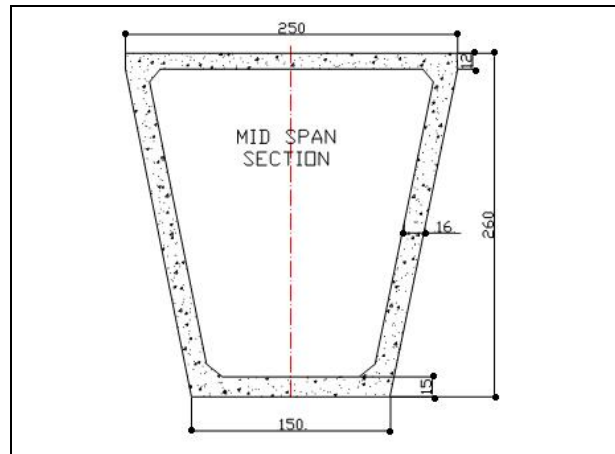


Figure 1. Typical cross-section of the box beam (dimensions in cm).

It is well known that developing a mathematical model concerning the behavior of the air subjected to fire action is not simple and involves flow dynamics. It has been decided to carry out an experimental test to determine the temperature in the concrete beam and in the tendons during a fire.

Due to size (and shape) issues, it has been impossible to introduce in the furnace a full scale portion of the box beam mainly because of his total height (260 cm).

For this reason some numerical analyses have been carried out with the aim to find out a concrete cross section smaller than the real one but with equivalent behaviour, suitable for being introduced into the furnace and being correctly exposed to fire action.

In order to achieve the best fitting model, we have considered that:

- the temperature inside the hollow core of the section depends on the temperature reached by internal walls;
- inside the core the heat diffuses mainly by convection rather than radiation or diffusion;
- the shape of isotherms is nearly parallel to the exposed surface, with the exception of the edges;
- therefore the temperature inside the cavity depends on the thickness of the slab.

Under these hypothesis, a physical model of the box was designed so that the following conditions were fulfilled:

- the material is the same of the actual box (concrete);
- the thickness of the walls S is the same of the actual box;
- only the length L (sum of lateral walls and bottom slab length) is reduced to make the specimen fit the furnace.

The problem of defining the model has been curtailed to define the minimum ratio L/S compatible with the thermal response of the actual beam.

NUMERICAL ANALYSIS

Four FEM thermal analyses (named MG0, MG1, MG2, MG3) have been performed in order to evaluate which are the main variations of the temperature in

the concrete section and how the temperature in some specific points of the section varies, when varying the dimensions of the concrete section itself described by the FEM models.

In MG0 the actual size of the cross section of the box beam are adopted;

in MG1 the ratio between the length L and the thickness S is $L/S = 6$;

in MG2 the ratio is $L/S = 5$;

in MG3 the ratio $L/S = 4$.

The thickness of the bottom slab, the thickness of the top slab and the thickness of the two lateral walls of the section are the same in all models and equal to the real ones. The width of the top slab is the same in all models. In all FEM models, for the evaluation of the temperature, reinforcing bars have been disregarded.

In Figure 2 the cross sections of the concrete box beam taken into account in the four FEM models are illustrated.

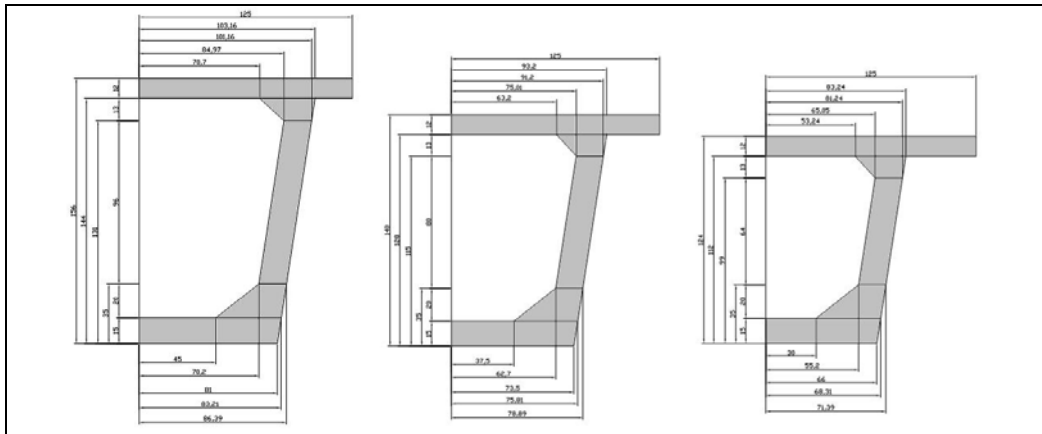


Figure 2. Cross section dimensions of models MG1, MG2 and MG3 (from left).

Table I. Thermal characteristics for concrete.

Siliceous concrete: constant values				
	Convection coeff. (exposed surfaces.)		25.0 W/m ² °C	
	Convection coeff. (not exposed surf.)		9.0 W/m ² °C	
	Resultant emissivity coefficient.		0.56	
	Radiating coefficient.		31.8 · 10 ⁻⁹	
Siliceous concrete: values depending on temperature				
	Temperature °C	Mass kg/m ³	Conductivity W/m ² °C	Spec. heat J/Kg°C
	0	2300	2.000	900.0
	275	2250	1.513	1062.0
	550	2250	1.152	1183.0
	825	2250	0.888	1261.0
	1100	2250	0.808	1297.0

Table II. Thermal characteristics for dry air.

Dry air: constant values				
	Convection coeff. (exposed surfaces.)		5.0 W/m ² °C	
	Convection coeff. (not exposed surf.)		5.0 W/m ² °C	
	Resultant emissivity coefficient.		0.56	
	Radiating coefficient.		31.8 · 10 ⁻⁹	
Dry air: values depending on temperature				
	Temperature °C	Mass kg/m ³	Conductivity W/m ² °C	Spec. heat J/Kg°C
	0	1.3	0.020	1050.0
	275	1.3	0.024	1004.0
	550	0.6	0.042	1040.0
	825	0.6	0.060	1080.0
	1100	0.5	0.075	1120.0

In Table I and Table II are reported the thermal characteristics of the materials involved in the numerical analyses.

The fire action has been simulated according to the ISO 834 temperature-time law. The analyses have been carried out using the code thermoCAD 4.1.

In Figure 3 the values of the temperature after 120 minutes of fire are illustrated for the original section and in Figure 4 the thermal maps for the reduced models.

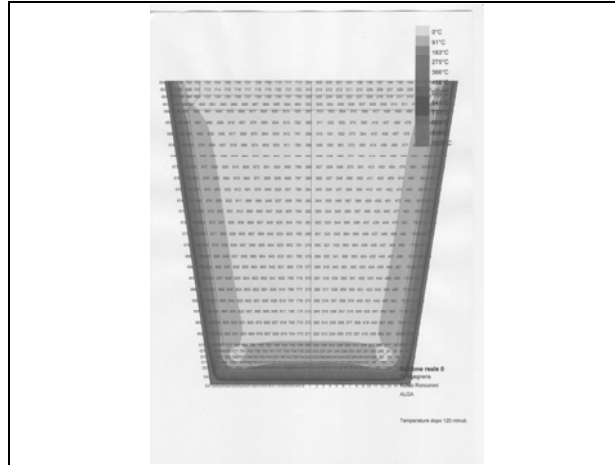


Figure 3. Thermal map of the original shape of the section, computed after 120'.

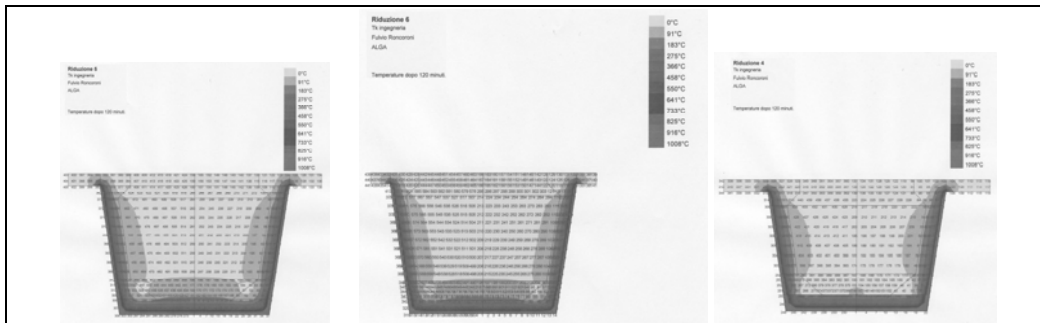


Figure 4. Thermal map of the models MG1, MG2 and MG3 (from left), after 120'.

It can be seen that in all FEM models the general pattern of the temperature is quite similar. Referring to all models, in the bottom slab the isothermal lines, with the exception of the corner zones, are parallel to the midline of the bottom slab itself; in each of the two lateral walls the isothermal lines, with the exception of the corner zones, are parallel to the midline of the lateral wall itself. This means that the length of the bottom slab and of the walls L is not a critical parameter in the thermal analyses.

Inside the box of the beam the values of the temperature are quite similar.

If we consider a line in the middle of the bottom slab and a line in the middle of each lateral wall, we notice that the values of temperatures in the four FEM models, along these lines, are quite similar.

Comparing the temperature patterns, we have recognized that the difference of thermal situations in MG0 and in MG3 analyses are not important, thus being possible to reduce the dimensions of the cross section of the box beam to be tested according to MG4.

EXPERIMENTAL TEST.

Test specimen

Consequently, the smaller proof element was constructed respecting the actual section and it proved to be better exposed to the fire in furnace and results may be considered meaningful nonetheless (Figure 5).

The actual mechanical characteristics of the concrete of the portion of the beam subjected to fire test were: $R_{ck} = 35$ MPa, $R_{cm} = 47.5$ MPa with siliceous aggregate.

Inside the cavity an external tendon was set. It was composed by high strength steel strands, each of them was greased and is inserted in a plastic sheet; all of them were inserted in a HDPE tube (Figure 5).



Figure 5. Test element and internal location of thermocouples (concrete walls and cable).

We remind that the main goal of the test was the measure of the temperature in tendons and specifically in strands; therefore only one of the several tendons which are usually provided for structural need of the actual box beam has been inserted.

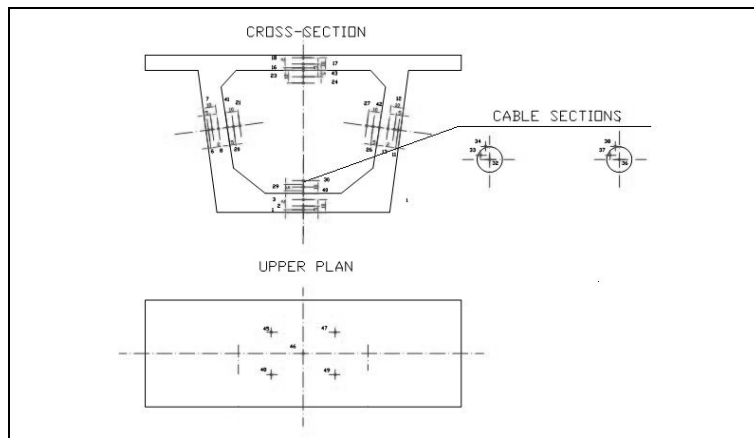


Figure 6. Location of thermocouples on concrete and on cables.

In order to obtain a complete view of the thermal behavior of the box beam, 49 thermocouples have been used during the test. We point out that the thermocouples have been positioned with the maximum accuracy. For example some thermocouples have been positioned in laboratory into prisms of concrete (one thermocouple for each prism) before casting the portion of concrete beam subjected

to fire test; then these prisms (with their thermocouples embedded inside) have been inserted in the reinforcing cage of the box beam, before casting.

Figure 6 shows the location of the thermocouples:

three inside each slab (upper, lower and laterals);

five on the upper surface of the element;

three in the cavity corresponding to the middle point of each slab (on the internal surface of the slab and 50 and 100 mm distance from that surface);

three for each cable (on the surface of the sheath, one on the external surface of the cable and one in the middle).

Test results

In Figure 7 are plotted the values of temperature recorded inside the furnace during the test. From 0 to 180 minutes the actual temperature inside the furnace approximates well enough the ISO 834 temperature-time curve (with temperature which remains a little less than the ISO 834 ones, because the particular size of the specimen has modified the inner shape of the furnace). After 180 minutes from the beginning of the test, the burners of the furnace have been turned off. Recording thermocouples signals has been stopped 360 minutes after the beginning.

In Figure 8 are shown the values of the temperature recorded during the test in the most significant thermocouples.

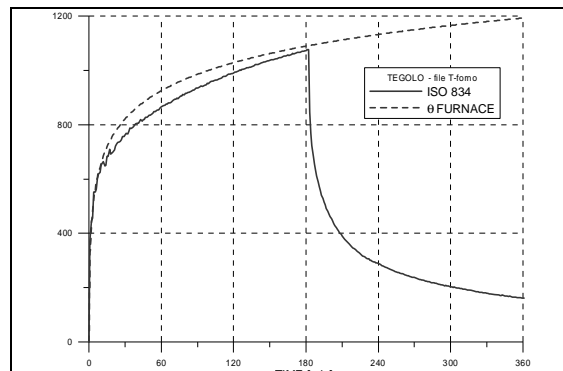


Figure 7. Temperature-Time curve in furnace.

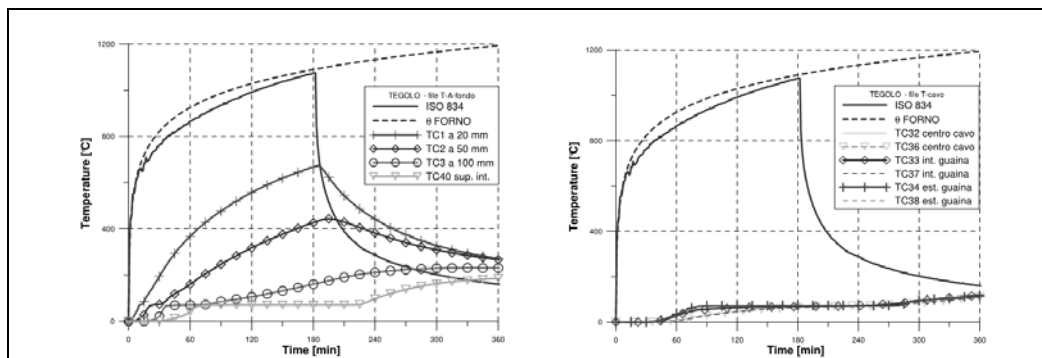


Figure 8. Temperature records in the slab bottom (left) and in the cable (right).

Some comments concerning the results of the test are reported hereafter.

The measures of the thermocouples are generally symmetric.

The temperature of the air inside the box of the beam does not vary significantly on varying the position of the points in which the measures are recorded (on or near the internal surface).

The temperature inside the box remained approximately equal to 100°C for more than 180 minutes. The water inside the mass of the concrete (the quantity of water in the concrete usually varies in the range of 2 - 3 %) moved from the external side of the beam to the internal box and evaporated. We point out that the temperature remains, for a long time almost constant and approximately equal to 100°C.

We note that evaporation of the water has been concluded about 200 minutes after the beginning of the test, after having turned off the burners, due to the residual heat inside the mass of the concrete.

We note that in the first 30 - 35 minutes from the beginning of the test, spalling effects have reduced the thickness of the bottom slab and of some parts of the two lateral walls of about 20 mm.



Figure 9. The test specimen after proofing: some spalling occurred on the bottom concrete (left); cable in almost good condition.

CONCLUSIONS

The study presented in this paper comprises both numerical analyses and an experimental test which have allowed to determine the values of the temperature inside the box beam subjected to a standard ISO fire.

The numerical analyses have mainly permitted to reduce the dimensions of the portion of the box beam tested in the furnace, without introducing unacceptable errors.

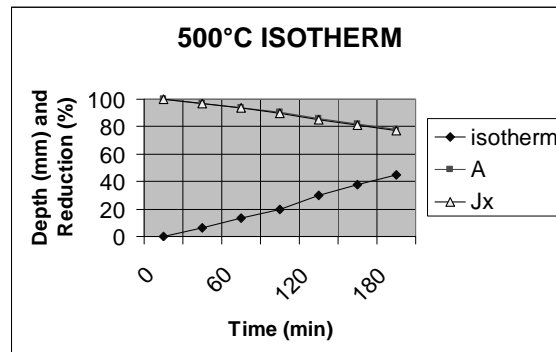


Figure 10. Position of 500°C isotherm from exposed surface with time and reduction of geometrical characteristics of the cross-section (Area A and Moment of Inertia J_x).

The experimental test has shown that the temperature inside the concrete beam remains low for more than three hours. This phenomenon is due to the water that is inside the mass of the concrete. We point out that the temperature of the external tendon, which is inside the box beam, has remained low for more than three hours, allowing the tendon to maintain almost unchanged the strength characteristics that it has at 20°C.

Without drawing any hurried conclusion, we think that the typology of concrete box beam prestressed by unbounded internal tendons, may generally be a good solution regarding fire resistance. As a matter of fact we observed that the 500°C isotherm has a rate of penetration almost linear with time (**Figure 10**) and consequently the reduction of area A and inertial moment J_x doesn't exceed 15% after 2 hours of standard fire.

REFERENCES

1. Kordina K., Meyer-Ottens C., "Beton Brandschutz Handbuch", *Beton Verlag*, Düsseldorf 1981.
2. Richter E., "Zur Berechnung der Biegetragfähigkeit brandbeanspruchter spannbetonbauteile unter Berücksichtigung geeigneter Vereinfachungen für die Materialgesetze" *IBMB, Braunschweig*, Heft 80 1987
3. Iding R., Bresler B., Nizamuddin Z., "Fires-T3. A Computer Program for the Fire Reponse of Structures-Thermal", *Fire Research Group, Un. of California, Report n°UCB FRG 77-15*, October 1977.
4. Italian Code UNI 7677 "Prove al fuoco. Termini e definizioni."
5. Italian Code UNI 7678 "Elementi costruttivi. Prove di resistenza al fuoco."
6. EN 1992-1-2 "Progetto al fuoco di strutture in c.a."
7. Buchanan A. H., "Structural Design for Fire Safety", *John Wiley & Sons Ltd*, Chicester UK, 2002
8. Tattoni S., "Fire Resistance of Precast Elements: Research Activity within th Italin Project ULISSE". *Proc. Workshop Fire Design of Concrete Structures: What now? What next?*, Milano, Italy, dec 2-3, 2004.

Behavior of Concrete Columns Subjected to Fire

A. M. B. MARTINS and J. P. C. RODRIGUES

ABSTRACT

This paper presents the results of an experimental and numerical study to clarify the influence of the surrounding building structure in the behavior of reinforced concrete columns subjected to fire. The parameters studied were: the longitudinal reinforcement ratio, the slenderness of the column and the stiffness of the surrounding structure to the column in fire. The experimental study was complemented by a numerical study carried out using the finite element program SAFIR.

The results of the numerical and experimental study are compared in this paper.

INTRODUCTION

The performance of a building structure in a fire event depends greatly on the behavior of the columns. The fire action on a building column can lead to severe consequences because its collapse can lead to the progressive collapse of the whole building [1-2]. A column in a building when subjected to fire tends to elongate, however the remaining structure that might remain at lower temperature will impose restraint to its elongation. The influence of the thermal restraining on the behavior of steel columns subjected to fire has been studied previously by many authors [3-4]. But the same cannot be said for reinforced concrete (RC) columns where only few studies were conducted [5-7].

In the past, the verification of the fire resistance of structures could only be made by subjecting structural members to standard fire resistance tests. Nowadays, the Eurocodes make it possible that the structural engineer can use tabulated data, simplified and advanced calculation methods. The tabulated data and the simplified calculation methods are used to single elements and don't take into account with the influence the building surrounding structure to the column under fire.

Alberto Miguel B. Martins and João Paulo C. Rodrigues (jpaulocr@dec.uc.pt). Department of Civil Engineering, Faculty of Sciences and Technology, University of Coimbra, 3030-788 Coimbra, Portugal

This paper presents some results of a research work concerning the fire behavior of RC columns with restrained thermal elongation that was carried out in the University of Coimbra, Portugal [8]. Experimental tests were performed and numerical models were developed. Simplified calculation methods proposed in the EN1992-1-2 [9] were also applied and the results analyzed and some conclusions drawn.

EXPERIMENTAL PROGRAMME

The experimental research carried out had the main objective of studying the behavior of RC columns with restrained thermal elongation subjected to fire.

In the tests the study parameters were the longitudinal reinforcement ratio, the slenderness of the columns and the stiffness of the surrounding structure (restraint level).

Test Specimens

The test specimens were RC columns of 3000 mm tall and with two different cross-sections (250 mm×250 mm and 160 mm×160 mm). They were connected to the restraining frame by a steel plate at each end. The steel end plates measured 450 mm×450 mm×30 mm and were made of class S355 steel. The connection between the concrete columns and the steel end plates was strengthened by welding the longitudinal steel reinforcement bars and a steel hook to them before concrete casting. Table I summarizes the characteristics of the specimens tested.

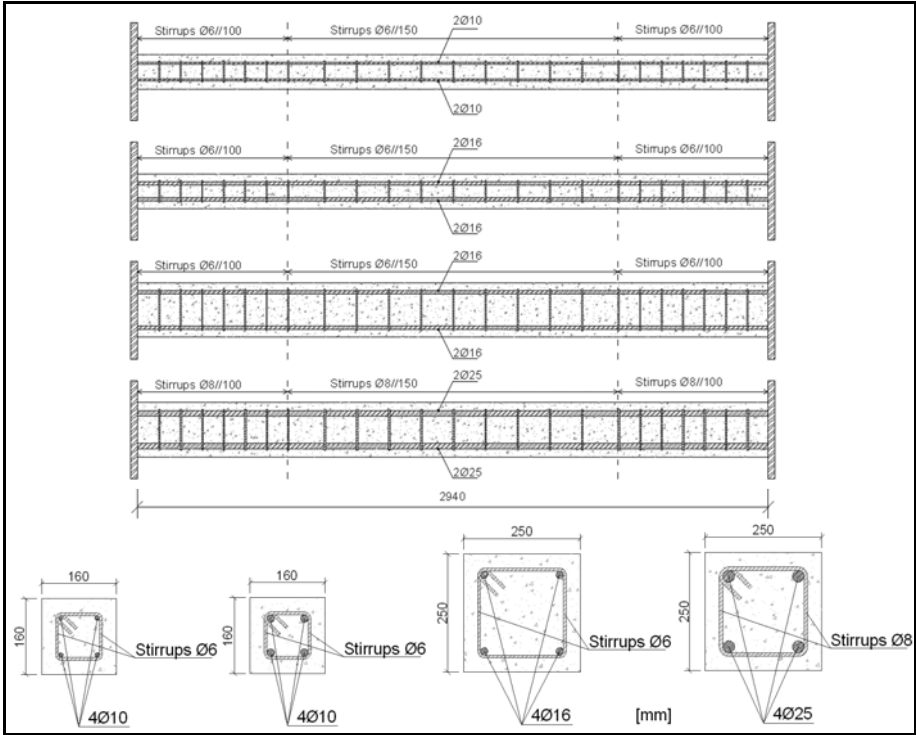
TABLE I. Characteristics of the test columns.

Column Reference	Cross-section		Longitudinal Reinforcement		Reinforcement ratio A_s/A_c [%]
	$h \times b$ [mm] × [mm]	Area, A_c [mm ²]	Number and Diameter	Area, A_s [mm ²]	
C16-10-K13	160 × 160	25600	4 10	314.2	1.23
C16-10-K45	160 × 160	25600	4 10	314.2	1.23
C16-16-K13	160 × 160	25600	4 16	804.2	3.14
C16-16-K45	160 × 160	25600	4 16	804.2	3.14
C25-16-K13	250 × 250	62500	4 16	804.2	1.27
C25-16-K45	250 × 250	62500	4 16	804.2	1.27
C25-25-K13	250 × 250	62500	4 25	1963.5	3.14
C25-25-K45	250 × 250	62500	4 25	1963.5	3.14

The first column indicates the specimen reference. Thus, as an example, reference C25-16-K45 indicates that the dimensions of the cross-section of the specimen are 250 mm×250 mm, the diameter of the longitudinal steel reinforcement is 16 mm and the stiffness of the surrounding structure is 45 kN/mm.

Figure 1 shows a longitudinal and a cross-sectional view of the specimens and details of the steel reinforcement. C20/25 calcareous aggregate concrete and

A500NR reinforcing steel bars were used for all test specimens. The concrete covering of all tested columns was 30 mm.



Test Set-up

In Figure 2 is presented a general view of the experimental test set-up.

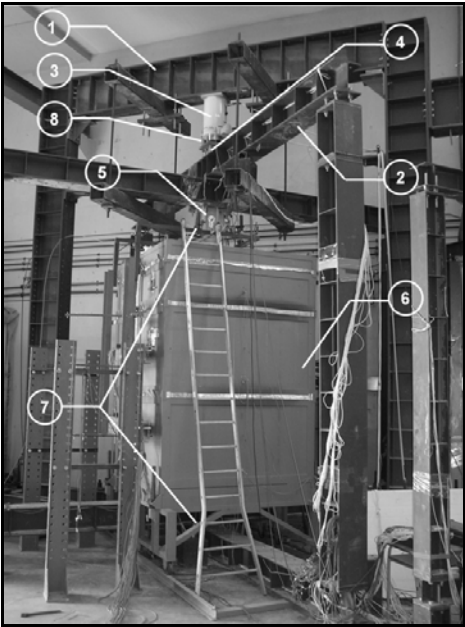


Figure 2. Experimental set-up.

The system comprised a two-dimensional reaction frame (1) with two HEB500 columns and an HEB600 beam of class S355 steel. This reaction frame was used to support a hydraulic jack that applied a compression load to the column. The load that was kept constant for the entire test, intended to simulate the serviceability load of the column when in a real building. The load was considered as 70% of the value of the columns' design load at room temperature, calculated according to EN1992-1-1 [10].

The hydraulic jack (3) used to apply the load had a maximum capacity of 3 MN and was controlled by a hydraulic central unit. A compression load cell of 1 MN (4) placed between the hydraulic jack and the top of the upper beams of a three-dimensional restraining frame (2) monitored the load.

The three-dimensional restraining frame was designed to simulate the structure surrounding the column in a fire case. It was composed of four columns and four HEB300 beams of class S355 steel, orthogonally arranged. Two stiffness values of the surrounding structure were tested: 13 kN/mm and 45 kN/mm. These stiffness values were achieved by changing the position of the columns of the three-dimensional restraining frame between tests. The elements in the experimental set-up were connected by means of M24 class 8.8 bolts.

The restraining forces developed due to the heating of the columns were measured by a compression load cell of 3 MN placed inside a special device built for the purpose (5).

The thermal action was applied to the specimens by means of a modular electric furnace (6) of internal dimensions 1500 mm×1500 mm×2500 mm, capable of temperatures up to 1200°C and able to follow fire curves with different heating rates. The heating curve applied was the standard fire curve ISO 834.

The axial displacements were also measured at the ends of the columns (7) by two sets of linear variable displacement transducers (LVDTs). Four LVDTs were located in the bottom and three in the top. They were arranged orthogonally to form a deformation plane to enable the calculation of both the axial displacements and the rotations at the ends of the columns. Another LVDT was placed near the point where the load was applied so to control the vertical displacement at that point (8).

The temperatures in the test specimens were registered by type K thermocouples placed in three sections in the vertical direction of the test columns (Figure 3).

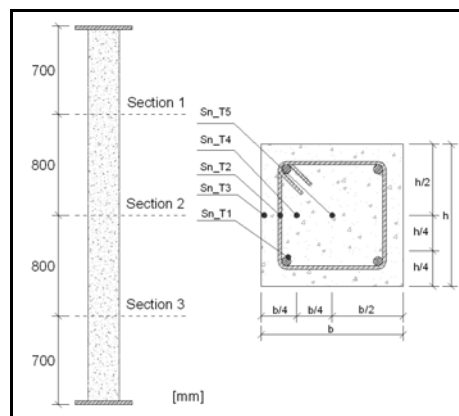


Figure 3. Location of the thermocouples in the test columns (n indicates the section number).

Five thermocouples were placed in each section, two welded to the longitudinal and transverse reinforcement bars and the other embedded in the concrete at various depths (one near surface, another in the centre and a third midway between them).

NUMERICAL SIMULATIONS

As stated in the EN1992-1-2 [9] the numerical models are classified as advanced calculation methods and they must allow the calculation of the temperature evolution in the structural members and also the evaluation of their mechanical behavior due to the fire. Considering that the temperature distribution is not dependent of the stress distribution in the members, it is possible to solve the problem of a structural member or structure subjected to fire in two separate steps [11–12]. First, the temperature distribution due to the thermal action is determined and then the mechanical analysis is carried out taking into account the mechanical actions and the temperatures calculated previously.

The numerical simulations were carried out with the SAFIR computer program developed in the University of Liège. The program is based on the finite element method and allows the non-linear thermo mechanical analysis of concrete, steel and composite steel and concrete structures subjected to fire [13].

Thermal Analysis

The thermal analysis was made by using 2D numerical models. The analysis was performed for the cross-section of each tested column. Quadrilateral isoparametric finite elements of 4 nodes were used.

The relevant physical and thermal properties of concrete and steel used were the ones stated in the EN1992-1-2 [9]. For the convection coefficient and emissivity of the concrete were used $25 \text{ W/m}^2\text{K}$ and 0.7, respectively.

The thermal action used in the models was the gas temperature registered in the furnace during the experimental tests.

Mechanical Analysis

The experimental system (test column and restraining frame) was modeled as a 3D framed structure using 3-node Euler-Bernoulli beam elements. The concrete and reinforcing steel were modeled using the non-linear stress-strain relationships proposed in the EN1992-1-2 [9]. Several authors refer the importance of the transient strain in the structural analysis of concrete elements, mainly columns. The constitutive law adopted contains implicitly the various strain components including the transient strain.

SIMPLIFIED CALCULATION METHODS

In the EN1992-1-2 [9] are proposed various simplified calculation methods to evaluate the fire resistance of RC columns, namely the zone method, the $500 \text{ }^\circ\text{C}$

isotherm method and two tabulated data methods (method A and method B). In this research work, the 500 °C isotherm and the method A were used.

To enable the application of the 500 °C isotherm method, a FORTRAN computer program was developed. The isotherm position and the temperatures of the steel reinforcement bars were assessed using the numerical results of the thermal analysis models performed with program SAFIR.

RESULTS AND ANALYSIS

Temperature Distribution

Figure 4 gives, as an example, the evolution of temperature, in cross-section S3 for column C25-16-K13, obtained in the test and numerical simulation. The standard fire curve ISO 834 and the furnace temperature are also presented. It can be stated that the numerical results (dashed lines) are close to the experimental measurements.

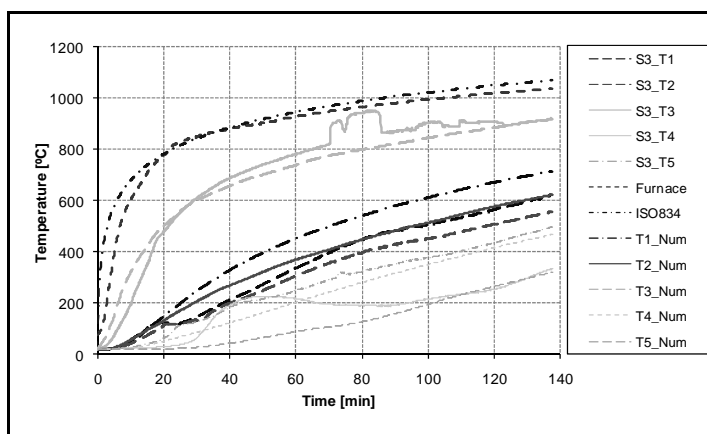


Figure 4. Temperature in cross-section 3 of column C25-16-K13 as a function of time (experimental vs numerical).

Fire resistance and restraining forces

In Figure 5 is presented, as an example, the evolution of the relationship (P/P_0) in function of time obtained in the experimental tests and numerical simulations.

In the experimental tests the fire resistance was defined as the time when the restraining force (P) drops to the initial value of the applied load (P_0). The numerical simulation predicts satisfactorily the maximum restraining forces and the fire resistance of the columns tested.

From the graphs it can be observed that increasing the cross-section from 160mm×160mm to 250mm×250mm led to an increase of the fire resistance from 90 to 135 min (Fig. 5 (a) and (b)). The increase of the diameter of the longitudinal reinforcement bars from 16 to 25mm led to a small increase of the fire resistance from 135 to 140 min (fig 5 (b) and (d)). The increase of the stiffness of the surrounding structure from 13 to 45kN/mm led to an increase of the restraining forces but nothing was observed in relation to the fire resistance (fig 5 (b) and (c)).

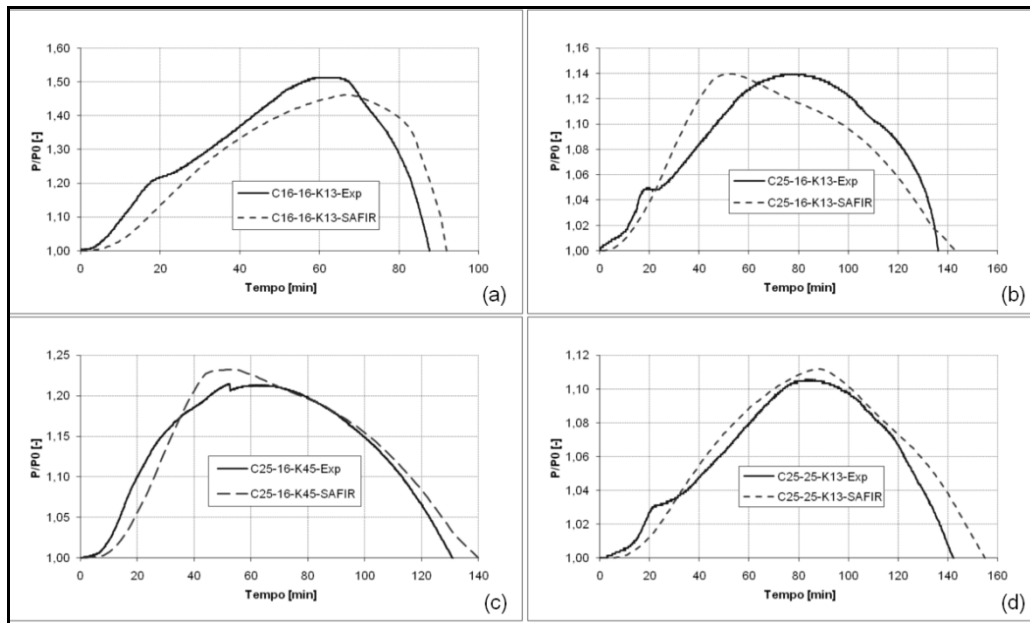


Figure 5. Relationship (P/P_0) in function of time (experimental vs numerical).

Tables II and III summarize the results obtained for the restraining forces and fire resistance of the tested columns.

TABLE II. Fire resistance and maximum restraining forces (experimental vs numerical).

Column reference	P_0 [kN]	Fire resistance [min]			Restraining forces [kN]		
		Experimental	SAFIR	Diff. [%]	Experimental	SAFIR	Diff. [%]
C16-16-K13	181.06	87.73	88.70	1.11	92.72	83.64	9.79
C25-16-K13	494.71	136.22	143.00	4.98	68.85	73.19	-6.30
C25-16-K45	507.40	131.67	140.00	6.33	108.78	108.70	0.07
C25-25-K13	656.34	143.53	155.00	7.99	69.36	73.36	-5.77

TABLE III. Fire resistance obtained with the calculation methods used.

Column reference	Fire resistance [min]			
	Experimental	SAFIR	Isotherm 500°C	Method A
C16-16-K13	87.73	88.70	56.93	45.26
C25-16-K13	136.22	143.00	84.26	52.49
C25-16-K45	131.67	140.00	83.82	52.49
C25-25-K13	143.53	155.00	93.33	69.10

CONCLUSIONS

From the experimental results obtained in this research work the following conclusions can be drawn:

- Increasing the longitudinal reinforcement ratio increases the fire resistance of RC columns and also the restraining forces, however, the increase in the restraining forces is not relevant.
- The slenderness increasing causes a significant reduction on the fire resistance and an increase in the restraining forces.
- As expected, increasing the restraint against thermal elongation, higher restraining forces were generated. Concerning the fire resistance a small

reduction was observed. This reduction was not higher due to the fact that in this experimental set-up associated to an increase of the axial stiffness is an increase of the rotational stiffness to the column in test. The increase of the axial stiffness reduces while the increase of the rotational stiffness increases the fire resistance.

The numerical models were developed assuming certain hypotheses, however, the results obtained are satisfactory since the simulations predict adequately the maximum restraining forces, the fire resistance and the temperature distribution.

In the thermal analysis the differences observed may be due to the disregard in the modeling of the concrete cracking, of the spalling phenomenon and of the vapor flux and change of phase inside the concrete mass. The concrete cracking and spalling were not taken into account in the mechanical models which can justify the differences obtained. However, the numerical results obtained for the restraining forces and for the fire resistance are close to the obtained with the experimental tests. It can also be referred that the constitutive model adopted for the concrete and proposed in the EN1992-1-2 [13] was adequate to model the experimental behavior observed.

From the application of the 500 °C isotherm method proposed in EN1992-1-2 [9] it can be noticed that these method led to smaller values of the fire resistance than those obtained in the experimental tests. The method A proved to be very conservative.

REFERENCES

1. Usmani, A.S., Rotter, J.M., Lamont, S., Sanad, A.M. e Gillie, M., 2001. "Fundamental principles of structural behaviour under thermal effects", *Fire Safety Journal*, 36: 721–744.
2. Kodur, V.K.R., Wang, T.C., Cheng, F.P., 2004. "Predicting the fire resistance behaviour of high strength concrete columns", *Cement & Concrete Composites*, 26: 141–153.
3. Correia Rodrigues, J.P., Cabrita Neves, I., Valente, J.C., 2000. "Experimental research on the critical temperature of compressed steel elements with restrained thermal elongation", *Fire Safety Journal*, 35: 77–98.
4. Cabrita Neves, I., Valente, J.C., Correia Rodrigues, J.P., 2002, "Thermal restraint and fire resistance of columns", *Fire Safety Journal*, 37: 753–771.
5. Lie, T.T., Lin, T.D., 1985. "Influence of Restraint on Fire Performance of Reinforced Concrete Columns", *Fire Safety Science—Proceedings of the First International Symposium*, Gaithersburg.
6. Ali, F., Nadjai, A., Silcock, G., Abu-Tair, A., 2004. "Outcomes of a major research on fire resistance of concrete columns", *Fire Safety Journal*, 39: 433–445.
7. Benmarce, A., Guenfoud, M., 2005. "Behaviour of axially restrained high strength concrete columns in fire", *Construction and Building Materials*, article in press.
8. Martins, A.M.B., 2009. *Fire Resistance of Reinforced Concrete Columns with Restrained Thermal Elongation*, MSc Thesis, University of Coimbra, Portugal (in Portuguese).
9. CEN, 2004. *Eurocode 2: Design of Concrete Structures—Part 1-2: General rules—Structural Fire Design*, CEN – Comité Européen de Normalisation, Brussels.
10. CEN, 2004. *Eurocode 2: Design of Concrete Structures—Part 1-1: General rules and rules for buildings*, CEN—Comité Européen de Normalisation, Brussels.
11. Terro, M.J., 1998. "Numerical modelling of the behaviour of concrete structures in fire", *ACI Structural Journal*, Vol. 95, No. 2: 183–193.
12. Zha, X.X., 2003. "Three-dimensional non-linear analysis of reinforced concrete members in fire", *Building and Environment*, 38: 297–307.
13. Franssen J.-M., 2005. "SAFIR. A Thermal/Structural Program Modelling Structures under Fire", *Engineering Journal*, A.I.S.C., 42, 3: 143–158.

The Influence of Travelling Fires on the Response of a Concrete Frame

A. LAW, J. STERN-GOTTFRIED, M. GILLIE and G. REIN

ABSTRACT

Experimental and theoretical work, as well as real fires such as occurred in the Windsor tower and TU Delft, show that compartment fires travel around the floor plate of structures. Despite this evidence, structural fire design almost without exception assumes uniform, single-curve design fires. This paper adopts an alternative methodology for studying the effect of fire on a concrete frame structure. The fifth floor (42 m by 28 m and 3.6 m high) of a nine storey building is analysed when subject to a variety of “travelling” design fires whose temperatures vary with space and time.

The structural effects on the frame of five travelling fires whose behaviour is based on fundamental fire dynamics are compared with the structural effects of uniformly distributed parametric fire and Standard Fire curves. Each part of the concrete frame is assessed using several different measures of structural behaviour for each fire scenario. The differences in the structural response for the multiple fires are then compared. Additionally, the structure is analysed after returning to ambient temperature for each fire scenario. This allows a residual-state analysis to be conducted on the structure. It is concluded that there are clear needs and benefits in using a travelling design fire as the basis for a comprehensive structural design.

INTRODUCTION

Current methods of structural design allow the development of large finite-element models that are used to assess the performance of the building in fire conditions. Designers subject these models to temperature-time curves (design fires) and study the response of the structure to these fires. While the commonly

Angus Law, PhD Student, BRE Centre for Fire Safety Engineering, University of Edinburgh, UK, email: A.Law@ed.ac.uk

Jamie Stern-Gottfried, PhD Student, BRE Centre for Fire Safety Engineering, University of Edinburgh, UK; Senior Fire Engineer, Arup Fire, London, UK, email: Jamie.Stern-Gottfried@arup.com

Martin Gillie, Lecturer, BRE Centre for Fire Safety Engineering, University of Edinburgh, UK, email: M.Gillie@ed.ac.uk

Guillermo Rein, Lecturer, BRE Centre for Fire Safety Engineering, University of Edinburgh, UK, email: G.Rein@ed.ac.uk

used temperature-time curves are useful, and represented breakthroughs in the discipline at their times of adoption, they have inherent limitations with regards to their range of applicability [1].

An assumption inherent to the traditional design fires is that uniform temperature conditions are developed throughout the whole floor of the compartment. A fire that would cause these types of conditions would burn uniformly within the enclosure and generate high temperatures for only relatively short duration. This is opposed to a travelling fire that burns locally but spreads through the enclosure with time, generating lower temperatures for longer times. Buchanan [4] notes that post-flashover fires in open plan offices are unlikely to burn throughout the whole space at once. Real, large fires that have lead to structural failure, such as those in the World Trade Center towers 1, 2 [2] and 7 [3] in September 2001, the Windsor Tower in Madrid, Spain in February 2005 [4] and the Faculty of Architecture building at TU Delft in the Netherlands in May 2008 [5] were all observed to travel across floor plates.

To better address the limitations of traditional design fires, a methodology [6-8] has been developed that allows for a wide range of possible fires, including both uniform burning and travelling fires, by considering the fire dynamics within a given building. This methodology also facilitates the collaboration between fire safety engineers and structural fire engineers, which is an identified need within the structural fire community, to jointly determine the most challenging fire scenarios for a structure [9].

There are a large number of different fires that could potentially occur in a building. It is only the most severe fires that are of interest for design. As for non-thermal loads, the structural engineer must identify which of the possible scenarios is likely to be the most severe condition for a structure and design on this basis. This paper begins the process of identifying which travelling fires induce a high level of structural distress.

FIRE METHODOLOGY

The new approach to design fires divides the effect of a fire on structural elements into the near-field and the far-field [1, 6, 7]. Near-field temperatures occur when a structural element is exposed directly to the flames of the fire (approximately 1200°C) and far-field temperature when it is exposed to the smoke layer. By varying the size of the near-field, a family of fires that covers the range of possible fires in a structure can be developed. It was assumed here that each fire in the family would burn over a fixed percentage of the total floor area of the building, ranging from 2.5% to 100%. The burning area of the fire that is equal to 100% of the floor area is a well distributed fire. The fires that only burn a proportion of the total floor area are represented by the changing location of the near-field. As fuel is consumed, the fire moves to another part of the building; these are travelling fires.

For simplicity, the far-field of each fire case is represented by a constant temperature calculated using a radiation biased average.

STRUCTURAL ASSESSMENT

Once the designer has selected a fire, finite element software can be used to model the impact of changing temperatures on the structure. The designer can then interpret the results of these analyses to decide whether the structure has the required resilience to the effect of extreme heating, or whether a redesign is required. It is the interpretation of the results where some ambiguities exist. Quantification of the effect of fire on the structure can be assessed a number of measures: rebar temperature [10]; midspan deflection; rate of deflection [11]; and rebar strain [12].

Although each of these methods is a useful indicator of some degree of structural distress, none of them are definitive indices that allow absolute structural failure to be determined. Sectional analysis is probably the most effective method for the assessment of how close a structure is to failure. However, even this does not allow the shear resistance of the structural elements to be assessed. For the purposes of this study, the measures used to assess the structure are rebar temperature and strain.

PROPOSED STRUCTURE

The methodologies outlined above were implemented on a nine story concrete structure. This was designed in accordance with the Eurocode [13-15]. The plan for the structure is shown in Figure 1; the total floor-plate was 42x28m. Every floor was of flat slab construction and each floor slab was 200mm thick; the interior columns were 400x400mm; and the exterior columns were 300x300mm. The design strength of the concrete in the columns was 48MPa, and the design strength of the concrete in the slabs was 40MPa. As the intended fires were to take place on the mid-floors of the structure, the foundations were not designed, and the columns were assumed to be rigidly fixed at the base. To allow the study of the different fires and their effects, a finite element model of the structure was created.

As the fires were restricted to fourth floor burning, it was possible to create a finite element model of the central region of the structure. The finite element model used throughout this paper extended from a height of 11.4m to 22.6m. The slab was modelled using shell elements, and the columns were modelled using three-dimensional solid elements. The rebar were modelled using truss elements. The model was created using the commercially available finite-element software, Abaqus [16]. All of the material properties used in the model were in accordance with EC2, and the yield criterion used for the concrete throughout the structure was the “damaged plasticity” model available in Abaqus, based on the work of Lubliner [17]. The concrete fracture energy used throughout this study was artificially high. A sensitivity study was conducted to analyse the impact of the using different fracture energies on the global behaviour of the structure. The error, in terms of total deflections, introduced by the sensitivity was 3.9% in the case of the columns, and less than 2% in the case of the slabs. It was decided, therefore, that the artificially high fracture energies were acceptable as the impact structural trends was minimal.

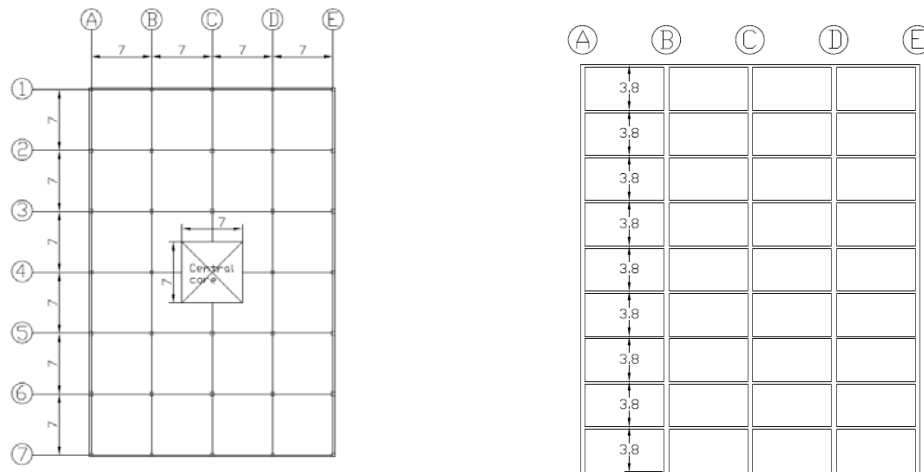


Figure 1. Plan and elevation.

The base of each column was assumed to be fixed in translation and rotation, and the top of each of the columns was fixed in all directions other than the vertical. As the higher stories of the structure were not modelled, the equivalent loads that would have been transferred into the column heads were calculated using a full frame elastic model and applied to the remaining structure during the loading phase of the analysis. The central core of the building was not modelled discretely; instead it was assumed to provide rigid restraint to the adjoining structure.

BASIC TRAVELLING FIRES

Initially a family of travelling fires (Figure 2) were applied to the model. In the case of the building described above, these fires were represented by a near-field which moved linearly from one side to another as illustrated in Figure 3. The near-field had a temperature of 1200°C; the temperature of the far-field was constant within each case. To quantify the degree of structural distress, two of the basic measures described above were used; the average tension rebar temperatures and the strain in the tensile rebar.

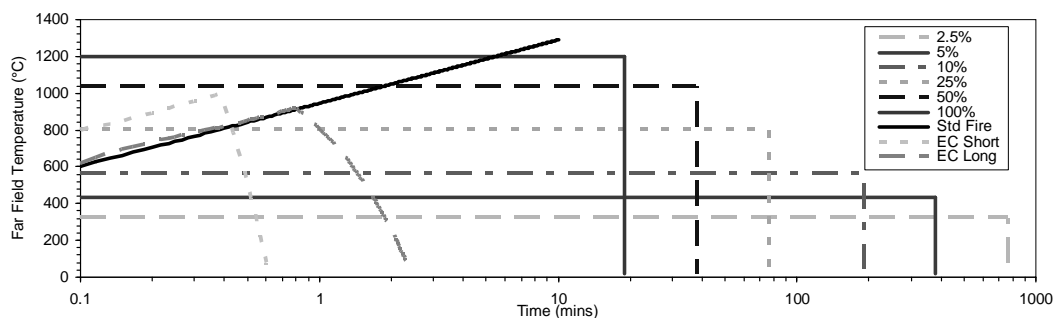


Figure 2. Base case fire far-field temperature.

For comparison, three of the more conventional design fires were also considered. The structure was subject to a two-hour standard fire; a “short-hot” parametric fire of duration 36 minutes with a peak temperature of 990°C; and a

“long cool” parametric fire of duration 145 minutes with a peak temperature of 915°C.

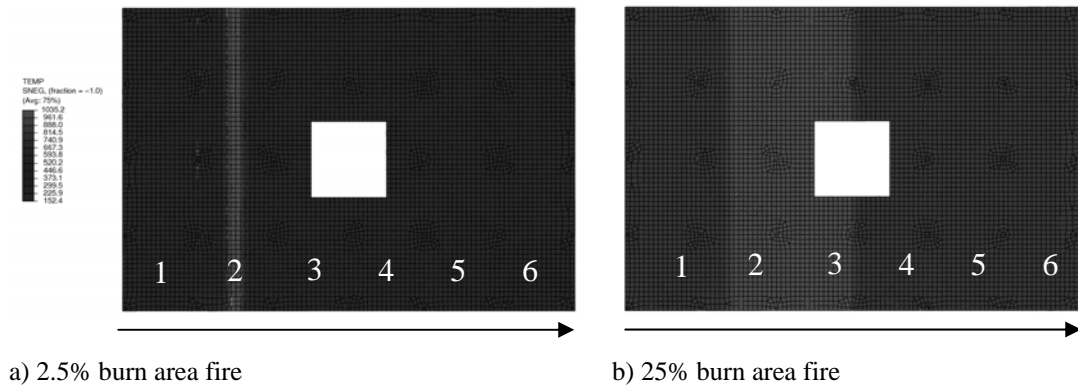


Figure 3. Fire progression across floor-plate. Structural bay numbers are also indicated.

Heat Transfer Analysis

A series of heat transfer analyses were conducted using the finite-element software, Abaqus. The temperature of the lower rebar layer for each bay was averaged. The bay which reached the average highest temperature is given as the result for the whole fire scenario. In all cases, except where stated, this corresponds with the final bay to be heated, bay six. The bay temperatures were averaged to prevent the results from being skewed by localized high temperature. For example, if a small fire were to heat the mid-span of one of the bays, very high temperatures would be recorded locally in the rebar, despite a negligible overall effect on the rest of the structure.

Table I presents the maximum average-rebar-temperatures for bay six for each of the base case burn areas. Also presented are the maximum temperatures reached during the Standard Fire, the “short-hot” and the “long-cool” parametric fires. It can be seen that the maximum rebar temperature is obtained during the Standard Fire exposure. The burn time for the Standard Fire in this case was two hours.

TABLE I. REBAR TEMPERATURES AND FIRE TIMES.

Fire Type	Standard Fire	Short Hot	Long Cool	2.5% Base	5% Base	10% Base	25% Base	50% Base	100% Base
Fire Duration (minutes)	120	36	145	760	380	190	76	38	19
Max. Bay Temperature (°C)	496	246	325	333	403	448	450	374	299

It is clear from Table I that some of the fires developed using the new methodology induce higher average-rebar-temperatures than both of the parametric fires. Of the travelling fires, the 10% and 25% burn areas induce the highest average-rebar-temperatures—these cases are highlighted.

Rebar Strain

For the same fires, the sagging rebar strains were also analysed. The maximum sagging strain that occurred in a bay at any time is shown in Figure 4. In all cases—apart from the 2.5% fire—the highest strains were recorded in bay four. It can be seen that the results show a similar trend to the temperature profiles for the steel. However, it must be noted that the maximum strains occur during the cooling phase of each fire. The strains which occurred during the Standard Fire are the largest, while those that occurred due to the parametric fires are significantly smaller—particularly the “long cool” fire. Of the fires developed using the new methodology the 10% and 25% fires induced the highest sagging strains in the model. It was also found that the 5% fire caused significant strains, while the 2.5%, 50% and 100% fires caused the lowest strains.

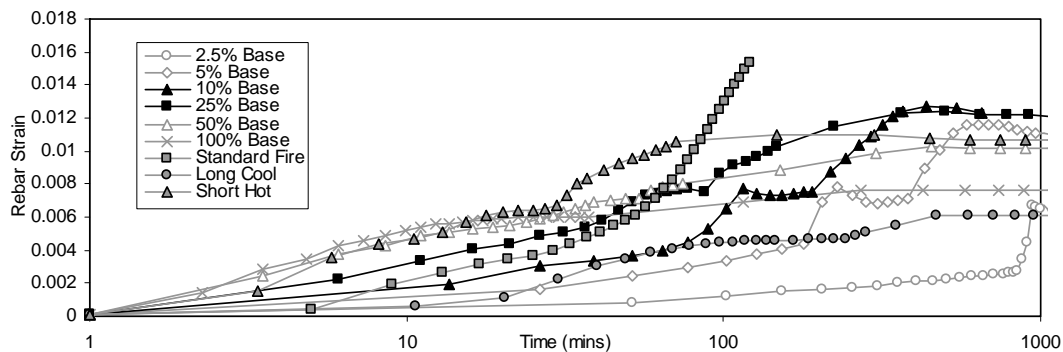


Figure 4. Maximum strain profiles for base cases and traditional fires.

OTHER TEMPERATURE PROFILES

It should be emphasised that the “base case” fires above do not represent a complete design approach for an engineer, but rather serve to help identify the potentially more critical fires which a structure could undergo. As such, there are many other scenarios to which the building could be exposed. A parametric study was conducted to analyse the effects of non-uniform far-field exposure and several different fire paths. As the 25% burn area fire was found to be one of the most critical base cases fires, each analysis in the parametric study was conducted only with this burn area.

The effect of several parameters was studied: the influence of a non-uniform far-field temperature field; the influence of a gradually moving fire (rather than suddenly moving); and the influences of different fire shapes. The non-uniform far-field was defined using the ceiling jet correlation developed by Alpert [18]. The gradually moving fire was represented by the near-field moved gradually between burn zones as opposed to suddenly jumping from one to the next. A far-field defined using two different temperatures was also used.

It was found that the base case (single far-field) fire induced higher temperatures than any of the fires that varied way that far-field was applied (Table II). The maximum sagging rebar strains induced by these fires were very similar—within 2.5% of each other as is demonstrated in Figure 5a.

In addition to the different far-field definition methods, several different fire shapes were represented by: a ring of fire gradually moving inwards/outwards; and

the fire moving clockwise around the structure. The rebar temperatures induced by these fires were very similar. This was unsurprising as each of the fire shapes induced a very similar heating regime in the most critical bay as is shown in table II. As with the different far-field heating profiles, the difference in the maximum strains was very small (Figure 5b); the outwardly progressing ring produced marginally higher strains.

TABLE II. MAXIMUM TEMPERATURES FOR DIFFERENT PROFILES.

Fire Type	25% Base	Gradually moving monotonic	Suddenly moving monotonic	Two Far-Field	Ring Inwards	Ring Outwards	Corners
Fire Duration (minutes)	76	93	76	76	76	76	76
Max. Bay Temperature (°C)	450	409	434	452	456	421	456

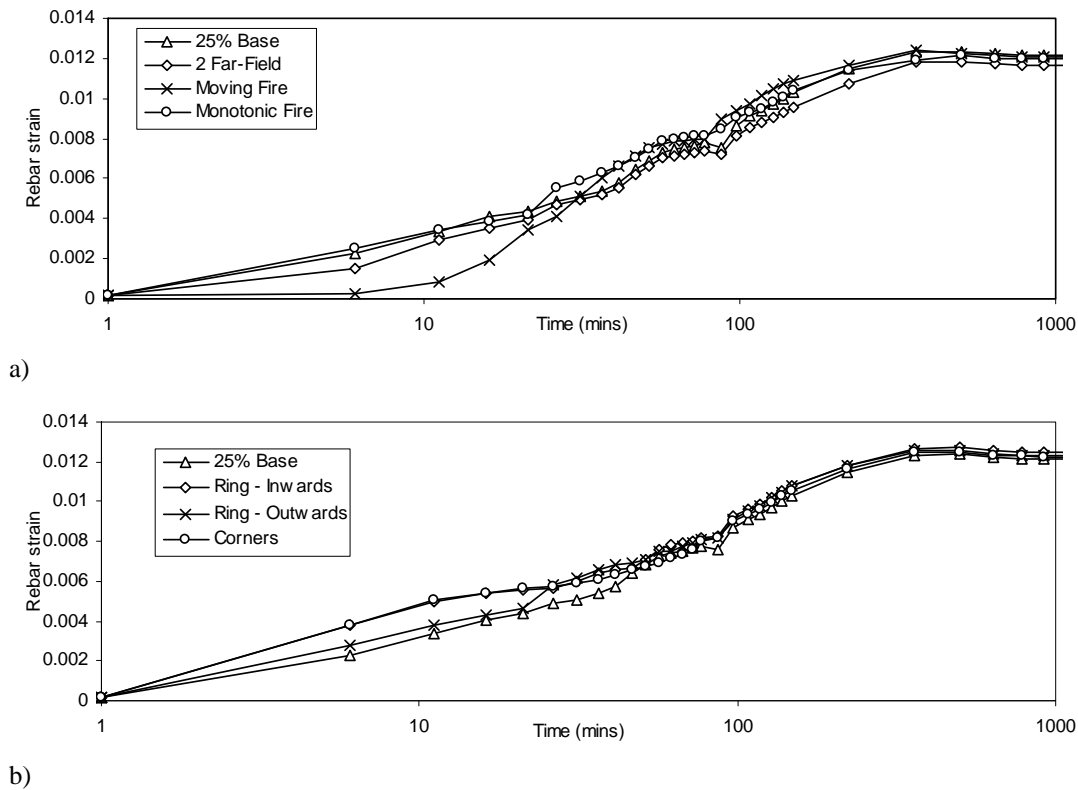


Figure 5. Maximum strain profiles for different far-field definitions and fire paths.

CONCLUSIONS

This paper presents a study of the impact of different design fires—including travelling fires—on the behaviour of a concrete frame. Several conclusions can be drawn:

The impact of travelling fires on a structure can be more severe than the equivalent parametric fires, and a similar to those of a 100 minute standard fire.

The 10% and 25% burn area fires induced the highest rebar-temperatures and sagging strains and can, thus, be considered to have the greatest impact on structural performance.

The parametric study showed that the detailed definition of the far-field temperature profiles does not have a major impact and takes secondary importance to the percentage burn area.

The implication of these conclusions is that the time temperature curves typically used in design cannot be assumed to give a conservative result.

REFERENCES

1. Rein G, Zhang X, Williams P, Hume B, Heise A, Jowsey A, Lane B, Torero JL. Multi-Story Fire Analysis for High-Rise Buildings. Proceedings of the 11th International Interflam Conference. London, 2007.
2. Gann RG. Reconstruction of the Fires in the World Trade Center Towers. NIST NCSTAR 1-5, 2005.
3. McAllister TP. Structural Fire Response and Probably Collapse Sequence of the World Trade Center Building 7. NIST NCSTAR 1-9, 2008.
4. Fletcher I, Welch S, Capote JA, Alvear D, Lazaro m. Model-Based Analysis of a Concrete Building Subjected to Fire. Advanced Research Workshop on Fire Computer Modelling. Santander, Spain, 2007.
5. Zannoni M. Brand Bij Bouwkunde. COT Instituut voor Veiligheids – en Crisismanagement, 2008.
6. Stern-Gottfried J, Rein G, Lane B, Torero JL. An Innovative Approach to Design Fires for Structural Analysis of Non-Conventional Buildings. In: Wald F, editor. Applications of Structural Fire Engineering. Prague, 2009.
7. Stern-Gottfried J, Rein G, Torero JL. Travel Guide. Fire Risk Management, 2009. p.12.
8. Stern-Gottfried J, Law A, Rein G, Gillie M, Torero JL. A Performance Based Methodology Using Travelling Fires for Structural Analysis. 8th International Conference on Performance-Based Codes and Fire Safety Design Methods. Lund, 2010.
9. Buchanan A. The Challenges of Predicting Structural Performance in Fires. Ninth International Symposium for Fire Safety Science, vol. 9. Karlsruhe, 2008.
10. Kodur V, Dwaikat M, Raut N. Macroscopic Fe Model for Tracing the Fire Response of Reinforced Concrete Structures. Engineering Structures 2009;31:2368.
11. BS476-20:1987. Fire Tests on Buildings Materials and Structures - Part 20: Method for Determination of the Fire Resistance of Elements of Construction: BSI, 1987.
12. EN1993-1-2. Eurocode 3: Design of Steel Structures - Part 1-2: General Rules - Structural Fire Design, 2005.
13. EN1992-1-2. Design of Concrete Structures - Part1-2: General Rules- Structural Fire Design, 1992.
14. EN1991-1-2. Eurocode 1: Actions of Structures - Part 1-2: General Actions - Actions on Structures Exposed to Fire, 1999.
15. EN1992-1-1. Eurocode 2: Design of Concrete Structures - Part 1-1: General Rules and Rules for Buildings, 1999.
16. Abaqus. Abaqus Analysis User's Manual. Providence: Dassault Systemes Simulia Corp, 2008.
17. Lubliner J, Oliver J, Oller S, Onate E. A Plastic-Damage Model for Concrete. International Journal of Solids and Structures 1989;25:299.
18. Alpert RL. Calculation of Response Time of Ceiling-Mounted Fire Detectors. Fire Technology 1972;8:181.

Simplified Procedure for Shear Failure Assessment of RC Framed Structures Exposed to Fire

R. FARIA, H. F. XAVIER and P. V. REAL

ABSTRACT

Real fire events have shown that shear failure of reinforced concrete (RC) columns due to thermal elongation of the adjacent beams and slabs is not a rare event. In this work evolution of shear forces on the elements of a RC frame are traced during a standard fire. As the advanced thermo-mechanical analysis used is unable to predict shear failure, a simplified method is proposed, based on the guidelines drawn in Eurocode 2 (EC2) for verification of shear strength of RC elements under ambient temperature, but extended to account for the detrimental effects of fire induced temperatures on the resistances of the stirrups (or links) and diagonal concrete struts. Shear forces are computed in all beams and columns of the analyzed RC frame with the FEM code SAFIR, and the corresponding shear strengths are evaluated in a post-process fashion with the proposed simplified method.

INTRODUCTION

Past real fire events have proved that shear failure of RC columns due to thermal elongation of beams and slabs constitutes a critical mechanism inducing structural collapse [1], [2]. Nonetheless, shear failure assessment is often neglected during design for fire safety, even when advanced thermo-mechanical analyses are performed. In another work of the same authors [3] it was noticed that quite relevant shear forces develop at the columns due to the drift imposed by the beam's

Rui Faria (corresponding author), Associate Professor, Faculty of Engineering, University of Porto, Rua Dr. Roberto Frias, 4200-465 Porto, Portugal

Hélder F. Xavier, MSc, Faculty of Engineering, University of Porto, Rua Dr. Roberto Frias, 4200-465 Porto, Portugal

Paulo Vila Real, Full Professor, University of Aveiro, Departamento de Engenharia Civil, Campus Universitário de Santiago, 3810-193 Aveiro, Portugal

thermal elongation, but the advanced thermo-mechanical method applied, based on the FEM code SAFIR [4], does not foresee any sort of shear failure. This is an important drawback in the analysis of RC structures subjected to fire. On an attempt to overcome this limitation a simplified procedure is here proposed, based on the EC2 [5] guidelines for verification of the shear strength of RC members at ambient temperature, but extended further to account for the unfavorable effects of elevated temperatures on the strengths of the steel stirrups and diagonal concrete struts. This procedure is implemented in a post-process fashion, where at each time-step shear forces predicted by SAFIR at every RC element are compared with the actual shear strengths affected by fire.

SHEAR FAILURE AT AMBIENT TEMPERATURE - EC2 APPROACH

At ambient temperature the EN1992-1-1 [5] prescribes a model for shear capacity assessment of RC elements (see Fig. 1) with stirrups D based on the Mörsh truss, where inclination of the concrete struts B may vary within the interval $1.0 \leq \cot \theta \leq 2.5$. The shear strength of a RC member with stirrups (or links) perpendicular to the longitudinal axis is given by the minimum of the capacities of the shear reinforcement ($V_{Rd,s}$) and of the inclined concrete struts ($V_{Rd,max}$), expressed by:

$$V_{Rd,s} = \frac{A_{sw}}{s} z f_{ywd} \cot \theta \quad (1)$$

$$V_{Rd,max} = \frac{\alpha_{cw} b_w z v_1 f_{cd}}{\cot \theta + \tan \theta} \quad (2)$$

In Eq. (1) A_{sw} is the shear reinforcement area, s denotes the stirrups spacing, z is the internal lever arm (distance between the longitudinal truss chords A and C – see Fig. 1) and f_{ywd} is the design tensile strength of steel. In Eq. (2) b_w is the minimum width of the concrete cross-section between the tension and compression chords,

$$v_1 = 0.6 \left(1 - \frac{f_{ck}}{250} \right) \quad (3)$$

(where the characteristic compressive strength of concrete f_{ck} is expressed in MPa) and f_{cd} is the design compressive strength of concrete. Coefficient α_{cw} accounts for the beneficial or unfavorable influence on $V_{Rd,max}$ due to the mean compressive stress σ_{cp} installed in concrete by the axial load, being defined as (see [5] and [6] for further details):

$$\alpha_{cw} = 1.0 \quad \text{if } \sigma_{cp} = 0 \quad (4a)$$

$$\alpha_{cw} = 1 + \frac{\sigma_{cp}}{f_{cd}} \quad \text{if } 0 < \sigma_{cp} \leq 0.25f_{cd} \quad (4b)$$

$$\alpha_{cw} = 1.25 \quad \text{if } 0.25f_{cd} < \sigma_{cp} \leq 0.5f_{cd} \quad (4c)$$

$$\alpha_{cw} = 2.5 \left(1 - \frac{\sigma_{cp}}{f_{cd}} \right) \quad \text{if } 0.5f_{cd} < \sigma_{cp} \leq 1.0f_{cd} \quad (4d)$$

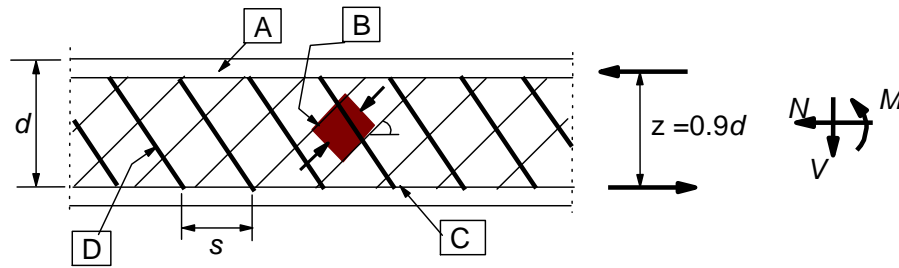


Figure 1. Truss model [5].

SHEAR FAILURE ASSESSMENT AT ELEVATED TEMPERATURES

The EC2 – Part 1.2 simplified approach

In EN1992-1-2 [7]—and although not fully verified—a simplified approach for shear strength assessment is provided in Annex D, relying on the assumption that the shear capacity of a RC member under fire conditions may be derived from the method reproduced in previous section for ambient temperature, yet considering that the fire induced temperatures reduce the stirrups' strength and the concrete cross-section effectiveness.

First step for assessing the shear capacity of a RC element is, therefore, to compute the reduced cross-section of concrete. The 'Zone method' of EC2 [7] is acknowledged to be more suitable for the analysis of fire exposed columns, when loaded in bending and axial compression. Yet, as far as the shear capacity is concerned this consideration is of reduced importance, so, for the sake of simplicity the isotherm of 500°C will be applied for the analysis of either beams or columns. Accordingly, at every time-step the effective concrete cross-section of each RC element is updated considering solely the fibers with temperatures $T \leq 500^\circ\text{C}$; inside the reduced cross-section concrete is considered with the compressive strength at ambient temperature. The next step is to update the stirrups' strength, and for this purpose temperatures at two points (as to be discussed later) are read from the sectional thermal files. Reduction of the steel strength as function of the temperature is made in accordance to standard procedures described in [7].

Considering the reduced concrete cross-section, as well as the reduced steel strength at the orthogonal stirrups, Eqs (1-2) are applied regarding the following features: (i) coefficient α_{cw} is determined at each time-step as a function of the average normal stress acting on concrete, according to Eqs (4); (ii) right-hand sides of Eqs (1) and (2) are set equal to extract the maximum allowable $\cot \theta$ at every time-step, taking into due account the reference interval $1.0 \leq \cot \theta \leq 2.5$; (iii) finally, upon determination of $\cot \theta$ shear strengths $V_{Rd,s}$ and $V_{Rd,max}$ are computed with Eqs (1-2), and compared against the shear force V_{Ed} acting on the RC element under study.

Temperature in the shear reinforcement

When shear capacity of a RC element is ruled by the strength of stirrups $V_{Rd,s}$, it is mandatory to appropriately account for steel properties under fire conditions. Accordingly, it is of vital importance to express the changes in the shear reinforcement strength with the evolution of temperature within the stirrups. As referred in Annex D of [7], the transversal reinforcement passes through concrete zones with different temperatures, leading to transferences of heat from the warmer to the cooler zones. Thanks to this, the link's temperature is lower than that of the surrounding concrete, and tends to become uniform along its length. In spite of this favorable effect, the link is not uniformly strained, and the maximum stress occurs near a shear crack [7]. To account for these peculiarities, in Annex D of EN199-1-2 a 'reference point' P is proposed within the concrete cross-section to characterize the link's temperature (see Fig. 2a). This point is located at the intersection of the links with line $a-a$, the latter being the upper boundary of the 'effective tension area' A of concrete effectively bonded to the longitudinal tensile reinforcement (see Fig. 2b), where tension-stiffening effects take place. According to EN1992-1-1 the height $h_{c,ef}$ of line $a-a$ is the minimum of $[2.5(h-d); (h-x)/3; h/2]$ – see definition of h , d and x in Fig. 2b.

To check the changes in the cross-sectional temperatures induced by the presence of links, several thermal analyses were performed with SAFIR, imposing a standard fire along the whole perimeter of a column with a $0.40 \times 0.40\text{m}^2$ concrete cross-section (see half of this section in Fig. 3a), reinforced with 8 20mm longitudinal rebars and a peripheral set of 8mm/200mm links. Fig. 3b allows to compare the evolution of temperatures at points 1-6 (see locations in Fig. 3a), with and without links: point 2 coincides with a corner longitudinal rebar (analysis without links); point 1 stands on the corner of the link that embraces rebar at point 2; point 6 coincides with the mid-height rebar (analysis without links); point 5 is placed on the link passing aside rebar at point 6; and point 3 (analysis with links) and point 4 (analysis without links) stand at the exact position of reference point P . In Fig. 3b a good correlation between temperatures in points 1 and 2 is recorded, which means that to determine the temperature in the corner of a link good approximation is obtained from a thermal analysis without discretization of the transversal reinforcement, just taking the temperature at the appropriate longitudinal rebar. Focusing on temperatures in points 3 and 4, it is possible to conclude also that they are very similar, considering or not the presence of links. Conversely, evolutions of temperatures in points 5 and 6 present a somewhat larger deviation, as each steel link constitutes a 'channel' of higher thermal conductivity within the concrete cross-section, enabling a temperature redistribution from hotter regions (like at point 1) to cooler ones (as at point 5).

From this preliminary study one arrives to the conclusion that for shear failure assessment, and particularly within the context of a simplified procedure, hereinafter thermal analyses need not to explicitly account for the presence of links.

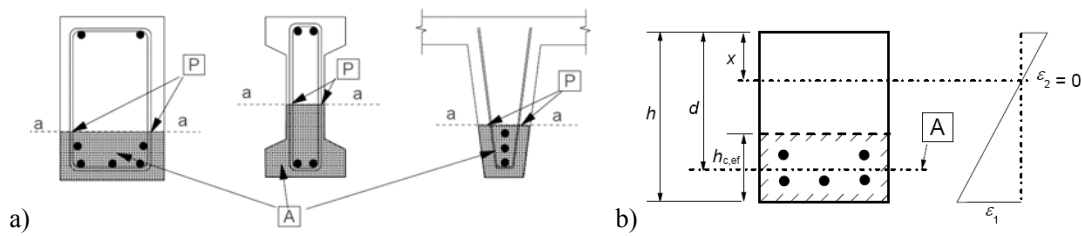


Figure 2. a) Point P to evaluate the reference temperature for links [7]; b) Effective tension area [5].

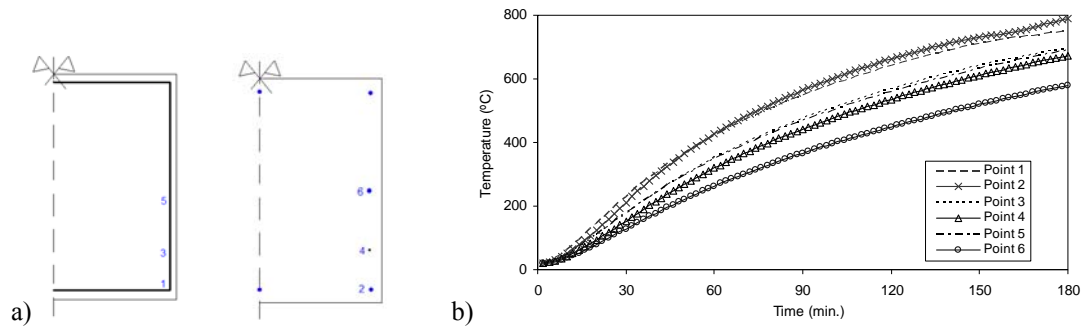


Figure 3. Evolution of temperatures in several points, with (1-3-5) and without (2-4-6) links.

Furthermore, and in order to update steel's strength at the shear reinforcement, if one takes the temperatures at the corner (point 2) and at mid-height (point 6) of the concrete cross-section, upper and lower bounds for the reference temperature in the links are obtained. Therefore, evaluation of temperatures at point P may be circumvented, which allows a considerable simplification, since as $h_{c,ef}$ is not constant during the course of the fire an extra computational effort would otherwise be required to define the 'variable' location of P , to extract the corresponding reference temperature. In the procedure here proposed this is not necessary, as the cross-section points 2 and 6, where the upper and lower bound temperatures are read, remain constant during the analysis.

APPLICATION

Three-bay RC frame

The simplified shear assessment procedure here proposed was applied to the columns of the RC frame reproduced in Fig. 4, analyzed in [3] under the standard fire. As far as the beams is concerned shear failure assessment will not be discussed, as in these members shear forces stood well below their shear strengths during the whole fire. The frame and loading reproduced in Fig. 4 are inspired on the ones adopted in [8], to which a number of modifications was applied. The first modification is related to the number of bays, augmented from 1 to 3. The second modification was the introduction of a lateral restraint against horizontal displacements of the floors, intended to simulate the presence of a highly stiff

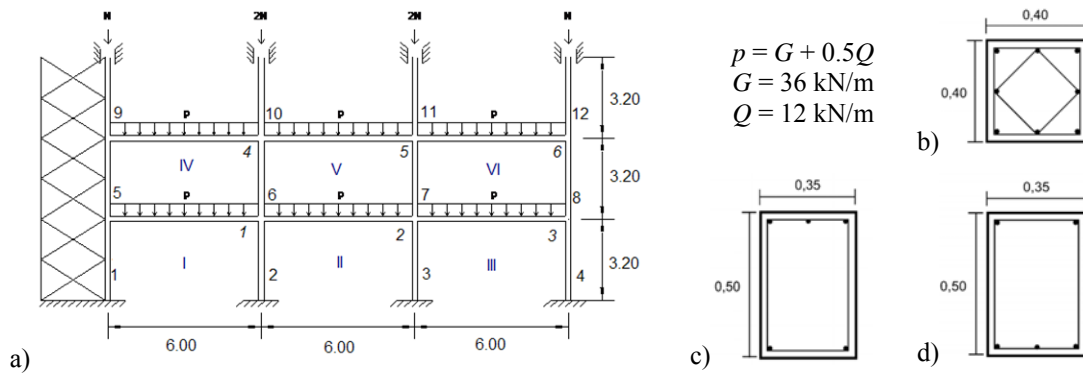


Figure 4. Three-bay frame and RC cross-sections (dimensions in [m]).

bracing system. With this restraint thermal elongations of the beams are directed towards one side, which is obviously an unfavorable condition to the structure, as it prescribes greater drifts to the outermost columns. Loading from the upper floors is reproduced by the vertical axial forces N and $2N$, being $N = 880\text{kN}$ (the upper columns are allowed to deform vertically, but restrained against horizontal displacements and rotations on the top extremities—see Fig. 4a). The concrete and steel strength grade classes are C30/37 ($f_{ck} = 30\text{MPa}$) and A500 (characteristic yield strength $f_{yk} = 500\text{MPa}$), respectively. The cross-section of the columns is constant (reproduced in Fig. 4b), as well as constant the beam cross-sections at the supports (Fig. 4c) and at mid-spans (Fig. 4d); all represented longitudinal rebars are 20mm. Shear reinforcement is constant for all the columns, corresponding to a value $A_{sw}/s = 5.03\text{cm}^2/\text{m}$ (8mm/200 mm, closed stirrups). In Fig. 4a notations I-II-(...) refer to compartment numbers, 1-2-(...) to column numbers and 1-2-(...) to beam numbers.

Scenario A: standard fire in compartments I, II and III

Fig. 5a illustrates the evolutions of the shear force and shear capacities in the top of column 4 (the one with the greatest drift) when only the ground floor is subjected to the standard fire (Scenario A). It is possible to see that failures due to lack of capacity of the shear reinforcement are recorded: (i) at approximately 33 minutes after the beginning of fire the design shear force V_{Ed} reaches $V_{Rd,s}$ if the temperature at the links is considered at point 2 (see curve $V_{Rd,s(2)}$); (ii) after 44 minutes of exposure V_{Ed} reaches $V_{Rd,s}$ if the temperature at point 6 is chosen (see curve $V_{Rd,s(6)}$). From the same figure it is also possible to observe that shear failure due to crushing of concrete is far from being the cause of collapse (see curve $V_{Rd,max(2,6)}$). Fig. 5b presents the evolution of the shear force and capacities in the top of column 8 for the same Scenario A: as this column is not exposed to fire shear capacities $V_{Rd,s}$ and $V_{Rd,max}$ remain constant during the analysis. It is observed that although an increase of the shear force is recorded during the fire, no shear failure of this column is expected.

Scenario B: standard fire in compartments IV, V and VI

Considering the standard fire acting solely in the 1st floor (Scenario B), Fig. 6a points to the possible occurrence of shear failure in the top of column 8 after approximately 29 minutes of exposure, and almost independently of points 2 or 6

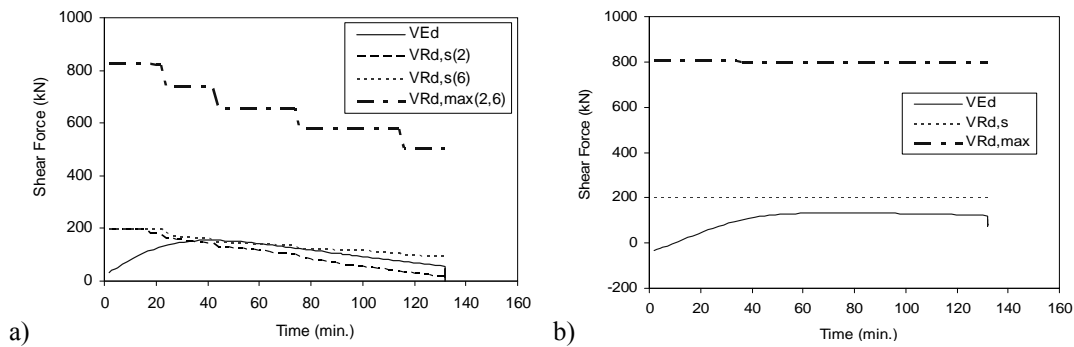


Figure 5. Evolutions of shear force and capacities (Scenario A) in the top of columns: a) 4, b) 8.

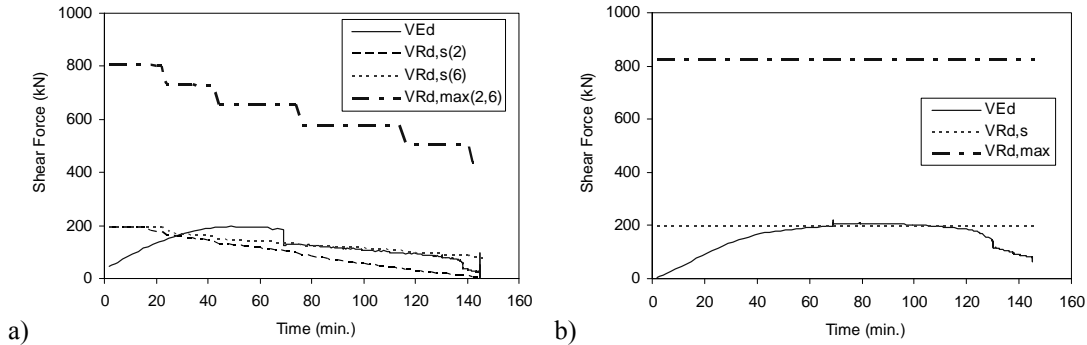


Figure 6. Evolutions of shear force and capacities (Scenario B) in the top of columns: a) 8, b) 11.

where temperature might be taken for the strength reduction on shear reinforcement. In Fig. 6b evolutions of the shear force and capacities are plotted in the top of column 11: however not directly exposed to fire, it is important to remark that the maximum shear force was recorded precisely at this column. This means that shear failures may occur also in the ‘cold part’ of the building. This shall be taken just as an indication of possible anomalies that the cold part of the structure could suffer due to indirect effects of fire; in fact, with regards to shear failure the analysis should have been stopped before column 11 reaches collapse, as shear failure in column 8 would have occurred before (compare Figs 6a and 6b).

Scenario C: standard fire in compartments I, II, III, IV, V and VI

If the standard fire acts in both the ground and 1st floor (Scenario C), evolutions of the shear force and capacities in the top of column 4 are reproduced in Fig. 7a: failure due to lack of links’ capacity is observed after 36 minutes of exposure if the temperature is considered at point 2, and after circa 44 minutes if temperature is taken at point 6. Similar comparative evolutions in the top of column 8 are presented in Fig. 7b: in this case only if the most unfavorable temperature at point 2 is considered shear failure might be expected at a later stage of the fire, meaning that for this column shear failure is not limitative if compared to the SAFIR analysis performed in [3], where influence of shear was disregarded and a fire resistance of 158 minutes was predicted for this scenario. This was expected, as both top and bottom of column 8 experience approximately the same drift during Scenario C, which reduces bending and shear.

CONCLUSIONS

A simplified procedure for shear failure assessment of RC elements under fire conditions was proposed, based on the recommendations of EN1992-1-1 and EN1992-1-2, which takes into consideration the detrimental effects of fire induced temperatures on the strengths of the stirrups (or links) and diagonal concrete struts. With such simplified procedure the risk of failure of a RC frame was checked, by comparing (in an *a posteriori* fashion) the evolutive shear strength of each column with the shear forces predicted by the advanced calculation code SAFIR.

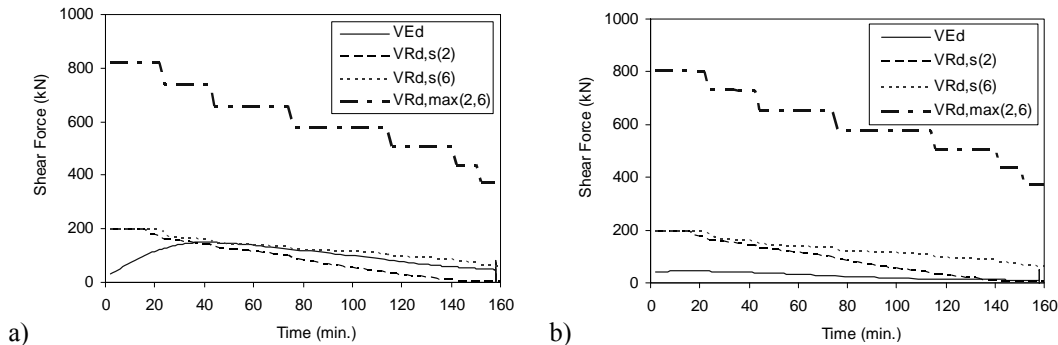


Figure 7. Evolutions of shear force and capacities (Scenario C) in the top of columns: a) 4, b) 8.

It was observed that the thermal elongation of beams may induce significant shear forces on the outermost columns, causing failure of the latter due to exhaustion of their shear reinforcement capacities. The points on the links where temperatures were taken to update the corresponding steel strengths under fire played a marginal role in the obtained results. However, while recommendations of EN1992-1-2 are not clarified, the most severe temperatures on the links (that is, close to the corners of the column cross-section) could be considered.

The simplified procedure for shear failure assessment here proposed should be considered at an initial development stage, still lacking for further experimental validation. Furthermore, as even at ambient temperatures shear calculation models have shown to be of limited accuracy, their extrapolation to fire conditions shall be considered with care.

ACKNOWLEDGEMENTS

Funding provided by the Portuguese Foundation for Science and Technology to the Research Unit LABEST—Laboratory for the Concrete Technology and Structural Behavior is gratefully acknowledged.

REFERENCES

1. Taerwe, L. 2007. "From Member Design to Global Structural Behaviour," in *fib Workshop on "Fire Design of Concrete Structures—From Materials Modelling to Structural Performance"*: University of Coimbra, pp. 253-270.

2. Mostafaei, H., Sultan, M. A. and Bénichou, N. 2009. "Performance of Structural Systems in Fire," in *International Conference Applications of Structural Fire Engineering*: Prague, pp. 604-609.
3. Xavier, H. F., Faria, R. and Vila Real, P. 2010. "Influence of Thermal Elongation of Beams on the Fire Resistance of RC Frames," in *6th International Conference on Structures in Fire*: Michigan State University, East Lansing.
4. Franssen, J.-M. 2005. "SAFIR: A Thermal/Structural Program Modeling Structures under Fire," *Engineering Journal, A.I.S.C.*, 42(3): 143-158.
5. EN1992-1-1. 2004. *Eurocode 2: Design of Concrete Structures - Part 1-1: General Rules and Rules for Buildings*. European Committee for Standardization.
6. Xavier, H. F. 2009. *Analysis of Reinforced Concrete Frames Exposed to Fire Based on Advanced Calculation Methods*. MSc Thesis, Faculty of Engineering, University of Porto, Portugal.
7. EN1992-1-2. 2004. *Eurocode 2: Design of Concrete Structures—Part 1-2: General Rules - Structural Fire Design*. European Committee for Standardization.
8. Riva, P. 2008. *Structural Behaviour of Continuous Beams and Frames*. fib bulletin 46: Fire design of concrete structures - Structural behaviour and assessment.

Modeling the Fire Response of Reinforced Concrete Columns Under Biaxial Bending

N. RAUT and V. KODUR

ABSTRACT

Reinforced concrete (RC) columns, under fire conditions, are often subjected to biaxial bending arising from eccentricity in loading, 1-, 2-, 3- side fire exposure or due to non-uniform spalling. Effect of such biaxial bending is often not taken into consideration in evaluating fire resistance of RC columns. Also, current fire provisions in codes and standards do not provide clear and specific guidelines for fire resistance evaluation under biaxial bending. An approach is presented for modeling the fire response of RC columns under biaxial bending. This approach accounts for high temperature material properties, geometric and material nonlinearity, fire induced spalling, and restraint effects and can be applied under realistic fire and loading scenarios. The validity of the approach is established by comparing the predictions from the model with results from full-scale fire resistance tests. The model is applied to study the effect of fire exposure on fire response of RC columns. Also, fire resistance predictions from the numerical model are compared with those from code provisions. These comparisons indicate that the current codes and standards neglect the effect of uniaxial/biaxial bending and thus may not yield reliable fire resistance predictions.

INTRODUCTION

Provision of appropriate fire safety measures for structural members is an important aspect in building design since fire represents one of the most severe environmental conditions to which structures may be subjected in their life time. Reinforced concrete columns form the main load bearing component of a structural frame and hence, the provision of appropriate fire resistance measures for these columns is one of the major safety requirements in building design. The basis for this requirement can be attributed to the fact that, when other measures for containing the fire fail, structural integrity is the last line of defense.

Nikhil Raut, Ph.D. (corresponding author), Candidate, CEE, Michigan State University, East Lansing, MI
Venkatesh Kodur, Professor, CEE, Michigan State University, East Lansing, MI

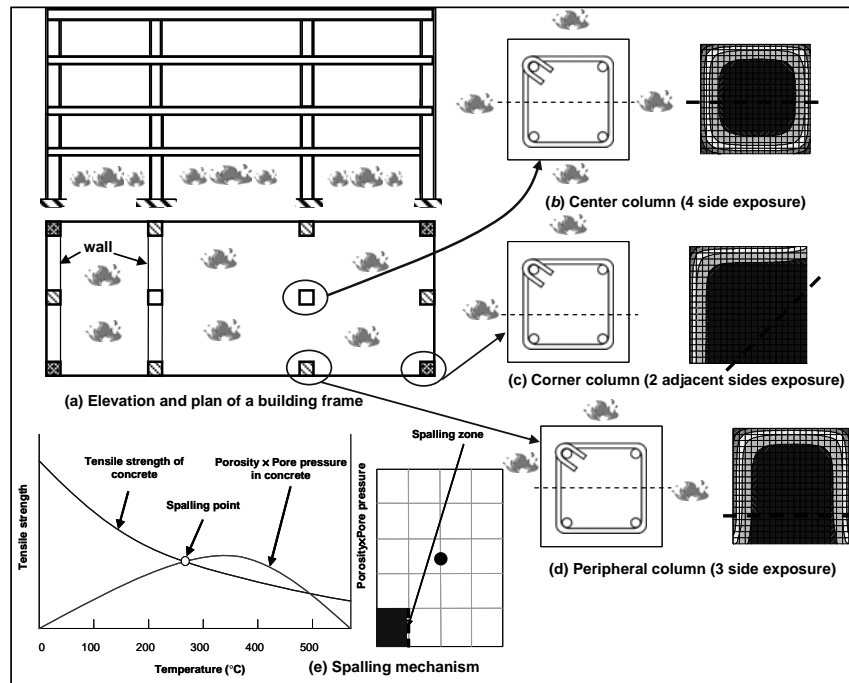


Figure 1. Fire induced biaxial bending situations for an RC column.

A RC column is often treated as a two-dimensional planar structure and therefore designed to resist bending moments acting in the plane of the frame. While this idealization is true for peripheral columns, in an actual building framework columns are frequently subjected to bending moments, acting in two perpendicular directions (biaxial bending), in addition to an axial compression. The obvious example is a corner column in a space frame of a building. Also under fire conditions a column may be exposed heat on 1-, 2-, 3-, or 4-sides. The 1-, 2-, or 3-side fire exposure causes development of thermal gradients which can result in uniaxial (1- or 3-side) or biaxial (2 adjacent sides) bending of the column. Also uneven spalling of the concrete cross-section can cause bending (uniaxial or biaxial) of the column. Hence the effect of biaxial bending can play a significant role in determining the fire response of RC columns.

The build-up of such biaxial bending effects in a RC column is illustrated in Figure 1 where a structural frame in a building is exposed to fire (Figure 1-a). Figure 1(b-d) illustrate the development of thermal gradients in center, peripheral and corner column respectively under fire conditions. It can be seen that the occurrence of uniaxial bending (peripheral column) and biaxial bending (corner column) can be common in most practical scenarios in buildings. The current fire resistance provisions in codes and standards are based on standard tests with all sides exposed to fire and hence may not be applicable to one, two or three-side fire exposure.

The presence of uniaxial bending induces an eccentricity in an originally axially loaded column due to the shift in neutral axis resulting from the degradation of constitutive properties of concrete and reinforcing steel. Thus the column is subjected to an additional moment along with the applied load and thus leads to reduction in fire resistance of the column. In the case of corner columns (biaxial bending) the neutral axis shifts and also rotates thus inducing eccentricity along both the axes. This causes the column to experience additional moments along both the axes. The induced eccentricity in both cases also increases lateral and axial deformations due to P- δ effects.

In addition to fire exposure, uneven fire induced spalling can also produce significant uniaxial or biaxial bending on the column. Such fire induced spalling may be more prevalent in columns made of HSC which is more prone to spalling. Spalling occurs due to development of pore pressure under some fire conditions. As the cross-sectional temperatures rise, the moisture in concrete turns in to vapor which creates pore pressure. When this pore pressure exceeds the tensile strength of concrete chunks of concrete peel off from the column and this process is referred to as spalling. The spalling mechanism is illustrated in Figure 1(e). Spalling depends on a number of factors including thermal gradients, porosity, moisture distribution and strength of concrete. Depending on these factors the columns may undergo non-uniform spalling thus causing the applied load to act eccentrically. For example if the column is concentrically loaded and a piece of concrete disintegrates from one side of the column as a result of spalling, the applied load will then become eccentric due to shift in the neutral axis. Therefore, 1-, 2-, or 3-side fire exposure and uneven spalling can produce uniaxial/biaxial bending effects in an RC column and should be accounted in fire resistance predictions.

FIRE RESISTANCE PROVISIONS IN CODES AND STANDARDS

Specifications for fire design of structural members are provided in building codes and national standards. The current fire provisions in most codes and standards are based on standard fire resistance tests and are thus valid for standard fire exposure and under axial loading only.

In the USA, prescriptive based fire provisions for concrete structures are provided in ACI 216.1 [1] standard which specifies concrete cover thickness and minimum column dimensions required for achieving a given fire resistance rating for either 4 sides or 2 (opposite) side fire exposure. Eurocode 2, Part 1–2 [2], gives a choice of simplified, tabular (tables) or advanced methods for determining fire resistance of RC columns. Tables and simplified empirical equations, which are based on prescriptive provisions, provide specifications for calculating the fire resistance of RC columns based on minimum dimensions, cover thickness, load level and reinforcement level in RC columns. The advanced methods recommends the use of detailed analysis for evaluating fire resistance, but no specific guidelines are provided on uniaxial/biaxial bending arising from thermal gradients or spalling. Australian Code AS 3600 (2001), similar to Eurocode, provides a simple equation to calculate the fire resistance of RC columns based on steel ratio, compressive strength of concrete, dimensions of column, axial load on the column and the effective length.

None of the current provisions in codes and standards specifically address the issue of bi-eccentric loading and biaxial bending under fire exposure. Though ACI 216.1 provides different (minimum) size requirements for columns exposed to fire from two parallel faces, it doesn't consider bending since the thermal gradients for this case are symmetric about both the axes. Under ambient temperature design, codes and standards provide specific provisions to account for uniaxial/biaxial bending in RC columns. Thus there is a need for specific provisions to evaluate fire resistance under uniaxial/biaxial bending.

MODEL FOR PREDICTING FIRE RESPONSE

A numerical model based on macroscopic finite element approach has been developed for tracing the response of RC columns exposed to fire [4]. In this approach, time dependent moment-curvature relationships are generated first and then utilized to trace the response of RC

structural members in the entire range of loading up to collapse under fire. The RC column is divided into a number of segments along its length and the mid-section of the segment is assumed to represent the behavior of the whole segment. The fire resistance analysis is carried out by incrementing time steps. At each time step, the model performs the analysis through three main steps; 1) Establishing fire temperature due to fire exposure, 2) Carrying out heat transfer analysis to determine temperature distribution and spalling and, 3) Performing strength analysis. Fire induced spalling is accounted for in the model through hydrothermal analysis that involves the calculation of pore pressure in concrete [5]. Various strain components including mechanical, thermal, and creep strains for both concrete and reinforcing steel and the transient strain in concrete are accounted for in the computer model based on the constitutive relationships proposed by Harmathy [6,7], and Anderberg and Thelandersson [8], for creep and transient strain respectively. The strength analysis involves calculating fire induced axial restraint force in the RC structural member, generation of M- κ relationship (utilizing the axial force computed above) for each segment, performing structural analysis of the overall member to compute lateral and axial deformations and internal forces. At every time step, each segment of the column is checked for failure under thermal and strength failure limit states.

The above model was extended to incorporate biaxial bending effects resulting from eccentric loading, 1-, 2-, 3-side exposure or due to uneven spalling on the column faces. The model utilizes 3D frame element in order to account for the biaxial bending of the column. The solution to a biaxially loaded column (representing the case of a beam-column) requires due consideration of geometry, compatibility, equilibrium and constitutive relationships. The instability of the member arising from the magnification of the primary moments by the axial load acting on laterally deflecting beam-column must be considered. The segment stiffness matrix $[k(10 \ 10)]$ [9] is computed considering axial and bending deformations separately. The sectional properties are assumed to be constant within the segment at a given time step and thus sequential elastic analysis can be used. The segmental matrix is derived by solving separately the axial and flexural components, using the force-displacement relations. The flexural components in Y and Z directions and the three force components in X, Y, Z directions are given by:

$$P = -EAu'_x; \quad m_y = -EI_y u''_z; \quad m_z = -EI_z u''_y \quad [1]$$

where: P = axial force acting on the column; m_y = moment about the Y axis; m_z = moment about the Z axis; EA = axial rigidity of the segment; EI_y = flexural rigidity of the segment about Y axis; EI_z = flexural rigidity of the segment about Z axis;

The flexural rigidities are calculated using secant stiffness method [10] and the final stiffness matrix for each segment can be written as

$$[k(10 \times 10)] = \begin{bmatrix} k_{AA}(5 \times 5) & k_{AB}(5 \times 5) \\ k_{BA}(5 \times 5) & k_{BB}(5 \times 5) \end{bmatrix} \quad [2]$$

In the above matrix the components K_{AA} , K_{BB} and K_{AB} are expressed as:

$$[k_{AA}] = \begin{bmatrix} \frac{EI_y k_y^3 S_y}{2-2C_y - k_y L S_n} & 0 & 0 & 0 & \frac{EI_y k_y^2 (1-C_y)}{2-2C_y - k_y L S_n} \\ 0 & \frac{EI_z k_z^3 S_z}{2-2C_z - k_z L S_z} & 0 & -\frac{EI_z k_z^2 (1-C_z)}{2-2C_z - k_z L S_z} & 0 \\ 0 & 0 & \frac{EA}{L} & 0 & 0 \\ 0 & -\frac{EI_z k_z^2 (1-C_z)}{2-2C_z - k_z L S_z} & 0 & \frac{EI_z k_z (S_z - k_z L C_z)}{2-2C_z - k_z L S_z} & 0 \\ \frac{EI_y k_y^2 (1-C_y)}{2-2C_y - k_y L S_n} & 0 & 0 & 0 & \frac{EI_y k_y (S_y - k_y L C_y)}{2-2C_y - k_y L S_y} \end{bmatrix} \quad [3]$$

$$[k_{BB}] = \begin{bmatrix} \frac{EI_y k_y^3 S_y}{2-2C_y - k_y L S_n} & 0 & 0 & 0 & \frac{EI_y k_y^2 (1-C_y)}{2-2C_y - k_y L S_n} \\ 0 & \frac{EI_z k_z^3 S_z}{2-2C_z - k_z L S_z} & 0 & -\frac{EI_z k_z^2 (1-C_z)}{2-2C_z - k_z L S_z} & 0 \\ 0 & 0 & \frac{EA}{L} & 0 & 0 \\ 0 & -\frac{EI_z k_z^2 (1-C_z)}{2-2C_z - k_z L S_z} & 0 & \frac{EI_z k_z (S_z - k_z L C_z)}{2-2C_z - k_z L S_z} & 0 \\ \frac{EI_y k_y^2 (1-C_y)}{2-2C_y - k_y L S_n} & 0 & 0 & 0 & \frac{EI_y k_y (S_y - k_y L C_y)}{2-2C_y - k_y L S_y} \end{bmatrix} \quad [4]$$

$$[k_{BA}] = [k_{AB}] = \begin{bmatrix} -\frac{EI_y k_y^3 S_y}{2-2C_y - k_y L S_n} & 0 & 0 & 0 & -\frac{EI_y k_y^2 (1-C_y)}{2-2C_y - k_y L S_n} \\ 0 & -\frac{EI_z k_z^3 S_z}{2-2C_z - k_z L S_z} & 0 & \frac{EI_z k_z^2 (1-C_z)}{2-2C_z - k_z L S_z} & 0 \\ 0 & 0 & -\frac{EA}{L} & 0 & 0 \\ 0 & \frac{EI_z k_z^2 (1-C_z)}{2-2C_z - k_z L S_z} & 0 & \frac{EI_z k_z (S_z - k_z L C_z)}{2-2C_z - k_z L S_z} & 0 \\ -\frac{EI_y k_y^2 (1-C_y)}{2-2C_y - k_y L S_n} & 0 & 0 & 0 & \frac{EI_y k_y (S_y - k_y L C_y)}{2-2C_y - k_y L S_y} \end{bmatrix} \quad [5]$$

Where: $C_y = \cos k_y L; S_y = \sin k_y L; C_z = \cos k_z L; S_z = \sin k_z L; k_y = \sqrt{\frac{P}{EI_y}}; k_z = \sqrt{\frac{P}{EI_z}}$ [6]

The global stiffness matrix for the column is arrived by assembling the stiffness matrices for each segment and can be expressed as:

$$([K_g] - [K_{geo}])\{\delta\} = \{P_f\} \cdot [K_g]\{\delta\} = \{P_f\} + \{P_s\} \cdot \{P_s\} = -[K_{geo}]\{\delta\} \quad [7]$$

where: $[K_g]$ = global stiffness matrix, $[K_{geo}]$ = geometric stiffness matrix, $\{\delta\}$ = nodal displacements, $\{P_f\}$ = equivalent nodal load vector due to applied loading, and $\{P_s\}$ = equivalent nodal load vector due to P - effect.

The failure of an RC column is said to occur when the applied axial load (or moments) exceeds the load (or moment) carrying capacity of the column. This is checked at every time step at the end of the structural analysis. If the column does not fail, the strains and curvature are calculated and the analysis continues to the next times step. The time (time step) at which the column fails is considered as the fire resistance of the column.

MODEL VALIDATION

There is no test data on RC columns under uni/biaxial bending arising from 1-, 2-, 3-side fire exposure. Hence, the validity of the above macroscopic finite element model is established by comparing the predictions from the analysis with test data reported by Lie and Woolerton [11] and Kodur et al.[12] for eccentrically loaded NSC column III3 and HSC column HS2-8 respectively. The geometric and material properties of the tested columns are taken from the literature and are summarized in Table 1. The eccentrically loaded columns were analyzed by simulating 4-side exposure to the standard time-temperature curve specified in ASTM E119 (2001). Both columns had axial load applied eccentrically along one axis. Predicted results from the analysis are compared to the measured values from the fire test in Figure 2 (a-d).

The predicted temperatures at three different cross-sectional locations (mid-depth, quarter-depth and on rebar), for column III3, are compared with the measured values, in Figure 2 (a). It can be seen that the predicted temperatures are generally in good agreement with the measured values. The temperatures follow expected trend with higher values close to the exposed surface. The rebar temperatures are higher than that in concrete (at quarter-depth and mid-depth) as the rebars are closest to the fire exposed column surface. Figure 2 (b) shows axial deformations as a function of fire exposure time for NSC column III3. It can be seen that model predictions are in close agreement with the measured axial deformations throughout the fire exposure time. The column expands initially and this is primarily due to significant thermal strain in rebars which results from increasing temperatures. This is followed by a decrease in the axial deformations (contraction) as a result of loss of strength and stiffness in the column. The faster rate of increase in deformation prior to failure of the column is mainly due to significant creep deformations resulting from the decreased stiffness and high temperatures. Also the increased P- δ effect, resulting from bending of the column, contributes to faster increase in deformations prior to failure of the column.

Figure 2 (c) shows the temperature variation comparison for HSC column HS2-8. Predictions from the model are in good agreement with the measured temperatures. Since this is an HSC

Table 1. Properties and Results for RC Columns used in the Validation Study.

Property	Column III3	Column HSC2-8
Description	Tested by Lie and Woolerton [11]	Tested by Kodur et al. [12]
Cross-section (mm)	305 305	406 406
Length (m)	3.8	3.8
Support condition	Fixed-Fixed	Pinned-Pinned
Reinforcement	4 25mm bars	8 25 mm bars
f'_c (MPa)	34.8	127
f_y (MPa)	444	400
Applied total load (kN)	800	4981
Load eccentricity (mm)	25	25
Concrete cover thickness (mm)	48	48
Aggregate type	Siliceous	Carbonate
Fire Resistance (minutes)	Test	185
	MFEM	176
		118
		123

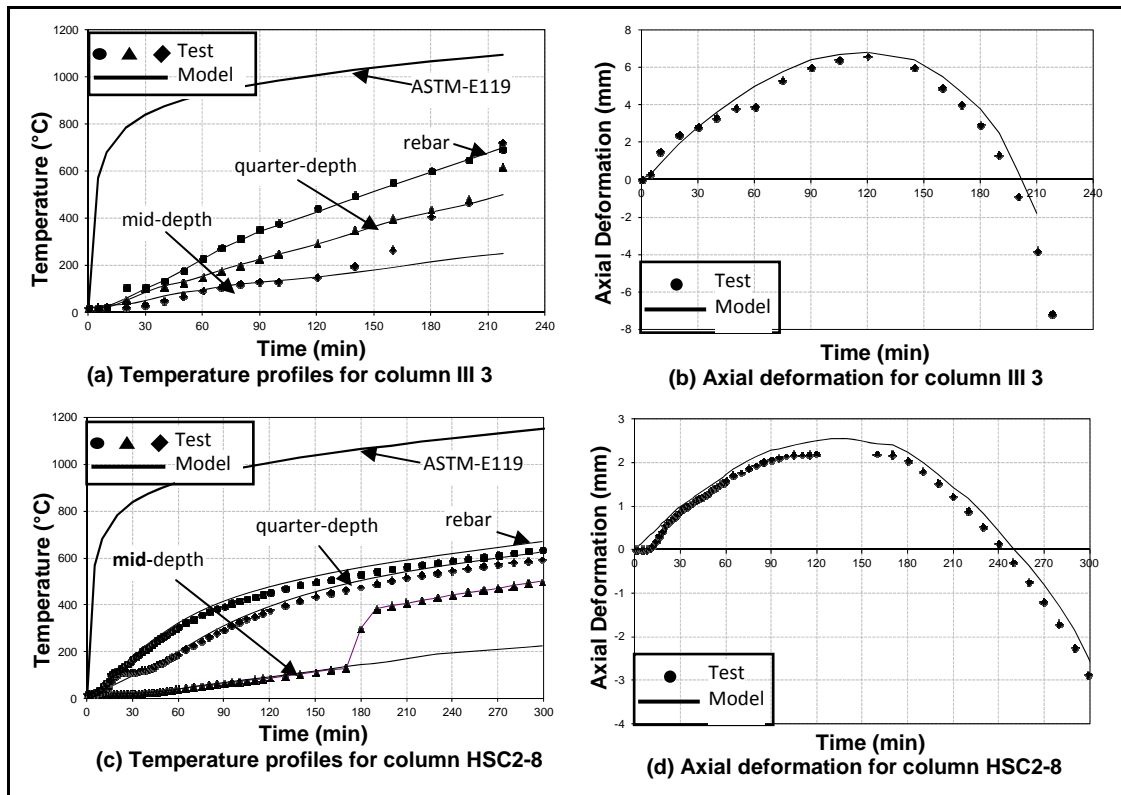


Figure 2. Comparison of predicted and measured temperatures and deformations for RC columns.

column, fire induced spalling occurred during the fire tests. The model predictions indicate that fire induced spalling starts at about 13 minutes, which is close to the observed time (10 minutes) recorded in test [12]. The temperature profile at mid-depth of the column has a sudden rise in temperature in the test after 180 minutes as seen in Figure 2 (c). This can be attributed to possible damage to the thermocouple or due to occurrence of large cracks in concrete resulting from reduced strength/stiffness which would expose the thermocouple to higher temperatures. This effect is not captured as the model cannot account for the occurrence of load induced cracks or their propagation. The effect of this variation in the temperature is reflected partially in higher fire resistance predicted by the model. Figure 2 (d) shows the axial deformation comparisons for HSC column HS2-1. The column shows similar trend to that of NSC column with expansion in the early stages followed by contraction of the column. There is lesser expansion in the HSC columns due to faster degradation of strength thus leading to high axial compression. Also the applied load ratio is higher for the HSC column causing higher compression in the column. The prediction from the model is in good agreement with the measured axial deformation. The comparisons indicate that the proposed macroscopic finite element model is capable of predicting the fire behavior of RC columns under eccentric loading conditions.

CASE STUDIES

To illustrate the effect of biaxial bending on fire response of RC columns four RC columns (CE1 – CE4) were selected and subjected to ASTM – E119 [13] standard fire under different exposure conditions. The geometric properties of these RC columns are shown in Figure 3 and

Table 2. All columns were assumed to be made of concrete with compressive strength of 30 MPa and were assumed to have a permeability of the order 10^{-17} . The columns were reinforced with 4 25 mm rebars having yield strength of 400 MPa and carried a concentric load of 800KN. The columns were designed as per ACI 318 [14] specifications. The fire resistance predictions from the model were also compared with the fire resistance values computed from current codes of practice.

Table 2. Properties and Results for RC Columns used in the numerical study.

Column	Faces Exposed	Fire resistance (mins)			
		Model	ACI 216.1	EC2*	AS3600
CE1	4	221	180	131	191
CE2	3	189	180	131	191
CE3	2 (adj)	138	180	131	191
CE4	1	198	180	131	191

* Simplified equation

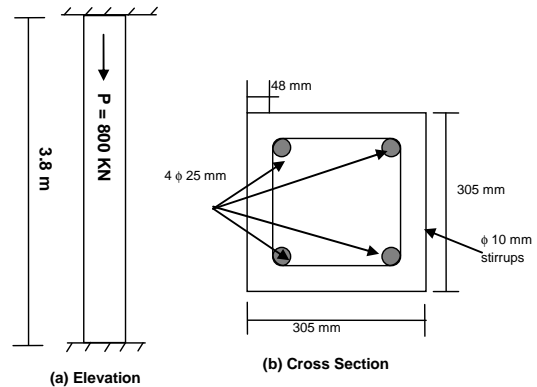


Figure 3. Elevation and cross-section of the RC column used in the case study.

Since all four columns have different number of faces exposed to fire, thermal gradients develop differently for these columns. It can be seen from Figure 4 that the thermal gradients in column CE1 (exposed on 4 sides) are symmetric about both the axes, the thermal gradients for column CE2 and CE4 (exposed on 3-sides and 1-side respectively) are symmetric about one axis and thus this will cause the column to bend along that axis. The thermal gradients for column CE3 (exposed on 2 adjacent sides) are not symmetric about any axes along the member orientation. The axis of symmetry is oriented at an angle to the member axes and thus this will cause the column to experience biaxial bending.

Figure 5 shows the variation of the axial deformation of columns CE1 – CE4 as a function of fire exposure time for different fire exposure. It can be seen that the columns undergoing bending have shorter expansion zone since the eccentricity causes bending and thus the total downward deformation of the column is higher (see Figure 5). Column CE3 undergoes biaxial bending and thus has significantly less area of concrete resisting bending. Therefore this column suffers higher compressive axial deformation as compared to columns CE2 and CE4 (uniaxial bending) and thus demonstrates lesser fire resistance.

Figure 6 shows progress of lateral deformation in the four columns as a function of time. It can be seen that the lateral deformations of all the columns are zero till the columns are expanding. This is as expected as an expanding column cannot deform laterally. The lateral deformations occur after the column begins to contract. These lateral deformations are very small until just prior to failure, where the high temperature creep strains play a higher role and concrete has lost significant stiffness. Also, the moments acting on the column get magnified with time due to the P- δ effect and thus the lateral deformations increase exponentially. It should be noted that, even though the thermal gradients of column CE1 are symmetric it undergoes lateral deformation as all the columns were analyzed with a load subjected to some minimum eccentricity in order to account for geometric nonlinearity and represent the realistic conditions.

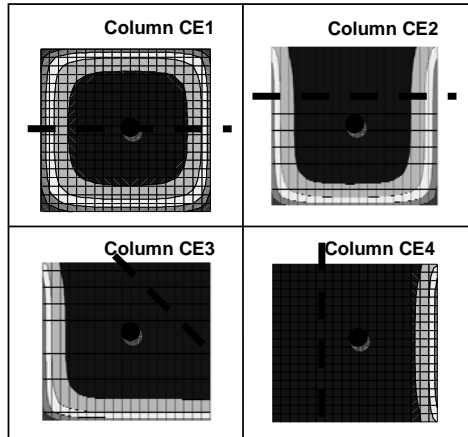


Figure 4: Thermal gradients after 60 minutes in RC columns CE1-CE4.

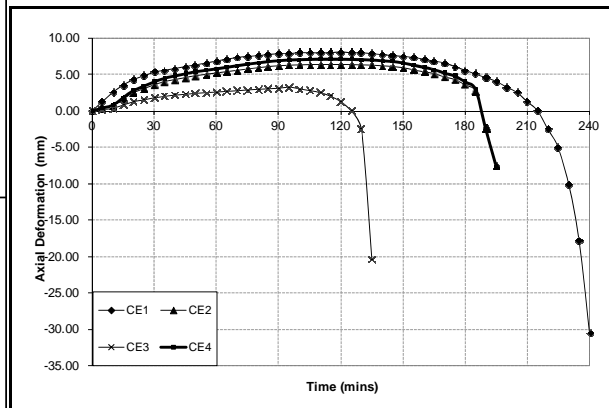


Figure 5: Axial deformation of RC columns (CE1-CE4) exposed to different fire scenarios.

It can be seen from Table 2 that exposure condition (1-, 2-, 3-, or 4-side exposure) has significant influence on the fire resistance of RC columns. The fire resistance reduces from 221 minutes, under four side exposure, to 189, 138 and 198 minutes when subjected to 3-, 2-, 1-side fire exposure respectively. As discussed above, this reduction can be attributed to the development of thermal gradients and associated bending (uniaxial or biaxial) effects.

Fire resistance of the four columns was evaluated based on the provisions in ACI, EC and AS codes and these are presented in Table 2. It can be seen that the predicted fire resistance remains the same for all the four columns using the simplified provisions in the different codes of practice. This is because the effect of biaxial bending is not taken in to consideration in these fire resistance provisions.

The macroscopic FEM, presented here, is being applied to conduct a series of parametric studies to quantify the influence of various parameters on the fire resistance of RC columns. Data

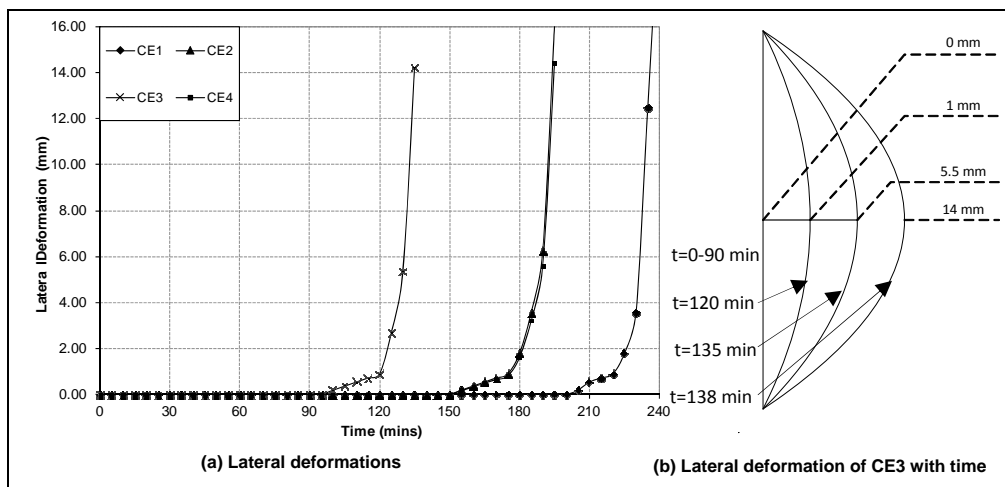


Figure 6. Lateral deformation of RC columns (CE1-CE4) exposed to different fire scenarios.

from such parametric studies will be used to develop rational and cost-effective fire design guidelines for incorporation in codes and standards.

CONCLUSIONS

RC columns in a structural frame can experience biaxial bending either due to 1-, 2-, 3-sided fire exposure, uneven spalling or eccentric loading. Such biaxial bending which is often not accounted for in fire resistance evaluation can have significant influence on response of RC columns.

The proposed macroscopic finite element model is capable of accounting for biaxial bending of RC columns arising from 1-, 2-, 3-side exposure, spalling or eccentric loading. Also, the model accounts for other critical parameters such as different fire scenarios, high temperature material properties, various strain components, fire induced spalling and restraint effects.

For a typical RC column, the fire resistance can decrease by about 15%, 40%, and 10% when the fire exposure changes from 4-sided to 3-, 2-, or 1-sided exposure respectively.

Specifications in current codes and standards do not account for the effect of uniaxial/biaxial bending and do not provide specific guidelines for undertaking detailed analysis and thus provide unrealistic fire resistance predictions.

ACKNOWLEDGMENTS

The research presented in this paper is primarily supported by the National Science Foundation CMMI program (Grant number CMS 0601178). Any opinions, findings, and conclusions or recommendations expressed in this paper are those of the authors and do not necessarily reflect the views of the sponsors.

REFERENCES

1. ACI/TMS Committee 216.1. 2007, Code requirements for determining fire resistance of concrete and masonry construction assemblies, American Concrete Institute, Detroit, MI, USA.
2. EN 1992-1-2. 2004, Design of concrete structures – Part 1-2, General rules – Structural Fire design, CEN.
3. AS-3600, “Concrete Structures”, Australia, Committee BD-002.
4. Kodur V., Dwaikat M. & Raut N. 2009, “Macroscopic FE Models for Tracing the Fire Response of Reinforced Concrete Members”, *Engineering Structures Journal*, V. 31 No. 10, pp. 2368–2379.
5. Dwaikat, M.B. & Kodur, V.K. 2008, "Hydrothermal Model for Predicting Fire Induced Spalling in Concrete Structural Systems", *Fire Safety Journal*, V. 44, No. 3, pp 425–434.
6. Harmathy T.Z. 1967, "A comprehensive Creep Model", *Journal of Basic Engineering*, V. 89, No. 2, pp. 496–502.
7. Harmathy T.Z. 1993, "Fire Safety Design and Concrete", *Concrete Design and Construction Series*, Longman Scientific and Technical, UK.
8. Anderberg Y., & Thelandersson S. 1976, "Stress and Deformation Characteristics of Concrete at High Temperatures, 2. Experimental Investigation and Material Behavior Model", Lund Institute of Technology, Sweden.
9. Chen, W.F., & Atsuta T. 1976, *Theory of beam-columns: Vol 2 Space behavior and design*, McGraw Hill, USA.
10. Campbell T.I., and Kodur V. 1990, Deformation Controlled Nonlinear Analysis of Prestressed Concrete Continuous Beams. *PCI Journal*, PCI, pp. 42–55.
11. Lie T.T., Woolerton J.L. 1988, "Fire Resistance of Reinforced Concrete Columns – Test Results", National Research Council Canada, Internal Report No 569.
12. Kodur V.R., McGrath R., Leroux P., & Latour J.C. 2005, "Experimental Studies for Evaluating the Fire Endurance of High-Strength Concrete Columns", National Research Council Canada, Internal Report No 197.
13. ASTM. 2001, "Standard Methods of Fire Test of Building Construction and Materials", Test Method E119-01, American Society for Testing and Materials, West Conshohocken, PA.
14. ACI Committee 318. 2005, “Building code requirements for structural concrete and Commentary”, American Concrete Institute, Detroit, MI, USA.

Modelling the Fire Resistance of Prestressed Concrete Floors Using Multi-Spring Connection Elements

J.-K. MIN, P. MOSS, R. DHAKAL and A. BUCHANAN

ABSTRACT

Despite big advances in analytical modelling of the performance of structures exposed to fire, there has been difficulty in modelling the fire performance of precast prestressed concrete floor slabs in multi storey buildings. The fire resistance of these floor systems is heavily influenced by the end connections and the stiffness of the surrounding structure, both of which must be considered in any analysis.

Previous “traditional” studies have modelled the floor slabs with beam or shell elements in which the end nodes share the nodes of the beam elements representing the supporting beams. This is acceptable for cast-in-situ or precast flooring system without prestressing, but leads to a major problem for precast prestressed flooring systems where the steel tendons terminate at the end of the flooring units, because the approach of sharing nodes of the supporting beam and floor assumes that these tendons are anchored into the supporting beams.

In order to solve this problem, a “multi-spring” connection element has been developed. The multi-spring connection element consists of several parallel axial springs sandwiched between two rigid plates. Each spring represents either a steel reinforcing layer or a segment of concrete in the floor cross-section. The concrete springs have compression-only properties. This multi-spring connection is placed between the end nodes of the floor and the nodes of the supporting beam. With this element, it is possible to terminate the prestressing tendons at the end node of the floor elements and to anchor only the topping reinforcement into the supporting systems predicted using the traditional approach and the newly developed multi-spring connection, with applications to different forms of precast concrete floors in multi storey buildings.

Jeong-Ki Min, PhD Candidate, Dept. of Civil and Natural Resources Engineering, University of Canterbury, Private Bag 4800, Christchurch, New Zealand

Peter Moss, Associate Professor

Rajesh Dhakal, Associate Professor

Andrew Buchanan, Professor

INTRODUCTION

The use of precast prestressed concrete flooring systems in multi-storey buildings has become very common in New Zealand due to several advantages, such as high quality control and the saving of labour. Recently, a considerable number of studies [1-3] have been conducted on the structural performance of precast prestressed concrete flooring system against earthquake actions at ambient temperatures. Nonetheless, relatively little attention was paid to fire performance of prestressed concrete flooring building systems in New Zealand [5].

The hollowcore concrete slabs, one of the most widely used prestressed concrete flooring systems in multi-storey buildings, has been studied by a few researchers [7, 8]. The studies, which were only limited to one or two units, have shown that some failure modes, such as debonding, shear and spalling, are more critical in prestressed hollowcore concrete slab exposed to fire. The failure mode of hollowcore slab exposed to fire has recently been questioned by some full-scale frame tests [4, 6] carried out at the Building Research Establishment (BRE) Cardington test facility in the UK. According to the BRE results of a series of full-scale frame test on hollowcore floors, the fire performance of hollowcore floors in a full-scale frame exposed to serious fires was satisfactory and there was no premature failure or shear failure or significant spalling.

Despite big advances in analytical modelling of the performance of structures exposed to fire, there has been difficulty in modelling the fire performance of precast prestressed concrete floor slabs in multi storey buildings. The fire resistance of these floor systems is heavily influenced by the end connections and the stiffness of the surrounding structure, both of which must be considered in any analysis.

Previous study [9] has modelled the floor slabs with beam or shell elements whose end nodes share the nodes of the beam elements representing the supporting beams. This is acceptable for cast-in-situ or precast flooring system without prestressing, but leads to a major problem for precast prestressed flooring systems where the steel tendons terminate at the end of the flooring units, because the approach of sharing nodes of the supporting beam and floor assumes that these tendons are anchored into the supporting beams.

This paper presents the development of a multi-spring connection element which is able to take into account the discontinuity of prestressing steel tendons between hollowcore slabs and their supporting end beams. The multi-spring connection model is verified against experimental data from a furnace test on hollowcore slabs connected to end beams obtained from literature.

TYPICAL STRUCTURAL CONNECTION DETAILS OF PRESTRESSED HOLLOWCORE SLAB

Precast prestressed hollowcore floor units seated on reinforced concrete moment resisting frames have been widely used as one of most common construction types in New Zealand during the last few decades. In order to investigate the seismic adequacy in different construction types, a series of experiments have been performed [1-3]. As a result, two acceptable solutions for hollowcore seating connections have been implemented in Amendment 3 within NZS3101:1995 and NZS3101:2006 for 'new' construction practice in New Zealand.

Simple connection detail

Traditionally, simply supported precast prestressed hollowcore slabs in New Zealand have been widely used as shown in Figure 1(a) [10]. The simple connection details comprised of the floor unit seated on a mortar bed, core end plugs to prevent concrete from entering the cores, and conventional starter bar reinforcement in the topping slab [1]. As shown in the Figure 1(a), a hollowcore slab is not directly anchored to the supporting beam; only the starter bars from the topping concrete are connected to the supporting beam. The gap between the supporting beam and the hollowcore slab is filled with normal concrete in order to provide flexibility of lateral movement in earthquakes.

Continuous connection detail

While the simple connection detail of prestressed hollowcore floors has been widely used, a continuous floor-end beam connection solution has also been proposed in order to improve seismic performance as shown in Figure 1(b). This continuous connection features hollow cores reinforced and filled with concrete [3]. For 200 mm deep hollowcore slabs, two cores of the six hollow cores are reinforced with hooked bars placed close to the bottom of the cores. The topping slab consists of reinforcement which is lapped with the starter bars. To construct the continuous connection, more effort, such as pre-cutting of cores and placing of extra reinforcement, are required in comparison to simple connection detail. However, the continuous connection provides redundancy by being tied into the supporting beams [3].

MODELLING OF PRECAST PRESTRESSED FLOORS FOR FIRE ANALYSIS

General

A special purpose, non-linear finite element program, SAFIR [11], which has been developed at the University of Liege, Belgium and is capable of conducting both thermal and structural analysis of structures, was used to carry out this numerical analysis. It includes two different types of elements which are used in this study: beam and spring elements.

Structural elements

The beam element has a constant section along the longitudinal axis that is a straight line extending between the two end nodes. In previous research [9] a beam grillage system was used to model the hollowcore units and shell elements were used for the topping concrete, whereas topping concrete is incorporated into the beam grillages in this study, as shown in Figure 2. Detailed information on the beam grillage model of hollowcore slabs can be found in references [5, 9].

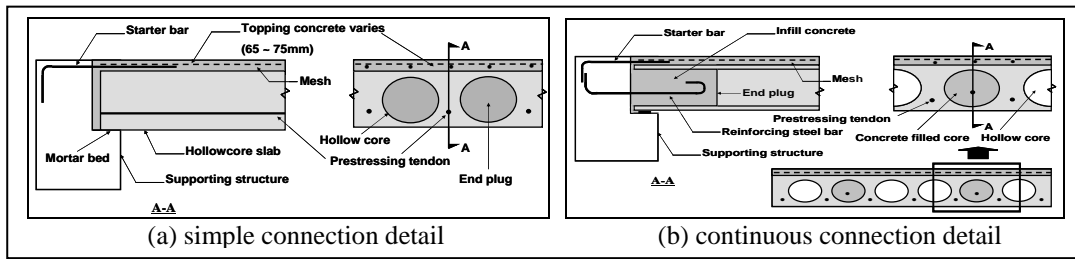


Figure 1. Floor-end beam connection detail of hollowcore floors.

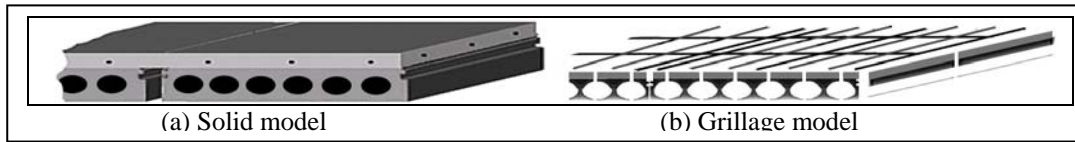


Figure 2. Grillage system for hollowcore system and topping concrete.

Limitations of SAFIR

Material models included in SAFIR program have some inherent assumptions, as is the case with all analytical models. The possible limitations of SAFIR resulting from these assumptions are:

- 1) SAFIR assumes perfect bond between two materials and cannot account for slippage between concrete and the steel.
- 2) SAFIR cannot predict spalling of concrete.
- 3) Because SAFIR is based on the Bernoulli hypothesis, the beam finite element cannot detect shear failure.

TABLE I. PROPERTIES OF THE HOLLOWCORE FLOOR UNIT.

Hollowcore	Cross-sectional area	0.121 m ²
	Self weight	3.88 kPa
	Compressive strength	45 MPa
Prestressing strands	Type	Stress relieved 7-wire strand
	Strength	1.87 GPa
	Prestressing level	70%
	Cross-sectional area	100 mm ²
Reinforced concrete topping slab	Concrete compressive strength	30 MPa
	Reinforcement strength	450 MPa

Dimensions and material properties

A typical 200 mm deep and 1200 mm wide prestressed hollowcore unit is used while the properties of such units are listed in Table I.

DEVELOPMENT OF MULTI-SPRING CONNECTION MODEL

As explained earlier, the current New Zealand concrete code has two different types of connection details. Analytical models for both connection details are developed in this study.

Multi-spring connection model for simple connection detail

A schematic of the multi-spring model for a simple connection is shown in Figure 3. In using the grillage model, beam elements, as shown in Figure 3, are expressed as fibres which include the geometrical and mechanical properties of the hollowcore cross-section as well as its thermal properties at elevated temperature. Here, the vertical faces in either side of the gap between the hollowcore slabs and seating beams are modelled as rigid surfaces, which are connected to each other through a series of springs representing the concrete and the starter bars. The use of rigid beam elements is able to avoid unnecessary small displacements at the vertical faces. Both rigid faces are vertically supported at the bottom, but the internal face is allowed to move horizontally and rotate freely to capture the variation of the gap at the end of the hollowcore slabs. On the other hand, the external rigid beam element at the vertical surface of the seating beam can be assumed to be either fully fixed at the end boundary or connected to the supporting beam depending on the conditions.

In order to employ spring elements into the new connection model, the cross-section of the gap between hollowcore slabs and seating beams is divided into nine segments as shown in Figure 4. The temperature developments obtained from thermal analyses, as shown in Figure 5, are applied to each of nine spring elements.

Multi-spring connection model for continuous connection detail

Most details of the multi-spring model for the continuous connection detail are principally based on the multi-spring connection model used for the simple connection detail. Continuous connection detail has some differences compared to the simple connection detail. Two steel spring elements (second from the top and third to bottom spring elements) were used to model the starter bar and reinforcing bar within the core. In current connection detail, the gap between the hollowcore slabs and the end beams is filled with concrete. Area of the spring elements, therefore, is modified as shown in Figure 7. Due to the filled concrete in the voids, there is a change in terms of temperature assessment.

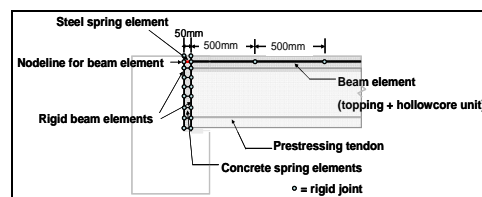


Figure 3. Schematic of multi-spring connection model for simple connection detail.

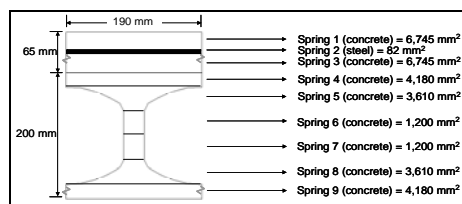


Figure 4. Division of the hollowcore slab cross-section for simple connection (white segment: concrete; black segment: steel).

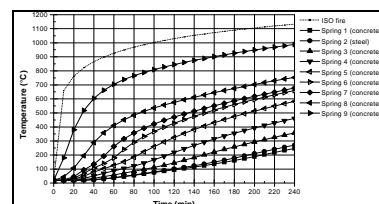


Figure 5. Temperature variation of each spring element for simple connection.

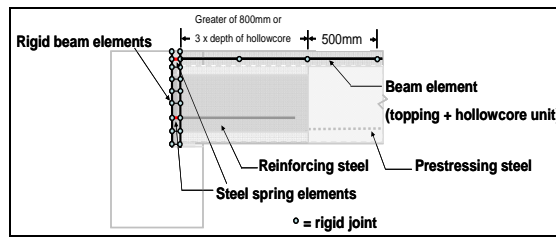


Figure 6. Schematic of multi-spring connection model for continuous connection detail.

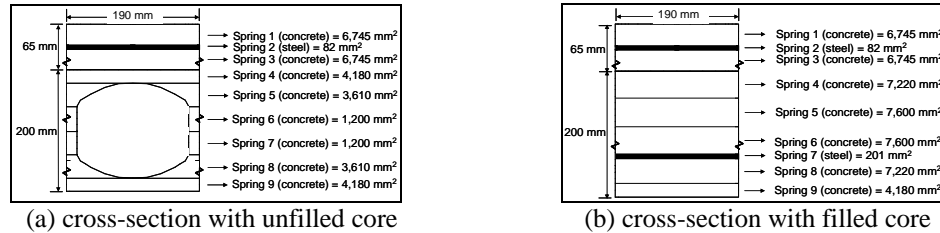


Figure 7. Division of the hollowcore slab cross-section for filled and unfilled core of current connection (white segment: concrete; black segment: steel).

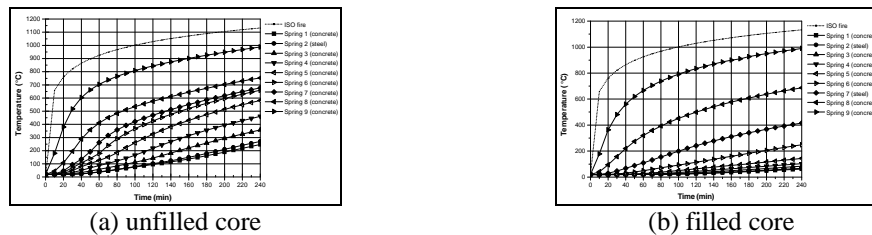


Figure 8. Temperature variation of each spring element for continuous connection for unfilled and filled core.

Comparison of traditional approach with the developed multi-spring connection model

The structural behaviour of a prestressed 200 mm hollowcore slab unit, which is restrained against horizontal and vertical movements at the end supports, is numerically investigated with and without the multi-spring connection elements. The analysis with fixed-fixed end supports based on traditional approach assumes that the prestressing strands in the hollowcore slab are anchored in the supporting beams. Figure 9 shows the comparison of structural behaviour in fire between the traditional approach and the newly developed multi-spring connection models. The mid-span vertical displacement for the fixed-fixed end condition suddenly increases after 60 minutes and then stabilises to a slow but gradual increase without any sign of failure up to 4 hours. This unconvincing response does not happen in reality because the analysis with fully fixed end supports gives rise to catenary action after the failure of starter bars when the hanging slab is supported by the tensile capacity of the prestressing steels anchored to the fixed supports. On the other hand, the newly developed multi-spring connection models resulted in failure after 62 and 87 minutes respectively. Therefore, the comparison of results indicates that the multi-spring connection elements model is more appropriate than the traditional approach because the displacement predicted by the multi-spring connection model shows a more realistic trend of the slab deflection with time.

VALIDATION AGAINST EXPERIMENTAL DATA

Four full-scale fire tests were performed at the Technical Universities of Liège and Gent in Belgium, taking into account the influence of connections and surrounding structures on the fire resistance of prestressed hollowcore slabs. Among these test results, one fire test result [13] which includes reinforced topping slab, as shown in Figure 10, has been chosen to validate the multi-spring connection model. The connection features two of the six hollow cores reinforced and filled with concrete. Even though the test consisted of two prestressed hollowcore floor spans of 3 m with three supporting beams, only one span was covered with reinforced topping slab. The hollowcore units were 200 mm thick with a 50 mm thick reinforced topping slab and the cross-section. The reinforcing bars of 40 mm diameter which were used to simulate the influence of the neighbouring structure were not considered in this analysis. Detailed information on material properties can be found in reference [13].

The multi-spring connection model was used to carry out the simulation of the experimental work, using the continuous connection model shown in Figure 6. In this model, grillage beam elements were connected to reinforcing steel bars within the cores as shown in Figure 11.

Figure 12 shows the comparison between the experimentally measured and analytically predicted structural behaviour of the slab in fire. As can be seen, the behaviour of the prestressed concrete slab in fire observed from the test is in good agreement with the numerical results in terms of fire resistance time. On the other hand, the experimental and numerical mid-span vertical deflections are different.

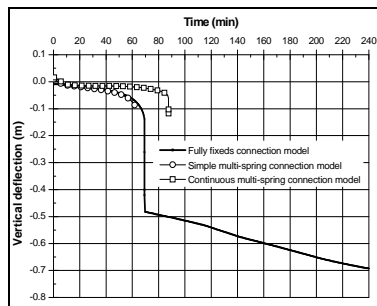


Figure 9. Comparison between vertical deflections of with and without the multi-spring connection model with respect to Fixed-Fixed end conditions.

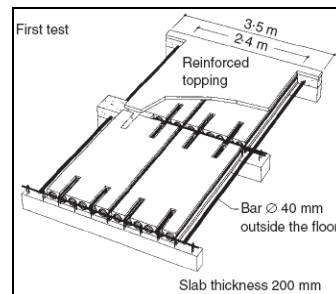


Figure 10. Fire test set-up [13].

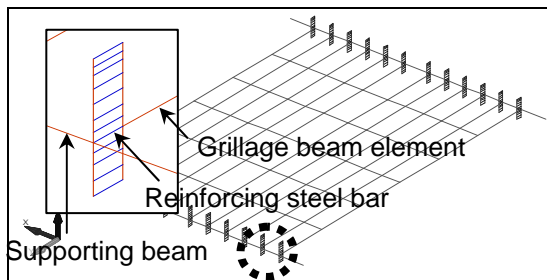


Figure 11. Modelling of the prestressed hollowcore slabs for the test.

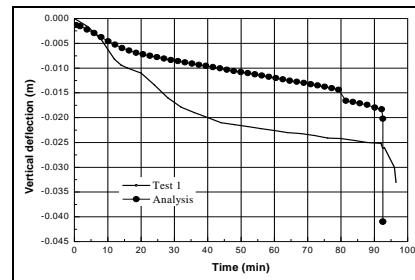


Figure 12. Comparison of structural behaviour against time.

Basically, beam elements in SAFIR program adopt the Bernoulli's hypothesis which means plane section remains plane so that shear deformation is not captured; and anchorage, bond and spalling effects are also not taken into account [9]. The difference with respect to vertical deflections, therefore, is attributed to these factors.

CONCLUSION

- The traditional approach of modelling fixed-fixed end condition cannot predict the structural behaviour of prestressed flooring systems in fire.
- A multi-spring connection model has been developed to predict the end connection behaviour of prestressed hollowcore slabs under fire exposure.
- Comparison of analytical results using the traditional approach and the newly developed multi-spring connection models has been made.
- The newly developed multi-spring connection model accounts for the yielding of starter bar or reinforcing steel bar between the prestressed units and the supporting beams.
- The model has been validated against an experiment, which showed good agreement in terms of fire resistance time.
- The newly developed multi-spring model can potentially be utilised to investigate the global behaviour of multi storey buildings in fire.

REFERENCES

1. Matthews, J. G. 2004. *Hollow-core floor slab performance following a severe earthquake*, PhD Thesis, Dept. of Civil Engineering, University of Canterbury, Christchurch, New Zealand.
2. Lindsay, R. 2004. *Experiments on the Seismic Performance of Hollow-core Floor Systems in Precast Concrete Buildings*, ME Thesis, Dept. of Civil Engineering, University of Canterbury, Christchurch, New Zealand.
3. Mac Pherson, C. J. 2005. *Seismic performance and forensic analysis of a precast concrete hollow-core floor super-assembly*, ME Thesis, Dept. of Civil Engineering, University of Canterbury, Christchurch, New Zealand.
4. Lennon, T. 2003. "Precast concrete hollow core slabs in fire," *The Structural Engineer*, 81(6): 30–47.
5. Chang, J. 2007. *Computer simulation of hollowcore concrete flooring systems exposed to fire*, PhD Thesis, Dept. of Civil Engineering, University of Canterbury, Christchurch, New Zealand.
6. Bailey, C. G. and Lennon, T. 2008. "Full-scale fire tests on hollowcore floors," *The Structural Engineer*, 86(6): 33–39.
7. Andersen, N. E. and Lauridsen, D. H. 1999. *Danish Institute of Fire Technology Technical Report X 52650 Part 2 – Hollow core Concrete Slabs*, Danish Institute of Fire Technology, Denmark.
8. Fellingner, J. H. H. 2004. *Shear and Anchorage Behaviour of Fire Exposed Hollow Core Slabs*, DUP Science, Delft, Netherlands.
9. Chang, J., Buchanan, A. H., Dhakal, R. P. and Moss, P. J. 2008. "Hollow-core concrete slabs exposed to fire," *Fire and Materials*, 32(6): 321–331.
10. Herlihy, M. D. 1999. *Precast concrete floor support and diaphragm action*, PhD Thesis, Dept. of Civil Engineering, University of Canterbury, Christchurch, New Zealand.
11. Franssen J.M. 2005. "A Thermal/Structural Program Modelling Structures under Fire," *Engineering Journal, A.I.S.C.*, 42(3): 143–158.
12. Franssen, J.M. 2007. *User's Manual for SAFIR 2007: A Computer Program for Analysis of Structures Subjected to Fire*, Liège: University of Liège, Belgium.
13. Van Acker, A. 2003. "Shear resistance of prestressed hollow core floors exposed to fire," *Structural Concrete – Journal of the fib*, 1(4): 65–74.

Behaviour of Earthquake Damaged Reinforced Concrete Structures in Fire

A. ERVINE, M. GILLIE and PANKAJ

ABSTRACT

In the interest of life safety, modern structures are designed and built to resist extreme events such as earthquakes without collapse. However, due to economic considerations limited structural damage is permissible. In seismic regions, a fire following an earthquake is considered to be a major threat due to the risk of ignition of damaged gas and/or fuel services. Design codes do not account for this scenario where these two extreme events occur consecutively on a structure and do not address the situation of the structure having some initial damage when being subject to a fire load.

This study examines and numerically models the effect of a fire following an earthquake on a reinforced concrete frame. This has been carried out by examining the type and magnitude of local damage the reinforced concrete frame undergoes, how this affects its thermal profile and hence the overall thermo-mechanical behaviour.

INTRODUCTION

Whilst the thermal properties of concrete have been well documented for a wide variety of concrete types and strengths, most available data relates to intact and undamaged concrete. As a reinforced concrete structure becomes damaged, the cover to the reinforcement may be significantly reduced or removed completely. This may lead to the reinforcement being subjected to higher temperatures or being directly heated, resulting in a reduced time to structural failure. Essentially this scenario can be modelled using the finite element method in two ways. First, removal of elements can be used to represent the concrete cover being diminished. This method can be time

Adam Ervine. PhD, BRE Centre for Fire Safety Engineering, University of Edinburgh
Email: a.ervine@see.ed.ac.uk

Dr. Martin Gillie., Lecturer, BRE Centre for Fire Safety Engineering, University of Edinburgh
Email: m.gillie@see.ed.ac.uk

Dr. Pankaj. Lecturer, BRE Centre for Fire Safety Engineering, University of Edinburgh
Email: p.pankaj@see.ed.ac.uk

consuming and lead to numerical instabilities. Instead of removing elements, the second method changes material properties such as conductivity, specific heat capacity and density of the damaged elements such that their thermal diffusivity becomes large and mechanical strength minimal. With this method, these properties can no longer be considered purely as material properties but ones that depends on the structural state of the concrete.

The numerical models presented in this paper include a quantification of damage that is established from the build up of plastics strains. Variations in conductivity, specific heat capacity and density are scaled appropriately with damage as later detailed. The thermal propagation and overall mechanical behaviour is then compared with the traditional model whereby the diffusivity is independent of damage.

PREVIOUS WORK

There has been much research into the mechanical properties and behaviour of concrete and how they vary with temperature. Such research has lead to guidelines being produced for a concrete crushing strain. Eurocode 2 states that for the purpose of design, concrete should have a maximum compressive strain of 0.0035. However, as this value is intended for design at ambient temperature it is conservative; hence the strains developed within the concrete compressive state can in fact be much greater.

Many papers have investigated the stress-strain relationship of concrete under static, impact and blast loading. Sukontasukkul et al. performed tests on purely concrete specimens under various rates of impact loading. Results showed that as the impact becomes more rapid the concrete specimens were able to resist greater and greater stresses and strains when compared to concrete subjected to static loading. Grote et al. also concluded that concrete has the ability to resist greater stresses and strains in both compression and tension as the strain rates are increased from static through to blast.

The strain rates undergone by a reinforced concrete structure subjected earthquake loading are of the order of 10^{-2} - 10^0 therefore it may be assumed that for this scenario the concretes stress strain-relationship is independent of loading rate thus design material properties may be used.

DETERMINING THE CRUSHING LIMIT

As a reinforced concrete section is loaded beyond its designed capabilities there are a number of damage modes that can occur, such as tensile cracking, loss of concrete cover and crushing of the concrete core. This paper is focuses on how the loss of concrete cover affects the thermal propagation through a section and subsequently the mechanical behaviour.

As the concrete cover crushes and becomes removed it may be considered that the front of the thermal boundary has been altered to the point that the reinforcement is directly heated as shown in Fig 1. To determine the point at which crushing failure occurs; an experimental program was undertaken to establish the plastic strains developed running up to and including the instance of crushing of a concrete specimen with a nominal compressive strength of 35MPa.

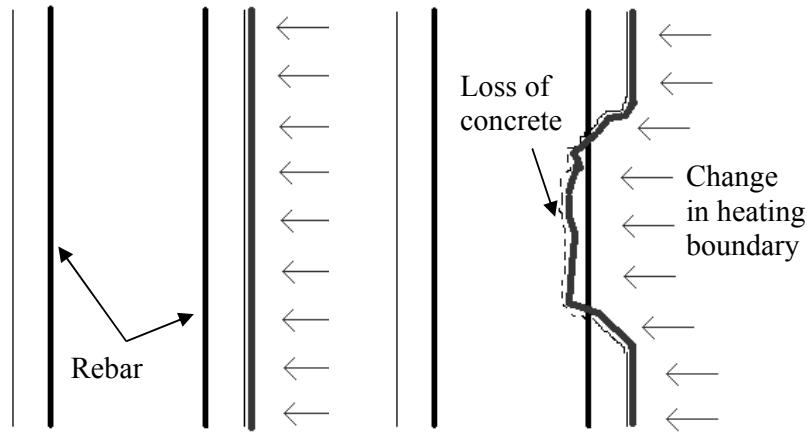


Figure 1. Illustration concrete thermal boundary alterations that may occur due to loss of reinforcement cover.

To achieve this, reinforced concrete beams were subjected to four point bending and the region of zero shear was monitored by cameras as shown in Fig 2. The beams used were doubly reinforced 35MPa (nominal) concrete with dimensions of 90×160×870mm. The reinforcement was 10Φ mm 460MPa steel. Concrete cover was 20mm on all sides with the exception of the tensile face which had a cover of 40mm. Loads were recorded from load cells placed under the loading jacks and deflections from gauges placed at the mid-span and other key locations. Load and deflection data was recorded at 2s intervals. Strains fields within the area of zero shear were recorded using image correlation by taking photographs of both sides of the beam at 5s intervals over the loading to failure time of ten minutes and processing these with a program developed by Bisby and Take (2009).

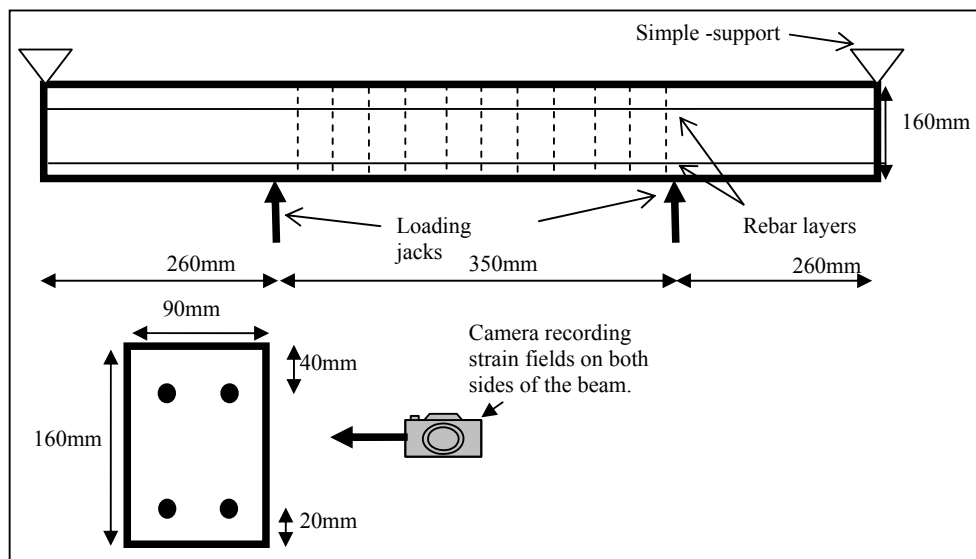


Figure 2. Experimental setup showing side view of loading beam and typical cross-section.

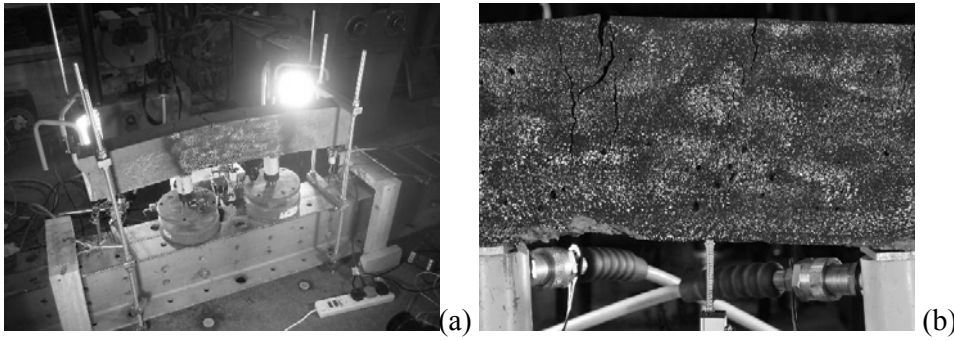


Figure 3. (a) General mechanical setup, (b) Side view of beam that enables the calculation of the strain fields. Also shows crushing on the compressive face.

From the data gathered, the load-deflection relationship was determined as well as the magnitude and location of the strains and plastic strains that are developed; these are illustrated Fig 4. From this it can be seen that the instant at which the concrete crushes is at a load of approximately 76kN and a mid-span deflection of 11mm. At this point the plastic strains developed at the compressive surface of the specimen reached approximately 0.004.

As stated previously it can be considered that the front of the thermal boundary is altered to follow profile of cover loss. However, to represent this numerically by removing of elements when a predefined plastic strain is reached can be not only time consuming but can lead to numerical instabilities. The procedure used in this investigation is to alter the conductivity, specific heat capacity, density and expansion of the material as it reaches this predefined plastic strain of 0.004 in compression. At this point the conductivity of the removed section is increased to infinity (numerically an extremely large number), whilst the specific heat capacity, the density and coefficient of thermal expansion reduce to zero.

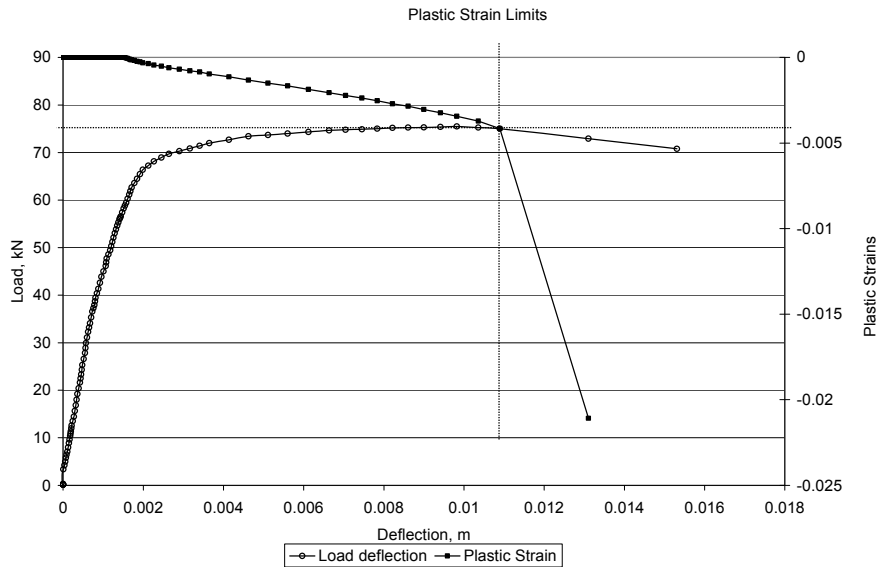


Figure 4. Load deflection relationship (left axis), Plastic strains developed (right axis). Point of crushing of the compressive face indicated with dotted lines.

NUMERICAL STUDY

A numerical study was set-up to investigate how localised crushing and removal of concrete cover due to some initial mechanical event affected the thermal and thermo-mechanical behaviour of a simple concrete frame (Fig 5). The frame was designed with non-linear Eurocode material properties. However, as it is the compression behaviour that is being explored, the tensile properties were enhanced to force yielding to occur in compression and to reduced numerical instabilities.

The frame was subjected to a uniformly distributed vertical load of 1MN together with a displacement controlled lateral force at beam height. “Minor damage” was produced by pushing the frame by 0.015m (i.e. 10% of the column width) whilst a push of 0.075m (i.e. 50% of the column width) was used for “major damage”. For both scenarios the frame was brought back to the point where there was no horizontal reaction force but some residual horizontal deflection (due to plasticity) thereby simulating in a simple manner the loading an earthquake might produce. The internal surfaces of the frame were then subjected to a thermal load of 800°C (ramped over five minutes and held constant for the remainder of an hour).

Due to the loading applied there were plastic strains developed in the frame as shown in Fig 6(a) and Fig 7(a). The magnitude of these plastic strains was sufficient to cause crushing and hence removal of the damaged section as outlined previously. For the minor scenario the ‘damaged’ portion was localised to the beam and with a length approximately 4% of the internal span whereas the ‘damaged’ portion of the major scenario was significantly more extensive.

Comparisons in mid-span deflections are made between models where the assumption is that the thermal propagation is independent of damaged and where the thermal propagation is dependent on damage.

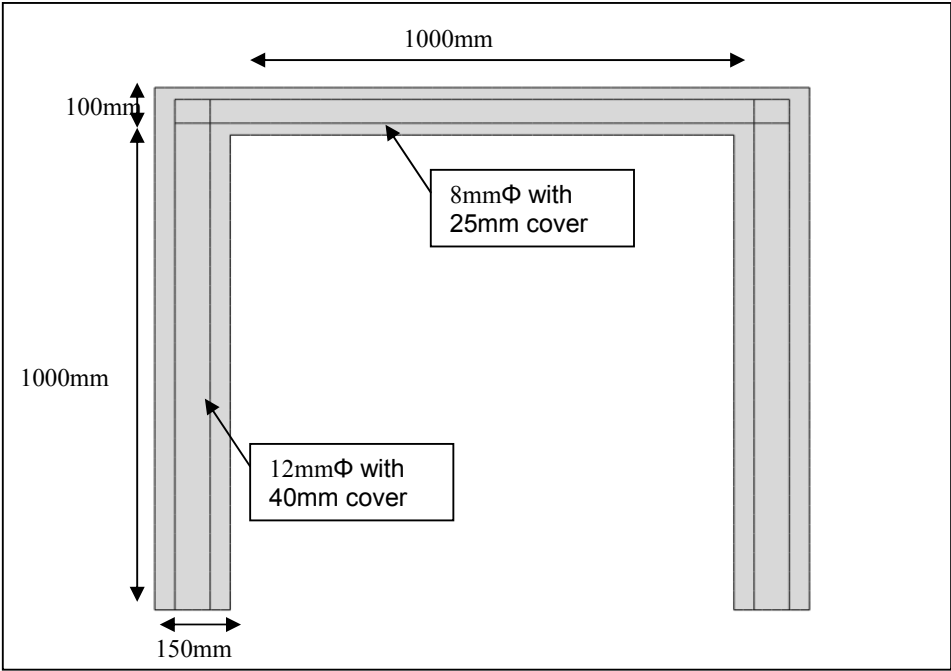


Figure 5. Numerical model setup showing dimensions and reinforcement.

Results

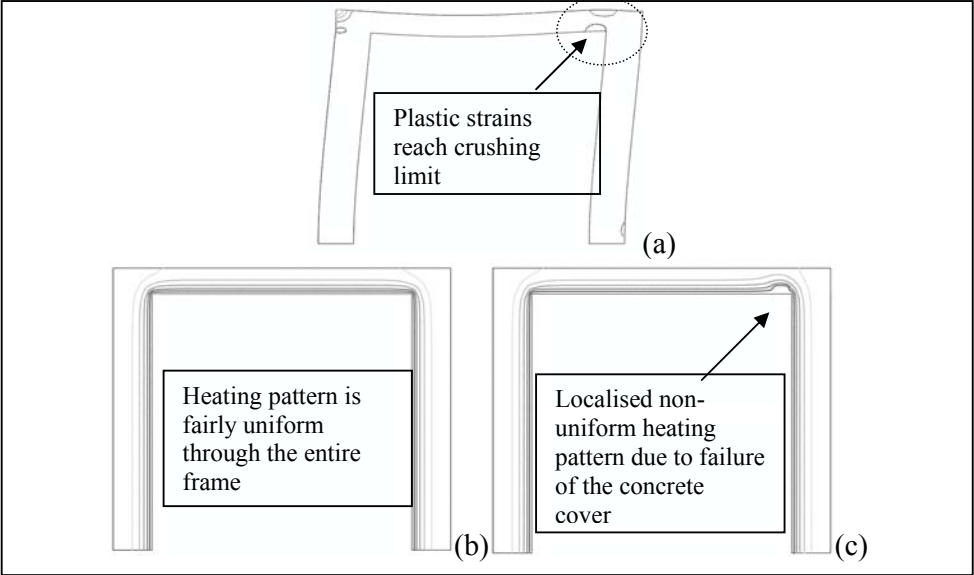


Figure 6. (a) Plastic strains developed within the frame during minor damage, (b) Thermal profile assuming material properties are independent of damage, (c) Thermal profile assuming material properties are dependant on damage.

The removal of cover caused an inconsistency within the thermal profile of the frame within the area of damage as seen when comparing Fig 6 (b) and (c). This is also observed in Fig 7(b). Within the area of damage, the diffusivity increases rapidly and hence the thermal boundary is effectively shifts into the beam to the point whereby locally the steel is being directly heated. This behaviour is even more prominent when the frame undergoes larger loads whereby more extensive loss of cover is observed. This is illustrated in Fig 7.

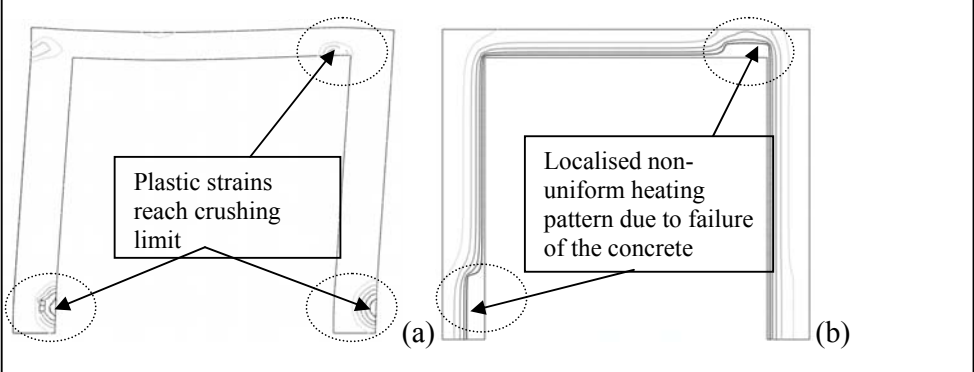


Figure 7. (a) Plastic strains developed within the frame during major damage, (b) Thermal profile assuming material properties are dependent on damage.

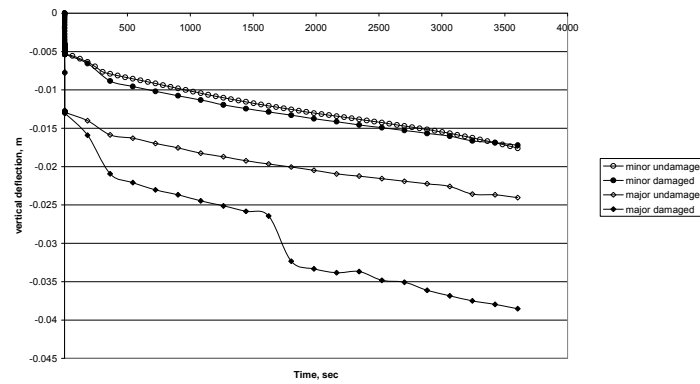


Figure 8. Comparisons of mid-span deflections for minor and major compressive damage.

CONCLUSIONS

The results of the numerical study show that damage to the cover of a reinforced concrete structure can severely alter the thermal profile and hence the overall thermo-mechanical behaviour. For a major event, Fig 8 shows a 60% increase in mid-span deflection when the thermal behaviour is assumed to be dependant on damage. Hence when the structure experiences large plastic deformations it has been shown that it is essential to consider the damage in terms of loss of concrete cover. However, for a scenario where there is some minor damage, the difference in behaviour when subjected to a thermal load is negligible as shown in Fig 8. Therefore, it is vital that the possible damaged state of the structure is determined before analysis under thermal load is undertaken.

Comparing the minor and major damage states, it can be concluded that the damaged state has to be sufficient to cause extensive plastic hinges that mean the structure approaches forming a mechanism for damage to have a significant effect. Thus, the effect of damage on the response of heated concrete structures does not depend in a linear manner on the degree of damage. Further investigation into the limits of the damaged states and relevance of their location is planned to achieve a more complete picture.

ACKNOWLEDGEMENTS

The authors acknowledge the financial support of EPSRC and the BRE Trust in funding this work.

REFERENCES

1. CEN, 2004, Eurocode 2: Design of concrete structures—Part 1.1 General rules and rules for buildings. *European Committee for Standardization*, Table 3.1, pp 2–18.
2. Sukontasukkul, P., Nimityongskul, P. and Mindess, S., 2004. Effect of loading rate on damage of concrete. *Cement and Concrete Research*, 34(11), p.2127–2134.
3. Grote, D., Park, S. and Zhou, M., 2001, Dynamic behaviour of concrete at high strain rates an pressures. *Journal of Impact Engineering*, Vol. 25, Pergamon Press, New York, pp. 869–886.
4. Bisby, L. A. & Take, W. A., 2009. Strain Localizations in FRP Confined Concrete: New Insights. *Structures and Buildings* 162(5): 301–309.

Fire Testing of an Earthquake Damaged RC Frame

P. BHARGAVA, U. K. SHARMA, Y. SINGH, B. SINGH, A. USMANI,
J. TORERO, M. GILLIE, PANKAJ, I. MAY and C. S. MANOHAR

ABSTRACT

Fires are a relatively likely event consequent to earthquakes in urban locations and in general are an integral part of the emergency response strategies focused on life safety in most developed economies. Similarly building regulations in most countries require engineers to consider the effect of seismic and fire loading on the structures to provide an adequate level of resistance to these hazards, however only on a separate basis. To the authors knowledge there are no current regulations that require buildings to consider these hazards in a sequential manner to quantify the compound loading and design for the required resistance. It is accepted that in many cases this may not be feasible or even desirable, but on the other hand there will be many high value structures where it would be economically and technically sensible to provide such resistance. This paper will describe a collaborative project currently underway involving two universities in India (IIT Roorkee and IISc) and the University of Edinburgh to investigate the fire resistance of earthquake damaged RC structures.

Pradeep Bhargava, Professor, Department of Civil Engineering, Indian Institute of Technology Roorkee, Roorkee, India 247667

Umesh Kumar Sharma, Assistant Professor, Department of Civil Engineering, Indian Institute of Technology Roorkee, Roorkee, India 247667

Yogendra Singh, Associate Professor, Department of Civil Engineering, Indian Institute of Technology Roorkee, Roorkee, India 247667

Bhupinder Singh, Assistant Professor, Department of Civil Engineering, Indian Institute of Technology Roorkee, Roorkee, India 247667

Asif Usmani (corresponding author), Professor, School of Engineering, The University of Edinburgh, Edinburgh EH9 3JF, United Kingdom

Jose Torero, Professor, School of Engineering, The University of Edinburgh, Edinburgh EH9 3JF, United Kingdom

Martin Gillie, Lecturer, School of Engineering, The University of Edinburgh, Edinburgh EH9 3JF, United Kingdom

Pankaj, Senior Lecturer, School of Engineering, The University of Edinburgh, Edinburgh EH9 3JF, United Kingdom

Ian May, Professor, School of Built Environment, Heriot-Watt University, Edinburgh EH14 4AS, United Kingdom

CS Manohar, Professor, Department of Civil Engineering, Indian Institute of Science, Bangalore, India 560012

INTRODUCTION

The risk of fires in the aftermath of earthquakes is well known. The fires following the 1906 San Francisco and the 1923 Tokyo earthquakes led to major conflagrations and widespread devastation resulting in far greater damage than caused by the original shaking. Fortunately the scale of those events have not been repeated, however there have been many major earthquakes which have been followed by fires. Nearly all major Californian earthquakes have been followed by multiple ignitions, most notably, the 1971 San Fernando and 1994 Northridge earthquakes were both followed by over 100 ignitions. The 1995 Hanshin (Kobe) earthquake was also followed by over 100 ignitions in Kobe City and a similar number of fires in other cities in a highly populated area (over 2 million) and several conflagrations developed. Scawthorn *et al.* [1] provide a relatively comprehensive treatment of the post-earthquake fires from an emergency response, societal preparedness and disaster mitigation point of view and include discussions of the major historical fire following earthquake (FFE) events.

Another thing that comes out rather starkly from the study of FFE events is that the risk of FFE is very non-uniform. Many recent earthquakes were not followed by widespread fire events, for example 1999 Izmit (Turkey) (although a number of crude and naphtha tanks burned), 2001 Gujrat (India), 2005 Kashmir (Pakistan and India) and 2008 Wenchuan (China) earthquakes were not followed by significant fire events. The level of urbanization and industrialization may be an obvious factor which possibly explains this anomaly (most certainly for the relatively remote and backward mountainous regions of Kashmir – even here, however, the main market in the town of Uri suffered a major fire following the earthquake which caused extensive damage). There may be other factors that are responsible for this apparent anomaly but a full explanation perhaps requires a careful and detailed study of the kind by Scawthorn *et al.* [1]. If urbanization (and concomitant density of gas, fuel and electrical supply networks) is indeed one of the key reasons, the risk of fire after earthquakes must then be considered as a rapidly increasing risk to life, livelihoods and to the sustainability of growth and development in some of the world's most densely populated regions. With an increasing integration of the world economy major disasters of the future could have repercussions far beyond the local region. FFE events have the potential to create such disasters and should certainly be considered in the overall disaster mitigation strategies by governments and agencies with such a remit. Considerable new research effort is required to properly address the challenge posed by FFE events, some which is discussed in [2].

This paper will describe the progress on a collaborative project between University of Edinburgh, Indian Institute of Technology Roorkee and Indian Institute of Science which started in Autumn 2008. The key aim of this project is to carry out possibly the first ever large-scale tests to understand the behaviour of damaged reinforced concrete frames in fire. The first of these tests will be carried out in the summer of this year (2010) and full testing programme is likely to end by spring 2011. The earthquake and fire research community will be invited to join a blind round-robin modeling exercise culminating in a workshop in India in the summer or Autumn of 2011, where the all the experimental data will be made available to the participants (and the wider research community).

PLAN FOR LARGE SCALE TESTING OF DAMAGED RC FRAMES

A number of identical reinforced concrete frames consisting of four columns (3m apart in plan) supporting four beams and a slab, all monolithically constructed, will be built at IIT Roorkee in India. These structures will then be subjected to cyclic quasi-static loading against a reaction wall to simulate seismic damage. Table 1 shows the tests to be carried out.

Table 1: Frame tests planned.

	Simulated seismic damage	Fire loading	Aftermath
1	Displacement beyond peak lateral force	900°C -1000°C*	Residual lateral capacity test*
2	None	900°C -1000°C for 1 hr	Residual lateral capacity test
3	Moderate (x% of the displacement corresponding to peak lateral force)†	900°C -1000°C for 1 hr	Residual lateral capacity test
4	Severe (y% of the displacement corresponding to peak lateral force)†	900°C -1000°C for 1 hr	Residual lateral capacity test

*for as long as considered safe

†applied incrementally and cyclically (as in Figure 7)

Moderate and severe damage levels will correspond to a percentage of the horizontal slab displacement achieved at peak lateral force (established in the first test). Efforts will be made to keep fire the exposure for all the tests broadly similar as far as possible. Figure 1 shows a schematic of the front elevation and plan of the test frame with key dimensions.

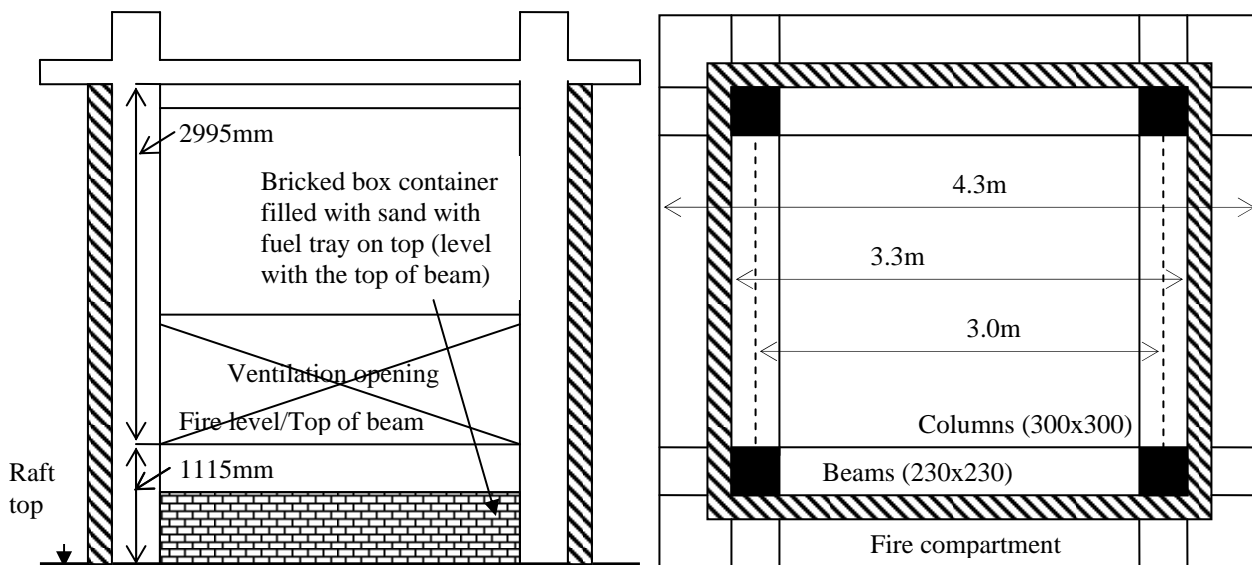


Figure 1. Schematic front elevation and plan of the test compartment.

Fire testing

The fire will be continuously fed by a 1m square tray of kerosene in a roughly 3m cube compartment with a 1m high opening along the full length of the wall at the bottom of one side (see Figure 1). To maintain a post flashover temperature of 900 °C to 1000 °C the peak burning rate for the chosen opening configuration is approximately 0.117kg/m²s. This requires a peak flow rate of kerosene into the tray of 1.43x10⁻⁴m³/s which will be maintained using a fixed head.

0.51m³ of kerosene will be required for maintaining the post flashover temperatures within the above range for 1 hour. It is anticipated that with the chosen configuration flashover will be achieved within 5 minutes.

A number of mock fire tests have been carried out at the location of the test to ensure that the expected fire behaviour is achieved and is repeatable. The first mock test carried out in July 2009 did not succeed as the brickwork walls were very damp because of rain and much of the radiant heat from the fire was being absorbed by the wall leading to an inordinate delay in flashover and low peak temperatures. The test was repeated in November 2009 and this time the results were as expected as shown in Figure 2.

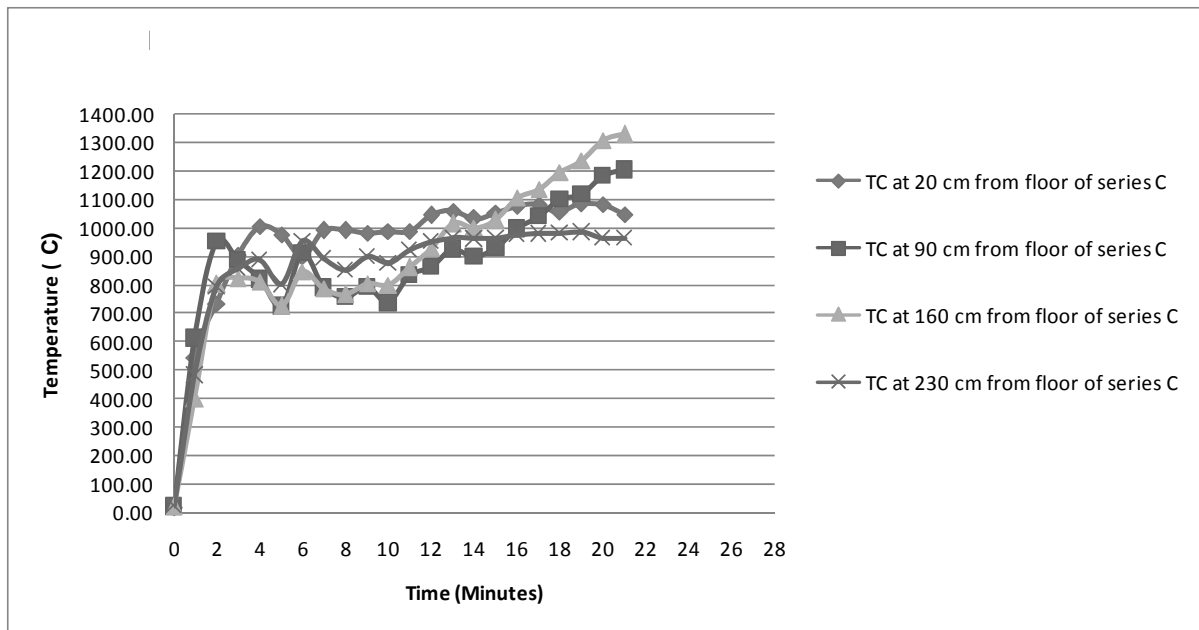


Figure 2. Temperatures inside the fire compartment (near the centre of the back wall opposite to opening).

Structural testing

No structural tests have been completed so far as the test rig is still under construction. The test frame will be built upon a 1.2m thick raft of dimensions 6.75mx8.55m and will be subjected to an increasing cyclic lateral displacement applied through jacks reacting against a stiff 1.2m thick reaction wall (monolithic with the base of the raft). The cyclic displacements will be applied at the slab level. It is expected that the first of the set of four tests will be carried out in early summer 2010.

COMPUTATIONAL MODELLING OF THE TEST FRAMES

A number of different models of the test frame have been developed to investigate the expected behaviour of the frame under the imposed cyclic mechanical displacements simulating quasi-statically the damage that may occur under seismic loads. The frame was designed as part of a four storey frame located in seismic zone IV according to Indian Standard IS 1893 (Part 1):2002. The beam and column reinforcement detail obtained from the first design cycle is shown in Figure 3. The design was checked against Eurocode 8 and found to be sufficiently ductile to withstand the assumed earthquake loading.

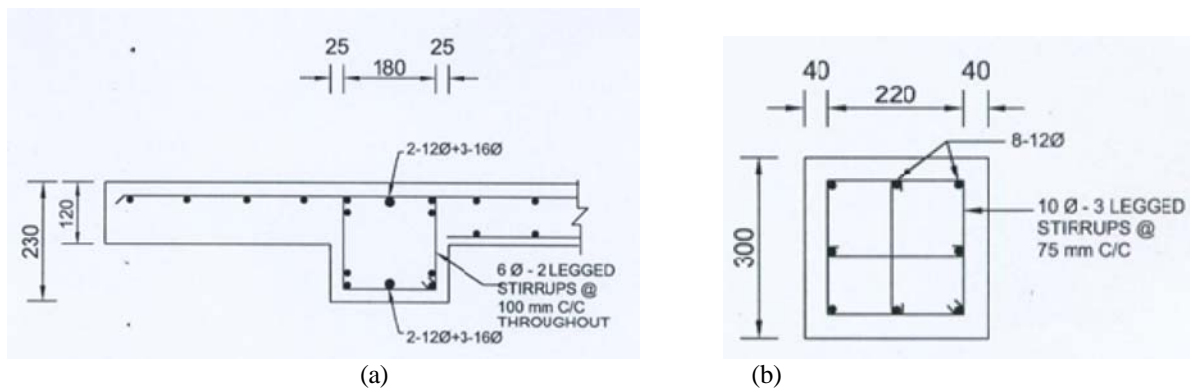


Figure 3. Details of (a) beam and (b) column reinforcement.

Although not explicitly stated in the standard, it was expected that if the code based design recommendations were followed, a strong-column weak-beam type behaviour would be obtained, *i.e.* the first hinge would form in the beams. A simple plastic analysis showed that this was not the case for the one storey test structure and this was later confirmed by more detailed finite element frame analyses as shown in Figure 4.

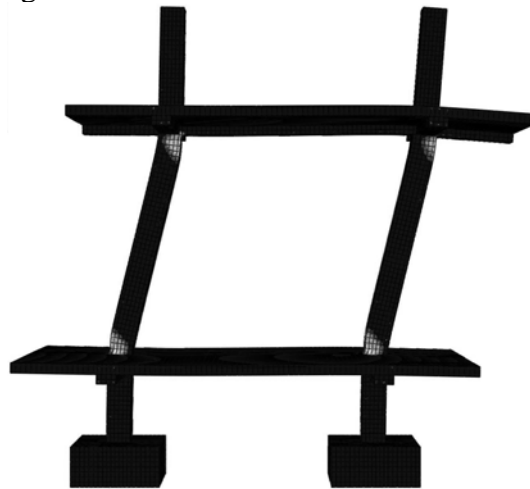


Figure 4. Finite element model of the frame showing hinges in columns.

There are two main reasons for this discrepancy: firstly the design is based on a four-storey structure where the beam moments at the joints are balanced by the sum of moments in two columns (upper and lower), while for the single bay single storey structure the moments in the beam and column must be the same; secondly frame analysis, which is the usual method for analysing structures under earthquake loads, does not fully account for the significant additional contribution from the monolithic slab acting compositely with the beam. This issue was discussed in detail between the UK and Indian teams and it was decided to ensure proper seismic behaviour of the frame and to ensure that first hinge formation occurs in the beam and therefore the reinforcement in the column was increased (to 8-20 bars) and that in the beam was decreased (to 3-16 bars top and bottom). Now the results from a single storey frame model analysis in SAP showed that first hinges formed in the beams, however the detailed finite element model (using brick elements for columns, beams and slabs) was inconclusive with plastification starting at joints (as shown in Figure 5) where the beam is composite with the slab (lower beams without slab clearly get hinges first).

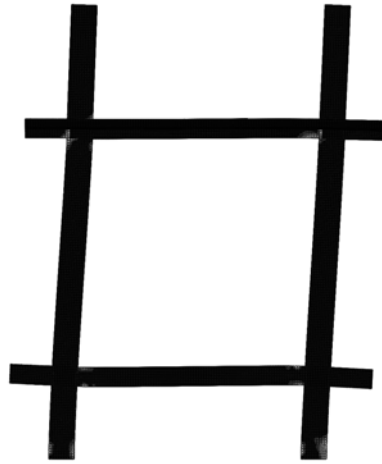


Figure 5. Finite element model of the modified RC frame (with stronger columns and weaker beams)

Peak load and displacement

The computational models have allowed estimates of peak lateral load and displacement curves to be plotted. The peak load from a plastic analysis calculation for the original frame (before the modification mentioned above) was found to be approximately 140kN. Figure 6 shows the results from a SAP frame model and a detailed finite element model (using ABAQUS) for the modified design. The ABAQUS model seems to overestimate the peak load considerably, however at a displacement of roughly 50mm the two models are somewhat in agreement (200kN and 260kN), the displacement at peak load are also similar (~100mm). It is possible that the ABAQUS model, constructed of brick elements, is over-stiff (despite using non-conforming elements and a relatively fine mesh). An ABAQUS beam and shell model provides results comparable to the SAP model.

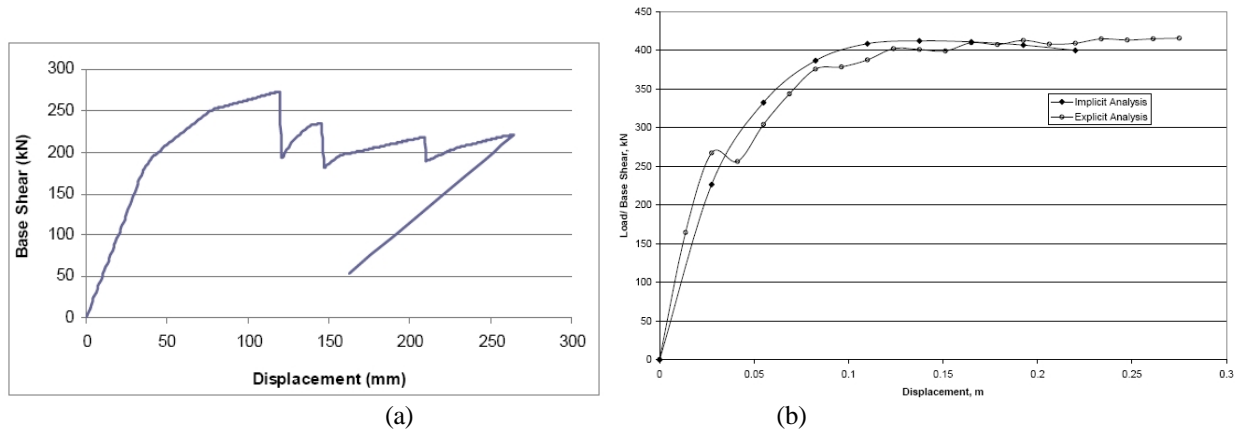


Figure 6. Load displacement curves from, (a) frame model and (b) detailed finite element model.

Further detailed analyses are being carried out with the modified model using a cyclic loading procedure, where the maximum displacement (corresponding to the peak load) will be applied in both directions in increasingly larger increments, reaching the target maximum displacement in an agreed number of cycles as shown in Figure 7.

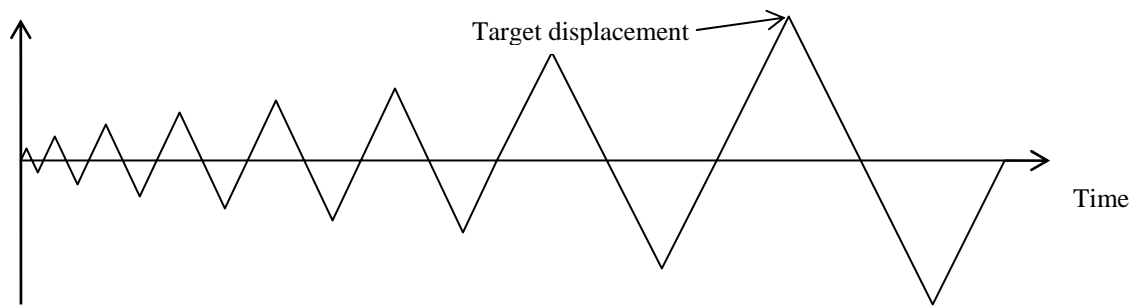


Figure 7. Incremental cyclic loading of the frame.

INSTRUMENTATION AND ROUND-ROBIN MODELLING EXERCISE

When the tests are carried out, detailed thermal and mechanical history will be recorded. A detailed set of displacements will be measured by erecting a secondary steel frame around the test frame, during both the damage inducing and fire phases. During the lateral displacement phase (to induce damage) a large number of strain gauges will be installed to obtain a detailed picture of strains at key locations. PIV equipment (high resolution camera and image analysis software) will also be used to create an independent set of data for comparison with the mechanical data using traditional methods.

Thermal instrumentation will consist of three thermocouple trees in the fire compartment to capture the gas temperature history inside the compartment during the fire testing phase. Adequate numbers of thermocouples will also be embedded in the structural members to obtain detailed structural temperature evolution for the whole heating and cooling cycle. It is unlikely that mechanical strain gauges will survive during the fire phase, therefore PIV equipment will be relied upon for obtaining some measure of strains during this phase.

The casting of the raft slab and the reaction wall is currently underway and it is expected that the first test will be carried out in May 2010. Producing numerical models of the structural response of buildings to sequential fire and earthquake loading is a challenging task. The proposed test programme will produce the first set of experimental data that can be used for benchmarking such models. It is anticipated that these tests will be of considerable interest to the wider international research community, therefore the project team wishes to offer an opportunity to all interested parties to participate in an international round-robin modelling competition. The task to be set for the exercise will primarily be to computationally predict aspects of behaviour witnessed in the test programme described above, initially without access to the experimental data. All participants in the competition will be invited to attend a workshop in India in summer or autumn 2011 and present their results (which will be published in a compendium). The full experimental results will also be made available to all participants at the workshop (and also published on the workshop webpage). We hope to be able to formally announce the workshop at the SiF conference.

CONCLUSIONS

As this work is in progress there are no final conclusions as such however some of the key lessons that have been learnt so far are perhaps the usual ones that one learns in any large-scale

testing program, i.e. the unpredictability of the whole process. It is difficult to foresee all the problems that may occur in advance. There have been the usual problems of communication between teams given the distance, time difference and different timetables of the UK and Indian partners, but this has not been a major issue and so far this has been an excellent overall collaboration. The real test is however yet to come, in more ways than one!

ACKNOWLEDGMENTS

This work has been funded by the UK-India Education and Research Initiative (UKIERI). Thanks to Adam Ervine and Mariyana Aida Abdel-Kadir for carrying out many of the analyses reported in this paper.

REFERENCES

1. Scawthorn, C., Eidinger J.M. and Schiff, A.J., editors, Fire Following Earthquake, ASCE Publications (2005).
2. Usmani, A.S., Research priorities for maintaining structural fire resistance after seismic damage, The 14th World Conference on Earthquake Engineering, Beijing, China, October 12–17, 2008.

A Simplified Sectional Analysis Approach for RC Elements During Fire Events

S. F. EL-FITIANY and M. A. YOUSSEF

ABSTRACT

Sectional analysis is widely used to assess the design of Reinforced Concrete (RC) members at ambient temperature. During fire exposure, a heat gradient is created within the concrete mass that induces non-uniform thermal and mechanical strains. These strains complicate using the same approach to predict the fire resistance of RC members. A simplified sectional analysis that tracks the axial and flexural behavior of RC elements during fire events is presented in this paper. The proposed method is based on using the Finite Difference (FD) analysis to estimate the temperature distribution within a concrete section. A rational approach is then proposed to convert the FD two-dimensional temperature distribution to one-dimensional distribution. This modification converts a complex problem to a simplified one and thus enables engineers to better understand the behavior and have higher confidence in the results. This paper covers the use of the simplified method for square columns subjected to fire from four sides and for rectangular beams exposed to fire from three sides. The validation of the proposed method is presented by comparing its predictions with other experimental and analytical results.

INTRODUCTION

Concrete as well as steel reinforcement experience significant deterioration when subjected to elevated temperatures. The strength reduction is accompanied with induced thermal and transient strains [1, 2].

S.F. El-Fitiany (corresponding author), Ph.D. Candidate, Department of Civil and Environmental Engineering, The University of Western Ontario, London, Ontario, Canada N6A 5B9

M.A. Youssef, Associate Professor, Department of Civil and Environmental Engineering, The University of Western Ontario, London, Ontario, Canada N6A 5B9

Concrete structures are currently being designed for fire using prescribed methods that are based on experimental tests. These methods specify minimum cross-section dimensions and minimum clear cover to the reinforcing bars. As new codes are moving towards performance-based design, engineers are in-need of new design tools to achieve specific performance criteria for a defined fire scenario. These tools must be analytical as conducting experimental tests to satisfy different fire scenarios would be an expensive solution. The Finite Element Method (FEM) has proven to be a powerful method to predict the behaviour concrete structures during exposure to fire events [3, 4]. Drawbacks of using the FEM, including the need to have a coupled thermal-stress analysis computer program and difficulty to comprehend its results and identify potential modelling errors, make it impractical for design engineers.

An approach that relies on using both Finite Difference Method (FDM) and a modified sectional analysis was proposed by the authors in a recent publication [5]. FDM is considered a simple method for evaluating the temperature variation within a concrete cross-section [6]. Sectional analysis allows evaluating the axial and/or flexural behaviour of concrete elements and is based on simple equilibrium and compatibility equations that can be easily applied by design engineers [5]. The modified sectional analysis was validated for concrete square columns exposed to fire from four faces [5]. To study RC beams at elevated temperatures, simple modifications to the proposed approach are introduced and validated in this paper..

The research conducted in this paper is limited to rectangular concrete sections exposed to a standard ASTM-E119 fire from three or four sides. Normal strength concrete is assumed and, thus explosive spalling is not considered [7].

SECTIONAL ANALYSIS AT AMBIENT TEMPERATURE

At ambient temperature, RC sections can be analyzed using the well-known sectional analysis approach [8]. For cases of single curvature, i.e. bending about horizontal axis, the concrete section is divided into horizontal discrete fibers as shown in Figure 1. Utilizing the uniaxial stress-strain relationship for each fiber and taking into account equilibrium and kinematics, the mechanical behavior of the section can be predicted. To simplify the analysis, two variables are assumed: incremental centroidal axial strain ($\Delta\epsilon_c$) and incremental curvature ($\Delta\psi$). Assuming a linear strain distribution, the incremental moment and axial force are obtained using Eq. (1).

$$\begin{pmatrix} \Delta M \\ \Delta P \end{pmatrix} = \begin{pmatrix} \sum_{i=1}^n E_i \times A_i \times y_i^2 & - \sum_{i=1}^n E_i \times A_i \times y_i \\ - \sum_{i=1}^n E_i \times A_i \times y_i & \sum_{i=1}^n E_i \times A_i \end{pmatrix} \times \begin{pmatrix} \Delta \psi \\ \Delta \epsilon_c \end{pmatrix} \quad (1)$$

Where E_i is the modulus of elasticity of layer i , A_i is the area of layer i , y_i is the distance between the centroid of layer i and the centroid of the cross-section.

For a given axial load, the moment-curvature behavior is obtained in two stages. In the first stage, the axial strain is increased incrementally while curvature is kept equal to zero until reaching the given axial load. In the second stage, the axial load is kept constant and the applied curvature is increased. The corresponding changes in the axial strain and the moment are calculated using Eq. (1). This process is repeated until reaching a predefined curvature value.

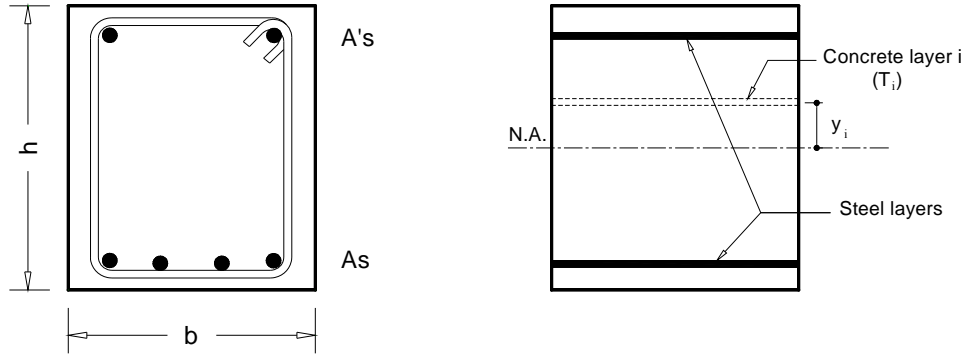


Figure 1. Cross-section and fiber model of the analyzed RC beam.

SECTIONAL ANALYSIS AT ELEVATED TEMPERATURES

To apply the same sectional analysis approach to RC columns at elevated temperatures (fire from four sides), a number of modifications were proposed and validated by El-Fitiany and Youssef [5]. Additional modifications are presented in the following sections to analyze RC beams at elevated temperatures (fire from three sides). The 6.1 m simply supported beam tested by Lin et al. [9] is considered for illustration, Figure 2a.

Heat Transfer Model

The first step to analyze a RC section subjected to elevated temperature is to estimate the heat gradient within the concrete mass. The Finite Difference Method (FDM) has the advantage of accounting for irregular shapes with good accuracy in addition to the ease of implementation in any programming code [6]. The implementation of this method in the proposed sectional analysis approach was discussed in-details by El-Fitiany and Youssef [15]. Figure 2b shows the FDM square mesh, where the temperature of each element is represented by the temperature at its center of area. A contour map for the heat gradient within the studied beam, after 1hr ASTM-E119 fire exposure, is shown in Figure 2c.

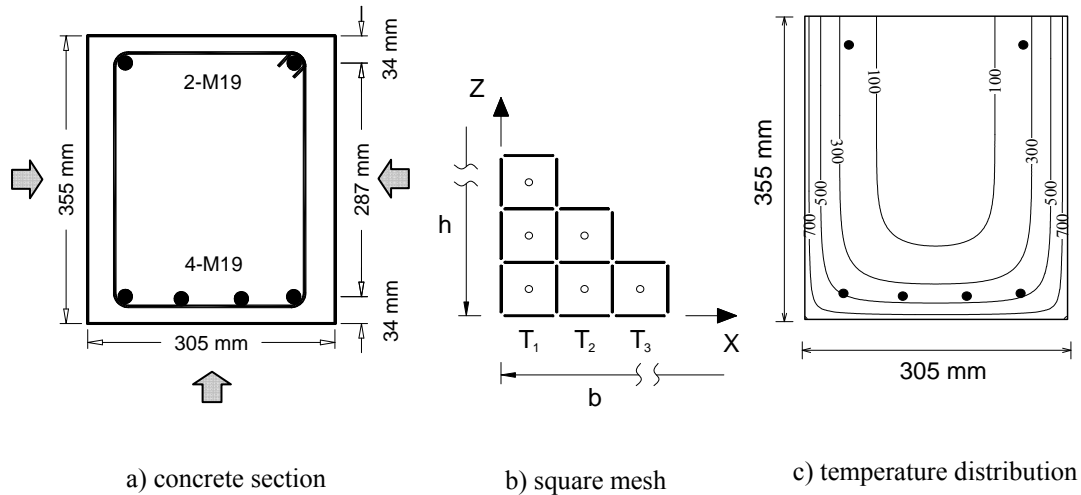


Figure 2. Heat transfer analysis of a concrete beam exposed to fire from three sides.

Concrete and Steel Constitutive Models

Based on the temperature reached in each square element, the mechanical properties of concrete and/or steel can be estimated. Youssef and Moftah [1] provided an assessment of available constitutive models for concrete and steel at elevated temperatures. The authors have utilized the material models recommended by Youssef and Moftah [1] in this study.

Average Layer Temperature

The square mesh elements are grouped into horizontal fibers to conduct sectional analysis. Therefore, an equivalent temperature T_i has to be assigned for each fiber. El-Fitiany and Youssef [5] suggested utilizing two temperature distributions, Figure 3.

The first temperature distribution is based on the fiber temperature producing the same average compressive strength (f'_{cT}) for the square mesh elements composing this fiber, Figure 2b. As f'_{cT} is proportional to the modulus of elasticity, this temperature distribution is representative of the average stiffness of the fibers.

Thermal and transient strains of a given fiber are proportional to its average elevated temperature. Thus, a second temperature distribution can be estimated using the algebraic average temperature of the square elements within the fiber.

Figure 3 shows the distribution of the two proposed average temperatures for the analyzed beam after one hour of ASTM-E119 standard fire exposure. The temperature of the steel bars can be assumed to be the same as the temperature of the square mesh element within which they are located [6].

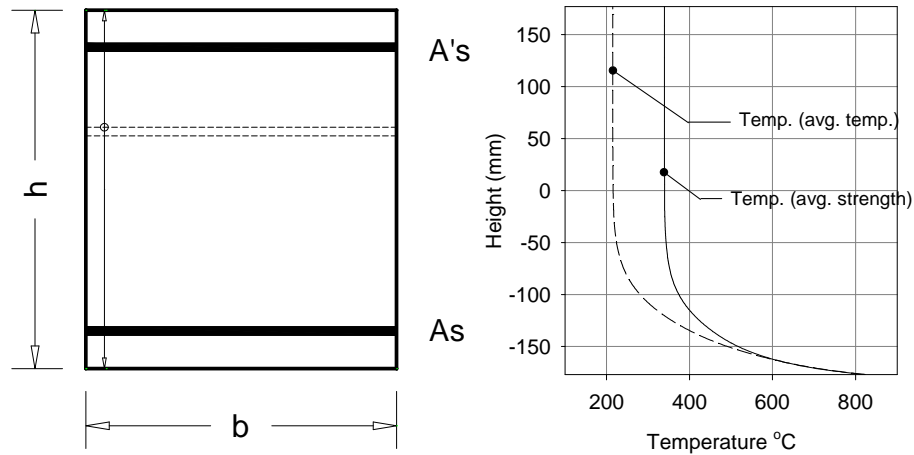


Figure 3. Average temperature distributions for beams during fire exposure.

Thermal and effective strains

Total concrete strain at elevated temperatures (ϵ_{tot}) is composed of three terms: instantaneous stress related strain (ϵ_{fT}), unrestrained thermal strain (ϵ_{th}), and transient creep strain (ϵ_{tr}). Figure 4 shows the expected linear distribution of the total strain (ϵ_{tot}) under a pure bending moment (M). This linear shape is based on the fact that plane sections remain plane after loading, which is still valid at elevated temperatures [10,11]. Knowing the average temperature for each layer, concrete and steel thermal strains (ϵ_{th}) can be evaluated. A schematic distribution of (ϵ_{th}) for typical RC beams exposed to fire temperature from three sides is shown in Figure 4. For the previously reported case of interior columns subjected to fire from four faces, the thermal strain distribution is symmetric about the section mid-height [5].

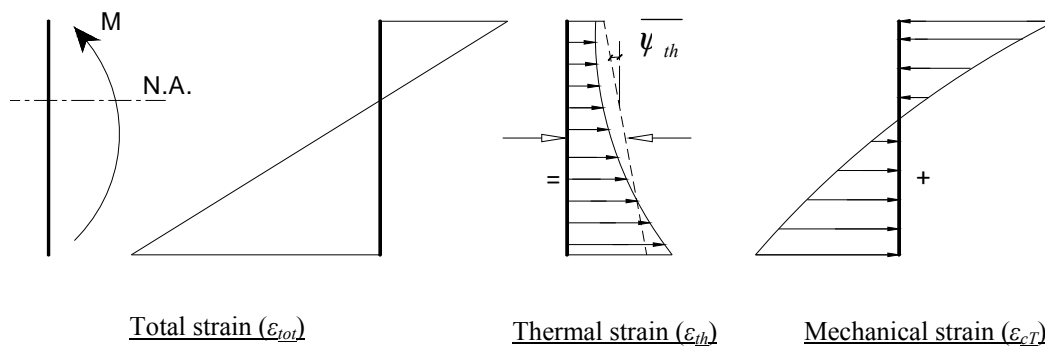


Figure 4. Components of total strain at elevated temperatures.

Youssef and Moftah [1] proposed concrete material model accounts for the transient creep strain (ϵ_{tr}). For unrestrained concrete sections, the effective strain (ϵ_{cT}) can be calculated by subtracting concrete and steel thermal strains from the

total strain. The nonlinear distribution of thermal strains results in a nonlinear effective (mechanical) strain distribution, Figure 4. As Eq. (1) is only applicable for linear strain distributions, the following sub-section present a method to convert the nonlinear thermal strain distribution into an equivalent linear strain distribution.

Isolation of Thermal Strain Component

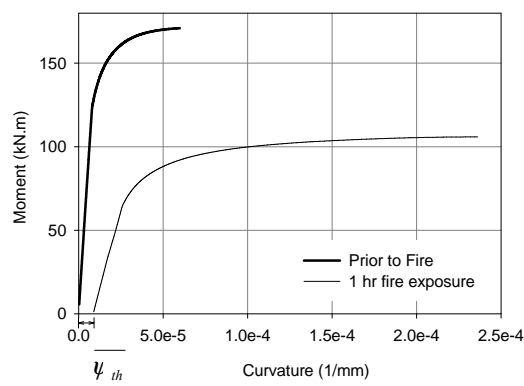
The equivalent thermal strain distribution is defined by the mid-height axial strain ($\overline{\varepsilon_{th}}$) and the curvature ($\overline{\psi_{th}}$), Figure 4. The values of $\overline{\varepsilon_{th}}$ and $\overline{\psi_{th}}$ are evaluated such that the forces in the concrete and steel fibers resulting from the difference between the actual thermal strain and $\overline{\varepsilon_{th}} - \overline{\psi_{th}}$ distribution are in self-equilibrium. An iterative procedure is used to calculate the values of $\overline{\varepsilon_{th}}$ and $\overline{\psi_{th}}$. Concrete tensile strength is neglected. The $\overline{\varepsilon_{th}} - \overline{\psi_{th}}$ distribution reflects the actual deformation of the concrete section under zero external loads and moments. Differences between the non-linear and the $\overline{\varepsilon_{th}} - \overline{\psi_{th}}$ distribution represent internal stresses in the concrete and steel materials that are in-equilibrium.

PERFORMANCE OF RC ELEMENTS DURING FIRE EXPOSURE

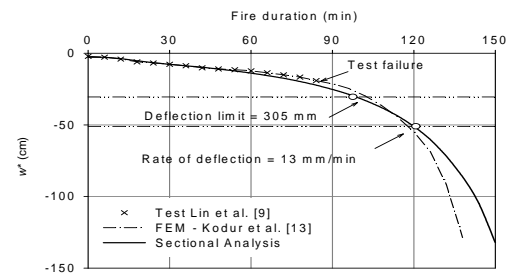
Sectional analysis can be conducted to construct the axial load-axial strain and moment-curvature diagrams. Figure 5a shows the effect of 1 hr standard ASTM-E119 fire exposure on the studied unrestrained beam section (load level, λ , equals to zero). As shown in Figure 5a, elevated temperatures have increased the ductility and reduced the capacity of the RC beam. The initial point of the moment-curvature diagram defines the equilibrium curvature $\overline{\psi_{th}}$. This curvature value represents the initial rotation of the fire-damaged beam due to the non-linear thermal distribution.

VALIDATION

The moment-curvature diagrams for the beam tested by Lin et al. [12] were constructed at different fire durations. The vertical deflection (w^*) at each duration was evaluated using the moment-area method. The obtained results were compared with the experimental results, Figure 5b. An excellent matching is found between the sectional analysis and the FEM conducted by Kodur and Dwaikat [13], and the experimental results (up to 80 minutes). Failure criteria proposed by BS 476 [14] and adopted by Kodur and Dwaikat [13] are used. These criteria are setting limits for the maximum allowable deflection and maximum rate of deflection. As shown in Figure 5b, the proposed sectional analysis results in about 17 minutes difference in predicting failure compared with the test failure and about 5 min difference with Kdour et al. [13]. Additional analytical and experimental work is required for further validation of the proposed methodology and the BS 476 failure criteria.



a) moment–curvature relationship



b) deflection of the studied beam [9]

Figure 5. Flexural and axial behavior of RC sections at elevate temperatures.

CONCLUSIONS

The sectional analysis approach, proposed by the authors in a previous publication, is extended in this paper to cover RC beams subjected to fire from three sides. The proposed approach is found to be a simple yet accurate method to track the behavior of rectangular RC beams at elevated temperatures. Analysis of RC section during fire exposure can be concluded into three main steps:

1. The heat transfer model is applied and the heat gradient through the cross section is predicted. The average temperatures $\overline{\varepsilon_{th}}$ for each layer are then obtained.
2. The equivalent uniform thermal strain $\overline{\varepsilon_{th}}$ and curvature $\overline{\psi_{th}}$ are then calculated by equilibrating the forces in the concrete and steel layers resulting from the actual thermal strain distribution. The difference between the actual and uniform strain distributions represents the induced strains $\varepsilon_{\sigma th}$ in concrete and steel layers to satisfy the section geometry. These strains are considered as initial strains in the following step.
3. Sectional analysis is conducted to construct the axial load-axial deformation and/or moment-curvature diagrams.

Additional tests are needed to further validate and improve the method for different concrete mixtures, aggregate types, fire scenarios, cross-section dimensions, number of exposed surfaces, and loading conditions. Extensive research is also needed to utilize this method at the structure level which requires accounting for fire-induced deformations.

ACKNOWLEDGMENTS

This research was funded by the Natural Sciences and Engineering Research Council of Canada (NSERC).

REFERENCES

1. Youssef, M.A. & Moftah, M. 2007, "General stress-strain relationship for concrete at elevated temperatures", *Engineering Structures*, vol. 29, no. 10, pp. 2618–2634.
2. Khoury, G.A. 2000, "Effect of fire on concrete and concrete Structures", *Progress in Structural Engineering and Materials*, vol. 2, no. 4, pp. 429–447.
3. Bratina, S., Saje, M., Planinc, I. 2007, "The effects of different strain contributions on the response of RC beams in fire", *Engineering Structures*, vol. 29, no. 3, pp. 418–430.
4. Bratina, S., Cas, B., Saje, M., Planinc, I. 2005, "Numerical modelling of behaviour of reinforced concrete columns in fire and comparison with Eurocode 2", *International Journal of Solids and Structures*, vol. 42, no. 21-22, pp. 5715–5733.
5. El-Fitiany, S., Youssef, M.A. 2009, "Assessing the flexural and axial behaviour of reinforced concrete members at elevated temperatures using sectional analysis", *Fire Safety Journal*, vol. 44, no. 5, pp. 691–703.
6. Lie, T.T. 1992, "Structural Fire Protection", *ASCE Manuals and Reports on Engineering Practice*, no. 78, New York, NY, USA, 241 pp.
7. Kodur, V.K.R., Sultan, Ma. 2003, "Effect of temperature on thermal properties of high-strength concrete", *ASCE Journal of Materials in Civil Engineering*, vol. 15, no. 2, pp. 101–107.
8. Youssef, M.A., and Rahman, M., "Simplified seismic modelling of reinforced concrete flexural members," *Magazine of Concrete Research*, vol. 59, no. 9, 2007, pp. 639–649.
9. Lin, T.D., Gustaferro, A.H., and Abrams, M.S., "Fire Endurance of Continuous Reinforced Concrete Beam", *Portland Cement Association, Bulletin RD072.01B*, Skokie, 1981.
10. Collins, M.P., Mitchell, D. 1987, "Prestressed Concrete Basics," *Canadian Prestress Concrete Institute*, Ottawa, ON, Canada.
11. Tassios, T.P., Chronopoulos, M.P., "Structural response of RC elements under fire," *The Structural Engineer*, vol. 69, no. 15, 1991, pp. 277–281.
12. Lin, T.D., Gustaferro, A.H., and Abrams, M.S., "Fire Endurance of Continuous Reinforced Concrete Beam", *Portland Cement Association, Bulletin RD072.01B*, Skokie, 1981.
13. Kodur, V.K.R., and Dwaikat, M., "Performance-based fire safety design of reinforced concrete beams," *Journal of Fire Protection Engineering*, vol. 17, no. 4, 2007, pp. 293–320.
14. Eurocode 2, "Design of Concrete Structures," *ENV EC2*, 1992.

Moment Curvature Relationships for Fire Damaged Reinforced Concrete Sections

D. M. S. PHANI PRASAD, V. KUMAR, U. K. SHARMA
and P. BHARGAVA

ABSTRACT

Once fire breaks out in a structure, it results in the loss of strength of the structure and as it may not be possible to use the structure safely, repair and rehabilitation options are to be chosen. To check for the feasibility options, it is often necessary to study the behavior of the structural elements after fire exposure. The relationship between moment and curvature demonstrates the strength and deformation characteristics of a given reinforced concrete section. If a complete moment-curvature relationship of fire damaged reinforced concrete section is available, one can determine the residual strength and ductility of the structural element. To this end, this paper reports the results of an experimental study carried out to determine the moment curvature relationships for fire damaged reinforced concrete beams. A total of 12 reinforced concrete beams of 100 mm x 200 mm x 2000 mm size were cast and tested under this test program. Test parameters were grade of concrete, lateral spacing of ties and duration of fire exposure. The doubly reinforced concrete beams were first exposed to standard fire in a full scale fire furnace. Subsequently after cooling, their moment curvature responses were recorded under two point loading. Based on the results, it has been found that the grade of concrete, transverse reinforcement spacing and duration of fire have considerable amount of influence on the moment carrying capacity and curvatures of the sections. The yield and the ultimate moment capacities of all the fire damaged beams decreased with an increase in fire duration. While the yield and ultimate curvatures increased with an increase in fire duration, the overall curvature ductility reduced.

D M S Phani, Student (M. Tech), Department of Civil Engineering, Indian Institute of Technology Roorkee, India 247 667.

Virendra Kumar, Research Scholar, Department of Civil Engineering, Indian Institute of Technology Roorkee, India 247 667.

Umesh Kumar Sharma, Assistant Professor, Department of Civil Engineering, Indian Institute of Technology Roorkee, India 247 667.

Pradeep Bhargava, Professor, Department of Civil Engineering, Indian Institute of Technology Roorkee, India 247 667.

INTRODUCTION

The fire safety of RCC structures largely depends on their fire resistance, which in turn depends on the combustibility and fire resistance of their main structural elements i.e., the beams and columns [1]. The residual bending moment and shear force of fire damaged concrete members are important factors in determining the safety of the structure [2]. The strength and deformation characteristics of the elements in a fire damaged structure are essential to decide about their repair feasibilities [3], [4], [5]. After a fire, the moment curvature relationship of the reinforced concrete sections may provide valuable information for post fire strength [6]. The ductility in reinforced concrete beams depends mainly on the shape of the moment—curvature curve as ductility is defined as the ability to undergo deformations without a substantial reduction in the flexural capacity of the member. Hence, it is important to know these relations to decide upon the feasible solutions regarding the repair and rehabilitation of the fire damaged reinforced concrete members, especially from the point of view of post fire life expectancy of the structure. In the present study, the moment curvature curves were experimentally determined for doubly reinforced beam sections, both for unexposed and fire exposed sections, so as to study the effect of fire on the strength-deformation characteristics reinforced concrete sections.

EXPERIMENTAL PROGRAMME

The experimental programme consisted of casting sixteen beams of M30 and M60 concrete strengths in which 6 mm two-legged stirrups were used for lateral reinforcement at spacing of 100 mm and 150 mm. The size of doubly reinforced concrete beams were 100 mm x 200 mm x 2000 mm, with effective span of 1970 mm c/c. The main longitudinal reinforcement of grade Fe415 consists of 16 mm bars in the beams of both the grades. While the M30 beams contain 12 mm bars at the top, M60 beams contain 8 mm bars as the compression reinforcement. A cover of 20 mm (clear) was provided at the bottom while a side clear cover of 19 mm was made available. The beams were tested under three- point symmetrical loading under flexure. Two LVDTs were installed at the top and bottom edges to calculate the strains at the top and bottom. The LVDTs recorded the displacements over a length of 200 mm which is the depth of the beam. Also, LVDTs were incorporated at the bottom of the beam to know the displacements of the beam under the loading. The LVDTs were connected to a data logger, which recorded the readings of displacements and also the loading values through a load cell. Figure 1 shows the schematic view of test set-up of experimentation. Designed mixes, M30 and M60 were cast in the present experimental study with 43 Grade Cement (OPC), Zone II sand and 10 mm down well graded coarse aggregate. After casting all the beam specimens in the laboratory, they were put in the furnace to expose them to fire as shown in Figure 2. The beams were exposed to the fire for durations of 0.50 hour, 1.0 hour and 1.5 hour. They were exposed to fire on three faces while being supported on 150 mm thick walls. The top of the furnace was covered with necessary insulating material so that the top face of the beam is not exposed to fire while exposing the three faces of the beam. The fire exposed simply supported beams, along with the virgin specimens were tested under three point loading. The

readings could be taken as long as the concrete in the central region was intact and as the loading continued, concrete started spalling and hence the readings could no more be recorded any more. This point was considered as the ultimate point.

TEST RESULTS

Beams which were exposed to fire for durations of 1.0 hour and 1.5 hour showed signs of spalling. In general a number of thermal cracks were observed for all the specimens exposed to fire. In the case of beams exposed to 1.5 hour duration, surface colour of concrete was observed to be brownish pink while it was brownish for the other duration's specimens. During the load test, the cracks travelled in the direction of the load, i.e. towards the top, originating from the bottom. The first crack in almost all the specimens was observed at the centre exactly under the load. During the load testing of fire exposed beams (after the load reaches the maximum capacity and when the load was released) a tremendous amount of concrete spalling was observed, which exposed the reinforcement at the top and at the bottom. The buckling of reinforcement in the compression zone was also observed. The measured moment-curvature curves for beams unexposed to fire are shown in Figure 3(a) to 3(d). Figure 4 (a) to (d) shows the experimental moment-curvature curves for M30 and M60 beams with 100 mm and 150 mm lateral spacing exposed to 0.5 hour fire respectively. The moment curvature for different beams exposed to 1.0 hour fire exposure are shown figure 5(a) to 5(d). Figure 6(a) to 6(d) shows the moment curvature relationship of the four types of beams exposed to 1.5 hour fire. The measured values of yield moment, maximum moment, yield curvature, ultimate curvature and curvature ductility are shown in Table I. For virgin samples, due to the limitations of the test set up, the loading could not be carried till failure; hence the curvature could not be computed in the case of virgin samples. It was observed that with the increase in fire duration, the ultimate moment as well as the yield moment of the beams reduced. For beam B3-10, the yield moment reduced by 53.5% , 58% and 60% after 30 minutes, 60 minutes and 90 minutes exposure to fire respectively while it reduced by 46%, 54.2% and 58% for the fire durations 30 minutes, 60 minutes and 90 minutes respectively for beam B3-15. Whereas for beam type of B6-10, yield moment reduced by 29.6%, 52.64% and 55% for fire durations of 30 minutes, 60 minutes and 90 minutes respectively while it reduced by 39.3%, 59.5% and 60% for 30 minutes, 60 minutes and 90 minutes durations respectively in the case of beam B6-15.

CONCLUSIONS

The yield and maximum moment capacities did not vary much for M30 beams for both the lateral tie spacings of 100 mm and 150 mm for a particular duration of fire. While the yield curvature and ultimate curvature of the beams increased with fire duration, the curvature ductility of all the beams reduced. The curvature ductility of the beams reduced with an increase in the grade of concrete and also with an increase in fire duration. However, after 60 minutes exposure to fire, not much difference in the maximum moment capacities of the M30 beams and M60 beams were observed.

TABLE I. MOMENT AND CURVATURE VALUES FOR BEAM.

Fire duration (minute)	Concrete strength (MPa)	Lateral tie spacing (mm)	Beam details	Yield moment (kNm)	Yield curvature (1/mm) $\times 10^{-5}$	Maximum moment (kNm)	Yield curvature (1/mm) $\times 10^{-5}$	Yield curvature (1/mm)
0	30	100	B3-10	30.40	2.38	33.16	---	---
0	30	150	B3-15	28.26	3.44	31.68	---	---
0	60	100	B6-10	34.63	2.94	38.78	---	---
0	60	150	B6-15	34.77	2.67	36.10	---	---
30	30	100	B3-10	14.13	3.55	14.90	61.8	19.15
30	30	150	B3-15	15.25	3.51	16.56	72.6	20.66
30	60	100	B6-10	24.36	2.95	26.98	33.6	11.38
30	60	150	B6-15	21.08	4.51	21.70	---	---
60	30	100	B3-10	12.76	3.76	13.79	62.9	16.46
60	30	150	B3-15	12.93	3.65	14.43	---	---
60	60	100	B6-10	16.40	2.95	16.50	36.2	12.28
60	60	150	B6-15	14.08	3.13	14.77	54.0	17.23
90	30	100	B3-10	11.97	4.15	13.74	67.2	16.19
90	30	150	B3-15	11.76	4.31	12.12	62.6	14.51
90	60	100	B6-10	15.57	3.43	17.10	69.8	20.35
90	60	150	B6-15	13.88	3.82	14.80	54.3	14.20

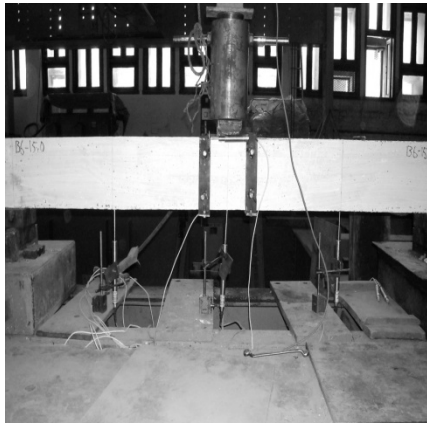
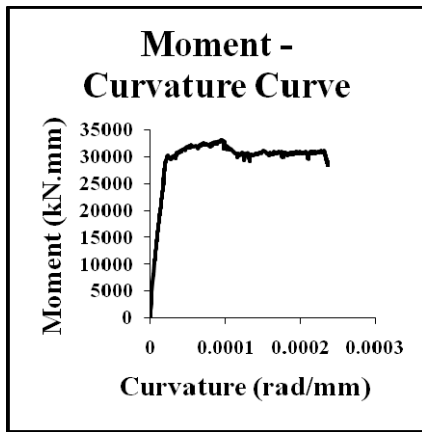


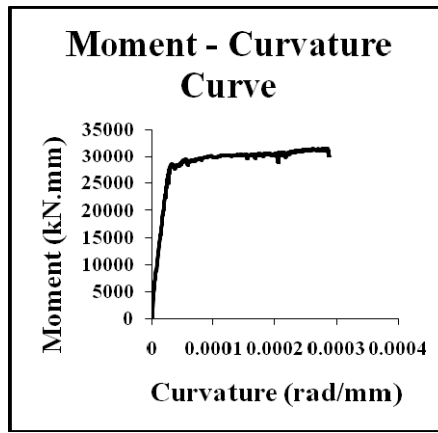
Figure 1. Test set up of the beam.



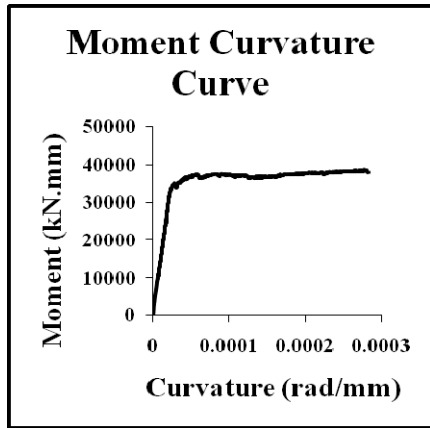
Figure 2. Beams for fire exposure extreme.



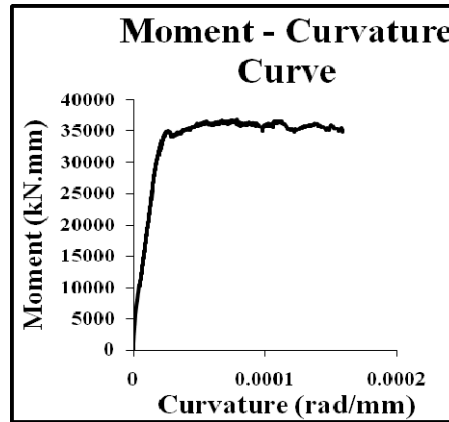
(a)



(b)

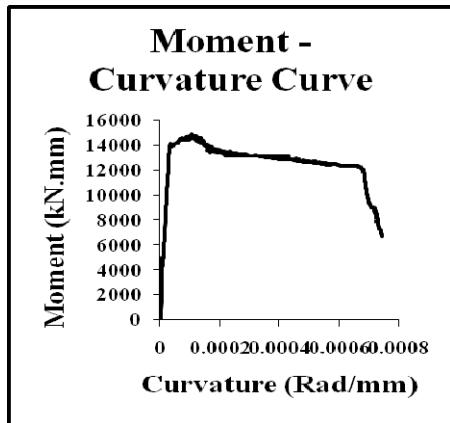


(c)

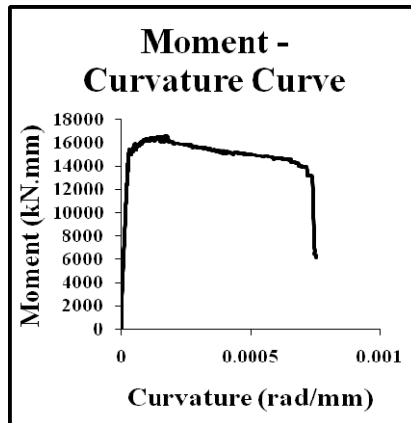


(d)

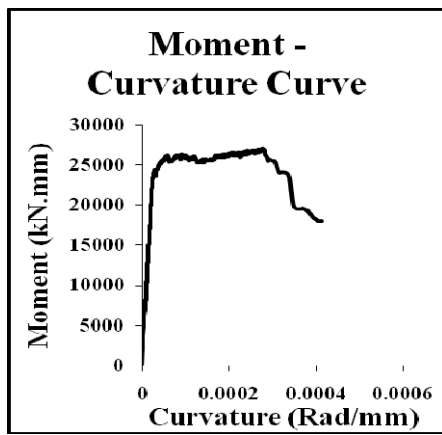
Figure 3. Moment-curvature relationship for virgin beams without fire exposure (a) B3-10, (b) B3-15, (c) B6-10, (d) B6-15.



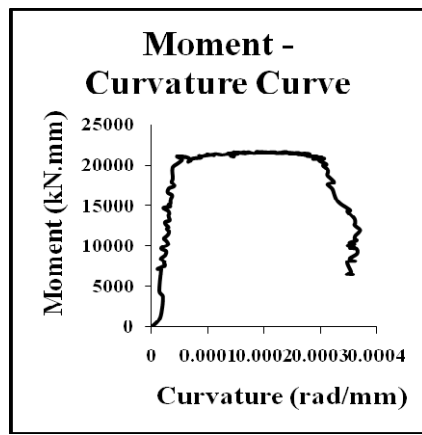
(a)



(b)

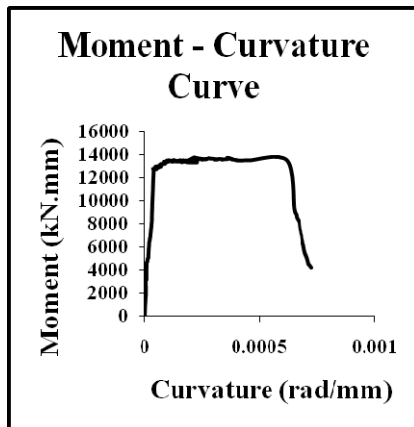


(c)

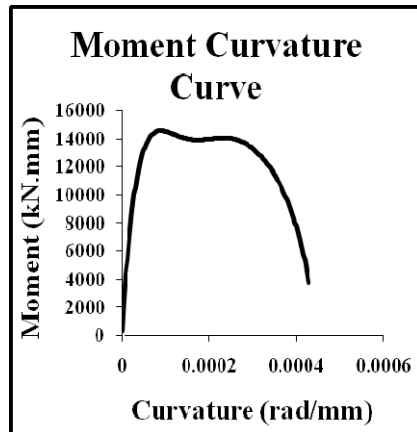


(d)

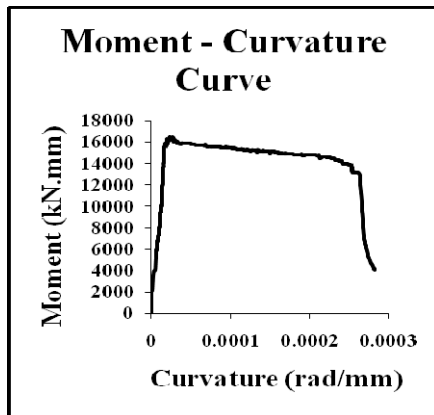
Figure 4. Moment-curvature relationship for beams exposed to fire for 30 minutes (a) B3-10 (b) B3-15 (c) B6-10 (d) B6-15.



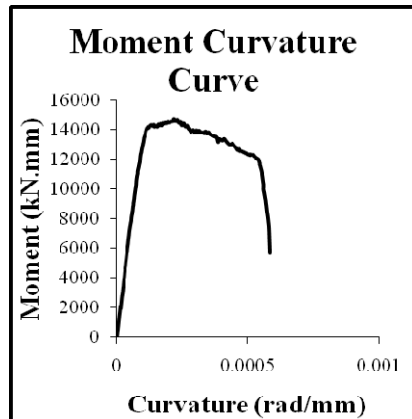
(a)



(b)



(c)



(d)

Figure 5. Moment-curvature relationship for beams exposed to fire for 60 minutes (a) B3-10 (b) B3-15 (c) B6-10 (d) B6-15.

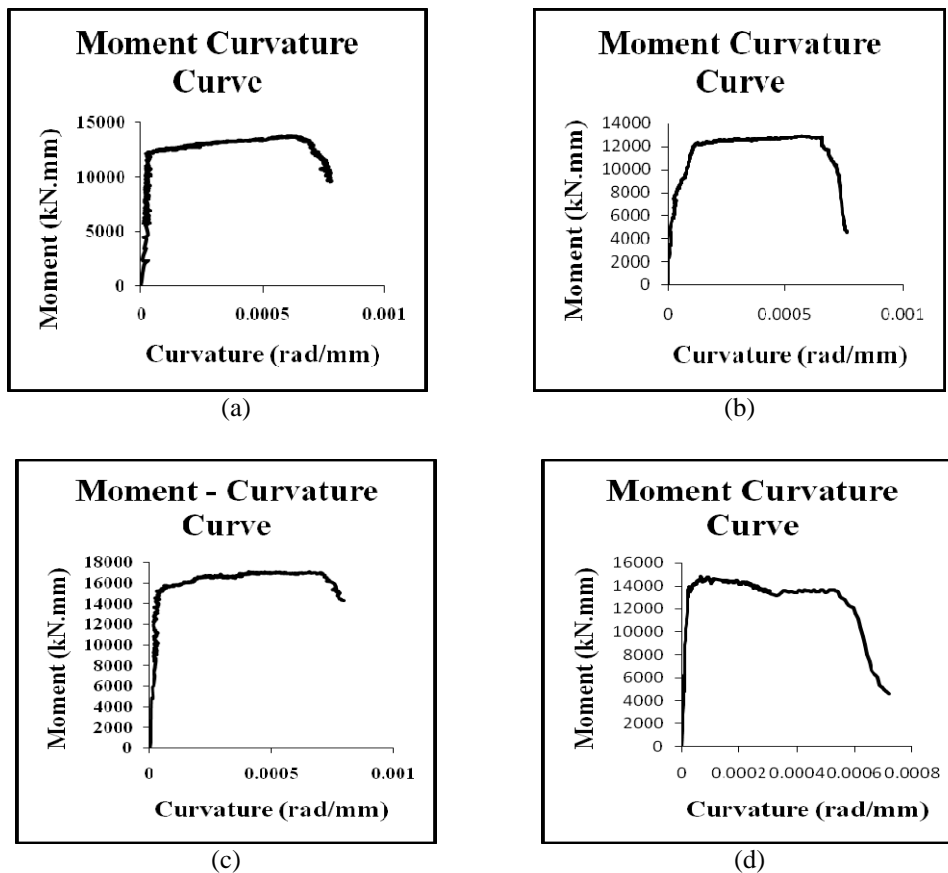


Figure 6. Moment-curvature relationship for beams exposed to fire for 90 minutes (a) B3-10 (b) B3-15 (c) B6-10 (d) B6-15.

REFERENCES

1. Buchanan, A. H. 2001. *Structural Design for Fire Safety*. John Wiley and Sons Inc. pp.225–256.
2. Georgali, B., Tsakiridis, P. E., 2005. “Microstructure of Fire-Damaged Concrete”, *A Case Study, Cement and Concrete Composites*, 27(2): pp 255–259.
3. Kumar, A., and Kumar, V. 2003, “Behaviour of RCC Beams after Exposure to Elevated Temperatures”, 84: pp 165–170.
4. Khoury, G. A. 2000, “Effect of Fire on Concrete and Concrete Structures”, *Progress in Structural Engineering and Materials*, pp 429–447.
5. Suprenaut, Bruce A. 1994, “Assessing the condition and repair alternatives of fire –exposed concrete and masonry members”, *Fire Protection and Planning Report*, National Codes and Standards Council of the Concrete and Masonry Industries.
6. Ian A. Fletcher, Welch Stephen, Torero, José L., Carvel, Richard O. and Usmani, Asif, 2007, “Behaviour of Concrete Structures in Fire”, *Review Paper, Thermal Science*, 11(2): pp 37–52.

Experimental Examination of Residual Load Bearing Capacity of RC Beams Heated Up to High Temperature

R. KOWALSKI and P. KROL

ABSTRACT

This paper shows the description and results of tests which were done on reinforced concrete beams loaded and simultaneously heated up to high temperature and then (after cooling) loaded once again in the room temperature. Two types of concrete C30/37 and C60/75 with siliceous aggregate were used. The cross-section dimensions of the beams were $b \times h = 12 \times 14$ cm. The span length was 105 cm. The beams were loaded to the level of 54% of their load bearing capacity and then they were kept in the furnace chamber in the temperature of 800°C for about 30 minutes. During this time the temperature of reinforcing bars reached the value of about 500 °C and the deflections of beams were about 60 mm (1/17.5 of the span). Despite this, the beams still were able to carry the load but they were nearly destroyed. After the tests in high temperature the beams were unloaded, removed out of the furnace chamber and cooled freely in the air. On the next day the load bearing capacity of beams in room temperature was tested. The beams were able to carry 35 or 87% respectively of their load bearing capacity before heating, depending on whether the failure occurred due to the damage of the concrete compressed zone or the yield of the reinforcement.

1. INTRODUCTION

Although fire safety problems are becoming more and more important, it is still impossible to eliminate the risk of fire in buildings completely. Total collapse of reinforced concrete structures due to fire occurs rather rarely, however, the

Robert Kowalski, Ph.D., Civ. Eng., Pawel Krol, Ph.D., Civ. Eng., Warsaw University of Technology, Civil Engineering Faculty, Al. Armii Ludowej 16, 00-637 Warsaw, Poland.
E-mail address: r.kowalski@il.pw.edu.pl; p.krol@il.pw.edu.pl

necessity of technical evaluation of structural elements after fire still appears quite often. The residual (after fire) load bearing capacity of reinforced concrete elements strongly depends on the material mechanical properties which values decrease due to high temperature influence.

This paper briefly discusses the residual concrete compressive strength and the residual steel yield strength after heating. Then it shows description and results of tests of residual load bearing capacity of reinforced concrete beams heated up with simultaneous action of load and afterwards cooled freely in the air.

2. RESIDUAL MATERIAL MECHANICAL PROPERTIES

2.1. Concrete

The key data for structural design of reinforced concrete structures in fire is given in [1-3]. The extensive summary of the state-of-the-art knowledge and experimental research of concrete behaviour and its strength decrease due to high temperature can be found in [4-6]. Among others, the works [7-11] have to be mentioned as the ones of fundamental importance for the development of the knowledge of influence of high temperature on the mechanical properties of concrete.

Figure 1 shows Eurocode [1] recommendations for prediction of concrete compressive strength decrease while this concrete is heated to high temperature. However, when concrete is cooled down, an additional decrease of its compressive strength can occur and finally the residual concrete compressive strength is usually lower than the one observed when concrete is hot [7, 10, 11]. Additional strength decrease of concrete compressive strength occurs after cooling as the result of two key reasons.

If the process of cooling down is sharp, the concrete may suffer mechanical damage due to the high temperature gradients (as a result of self-equilibrating stress). From the practical point of view, sudden cooling can be particularly dangerous when concrete is heated to a relatively low temperature, such as 200–300°C. The decrease of concrete strength is not high then, and the effect of heating would be hardly significant for slow cooling. However, sudden cooling may cause considerable structural damage to concrete. Such a situation may occur during fire-fighting when structural elements can be heated several times and then violently cooled with water.

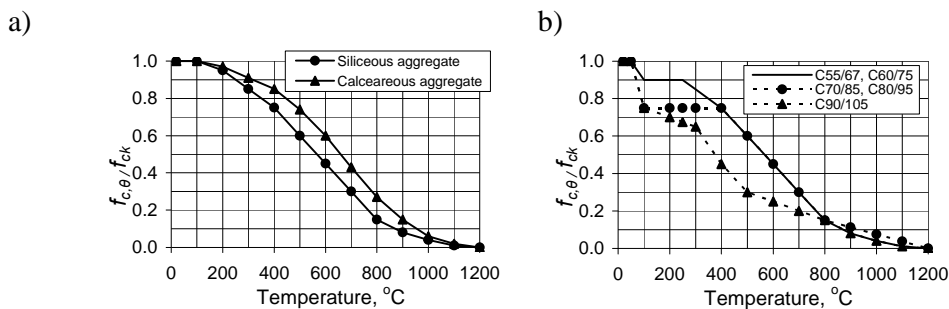


Figure 1. Relative concrete compressive strength decrease in high temperature [1]: a) ordinary strength concrete, b) high strength concrete.

If the cooling process is slow, the concrete retains high temperature for a longer time which prolongs the duration of unfavourable chemical and physical transformations. It is worth considering that due to thermal inertia of concrete, the maximum temperature zone may still progress into the structural element after high temperature ceases to affect its surface. While doing so, it may further destroy the structure of concrete in the middle part of the element cross-section, even for some hours after the end of fire.

2.2. Reinforcing steel

General guidelines for the prediction of steel mechanical properties decrease in high temperature can be found in Eurocode [1] and [12]. Due to the temperature increase both the value of steel yield strength and of the steel Young modulus drop significantly. However after fire, when the structure is cooled down, the behaviour of steel is completely different than in the case of concrete. Reinforcing steel heated up to high temperature and subsequently let to cool down, usually recovers its mechanical properties. According to [13] ordinary hot-rolled bars tend to recover their mechanical properties completely after being heated to the temperature of 550-600°C and almost completely after being heated to 800°C. Hot-rolled bars tested in [14] recovered their strength after being heated to 600°C. In the author's opinion one can securely assume that hot-rolled bars heated to the temperature of 500-700°C after cooling should recover 85–95% of their original strength.

3. TEST DESCRIPTION

3.1. Testing the beams in high temperature

Tests described in this paper are the part of a wider experimental program that aimed at recognising the behaviour of RC beams under simultaneous action of load and high temperature. Examinations of two series of beams are presented below.

The beams were made of two types of concrete: C30/37 and C60/75, with siliceous aggregate. They were 12 x 14 cm in the cross-section and 120 cm in the length. The main reinforcement of each beam consisted of two hot-rolled bars, 10 mm in diameter. The average yield strength of steel was 583 MPa. The concrete cover was 15 mm. The reinforcement ratio was 1.09%. In Figure 2 the reinforcement and the loading scheme of beams are shown. Each series consists of six beams. Three of them were used for tests in high temperature and three others were used for pre-tests, performed in room temperature. The tests were performed about five months after the beams were cast.

In the first part of tests three beams of each series were tested in room temperature. At the beginning each beam was loaded and unloaded seven times to the load level of 54% of calculated load bearing capacity. It was done to simulate the action of permanent load. The value of 54% of maximal load is the probably value of permanent load, recommended for consideration of many kinds of building structures. Finally, each beam was loaded up to the failure. In Table 1 the values of calculated maximal bending moment and average values of maximal bending moments obtained experimentally are shown.

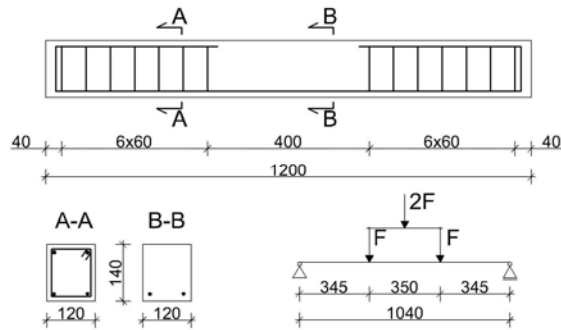


Figure 2. The reinforcement and the loading scheme of the beams.

TABLE 1. BENDING MOMENTS APPLIED IN TESTED BEAMS.

Type of beam	Bending moments, kNm		
	Load bearing capacity		Applied during tests in high temperature
	Calculated	Average obtained experimentally in room temperature	
C30/37, 2#10	10.18	9.54	5.15
C60/75, 2#10	10.56	10.39	5.61

In the second part of tests three beams of each series were tested in high temperature. Before hot tests each beam was loaded and unloaded seven times to the load level of 54% of load bearing capacity obtained experimentally (the simulation of permanent load action).

At the beginning of hot tests the furnace chamber was heated up to the temperature of 800°C. Then it was opened and the beam was put inside as quickly as possible. During the time when the furnace chamber door was closed the load was applied statically. The above described process took about 2-3 minutes.

The beams were kept in the furnace chamber in the constant temperature of 800°C under the constant load. The load level was taken as 54% of the average load bearing capacity of beams obtained in room temperature (Table 1). The value of 54% of maximal load is the probably value of load, recommended for consideration of many kinds of building structures in fire design situation.

During the tests the temperature of the reinforcement and the deflections of the mid-span of the beams were measured. In Figure 3 the graphs of the temperature in the furnace chamber, the temperature of the reinforcement and the deflection increase against time of testing are shown.

After about 30 minutes of keeping the beams in the furnace chamber, the deflections of the mid-spans reached the value of 60 mm and the temperature of the reinforcement exceeded 500°C. Despite this the beams still carried the load, but the deflection increase became very sharp. In the presence of the deflection value of about 70 mm there was the danger of the measurement equipment damage. It was the reason for stopping the tests when the deflections of beams exceeded 60 mm. The load was taken out, the furnace chamber was opened and the beams were put out. Then they were cooled freely in the air. Figure 4 shows the exemplary views of beams after the test in high temperature.

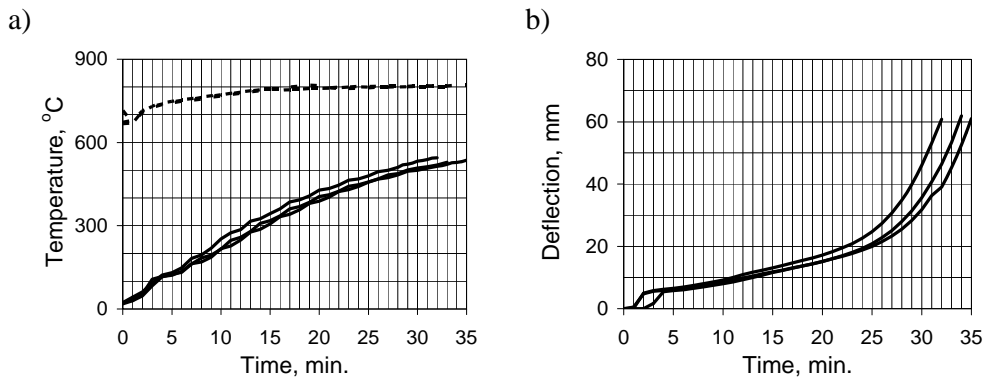


Figure 3. a) Temperature of the reinforcement (solid line) and the temperature of the furnace chamber (dotted line), b) Deflections of the mid-span of beams.

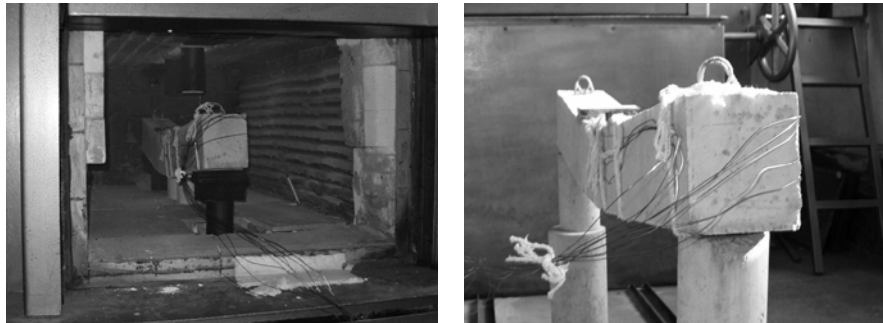


Figure 4. The views of beams after the test in high temperature.

3.2. Testing the residual load bearing capacity of the beams

In the third part of the tests the residual load bearing capacity of the beams was determined experimentally. The tests were performed one day after tests carried out in high temperature. The beams were loaded statically up to the damage. During the tests the deflections in the mid-span of beams were measured.

In Table 2 the main test results are summarised. The beams made of ordinary strength concrete (C30/37) were destroyed due to the damage of the concrete compressed zone. The beams made of high strength concrete (C60/75) were destroyed due to the damage of the reinforcement.

TABLE 2. TEST RESULTS.

Type of beam	Load bearing capacity of tested beams (bending moments, kNm)			
	Before hot tests (average)	After hot tests (residual)		Ratio after / before
		Test result	Average	
C30/37, 2#10	9.54	3.64 3.29 3.23	3.39	0.35
C60/75, 2#10	10.39	9.16 8.90	9.03	0.87

In Figure 5 the graphs of the bending moment against the deflection of beams are shown. The dotted line presents the average values obtained during the first part of the tests, performed in room temperature. The solid line presents the results obtained during the third part of tests, performed on pre-heated beams.

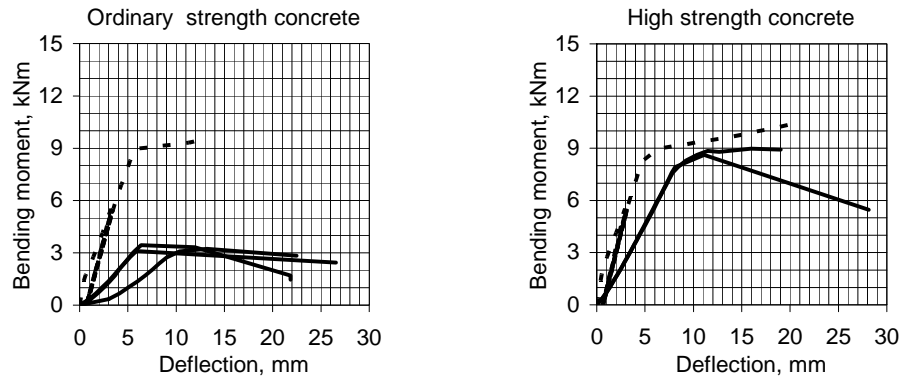


Figure 5. Bending moment against the deflection of beams (dotted line—tests in room temperature, solid line—tests on pre heated beams).

4. DISCUSSION OF THE TEST RESULTS

First of all, it is necessary to emphasise the fact that during tests in the furnace chamber the beams were nearly destroyed. The temperature of their reinforcement was higher than 500°C . In fire design situation the temperature of 500°C is usually considered as the critical temperature of the structure. The mid-span deflections of the beams reached the value of 60 mm. It is about 1/17.5 of the span length. It is also possible to estimate that the sum of the average elongation of concrete in compressed fibre and the average elongation of reinforcing steel reached the value of about 60‰. This value seems to be very high.

The tests performed on the beams after cooling showed that the value of their residual load bearing capacity might be much lower or almost the same as their load bearing capacity before heating.

The beams made of ordinary strength concrete (C30/37) had relatively low residual load bearing capacity. They were destroyed due to the damage of the concrete compressed zone. All values of the maximal residual bending moments were significantly lower than the bending moments obtained before heating and applied during the tests in high temperature. (See Table 1 and 2). This phenomenon took place due to the additional decrease of the concrete compressive strength that occurred when the beams were cooled freely in the air.

The residual load bearing capacity of beams made of high strength concrete (C60/75) was only slightly lower than this one measured before heating (See Table 2). The beams were destroyed due to the yield of the reinforcement. This shows that the steel heated to the temperature of about 500°C after cooling recovered the majority of its strength. In this case the additional decrease of the concrete compressive strength also occurred, but its influence on the load bearing capacity of beams was not significant.

In both cases, of the ordinary strength concrete and the high strength concrete, the stiffness of pre-heated beams was much lower than the stiffness of beams which were not heated (See deflections shown in Fig. 5). This phenomenon should be taken into consideration when reassessment of the beams or slabs after fire is performed.

The softening of the reinforcing bars due to fire usually results in a significant increase of the element deflection. Whenever it is possible for the elements to deflect freely and without any limits, the increase in the reinforcement temperature up to the value between 450 and 600°C should lead to the collapse of the element. However, sometimes in practical cases, the secondary scheme of the structure can occur, as a result of high element deflection. This situation usually occurs when hot deflected flexural elements can be supported by another part of building (for example by a partition walls). In such case, the total destruction of the element can be stopped till the end of fire. Figure 6 shows schematically the situation when simply supported slab can be destroyed in the result of fire (Fig. 6.a) or when it can be saved as a result of the occurrence of the secondary scheme of the structure (Fig. 6.b). It is important to remember that the stresses in the reinforcing bars could be relaxed when the destruction of flexural structural elements was avoided due to the occurrence of the secondary scheme of the structure.

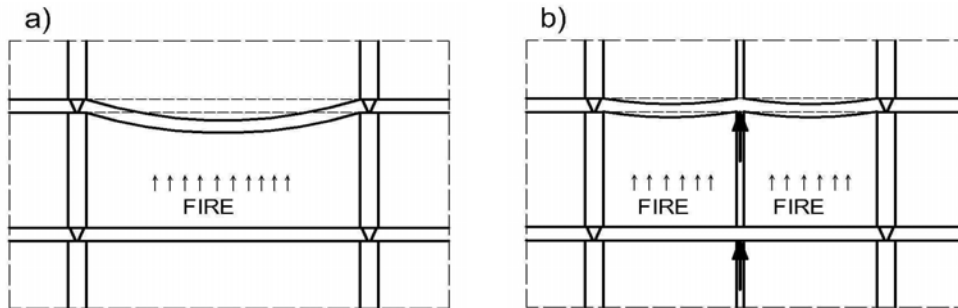


Figure 6. Simply supported slab in fire: a) destruction resulting from fire b) occurrence of the secondary scheme of the structure,

4. CONCLUSIONS

After fire the residual load bearing capacity of structural elements with pre-heated compressed zone of concrete might be much lower than the load bearing capacity in high temperature.

When the destruction of structural element occurs due to the yield of the reinforcing bars, after fire a significant recover of the load bearing capacity should be expected.

The stresses in the reinforcing bars could be relaxed when the destruction of flexural structural elements was avoided due to the occurrence of the secondary scheme of the structure.

REFERENCES

1. EN 1992-1-2: 2004: Eurocode 2: Design of concrete structures—Part 1-2: General rules - Structural fire design.
2. Buchanan A.H.: Structural Design for Fire Safety. John Wiley and Sons Ltd., 2002.
3. fib Bulletin 46/2008. Fire design of concrete structures—structural behaviour and assessment.
4. Khoury G.A., Majorana C.E., Pesavento F., Schrefler B.A.: Modelling of heated concrete. Magazine of Concrete Research, 2002, Vol. 54, No. 2, p. 77–101.
5. fib Bulletin 38/2007. Fire design for concrete structures—materials, structures and modelling.
6. Bamonte P., Gambarova P.G., Meda A.: Today's concretes exposed to fire—test results and sectional analysis. Structural Concrete. Journal of the fib. 2008, Vol. 9, No 1, p. 19–29.
7. Malhotra H.L.: The effect of temperature on the compressive strength of concrete. Magazine of Concrete Research, Vol. 8, No. 23, 1956, p. 85–94.
8. Zoldners N.G.: Effect of High Temperatures on Concretes Incorporating Different Aggregates. American Society of Testing Materials, 60/1960, p. 1087–1108, Sixty-third Annual Meeting of the Society 1960.
9. Abrams M.S.: Compressive Strength of Concrete at Temperatures to 1600 F. ACI Publication SP25, paper SP25-2, Detroit 1971.
10. Schneider U.: Concrete at High Temperatures—A General Review. Fire Safety Journal, 13/1988, p. 55–68.
11. Bazant Z.P., Kaplan M.F.: Concrete at High Temperatures. Material Properties and Mathematical Models. Longman Group Ltd. 1996.
12. Hertz. K.D.: Reinforcement data for fire safety design. Magazine of Concrete Research, 2004, Vol. 56, No. 8, p. 453–459.
13. Meda A., Gambarova P. G., Bonomi M.: High-Performance Concrete in Fire-Exposed Reinforced Concrete Sections. ACI Materials Journal, Vol. 99, No. 3, 2002, p. 277–287.
14. Elghazouli, A.Y., Cashell, K.A., Izzuddin B.A. Experimental evaluation of mechanical properties of steel reinforcement at elevated temperature. Fire Safety Journal, Vol. 44 (2009), p. 909–919.

Influence of Thermal Elongation of Beams on the Fire Resistance of RC Frames

H. F. XAVIER, R. FARIA and P. V. REAL

ABSTRACT

Based on design codes like Eurocode 2 (EC2), engineers are able to assess fire resistance of reinforced concrete (RC) frames via several methods, ranging from simplified cross-section approaches up to advanced thermo-mechanical analyses. Fire resistance assessment may be performed over the entire structure (or part of it) or, in a simplified manner, over each RC member considered as isolated. Although it is commonly accepted that the proper inclusion of structural continuity and fire induced effects is vital for an accurate evaluation of the RC building's response, the approach where each beam or column is handled as an independent member under fire conditions is often applied due to its simplicity, meaning that global behavior is disregarded. In this work three RC frames attached to a rigid bracing system are submitted to a standard fire, and analyzed with the advanced thermo-mechanical code SAFIR. Influence of the thermal elongation of beams, which impose considerable drifts to the outermost columns, is investigated. Fire resistances of the beams and columns of the same frames are assessed with the 'Zone method' of EC2, and compared to the results obtained with SAFIR.

INTRODUCTION

Recent research and real fire events have outlined thermal elongation of beams and structural continuity as key phenomena, influencing the performance of RC structures in fire [1], [2]. As a result of this, advanced thermo-mechanical

Hélder F. Xavier, Faculty of Engineering, University of Porto, Rua Dr. Roberto Frias, 4200-465 Porto, Portugal

Rui Faria (corresponding author), Associate Professor, Faculty of Engineering, University of Porto, Rua Dr. Roberto Frias, 4200-465 Porto, Portugal

Paulo Vila Real, Full Professor, University of Aveiro, Departamento de Engenharia Civil, Campus Universitário de Santiago, 3810-193 Aveiro, Portugal

methods accounting for the whole structural response are being increasingly applied, when fire resistance is to be assessed.

Nonetheless, design codes such as the EC2 Part 1-2 (EN 1992-1-2) [3] allow fire resistance of RC frames to be evaluated by means of simplified cross-section methods, where the several structural elements are regarded as isolated, thus neglecting structural continuity and influence of fire induced thermal elongation on the internal forces that develop in beams and columns. It is believed that the proper inclusion of thermal elongation effects and structural continuity is vital for the accurate simulation of structures in fire. However, as computational codes available for application of advanced thermo-mechanical analyses still demand considerable expertise and are large time consuming, simplified procedures like the ‘Tabulated method’, de ‘500°C isotherm method’ or the ‘Zone method’ are certainly more attractive for design engineers. Moreover, it is somehow widespread the idea that considering structural redundancy during the course of a fire, enabling the redistribution of internal forces from thermally affected members to other parts of the structure, leads to an enhanced fire resistance, and that considering isolated member analyses yields conservative results. Nevertheless, real fires on RC structures [1] have shown that thermal elongation of beams may anticipate structural collapse in continuous frames, in comparison to what might be expected from isolated member analyses.

To clarify this controversial aspect, in this paper three RC frames submitted to the standard fire are analyzed with the FEM code SAFIR [4]. Thermal elongation of beams is allowed to occur just in the left-to-right direction, due to the existence of a highly stiff core – as it is common in standard braced RC framed buildings –, which promotes considerable drifts on the columns. Fire resistances of the same frames are assessed with the Zone method of EC2 [3] (the more accurate of the simplified methods provided in this code), and compared to the ones predicted by SAFIR.

THREE-BAY RC FRAME UNDER THE STANDARD FIRE

Geometry and loading

Fig. 1 reproduces the geometry of a three-bay RC frame analyzed in this work, inspired on the one in [5] but augmenting the number of bays from 1 to 3, and adding on the left hand-side a lateral restraint against horizontal displacements of the floors (to simulate a bracing system, such as a RC core around the elevators or stairs). With this restraint thermal elongations of the beams are directed towards the right, prescribing relevant drifts to the rightmost columns. In Fig. 1 notations I-II-(...) refer to compartment numbers, 1-2-(...) to column numbers and 1-2-(...) to beam numbers.

Vertical loading for the relevant combination in fire conditions [6] is reproduced by the uniformly distributed load $p = G + 0.5Q$ acting on the beams, being $G = 36\text{kN/m}$ the dead load and $Q = 12\text{kN/m}$ the live load. To simplify the numerical model the beams of the 1st and 2nd floors and the adjacent columns are fully reproduced at SAFIR by finite elements (FE), but the upper floors are

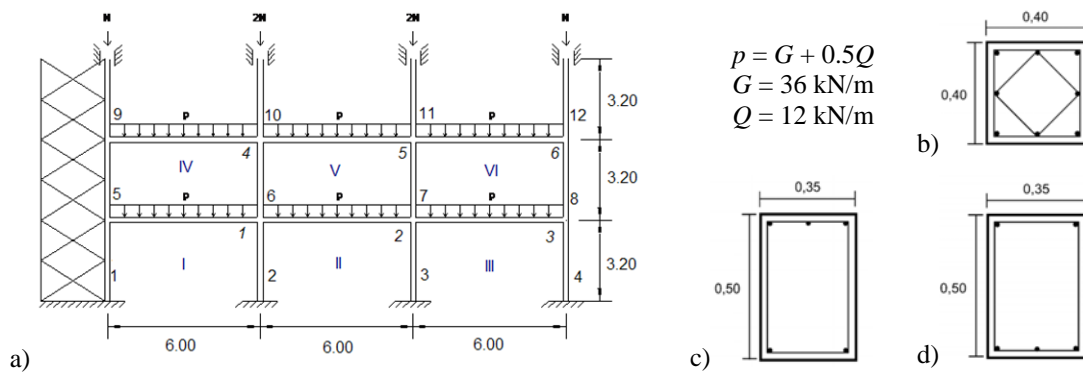


Figure 1. Three-bay frame and RC cross-sections (dimensions in [m]).

simulated in an approximate fashion, by just inputting on the top of columns 9-12 vertical forces N and $2N$, being $N = 880\text{kN}$. All beams and columns are discretized with 10 beam-type FE, with due account to material and geometrical nonlinearities. Bases of columns 1-4 are assumed fully fixed, and at the top of columns 9-12 supports are considered in such a way that rotations and horizontal translations are prevented, but vertical displacements are allowed to occur freely—see Fig. 1. Influence of the RC bracing is simulated by restraining the horizontal displacements on the left extremities of beams 1 and 4.

The concrete and reinforcement strength grade classes are C30/37 (characteristic compressive cylinder strength $f_{ck} = 30\text{MPa}$) and A500 (characteristic yield strength $f_{yk} = 500\text{MPa}$), respectively. For the advanced calculation in SAFIR the mechanical and thermal properties of concrete (siliceous aggregates) and rebars were taken from EN 1992-1-2 [3]. The cross-section of the columns is constant (reproduced in Fig. 1b), as well as constant the beam cross-sections at the intersection with the columns (Fig. 1c) and at mid-spans (Fig. 1d). In Fig. 1 all represented longitudinal rebars are 20mm.

The fire action to represent the evolution of the compartment gas temperature corresponds to the ISO 834 standard fire curve [7]. All columns within the fire compartments are considered to be exposed along all lateral surfaces, while the ones standing out of the fire compartments are admitted to remain at ambient temperature (20°C). As far as the beams are concerned, they are considered to be exposed on three sides.

Analyses with SAFIR for three fire scenarios

Three scenarios assuming the standard fire acting just in the ground floor (Scenario A), just in the 1st floor (Scenario B) or in both the ground and 1st floor (Scenario C) were considered, to check the performance of the RC frame with due account to the influence of structural continuity, thermal elongation of members and deterioration of material properties induced by elevated temperatures. Table I summarizes the fire scenarios and the time to failure reached in each of them, relying on global advanced thermo-mechanical analyses performed with SAFIR.

The deformed structural configurations immediately prior to collapse, and regarding the mentioned fire scenarios, are depicted in Fig. 2. It is rather clear how failure is influenced by the thermal elongation of beams, pushing off the outer

TABLE I. STANDARD FIRE RESISTANCES OF THE THREE-BAY RC FRAME.

Scenario	Compartments in fire	Time to failure (min)
A	I, II, III	132
B	IV, V, VI	145
C	I, II, III, IV, V, VI	158

columns. To further acknowledge how this phenomenon governs the structural fire response, evolution of the horizontal displacement in the top of column 4 is plotted in Fig. 3 for the three fire scenarios. It may be seen that close to failure the drift between both extremities of column 4 surpasses 8.5cm in Scenario A and 13.5cm in Scenario C, which are rather significant when compared to the member length (3.2m, see Fig. 1); in fire Scenario B the drift of column 4 is almost irrelevant (see Fig. 2*b* and Fig. 3), as in this case beams of the 1st floor are not exposed to fire.

A noteworthy remark shall be directed to the fact that in Scenario A a smaller fire resistance was achieved (132 minutes – see Table I) than in Scenario C (158

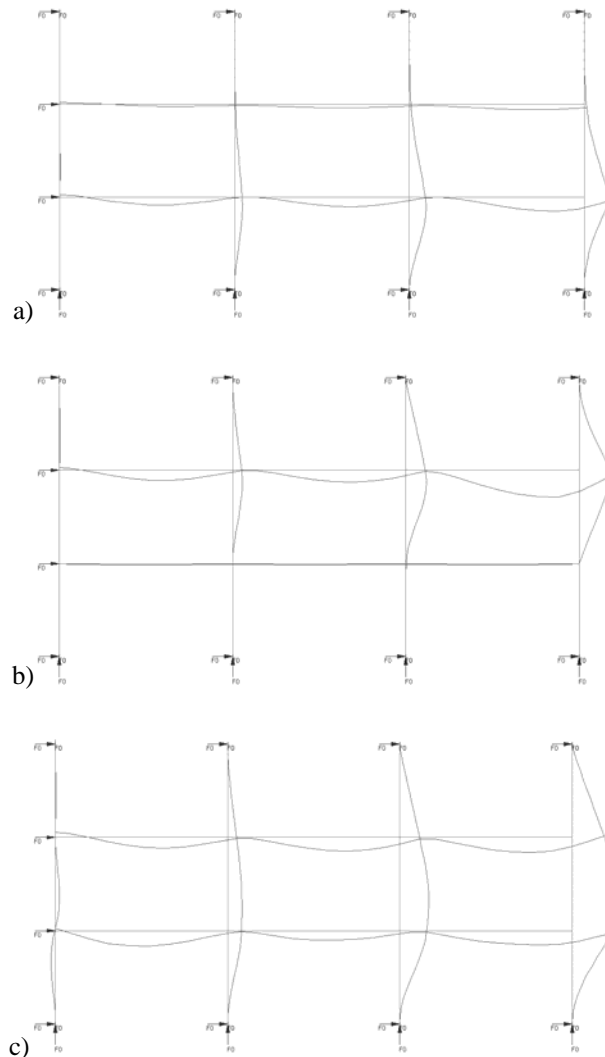


Figure 2. Deformed configurations immediately prior to collapse in Scenarios: a) A, b) B, c) C.

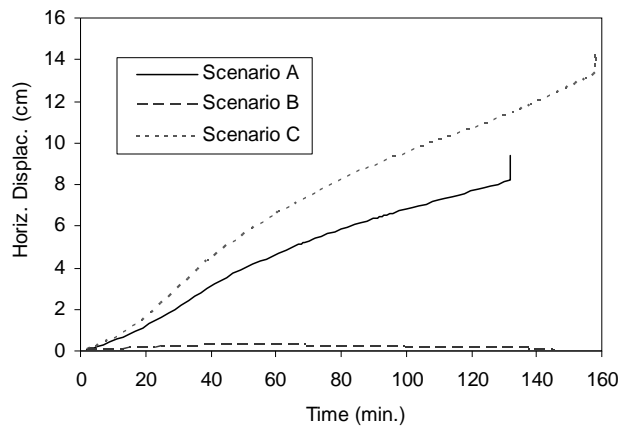


Figure 3. Evolution of horizontal displacement in the top of column 4.

minutes), even though in the latter a greater number of structural elements are exposed to fire. This demonstrates that in case of restrained structures more compartments simultaneously exposed to fire do not necessarily mean more severe fire scenarios. To better clarify this, evolution of the bending moment in the top of column 4 regarding the three scenarios is presented in Fig. 4a: focusing on the curve related to Scenario A, it is possible to observe that a steeper increase of the bending moment is recorded, as compared to what occurs in Scenario C. This is due to the fact that in Scenario A thermal elongation of the 1st floor is restrained by a stiffer structure than in Scenario C, as in the former there is a greater number of RC members remaining at the ambient temperature. Fig. 4b shows the shear force evolution in the top of column 4, which reaches important (and rather similar) values in Scenarios A and C, although the advanced thermo-mechanical analyses performed do not predict failure due to shear in RC members.

Having in mind that in the three scenarios onset of failure occurred always in one of the outermost columns, and that the drifts imposed by the beams played a fundamental role on the structural collapse, the analyses of the present non-sway frame emphasize importance of thermal elongation of RC members on the structural performance, as it may induce evolutions of internal forces that otherwise are strongly distorted if fire resistance is assessed disregarding that phenomenon (like in simplified methods that account for fire resistance of the RC members acting as isolated).

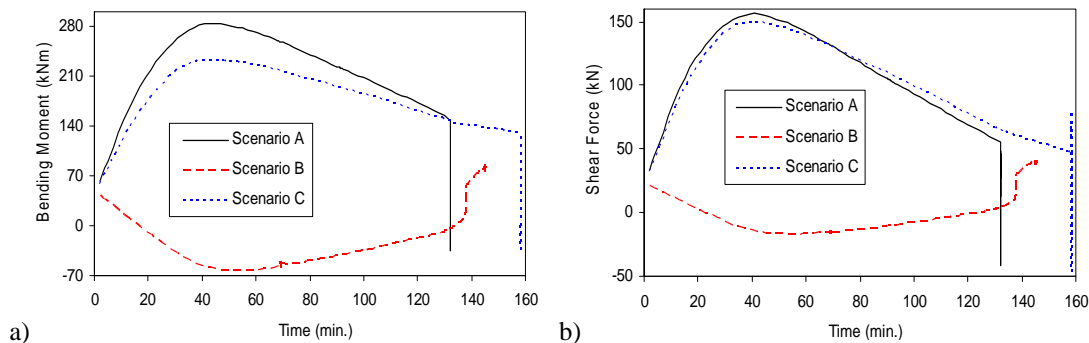


Figure 4. Internal forces in the top of column 4: a) bending moment, b) shear force.

FOUR AND FIVE-BAY RC FRAMES UNDER THE STANDARD FIRE

Analyses with SAFIR for fire Scenario A

As in the previous section thermal elongation of beams played a fundamental role on the structural behavior under fire of the studied frame, in this section this influence is further analyzed by adding one and two bays (and the corresponding distributed loads p) to the right of the RC braced frame of Fig. 1. Every added bay keeps the length of 6m adopted in the basic geometry of Fig. 1; so, one gets a four-bay frame with a horizontal length of 24m, and a five-bay frame with a horizontal length of 30m. The added columns have the same cross section reproduced in Fig. 1b; at the level of the 3rd floor the internal columns are loaded by vertical forces $2N$, whereas the outer ones by forces N , similarly as in Fig. 1. These modifications to the initial geometry are designed not only to check how thermal elongation of beams influences the structural response, but mainly to acknowledge if imposing greater drifts at the outer columns (due to larger horizontal lengths of the RC frames) leads to smaller fire resistances (thus underlining the detrimental effect of thermal elongation of beams). The new analyses concern solely fire Scenario A (which proved to be the most unfavorable one), so in the four and five-bay frames the standard fire is assumed to act just in the ground floor. For a clear identification hereinafter the analyses concerning the four and five-bay frames will be referred to as Scenarios A4 and A5, respectively.

Times to failure reached on these scenarios, according to the advanced analysis performed with SAFIR, are summarized in Table II. It is concluded that more bays (and subsequently more drifts imposed to the outer columns) induced smaller fire resistances. In Fig. 5 the deformed structural configuration immediately prior to collapse for the five-bay frame (Scenario A5) is presented, showing once more that failure affects primarily the rightmost lower column. Evolutions of the horizontal displacements in the top of the rightmost lower columns for Scenarios A4 and A5 are illustrated in Fig. 6a; evolutions of the corresponding bending moments are

TABLE II. STANDARD FIRE RESISTANCES (FOUR AND FIVE-BAY RC FRAMES).

Scenario	Number of bays	Time to failure (min)
A4	4	113
A5	5	97

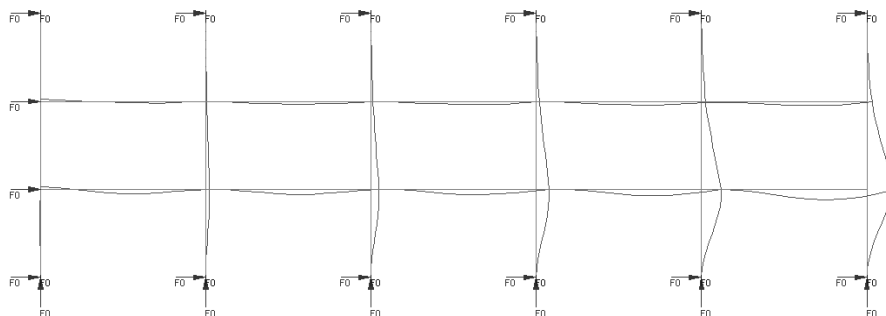


Figure 5. Deformed configuration immediately prior to collapse in Scenario A5.

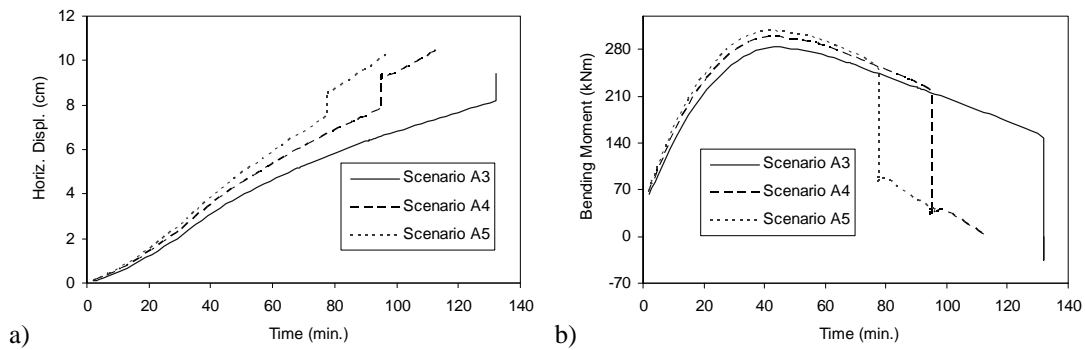


Figure 6. Evolutions in the top of the rightmost lower columns: a) horizontal displacement, b) bending moment.

reproduced in Fig. 6*b*. For comparison purposes Figs 6*a,b* include also the evolutions for the three-bay frame (curves indicated as ‘Scenario A3’). In Fig. 6*a* one may observe that as the number of bays increases the drift evolution on the outermost column becomes steeper, which reflects the influence of the thermal elongation of beams.

These analyses point to the conclusion that as the number of bays increases lesser resistances to failure are to be expected from braced RC frames exposed to the standard fire. In the analyses performed with SAFIR this is illustrated by the continuous reduction of time to failure under fire conditions: 132 minutes for Scenario A3, 113 minutes for Scenario A4 and 97 minutes for Scenario A5.

APPLICATION OF THE ZONE METHOD OF EC2

The observation made at the end of previous section raises a fundamental doubt: if thermal elongation of beams leads to a reduction of fire resistance of RC frames with an increased number of bays, and this structural effect is disregarded when performing fire assessment analyses with simplified cross-section methods, the latter may lead to unsafe conclusions with regards to the evaluation of fire resistances of long braced frames.

To clarify this aspect the standard fire resistance of the three RC frames was assessed by means of the Zone method provided in EN 1992-1-2 [3]. As implicit in this simplified procedure, under fire every RC beam and column is regarded as isolated, and accordingly the Zone method is intrinsically incapable of distinguishing Scenario A3 from Scenarios A4 and A5. The time of fire exposure admissible at the most unfavorable RC member was then computed, which lead to the conclusion that the three frames should be classified as R120. Therefore, compared to the advanced analysis of SAFIR, which predicted Scenario A5 as being considerably more limitative (pointing to a classification of R90 for the five-bay RC frame), the Zone method leads to an unsafe fire resistance evaluation. This is a direct consequence of the strong influence of thermal elongation of beams and structural continuity under fire, duly accounted in SAFIR but neglected in the simplified method.

CONCLUSIONS

A three-bay braced RC frame was analyzed with the advanced thermo-mechanical code SAFIR in three scenarios, assuming the standard fire acting just in the ground floor (Scenario A), in the 1st floor (Scenario B) or in both (Scenario C). The results for these scenarios highlighted the influence of thermal elongation of beams as a key phenomenon governing structural response, in the way it imposes relevant drifts to the outer columns, leading to failure of the latter. It was concluded also that more compartments simultaneously exposed to fire do not necessarily mean more severe fire scenarios. Moreover, considering Scenario A but augmenting the number of bays in the frame, smaller fire resistances were obtained.

On the other hand, the standard fire resistance of the analyzed frames (with three, four and five-bays) was assessed via the Zone method, which rendered a classification as R120. Therefore, with respect to the four and five-bay frames an unsafe evaluation of fire resistance was obtained with this simplified method, since it disregards the influence of thermal elongation of members and structural continuity under fire.

ACKNOWLEDGEMENTS

Funding provided by the Portuguese Foundation for Science and Technology to the Research Unit LABEST—Laboratory for the Concrete Technology and Structural Behavior is gratefully acknowledged.

REFERENCES

1. Taerwe, L. 2007. “From Member Design to Global Structural Behaviour,” in *fib Workshop on “Fire Design of Concrete Structures—From Materials Modelling to Structural Performance*: University of Coimbra, pp. 253–270.
2. Mostafaei, H., Sultan, M. A. and Bénichou, N. 2009. “Performance of Structural Systems in Fire,” in *International Conference Applications of Structural Fire Engineering*: Prague, pp. 604–609.
3. EN1992-1-2. 2004. *Eurocode 2: Design of Concrete Structures—Part 1-2: General Rules—Structural Fire Design*. European Committee for Standardization.
4. Franssen, J.-M. 2005. “SAFIR: A Thermal/Structural Program Modeling Structures under Fire,” *Engineering Journal, A.I.S.C.*, 42(3): 143–158.
5. Riva, P. 2008. *Structural Behaviour of Continuous Beams and Frames*. fib bulletin 46: Fire design of concrete structures - Structural behaviour and assessment.
6. EN 1991-1-2. 2002. *Eurocode 1: Actions on Structures—Part 1-2: General Rules—Actions on Structures Exposed to Fire*. European Committee for Standardization.
7. ISO 834. 1975. *Essais de Résistance au Feu: Organisation Internationale de Normalisation*. Norme Internationale. Genève.

Stability of RC Structure Under Non-Uniform Thermal Exposure

S. DEENY and T. STRATFORD

ABSTRACT

This paper investigates the effect of a uniform temperature design fire assumption upon structural response. The structural behaviour when exposed to the non-uniform gas temperatures above a fire plume (the Alpert correlation [1]) is compared with the structural behaviour when exposed to uniform gas temperature, using either the average or maximum of the non-uniform gas temperatures. A two-way spanning reinforced concrete slab is used as the test case. It is found that the non-uniform gas temperature distribution causes localised failures underestimated by the average gas temperature assumption. The maximum gas temperature assumption provides a conservative estimate of behaviour. The varied response elicited by differing assumptions concerning the thermal exposure highlights the need for an improved design philosophy for structures in fire.

INTRODUCTION

The design of structures to resist the debilitating effects of fire has evolved from (1) a purely empirical approach of fire resistance testing to (2) calculations of strength based on high temperature material properties and more recently (3) estimating structural behaviour based on material strength, thermal expansion and structural interactions. Design methods still make use of all three approaches [2].

From the perspective of a structural engineer these methods represent a spectrum of increasing complexity facilitated by our increasing understanding of material and structural behaviour at high temperatures and increased computational capabilities. A fundamental input to all three methods is the definition of the fire. Although the field of fire science has correspondingly experienced an increase in understanding of behaviour and calculation capabilities, the design fire for structural analysis has remained strongly tied to its original incarnation: the

Susan Deeny, BRE Centre for Fire Safety Engineering, School of Engineering, The University of Edinburgh, The King's Buildings, Edinburgh, EH9 3JL
Tim Stratford, Ph.D., BRE Centre for Fire Safety Engineering, School of Engineering, The University of Edinburgh, The King's Buildings, Edinburgh, EH9 3JL

standard-temperature time curve. The refinements in structural modelling under fire conditions should be accompanied by a better understanding of the worst case fire scenario for structures, especially where fire protection measures are specified on the basis of the model predictions. Thus, we need to investigate the effect of different fire scenarios upon structural behaviour to establish which aspects of fire behaviour are worst from the perspective of the structure. In this paper the ‘uniform fire’ assumption is investigated by contrasting detailed finite element analyses of a structural element under non-uniform and equivalent uniform thermal loadings.

DESIGN FIRES FOR STRUCTURAL ANALYSIS

The design fires for structural analysis are universally based on the format of a single temperature evolving with time. The original design fire and one of the simplest, the standard temperature curve, is found in Eurocode 1 [3], which rises quickly to approximately 900°C then continues to rise infinitely at a slow rate. It was used originally to provide standardisation in fire resistance tests; as fire resistance estimation began to employ calculation methods, the standard fire was utilised to define fire loading. The parametric fire curve (also found in Eurocode 1 [3]) is a recent modification of the standard fire. This design fire adopts different rates of temperature rise, maximum temperature and a cooling branch. These features are varied in accordance to the ventilation area, fuel load, burning rate and compartment thermal behaviour.

The ventilation conditions, fuel layout and compartment size strongly influence the burning behaviour of a compartment fire and consequently the thermal variation that exists within that compartment. This is generally acknowledged [4]; however, the single temperature fire is a convenient simplification in the complex analysis of structures at high temperatures. For design purposes, the assumption of a single temperature fire is justified on the basis that it assumes burning to be occurring everywhere and that this is the worst case scenario, but little to no research has previously focused on whether the standard fire or the assumption of burning everywhere actually represents the worst case scenario for structural stability. As our understanding of and capabilities to analyse *structures at elevated temperatures* has improved significantly in the last two decades, it is now appropriate that we consider the implications of realistic fire definitions in more detail to improve our understanding and design of *structures in fire*.

MEMBRANE BEHAVIOUR OF SLABS

Structural behaviour at elevated temperatures is complex, due to the combination of changing material properties at elevated temperatures and thermal expansion. To consider the effects of non-uniform thermal definitions for structural behaviour, therefore, it is convenient to use initially a structural form that is already well understood. Two-way spanning reinforced concrete slabs have been studied extensively in the context of steel-concrete composite structures in fire due to performance enhancing stability mechanisms such as compressive membrane action and tensile membrane action [5-7].

At low deflections, laterally restrained reinforced concrete slabs experience compressive membrane action due to restraint of thermal expansion. When the

central deflections increase beyond the line of thrust provided by the horizontal restraint tensile stresses and cracking develops at the mid span of the slab. The portion of the slab in tension hangs in a catenary, anchored by either the surrounding ring of compression or lateral restraint where it exists; this is referred to as tensile membrane action. Slender slabs develop catenary action more rapidly whereas compressive membrane action dominates for stockier slabs.

FINITE ELEMENT MODEL

In this investigation the general purpose finite element software ABAQUS [8] is used to analyse both the thermal and mechanical response of a slab to heating. The structural model used is based on those demonstrated by Cameron and Fox [9, 10].

The reinforced concrete slab is 6m \times 6m \times 0.1m, and a 12mm diameter reinforcing mesh at 200 mm spacing is provided at the top and bottom of the slab. The axis distance (from the surface to the mesh mid depth) is 30 mm for the top and bottom reinforcement, summarised in figure 1. A load of 5 N/m² was applied to the slab. Symmetry is taken advantage of and half of the slab is modelled. The slab is unrestrained laterally and rotationally at the edges.

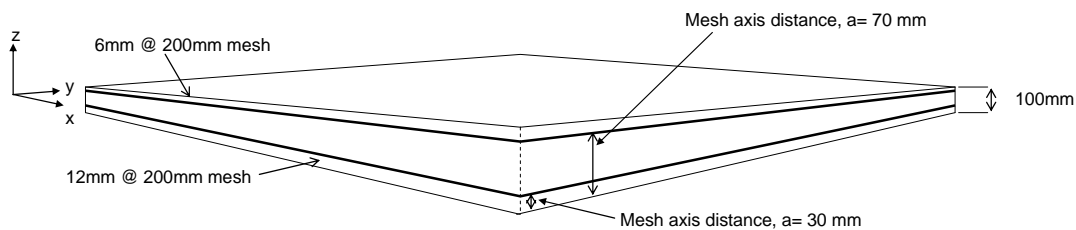


Figure 1. RC slab geometry and FE representation for heat transfer and stress-displacement analysis.

The thermal response of the slab was modelled using 4 node heat transfer shell elements (ABAQUS DS4) and temperatures calculated at 5mm increments to capture the highly non-linear thermal profile typical of concrete in fire. Eurocode 2 [2] temperature dependent thermal properties for siliceous concrete are used, with a moisture content of 3% is assumed.

The mechanical properties of the reinforcement and the siliceous concrete at elevated temperatures are similarly taken from Eurocode 2 [2]. The ambient compressive strength of concrete is 30 N/mm², the ambient tensile strength is calculated from [11] as 3.39 N/mm². Tension stiffening is incorporated into the analysis by decreasing the slope of the linear tensile softening branch, with the amount of tension stiffening determined from a sensitivity analysis. A small amount of tension stiffening was found to result in a numerically unstable response; a large amount resulted in an overly stiff response. The lowest value of tension stiffening that provided a numerically stable response was chosen; in this case, the ultimate strain was taken as ten times the failure strain. The analysis uses quadrilateral ABAQUS general purpose stress/displacement shell elements (S4R) with reduced integration and a large strain formulation. Transverse shear strength is calculated at the start of the analysis and cannot therefore change [8]. The S4R element uses a fully non-linear formulation allowing large-displacement analyses to be conducted; geometric non-linearity has been shown to be important for the prediction of RC

slab catenary action [5, 6]. The reinforcement is modelled as a smeared layer with only axial strength; the layer is equal to the area of one reinforcing bar divided by the spacing.

The concrete biaxial material model is the ABAQUS concrete damage plasticity model, which provides a good description of the failure surface under both tension and compression. The mechanical analysis is solved using explicit dynamics (ABAQUS/Explicit) which is more efficient than implicit integration (ABAQUS/Standard) for extremely discontinuous events or processes.

THERMAL DEFINITIONS

The Alpert correlation [1] is used to define a non-uniform gas temperature profile to which the structure is exposed. The Alpert correlation relates the maximum ceiling temperature at a radial distance r from a fire plume axis to the burning rate of that fire. It was developed from a series of full scale fire tests of substantial fires (4.2 up to 98 MW) under flat ceilings. (4.6m to 15.5 m high). For this investigation, the Alpert correlation has been normalised as shown in figure 2. In this case, the peak temperature, T_{peak} , is 900°C and the ceiling height, H , is 6m. The correlations do not apply where the horizontal flow of the smoke layer is impeded or a static layer of smoke develops [12], but are a good starting point to investigate the significance of a non-uniform fire upon structural behaviour.

The spatial variation in gas temperature does not vary with time; therefore it is applied as a constant exposure for 60 minutes. It is applied to the two way spanning slab in one direction only. The same slab is subjected to two uniform temperature exposures, using the average Alpert profile temperature and the maximum Alpert profile temperature.

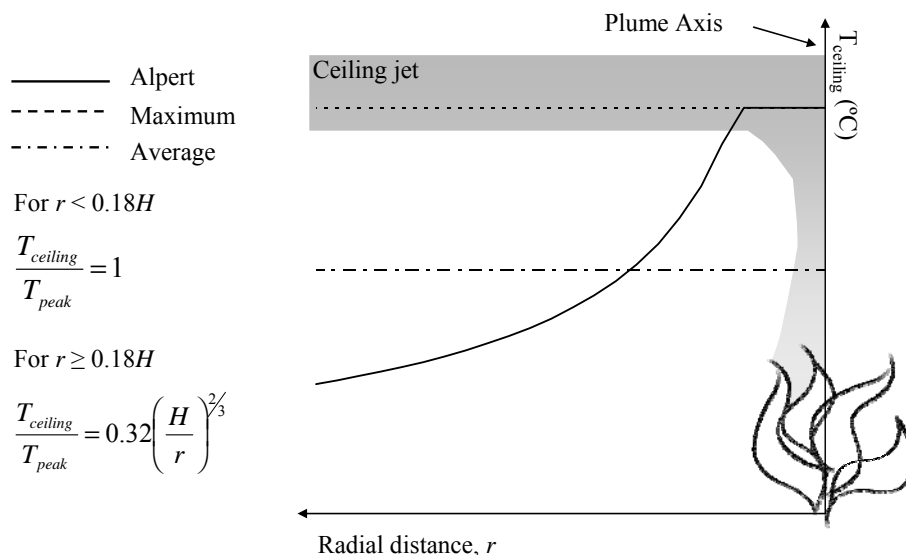


Figure 2. Normalised gas temperature distribution as proposed by Alpert [1].

THERMAL RESPONSE OF THE SLAB

The thermal response of the slab to the three thermal load cases is presented in terms of the concrete average temperature rise and a linear approximation of the thermal gradient at each nodal coordinate in the direction of thermal variation (figure 3).

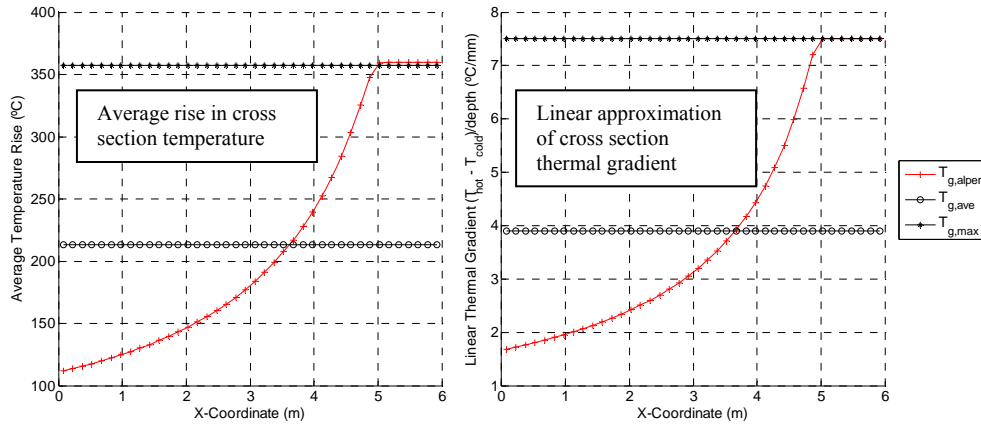


Figure 3. (a) Average rise in cross section temp (b) linear approximation of cross section thermal gradient.

The average temperature rise and the thermal gradient dictate the degree of thermal expansion and thermal bowing respectively [13]. Both the average temperature rise and the thermal gradient strongly reflect the spatial variation in gas temperature, indicating that lateral heat transfer is negligible. The average temperature rise is responsible for the lateral expansion of the slab, therefore, a non-uniform distribution will cause the same lateral expansion as the average of that non-uniform distribution (for a constant co-efficient of thermal expansion). The thermal gradient induces curvature in the slab; therefore the variation of thermal gradient along the length of slab indicated in figure 3 will cause local bowing.

MECHANICAL RESPONSE OF THE SLAB

The behaviour of this slab is characterised by decreasing flexural strength due to material degradation, in combination with increasing deflections resulting from thermal expansion, and hence the development of tensile membrane action.

The tensile membrane behaviour of slabs is heavily dependent upon the slab deflected shape. The double curvature caused by bi-directional bending results in the formation of a self supporting ring of compressive stress at the slab perimeter [6]. This ring supports the central portion of the slab which hangs in catenary action, relying upon the tensile strength of the reinforcement. Previous research [14] has shown the failure of lightly reinforced slabs in tensile membrane action to be by rupture of reinforcement at mid-span. The reinforcement ratio of this slab is relatively high therefore failure by crushing of the concrete within the compressive ring is also a possible failure mechanism. The implications of the non-uniform thermal load case upon membrane behaviour of the slab is shown in terms of the slab deformation, the concrete section minimum principle stresses, concrete plastic strains and the reinforcement mechanical strain in figure 4 to figure 6 and table I.

The distortion of the slab's deformation due to a non-uniform thermal profile is evident from the central span deflection profiles in figure 4. The increased thermal gradient caused by the peak temperature causes a corresponding increase in curvature. The resulting slab deflection is less than that of the uniform maximum temperature case, however, as compatibility with the cooler portion of the slab reduces the slab maximum deflection to a magnitude similar to that of the average temperature case.

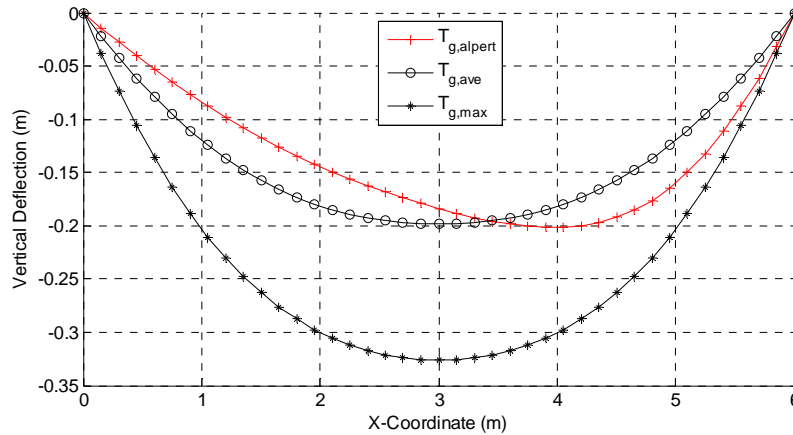


Figure 4. Central span deflection profile after 60 minutes exposure.

This distorted shape affects the development of the concrete compressive ring; this is evident in figure 5, which plots in plan the concrete minimum principle section stresses for the uniform maximum temperature case and the non-uniform case. The stresses through the section depth are integrated and from these the principle section stress values calculated using Mohr's circle. In the region of the peak temperature stresses are lower for the non-uniform case as a result of increased concrete straining.

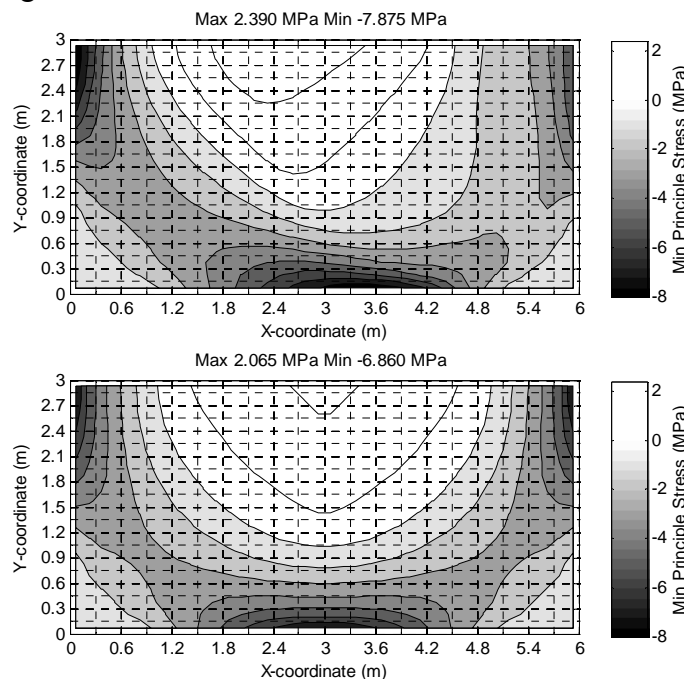


Figure 5. Concrete minimum principle section stress (a) Non-uniform case (b) Uniform average case.

The crushing strains are examined by plotting the plastic equivalent compressive strains as a proportion of the peak strain. A value greater than 1 indicates the onset of crushing. In figure 6 these have been plotted in two cross-section contour plots for the non-uniform case. From this figure, it is evident that crushing strains in the region of the peak are more substantial than at the cooler end with proportional peak strains of 6.54 and 2.35 respectively. The corresponding values for the average and maximum temperature cases are 4.191 and 7.53 respectively. The average gas temperature assumption underestimates the strains, and the maximum gas temperature assumption provides a conservative estimate.

The peak sagging mechanical strains for the top and bottom reinforcement are summarised in Table I. The bottom reinforcement mechanical strains are notably lower than the top reinforcement due to the relief of mechanical strains by increased thermal expansion. Much higher reinforcement strains develop in the non-uniform case when compared to the average uniform exposure case despite similar deflections. The maximum uniform exposure results in the highest reinforcement strains. For all cases, however, the strains remain relatively small with respect to the Eurocode 2 [2] rupture strain of 15%, although the modelling approach has a limited capability to capture rupture due to the smeared reinforcement approach.

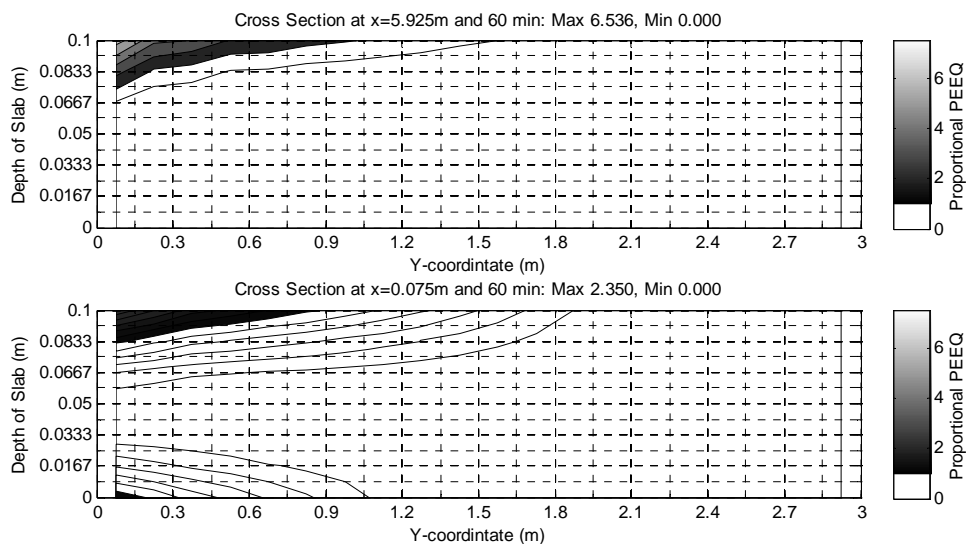


Figure 6. Proportional plastic equivalent concrete strains cross-section contour for the non-uniform case.

Table I. Peak reinforcement mechanical strains.

	Alpert distribution		Average Symmetrical	Maximum Symmetrical
	X direction	Y direction		
Top Rebar	0.18 %	0.46 %	0.47 %	1.95 %
Bottom Rebar	0.4 %	0.18 %	0.1 %	0.19 %

CONCLUSIONS

In this paper the response of a two way spanning slab to a non-uniform gas temperature distribution has been compared with the response when uniformly exposed to the average gas temperature and the maximum gas temperature. The variation in exposure temperature distorts the deflection profile of the slab leading to locally high crushing strains in the compressive ring which is not captured by assuming an average gas temperature exposure. The uniform maximum temperature had the most detrimental effect for the slab, providing a conservative estimate of behaviour. The study is being extended currently to consider transient variation also. This study has highlighted the potential variation different assumptions regarding the design fire may have for the structural fire performance of a single element. It is therefore critical that current design fire assumptions such as the single temperature fire are well understood to allow better judgment of the worst case scenario.

ACKNOWLEDGMENTS

The authors gratefully acknowledge sponsorship and support of the first author by Buro Happold FEDRA Ltd and EPSRC.

REFERENCES

1. Alpert, R.L., *Calculation of response time of ceiling-mounted fire detectors*. Fire Technology, 1972. **8**: p. 181–195.
2. European Committee for Standardisation, *Eurocode 2: Design of Concrete Structures- Part 1-2: General Rules - Structural Fire Design*. 2004, BS EN 1992-1-2:2004.
3. European Committee for Standardisation, *Eurocode 1: Actions on Structures: General Actions- Part 1-2: Actions on Structures Exposed to Fire*. 2002, BS EN1991-1-2:2002.
4. Buchanan, A., et al., *The effect of stress-strain relationships on the fire performance of steel beams*. Engineering Structures, 2004. **26**(11): p. 1505–1515.
5. Gillie, M., A.S. Usmani, and J.M. Rotter, *A structural analysis of the first Cardington test*. Journal of Constructional Steel Research, 2001. **57**(6): p. 581–601.
6. Huang, Z.H., I.W. Burgess, and R.J. Plank, *Modeling membrane action of concrete slabs in composite buildings in fire. I: Theoretical development*. Journal of Structural Engineering-Asce, 2003. **129**(8): p. 1093–1102.
7. Foster, S., et al., *Thermal and structural behaviour of a full-scale composite building subject to a severe compartment fire*. Fire Safety Journal, 2007. **42**(3): p. 183–199.
8. ABAQUS, *ABAQUS 6.8*. 2008, Dassault Systemes Simulia Corp: Providence.
9. Cameron, N.J., *The behaviour and design of composite floor systems in fire*. 2003, University of Edinburgh.
10. Fox, D., *Investigation into factors affecting membrane stress development in concrete floor slabs in fire*. 2006, The University of Edinburgh.
11. Shah, S.P., S.E. Swartz, and C. Ouyang, *Fracture Mechanics of Concrete*. 1995, New York: John Wiley & Sons.
12. Drysdale, D., *An Introduction to Fire Dynamics*. 2nd ed. 1998, London: John Wiley and Sons Ltd.
13. Usmani, A.S., et al., *Fundamental principles of structural behaviour under thermal effects*. Fire Safety Journal, 2001. **36**(8): p. 721–744.
14. Bailey, C.G. and W.S. Toh, *Small-scale concrete slab tests at ambient and elevated temperatures*. Engineering Structures, 2007. **29**(10): p. 2775–2791.

The Fire Performance of Polymer Fibre Reinforced Composite Concrete Slabs

D. FOX and T. STRATFORD

ABSTRACT

Dispersed polymer macro-fibres have recently started to be used within steel-concrete composite slab floors to reduce the need to lift, position and fix steel reinforcing fabric. Polymer fibres can be used to replace light reinforcing meshes required for crack control. This paper investigates the performance in fire of a macro-synthetic polymer-fibre-reinforced composite slab system.

The performance-based fire design of a composite floor slab can take advantage of secondary load carrying mechanisms that develop during a fire, the most significant of these being catenary (tensile membrane) action. For a slab to act in tensile membrane action, it must contain sufficient reinforcing to provide the required tensile capacity.

The polymer macro fibres used to reinforce concrete typically soften with increasing temperature and melt by around 160°C. There is therefore a concern that by replacing a steel reinforcing mesh with the polymer fibres, there will be no secondary load-carrying mechanism and the slab may be more vulnerable than a traditional slab exposed to the same fire condition. However, the interaction between the thermal gradient in the slab, the thermo-mechanical properties of the concrete including the fibres, and the restraint condition at the slab boundary is far from clear.

This paper presents preliminary results from computational research into the performance of polymer fibre reinforced concrete slabs. It focuses upon model slabs designed to capture the underlying mechanisms that govern their thermal and structural behaviour during a fire, and demonstrates that the introduction of polymer fibres into concrete enhances the ability of a floor slab to carry load during a fire. The performance of the polymer fibre-reinforced concrete slab considered is comparable to that of an equivalent slab with traditional steel fabric reinforcement.

David Fox, Tim Stratford, PhD

BRE Centre for Fire Safety Engineering, School of Engineering, The University of Edinburgh, The King's Buildings, Edinburgh, EH9 3JL, UK

INTRODUCTION

Polymer fibre reinforcement has recently started to be used in the construction of composite steel-concrete floor slabs. Dispersed polymer macro fibres (around 50mm long) can be used in place of traditional anti-crack reinforcement, which usually takes the form of welded steel fabric that is placed above the steel deck prior to pouring. The fibres are added at the batching plant, and remove the need to lift and fix sheets of steel fabric. The fire resistance of polymer fibre reinforced composite slabs have been evaluated by the manufacturers using isolated element tests, and design tables for polymer fibre reinforced concrete (FRC) composite slabs have been produced.

The polymer macro fibres used to reinforce concrete typically have a glass transition temperature of around 100°C and decompose at around 160°C. This raises concerns about the performance of polymer FRC composite slabs during a fire. In particular, it is not clear whether a polymer FRC composite slab could support the secondary load-carrying mechanisms that can be established within a steel fabric reinforced concrete slab during a fire. Secondary mechanisms such as catenary or tensile membrane action can be used in performance-based design methods to enhance the fire performance of a structure, or reduce the need for fire protection [1].

A polymer FRC may lose tensile strength as the fibres are heated; however, it is far from clear what effect this will have upon its fire performance. Firstly, only part of the depth of the slab will have exceeded the glass transition temperature of the fibres; the fibres towards the unheated side of the slab may retain tensile strength. Secondly, restraint conditions around the slab may reduce the reliance of the slab upon catenary action.

This paper investigates the relative performance of steel fabric and polymer fibre reinforced model-scale concrete slabs. (Model scale slabs are here considered in support of a subsequent model scale experimental investigation). The paper focuses upon the constitutive behaviour of the FRC, how it differs from plain concrete and how it changes with temperature. Experimental results are used to modify existing concrete constitutive models to give a temperature-dependent material model for polymer FRC suitable for numerical analysis.

MATERIAL PROPERTY DEFINITIONS

Material Definitions for Plain Concrete and Steel

Eurocode 2 [2] expresses ultimate tensile stresses in terms of compressive strength, and gives reduction factors that reduce these strengths depending upon temperature up to 600°C. The Eurocode 2 approach, however, is intended for design, and does not give any information on the post-peak behaviour of concrete in tension, which is particularly important for modelling (i) concrete in fire and (ii) polymer fibre reinforced concrete. Rots *et al.* (1984) express the softening response of concrete in tension in [3]. Rots' model is expressed in terms of stress-strain curves, the area under which describes the fracture energy G_f of the concrete. This model assumes a length over which strain localisation occurs, and thus can also be

interpreted as a stress-displacement model. Rots' model compares well to other stress-displacement models found in the literature, such as Trunk *et al.*, 1999 [4] and Wittmann, 2002 [5].

The constitutive response of concrete in compression used in this paper are taken from Eurocode 4, Part 1-2, Figure 3.2 [6]. Eurocode 4 also gives a material model for traditional steel reinforcement.

Material Definition for Polymer Fibre Reinforced Concrete

The polymer fibres considered in this study are a polyethylene/polypropylene blend with a high surface area to volume ratio. They affect the concrete's properties primarily by bond with the cementitious matrix and the frictional work associated with fibre pull-out during crack opening [7]. During a split-tension test [8], for example, fibre bridging allows the cracked specimen to carry sustained load after first cracking, unlike a brittle plain concrete specimen, because the fibres are able to bridge a 20mm crack width. The effectiveness of the fibre in toughening concrete depends upon the fibre orientation and bond with the matrix, which is in turn related to the matrix strength.

Figure 1 plots the stress-displacement of polymer FRC in tension. The 20°C curve shows that polymer FRC has a far greater deformation capacity than plain concrete. The tensile response of plain concrete is similar to the curves shown for temperatures > 200 °C, in the bottom left of the figure.

The fibres have a relatively low degradation temperature (160°C) and glass transition temperature (~100°C), which give loss in stiffness and strength upon heating. Consequently, the magnitude of the stress-displacement curves in Figure 1 reduces with temperature. The curves in Figure 1 were obtained by conducting wedge splitting tests on polymer FRC at various temperatures up to 140°C [9]. These results were used to derive a stress-displacement based constitutive response

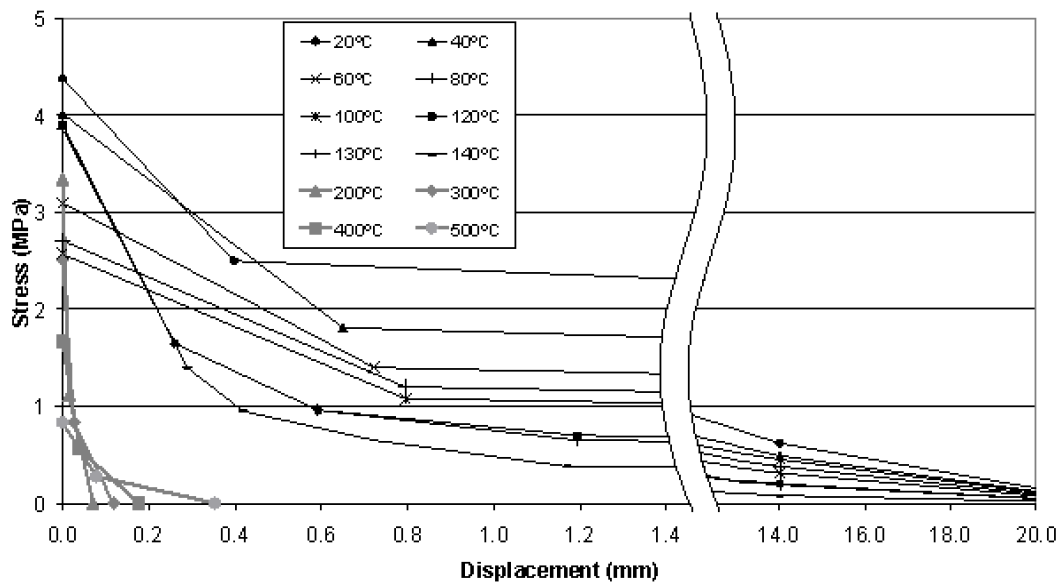


Figure 1. Stress-displacement formulation for polymer fibre reinforced concrete.

for polymer FRC in tension. Above 140°C the polymer fibres have softened and no longer provide a noticeable mechanical contribution to the composite behaviour; consequently, the plain concrete model is used for temperatures above 140°C to give a full description of the behaviour of PFRC up to 500°C. This seems to be a reasonable assumption for the present purposes; however, it should be noted that there will be residual porosity due to the voids left by melted fibres. This may have an appreciable effect on the material behaviour which is not taken into account with this model. The loss in fibre strength at 140°C gives an abrupt jump in the stress-displacement curves and this part of the model is likely to be revisited in the future.

An interesting result is observed in the data upon which the stress-displacement model is based. The peak tensile stress reduces with temperature, as expected, up to 100°C. But at higher temperatures, the peak stress rises in an erratic way, and the peak value at 130°C and 140°C is very close to the value at 40°C. This is non-intuitive, but in the absence of other data, is included in the stress-displacement model. The compressive behaviour of fibre reinforced concrete is assumed to be the same as plain concrete for the present model.

MODEL DESCRIPTION AND FINITE ELEMENT ANALYSIS

This paper examines three model scale, 40mm thick by 1400mm square slabs with different reinforcement properties, listed in Table I. The traditional, steel fabric reinforced concrete slab uses the plain concrete stress-displacement material model with a smeared layer of steel reinforcement. In the plain slab, this reinforcement is removed. The fibre reinforced slab uses the fibre reinforced stress-displacement material model from Figure 1 with a compressive strength of 35MPa. The boundaries of the slabs have translational and rotational fixity to simulate a heated panel surrounded by a cool rigid structure.

Slab	Reinforcement type
Traditional	A mesh of 3mm diameter mild steel with 50mm spacing is placed at mid-depth of the slab. This gives a reinforcement percentage of 0.35%.
Plain	There is no reinforcement applied to this slab.
Fibre	Polymer fibre reinforced concrete, using the constitutive response in Figure 1.

Table I. Summary of analyses

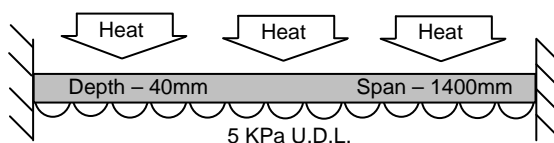


Figure 2. Schematic of test setup.

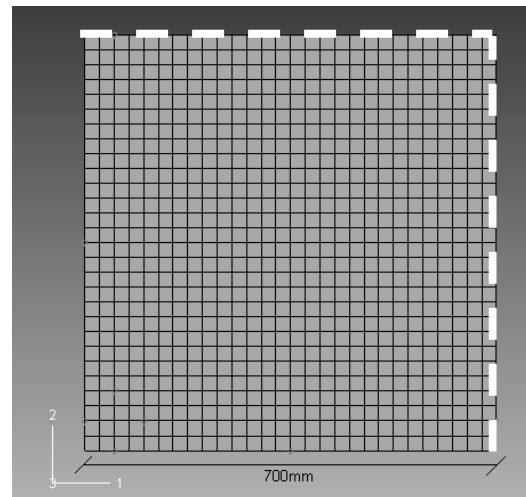


Figure 3. Mesh schematic. White lines indicate symmetry boundary conditions.

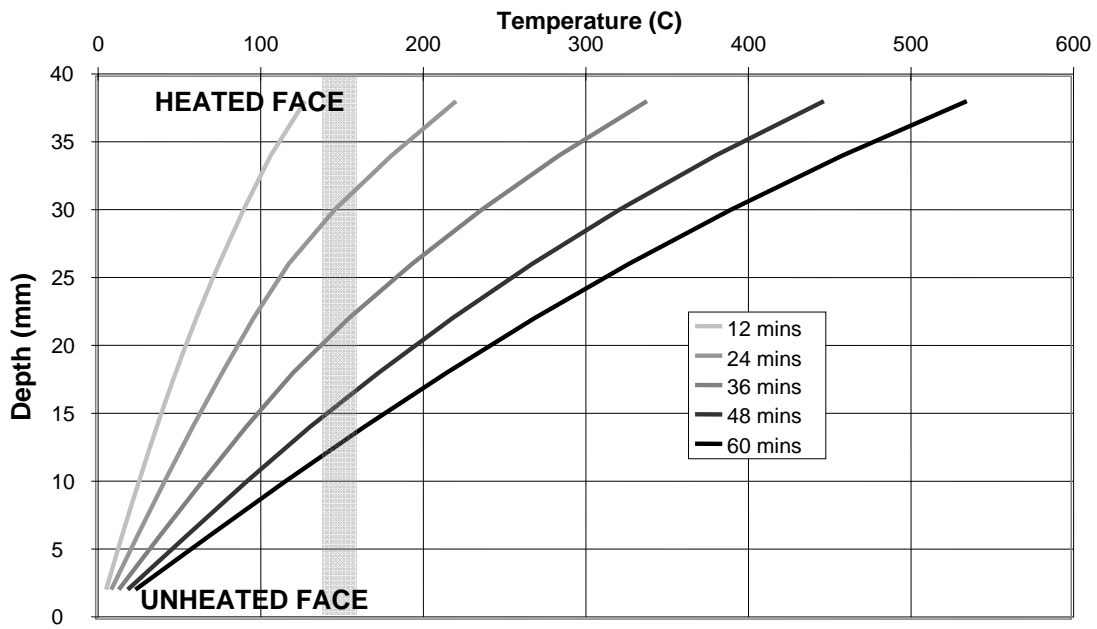


Figure 4. Temperature evolution throughout model scale slab.

The slabs were subjected to a one-hour exposure to the BS 476 time-temperature curve [10], followed by a one-hour cooling period, in which the applied temperature falls linearly from a peak of 945°C to ambient (20°C). The general arrangement of the test is shown in Figure 2. Note that the slab is inverted from its normal orientation to reflect the arrangement that will be used in subsequent testing, thus, the load is applied from *below*, and the slab is heated from *above*. Position within the slab depth is defined upwards from the loaded surface.

The slabs were modelled using the finite element software Abaqus [11], with only a quarter slab modelled with the appropriate symmetry conditions to reduce computational demand. A schematic of the mesh is given in Figure 3.

The temperature and mechanical analyses could be uncoupled, hence, the temperatures were first calculated using a separate heat transfer analysis. The spatial and temporal variation in temperature through the depth of the slab is shown in Figure 4. The grey region between 140°C and 160°C indicates the transition zone where fibres become ineffective as reinforcement. It can be seen that even after one hour of heating, approximately 35% of the depth of the slab remains cool enough for the fibres to retain some strength and thus contribute to the load carrying mechanisms within the slab.

RESULTS AND DISCUSSION

Slab Deflection Behaviour

Figure 5 compares the deflection-time response of each of the three slabs. The analysis predicts that all three slabs undergo similar deflections up to 40 minutes of heating. After this time, hogging cracks form around the perimeter of the slab. The plain concrete slab undergoes a rapid runaway failure. Both the fibre and steel mesh reinforcement provide capacity across the hogging cracks, and their deflection-time

responses are very similar to the end of heating, with 41mm and 37mm maximum deflection respectively. These deflections do not recover during cooling.

The deflection response plots demonstrate that the polymer fibre reinforcement has a significant beneficial effect on the performance of the slab during fire, and there is a near equivalence with the steel fabric reinforced slab.

Stress Profiles through Depth

The deflection-time response of the polymer FRC slab suggests that its performance is comparable to traditional steel reinforced concrete; however, it is important to understand the load carrying mechanisms that act within the slab. As discussed in the introduction of this paper, whilst the polymer fibres degrade at elevated temperatures, fibres close to the unheated face of the slab will be sufficiently cool to maintain some strength and deformation capacity. Furthermore, restraint by the boundary conditions around the slab may reduce reliance upon catenary action.

Stress profiles give an indication of how the slab carries load, and stress profiles (tension positive) have been plotted through the thickness of the slab in Figure 6 and 7, at times that correspond to the temperature profiles in Figure 4. Figure 6 plots stress profiles at the centre of the slab; Figure 7 plots the stress near the boundary, perpendicular to the slab's edge.

Figure 6 shows how, in the initial stages of heating, the unheated face at the centre of the slab experiences compression, due to bending action to carry the applied load. As heating continues, compression develops throughout the depth of the slab. Towards the end of the heating period (60 minutes), the heated side is in compression due to restrained thermal expansion, and there is a combination of compression at the unheated face and tension towards the centre of the slab, required to maintain axial and moment equilibrium of the cross-section. Compressive behaviour dominates the slab response in this case, removing the need for the fibres to contribute to the load-carrying mechanisms of the slab.

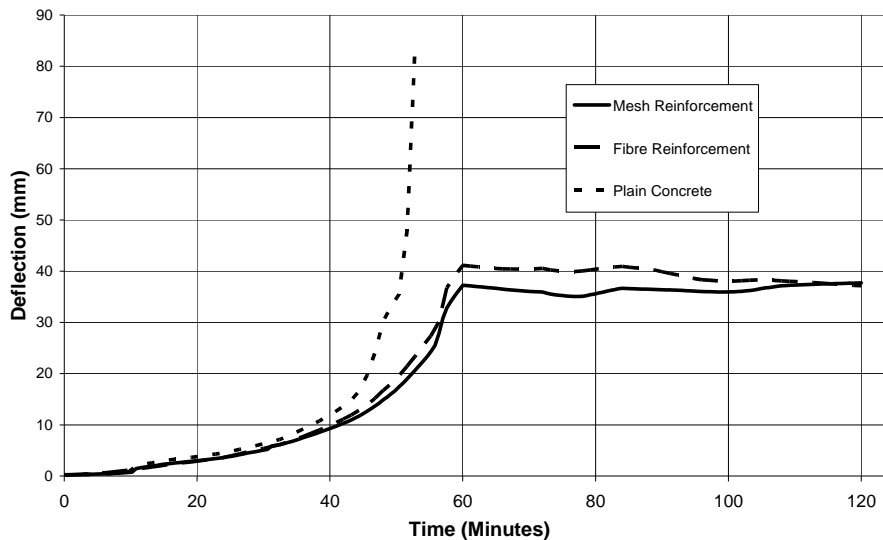


Figure 5. Deflection histories of heated slabs with different kinds of reinforcement.

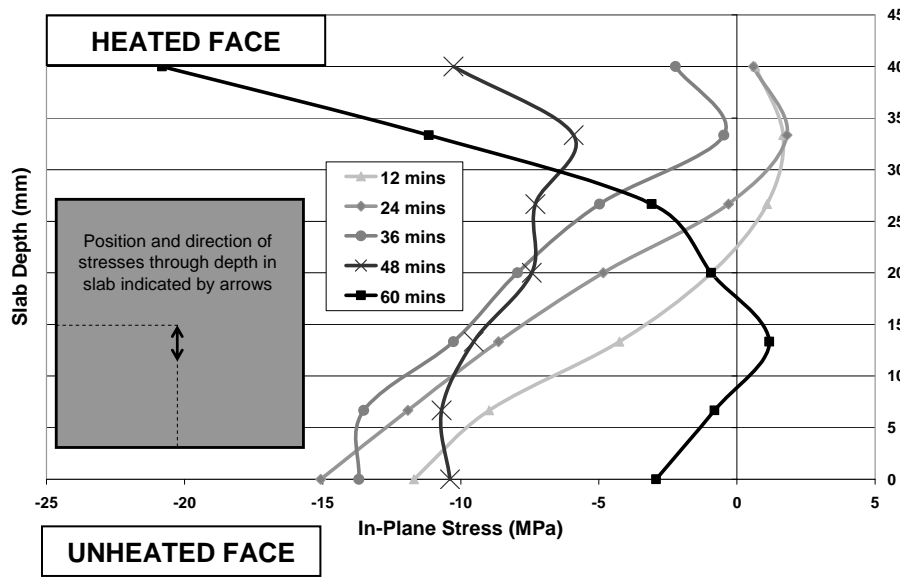


Figure 6. Stress profiles through depth on midline 25mm from centre of slab.

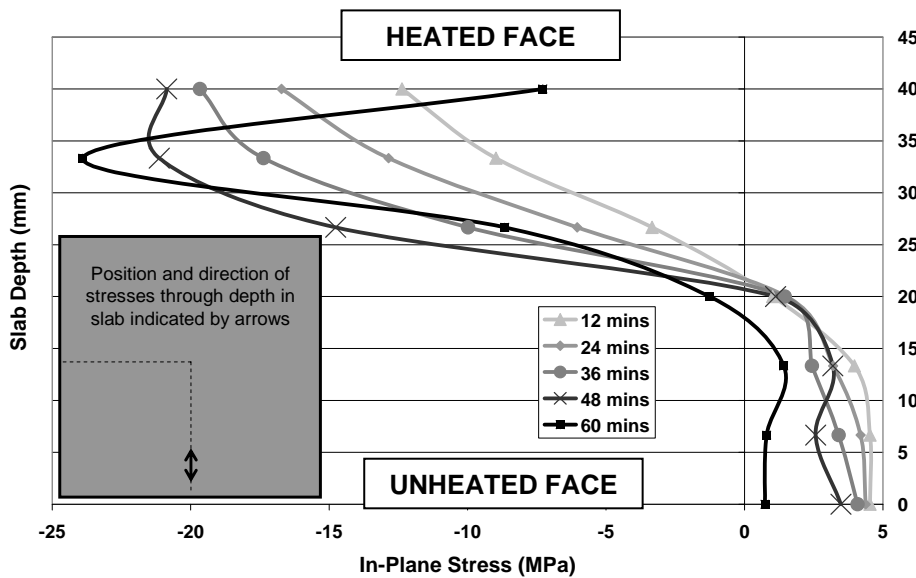


Figure 7. Stress profiles through depth at midpoint of supported edge, hogging zone.

At the edge of the slab (Figure 7), the slab initially carries load by bending, giving tension on the unheated face of the slab and compression on the heated face. As the temperatures rise, restrained thermal expansion causes increasing compression on the heated face, but the tensile stress is mostly constant. The polymer fibres in the 20mm closest to the unheated face are able to carry sustained tensile stress as their temperature does not cause degradation of the fibres (Figure 4). The fibres do not alter the tensile strength of the concrete, compared to plain concrete without fibres, but they enhance its deformation capacity, which prevents the formation of hogging cracks at the slab boundaries from causing catastrophic behaviour (Figure 5), and thus increases the slab resistance to fire.

Also, examination of the strains at the boundary support indicates that the fibre reinforced slab distributed hogging strains over a wider area than the steel mesh or unreinforced slabs.

CONCLUSIONS

This paper has presented the results of preliminary finite element analyses that investigate the performance of polymer fibre reinforced concrete during fire to plain concrete and concrete containing traditional steel reinforcement. The effect of the polymer fibres has been included by means of a stress-displacement based material model for the tensile performance of polymer fibre-reinforced concrete.

Initial results from the finite element analyses of a model scale concrete slab predict that including polymer fibres in the concrete enhances its fire resistance compared to an unreinforced slab. Near-equivalence with the steel mesh reinforced slab was observed in the deflection-time response. The research points to the significance of maintaining a low temperature in the fibres near the unheated surface for the purpose of providing ductility at the slab boundary. The fibres can distribute the concrete tensile strains over a much wider area.

The models presented here are preliminary, for the purpose of designing and predicting the experimental behaviour. After conducting the tests, the results will be used to refine the various constitutive models in this analysis to better reflect the true behaviour. Of significant importance are the heat transfer within the slab, the tensile characteristics of the concrete around the fibre melting temperature, and the extent of distributed cracking and toughness provided by the fibres at the slab support.

REFERENCES

1. Usmani, A.S, Cameron, N.J.K, "Limit Capacity of Laterally Restrained Reinforced Concrete Floor Slabs in Fire", *Cement and Concrete Composites*, Vol. 26, 2004 pp 127–140.
2. British Standards Institution (2004) Eurocode 2—Design of concrete Structures. General Rules and Rules for Buildings. BS EN 1992–2004.
3. Rots, J.G, Kusters, G.M.A, Blaauwendraad, J. "The Need for Fracture Mechanics Options in Finite Element Models for Concrete Structures", *Proc. of the Int'l Conf. on Computer-Aided Analysis and Design of Concrete Structures: Split, Yugoslavia, 17th-21st September, 1984*, Volume 1 pp 19–32.
4. Trunk, B, Schober, G, Helbling, A.K, Whittman, F.H. "Fracture Parameters of Autoclaved Aerated Concrete". *Cement and Concrete Research* 29 (1999) 855–859.
5. Wittmann, F.H. "Crack Formation and Fracture Energy of Normal and High Strength Concrete", *Sadhana*, Vol 27, Part 4, August 2002, pp 413–423.
6. British Standards Institution (2005) Eurocode 4—Design of composite steel and concrete structures. Part 1-2: General Rules – Structural fire design BS EN 1994-1-2:2005.
7. Guidance on the use of Macro-Synthetic-Fibre-Reinforced Concrete, Technical Report No. 65, The Concrete Society, April 2007.
8. British Standards Institution (2000) Testing Hardened Concrete Part 6—Tensile Splitting Strength of Test Specimens. BS EN 12390-6:2000.
9. Rieder, K.A. Fracture behavior at elevated temperatures of STRUX® 90/40 reinforced concrete, Grace Construction Products, 2004.
10. British Standards Institution (1972) BS 476 Part 8—Test Methods and Criteria for the Fire Resistance of Elements of Building Construction, BS 476 Part 8: 1972.
11. Abaqus version 6.8, Simulia, Dassault Systemes, 2008.

Estimating the Response of Flat Plate Concrete Slab Systems to Fire Exposure

M. GHOREISHI, A. BAGCHI and M. A. SULTAN

ABSTRACT

Two-way flat plate slabs provide a number of benefits for office buildings and apartments—for example, reducing formwork, flexibility of partitions, relatively high ceiling, and prompt erection. This paper shows that the fire resistance of flat plate slab structures is affected by many factors including concrete cover, cross section of the structural elements which is not essentially constant during fire exposure, and the material properties of concrete and reinforcing steel. Concrete has fairly excellent fire resistance properties. However, the strength of concrete reduces as temperature rises. There is a lack of studies, both analytical and experimental, on flat plate concrete slabs in the literature. The objective of this research is to investigate the effects of concrete and steel behavior of slab in fire and the tensile membrane action conditions.

INTRODUCTION

Performance of structures exposed to fire is usually studied based on the performance of single structural elements. In recent years, various studies have been undertaken on the overall behavior of structures when subjected to fire. Concrete is considered to be comparatively fire resistant, while steel is adversely affected by fire exposure. Now the question is: is fire resistance of a complete concrete structure different from that of a single member? Does a structural system as a whole, concrete or steel, enhance the fire safety of structure? Which parameters are influencing the fire resistance of reinforced concrete structure? This article presents a study on two-way flat plate concrete slabs to address some of the above questions. Although there are studies on fire resistance of reinforced concrete

Mehrafarid Ghoreishi, Dept. of Building, Civil and Environmental Eng., Concordia University, Montreal, Canada

Ashutosh Bagchi, Dept. of Building, Civil and Environmental Eng., Concordia University, Montreal, Canada

Mohamed A. Sultan, Institute of Research in Construction, National Research Council, Ottawa, Canada

components at the element levels, including different materials such as high strength concrete, concrete columns and beams strengthened with fiber reinforced polymer, there is a lack of analytical and experimental studies on assemblies or whole structural systems with flat plate slabs. This paper presents the non-linear analysis of reinforced concrete flat slabs at high temperature and service loads. Predictions from this analysis compared with the available experimental results which resulted in a good agreement.

LITERATURE REVIEW

In recent years, a number of studies on numerical analysis of behavior of reinforced concrete structures in fire have been carried out. A brief summary of the state of the art is provided in this paper. Nwosu and Kodur in 1997 [1] presented an extensive review of available studies for steel structures. Ghoreishi et al. in 2009 [2] provided a review of available experimental and numerical studies on whole structural systems under fire, and observed that there is a lack of experimental studies on whole structural systems, particularly for concrete. Nizamuddin [3] in 1976 developed a non-linear layered finite element approach based on the Kirchoff's thin plate theory, while Huang et al. in 2003 [4] used Mindline-Reissner's theory and Reynournd and Nechnech in 2002 [5] used elasto-plastic damage model to analyze R.C. slabs in fire. Effects of different aggregates reinforced concrete slabs was studied in two experimental ISO-834 fire tests by Wade in 1992 [6]. Cooper and Franssen studied on 1-D, 2-D and 3-D of concrete slabs in 1999 [7]. Issen et al. in 1970 [8] explained that axial restraint increases the fire resistance of reinforced concrete floor systems. However, analytical studies by Anderberg and Forsen in 1982 [9] have shown increase of axial restraint does not always increase the fire resistance of flat slabs. Experimental fire tests on restrained flat slabs by Cooke in 1993 [10] have shown that position of the restraint force at the supports is beneficial to the fire resistance. In 2004, Lim et al. [11] studied axially restrained one-way reinforced concrete slabs broadly in fire conditions.

While fire behavior of reinforced concrete slabs has been previously studied by various researchers, most studies focused on one-way reinforced concrete slabs. Also, research on the fire performance of reinforced concrete structures has been mainly focused on material properties rather than structural performance. Although there are some studies on the element level fire resistance, there is a lack of analytical and experimental studies on assemblies or whole structural systems with flat plate slabs.

EXISTING EXPERIMENTAL STUDY

An experimental test on whole structure under fire was carried out in 2001 for a seven storey in-situ reinforced concrete building constructed at the Building Research Establishment (BRE) laboratories in Cardington, UK [12]. The design of fire was based on the parametric approach provided in Annex A of the fire part of Eurocode [13]. The predicted time-temperature response from the Eurocode and ISO standard curve is shown in Figure 1. The test showed that spalling of the floor slab was extensive which resulted in exposure of the bottom reinforcement.

Although concrete spalling considerably reduced the flexural strength of the slab, collapse did not occur. This could be attributed to the slab behaving in compressive membrane action, which is currently not considered in codified design methods.

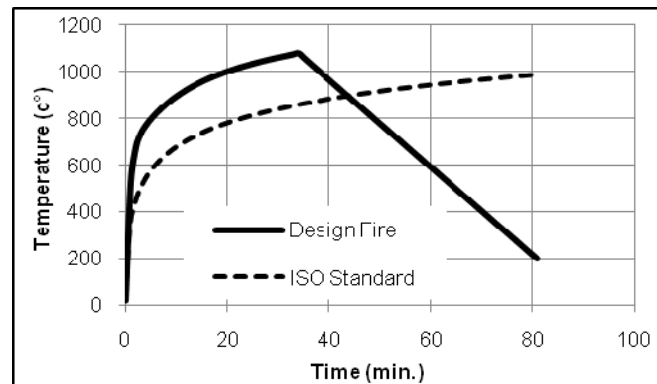


Figure 1. Design fire curve and ISO standard curve.

ANALYTICAL/NUMERICAL MODEL

At present, considerable attention has been given to simulate the behavior of structures in fire by analytical and numerical approaches. In this paper a 250 mm thick two-way flat plate slab is considered and the finite element (FE) method is used for modeling the slab. Details of the slab and the modeled area are shown in Figure 2a, 2b. Double layers (top and bottom) of 12 mm diameter reinforcing bars at 100 mm spacing around columns and 16 mm diameter bars at 300 mm spacing elsewhere in the slab have been provided. The concrete compressive strength is assumed to be 37 MPa. The reinforcing steel is modeled as hot-rolled reinforcing bars with yield strength of 400 MPa with 22 mm concrete cover. The thermal and mechanical properties of the concrete and reinforcing steel are assumed based on Eurocode 2. The slab is considered to be subjected to uniformly distributed load of 9.62 KPa which includes the self-weight, superimposed dead load and live load for an office building.

SAFIR, a finite element based computer program developed at the University of Liege in Belgium [14], has been used for thermal and structural analysis of fire resistance of slabs for performing nonlinear two and three dimensional analysis of steel, concrete, and composite structures. The behavior of a structure in fire is simulated in the program as a function of time using the temperature distributions in the structural elements evaluated from a thermal analysis.

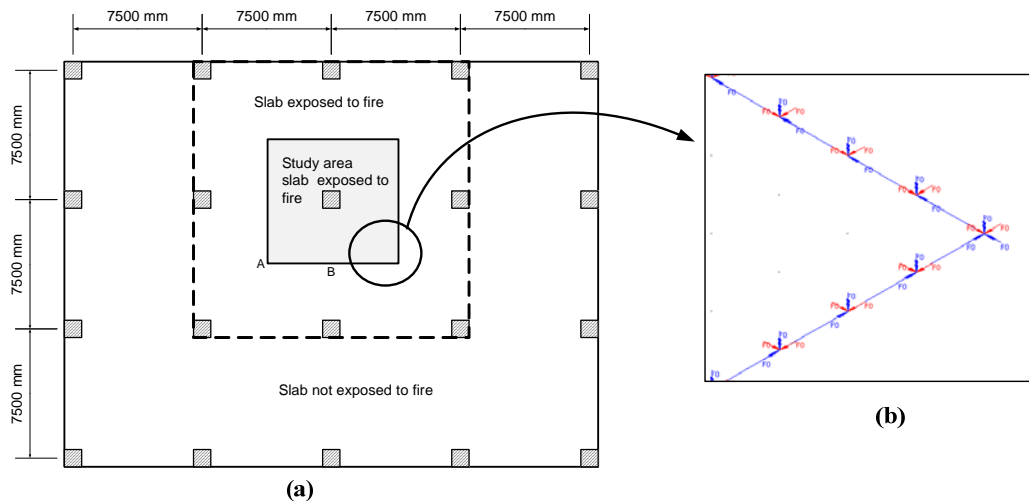


Figure 2. a) Study area of concrete slab and b) boundary condition of proposed model.

In this paper, other software, SAFE [15] and Direct Design Method (DDM) [16] have been used to compare the results with the base results obtained by SAFIR to check SAFIR model. A mesh size of 250 mm is found to be appropriate to obtain a reasonable accuracy with acceptable computational time. Figure 2a shows the proposed model for a two-way flat plate concrete slab with a 400 mm rectangular column in the middle of the 7.5 m span and boundary conditions, for modeling tensile membrane action. Symmetrical boundary conditions are applied on the four edges of the meshed domain. The centerlines of a slab panel are assumed to represent the lines of symmetry for the panel, and they are considered to have transverse (vertical) movement only (Figure 2b).

Using the present FE model, the deflection at the center of the slab (point A) was found to be 0.551 mm and that at the midway between columns (point B) is 0.426 mm under service loads condition. Based on Eurocode, the following reinforcements are provided in the slab: 1200 mm²/m steel bars on the top face around the columns, and 430 mm²/m for on the top face between the columns. A minimum reinforcement of 340 mm²/m is provided for all other sections including mid span.

FE MODEL EXPOSED TO FIRE

Experimental results show that the vertical displacement at position A is 24 mm and that at B is 22 mm for fire duration of 21 minutes [12]. Displacement in this paper refers to the deflection under fire loads only (after filtering the deflection due to service loads). After 21 minutes, the instruments malfunction and no further data could be recorded. As observed in the test, spalling of concrete from soffit of slab occurred after 12 minutes of fire followed by large displacements in slab especially in areas where tensile membrane action could not prevent such deflections. Displacements at 10 minutes before spalling were reported to be between 1 to 2 mm at the center of the slab and between the columns [12]. In this period of time the proposed FE model under parametric fire shows 1.86 mm deflection in center and 1.57 mm between columns (Figure 3).

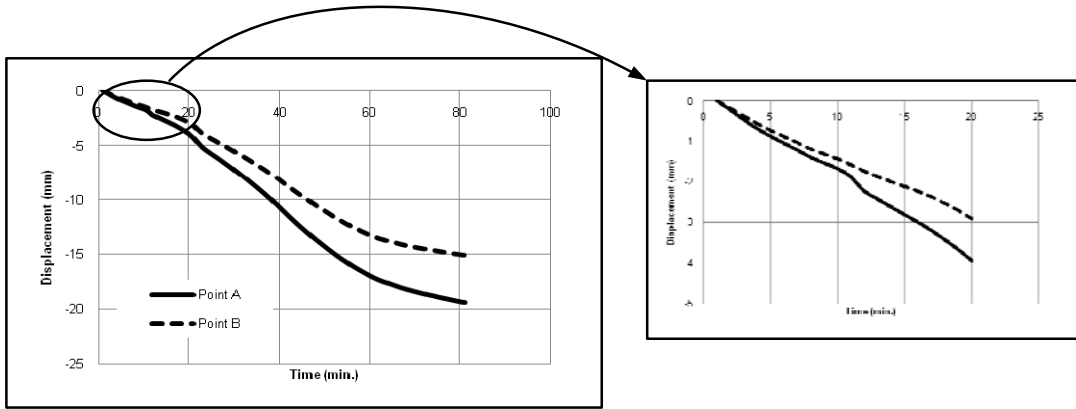


Figure 3. Displacement of the slab at A (slab center) and B (between columns) under design fire.

Both UK and European codified design methods suggest that concrete spalling within the fire compartment could be ignored during the design. It is clear in the numerical results that a displacement of 20 mm is reached at 80 minutes when spalling is not considered, while the same displacements occur in just 17 minutes in the test where spalling occurs. Although SAFIR can be used to predict the fire response of slab, the model does not account for fire to include spalling of concrete.

The experimental test conducted in [12] shows that the temperature is reduced initially for 12 to 13 minutes, and after that the average atmosphere temperature, at 300 mm below the soffit of the slab, remains between the design fire and ISO curve for 25 minutes until the instruments stop working. Figure 4 shows the displacements from the current numerical analysis at the midpoint of the slab (A) under standard and parametric fire curves. The full length of the slab in this paper is assumed to be exposed to parametric (design) fire from the bottom face. While only one type of slab is considered here, it is analyzed for cases with different values of the parameters considered. The available experimental results that is described before is used to verify the base case in the numerical approach.

PARAMETERS CONSIDERED

Concrete generally provides relatively fire resistance properties. It does not burn and emit any toxic fumes, smoke or drip molten particles when exposed to fire.

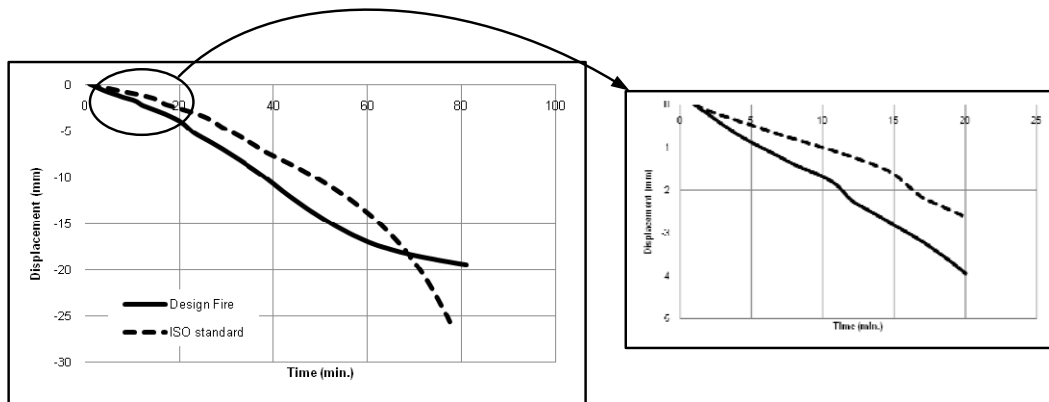


Figure 4. Analytical displacement of A under parametric and design fire.

F

The parametric fire used in this study has a high maximum temperature and relatively short duration (30 minutes). A high temperature, short duration fire, may induce concrete spalling due to the thermal shock, whereas a lower temperature but longer duration will result in a greater average temperature in the concrete members.

Compressive strength of concrete

Fire performance of concrete is controlled by type of aggregate and the cement paste. Concretes are conventionally classified as normal-weight concrete (NWC), lightweight concrete (LWC), depending on the density of the aggregates used. Concrete has a low thermal conductivity (50 times lower than steel) and therefore heats up very slowly during a fire [17]. The behavior of reinforced concrete slabs under high temperature is mainly affected by the strength of the concrete.

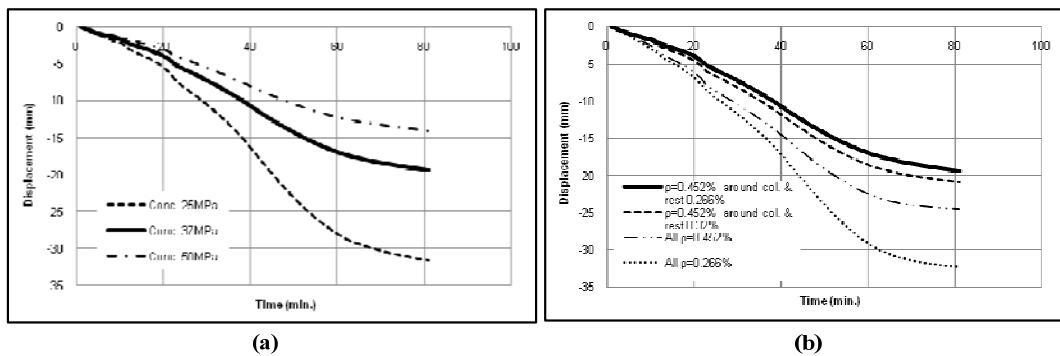


Figure 5. Vertical displacement of slab (point A) under various a) compression strength b) reinforcing slab scenarios.

Normal density concrete with a crushing strength of 37 MPa was used in the experimental test. In the current study, the compressive strength of concrete is varied. Figure 5a shows the vertical displacement at the center of the slab for various compressive strength. The displacement increases faster for low compressive strength of concrete. In Location “A” for 25 MPa concrete, the displacement is about 34 mm in 80 min and that for 37 MPa concrete is 20 mm.

There has been significant interest recently in high-strength concrete (HSC) as a high performance construction material due to its superior strength (with compressive strength at least 50 MPa), stiffness and durability. High strength concrete has a relatively higher strength loss when exposed to the same heating condition than normal strength concrete, since high strength concrete is prone to explosive spalling [17]. As seen in experimental test, high temperatures affect the strength of the HSC by explosive spalling which affects the integrity of the structure.

Reinforcement Steel

Area of reinforcing steels has significant effects on the performance of two-way flat plate slabs. The base FE model has a 0.452% reinforcing steel around columns and 0.266% in other areas. Figure 5b shows displacement of slab under various

reinforcing scenarios. It is clear from the figure that the smallest displacement occurs when ratio of reinforcement is around the standard design. Higher reinforcement at the center of slab, and/or lower reinforcements around the columns results in larger displacement at center of the slab.

Imposed Load

The loads on the experimentally tested structure represented an office building with imposed live load of 2.5 KPa. The behavior of structures subjected to fire can be treated as an accidental limit state, with appropriate load factors. These factors are specified by the design codes (e.g., ENV 1991-1 [18] and BS5950 part 8 [19]). Various imposed load scenarios are shown in Figure 6a. As shown in this figure, an increase of 21.5% in imposed loads from 9.25 KPa to 11.25 KPa results in 46% increase in displacement in 30 minutes fire and 63% in 60 minutes. Also 43% increase in such loads causes 205% increase in displacements in 30 minutes fire and 286% increase in 60 minutes fire. Thus it is important for heavy live load areas such as cinema, and parking garages to give special attention for fire safety design.

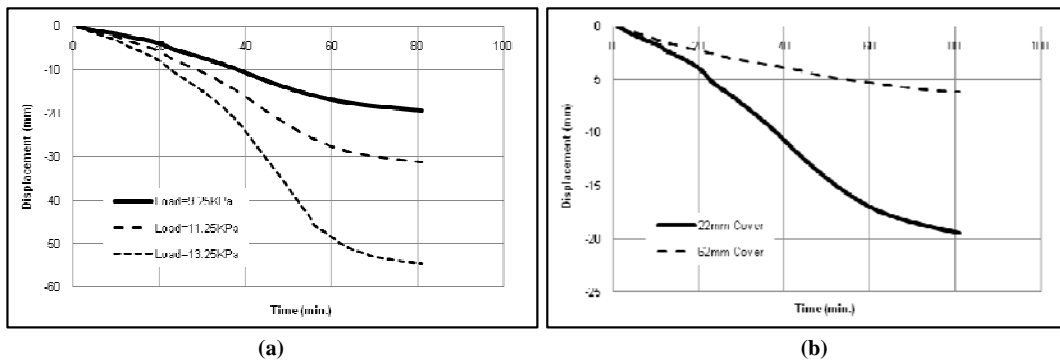


Figure 6. Vertical displacement of slab (point A) under various a) service load b) concrete cover scenarios.

Concrete Cover

For reinforced concrete members such as slabs, the fire resistance is principally based on the amount of flexural reinforcements and the concrete cover to the reinforcing steel. According to Eurocode 2, the minimum thickness of clear cover provided to steel reinforcements for concrete flat slab for a fire rating of 90 min should be 20 mm [13]. As shown in Figure 6b, providing 62 mm instead of 22 mm cover of bottom reinforcement results in 56% decrease in the mid span displacement in 30 minutes and 69% in 60 minutes fire.

CONCLUSION AND RESEARCH NEEDS

While concrete structures are assumed to be very robust in fire exposure, there are many issues that need to be considered for safer design. Thermal exposure may cause sudden failure of the concrete structural units. The behavior of two-way flat plate slab under combined elevated temperatures and gravity loading was studied in this paper. Combined fire and imposed loading can severely change structural

behavior. FE model in SAFIR program has been utilized to study various scenarios such as the effects of compressive strength of concrete, amount of reinforcing steel, magnitude of imposed loads, and the thickness of concrete cover. It was found that the fire performance of a concrete flat plate slab is very sensitive to the the above mentioned parameters. Further investigation needs to be conducted to simulate more complex scenarios to include spalling and hygrothermal effects.

REFERENCES

1. Nwosu, D.I., Kodur, V.K.R. 1997. "Steel Structures Exposed to Fire—a state-of-art report" IRC, National Research Council of Canada, Ottawa, Ont., Internal Report No. 749, pp. 1–32.
2. Ghoreishi, M., Bagchi, A., Sultan, M.A. 2009. "Estimating the Response of Structural Systems to Fire Exposure: State-of-the-Art Review", 11th Int. Conf. on Fire and Materials, San Francisco, CA., pp. 475–483.
3. Nizamuddin, Z. T. 1976. "Thermal and structural analysis of reinforced concrete slabs in fire environments". Ph.D. thesis, University of California, Berkeley, CA.
4. Huang, Z., Burgess, I. and Plank, R.J. 2003, "Modeling membrane action of concrete slabs in composite building in fire. I: Theoretical development", ASCE J of Structural Eng, V 129, No.8.
5. Nechnech, W., Meftah, F., Reynouard, J.M. 2002. "Elasto - plastic damage model for plain concrete subjected to high temperatures", Engineering Structures 24, pp. 597–611.
6. Wade, C., 1992. "Fire resistance of New Zealand concretes (Study Report No. 40)", Judgeford: BRANZ, The Resource Centre for Building Excellence.
7. Cooper, L. Y., Franssen, J-M. 1999. "A Basis for using Fire Modeling with 1-D Thermal Analyses of Partitions to Simulate 2-D and 3-D Structural Performance in Real Fires". Fire Safety Journal. 33-2, pp.115–128.
8. Issen, L.A., Gustaferro, A. H., Carlson, C.C. 1970. "Fire tests of concrete members: An improved method for estimating thermal restraint forces." Fire Test Performance, ASTM, STP 464, American Society for Testing and Materials, Philadelphia, pp. 153–185.
9. Anderberg, Y., Forsen, N. E. 1982. "Fire resistance of concrete structures." Division of Structural Mechanics and Concrete Construction, Lund Institute of Technology, Lund, Sweden.
10. Cooke, G.M.E. 1993. "Results of tests on end-restrained reinforced concrete floor strips exposed to standard fires." Report prepared for the Construction Directorate of the Department of the Environment, Fire Research Station, Hertfordshire, U.K.
11. Lim, L., Buchanan, A., Moss, P., Franssen, J.M. 2004. "Computer Modeling of Restrained Reinforced Concrete Slabs in Fire Conditions" ASCE J of Structural Eng. 130, p.p. 1964–1971.
12. Bailey, C., 2002. "Holistic Behavior of Concrete Buildings in Fire". Proceedings of the Institution of Civil Engineers, Structures and Buildings. 152 Issue 3, pp.199–212.
13. Eurocode 2, 2002. Design of concrete structure, Part 1-2: General rule—structural fire design, prEN 1992-1-2.
14. Franssen, J.M. 2003. "SAFIR: A thermal/structural program modeling structures under fire". Proc., North American Steel Construction Conf., American Inst of Steel Constr, Baltimore.
15. SAFE, 2010, Computers and Structures Inc., Berkeley, CA., USA.
16. CAN/CSA A23.3-04, "Design of concrete structure.", Can Standards Assoc, Rexdale, ON.
17. Moore, D., Lennon, T., Wang, Y. 2007. "Designers' Guide to En 1991-1-2, 1992-1-2, 1993-1-2 and 1994-1-2: Handbook for the Fire Design of Steel, Composite and Concrete Structures to the Eurocodes", Thomas Telford Services Ltd.
18. DD ENV 1991-1: 1996. "Eurocode 1. Basis of design and actions on structures. Basis of design (together with U.K. national application document)". British Research Institution, London.
19. BS5990 Part 8: 1990. "Structural use of steelwork in buildings: Part 8: Code of practice for fire resistant design. British Standard Institution, London.

Structural Behavior of Reinforced Pre-Compressed Concrete (r.c.) Structures in Fire: Paradigms and Lessons from Experience

D. MAXIA¹, A. PORCU², R. PORCU³ and S. TATTONI⁴

ABSTRACT

In this paper two case studies are discussed with particular regard to the structural behavior of reinforced concrete during fire; remarks are based on the reports of the fire brigade. The fire load was recreated and the fire spread simulated in order to understand the true thermal load acting on the structural elements.

As a preliminary result we ascertained a considerable difference between the actual fire resistance R and the requested one (usually 120 min). The reason for such a difference is frequently found in the lack in design details and in insufficient care in assembling the elements of the structure.

As a consequence some elements can fall abruptly from their position without the development of plastic hinges, as assumed by the current calculation methods.

FOREWORD

Following current technical rules (EN 1992-1-2), it is possible to assess fire resistance of ordinary reinforced concrete structures by means of member analysis (tabular methods or simplified calculation methods) subjected to a conventional time-temperature curve (standard fire). Nevertheless, this approach does not lead necessarily to a safe design for situations of fire, in particular when dealing with pre-cast structures. For this type of structure damage often exceeds causal circumstances.

CASE HISTORY 1

Description of the structure

The structure is an 8m high rectangular industrial warehouse (30m × 100m)

¹Structural Engineer, Fire Department – Cagliari—Italy

²Chief Structural Engineer, Fire Department – Cagliari—Italy

³Phd student - Cagliari University—Italy

⁴Professor of Structural Engineering, Cagliari University, via Marengo 2, 09123 Cagliari (CA)—Italy

with a shed roof supported by pre-compressed V section beams on r.c. pillars (fig. 1). The roof is made of ribbed slabs in pre-stressed reinforced concrete with 25mm minimum thickness (fig. 2).

The roof slabs rest on the beam edge concrete stamp whereas at the shed window the beams are supported by simple steel square-sectioned 50×50×2mm struts.

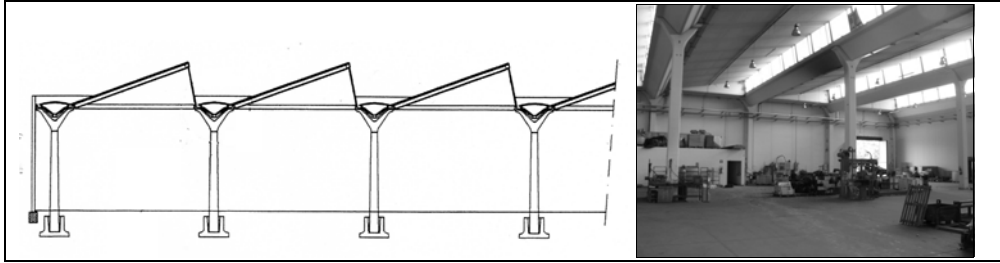


Figure 1. Transverse section and general view.

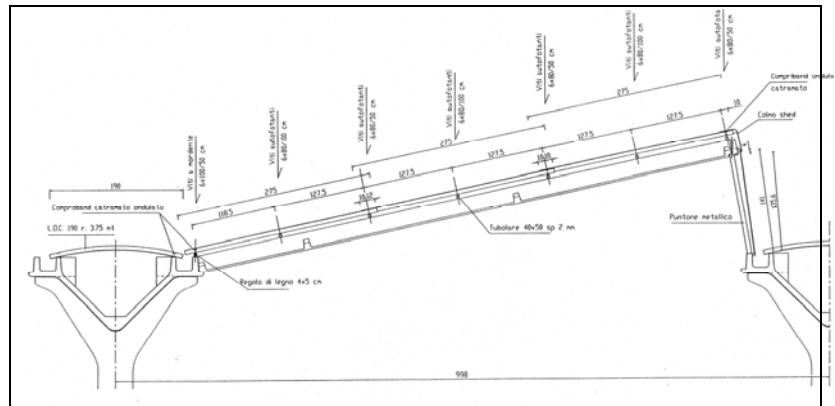


Figure 2. Transverse section on the shed cover.

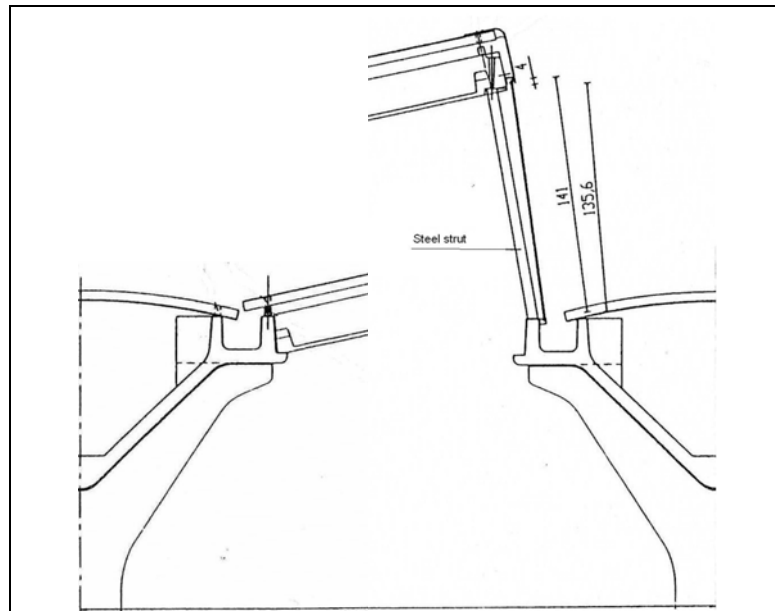


Figure 3. Details of supports of the cover slab: left on the beam, right on the shed window.

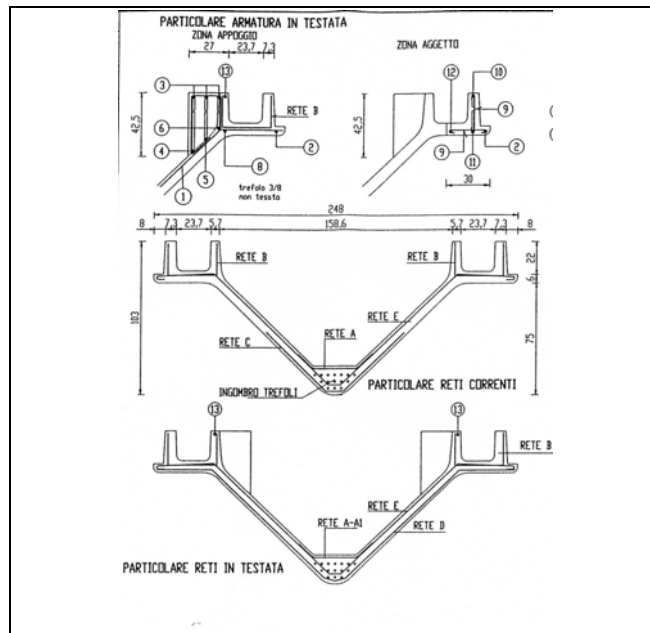


Figure 4. Transverse section of the main beams in pre-stressed reinforced concrete.

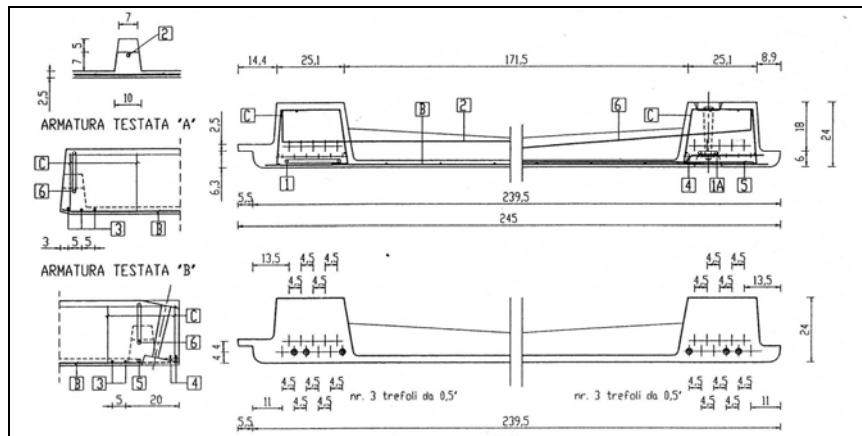


Figure 5. transverse section of the cover slab in pre-stressed reinforced concrete.

Following Fire Department guidelines, the structure was designed for REI 120 destined for the assembly of electrical equipment.

This performance conforms to resistance to fire requirements for the necessary time to manage an emergency for a fire load $q_{fd} \leq 1800 \text{ MJ/m}^2$ (Italian standard LIV. III, D.M. 9/03/2007).

Fire description

As well as equipment, combustible packaging materials for the finished products were accumulated in a limited area of the warehouse.

The fire developed in this area and therefore was limited and isolated. Maximum temperature was estimated not to be higher than 400°C (Fire department estimate).

Damage to scaffolding resulted compatible with the temperatures indicated above.



Figure 6. Shelves partially deformed by heat.

Structural damage

Despite the structure having an elevated resistance to fire and the fire load itself being low, significant structural damage was seen to the scaffolding with panels collapsing and important deformation clearly visible in both the areas directly affected by the fire and surrounding areas.

These deformations involved main beams probably due to loss of pre-compression and the ribbed slabs of minor height.

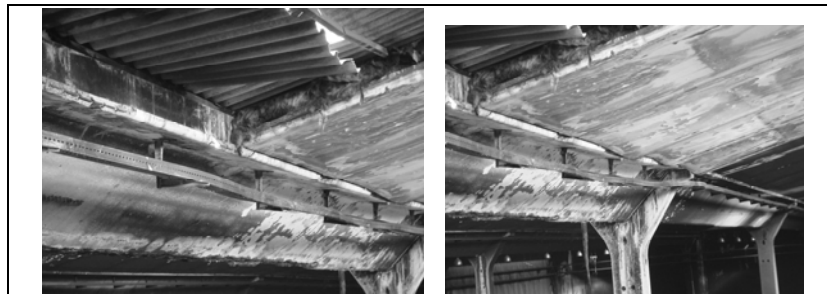


Figure 7. Slabs fell from their supports breaking the concrete stamp. In the photo on the right we can see the deformation of the 25mm concrete slab.

Critical points

REI 120 resistance had been verified by analytic calculus limited to the single structural elements (pillars, main beams, ribs, cover ribbed slabs) independently of each other.

No specific exam, nor particular observations regarding the connections between various elements were adopted.

In particular the structure revealed its vulnerability: for the unprotected metallic struts that did not collapse thanks to the modest temperature developed and to the relatively short duration of the fire.);

for the fragility of the concrete prominence of modest dimensions without any form of reinforcement.



Figure 8. On the left view of left metallic strut about to collapse due to buckling, on the right view of the split prominence.

CASE HISTORY 2

Description of the structure

Eight-storey office tower block built in the 70's. From a structural viewpoint the building is characterized by metallic floor structure (beams and corrugated steel shed with cast concrete cooperative) suspended by a system of stainless tie along the perimeter and reinforced concrete core.

The linking system of suspended stainless tie is made of two serrate shells against the stainless tie that are continuous for the whole height of the building. The transmission of the binding reaction on the deck to the suspension stainless tie is therefore dependant on the friction between the steel wires and shells.



Figure 9. On the left general view of the building and effect of fire, in the center the main structure, on the right the suspension device.

When the structure was built no specific regulations were in force concerning resistance to fire for office buildings. At present, it corresponds to the III performance level (Italian standard LIV. III, D.M. 9/03/2007). This level conforms to a fire load of $q_{fd} \leq 450 \text{ MJ/m}^2$.

Fire description

Effective fire load was well below the above mentioned level, equal to resistance REI 30.

Combustible material was scarce and equally distributed and comprised primarily by office furniture. No archives or files were present.

The fire developed in one room and the maximum estimated temperature did not exceed 500–600°C except for a few minutes, if at all. Given that the glass windows shattered almost instantly, flames spread to the office above without causing significant damage.



Figure 10. on the left view of fire effects on façade, in the center damage in the room where fire developed, on the right damage in the office above.

Structural damage

The main structure (steel beams and corrugated steel shed) did not suffer any significant damage.

The steel rods did not resent the effect of heat although their protective covering was totally destroyed or completely absent in certain points.

Critical points

The danger of the steels wires plastic collapsing or, even worse, the sliding of the shells along the steels wires or their loss or friction reduction, was avoided thanks to the short duration of the fire.

The critical points of the system can be found in the scarce protection from fire of the stainless tie and in the floor-stainless tie connection system based entirely on friction and 6 high- resistance steel bolts that lost effectiveness due to the heat.



Figure 11. Particular of the shells joint.

CONCLUSION

In the illustrated examples it is clear how scarce attention to construction details and in particular to connection systems between the various structural components can cause greater or non-proportional damage to an accidental fire of modest entity.

Therefore, verification of the REI resistance requisites of the main structural components is a necessary condition but is not sufficient in order to guarantee the required requisites of the whole structure.

REFERENCES

1. EN 1992-1-2
2. Italian Standard D.M. 9/03/2007
3. Italian Standard D.M. 16/02/2007
4. Dassori E., "La prefabbricazione in calcestruzzo, guida all'utilizzo nella progettazione", *Assobeton BE-MA editrice*, 2001.

Spalling of Normal Strength Concrete Walls in Fire

M. GUERRIERI and S. FRAGOMENI

ABSTRACT

A standard fire test was conducted on four slender concrete walls incorporating two different loading conditions: The first loading condition considered the effect of in-plane loading at the midspan, uniformly distributed load at two edges in addition to self weight. This loading condition is representative of a load bearing wall which supports the above floors and roof structures. The second load case considered the effect of self weight only which is representative of tilt-up wall panels. In each loading condition, two identical samples were tested in regards to their spalling performance. The specimens (1300 x 1300 x 50 mm) were tested at an age of six months when the compressive strengths were in the order of 40 MPa. The specimens were exposed to the standard fire on one side (compression side).

Explosive spalling only occurred in one of two panels which were exposed to fire under self weight only. In comparison, no spalling occurred on the walls which were loaded both in-plane and due to self weight and exposed to fire. This is due to the flexural cracking which occurred on the unexposed surface of these walls thus allowing significant amounts of steam and water migrating out of the specimen on the unexposed side during the testing. This water and steam migration eliminated the build-up of pore water pressure thereby eliminating the threat of explosive spalling.

The results show that pore pressure build-up and flexural cracking due to support conditions plays a major role in the spalling performance of concrete walls exposed to fire. In addition, the fact that the compressive strength was quite low and the specimens were very slender (both conditions which normally reduce spalling) suggests explosive spalling occurs when all contributing factors coincide at a converging point during the heat exposure. This explains why explosive spalling occurs randomly in a majority of tests reported.

Maurice Guerrieri, Ph.D., Postdoc Research Fellow, CESARE, Victoria University, Werribee, PO Box 14428, Melbourne 8001, Victoria, Australia
Sam Fragomeni, Ph.D., A/Professor in Structures, School of Engineering and Science, Victoria University, Footscray Park, PO Box 14428, Melbourne 8001, Victoria, Australia

INTRODUCTION

Concrete is the most widely used construction material for the nation's physical infrastructure, especially when compared to alternatives such as steel and timber. In addition, concrete is generally considered to have good fire resistance properties as it does not melt or burn like steel and timber. However, concrete is susceptible to a less known phenomenon termed *spalling* in fire. Spalling of concrete in fire is the dislodgement of small pieces of concrete up to 50 mm (popping out) from the surface of the concrete, often explosive in nature. If the degree of spalling is significant, the load bearing capacity of the concrete member can be reduced due to: (1) reduction in its cross-sectional size, and (2) rapid increase in temperatures of the reinforcement. Spalling of concrete in fire is a poorly understood phenomenon that occurs due to a complex interplay between numerous parameters in the material and/or structure [1] and as a result, has been often overlooked in international building codes, including the Australian concrete code (AS3600) [2].

Slender reinforced concrete walls have been used widely in the form of tilt-up and precast walls due to their low cost, ease of placement and architecturally pleasing benefits [3]. These walls typically serve two main purposes in a building. Firstly, these walls carry the structural loads which consist of lateral loads due to shear and wind loads, in addition to eccentric inplane loads from the floors and roof above. Their second purpose which is often overlooked is that they work as a fire wall in preventing the migration of a fire spreading to adjacent rooms within the structure. According to the current Australian Standards, (AS3600) [2], walls with height-to-thickness ratios between 20-50 can be subjected to inplane loads of up to 3% of their crushing strength, irrespective of the load's eccentricity and fire resistance period [3]. In regards to the fire resistance level, AS3600 [2] specifies fire resistance levels (FRL in mins) in which a structural concrete component has to perform regarding its structural adequacy, integrity and insulation. These FRLs are based on tabulated values for minimum dimensions and cover to reinforcement depths which in essence are concerned with delaying the temperature increase of the reinforcing or prestressing steel (insulation criteria) in order to sustain the load bearing capacity of the reinforcement (adequacy criteria). In reality, whilst sufficient cover may hinder the transfer of high temperatures to the reinforcement and provide higher fire resistance periods, the issue of concrete spalling and the performance of concrete at elevated temperatures are of much greater significance. Both of these issues begin from the onset of the concrete being exposed to the fire whereas the temperature increase of the reinforcement is a time delayed process. These issues are really only raised in the design of concrete tunnels, however, they are just as critical in the design of all concrete members exposed to fire, for example, tilt up walls.

LITERATURE REVIEW

The work carried out by Crozier & Sanjayan [3] is the only published experimental study to date which has investigated the fire performance of slender normal strength (NSC) and high strength (HSC) concrete load bearing walls, which were placed horizontally and exposed to fire on the tension side. The aim of their work was to investigate experimentally the behavior of slender walls subjected to the standard fire conditions specified in ISO 834-1 [4] under

(1) eccentric in-plane loading + lateral loading conditions, and (2) lateral loading only.

Eighteen slender reinforced concrete walls measuring 3.6m x 1.2m were prepared at varying slenderness ratios i.e. by varying the thickness from 75 mm, 100 mm and 150 mm while keeping the dimensions constant. Along with the wall thickness, the influence of the compressive strength (44 – 70 MPa), reinforcement covers, level of eccentric in-plane load and three supporting conditions were investigated. Eight walls were simply supported along two short edges which were tested under combined in-plane and lateral loads in order to investigate the influence of fire on the bending moment and the in-plane capacity. Another eight walls were also simply supported along two short edges and were only loaded laterally in order to investigate the influence of spalling and thermal bowing [3]. In order to investigate the influence of flexural cracking on spalling and thermal bowing, two walls were simply supported on three edges, two short and one long and were testing under lateral loading only.

In this investigation, structural collapse of the loaded specimen was deemed to have occurred if the specimen collapsed or if the deflection and rate of deflection were outside the limits imposed by AS 1530.4 [5]. The insulation and integrity criteria were not considered. From this investigation, Crozier & Sanjayan [3] showed that the NSC walls experience major spalling as compared to the HSC walls which had minor degrees of spalling. This is contrary to the well accepted theory that HSC is more susceptible to spalling due to the inability of the pore pressure build-up being able to dissipate as much in low permeable HSC than higher permeable NSC [6-9].

It was postulated by Crozier & Sanjayan [3] that the HSC walls had higher amounts of flexural cracking occurring which allowed the escape of pore water pressure and thus reduced the spalling tendency. Flexural cracking was higher in the HSC walls than the NSC as they were supported along two edges compared to three edges for the NSC walls. It was also shown that spalling was more dominant in thicker concrete walls which is due to the increased length in which the pore water pressure needs to travel in order to escape. Based on this theory, the investigation presented in this paper was conducted on the fire performance of slender reinforced walls which would be exposed to fire on the compression side. This would represent the worst case scenario in regards to spalling due to the pore water pressure build-up being hindered to escape due to the compression forces.

SIGNIFICANCE WITHIN THE RESEARCH FIELD

Concrete spalling has caused severe damage to concrete lining due to three major fire tunnel accidents in Europe, namely, Channel Tunnel in 1996, Mount Blanc Tunnel in 1999, and the St. Gotthard Tunnel in 2002 [10]. Slender reinforced concrete walls have been used widely in the form of tilt-up and precast construction due to their low cost, ease of placement and architecturally pleasing benefits [3]. These walls typically serve two main purposes in a building. Firstly, these walls carry the structural loads which consist of lateral loads due to shear and wind loads, in addition to eccentric in-plane loads from the floors and roof above. Their second purpose is that they act as a fire wall in

preventing the migration of a fire spreading to adjacent rooms within the structure.

As evident from the works of Crozier & Sanjayan [3], it is clear that serious considerations are warranted in regards to investigating effective measures to combat spalling of load bearing slender concrete walls in fire. Whilst these investigations have made significant contributions in this field, it is still unclear which parameters and variables and the combination of these influence the degree of spalling. This is because spalling has not been witnessed on a consistent basis on identical specimens exposed to identical fire conditions [11]. This research adds important experimental data to the existing knowledge on the behavior of load-bearing slender reinforced concrete walls in fire.

EXPERIMENTAL PROGRAM

CEMENTITIOUS MATERIALS

The chemical and mineral compositions of the cementitious material (binder) used as determined by XRF analysis is shown in Table 1. The binder used was ordinary portland cement (OPC) which was produced in Australia.

Table 1. Chemical and mineral compositions of cement.

Constituent/property %	OPC
SiO ₂	19.90
Al ₂ O ₃	4.70
Fe ₂ O ₃	3.38
MgO	1.30
CaO	63.93
Na ₂ O	0.17
TiO ₂	0.25
K ₂ O	0.45
MnO	0.08
P ₂ O ₅	0.06
SO ₃	2.54
LOI	2.97

MIX DESIGN, SPECIMEN GEOMETRY AND COMPRESSIVE STRENGTH MEASUREMENTS

The fine aggregate consisted of river sand, locally produced at Lynhurst with a specific gravity of 2.65, 24 hour water absorption of 0.5%, and a fineness modulus of 2.19. The coarse aggregate consisted of 14 mm maximum size basalt with a specific gravity of 2.95 and 24 h water absorption of 1.2%. The mix proportions used in this experimental program are given in Table 2.

Table 2. Mix proportions of mix concrete.

Constituent	kg/m ³
Cement	360
Slag	-
Fly ash	-
Coarse aggregate, SSD*	1130
Fine aggregate, SSD*	830
Free water	180
w/b	0.50

* SSD = Saturated Surface Dry Condition

The four slab specimens (1300 x 1300 x 50 mm) were reinforced with ribbed-wire mesh (100 x 100 mm spacing's and 6 mm diameter), the standard mesh reinforcement available in Australia. All specimens had one layer of reinforcement placed at approximately the mid-depth of the thickness.

The specimens were stripped at 24 hours and moist cured in a fog room at 23°C and 100% RH for 28 days. The wall specimens were then removed from the fog room and kept exposed to laboratory air at room temperature (approximately 23°C and 50% RH) until the test date (approximately six months where the compressive strengths were of the order of 40 MPa) . The weight measurements indicated that by 180 days, the specimen weight losses were stabilized indicating that the specimens were in dry condition avoiding the possibility of any spalling due to steam pressure build-up.

SPALLING TEST SETUP

The spalling test was conducted in a gas firing furnace that was programmed to follow the standard fire curve ISO 834-1 [4] as shown in Fig.1 which also shows the furnace fire curve. The specimens were tested in a vertical position with fire exposed on one side. This represents fire exposures commonly associated with wall fires in building.

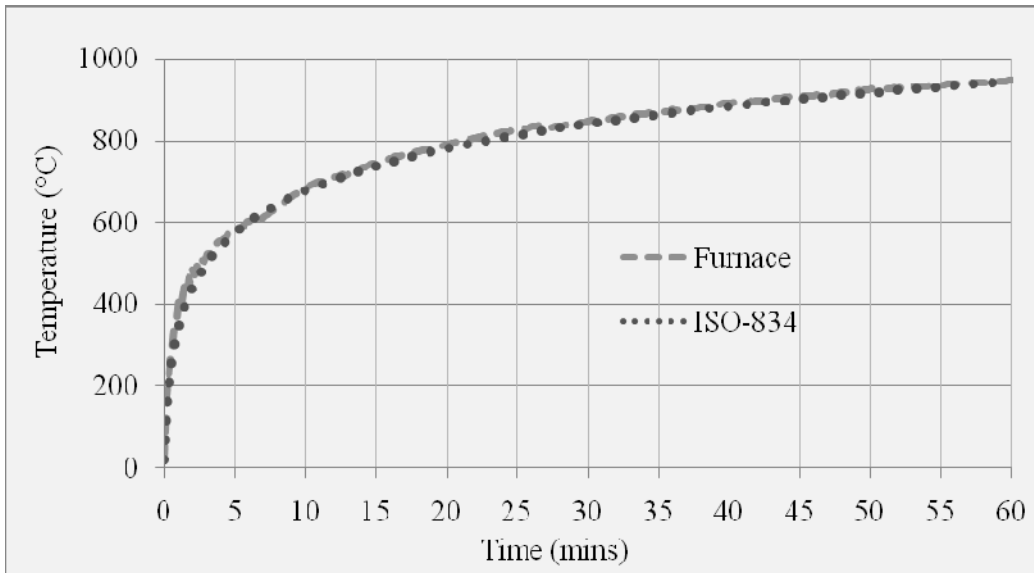


Figure 1. Comparison between ISO-834 and furnace fire curves.

Two of the four specimens were loaded during the fire exposure (compression side was exposed to fire) to consider the effect of in-plane load at the midspan, i.e. uniformly distributed load at two edges in addition to self weight. This loading condition is representative of a load bearing wall which supports the above floors and roof structures. Previously, Crozier & Sanjayan [3] exposed the tension side of walls to fire. The results from these authors were used for comparison reasons. The second load case considered the effect of self weight only which is representative of tilt-up wall panels. The idealized and actual fire setup can be seen in Fig. 2 and Fig. 3 respectively.

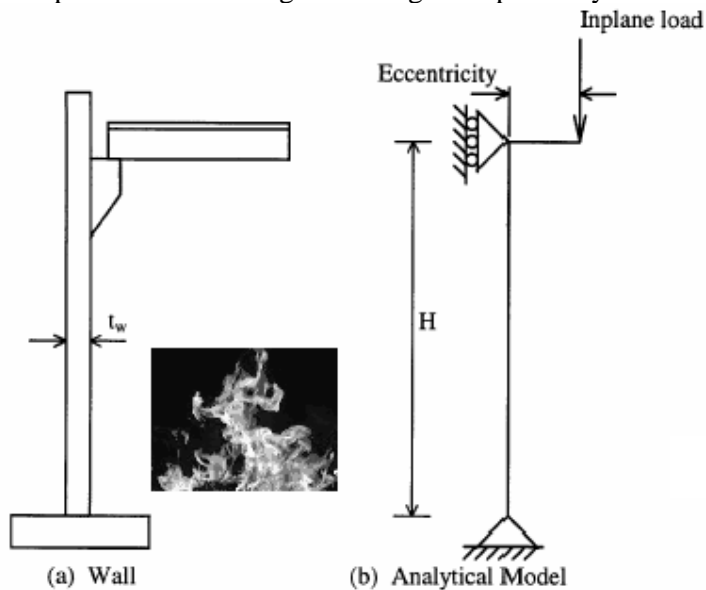


Figure 2. Ideal fire test setup.

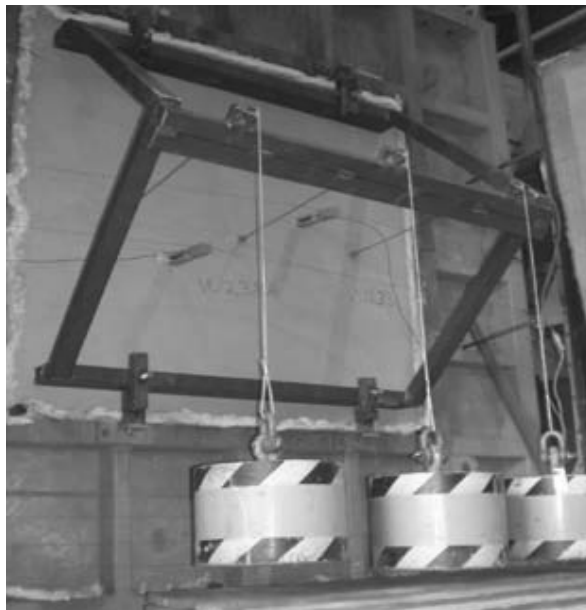


Figure 3. Actual inplane loading setup.

EXPERIMENTAL RESULTS AND DISCUSSION

SPECIMENS LOADED DUE TO SELF WEIGHT AND IN-PLANE LOADING

Flexural cracking on the unexposed surface was observed in both of the wall panels which were loaded both in-plane and by self weight. As a result, significant amounts of steam and water migrated out of the specimen on the unexposed side during the testing. Both panels were seen to undergo reduced curvature and pull in towards the direction of the fire exposure. This is due to the reduction in bending moment and elastic modulus which progressively decreases as a function of fire duration and temperature [12, 13].

One of the two panels tested failed due to brittle failure whilst the other panel survived the fire test. In both instances, surface spalling was observed to have occurred on the side exposed to fire. Explosive spalling did not occur due to both specimens experiencing sufficient flexural cracking to avoid the build-up of pore pressure. The brittle failure observed may have been caused by the thermo-incompatibility between the cement paste and aggregates and the thermal gradient across the 50 mm thick section. This is in addition to the strength deterioration of the concrete itself due to the decomposition of the hydrates [14, 15].

SPECIMENS LOADED DUE TO SELF WEIGHT

Both specimens loaded only by their self weight, failed the fire test after a fire exposure of 15 minutes. In specimens, flexural cracking and steam release occurred on a significantly smaller scale than the specimens which were loaded in-plane. Explosive spalling occurred in one of the two specimens which in addition to the reduce levels of flexural cracking, adds weight to the argument that the explosive spalling occurred due to the build-up of pore water pressure.

However, brittle failure was the cause of structural failure in the other specimen which was possibly caused by the thermal-incompatibility between the concrete *paste* and aggregate. Hence, it is unclear to scientifically establish the cause of explosive spalling. However, it is well regarded that explosive spalling is due to the combination of pore pressures and differential thermal stresses as first described by Bazant and Thonguthai [16] and later adapted by Anderberg [17], Harada and Terai [18], Consolazio, McVay and Rish [8], Ulm, Coussy and Bazant [19], Khoury [20], Kalifa, Chene and Galle [9], Phan and Carino [21], Tenchev, Li and Purkiss [22], Khoury et al. [23] and Yanko [24]. These authors believe that spalling is largely due to a combination of the moisture presence and rapid heating rates. The high heating rates cause thermal gradients in addition to accelerating the moisture release and the build-up of the pore pressures.

These two mechanisms can act singly or in combination depending upon the section size, the type of concrete, and the moisture content. Explosive spalling occurs when the combination of these pressures exceed the tensile strength of the concrete material. In most structures, compressive loading is present, e.g. concrete tunnel lining, which in addition to the induced pore water pressures and thermal stresses, can increase the probability of explosive spalling occurring [20]. The theory behind the combined pore pressure and thermal stress mechanisms is that explosive spalling is a result of pore pressure compression in the region closest to the surface (caused by thermal stresses and external loading), and internal cracking [25]. During heating, cracks form in the material as the sum of the stresses exceeds the tensile strength of the material. The formation of cracks is accompanied by a sudden release of energy which can cause explosive spalling [25].

It is quite clear that pore pressure build-up and flexural cracking due to support conditions plays a major role in the spalling performance of concrete walls exposed to fire. In addition, the fact that the compressive strength was quite low and the specimens were very slender (both conditions which normally reduce spalling) suggests explosive spalling occurs when all contributing factors coincide at a converging point during the heat exposure. This explains why explosive spalling occurs randomly in a majority of test reported [6, 11, 21, 26, 27].

Figs. 4a-d respectively show the bowing of the specimens, the flexural cracking, pore water pressure release, surface spalling and explosive spalling of the specimens tested.

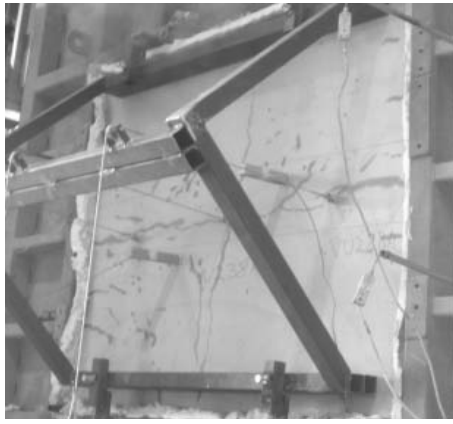


Figure 4a. Bowing, flexural cracking and pore water pressure release.

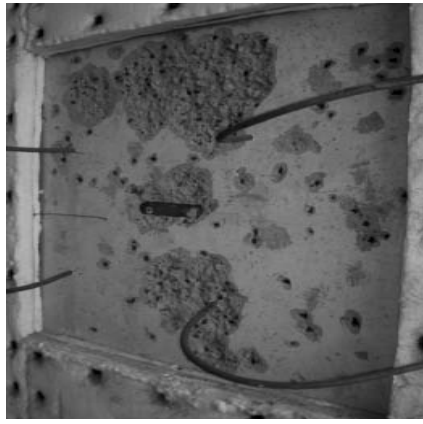


Figure 4b. Minor surface spalling.



Figure 4c. –Severe surface spalling.



Figure 4d. Explosive spalling.

CONCLUSIONS

Explosive spalling only occurred in one of two panels which were exposed to fire under self weight only. In comparison, no spalling occurred on the walls which were loaded both in-plane and due to self weight and exposed to fire. This is due to the flexural cracking which occurred on the unexposed surface of these walls, thus allowing significant amounts of steam and water migrating out of the specimen on the unexposed side during the testing. This water and steam migration eliminated the build-up of pore water pressure thereby eliminating the threat of explosive spalling.

The results show that pore pressure build-up and flexural cracking due to support conditions plays a major role in the spalling performance of concrete walls exposed to fire. In addition, the fact that the compressive strength was quite low and the specimens were very slender (both conditions which normally reduce spalling) suggests explosive spalling occurs when all contributing factors coincide at a converging point during the heat exposure. This explains why explosive spalling occurs randomly in a majority of test reported.

ACKNOWLEDGMENTS

The research work presented in this paper was carried out as part of a final year project with the majority of the laboratory work conducted by the final year students; Sinapati Ulberg, Dean Stefanovic, Adrian Brincat and Daniel Zdraveski whilst they were at Victoria University. The authors of this paper were the co-supervisors and were responsible for the analyses of the experimental program

REFERENCES

1. Jansson, R., *Liquid / steam pressure measurement inside concrete exposed to fire*, in *Fourth International Workshop on Structures in Fire*. 2006: Aviro, Portugal. p. 747–755.
2. *Standards Australia. AS 3600 Concrete Structures*. 2009.
3. Crozier, D.A. and J.G. Sanjayan, *Tests of load-bearing slender reinforced concrete walls in fire*. *ACI Structural Journal*, 2000. 97(2): p. 243–251.
4. *ISO 834-1 Fire-Resistance Tests - Elements of Building Construction—Part 1: General Requirements*, 1999. 1999.
5. *AS 1530.4: Methods for fire tests on building materials, components and structures - Fire-resistance test of elements of construction* 2005.
6. Phan, L. and N. Carino, *Mechanical properties of high strength concrete at elevated temperatures*. 2001, Building and Fire Research Laboratory, National Institute of Standards and Technology: Gaithersburg, Maryland.
7. Harmathy, T., *Effect of moisture on fire endurance of building elements*. 1965, American Society for Testing and Materials: Philadelphia. p. 74–95.
8. Consolazio, G., M. McVay, and J. Rish, *Measurement and prediction of pore pressures in saturated cement mortar subjected to radiant heating*. *ACI Materials Journal*, 1998. 95(5): p. 525–536.
9. Kalifa, P., G. Chene, and C. Galle, *High-temperature behaviour of HPC with polypropylene fibres - from spalling to microstructure*. *Cement and Concrete Research*, 2001. 31(10): p. 1487–1499.
10. Houry, G.A., C.E. Majorana, F. Pesavento, and B.A. Schrefler, *Modelling of heated concrete*. *Magazine of Concrete Research*. 2002. 54(2): p. 77–101.
11. Phan, L., *Fire performance of high-strength concrete: a report of the state-of-the-art*. 1996, Building and Fire Research Laboratory, National Institute of Standards and Technology: Gaithersburg, Maryland.
12. Hsu, J.-H. and C.-S. Lin, *Effect of fire on the residual mechanical properties and structural performance of reinforced concrete beams*. *Journal of Fire Protection Engineering*, 2008. 18(4): p. 245–274.
13. Hj, N.P., *Recent development in fire design of concrete structures*. *Structural Concrete*, 2008. 9(1): p. 3–9.
14. Mendes, A., J. Sanjayan, and F. Collins, *Phase transformations and mechanical strength of OPC/Slag pastes submitted to high temperatures*. *Materials and Structures/Materiaux et Constructions*, 2008a. 41(2): p. 345–350.
15. Guerrieri, M., J. Sanjayan, and F. Collins, *Effect of slag on the performance of concretes in hydrocarbon fire*. *ACI SP-255: Designing Concrete Structures for Fire Safety*, ACI-TMS Committee 216: Fire Resistance and Fire Protection of Structures, 2008. Paper number 2(2): p. 23–45.
16. Bazant, Z. and W. Thonguthai, *Pore pressure in heated concrete walls: theoretical prediction*. *Magazine of Concrete Research*, 1979. 31(107): p. 67–76.
17. Anderberg, Y., *Spalling phenomena of HPC and OPC*. 1997, Building and Fire Research Laboratory, National Institute of Standards and Technology: Gaithersburg, MD. p. 69–73.
18. Harada, K. and T. Terai, *Heat and mass transfer in the walls subjected to fire*. 1997, Building and Fire Research Laboratory, National Institute of Standards and Technology: Gaithersburg, MD. p. 423–435.
19. Ulm, F., O. Coussy, and Z. Bazant, *Chunnel fire, Part I: chemoplastic softening in rapidly heated concrete*. *Journal of Engineering Mechanics*, 1999. 125(3): p. 272–282.
20. Houry, G., *Effect of fire on concrete and concrete structures*. *Progress in Structural Engineering and Materials*, 2000. 2(4): p. 429–47.

21. Phan, L., J. Lawson, and F. Davis, *Effects of elevated temperature exposure on heating characteristics, spalling, and residual properties of high performance concrete*. Materials and Structures, 2001. 34(2): p. 83–91.
22. Tenchev, R., L. Li, and J. Purkiss, *Finite element analysis of coupled heat and moisture transfer in concrete subjected to fire*. Journal of Numerical Heat Transfer, Part A (Applications), 2001. 39(7): p. 685-710.
23. Khoury, G., C. Majorana, F. Pesavento, and B. Schrefler, *Modelling of heated concrete*. Magazine of Concrete Research, 2002. 54(2): p. 77–101.
24. Yanko, W., *Experimental and numerical evaluation of concrete spalling during extreme thermal loading*, in *Department of Civil Engineering*. 2004, University of Florida: Florida, USA.
25. Larsson, K., *Fires in tunnels and their effect on rock*. 2006, Lulea University of Technology, Department of Civil and Environmental Engineering: Lulea, Scandinavia. p. 60.
26. Phan, L. and N. Carino, *Review of mechanical properties of HSC at elevated temperature*. Journal of Materials in Civil Engineering, 1998. 10(1): p. 58–64.
27. Phan, L., N. Carino, D. Duthing, and E. Garboczi, *International workshop on the fire performance of high strength concrete*. 1997, Building and Fire Research Laboratory, National Institute of Standards and Technology: Gaithersburg, Maryland.

A Material Model for the Numerical Simulation of High Strength Concrete Columns Subjected to Fire Loading

S. HUISMANN, M. KORZEN and U. SCHNEIDER

ABSTRACT

This paper presents a material model for high strength concrete (HSC) at high temperatures. It includes all strain components in the mathematical stress-strain relationship. The main parameters of the model are the compressive strength and the modulus of elasticity. Their identification is based on own experimental tests [3]. The validation of the model was achieved with the results of a fire test of an axially loaded HSC column [4]. For the material behaviour of the reinforcement the Eurocode 2 (EC 2) [2] model with its properties was applied. The calculated displacements and the fire resistance time of the column as well as the material tests correlates well with the experimental results. Thereby it was found that the compressive strength has to be derived from transient creep and compressive strength tests.

1. INTRODUCTION

The EC 2 proposes a material model for concrete together with its parameters for advanced calculation methods. However, it is addressed to normal strength concrete. For HSC we have observed that the application this model including its parameters lead to results that are significantly unsafe. Therefore, a new material model was developed. The characteristic parameters of this model were obtained from own material tests [3]. In this paper it is shown that the use of this material model results in a realistic approximation of the deformation and the fire resistance time of HSC columns. Furthermore it will be demonstrated, which type of material tests have to be applied to identify the material properties of such a material model.

Sven Huismann (corresponding author), Ph.D. candidate, BAM Federal Institute for Materials Research and Testing, Unter den Eichen 87, 12205 Berlin, Germany.

Manfred Korzen, Ph.D., BAM Federal Institute for Materials Research and Testing, Unter den Eichen 87, 12205 Berlin, Germany.

Ulrich Schneider, Professor, University of Technology Vienna, Research Centre of Building Materials, Material Technology and Fire Safety, Karlsplatz 13/E206, 1040 Vienna, Austria.

2. MATERIAL MODELLING

For the material modelling the experimental investigations of [3] were taken as the basis. In the material tests the thermomechanical properties for temperatures up to 750°C were determined for HSC with polypropylene fibres and quartzite aggregates. The compressive strength was 110 MPa. The same HSC was used for the column in the fire test.

The parameters characterizing the thermal boundary conditions of the column were taken from the EC 2. However, the thermal conductivity λ and the specific heat c were modified in the temperature range from 20°C to 200°C. This modification is based on moisture effects in the high dense HSC. With these changes the calculated temperatures correlate well with the experimental results of the fire exposed concrete column [3], [4].

The material model for the thermomechanical behaviour of the HSC will be described with stress-strain-curves. They were developed on the basis of transient creep tests and compressive strength tests. The results of the transient creep tests are presented in Figure 1 (left). The total strain ϵ_{tot} can be separated according to (1) in the thermal strain ϵ_{th} , the elastic strain ϵ_{el} , the plastic strain ϵ_{pl} , and the transient creep strain $\epsilon_{tr,k}$ [7]. Because ϵ_{el} , ϵ_{pl} , and $\epsilon_{tr,k}$ are mechanically induced strains they can be merged in (2) to the mechanical strain ϵ_m (see Figure 2 (right)). The thermal strain corresponds to the total strain ϵ_{tot} with a load level $\alpha = 0$ ($\alpha = \sigma_i / f_c(20^\circ\text{C})$).

$$\epsilon_{tot} = \epsilon_{th} + \epsilon_{el} + \epsilon_{pl} + \epsilon_{tr,k} \quad (1)$$

$$\epsilon_m = \epsilon_{tot} - \epsilon_{th} = \epsilon_{el} + \epsilon_{pl} + \epsilon_{tr,k} \quad (2)$$

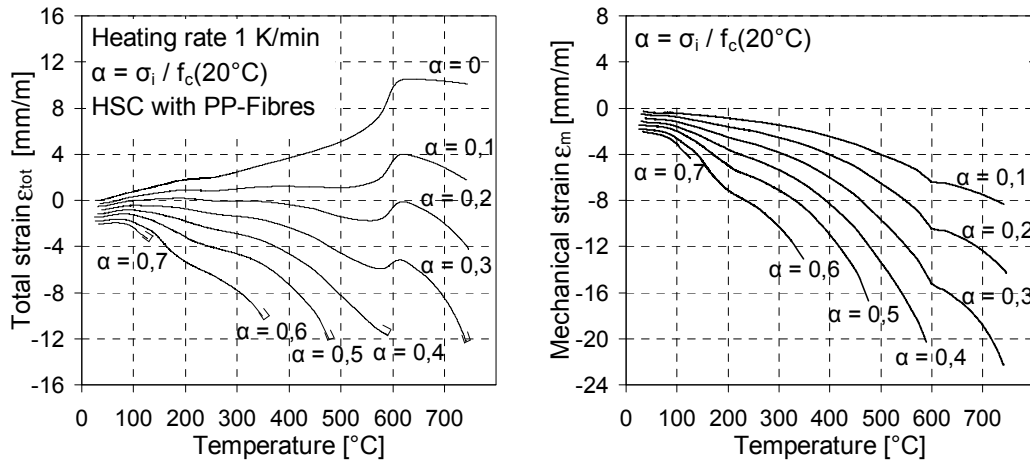


Figure 1. Total strain (left) and mechanical strain (right) according to (2) for HSC with pp-fibres under transient heating [3].

For each temperature T the mechanical strain with the corresponding stress will be transferred in a stress-strain-diagram. The mathematical description was done using (3) according to Thorenfeldt et al. [8]. It corresponds to the equation in Figure 3.1 from the EC 2 whereby n is a constant value ($n = 3$) and ϵ_{c1} is a given function of temperature, but in variance with (4). The parameter k describes the post peak behaviour of the stress-strain relation.

$$\sigma = f_c \cdot \frac{\varepsilon}{\varepsilon_{c1}} \cdot \frac{n}{n-1 + \left(\frac{\varepsilon}{\varepsilon_{c1}}\right)^{nk}} \quad (3)$$

$$\text{with } \varepsilon_{c1}(T) = \frac{f_c(T)}{E(T)} \cdot \frac{n(T)}{n(T)-1} \quad (4)$$

$$n(T) = 0,80 + \frac{f_c(T)}{17} \quad (5)$$

$$k(T) = \begin{cases} 1 & \text{for } \varepsilon_{c1}(T) > \varepsilon(T) > 0 \\ 0,67 + \frac{f_c(T)}{62} & \text{for } \varepsilon(T) \geq \varepsilon_{c1}(T) \end{cases} \quad (6)$$

$$20^\circ\text{C} \leq T \leq 1200^\circ\text{C}$$

The characteristic parameters of the concrete model are the compressive strength $f_c(T)$ and the modulus of elasticity $E(T)$. The peak stress strain $\varepsilon_{c1}(T)$ is defined by these functions.

The modulus of elasticity $E(T)$ equates with the tangent of (3) in the point of origin. The described approach considers all mechanical induced strain components under transient heating.

The compressive strength $f_c(T)$ corresponds with the peak stress of the stress-strain relation. There are different possibilities to estimate $f_c(T)$. One is to take it from stationary tests. Thereby the specimen is heated up with the constant load level α and after reaching the desired temperature T it will be loaded until failure [5]. The peak stress at this temperature is $f_c(T)$. The other way is to derive $f_c(T)$ from transient creep tests [6]. In this case $f_c(T)$ corresponds to the constant stress during heating at which the specimen fails at the temperature T . The different functions for $f_c(T)$ as well as the one from the EC 2 and a “lower bound” function are presented in Figure 2. They are labelled as “stationary”, “transient”, “lower bound”, and “EC 2”.

The “transient” function lies below the “stationary” curve for temperatures lower than 350°C . The difference originates from the evaporation behaviour of the free and physical bound water. Thereby the water wets the interior concrete surfaces whereby the surface energy is strongly reduced. If there is a stationary temperature condition for a longer period, like in the stationary tests, the water can partly evaporate from the specimen. This leads to an increase of the surface energy and thus to a higher compressive strength under “stationary” than under “transient” temperature conditions. For temperatures above 350°C the “transient” function lies between the “stationary” curves with $\alpha = 0$ and $\alpha = 0.2$ in the measured temperature range. The “lower bound” function corresponds with the “transient” function until 350°C and from 350°C to 600°C with the “stationary” curve with $\alpha = 0$. Above 600°C it merges with the EC 2 properties. This is constituted by the strong cracking at the outer parts of the column cross section, which exhibit such temperatures at the moment of failure. It can be assumed that the compressive strength in this area is lower than expectable from the material experiment without such cracks.

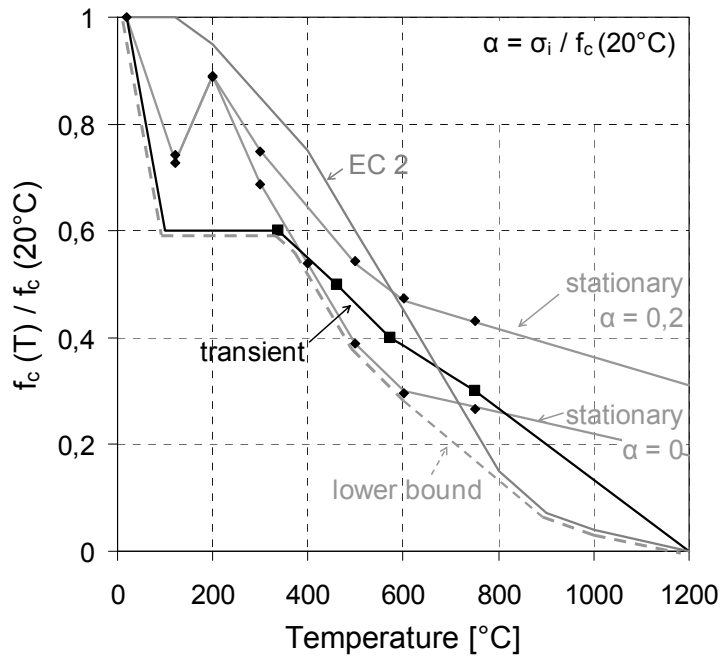


Figure 2. Compressive strength obtained from different tests [3].

With the presented properties of the HSC the stress-strain-curves can be generated. They are exemplary presented for the “transient” values in the loading range in Figure 3. The corresponding parameters are listed in Table I.

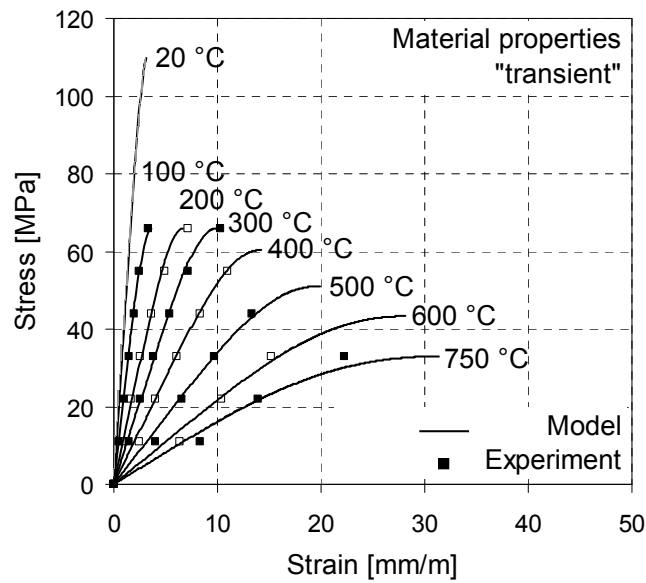


Figure 3. Constitutive stress-strain relationship and experimental data.

TABLE I: CONSTITUTIVE PROPERTIES FOR THE MATHEMATICAL STRESS-STRAIN-RELATIONS.

T [°C]	20	100	200	300	400	500	600	750	1000	1200
$f_c(T) / f_c(20^\circ\text{C})$	1,00	0,6	0,6	0,6	0,55	0,46	0,38	0,30	0,13	0,00
$E(T) / E(20^\circ\text{C})$	1,00	0,65	0,31	0,21	0,14	0,09	0,06	0,04	0,02	0,00
$\varepsilon_{c1}(T) [\%]$	3,2	3,2	6,8	10,0	14,2	20,0	27,6	31,5	50,1	∞

Whether the “stationary”, the “transient”, or the “lower bound” function leads to more realistic results for modelling concrete columns under fire conditions is shown in chapter 3.2.

The thermal strain is estimated from the transient tests (Figure 1) with a load level $\alpha = 0$. For temperatures above 750°C it will be extrapolated. For the reinforcement material behaviour the EC 2 model with its properties was used.

3. NUMERICAL SIMULATIONS

The numerical simulation for the validation of the model will be performed with the nonlinear three dimensional finite element program DIANA 9.2 from TNO. The proposed concrete model including its material parameters were implemented in that code.

3.1 Simulation of material tests

The validation of the concrete model was performed for transient creep tests. A comparison of the calculations and the experimental results is presented in Figure 4. The calculated strain correlates well with the experimental results since the modulus of elasticity was determined from these test results.

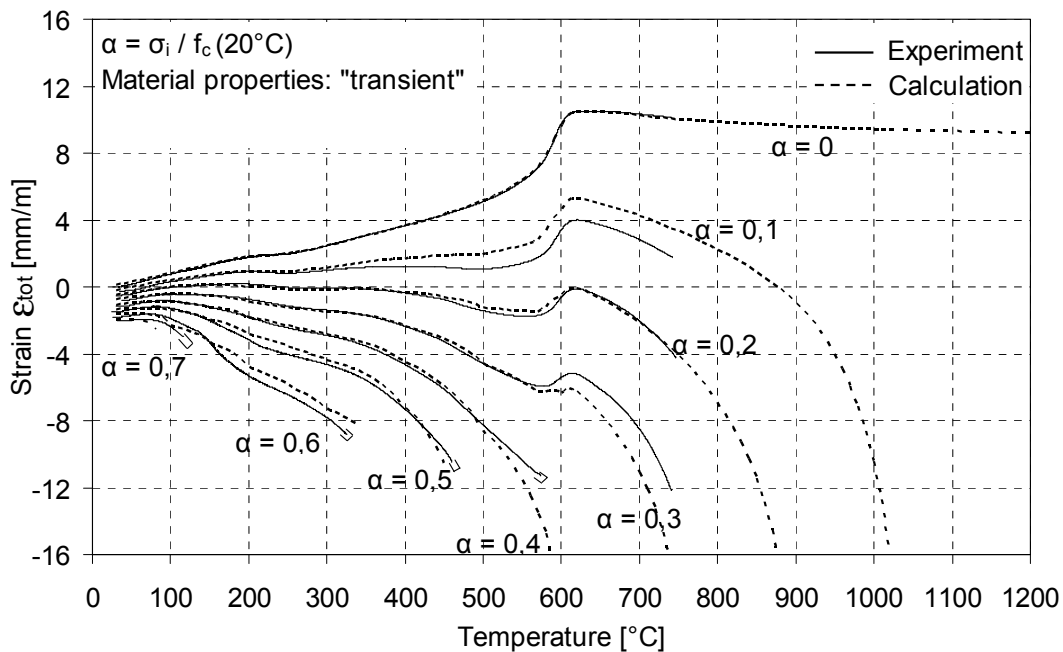


Figure 4. Measured and calculated strains in the transient creep tests.

3.2 Simulation of a concrete column

The validation of the model will be performed in addition to the material tests on the basis of a column fire test [4]. It was made of the same HSC as the specimens for the material tests. The column had a cross section of 300 x 300 mm² and a height of 3600 mm. The longitudinal reinforcement bars had a diameter of

25 mm and an axis distance to the surface of 50 mm. The bars were tied with 10 mm ties at a spacing of 150 mm at both ends and 300 mm in the middle. The load of 3200 kN was kept constant during the ISO fire exposure. The column failed in compression mode after 116 minutes. During the heating no spalling occurred.

The finite element discretisation of the column was done with twenty-node isoparametric solid elements. They are $25 \times 25 \text{ mm}^2$ in the cross section and 100 mm in height. To reduce the computing time only one half of the cross section was discretised. Imperfections were considered with an eccentricity $e = 1/800$ according to [1].

Figure 5 presents the calculated axial displacements of the column for different material properties in comparison to the experimental results. Assuming the material model presented in chapter 2 as well as the material properties from own tests the calculated axial displacement of the column correlates well with the experimental results. If the EC 2 material properties - thermal strain, ultimate strain and compressive strength - were assumed significant differences compared to the experimental results can be observed. This is a result of the higher thermal strain and lower transient creep strain in the EC 2 material properties.

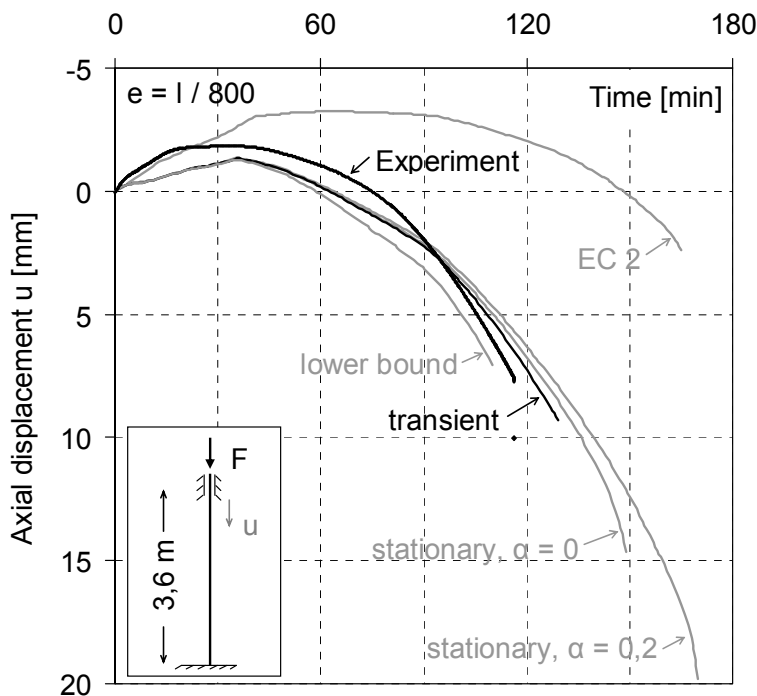


Figure 5. Axial displacement for different material properties and the experimental results.

The calculated fire resistance time for the different material functions is compared in Figure 6. Thereby for each function the calculations were performed on the one hand for an eccentricity of $e = 1/800$ and on the other hand without an eccentricity, i.e. no geometrical nonlinear effects were considered. With the EC 2 material properties as well as with the “stationary” function for the compressive strength the fire resistance time was overestimated. However, if the “transient” parameters were chosen the calculation results are only about 10 % higher than the experimental result and 5 % lower than those of the “lower bound” function.

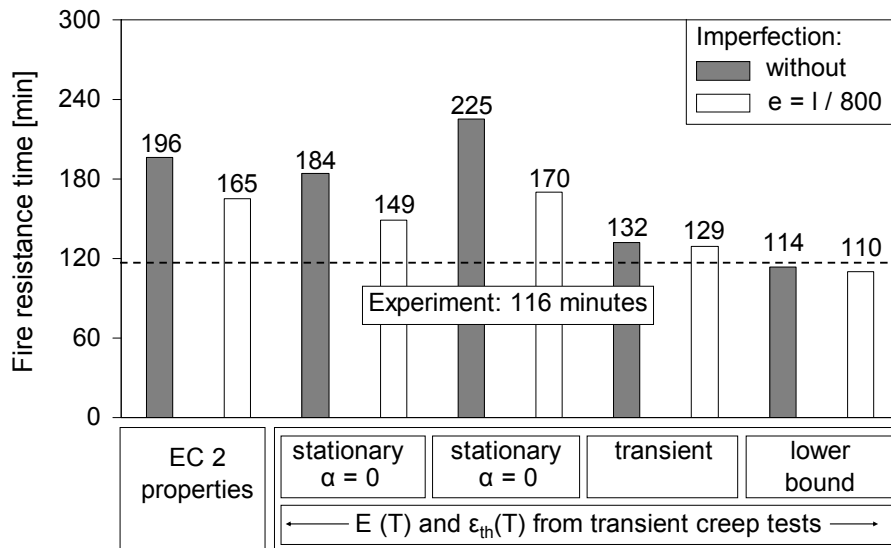


Figure 6. Fire resistance time for different material properties.

The reason for the overestimation of the fire resistance time assuming “stationary” material properties can mainly be found in the wrong approximation of the compressive strength especially between 100 °C and 350 °C. This temperature range is very important since the inner cross sectional part of the column exhibits this temperature and contributes mostly to the load bearing behaviour. Therefore good results were obtained for the “transient” and the “lower bound” functions.

The reason for the wrong approximation of the fire resistance time assuming the EC 2 material properties is on the one hand the function for compressive strength which overestimates the HSC behaviour. On the other hand the ultimate strain of the EC 2 does not include the high transient strain of the HSC. Therefore these material properties are not suitable for calculation of the behaviour of concrete columns under ISO fire conditions.

The calculated lateral displacements are presented in Figure 7.

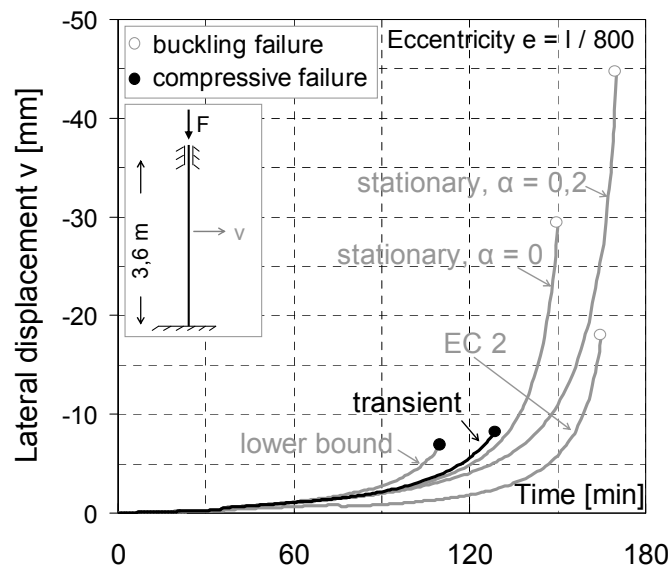


Figure 7. Lateral displacement for different material properties.

The analysis of these curves indicates the failure mode of the column. If the slope of the lateral displacement curve just before failure has nearly an infinite value it is a buckling failure and if not it is a compressive failure. The calculations with the EC 2 material properties as well as the “stationary” properties indicate a buckling failure whereas the “transient” and “lower bound” properties indicate the failure in compression mode. Since the compressive failure mode corresponds to the observation in the experiments, the material parameters from the “transient” and “lower bound” functions for the compressive strength can be approved as realistic values.

4. SUMMARY AND CONCLUSIONS

A simplified material model with its characteristic parameters was presented for HSC, which was developed on the basis of own material tests. It was validated with the results of material tests as well as a fire test of a HSC column.

The deformation behaviour and the fire resistance time of the column under fire conditions could be approximated in relative good agreement with the experimental results. For the realistic calculation of the deformation behaviour it is necessary to determine the modulus of elasticity from transient creep tests. The compressive strength has to be determined up to 400 °C from transient creep tests and above from stationary tests with a zero preload during heating. Besides it should not exceed the EC 2 properties.

It was pointed out that the application of the EC 2 material properties results in an overestimation of the fire resistance time and too low axial deformations of the HSC column. These properties are not suitable for HSC. The right approximation of the deformations is particularly required with increasing importance of geometrical nonlinear effects, which is for instance the case for cantilever columns.

REFERENCES

1. Eurocode 2: Design of concrete structures - Part 1-1: General rules and rules for buildings, 2005.
2. Eurocode 2: Design of concrete structures - Part 1-2: General rules—Structural fire design, 2006.
3. Huismann, S.: "Materialverhalten von hochfestem Beton unter thermomechanischer Beanspruchung", Ph.D. Thesis, Technical University of Vienna, 2010. (in preparation)
4. Huismann, S.; Korzen, M.: "Experimental and numerical study of high performance concrete columns subjected to fire loading", in *Applications of Structural Fire Engineering*, Prag, S. 246-251, 2009.
5. RILEM TC 129 MHT: "Test methods for mechanical properties of concrete at high temperatures: Part 3: Compressive strength for service and accident conditions", *Materials and Structures*, Vol. 28 (7), S. 410–414, 1995.
6. RILEM TC 129 MHT: "Test methods for mechanical properties of concrete at high temperatures: Part 7: Transient creep for service and accident conditions", *Materials and Structures*, Vol. 31 (5), S. 290-295, 1998.
7. Schneider, U.: "Concrete at high temperatures - A general review", *Fire Safety Journal*, Vol. 13, S. 55–68, 1988.
8. Thorenfeldt, E.; Tomaszewicz, A.; Jensen, J.J.: "Mechanical properties of high-strength concrete and application in design", *Utilization of high strength concrete*, Stavanger, S. 12, 1987.

Modeling R/C Columns in Fire According to Different Constitutive Models for Heated Concrete

P. BAMONTE and F. LO MONTE

ABSTRACT

Several analytical formulations aimed to describe concrete behavior at high temperature have been proposed in the past two decades, all of them taking into account transient and creep strains, either explicitly or implicitly. The main objective of this paper is to compare some of the different models available in the literature, with reference to the structural behavior of long R/C columns exposed to fire, since these structural members are rather sensitive to thermally-induced deformations. To this end, a number of significant examples based on real-scale fire tests, characterized by well-defined geometry, loads and boundary conditions, were simulated numerically, by adopting different formulations for concrete behavior in compression. In terms of displacements and time to failure, the comparisons clearly show that by using accurate constitutive laws (including—implicitly or explicitly—all strain components) a correct evaluation of the time to failure is possible. At the same time, no significant differences are observed among the various models, which means that the development of further models is not fully justified.

INTRODUCTION

Since the earliest studies on concrete behavior at high temperature, it was clear that any sound constitutive model should not neglect such strain components as the temperature-induced transient strain and the time-dependent (or creep) strain, both leading to a significant reduction of concrete stiffness and – consequently – to the “relaxation” of the thermal stresses.

Hence, the use of accurate constitutive models to describe the relationship between the deformation and the stress in the concrete is mandatory, whenever deformations and displacements are at issue, as it is the case in those R/C elements, whose internal forces are significantly dependent on the displacements. This is the case, for example, of long columns subjected to an eccentric axial force. On the

Patrick Bamonte, Francesco Lo Monte; Department of Structural Engineering
Politecnico di Milano, Piazza Leonardo da Vinci 32, 20133 Milan, Italy

contrary, whenever statically-determinate elements are at issue, the constitutive laws can be somewhat simplified, since the failure is generally controlled by the bearing capacity of one single critical section.

In the past two decades, several analytical formulations for the “hot” behavior of concrete in compression have been proposed. These models can be subdivided into (a) *explicit* models, where transient and creep strains are introduced separately from the stress-related strain (*mechanical strain*) and from the free thermal strain, and (b) *implicit* models, that “lump” all the strain components into a single component (with the exception of the free thermal strain). The traditional models by Anderberg-Thelandersson [1], Khoury-Terro [2], and the very recent model by M. Schneider, U. Schneider and Franssen [3] belong to the first group, while the model proposed in the Eurocode 2—Fire Design [4] is the most popular example of implicit model.

For several types of structural members, explicit and implicit models have been shown to bear no significant differences in terms of structural behavior. Hence, the reasons why so many explicit models have been proposed, is still an open question.

Within this context, the main objective of the present paper is to make comparisons among the most popular explicit models proposed in the literature, using—as a benchmark—several real-scale tests on R/C columns exposed to the standard fire. To this end, a number of significant fully-documented examples are simulated numerically, and then are compared with reference to the time to failure.

CONCRETE BEHAVIOR IN COMPRESSION AT HIGH TEMPERATURE

The basic assumption used for concrete to describe its “hot” behavior in compression is that the principle of superposition of the different strain components be applied. Therefore, the total strain ϵ_{tot} in any given concrete fiber is the sum of four components:

- the thermal strain $\epsilon_{\text{th}}(T)$;
- the stress-related strain $\epsilon_{\sigma}(\sigma, T)$;
- the transient strain $\epsilon_{\text{tr}}(\sigma, T)$;
- the creep strain $\epsilon_{\text{cr}}(\sigma, T, t)$.

The *thermal strain* ϵ_{th} is a function of the temperature, and can be adequately described by means of the provisions given in the EC 2 – Fire Design, that take into account the type of the aggregate (*siliceous* or *calcareous* aggregates).

The *stress-related strain* ϵ_{σ} is the strain occurring in a heated specimen during the application of the load (= *instantaneous load-induced strain*).

The irreversible time- and stress-dependent *transient strain* ϵ_{tr} occurs only during the first heating of the material and predominates over the stress-related strain. This phenomenon seems to be related to the cement paste, as demonstrated by the fact that it can be reduced by increasing the quantity of the aggregates [5].

The *creep strain* ϵ_{cr} is somewhat similar to the basic creep observed at ambient temperature, as it depends mainly on time, provided that the applied stress be constant. Usually, the creep strain plays a minor role compared to the other compo-

nents; hence, it is often neglected, or it is lumped into the transient strain (*implicit* formulation, as shown in [6]).

It is worth observing that, from a structural point of view, transient and creep strains bring in a significant reduction of the apparent stiffness, to the advantage of the relaxation of the stresses induced by the thermal strains. (In other terms, transient and creep strains bring in a favorable *stress redistribution*). Moreover, since these strain components are related to the stress, they can be implicitly included into one single stress-related strain.

The most important models implicitly or explicitly including thermal-creep phenomena and considered in this paper are four:

1. Anderberg and Thelandersson's model [1];
2. Khoury et al.'s model, developed at the beginning of the 80's, and later refined by Terro [2] for structural applications;
3. U. Schneider, M. Schneider and Franssen' model [3];
4. EC-2's model [4].

In the model by Anderberg and Thelandersson, the transient and creep strains are defined as follows:

$$\varepsilon_{tr}(\sigma, T) = k_{tr} \frac{\sigma(\varepsilon_{\sigma})}{f_c^{20}} \varepsilon_{th} \quad (1)$$

$$\varepsilon_{cr}(\sigma, T, t) = 5.3 \cdot 10^{-4} \cdot \frac{\sigma(\varepsilon_{\sigma})}{f_c^T} \cdot \sqrt{\frac{t}{3}} e^{3.04 \cdot 10^{-5} \cdot (T-20)} \quad (2)$$

where k_{tr} is a constant (ranging from 1.80 to 2.35), that depends mostly on the type of aggregate (for siliceous aggregates $k_{tr} = 2.35$); f_c^{20} is the cylindrical compressive strength at 20°C; f_c^T is the cylindrical compressive strength at the temperature T; and t is the time expressed in hours.

The model by Khoury and Terro – who introduced the concept of *load-induced thermal strain (LITS)* - has a phenomenological basis, because it was developed starting from the analysis of many experimental results at high temperature (up to 600°C):

$$LITS = \varepsilon_{\sigma}(\sigma, T) + \varepsilon_{tr}(\sigma, T) + \varepsilon_{cr}(\sigma, T, t) - \frac{\sigma}{E_0} = \varepsilon_{tot}(\sigma, T, t) - \varepsilon_{th}(T) - \frac{\sigma}{E_0} \quad (3)$$

where E_0 is the initial tangent modulus of concrete stress-strain law at room temperature. It is worth noting that the instantaneous load-induced strain is assumed to be (a) purely elastic and (b) related to the stress through the elastic modulus at ambient temperature. (In the elastic phase, the dependence of the elastic modulus on the temperature is neglected). The remaining part of the strain (namely the stress-induced strain at higher temperatures, the transient strain and the creep strain) are “lumped” into a single component, which is called LITS.

In the model by U. Schneider, M. Schneider and Franssen, the instantaneous load-induced strain is decomposed into an instantaneous elastic strain $\varepsilon_{el}(\sigma, T)$, and an instantaneous plastic strain $\varepsilon_{pl}(\sigma, T)$:

$$\varepsilon_{tot}(\sigma, T, t) = \varepsilon_{th}(T) + \varepsilon_{pl}(\sigma, T) + \varepsilon_{tr}(\sigma, T) + \varepsilon_{cr}(\sigma, T, t) \quad (4)$$

where:

$$\varepsilon_{pl}(T, \alpha) = \kappa \frac{\sigma(t)}{E(T, \alpha)} \quad ; \quad \varepsilon_{tr}(T, \alpha) + \varepsilon_{cr}(T, \alpha) = \varphi \frac{\sigma(t)}{E(T, \alpha)}$$

where κ is a numerical coefficient, and φ is a sort of “transient creep function”. Summing up:

$$\begin{aligned} \varepsilon_{in}(t, \sigma, T) &= \frac{\sigma(t)}{E(T, \alpha)} + \kappa \frac{\sigma(t)}{E(T, \alpha)} + \varphi \frac{\sigma(t)}{E(T, \alpha)} = (1 + \kappa + \varphi) \frac{\sigma(t)}{E(T, \alpha)} \\ &= (1 + \kappa + \varphi) \varepsilon_{el}(\sigma, T) \end{aligned}$$

In the Eurocode, the total strain in the concrete is the sum of two components:

$$\varepsilon_{tot}(\sigma, T, t) = \varepsilon_{th}(T) + \varepsilon_{\sigma, trcr}(\sigma, T) \quad (5)$$

where $\varepsilon_{\sigma, trcr}$ includes all the strain components induced by the load, such as the instantaneous elastic-plastic strain, the transient strain and the creep strain.

When using explicit models, an effective way of relating the stress to the *stress-related strain*, $\varepsilon(\sigma, T)$ is to use the relationship proposed in the EC 2 – Fire Design (Figure 1a):

$$\sigma(T) = \frac{3 \varepsilon f_{c,T}}{\varepsilon_{c1,T} \left[2 + \left(\frac{\varepsilon}{\varepsilon_{c1,T}} \right)^3 \right]} \quad (6)$$

where $f_{c,T}$ is the compressive strength, and $\varepsilon_{c1,T}$ is the strain at the peak stress, calculated by means of the expression suggested by Franssen ([7], Figure 1a):

$$\varepsilon_{c1,T} = 2.5 \cdot 10^{-3} + 4.1 \cdot 10^{-6}(T - 20) + 5.5 \cdot 10^{-9}(T - 20)^2 \leq 10 \cdot 10^{-3} \quad (7)$$

In the fourth model, the strain $\varepsilon_{,trcr}$ (that includes all the strain components, directly or indirectly induced by the loads, such as the elastic-plastic strain, the creep strain and the transient strain) is once again expressed by means of Eq.(8), up to the peak strain, and by a descending – linear or nonlinear - branch going to zero when the ultimate strain $\varepsilon_{cu,T}$ is attained.

In particular, the descending branch can be expressed by both a linear or non linear model. The values of $f_{c,T}$, $\varepsilon_{cu,T}$ and $\varepsilon_{c1,T}$ are given in the EC 2 – Fire Design. It is worth observing that the values of the peak strain given by the EC 2 – Fire Design

are by far larger than those suggested by Franssen (Figure 1b): in this way the stress-strain curve proposed by the EC 2 – Fire Design is less stiff, and implicitly takes into account both transient and creep strains.

In order to investigate the structural implications that the four models presented in the previous section have on the response of rather simple members (such as beams and columns) a finite element code was developed. The basic assumption is that the thermal behavior influences the mechanical behavior, but not viceversa. Therefore, the thermo-mechanical analysis is sequentially-coupled, and the solution of the problem can be subdivided into two parts.

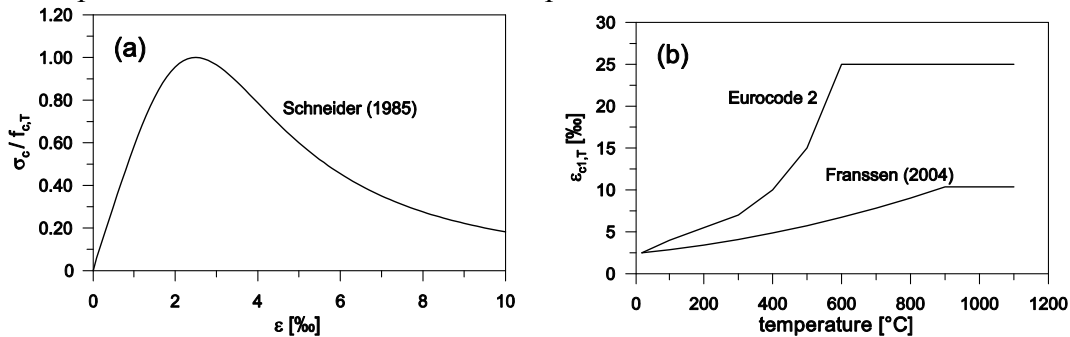


Figure 1. (a) Stress-strain diagram proposed by Schneider (1985), used to evaluate the stress-related strain in explicit models; and (b) peak strain to be used in the previous stress-strain diagram for implicit models (EC2) and explicit models [7].

The first part has to do with the thermal FE analysis of the cross-section of the member. The algorithm used is implicit (to allow unconditioned stability); the boundary conditions are those commonly adopted in fire problems (convection and radiation), and the thermal properties of the concrete are assumed to be nonlinear functions of the temperature [4]. As it is usually done in R/C thermal analysis, the reinforcement is neglected. Heat transfer in the longitudinal direction (i.e. along the axis of the member in question) is neglected as well.

Once the thermal analysis has been carried out, and the thermal field is known in any given point and for any fire duration, the mechanical analysis is carried out, on the basis of the traditional assumptions concerning slender Euler-Bernoulli structural members (plane sections remain plane, and the shear strain are neglected). As for the deformed configuration in the longitudinal direction, it is a function of the 6 nodal degrees of freedom (two translations, and one rotation per node) via the usual linear and cubic shape functions (for the axial and flexural behaviors, respectively).

GENERAL CONSIDERATIONS ON THE STRUCTURAL BEHAVIOUR OF COLUMNS

To make some general considerations on the different models presented in the previous sections, a real column tested at the Technical University of Braunschweig [8], exposed to a ISO 834 Standard Fire acting on the four sides, and subjected to an eccentric axial load is first studied (square section: side = 300 mm; reinforcement:

6 16 mm bars; concrete and steel strengths: $f_c^{20} = 24$ MPa and $f_y^{20} = 487$ MPa; applied load: $P = 710$ kN; and load eccentricity: $e = 30$ mm).

The results, concerning the evolution of the 1st-order axial displacement at mid-height, are shown in Figure 2 (continuous lines). Model 1 and 2 lead to very close results, and are characterized by the highest deformability, while Model 4 brings in the stiffest response. For each model, the introduction of second-order effects (dashed lines) causes a very strong decrease of the fire resistance. It is worth noting, however, that the differences between the four models are minimal, especially in the ascending branch, where the deformations are controlled by the thermal dilation (that was assumed to be the same in all four cases). Moreover, using the four models both 1st-order and 2nd-order calculations bring in time-to-failure values, which are comprised within rather narrow bands (grey shaded areas in Figure 2); these values are comprised between 175 and 205 minutes if attention is limited to 1st-order effects, and between 70 and 80 minutes, if 2nd-order effects are included.

Figure 3 illustrates the results concerning the same column in terms of lateral deflection at mid-height. The considerations made with reference to the axial displacement are still valid. In this case, the failure becomes more evident, with the typical increase of the displacement rate (*runaway failure*), particularly if 2nd-order effects are taken into account (dashed curves).

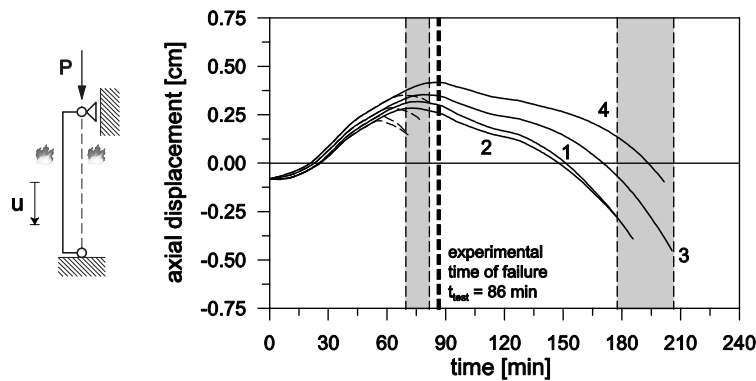


Figure 2. Plots of the axial displacement of the mid-height section of the reference column, according to the four models considered in this study.

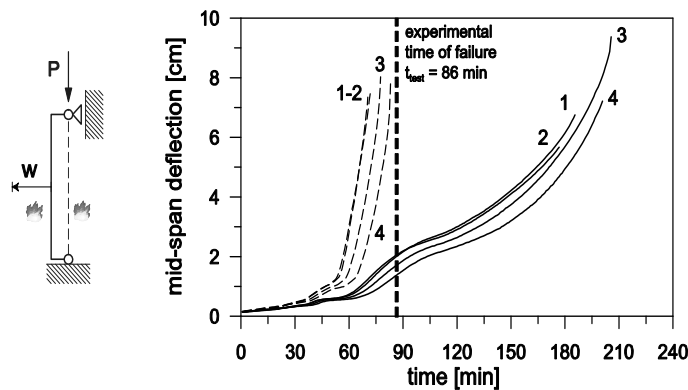


Figure 3. Plots of the maximum lateral deflection of the reference column, according to the four models considered in this study.

FITTING OF THE EXPERIMENTAL RESULTS

So far, all considerations were focused on the differences between the 4 constitutive models. It is now interesting to compare the predictions of the models with some well-documented test results. To this end, the structural behavior of approximately 60 columns [8] tested in the laboratories of the Technical University of Braunschweig (39 tests), of the University of Ghent (16 tests) and of the University of Liège (5 tests) was simulated numerically, and the time to failure was calculated. The results are presented - as it is usually done in the literature - through the ratio between the calculated time to failure (t_{num}) and the time to failure measured during the tests (t_{test}). The values of the ratio t_{num}/t_{test} were calculated by using each of the four models, and four statistical distributions were obtained (Figure 4; range 0-2). Clearly, the results characterized by $t_{num}/t_{test} > 1.00$ are on the safe side.

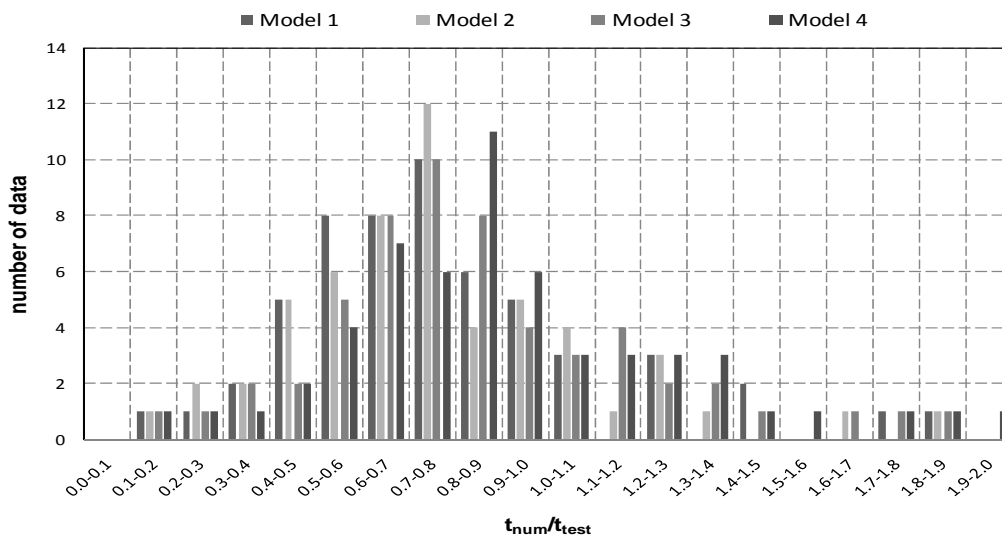


Figure 4. Values of the time to failure of roughly 60 columns, according to the four models considered in this study, and to Tan and Tang simplified equation.

The four models taking into account creep and transient strains tend to give smaller values of fire resistance than those measured experimentally, especially in the case of columns subjected to eccentric axial loads. With small eccentricities, however, they tend to slightly overestimate the fire resistance. This is probably due to the fact that in the columns subjected to a purely axial load, the role of accidental eccentricities or geometrical imperfections is likely to play a more significant role.

In any case, the overall agreement between the numerical analysis and the experimental results is satisfactory. In the case of eccentric axial loads, the different models tend to underevaluate the fire resistance, more according to Models 1 and 2, and less according to the model proposed by the Eurocode 2 (Model 4).

Among the four models, Model 1 and 2 are the most conservative, with a mean value of t_{num}/t_{test} equal to 0.78 and to 0.77, respectively. The model proposed by

EC2 brings in the best fitting (mean value of 0.92). Finally, the model proposed by the Schneiders and by Franssen is in an intermediate position (mean value of 0.85).

CONCLUSIONS

The numerical results shown in the present paper allow to conclude that the explicit models by Anderberg and Thelandersson, and by Khoury and Terro lead to results that are in perfect agreement to each other, and that are characterized by a greater deformability and by smaller values in terms of fire resistance (expressed in terms of time to failure). The model proposed by the EC 2 – Fire Design is the stiffest and leads to the highest values of time to failure, while the model formulated by the Schneiders and by Franssen leads to an intermediate situation. On the whole, however, no significant differences were observed among the different explicit models, something that may suggest further justifications of the various models to those found in the literature.

In terms of test fitting, the mechanical model proposed in EC 2 – Fire Design appears to be the best; it is fair to say, however, that the data base of the experimental results used in this paper is probably the same that was used to calibrate the stress-strain diagram proposed in the EC 2 – Fire Design.

REFERENCES

1. Anderberg, Y., and Thelandersson, S. 1976. “*Stress and Deformation Characteristics of Concrete at High Temperatures—2. Experimental Investigation and Material Behaviour Model*,” Report No. 34, Division of Structural Mechanics and Concrete Construction, Lund Institute of Technology, Lund (Sweden).
2. Terro Mohammad J. 1998 “Numerical modelling of the behaviour of concrete structures in fire”, *ACI Structural Journal*, Vol. 95, No. 2, pp. 183–193.
3. Schneider U., Schneider M., Franssen J. M. 2008. “Consideration of nonlinear creep strain of siliceous concrete on calculation of mechanical strain under transient temperatures as a function of load history”, *Proceedings of the Fifth International Conference on Structures in Fire – SiF’08*, Singapore, May 28-30, 2008, pp. 463–476.
4. European Committee for Standardization (2004). Eurocode 2: Design of Concrete Structures, Part 1.2: General rules - Structural Fire Design. Central Secretariat: rue de Stassart, 36 B-1050 Bruxelles.
5. Law A., Gillie M. 2008. “Load Induced Thermal Strain: Implications for Structural Behaviour”, *Proceedings of the Fifth International Conference on Structures in Fire – SiF’08*, Singapore, May 28-30, 2008, pp. 488–498.
6. Anderberg Y. 2008. “The impact of various material models on structural fire behaviour prediction”, *Proceedings of the Fifth International Conference on Structures in Fire – SiF’08*, Singapore, May 28-30, 2008, pp. 253–265.
7. Franssen J. M. 2004. “Plastic analysis of concrete structures subjected to fire”, *Proceedings of the Workshop “Fire design of concrete structures: What now? What next?”*, Milan (Italy), December 2-3, 2004, pp. 133–146.
8. Tan K. H. and Tang C. Y. 2004. “Interaction formula for reinforced concrete columns in fire condition”, *ACI Structural Journal*, Vol. 101, No. 1, pp. 19–28.

Performance of FRP-Strengthened Reinforced Concrete Beams Under Design Fire Exposure

A. AHMED¹ and V. KODUR²

ABSTRACT

Results from fire resistance experiments on two full-scale FRP-strengthened reinforced concrete (RC) beams are presented in this paper. The rectangular RC beams strengthened with CFRP and insulated with Tyfo[®] WR Advanced Protection (AFP) system, were tested under a design fire exposure. Data from fire tests is used to evaluate the thermal and structural response, as well as failure patterns in FRP-strengthened RC beams. Test results indicate that effectiveness of anchorages play a critical role in limiting the debonding of FRP under fire conditions. FRP-strengthened RC beams supplemented with 25 mm thick spray-applied Tyfo[®] WR AFP system can survive failure under non-standard fire (design fire) conditions, comprising of 3 hours of ASTM E119 growth phase followed by a cooling phase.

INTRODUCTION

In recent years, Fiber Reinforced Polymers (FRP) are finding wide applications in civil infrastructure applications. FRP are quite attractive for strengthening and retrofitting of RC structures, through externally bonded FRP, due to ease of application, cost effectiveness and high performance levels. Currently, most applications of FRP are in bridges and other infrastructures where fire safety is not a critical issue. However, when used in buildings, FRP have to satisfy fire resistance requirements specified in building codes and standards.

In the last decade, a few fire tests have been conducted on FRP-strengthened RC members to generate fire endurance ratings. Most of these tests were under standard fire exposure aimed at obtaining fire resistance ratings rather than understanding the response of FRP-strengthened members under fire conditions.

¹Ph.D. Candidate, Department of Civil and Environmental Engineering, Michigan State University, East Lansing, Michigan, Email:ahmedaqe@msu.edu

²Professor, Department of Civil and Environmental Engineering, Michigan State University, East Lansing, Michigan, Email:kodur@egr.msu.edu.

Thus, there is lack of understanding on the response of FRP-strengthened RC beams under realistic fire, loading and failure limit states. This lack of knowledge is posing a major obstacle for the use of FRP in buildings and parking structures.

To overcome the current knowledge gaps, a comprehensive research project is currently underway at Michigan State University to quantify the influence of various parameters on the fire performance of FRP-strengthened RC beams. This paper presents results from fire tests on two FRP-strengthened RC beams exposed to design fire (non-standard fire) conditions. The effectiveness of new insulation system (Tyfo[®] WR Advanced Fire Protection (AFP)) and anchorage patterns on fire resistance of FRP-strengthened RC beams are specifically evaluated.

PREVIOUS RESEARCH

The few notable experimental studies on FRP-strengthened RC beams were conducted by Deuring [1], Blontrock et al. [2], Barnes and Fidell [3] and Williams et al. [4]. Initial experimental studies in this area were performed in Europe by Deuring [1], who conducted fire tests on six RC beams strengthened with external carbon fiber reinforced polymer (CFRP) strips and steel plates under ISO 834 standard fire exposure to assess post-fire residual strength of the beams. Through these fire tests, Deuring demonstrated that interaction between FRP and concrete is lost in early stages of fire exposure. Thus, he recommended application of external thermal insulation to maintain effective bond under fire conditions.

Blontrock et al. [2] conducted fire tests on FRP-strengthened RC beams using a variety of supplemental fire insulation schemes. Based on the results from fire tests, the authors concluded that supplemental fire insulation is needed for externally bonded FRP to limit temperature rise at FRP-concrete interface below glass transition temperature (T_g).

Barnes and Fidell [3] tested CFRP-strengthened RC beams under standard fire conditions to study the effectiveness of insulation and mechanical bolting of CFRP plate. Beams were exposed to fire for 1 hour without any applied loading and later subjected to four point bending loads till failure occurred in the beams. The test data indicated that no transfer of stresses occurred from concrete to CFRP plate once the bond between FRP and concrete was lost at temperature exceeding T_g .

Williams et al. [4, 5] conducted full-scale fire tests on four FRP-strengthened beam-slab assemblies (T-beams) and protected with VG-EI-R insulation, under standard fire exposure. The beams were applied with 100 mm wide layer of CFRP for flexural strengthening and two layers of GFRP to provide U-wrap anchorages. The study concluded that FRP-RC beams with appropriate insulation (38 mm of VG-EI-R insulation) are capable of achieving 4 hours of fire resistance rating although T_g of the adhesive exceeded in about 1 hour of fire exposure.

The above review illustrates that there have been only limited tests conducted to evaluate fire performance of FRP-strengthened RC beams. Most of these tests have been conducted under standard fire exposure without any due consideration realistic fire, loading, and restraint scenarios. Further there is no data on the FRP-strengthened beams protected with improved (Tyfo[®] WR AFP) fire insulation.

EXPERIMENTAL STUDIES

To overcome some of the above drawbacks, fire resistance experiments on FRP-strengthened RC beams are currently underway at Michigan State University (MSU). Results from fire resistance tests on two CFRP-strengthened RC beams under design fire exposure are discussed here. Details of test specimens and test procedure are presented below.

Test Specimens

The specimens for fire resistance tests consisted of rectangular RC beams strengthened with CFRP. The beams were designed to be as close to typical building geometries as possible, in order to maximize the usefulness of the test results. The beams were of 254 mm width and 406 mm depth and had 3.96 m span length. The RC beams were designed as per ACI 318 [6] specifications and were fabricated at the Civil Infrastructure Laboratory at Michigan State University. The RC beams had three 19 mm dia. rebars as flexural reinforcement and two 13 mm rebars as compressive reinforcement. The stirrups used as shear reinforcement were of 6 mm dia. and were spaced at 150 mm. The elevation and cross sectional details of the beams are shown in Figure 1.

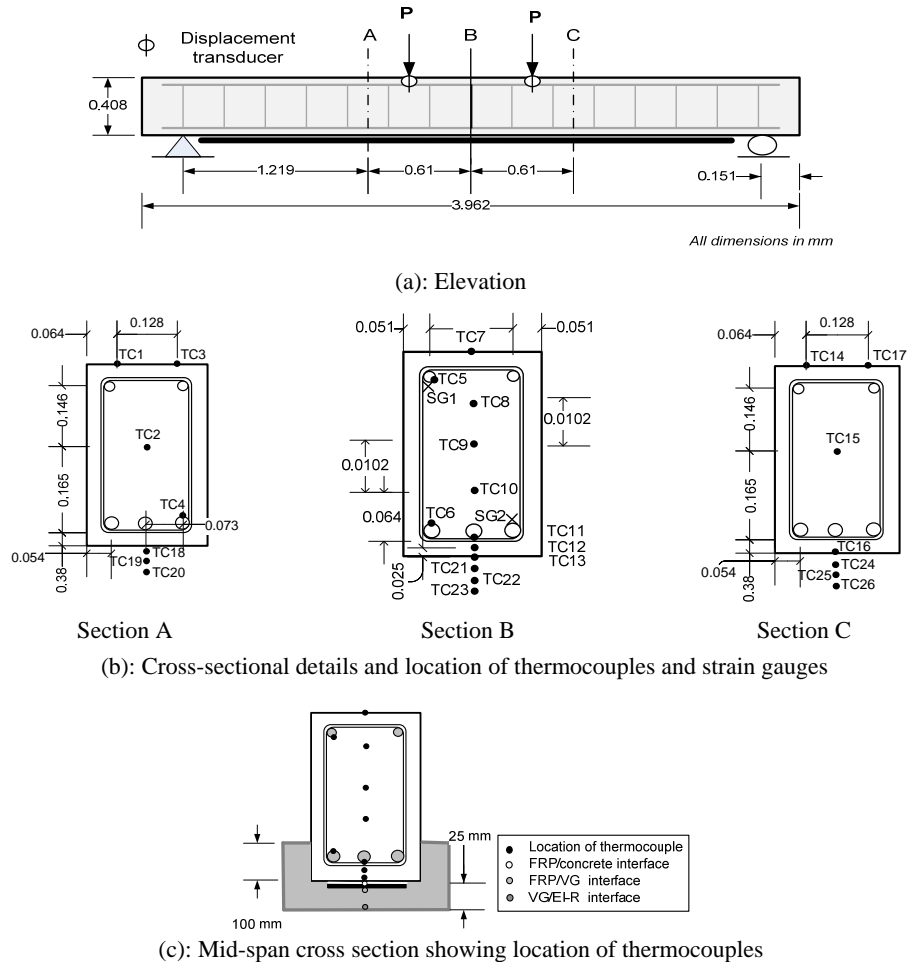


Figure 1. Elevation and cross-sectional details of tested FRP-strengthened RC beam.

The RC beams were fabricated with concrete having a design compressive strength of 42 MPa. Type I Portland cement and carbonate based coarse aggregate was used in concrete. The measured compressive strength of concrete at 28 days was 52 MPa, while on the day of test (after 2 years), it was 55 MPa. The mix proportion of concrete comprised of:

Cement	390 (kg/m ³)
Coarse aggregate	1038 (kg/m ³)
Fine aggregate	830 (kg/m ³)
Water	156 (kg/m ³)
Water reducing agent	2 (kg/m ³)

The casted beams were sealed within the forms for the first 7 days. Thereafter, the beams were lifted out from the forms and stored in the laboratory, at about 25°C (40% relative humidity), for about 18 months before retrofitted with CFRP. The details of specimen and testing parameters are provided in Table I.

TABLE I. SUMMARY OF TEST PARAMETERS AND RESULTS.

Designation	CFRP strengthening	Insulation type	Insulation thickness (mm)		Fire scenario	Failure time (min)
			VG	EI-R		
Beam I	2 layers of 203 mm wide	Tyfo® WR AFP-Type A	25	0.1	Design	NF*
Beam II	2 layers of 203 mm wide	Tyfo® WR AFP-Type B	25	0.1	Design	NF*

* NF – No failure

Strengthening and Insulation of Beams

The two RC beams were strengthened with CFRP sheets to enhance their flexural strength capacity by 50%. The concrete surface, which was fairly smooth due to form work, was roughened by sand blasting to partially expose the aggregate at beam soffit. Then, two CFRP sheets of 2 mm thick and 203 mm width, saturated in S- epoxy were roller-applied at the beam soffit as flexural strengthening. The ultimate tensile modulus (in fiber direction) and tensile modulus of FRP were 986 MPa and 96 GPa, respectively. The resin used to bond fibers was two-component epoxy material with a glass transition temperature (T_g) of 82°C. The CFRP was applied on the entire unsupported length of the beam (3.66 m) terminating at a distance d from the supports. Unlike in previous tests, no shear strengthening was provided to study the case of failure patters under only flexural strengthening of the beams.

The strengthened beams were cured for 72 hours and then spray-applied with Tyfo® WR AFP system, an improved version as compared to previously developed Tyfo® AFP system [4]. The Tyfo® WR AFP system comprises of vermiculite based insulation (VG insulation) and EI-R coating. It is available in two forms, Tyfo® WR AFP-Type A and Tyfo® WR AFP-Type B. The insulation is non-combustible and non-flammable lightweight material available in a powdered form. Beam I was spray-applied with Tyfo® WR AFP-Type A, while Tyfo® WR AFP-Type B was used for Beam II. On top of insulation, spray-on EI-R coating was applied. This EI-R coating is a crack resistant surface coating with excellent adhesion and fire resistance properties and provides additional stability to insulation.

This insulation application comprised of spraying a thin coat of VG primer, followed by a dash coat, on the FRP-strengthened beam soffit to enhance FRP/insulation bond. Thereafter,

insulation material, which is available in powdered form, was mixed with appropriate amount of clear water and spray-applied on the beams using a hopper gun. Special attention was taken to maintain uniform thickness throughout the beam length. The insulation layout comprised of 25 mm at the bottom surface of the beam extending 105 mm on the two sides (refer to Figure 1(c)). This sprayed insulation was cured for 24 hours before final coat of EI-R was applied.

Instrumentation

The beams were instrumented at three different sections along the span of the beam with Type-K thermocouples to measure the temperatures at various depths in concrete, reinforcement, and concrete-FRP and FRP-insulation interfaces. A total of 27 thermocouples were installed for each beam. In addition, normal and high temperature strain gauges were placed to record strains in compression and tension rebars respectively, as shown in Figure 1(b). The locations and numbering of thermocouples and strain gauges are shown in Figure 1(b). In addition, three “Linear Variable Differential Transducers (LVDT’s)” were installed for each beam, one at mid-span and two under point loads to measure deflections.

Furnace Details

The fire resistance tests on FRP-strengthened RC beams were conducted at MSU’s structural fire testing furnace. The test furnace is specially designed to produce conditions, such as temperature, structural loads and heat transfer, to which a member might be exposed during a fire. The furnace, shown in Figure 2, consists of a steel framework supported by four steel columns, with a fire chamber that is 2.44 m wide, 3.05 m long, and 1.68 m high. Six propane burners located within the furnace provide thermal energy, while six thermocouples, distributed throughout the test chamber, monitor the furnace temperature during a fire test. The furnace temperature can be maintained along a desired time-temperature curve as in a standard or design fire. Two small view ports on either side of the furnace wall facilitate visual monitoring of the fire-exposed test specimens during fire tests. The furnace accommodates two beams at a time and different load levels and restrained conditions can be simulated for each beam.

Test Setup and Procedure

Both FRP-strengthened RC beams were tested simultaneously under loading and fire conditions. The beams were simply supported at the ends with an unsupported length of 3.66 m, of which 2.44 m was exposed to fire in the furnace. The beams were subjected to two point loads, each of 70kN, which represents 50% of the strengthened beam nominal capacity according to ACI 440.2R [7]. The point loads were applied at a distance of 1.4 m from the end supports as shown in Figure 1(a). The loading was applied approximately 30 minutes before the start of the test until steady condition (no increase in deflection with time) was reached.

After about 30 minutes, the beams were exposed to a design fire from three sides. The design fire comprised of a rising temperature (growth) phase followed by a cooling phase. In growth phase, the time-temperature curve as that of ASTM E119 standard fire [8] was simulated for the first 180 minutes. Thereafter, a decay phase was introduced at a cooling rate of 10°C/minute. During the test, temperatures at various locations of the beam cross section, strains and deflections were recorded at 5-second intervals. Also, visual observations were made through view ports in the furnace to record progression of cracks in the insulation, localized burning of FRP, and delamination of insulation and FRP.

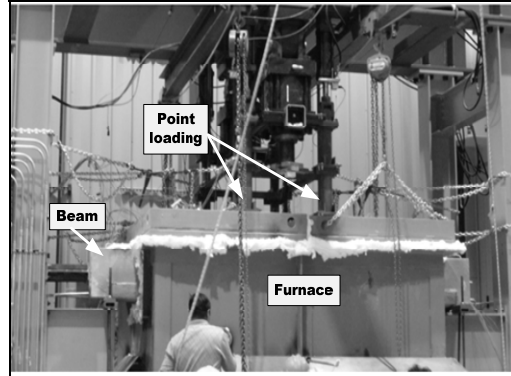


Figure 2. Structural fire test furnace at MSU Civil and Infrastructure laboratory.

RESULTS AND DISCUSSION

Data generated from above fire tests can be used to study thermal and structural response of FRP-strengthened RC beams. Test conditions in the tested beams represented a typical compartment fire in a building where a portion (center) of the beam is exposed to fire, while terminating ends of CFRP near supports (outside fire zones) acted as anchorages.

Thermal Response

Figure 3 shows time-temperature progression for Beam I at FRP/VG and FRP/concrete interface, corner rebar and at mid-depth of the beam for section B. In the first 20 minutes of fire exposure, temperatures at FRP/VG and FRP/concrete interfaces increases slowly followed by a plateau around 100°C. This temperature plateau can be attributed to evaporation of free and chemically bonded water in the insulation that consumes significant amount of energy. The VG insulation, which is spray-applied in the form of slurry, contains free moisture. Most of the free water in the insulation close to exposed surface, dries-out at room temperature, however, remaining free and chemically bonded water consumed significant energy from fire to evaporate.

Beyond 100°C, temperature increase at FRP/VG interface was very rapid as compared to that at FRP/concrete interface. This can be attributed to progression of cracks in insulation that allows rapid transfer of heat. The slow temperature increase at FRP/concrete interface is due to formation of protective char layer as a result of pyrolysis process of matrix [9]. This char layer acts as a thermal barrier and insulates the interior interface between FRP and concrete which is critical in maintaining bond at elevated temperatures. When the temperature at FRP/concrete interface reaches 400°C, another short temperature plateau develops and this can be attributed to thermal decomposition of matrix/adhesive occurring in 300-500°C range. After about 3 hours of fire exposure, temperatures at various levels of the beam cross section decreases after attaining a peak temperature. This is due to the commencement of decay (cooling) phase of the fire which starts at 180 minutes of fire exposure.

Figure 4 shows temperatures measured at various levels in FRP-RC Beam II, which was insulated Tyfo[®] WR AFP-Type B. The temperature progression is slightly different than that in Beam I. Rise of temperature at FRP/VG interface is very rapid (as compared to Beam I) after 20 minutes of fire exposure. This is due to early development and faster widening of cracks in the insulation. These wide cracks expose CFRP polymer matrix to heat flux resulting in localized burning of matrix and thus raises the temperature at FRP/VG interface abruptly. The temperature increase in Beam II at FRP/concrete interface was steady and closely matched with the measured

temperatures for Beam I. This can be attributed to pyrolysis process that played an effective role in insulating inner interface between FRP and concrete. By about 60 minutes, most part of the FRP at the beam soffit was engulfed in fire. This sudden increase in temperatures as a result of FRP matrix burning accelerated temperature progression throughout the beam cross section including the rebars.

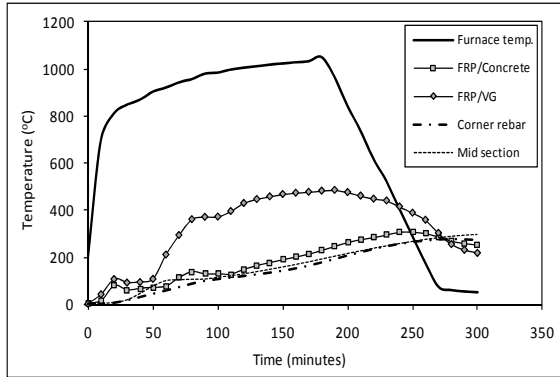


Figure 3. Measured temperatures as function of time for FRP-RC Beam I.

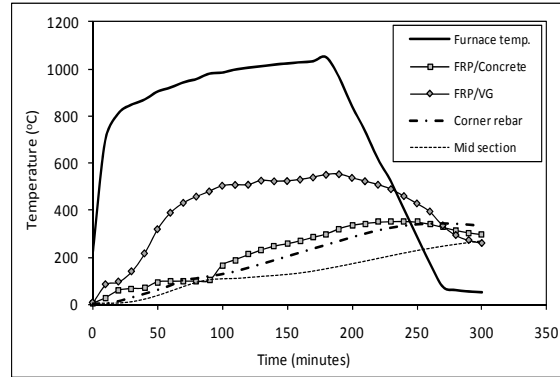


Figure 4. Measured temperatures as function of time for FRP-RC Beam II.

Fire resistance of FRP-strengthened flexural members is mainly influenced by strength and stiffness properties of FRP and steel reinforcement and these properties degrade with temperature. In FRP, the rate of degradation of strength and stiffness properties is faster as compared to concrete and steel due to low tolerance of the polymer matrix to high temperature. Therefore, after FRP loses contributing to flexural capacity of the beam that happens at early stages of fire exposure, rebars temperatures becomes an important indicator of fire resistance of FRP-RC beams. Figure 5 shows that temperature progression in corner rebar as a function of time. For both beams, temperature rises at slow pace up to about 2 hours, which can be attributed to the insulation effect from Tyfo[®] WR AFP system. Beyond 2 hours, rebar temperatures in Beam II are higher, as compared to Beam I, due to early development of cracks in insulation (Tyfo[®] WR AFP-Type B) that resulted in transfer of more heat flux. For full duration of the test, the average rebar temperature in both beams remained less than 400°C. Since rebars does not lose any significant strength up to 400°C, therefore, the beams maintained full strength capacity for the test duration.

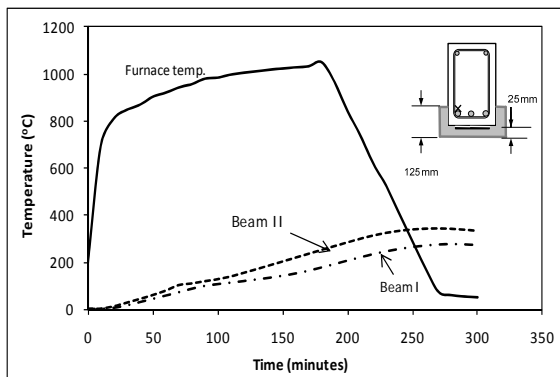


Figure 5. Progression of corner rebar temperatures in Beam I and II.

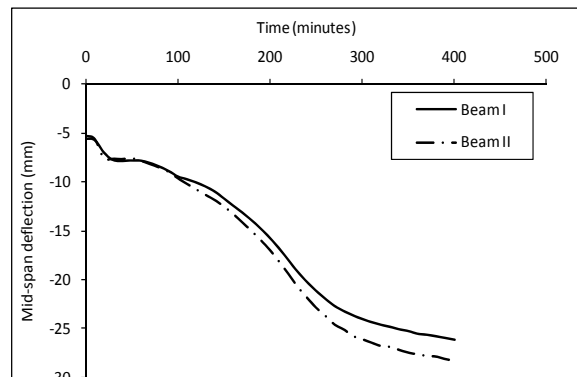


Figure 6. Mid-span deflection as a function of time in Beam I and II.

Structural Response

The structural response of the beams can be gauged through deflection progression with fire exposure time. Figure 6 shows variation of mid-span deflection as function of time for the two tested beams. The beams were loaded by applying two point loads (70 kN each) that represents about 50% of the ultimate capacity of the beams calculated as per ACI 440.2R-08 provisions. The initial deflections in Beam I and Beam II prior to fire exposure was 5.6 mm and 5.3 mm, respectively. Under fire, the deflections increased gradually and around 20 minutes, both beams experienced a sudden increase in deflections. This can be attributed to loss of bond at FRP/concrete interface with temperature. A closer examination of measured temperature in FRP indicated that the temperature at FRP/concrete interface had exceeded the glass transition temperature of epoxy ($T_g = 82^\circ C$) at about 20 minutes of fire exposure. When the temperature of polymer matrix approaches close to glass transition temperature, the matrix becomes soft and viscous. This results in reduced capability of the polymer matrix to transfer forces between the fibers and interaction between FRP and concrete substrate is lost due to degradation of bond. This leads to sudden increase in deflections.

After 20 minutes, rate of increase in deflection is gradual. This is contrary to the response of unstrengthened and uninsulated RC beam under fire where deflections continue to increase at faster rate. This can be attributed to factors slow degradation of strength and stiffness properties of concrete and rebars resulting from lower temperatures facilitated by insulation protection. The insulation effectively slows down the temperature rise in concrete and rebars and thus the deflections does not increase significantly. Also, the formation of char layer resulting from pyrolysis process provides thermal barrier to inner layers of the beam cross section and limits the rise in temperature. Another factor that contributed to slower deflections is the contributed load sharing by FRP fibers through cable (similar to tensile membrane action in slabs) action. Typically, char layer decomposes after prolonged exposure to high temperatures (for a typical polyester resin it is above approximately $500^\circ C$), however, carbon fibers have high tolerance against thermal decomposition and are less sensitive to temperatures up to $900^\circ C$ [9]. Therefore, in absence of any delamination of FRP due to the location of anchorages outside the fire zone, the unbonded continuous fibers at the beam soffit continue to contribute towards tensile strength of the beam through 'cable' mechanism. However, if the anchorages are not effective, delamination of FRP is likely to occur and any strength contribution from FRP is unlikely.

FIRE RESISTANCE AND FAILURE PATTERN

Both FRP-strengthened beams with Tyfo[®] WR AFP system, did not experience failure and survived the fire exposure. The glass transition temperature (T_g) in FRP exceeded in first 20 minutes, however, the beams resisted applied loading for the entire duration of the test. In the first 20 minutes of fire exposure time, cracks started to appear in insulation for Beam II. These cracks widened at 30 minutes which initially resulted in localized burning of matrix (epoxy) followed by complete burning of epoxy at the soffit after 60 minutes as shown in Figure 7. For Beam I, development of cracks initiated after 45 minutes of fire exposure time. After the bond between FRP and concrete substrate was lost, carbon fibers continued to contribute to flexural capacity through cable mechanism as a result of protected anchorages. These results suggest that in evaluating fire endurance of FRP-strengthened RC beams, reaching T_g at FRP/concrete interface does not indicate failure of the beam. However, it should be noted that in these tests, both the anchorages (terminating ends of FRP) were outside the fire zone. This might have

played a positive role in controlling FRP delamination that generally starts at FRP terminating ends. To further study the effect of anchorages, additional fire resistance tests on FRP-RC beam are currently underway under different anchorage schemes.

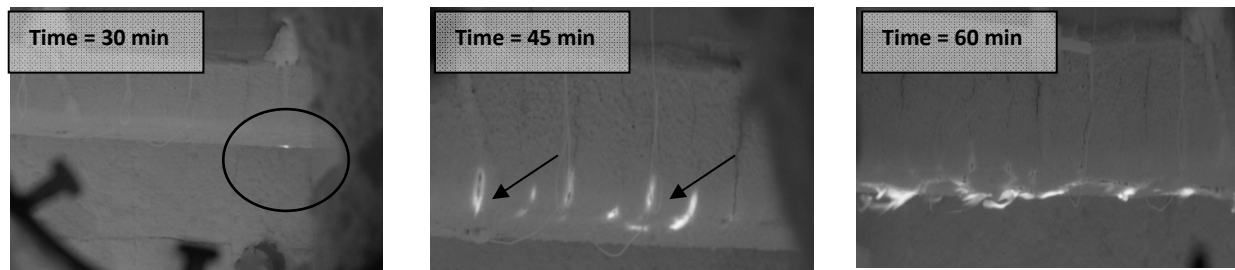


Figure 7. Crack development in insulation of FRP-strengthened beam (Beam II).

CURRENT STUDIES

Experimental studies, such as the one presented in this paper, provide an insight into the response of FRP-strengthened RC beam under realistic fire scenarios. However, the availability of wide varieties of FRP and insulation materials in the market requires numerous fire tests to characterize performance of each combination under fire. An alternative to fire tests is the use of numerical models for evaluating the resistance of FRP-strengthened RC structures. At present, there is limited information in the area of fire resistance modeling on FRP-strengthened structures.

As part of ongoing research, a finite element (FE) model is being developed to trace the fire response of FRP-strengthened RC beams. Data from the above experimental studies will be used to validate the model. The validated model will be applied to investigate and quantify influence of different parameters on fire performance of FRP-RC members.

CONCLUSIONS

Based on experimental studies, following conclusions can be drawn:

FRP-strengthened RC beams, supplemented with 25 mm thick spray-applied Tyfo[®] WR Advanced Fire Protection system can survive failure under non-standard fire (design fire) conditions comprising of 3 hours of ASTM E119 growth phase followed by a decay (cooling) phase.

Reaching glass transition temperature (T_g) in CFRP does not lead to strength failure in insulated CFRP-strengthened RC beams.

Presence of cooler anchorages outside the fire zone helps in contributing to load carrying capacity of FRP-RC beams through cable mechanism provided by unbonded continuous fibers at the beam soffit.

Formation of char layer resulting from pyrolysis process in FRP (matrix) provides an effective thermal barrier and delays heat transfer across FRP.

ACKNOWLEDGMENTS

The research presented in this paper is supported by the National Science Foundation (Grant No. CMMI 0855820) and Michigan State University through Strategic Partnership Grant (Award No. SPG 71-4434). The authors would also like to thank Fyfe Company LLC, USA, for supplying Tyfo[®] WR Advanced Fire Protection system. Any opinions, findings, and conclusions or recommendations expressed in this paper are those of the authors and do not necessarily reflect the views of the sponsors.

REFERENCES

1. Deuring, M., *Brandversuche an nachtraglich verstärkten tragern aus beton*, in *Research Report EMPA No. 148,795*. 1994, Swiss Federal Laboratories for Materials Testing and Research: Dubendorf, Switzerland.
2. Blontrock, H., L. Taerwe, and P. Vandevelde. *Fire tests on concrete beams strengthened with fibre composite laminates*. in *Third PhD Symposium*. 2000. Vienna, Austria.
3. Barnes, R. and J. Fidell, *Performance in fire of small-scale CFRP strengthened concrete beams*. *Journal of Composites for Construction*, 2006. 10: p. 503–508.
4. Williams, B., V.K.R. Kodur, M.F. Green, and L. Bisby, *Fire endurance of fiber-reinforced polymer strengthened concrete T-Beams*. *ACI Structural Journal*, 2008. 105(1): p. 60–67.
5. Williams, B., L. Bisby, V.K.R. Kodur, M. Green, and E. Chowdhury, *Fire insulation schemes for FRP-strengthened concrete slabs*. *Composites Part A*, 2006. 37(8): p. 1151–1160.
6. ACI 318-08, *Building Code Requirements for Reinforced Concrete and Commentary*. 2008, American Concrete Institute: Farmington Hills, MI.
7. American Concrete Institute (ACI), *Guide for the design and construction of externally bonded FRP systems for strengthening concrete structures* 2008, ACI 440.2R-08, ACI Committee 440: Farmington Hills, MI. p. 1–45.
8. American Society for Testing and Materials (ASTM), *Standard test methods for fire tests of building construction and materials*. 2007, ASTM E119: West Conshohocken, PA.
9. Davies, J.M., Y.C. Wang, and F.M.H. Wong. *Polymer composites in fire*. in *Proceedings of Advanced Composites for Structural Applications in Construction*. 2004. Guildford, Surrey, UK.

COMPOSITE STRUCTURES

Composite Columns Made of Partially Encased Steel Sections Subjected to Fire

M. KORZEN, J. P. C. RODRIGUES and A. M. CORREIA

ABSTRACT.

The behaviour of composite steel-concrete columns in comparison to bare steel columns subjected to fire is in general much better. The stiffness of the surrounding structure plays an important role in this behaviour. Therefore, a set of fire resistance tests on composite steel-concrete columns with restrained thermal elongation were carried out at the University of Coimbra, in Portugal, and the Federal Institute for Materials Research and Testing, in Berlin, Germany. Especially the influence of the restraining stiffness of the surrounding structure on the fire resistance of the columns was analyzed. The conclusions drawn in this study intended to show how the fire resistance of composite steel-concrete columns is influenced by their interaction with the building structure in a fire event.

INTRODUCTION

The composite steel-concrete columns subjected to fire behave different from the bare steel columns, because the concrete besides the resistant function has also a fire protection function. The fire resistance of composite steel-concrete columns is usually much higher than bare steel columns [1].

The stiffness of the surrounding structure plays an important role in the global failure of structural elements in case of fire [2, 3]. A set of fire resistance tests on composite steel and concrete columns made of partially encased steel sections with restrained thermal elongation were carried out at the Laboratory of Testing Materials and Structures of the Faculty of Sciences and Technology of the University of Coimbra (FCTUC), in Portugal, and the Laboratory of Fire Resistance of the Bundesanstalt für Materialforschung und -prüfung (BAM). Besides the

Manfred Korzen, BAM - Federal Institute for Materials Research and Testing, Unter den Eichen 87, 12205 Berlin, Germany.

João Paulo C. Rodrigues & António M. Correia, Department of Civil Engineering, Faculty of Sciences and Technology of Univ. of Coimbra, Rua Luis Reis Santos, 3030-788 Coimbra, Portugal.

influence of the stiffness of the surrounding structure in the fire resistance of the columns other parameters such as the load level and the slenderness of the column were analyzed. The results of the fire resistance tests carried out in both institutions are compared in the paper.

EXPERIMENTAL SET-UP AT FCTUC

A new test set-up was used at FCTUC to assess the fire resistance of the columns (Fig. 1). The system comprised a restraining frame of variable stiffness (1) that had the function of simulating the stiffness of the surrounding structure to the column in fire. The columns were subjected to a constant compressive load that intended to simulate the serviceability load of the column when part of a real structure. This load was controlled by a load cell of 1 MN located on the head of the hydraulic jack (6). The load was applied by the hydraulic jack (2) controlled by a servo hydraulic system. The thermal action was applied by a modular electric furnace (3) that could closely follow the ISO 834 fire curve. The restraining forces generated in the column due to heating were measured by a load cell of 3 MN located inside of a void steel cylinder of high stiffness compressed by a massive steel cylinder that entered in the first one due to the column elongation (4). This system was located between the testing column and the restraining frame. The axial displacements and rotations on the top and base of the column were also measured by displacement transducers (5) orthogonally arranged in three different points, forming a deformation plane.

EXPERIMENTAL SET-UP AT BAM

A central role of the substructuring method plays the BAM column furnace (Fig. 2 (a) – (b)). Mechanical and thermal actions are applied through this device to the specimen under test. Whereas the thermal set point is a known function of time for the mean gas temperature, which is realized through six oil burners, before starting the test, the mechanical set point has to be calculated online during a fire test in substructuring mode. Six electro-hydraulic control channels equipped with displacement and force sensors are available to influence the mechanical boundary conditions, i.e. two bending rotations each at top and bottom, one axial displacement at the bottom and one horizontal displacement at the top. During a substructuring test, forces and moments at the boundaries of the specimen, i.e. at the upper and lower bearings of the column, are measured and utilized for the computation of the corresponding displacements and angles, which are sent to the specimen in order to keep the entire building in mechanical equilibrium with its prescribed overall boundary conditions [4].

This closed loop for only one channel in substructuring mode is displayed in Fig. 2 (b) – (c). According to the free body diagram in Fig. 2 (c), the experiment is driven by the thermal displacement, which is diminished by the mechanical displacement u^{mech} due to the stiffness c^{mod} of the surrounding environment resulting in a compressive force on the column under test. The function of the control loop is to change the (total) displacement u by moving the position of the electro-hydraulic axial cylinder in such a way that the model force f^{mod} is equal to the measured force f .

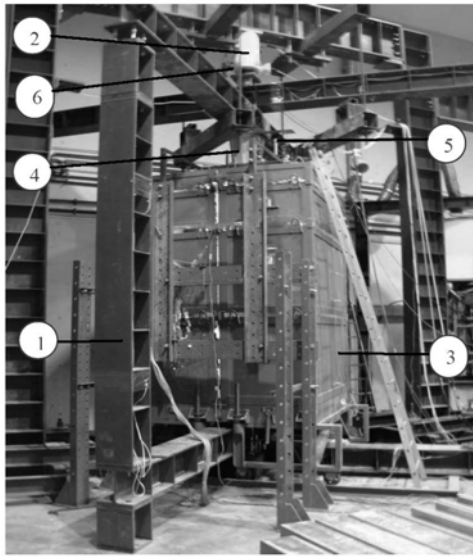


Figure 1. Experimental Set-Up at FCTUC.

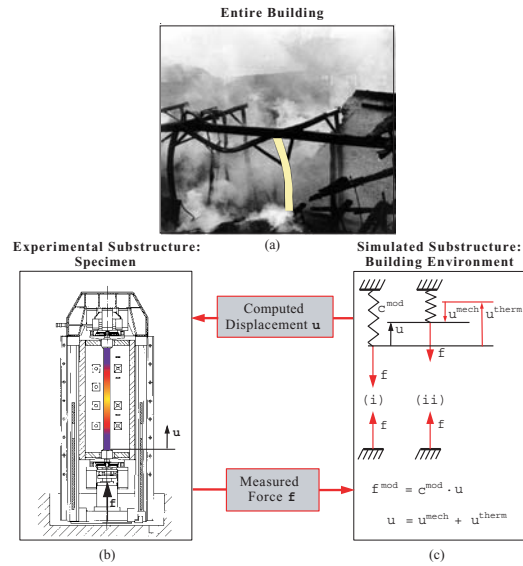


Figure 2. Experimental Set-Up at BAM.

TEST PLAN

The main objective of the test series was twofold: (i) the study of the influence of the surrounding stiffness on the fire resistance and (ii) the comparison of the performance of both experimental systems.

One of the main correlation parameters identified was the non-dimensional stiffness ratio R , defined as the ratio between the axial stiffness K of the external system (external restraining frame in the case of the FCTUC tests, virtual structure in the case of the BAM tests) and the axial stiffness C of the tested composite columns, i.e.

$$R = \frac{K}{C}. \quad (1)$$

Table I. summarizes the values of the parameters used in the tests.

TABLE I. Experimental Parameters

Reference	BAM-A	FCTUC-I	FCTUC-III	BAM-B	FCTUC-II
Length [mm]	3560	2940	2940	3560	2940
Relative Slenderness $\bar{\lambda}_z$	0.856	0.866	0.866	0.856	0.866
Initial Load [kN]	1200	1185	1185	1200	1185
K [kN/mm]	11	13	45	59	128
C [kN/mm]	664.7	788.8	788.8	664.7	788.8
R [-]	0.016		0.057	0.089	0.162

Four values for R were chosen: 0.016, 0.057 and 0.089 and 0.162. The average stiffness ratio R found in practice is between 0.05 – 0.1 [5]. Our chosen values are in this range, except for $R = 0.016$ and $R = 0.162$, which were chosen to be extreme values, one very low and the other very high.

All the FCTUC and BAM columns were made of partially encased 2940 mm

and 3560 mm long HEM 200 steel profiles, respectively (fig. 3). The steel class of the testing columns was S355 and the concrete C25/30.

The column temperature distribution was measured by type K wire thermocouples at five sections S1 to S5 (fig. 3).

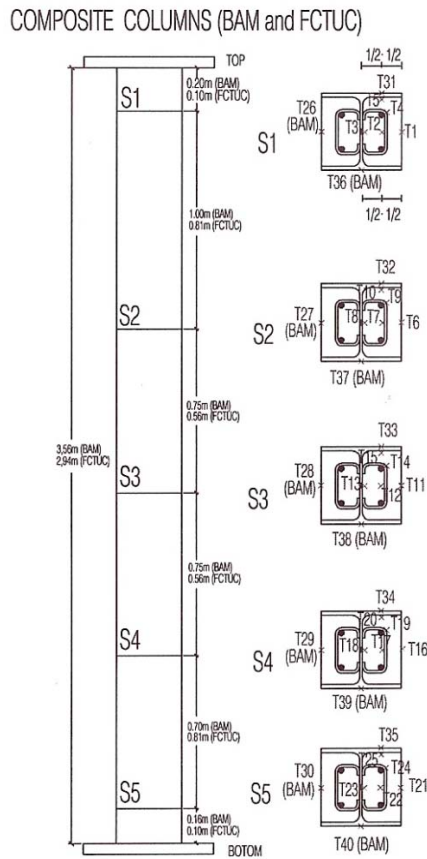


Figure 4. Specimen I (FCTUC) after test.



Figure 5. Specimen A (BAM) after test.

Figure 3. Specimens in FCTUC and BAM tests.

All the tests were run with a serviceability load of 70 % of the design value of the column buckling resistance at room temperature [1].

TEST RESULTS

Two representative examples of specimens after fire resistance tests, i.e. column I (FCTUC) and column A (BAM), are shown in Figures 4 and 5, respectively.

The temperature development in specimens FCTUC-II and BAM-A as a function of the test duration are visualized in Figures 6 and 7, respectively. Both diagrams show specimen temperatures, mean furnace temperatures and target temperatures due to the ISO 834 fire curve. Due to differences between the heating types, i.e. electrical heating at FCTUC and heating through oil burners at BAM, the FCTUC furnace temperatures are a bit in delay with respect to the target furnace temperatures. This may be the reason that the temperature distribution of the specimen BAM-A was more uniform in comparison to the FCTUC-II. The expected thermal gradients in depth in the cross-section are observed (thermocouples 11, 12 and 13) (figs. 6 and 7). However, the heating was quite uniform around the cross-section (thermocouples 33 and 38, 11 and 28 of BAM tests).

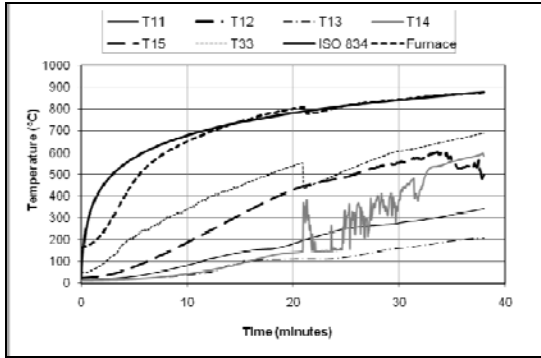


Figure 6. Furnace and specimen (Section S3) temperatures of specimen FCTUC-II.

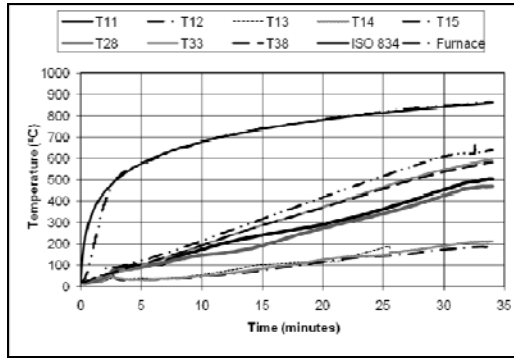


Figure 7. Furnace and specimen (Section S3) temperatures of specimen BAM-A.

Figures 8 and 9 present the evolution of temperatures along the height of columns BAM-A and FCTUC-II. It can be observed that in tests performed in FCTUC there is a higher thermal gradient in height than in BAM. This is due to the fact that the columns in FCTUC were tested with the ends in an area of the furnace not directly exposed to the electrical resistances, 0.25m in each end. In BAM, the columns were totally heated leading to lower thermal gradients along the height.

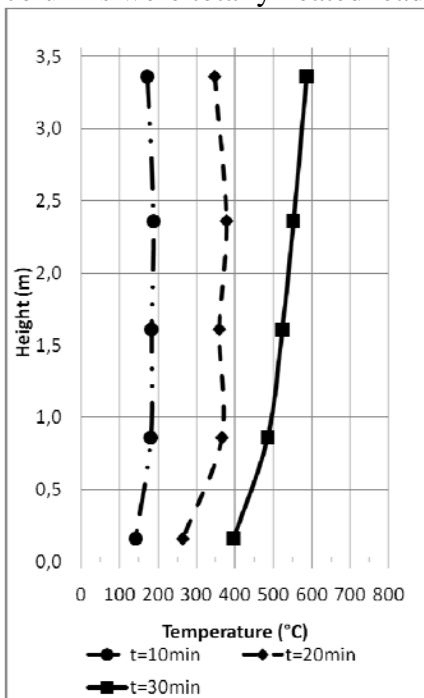


Figure 8. Thermal gradients in column's height, BAM-B.

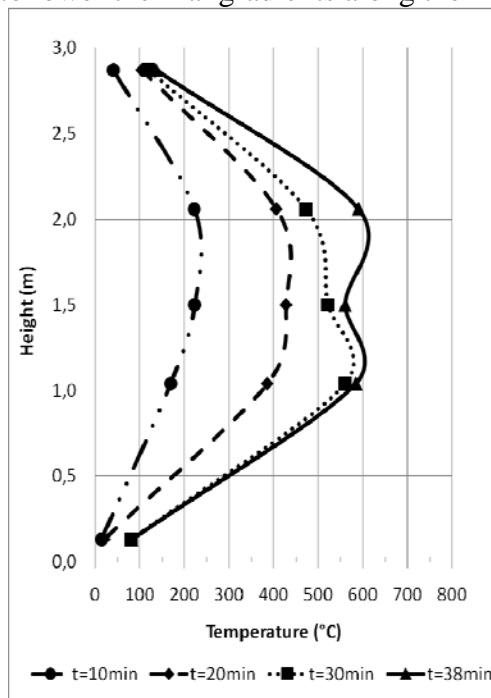


Figure 9. Thermal gradients in column's height FCTUC-II.

The evolution of the non-dimensional restraining forces, defined as the ratio between the axial restraining forces registered during the test and the initial applied load, at FCTUC and BAM tests, are presented in function of the test duration (fig. 10).

Figure 11 presents the evolution of the axial displacements as a function of the test duration. The main finding is that the axial displacements experienced by the BAM specimens were in general higher than the ones of FCTUC specimens.

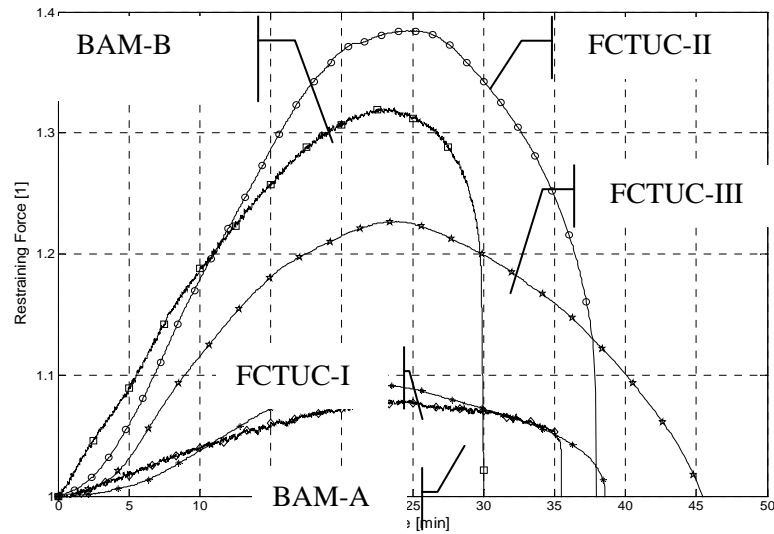


Figure 10. Test results—Dimensionless restraining forces as a function of test duration.

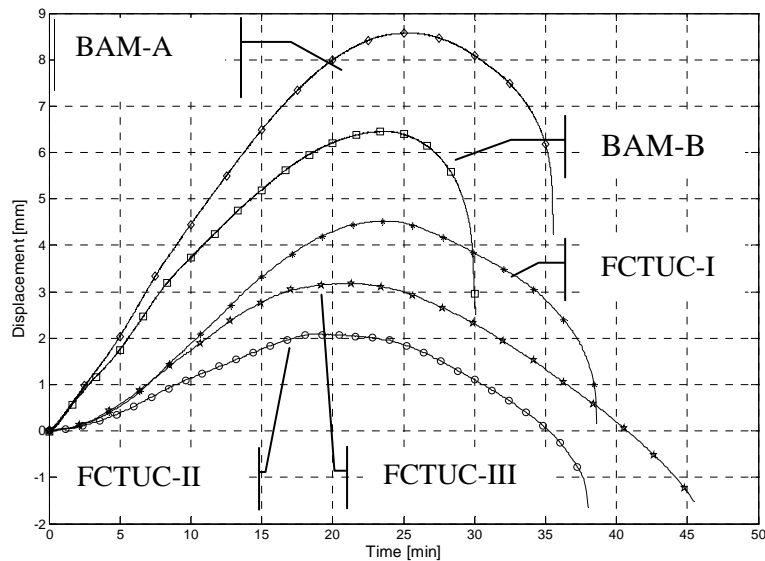


Figure 11. Test results—Vertical displacements as a function of test duration.

In figure 10 can be observed that the restraining forces were higher for the higher values of the non-dimensional stiffness.

Here we define the fire resistance as the time instant when the restraining forces has reached its initial value. It is difficult to define a pattern of variation of the fire resistance of the columns in function of the non-dimensional stiffness for the different FCTUC tests. The difference in the fire resistance in the FCTUC tests is very small, because associated to an increase of the axial stiffness is an increase of the rotational stiffness. These two stiffness play in the opposite

directions, the increase of the axial stiffness reduces while the increase of the rotational stiffness increases the fire resistance. In BAM tests the increasing of the non-dimensional stiffness ratio led to a reduction of the fire resistance.

Comparing for constant stiffness ratios the performance of the two testing systems at FCTUC and BAM one can say that the BAM system produces smaller fire resistances. The good correlation between FCTUC and BAM tests can be found for the smallest stiffness ratio, i.e. $R = 0.016$.

Concerning the axial displacements (fig. 11) the increase of the non-dimensional stiffness led to a decrease of their maximum value. The maximum axial displacements in the BAM tests were in general 4mm higher than in the FCTUC tests. The displacements in the FCTUC tests, after increase and decrease, cross the line of the initial displacement, while in the BAM tests this didn't happen and a residual displacement remained in the specimens after test (fig. 11).

Figure 12 to 15 present the force-displacement diagrams for several cases studied. In the FCTUC tests it was observed a hysteresis phenomenon in the loading unloading process, which did not occur in BAM tests. This is probably due to the fact that in FCTUC, the restraint to thermal elongation is provided by a real structure, and in BAM is a computer controlled hydraulic jack which controls the test.

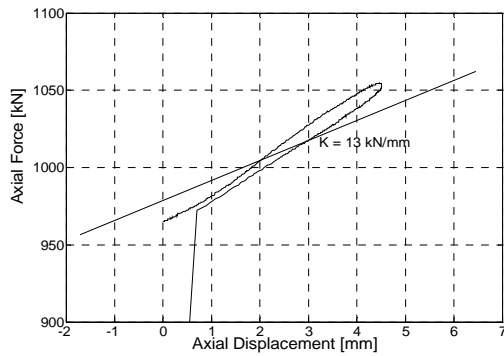


Figure 12. Force-displacement diagram of specimen FCTUC-I ($R = 0.016$).

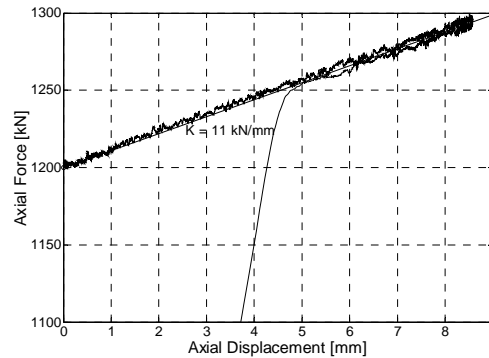


Figure 13. Force-displacement diagram of specimen BAM-A ($R = 0.016$).

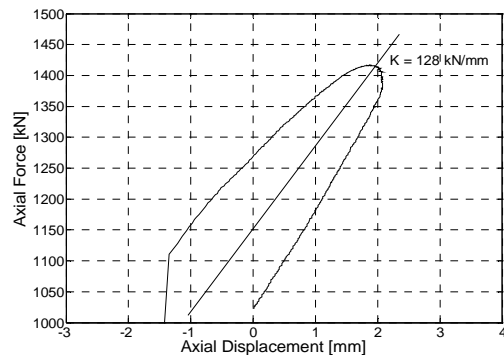


Figure 14. Force-displacement diagram of specimen FCTUC-II ($R = 0.162$).

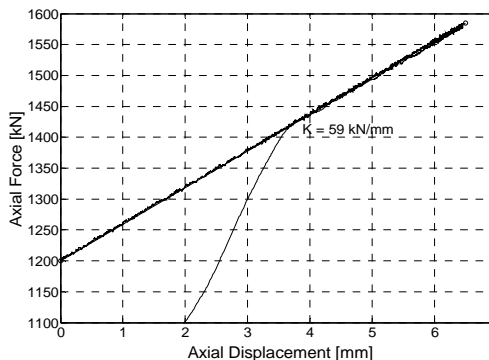


Figure 15. Force-displacement diagram of specimen BAM-B ($R = 0.089$).

Another interesting remark that should be pointed out is that the columns in BAM set-up were built-in while in FCTUC set-up the connection column-beam had

a certain rotational stiffness. This fact, although it was not quantified, must have an influence in the fire resistance of the columns.

CONCLUSIONS AND FINAL REMARKS

Concerning the comparison of the two test set-ups it can be said that they are very similar leading to very similar curves for the restraining forces. The main difference observed in the experimental set-ups was the fact that the specimen in the BAM furnace is heated along its whole length while in FCTUC furnace around 8% of the column length in each end is not heated. This fact has influence in the fire resistance, being smaller for the same testing conditions, in the BAM test set-up.

The influence of the surrounding structure has a major influence in the development of axial forces in the test columns. This can be observed in the results of the evolution of restraining forces in the five experimental tests presented in this work. With no exception, the higher the stiffness of the surrounding structure the higher the axial forces generated during the fire.

ACKNOWLEDGMENTS

The authors gratefully acknowledge the Portuguese Foundation for Science and Technology—FCT—MCTES, S.A., METALOCARDOSO S.A. and A. COSTA CABRAL S.A., Portugal, for their support.

REFERENCES

1. CEN-EN1994-1-2. 2005. "Design of composite steel and concrete structures—part 1-2: General Rules—Structural fire design", Brussels.
2. Rodrigues, J. P. C.; Neves I. C. and Valente J. C.. 2000. "Experimental research on the critical temperature of compressed steel elements with restrained thermal elongation," *Fire Safety Journal*, 35(2):77–98.
3. Huang, Zhan-Fei; Tan, Kang-Hai and Phng, Guan-Hwee. 2006. "Axial Restraint Effects on the Fire Resistance of Composite Columns Encasing I-section Steel" *Fire Safety Journal*, doi:10.1016/j.jcsr.2006.07.001.
4. Korzen, M.; Magonette G. and Buchet Ph.. 1999. "Mechanical loading of columns in fire tests by means of the substructuring method," *Zeitschrift für Angewandte Mathematik und Mechanik*, 79: S617-S618.
5. Ali, F.; Nadjai, A.; Silcock, G. and Abu-Tair, A.. 2004. "Outcomes of a major research on fire resistance of concrete columns," *Fire Safety Journal*, 39(6):433–445.

Parametrical Study on the Behaviour of Steel and Composite Cellular Beams Under Fire Conditions

O. VASSART, C. G. BAILEY, G. BIHINA, M. HAWES, A. NADJAI, C. PEIGNEUX, W. I. SIMMS and J.-M. FRANSSSEN

ABSTRACT

This paper describes an extensive parametric study on the behaviour of cellular beam under fire conditions.

Different finite element models using shell elements were developed considering both material and geometrical non-linearity; CAST3M [1], ANSYS [2] and another one in SAFIR [3]. They were calibrated on the basis of a new experimental test campaign performed in the scope of the project FICEB+ [4] funded by the Research Fund for Coal and Steel

The comparison between the finite element prediction and actual experimental results showed a good agreement in terms of failure modes, load deflection relationship and ultimate loads. At failure, temperature measured during the fire tests indicated that failure arising by web post buckling of cellular beams in fire cannot be simply estimated by applying temperature dependent reduction factors on strength alone, as given in codes.

A design model representing the behaviour of cellular beam in fire conditions has been developed by Vassart [5-7]. This design model is able to predict the complex behaviour of cellular beam in case of fire comprising web-post buckling and Vierendeel bending, as well as standard flexural bending.

The results of the Finite Element Models are compared in terms of critical temperatures and failure mode obtained using the design model.

This paper also contains some tests results that were used to calibrate the FEM model and the comparison between analytical and FEM models.

O. Vassart (ArcelorMittal R&D, G.-D. of Luxemburg)
C. G. Bailey (University of Manchester, UK)
G. Bihina (CTICM, France)
M. Hawes (ASDWestok Limited, UK)
A. Nadjai (University of Ulster, UK)
C. Peigneux and J.-M. Franssen (University of Liège, Belgium)
W. I. Simms (SCI, UK)

EXPERIMENTAL TEST CAMPAIGN

Beam geometric and material properties

An overall view of the four beams is shown in Fig. 1. As part of the composite floor plate, beams 1, 3 and 4 were considered to be secondary beams, and beam 2 was considered as a primary beam. They were fire designed according to [8].

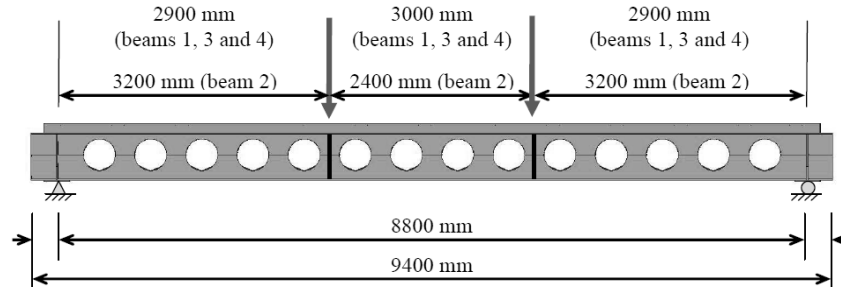


Figure 1. elevation view of the composite beams.

	Beam 1	Beam 2	Beam 3	Beam 4
Top tee section	IPE 360	IPE 450	IPE 360	IPE 360
Top tee depth h_{top} (mm)	255	275	255	255
Bottom tee section	IPE 450	IPE 450	HEB 450	IPE 450
Bottom tee depth h_{bot} (mm)	300	275	300	300
Stiffener thickness (mm)	20	20	20	20 / 15
Span : L (mm)	8800			
Overall slab length: L_t (mm)	9100			
Slab width : b_{eff} (mm)	2200			
Number of openings	13	13	13	14
Number of circular openings	12	11	12	14
Number of elongated openings	1	2	1	0
Number of semi-infilled openings	0	2	0	0
Cell diameter (mm)	375	335	375	375
Reinforcement mesh	A252			
Number of shear studs	59			
Shear stud diameter (mm)	19			
Shear stud length (mm)	100			
Shear stud spacing (mm)	150			
Mechanical load (kN)	140	160	160	140
Steel grade	S355			
NWC compressive strength (MPa)	31.0	33.0	33.5	29.5

Table 1. Geometries and properties of the tested beams.

The main geometric and material properties of the beams are shown in Table 1. In addition to the web stiffeners at load points and at its end supports, for beam 4, there was a one side stiffener at each web-post. The upper steel flange was fully connected to the 120mm deep composite slab, which comprised a COFRASTRA 40 ® re-entrant deck, via Nelson headed studs.

The slab width was 2.20 m which equals to the effective width b_{eff} according to Eurocode 4 part 1.1. [9], i.e. $2 L/8$. As for the reinforcement steel, a mesh of 252 mm²/m was used.

Failure mode

For both beam 1 and beam 3, the failure was due to web-post buckling near the beam supports (Figure 2), which is one of the usual modes of failure observed for such beams in fire situation..

Besides, because of its web-post stiffeners, beam 4 could only have a flexural bending failure, as it behaved like an “ordinary” beam. Hence, as beam 1 and beam 4 had the same cross-section, and as their deflection vs. time graphs are very close, beam 1’s collapse might have been caused by combined web-post buckling and flexural bending.

As for the primary beam, i.e. beam 2, no web-post buckling was observed, which leads to the conclusion that this beam also failed by flexural bending.

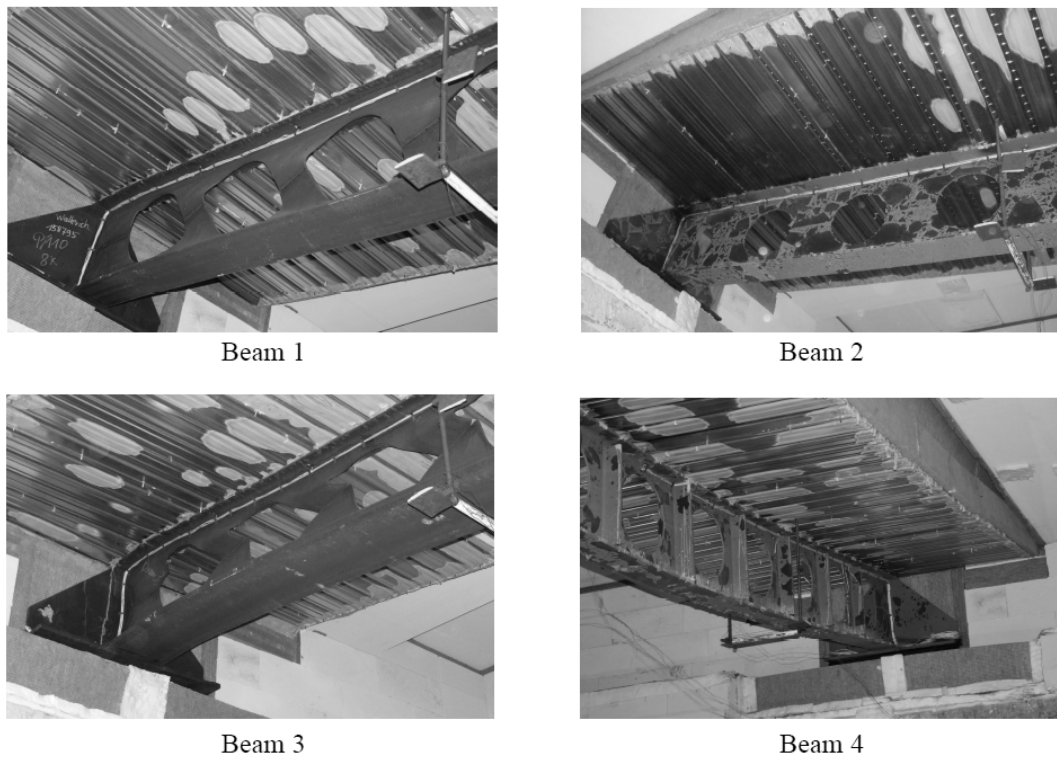


Figure 2. Deformed beams.

NUMERICAL MODELING

The parametric study was run conducted using SAFIR (version 2007a), CAST 3M and Ansys.

SAFIR Mechanical model

For the mechanical model of the steel profile, 4-node shell finite elements were used, as shown in Figure 3.

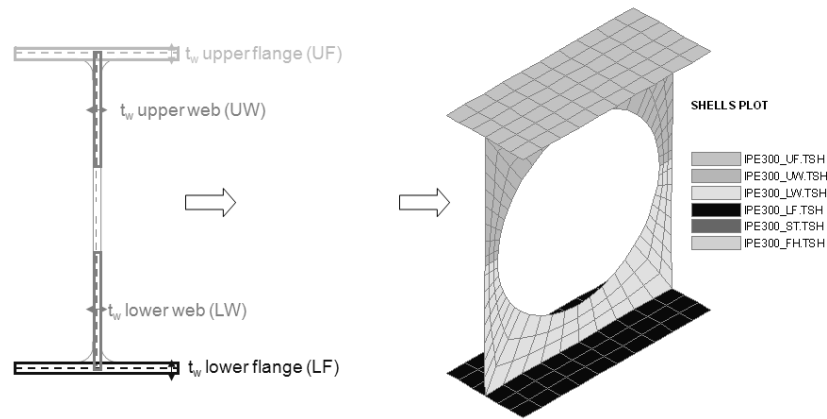


Figure 3. Mechanical model.

The beam was simply supported. Symmetry was used at the mid-span and the lateral displacement of the upper flange was restrained to avoid any lateral torsional buckling (Figure 3).

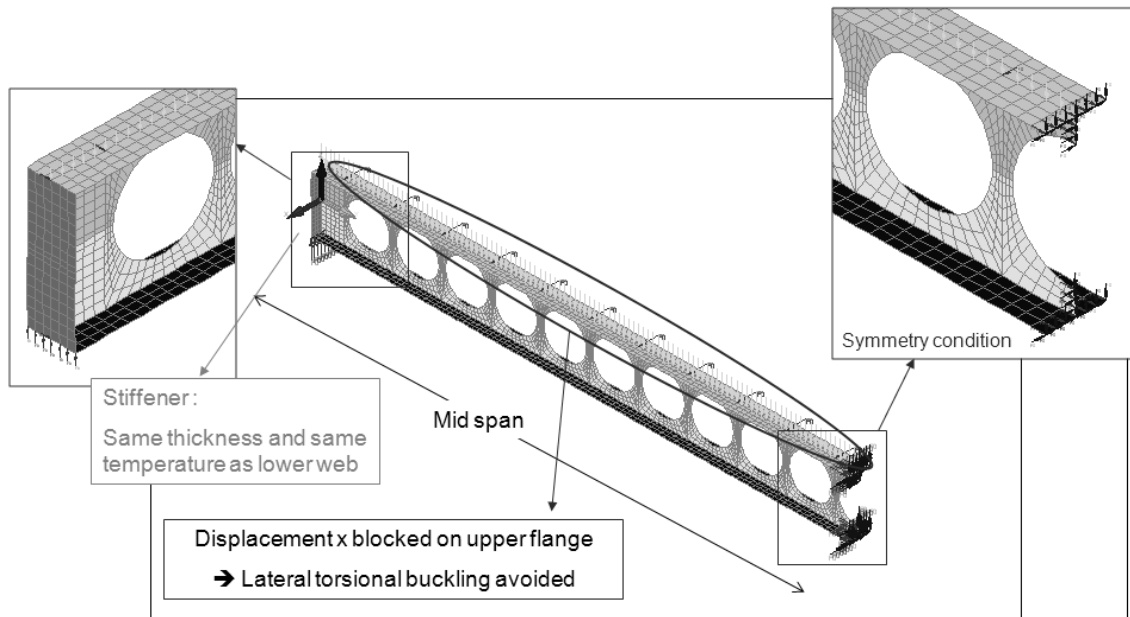


Figure 3. Boundary conditions for modelled beam.

An initial deformation was given to the beam (Figure 4a). This deformation results from the product of a sine curve on the height of the profile (Figure 4b) and of a cosine curve on the length of the beam. The maximum amplitude was 2 mm.

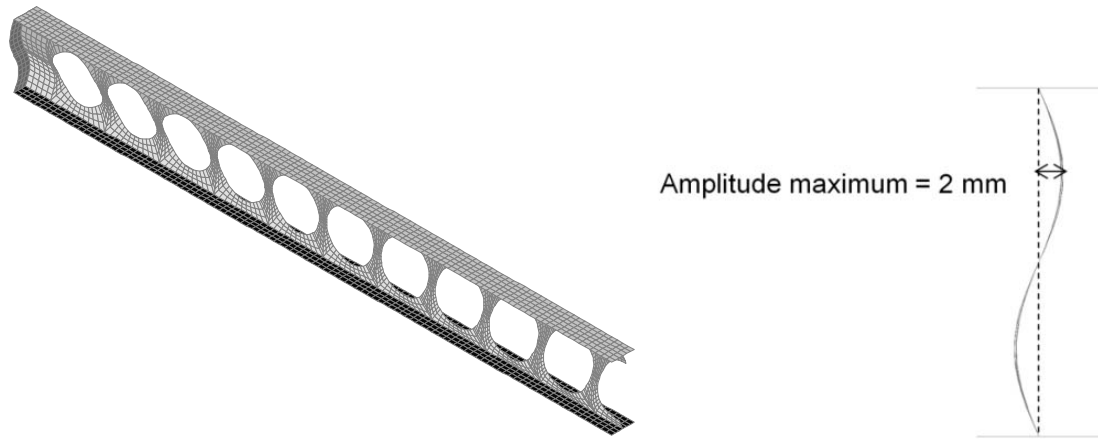


Figure 4: a) CB with amplified initial deformation (x 15) and b) initial deformation of the web-post.

The assumed material properties of the steel were taken according to Eurocode EN1993-1-2 [10], with the variation of different parameters with temperature taken from Eurocode EN1993-1-2.

The Figure 5 shows the comparison between FEM model and the fire test beam 2.

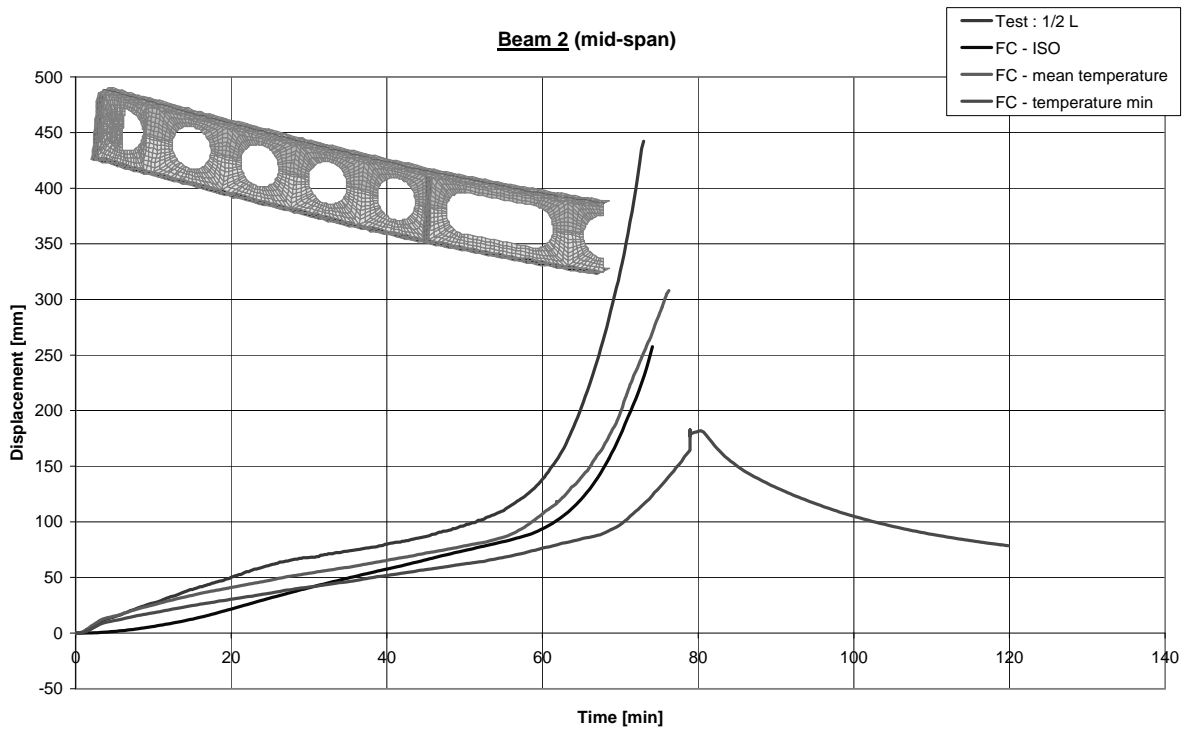


Figure 5. Time-Displacement diagram of the beam 2 at mid-span.

Anslys Numerical Model

The Ansys model was based on a 3D mesh made of shell and beam elements (Figure 6a). As the ribs were neglected in the model, only the concrete part above the steel deck was modelled (Figure 6b). The experimental measured yield strengths were used.

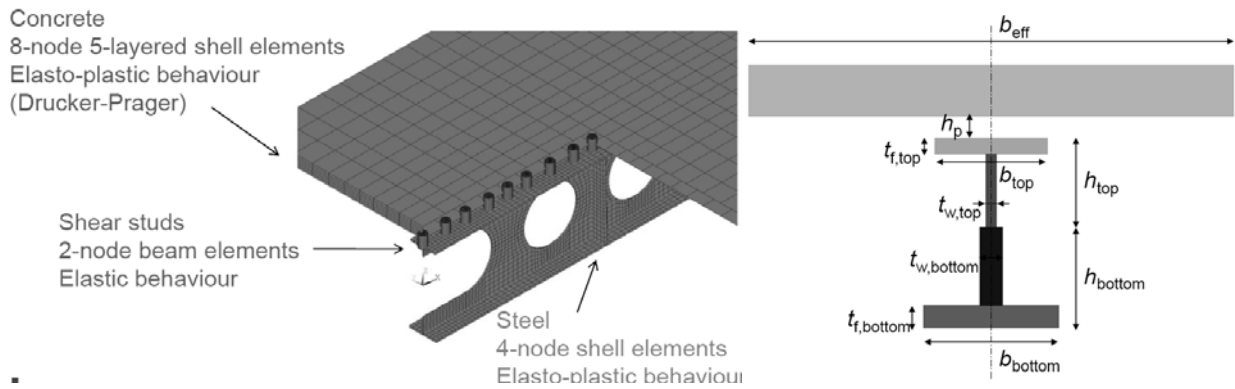


Figure 6. a) Mechanical analysis model and b) Mechanical analysis cross-section.

Due to mid-span symmetry, axial restraints and rotational restraints about the two axes of mid-span cross-section were applied. Support conditions were modelled by restraining vertical displacements. Also, so as to prevent lateral torsional buckling, flange-web junctions in both tees were laterally restrained. The mechanical load was applied to the top steel flange, including self-weight. The analysis was run until numerical failure. Figure 7 shows the comparison between the FEM model and the fire test beam 2.

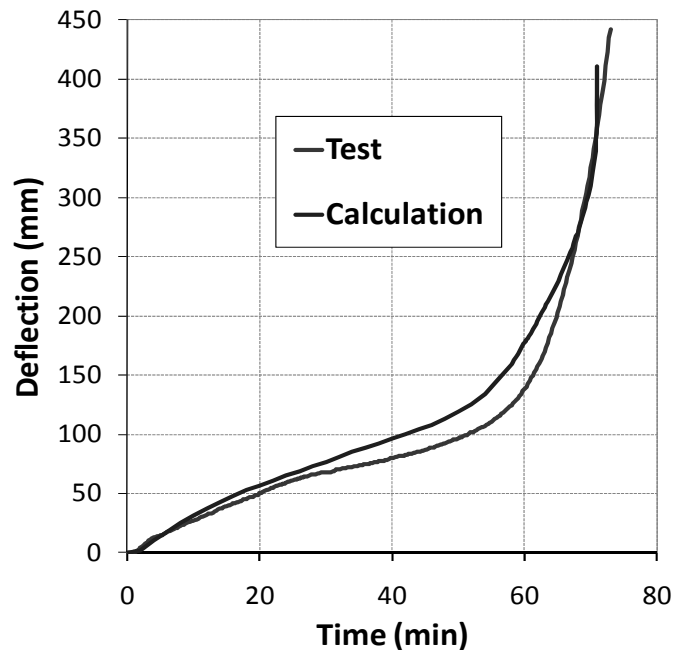


Figure 7. Time-Displacement diagram of the beam 2 at mid-span.

Conclusion on FEM Modelling

A good agreement between the tests and both FEM models is observed, in terms of failure modes and critical temperatures. Thus, these models can accurately predict the mechanical behaviour of a simply-supported composite cellular beam at elevated temperatures, and can be used for the parametric study which aims to check the relevance of the simplified design method.

PARAMETRICAL STUDY

This parametrical study was made varying the following parameters:

- steel profile
- geometry of the web-post
- steel strength limit
- loading type
- slab type

Table 2 is summarising the different calculated cases.

Sum-total, 192 simulations are foreseen for pure steel beams and 192 simulations for composite beams.

Results of the parametrical study

The critical temperature and the failure modes were assessed using finite element models and compared with analytical model using the following formula:

$$\frac{(\mathit{Crit_Temp}_{FEM} - \mathit{Crit_Temp}_{Analytical})}{\mathit{Crit_Temp}_{FEM}} \times 100 = \Delta$$

This means that when the points are positive, the analytical model predicts a lower critical temperature than the finite element model and so is considered conservative (i.e safe sided).

Figure 8 shows the comparison of the results between FEM and analytical model.

Analysing Figure 8, it can be pointed out that the analytical models can predict the critical temperature of steel cellular beams. The analytical model, based on Eurocodes principles, provides safe sided results with acceptable level of accuracy.

It can also be pointed out that the analytical models can also predict the critical temperature of composite cellular beams.

Some numerical simulations still running and points of comparison with analytical models will be added for composite sections. Moreover, the numerical modelling are still analysed because some discrepancies in the results appeared between the different finite elements models for composite sections.

CONCLUSIONS

The different FEM models were able to reproduce with an acceptable level of accuracy the complex behaviour of cellular beams in fire conditions.

On the basis of theses different FEM models, a parametric study was made to validate the developed analytical model.

Parameter	minimum value	maximum value	step	number of different beams	
				PS (Pure steel)	CB (Composite Beam)
general properties	span	8 m	20 m	4	4
	Pure Steel beam or Composite Beam			1	1
	fire curve		ISO fire curve	1	1
	loading		PS : 2 concentrated loads - distributed load (load ratio = 0.5) CB : distributed load (load ratio = 0.5)	2	1
	steel profile	IPE ... - HE ...	PS : IPE300 - HEA400 - HEM900 CB : IPE300 - HEA400 - IPE300/HEA400	3	3
	steel grade of the profile	f_y	IPE300 : S275 - S355 HEA400 et HEM900 : S355 - S460 IPE300/HEA400 : S355/355 - S355/460	2	2
	total height of the profile	H_t	depending of the steel profile, a_0 and w	1	1
	height lower profile	H_{LP}	depending of the steel profile	1	1
	upper flange thickness	t_{UF}	depending of the steel profile	1	1
	upper web thickness	t_{UW}	depending of the steel profile	1	1
steel profile	lower web thickness	t_{LW}	depending of the steel profile	1	1
	lower flange thickness	t_{LF}	depending of the steel profile	1	1
	diameter of openings	a_0	a_0 "normal"	2	2
	position of the first opening	w_0	-	1	1
	web post width	w	for a_0 "normal" : w_{max} and w_{min} (>50) for a_0 max : $w_{optimum}$ and $w_{small\ value}$	2	2
	protection			1	1
	concrete slab thickness	h_c	$h_p = 59\text{mm}$ $h_c = 61\text{mm}$		2
	overall depth of the profiled steel sheeting	h_p	$h_p = 0\text{mm}$ $h_c = 120\text{mm}$	60	
	concrete effective width	b_{eff}	min (2 m ; $L/4$)	-	1
	concrete grade	f_{ck}	C25/30 if S275 and S355 - C30/37 if S460		1
concrete slab	concrete slab reinforcement	A_s	0.00%		1
	reinforcement grade	f_{sk}	S500		1
	degree of shear connection	h	100%		1
				192	192
				= total number of simulations for steel CB	= total number of simulations for composite CB

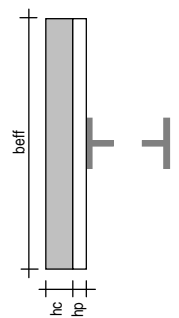
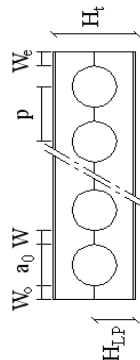


Table 2. Parametrical study cases.

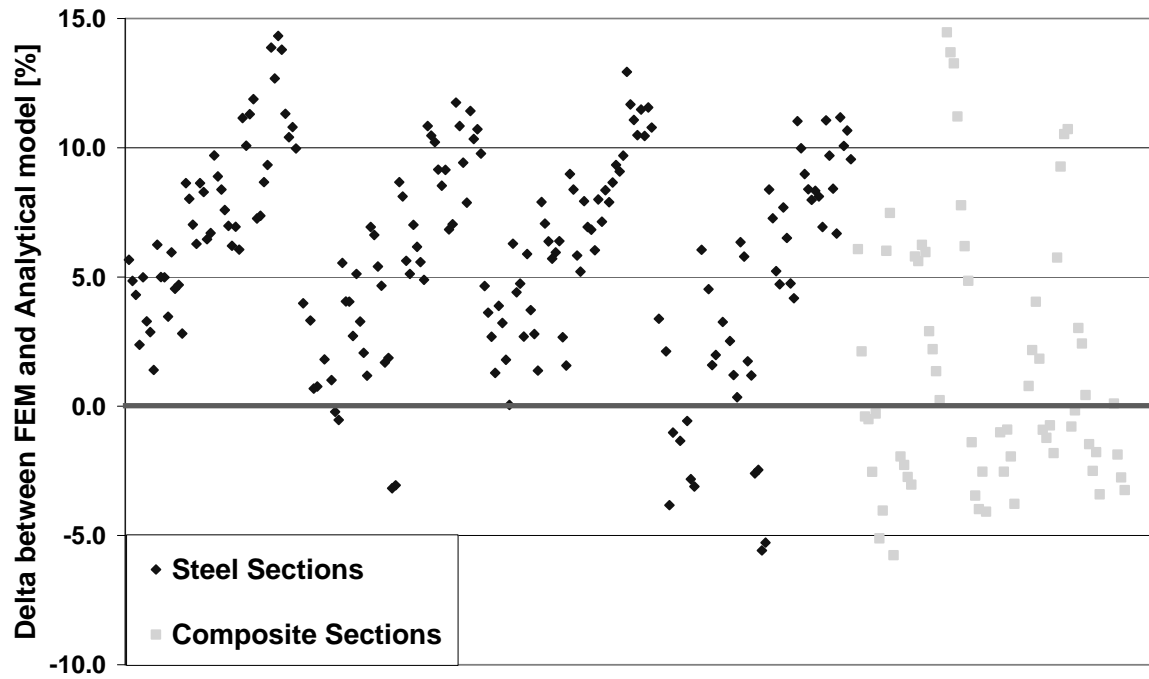


Fig. 8: Time-Analytical model Vs FEM Modelling

The analytical model was again validated by this parametrical study and can be used for the prediction of the critical temperature of cellular beam in case of fire. This model takes into account the complex behaviour of cellular beams in fire conditions and is based on the Eurocodes principles taking into account the loss of material properties and stiffness required in the Eurocodes. This model was implemented in a design software called ACB+ and can be downloaded for free on www.arcelormittal.com/sections .

REFERENCES

1. CAST 3M - GUIDE D'UTILISATION : CEA/DMT/LAMS
2. Ansys, Inc. (2006). "ANSYS Academic version, Release 10.0, Help System".
3. SAFIR. A Thermal/Structural Program Modelling Structures under Fire, Franssen J.-M., Engineering Journal, A.I.S.C., Vol 42, No. 3 (2005), 143–158.
4. Technical annex of RFCS project FICEB+ (Fire resistance of long span Cellular Beam made of hot rolled profiles), ArcelorMittal, WESTOK, SCI, CTICM, ULG, Ulster University, 2006.
5. Nadjai A, Vassart O., Ali F., Talamona D., Allam A., Hawes M. "Performance of Cellular composite floor beams at elevated temperatures" Fire Safety Journal, Volume 42, Issues 6-7, September-October 2007, Pages 489–497.
6. Vassart O. , Bouchair A., Muzeau J-P and Nadjai A. "Analytical model for the web post buckling in cellular beams under fire" Fifth International workshop Structures in Fire, Singapore 2008.
7. Vassart O. "Analytical model for cellular beams made of hot Rolled sections in case of fire" PhD thesis Université Blaise Pascal, Clermont Ferrand, 2009.
8. ASDWestok Cell Beam Software, V 3.01, Steel Construction Institute.
9. CEN, Eurocode 4 - Design of composite steel and concrete structures—Part 1-1: General rules and rules for buildings, 2005.
10. EN1993-1-2 "Eurocode 3: Design of steel structures - Part 1–3: General rules and structural fire design.

Performance of RC Beam to Concrete Filled Steel Tubular (CFST) Column Frames Subjected to Fire

L.-H. HAN, W.-H. WANG and H.-X. YU

ABSTRACT

This paper describes a test program carried out on reinforced concrete (RC) beam to concrete filled steel tubular (CFST) column planar frames under ISO-834 standard fire. These tests were meant to reproduce the conditions of the CFST columns and RC beams in multi-storey composite buildings commonly used in China. The columns in four of the framed specimens used circular steel tubes while the rest two were square tubes. Other test parameters include the level of axial load in the CFST column, the load level in the RC beam and the beam-column stiffness ratio. A finite element analysis (FEA) model was developed and a comparison of results from this model with the test results shows generally good agreement.

KEYWORDS:

Concrete filled steel tubes (CFST); Reinforced concrete (RC); Frames; Fire resistance; Finite element model (FEA); Analysis.

Lin-Hai Han (corresponding author), Professor, Department of Civil Engineering, Tsinghua University, Beijing, 100084, P. R. China, Tel: 86 10 62797067, Fax: 86 10 62781488, E-mail: lhhan@tsinghua.edu.cn

Wei-hua Wang, Ph.D., Department of Civil Engineering, Tsinghua University, Beijing, 100084, P. R. China, Email: wangwh@tsinghua.edu.cn

Hong-xia Yu, Ph.D., Department of Civil Engineering, Tsinghua University, Beijing, 100084, P. R. China, Email: yuhx@tsinghua.edu.cn

1. INTRODUCTION

Concrete filled steel tubular (CFST) columns have a high load bearing capacity and naturally obtain excellent fire resistance, which make them particularly suitable to be applied in high-rise buildings and subway constructions. Previously, a large number of studies have been performed to understand the realistic behaviour of CFST columns under fire conditions, such as Lie and Caron [1], Hass [2], O’Meagher et al. [3], Lie and Chabot [4], Lie and Stringer [5], Kodur [6], Kim et al. [7], Tan and Tang [8], Han et al. [9], Ding and Wang [10] etc. However, research is rare on the fire performance of CFST frames with RC slabs.

This paper is thus an attempt to investigate the interactions between the RC beam and the CFST column by conducting six planar frame tests subjected to ISO-834 standard fire [11]. The test setup is introduced and test results reported. After that, a finite element analysis (FEA) model is developed and shown to reproduce the test results with good accuracy. Failure mechanisms of RC beam to CFST column frames are at last investigated by looking into the test observations and FEA results.

2. EXPERIMENTAL STUDIES

2.1 Specimen information

Six RC beam to CFST column framed specimens have been tested, four of them used circular columns, and the rest two used square columns. Fig. 1 shows a schematic view of the composite frame under loading with its relative position in the furnace. The test parameters were shown in Table I, including the column cross-sectional type, the level of axial load in the column (n), the load level in the beam (m) and the beam-column stiffness ratio (k).

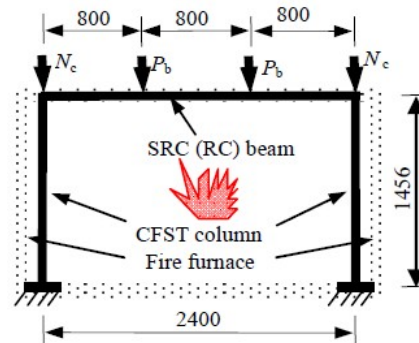


Figure 1. A schematic view of the frame (unit: mm).

TABLE I. SUMMARY OF SPECIMEN INFORMATION.

Specimen label	Column dimension $D \times t_s$ (mm)	Beam dimension $b \times h$ (mm)	Beam to column stiffness ratio k	Load level in column $n(N_c/kN)$	Load level in beams $m(P_b/kN)$
CFRC-1	140 × 3.85 (7)*	180 × 100	0.95	0.58(760)	0.3(19.5)
CFRC-2	140 × 3.85 (6)*	180 × 100	0.95	0.29(380)	0.3(19.5)
CFRC-3	140 × 3.85 (3)*	180 × 100	0.95	0.29(380)	0.6(39)
CFRC-4	140 × 3.85 (6)*	160 × 100	0.45	0.29(380)	0.3(11.5)
SFRC-1	140 × 3.51 (4)*	200 × 120	0.85	0.27(330)	0.3(22)
SFRC-2	140 × 3.51 (11)*	200 × 120	0.85	0.54(660)	0.3(22)

*The number in the “()” represents the thickness of the fire protection to the CFST columns.

In table I, k is calculated as $k = ((EI)_{beam}/L)/((EI)_{column}/H)$, where $(EI)_{beam}$ and

$(EI)_{\text{column}}$ are the flexural stiffness of the beam and the column, respectively; $n = N_c/N_u$, where N_c is the axial load and N_u is the axial compressive capacity of the column at ambient temperature; $m = P_b/P_u$, P_b is the vertical load applied on the beam and P_u represents the load to reach the bending capacity of the same beam, but with simply supported boundary condition at ambient temperature; D and t_s are the overall dimension and thickness of the steel tubes. The diameters of the upper and lower longitudinal bars in the RC beams were 12 mm and 16 mm for all specimens but CFRC-4, for which the diameters were 10 mm and 12 mm, respectively.

Details of the framed specimens are shown in Fig. 2. The columns were made of cold formed steel tubes (for square sections, the inner radius of corners for square tubes is 5 mm). Steel brackets were provided at the beam-to-column junctions to help transfer the shear force from the beam to the columns. Two semi-circular holes of 20 mm in diameter were drilled in the wall of the column, adjacent to the top and bottom plate respectively. The corner longitudinal steel bars of the RC beam were designed to enclose the column without passing through them. The concrete cover for the trapezoidal brackets was 40 mm and the thickness of the steel plates was 4 mm in all brackets, which were welded to the steel tubes. The longitudinal and transverse reinforcements in the RC slab were at 200 mm interval with a diameter of 8 mm. The thermal conductivity (k_p), specific heat (c_p) and density (ρ) of the sprayed fire protection applied to the columns are $0.116 \text{ W/(m}\cdot\text{k)}$, $1.047 \times 10^3 \text{ J/(kg}\cdot\text{k)}$, and $400 \pm 20 \text{ kg/m}^3$, respectively. Its water content is 5 percent.

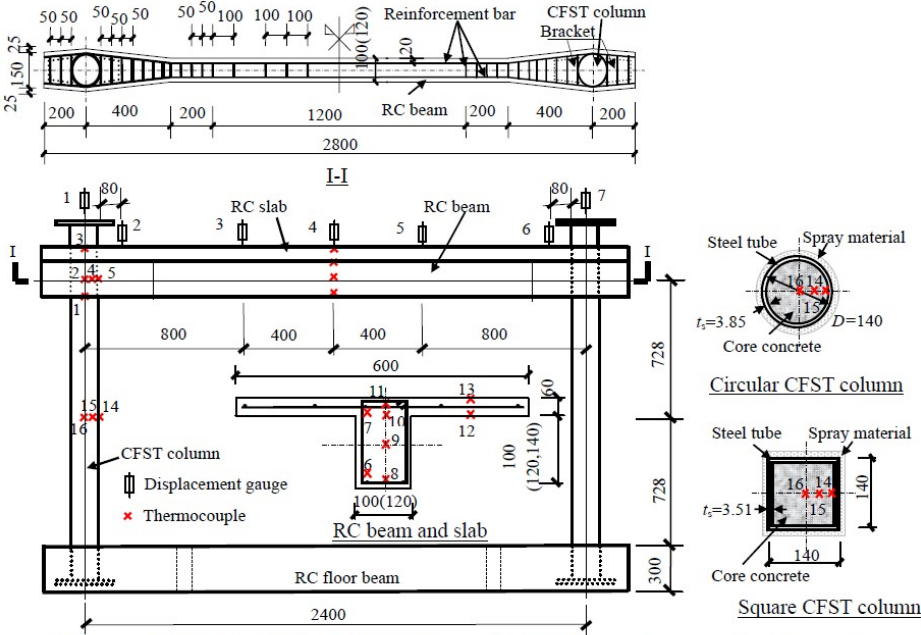


Figure 2. Details of the CFST Column to RC Beam Frames (unit: mm).

Table II lists the measured average values for the yield strength (f_y), ultimate strength (f_u), modulus of elasticity (E_s) and Poisson's ratio (ν_s) of the steel tubes and reinforcements. The fine aggregate and coarse aggregate used in concrete were silica-based sand and carbonate stone. The average cube strength at 28-day and the time of testing (the tests were carried out with a concrete curing age of about two months) were 47.4 MPa and 56.7 MPa, respectively.

TABLE II. MATERIAL PROPERTIES OF STEEL.

Steel type	Thickness/ Diameter (mm)	f_y (MPa)	f_u (MPa)	E_s (N/mm ²)	s
Circular tube	3.85	412	489.67	2.11 10 ⁵	0.283
Square tube	3.51	263.1	389.6	2.05 10 ⁵	0.301
Reinforced bar (16)	16	427.7	641.3	2.02 10 ⁵	0.282
Reinforced bar (12)	12	445.0	691.5	2.03 10 ⁵	0.270
Reinforced bar (10)	10	445.9	642.1	2.00 10 ⁵	0.277

2.2 Test results

At the start of the tests the furnace air temperature was about 20°C, and only the space under the RC slab was heated. During the testing, the specimen was exposed to fire controlled with the average temperature in the furnace following as closely as possible to the ISO-834 Standard fire [11], and the failure criteria specified by this Standard for elements subjected to axial actions and flexural loads were adopted to determine the failure time of the CFST column and RC beam respectively. The fire tests were stopped when the tested specimen could not withstand the loads applied on the CFST columns and RC beam. The test measured results and the FEA predicted fire resistance, which will be described later in Section III, are presented in Table III. In the table, Δ_{ctu} is the ultimate axial deformation of the left or right column (point 1 or 7 in Figure 2) measured in the tests, Δ_{btu} is the ultimate mid-span deflection (point 4 in Figure 2) of the beam.

TABLE III. TEST RESULTS OF CFST FRAME SPECIMENS.

Specimen label	exposure time t (min)	Fire resistance (min)				Δ_{ctu} (mm)	Δ_{btu} (mm)	Limiting temp (°C)	First Failure
		Measured	Predicted	Designed Column	Designed Beam				
CFRC-1	41	40	35	90	57	15.6	73.4	230	Column
CFRC-2	80	79	86	150	57	2.8	89.8	493	Beam
CFRC-3	48	40	42	90	13	15.6	131.5	344	Beam
CFRC-4	95	83	86	150	29	14.3	136.6	563	Beam
SFRC-1	70	70	-	90	71	2.0	83.9	518	Beam
SFRC-2	72	72	-	90	71	5.7	80.3	239	Beam

It can be seen from Table III that the tested fire resistances were between those designed values for the individual columns (determined by Han [12]) and the simply supported isolated beams (calculated with FEA methods), except CFRC-1. This happened because the restraints to the RC beam provided by the CFST columns were favorable to the fire resistant behaviour of the beam, but put the column in a disadvantaged condition. For CFRC-1, the columns were at the same time subjected to a high amount of axial load, which caused a very early failure of the columns and subsequently the beam.

Figure 3 shows the measured temperature distributions (dashed lines) in CFRC-2, which is typical of other specimens. It can be found that the

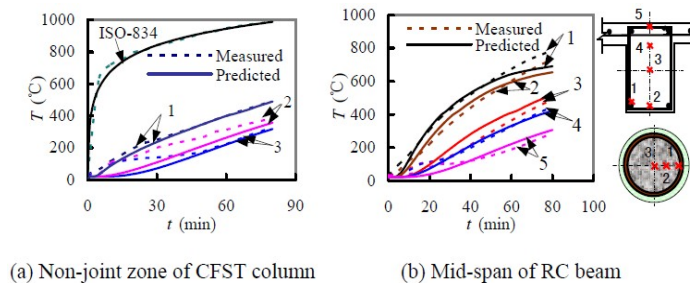


Figure 3. Temperature Distributions (CFRC-2).

temperature development of the core concrete were far delayed by the fire protection coating, and because of the complex influence of the water vapour, the temperature curves show a platform when the temperatures increase to about 100°C, and this platform lasts longer when the distance from the fire exposed surface is larger. Over the beam section, the corner (point 1) shows the highest temperature. From the bottom to the top along the middle line, the measured temperature decreased quickly.

The measured displacement versus time curves are shown in Figure 4. Due to the interaction between the steel tube and the core concrete, composite columns show a slower and smoother failure than pure steel columns. It can be seen from the figure that irrespective of the load level of the RC beam, the deflection at the mid-span of the beam increased quickly near failure time. However, when the beam to column stiffness ratio was low, such as CFRC-4, the slope of deflection increasing was smaller than other specimens.

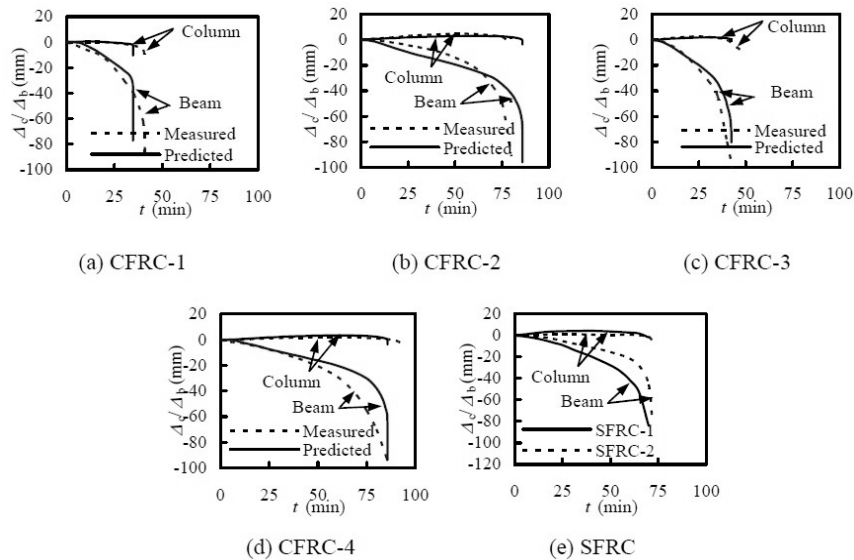


Figure 4. Deformation versus Time Relationship of Columns and Beams.

Two failure modes: column failed first (mode I) or beam failed first (mode II) were shown in Figure 5 according to the test results. Differences can be observed by comparing these two failure modes. The beam near the joint cracked severely in mode I, while no such cracks were observed in mode II, and the cracks in mid-span of the beam were lighter in mode I than that in mode II.

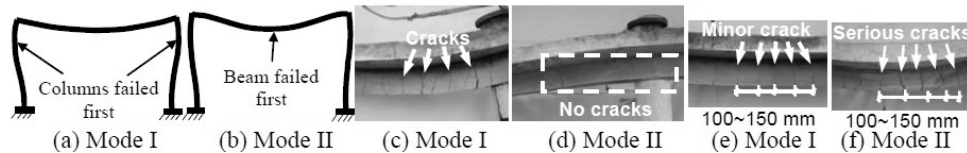


Figure 5. Typical Failure Modes.

3. FINITE ELEMENT ANALYSIS (FEA) MODEL

3.1 General descriptions of the FEA model

A FEA model was developed using the commercial program ABAQUS/Standard 6.5. Elastic-plastic model was used to describe the constitutive behaviour of the steel with its high temperature stress-strain relationship following that by Lie[13]. The damaged plasticity model predefined

in ABAQUS for concrete (Hibbitt et al [14]) was used here. The uniaxial compressive behaviour of core concrete for CFST followed that presented by Song et al. [15]. The compressive property of RC concrete and tensile behaviour of all concrete followed that presented by Han et al. [16].

The FEA models are shown in Figure 6. The 8-node brick elements, with three translation degrees of freedom at each node was used for the concrete. The 4-node shell elements were used for the steel tubes and brackets, and the 2-node truss elements were used to model all the steel bars. The applied loads N_c and P_b were applied through a rigid patch attached to the corresponding loading position.

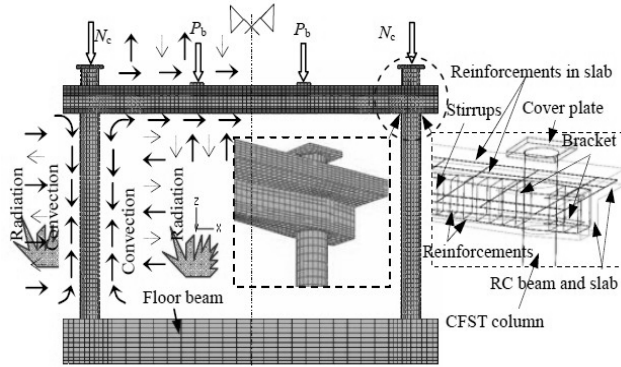


Figure 6. FEA Model of the CFST Frames.

3.2 Verifications of the FEA model

The predicted and measured fire resistances are shown in Table III, and the predicted and measured typical temperature distributions in structural members are compared in Figure 3 for CFRC-2. The deformation versus time relationships for the columns and the beams are shown in Figure 4. From all above three aspects, the predicted results show generally good agreement with the measured results.

General view comparisons of the deformed shapes of the circular framed specimens are shown in Figure 7. It can be seen that generally they match well in terms of the failure modes.

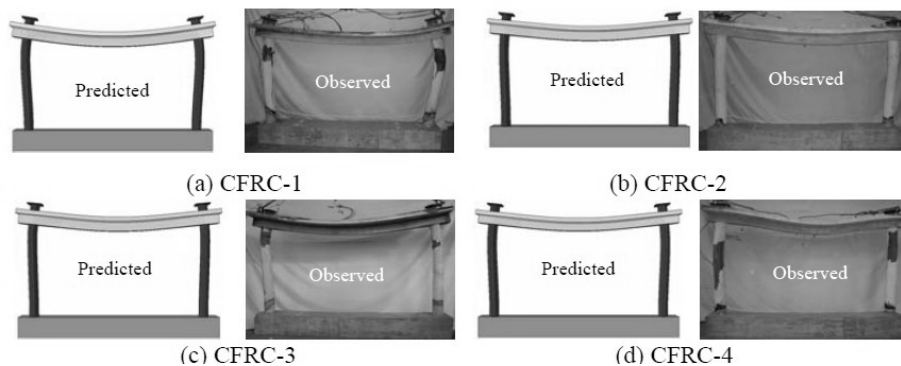


Figure 7. Comparisons between Predicted and Observed Failure Modes.

3.3 Analytical Behaviour

Under fire environments, concrete would crack at the locations of maximum tensile stresses when they reached the tensile resistance under the combined action of high temperature and the mechanical loading. Therefore, the distribution of the tensile stresses gives a good indication of the crack pattern and crack severity. Figure 8 shows a comparison of the tensile stress distribution against the observed crack pattern for specimen CFRC-1 at a heating time of 33

minutes. In Figure 8 (b), it could be seen that the tensile stress near the CFST columns along the RC beam axial line was higher than that in both sides, which coincides with the crack pattern at the top of joint zone.

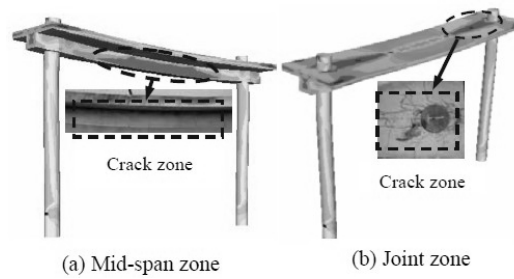


Figure 8. Predicted Tensile Stresses versus Test Phenomena (CFRC-1).

Based on the FEA modelling results, many aspects that could not be measured during the fire

tests can now be presented, such as the mid-span moments and the joint internal moments of the RC beams, as shown in Figure 9 for all circular framed specimens. The sagging moments at the mid-span of the RC beams decreased in the initial heating phase. After about 20 min, the sagging moments reached their lowest values. Then the sagging moments increased with heating time until the framed specimens failed, as shown in Figure 9 (a). Near failure, the sagging moments increased very quickly. The hogging moment in the joint zone of the RC beams increased in the initial heating stage, due to the non-uniform thermal expansion in the lower section and the axial extension of the RC beams. The development of hogging moments at the ends of the beam was because of the rotational restraint due to the existence of the column. Therefore, the amount of the hogging moments that can be maintained at the beam ends provides a strong indication of the column restraint stiffness. From Figure 9 (b), it could be seen that the hogging moment started to decrease from about 20 min, which seems to indicate the start of the column weakening.

By failure, the hogging moment of CFRC-1 turned to a sagging moment, which indicates complete failure of the columns. This is in agreement with the test observations.

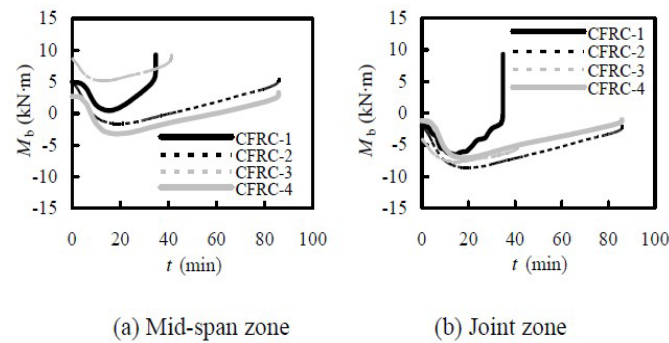


Figure 9. Internal Forces of RC Beams.

4. CONCLUDING REMARKS

This paper reported six tests on composite frames with circular or square columns and RC beams subjected to ISO-834 Standard fire. Two failure modes were observed for the framed specimens: column fails first, or the beam fails first. The test results show that the fire resistances of the frame were generally lower than those of individual CFST columns and higher than those of isolated RC beams. A FEA model was established and its accuracy was validated by comparing to the test results. This FEA modelling technique can be used to further investigate the performance of the composite frames under fire.

ACKNOWLEDGEMENTS

The research reported in the paper is part of the Project 50738005 supported by National Natural Science Foundation of China, and the Technical Supporting Programs Funded by Ministry of Science & Technology of China (No. 2008BAJ08B014-07). The financial support is highly appreciated.

REFERENCES

1. Lie, T.T. and Caron, S.E.. 1988. "Fire Resistance of Hollow Steel Columns Filled with Siliceous Aggregate Concrete: Test Results," NRC-CNRC Internal Report, No. 570, Ottawa, Canada.
2. Hass, R.. 1991. "On Realistic Testing of the Fire Protection Technology of Steel and Cement Supports," Translation BHPR/NL/T/1444, Melbourne, Australia.
3. O'Meagher, A. J., Bennetts, I. D., Hutchinson, G. L. and Stevens, L. K.. 1991. "Modelling of HSS Columns Filled with Concrete in Fire," BHPR /ENG/R/91 /031/ PS69, Melbourne, Australia.
4. Lie, T. T. and Chabot, M.. 1992. "Experimental Studies on the Fire Resistance of Hollow Steel Columns Filled with Plain Concrete," NRC-CNRC Internal Report, No.611, Ottawa, Canada.
5. Lie, T. T. and Stringer, D.C.. 1994. "Calculation of the Fire Resistance of Steel Hollows Structural Section Columns Filled with Plain Concrete," *Canada Journal of Civil Engineering*, 21(3):382-385.
6. Kodur, V. K. R.. 1999. "Performance-based Fire Resistance Design of Concrete-filled Steel Columns," *Journal of Constructional Steel Research*; 51(1): 21-26.
7. Kim, D. K., Choi, S. M. and Chung, K. S.. 2000. "Structural Characteristics of CFT Columns Subjected Fire Loading and Axial Force," presented at the 6th ASCCS Conference, ASCCS, Los Angeles, USA: 271-278.
8. Tan, K. H. and Tang, C. Y.. 2004. "Interaction Model for Unprotected Concrete Filled Steel Columns under Standard Fire Conditions," *Journal of Structural Engineering, ASCE*; 130 (9): 1405-1413.
9. Han, L. H., Zhao, X. L., Yang, Y. F. and Feng, J. B.. 2003. "Experimental Study and Calculation of Fire Resistance of Concrete-filled Hollow Steel Columns," *Journal of Structural Engineering, ASCE*; 129(3): 346-356.
10. Ding J. and Wang Y. C.. 2007. "Experimental Study of Structural Fire Behaviour of Steel Beam to Concrete Filled Tubular Column Assemblies with Different Types of Joints," *Engineering Structures*, 29 (12): 3485-3502.
11. ISO 834-1. 1999. "*Fire-resistance Tests-elements of Building Construction-Part 1: General Requirements*," International Organization for Standardization, Geneva, Switzerland.
12. Han L. H.. 2007. "*Concrete filled steel tube structures: theory and experience*," Beijing: Science Press (in Chinese).
13. Lie T. T. 1994. "Fire Resistance of Circular Steel Columns Filled with Bar-reinforced Concrete," *Journal of Structural Engineering, ASCE*, 120(5):1489-1509.
14. Hibbitt, Karlson, Sorenson.. 2005. "*ABAQUS Version 6.5: Theory Manual, Users' Manual, Verification Manual and Example Problems Manual*," America: HKS Company.
15. Song T. Y., Han L. H. and Yu H. X. 2010. "Concrete Filled Steel Tube Stub Columns under Combined Temperature and Loading," *Journal of Constructional Steel Research*, 66(3): 369-384.
16. Han L.H., Zheng Y.Q. and Tao Z.. 2009. "Fire Performance of Steel-reinforced Concrete Beam-column Joints," *Magazine of Concrete Research*, 61(7):499-518.

Experimental and Analytical Investigations of the Behaviour of Protected Composite Floor Beams with Web Openings in Fire

V. Y. B. WONG, I. W. BURGESS and R. J. PLANK

ABSTRACT

Intumescent coating is the most common of the passive fire protection options for cellular beams. Applying intumescent coating to cellular beam has generally followed a tabulated method which is only available for beams with circular web openings, and applies geometrical limitations to the positions and sizes of the openings. A full-scale fire test has been conducted recently to investigate the behaviour of an intumescent-protected composite floor beam with rectangular web openings. The loaded test specimen was protected with a specified coating thickness determined on the basis of a multi-temperature assessment, taking into consideration the actual loading condition, as well as the exact position of the web openings. It was observed that the predicted behaviour of the protected beam was in reasonably close agreement with the test result. Observations from the test suggested that the inconsistency of web temperatures along the beam was due to local detachment of the intumescent char from the bottom-flange. The study has been extended to carry out finite element simulations of the fire test, considering material and geometrical non-linearities. The result is directly compared against the experimental results.

V.Y. Bernice Wong, Department of Civil and Structural Engineering, University of Sheffield S1 3JD, UK

Ian W. Burgess, Department of Civil and Structural Engineering, University of Sheffield, S1 3JD, UK

Roger J. Plank, School of Architectural Studies, University of Sheffield, S10 2TN, UK

INTRODUCTION

The use of steel beams with regular web openings is becoming more popular in multi-storey building construction, because it is possible to achieve long spans and the system is capable of providing through-passage for service ducts, reducing overall building height. In practice, web-openings in beams result in different stress distributions within the webs from solid-web sections, and these create unique failure modes. In fire, the degradation of strength and stiffness of unprotected structural steel happen at different rates, and this can cause not only early structural collapse but also a change of failure mechanism compared to ambient-temperature performance.

Numerous fire protection technologies are available to protect steel structures. Intumescent coating is the most common of the passive fire protection options for perforated steel beams. This has the advantage of allowing the structural form to remain visible as an architectural feature. In fire, the thin dry film layer foams and expands to 15-30 times its original thickness, developing an insulating char layer.

The current approach provides detailed guidance to determine dry film thicknesses of intumescent coating required for composite beams with web openings. This is generally based on a tabulated method [1], [2], [3], [4] which uses a range of design parameters to estimate limiting bottom flange temperatures, from which the protection requirements of cellular beams may be obtained. These tables only exist for beams with circular web openings, and limit the positions and sizes of the openings. There is clearly a need for rules which incorporate realistic structural behaviour during a fire, considering the actual loading condition and the exact positions of the web openings.

Simulations are presented of a fire test carried out to investigate the behaviour of an intumescent-protected composite floor beam with rectangular web openings.

EXPERIMENTAL INVESTIGATIONS

The fire test involved the heating of a protected composite floor beam with rectangular web openings. The beam's span was 4.2m, with relatively narrow web-posts to induce web-post failure. The beam was an asymmetric composite section with a 200mm x 15mm top-flange, 250mm x 15mm bottom-flange and 6mm x 370mm web. The concrete slab was 130mm thick x 700mm wide, using C25/30 concrete with A142 reinforcing mesh (yield strength 460N/mm²) and 1.2mm thick Metfloor 55 steel decking. Shear connectors 19mm diameter x 100mm long were used. The nominal and measured yield strengths of the steel beam were 275N/mm² and 433N/mm² respectively. A total load of 90kN was applied to the top of the concrete slab as four point loads. The beam was tested in a 4m x 3m furnace (Fig. 3) using the ISO 834 standard fire. The target dry film thickness of the specified intumescent was 2.47mm, although its measured average dry film thickness was 2.206mm. The target thickness was determined through a simplified model which takes into account the actual beam loading and the locations of the web openings.

Loads were applied at ambient temperature and maintained during the fire test, which lasted 142 minutes; thermocouples were positioned on the section to record the temperatures throughout the fire test. Figs.1 and 2 illustrate the composite beam geometries and the locations of the thermocouples.

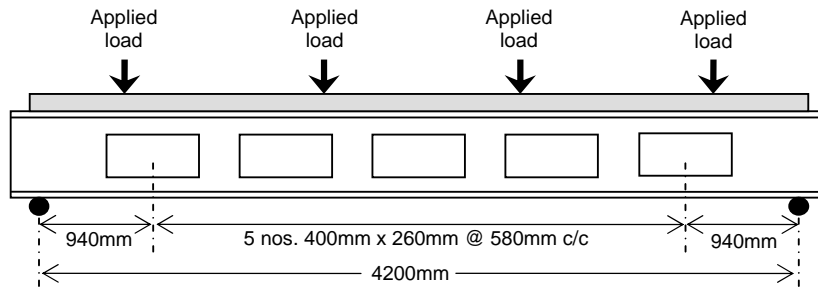


Figure 1. Beam geometries.

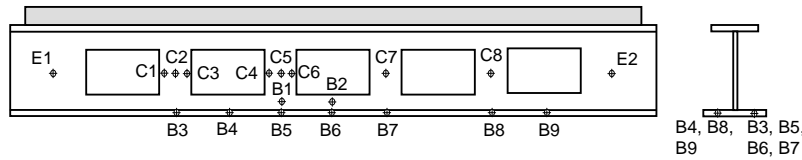


Figure 2. Location of the thermocouples.



Figure 3. Experimental setup: Beam within the furnace, apply loads on beam.

The fire test lasted 142 minutes. It was observed that 20% of Intumescent on the bottom-flange fell off the beam near to a support at 20 minutes (Fig. 4). After 60 minutes, small amounts of Intumescent continued to fall off the bottom-flange.

Fig. 5 shows the recorded temperatures at the centres of the web-posts (positions C2, C5, C7 and C8), averaged end-posts (positions E1 and E2) and the average furnace temperature. Fig. 6 shows the recorded temperatures at the bottom-flange of the beam (positions B4, B6 and B9) below the openings. The higher temperature at B9 is due to the intumescent falling off the bottom-flange of the beam. Comparisons of the measured temperatures at the bottom-flange (positions B3, B5, B7 and B8) measured below the web-posts are shown in Fig. 7. Once again higher temperature at position B8 is caused by the local loss of char



Figure 4. Intumescent on the bottom-flange fell off the beam near the support.

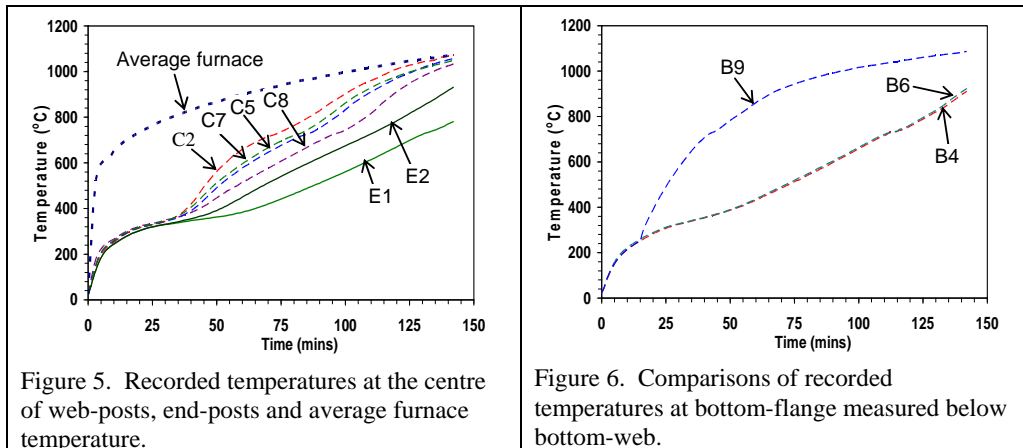


Figure 5. Recorded temperatures at the centre of web-posts, end-posts and average furnace temperature.

Figure 6. Comparisons of recorded temperatures at bottom-flange measured below bottom-web.

A comparison of the average temperatures at the bottom-flange (positions B3 to B8) against temperatures at the centre of web-posts (position C2, C5, C7 and C8) is shown in Fig. 8. The difference in temperatures between the average bottom-flange and centre of web-post is less than 45°C before 40 minutes. After 50 minutes the web-post was on average 205°C hotter than the bottom-flange. Note that the average temperature at the bottom-flange does not include the temperature at position B9.

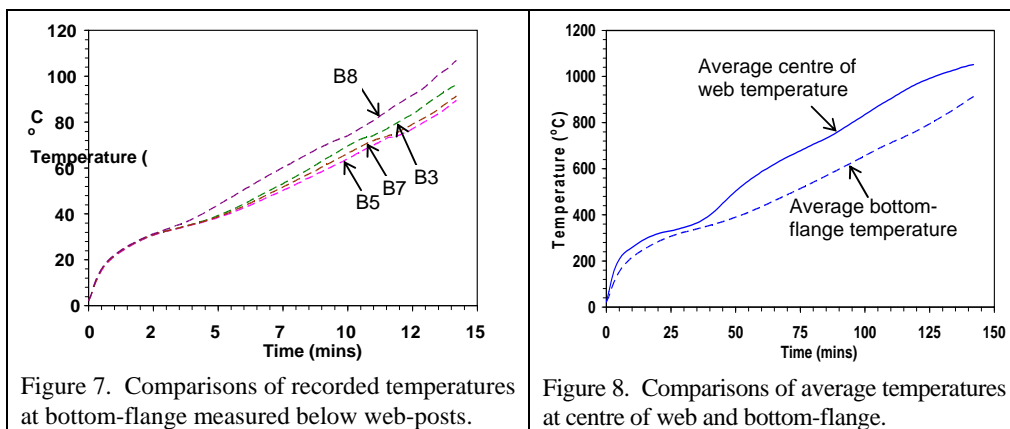


Figure 7. Comparisons of recorded temperatures at bottom-flange measured below web-posts.

Figure 8. Comparisons of average temperatures at centre of web and bottom-flange.

Fig. 9 compares the recorded temperatures at the first and second web-posts (positions C1–C3 and C4–C6). The temperatures at the three positions on the each web-post remain within 70°C of each other.

Comparison of the recorded temperature at the bottom-flange (positions B5 and B6) against the bottom-web temperatures (positions B1 and B2) is shown in Fig. 10. The temperatures below openings (positions B2 and B6) are hotter than those measured below a web-post (positions B1 and B5). The difference in temperatures between the bottom-web and bottom-flange was about 80°C after 50 minutes.

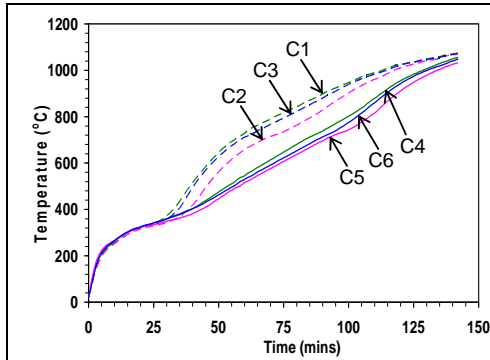


Figure 9. Comparisons of recorded temperatures at first and second web-post.

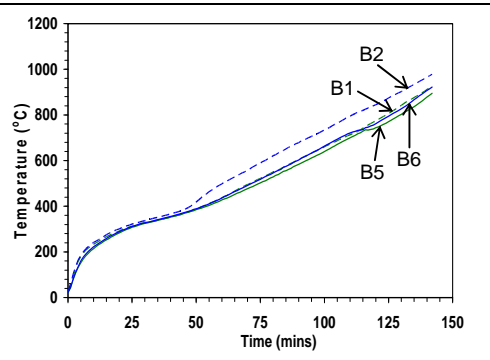


Figure 10. Comparisons of temperatures at bottom-flange against bottom-web temperatures.

ANALYTICAL INVESTIGATION

The current approach for determining the thickness of intumescent coating required for composite beams with web openings is based on the relationship between web-post temperature and bottom-flange temperature for each protection product. This relates the web-post temperature to the width of the web-post [3] and [4]. Based on the currently available guidance [5], [6], [7] and [8] for composite cellular beam at ambient temperature, an analytical model to predict intumescent thickness for composite beams with web openings has been developed, taking into consideration the actual structural behaviour during a fire. Where web-post buckling is critical, the limiting temperature of the most critical web-post is determined. A limiting bottom-flange temperature is predicted using the web-post factor for the product used.

Assuming that the design of the composite beam with openings is adequate for its overall shear, bending and local Vierendeel resistance requirements, the following simple method is proposed for calculating the resistance of the zone influenced by web-post buckling. In cellular beam design, the resistance of each web-post to local buckling is checked using an ‘equivalent strut’ principle, by considering the compressive force acting over its width S_o (Fig. 12). At high temperature, the shear resistance of the web reduces at a faster rate than bending resistance of the bottom-flange, and thus the web is more influenced by local buckling. In fire, the capacity of a web-post ($V_{h,buck,fi}$) is defined as:

$$V_{h,buck,fi} = \chi_{fi} f_{y,fi} S_o t_w \quad (1)$$

where:

$f_{y,fi}$ is the design yield strength of the perforated section at high temperature
 t_w is the thickness of the web-post

The buckling stress acting across the web-post ($f_{E,fi}$) is defined as:

$$f_{E,fi} = \frac{\pi^2 E_{fi}}{\lambda_{fi}^2} \quad (2)$$

Slenderness of the web-post (λ_{fi}) for a web with a rectangular opening is:

$$\lambda_{fi} = \frac{3.5d_o}{t_w} \quad \text{for } S_o > d_o \quad (3)$$

$$\lambda_{fi} = \frac{\sqrt{12}l_{e,fi}}{t_w} \quad \text{for } S_o \leq d_o \quad (4)$$

in which d_o is the opening depth and $l_{e,fi}$ is web-post effective length at elevated temperature, given by:

$$l_{e,fi} = 0.9l_e \quad (5)$$

l_e is the web-post effective length at ambient temperature, for beam with rectangular web opening, it is calculated from:

$$l_e = 0.7\sqrt{S_o^2 + d_o^2} \quad (6)$$

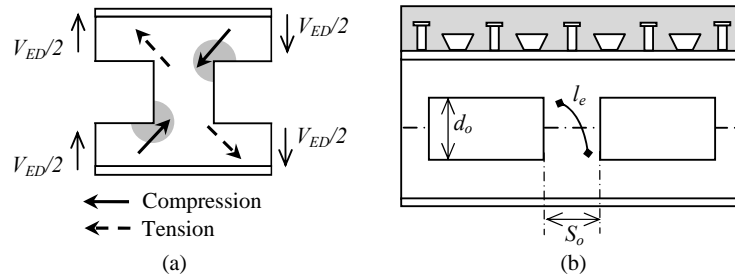


Figure 12. Web-post buckling (a) Mode of Failure; (b) Web-post geometries.

The applied vertical compressive force acting across the web-post (V_t) is calculated by $V_{ED}/2$; where V_{ED} is the design shear force at a distance x from the support.

FINITE ELEMENT (FE) MODELLING

Based on the results obtained from the fire test, geometrically non-linear finite element simulations have been carried out using ABAQUS [9] with non-linear material properties. Three-dimensional 8-noded solid elements and 4-noded quadrilateral shell elements with reduced integration were used to represent the concrete slab and cellular steel beam respectively. Reinforcing mesh in the solid slab element was defined as a layer of steel of equivalent area in each direction. Slip between the concrete slab and steel beam is not considered in this analysis; full composite action was achieved by using a tying constraint to tie the surfaces of both components together. The support and loading conditions in the FE models simulated the experimental conditions, restraining the appropriate degrees of freedom. Temperatures of each part of beam section measured in the test were introduced into the finite element models. For the

concrete slab, an effective flat slab thickness and an assumed linear distribution of temperature through the thickness were adopted in the FEA models. The measured temperatures at the top and bottom surfaces of the slab were directly applied in the FEA model. The measured yield strength of the steel beam (433N/mm^2) was used in the FEA model. Fig. 13 illustrates the type of failure mode predicted by the FE modelling.

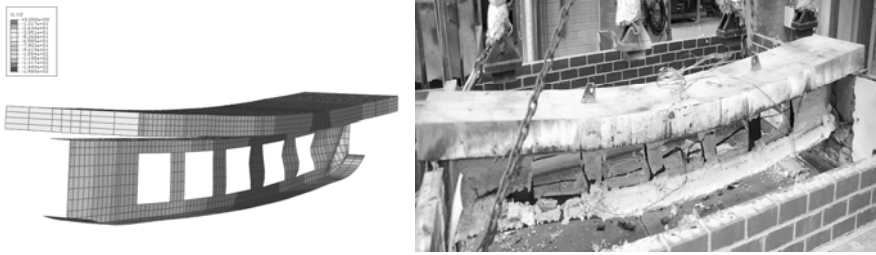


Figure 13. Web-post buckling failure in FE modelling and experimental.

RESULTS

A summary of the results obtained from experimental, FE modelling and predicted limiting web temperature are illustrated in Fig. 14. The critical temperatures generated by the proposed analytical model are also shown. The specified intumescent thickness, was expected to provide a fire resistance of 90 minutes, for which the web temperature of the beam needs to be lower than the predicted limiting web temperature. The structural behaviour of the composite perforated sections observed from the experiments was in good agreement with the finite element results in terms both of failure modes and overall behaviour. Web-post buckling was clearly observed in the experiment (Fig. 15). The measured web temperature of the beam at 90 minutes was 25 C higher than the predicted temperature. However, it should be noted that the average measured web temperature is used for comparison, and that this was affected by the inconsistency of web temperatures due to local detachment of the intumescent char from the bottom-flange.

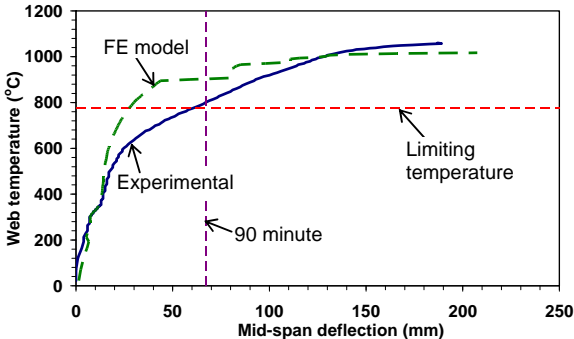


Figure 14. Comparison of mid-span deflection and limiting temperature.



Figure 15. Web-post buckling failure mechanism.

CONCLUSION

The final failure conditions of the composite cellular beam predicted by the analytical model agree well with the experimental observations and the FE simulation. All failure modes are accurately predicted by the FE models. The average measured web temperature of the tested beam was 25°C higher than the predicted temperature at the target fire resistance period, although it seems likely that the inconsistency of web temperatures along the beam was due to local detachment of some intumescent char from the bottom-flange.

ACKNOWLEDGEMENTS

The authors gratefully acknowledge the support from the Engineering and Physical Sciences Research Council of the United Kingdom for providing funding for this research work under Grant EP/F001711/1.

REFERENCES

1. ASFP/SCI/FTSG. 2007. “Fire Protection for Structural Steel in Buildings, 4th Edition”, ASFP Publication.
2. Steel Construction Institute. 2004. “Fire design of cellular beams with slender web posts”, Publication RT1006 Version 02.
3. Steel Construction Institute. 2007. “Guidance on the use of intumescent coatings for the fire protection of beams with web openings”, Publication RT1085 Version 04.
4. Steel Construction Institute. 2008. “Guidance on the fire protection of beams with web openings”, Publication RT1187 Version 01.
5. Lawson, R.M. 1987. “Design for openings in the webs of composite beams”, SCI/CIRIA publication P068.
6. Ward, J.K. 1999. “Design for composite and non-composite cellular beams”, SCI publication P100.
7. Chung, K.F. and Lawson, R.M. 2001. “Simplified design of composite beams with large web openings to Eurocode 4”. *Journal of Constructional Steel Research*, 59, pp. 135–163.
8. Lawson, R.M., Lim, J., Hicks, S.J. and Simms, W.I. 2006. “Design of composite asymmetric cellular beams and beams with web openings”. *Journal of Constructional Steel Research*, 62, pp. 614–629.
9. Pawtucket, R.I. 2001. “ABAQUS user’s manual version 6.2”, Hibbitt, Karlsson and Sorensen Inc.

Influence of Reinforcement Properties on the Failure of Composite Slabs in Fire

K. A. CASHELL¹, A. Y. ELGHAZOULI² and B. A. IZZUDDIN³

ABSTRACT

This paper examines the influence of the properties of steel reinforcement on the response of composite floor slabs under idealised fire conditions, with emphasis on ultimate failure considerations. An experimental investigation into the effect of elevated temperatures on the mechanical characteristics of steel reinforcement is firstly described. The study includes tests carried out at ambient temperature as well as under steady state and transient elevated temperature conditions. Apart from the evaluation of stress-strain response and degradation of stiffness and strength properties, particular emphasis is given to assessing the influence of elevated temperature on enhancing the ductility of steel reinforcement. The implications of the specific reinforcement properties on the ultimate behaviour of composite floor elements and assemblages in fire are then discussed. For this purpose, novel analytical models are used to assess the ultimate behaviour of members incorporating different types of reinforcement.

1 INTRODUCTION

The structural response of buildings to fire conditions has been the focus of intensive research activity in recent years. For composite steel/concrete buildings, this has been largely motivated by the desire to achieve more cost-effective designs which are based on the actual structural performance rather than typical prescriptive methods which are based on unrealistic idealisations of isolated elements. This is particularly relevant at elevated temperature, when the interactions between various structural components may have a direct influence on the response and are potentially advantageous to the overall building performance. However, before the potential benefits can be incorporated in to design methods, it is necessary to gain a detailed understanding of the underlying behavioural mechanisms in fire conditions.

Towards this end, significant insights into the actual structural response of buildings in fire were provided through the large-scale tests at Cardington [1, 2]. The findings of these tests identified the important role played by the composite floor slab in carrying the gravity loading within the fire compartment after the loss of strength in the supporting secondary steel beams due to elevated temperature.

¹High-Point Rendel Ltd., London, email: k.cashell@hprconsult.com

²Dept. of Civil Engineering, Imperial College London, e-mail: a.elghazouli@imperial.ac.uk

³Dept. of Civil Engineering, Imperial College London, e-mail: b.izzuddin@imperial.ac.uk

It was shown that the floor slab continues to support load through membrane action even after the loss of the deck and steel beams, thereby enabling alternative load paths to develop after conventional strength limits have been reached.

Before the above-mentioned secondary load-carrying mechanisms can be relied upon in design, it is necessary to understand the limiting failure criteria. Apart from compressive mechanisms that may occur in the slab, a key failure condition is related to fracture of the steel reinforcement in tension. In this respect, fundamental analytical approaches have recently been proposed which are capable of predicting the level of deformation and load corresponding to failure by reinforcement fracture at elevated temperature [3-6]. The reliability of these methods, however, is directly dependent on the availability of information pertaining to the key material characteristics at elevated temperature.

In this context, this paper describes the observations from an experimental investigation into the effect of elevated temperature on reinforcing bars tested to fracture. A primary objective of the study is to gain an insight into the effect of elevated temperature on the ductility properties of steel reinforcement. Following this, the findings of the tests are employed, together with the analytical models, to investigate the behaviour of idealised reinforced concrete members under simulated fire conditions.

2 TEMPERATURE-DEPENDENT PROPERTIES

Elevated temperature has the effect of reducing the strength and stiffness of steel reinforcement [6, 7]; the reduction is directly related to the manufacturing process of the bars. For example, in Eurocode 2 [7] an idealised stress-strain relationship is assumed as depicted in Figure 1. A linear relationship is initially considered followed by an elliptical representation until the maximum stress is achieved at a strain of $\epsilon_{sy,\theta}$, after which a constant strength is assumed between $\epsilon_{sy,\theta}$ and $\epsilon_{st,\theta}$. The main parameters related to stiffness and strength (i.e. $E_{s,\theta}$, $f_{sp,\theta}$ and $f_{sy,\theta}$) are assigned reduction factors for increasing temperatures. These reduction factors are discussed in subsequent parts of the paper.

More importantly, in terms of ductility, the Eurocode approach considers $\epsilon_{sy,\theta}$, $\epsilon_{st,\theta}$ and $\epsilon_{su,\theta}$ as constant values irrespective of the temperature; these are stipulated as 0.02, 0.15 and 0.2, respectively (for Class B and C reinforcement) and 0.02, 0.05 and 0.1, respectively (for Class A reinforcement). Accordingly, it is assumed that the ductility of reinforcement is unaffected by the level of temperature, an assumption which is examined in more detail in the experimental investigation described in this paper.

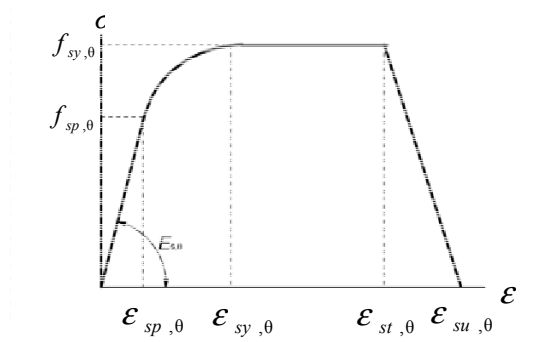


Figure 1. Stress-strain relationship for reinforcement at elevated temperature [13].

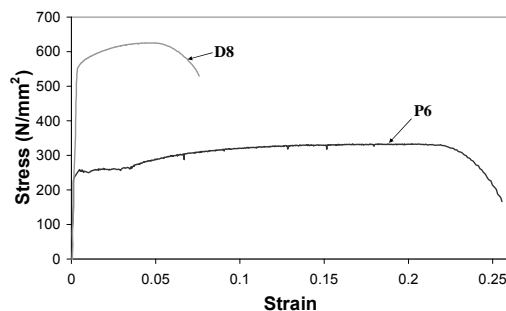


Figure 2. Typical stress-strain relationships at ambient temperature.

3 EXPERIMENTAL STUDY

The main objective of the material tests was to examine the variation in key properties of steel reinforcement with temperature. Particular emphasis is given to the influence of temperature on ductility, in terms of ultimate strain at fracture, which is critical for the reliable assessment of the performance of structural members under fire conditions. The full test program included (i) steady-state elevated temperature tests; (ii) transient elevated temperature tests at a constant load; and (iii) steady-state tests for assessing residual properties. For brevity, this paper focuses on the results of (i) only; the other tests are described elsewhere [8].

3.1 Experimental Response at Ambient Temperature

In order to assess the behaviour of steel reinforcement of different characteristics, two bar types are considered, namely 6mm plain hot-rolled bars (P6) and 6mm ribbed cold-worked bars (D6). Other bars were also included in the full test programme but are not included in this paper for brevity (see [8]). The results from these two bars are indicative of the general observations during the full test programme. Ambient tensile tests were conducted for each bar type to ascertain the mechanical characteristics; typical stress-strain relationships obtained for each of the reinforcement configurations are presented in Figure 2. In addition, the key mechanical characteristics are summarised in Table 1 where f_{sy} and f_{su} are the yield and ultimate strengths at ambient, respectively, and ϵ_{su} is the corresponding ultimate strain, measured through an extensometer. The values given in the table are the average obtained from at least three specimens for each bar-type.

Table I: AMBIENT STEEL REINFORCEMENT PROPERTIES.

	f_{sy}	f_{su}	ϵ_{su}
P6	251	328	0.20
D6	551	592	0.04

3.2 Steady-State Elevated Temperature Tests

The test arrangement is shown in Figure 3. A hydraulic testing machine was utilised and the temperature was applied using an electric furnace. Each specimen had a full length of 1000mm with a heated segment of 325mm. As well as overall load and displacement readings, the extension in the heated part of the bar was measured using the arrangement shown in Figure 4. In addition, the reinforcement was marked at 30 mm intervals prior to testing to facilitate the measurement of ultimate strain after cooling. Once the specimen and furnace were in position, the temperature was increased to the required level at a rate of 10°C/minute. This temperature was then maintained for 30 minutes before tensile loading was applied, through displacement control, at a rate of 4mm/minute until fracture occurred. In this paper, the stress-strain relationship at a given temperature, θ , is defined by four key parameters: (i) the slope in the linear-elastic range ($E_{s,\theta}$); (ii) the proportional limit ($f_{sp,\theta}$) after which non-linear behaviour is exhibited; (iii) the ultimate stress ($f_{su,\theta}$) corresponding to the maximum capacity of the bars; and (iv) the ultimate mechanical strain at fracture ($\epsilon_{su,\theta}$).

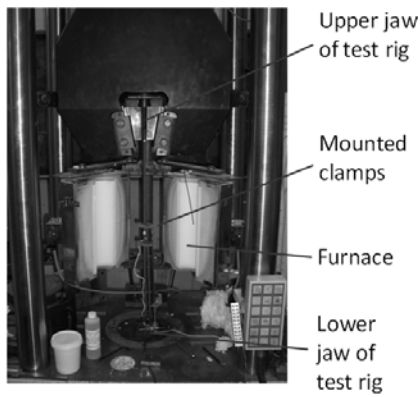


Figure 3. Elevated temperature testing arrangement.

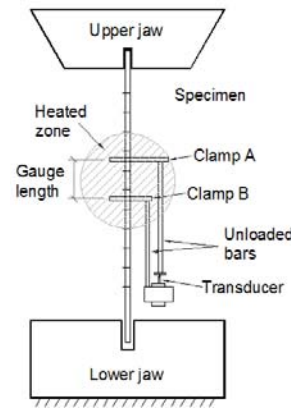


Figure 4. Arrangement for measuring bar extension.

3.2.1 EVALUATION OF STRENGTH AND STIFFNESS

The experimental response curves obtained for P6 and D6 are shown in Figures 5 and 6 respectively, presented in terms of stress against extension. In addition, the degradation of reinforcement properties with elevated temperature are presented in Figures 7 and 8 for P6 and D6 respectively, where the reduction factors are normalised by their corresponding values at ambient conditions, and plotted against the temperature (θ). For comparison purposes, the plots also include the reduction factors suggested in Eurocode 2 [13] for hot-rolled and cold-worked bars.

With reference to the overall shape of the stress-strain response depicted in Figures 5 and 6, it is evident that the clear yield-plateau, demonstrated by the hot-rolled bars (P6) at ambient temperature, disappeared at temperatures above 200 C and the behaviour became more continuous. Furthermore, strain-hardening diminished for both bar-types from around 400-500 C. This conflicts with the Eurocode which assumes that strain hardening is negligible at all temperatures and hence the maximum stress level is essentially treated as an ‘effective yield strength’, referred to as $f_{sy,\theta}$. The test results shown in this paper suggest that strain hardening becomes insignificant only when temperatures above 400 C are reached. Characterisation of a representative effective yield strength at elevated temperature from the experimental results is not possible without either: (i) defining a limiting strain criteria, which is difficult due to the variable $E_{s,\theta}$, or (ii) ignoring the presence of strain hardening characteristics as assumed in EC2.

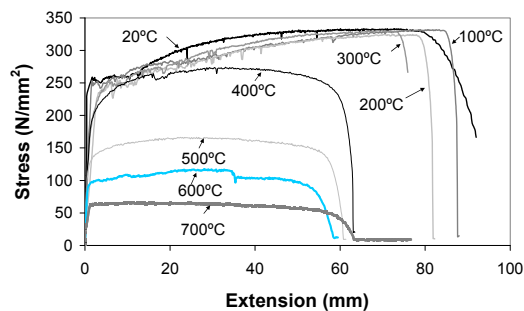


Figure 5. Stress versus extension response for P6 bars at various temperatures.

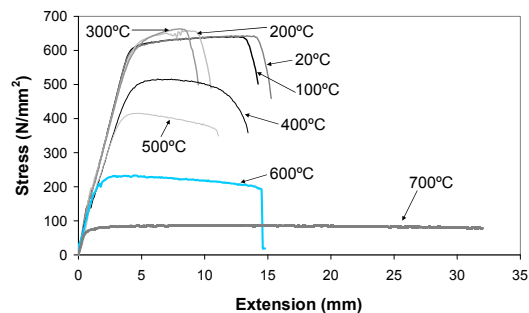


Figure 6. Stress versus extension response for D6 bars at various temperatures.

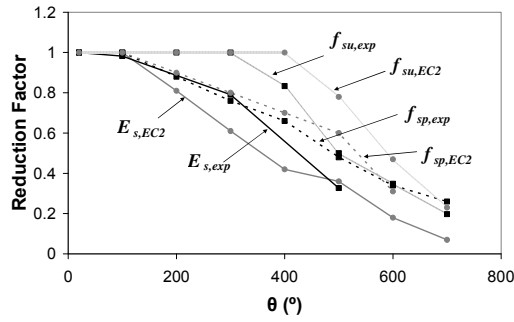


Figure 7. Effect of elevated temperature on properties of P6 reinforcement.

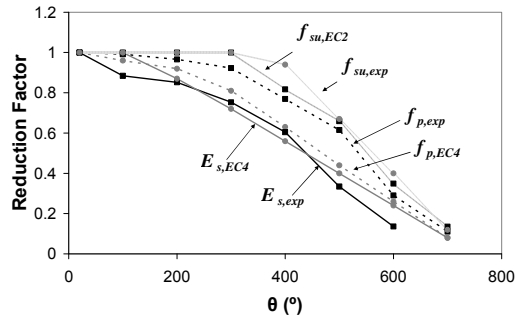


Figure 8. Effect of elevated temperature on properties of D6 reinforcement.

In terms of $E_{s,\theta}$, $f_{sp,\theta}$, and $f_{su,\theta}$, Figures 7 and 8 indicate that each of these properties decrease gradually with temperature. $E_{s,\theta}$ and $f_{sp,\theta}$ reduce at a relatively constant rate at temperatures above 100-200 C and are largely in agreement with the corresponding Eurocode values. On the other hand, $f_{su,\theta}$ does not reduce until around 300-400 C after which it degrades at a similar rate for both bar-types. The ‘effective yield strength’ of cold-formed bars typically reduces more than that of hot-rolled reinforcement at elevated temperature. However, for the bars in this study, this is counterbalanced by the greater strain-hardening capacity of the P6 bars at ambient temperature. Consequently, both types display similar trends of ultimate strength when the normalised values are assessed. It is noteworthy that the test results for P6 (hot-rolled) bars show that the corresponding Eurocode values appear to be un-conservative.

3.2.2 REINFORCEMENT DUCTILITY

Figure 9 illustrates the effect of elevated temperature on the ultimate strain for both P6 and D6. It is shown that the behaviour of both the hot-rolled and cold-formed bars is similar until around 500 C, with the ultimate strain reaching around twice the corresponding ambient value. At higher temperatures, the enhancement increased significantly for the D6 bars, reaching values of between 7 to 9 times the ambient value at 700 C whereas the hot-rolled bars only increased by a factor of 2 or 3 in the same range. Clearly, when the cold-working effect is alleviated at temperatures exceeding around 500 C, the ductility increased significantly in comparison with the characteristically low values exhibited at ambient temperature for this type of reinforcement.

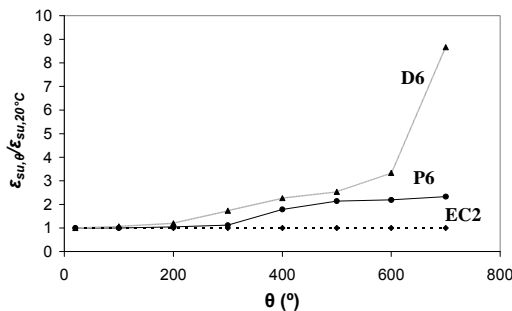


Figure 9. Effect of elevated temperature on $\epsilon_{su,\theta}$

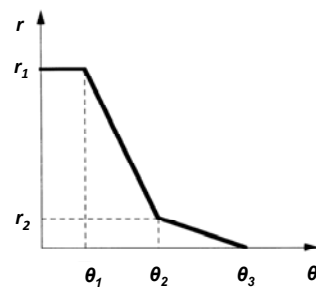


Figure 10. Variation of material reduction factors with temperature.

The findings of this experimental programme are critical for the reliable assessment of the performance of structural members in fire. The subsequent section employs some of the key

results to describe a brief analytical investigation into the response of reinforced concrete slab members under idealised fire conditions.

4 MEMBER RESPONSE

As previously discussed, simplified analytical models have been developed which can predict the ultimate behaviour of one- and two-way spanning slab components at ambient and elevated temperature. The models enable a fundamental assessment of the large-displacement behaviour of reinforced concrete members in fire conditions, including the failure conditions. This section provides an analysis of the behaviour of one-way spanning slab strips at elevated temperature. For compactness, the simplified analytical model (hereafter referred to as the SAM) is only briefly discussed herein; more detailed discussions can be found elsewhere [3, 4, 9]. However, the model is utilised, together with the material data presented in this paper, to investigate the influence of several parameters on the failure behaviour of slabs under realistic fire conditions.

The SAM accounts for the effects of elevated temperature including the variation in material properties as well as thermal expansion and thermal curvature. It also considers the influence of complex relationships such as bond-slip. Extensive validation of the predicted load deflection response has been carried out elsewhere [4]. In this section, focus is given to examining the influence of restraint conditions and the degradation of material properties on the ultimate response, at elevated temperature. In order to investigate the ensuing phenomena, and to illustrate important behavioural aspects, the properties of a reference configuration adopted to facilitate the interpretation of the results are presented in Table 2. The table gives details of the half-length (L), width (b), depth (h), depth of the reinforcement from the compressive face (d_s), area of steel (A_s) and reinforcement ratio (ρ). It also indicates the effective bond strength (σ_b) as well as the compressive strength of concrete (f_c'). The steel characteristics adopted replicate those of P6 reinforcement.

Table II: DETAILS OF CONTROL MODEL.

Member configuration		Ambient material properties	
L	1500mm	E_s	$2.1 \times 10^5 \text{N/mm}^2$
h	60mm	f_{sy}	252N/mm^2
b	600mm	f_{su}	330N/mm^2
d_s	30mm	ϵ_{su}	0.2
ρ	0.23%	f_c'	40N/mm^2
A_s	85mm^2	σ_b	0.9N/mm^2

The degradation of material properties with elevated temperature are represented in the analysis through tri-linear reduction curves (Figure 10), as summarised in Table 3. The temperature-dependent material properties related to bond and concrete are taken from available information [7, 10]. In subsequent analysis, the temperature distribution is assumed to be linear within the cross-section and constant along the length.

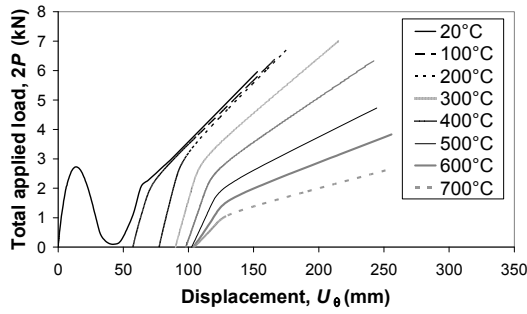


Figure 11. Response of unrestrained control model at various temperatures.

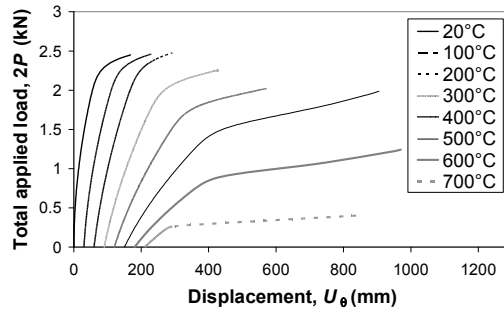


Figure 12. Response of restrained control model at various temperatures.

Figure 11 presents the relationship between the total applied load ($2P$) versus the temperature-dependant deflection (U_θ) for various steel reinforcement temperatures θ . The last point on each curve corresponds to the attainment of ultimate strain in the steel and hence indicates failure. Evidently, the member capacity reduces with increasing temperature owing to material degradation whereas the failure displacement increases significantly (until about 600 C) as a result of the improved material ductility. It is noteworthy that the increase in temperature causes the member to deform even before gravity loading has been applied, resulting in a significant initial displacement. Rupture of the reinforcement depends directly on the combination of the thermal expansion characteristics together with the variation in the relevant material properties. It is seen that for the particular material properties employed in these analyses, as the temperature approaches 700°C, the failure deflection reduces again.

The effect of boundary conditions on the ultimate behaviour, at various levels of elevated temperature, is investigated by examining the response of the control model using the axially-restrained SAM (Figure 12). As before, it is evident that the response is significantly influenced by the increase in temperature, in terms of the initial and ultimate deflection, failure load and the overall response history. Most notably, the compressive arching effect is lost at elevated temperatures. The initial deformation due to the increase in temperature is sufficient to take the member beyond the range within which compressive arching can develop. Furthermore, at relatively low levels of elevated temperature, the initial deformations are more significant in this case than in the previous unrestrained model as the restraint against thermal expansion causes the member to buckle at a relatively early stage.

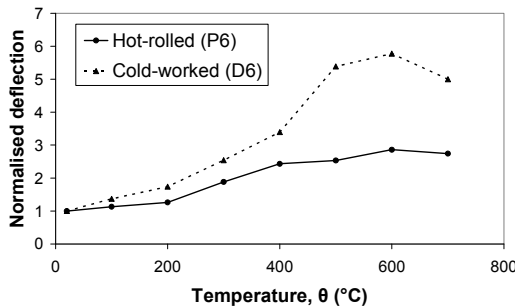


Figure 13. Effect of bar type on failure displacement at elevated temperature.

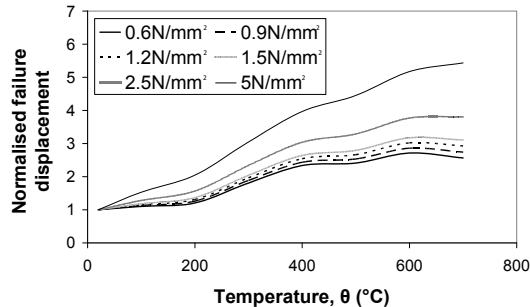


Figure 14. Effect of bond strength on failure displacement at elevated temperature.

In order to investigate the effect of reinforcement type, the bars employed in the control model are varied by considering a cold-worked material with properties similar to D6. All of the

other properties are retained from the previous analysis. The effect is illustrated in Figure 13 in which the failure displacements have been normalised to their corresponding values at ambient temperature and plotted against θ . Clearly, elevated temperature has a greater influence on the failure of strips with cold-worked bars than those with hot-rolled reinforcement.

It has been shown elsewhere [4, 9] that bond strength has only a marginal influence on the load-deflection response whereas, more importantly, it has a pronounced influence on the failure level. The influence of bond on the failure displacement at various levels of elevated temperature is presented in Figure 14. The ambient bond strength is varied between 0.5 and 5N/mm². As the bar type is unchanged, the degradation of bond with elevated temperature is assumed to be identical in each case. Evidently, the normalised failure deflection increases proportionally to the level of bond strength. In other words, elevated temperature has a greater influence on failure when the bond strength is relatively higher.

5 CONCLUDING REMARKS

This paper has provided an insight into the effects of elevated temperature on the characteristic properties of steel reinforcement and the consequent effect on member behaviour. Generally, the stiffness and strength of steel reduce progressively with increasing temperature whereas the ductility increases. The study also a brief analytical investigation into the effect of elevated temperature on the response of one-way spanning reinforced concrete members under idealised fire conditions.

REFERENCES

1. Kirby B.R. (1997). "British steel technical European fire test programme – Design, construction and results." *Fire, static and dynamic tests of building structures*, G. Armer and T. O'Neill, eds., Spon, London.
2. O' Connor, M. A. and Martin, D. M. (1998). "Behaviour of multi-storey steel framed buildings subjected to fire attack." *Journal of Constructional Steel Research* 46(1-3). Paper No: 169.
3. Izzuddin, B. A. and Elghazouli, A. Y. (2004). "Failure of lightly reinforced concrete members under fire. I: Analytical modelling." *Journal of Structural Engineering*, 130(1):3–17.
4. Elghazouli, A. Y. and Izzuddin, B. A. (2004). "Failure of lightly reinforced concrete members under fire. II: Parametric studies and design considerations." *Journal of Structural Engineering*, 130(1):18–31.
5. Omer, E. (2006). "Failure of composite steel-concrete slabs under elevated temperatures." PhD Thesis, Imperial College London
6. Buchanan, A.H. (2001). "Structural Design for Fire Safety." Wiley, UK.
7. EN 1992 Eurocode 2 (2004). "Design of concrete structures: Part 1.2: General rules—Structural fire design." *European Committee for Standardization*, Brussels.
8. Elghazouli A.Y., Cashell K.A. and Izzuddin B.A. (2009). "Experimental evaluation of the mechanical properties of steel reinforcement at elevated temperature." *Fire Safety Journal* 44(6): 909–919.
9. Cashell, K.A. (2009), "Failure assessment of floor slab systems under extreme loading conditions." PhD Thesis, Imperial College London.
10. Giroldo, F. and Bailey C.G. (2008). "Experimental bond behaviour of welded mesh reinforcement at elevated temperatures." *Magazine of Concrete Research*, 60(1): 23–31.

Collapse Mechanisms of Composite Slab Panels in Fire

A. ABU, V. RAMANITRARIVO and I. BURGESS

ABSTRACT

The identification of tensile membrane action as a sustainable, high-capacity load-bearing mechanism of composite floors under fire conditions has led to the development of a number of simplified design solutions, because of the unsuitability of finite element analysis for routine design. Prominent amongst these is the Bailey-BRE method, which predicts composite slab capacity by calculating the enhancement of its traditional yield-line load capacity due to tensile membrane action. This method assumes that the two-way bending slab panel, composed internally of parallel unprotected composite beams, is supported on edges which resist vertical deflection. In practice, the protected composite beams which simulate this vertical edge support in fire deflect under the combination of heating and load, and this loss of vertical support induces single-curvature bending, which leads to an eventual structural failure by folding of the slab panel.

A simple folding mechanism, which considers the contributions of the internal unprotected beams and the protected edge beams, has been developed for isolated slab panels. In the current study the mechanism has been extended to include the reinforcement in the slab as well as its continuity across the protected edge beams. Structural failure of the panel depends on the applied loads, the relative beam sizes, their locations within the building, their arrangement in the slab panel considered, the location of the slab panel and the severity of fire exposure. These factors are considered in developing a number of collapse mechanisms as an additional check within the Bailey-BRE design method. Comparisons are made with the finite element software *Vulcan* and other acceptance criteria.

Anthony Abu PhD, Lecturer, Department of Civil and Natural Resources Engineering, University of Canterbury, Private Bag 4800, Christchurch 8140, New Zealand

Verotiana Ramanitarivo, Structural Designer, MDCI Concept Industry, 53-55 Rue du Capitaine Guynemer, 92400 Courbevoie, Paris, France

Ian Burgess PhD, Professor, Department of Civil and Structural Engineering, University of Sheffield, Sir Frederick Mappin Building, Mappin Street, Sheffield S1 3JD, United Kingdom

INTRODUCTION

Recent advances in structural fire engineering have paved the way for innovation and an increased use of performance-based design, especially in steel-framed buildings. Research and observations of structural behaviour under fire conditions over the past 20 years have shown that load redistribution and large deflections of parts of the structure at the Fire Limit State are essential to the survival of the entire structure. Both accidental fires and tests on full-scale buildings have shown that designing composite floors for tensile membrane action yields considerable savings in protection costs, and structural stability is maintained by taking advantage of this real building behaviour in fire [1]. Tensile membrane action is a mechanism that produces increased load-bearing capacity in thin slabs undergoing large vertical displacements, in which radial tension in the central area of a slab induces an equilibrating peripheral ring of compression. The conditions necessary for the effective use of this mechanism are two-way bending of the slab and vertical support along all of its edges. Due to its self-equilibrating nature, horizontal edge restraint is not required to mobilise tensile membrane action.

To optimise composite floors to take advantage of this higher load capacity in structural fire engineering design, a composite floor is divided into several fire-resisting rectangular zones of low aspect ratio, called slab panels, each usually comprising a set of parallel adjacent unprotected composite beams in the interior of the panel, with edges which primarily resist vertical deflection [2]. This vertical support is usually provided by protected composite beams along all four edges, and the panels are generally set out to align with the column gridlines, as shown in Figure 1.

In fire the unprotected beams lose strength and stiffness rapidly, and their loads are then borne by the concrete slab, which undergoes two-way bending and increases its resistance as its deflections increase. At large deflections and high temperatures, the slab panel's capacity is dependent on the tensile strength of the reinforcement, provided sufficient vertical support is available at the slab panel boundary. The benefits of incorporating tensile membrane action into fire engineering design have inspired the development of several software packages to help quantify slab capacities in fire. Whole-structure behaviour in fire can be modelled in a three-dimensional framework with sophisticated finite element software (such as *Vulcan* [3], TNO DIANA, ABAQUS and SAFIR) which incorporates geometric and material nonlinear properties of structures.

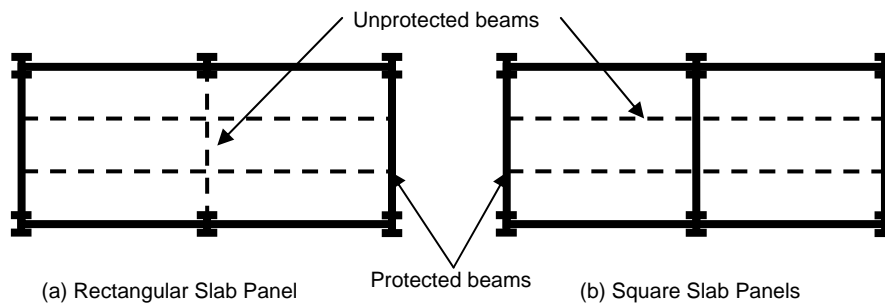


Figure 1. Rectangular and square slab panels.

Although these simulations provide useful information on complete load-deformation and stress development at elevated temperatures, they can be very costly processes; simpler methods [2, 4-6] are often preferred for routine design.

Prominent among these simplified approaches is the Bailey-BRE Method. It treats slab panels as isolated, because the large hogging moments which may be generated at the edges at large deflections are assumed to fail the slab reinforcement over the edge beams, eliminating any continuity with adjacent panels. The method analyses the panels on the assumption that the protected edge beams offer sufficient vertical restraint throughout the fire exposure. The limiting condition is the formation of a central through-depth tensile crack across the short span of the slab, which constitutes a failure of the integrity of compartmentation rather than a real structural stability failure.

However, a combination of the redistributed applied loads and long-term thermal exposure can cause significant deflections of some of the edge beams, resulting in the loss of the sustained double-curvature, which may lead to a local structural collapse. Finite element investigations of composite slab systems have confirmed this, and a simple folding mechanism has been proposed for isolated panels [7].

This paper extends the proposal to cover reinforcement, slab continuity, and to examine other potential collapse mechanisms which could be incorporated into the Bailey-BRE method to make it more robust.

COLLAPSE MECHANISMS

Structural collapse of a slab can be modelled using plastic folding mechanisms, which allow collapse without generating membrane forces in the slab. It is not a unified concept. It requires work-balance calculations for a range of failure modes, selecting the one which occurs first; this depends on the layout of the slab and its support conditions.

After postulating a failure mode, the algebraic expressions for external and internal work done are derived, and equating these unearths the appropriate collapse load. In fire, the load intensity is invariant at the Fire Limit State loading. However, the resistance of each structural component varies as its thermal exposure changes. For a slab panel, the overall resistance depends on the relative temperatures of its components; the slab, its reinforcement, and the protected and unprotected beams. In addition, continuity would increase the panel's capacity due to the hogging moments generated across the edge beams not involved in folding.

The development therefore calculates the reduced internal work done due to the thermal exposure at each time step, and then compares it with the 'constant' external work done for a given deflection. The point at which the internal work done ceases to exceed the external work done defines failure of the panel, and hence the failure 'time'.

Figure 2 presents a summary of the mechanisms discussed in this paper:

1. Collapse Mechanism 1 is for the isolated slab panel case.
2. Collapse Mechanism 2 follows the principles of the isolated panel, but includes continuity across two opposite sides of the slab panel. Although uncommon, this type of failure occurs in large compartments, such as open-plan offices where the fire can cover very large areas.

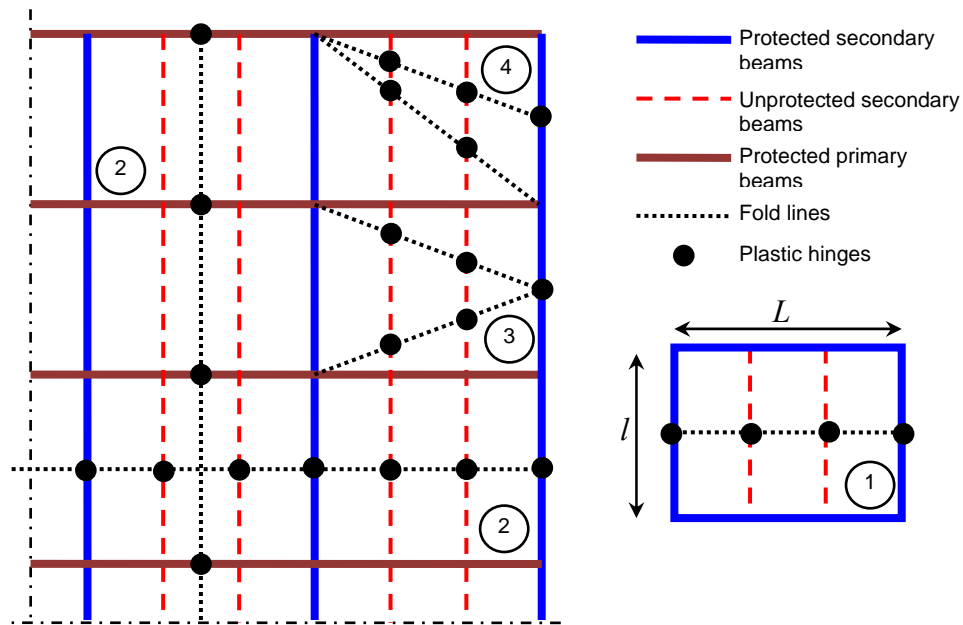


Figure 2. Proposed Collapse mechanisms.

3. Collapse Mechanism 3 is appropriate to slab panels at the edge of a building, subjected to fires which are local to that compartment.
4. Collapse Mechanism 4 would cover a similar fire exposure scenario, but resulting in a different response of the slab panel, due to its location and the relative sizes of its beams.

These simplified mechanisms have been verified with *Vulcan* [3], and checked against the Bailey-BRE Limit and the conventional span/20 deflection limit. The design data for the example case are: dead load = 4.33kN/m²; live load = 5.0kN/m²; trapezoidal decking profile with a trough depth of 60mm; overall slab thickness of 130mm, and a concrete cube strength of 40N/mm². The floor beams were designed to BS5950 Parts 3 and 8, and the edge beams were protected to reach a maximum temperature of 550°C at 60min Standard Fire exposure.

Two slab panel sizes (9m x 9m and 12m x 9m, with properties listed in Table 1) were used for the verification. Intermediate secondary beams were spaced at 3m.

TABLE I. SLAB PANEL DESIGN DATA.

Slab Panel Size	Beam Type	Beam Section	Load Ratio	Temperature at 60 minutes	Span (m)
9m x 9m	Intermediate	305 x 127 x 48 UB	0.471	940°C	9
	Secondary	356 x 171 x 67 UB	0.442	550°C	9
	Primary	533 x 210 x 101 UB	0.446	548°C	9
12m x 9m	Intermediate	457 x 152 x 67 UB	0.470	941°C	12
	Secondary 1	406 x 178 x 67 UB	0.443	548°C	12
	Secondary 2	533 x 210 x 101 UB	0.469	550°C	12
	Primary	610 x 305 x 179 UB	0.471	547°C	9

In the equations that follow, the following notation is used:

- L length of primary beam
- l length of secondary beam
- w applied floor load at the fire limit state
- w_{eff} effective width of composite beam
- δ maximum deflection of the slab (or beams)
- θ beam or slab rotation
- M_{pp} plastic moment capacity of the protected primary beam at time t
- M_{ps} plastic moment capacity of the protected secondary beam at time t
- M_u plastic moment capacity of the unprotected beam at time t
- m^+ sagging moment capacity of the slab
- m^- hogging moment capacity of the slab
- n number of intermediate unprotected beams in the slab panel

Collapse Mechanism 1 (see Figure 2)

Folding across secondary beams:

$$\frac{wLl}{2} - \left[8M_{ps} \frac{1}{l} + 4nM_u \frac{1}{l} + 4m^+ \frac{1}{l} \left[L - (n+1)w_{eff} \right] \right] \geq 0 \quad (1)$$

Folding across primary beams:

$$\frac{wLl}{2} - \left[8M_{pp} \frac{1}{L} + 4m^+ \frac{1}{L} l \right] \geq 0 \quad (2)$$

In the equations above, the plastic capacities of the composite beams include the contribution of the reinforcement in the slab which forms the upper flange. The term $(L-(n+1)w_{eff})$ therefore accounts for the parts of the reinforced concrete slab which do not form parts of the effective upper flange widths.

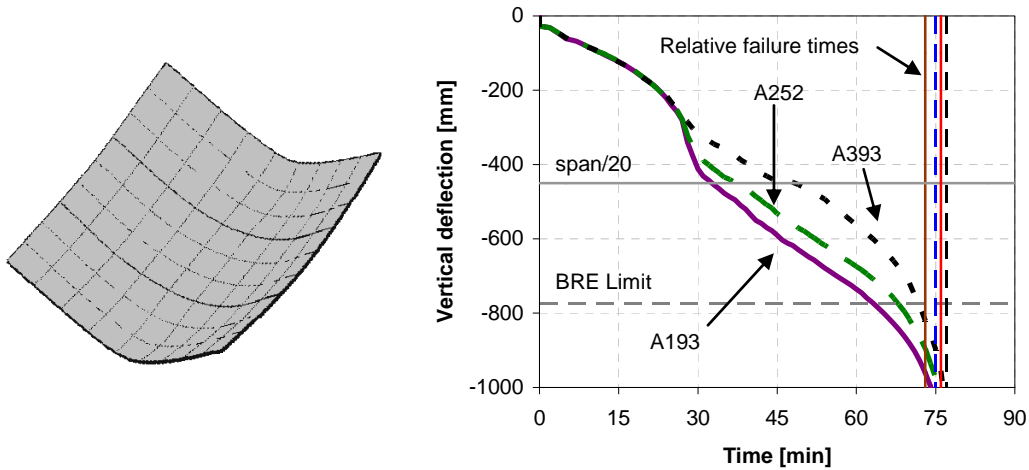


Figure 3. Collapse mechanism 1-comparisons.

Figure 3 shows a snapshot from the *Vulcan* analysis of the single-curvature folding of the isolated 9m x 9m slab panel. Following from the previous study [7] the analysis was conducted with 3 mesh sizes—A193, A252 and A393 (193, 252 and 393 mm²/m in each direction, respectively). It is observed that the mesh size influences the failure time—a feature which is picked up by the improved proposal. The four vertical lines in the plot signify the failure times without reinforcement (73min), with A193 (75min), A252 (76min) and A393 (77min) respectively from left to right.

Collapse Mechanism 2 (see Figure 2)

Failure across secondary beams:

$$\frac{wLl}{2} - \left[8M_{ps} \frac{1}{l} + 4nM_u \frac{1}{l} + 4m^+ \frac{1}{l} \left[L - (n+1)w_{eff} \right] + 4m^- \frac{1}{l} L \right] \geq 0 \quad (3)$$

Failure across primary beams:

$$\frac{wLl}{2} - \left[8M_{pp} \frac{1}{L} + 4(m^+ + m^-) \frac{1}{L} l \right] \geq 0 \quad (4)$$

It is assumed that the net compressive force (for hogging moment) acts at the centroid of the unprotected beam connection

A verification of Collapse Mechanism 2 is shown in Figure 4. The *Vulcan* analysis on the left is of two bays of 9m x 9m slab panels, with continuity across one edge of primary beams. This simulates a fire in a large compartment in the outer bays of a building. The graph on the right shows deflections of the centre of the 9m x 9m slab panel and the protected secondary beam between the two panels. It is observed that, due to the redistribution of loads that takes place, coupled with thermal exposure, the protected beam deflection ‘runs away’, resulting in another single-curvature failure. The proposed collapse mechanism is seen to give a good approximation of the failure time (82min) of the multi-bay model.

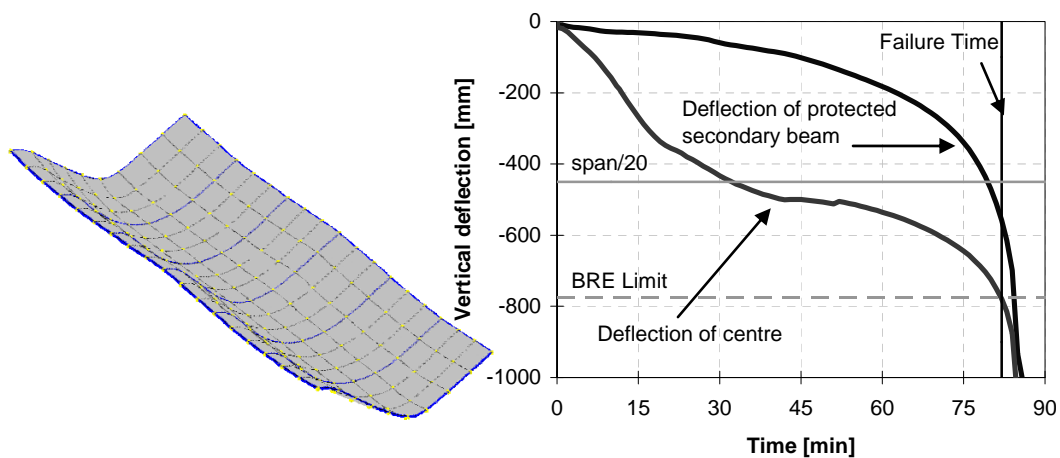


Figure 4. Collapse Mechanism 2—comparisons.

Collapse Mechanism 3 (see Figure 2)

Failure of protected secondary beam:

$$\frac{wLl}{3} - \left[\begin{array}{l} 4M_{ps} \frac{1}{l} + 4nM_u \frac{1}{l} + 4m^+ \frac{1}{l} [L - (n+1)w_{eff}] \\ + 4m^- \frac{1}{l} L + 2(m^+ + m^-) \frac{l}{L} \end{array} \right] \geq 0 \quad (5)$$

Failure of protected primary beam:

$$\frac{wLl}{3} - \left[\begin{array}{l} 4M_{pp} \frac{1}{L} + 4(m^+ + m^-) \frac{1}{L} l + m^- \frac{L}{l} \\ + m^+ [L - (n+1)w_{eff}] \frac{1}{l} \end{array} \right] \geq 0 \quad (6)$$

A comparison of deflections of the 12m x 9m *Vulcan* model and the limiting deflections is shown in Figure 5. Relative to the span/20 criterion, the slab panel fails at about 25min, while the Bailey-BRE limit suggests the panel can adequately survive a 120min exposure to the standard fire. However, the deflection-time plot shows no clear sign of failure until about 150min into the fire when the deflections of the centres of both the panel and the edge beam accelerate. The proposed collapse mechanism gives a very conservative prediction. In the derivations so far, the fold lines have been perpendicular to the orientation of either the failing secondary or primary beams. In this particular case, they are at an angle, and could especially influence the capacities of the unprotected beams. The *Vulcan* models show a twisting of the unprotected beams at the plastic hinges; the next update of these collapse mechanisms will explore the possibility of incorporating this in the method to improve predictions.

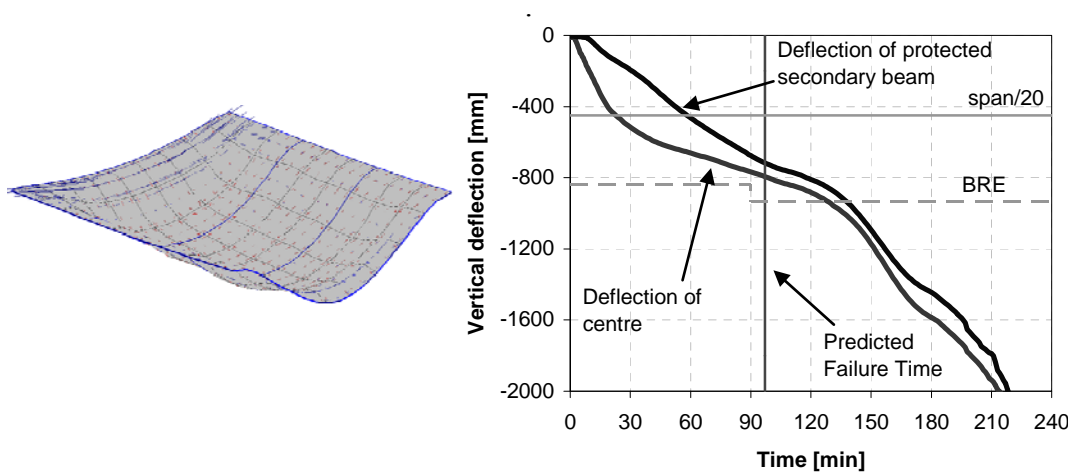


Figure 5. Collapse Mechanism 3—comparisons.

Collapse Mechanism 4 (see Figure 2)

Collapse Mechanism 4 is proposed to predict the failure of corner panels. The aim is to determine the influence of different support conditions and beam sizes on slab panel failure. The suggested failure mechanism is shown in Figure 2. However, comparisons using the numerical models have shown failure modes similar to those of isolated slab panels, folding in single-curvature directly across secondary beams, regardless of the support conditions at the edges of the panel. More investigation will be carried out to ascertain this and evaluate how aspect ratios and the degrees of protection or relative capacities of beams may influence this behaviour.

CONCLUSION

A number of collapse mechanisms have been proposed for inclusion into the Bailey-BRE Method to act as an extra check against structural collapse, as distinct from the compartment integrity failure on which the existing method is based. Two of the proposals, for isolated panels and for large compartments, give accurate predictions, but those for edge panels and panels in the corner of a building require improvement.

In the study, the effects of columns were not considered. The presence of columns will provide some axial restraint to the beams and the slab panels as a whole. Depending on the loads on the beams attached to the columns and the columns themselves, coupled with fire severity, the beams could fail, pulling the columns inwards which could potentially fail due to $p-\Delta$ effects. This is however a subject for future research.

REFERENCES

1. Newman, G. M., J. T. Robinson, and C. G. Bailey. 2006. *Fire Safe Design: A New Approach to Multi-Storey Steel-Framed Buildings*, Second Edition, SCI Publication P288, The Steel Construction Institute, UK.
2. Bailey, C. G. 2000. *Design of Steel Structures with Composite Slabs at the Fire Limit State, Final Report No. 81415, prepared for DETR and SCI*, The Building Research Establishment, Garston, UK.
3. Huang Z., I. W. Burgess and R. J. Plank. 2003. "Modelling membrane action of concrete slabs in composite slabs in fire. I: Theoretical Development", *ASCE Journal of Structural Engineering*, 129 (8), pp. 1093–1102.
4. Cameron, N. J. K. and A. S. Usmani. 2005. "New design method to determine the membrane capacity of laterally restrained composite floor slabs in fire; Part 1: Theory and method", *The Structural Engineer* 83 (19), pp. 28–33.
5. Omer, E., B. A. Izzudin, and A. Y. Elghazouli. 2006. "Failure assessment of simply supported floor slabs under elevated temperature" *Structural Engineering International* 16 (2), pp. 148–155.
6. Li, G. Q., S. X. Guo and H. S. Zhou. 2007. "Modelling of membrane action in floor slabs subjected to fire", *Engineering Structures* 29, pp. 880–887.
7. Abu A. K., I. W. Burgess and R. J. Plank. 2008. "Effects of edge support and reinforcement ratios on slab panel failure in fire", *Proceedings of the 5th Structures in Fire Conference*, Singapore, 380–391.

Planning for a Large-Scale Fire Test on a Composite Steel-Frame Floor System

D. J. PROE and I. R. THOMAS

ABSTRACT

A large-scale fire test is to be conducted in Melbourne, Australia late in 2010. This paper describes the physical details of the test and its purpose. The test will facilitate investigation of the fire behaviour of one storey of a typical office building structure as used in Australia for a particular configuration of unprotected steel beams. The test structure will be a steel-frame composite concrete floor system suspended 3 m above the floor of the test building. It will have plan dimensions of 20 m by 16 m, divided into two bays in each orthogonal direction.

INTRODUCTION

A series of six large-scale fire tests conducted within a purpose-built test building at Cardington in the UK in 1995 and 1996 [1] indicated that the structural performance in fire of the whole structure may be superior to that of the individual members. It may thus be possible that adequate performance can be achieved with some steel beams not being protected, thus saving the cost of this protection. The application of the benefits of the Cardington tests to building design requires an understanding of the structural principles by which the improved performance was achieved, in order that they may be reliably replicated in the real building. Essentially a design method is required, by which the normal structural design of the building for ambient temperature conditions is extended to ensure adequate structural performance under elevated temperature conditions. A research project is currently under way to develop such a design method.

David J Proe, Prof Res Fellow, CESARE, Victoria University, Melbourne, Australia.
Ian R Thomas, Professor, CESARE, Victoria University, Melbourne, Australia.

SCOPE AND ASSUMPTIONS OF RESEARCH PROJECT

This research project focuses on a particular fire protection scheme in a multistorey office building satisfying particular geometric conditions. This scheme involves protection of all columns and all main grid beams (those framing directly into columns), with all other beams unprotected. It includes a greater proportion of protected beams than were incorporated in most of the Cardington tests. The building is required to have a central core which is capable of ensuring global stability of the building in the event of a fire over the whole area of one storey. The beam layout is required to be regular, with each column having beams connected in both orthogonal directions. The form of construction is required to be similar to that used in the Cardington tests, incorporating steel columns, steel beams, a composite floor slab and shear studs between the steel beams and the slab. The slab must incorporate reinforcement which is continuous throughout the floor plate.

It is assumed for this project that the entire underside of the floor system is exposed to uniform fire conditions (as this is considered to be the worst case condition) and that the fire exposure is defined by the standard time-temperature curve as given in the Australian Standard for fire testing, AS1530.4. This project does not consider the many variables affecting fire growth in a real building. It is assumed that the Fire-Resistance Level (FRL) is stipulated by others and that its structural adequacy component is either 60, 90 or 120 minutes.

It is assumed furthermore that the building is sprinkler-protected throughout, as required in Australia for buildings with at least six or seven storeys above ground. In some applications, isolation valves on each storey may also be required. Associated with these assumptions, fire on only one storey is considered to occur and the insulation and integrity failure criteria are ignored.

The sole acceptance criterion for application of the proposed solution to a real building is that, for a fire at any one storey, all storeys above should remain stable throughout the fire duration of the fire. This requires that all columns passing through the fire-affected storey should remain stable. The condition of the floor directly above the fire is only important to the extent that it affects the stability of the columns attached to this floor.

Numerous aspects of the structural performance in fire of this floor system could be studied. Based on the extensive analysis and further testing which has occurred since the Cardington tests, it appears likely that the principle contributing most to the enhanced performance in fire is tensile membrane action in the slab. This mode of support is the main focus of the research project. Aspects closely associated with tensile membrane action will be given more emphasis, including the following:

- ability of protected beams to support load being shed from unprotected beams
- effect of beam deflection at slab perimeter on tensile membrane action
- effect of reinforcement ductility and strain localisation on slab failure deflection
- effect of perimeter horizontal displacement and forces on column capacity

To enable development of the design method and demonstrate the adequacy of the proposed approach, a large-scale fire test will be conducted late in 2010.

PHYSICAL DETAILS AND PURPOSE OF PROPOSED FIRE TEST

The proposed test will be conducted within the Fiskville fire test building, which has plan dimensions of 40 m by 70 m and a height of 20 m. The test structure will be a steel-frame floor system suspended 3 m above the floor of the building. It will have horizontal dimensions of 20 m by 16 m, divided into 2 equal bays in each orthogonal direction (see Figure 1). It will incorporate 9 columns, supported at the top by a braced steel frame. The beams and columns will be steel I-sections. A composite slab with a dovetail profile will be used. All structural members will be sized in accordance with Australian codes. All beams except some perimeter beams will be constructed to achieve full composite action with the slab. All internal secondary beams will incorporate web penetrations, with some reinforced (plated) and others unreinforced. Insulation material will be applied to all columns and to the main grid beams. Beams internal to each bay will be left unprotected. This four-bay structure will be loaded as per Australian codes and will realistically model the continuity achieved over the internal edges of a corner bay. It will not be possible to apply realistic loads to the columns, however, and so their performance will not form part of the test but will be evaluated afterwards by analysis.

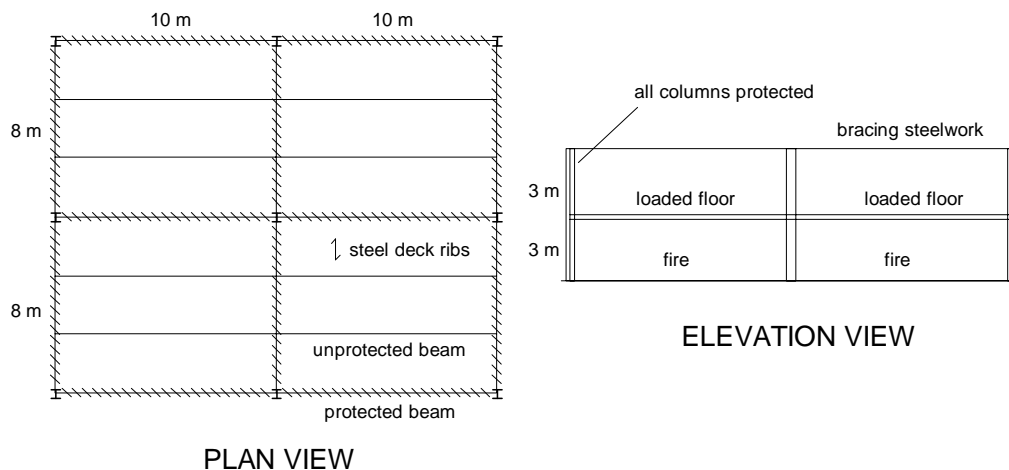


Figure 1. Test Structure.

The entire underside of the floor system will be exposed to fire. Test burns and CFD modelling are being performed with the objective of producing temperature conditions which are as uniform as possible throughout the structure. Ideally the time-temperature curve of the fire would approximate that of the standard fire test, but this may not be practically achievable. It is envisaged at least that the temperature of the unprotected steel beams will reach 900-1000°C for 30 minutes or more. At this stage it is expected that the fuel will be liquid kerosene, continuously piped into the test enclosure, with provision for ventilation conditions to be adjusted during the test. The FRL of the protection material on the beams will be selected based on the likely fire severity which can be achieved, but it is expected to be approximately 60–90 minutes.

Instrumentation of the test will include approximately 500 thermocouples and 50 displacement transducers, as well as about 6 cameras. Displacements will be

measured relative to unprotected stainless steel cables under gravity loading which will be stretched above the floor across the entire structure in both orthogonal directions. Loading will be via 360 steel drums, each containing 200 litres of water.

The purpose of the test is to focus on the particular protection scheme considered and to investigate a fire over the whole floor plate. The Cardington tests did not enable the latter possibility to be evaluated. It will check that this type of solution can be applied to Australian materials and design methods, particularly low ductility, high bond reinforcement. It will check the boundary conditions (moment continuity and axial restraint) to be used at the internal edges of each bay.

SURVEY OF RELEVANT LITERATURE

Extensive technical literature is becoming available on this subject. The discussion below focuses on those publications which are most directly applicable to predicting the likely performance of the structure in the proposed fire test.

Park and Gamble [2] have described tensile membrane action in reinforced concrete construction and presented a theoretical solution for the ambient temperature capacity of a rectangular reinforced concrete slab, assuming perimeter support on walls and full lateral restraint. These boundary conditions are likely to produce a greater load capacity than those available in the floor system under consideration, and so the solution presented is likely to be a “best-case” scenario. The solution has the form of the classical catenary equation and may be amenable to adaption for a design method for fire, provided that allowance can be made for the relevant boundary conditions and for various reinforcement ductility limits. Importantly the recommended deflection limit for this case is 10-15% of the smaller span, based on a review of test results.

A method of slab design in fire has been proposed by Bailey [3]. This method applies only to slab bays with protected steel beams on all four sides. At continuous internal edges of these bays, the method assumes that under fire conditions any reinforcement will fracture, resulting in internal bays, edge bays and corner bays all having the same load capacity (ie no moment continuity or lateral restraint over supports). Unpublished fire testing by D J Proe and M Patrick at BHP Melbourne Research Laboratories in 1997 found that fracture of slab reinforcement over beam supports did not occur. A one-way slab which was continuous over beam supports at each end of the middle span was subjected to standard fire exposure from below. Each cantilever end of the slab was held down by a loading jack such that zero rotation was maintained over the supporting beams. A type of reinforcement considered to be low ductility was used in the slab. The expected FRL of the slab was 120 minutes but heating was continued for nearly 240 minutes without collapse. Whereas fracture of the reinforcement over the beams could have been expected under these onerous conditions, none occurred. The cracked zone above the beam had a length which was greater than expected, and the required rotation was achieved by a long plastic hinge with a small curvature rather than a shorter hinge with a larger curvature.

Bailey's method is based on ambient temperature solutions from an earlier paper by Hayes [4], who in turn based his work on a proposal from Sawczuk. This method has been adapted to elevated temperature conditions. A deflection limit directly

controls the load capacity. Given limited information on ductility at the time, a number of assumptions have been made in calculating this deflection limit, and it is considered that this limit should now be revisited given the new information becoming available. The paper by Hayes appears to assume a limit of about 3-5 times the effective depth of the slab.

Na-Si Zhang et al [5] have published an analytical solution for tensile membrane action in rectangular slabs with roller edge support. The capacity limit is based on reinforcement ductility and uses the specified uniform elongation value, taking no account of strain localisation. Some input assumptions appear to be unconservative, including the calculation of different applied loads in various parts of the slab (whereas uniform loading is applied). The slab is divided into a central membrane in tension which is supported by rigid plates around the edges. No calculation of the strength of these rigid plates is performed. A check of the in-plane moment capacity of the edge plate at the mid-length of the long side under the influence of the assumed applied loads indicates that it is unlikely to be adequate.

Gilbert has published ambient temperature slab test results for low ductility reinforcement [6]. Although concerned about ductility issues in one-way slabs, he appears less concerned about two-way slabs, where the occurrence of more closely spaced cracks has been found to improve the ductility.

Cashell [7] has discussed reinforcement ductility in relation to the low reinforcement ratio in composite slabs after the steel sheeting has reached a high temperature and become ineffective. The ultimate tensile capacity and moment capacity of the slab will typically be below those at first cracking in this case, a condition closely associated with strain localisation and low cross-section ductility. This work is continued in the paper by Elghazouli et al [8], where measurements of the effect of elevated temperature on reinforcement ductility are reported, indicating ultimate strains for cold-worked reinforcement of twice ambient values at 500°C and 7-9 times ambient values at 700°C. This is important, as it is the cold-worked reinforcement which is typically the lowest in ductility. Further work at Imperial College by Omer [9] has produced a method of calculating the effect of strain localisation. Slab deformations are calculated using the geometry of the yield lines (similar to Bailey's approach) and bond-cracking theory is used to calculate the required reinforcement ductility. This may prove a useful approach, depending on the accuracy of the bond model used.

Numerous papers have been published on finite element analysis of the Cardington fire tests, particularly from Sheffield University, Edinburgh University and Imperial College [10,11,12]. Analysis work which is able to replicate the Cardington tests is useful as it may demonstrate that the observed structural performance is a true indication of the performance of the structure as reported and is not due to some extraneous factor which would not exist in a real building. Such extraneous factors are mentioned on the Vulcan Solutions website [13]. This website shows analysis of all six Cardington tests using the finite element program, VULCAN. In all cases, reasonable agreement is indicated between the calculated and measured deflections. For Test 4 (BRE Corner Test), it is stated that external wind posts supported the perimeter beam, and its effect is included in the analysis. For Test 6 (BRE Demonstration Office Test), it is stated that a part of the slab came into contact with the block walls forming an internal boundary of the fire enclosure. Again it is assumed that this effect was included in the analysis, as good agreement

with the test deflection was obtained. The VULCAN analysis of Cardington Test 3 (British Steel Corner Test) is corroborated by Elghazouli et al [12] using the program ADAPTIC. The deflection results obtained are similar to the VULCAN results and to the measured values.

The structural performance in many of the Cardington tests is difficult to understand in the context of the currently available theory. Both Bailey's method and that proposed by Zhang et al address the case of protected beams on all four sides of a bay. None of the Cardington tests satisfied this requirement, and the performance was therefore much better than expected. In particular Tests 3 and 4 included exposure of one corner bay, with the two perimeter beams protected in Test 3 and no beams protected in Test 4 (but some support from wind posts at an edge beam). Test 6 included fire exposure of two complete bays and part of two further bays, with none of the main grid beams protected. Even with support from the block wall at one location, the extent of unprotected floor was large enough that collapse could have been expected. Test 5 included exposure of the largest section of floor, extending across the full width of the building and along 40% of its length, representing 6 bays. None of the steel beams in this area were protected. Unfortunately the beam temperatures achieved were too low to be of interest in this test. A further Cardington test was conducted in 2003. This test include exposure of one edge bay, with no steel beams protected. High steel temperatures were achieved and no collapse occurred. Some support from wind posts at the edge beam was considered to have occurred. Nevertheless, the performance was again much better than could be expected for a bay without edge beams protected. Since the Cardington tests, other relevant fire tests have been performed, again showing excellent slab performance. These tests included those by Lim [14], Zhao [15] and Wald [16].

It therefore appears that the support mode demonstrated in the Cardington tests may have been associated with the fact that only part of the storey was exposed to fire. The remaining cool parts of the floor slab may have provided almost rigid in-plane restraint in two directions and this may have been sufficient to maintain stability. This conclusion assumes that support from the block walls did not occur to any significant extent, but this appears unlikely as great care was taken to ensure that this did not occur. In any case, the plots of deflection versus time would be likely to show a sudden change if this had occurred.

Another useful paper is that by Quiel and Garlock [17], who analyse the important problem of the effect of horizontal floor deformation on column strength. For the case analysed, it was shown that failure of unprotected beams may result in the column remaining deflected outward and therefore stable throughout the fire.

STRUCTURAL PERFORMANCE CALCULATIONS

The equations from Park and Gamble [2] indicate that, for the best case scenario where all edges remain straight and full horizontal restraint is available, high load capacity can be achieved with only a small quantity of slab reinforcement. The catenary equation and deflection limit shown below apply to a square panel with equal reinforcement in both orthogonal directions:

$$\frac{wL^2}{14} T \quad \text{and} \quad 0.15L \quad \text{give} \quad T = wL/2 \quad \text{and} \quad A_{st} = T/(Rf_{sy})$$

Assuming a slab span (L) of 9 m in each direction and a uniform load at the fire limit state (w) of 6 kPa, along with 500 MPa reinforcement (f_{sy}) and 50% strength reduction (R) due to heating, the required reinforcement quantity (A_{st}) at deflection (ϵ) is only 108 mm²/m, whereas at least 200 mm²/m is typically used. To calculate the width of the compression ring to support the catenary force (T), elastic equations for hoop stress and radial stress have been used to calculate that, for a slab depth of 120 mm and concrete strength of 40 MPa, the required width of the concrete compression ring is only 60 mm

The above results appear positive for tensile membrane action. On the other hand, the ability of the slab to support the applied area loading depends the ability of the protected beams on all four sides to carry their applied loads. For the proposed beam layout, if the heated unprotected beams are assumed to carry no load and the tributary area assumption is made as for ambient conditions, then the bending moment in the protected secondary beams is doubled due to this load shedding alone. Given that their load ratio is typically about one-half, this extra load would cause these beams to fail as soon as any strength was lost due to heating. This effect does not appear to have caused failure in the Cardington tests nor in the VULCAN simulations conducted, however. The way that tensile membrane action distributes the load to the perimeter beams is an important part of the study.

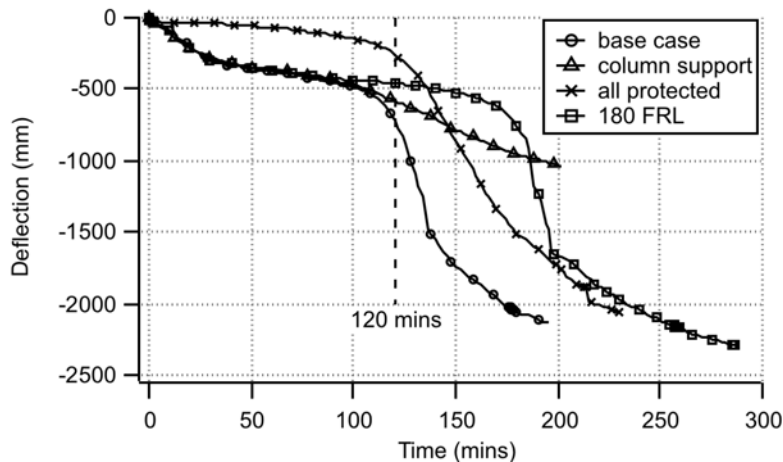


Figure 2. VULCAN Results.

Several VULCAN runs have been performed on a model representing one-quarter of the proposed structure. The slab reinforcement area was 252 mm²/m in each direction. Temperatures as for standard fire exposure were used. Protected beams were assumed to reach bottom and top flange temperatures of 593°C and 421°C respectively at 120 minutes (representing 120 FRL), while unprotected beams reached 1043°C and 941°C respectively at 120 minutes. The slab soffit was assumed to follow the standard time-temperature curve and a realistic non-linear profile through the slab was adopted. Slab element sizes were approximately 1 m in

each plan dimension. For the base case (Run 1), the slab was supported at its corners on rollers and the beam protection layout was as per Figure 1. For Run 2, the slab was supported on ambient-temperature columns, which provided resistance to horizontal translation. For Run 3, all beams were protected. For Run 4, 180 FRL was applied to the protected beams. The calculated performance appeared reasonable in all cases (see Figure 2).

CONCLUSION AND ACKNOWLEDGEMENTS

A proposed large-scale fire test has been described, along with its context within the international technical research. Preliminary analysis has been presented.

This document has been prepared with funding provided by the Australian Department of Tourism and Resources (AusIndustry) under the Industry Cooperative Innovation Program (ICIP). The valuable contributions of Anthony Ng of OneSteel Pty Ltd and Michael Culton of CESARE are acknowledged.

REFERENCES

1. Kirby, B et al, "The Behaviour of Multi-Storey Steel Framed Buildings in Fire", British Steel Corporation, 1999.
2. Park, R and Gamble, W L, "Reinforced Concrete Slabs", Wiley, 1980.
3. Bailey, C G, "Efficient Arrangement of Reinforcement for Membrane Behaviour of Composite Floor Slabs in Fire Conditions", Journal of Constructional Steel Research, Vol 59, 2003.
4. Hayes, B, "Allowing for Membrane Action in the Plastic Analysis of Rectangular Reinforced Concrete Slabs", Magazine of Concrete Research, Vol 20, No 65, 1968.
5. Na-Si Zhang And Guo-Qiang Li, A New Method to Analyze the Membrane Action of Composite Floor Slabs In Fire Condition, Structures in Fire Conference, Singapore, 2008.
6. Gilbert, R I, "The Treatment of Ductility in the Analysis and Design of Reinforced Concrete Beams and Slabs—Why AS3600-2001 Got It Wrong", Concrete Institute of Australia Conference, 2007.
7. K.A. Cashell, A.Y. Elghazouli And B.A. Izzuddin, Ultimate Behaviour Of Composite Floor Slabs at Ambient And Elevated Temperature, Structures in Fire Conference, Singapore, 2008.
8. Elghazouli, A Y, Cashell, K A and Izzuddin, B A, "Experimental Evaluation of the Mechanical Properties of Steel Reinforcement at Elevated Temperatures", Fire Safety Journal, Vol 44, 2009.
9. Omer, E, "Failure of Composite Steel-Concrete Slabs Under Elevated Temperatures", PhD thesis, Imperial College, 2006.
10. Huang, Z, Burgess, I W and Plank, R J, "Modelling Membrane Action of Concrete Slabs in Composite Building in Fire, I: Theoretical Development", Journal of Structural Engineering, ASCE, 2003.
11. Gillie, M, "The Behaviour of Steel-Framed Composite Structures in Fire Conditions", PhD thesis, University of Edinburgh, 2000.
12. Elghazouli, A Y, Izzuddin, B A and Richardson, A J, "Numerical Modelling of the Structural Fire Behaviour of Composite Buildings", Fire Safety Journal, Vol. 35, 2000.
13. VULCAN Solutions website (<http://www.vulcan-solutions.com/cardington.html>), Mar 2009.
14. Lim, L C S, "Membrane Action in Fire Exposed Concrete Floor Systems", PhD thesis, University of Canterbury, 2003.
15. Bin Zhao, Mohsen Rosefid And Olivier Vassart , "Full Scale Test of A Steel and Concrete Composite Floor Exposed to ISO Fire", Structures in Fire Conference, Singapore, 2008.
16. Wald, F and Kallerova, P, Draft Summary of Results from Fire Test in Mokrsko 2008", http://fire.fsv.cvut.cz/firetest_Mokrsko, 2009.
17. Quiel, S E and Garlock, M E, "A Closed-Form Analysis of Perimeter Member Behaviour in a Steel Building Frame Subject to Fire", Engineering Structures, Vol. 30, 2008.

Large-Scale Fire Test of Unprotected Cellular Beam Acting in Membrane Action

O. VASSART, C. G. BAILEY, M. HAWES, A. NADJAI, W. I. SIMMS,
B. ZHAO, T. GERNAY and J.-M. FRANSSSEN

ABSTRACT

This paper describes a full scale fire test performed recently on a composite floor for analysing the possibility of tensile membrane action to develop when the unprotected steel beams in the central part of the floor are made of cellular beams.

The natural fire was created by a wood crib fire load of 700 MJ/m² and the 9 x 15 m floor survived the fire that peaked at 1000°C and lasted for 90 minutes.

Blind predictions of the air temperature development by the software Ozone and of the structural behaviour by the software SAFIR which proved quite satisfactory are also described.



Figure 1. Fire test and structural elements after the fire.

O. Vassart (ArcelorMittal R&D, G.-D. of Luxemburg)
C. G. Bailey (University of Manchester, UK)
M. Hawes (ASDWestok Limited, UK)
A. Nadjai (University of Ulster, UK)
W. I. Simms (SCI, UK)
B. Zhao (CTICM, France)
T. Gernay and J.-M. Franssen (University of Liège, Belgium)

INTRODUCTION

As spans become longer, steel framed buildings become then more competitive compared with reinforced concrete framed buildings. For maximum economy, steel beams should be designed to act compositely with the floor slab. The increased use of long span composite beams leads to large open plan offices with minimal columns. However, as the span increases, the beam depth will also increase which, in turn, can lead to increased storey heights. The use of cellular beams (CB) largely overcomes this problem because ducts, pipes and other services can pass through the openings in the web. Also, as CB are constructed from hot rolled sections, the increased section depth results in added strength without additional material and thus tends to reduce the total weight of steelwork. Efficient assessment of structures in fire conditions is becoming more and more relevant and is covered by the use of numerical models. However, numerical models are based on small scale tests and experience. To date, no rigorous research into the performance of cellular beams in fire has taken place. The design assumptions are still largely based on the performance of solid web beams in standard fire tests.

A large scale composite floor using cellular beams connected to composite slabs was tested under a natural fire. The two central secondary beams were left unprotected. As cellular beams behave in a very different way compared to traditional steel beams in fire conditions, the test also provided unique experimental data on the performance of the cellular beams acting in membrane action. All the beam sections (protected and unprotected) and the slab were instrumented in order to measure the evolution of temperatures and displacements during the fire.



Figure 2. Inside view of the compartment before the test.

The fire test was conducted on the 27th of February 2010 by the University of Ulster (Figure 1). The information recorded during the test will be used to validate the natural fire safety concept and provide design rules and guidance for protected and unprotected cellular beams. The work is supported by the Research Fund for Coal and Steel and six partners are involved in this project.

The compartment covers an area of 15 by 9 m with a floor to soffit distance of 3m. It can be located near the central zone of any office building. The surrounding walls of the compartment were made of normal weight concrete block works with three 3 x 1.5 m openings in the front wall. The

surrounding walls were not fixed to the composite floor at the top which allowed vertical movement of the floor without interaction with the walls. All the columns and solid beams on the opening side were protected for a standard fire of two hours using fibre boards of 20 mm. The surrounding cellular beams were also protected using ceramic fibres.

STRUCTURE

The slab is made of 51 mm deep profile of the Kingspan Multideck 50 type with a concrete cover of 69 mm on the profile, which makes a total depth of 120 mm. A steel mesh of 10 mm with a spacing of 200 mm in each direction made of S500 steel was used as reinforcement. It was located at a vertical distance of 40 mm above the steel sheets. The slab was fixed on all steel beams by means of steel studs welded on the upper flanges (full connexion). All connections from secondary beams to main beams and from beams to columns are simple connections. Horizontal bracing was provided in 4 positions leaving the slab completely free of external horizontal restraint.

DESIGN LOADS

The loads applied on the slab are those which are commonly used in the design of office buildings, see Table 1.

description	Characteristics KN/m ²	Fire Factor	Design Load KN/m ²
Partition	1.0	1.0	1.0
Services & Finishes	0.5	1.0	0.5
Live Load	3.5	0.5	1.75
		Total	3.25

Table 1: Design Loads.

The applied load of 3.25 kN/m² was achieved using 44 sandbags of 1 ton evenly positioned over the floor plate, as shown in Figure 3a. The self weight of the slab of 120 mm thickness is about 2.90 KN/m².

FIRE LOAD

Assuming the design for an office, the fire load density would be 511 MJ/m² according to Table E.2 of EN 1991-1-2 [1]. However for this test, the fire load was increased by using 45 standard (1 m x 1 m x 0.5 m high) wood cribs, comprising 50 mm x 50 mm x 1000 mm wooden battens, positioned evenly around the compartment (Figure 3b), yielding a fire load was 40 kg of wood per square metre of ground area. The wood density provided was 510 kg/m³ with a calorific value of 17.5 MJ/kg for wood, which corresponds finally to a fire load of 700 MJ/m². This is consistent for multi-storey office accommodation [2] and allows a direct comparison with previous test carried out on the steel building at Cardington [3]. The figure is well established from the statistical data and a

number of tests have been carried out considering the quantity of fire load as the variable parameter [4].



Figure 3. a) Vertical static load, b) Wooden cribs used for the fire load.

METHOD OF IGNITION AND TEMPERATURE IN THE COMPARTMENT

The fire was started from a single ignition source (Figure 4). After 5 minutes two additional ignitions sources were started in different places and the rest of cribs were left to ignite naturally. Each crib was connected to its neighbours by mild steel channel section with porous fibre board laid into the channels and, approximately 30 minutes before ignition, some 20 litres of paraffin was poured into channel.



Figure. 4. Ignition and fully engulfed fire.

A blind prediction of the temperature development was made using the software OZone [5, 6] with the following hypotheses:

The fire load density: 570 MJ/m²
Combustion model: extended fire duration
Fuel height: 0.5 m
RHRf: 1250 kW/m²

Combustion heat of fuel: 17.5 MJ/kg
Fire growth: medium
Combustion efficiency: 0.8

As the fire test was conducted with a fire load of 700 MJ/m², a second calculation was performed with this fire load without changing other parameters. Figure 5 shows the comparison between the measured temperatures in the compartment and the OZone predictions:

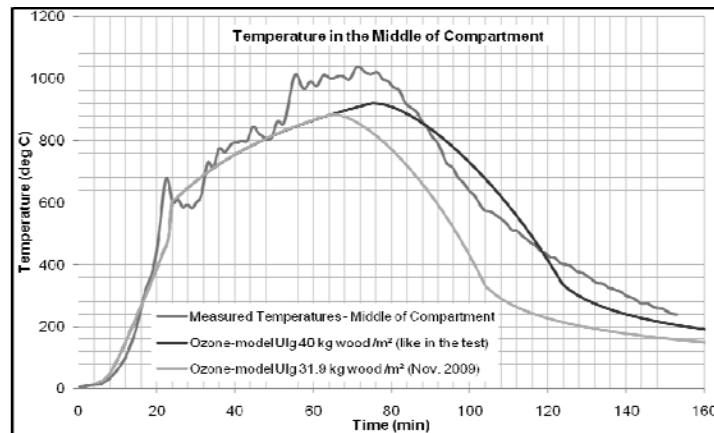


Figure 5. Measured temperature in the compartment Vs Ozone prediction.

LONG CELLULAR BEAM BEHAVIOUR

Under fire conditions, the deflection in the steel beam is the result of two causes: the thermal bowing and the mechanical deflection. The mechanical deflection is the increase in deflection under constant load due to reduced steel strength and stiffness with increasing temperatures. It is expected that at low temperatures (less than 500°C), the beam deflection is controlled essentially by thermal bowing. At higher temperatures, mechanical deflection dominates and the beam deflection increases at a faster rate (Figure 6) with a rise in the beam temperature (Figure 7). The unprotected cellular beams became as cables with only top flange considered working at very temperature around 800°C. Therefore, the bottom flange became very weak; the vertical shear forces induced by each web post combined with longitudinal restraint provided by the concrete slab caused a rotation of the lower beam, see Figure 6

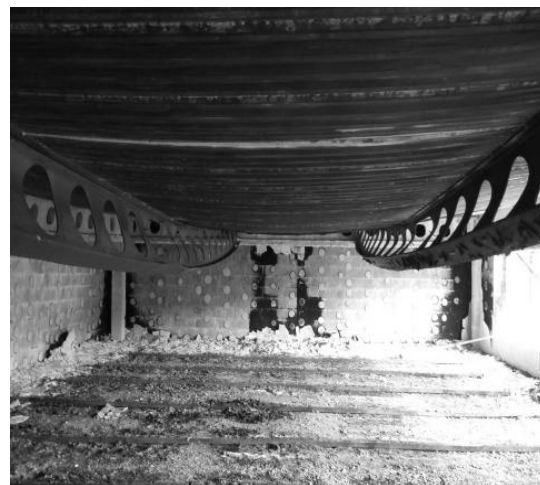
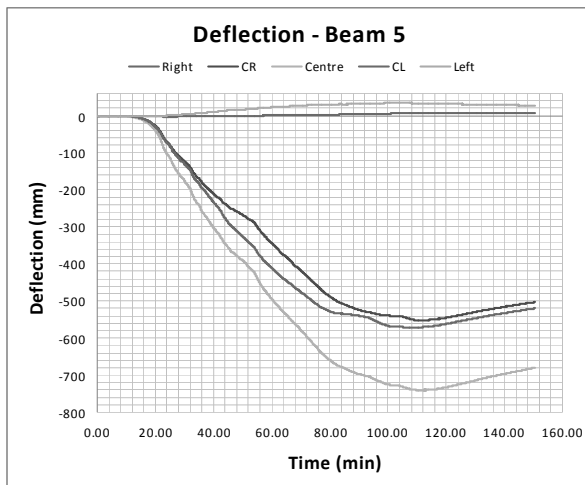


Figure 6. deflection of the unprotected beam and slab.

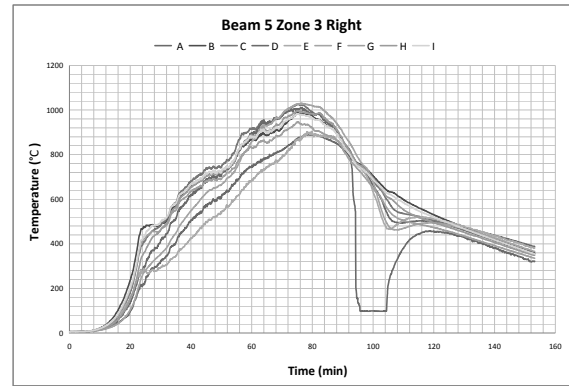


Figure 7. a) post web buckling , lateral and torsional effect, b) temperature distribution at the steel cross section

FLEXURAL STRENGTH OF THE COMPOSITE SLAB

The concrete slab had a nominal thickness of 120 mm and was constructed using normal-weight concrete. The average cube strength was 54.8 N/mm² at 28 days. The slab was exposed in an external environment and, at the time of the test, the measured moisture content of the concrete slab was 6.4% by weight. The slab reinforcement consisted of welded wire mesh reinforcement A393 (10mm diameter ribbed bars at 200mm centres) having nominal yield strength of 500N/mm². Full interaction between the slab and beam was ensured in all specimens by the use of a high density of shear connectors of 19 mm diameter studs at height 95 mm. The shear studs have been equally distributed in one row with spacing of 150 mm over the beam length. A trapezoidal steel deck with a thickness of 1.0 mm was used as sheeting.

Recorded results show very high temperatures in the steel decking, reaching the maximum of about 1100°C. The steel decking was also observed to have debonded from the concrete slab in most areas. Thus it may be assumed that the steel decking contributed very little to the slab strength at the maximum fire severity.

It was clear from the test that membrane action occurred in the floor plate supporting the current design approaches [7-10] which utilise this mode of behaviour to allow a significant number of steel beams to be left unprotected.

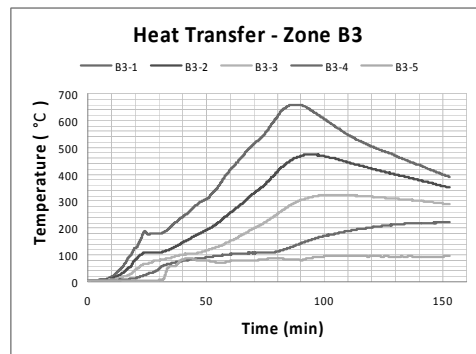
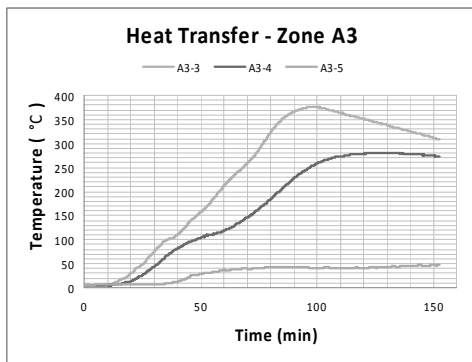


Figure 8. Temperatures at the slab decking.

SAFIR FINITE ELEMENT PREDICTION

A finite element model was built in the SAFIR software [11]. This model was made blind before the test in order to predict the behaviour of the structure. Figure 9 shows the numerical modelling with different types of elements.

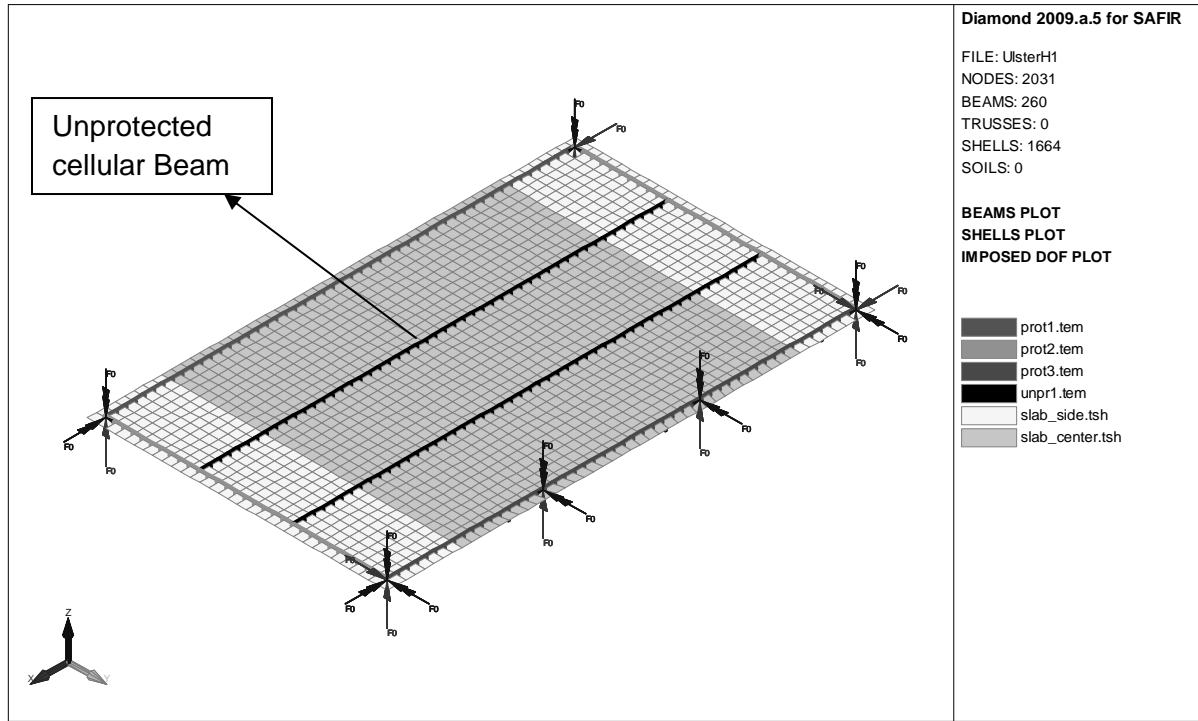


Figure 9. Finite element model built in SAFIR.

The unprotected cellular beams were simulated using BEAM finite Element which does not allow taking into account the web post buckling instabilities. This was why the simulation was run twice, once with cellular beams modelled as the double tee section (figure 10 a) and once as only the upper tee section (figure 10 b)



Figure 10. a) double tee section

b) upper tee section

The lower curve on the Figure 11 is obtained by modelling only the upper tee of the unprotected beams, what is justified by the fact that web post buckling will appear in these sections and will prevent the bottom tee from playing any structural function. In this case the deflection at room

temperature has no physical signification since the real contribution of the secondary beam is largely underestimated. But in fire situation, the results are interesting. For example, it can be observed that the deflection does not decrease when the temperature decreases, because the steel profiles do not recover their stiffness. This model can be considered as a reasonable model for a simulation of such type of floor system in the fire situation since the cellular beams, after the web post buckling, will probably not be able to recover their initial stiffness when the temperature decreases.

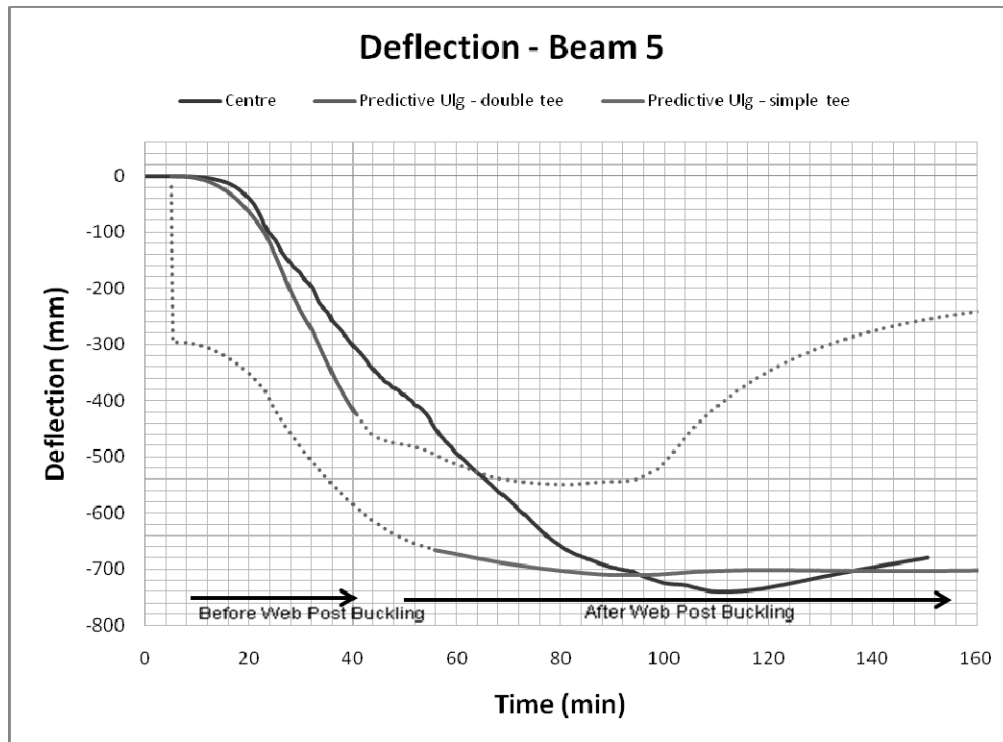


Figure 11. Influence of the model of the unprotected beams and comparison with test results.

Figure 11 shows a good correlation between the FEM model and the real behaviour of the test. Of course, some parameters of the finite element model can be adapted in order to fit with the real properties of the material used during the test, the real measured temperatures in the element, etc.... But it already gives some confidence that this model is capable of predicting the fire behaviour of such type of floor system with a satisfying level of accuracy.

It would also be possible to model the steel cellular beams in detail with shell elements, but such model would be too large for practical applications.

CONCLUSION

This fire test provided a unique opportunity to study the behaviour of long cellular steel beams in a complete compartment office in building structure under realistic fire conditions. The test was very successful, fire was more intense and of longer duration that assumed in the initial studies yet the structure performed as predicted. The test results are still being intensively analysed by partner

researchers, thus it is not yet possible to draw a comprehensive list of conclusions at this stage. It appears anyway clear already that the fact to use cellular beams to support the composite slab does not jeopardise the tensile membrane action that develops in the slab in a fire situation.

The Ozone model provides a rather estimation of the fire development, provided that the correct amount of fire load is introduced.

The SAFIR model was capable of predicting with an acceptable level of accuracy the complex behaviour of cellular beams acting in membrane action.

ACKNOWLEDGEMENTS

The authors thank Mr Seamus O'Connor, Martin Cox and Thomas Farrell from the Fire Direct Glass and Mr Sam Kelly from the composite decking and Kingspan ltd.

REFERENCES

1. EN1991-1-2 "Eurocode 1: Actions on structures—Part 1–2: General rules—Fire design"
2. CIB W14 Workshop Report. Design guide: structural fire safety. *Fire Saf J* 1986;10(1):77–154.
3. Bailey C.G., Lennon T., and Moore D.B. The behaviour of full-scale steel-framed buildings subjected to compartment fires. *The Structural Engineer* Vol. 77 No. 8 April 1999 pp. 15 - 21.
4. Natural fires in large scale compartments—A British Steel Technical, Fire Research Station Collaborative Project. Contract Report for the Department of the Environment.
5. A tool to design steel elements submitted to compartment fires—OZone V2. Part 1: pre- and post-flashover compartment fire model, Cadorin J.-F. & Franssen J.-M., *Fire Safety Journal*, Elsevier, 38 (2003), 395–427, <http://hdl.handle.net/2268/29650>.
6. A tool to design steel elements submitted to compartment fires—OZone V2. Part 2: Methodology and application, Cadorin J.-F., Pintea D., Dotreppe J.-C. & Franssen J.-M., *Fire Safety Journal*, Elsevier, 38 (2003), 429–451, <http://hdl.handle.net/2268/29651>.
7. Bailey C.G. and Moore D.B. The structural behaviour of steel frames with composite floorslabs subject to fire: Part 1: Theory. *The Structural Engineer* Vol. 78 No. 11 June 2000 pp. 19 – 27
8. Newman G.M., Robinson J.T. and Bailey C.G., *Fire Safe design: A New Approach to Multi-Storey Steel-Framed Buildings* (Second Edition). SCI Publication P288. The Steel Construction Institute, Ascot. 2006. ISBN 1 85942 169 5.
9. Bailey C.G. *Steel Structures supporting composite floor slabs: design for fire*. BRE Digest 462. December 2001. ISBN 1 86081 527 8.
10. Bailey C G, Toh W.S. "Behaviour of concrete floor slabs at ambient and elevated temperatures". *Fire Safety Journal*. Vol. 42. Issue 6-7. 2007 pp 425–436.
11. SAFIR. A Thermal/Structural Program Modelling Structures under Fire, Franssen J.-M., *Engineering Journal*, A.I.S.C., Vol 42, No. 3 (2005), 143–158.

Experimental and Numerical Investigations of Steel and Concrete Composite Floors Subjected to ISO Fire Condition

B. ZHAO and M. ROUSEFID

ABSTRACT

The very positive membrane action of steel and concrete composite floor systems (concrete slabs connected to steel beams by means of headed studs) has been clearly demonstrated through various Cardington real fire tests. However, little evidence is established for fire performance of such structural system exposed to ISO fire condition, the lack of which still constitutes an obstacle for certain national authorities to accept totally the application of the design concept derived from above real fire tests, in particular for long duration ISO fire.

On the basis of above situation and in order to enlarge the application of the design concept based on membrane action to all types of fire, CTICM, within the scope of two different research projects FRACOF and COSSFIRE, performed successively two full scale ISO fire tests, both of which lasted for more than 120 minutes, with two different steel and concrete composite floor systems designed according to Eurocode. The observed fire performance of these floor systems during the tests was extremely satisfactory and revealed a solid robustness of such type of structure systems in fire situation. Considering the fact that the fire test of FRACOF project has been already presented in detail during previous SIF conference, this paper is focused especially on the comparison of above two tests with regard to structural configuration, loading condition, structural behaviour and the failure modes.

In addition, these tests have been subjected to a specific numerical investigation with help of a 3D hybrid structural FE model. It is illustrated through this numerical investigation that the actual advanced modelling technique is accurate enough to reproduce precisely the fire behaviour of complex structural systems and may be applied to fire safety engineering with high level of confidence.¹

INTRODUCTION

Since the natural fire tests on the eight-storey building at Cardington in UK [1-3], a new design concept on the basis of membrane action has been

Bin ZHAO and Mohsen ROUSEFID, CTICM, Espace technologique, L'orme des merisiers, Immeuble Apollo, 91193 Saint-Aubin, France
email : binzhao@cticm.com and mrousefid@cticm.com

developed and applied firstly in UK with help of a specific design tool [4]. Nowadays, the same design concept is being extended also to other European countries and of great interest to a lot of researchers around the world.

In order to provide solid evidence about the robustness of such design concept for facilitating its acceptance by different national authorities, a special full scale fire test was conducted within the scope of the project FRACOF and the corresponding experimental results have been largely described in [5]. Despite the very positive results from this test with respect to global load-bearing capacity of steel and concrete composite floor system under membrane action even for a long duration fire, an important open crack appeared at the middle part of the floor due to a joint failure of reinforcing steel mesh for lack of appropriate construction detail.

More recently another full scale steel and concrete composite floor system was fire tested in the scope of European RFCS research project COSSFIRE dedicated to the investigation steel and composite joints under natural fire conditions. As the two fire tests have quite a lot of similarities, it will be thus very instructive and inspirational to compare, on the one hand, the test set-ups and on the other hand, the corresponding experimental results.

Moreover, these tests have also provided the possibility to check the validity of the advanced modelling technology which is more and more widely applied to investigate such type of structure systems in fire safety engineering. In consequence, a numerical model developed on the basis of a general computer code has been applied to these tests. The calculated results were then compared to experimental ones, from which one can get an accurate idea about the precision of the numerical model.

TEST ARRANGEMENT OF TWO STEEL AND CONCRETE COMPOSITE FLOORS

As the two tests were performed upon the same furnace, their global sizes were close but the adopted steel frames were quite different (see figure 1).

TABLE I. EXPERIMENTAL DATA OF FRACOF AND COSSFIRE FIRE TESTS.

Item		FRACOF	COSSFIRE
Composite slab	Total depth	155 mm	135 mm
	Thickness of steel deck	0.75 mm	
	Size of reinforcing mesh	7 and a grid of 150 mm	
	Axis distance of reinforcing steel from top of the slab	50 mm	35 mm
Shear stud	Size	19 and h=125 mm	
	Spacing in secondary beams	207 mm	
	Spacing in main beams	100 mm	300 mm
Material properties	Steel grade of main beams	423 MPa	320 MPa
	Steel grade of secondary beams	311 MPa	320 MPa
	Steel grade of reinforcing steel	594 MPa	590 MPa
	Compressive strength of concrete	36.7 MPa	38.0 MPa
Steel joints	Main beams to column flange	Flexible end-plate	
	Secondary beams to column web	Double angle web cleats	
	Secondary beams to main beams	Double angle web cleats	

Applied load during test (without self-weight)		3.87 kN/m ²	3.75 kN/m ²
FRACOF		COSSFIRE	

Figure 1. Steel frames as well as the composite floors of FRACOF and COSSFIRE fire tests.

As it is shown in figure 1, the two steel frames were covered then by a composite slab with the profiled steel sheet COFRAPLUS60 (trapezoidal). The other experimental data with respect to these two specimens are summarized in table 1. It is necessary to point out here that all structural members (beams, columns slab and joints) have been designed in accordance with concerned Eurocodes [6-8] and the reinforcing steel mesh is defined mainly on the basis of the simple design rules in [4].

FRACOF	COSSFIRE
15 sand bags and each weighs 15 kN	20 sand bags and each weighs 11 kN

Figure 2. Loading conditions of FRACOF and COSSFIRE fire tests.

With respect to heating conditions of two specimens, the central part of the floor, including steel members, is submitted directly to ISO fire but the fire exposure condition of edge part of the floors was quite different. In fact, in

FRACOF fire test, the furnace wall was built just behind all perimeter steel beams without any gap while in COSSFIRE fire test, these beams were put inside the furnace so more exposed to fire. Moreover, the steel joints in COSSFIRE test were much less protected than those in FRACOF test for the purpose of getting more realistic information about the fire behaviour of steel joints under membrane action.

The mechanical load were realised for both tests with help of sand bags as shown below (see figure 2).

Important means of measurement were undertaken to record the test results not only relative to heating of all structural members, like composite slab, steel members and steel joints, but with respect also to structural behaviour during both heating and cooling phases of these floors in terms of displacements.

EXPERIMENTAL RESULTS OF THE FIRE TESTS AND THEIR COMPARISONS

As FRACOF fire test has been explained in detail in [5], the description here is focused then on the comparison of experimental results obtained from above two fire tests.

For both of these fire tests, the ISO fire curve was applied during the heating period and a natural furnace cooling was followed until the total cool-down of the floor. In fact, the stopping of heating phase was decided on the basis of the observation of the floor behaviour during the test. However, with an entire coincidence, their heating phases lasted for about the same duration, that is, 120 and few minutes more.

If the average furnace temperatures recorded during the tests are compared, one can find that they are very close one to another except that for FRACOF test, the cooling speed is slightly higher (see figure 3). However, if more attention is paid to the temperatures of unprotected steel beams, they seems to be very close even during the cooling phase.

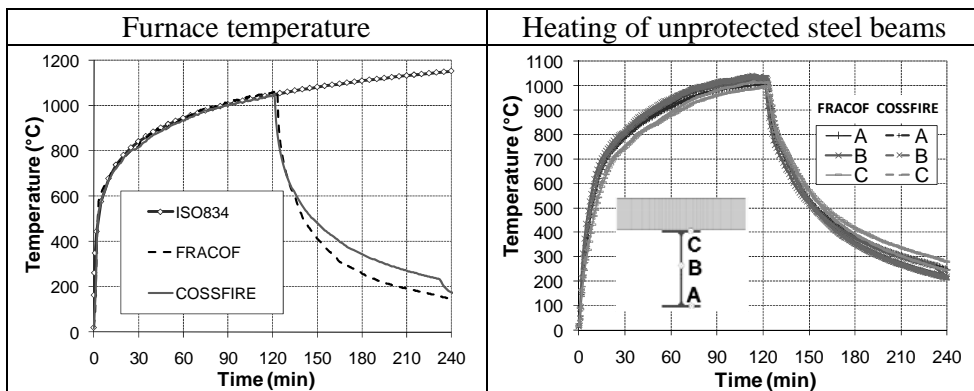


Figure 3. Comparison of fire curves and heating of unprotected steel beams.

In fact, the heating difference between two tests lies in edge steel members. As these members were more protected in FRACOF test, they were much less heated (see figure 4). In general, the maximum temperature rise of edge steel beams in FRACOF test was about 300°C while in COSSFIRE test, it was about 550°C. In particular the temperature recorded in one of edge beams during COSSFIRE test indicated that its heating was up to about 630°C. In

consequence, the global structural behaviour obtained during two tests was largely influenced by this different heating behaviour.

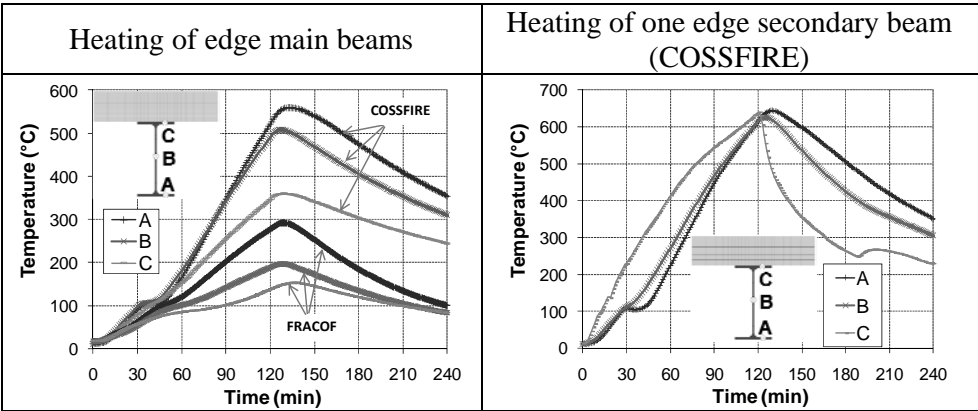


Figure 4. Comparison of heating of edge steel beams.

This observation remains equally true for all steel joints which were heated in general up to around 300 °C in FRACOF test and on the contrary to more than 800 °C for certain joints in COSSFIRE test.

As it has been indicated earlier (see table 1), the total slab depth is different between two floors (155 mm for FRACOF test and 135 mm for COSSFIRE test), so the temperatures measured in composite slabs differ also quite a lot (see figure 5) and in particular the reinforcing steel mesh in COSSFIRE test was apparently much hotter (500 °C against 300 °C in FRACOF test). The same tendency was equally observed for unexposed side of the slab (about 200°C after 120 minutes of fire in COSSFIRE test against only around 100°C in FRACOF test).

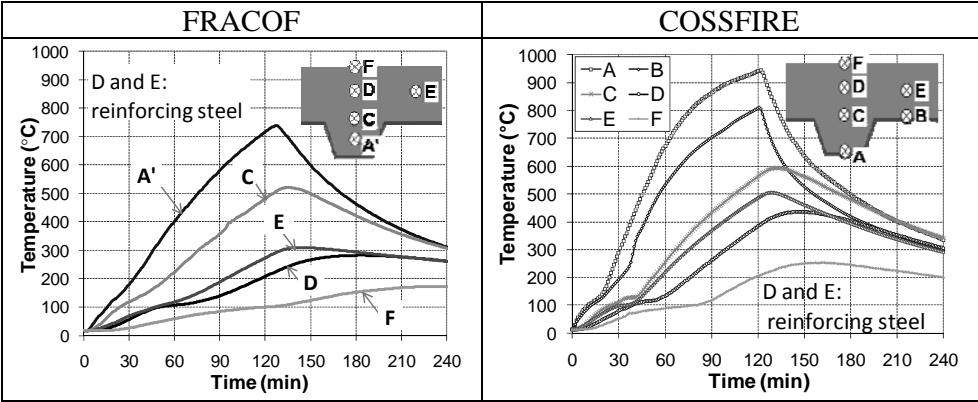


Figure 5. Comparison of heating of composite slab.

The investigation of the structural behaviour constituted the principal objectives of these tests. It is therefore inevitable to compare the two tests in this field by means of recorded deflections of the floors as well as the visual observations made during the tests.

With respect to the structural behaviour of the floor, it is well known that large deflection undergoes under membrane action. Such phenomenon was inevitably observed in both tests (see figure 6). However, if closer attention is paid to the measured deflections of these floors, one can find that during the first

60 minutes of fire, the two floors deflected nearly at the same speed and then progressively the floor in COSSFIRE test got more deflection than that in FRACOF test but the maximum deflection seemed to be reached once again at the same instant, that is about 15 minutes after the stopping of heating phase. In fact, such deformation difference could be explained by the fact that at the beginning of fire, the temperature gradient induced bowing due to sharp temperature increase of unprotected steel beams dominated the deflection behaviour of both floors and once these steel beams lost a lot of their strength, the floor entered into membrane action which relies mainly on the strength of reinforcing steel mesh. As the reinforcing steel mesh in COSSFIRE test was heated much more quickly from about 60 minutes of fire, it resulted correspondingly in more deflections of the floor. During the cooling phase, as the reinforcing steel mesh in both tests started to cool down around 15 minutes after the fire was stopped, the total deflections of both floors began to decrease in consequence at the same moment.

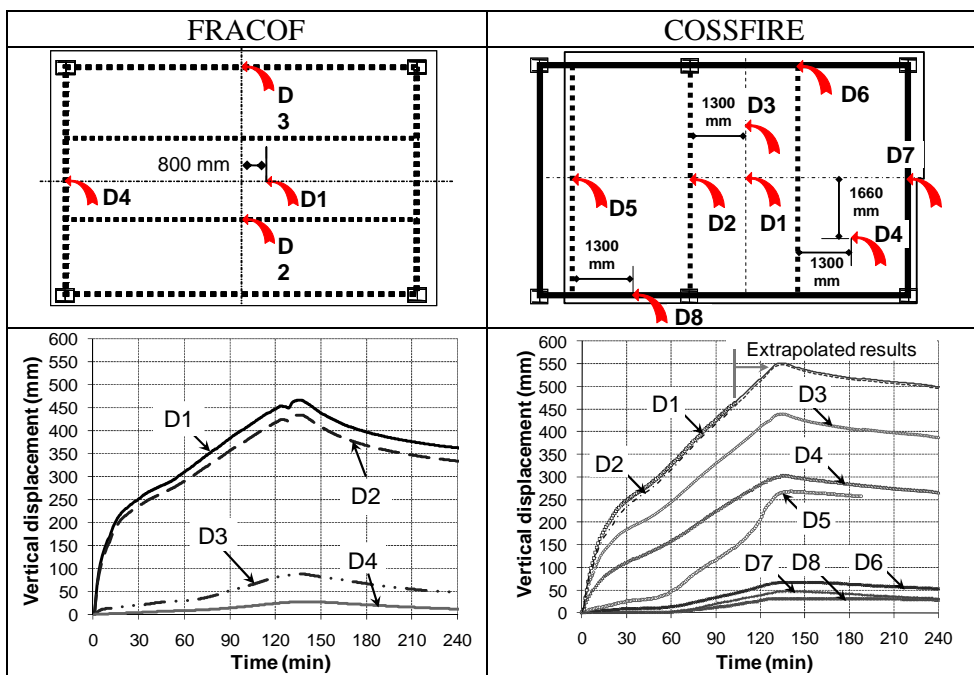


Figure 6. Comparison of floor deflections.

As far as FRACOF fire test is concerned, an open crack of composite slab at the central part of the floor in the direction of short span (parallel to rib of steel deck) appeared at about 105 minutes of fire (see left part of figure 7) which has led to the stopping of heating phase just after 120 minutes of fire, predicted as the fire rating of this floor according to the design rules of [4]. As it was explained in detail in [3], this crack was caused by the joint failure of reinforcing steel mesh for lack of enough overlapping.

For COSSFIRE test, the heating phase was stopped as it was observed that one of two secondary edge beams was collapsing (see the displacement measurement D5 in figure 6) under a heating of more than 600°C at 120 minutes of fire (see right part of figure 4). Despite this collapse, the load-bearing capacity of the floor seems to be still adequate because it remained stable during the whole period of cooling phase under the same loading condition. It must be pointed out here that this floor meets only a fire rating of 90 minutes according

to the design rules given in [4]. Also during the test, an important concrete crushing at mid-span of this edge beam was observed (see right part of figure 7) but there was no visible concrete cracking in the central part of the floor though the reinforcing steel mesh was much more heated. This excellent behaviour is certainly due to the appropriate overlapping of reinforcing steel meshes.

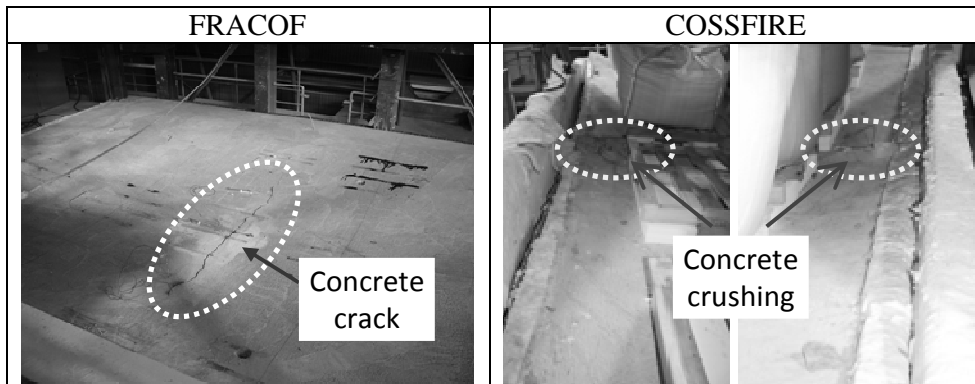


Figure 7. Local failure modes of tested composite floors.

From the experimental results of above tests, it can be derived that steel and concrete composite floor systems based on membrane action are robust and the existing design rules are conservative for global structural performance. Nevertheless, particular attention must be paid to construction details, such as the overlapping of reinforcing steel mesh, the anchorage of the same reinforcing steel mesh to boundary steel beams etc. to guarantee the good working order of such type of structural performance.

NUMERICAL INVESTIGATION OF THE FIRE TESTS

Nowadays, with the advancement of numerical modelling technology, the fire safety engineering relies more and more on advanced calculation models in fire assessment of steel framed buildings. However, the validation of these modern design tools based on global structural behaviour raises still questions not only for engineers but also for authorities who are not familiar yet with such type of analysis approach. The two fire tests described above constitutes then ideal experimental evidence to check the validity of numerical design tools

Here the results obtained with a numerical model developed under the computer code ANSYS will be explained and discussed. This model is based on a hybrid structural model which takes account of steel beams, steel sheet, concrete rib, concrete slab and reinforcing steel mesh with different types of finite elements (see figure 8). In this structural model, the steel members (beams and columns) are represented by 3D non-linear elasto-plastic line element of BEAM24 and the same element is also used for concrete ribs and steel decking of the composite slab. As for concrete part over the steel sheet including the reinforcing steel mesh, a multi-layered orthotropic shell element SHELL91 is used. The connection between steel beams and concrete slab was modeled using 3D elastic line element PIPE16.

In order to perform whole fire analysis of such floor system, the developed numerical model is in fact divided into two different steps, one for heat transfer analysis and another one for structural analysis. The heat transfer analysis is conducted on the basis of 2D model which means that the temperature is

calculated only with all cross sections taking into account nevertheless the protection condition of each structural member. The cross-section temperature field obtained in such way is then imposed to whole length of each structural member and the border effect is thus neglected.

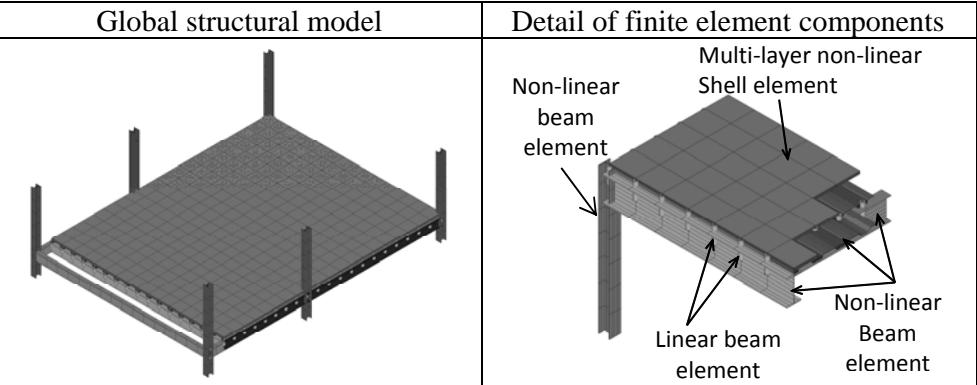


Figure 8. Numerical model developed under the computer code ANSYS.

The global structural behaviour of the floor is then analysed on the basis of previously calculated temperature field. The simulated results of the two steel and concrete composite floor systems are shown together in figure 9 which illustrates on the one hand, the deformed shapes of the floors predicted by the numerical model at 120 minutes of ISO fire and on the other hand, the vertical displacements of several representative points of the floor versus time, such as the deflection at the centre of the floor, the bowing of edge beams etc.

In both heat transfer and structural analysis, the thermal and mechanical laws of Eurocode 4 part 1.2 [7] have been used for all materials of the floor.

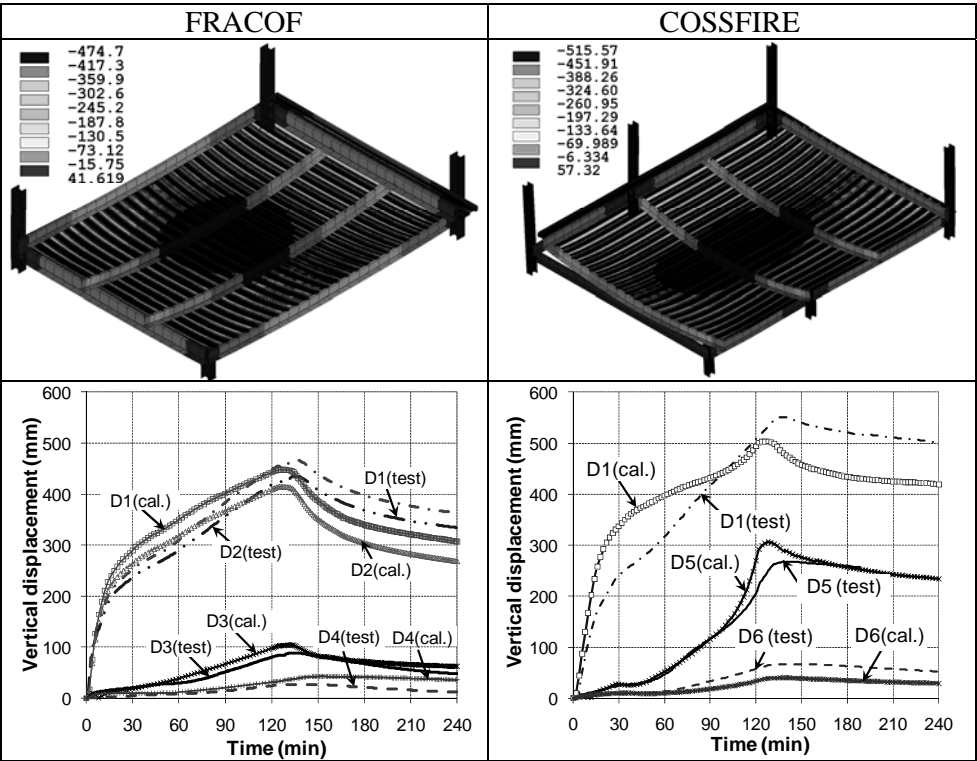


Figure 9. Numerical results of FRACOF and COSSFIRE tests.

A comparison of floor vertical displacements between numerical calculation and tests is also shown in figure 9. It can be observed that globally the numerical simulations follow quite closely the experimental results. However, for FRACOF test, a very slight discrepancy occurs after 90 minutes of fire and the deflection speed of test is higher than that predicted by the numerical model. This phenomenon is maybe the results of the joint failure of reinforcing steel mesh as it was explained in paragraph 3, which induces a small change in the floor behaviour as well as the sudden increase of floor deflection during the cooling phase of it.

With respect to the comparison between the numerical model and COSSFIRE test (see the right part of figure 9), the total deflection of the floor at the end of heating phase is quite close each other but there is more discrepancy during the first period of fire. This difference is very possibly and mainly due to the fact that in the numerical model, unprotected steel beams as well as all steel columns are considered fully restrained in particular for the beam between steel columns which leads inevitably to a large deflection but in reality this effect is tremendously reduced by the important buckling of steel beam connected to steel columns (see the right part of figure 10) whereas in FRACOF test, such phenomena did not occur (see the left part of figure10). Another important feature is that the numerical model predicts quite well the behaviour of all perimeter beams including the collapsed secondary beam (see D5 for COSSFIRE test in figure 9). In addition for COSSFIRE test, the bowing of all main edge beams in numerical analysis is apparently underestimated in comparison with measured deflection. In fact, as the joint parts of central steel columns were much more exposed to fire, slight flange local buckling occurred during the test which may decrease the rotation stiffness of main edge beams connected to them and increase then the deflection of these beams.

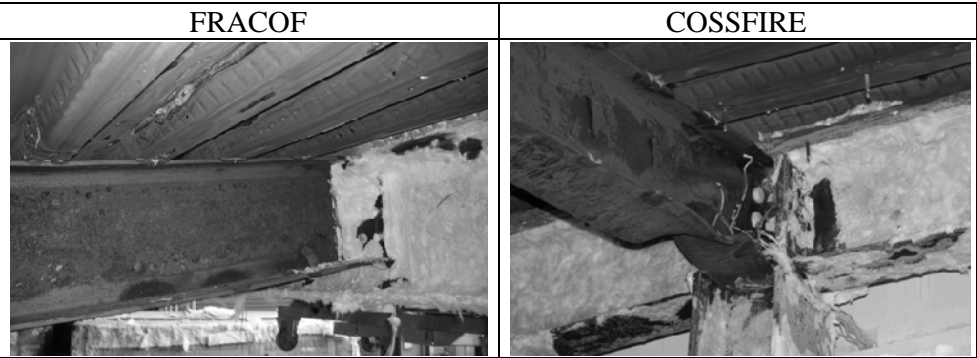


Figure 10. Deformed shape of unprotected beams near beam ends.

In conclusion, it can be derived from all above comparisons that the accuracy of the numerical model for predicting the global fire behaviour of steel and concrete composite floor system is satisfactory but some local phenomena, in particular the cracking of concrete can not be dealt with in detail, which needs however to use very specific model and cannot be applied to a structural model of such scale. In consequence, it seems to be necessary to define the application field of such type of numerical analysis, for example, to establish the limit values for global deflection as well as the maximum strain in reinforcing steel etc on the basis of obtained experimental evidence in the fire tests like those presented in this paper.

CONCLUSION

Two important full scale fire tests have been conducted respectively within the scope of the projects FRACOF and COSSFIRE on steel and concrete composite floor systems. The experimental results have provided the evidence about:

- the robust behaviour of such type of structural system under membrane action
- the conservativeness of the existing design rules
- the necessity of applying appropriate construction details especially for reinforcing steel mesh

As far as the advanced numerical calculation is concerned, it appears that the modern numerical modelling technology is fully adequate to predict the global structural behaviour of steel and concrete composite floor systems exposed to fire but the local behaviour such as cracking of concrete and local buckling of steel members can not be taken into account in accurate way. In consequence, it has to take some care when such type of approach is applied in practical fire safety engineering.

ACKNOWLEDGMENT

The authors of the paper would like to give their gratitude to all companies or organisations which have contributed financially to the fulfilment of the fire tests in particular the sponsorship from ArcelorMittal and RFCS programme of the European Commission. In addition, they are also very grateful for the scientific support from Messrs O. Vassart, LG. Cajot (ArcelorMittal) and JM. Franssen (Université de Liège) in the design of these fire tests.

REFERENCE

1. 'The behaviour of Multi-storey steel framed buildings in fire', A European joint research programme, British Steel Swinden Technology Centre, 1999.
2. Lennon, T., 'Cardington fire tests: instrumentation locations for large compartment fire test.', Building Research Establishment Report N100/98, June 1996.
3. Lennon, T., 'Cardington fire tests: instrumentation locations for corner fire test.', Building Research Establishment Report N152/95, June 1996.
4. Fire Safe design: A new approach to multi-storey steel-framed buildings, Steel Construction Institute Publication no 288.
5. Zhao B., Roosefid M. and Vassart O., Full scale test of a steel and concrete composite floor exposed to ISO fire and corresponding numerical investigation, Eurosteel Conference proceeding, 2008.
6. CEN, EN 1994-1-1, Eurocode 4: Design of composite steel and concrete structures"—Part 1-1: General rules and rules for buildings, European Committee for Standardisation , 2004.
7. CEN, EN 1994-1-2, Eurocode 4: Design of composite steel and concrete structures, Part 1-2: General rules - Structural fire design, European Committee for Standardisation, 2005.
8. EN 1993-1-8, Eurocode 3 Design of steel structures – Part 1-8: Design of joints, CEN.

Experimental Evaluation of Composite Floor Assemblies Under Fire Loading

E. WELLMAN, A. H. VARMA, R. FIKE, P. PAKALA and V. KODUR

ABSTRACT

This paper presents the results of experimental investigations on the structural behavior of composite beam and floor systems subjected to gravity and thermal loading through experimental testing. A floor slab, 3.96 m by 4.57 m in plan with single plate, beam-to-girder shear connections was tested under a realistic fire without fire-protection on the interior beam. The results show that the lack of fire proofing on the interior beam and the “realistic fire” caused: (i) slower cooling of all elements in the system including the connection elements; and (ii) permanent deformations in the beam and the girders. The connection did not fail in the specimen although deformations were present as a result of the cooling portion of the realistic fire, indicating that the composite slab carries a significant portion of the shear from the beam to the girder.

INTRODUCTION

The use of composite floor systems in structures is a common construction practice due to structural and economic advantages. Steel deck panels act as formwork and bottom slab reinforcement while the slab itself is able to act compositely with the steel beam. As a result of potential savings in fire protection for tall buildings, there has been recent interest in the behavior and design of these systems with protected girders and columns and unprotected beams. Such construction is becoming popular in New Zealand, the U.K., and Australia; however there are issues present when considering using this type of construction in the U.S. Current building codes do not require any reinforcement for fire in composite slabs. Shrinkage reinforcement that in composite slabs is also very light. The beam-to-girder connections are designed for shear with no consideration of additional tensile and compression forces that may be present during fire events.

Wellman and Varma - Bowen Laboratory, School of Civil Engineering, Purdue University, 1040 South River Road, Lafayette, IN 47907

Fike, Pakala and Kodur - MSU Center for Structural Fire Engineering and Diagnostics, Department of Civil and Environmental Engineering, Michigan State University, 3580 Engineering Building, East Lansing, MI 48824

The goal of this study is to determine the structural behavior of composite beam and floor systems subjected to both gravity and thermal loading through experimental testing. This paper presents the response of these systems with both protected and unprotected beams under both standard and realistic fire loading.

SPECIMEN DESIGN AND INSTRUMENTATION

A 3.96 m by 4.57 m floor system was constructed to study the behavior of composite floor assemblies under fire loading. All flexural members were ASTM A992 steel with W10X15 beams and W12X16 girders, as shown in Figure 1. The pinned beam-to-girder connections are detailed in Figure 2. 6.35mm ASTM A36 steel plates were shop welded to the girder web and bolted to the beam web with (2) 19.05mm ASTM A325 bolts. The slab was composed of Vulcraft 1.5VLR composite decking with 101.6mm of lightweight concrete topping, 63.5mm above the top rib of the deck. Shrinkage reinforcement of 6x6-W1.4xW1.4 welded wire fabric was placed at 38.1mm from the top of the slab. The steel beams were designed for partial composite action with the slab using 76.2mm long, 15.9mm diameter headed shear studs (Figure 3).

Design Philosophy

The geometric design of the test specimens was dictated by dimensional constraints imposed by the furnace. As shown in Figure 4, the furnace is able to support two beams of a maximum length of 3.96 m at a spacing of 2.13 m.

Loading conditions were also dictated by the test furnace. The actuator layout over the furnace is shown in Figure 5. To load the interior beam, the available loading pattern was a point load at mid-span. Each girder could be loaded with two point loads at a spread of 870mm.

The fundamental basis of the design philosophy was to design the composite beams, girders, and connections at ambient conditions according to the AISC Specifications for Structural Steel Buildings [1] such that during testing the connection would fail first, followed by the interior beam, and finally the girders.

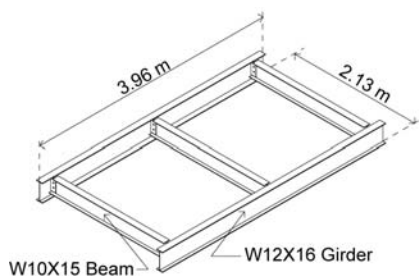


Figure 1. Layout of steel framing.

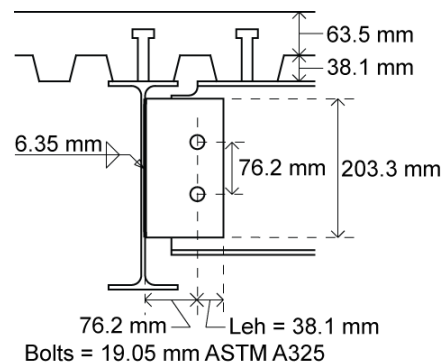


Figure 2. Shear tab connection design.

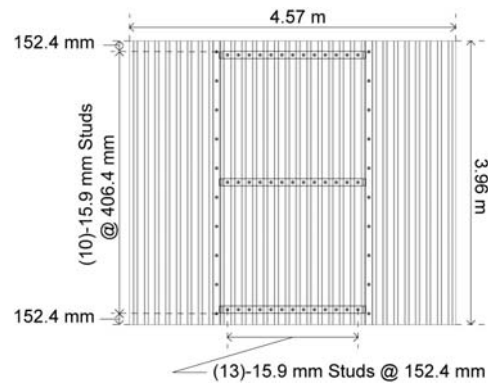


Figure 3. Shear stud layout for Slabs 1 and 2.

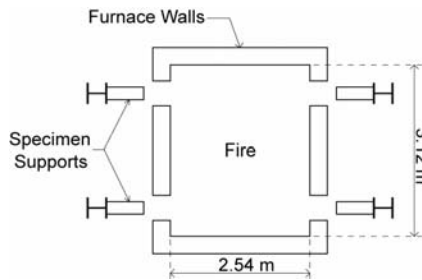


Figure 4. MSU furnace plan view.

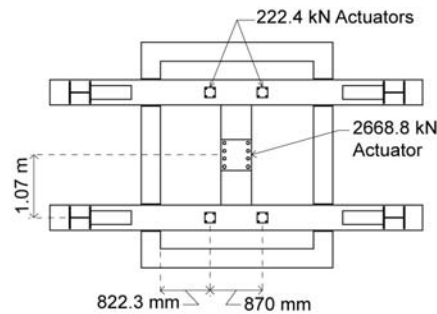


Figure 5. Layout of utilized actuators in Tests 1 and 2.

A minimum shear connection consisting of a 6.35mm plate with two 19.0mm bolts was selected initially. Due to the short span of the member and the relatively high predicted strength of even the smallest connection, a small section size with low composite action was needed for the beam and the W10X15 was selected. The ribs of the composite decking ran perpendicular to the beam, limiting number and spacing of shear studs. The resulting beam had a percentage of composite action of 32.5% and an ultimate moment capacity of 147.5 kN-m.

The girders were sized to hold the reaction force that would be present at the failure of the beam resulting in the selection of a W12X16 section. Here, the ribs of the composite decking ran parallel to the girder and as such imposed no limitations on the number or spacing of shear studs. The resulting girder had a percentage of composite action of 25.4% and an ultimate moment capacity of 180.6 kN-m.

Once the beams and girders had been designed, the connection was further detailed and its ultimate shear strength was found to be 200 kN. Since the beam was not stronger than the connection at ambient temperatures, a projection of elevated temperature behavior under loading needed to be determined.

Loading values were developed by back-calculating service load values from the ambient ultimate moment capacities of the members assuming equal dead and live loads and considering both the load case for fire and the load reduction factors applied in determining ultimate moment capacity [1]. For the interior beam, this resulted in a load of 133 kN spread at 304.8mm over the mid-span for Slab 1 and 111 kN at mid-span for Slab 2.

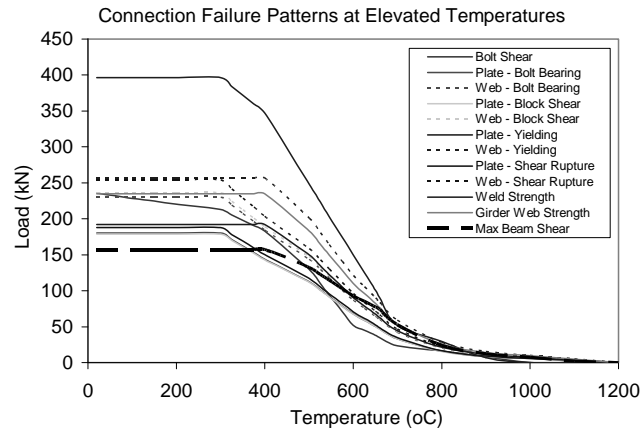


Figure 6. Ultimate strength of connection with increasing temperature.

Using the elevated temperature material property reduction factors suggested by Eurocode 3 [2] and the strength equations in AISC 360 [1], an estimation of the behavior of the connection and the beam under fire loading was developed. Figure 6 shows a plot of the ultimate shear strength of the connection's failure modes as temperatures increase and the shear reaction force on the connection at beam failure. From this figure it can be seen that at temperatures over 400°C and reaction loadings under 150 kN, the connection is the weakest link and should fail in shear before the beam develops a plastic hinge.

Fireproofing of the steel members was designed to meet a one-hour rating according to AISC Steel Design Guide 19 [3]. Carbolite Type 5GP spray-applied fire resistance material (SFRM) was applied at a thickness of 14.3 mm only on the girders, while the interior beam was left unprotected.

Instrumentation

Measurements for temperature, displacement, and strain were taken to evaluate the behavior of the floor system. Sections were defined at different locations on the slab, each having its own instrumentation layout. These locations are shown in Figure 7. The sections are further detailed in Table I.

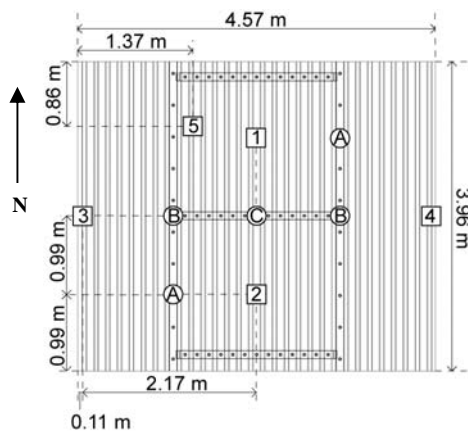


Figure 7. Instrumentation locations.

Table I. Properties measured at Sections A-C and 1-5.

Section	Temp.	Disp.	Strain NS	Strain EW
A	Yes	Yes	No	No
B	Yes	Yes	Yes	Yes
C	Yes	Yes	Yes	Yes
1	No	Yes	Yes	No
2	No	No	Yes	No
3	No	Yes	No	No
4	No	Yes	No	No
5	No	No	Yes	Yes

TESTING

Furnace

The specimen was tested at the Michigan State University Center for Structural Fire Engineering and Diagnostics. Furnace details were discussed in the **Design Philosophy** section and Figures 4 and 5.

Loading Scheme

The slab began with 111.2 kN applied at the mid-span of the beam and 22.2 kN applied at two points on each girder (the additional loading to reach the service load of the girder). This loading was maintained until failure was reached in the beam. Temperatures were then held static while loading was removed from the beam and increased to 44.5 kN in the girder. Loading continued until failure was reached in the girders, after which all loading was removed and the cooling curve (see Figure 8) was implemented.

Failure was defined using the criteria recommended by BS-476 [5]. Values for the beam and girder failure as defined by this standard are shown in Table II. Failure occurs when either of the two criteria is met.

RESULTS

Observations

Cracking presented initially in an ovular or circular pattern with steam and boiling water being emitted from the cracks. Testing continued for 27 minutes when beam failure was reached. Beam loading was then removed and girder loading was increased. Testing continued until 110 minutes when the actuators reached their full extension and no further loading could be applied. At this time, no visible deformations were present in the connections. The cooling phase of the heating curve was entered and maintained until 270 minutes when the furnace reached its ambient temperature. Images from the test are shown in Figure 9 (a) and (b). When the specimen was removed from the furnace, visible rotational deformations were present in the shear connections as shown in Figure 10.

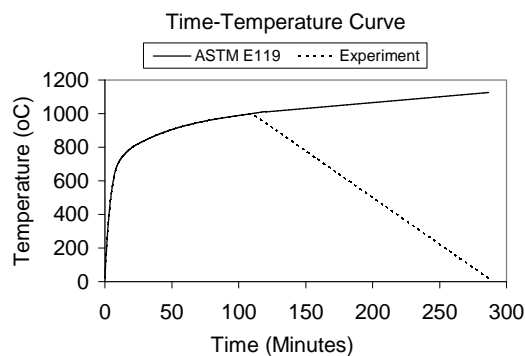
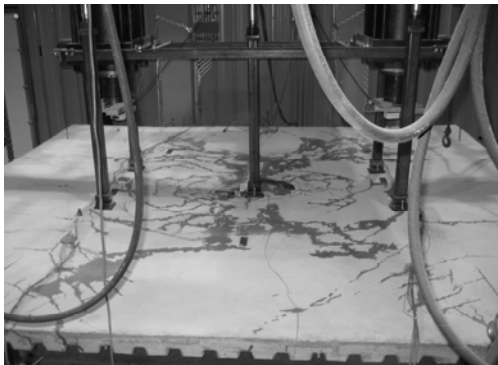


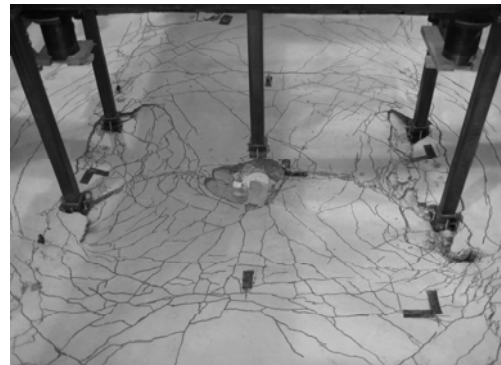
Figure 8. Design time-temperature curve.

Table II. Failure criteria for flexural members per BS-476.

Member	Member Dimensions		BS 476 (Meet either 1 OR 2)		
			1	2	
	L (mm)	d (mm)	L/20 (mm)	L/30 (mm)	L ² /(9000d) (mm/min)
W10X15 - Beam	2133.6	254.0	106.7	71.1	2.0
W12X16 - Girder	3962.4	304.8	198.1	132.1	5.7



(a)



(b)

Figure 9. Images from testing, (a) Initial cracking (b) Final cracking pattern after slab cooling.



Figure 10. Shear connections following testing.

Deformations

Figure 11 shows the progression of displacements of the slab. When loading was removed, the overall displacement of the beam was 131.0 mm with a deflection of 115.4 mm. The beam had reached its failure definition as defined in Table III, Criterion 2. The rate of deflection at this time was 105.6 mm/min. After the loading was removed from the beam, displacements continued to increase.

Girder D reached a maximum displacement of 120.7 mm at 107.9 minutes. The rate of deflection at this time was 4.0 mm/min. Girder E reached a maximum displacement of 143.8 mm at 107.3 minutes. The rate of deflection at this time was 0.6 mm/minute. After the test ended, the beam and girders rebounded slightly, but

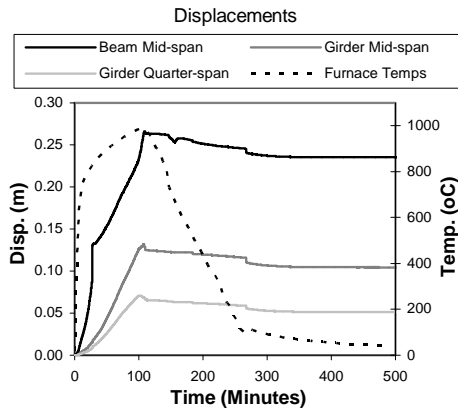


Figure 11. Section displacements.

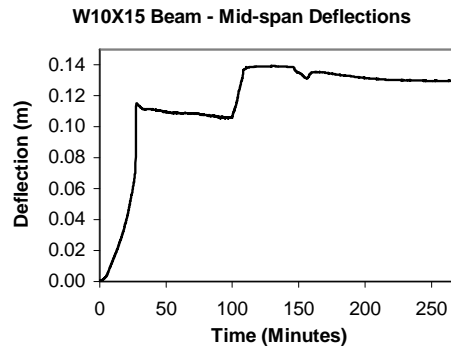


Figure 12. Beam mid-span deflection comparisons.

displayed permanent deformations. The beam retained a permanent deflection of 130.8 mm. Girder D retained a permanent deformation of 91.2 mm. Girder E retained a permanent deformation of 118.0 mm.

The slab demonstrated interesting behavior between beam failure and the end of the heating portion of the test. After reaching their initial peak, beam deflections (Figure 12) decreased as a result of the difference in rate of the deflection of the girders and the beam which was caused by the beam rebounding slightly once its loading was removed. A secondary spike occurred between 100 and 110 minutes. At this point the girders were reaching their maximum deflections, their loading had not yet been removed, and the average bottom flange temperature of the steel beam section increased from 987°C to 1004°C. The jump in beam deflections was a result of the loss of the strength needed to carry self-weight due to increased temperatures.

CONCLUSIONS

A 3.96 m x 4.57 m composite floor system was tested under gravity and fire loading to determine the elevated temperature behavior of the system. Time-temperature profiles and displacements were reported for various locations within the system.

The results indicate that the presence of a realistic fire caused slower cooling of all elements in the system including the connection elements. It also caused permanent deformations in the beam and the girders. The connection did not fail in the specimen although deformations were present as a result of the cooling portion of the realistic fire. As connections were expected to fail before the beam, this indicates that the composite slab carries a significant portion of the shear from the beam to the girder and that the connection did not see the shear force required for it to fail.

The tested slab considered only one type of shear connection and did not include the restraining effects of such a slab within a full building structure. Currently in progress and future testing will address these parameters.

ACKNOWLEDGEMENTS

The experimental work presented in the paper was performed in the MSU Center for Structural Fire Engineering and Diagnostics, Department of Civil and Environmental Engineering, Michigan State University. The research presented in this paper is based upon work funded by the National Science Foundation Grant No. 0758461 and NSF CMMI 0758409. Any opinions, findings, and conclusions or recommendations expressed in this paper are those of the authors and do not necessarily reflect the views of the sponsors.

REFERENCES

1. AISC 360 (2005), Specification for Structural Steel Buildings. American Institute of Steel Construction, Chicago, IL.
2. CEN (2005), Eurocode 3: Design of Steel Structures, Part 1-2: General Rules—Structural Fire Design, European Committee for Standardization, Brussels, Belgium.
3. Ruddy, J., Marlo, J., Ioannides, S., Alfawakhiri, F. (2003), Steel Design Guide 19: Fire Resistance of Structural Steel Framing, American Institute of Steel Construction, USA.
4. ASTM (2008), Standard Test Methods for Fire Tests of Building Construction and Materials, E119, American Society for Testing and Materials, West Conshohocken, PA.
5. CEN (1987), BS 476-20 Fire tests on building materials and structure—Part 20: Method for determination of the fire resistance of elements of construction, European Committee for Standardization, Brussels, Belgium.

A Numerical Model for Unbraced Composite Frames in Fire

P. SCHAUMANN¹ and O. BAHR²

ABSTRACT

A numerical model was established in the non-linear software Safir for unbraced composite frames in fire. The model considers the sequence of construction and load history of the composite frames. In addition, it includes a local model taking semi-rigid composite joints into account. This contribution presents the key features of the model. Furthermore, the model is validated against fire tests and used to study the fire performance of unbraced composite frames. The investigations focused on the influence of base support, geometry of the frames, and location of the fire on the fire performance of unbraced composite frames. This research work is part of the ongoing European project 'Unbraced Composite Structures in Fire'.

1. INTRODUCTION

Unbraced composite frames are an interesting alternative to traditional bracing. If properly designed, their lateral stiffness is sufficient to meet requirements of limit state and serviceability. In addition, unbraced frames offer large possible spans without internal columns. Since bracing is not necessary, the flexibility of the building's use is hence significantly increased. Finally, the frames provide an inherent fire resistance due to the concrete that slows the heating down.

Nevertheless, current design rules in the fire-related part of Eurocode 4 [1] are limited to braced buildings. To date, there is little research on the fire performance of unbraced composite frames. As a result, there are only few examples of buildings with unbraced composite frames as load-bearing structure.

Therefore a numerical model in the non-linear software Safir [2] was established to study the fire performance of unbraced composite frames in detail. The model considers both the sequence of construction and load history of the composite frames. In addition, it includes a local model taking semi-rigid composite joints into account. This research work is part of the ongoing European project 'Unbraced Composite Structures in Fire' [3].

The model was validated against fire tests and used to study the fire performance of unbraced composite frames. The investigations focused on the influence of base support, geometry of the frames, and location of the fire on the fire performance of unbraced composite frames. In addition, accompanying experimental and numerical studies on the fire performance of external semi-rigid composite joints for the unbraced composite frames were carried out [4, 5].

¹Professor, Leibniz University Hannover, Institute for Steel Construction, Hannover, Germany

²Research Assistant, Leibniz University Hannover, Institute for Steel Construction, Hannover, Germany,

2. SCOPE OF APPLICATION AND PARAMETER RANGE

In this contribution, the regarded unbraced composite frames are assumed to be the load-bearing structure of office buildings. There are three reasons for this decision. First of all, offices are built frequently. Second, numerous normative regulations and recommendations for office buildings set a clear parameter range for the layout of office buildings. Third, the fire loads in office buildings are well-defined. Nevertheless, the frames are also suitable for other building types, for instance industrial and school buildings.

Furthermore, investigations focused on low- and medium-rise buildings with three storeys at most. This is because normative regulations often demand for elevators in higher buildings, where the massive elevator shaft stabilizes the building against wind loads and significantly reduces sway of the frames. Even in the absence of an elevator, wind loads increase sharply for higher buildings so that often stiffer load-bearing systems than frames are required.

In low- to medium-rise buildings, two- or three-loaded cellular offices or three-loaded combination offices are reasonable. To comply with current recommendations, the frames should span over a building depth from 12 to 16 m. In the numerical studies, this range was extended from 10 to 18 m to examine the load response of the fire-exposed frames. In general, the frames should fulfill the demand for maximum flexibility, which requires large column spacing and spans. Thus, unbraced composite frames with one bay were regarded.

Besides the span, the storey height influences the geometry of the frames. For the regarded office types the level of installation will be relatively low. Thus, storey heights between 3.0 m and 4.5 m were taken into consideration.

Finally, the frames should meet the requirements for a fire rating R60, which agrees with most European normative regulations. For this reasons, new external semi-rigid composite joints were established. Further details are given in [4, 5].

3. NUMERICAL MODELING OF UNBRACED COMPOSITE FRAMES

3.1 Modeling of unpropped composite constructions

Composite frames can be constructed with and without propping the steel beams during the casting of the slabs. Since it is time-consuming and hence expensive to install the propping, construction companies prefer unpropped constructions. Despite the wide-spread use of unpropped constructions, there are very few numerical models that are capable to consider the sequence of construction. For instance, Burgess et al. report on a numerical model for the design at room temperature [6]. However, to the best knowledge of the authors, there are to date no numerical models for the fire design that include the sequence of construction and load history.

One main difficulty with the numerical modeling of unpropped constructions is that the steel section alone supports the dead loads, while the composite action only resists the imposed loads. Thus, the model has to change cross-sections from steel to composite beams. Furthermore, the stresses and deformations of the steel beam have to be stored as initial stage for the composite beam.

3.2 Modeling of composite joints

Another problem arises if the joints should be included realistically in the numerical model. In most numerical simulations, the joints are assumed to be either rigid or hinged. However, it is clear that this assumption is idealistic since the joints range between these two limits. Furthermore, it is particularly important to use semi-rigid instead of rigid external joints in unbraced composite frames. Thus, the established model is enabled to consider such joints. This means that the joints are hinged during construction stage and semi-rigid at final stage. The numerical model hence covers the system change of the frames.

In fire design software such as Safir, cross-sections are discretized into fibres with uniaxial material laws. For the used beam finite elements, shear energy and shear deformations are not taken into account. Although shear forces can be derived from the moment distribution, they are not considered for the utilization of the cross-section. This common approach is valid for flexural and compressive members, where the shear forces are negligible. This assumption is valid for the beams in the regarded unbraced composite frames, but not for the joint, where the beam introduces high shear forces into the column. Therefore particular attention was paid on developing this local region that plays a crucial role for the fire performance of the unbraced composite frames.

3.3 Established submodel of the external composite joint

Figure 1 shows the established numerical submodel for the joints, which is used in the global frame analysis of fire-exposed unbraced composite frames with Safir. The top line in Figure 1 shows the joint at construction stage and the bottom line at final stage after the concrete has hardened. The figure also depicts the elevation of the joint and the cross-section of the beam at construction and final stage. The chain line in Figure 1 refers to the numerical abstraction of the real load-bearing parts.

As it can be seen in Figure 1, the submodel of the joint is divided into several elements that refer to the real structure. It consists of two truss elements representing the reinforcement and the substitute flange of the beam that is active in fire. Moments in the exterior joints are hence represented by a pair of normal forces that are attributed to the reinforcement and the substitute flange for the fire case. Moreover, vertical loads are transferred by an element into the column that represents the cleat. A very stiff artificial element couples the three elements and transfers the loads from the beam into the reinforcement and flange of the beam. In this way, the load introduction is clearly divided into tension, compression, and vertical forces facilitating the design of the column. Moreover, a fifth element is denominated as 'switch element'. As the switch element has negligible stiffness during construction stage, the attached truss elements representing the slab reinforcement and the substitute flange are also not active. During the construction, the submodel hence introduces only vertical forces into the column, which is underlined by the schematic moment distribution below the submodel. Regarding the cross-section of the beam in Figure 1, the composite slab is not active at construction stage. Thus, the steel section alone bears the applied construction loads.

After a defined small time increment, the switch element is activated to simulate the load-bearing behaviour at final stage. In this way, the joint becomes semi-rigid so that the additional imposed and wind loads at the final stage induce bending moments in the joints. Moreover, the concrete slab is activated, which is depicted in the elevation of the joint and the cross-section of

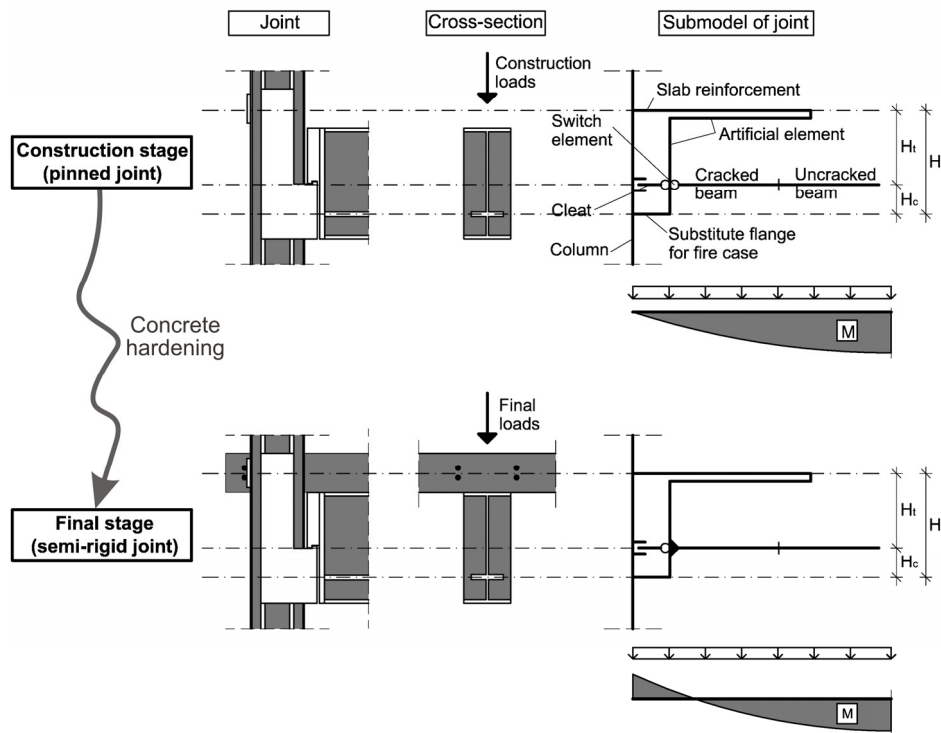


Figure 1 - Submodel in Safir for the external composite joint.

the beam, respectively. For the composite beam both cracked and uncracked regions are taken into account.

3.4 Benefits of the established numerical model for unbraced composite frames

The established numerical model is beneficial to realize a competitive fire design of unbraced composite frames. In this context, the joints are very important. Although rigid external joints are useful in reducing the lateral sway of the unbraced frames, resulting hogging moment in the joints would be very high for composite frames with practical load ratios and competitive span of at least 10 m. As the moment is transferred by a pair of forces into the column, it would be difficult to resist the resulting shear forces with economical composite cross-sections. Even if the columns would be strengthened, their increased stiffness would again attract higher bending moments. On the other hand, hinged joints are also not feasible because such frames fail early due to global instability.

Contrary, semi-rigid joints restrict the hogging moment in the joint to a well-defined measure to achieve compact and therefore competitive composite columns. Accordingly, the field moment increases so that the full flexural capacity of the composite beam may be employed. The joint moment may be defined in two ways. Either the amount of slab reinforcement is restricted or the leverage between the reinforcement and the lower flange is reduced. In case of fire, the lower flange within the chambers of the beam will substitute the lower flange of the beam that is directly exposed to fire (see Figure 1). Overall, the joints are designed to fulfill the interaction of normal forces, shear forces, and moments into the joint.

Finally, the submodel of the joint is continuous and not a zero-length spring element as in other numerical models. Thus, the slab reinforcement is modeled with its real length, which has

two advantages. First, it is not necessary to perform fire tests to gain moment-rotation characteristics of composite joints that describe the evolution of the spring stiffness. Besides, such temperature-dependent formulations are difficult due to the inhomogeneous temperature field into composite joints. Second, realistic strains of the slab reinforcement can be taken into account, which is important to consider the realistic fire performance of the joint and its rotational capacity.

3.4 Validation of the numerical model

Within the scope of the European project ‘Unbraced Composite Structures in Fire’, four fire tests on isolated joints were conducted by CTICM [4, 5]. The test data was used to establish the accuracy of the presented numerical submodel of the joint. Two large-scale fire tests on unbraced composite frames will be carried out in the near future by CTICM. In the absence of fire tests on large-scale unbraced composite frames, this data will be valuable to further validate the numerical model of the whole unbraced composite frame.

The validation included both the prediction of temperatures and deformations. In general, the numerical model reasonably predicted the temperature development into the different sections. In this paper, only the validation of the deformations is shown here. Figure 2(a) shows test specimen ‘P1’ with semi-rigid joints according to Figure 3(b) after the fire test. For details regarding the construction of the joints, please refer to [4, 5]. During the test, combined bending of the beam and lateral drift of the column was observed. Deformations were captured with displacement transducers located according to Figure 2(b). Furthermore, the static system and load application is shown in this figure. Figure 3 shows the deflection of the slab at the end of the cantilever beam, the horizontal movement of the column, and the jack force ‘F’. The applied load was increased towards the end of the fire tests.

The numerical model is conservative in predicting less fire resistance times than observed in the real tests. For fire tests ‘C1’ and ‘P1’ in Figure 3, the calculation stopped after 74 and 101 min due to global instability of the frames, as opposed to 78 and 101 min in the fire tests, respectively. In addition, the model predicted the deformations with a sufficient accuracy. However, the maximum deformations close to failure were partially underestimated although Safir is capable to take large deformations into account. This is due to the very steep gradient of the deformations in Safir, where runaway failure occurs.

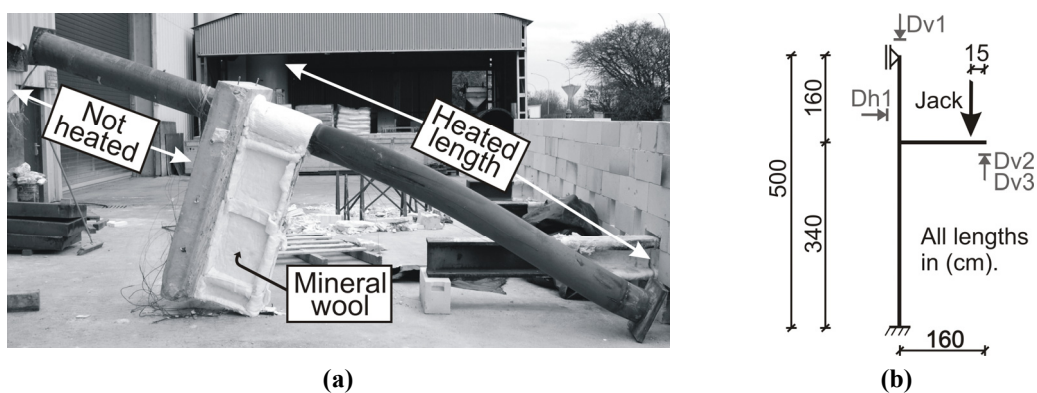
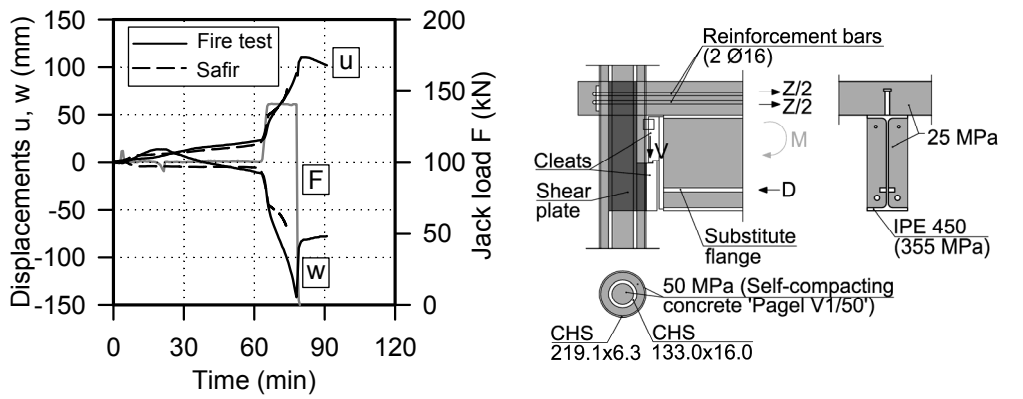
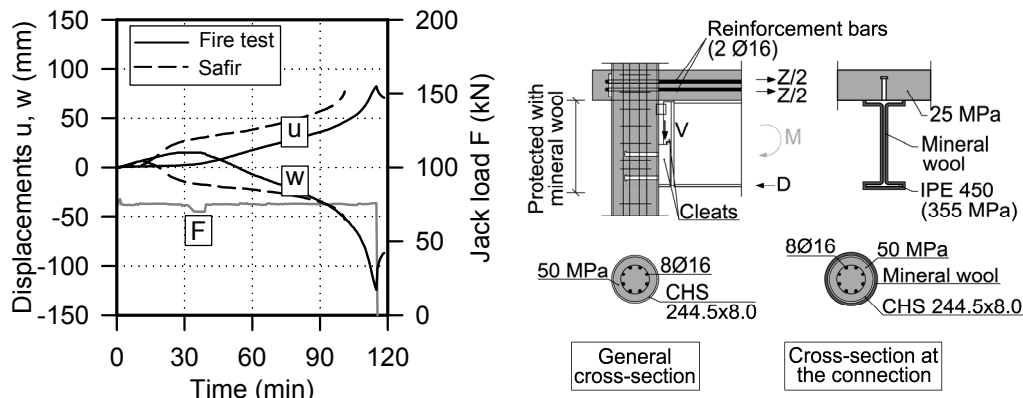


Figure 2 - Specimen ‘P1’ after the fire test (a) and static system of the fire tests (b).



(a) Joint 'C1' with circular concrete-filled double skin steel tubular columns.



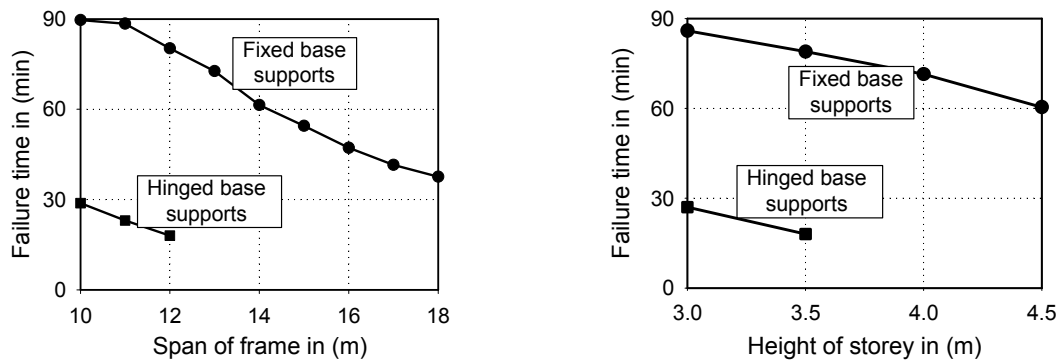
(b) Joint 'P1' with protected composite joint with concrete-filled steel tubular columns.

Figure 3 - Validation of numerical model against results from two fire tests on isolated joints.

4. STUDIES ON FIRE-EXPOSED UNBRACED COMPOSITE FRAMES

4.1 Influence of base support and geometry of the frames

This study investigates how the base support and geometry influence the fire rating of a one-bay three-storey unbraced composite frame with joints according to Figure 3(a) and spacing of 3.60 m between the frames. Overall, Figure 4(a) and (b) show that fixed base supports allow for high fire ratings, whereas hinged base supports are not feasible. Additionally, it can be seen that both span and height of storey greatly impact the fire performance of the frames.



(a) Storey height of 3.50 m height and varying span.

(b) Span of 12.00 m and varying height.

Figure 4 - Influence of base support and geometry on the fire performance of unbraced frames.

4.2 Influence of location of the fire

In addition, the numerical model was used to investigate the influence of location of the fire. For this study, the basic layout of the frames is shown in Figure 5(a). Again, joints according to Figure 3(a) and spacing of 3.60 m between the frames were assumed. For the inner tube, circular hollow sections with 133.0×16.0 mm and 219.1×12.5 mm were considered. Three different fire scenarios were considered. It was assumed that compartment fires occur either in the ground storey, the first storey, or in both storeys simultaneously. The lateral sway of the frames ‘u’ was measured at the top of the right column and is plotted in Figure 5(c) for the three different fire scenarios. For simultaneous fire in both storeys, the sway sharply increases in comparison to the other scenarios. Apart from this, fire in the ground storey is for two reasons more critical than in the first storey. First, the load ratio of the columns in the first storey is lower than in the ground storey, which delays global instability problems. Second, the ground and second storey provide lateral restraint for a fire in the first storey. Regarding Figure 5(d), it can be seen that the location of the fire has less influence on the deflection of the beam. In the comparison, the beam in the fire-exposed storey was chosen. It should be noted that for the larger diameter of 219.1 mm for the inner tube, the plots were very close to each other. For clarity, only the curve for simultaneous fire is plotted in Figure 5(d).

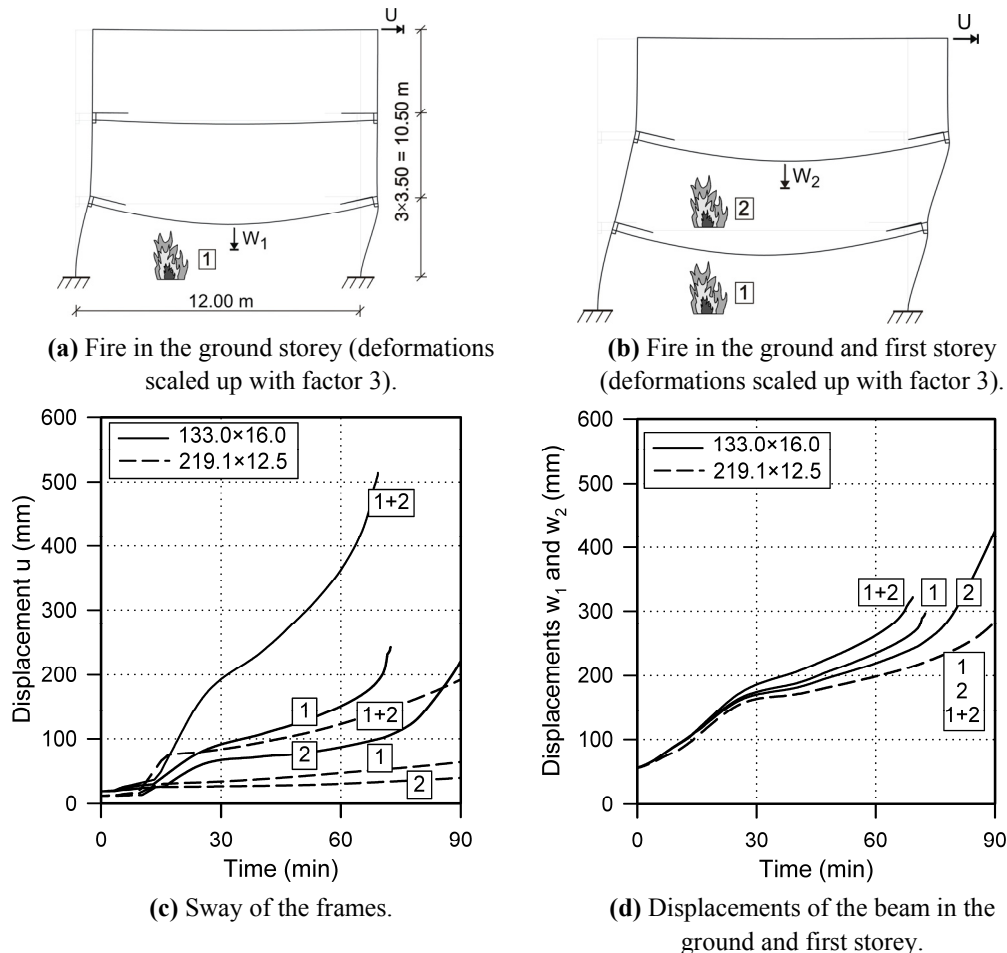


Figure 5 - Influence of location of the fire on the fire performance of unbraced composite frames.

6. CONCLUSIONS

Based on the information presented, the following conclusions may be drawn:

- A numerical model for unbraced composite frames in fire was established. The validation against results from fire tests showed that the model is suitable to simulate the fire performance of the investigated composite joints with a reasonable accuracy.
- To achieve a fire rating of 60 min, fixed base supports are a crucial factor.
- Fire tests and numerical simulations confirmed that this fire rating may be achieved even for large spans of the frames with an appropriate inner tube.
- If a fire in both storeys might occur for example due to loss of compartmentation, it is most critical. Otherwise, fire in the ground storey is critical.
- Overall, unbraced composite frames offer large flexibility regarding the building's use and fast construction times. Thus, these frames are a serious alternative to traditional load-bearing structures of low- and medium-rise buildings.

ACKNOWLEDGEMENTS

The work presented here has been carried out with a financial grant from the Research Fund for Coal and Steel (RFCS) of the European Community. The authors gratefully acknowledge the financial support and appreciate the intensive cooperation among the project partners.

Furthermore, the authors greatly acknowledge the support from the company 'Pagel Spezial-Beton', which included supply of material and concreting of the test specimens in France and Germany.

In addition, the authors thank Professor Jean-Marc Franssen for his valuable support regarding the establishment of the numerical model and for the provision of the academic version of Safir.

REFERENCES

- [1] European Committee for Standardization. 2006. EN 1994-1-2 'Design of composite steel and concrete structures, Part 1-2: General rules - Structural fire design'.
- [2] Franssen, J.-M. 2005. 'Safir. A thermal/structural program modelling structures under fire', *Engineering Journal*, A.I.S.C., 42(3):143-158.
- [3] European Commission. 2007-2010. Research project 'Unbraced Composite Structures in Fire' (UCoSiF). Research Fund for Coal and Steel, Contract N° RFSR-CT-2007-00044, Brussels.
- [4] Schaumann, P. and Bahr, O. 2010. 'Fire performance of external semi-rigid composite joints'. Structures in Fire 2010, Michigan, USA (*accepted for publication*).
- [5] Schaumann, P. and Bahr, O. 2010. 'Fire design of external semi-rigid composite joints'. ISTS13, Hong Kong, 2010 (*accepted for publication*).
- [6] Burgess, I. W., Dissanayake, U. I., and Davison, J.B. 2005. 'Modelling of plane composite frames in unpropped construction'. *Engineering Structures* 22: 287-303.

Fire Resistance of Axially Loaded Slender Concrete Filled Steel Tubular Columns

G. S. LEITE, JR., K. A. GOMIDE, A. L. MORENO, JR. and V. P. SILVA

ABSTRACT

The concrete filled steel tube (CFST) column is a composite member that consists of a steel tube filled with concrete. Concrete inside the steel tube enhances the stability of the steel tube, and the steel tube in turn provides effective lateral confinement to the concrete. Compared to conventional thin walled steel tube columns or reinforced concrete columns, the CFST column thus has the advantages of high load-carrying capacity, inherent ductility and toughness. Small diameters for these CFST columns, outside the range of design Codes validity, have been used.

In this paper are presented the results obtained in the experimental research of concrete filled steel tube (CFST) columns of 114.3 mm and 168.3 mm in diameter, subjected to loading levels corresponding to 30%, 50% and 70% of the ultimate loading at ambient temperature, filled with the usual concrete strength (25 MPa) and high compressive strength (75 MPa). The experimentally discovered effects of these parameters are discussed and the validity of Eurocode procedures for FCST columns with small diameters has been established by comparing the experimental results and analytical results.

Geraldo Silveira Leite Junior, Under Graduate Student, Department of Structural Engineering, State University of Campinas, UNICAMP, Rua Albert Einstein, 951, CP 6021, CEP 13083-952, Campinas, São Paulo, Brasil.

Kleber Aparecido Gomide, Under Graduate Student, Department of Structural Engineering, State University of Campinas, UNICAMP, Rua Albert Einstein, 951, CP 6021, CEP 13083-952, Campinas, São Paulo, Brasil.

Armando Lopes Moreno Junior (corresponding author), Professor, Department of Structural Engineering, State University of Campinas, UNICAMP, Rua Albert Einstein, 951, CP 6021, CEP 13083-952, Campinas, São Paulo, Brasil, E-mail: almoreno@fec.unicamp.br

Valdir Pignatta Silva, Professor, Department of Structural Engineering, State University of São Paulo, USP, Av. Prof. Almeida Prado, travessa 2, 271, São Paulo, São Paulo, Brasil, E-mail: valdirps@usp.br

INTRODUCTION

The steel structures clearly require an expensive fire protection since the steel is an excellent heat conductor. At the temperature near of 500 °C, it can lose half of its initial resistance of the ambient temperature.

In this context, the mixed steel and concrete structures show a huge differential: the present concrete on the structure can act as an additional fire protection, slowing down the steel temperature increase.

The composite steel columns filled with concrete has the advantage of an ease constructive (in the absence of molds, reduced structure's self-weight, etc.), and better structural behavior, as the concrete core is responsible for increasing the rigidity and resistance the tubular profile, a marked improvement in its isolated behavior.

Besides the advantages mentioned above, international experimental research point to a better behavior of composite columns filled in a fire condition when compared to unfilled (LIE & CHABOT (1992)[1], HAN *et al* (2003)[2], GOMIDE (2008)[3], LEITE JR. (2009)[4], SANT'ANNA (2009)[5]).

In this context, the State University of Campinas, UNICAMP, and the University of São Paulo, USP, have developed a survey comprising a theoretical study, based on existing literature and an experimental study addressing the behavior of slender columns of small diameter filled with concrete, mixed in the usual resistance and high compressive strength, in a fire condition.

In this paper are presented the results obtained in the experimental research of concrete filled steel tube (CFST) columns of 114.3 mm and 168.3 mm in diameter, subjected to loading levels corresponding to 30%, 50% and 70% of the ultimate loading at ambient temperature, filled with the usual concrete strength (25 MPa) and high compressive strength (75 MPa).

DESIGN OF CFST COLUMNS IN FIRE CONDITION

The fire resistance of the column is derived by calculating the strength of the column as a function of the time of exposure to fire. The strength reduces gradually with time and eventually reaches a point at which the strength becomes so low that the column can no longer support the load. At this point, the column becomes unstable and is assumed to have failed either by buckling or by compression. The time required from the initial fire exposure to reach the point at which a column becomes unstable, leading to failure under a given load, is taken as the fire resistance.

The EUROCODE 4 [6] presents analytical method for fire resistance CSFT columns determination. Fire resistance calculation involves the computation of the cross-sectional temperature. In the specific case of concrete filled steel tubes, the determination of temperatures in the cross section is very complex because there is a heat exchange between the concrete core and steel profile, due to the thermal gradient between the two materials. Added to this, the concrete moisture content influence modifies the heat flow.

By specifying the mechanical and thermal properties of structural steel and concrete, at elevated temperatures, the cross sectional temperature can be evaluated by software that uses a finite difference technique like STC, SuperTempCalc.

In this paper the validity of Eurocode procedures for FCST columns with small diameters has been established by comparing the experimental results and analytical results. The analytical results had been obtained with cross sectional temperature evaluated by software STC and experimental time-temperature curve (as closely as possible to the ISO 834 curve) recorded by thermocouple located 10 cm (+ 5cm ou – 5cm) to external face tube.

MATERIALS AND METHODS

Twenty-four concrete-filled steel tube (CFST) columns were tested. subjected to loading levels corresponding to 30%, 50% and 70% of the ultimate loading at ambient temperature.

The columns had circular cross-sections and were filled with two types of concrete compressive strength, normal and high strength. The outside diameter of the circular columns was 114.3 mm and 168.3.

All tubes were 6.4 mm wall thichnes. The columns height were variable and calculated to conserve the same 0.56 non-dimensional slenderness ratio under fire.

No external fire-proofing was provided for the steel.

The test variables were column sectional dimensions, load intensity and concrete compressive strength.

The concrete mix used for fabricating the columns was made with Portland cement, normal weight aggregate (siliceous stone of 19 mm maximum size), and silica-based sand.

The tests were carried out by exposing the concrete-filled columns to heat in electrical furnace especially built for testing loaded columns (Fig. 1 a). The furnace was constructed in three parts and different height columns can be tested (Fig. 1b). The columns extremes and upper side furnace can be isolated (Fig. 1c).

The test furnace was designed to produce conditions such as temperature, structural loads and heat transfer, to which a member might be exposed during a fire. It consists of a steel framework with the furnace chamber inside it. The furnace facility includes a hydraulic loading system with a capacity of 2500 kN.

During the test, the column was exposed, under a load, to heating controlled in such a way that the average temperature in the furnace followed, as closely as possible, the ISO 834[7] standard temperature–time curve.

The load was maintained constant throughout the test. The columns were considered to have failed and the tests were terminated when the hydraulic jack, which has a maximum speed of 76 mm/min, could no longer maintain the load. The furnace temperatures as well as the axial deformations were recorded until failure of the column.

The test specimens are shown in Table 1. The series is identified by name, FC-Ti-Cxx- η -j, where:

- FC: Fire Condition especification;
- T: tubular section;
- i: Diameter of the section, taken their entire value, ie, 114 or 168 mm;
- Cxx: concrete compressive strength “xx”, 25 for 25 MPa for example;
- η : load level used, ie, 30, 50 or 70%
- j: specimen number, 1 or 2.

Profiles of steel had yield strength of 30.3 kN/cm² and 34.0 kN/cm² for the tube diameters of 114.3mm and 168.3mm, respectively. The Yong’s modulus was 20500 kN/cm².

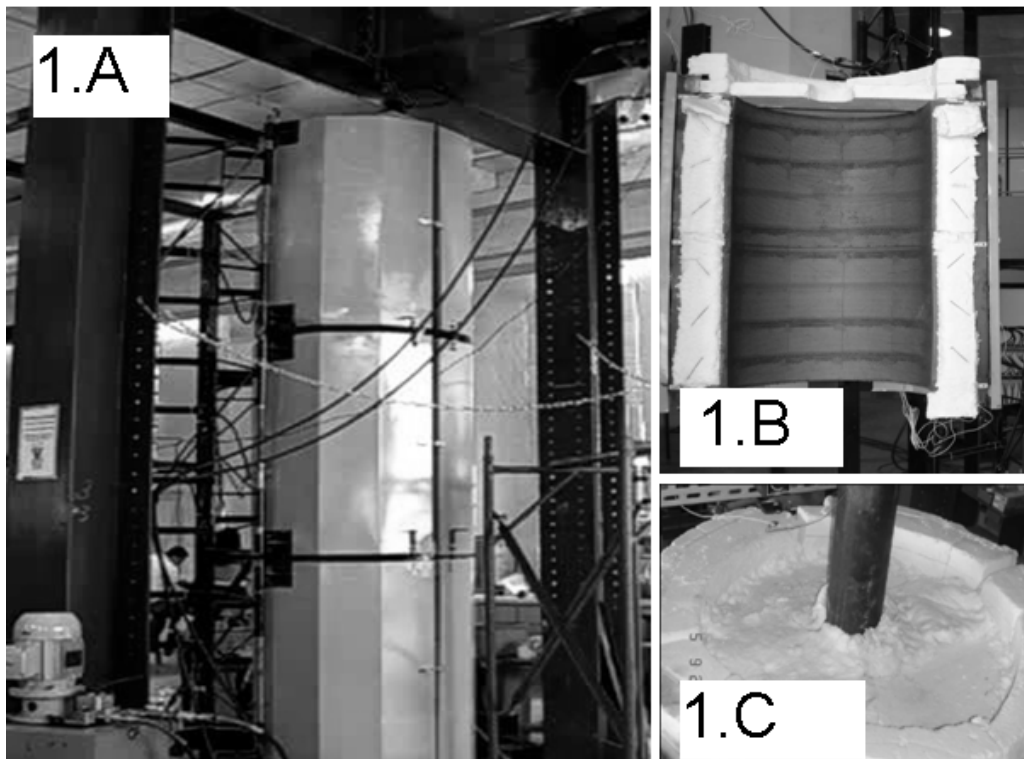


Figure1. (a) Electrical Furnace used, (b) Upper part Furnace; (c) Specimen isolation.

Four CFST columns were tested in the ambient temperature to determine the ultimate loading to axial compression. The values found in the room temperature and the mechanical characteristics of concrete used are shown in Table 2.

Table 1. Series of tests in fire condition.

Specimen	Geometry	Specimen	Geometry
FC-T114-C25-30-1	Diameter: 114,3 Thickness: 6,4 Height: 1660	FC-T114-C75-30-1	Diameter: 114,3 Thickness: 6,4 Height: 1440
FC-T114-C25-30-2		FC-T114-C75-30-2	
FC-T114-C25-50-1		FC-T114-C75-50-1	
FC-T114-C25-50-2		FC-T114-C75-50-2	
FC-T114-C25-70-1		FC-T114-C75-70-1	
FC-T114-C25-70-2		FC-T114-C75-70-2	
FC-T168-C25-30-1	Diameter: 168,3 Thickness: 6,4 Height: 2410	FC-T168-C75-30-1	Diameter: 168,3 Thickness: 6,4 Height: 2000
FC-T168-C25-30-2		FC-T168-C75-30-2	
FC-T168-C25-50-1		FC-T168-C75-50-1	
FC-T168-C25-50-2		FC-T168-C75-50-2	
FC-T168-C25-70-1		FC-T168-C75-70-1	
FC-T168-C25-70-2		FC-T168-C75-70-2	

Table 2. Results in room temperature and mechanical properties of concrete.

Diameter	Specimen	Ultimate Load (kN)	Mechanical properties	
114,3 mm	C25	773,16	$E_c = 2094,25 \text{ kN/cm}^2$	$f_c = 2,28 \text{ kN/cm}^2$
	C75	1089,10	$E_c = 3750,00 \text{ kN/cm}^2$	$f_c = 7,28 \text{ kN/cm}^2$
168,3 mm	C25	1483,35	$E_c = 2685,64 \text{ kN/cm}^2$	$f_c = 3,14 \text{ kN/cm}^2$
	C75	1955,15	$E_c = 3750,00 \text{ kN/cm}^2$	$f_c = 7,48 \text{ kN/cm}^2$

The furnace, concrete and steel temperatures as well as the axial deformations and rotations were recorded until failure of the column. Figure 2 shows the arrangement of thermocouples and LVDT.

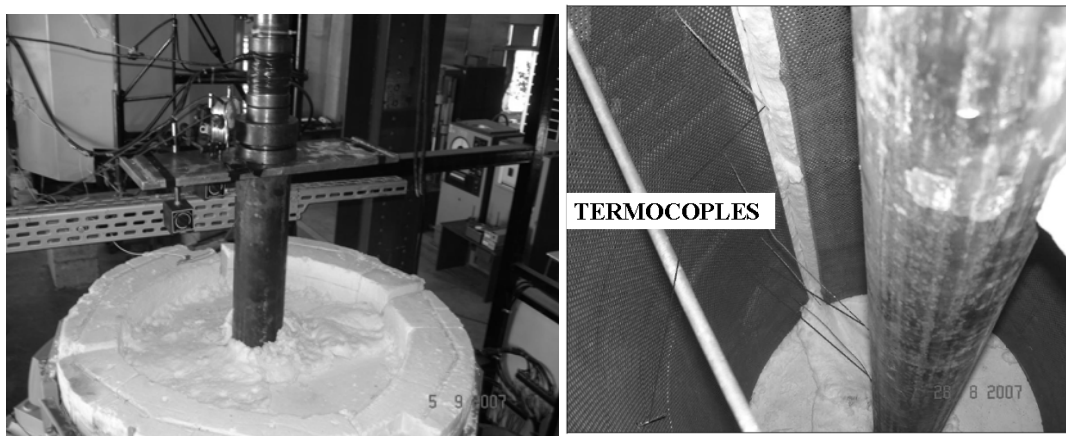


Figure 2. Instrumentation details (a) LVDT s (b) Termocoples.

RESULTS

The CFST columns failure were for global instability of the specimen, except for specimen FC-T168-C25-30-1 that presented local buckling of the steel profile, characterized by a bulge in the profile. Figure 3 illustrates the final aspect of some specimens. The results for specimens tested in fire condition are presented in Table 4.

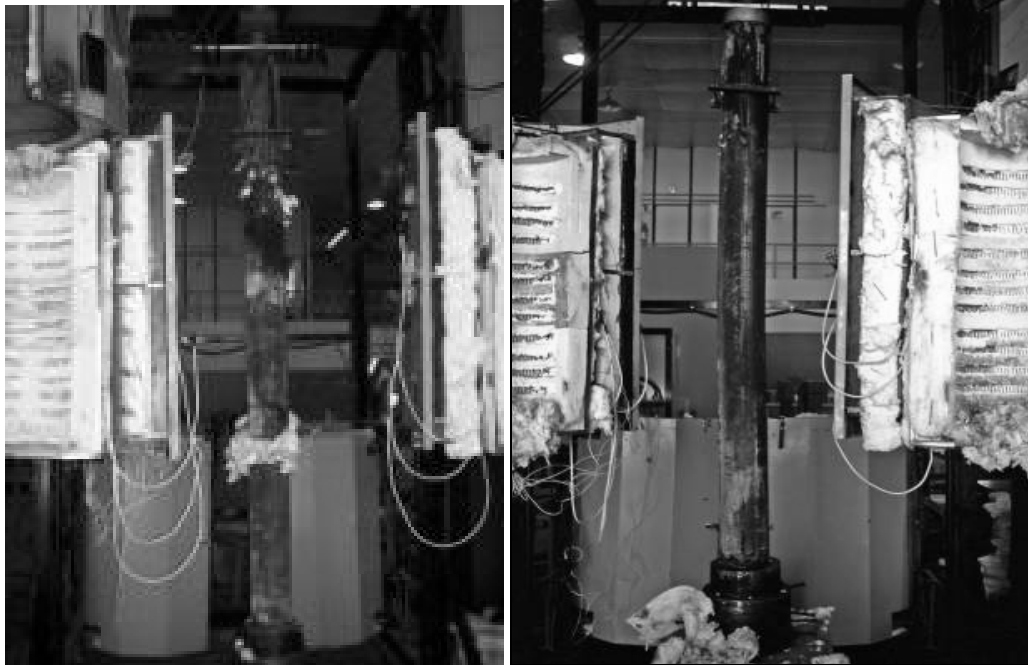


Figure 3. Specimen final appearance before fire test: FC-T168-C25-30-1 and - FC-T168-C75-70-1.

Table 4. Tests results and EUROCODE 4 results.

Specimen	Test Load (kN)	Fire Resistance (min)	Load EC-4 1-2 (kN)	$\frac{N_{R,exp}}{N_{R,EC-4}}$
FC-T114-C25-30-1	231,95	-	-	-
FC-T114-C25-30-2	231,95	-	-	-
FC-T114-C25-50-1	386,58	25,0	311,70	1,24
FC-T114-C25-50-2	386,58	27,0	331,48	1,17
FC-T114-C25-70-1	541,21	20,5	345,23	1,57
FC-T114-C25-70-2	541,21	20,5	385,83	1,40
FC-T114-C75-30-1	326,73	43,5	260,93	1,25
FC-T114-C75-30-2	326,73	40,5	256,07	1,28
FC-T114-C75-50-1	544,55	-	-	-
FC-T114-C75-50-2	544,55	27,4	499,67	1,09
FC-T114-C75-70-1	762,37	20,2	896,32	0,85
FC-T114-C75-70-2	762,37	17,2	952,82	0,80
FC-T168-C25-30-1	445,01	32,0	529,61	0,84
FC-T168-C25-30-2	445,01	-	-	-
FC-T168-C25-50-1	741,68	25,0	721,20	1,03
FC-T168-C25-50-2	741,68	21,0	947,11	0,78
FC-T168-C25-70-1	1038,35	9,0	1234,08	0,84
FC-T168-C25-70-2	1038,35	13,0	1116,09	0,93
FC-T168-C75-30-1	586,55	41,0	569,22	1,03
FC-T168-C75-30-2	586,55	-	-	-
FC-T168-C75-50-1	977,58	22,4	1321,59	0,74
FC-T168-C75-50-2	977,58	22,2	1303,41	0,75
FC-T168-C75-70-1	1368,61	14,4	1824,45	0,75
FC-T168-C75-70-2	1368,61	-	-	-

Note: The specimen pointed with ----- had their results discarded from this work because it's not in according to the requirement adopted in the Experimental Methodology.

Figure 4. presents the typical numerical analysis of a CFST column for fire resistance time by software SuperTempCalc – STC; the cross section distribution temperature are shown.

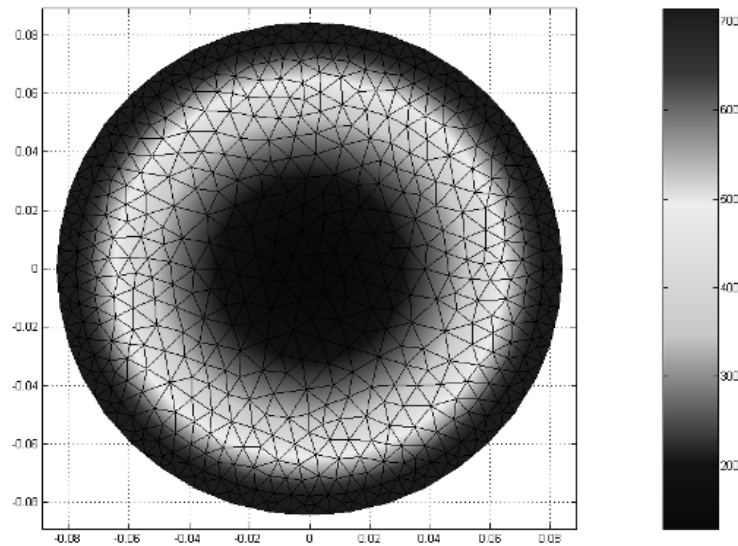


Figure 4. Cross section distribution for fire resistance (end of the test) – FC-T168-C75-30-1.

DISCUSSION

Experimental results presented in this paper were obtained by testing concrete filled steel tubes (CFST) columns under axial compression up to failure that have been exposed to standard ISO-834 fire. Three parameters are studied: concrete compressive strength, tube diameter and axial load level.

In this work was necessary a numerical analysis to determine the temperature field in the specimen for the columns filled with concrete mixed in a fire condition, which subsidized the comparison between the experimental values and theoretical values proposed by the normative codes evaluated.

By observing the results obtained experimentally (Table 4), no evidences were found on the effect of the concrete compressive strength on the CFST columns fire resistance. For the same diameter and load level, the fire resistance time for CFST columns was practically the same, for usual concrete compressive strength and high strength. Maybe, the same non-dimensional slenderness ratio under fire CFST columns can explain these tests results.

The fire resistance of the CFST columns was enhanced by the axial load level test columns. The most increase axial load level, the less CFST columns fire resistance.

Columns failure load were also predicted by design code EC4 Pt.1.2. (Table 4). Some of Code predicted failure load do not agree very well with test results. The CFST columns load test results are consistently smaller than the EC4 predicted loads results. In other words, EC4 values are not very accurate for the heating CFST columns of this study.

It should be noted that CFST tested in this study had small diameters and these fire resistance time were down or so close 30 minutes. Maybe the EC4 procedures there are not so adjustable for small diameters and small fire resistance time. The specimens of diameter 114.3 mm are outside the range of validity of the EC4 equations used.

CONCLUSIONS

This paper provides new test data concerning concrete filled steel tubes (CFST) columns that have been exposed to standard ISO-834 fire. The following conclusions can be drawn based on the experimental results of the study:

- (1) No evidences were found on the effect of the concrete compressive strength on the CFST columns fire resistance.
- (2) The fire resistance of the CFST columns was enhanced by the axial load level test columns. The most increase axial load level, the less CFST columns fire resistance.
- (3) The EC4 procedures are not so adjustable for small diameters and small fire resistance time CFST columns tested in this study.

Finally, there emphasize the needs for continuing this research, evaluating the influence of other parameters for fire resistance of CFST columns with small diameters (thickness, diameter, concrete strength, etc). The results, although alarming, should be added to those obtained by other national and international experts and, considered together, subsidize, if necessary, adjustments to the current regulatory Codes.

ACKNOWLEDGMENTS

This work was funded by FAPESP – Fundação para o Desenvolvimento Pesquisa do Estado de São Paulo.

REFERENCES

1. LIE, T. T.; CHABOT, M. Experimental Studies on the Fire Resistance of Hollow Steel Columns Filled with Plain Concrete. Internal Report n.º 611. National Research Council of Canada. Ottawa, 1992.
2. HAN, L.; ZHAO, X.; YANG, Y.; FENG, J. Experimental study and calculation of Fire Resistance of Concrete-Filled Hollow Steel Columns. Journal of Structural Engineering 129 n.3 – ASCE, 2003. p. 346 – 356.
3. GOMIDE, Kleber Aparecido. Colunas esbeltas de pequeno diâmetro mistas de aço preenchidas com concreto em situação de incêndio. Campinas: Faculdade de Engenharia Civil, Arquitetura e Urbanismo—UNICAMP, 2008. 247p. Dissertação de Mestrado—Faculdade de Engenharia Civil, Arquitetura e Urbanismo, UNICAMP, 2008.
4. LEITE JUNIOR, Geraldo Silveira; MORENO JUNIOR, Armando Lopes (orient.). Colunas mistas esbeltas de aço preenchidas com concreto de alta resistencia em temperatura ambiente e em situação de incendio . 261 p. Tese (doutorado) - Universidade Estadual de Campinas, Faculdade de Engenharia Civil, Arquitetura e Urbanismo, 2009.
5. SANT'ANNA, M. S.; “Pilares Mistos Esbeltos em aço Preenchidos com Concreto, de Seção Quadrada, em Situação de Incêndio” – Universidade Estadual de Campinas – Dissertação (Mestrado), Campinas-SP (2009).
6. EUROPEAN COMMITTEE FOR STANDARDIZATION (CEN). EUROCODE 4: Design of composite steel and concrete structures – Part 1.2: General Rules – Structural fire design. EN 1994-1-2. 2005.
7. INTERNATIONAL ORGANIZATION FOR STANDARDIZATION. Fire Resistance Tests—Elements of Building Construction—ISO 834-1—Part 1: General Requirements. Geneva: ISO/TC, 1999.
8. ASSOCIAÇÃO BRASILEIRA DE NORMAS TÉCNICAS. NBR 14432:2000 Exigências de resistência ao fogo de elementos construtivos de edificações – Procedimento. Rio de Janeiro, 2001. 14 p.

Performance Based Fire Resistance Design of CFT Columns in a Railway Station

C. ZHANG, S.-C. JIANG and G.-Q. LI

ABSTRACT

A simple calculation method has been proposed to evaluate the fire resistance of the CFT columns in the performance-based fire safety design of a railway station. Correlations recommended by EC1-1-2 are adopted to model the behavior of the design fire in the railway station. The concept of ‘t-equivalence’ is adopted to represent the severity of the design fire by standard fire duration time. Calculation method adopted by Chinese code CECS200 is used to calculate the load capacity of the CFT columns in fire. The method, by correlating real fires with standard fire, provides an easy and efficient way to evaluate the fire resistance of structures by performance-based approach.

INTRODUCTION

Concrete-filled steel tubular (CFT) columns have many advantages, including high load carrying capacity, fast construction, small cross-section, and high fire resistance. These attractions have enabled CFT columns to be used in many high-rise buildings.

Traditionally, the fire resistance of CFT columns is determined based on the results of standard fire resistance tests, which can be time consuming and expensive.

Chao Zhang (corresponding author), PHD Student, College of Civil Engineering, Tongji University, 1239 Siping Road, Shanghai 200092, China
Shou-Chao Jiang, Associate Professor, College of Civil Engineering, Tongji University, 1239 Siping Road, Shanghai 200092, China
Guo-Qiang Li, Professor, College of Civil Engineering, Tongji University, 1239 Siping Road, Shanghai 200092, China

In recent years, the behavior of CFT columns in fire conditions has been studied by many researches [1-6] and calculation methods have been developed to assess the fire resistance of CFT columns [7-9]. In many codes, such as eurocode EC4-1-2 [10], Chinese code CECS200 [11] etc., simple calculation methods for fire resistance evaluation of CFT columns are given.

Using the state-of-the-art knowledge in structural fire engineering (SFE), performance-based approach (PBA) has its capability of considering fire load, ventilation and robust mechanical behavior of real structures in fire conditions. PBA is preferable for large and complex buildings like sport stadium, airport terminal, and railway station, etc...

This paper proposes a calculation method to evaluate the fire resistance of CFT columns in a railway station. Design fire scenarios in the railway station are determined by PBA. Localized fire model given by EC1-1-2 [12] has been adopted to determine the fire properties. Temperature response of CFT columns exposed to design fires is calculated by FEM with assumptions that the CFT columns are fully engulfed by the fire plumes. The 't-equivalence' principle has been used to correlate design fire with the standard fire exposure. 't-equivalence' is defined as 'the exposure time in the standard fire resistance test which gives the same heating effect on a structure as a given compartment fire' [13]. Bridged by 't-equivalence' the design fire severity is represented by standard fire curves, correspondingly the simple calculation methods based on standard fire can be used in design fire scenarios. Simple method given by CECS200 [11] is adopted in our method. The proposed method is also valid and convenient to evaluate the fire resistance of structural members in other large spaces.

BACKGROUND AND METHODOLOGY

Fire modeling

The building fires are generally divided into two types, which are post-flashover fires in small/middle scaled compartments and pre-flashover fires in large scaled compartments (like large spaces in atria, railway station, airport terminal, stadium, etc...). In a post-flashover fire, gas properties throughout the compartment are approximately uniform that simple time-temperature curves such as ISO834, ASTM E119 are widely used to represent the fire environment. In a pre-flashover (or large space) fire, the fire is often localized near the fire source that localized fire model or two-zone model is often used to model the fire behavior.

Correlations given by EC1-1-2 [10] are adopted to determine the properties of fire plume in localized fire. The fire plume temperature is given by

$$T_z = 20 + 0.25Q_c^{2/3}(z - z_0) \leq 900 \quad (1)$$

where, Q_c is the convective part of the rate of heat release of the fire Q ; z is the

height along the flame axis; and z_0 is the virtual origin of the axis, given by

$$z_0 = -1.02D + 0.00524Q^{2/5} \quad (2)$$

where, D is the diameter of the fire.

Heat transfer

In standard fire environment, temperature gradient along the longitudinal direction of the member is always ignored, thus the governing differential equation for heat conduction is

$$\frac{\partial^2 T}{\partial x^2} + \frac{\partial^2 T}{\partial y^2} = \frac{\rho c}{k} \frac{\partial T}{\partial t} \quad (3)$$

where, k and ρc are thermal conductivity and thermal capacity.

The heat flux transferred from the fire to the exposed surfaces by convection and radiation is given by

$$q = q_c + q_r = (h_c + h_r)[T_g(t) - T_s(0, t)] \quad (4)$$

where, $T_g(t)$, $T_s(0, t)$ are temperatures of the surrounding hot gas and the exposed surface respectively; h_c is the convective heat transfer coefficient, often taken as 25 W/(m²K) [12]; and h_r is the radiative heat transfer coefficient, determined by

$$h_r = \sigma \varepsilon_{res} [(T_g(t) + 273)^2 + (T_s(0, t) + 273)^2] \times [T_g(t) + 273 + T_s(0, t) + 273] \quad (5)$$

where, σ is the Stefan-Boltzmann constant, taken as 5.67×10^{-8} W/(m²K⁴); and ε_{res} is the resultant emissivity for radiation heat transfer, taken as 0.7 [10].

The temperature of CFT columns in fire can be predicted by solving Eq.(3) with boundary condition given by Eq.(4). FEM program ANSYS is adopted to solve the heat transfer problem. 2D thermal solid element PLANE55 and thermal surface effect element SURF151 as used in a previous work [14] are adopted in numerical simulation.

Calculation method to evaluate the fire resistance of CFT columns in standard fire

The calculation method proposed by Han et al. [15] has been adopted by Chinese code CECS200 [11] to evaluate the fire resistance of CFT columns.

In [11], strength index k_t is defined to quantify the strength of the CFT columns subjected to standard fire, which is expressed as

$$k_t = \frac{N_u(t)}{N_u} \quad (6)$$

where, $N_u(t)$ is the ultimate strength corresponding to the fire resistance time t of the CFT columns; and N_u is the ultimate strength of the CFT columns at normal temperatures, which can be calculated using the equations given by design codes

such as DL/T5085-1999[16], CECS 28-90[17].

For the CFT columns without fire protection, the strength index can be calculated by the following expressions as [15]

$$k_t = \frac{1}{1 + at_0^{2.5}}, \quad \text{for } t_0 \leq t_1 \quad (7a)$$

$$k_t = \frac{1}{bt_0 + c}, \quad \text{for } t_1 < t_0 \leq t_2 \quad (7b)$$

$$k_t = kt_0 + d, \quad \text{for } t_0 > t_2 \quad (7c)$$

where

$$a = (-0.13\lambda_0^3 + 0.92\lambda_0^2 - 0.39\lambda_0 + 0.74)(-2.85D_0 + 19.45)$$

$$b = D_0^{-0.46}(-1.59\lambda_0^2 + 13.0\lambda_0 - 3.0); \quad c = 1 + at_1^{2.5} - bt_1; \quad d = 1/(bt_2 + c) - kt_2$$

$$k = (0.02\lambda_0^3 - 0.31\lambda_0^2 + 1.46\lambda_0 + 0.03)(0.01D_0^3 - 0.12D_0^2 + 0.48D_0 - 0.59)$$

$$t_1 = (0.0072D_0^2 - 0.02D_0 + 0.27)(-0.0131\lambda_0^3 + 0.17\lambda_0^2 - 0.72\lambda_0 + 1.49)$$

$$t_2 = (0.01D_0^2 - 0.03D_0 + 0.39)(-0.03\lambda_0^3 + 0.31\lambda_0^2 - 1.12\lambda_0 + 1.89)$$

$$t_0 = t/100; \quad D_0 = D_c/400; \quad \lambda_0 = \lambda/40$$

Here, D_c is the diameter of the circular section; and λ is the slenderness ratio.

Taking Eq.(7) into Eq.(6), we obtain the ultimate strength $N_u(t)$ of the unprotected CFT columns corresponding to fire resistance time t .

‘T-equivalence’ based method

In current codes [10-11], the concept of ‘t-equivalence’ has been adopted to relate real fire with standard fire. The equivalent time of a real fire is the time when a structural element is subjected to the standard fire exposure that would give the same critical temperature as the maximum temperature the structural element will get when subjected to the real fire exposure [18]. Fig. 1 illustrates this concept.

Using ‘t-equivalence’ concept, the fire resistance of CFT columns in real buildings can be evaluated by PBA with following the steps given below.

- Step 1: Determine the design fire scenario (including fire type, fire severity, fire duration etc.) by fire risk analysis;
- Step 2: Model the fire behavior and predict the temperature of the column in the design fire;
- Step 3: Predict the temperature of the column in the standard fire and determine the corresponding standard fire exposure time by t-equivalence;
- Step 4: Calculate the strength index of the CFT column k_t by Eq. (7) ;

- Step 5: Calculate the ultimate strength of the column in the design fire $N_u(t)$ from Eq.(6); (The ultimate strength of the column at normal temperature N_u is calculated separately)
- Step 6: Check the load bearing capacity of the CFT column in the design fire by comparing $N_u(t)$ with the action force in the design fire N_f . If $N_u(t) \geq N_f$, the CFT column has sufficient load capacity.

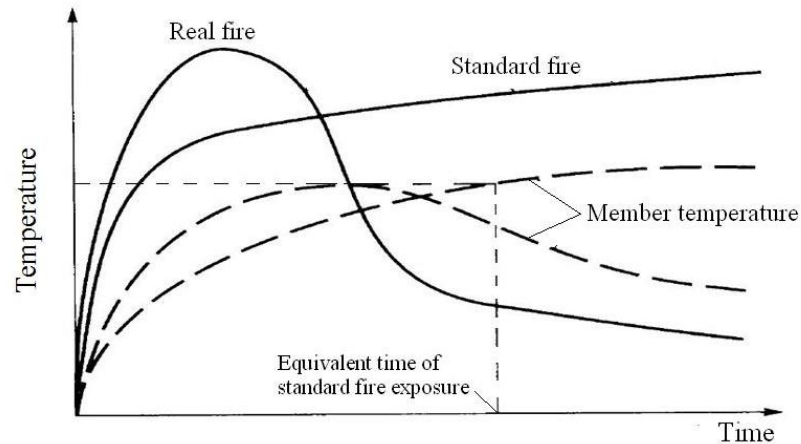


Figure 1. Concept of 't-equivalence'.

A CASE STUDY

The 't-equivalence' based method described above was used to design the fire resistance of CFT columns in Nanjing South railway station, as shown in Fig. 2. The construction area of the building is about 182340 m². The main station building is about 56.6m high. CFT columns are used to support the roof structure of the main station building. Performance-based approach has been adopted in the fire safety design of the building.

During the evaluation of the fire resistance of the CFT columns, the following simplifications and assumptions have been adopted,

- Steady-state fire scenario is considered. The fire duration time is taken as 3h.
- Localized fire model is adopted to model the fire behavior;
- The CFT columns are fully engulfed by the fire plumes and the temperature of the gas around the columns is taken as the plume temperature given by Eq.(1);
- Heat conduction along the length of the columns is safely ignored when calculating the maximum temperature of the column.

The dimensions of the CFT columns are 16m (height) × 1600mm (diameter) × 60mm (tube thickness). The filled concrete is plain weight normal concrete (NWC). The thermal properties of steel and NWC given by CECS200 [11] are used in temperature calculation.

Fig. 3 gives the FE model used for calculation of the maximum temperatures of the CFT columns in design fire and standard fire. Fig.3 also gives the result of the predicted maximum column temperature in design fire. Fig.4 shows the determination of the corresponding standard fire exposure time by t-equivalence. T_{smax} is the temperature of the outside wall of the steel tube. The corresponding standard fire exposure time is about 1.05h, which is much less than the required fire resistance time for columns determined by prescriptive code [19]. After calculation, the CFT columns are left unprotected.



Figure 2. Nanjing South railway station, Nanjing City, China.

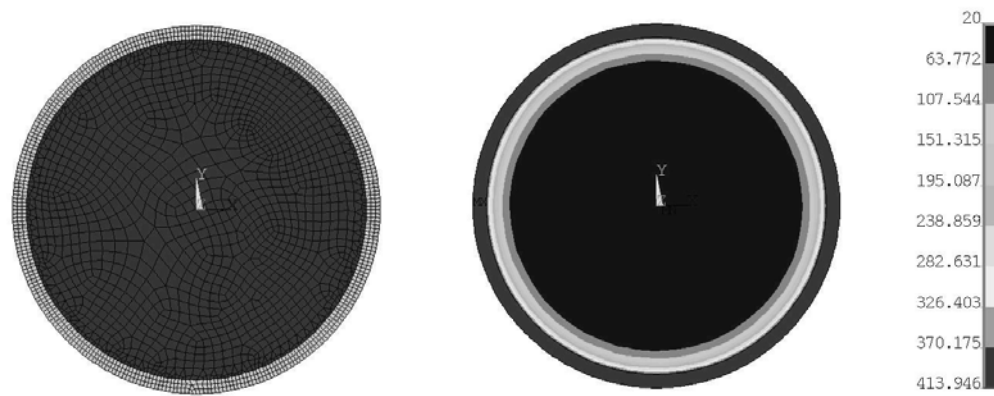


Figure 3. FE model (left) and the results of the predicted maximum temperature in design fire (right)

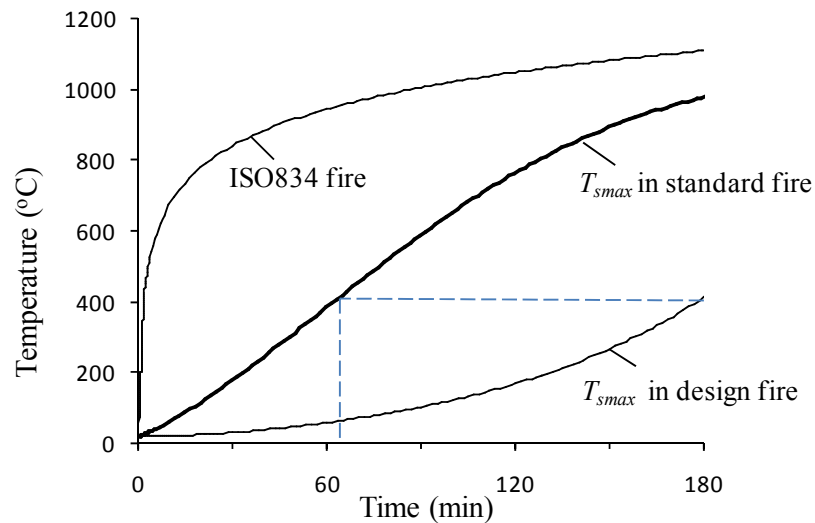


Figure 4. The corresponding standard fire exposure time determined by t-equivalence

CONCLUSIONS AND DISCUSSIONS

The proposed method adopts the concept of t-equivalence to correlate real fires with standard fire. This concept, although being widely used, its scientificity has not been investigated. In study the behavior of a composite steel frame structure in a “long-cool” and a “short-hot” fire, Lamont et al. [20] give results which go against the t-equivalence concept.

The temperature calculation of vertical members in large space fires is very complex and difficult, mainly due to the difficulty in fire modeling and radiation calculation. As a result, in the real design many assumptions have been adopted to simplify the calculation when predicting the temperature of CFT columns.

REFERENCE

1. Lie TT. Fire resistance of circular steel columns filled with bar-reinforced concrete. *Journal of Structural Engineering*, 1994; 120:1489–509.
2. Lie TT, Stringer DC. (1994). Calculation of fire resistance of steel hollow structural steel columns filled with plain concrete. *Canadian Journal of Civil Engineering*, 1994; 21:382–5.
3. Kodur VKR, Lie TT. Fire resistance of circular steel columns filled with fibre-reinforced concrete. *Journal of Structural Engineering*, 1996; 122:776–82.
4. Wang YC. The effects of structural continuity on the fire resistance of concrete filled columns in non-sway frames. *Journal of Constructional Steel Research*, 1999; 50:177–97.
5. Han LH. Fire performance of concrete filled steel tubular beam-columns. *Journal of Constructional Steel Research*, 2001; 57: 695–709.

6. Han LH, Huo JS. Concrete-filled hollow structural steel columns after exposure to ISO-834 fire standard. *Journal of Structural Engineering*, 2003; 129:68–78.
7. Lie TT, Chabot M. A method to predict the fire resistance of circular concrete filled hollow steel columns. *Journal of Fire Protection Engineering*, 1990; 2:111–26.
8. Kodur VKR. Performance-based fire resistance design of concrete-filled steel columns. *Journal of Constructional Steel Research*, 1999; 51: 21–36.
9. Wang YC. A simple method for calculating the fire resistance of concrete-filled CHS columns. *Journal of Constructional Steel Research*, 2000; 54: 365–86.
10. EN 1994-1-2. Eurocode 4: Design of composite steel and concrete structures—Part 1-2: General rules—Structural fire design. British Standard Institution . London. 2005.
11. China Association for Engineering Construction Standardization (CECS200). Technical code for fire safety of steel structure in buildings (in Chinese). Beijing, China Planning Press, 2006.
12. EN 1991-1-2. Eurocode 1: Actions on structures—Part 1-2: General rules—Actions on structures exposed to fire. British Standard Institution . London. 2002.
13. Law M. A relationship between fire grading and building design and contents. Technical report, 1971.
14. Guo-qiang Li, Chao Zhang. Thermal response to fire of uniformly insulated steel members: Background and verification of the formulation recommended by Chinese code CECS200. *Advanced Steel Construction, an International Journal*, Vol. 6, No. 2, June 2010. (*In Press, Corrected Proofs*)
15. Han LH, Zhao XL, Yang YF, Feng JB. Experimental study and calculation of fire resistance of concrete-filled hollow steel columns. *Journal of Structural Engineering*, 2003;129:346–56.
16. DL/T5085-1999. Chinese design code for steel-concrete composite structures (in Chinese). Beijing, Chinese Electricity Press.
17. China Association for Engineering Construction Standardization (CECS28-90). Specification for design and construction of concrete-filled steel tubular structures (in Chinese). Beijing, China Planning Press, 1991.
18. Wang YC. Some considerations in the design of unprotected concrete-filled steel tubular columns under fire conditions. *Journal of Constructional Steel Research*, 1997; 44:203–23.
19. GB 50016-2006. Code of design on building fire protection and prevention (in Chinese). Beijing, China Planning Press, 2006.
20. Lamont S, Usmani AS, Gillie M. Behaviour of a small composite steel frame structure in a “long-cool” and a “short-hot” fire. *Fire Safety Journal*, 2004;39:327–57.

Fire-Resistance Evaluation of Double CFT Columns Under Central Axial Load

Y. A. WON, S. H. KIM, S. K. JUNG, K. S. CHUNG and S. M. CHOI

ABSTRACT

Studies and tests (D.K. Kim et al. 2005; K.S. Chung et al. 2008; S.H. Park et al. 2008) have proved that unprotected CTF columns can resist a fire for up to two hours under strong axial load and heat. However, the fire-proof construction and management code recently established by the Ministry of Land, Transport and Maritime Affairs prescribes that the columns of high-rise buildings over twelve stories resist fire for three hours at least. Accordingly, double CFT columns using SPSR400 steel with concrete compressive strength of 36.1MPa are suggested in this study as a way to meet the fire-resistance requirement. In order to compare their fire-resistance with that of unprotected CFT columns, full-scale structural test and numerical analysis were conducted with the variables of central hollow ratio, concrete strength and steel tube strength. It is evaluated whether double CFT columns can resist fire for more than three hours and thus be appropriate to over 12 story high-rise buildings.

Key words: Central axial load, Double CFT column, Fire-resistance, Numerical analysis

Won, Yong An, Ph.D Candidate, Ministry of National Defence

Kim, Sun Hee, Ph.D Candidate, Department of Architecture at University of Seoul

Jung, Sang Keun, Master's Course, Department of Architecture at University of Seoul

Chung, Kyung Soo, Research Institute of Industrial Science & Technology of Korea

Choi, Sung Mo, Professor of Department of Architecture at University of Seoul, Ph. D

INTRODUCTION

Background & Purpose

CFT columns are considered to excel in fire-resistance thanks to the thermal storage enabled by in-filled concrete. One of the previous studies (D.K. Kim et al. 2005; K.S. Chung, S.H. Park et al. 2008) has proved that unprotected CFT columns resist fire for less than two hours under high axial load ratio. However, the Fire-proof Construction & Management Code (No. 2005-122) provided by the Ministry of Land, Transport & Maritime Affairs requires the columns of high-rise buildings over twelve stories to secure fire-resistance for three hours. Unprotected CFT columns with high axial load ratio can be employed to low/medium-rise buildings to provide fire-resistance for less than two hours, but they can not satisfy three hour fire-resistance requirement for high-rise buildings. Accordingly, fire-resistance of unprotected CFT columns should be improved in order for them to be employed to high-rise buildings. This study suggests CFDST (Concrete Filled Double Skin Tube) columns to improve the fire-resistance of unprotected CFT columns. Although experimental and analytical studies on the evaluation of the fire-resistance of CFDST columns have been recently made in China (Y.F. Yan and L.H. Han 2005; H. Lu et al. 2007), no studies have been conducted to evaluate the fire-resistance of the columns based on the comparison with CFT columns. The purpose of this study is to make a comparative analysis of fire-resistance improvement provided by CFDST columns and the influence of different sectional shapes through the loaded heating tests for full-scaled unprotected CFT column and CFDST columns.

TEST(Test Plan)

In this study, four specimens were planned as shown in Table 1 to conduct loaded heating tests for CFDST columns with the variables of reinforcement/unreinforcement of inner tube and sectional shape of inner and outer tube. Column length and end-plate thickness were 3,000mm and 49mm, respectively. S-N, S-S, S-C and C-C mean unprotected CFT square column, CFDST square column with square inner tube, CFDST square column with circular inner tube and CFDST circular column with circular inner tube which has concrete dimensions and sectional area of inner tube identical to its S-S counterparts. Central hallow ratio (D_i/D_o) of CFTST square and circular columns ranged between 0.39 and 0.40. Axial load ratio for all the four columns was 0.4.

Table I. VARIABLES.

Specimen	$D_o \times t_o$ (mm)	$D_i \times t_i$ (mm)	F_{ck} (MPa)	N_a (kN)	Axial load ratio (N_a/N_{c+s})
S-N	□ 360.0×9	-	36.09	1,670	0.40
S-S	□ 360.0×9	□ 140×6.0	36.09	1,687	0.40
S-C	□ 360.0×9	∅ 140×6.6	36.09	1,705	0.40
C-C	∅ 406.4×9	∅ 165×7.1	36.09	1,707	0.40

Fabrication of Specimens

Mass-produced circular column was used, while two bending-formed channel steel plates were butt-welded to make each of the square columns. The connection between end-plate and column was reinforced with four ribs. On

each surface of the columns, holes 20mm in diameter were made consisting of those at 340mm from the contact surface between upper/lower end-plate and column and that at the centre of column width. Seven ~ nine thermo couples were mounted around the center of the columns to measure sectional temperature (Fig. 4).

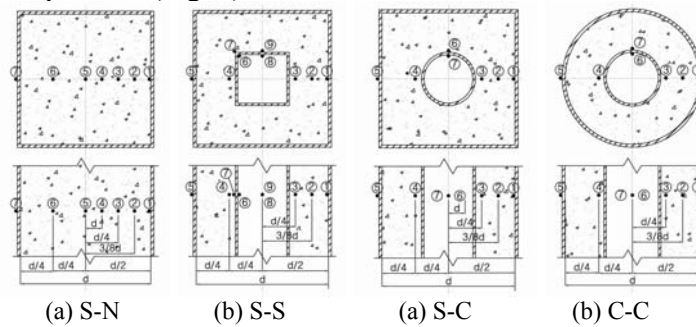


Figure 4. Location of thermo couples.

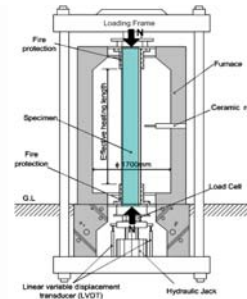


Figure 5. Loaded heating furnace

Test Process

Loaded heating furnace used for the test is shown in Fig. 5. The temperature of the furnace and inside the specimens and vertical displacement of the specimens were measured. Loading was applied by a 3,000kN hydraulic jack located under the furnace and Elongation caused by thermal expansion and shrinkage was measured by linear type displacement transducers installed at hydraulic cylinder. Heating was generated by four gas burners located at the four sides of each column.

TEST RESULTS & ANALYSIS

Temperature Distribution on Sectional Areas

The standard fire curve prescribed in ISO-834 and the curves obtained from the test. The fire temperature during the loaded heating test is within the deviation of 5% from the standard fire curve. There is a gap between the average temperature of the columns and standard fire temperature at the beginning, but the former gets closer to the latter from 60 minute point due to the influence of heat transfer and radiation. In addition, the average temperature of the columns is almost identical to standard heat temperature regardless of sectional shape and the length of column diameter.

Fig. 6 shows temperature distribution observed at different distances from the surface of concrete core. Because the thermal capacity of in-filled concrete restrains temperature rise, while the temperature at the surface of concrete core rose up to 1000°C in 180 minutes, temperature rise at the surface of inner tube was significantly smaller, with its peak marking below 300°C. Fig. 6 (b) ~ (d) show the difference in the temperature of in-filled concrete associated with reinforcement/unreinforcement of inner tube and type of reinforcement. As shown in Fig. 7 (b), all the specimens except C-C displayed almost identical distribution at the distance of 1/8 of concrete core diameter. It was because the distance from concrete surface in C-C was approximately 6mm longer than that in others. The increase in temperature nearer to the center of concrete core was more severe in S-S and C-C than in others and the two specimens exhibited almost identical temperature distribution except the outer surface of inner tube shown in Fig. 7(b). It is induced that the reason is that the two specimens have

identical sectional areas and the smallest concrete amount. In addition, S-N displayed the lowest temperature distribution.

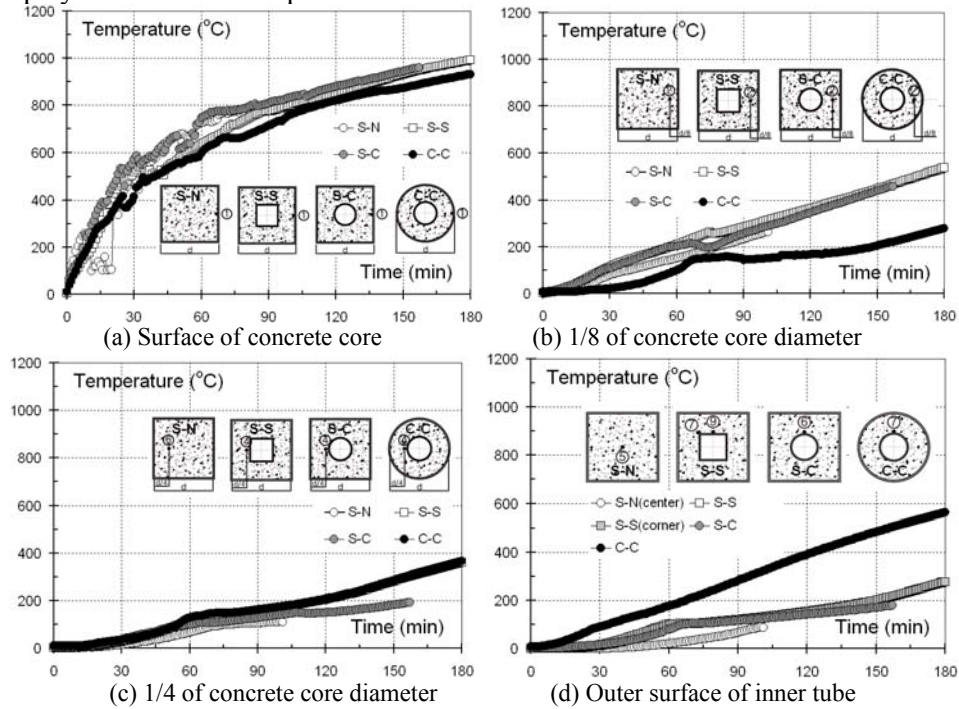


Figure 6. Temperature distribution on different points.

Axial Deformation

Axial expansion was observed in all specimens from 15 to 20 minutes due to the thermal expansion of outer tube after heating. As shown in Fig. 6, the temperature of outer tube surface rose up to 500-600°C. After that, axial expansion stopped due to the deterioration of load capacity caused by temperature rise and local buckling at the lower end of columns. Contraction progressed rapidly and the load which had been applied to outer tube was delivered to concrete and inner tube. Initial axial expansion of 10mm observed in S-N was larger than that of all the other specimens which was approximately 5mm in common. It is deduced that inner tube confined thermal expansion against initial axial expansion of outer tube in S-S, S-C and C-C CFDST specimens. While axial contraction in S-N specimen progressed most gradually, it ruptured as soon as the load capacity of concrete was exhausted as shown in Fig. 7 (a). In CFDST specimens, since concrete and inner tube resisted load after the load capacity of outer tube was exhausted, the columns maintained original length without contraction for more than one hour and deformation progressed gradually until rupture. The time until rupture was the shortest in S-C. S-S specimen did not rupture until the test was terminated at 180 minute point.

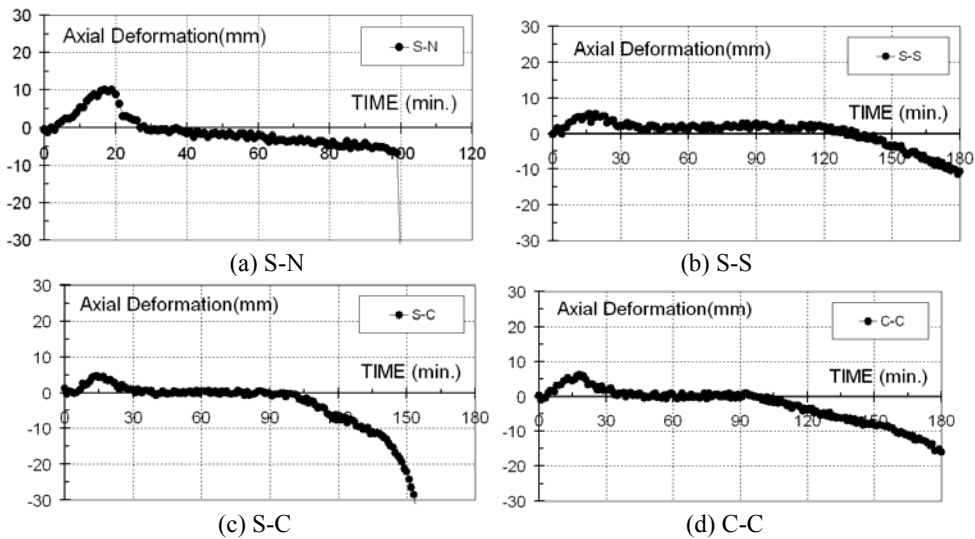


Figure 7. Resistance to axial deformation.

ANALYSIS OF INFLUENTIAL FACTORS ON FIRE-RESISTANCE

Reinforcement/Unreinforcement of Inner Tube & Sectional Shape

of sectional size was 0.3 in both S-S and S-C specimens. Therefore, axial load applied to S-S and S-C was stronger than that to S-N by 1% and 2%, respectively as shown in Fig. 8 (a). Fire-resistance time in S-S and S-C was 180 minutes and 153 minutes, respectively which were longer than that of S-N by 82% and 55%. In addition, square column with square inner tube was superior to square column with circular inner tube by 18% in terms of fire-resistance. As shown in 9 (b), the length of time that concrete and inner tube resisted axial load ('a') in S-S and S-C was 2.2 times and 1.5 times longer than that in S-N. And, the resistance to axial deformation in S-S was 1.5 times longer than that in S-C.

* a : Resistance of concrete & inner tube to applied load

Therefore, it is deduced that CFDST column can secure fire-resistance for more than three hours and can be regarded as an alternative to unprotected CFT column for improving fire-resistance. It is also determined that CFDST square column with square inner tube is more effective than that with circular inner

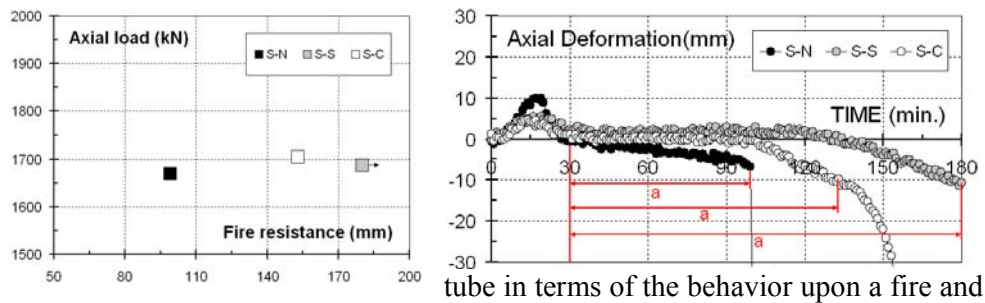


Figure 8. The influence of reinforcement & sectional shape.

Sectional Shape of Outer Tube

C-C and S-S specimens had the same sectional dimensions of in-filled concrete and inner tube, whereas the sectional area of S-C was larger by approximately 4%. In short, there was no gap among the specimens in terms of sectional area. As shown in Fig. 9 (a), applied axial load to S-S and S-C differed from that to C-C by about 1%. Fire-resistance time observed in S-S was 180 minutes which was similar to that in C-C, while fire-resistance time in S-C was 153 minutes which was shorter than that in C-C by 15%. As shown in Fig. 9 (b), the length of time that concrete and inner tube of S-S resisted applied load ('a') increased about 1.1 times when compared with C-C. Resistance to axial deformation in S-C was 0.75 times of C-C confirming the decrease in fire-resistance time. Accordingly, it is determined that CFDST square column with square inner tube is slightly superior to CFDST circular column with circular inner tube and CFDST circular column with circular inner tube is superior to CFDST square column with circular inner tube in terms of fire-resistance under identical axial load ratio.

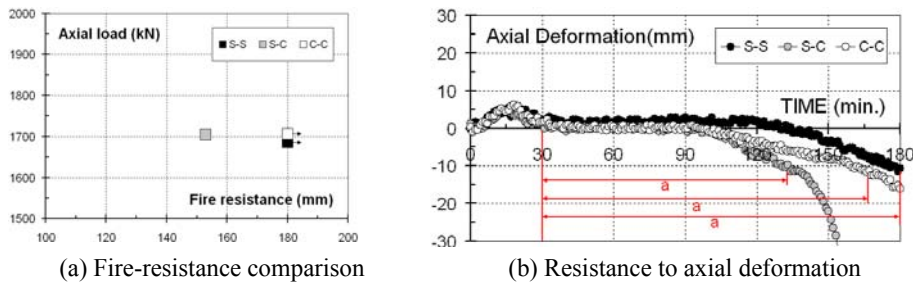


Figure 9. Influence of sectional shape.

NUMERICAL ANALYSIS OF CFDST SQUARE COLUMNS

Sectional area of each CFDST column was divided into sub-areas consisting of steel element and concrete element in order to calculate temperature distribution on the sectional area and axial deformation and stress of the column as shown in Fig. 10. After heat transfer analysis was conducted with the thermal characteristics of members taken into consideration to predict sectional temperature distribution, thermal stress analysis was conducted with the temperature distribution data and the dynamic characteristics of members taken into consideration to predict the behavior and fire-resistance of CFDST square columns. Standard fire curve complying with the KSF 2257-1 was used at the numerical analysis in order to realize an actual fire. In addition, numerical analyses of the fire-resistance of CFT square columns and double CFT columns under constant axial load were conducted in terms of maximum load capacity and axial deformation based on the sectional temperature distribution obtained from heat transfer numerical analysis. In order to verify the validity of the numerical analyses, the results were compared with those of fire-resistance tests for CFDST and CFT columns. Test and analysis variables were as shown in Table II.

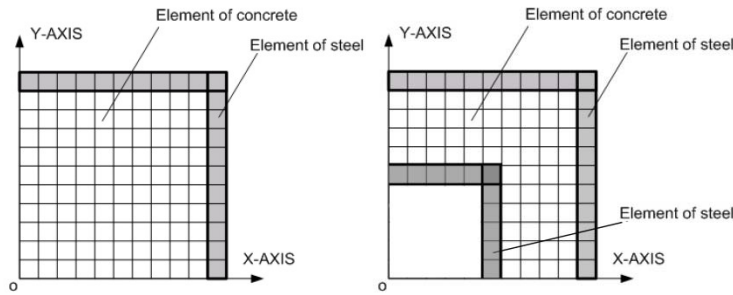
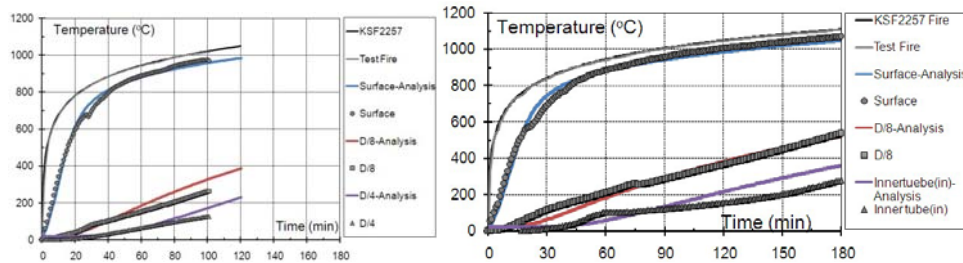


Figure 10. Analysis model (1/4 dissection).

Table II. CFT COLUMNS TO BE ANALYZED.

Specimen	Do×to (mm)	Di×ti (mm)	fck (MPa)	Na (kN)	Axial load ratio (Na/Nc+s)	Fire-resistance time (min.)	
						Test	Analysis
S-N	□360×9	-	36.1	1,670	0.4	99	89
S-S	□360×9	□140×6	36.1	1,687	0.4	180*	150

Table II and Fig. 11 show fire-resistance time obtained from the analyses and tests. Numerical analyses predicting fire-resistance time of 150 minutes and 89 minutes for Double CFT columns and unprotected CFT columns were more conservative than fire-resistance test.

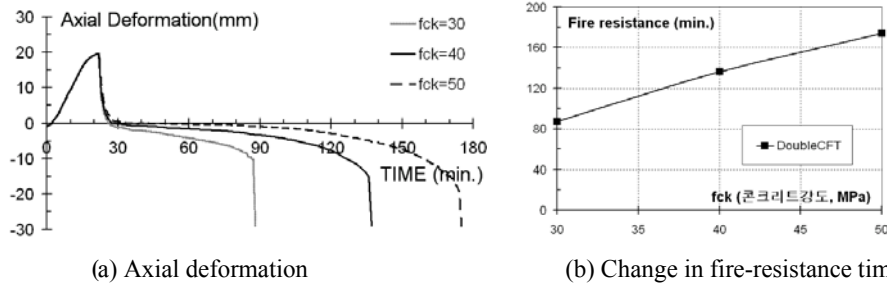


(a) Time-Temperature relation in unprotected CFT column
(b) Time-Temperature relation in double CFT columns

Figure 11. Comparison of analysis results.

The Influence of Concrete Strength

It was observed that higher concrete strength would result in a lot more gentle slope in axial deformation. Increase in concrete strength was accompanied with nearly proportional improvement of fire-resistance and increase from 30MPa to 50MPa resulted in the improvement of fire-resistance as much as twice as in the case of unprotected CFT columns.



(a) Axial deformation (b) Change in fire-resistance time
Figure 12. Axial deformation & fire-resistance time for different concrete strengths.

Influence of Inner Tube Strength

As the strength of inner tube increased in final rupture section, fire-resistance time increased by approximately 20 minutes because load delivery to concrete core was delayed as the strength of inner tube increased. It is determined that the temperature of inner tube exerts significant influence on the fire-resistance of double CFT columns.

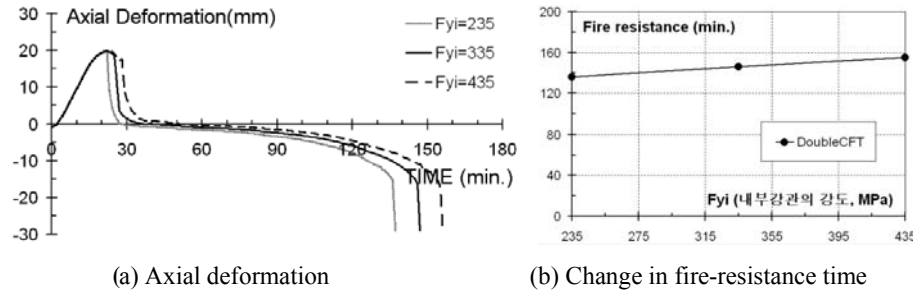


Figure 13. Axial deformation & fire-resistance time for different strengths of inner tubes.

CONCLUSION

The conclusion of this study covering loaded heating tests for full-scale unprotected CFT and CFDST column specimens to evaluate the improvement of fire-resistance associated with CFDST columns and the influence of sectional shape is as follows.

It is determined that CFDST column can secure fire-resistance for more than three hours and thus can be considered as a very effective alternative to unprotected CFT column for improving fire-resistance. CFDST square column with square inner tube is superior to that with circular inner tube in terms of the behavior upon a fire and fire-resistance. In addition, under identical axial load ratio, the fire-resistance of CFDST square column with square inner tube is slightly superior to CFDST circular column with circular inner tube of identical sectional area and CFDST circular column with circular inner tube is superior to CFDST square column with circular inner tube in terms of fire-resistance.

As the strength of inner tube increased in final rupture section, fire-resistance time increased by approximately 20 minutes because load delivery to concrete core was delayed as the strength of inner tube increased. It is deduced that the temperature of inner tube exerts significant influence on the fire-resistance of double CFT columns. CFDST columns displayed the improvement of fire-resistance by approximately 70-80% when compared with CFT column so they are expected to be employed to high-rise buildings for securing fire-resistance. As in the case of unprotected CFT columns, concrete strength is a major influential factor. In addition, width-thickness ratio of column and the strength of inner tube are deduced to be major factors to improve fire-resistance.

ACKNOWLEDGEMENT

This research was made possible by the second-year support for the 2008 research of the Ministry of Science and Technology entitled *Evaluation Technology for High-rise Structures* (Roa-2007-000-10047-0).

NOTATION

Do: Diameter of outer tube (mm)	Di: Diameter of inner tube (mm)
to: Thickness of outer tube (mm)	ti: Thickness of inner tube (mm)
f_{ck} : Concrete strength (MPa)	Nf(t) : Axial resistance upon a fire (kN)
N_a : Applied axial load,	Nc+s: Load capacity provided by concrete & inner tube
FR: Fire-resistance time	R= Fire-resistance (min.)
K= Effective length coefficient	L = Unraced length of column (mm)
C = Applied load	F1= Coefficient for taking into consideration
the components & sectional shape of HSS columns	Ac: Concrete sectional area

REFERENCES

1. ISO., "Fire Resistance Test-Elements of Building Construction" *ISO 834*,(1975).
2. V.K.R Kudur., "Design Equations for Evaluating Fire Resistance of SERC-filled HSS Columns", *Journal of Structural Engineering*, (1998).
3. V.K.R. Kodur., "Performance-based fire resistance design of concrete-filled steel columns", *Journal of Constructional Steel Research*, Vol. 51, No. 1, (1999).
4. Y.C Wang., "Steel and Composite Structures-Behavior and Design for Fire Safety", *Span press-Taylor & Francis Group*, (2002).
5. Choi S. M., Park S.H., Chung, K.S., and Kim, D.k., "Review of Material Properties for Predicting the Fire Resistance of Concrete-Filled Steel Square Tube Column using the Numerical Method", *8th Association for steel-concrete composite structures*, (2006).
6. Park S.H., Chung K. S., Choi S.M., "A Study on Failure Prediction and Design Equation of Concrete Filled Square steel Tube Columns under fire Condition", *International Journal of STEEL STRUCTURES*, (2007).
7. H. Lu, X.L. Zhao, and L.H. Han, "Experimental investigation on fire performance of self-consolidating concrete(SCC) filled double skin tubular columns", *Proceedings of the Fifth International Conference on Advances in Steel Structures*, Singapore(2007), pp. 944-949.
8. Park S.H., Chung K. S., Choi S.M., "A Study on the fire-resistance of concrete-filled steel square tube columns without fire protection under constant central axial loads", *Steel and Composite Structures*, (2008).
9. Chung K. S., Park S.H., Choi S.M., "Material effect for predicting the fire resistance of concrete-filled square steel tube column under constant axial load", *Journal of Constructional Steel Research*, (2008).

Fire Endurance Performance of Cellular GFRP Columns with Water-Cooling System

Y. BAI¹, E. HUGI², C. LUDWIG³ and T. KELLER⁴

ABSTRACT

Experimental results on the fire endurance of full-scale glass fiber-reinforced polymer (GFRP) composite columns are reported in this paper. The pultruded four-cell profiles were first loaded to axial compression (uniform serviceability stress of 5 MPa) and then simultaneously subjected to an ISO834 fire from one side until ultimate failure occurred or the planned duration of fire exposure was reached. An active water cooling system was integrated into two columns to improve the fire resistance duration. The time-dependent temperature responses and lateral deflections were recorded. The latter were caused by thermal expansion and load eccentricity due to material loss on the fire side. A non-cooled reference column failed after 50 min fire exposure while the two water-cooled columns did not fail within the planned 60 and 120 min. Previously developed models were capable of predicting the time-dependent temperature responses, modulus degradation and time-to-failure.

INTRODUCTION

Fire always constitutes a potential hazard for load-bearing structures, because all the commonly used structural materials—including timber, steel and concrete - show more or less degradation (in terms of stiffness and strength) in fire. Depending on the application, e.g. bridge or building construction, load-bearing structures have therefore to fulfill more or less stringent requirements regarding fire performance and fire safety. Corresponding codes and regulations have been established to guarantee a minimum level of fire safety. A simple and basic requirement in building construction is often a prescribed fire endurance time during which a building can safely be evacuated. This duration time normally depends on the building significance and number of stories, for example in Switzerland, 60 min for three-story buildings or 90 min for buildings taller than three stories [1].

^{1,4}Composite Construction Laboratory (CCLab), Ecole Polytechnique Fédérale de Lausanne (EPFL), BP 2220, Station 16, CH-1015 Lausanne, Switzerland.

^{2,3}Empa, Swiss Federal Laboratories for Materials Testing and Research, Laboratory for Building Science and Technology, Ueberlandstrasse 129, CH-8600 Dübendorf, Switzerland.

In recent years, fiber-reinforced polymer (FRP) composite materials have been increasingly considered in structural construction. The performance of FRP composites under elevated and high temperatures was first studied on the material level. It was shown that their thermophysical properties (density, specific heat capacity, and thermal conductivity) exhibit significant changes during decomposition [2, 3]. Investigations on FRP laminates also showed that the thermomechanical properties (modulus and strength) degrade considerably at glass transition, a temperature range much lower than the decomposition temperature [4, 5]. Especially in compression, FRP components are much more vulnerable because of early polymer softening and subsequent fiber buckling [6, 7]. Application of FRP composites in structural engineering further requires the understanding of their performances on the structural level. Full-scale structural fire endurance experiments were conducted by Keller et al. [8] on cellular GFRP panels in a four-point-bending setup and subjected to an ISO 834 fire from the underside (which was in tension in that case). The implementation of a water-cooling system in the panel cells extended the fire endurance time from 57min to at least 120min. Failure occurred only in the non-cooled panel, not on the (tensioned) fire side but on the (compressed) cold side at a temperature close to the glass transition temperature. The results confirmed that FRP structural components are much more sensitive to elevated and high temperatures on the compression than on the tension side.

While the former work concentrated on GFRP slab components (subjected to bending with one side, the fire side, in tension), this work focuses on column or wall components (with both sides, also the fire side, in compression). The paper reports on the results (thermal responses, stiffness degradation, time-to-failure) of cellular GFRP columns subjected to axial compression and an ISO834 fire from one side. Again non-cooled and water-cooled specimens were investigated.

EXPERIMENTAL INVESTIGATIONS

Material and Specimens

Three pultruded four-cell cross sections of the Dura Span®766 system were used, which are composed of two face sheets and alternating vertical and inclined webs of different thicknesses. A detailed material description can be found in [8].

Experimental Scenarios and Set-up

Specimen NC was tested without any fire-protection measures up to failure. Specimens WC1 and WC2, subjected to one and two hours of heating, were equipped with a water-cooling system. Water circulated in the cells at a low flow rate of 2.5 cm/s. A hinged steel joint was installed at the specimen ends. In order to protect the loading bearing facilities and also prevent failure at joint positions, stone wool blocks were used to isolate the joints up to a distance of 300 mm from the specimen ends. Figure 1 shows the experimental setup. First, an axial compressive load of 145 kN (corresponding to a uni-form stress level of 5 MPa) was applied and kept constant during the subsequent thermal loading. Then the water flow (if used) was started. When all the flow meters and thermocouples gave stable values,

thermal loading was applied following the ISO834 fire curve until structural failure occurred or the planned time duration was attained.

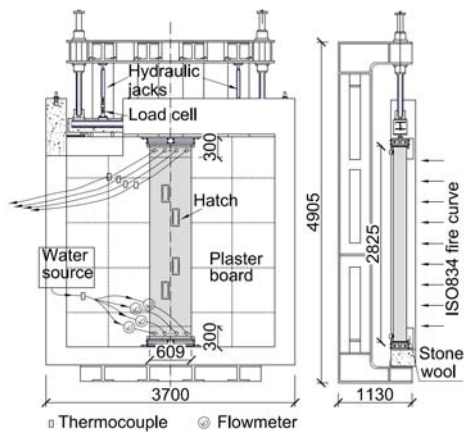


Figure 1. Experimental set-up and configuration of water cooling system.

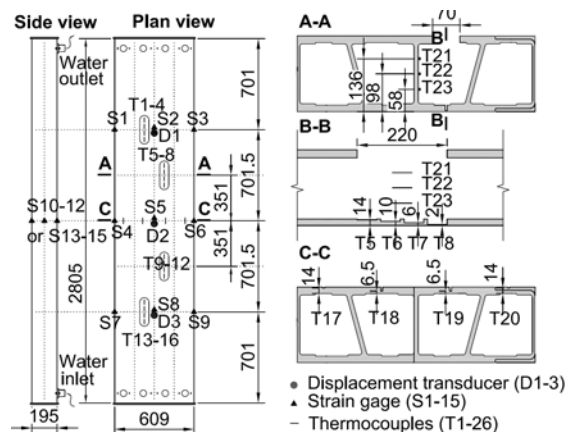


Figure 2. Measurement arrangement and Terminology.

Instrumentation

Thermocouples were placed at different depths through the thickness and designated T1, T2, etc. Strain gages (S1, S2, etc.) were placed in the pultrusion direction on the outer face sheets and the two outside webs to measure the axial strains, as indicated in Figure 2. Lateral displacements were measured at mid-height and axial deformations at the upper specimen end during the entire experimental process.

EXPERIMENTAL RESULTS

Non-Cooled Specimen NC

During the (pre-fire) mechanical loading, the lateral deflection at mid-height remained small: 1.4 mm towards the fire side. When fire exposure started (at time $t = 0$), lateral deflection towards the fire side started to increase due to the thermal expansion of the inner fire-exposed face sheet and reached a maximum of 8.1 mm after 20 min, see Figure 3. From this point on, lateral deflections started to decrease due to the loss of decomposed material on the inner face sheet, which moved the cross section's centroid towards the outer face sheet and resulted in an eccentricity that produced a deflection away from the fire side. Specimen ultimate failure occurred after 49 min at a lateral deflection of 2.0 mm towards the fire side.

The temperature progressions are shown in Figure 4. After less than 15 min the temperature through the whole inner face sheet exceeded T_g (117 °C) and T_d was exceeded at the hot face, suggesting that the inner face sheet completely lost its stiffness and decomposition started at the hot face. At ultimate failure, approximately 70% (12 of a total of 16.8 mm) of the inner face sheet depth had reached a temperature of above 300°C and therefore decomposed.

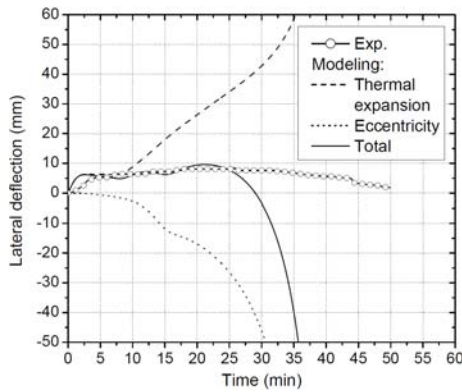


Figure 3. Measured mid-height lateral deflections with time and comparison to modeling results, non-cooled specimen NC.

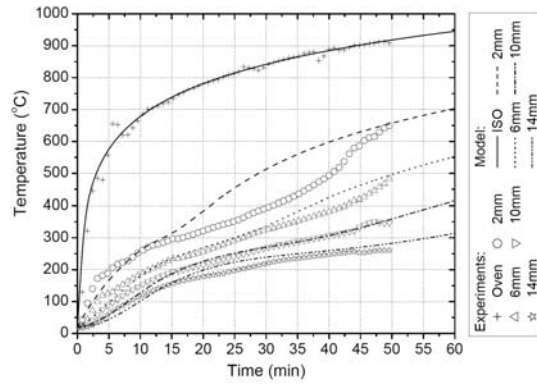


Figure 4. Temperature progression at different depths of inner face sheet of specimen NC and comparison to modeling results.

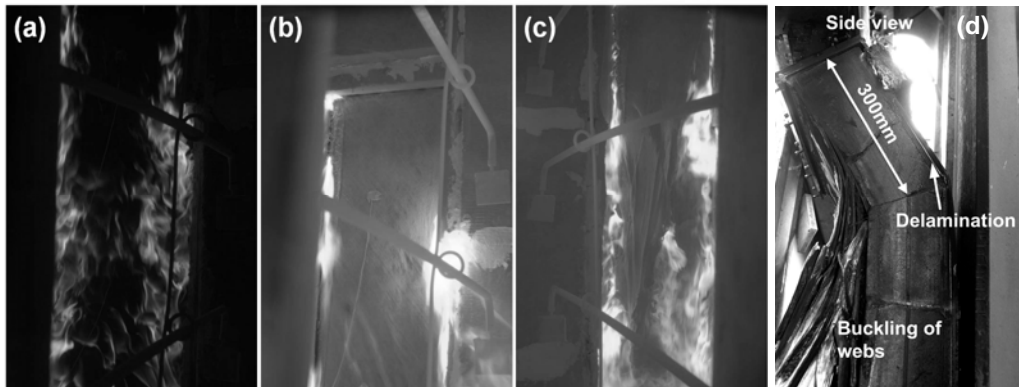


Figure 5. Visual observations of hot face of non-cooled specimen NC during mechanical and fire loading after: a) 5min, b) 25min, c) 45 min; and d) final failure mode.

Visual observations of the changes of the fire exposed surface with time are shown in Figure 5a-c. After 5 min of fire exposure, surface burning was noticed over the whole area (Figure 5a). After 25 min, the surface resin was burnt and only the first fiber layer remained visible (with the exception of some flames at the specimen edges, Figure 5b). This fiber layer was then separated from the inner face sheet after 35 min and finally melt and fell down after 45 min of fire exposure (Figure 5c). The furnace temperature at that time was approximately 900°C (see Figure 4), and therefore already beyond the softening temperature of the fibers (830°C). Ultimate failure occurred at 49 min and was very sudden without any prior warning. Globally, the whole specimen buckled, as shown in Figure 5d. This global buckling, however, was accompanied or even might have been caused by a series of preceding local failures at the end of the upper protective insulation block (approximately 300 mm from the upper specimen end): separation or delamination between outer face sheet and webs, and buckling of separated webs and outer face sheet were observed at this location.

Water-Cooled Specimens WC1 And WC2

The pre-fire mechanical responses of WC1 and WC2 were almost the same as for the NC specimen. Again similarly to the NC specimen, lateral deflections started increasing towards the fire side with increasing temperature and then decreasing after decomposition started on the hot face, as shown in Figure 5 for WC1 (WC2 results were similar). The maximum lateral deflection, however, was only approximately half that of NC specimen (4.8 mm for WL1 and 4.1 mm for WL2) since decomposition was delayed by the water cooling. After approximately 15 min, the lateral deflection of WC1 stabilized at 4.2 mm (3.0 mm for WC2) and remained almost constant up until the end of the experiment (60/120 min for WC1/2). The temperature progressions are shown in Figure 6 for WC2 (WC1 results were similar). The temperature development close to the hot face (at 2 mm remaining depth) was similar to that of the non-cooled specimen. A significant increase occurred after approximately 50 min close to the hot face (which was similarly visible in the NC specimen at 40 min) where the material was in the decomposition process and the resin above the first fiber layer almost burnt away. The easier heat transfer through this fiber layer might have caused this temperature increase. In contrast to specimen NC, the temperatures at the cold face of the inner face sheet (at 14 mm remaining depth) clearly remained below T_g throughout the experiments (duration of up to 120 min).

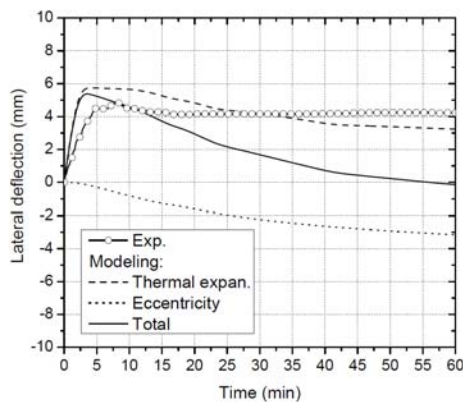


Figure 6. Measured mid-height lateral deflections with time and comparison to modeling results, water-cooled specimen WC1.

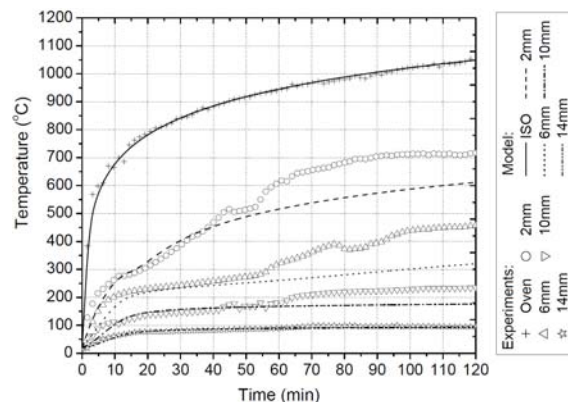


Figure 7. Temperature progression at different depths of inner face sheet of specimen WC2 and comparison to modeling results time.

The visual observations of the hot face of inner WC1/2 face sheets were similar as those for the non-cooled specimen up to 50 min (separation and detachment of one fiber layer). No further changes could be observed for WC1 (up to 60 min) while, after removal of the first fiber layer, the WC2 surface started burning again for approximately 15 min. Subsequently, the flames disappeared; the surface color changed to white and this status remained unchanged up to the end (120 min).

MODELING RESULTS AND DISCUSSION

Temperature responses

To obtain the through-thickness thermal responses of the inner and outer face sheets, the one-dimensional thermal response model proposed by the authors in [9] was applied. The NC modeling results are presented in Figure 4, while the WC2 results are shown in Figure 6. Generally, the predicted thermal responses compared well to the experimental results. The greatest differences were observed at the thermocouples closest to the hot face for layers where the resin had decomposed or was in the decomposition process. The subsequent significant temperature increase could not be captured in the model. The best predictions were obtained for layers below the glass transition temperature.

Time-dependent lateral deflection

During the thermal loading process, lateral deflections changed because of thermal expansion and load eccentricity resulting from the centroid shift due to material degradation. In view of the change of the non-dimensional specimen slenderness, second-order effects occurred.

Assuming the specimen as a hinged column, the time-dependent Euler buckling load $P_E(t_i)$ can be expressed as

$$P_E(t_i) = \frac{\pi^2 \cdot EI(t_i)}{L^2} \quad (1)$$

where L is the specimen height (2825 mm) and $EI(t_i)$ is the time-dependent effective bending stiffness of the specimen. Based on the thermomechanical property model presented in [5], the shift of the neutral axis and the decrease of the Euler buckling load were obtained, see Figure 7.

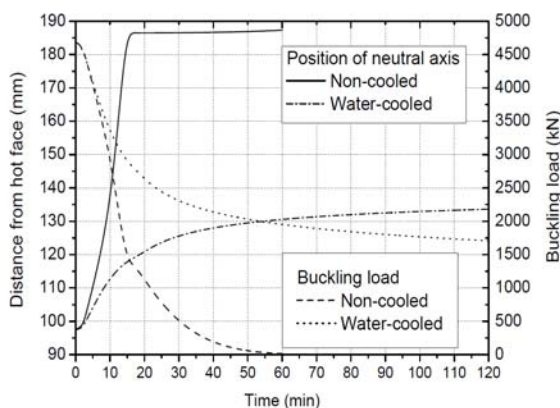


Figure 7. Modeling results for shift of neutral axis and decrease of Euler buckling load with time.

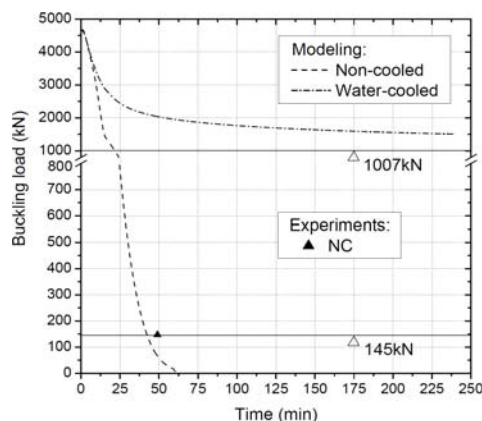


Figure 8. Time-to-failure prediction of NC and WC specimens and comparison to experimental results.

Based on the predicted temperature gradients, the mid-height lateral second-order deflection due to thermal expansion $w_T(t_i)$ at time step t_i was approached by:

$$w_T(t_i) = \frac{\lambda_{c,e}(t_i) \cdot L^2}{8} \cdot \left(\frac{\Delta T}{h} \right)_{t_i} \cdot \frac{1}{1 - P/P_E(t_i)} \quad (2)$$

where $\lambda_{c,e}(t_i)$ is the temperature-dependent effective coefficient of thermal expansion at time step t_i , and P is the applied compressive load.

Assuming that the compressive load always was uniformly distributed over the cross-section, the mid-height lateral second order deflection due to load eccentricity, $w_e(t_i)$, was estimated as follows:

$$w_e(t_i) = e_0(t_i) \left[\frac{1}{\cos\left(\left(\pi/2\right) \cdot \sqrt{P/P_E(t_i)}\right)} - 1 \right] \quad (3)$$

where $e_0(t_i)$ is the eccentricity at time t_i , corresponding to the shift of neutral axis from the initial position due to material degradation.

The calculated second-order lateral deflections due to thermal expansion and eccentricity are shown in Figure 3 for specimen NC and Figure 6 for WC1. The total lateral deflections were obtained by superposing both contributions. The total deflection agreed well with measurements of NC specimen during the first 25 min, but then, in contrast to the measurements, the predicted values greatly increased. For the WC specimen, only a moderately good agreement was found during the first 5-10 min and subsequently the measurements were underestimated. Several reasons may exist for these discrepancies. First of all, the lateral deflections were small, less than 10 mm for the NC and less than 5 mm for the WC specimens. In view of the scale of the experiments, the corresponding measurement accuracy and the complex processes which occurred during the fire exposure, it is difficult to accurately predict such small values. Furthermore, the slenderness of the NC specimen due to material loss largely increased. The corresponding amplification of small values due to second order effects can easily lead to large discrepancies. This may explain why the sharp increase of deflections was predicted to early, after 25 min and not after 49 min where failure occurred.

Time-to-failure

Figure 8 shows that, at ultimate failure, the buckling load of the non-cooled specimen approached the applied load. The 145 kN load level was reached after 43 min, which represents an underestimation of the measured time-to-failure (49 min) of 12%. The buckling load of the water-cooled specimens approached a value of 1007 kN, marked in Figure 8, which represents the buckling load of a specimen which completely lost one face sheet. After the maximum experimental duration (120 min), however, this critical load is still exceeded by almost 70%.

The applied load was limited by the test set-up. Compared to real loads in buildings it was quite small and approximately corresponded, for example, to the

dead load (1 kN/m²) and serviceability load (2 kN/m²) of two floors (in lightweight construction) with a 5-m column spacing. Higher loads would certainly decrease the time-to-failure in the non-cooled case. Using the water-cooling system, however, would allow increasing the load by at least a factor of ten (see Figure 8).

CONCLUSION

Structural fire endurance experiments were conducted on full-scale cellular GFRP columns under axial compression and subjected to ISO834 fire exposure. The following conclusions can be drawn:

1) It was demonstrated that unprotected cellular GFRP columns can resist for more than 30 min to an ISO834 fire from one side. This time-to-failure normally is sufficient for smaller buildings to evacuate occupants.

2) Lateral deflections, which normally accelerate the buckling process, remained small in all the cases due to two counteracting effects: deflections caused by an increasing eccentricity due to material loss were almost compensated by deformations due to thermal expansion.

3) Water-cooling proved to offer an effective active fire protection system. The structural function of the column could be maintained during two hours in the experiments and could easily be extended to four or five hours according to the model prediction.

4) Previously developed models can well describe the time-dependent temperature responses and modulus degradation in both the non-cooled and water-cooled cases, as well as the time-to-failure.

REFERENCES

1. SIA. 1997. "SN 520-183, La protection contre l'incendie dans la construction," Swiss Society of Engineers and Architects, Zurich.
2. Lattimer, B.Y., Ouellette J. 2006. "Properties of composite materials for thermal analysis involving fires," *Composite Part A*, 37: 1068–1081.
3. Bai, Y., Vallée, T., Keller, T. 2007. "Modeling of thermo-physical properties for FRP composites under elevated and high temperatures," *Composites Science and Technology*, 67(15-16): 3098–3109.
4. Feih, S., Mathys, Z., Gibson, A.G., and Mouritz, A.P. 2007. "Modeling the tension and compression strengths of polymer laminates in fire," *Composites Science and Technology*, 67: 551–564.
5. Bai, Y., Keller, T., and Vallée, T. 2008. "Modeling of stiffness of FRP composites under elevated and high temperatures," *Composites Science and Technology*, 68: 3099–3106.
6. Wong, P.M.H., Davies, M.J., Wang, Y.C. 2004. "An experimental and numerical study of the behavior of glass fiber reinforced plastics (GRP) short columns at elevated temperatures," *Composite Structures*, 63: 33–43.
7. Asaro, R.J., Lattimer, B., and Ramroth, W. 2009. "Structural response of FRP composites during fire," *Composite Structures*, 87(4): 382–393.
8. Keller, T., Tracy, C., and Hugi, E. 2006. "Fire endurance of loaded and liquid-cooled GFRP slabs for construction," *Composites Part A*, 37(7): 1055–1067.
9. Bai, Y., Vallée, T. and Keller, T. 2008. "Modeling of thermal responses for FRP composites under elevated and high temperatures," *Composites Science and Technology*, 68(1): 47–56.

Influence of Moisture Transport on Fire Resistance of Steel Concrete Composite Slab

T. HOZJAN, J. KOLSEK, M. SAJE, I. PLANINC, S. BRATINA
and S. SRPCIC

ABSTRACT

The paper discusses the effect of moisture transport in concrete on the fire resistance of a steel-concrete composite slab. A comprehensive model of slow transient phenomena involving a simultaneous heat and mass transport and the pore pressure increase in concrete, proposed by Tenchev et al. [Tenchev, R.T., Li, L.Y., Purkiss, J.A. (2001) Num. Heat Transfer Part A, 39: 685–710] is employed in the thermal analysis of a steel-concrete slab employing the trapezoidal thin sheet for panelling, and the results compared to the simplified thermal analysis in which only the heat flux is taken into account. This way the effect of moisture on the temperature field development in steel-concrete composite slab during fire is assessed. The further mechanical analysis reveals that the fire resistance of the steel-concrete composite slabs depends mainly on the time the temperature in additional reinforcement bars reaches the critical temperature. These bars which are placed in each wave are redundant at room temperature, but must be there to guarantee a sufficient fire resistance. The analysis shows that temperature in these bars depends mainly on the thickness of the protection layer of concrete. Finally, the position of these reinforcement bars is optimized.

Tomaž Hozjan, Ph.D., University of Ljubljana, Faculty of Civil of Geodetic Engineering, Jamova 2, SI-1115 Ljubljana, Slovenia

Jerneja Kolšek, Ph.D. Student, Kraški Zidar d.d., Kolodvorska ulica 1, SI - 6210 Sežana, Slovenia

Miran Saje, Professor, University of Ljubljana, Faculty of Civil of Geodetic Engineering, Jamova 2, SI-1115 Ljubljana, Slovenia

Igor Planinc, Associate Professor, University of Ljubljana, Faculty of Civil of Geodetic Engineering, Jamova 2, SI-1115 Ljubljana, Slovenia

Sebastjan Bratina, Ph.D., University of Ljubljana, Faculty of Civil of Geodetic Engineering, Jamova 2, SI-1115 Ljubljana, Slovenia

Stanislav Srpčič, Associate Professor, University of Ljubljana, Faculty of Civil of Geodetic Engineering, Jamova 2, SI-1115 Ljubljana, Slovenia

INTRODUCTION

Composite concrete–trapezoidal steel plate slabs are widely used construction elements in buildings and bridges. The main reason is their highly efficient design. During the course of construction, the trapezoidal steel plate replaces panelling, while after hardening of concrete, the two materials work as a composite slab, in which the steel plate represents an external reinforcement. For a better load redistribution and to minimize cracking, the composite steel–concrete slabs are nearly always additionally reinforced, typically with steel reinforcement meshes. The use of strong ribbed reinforcing bars for the purpose of increasing bending capacity is rare. If a composite slab is exposed to fire to achieve a sufficient fire resistance, an additional reinforcing with ribbed reinforcing bars is necessary because the steel plate is directly exposed to fire and the bearing capacity of steel rapidly decreases with an increasing temperature, especially beyond the temperature 400°C when viscous creep emerges in steel and, consequently, the beneficial effect of the steel plate on the composite slab is lost. Therefore, the reinforcing bars within the concrete slab constitute an essential reinforcement of the concrete cross-section. Typically one or two bars suffice in every wave of the slab. The distance between the bars and the exposed surface has to be large enough to reduce their heating rate during fire.

There are a number of mathematical models available to determine the temperature field in the composite concrete–trapezoidal steel plate slab. More complex models consider the moisture effect in concrete to determine the temperature field. One of the first models was presented by Luikov [8]. He described the coupled heat and mass transfer through permeable porous materials. Later a somewhat modified Luikov model, adapted for the study of temperature and pore pressure transport in concrete during fire was introduced by Bažant and Thonguthai [2]. Their model is capable of considering the dehydration process of chemically bound water in concrete, while the free water evaporation and condensation in concrete are neglected. This model was later on supplemented by Davie et al. [3] and Tenchev et al. [9], among others. The model can be considered rather complete for the analysis of concrete structures in fire. An even more advanced model where heat and mass transfer and mechanical deformations are considered as coupled is given in [5].

In this paper we present an improved numerical model for the analysis of steel–concrete composite slabs subjected to fire loads. For the description of slow transient phenomena involving heat and mass transport and the pore pressure increase in concrete, a somewhat modified thermo-hydro-chemical model of Tenchev [9] is employed. In this model the influence of moisture on temperature development is accounted for. A simplified thermal analysis in which only the heat flux is taken into account is also performed. When the results of the two models are compared, the influence of moisture on the distribution of temperature and consequently on fire resistance of steel–concrete composite slab is assessed.

HEAT AND MASS TRANSFER IN CONCRETE SLAB

A coupled heat and moisture transfer in concrete exposed to fire can be mathematically described with a system of mass conservation equations for each phase of concrete separately and with an energy conservation equation [9] as follows:

Water conservation:

$$\frac{\partial \bar{\rho}_L}{\partial t} = -\nabla \mathbf{J}_L - \dot{E}_L + \frac{\partial \bar{\rho}_D}{\partial t} \quad (1)$$

Water vapour conservation:

$$\frac{\partial (\varepsilon_G \bar{\rho}_V)}{\partial t} = -\nabla \mathbf{J}_V + \dot{E}_L \quad (2)$$

Air conservation:

$$\frac{\partial (\varepsilon_G \bar{\rho}_A)}{\partial t} = -\nabla \mathbf{J}_A \quad (3)$$

Energy conservation:

$$(\underline{\rho C}) \frac{\partial T}{\partial t} = -\nabla \cdot (-k \nabla T) - (\underline{\rho C v}) \cdot \nabla T - \lambda_E \dot{E}_L - \lambda_D \frac{\partial \bar{\rho}_D}{\partial t} \quad (4)$$

In Eqs. (1)–(4), ρ_i is the density of a phase i , \mathbf{J}_i is the mass flux of phase i per unit volume of gaseous material, $\varepsilon_G \bar{\rho}_V$ and $\varepsilon_G \bar{\rho}_A$ are mass concentrations of air and water vapour per unit volume concrete, \dot{E}_L is the rate of evaporation of free water (including desorption), t is time. Index i denotes each phase separately: L is free water, V is water vapour and A is dry air. In Eq. (4) $\underline{\rho C}$ is heat capacity of concrete, k is thermal conductivity of concrete, $\underline{\rho C v}$ relates to the energy transferred by fluid flow, λ_E is the specific heat of evaporation, λ_D is specific heat of dehydration and T is the absolute temperature.

The mass fluxes of dry air, water vapour and free water can be expressed in terms of pressure and concentration gradients assuming that Darcy's and Fick's law are applicable and that the diffusion of adsorbed water on the surface of solid cement phase skeleton is negligible:

$$\mathbf{J}_A = \varepsilon_G \bar{\rho}_A \mathbf{v}_G - \varepsilon_G \bar{\rho}_G D_{AV} \nabla \left(\frac{\bar{\rho}_A}{\bar{\rho}_G} \right) \quad (5)$$

$$\mathbf{J}_G = \varepsilon_G \bar{\rho}_V \mathbf{v}_G - \varepsilon_G \bar{\rho}_G D_{VA} \nabla \left(\frac{\bar{\rho}_V}{\bar{\rho}_G} \right) \quad (6)$$

$$\mathbf{J}_L = \bar{\rho}_L \mathbf{v}_L \quad (7)$$

The fluxes are defined per unit area of concrete. In Eqs. (5)–(7), D_{AV} and D_{VA} are the diffusion coefficients of dry air in water vapour and water vapour in dry air within the porous concrete, and \mathbf{v}_G and \mathbf{v}_L are the velocities of the gas and liquid water phases resulting from a pressure-driven flow as given by Darcy's law:

$$\mathbf{v}_G = -\frac{KK_G}{\mu_G} \nabla P_G \quad (8)$$

$$\mathbf{v}_L = -\frac{KK_L}{\mu_L} \nabla P_L \quad (9)$$

Here K is the intrinsic permeability of dry concrete, K_G and K_L are the relative permeabilities of the gas and liquid phase, μ_G and μ_L are their dynamic viscosities, and P_G and P_L are the corresponding pressures. As in the model proposed by Tenchev *et al.* [9,10], it is here assumed that the liquid pressure is equal to the gas pressure, $P_G = P_L$. It is also assumed that air and water vapour behave as an ideal gas and the content of free water, $\bar{\rho}_L$, is determined using sorption curves defined by Bažant *et al.* [1]. As already mentioned a simplified thermal analysis is also performed in which only the heat flux is taken into account. Mathematically the heat flux problem is described with Fourier's Law of thermal conduction:

$$(\underline{\rho C}) \frac{\partial T}{\partial t} = -\nabla \cdot (-k \nabla T) \quad (10)$$

By summing Eqs. (1) and (2) we end up with three partial differential equations. The solution is obtained numerically with the finite element method, where the primary unknowns of the problem are temperature T , pore pressure P_G and water vapour content $\bar{\rho}_V$. For a detailed description of the problem and its numerical formulation, see [9].

NUMERICAL EXAMPLE

We consider a steel–concrete composite slab exposed to standard fire ISO 834 [7]. Fig. 1 presents geometric data, load data and the 2D finite-element mesh, which was used to determine the heat and mass transfer in the composite slab. We consider two examples. In the first example (A1), we consider the steel sheet on the lower, heated surface to be a diffusion barrier. This way the mass flux through the lower surface (edge 1) is not allowed, i.e. the mass flux is equal to zero. Mass flux is, however, allowed on edge 2. In the second example (A2) we neglect the influence of moisture transport in heat transport, so that the time and space distributions of temperature in the composite slab is obtained by the solution of Eq. (10).

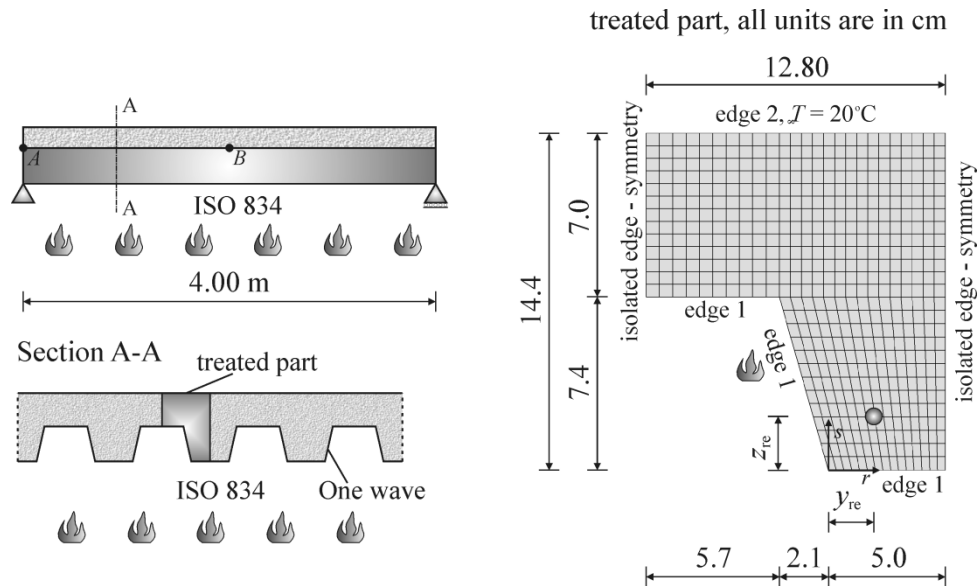


Figure 1. Scheme of composite plate and 2D finite element mesh.

The slab is heated from the lower side (edge 1), while at edge 2 an ambient temperature 20°C is assumed. A complete list of details about the boundary conditions is given in Table 1. The remaining data are: density of concrete $\rho_c = 2400 \text{ kg/m}^3$, density of cement $\rho_{\text{cem}} = 300 \text{ kg/m}^3$, temperature $T_0 = 20^\circ\text{C}$, initial pore pressure $P_{G,0} = 0.1 \text{ MPa}$, initial water vapour content $\bar{\rho}_{v,0} = 0.0111 \text{ kg/m}^3$, water vapour content on boundary $\bar{\rho}_{v,\infty} = 0.0089 \text{ kg/m}^3$, initial porosity of concrete $p_{\text{or}}^0 = 0.15$, initial permeability of concrete $K = 1 \cdot 10^{-16}$ and initial free water amount $\bar{\rho}_{L,0} = 10 \text{ kg/m}^3$. Heat transfer coefficient and emissivity on edge 1 is taken to be equal to $h_q = 25 \text{ W/m}^2\text{K}$ and $e = 0.6$, respectively; on edge 2, which is not exposed to fire, the heat transfer is $h_q = 9 \text{ W/m}^2\text{K}$. The time step is taken to be equal to 0.5 s in case A1 and equal to 20 s in case A2. The variation of specific heat and thermal conductivity of concrete with temperature was taken according to EC 2 [4]. Variation of the remaining temperature dependent parameters that are needed in the more advanced model (case A1) are taken as in [9].

To assess the effect of steel sheet as a diffusion barrier, in Fig. 3 we present the time development of temperatures in some characteristic points, whose positions are chosen such that they could present natural positions for additional reinforcing bars to achieve a sufficient bearing capacity of this type of a composite slab when exposed to fire. The coordinates of the points are presented in Table 1.

Table 1. Coordinates of characteristic points A, B, C, D and E.

point	y_{re} [cm]	z_{re} [cm]
A	2.5	2.5
B	2.5	3
C	2.5	4
D	2.5	5
E	2.5	6

The comparison of the results for cases A1 and A2 shows that the time development of temperature differs substantially. The differences between the models appear only above 100°C. In case A1 temperature is increasing slower than in case A2. An additional energy is needed for the phase change of liquid water into water vapour and this causes some delay in temperature development. Once liquid water is fully transformed into water vapour, the temperature difference between cases A1 and A2 appears almost constant. For instance, the difference in temperature in point D at time 30 min is 26°C, at 60 min 27°C and at 90 min 22°C. The illustration of the distribution of pore pressure over the cross-section at chosen times is presented in Fig. 3. The steel sheet as a diffusion barrier has a substantial effect on pore pressures. In this case the whole amount of free water and water vapour is pushed by the temperature and pore pressure gradients to the upper, free edge 4, where water evaporates to the outside. Beyond 200 °C, the chemically bounded water starts releasing and increases the volume of free water. At some moment of time, a full saturation in pores takes place which causes the rise of the pore pressure. The magnitude of pore pressure at 30 min is about 4.5 MPa and is almost homogeneous over the flange of the concrete slab (Fig. 3).

As the steel sheet is directly exposed to high temperatures, it loses its bearing capacity shortly after fire begins. The additional reinforcement bars, if any, are then essential to be there. That is

why fire resistance of composite slab in terms of the resistance time can rather well be estimated on the basis of actual temperatures in the additional reinforcement bars placed in the web.

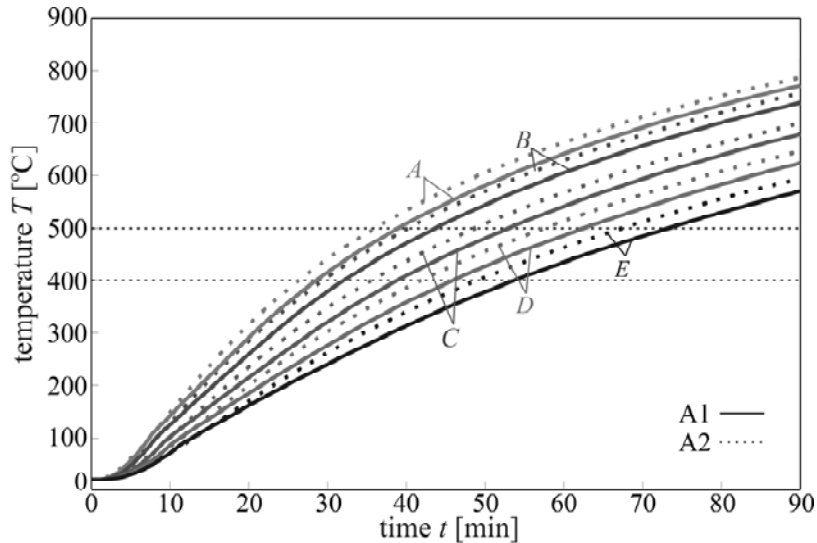


Figure 2. Variation of temperature with time in points *A*, *B*, *C*, *D* and *E*.

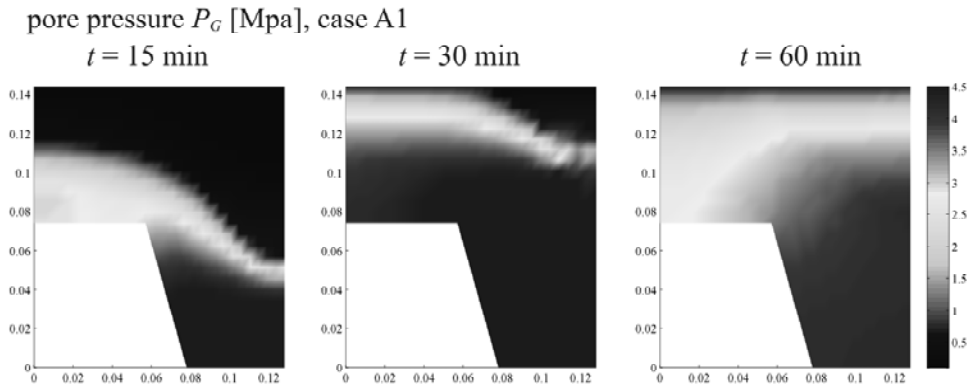


Figure 3. Distribution of pore pressures over the cross-section at chosen times in case A1.

The bearing capacity of the slab in fire is largely dependent on the temperature gradient. As we can see from Fig. 2, the temperature difference between the two neighbouring points is about 65°C per 1 cm at 90 min, which results in the temperature difference between points *A* and *E* to be roughly 200°C. These data can be used for determining an optimal position of an additional reinforcing bar in order to achieve a sufficient fire resistance of the composite slab. With a relatively small change in position of the reinforcing bar away from the lower surface of the composite slab, we can increase its fire resistance substantially. We have to be very careful, however, because the change of position means a somewhat smaller static height. The optimal position of an additional reinforcing bar was found in [6].

As the steel sheet is directly exposed to high temperatures, it loses its bearing capacity shortly after fire begins. The additional reinforcement bars, if any, are then essential to be there. That is why fire resistance of a composite slab in terms of the resistance time can rather well be estimated on the basis of actual temperatures in the additional reinforcement bars placed in the web. It is well known that creep strains of mild steel start increasing at about 400°C [10]. At

roughly 500°C, the creep strain rates become pronounced and dictate the failure of the slab. Therefore it is plausible to estimate the resistance time of the composite slab on the basis of the critical temperature in the additional reinforcement. That is, we may assume that loss of resistance is strongly related to the instant the temperature of the additional reinforcement bar reaches 500°C. If we look back to Fig. 2, where the time development of temperatures at various vertical locations, z_{re} , appropriate for placing additional reinforcement bars in the cross-section is presented, we observe, as expected, the rise of temperature in the reinforcement bar is smaller for bars placed higher. The critical temperature, $T_{cr} = 500^\circ\text{C}$, for $z_{re} = 4$ cm is reached in 58 min and for $z_{re} = 6$ cm in 83 min for case A1, while in case A2, the critical temperature is reached at 49 min and 68 min. Notice a big difference in time compared to a relatively small change in the vertical position. This becomes even more clear in Fig. 4a, where the relation between the temperature and the vertical position z_{re} is presented for $t = 30, 60,$ and 90 min. Using the simplified EC2 [4] Annex procedure gives us the minimum area of the steel bar. The minimum area of the steel bar is determined for the simply supported beam discussed here (Fig. 1), when subject to the uniform non-accidental external load $q = 1.52 \text{ kN/m}$ [6]. In the calculation, the following material parameters for concrete and reinforcement steel at room temperature were adopted: strength of concrete $f_{ck,20} = 3.0 \text{ kN/cm}^2$ and yield strength of steel $f_{yk,20} = 40 \text{ kN/cm}^2$.

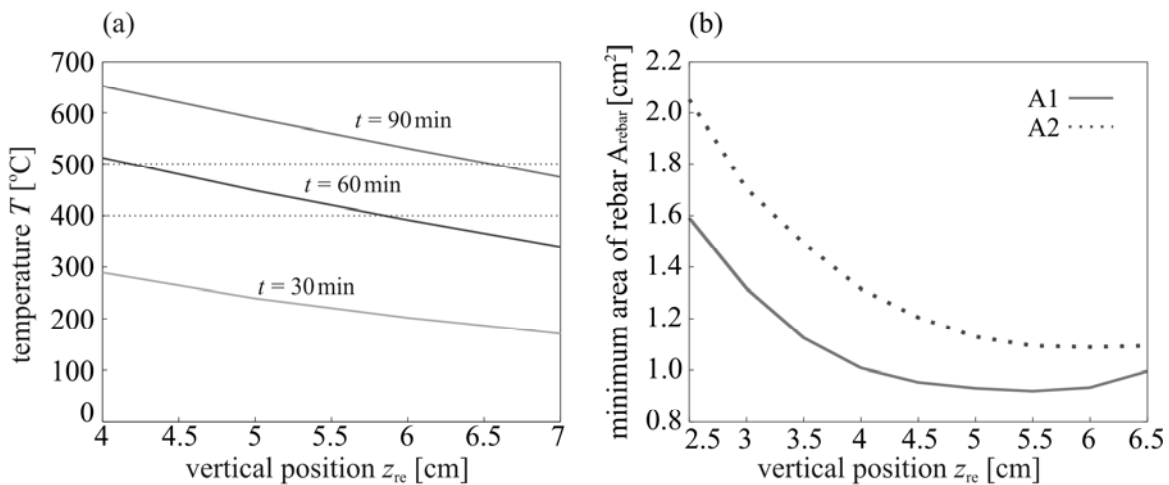


Figure 4. (a) Variation of temperature with vertical position z_{re} at $t = 30, 60,$ and 90 min for case A1. Minimum area of reinforcement bars in case A1 and A2.

In Fig. 4(b) the graphs of the minimum area of the reinforcement bar required are depicted. The comparison of results of cases A1 and A2 shows that, in case A2, the minimum area of the bar is bigger than in case A1. This difference can even grow further, up to 30%. We also observe that the minimum area of the reinforcement bar decreases with the rise of the vertical position z_{re} only up to a certain point and, afterwards, due to a smaller static height, increases again.

CONCLUSIONS

The simply-supported composite concrete–trapezoidal steel sheet slab is a widely used structural element in engineering. Often its resistance to fire applied from below is of prime importance. The objectives of the present study were hence to find the area and optimal position of the steel

reinforcement bar in the web such that its fire resistance is within a chosen time resistance class and to present the influence of moisture transport on the fire resistance of a trapezoidal steel plate-concrete composite slab. The temperature development in a steel-concrete composite slab was determined twice: first with the use of a more advanced coupled model of slow transient phenomena involving the heat and mass transfer which takes into account the influence of moisture and vapour transport, and then with a simplified model, where the heat flux was only taken into account. Due to a slow temperature diffusion in concrete, a big difference in the resistance time follows after a small change in the vertical position of the bar. As seen, the moisture transport has a noticeable influence on the results. For the composite slab investigated here, the error in the critical time estimated according to the critical temperature in reinforcement bars, $T_{cr} = 500$ °C, is around 10 minutes (18%) and in the required range of reinforcement bars amounts to 30%. From these results we can conclude that the effect of moisture on the fire resistance of steel-concrete composite slab is worth studying.

ACKNOWLEDGMENTS

The work of J. Kolšek was partly financially supported by the European Union, European Social Fund. The support is gratefully acknowledged.

REFERENCES

1. Bažant, Z.P. and Kaplan M.F., "Concrete at high temperatures: material properties and mathematical models," Longman, Harlow (1996).
2. Bažant, Z.P. and Thonguthai, W., "Pore pressure and drying of concrete at high-temperature," *J. Eng. Mech. Division – ASCE*, 104(5), (1978), pp. 1059–1079.
3. Davie, C.T., Pearce, C.J. and Bičanić, N., "Coupled heat and moisture transport in concrete at elevated temperatures – Effects of capillary pressure and absorbed water," *Num. Heat Transfer Part A*, 49, (2006), pp. 733–763.
4. Eurocode 2., "Design of Concrete Structures, Part 1.2: Structural fire design," European Committee for Standardization, (2004).
5. Gawin, D., Pesavento, F. and Schrefler, B.A., "Towards prediction of the thermal spalling risk through a multi-phase porous media model of concrete," *Compt. Methods Appl. Mech. Eng.*, 195, (2003), pp. 5707–5729.
6. Hozjan, T., "Nonlinear analysis of composite planar structures exposed to fire," University of Ljubljana, Faculty of Civil and Geodetic Engineering, Doctoral thesis, (in Slovene), (2009).
7. ISO 834. 1975. "Fire resistance tests – elements of building constructions," International Standard ISO 834.
8. Luikov, A.V., "Systems of differential equations of heat and mass transfer on capillary-porous bodies (review)," *Int. J. Heat Mass Transfer*, 18, (1975), pp. 1–14.
9. Tenchev, R.T., Li, L.Y. and Purkiss, J.A., "Finite element analysis of coupled heat and moisture transfer in concrete subjected to fire," *Num. Heat Transfer Part A*, 39, (2001), pp. 685–710.
10. Tenchev, R.T. and Purnell, P., "An application of a damage constitutive model to concrete at high temperature and prediction of spalling," *Int. J. Solids & Struct.*, 42, (2005), pp. 6550–6565.
11. Williams-Leir, G., "Creep of structural steel in fire: Analytical expressions," *Fire and Materials*, 7(2), (1983), pp.73–78.

Numerical Modelling of Membrane Action of Composite Slabs in Fire Situation

C. VULCU, TH. GERNAY, R. ZAHARIA and J. M. FRANSSSEN

ABSTRACT

Membrane action in fire is now an intensively researched area, for which more improvement is always necessary. The paper presents some numerical simulations, done with the SAFIR program, in order to derive more simple models for representing the partially protected composite floors in fire situation. The numerical models are calibrated using the results of three full scale tests that have been performed in recent years.

INTRODUCTION

Several full-scale fire tests on composite steel-concrete slabs have shown that the load transfer mode in the slab, that relies essentially on bending at room temperature, changes to membrane behaviour in the fire situation, due to the large deflections created by thermal gradients. Appropriate understanding and modelling of this particular behaviour allows a safe approach, but also substantial savings on the thermal insulation that has to be applied on the underlying steel structure.

A complete and detailed numerical modelling of the membrane effect is quite complex and CPU time consuming, due to the simultaneous presence of beams and of orthotropic shells. If such a numerical simulation can be done in research centres and universities, it is not practically applicable for real projects that have to be analyzed in shorter time.

The first objective of the research presented in this paper is to derive more simple models for representing the partially protected composite floors in fire situation that, on the price of simplifications and approximations, would nevertheless yield a sufficiently close to reality representation of the structural behaviour and a safe estimate of the load bearing capacity.

C. Vulcu, R. Zaharia, The "Politehnica" University of Timisoara, 2, Pta. Victoriei, Timisoara, Romania

Th. Gernay, J. M. Franssen, Université de Liège, 1, Chemin des Chevreuils, 4000, Liège, Belgium

The second objective is to highlight the influence of some critical parameters on the behaviour and fire resistance of composite slabs such as the amount of reinforcing steel in the slab, the thickness of the slab, the load level and the flexibility of the protected edge beams.

The calibration of the numerical models is based on the results of three full scale tests that have been performed in recent years in order to investigate various aspects of the tensile membrane action: two have been performed by CTICM in France, FRACOF [1] and COSSFIRE [1], and one by the Czech Technical University in Prague, in the Czech Republic [3]. Different parametric analyses have been performed on these tests with the advanced calculation model SAFIR of the University of Liege [4].

FRACOF TEST AND NUMERICAL SIMULATION

Considering the size of used fire furnace, the designed test specimen covered an area of 7.35 m by 9.53 m [1], see Figure 1. The specimen comprised 4 secondary beams, 2 primary beams, 4 short columns and a 155 mm thick floor slab incorporating a reinforcing steel mesh of 256 mm²/m located at 47 mm over the steel sheet. The composite steel and concrete slab was realised with open trapezoidal steel sheet of 0.75 mm thickness. A uniformly distributed load of 3.87 kN/m² was applied on the slab. The two central secondary beams and the composite slab were unprotected, while all other beams and the columns were fire protected. The ISO fire exposure lasted up to 120 minutes, moment when the fire was stopped due to integrity failure of the floor.

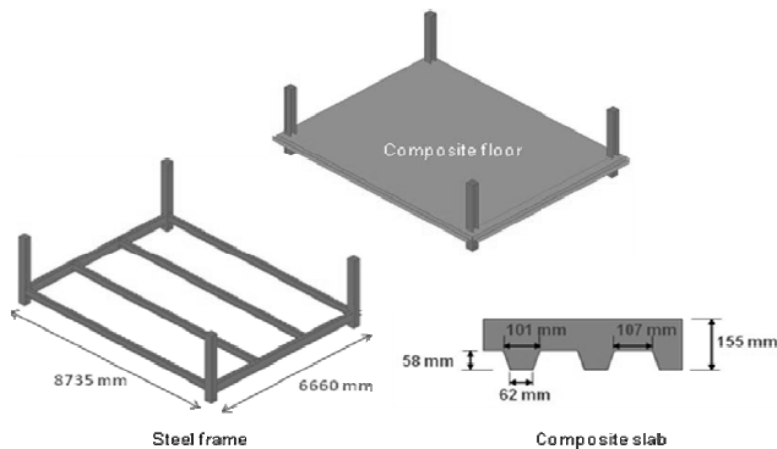


Figure 1. Tested structure.

For the temperature in protected beams, there is a certain level of uncertainty for *a priori* simulations because only the nominal values of thermal properties are known and some differences can be observed between the predicted and the measured steel temperature. The predictions are much more reliable for unprotected beams. For the thermal analysis, the cross section of the slab containing ribs has been replaced by a section with an average thickness calculated according to EC4-1-2 Annex D [5] which, for this profile, yielded sufficiently accurate estimation of the temperature at the level of the bars, see Figure 4.

The beams have been idealised using beam elements, and the slab using shell elements. According to the connection details from the test, the beam-to-column and beam-to-beam joints were modelled as simple connections. The bars have been modelled as smeared layer having only uniaxial strength and stiffness. For the material properties, the nominal values have been used, not the measured ones.

In Figure 2, the calculated deformed shape and the membrane stresses in the slab are shown, at 165 minutes, i.e. just before failure was reached in the numerical the simulation. At this moment, the structure failed due to large deflections of the secondary edge beams. The membrane action, characterised by the equilibrium between the compression of the concrete on the edges of the slab and the tension in the bars in the middle of the slab, was overreached, and the slab could not support the load any longer. The chart shows the comparison between the measured and the calculated deflection at the centre of the slab.

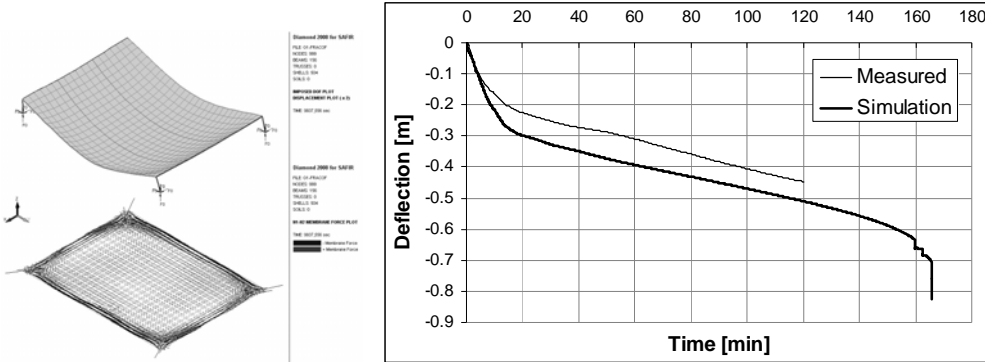


Figure 2. Deformed shape and membrane forces—Deflection in the middle of the slab.

COSSFIRE TEST AND NUMERICAL SIMULATION

The COSSFIRE test [2] was part of a project with the objective to propose design rules for the beam-to-column connections when exposed to a natural fire. The designed test specimen covered an area of 6.66 m by 8.5 m. A specific test specimen shown in Figure 3 was adopted, composed of 5 secondary beams, 4 primary beams, 6 short columns and a 135 mm thick deck incorporating a reinforcing steel mesh of 251 mm²/m located at 35 mm over the trapezoidal steel sheet Cofraplus60, with 0.75 mm thickness. A uniformly distributed load of 3.75 kN/m² was applied on the slab. The two middle secondary beams and the composite slab were unprotected, while all the boundary beams of the floor were fire protected. The ISO fire exposure lasted up to 120 minutes.

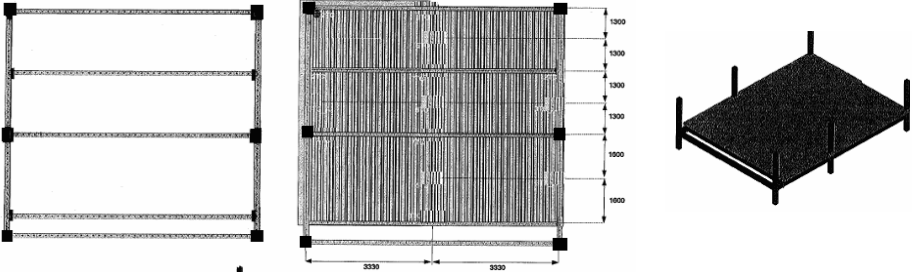


Figure 3. Tested structure.

Here also, the temperatures calculated in the unprotected beams were closer to the observed temperatures than those calculated in the protected edge beams and the temperatures calculated in the bars of the slab on the base of the equivalent thickness as recommended by Eurocode 4 were reasonably close to the temperatures observed during the test, see Figure 5.

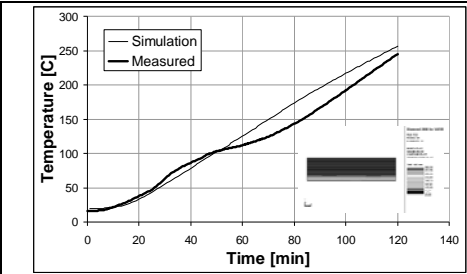


Figure 4. Temperature variation in the slab at rebar level (FRACOF).

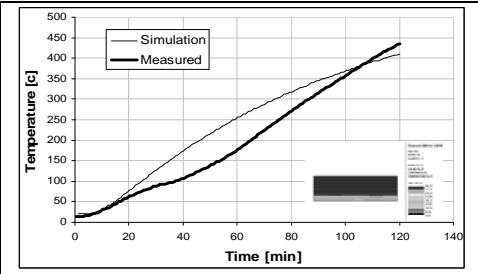


Figure 5. Temperature variation in the slab at rebar level (COSSFIRE).

In Figure 6, the deformed shape and the membrane forces of the slab after 150 minutes are shown. At this moment the composite slab failed, in the same manner as for the model of Fracof structure, due to the large deflections of the secondary edge beam. In the chart, a comparison between the measured and the calculated deflection of the middle of the slab is shown.

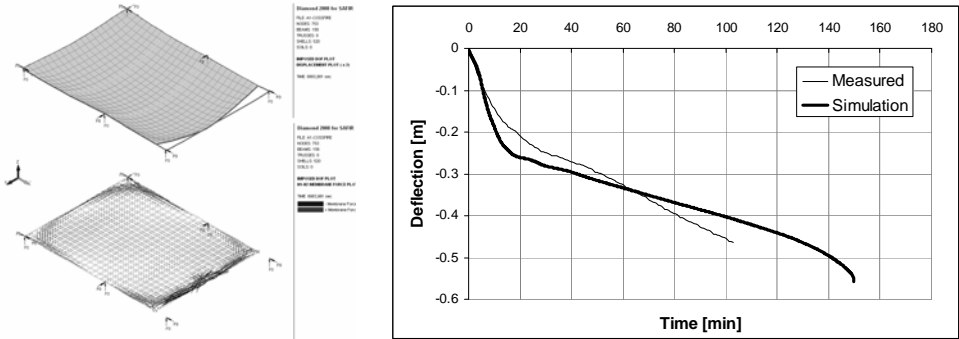


Figure 6. Deformed shape and membrane forces – Deflection in the middle of the slab.

PRAGUE TEST AND NUMERICAL SIMULATION

The aim of the fire test was to observe the overall behaviour of the structure, which may not be observed in tests performed on separate elements. Three types of flooring systems [3] and six wall structures with mineral wool were tested. The construction of the experimental building is documented on Figure 7.

The experimental structure represents one floor of an administrative building of 18 x 12 m. The composite slab on the castellated covered an area of 9 x 12 m² and beams with corrugated webs an area of 9 x 6 m². The deck was a simple trapezoidal composite profile of 60 mm depth with 60 mm of concrete over the profile, reinforced by a smooth mesh of $\phi 5$ mm 100/100 mm (i.e. 196 mm²/m) located 20 mm over the profile.

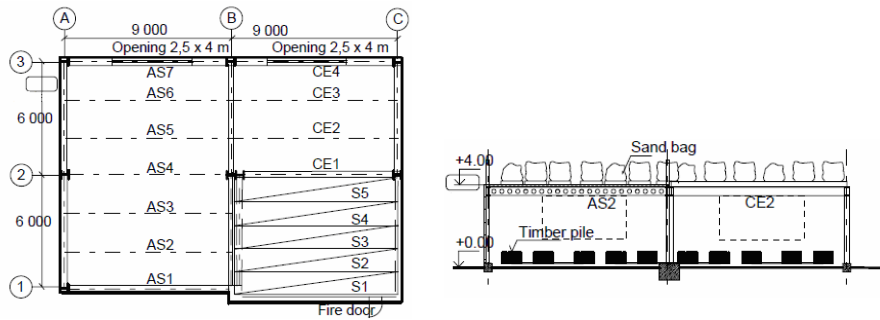


Figure 7. Tested structure.

The dead load of the tested structure reached 2,6 kN/m². The variable load of 3,0 kN/m² was simulated by sand bags. The fire load of 620 MJ/m² for this natural fire tests consisted wooden cribs. The openings of 2.54 m height and a total length of 8.00 m ventilated the compartment. To allow a smooth development of fire, no glazing was installed.

Under the composite slab with castellated beams, a temperature of 935°C was measured after 60 minutes. The collapse of the slab occurred after 62 minutes, at the beginning of the cooling phase of the fire, with the measured temperature of the lower flange of the beam at the mid span equal to 895 °C.

The numerical simulation was performed for the 9x6 m² zone where the slab is supported by Angelina beams. The columns and the cross braces were not modelled. Therefore, the analysis was realised only for the Angelina beams, the composite slab, and two types of protected edge beams.

A fire curve has first been obtained with OZone program and used further in the thermal analysis. This curve is compared in Figure 8.a) with the measured gas temperatures at the test. Figure 8.b) shows the comparison for the temperature in the lower flange of the Angelina beams.

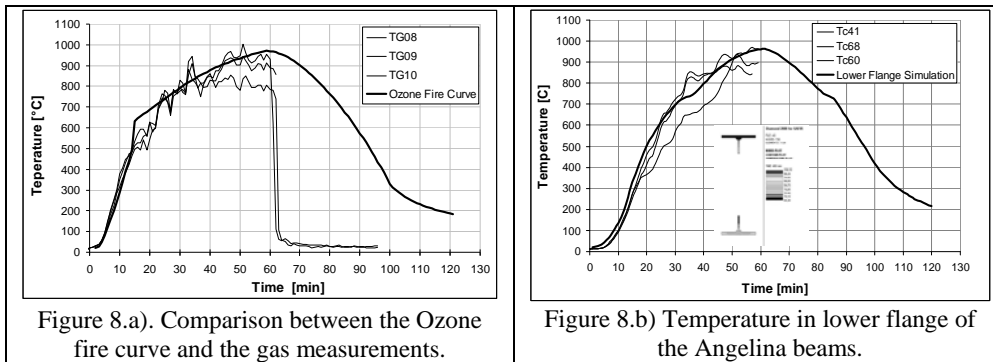


Figure 8.a). Comparison between the Ozone fire curve and the gas measurements.

Figure 8.b) Temperature in lower flange of the Angelina beams.

The castellated beams were modelled using the “minimum section” for the entire length of the beam. For the thermal distribution, the section of the slab containing ribs has also been replaced by a section with an average thickness.

In the numerical model, the edge beams and the unprotected Angelina beams were idealised using beam elements, and the slab using shell elements. Vertical supports have been used instead for the columns, and horizontal restrains for the cross braces and for the continuity of the slab.

Figure shows the deformed shape and the membrane forces of the slab at failure, namely a concrete failure in the corner of the slab, see Figure 9. The

chart shows the deflection curve from the simulation compared to the measured deflection from the test for the middle area of the slab.

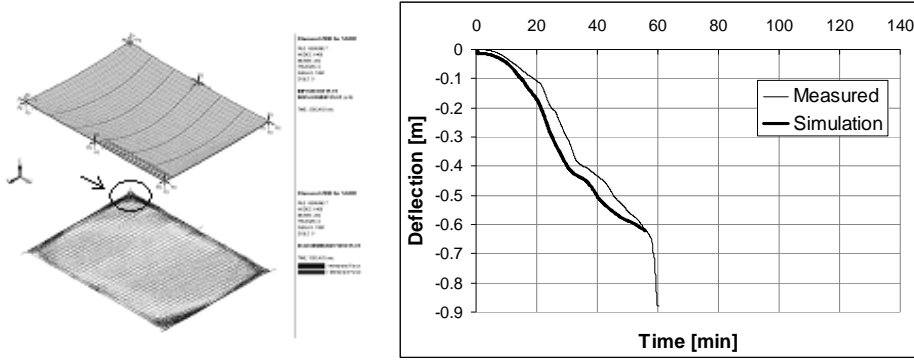


Figure 9. Deformed shape and membrane forces – Deflection in the middle of the slab.

PARAMETRIC STUDY

For the tree tests, a sensitive analysis has been performed in order to see the influence of a number of parameters on the mechanical response of a composite slab. For the Prague test, the study aimed also to identify what could have improved the behaviour of the slab. For each parameter, one or more simulations have been done and then compared with the reference numerical models presented above. The investigated parameters are:

- the vertical supports on the edges;
- the thickness of the slab;
- the amount of reinforcement;
- the modelling of the unprotected beam;
- the influence of the lateral restraints of the slab;

Influence of the vertical supports on the edges

For the three tests, a model was built in which all the edges of the composite slab were fully restrained vertically. The aim was to see how important the stiffness of the edge beam is. In all three cases, the slab with full vertical fixity on the edges resisted a longer time to the fire exposure, see Figure 10, because the plastic hinge that otherwise formed in the secondary edge beams was avoided. For the Fracof and Cossfire tests the collapse of the slab was not reached after 4 and respectively 3 hours of ISO fire exposure. For the Prague test, the collapse at 61 minutes was also avoided.

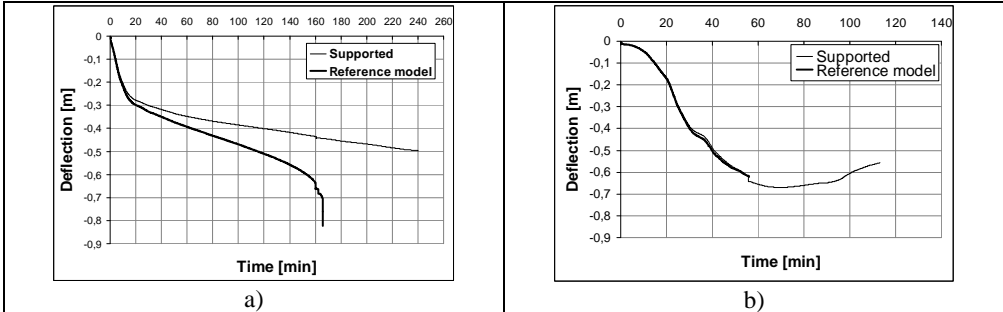


Figure 10. Influence of the supports on the edges: a) FRACOF c) PRAGUE.

Influence of the thickness of the slab

Models with different thickness of the slab were considered. Figure 11 shows that a higher thickness leads to lower deflections, with a minimum thickness being required to achieve stability, the value of this minimum thickness being somehow different in each test.

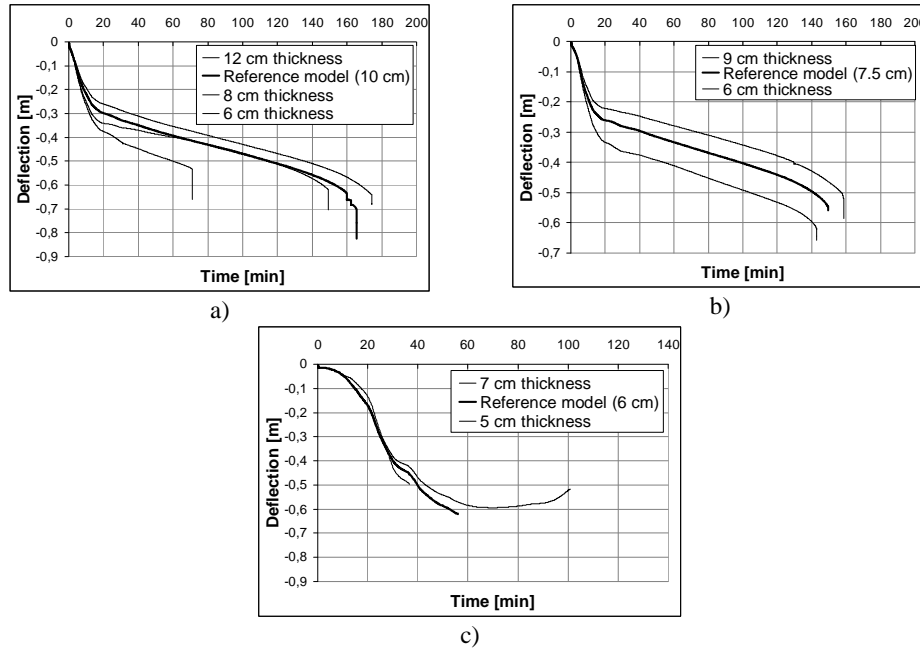


Figure 11. Influence of the slab thickness: a) FRACOF b) COSSFIRE c) PRAGUE.

Influence of the amount of reinforcement

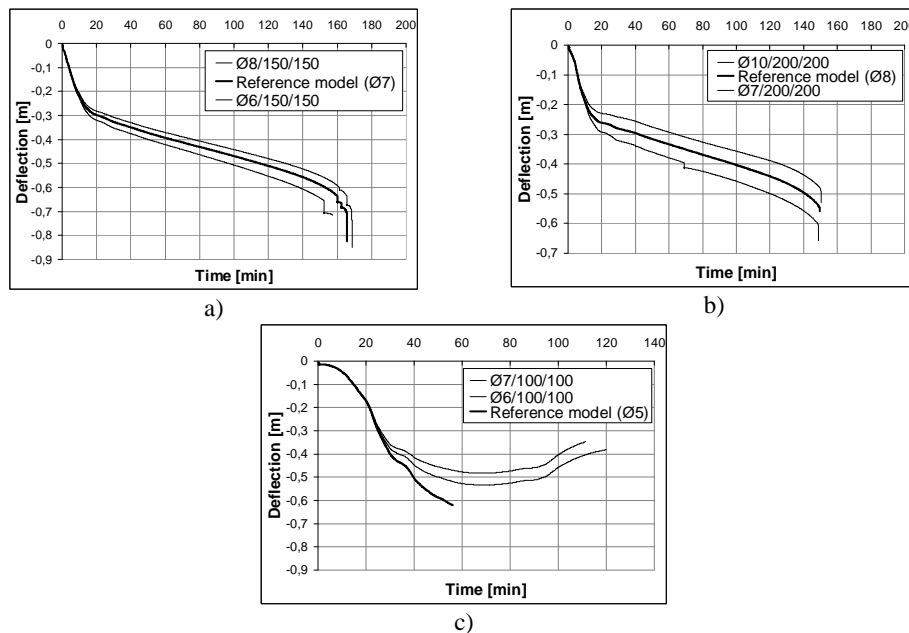


Figure 12. Influence of the reinforcement: a) FRACOF b) COSSFIRE c) PRAGUE.

Models with different quantities of reinforcements were considered with nearly unchanged results for the first 2 tests and a dramatic improvement in the test of Prague, see Figure 12.

Modelling of the unprotected beam

For the three tests, besides the reference model, a second model has been considered, in which the unprotected secondary beams were neglected, or just a part of the section has been modelled. For the Prague test, the secondary beams were castellated beams, and the question was how to model these, or whether it is really necessary to model these at all. Figure 13 shows the deflection for the reference models and the models without unprotected beam.

For the Fracof test, in case the unprotected beams were neglected, the transition from the compressive membrane to the tensile membrane was “violent” so that the yield lines formed leading to the failure of the slab before the total load could be applied.

For the Cossfire test, in case the unprotected beams were not present, the slab entered from the beginning into tensile membrane. As the fire develops, the deflection curve converged towards the same curve as the one obtained when the unprotected beams are present in the model.

For Prague test, using just the upper T for the castellated beams lead to large deflections at the beginning of the test, but the deflection curve did not converged to the same displacement and time resistance. Using the minimum section (the upper and lower T) for the Angelina beams lead to a good correlation with the test, but in the case where just the upper T was used, an early failure of the slab occurred.

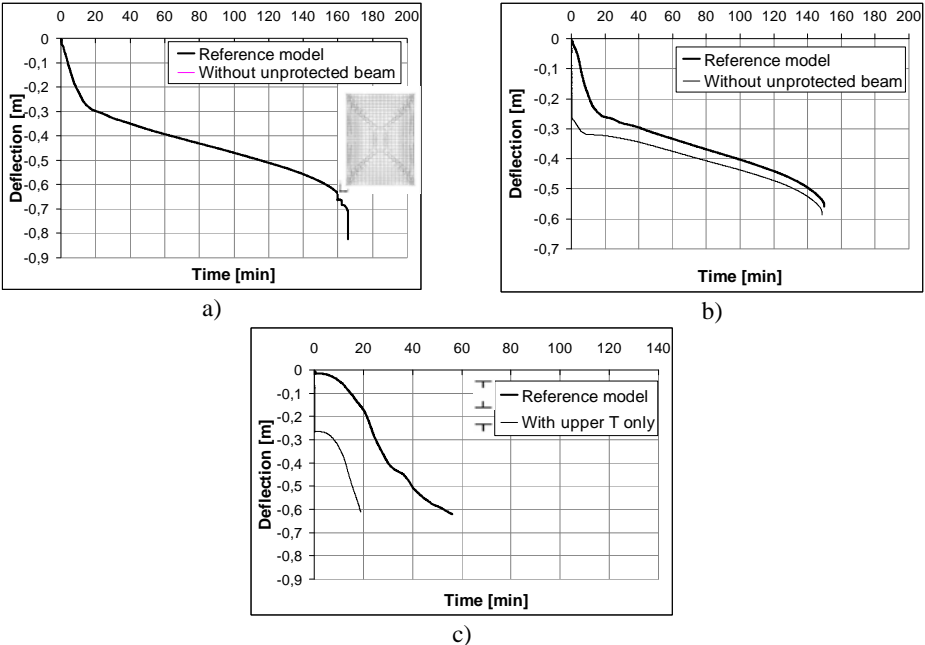


Figure 13. Modelling of the unprotected beam: a) FRACOF b) COSSFIRE c) PRAGUE.

Influence of the lateral restraints of the slab

For the three tests, beside the reference model, a second model has been considered in which the composite slab was laterally restrained on the four edges, with the aim to simulate an eventual continuity of the slab, assuming that there is no rupture of the bars on the supports. Figure 14 shows that the Fracof structure resisted up to 4 hours, while for the other structures a numerical failure occurred and the simulation could not be run until failure.

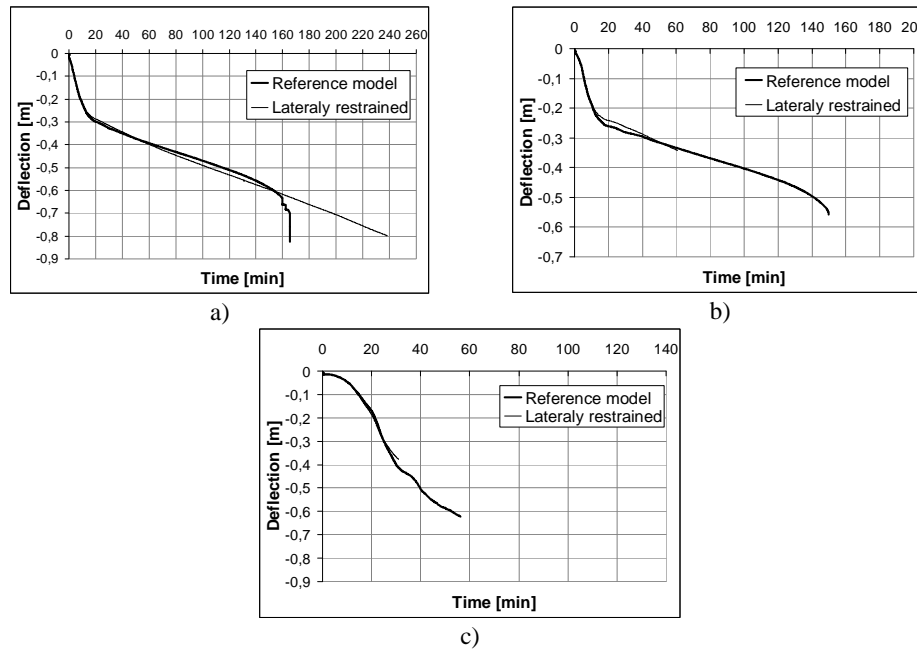


Figure 14. Influence of the lateral restraints of the slab: a) FRACOF b) COSSFIRE c) PRAGUE.

CONCLUSIONS

Using the available information from the three tests, Fracof, Cossfire and Prague, numerical simulations have been done using the SAFIR program. Differences of time resistance for Fracof and Cossfire tests could not be emphasised because the fire exposure in the tests was stopped after 120 minutes. For the Prague structure, the fire resistance time in the *a priori* numerical simulation is almost the same as the failure time observed in the test, with a difference of 5 minutes.

In order to see the influence of different parameters on the behaviour of the composite slabs when exposed to fire, a parametric study has been performed for each test.

Increasing the thickness of the slab improves the behaviour of the slab, with lower vertical deflections and higher fire resistance times. The average thickness for the section of the slabs containing ribs, calculated according to Annex D of EC4-1-2, may be used for the thermal distribution in the numerical simulation, at least with the open trapezoidal sections used in these tests.

For the Fracof and Cossfire tests the failure was caused by plastic hinge forming in the secondary edge beams. When the edges of the slabs are considered as completely restrained vertically, the plastic hinge forming in the

secondary edge beams is avoided and the fire resistance time is increased for the three slabs.

If lateral restrains are used in the numerical simulation, the failure is not reached after 4 hours of ISO fire exposure in the Fracof test. For the other two tests (Cossfire and Prague), the use of lateral restrains leads to early numerical failure.

If the secondary beams are not present in the numerical simulation, the transition from the compressive membrane to the tensile membrane is “violent” For the Fracof test so that the yield lines lead to early failure of the slab. For the Cossfire test, if the secondary beams are neglected, the slab enters from the beginning into tensile membrane. However, the failure time and evolution of vertical deflections are nearly the same than for the reference model. For Prague structure, using just the upper T for the castellated Angelina beams, large deflections are obtained at the beginning, like in the Cossfire test, but the vertical deflection curve does not converge to the same displacement and time resistance as in the reference numerical model. For the Prague test, using the minimum section (the upper and lower T) for the Angelina beam showed good correlation with the test.

Increasing the amount of reinforcement improves the behaviour of the slab (less vertical displacement and higher fire resistance times). However, if the collapse is not caused by failure of reinforcement but by compression in the concrete, using more reinforcement will not lead to a significant improvement (as can be seen in the case of the Fracof and Cossfire tests). For Prague test, using a higher amount of rebars lead to lower vertical deflection and the collapse was avoided.

REFERENCES

1. Zhao, B., Roosefid, M. and Vassart, O., Full scale test of a steel and concrete composite floor exposed to ISO fire, Proceedings of the 5th Structures in Fire Workshop SiF'08, Singapore City, Singapore, 2008, 539–550.
2. COSSFIRE, Connection of Steel and Composite Structures Under Natural Fire Conditions, RFCS research project N° RFSR-CT-2006-00028
3. Kallerova P., Wald F., Fire test on experimental structure in Mokrsko, CTU in Prague, August 2008
4. Franssen J. M., SAFIR—“A thermal/structural program modelling structures under fire”, Engineering Journal, AISC, Vol. 42, No 3, 2005, 143–158
5. EN 1994-1-2, Eurocode 4—Design of composite steel and concrete structures. Part 1–2. General rules – Structural Fire Design, CEN, Brussels, 2005

Fire Test of Composite Floor with Castellated Beams

J. BEDNAR, F. WALD and M. STUJBEROVA

ABSTRACT

The paper presents the comparison of the fire design of the unprotected castellated composite beam to the results of the fire test on administrative building. The transfer of heat into the structure shows a good conservative prediction of the test on real structure. The shear failure modes of the simplified mechanical prediction of the behaviour at elevated temperature are well visible on the load deformation curve. The slab was reinforced by ductile mesh to carry the load by its membrane action. The simple analysis shows the activation of the membrane action and the development of the slab deformations.

INTRODUCTION

The main goal of the fire test on a floor of an administrative building was the overall behaviour of the structure, which may not be observed on the separate tests on individual elements. A new building was erected in front of the Czech Technical University in Prague educational centre Joseph gallery in Mokrsko in Central Bohemia. The experiment followed the seven large fire tests in Cardington laboratory on steel frame conducted between 1998 and 2003, see [1]. The structure was design complex to allow a simple as well as advanced modelling of today modern buildings. Except of the three types of flooring systems were tested six wall structures with mineral wool. On one half of the floor was used the composite slab supported by the fire unprotected composite pretty castellated beams with large openings ArcelorMittal AngelinaTM, see Figure 1. The experimental structure represents a part of a floor of administrative building of size 18 x 12 m with height 2,68 m, see [2].

Tomáš Jána, František Wald,
Czech Technical University in Prague, Thakurova 7, CZ 166 29 Praha, Czech Republic
Magdaléna Štujberová,
Slovak Technical University in Bratislava, Radlinského 11, 813 68 Bratislava 1, Slovak Republic

The composite slab on the castellated beams was designed with a span 9 to 12 m and on beams with corrugated webs with a span 9 to 6 m. The deck was a simple trapezoidal composite slab of thickness 60 mm with the height over the rib 120 mm with sheeting CF60 (Cofraplus 0,75 mm) and concrete of measured cubic strength 34 N/mm^3 in 28 days reinforced by a smooth mesh $\varnothing 5 \text{ mm } 100/100 \text{ mm}$; with strength 500 MPa and coverage 20 mm. The castellated beams with sinusoidal shape openings were made from profile IPE 270 and its web height was 395 mm. The connections were design as simple with header plate connection partially encased in the concrete slab.

During the test were observed apart from other more then 300 thermocouples, twenty deflectometers, six flux density meters, two meteorological stations, ten video, and four thermo imagine cameras. The gas temperature round the castellated beam was measured by thermocouples TG08 and TG09 at the level of lower flange, see Figure 1. Round the experimental building was erected the structure from scaffold. The vertical deformations were measured from the twins of timber formwork beams, which were fixed on linear scaffolds and on bridged truss girders 1,5 m above the building floor.



Figure 1. Thermocouples located at the midspan on the castellated beams and its connections.

The mechanical load was designed for typical administrative building, where the variable action in Czech Republic reached usually from $2,5$ to $3,5 \text{ kN/m}^2$. The dead load of the composite slab and beams reached $2,6 \text{ kN/m}^2$. The load was created by bags. The load represents the variable load at ambient temperature $3,0 \text{ kN/m}^2$ and added permanent load $1,0 \text{ kN/m}^2$ in characteristic values. Mechanical load $3,0 \text{ kN/m}^2$ was represented by 78 sand bags; each bag had approximately 900 kg. These sand bags were put on wooden pallets and uniformly distributed on the composite slab and pre-stressed panels.

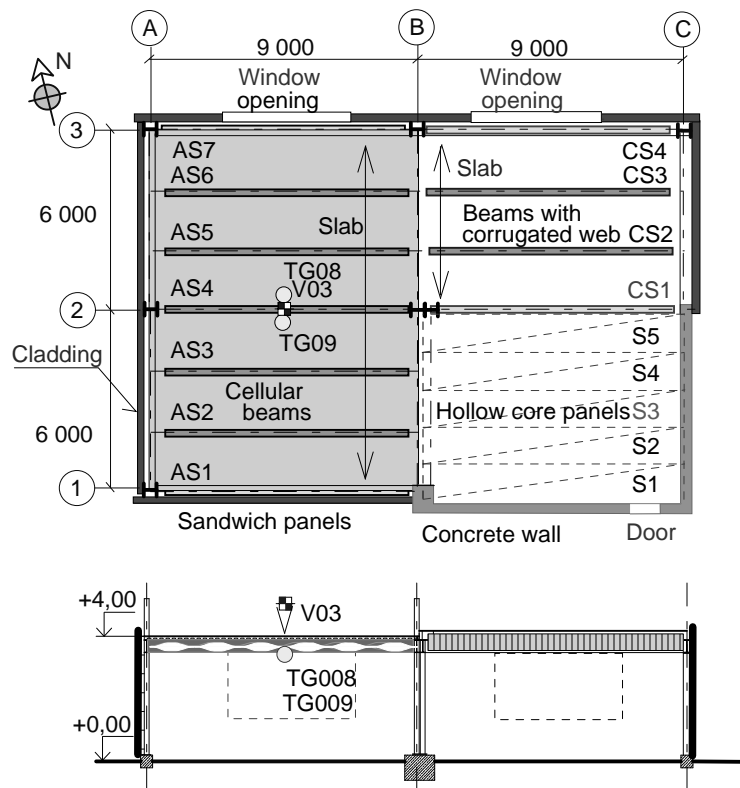


Figure 2. Structure of experimental building for fire test.

Two window openings in the front wall with dimension 2,43 x 4,0 m provided air supply into the fire compartment. Fire load was made of rough battens from soft pine wood, total volume of 15 m³. The usual characteristic value of the fire load for administrative building is 420 MJ/m², by the experiment the fire load reached 515 MJ/m².

The aim of this paper is to show the accuracy of simplified modelling of the heat transfer to the castellated beam, the shear behaviour of the composite castellated beam, the temperature development in the composite slab, and of the prediction slab catenary action on the presented fire test on administrative building.

HEAT TRANSFER INTO THE CASTELLATED BEAM

In fire, the temperature distribution across a composite member is non-uniform, since the web and bottom flange have thin cross-sections and a greater exposed perimeter than the top flange. The deterioration of the material properties of the web may therefore become an important effect on the overall performance of the member in the event of fire. The former fire resistance studies has been focussed to intumescent protection, see [3], as well as temperature developments in unprotected steel, see [4].

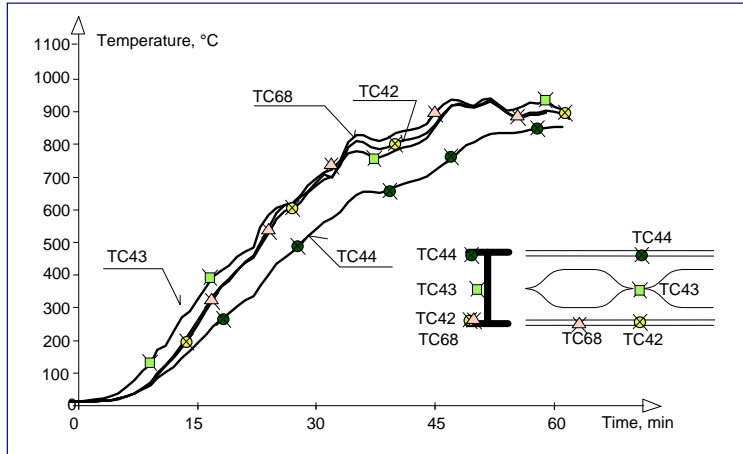


Figure 3. Temperatures measured at the midspan on the castellated beam AS4.

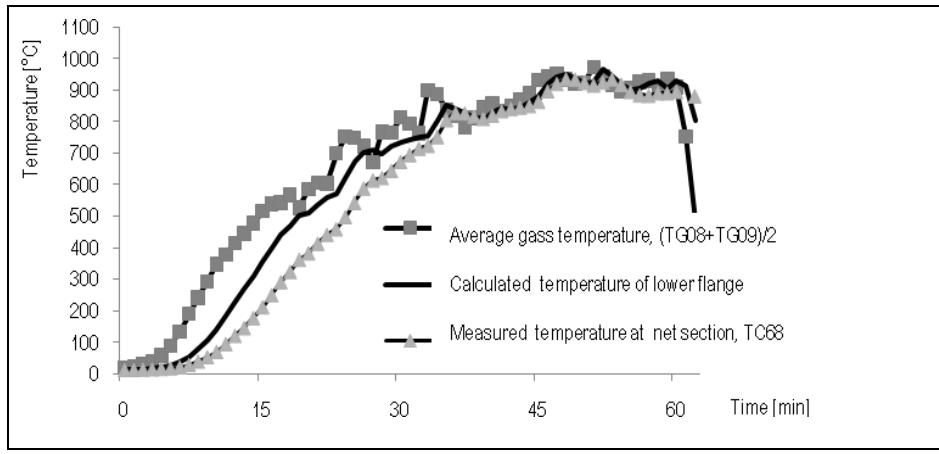


Figure 4. Calculated and measured temperature of the beam lower flange.

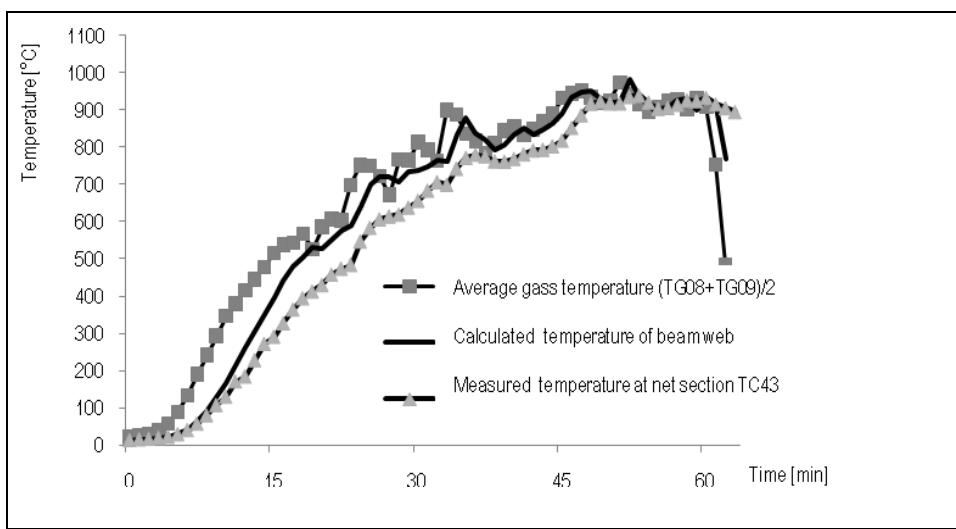


Figure 5. Calculated and measured temperature of the beam web.

In the described test was measured the gas temperature round the castellated beam by thermocouples TG08 and TG09 at the level of lower flange. The average gas temperature round the castellated beam was calculated from thermocouples as an average TG08 a TG09, see Figure 3. The step by step procedure according to EN 1993-1-2, see [5] was used to predict the parts of the structure temperature. For the lower flange was calculated the section factor $A_p/V = 232,1 \text{ m}^{-1}$, for the beam web $303,0 \text{ m}^{-1}$, for the upper flange exposed from the three sides $156,6 \text{ m}^{-1}$ and for the net section of the beam $178,3 \text{ m}^{-1}$. The comparison of this simple prediction to the measured values is shown at Figures 4 and 5.

BEAM RESISTANCE

Several investigations into the castellated beams structural behaviour have supported the widespread use of as structural members in steel to concrete composite frames. First studies at ambient temperature concentrated on in plane response in the elastic range and later plastic one as well. As a result of various series of tests a number of different failure modes have been observed, see [6]. The main failure modes are a Vierendeel collapse mechanism in which plastic hinges form at the section touching the four re-entrant corners of a castellation, buckling of a web-post, and web weld failure. Several prediction of collapse mechanisms have been proposed, see [7], and the lateral buckling of the web-posts has been analysed. Only limited investigations of composite floors using castellated steel beams at ambient temperature have been conducted, see [8]. The beams have been used widely in roof and composite construction without having been rigorously investigated under fire conditions. A composite concrete floor-slab has the effect of significantly increasing the flexural resistance of a steel section. Investigation of the behaviour of composite beams with isolated web openings in otherwise solid webs has shown that the slab significantly increases the shear-carrying capacity beyond that of the steel beam alone. This is due to the enhanced flexural and shear capacity of the upper part of the beam across an opening, although an unsupported webpost is more susceptible to buckling, see [9] and [4]. The simplified model for evaluation of the fire resistance of the beams was developed based on FE modelling approved by two fire tests, see [10].

In the fire test in Mokrsko 2008 were examined beams with large web openings which are sensitive to the shear resistance of the web and flanges. The advanced FE model was prepared to predict the behaviour before and after the fire test au University of Sheffield, see [2]. In the simplified calculation were utilised for the internal forces distribution by the Vierendeel analogy and the adequate failure modes were observed, see [11]. The measured deflection of the castellated beam AS4 at its midspan with marked shear resistances of horizontal shear, shear in opening and vertical shear is shown on Figure 6 for the reduction factor of the effective yield stress k_y , and proportional limit for steel at elevated temperature $k_{p,0,2}$.

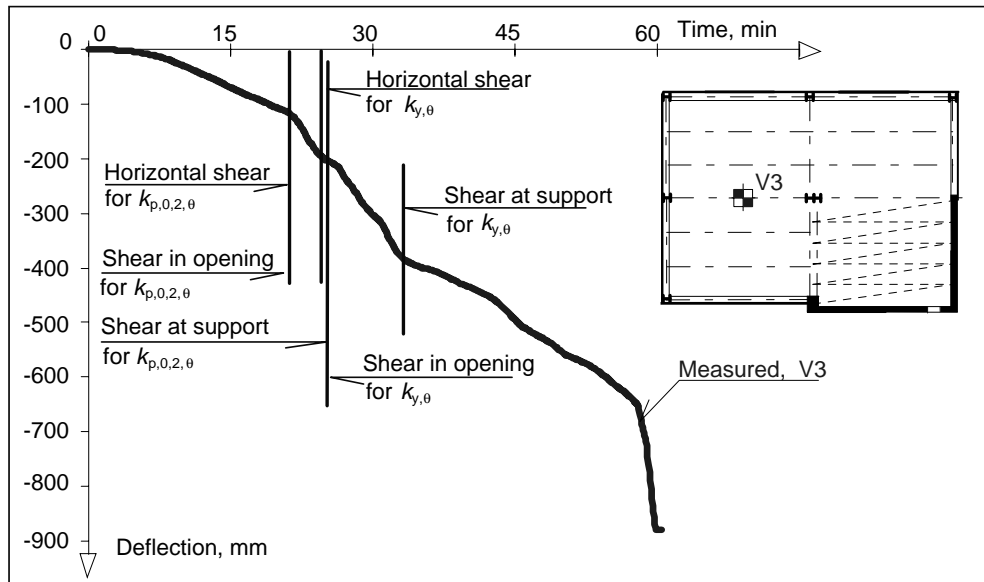


Figure 6: Measured deflection of the castellated beam AS4 at its midspan with reached shear resistances.

SLAB RESISTANCE

The steel sheeting temperature during the fire follows the gas temperature and the sheeting lost its bending stiffness and resistance in early stage of the fire. The sheeting deforms and separate from the concrete slab. The bending stiffness of the unprotected composite beam was decreasing. The beam web is losing its shear resistance and the beam flanges its bending resistance. Under the high deformations the upper mesh in the composite slab allows to help transfer the load by its catenary action, see [9]. The behaviour was predicted by simple, see [13], as well as advanced methods, see [14].

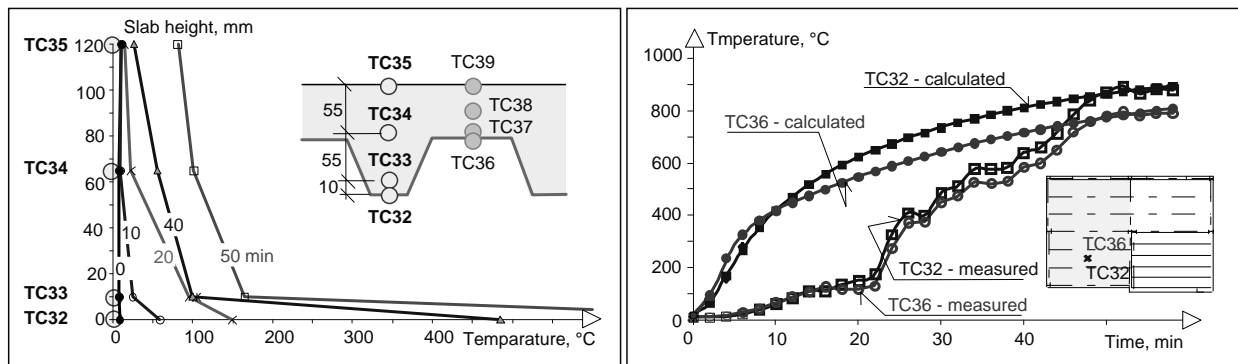


Figure 7. Measured temperatures in slab over the rib and comparison of predicted and measured temperatures of the bottom surface of slab.

For the simple prediction method were derived the temperature along its thickness by the differential method from the gas temperature measured under the slab. The moisture content was taken into account by the change of specific heat capacity between 100°C and 200°C. The measured thermal gradient in the composite slab is documented in Figure 7. The comparison of

predicted and measured temperatures of the bottom surface of slab shows, that the moisture affected the temperatures till 50 min of fire test.

In simplified slab model was the beam represented by its flanges only. The slab resistance including supported beams was calculated as $p_{fi,d} = 7,9 \text{ kN/m}^2$. The simplified model is based on evaluation of the deformations necessary to develop the membrane action. The maximal deflection limited by reinforcement ductility was calculated as 712 mm. The calculated deformations are on Figure 8 compared to values measured during the test. The fire resistance of slab was predicted based on advanced model, see [14].

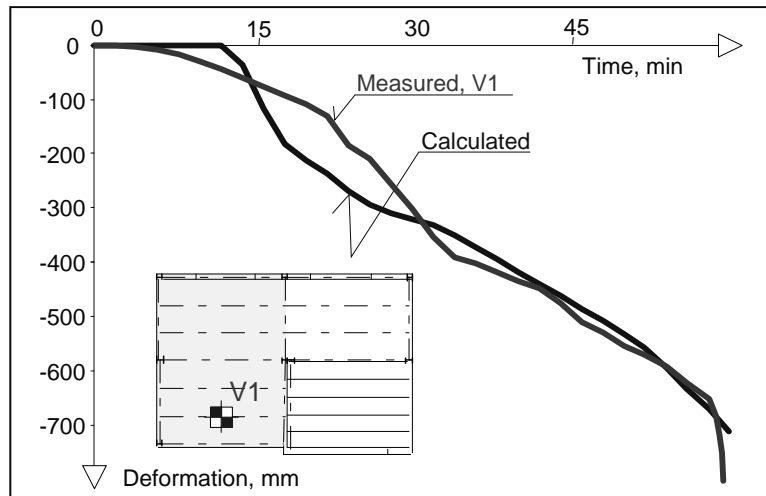


Figure 8. Predicted and measured deformation of the slab at its mid span.

The damage of the ceiling started in the Southeast corner. The slab lost the resistance in compression in 62 min of the experiment, see Figure 9. The edge beam buckled on its developed free length. Due to the spalling of the top of the concrete column lost the anchors the tensile resistance. The bolted connection of the primary box girder was exposed to torsion, which leads to the lost of the shear resistance of its bolts.

CONCLUSIONS

The fire test approved a good fire resistance of composite slab with unprotected castellated beams, which is higher compare to the separate composite beam resistance, see Figure 9. The slab resistance, designed for R60, was reached at 62 min and the beam shear resistance in 21 min.

The experimental data confirms a reasonable accuracy of prediction just by a simple model of the heat transfer to the castellated beam, the shear behaviour of the composite castellated beam, the temperature development in the composite slab, and of the prediction slab catenary action on the presented fire test on administrative building, even though the stresses of beam in structure are highly influenced be elements elongation/shortening.



Figure 9. The collapsed slab with removed mechanical load.

ACKNOWLEDGMENTS

This outcome has been achieved with the financial support of Grant Agency of Czech Republic No. P105/10/2159.

REFERENCES

1. Wald, F., Simoes da Silva, L., Moore D.B., Lennon, T., Chladna, M., Santiago, A., Beneš, M., Borges, L., Experimental behaviour of a steel structure under natural fire, *Fire Safety Journal*, 41, 509-522, 2006.
2. Kallerová P. a Wald F., Fire test on experimental building in Mokrsko, CTU in Prague, Prague. 2009, ISBN 978-80-01-04146-8, URL: fire.fsv.cvut.cz/firetest_Mokrsko
3. Bailey CG. Indicative fire tests to investigate the behavior of cellular beams protected with intumescent coatings, *Fire Safety Journal*, 39, 689-709, 2004.
4. Nadjaia, A., Vassart O., Ali F., Talamonab, D., Allamb A, Hawes, M., Performance of cellular composite floor beams at elevated temperatures, *Fire Safety Journal*, 42, 489-497, 2007.
5. EN 1993-1-2, Eurocode 3: Design of steel structures - Part 1-2: General rules - Structural fire design, CEN, 2005.
6. Kerdal D., Nethercot D.A. Failure modes for castellated beams, *Journal of Constructional Steel Research*, 4, 295-315, 1984.
7. RT1006 version 02, Fire design of cellular beams with slender web posts, Ascot, SCI; 2004.
8. Megharief, J. and Redwood R., Behaviour of Composite Castellated Beams, *Journal of Constructional Steel Research*, 46, 199-200, 1998.
9. Bitar, D., Demarco, T., Martin, P.O., Steel and non-composite cellular beams-novel approach for design based on experimental studies and numerical investigations. Proceedings. EUROSTEEL, Coimbra 2005.
10. Nadjaia, A., Goodfellow, N., Vassart, O., Ali, F., Choi, S., Simple calculation method of cellular composite floor beams at elevated temperatures, in *Structures in fire*, Singapore, 2008, 551-559, ISBN 978-981-08-0767-2.
11. Pelouchová A., Evaluation of fire resistance of cellular beams at Mokrsko fire test, part IV of Diploma theses, CTU in Prague, Prague 2010.
12. Newman GM, Robinson JT, Bailey CG. Fire safe design: A new approach to multi-storey steel-framed buildings. 2nd ed., Ascot: SCI, Publication P288, The Steel Construction Institute; 2006.
13. Wald, F., Štujberová, M., Bednář, J., Resistance of composite floor during fire test on experimental structure in Mokrsko, in *Czech, Konstrukce*. 8, 5, 11-14, 2009, ISSN 1213-8762.
14. Anthony Abu, Berenice Wong, Florian Block and Ian Burgess, structural fire engineering assessments of the Mokrsko fire tests, The University of Sheffield and Buro Happold Specialist Consulting.

The Slab Panel Method: Design of Composite Floor Systems for Dependable Inelastic Response to Severe Fires

G. C. CLIFTON, A. G. GILLIES and N. MAGO

ABSTRACT

The Slab Panel Method (SPM) covers design of steel/concrete composite floor systems for dependable inelastic response in severe fires, in which two-way action within a deformed region of the floor known as a slab panel is used to allow many of the supporting beams within that slab panel to remain unprotected. The SPM, in which significant deformation of the unprotected elements and supporting floor structure is anticipated and designed for, is suitable for desktop design office use.

This paper focuses firstly on a description of the features, application and limitations of the method, followed by details of the development steps taken from the first published method in 2001 to the latest draft in development, 2010. References are given to sources of further information to allow readers to study the method and each of the development steps undertaken in more detail

INTRODUCTION AND SCOPE OF PAPER

The Slab Panel Method (SPM) of designing composite floor systems for dependable inelastic response to severe fires is a general purpose method for determining whether a region of slab will, under a specified duration of severe fire exposure and two-way action, support the applied load in flexure and shear. The current version, presented in HERA Report R4-131 [1], has been developed from a 10 year research programme and further development work is underway.

Space limitations herein mean that this presentation is limited to brief written descriptions of the principal aspects of these developments and references are given to publically available source documents which include more details.

It is assumed that readers are generally familiar with the tensile membrane model developed by Bailey [2] as this paper covers only the changes to that model that have been made.

G Charles Clifton, The University of Auckland, 20 Symonds Street, Auckland 1142, New Zealand

Anthony G Gillies, Lakehead University, 955 Oliver Road, Thunder Bay, Ontario, Canada
Nandor Mago, New Zealand HERA, 17-19 Gladding Place, Manukau City, New Zealand

FEATURES, APPLICATION AND LIMITATIONS OF THE SLAB PANEL METHOD

Features of Method

The SPM comprises a generalised application of the tensile membrane model [2] in conjunction with the yieldline theory of Park [3] to a two-way region of a floor slab known as a *Slab Panel*; **Figure 1** shows an example.

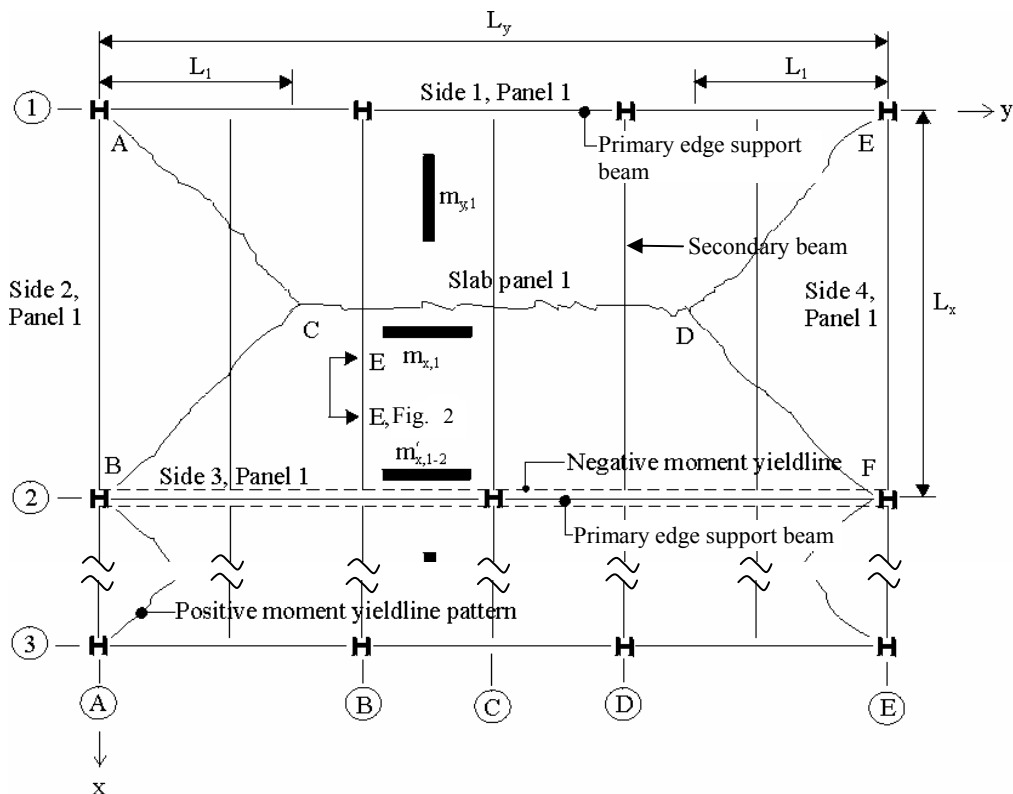


Figure 1. Reflected Floor Plan Showing Dimensions for Slab Panel Yield Line Pattern and Developed Moments.

Features of the method are:

1. The method is applicable to a wide range of concrete slabs supported on secondary and primary steel beams.
2. Types of concrete slabs covered are flat slab with reinforcement, slabs on steel deck with clipped pan (solid slab), trapezoidal profiles or deep ribbed deck profiles and a limited range of solid precast units incorporating a two way reinforced in-situ topping layer.
3. Normal weight and constructional light weight concrete are covered.
4. The supporting software allows two layers of slab reinforcement in the L_x and L_y directions, as well as individual reinforcing bars in each rib of a steel deck slab, and interior support bars over slab panel edges which are continuous across the support (eg side 3 in panel 1 in **Figure 1**).

5. Supporting unprotected secondary beams within the slab panel (see **Figure 1**) can be hot rolled or welded beams with discrete web openings or with continuous web openings or closely spaced cold formed steel joists.
6. The expected deformations of the slab panel and supporting edge beams are calculated for the end state and can be used in design of fire separating walls which must pass under the slab panel.
7. Structural detailing requirements to withstand the expected deformations without failure of the floor system is a key aspect of the procedure. This includes all supporting beams being connected by shear studs, reinforcement at the slab edges to tie the slab securely into the shear studs and prevent edge unzipping, minimum elongation requirements for reinforcement required to undergo yielding in fire and all supporting steel member connections having a minimum specified rotation capacity at room temperature without loss of load carrying capacity.
8. Design temperatures are calculated for all elements exposed to high temperatures and the reduced strength associated with those temperatures is used in the strength design checks.
9. The strength design checks on the slab panel involve a flexural/tensile membrane load carrying capacity check and a shear check.
10. The contribution of the secondary beams is included in the calculation of internal actions and hence slab panel capacity as described in the next section.

Application of Method

Application of the SPM involves the following steps (the full method is given in Appendix A of [1]):

- Step 1. Determine the fire emergency design loading, w^* , which is in accordance with the New Zealand Loadings Standard AS/NZS 1170.0 [4].
- Step 2. Determine the design structural fire severity, which uses the t_{eq} value calculated by EN 1991-1-2 [5] or as described in [6].
- Step 3. Determine the temperatures of all slab panel components and associated mechanical properties.
- Step 4. Determine the yieldline load carrying capacity of the slab panel at elevated temperatures. This involves the following sub-steps:
 - a. Determine the positive moment capacity within the slab panel per unit length in each of the x- and y- directions. For the L_x direction, the positive moment capacity in the x- direction includes directly the contribution of the unprotected secondary beams, as shown in **Figure 2**. This involves determining the total tension force from all steel components that can develop a dependable tension force across the span L_x , given as $R_{tsx,total}$, expressed as force/unit width of slab in the L_y direction and the distance to the centroid of this force from the top of concrete, e_{rx} . This is balanced by a compression force R_{cc} in the top of the slab, such that $R_{cc} = R_{tsx,total}$, whereupon the moment capacity is determined using standard reinforced concrete theory. These capacities are shown in **Figure 1** as $m_{x,1}$ and $m_{y,1}$.
 - b. For the slab panel sides which are continuous, determine the negative moment capacity per unit length in the appropriate direction. For the

slab panel shown in **Figure 1**, only side 3 is continuous and so $m'_{x,1-2}$ is the only negative moment capacity calculated for that slab panel.

- c. Calculate the yieldline load carrying capacity, using the equation for a general rectangular slab with either pinned or fixed edge supports given by Park [3]. This capacity is calculated for the slab panel with the actual edge support conditions, designated w_{yl} , and for the slab panel with all edges assumed simply supported, designated $w_{yl,ss}$. Tensile membrane enhancement is applied only to the latter.

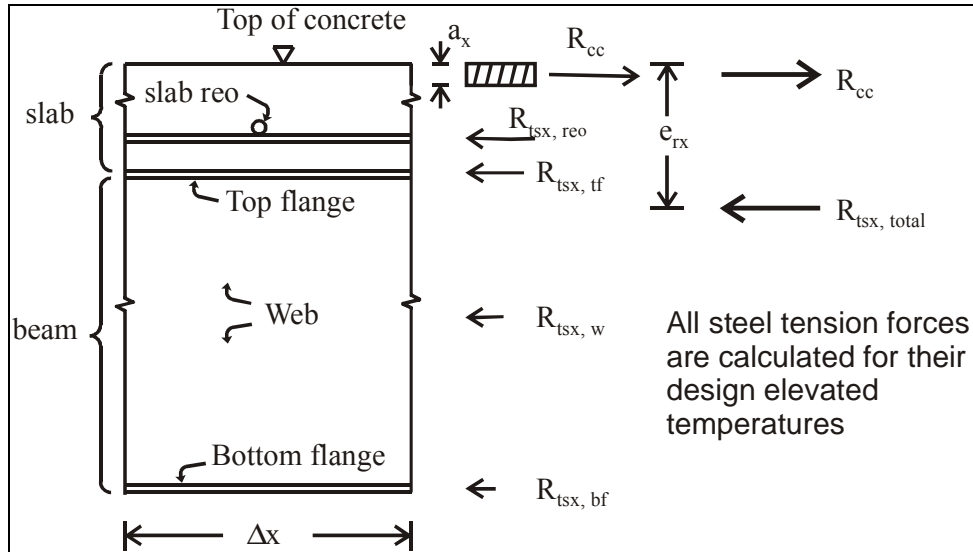


Figure 2. Section E-E Through Region of Floor Slab Incorporating Steel Decking, Showing Development of Positive Moment Capacity Using the General Slab Reinforcement and the Secondary Beams.

- Step 5. Determine the limiting and maximum deflection of the slab panel. This gives the maximum allowed vertical deflection of the slab panel relative to the pre-fire condition of the adjacent supports, used to calculate the tensile membrane enhancement. The limits have been modified from those of [2] on the basis of subsequent testing and analysis and include a dependence on the structural fire severity, t_{eq} , as described in the next section.
- Step 6. Determine the tensile membrane enhancement. In the currently published method [1] this uses the Bailey model for isotropic reinforcement given in [2], however the Bailey model for orthotropic reinforcement [7] has been incorporated into the next revision currently in draft development stage and described in the final section of the paper.
- Step 7. Determine the moment/tension membrane adequacy of the slab panel, w_u and check if it is adequate. This is given by equation (1).

$$w_u = (w_{yl\theta} - w_{yl\theta,ss}) + w_{yl\theta,ss} e \quad (1)$$

where e is the enhancement in simply supported slab panel load carrying

capacity due to tensile membrane action.

If $w^* \leq w_u$, then the moment/tension membrane capacity is adequate.

Step 8. Determine the shear capacity of the slab panel. This is determined for side 1 or side 3, **Figure 1**, where the decking, if present, is running parallel to the edge support beams and so the minimum thickness of slab is present. The procedure takes account of the loss of concrete load carrying capacity in the bottom of the slab due to the high temperatures developed. It also incorporates the elevated temperature contribution from the secondary beams if present, being calculated as the minimum of the contribution from the web of the beam or from the connections of the secondary beam into the primary edge beam.

Step 9. Determine the reinforcement content required for integrity (prevention of the passage of fire through any cracks in the slab). These provisions taken directly from the six slab panel furnace tests described by Lim [8].

Limitations of the Slab Panel Method

As a research tool the method has limited application, in that it determines the adequacy of the slab load carrying capacity at a given structural fire severity (t_{eq}) when a specified mid-panel maximum deflection is reached. It does not generate the behaviour of the slab panel throughout the period of fire exposure, unlike a finite element based approach such as VULCAN [9].

The method is very versatile as a design tool but with the following limitations:

- (1) Because the method is based on developing significant vertical deformation of the floor system to generate the required fire resistance it is not applicable where this deformation may compromise the life safety performance of elements underneath the fire separating floor.
- (2) To dependably resist the expected structural deformations the structural system must have sufficient ductility capacity as specified in [1]. Structural systems designed and detailed to resist severe earthquake demands meet these criteria. This is especially important for the building to withstand dependably the fully developed fire on more than one level at one time, which might occur.
- (3) The slab panel vertical edge supports must have sufficient strength to resist the applied loads generated from the slab panel tributary supported areas (eg for side 2, panel 1, **Figure 1**, this is the tributary area from region ACB) and must resist these loads with limited deformation (limit of span/100 is given).
- (4) Bare steel columns supporting the slab panel must be passive protected full height including the connection region.

DEVELOPMENT WORK UNDERTAKEN

The overall research programme for the SPM has involved the following steps:

1. The Cardington (UK) full scale fire tests in 1995/1996 [10] showed that composite floor systems with unprotected primary and secondary floor support beams can develop high fire resistance through inelastic action under severe fire exposure. However, these reports did not produce a design model for this observed behaviour.

2. Bailey published the tensile membrane model of floor system behaviour [2] and confirmed the postulated slab panel/tensile membrane behaviour in lightly reinforced large scale slab panel tests at ambient temperature.
3. Clifton et al [11] generalised Bailey's model into the first edition of the Slab Panel Method of design and detailing composite floor systems for dependable inelastic response under fully developed fires.
4. Finite element modelling [12] of the Cardington tests as an assemblage of linked composite members undertaken over 2002/2003 showed the three-dimensional nature of the floor system response, involving two-way action of the floor system, consistent with the Bailey model [2].
5. Six rectangular slab panels were designed to the first edition of the SPM procedure and tested at the Building Research Association of New Zealand fire test furnace in 2002 [8]. The panel supports on the 4 sides of the panel were rigid vertically, but free to translate horizontally and to rotate.
6. These 6 tests allowed the methods of temperature determination for the concrete and slab reinforcement and the requirements for integrity to be revised. Details are in [13]. These revisions were incorporated into the second edition of the SPM [14]. Prediction of the expected failure times of the tested slab panels by the first edition [11] and the second edition [14] showed both to be conservative, the first edition especially so.
7. Advanced Finite Element Analysis (FEA) of all 6 tested panels was undertaken, with the models validated through comparing the mid-panel deflection and then being used to compare edge lateral deflections and reinforcement strains. Accurate models were obtained in all cases; details are in [15].
8. FEA was then used to determine the influence of deforming supports on the slab panel behaviour. Details are in [16]. This influence is minor and is accounted for in the edition of the procedure currently published [1]. The influence of in-plane axial restraint on the slab panel deformation was determined and found to be significant, with even minor levels of restraint (less than 100kN/m stiffness) reducing the vertical deformation at the centre of the slab panel [16].
9. Modelling of a real floor system (similar to that shown in **Figure 1**) comprising unprotected secondary beams was next undertaken to confirm that the SPM approach of incorporating the unprotected secondary beams into the slab panel resistance, in the manner shown in **Figure 2**, is valid. Details are in [17]. This involved first validating the FE model for a slab on beams by accurately predicting [18] the standard fire test response of one non composite and two composite floor beams undertaken at the Warrington Fire Testing station.
10. FEA was then used to determine the performance of a complete floor system with unprotected secondary beams within the slab panel compared with the predicted response from the SPM second edition, with good agreement [19]. This modelling included determining the response under the Standard Fire exposure [20] up to and beyond the calculated time to failure and under a natural fire generating the same structural fire severity as the calculated time to failure.
11. FEA was used to determine the load distribution into the supporting beams of the slab panel under severe fire conditions and to compare this with the assumed load transfer mechanism for slab panel response. This comparison showed [17] that the yieldline basis of load transfer from the slab panel into the support beams (as determined from the tributary area shown in **Figure 1**) is more

accurate than the ambient temperature load transfer assumed in ambient temperature design, which assumes a series of 1 way load transfer systems, comprising slab secondary beams primary beams columns.

12. A tentative fire engineering design procedure incorporating unprotected slab panel supporting beams was developed. Representative slab panel systems with protected and with unprotected floor support beam were designed and analysed [21]. This model enabled a good prediction of the Cardington Large Enclosure test floor performance [10] to be made, however ensuring lateral stability of the unprotected edge beams and confirming the additional detailing requirements to ensure slab panel stability required too much additional research work for the benefit to be obtained and so this avenue has not been further developed.
13. Modification to the limiting deflection through the factor C_{ISO} was introduced. For slab panels with unprotected secondary beams, large temperature differentials in the beams early in the fire exposure drive rapid downwards deflection, the rate of which decreases with increasing time. This is stage 1 behaviour. It is followed by a period of stable slab panel behaviour, with a constant rate of deflection versus structural fire severity, t_{eq} . This is stage 2 behaviour. The increasing deflection generates increasing tension membrane resistance, which counters the loss of strength with increasing temperature and gives the stability to this stage of slab panel response. It is this effect which is incorporated through the C_{ISO} factor. Details are given in section CA4.2.3 of [1]. Finally, if the structural fire severity is sufficiently great, the rate of deflection increases with increasing time until final failure occurs. This is stage 3.
14. The SPM procedure has now been applied to all multi-storey steel framed office buildings built within the City of Auckland over the last 4 years. The Building Control Authority responsible for this jurisdiction required the procedure to be subjected to independent peer review prior to allowing the first application. This was undertaken in 2006 by Holmes Fire and Safety and the resulting recommendations were incorporated into the current procedure [1].

CURRENT DEVELOPMENT WORK AND CONCLUSIONS

The most recent revisions to the procedure, which are currently in draft form, involve the following:

- a. Incorporating orthotropic strength at fire design temperature into the tensile membrane enhancement factor, as recommended by Bailey in [7]. This is essential as every application is orthotropic due to the temperature effects.
- b. Ensuring that the tensile membrane failure mode is correctly determined when the tensile capacity in the x- direction (ie the direction $m_{x,1}$ in **Figure 1**) is less than that in the y- direction. The Bailey model [7] assumes that tensile membrane failure occurs mid-panel and parallel to the L_x direction. However, if the tensile capacity in the x- direction is the lower of the two, the Bailey model will overestimate the flexural/tensile membrane capacity.
- c. Maintaining equilibrium in the yieldlines at their intersections within the slab panel (eg at points C and D in **Figure 1**). This is not checked in [2, 7].

These provisions have been incorporated into a draft revision of the program, termed SPM0609, which has been used to predict with acceptable or better accuracy

the response of several recent large scale fire tests, such as the Mokrsko test [22] prior to the unzipping failure which prematurely ended the test (and which would have been suppressed by the detailing requirements in the SPM procedure for tying the slab onto the supporting edge beams).

REFERENCES

1. Clifton, G., *Design of composite steel floor systems for severe fires, HERA Report R4-131*. 2006, New Zealand HERA: Manukau City.
2. Bailey, C.G., *Design of steel members with composite slabs at the fire limit state*. 2000: Building Research Establishment.
3. Park, R., *Ultimate Strength of Reinforced Concrete Slabs, Volume 2*. 1970, The University of Canterbury: Christchurch, New Zealand.
4. AS/NZS1170.0, *Structural Design Actions Part 0 - General Principles*, N.Z. Standards, Editor. 2002, Standards New Zealand: Wellington, NZ.
5. ENV1991-1-2, *Eurocode 1: Actions on Structures Part 1-2: General Actions - Actions on Structures Exposed to Fire*, CEN, Editor. 2002, CEN, Brussels, Belgium.
6. Spearpoint, M.E., ed. *Fire Engineering Design Guide, Third Edition*. 2008, Centre for Advanced Engineering: Christchurch, NZ.
7. Bailey, C.G., *Efficient Arrangement of Reinforcement for Membrane Behaviour of Composite Floor Slabs in Fire Conditions*. *Journal of Constructional Steel Research*, 2003. 59: p. 931 - 949.
8. Lim, L. and C.A. Wade, *Experimental Fire Tests of Two-Way Concrete Slabs, Fire Engineering Research Report 02/12*. 2002, University of Canterbury: Christchurch, NZ.
9. Huang, Z., I.W. Burgess, and R.J. Plank, *Modelling Membrane Action of Concrete Slabs in Composite Action in Fire, Theoretical Development and Validations*. *ASCE Journal of Structural Engineering*, 2003. 129(8): p. 1093 - 1112.
10. Kirby, B., *The Behaviour of a Multi-Storey Steel Framed Building Subject to Fire Attack- Experimental Data: Also data from BRE, Cardington, on the Corner Fire Test and the Large Compartment Fire Test, 1996*. 1998, British Steel Swinden Technology Centre: Swinden.
11. Clifton, G.C., M. Hinderhofer, and R. Schmid, *Design of Multi-Storey Steel Framed Buildings with Unprotected Secondary Beams or Joists for Dependable Inelastic Response in Severe Fires*. *Steel Design and Construction Bulletin*, 2001. 60(February): p. 1 - 58.
12. Moss, P.J. and G.C. Clifton, *Modelling of the Cardington LBTF Steel Frame Building Fire Tests*. *Fire and Materials*, 2004. 28: p. 177 - 198.
13. Clifton, G.C. and C. Beck, *Revision of the Slab Panel Method - Comparison With Experimental Results*. *Steel Design and Construction Bulletin*, 2002. 70(October/November): p. 1 - 19, 47.
14. Clifton, G.C. and C. Beck, *Design of Multi-Storey Steel Framed Buildings with Unprotected Secondary Beams or Joists for Dependable Inelastic Response in Fires: Second Edition*. *Steel Design and Construction Bulletin*, 2003. 71(December02/January03): p. 3 - 72.
15. Mago, N. and G.C. Clifton, *Stage 2 development of the Slab Panel Design Method, HERA Report R4-118*. 2003, New Zealand HERA: Manukau City, NZ.
16. Mago, N., *Influence of slab panel edge sagging in fire - Stage 2 of the SPM: Concise summary, HERA Report R4-118.1*. 2004a, New Zealand HERA: Manukau City, NZ.
17. Mago, N. and G.C. Clifton, *Advanced Analysis of Slab Panel Floor Systems Under Severe Fire Attack*. *Steel Design and Construction Bulletin*, 2005. 77(March): p. 3 - 18, 23 - 24.
18. Mago, N., *FEA of three WRCSI fire tests: concise summary, HERA Report R4-118.2*. 2004b, New Zealand HERA: Manukau City, NZ.
19. Mago, N., *Composite floor system performance in ISO 100 min and natural fire test 44 min: concise summary, HERA Report R4-118.3*. 2004c, New Zealand HERA: Manukau City, NZ.
20. ISO834, *Fire Resistance Tests - Elements of Building Construction Part 1 General Requirements*, G. ISO, Switzerland, Editor. 1999, ISO, Geneva, Switzerland.
21. Mago, N., *DCB No 71 with secondary beams or Speedfloor joists: concise summary, HERA Report R4-118.4*. 2005, New Zealand HERA: Manukau City, NZ.
22. Wald, F. and P. Kallerova, *Draft Summary of Results from Fire Test in Mokrsko 2008*. 2009, CVUT: Prague, Czechoslovakia.

TIMBER STRUCTURES

Design Method for the Separating Function of Timber Structures

A. FRANGI, V. SCHLEIFER, M. FONTANA and E. HUGI

ABSTRACT

A comprehensive research project on the separating function of light timber frame wall and floor assemblies with cladding made of gypsum plasterboards and wood-based panels was carried out at ETH Zurich in collaboration with the Swiss Laboratories for Materials Testing and Research (Empa). The paper describes the developed design model for the verification of the separating function of light timber frame wall and floor assemblies. The proposed design method significantly extends the application range of the design method according to EN 1995-1-2 and permits the verification of the separating function of a large number of common timber assemblies.

INTRODUCTION

Light timber frame wall and floor assemblies are typical structural elements used in timber buildings. The assemblies consist of solid timber studs or beams with cladding made of gypsum plasterboards, wood-based panels or combinations of these layers. The cavities may be filled with insulation made of rock, glass or wood fibre or include voids. Unlike heavy timber structures in which the char-layer of fire-exposed members performs as an effective protection of the remaining unburned residual cross-section, the fire performance of load-bearing and non load-bearing light timber frame assemblies mainly depends on the protection provided by the cladding [1-3].

Andrea Frangi (corresponding author), PhD, ETH Zurich, Institute of Structural Engineering, Wolfgang Pauli-Strasse 15, 8093 Zurich, Switzerland.

Vanessa Schleifer, PhD, ETH Zurich, Institute of Structural Engineering, Wolfgang Pauli-Strasse 15, 8093 Zurich, Switzerland.

Mario Fontana, Professor, PhD, ETH Zurich, Institute of Structural Engineering, Wolfgang Pauli-Strasse 15, 8093 Zurich, Switzerland.

Erich Hugi, PhD, Empa, Swiss Laboratories for Materials Testing and Research, Uberlandstrasse 129, 8600 Dubendorf, Switzerland.

In order to limit fire spread by guaranteeing adequate fire compartmentation, elements forming the boundaries of fire compartments are designed and constructed

in such a way that they maintain their separating function during the required fire exposure (requirement on integrity E and insulation I). The required period of time is normally expressed in terms of fire resistance using the standard fire exposure [4] and is specified by the building regulations. While fire tests are still widely used for the verification of the separating function of light timber frame assemblies, design models are becoming increasingly common. For ISO-fire exposure criterion I (insulation) may be assumed to be satisfied if the average temperature rise over the whole of the non-exposed surface is limited to 140K, and the maximum temperature rise at any point of that surface does not exceed 180K, thus preventing ignition of objects in the neighbouring compartment. The criterion E (integrity) may be assumed to be satisfied if no flames or hot gases on the fire-unexposed side of the construction can be observed. Criterion I (insulation) is clearly defined and thus the verification can be made by heat transfer calculations instead of testing. On the other hand, criterion E (integrity) is mostly determined by observations, because calculations are still very complex. However, extensive experience of full-scale testing of wall and floor assemblies permitted to define some rules about detailing of wall and floor assemblies that have been included for example in EN 1995-1-2 [5]. Thus, the criterion E (integrity) may be assumed to be satisfied if the criterion I (insulation) has been satisfied and panels remain fixed to the timber structure on the unexposed side.

A comprehensive research project on the separating function of light timber frame wall and floor assemblies with cladding made of gypsum plasterboards and wood-based panels has been carried out at ETH Zurich in collaboration with the Swiss Laboratories for Materials Testing and Research (Empa). The objective of the research project was the development of an improved design model for the verification of the separating function of light timber frame wall and floor assemblies. A large number of small-scale fire tests permitted the analysis of different parameters (material, thickness, position and number of the layers) on the thermal behaviour of protective cladding made of gypsum plasterboards and wood-based panels [6]. The results of the fire tests allowed the verification and calibration of thermal properties used for thermal finite element (FE) analysis. Based on an extensive FE parametric study, the coefficients of the design model for the verification of the separating function of light timber frame wall and floor assemblies were calculated [7,8]. The design model was verified by means of full-scale fire tests.

DESIGN METHOD FOR SEPARATING FUNCTION OF TIMBER CONSTRUCTIONS

A comprehensive design method for the verification of the separating function of timber constructions has been developed based on an extensive experimental as well as finite element thermal analysis. The design method is capable of considering timber assemblies with an unlimited number of layers made of gypsum plasterboards, wood panels or combinations thereof. The cavity may be void or filled with insulation made of rock or glass fibre. The design method is valid for following materials:

- Solid timber panels (density $\geq 400 \text{ kg/m}^3$)
- Oriented Strand Board (OSB) (density $\geq 550 \text{ kg/m}^3$)
- Particleboards (density $\geq 500 \text{ kg/m}^3$)
- Plywood (density $\geq 400 \text{ kg/m}^3$)
- Gypsum plasterboards:
 - Type A, H und F according to EN 520 [9]
 - Type X according to ASTM C1396 [10] or CAN/CSA-82.27-M91 [11]
- Gypsum fibreboards according to EN 15283-2 [12]
- Rock fibre insulation (density $\geq 26 \text{ kg/m}^3$)
- Glass fibre insulation (density $\geq 15 \text{ kg/m}^3$)

The developed design method is based on the additive component method given in EN 1995-1-2 [5]. Thus, the fire resistance t_{ins} of the timber assembly is taken as the sum of the contributions from the different layers (claddings, void or insulated cavities) according to their function and interaction as follows (Fig. 1):

$$t_{ins} = \sum_{i=1}^{i=n-1} t_{prot,i} + t_{ins,n} \quad (1)$$

with $\sum_{i=1}^{i=n-1} t_{prot,i}$ Sum of the protection values $t_{prot,i}$ of the layers (in direction of the heat flux) preceding the last layer of the assembly on the fire-unexposed side [min]

$t_{ins,n}$ Insulation value $t_{ins,n}$ of the last layer of the assembly on the fire-unexposed side [min]

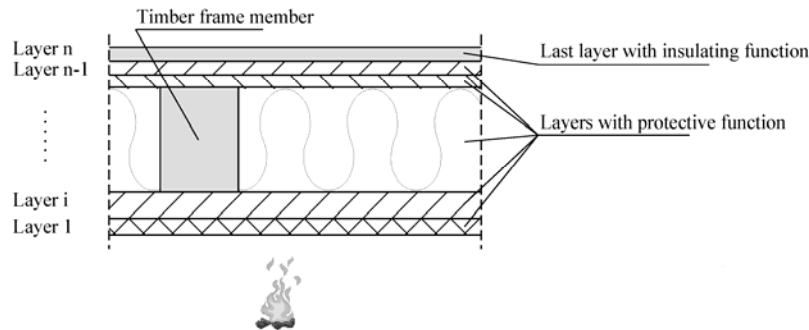


Figure 1. Timber frame wall and floor assemblies: numbering and function of the different layers.

Protection and insulation values of the layers can be calculated according to the following general equations taking into account the basic values of the layers, the coefficients for the position of the layers in the assembly and the coefficients for the joint configurations:

$$t_{prot,i} = (t_{prot,0,i} \cdot k_{pos,exp,i} \cdot k_{pos,unexp,i} + \Delta t_i) \cdot k_{j,i} \quad (2)$$

$$t_{ins,n} = (t_{ins,0,n} \cdot k_{pos,exp,n} + \Delta t_n) \cdot k_{j,n} \quad (3)$$

with	
$t_{\text{prot},0,i}$	Basic protection value [min] of layer i (Fig. 1 and Table I)
$t_{\text{ins},0,n}$	Basic insulation value [min] of the last layer n of the assembly on the fire-unexposed side (Fig. 1 and Table I)
$k_{\text{pos,exp},i}, k_{\text{pos,exp},n}$	Position coefficient that takes into account the influence of layers preceding the layer considered (Table II)
t_i, t_n	Correction time [min] for layers protected by gypsum plasterboards of type F or type X as well as gypsum fibreboards (Table III)
$k_{\text{pos,unexp},i}$	Position coefficient that takes into account the influence of layers backing the layer considered (Table IV)
$k_{j,i}, k_{j,n}$	Joint coefficient

BASIC VALUES

The basic insulation value $t_{\text{ins},0}$ corresponds to the fire resistance of a single layer without the influence of adjacent materials and joints, i.e. the average temperature rise over the whole of the non-exposed surface is limited to 140K, and the maximum temperature rise at any point of that surface does not exceed 180K. The basic insulation value can be assessed by tests or FE thermal analysis. For FE thermal analysis only the temperature criterion 140°C is used. Further, the temperature of the layer at the beginning of the analysis on the fire-exposed side as well as on the fire-unexposed side is assumed as 20°C.

Wall and floor assemblies with only one single layer are rarely used in buildings. Most wall and floor assemblies consist of assemblies having two or more layers (Fig. 1). The contribution to the separating function of the construction of each layer (except the last layer of the assembly on the fire-unexposed side) is mainly the protection of the following layers (Fig. 1). Therefore it seems more appropriate to introduce a basic protection value $t_{\text{prot},0}$ defined as the time until failure of the protective function. In analogy to the calculation for fire protective claddings of load-bearing timber constructions according to EN 13501-2 [13] the definition of the basic protection value $t_{\text{prot},0}$ is illustrated in Fig. 2. The testing method for fire protective claddings is performed with a particleboard with a thickness of 19 mm backing the layer studied. The contribution of the cladding to the fire protection of the particleboard may be assumed to be satisfied if the average temperature rise over the whole exposed surface of the particleboard is limited to 250K, and the maximum temperature rise at any point of that surface does not exceed 270K. For FE thermal analysis only the temperature criterion 250°C is used. Further, the temperature of the layer at the beginning of the analysis on the fire-exposed side as well as on the fire-unexposed side is assumed as 20°C (Fig. 2).

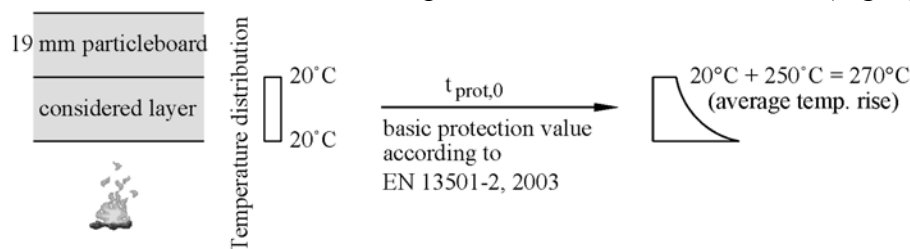


Figure 2. Definition of the basic protection value $t_{\text{prot},0}$ using FE thermal analysis.

Table I gives the equations for the calculation of the basic insulation value $t_{\text{ins},0}$ as well as the basic protection value $t_{\text{prot},0}$ for different materials, that were

systematically calculated using numerical finite elements simulations and verified with fire tests.

Table I. Basic insulation values $t_{ins,0,n}$ as well as basic protection values $t_{prot,0,i}$ for different materials. For rock and glass fibre insulation only the basic protection value $t_{prot,0,i}$ is given as wall and floor assemblies with the insulation as last layer of the assembly are rarely used in buildings.

Material	Basic insulation value $t_{ins,0,n}$ [min]	Basic protection value $t_{prot,0,i}$ [min]
Gypsum plaster-board, gypsum fibreboard	$24 \cdot \left(\frac{h_i}{15}\right)^{1.4}$	$30 \cdot \left(\frac{h_i}{15}\right)^{1.2}$
Solid timber panel	$19 \cdot \left(\frac{h_i}{20}\right)^{1.4}$	$30 \cdot \left(\frac{h_i}{20}\right)^{1.1}$
Particleboard	$22 \cdot \left(\frac{h_i}{20}\right)^{1.4}$	$33 \cdot \left(\frac{h_i}{20}\right)^{1.1}$
OSB, Plywood	$16 \cdot \left(\frac{h_i}{20}\right)^{1.4}$	$23 \cdot \left(\frac{h_i}{20}\right)^{1.1}$
Rock fibre	-	$0.3 \cdot h_i^{(0.75 \cdot \log(\rho_i) - \rho_i/400)}$
Glass fibre	-	for $h_i \leq 40$ mm: 0 for $h_i > 40$ mm: $(0.0007 \cdot \rho_i + 0.046) \cdot h_i + 13 \leq 30$

With h_i : Thickness of the layer considered [mm]
 ρ_i : Density of the layer considered [kg/m^3]

POSITION COEFFICIENTS

The position coefficient considers the position of the layer within the assembly (in direction of the heat flux), because the layers preceding and backing the layer considered have an influence on its fire behaviour. The influence of the layers preceding and backing the layer considered was analysed separately. The position coefficient $k_{pos,exp}$ considers the influence of the layers preceding the layer studied, while the influence of the layer backing the layer studied is considered by $k_{pos,unexp}$.

The position coefficients were systematically calculated using numerical finite elements simulations. The results of the numerical FE simulations showed that the position coefficient $k_{pos,exp}$ is mainly influenced by the furnace temperature at the time when the layer considered is exposed directly to fire as well as the material and thickness of the layer considered, while the influence of preheating is small. As the design model for the verification of the separating function of timber assemblies is developed for ISO fire exposure the furnace temperature is a function of the sum of the protection values of the preceding layers (i.e. $\sum t_{prot,i-1}$). The thickness of the layer considered is expressed by its basic protection value $t_{prot,0,i}$ or basic insulation value $t_{ins,0,n}$. Thus, it was possible to determine the position coefficient $k_{pos,exp}$ as a function of the sum of the protection values of the layers preceding the layer considered ($\sum t_{prot,i-1}$) and the basic values of the layer considered ($t_{prot,0,i}$ and $t_{ins,0,n}$), making the calculation of the position coefficient $k_{pos,exp}$ easy for the designer (Table II).

Table II. Position coefficient $k_{pos,exp,i}$ and $k_{pos,exp,n}$

Material	Position coefficient $k_{\text{pos,exp},i}$ and $k_{\text{pos,exp},n}$
Cladding (gypsum, timber)	$k_{\text{pos,exp},n}$ for $t_{\text{ins},n}$
	$1 - 0.6 \cdot \frac{\sum t_{\text{prot},i-1}}{t_{\text{ins},0,n}} \quad \text{for } \sum t_{\text{prot},i-1} \leq \frac{t_{\text{ins},0,n}}{2}$ $0.5 \cdot \sqrt{\frac{t_{\text{ins},0,n}}{\sum t_{\text{prot},i-1}}} \quad \text{for } \sum t_{\text{prot},i-1} > \frac{t_{\text{ins},0,n}}{2}$
Cladding (gypsum, timber); Rock fibre	$k_{\text{pos,exp},i}$ for $t_{\text{prot},i}$
	$1 - 0.6 \cdot \frac{\sum t_{\text{prot},i-1}}{t_{\text{prot},0,i}} \quad \text{for } \sum t_{\text{prot},i-1} \leq \frac{t_{\text{prot},0,i}}{2}$ $0.5 \cdot \sqrt{\frac{t_{\text{prot},0,i}}{\sum t_{\text{prot},i-1}}} \quad \text{for } \sum t_{\text{prot},i-1} > \frac{t_{\text{prot},0,i}}{2}$
Glass fibre for $h_i \geq 40\text{mm}$	$k_{\text{pos,exp},i}$ for $t_{\text{prot},i}$
	$1 - 0.8 \cdot \frac{\sum t_{\text{prot},i-1}}{t_{\text{prot},0,i}} \quad \text{for } \sum t_{\text{prot},i-1} \leq \frac{t_{\text{prot},0,i}}{4}$ $(0.001 \cdot \rho_i + 0.27) \cdot \left[\frac{t_{\text{prot},0,i}}{\sum t_{\text{prot},i-1}} \right]^{(0.75 - 0.002 \cdot \rho_i)} \quad \text{for } \sum t_{\text{prot},i-1} > \frac{t_{\text{prot},0,i}}{4}$

With ρ_i : Density of the layer considered [kg/m^3]

The position coefficients $k_{\text{pos,exp}}$ given in Table II were calculated assuming that the layers fall off when the temperature of 270°C is reached on the fire-unexposed side of the layers. Fire tests showed that this assumption is conservative for gypsum plasterboards of type F or type X (commonly used in North America) and gypsum fibreboards [7,8]. Therefore the protection or insulation values of layers protected by gypsum plasterboards of type F or type X as well as gypsum fibreboards can be increased using a correction time Δt (Eq. 2 and 3). Table III gives the correction times Δt that were systemically calculated using numerical finite element simulations. For the calculation of Δt it was assumed that for floor assemblies the gypsum plasterboards type F or type X and the gypsum fibreboards fall off when the temperature of 400°C is reached on the fire-unexposed side of the board, while for wall assemblies the falling-off of the boards was assumed by a temperature of 600°C . The temperature criteria were based on the evaluation of a large number of full-scale fire tests found in the literature [7,8].

The influence of the layer backing the layer studied is considered by the position coefficient $k_{\text{pos,unexp}}$. Results of fire tests supported by finite element thermal simulations showed that the influence of the layer backing the layer considered is small if the backing layer is made of gypsum or timber, while insulating batts backing the layer considered caused the layer to heat up more rapidly, reducing the protection time of the layer. Table IV gives the equations for the position coefficient $k_{\text{pos,unexp}}$ for different materials backed by insulating batts, that were systematically calculated using numerical finite elements simulations. For backing layers made of timber or gypsum $k_{\text{pos,unexp},i} = 1.0$ is assumed as a simplification.

Table III. Correction time Δt_i of protection values $t_{\text{prot},i}$ of layers protected by gypsum plasterboards of type F or type X as well as gypsum fibreboards. Correction time Δt_n of insulation values $t_{\text{ins},n}$ can be calculated in the same way.

Material	Δt_i for floor assemblies [min]	Δt_i for wall assemblies [min]
Cladding (gypsum, timber)	$0.06 \cdot t_{\text{prot},i-1} + 1.1 \cdot t_{\text{prot},0,i} - 5$ for $t_{\text{prot},0,i} < 8$ min	$0.06 \cdot t_{\text{prot},i-1} + 1.1 \cdot t_{\text{prot},0,i} - 5$ for $t_{\text{prot},0,i} < 8$ min
	$0.1 \cdot t_{\text{prot},i-1} - 0.035 \cdot t_{\text{prot},0,i} + 1.2$ for $t_{\text{prot},0,i} \geq 8$ min	$0.1 \cdot t_{\text{prot},i-1} - 0.035 \cdot t_{\text{prot},0,i} + 1.2$ for $t_{\text{prot},0,i} \geq 8$ min
Insulation (rock and glass fibre)	$0.1 \cdot t_{\text{prot},i-1} - 0.035 \cdot t_{\text{prot},0,i}$	$0.1 \cdot t_{\text{prot},i-1} + t_{\text{prot},0,i} - 1.0$ for $t_{\text{prot},0,i} < 6$ min
		$0.22 \cdot t_{\text{prot},i-1} - 0.1 \cdot t_{\text{prot},0,i} + 3.5$ for $t_{\text{prot},0,i} \geq 6$ min

Table IV. Position coefficient $k_{\text{pos,unexp},i}$.

Material of the layer considered	$k_{\text{pos,unexp},i}$ for layers backed by cladding made of gypsum or timber	$k_{\text{pos,unexp},i}$ for layers backed by insulation
Gypsum plasterboard, gypsum fibreboard	1.0	$0.5 \cdot h_i^{0.15}$
Solid timber panel		$0.35 \cdot h_i^{0.21}$
Particleboard		$0.41 \cdot h_i^{0.18}$
OSB, Plywood		$0.5 \cdot h_i^{0.15}$
Rock fibre		$0.18 \cdot h_i^{(0.001 \cdot \rho_i + 0.08)}$
Glass fibre		$0.01 \cdot h_i - \frac{h_i^2}{30000} + \rho_i^{0.09} - 1.3$

With h_i : Thickness of the layer considered [mm]

ρ_i : Density of the layer considered [kg/m^3]

VOID CAVITIES AND JOINT COEFFICIENTS

The influence of void cavities between two layers is considered in the design method by modifying the position coefficient $k_{\text{pos,exp}}$ for the layer on the fire-unexposed side of the cavity and the position coefficient $k_{\text{pos,unexp}}$ for the layer on the fire-exposed side of the cavity (Table V).

Table V. Modification of position coefficient $k_{\text{pos,exp}}$ und $k_{\text{pos,unexp}}$ in case of void cavities.

Material	Layer on the fire-exposed side of the cavity	Layer on the fire-unexposed side of the cavity	
Cladding	$k_{\text{pos,unexp},i}$ according to Table IV, column 3	$1.6 \times k_{\text{pos,exp},i}$ according to Table II	$3 \times t_i$ according to Table III
Insulation	$k_{\text{pos,unexp},i} = 1.0$		t_i according to Table III

The joint coefficient considers the influence of joints in panels (claddings) not backed by battens or structural members or panels and their influence on the protection and insulation time of these layers. According to EN 1995-1-2 joints with a gap width greater than 2 mm are not allowed. Results of the fire tests showed that the influence of joints with a gap width less than 2 mm backed by a layer is small. Thus, for simplicity the design method considers the influence of joints only for the last layer of the assembly on the fire unexposed side and for the layer preceding a void cavity. The same values according to EN 1995-1-2 are assumed. For all other layers it is assumed $k_{j,i} = 1.0$.

CONCLUSIONS

The proposed design method is based on physical submodels for each layer and the interaction between the layers forming the assembly. Thus, the total fire resistance is taken as the sum of the contributions from the different layers. The coefficients of the design method were calculated by extensive finite element thermal simulations based on physical models for the heat transfer through separating multiple layered construction. The design method was verified with full-scale fire tests, showing that the model is able to predict the fire resistance of timber assembly safely. The proposed design method significantly extends the application range of the design method according to EN 1995-1-2 by giving additional data as well as physical models for the basic protection and insulation values as well as the position coefficients and permits the verification of the separating function of a large number of common timber assemblies.

REFERENCES

1. Takeda, H. and Mehaffey, JR. WALL2D: A model for predicting heat transfer through wood-stud walls exposed to fire, *Fire and Materials* 1998; 22:133-140.
2. König, J. and Walleij, L. Timber frame assemblies exposed to standard and parametric fires, Part 2: A design model for standard fire exposure, Trätekt, Report I 0001001, Stockholm, 2000.
3. Young, S.A. and Clancy, P. Structural modelling of light-timber framed walls in fire, *Fire Safety Journal* 2001; 36: 241-268.
4. ISO 834-1, Fire-resistance tests—Elements of building construction—Part 1: General requirements, International Organization for Standardization (ISO), Geneva, 1999.
5. EN 1995-1-2, Design of timber structures, Part 1-2 General rules-Structural fire design, CEN, 2004.
6. Schleifer, V., Frangi, A. and Fontana, M. Experimentelle Untersuchungen zum Brandverhalten von Plattenelementen, Report No. 302, Institute of Structural Engineering, ETH Zurich, 2007.
7. Schleifer, V. Zum Verhalten von raumabschliessenden mehrschichtigen Holzbauteilen im Brandfall, PhD Thesis ETH No. 18156, ETH Zurich, 2009.
8. Frangi, A., Schleifer, V. and Fontana, M. Design model for the verification of the separating function of light timber frame assemblies, *Engineering Structures* 2010, 32: 1184–1195.
9. EN 520, Gypsum plasterboards - Definitions, requirements and test methods, CEN, 2004.
10. ASTM C1396 / C1396M - 06a, Standard Specification for Gypsum Board, American Society for Testing and Materials (ASTM), West Conshohocken, 2006.
11. CAN/CSA-82.27-M91, Gypsum Board, Canadian Standards Association, Etobicoke, 1991.
12. EN 15283-2, Gypsum boards with fibrous reinforcement - Definitions, requirements and test methods - Part 2: Gypsum fibreboards, CEN, 2008.
13. EN 13501-2, Fire classification of construction products and building elements—Part 2: Classification using data from fire resistance tests, excluding ventilation services, CEN, 2003.

Design Model for Fire Exposed Cross-Laminated Timber

J. SCHMID, J. KÖNIG and J. KÖHLER

ABSTRACT

Cross-laminated timber (CLT) is increasingly used in medium-rise timber buildings, among other reasons for cost effectiveness and robustness. This paper presents a simple design model using the effective cross-section method for the structural fire design, i.e. the determination of the mechanical resistance with respect to bending (floors). Performing advanced calculations for a large number of lay-ups of various lamination thicknesses, using the thermal and thermo-mechanical properties of wood, charring depths and the reduction of bending resistance of CLT were determined as functions of time of fire exposure. From these results zero-strength layers were derived to be used in the design model using an effective residual cross-section for the determination of mechanical resistance. The model also takes into account different temperature gradients in the CLT in order to include the effect of slower heating rate when the CLT is protected by insulation and/or gypsum plasterboard. The paper also gives results from fire-tests of CLT in bending using beam strips cut from CLT with adequate side protection in order to achieve one-dimensional heat transfer.

Reference tests at ambient temperature were performed to predict the moment resistance of the beams being tested in fire. Both, calculations and tests show that results can be highly dependent on the temperature profile caused by e.g. protection.

Schmid, Joachim, SP Trätekt, Drottning Kristinas väg 67, 11428 Stockholm, Sweden
König, Jürgen, SP Trätekt, Drottning Kristinas väg 67, 11428 Stockholm, Sweden
Köhler, Jochen, Swiss Federal Institute of Technology ETH, IBK - Chair of Risk and Safety,
Wolfgang-Pauli-Str. 158093 Zürich, Switzerland

INTRODUCTION

Cross-laminated timber (CLT) made of flatwise laminations which are held together by bonding are increasingly used both for floors and walls.

In structural fire design, for timber beams and columns EN 1995-1-2 [1] gives a simplified method for the calculation of the mechanical resistance (reduced cross-section model). Apart from charring that reduces the size of the cross-section of the member, the effect of elevated temperature in a ca. 40 mm deep zone below the char layer is taken into account by assuming a zero-strength layer of depth 7 mm immediately below the char layer, and ambient strength and stiffness properties in the remaining effective residual cross-section.

When EN 1995-1-2 was drafted, it was believed that the reduced cross-section method could be applied to timber slabs exposed to fire on one side using a constant zero-strength layer of 7 mm. At that time the use of CLT in housing was just in the beginning. It was not intended that the reduced cross-section method could be applied to this new type of construction without further investigation. A preliminary study [2] on timber decks in bending showed that the application of a zero-strength layer of 7 mm would give unsafe results in many applications. This paper presents an easy-to-use design model for CLT decks (floors) and a comparison with the results from fire tests. CLT walls will be subject of future publications.

COMPUTER SIMULATIONS

ASSUMPTIONS, THERMAL ANALYSIS, STRUCTURAL ANALYSIS

The thermal analyses were performed using SAFIR 2007 [3] using thermal properties of wood given by EN 1995-1-2 [1]. The thermal properties of gypsum plasterboard were similar to those given in [4], however further calibrated to fit test results, see [5].

For the structural analysis, a computer program CSTFire, written as a Visual Basic macro embedded in Excel, was developed, using the temperature output from the heat transfer calculations and the relative strength and stiffness values given by EN 1995-1-2 [1], i.e. compressive and tensile strengths, f_c and f_t , and moduli of elasticity in compression and tension, E_c and E_t . These values are given as bi-linear functions of temperature from 20 to 300°C with breakpoints at 100°C, also taking into account the effects of transient moisture situations and creep, see Fig. 1. The software takes into account the possibility of permitting ductile behavior of wood under elevated temperature since in the fire situation tensile failure of the outermost fibres won't cause immediate collapse of the member since a redistribution of internal stresses will take place as long as equilibrium is maintained.

Since the reduction of strength and stiffness properties is different for tension and compression, CSTFire uses an iteration process, increasing the curvature of the member until the maximum moment resistance is reached. The element size used for the thermal and structural analysis was chosen as 1 mm × 1 mm.

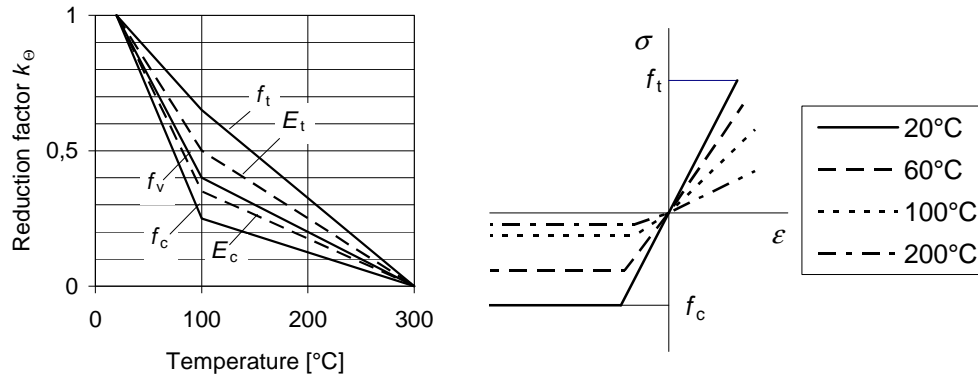


Figure 1. Reduction factors for strength and stiffness properties according to EN 1995-1-2 [1] (left), Temperature-dependent stress-strain relationships for wood for different temperatures (right).

The calculations were conducted assuming material properties that are representative for timber deck plates used in practice, using the stress-strain relationship shown in Fig 1. Since the values of tensile and compressive strength of solid timber given in design or product standards, e.g. EN 338 [6], are values related to the whole cross-section and were determined on the assumption of a linear relationship between stress and strain until failure, the use of these values in a finite element analysis would not be correct [4]. Therefore, compressive strength values were determined using the data from Thunell [7] dependent on density and moisture content as shown in [4]. Calculations in [5] were made assuming $f_t/f_c = (0,92)$. Since the ratio has only a small influence on the results, it can be neglected for practical application. For layers with the grain direction perpendicular to the longitudinal direction of the plate (cross-layers), the modulus of elasticity was assumed to be zero, while these layers were assumed to be completely effective with respect to shear stiffness, i.e. complete composite action of the longitudinal layers was assumed. This assumption is justified by the slenderness ratios of CLT occurring in practice. For deck plates of thickness 150 mm and a typical span of 5,5 m, the slenderness ratio is 30 which increases even more in fire. Due to shear deformations the maximum bending stress is increased by about 3 % [8]. This influence is neglected in the model presented here.

The calculations were carried out for members in bending with depths from 45 to 315 mm, layer thicknesses from 15 to 45 mm and layer numbers from 3 to 7, both for unprotected and protected CLT, and both for the fire-exposed side in tension or compression. Both regular and irregular lay-ups were studied, i.e. regular lay-ups with equal layer thicknesses of longitudinal and cross-layers, and irregular ones where layer thicknesses of longitudinal and cross-layers were different. In all cases, however, all longitudinal layers had the same thickness and the lay-ups were symmetrical.

RESULTS

In the following, some examples from [5] for unprotected and protected CLT with five layers (5x 20 mm) are shown. Definition of zero-strength layer d_0 is given in Fig. 2, simulation results for bending moment ratio M_{fi}/M and charring and d_0 and charring, respectively in Fig. 3.

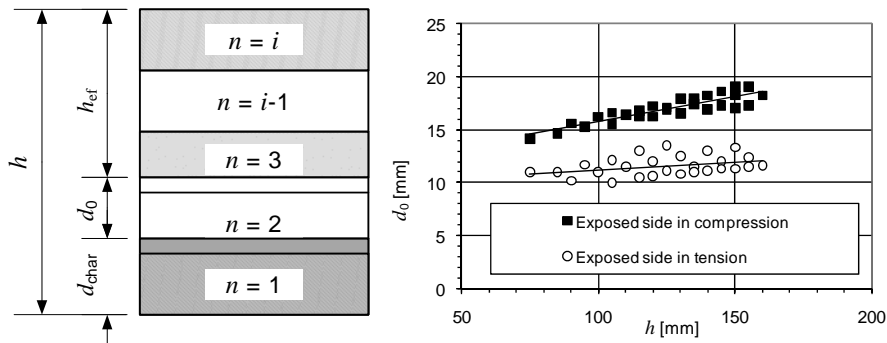


Figure 2: Effective residual cross-section obtained after reduction of original cross-section (left) with charring depth d_{char} and zero-strength layer d_0 (right), determination of linear expression for zero-strength layer d_0 vs. plate depth for unprotected CLT.

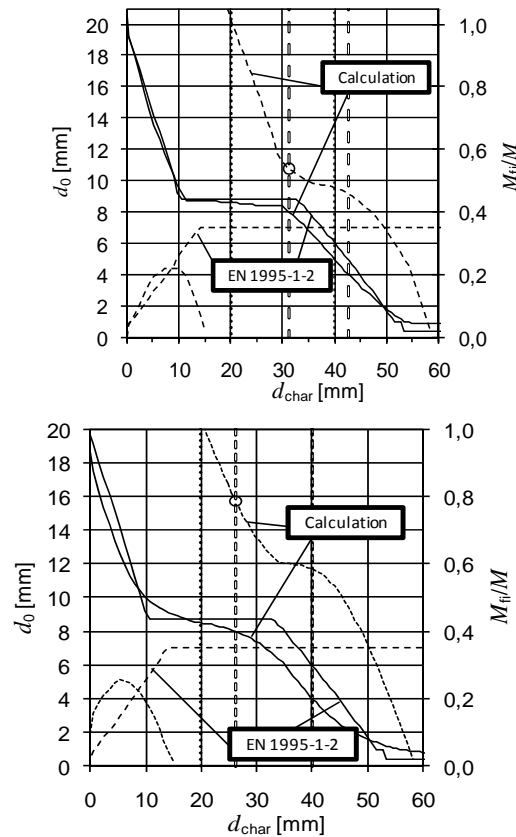


Figure 3: Results for CLT with 5 layers of thickness 20 mm with the fire-exposed side in compression. Broken curves show d_0 . The vertical dotted lines indicate charring of bondline. The black broken bars indicate the 20 and 40 % levels of bending resistance; Exposed side in tension (left) and compression (right).

For the examples shown here, during the first charring phase when charring takes place in the first (load-bearing) layer, the bending resistance is reduced to approximately forty percent of ambient resistance. In the beginning of the next charring phase when charring takes place in the second (non load-bearing) layer, the decay of bending resistance is very slow, but increasing considerably before the char

front has reached the second bond line. At that stage the bending resistance has dropped to twenty-five to twenty percent, depending on the state of stress on the fire-exposed side. When the fire-exposed side is in compression, the reduction of bending resistance is greatest. The charts also show the corresponding zero-strength layers d_0 that should be applied to the cross-section to get the same results using ambient strength and stiffness properties for the effective residual cross-section.

Since the value of d_0 varies considerable with time (or charring depth), in order to simplify the design model, the largest value within the bending resistance interval between 20 and 40 percent was chosen. In Fig. 3 these value is marked as a ring. For the CLT plates shown here, $d_0 = 10,5mm$ for the fire-exposed side in tension and $d_0 = 15,9mm$ for the fire-exposed side in compression can be derived. From the charts can be seen that, for the most relevant stage of relative resistances from 0,2 to 0,4, a constant value of 7 mm (compare [1]) would give non-conservative results in comparison with the results from the simulations.

Calculations were carried out for a large number of lay-ups with five layers. The data for d_0 where the plotted as functions of the depth h of the CLT plate, see Fig. 2.

The trendlines, somewhat modified and simplified, are given in millimeter as:

For unprotected CLT with five layers where the fire-exposed side is in tension

$$d_0 = \frac{h}{100} + 10 \quad (1)$$

For unprotected CLT with five layers where the fire-exposed side is in compression

$$d_0 = \frac{h}{20} + 11 \quad (2)$$

There is a large effect of the protection on the fire resistance since the start of charring is delayed and the charring rate behind the gypsum plasterboard is slower than in the unprotected case. Depending on the build-up the same charring depth (which are valid for different times), the bending resistance is smaller when the CLT is protected. Since the heating rate is smaller due to the protection provided by the gypsum plasterboard the temperature gradient in the wood is smaller than in the unprotected case. Therefore, failure of the gypsum plasterboard has a positive effect on the bending resistance (and the zero-strength layer), however the total effect of failure of the gypsum plasterboard may be negative, since the charring rate increases considerably during the post-protection phase.

The simulations for protected CLT were carried out for a large number of regular lay-ups and protective claddings consisting of one layer (12,5 mm or 15,4 mm thick) or two layers 12,5 + 15,4 mm thick gypsum plasterboard. The gypsum plasterboards were assumed to fall off when the temperature in the interface between gypsum plasterboard and wood was 270, 400, 600 and 800°C respectively. Long protection times lead to small temperature gradients where ambient temperature is reached in larger depths which may result in higher values for d_0 . Contrary char ablation which exposes following layers directly to fire without a protective char layer may lead to high gradients which may lead to lower d_0 .

TESTS

GENERAL

In order to verify the model by tests, two CLT products currently being on the market were chosen. The width of all specimens was 150 mm. The specimens of series M had a lay-up of five layers of equal thickness 19 mm (regular lay-up), i.e. the total thickness was 95 mm, while the lay-up of series S with a thickness of 150 mm was irregular. The width and length of the specimens chosen was governed by the test conditions in the fire situation deviating from EN 789 [9] which requires a span of 32 times the depth of the CLT panel, while the minimum width required by the standard is 300 mm. A sample of each product was subdivided into two groups, one of which was tested in fire (both series) while the other was tested at ambient conditions (both series) in order to provide data for the prediction of the ambient bending moment resistance of the specimens to be tested in fire.

In CLT panels lamellae finger joints are situated randomly. Since finger joints in a lamellae of series SF could have a considerable influence on the bending resistance in fire [10], the specimens of series SR and SF were produced or selected such that they did not contain any finger joints in the most stressed parts of the beams. Since the lamellae of CLT in series M, in practice normally used for walls, are butt-jointed; i.e. the butt-joints are non-loadbearing in tension), the test specimens were produced without any joints in the longitudinal layers. This product will therefore exhibit lower bending strength when the CLT contains butt-joints. All test specimens were conditioned at 20°C and 65 % relative humidity.

Reference tests under ambient conditions

The ambient reference tests of both series were carried out as four-point ramp load tests. The number of tests was 10 (series MR) and 15 (series SR), respectively.

Since two different failure modes were observed, either tensile failure in the outer lamella or shear failure in one or two of the cross-layers (compare Fig. 13) the results of both series were evaluated with respect to the relevant failure mode “failure of tensile lamella”. The parameters of a lognormal distribution have been estimated by using the censored using the Maximum Likelihood Method [11].

FIRE TESTS

GENERAL AND TEST PROCEDURE

Fire tests of specimens in bending were performed for the following cases:

1. Unprotected timber; fire-exposed side in tension (tsw);
2. Unprotected timber; fire-exposed side in compression (csw);
3. Protected timber; fire-exposed side in tension (tsw);
4. Protected timber; fire-exposed side in compression (csw).

In order to simulate the thermal conditions in a CLT plate in fire, i.e. the one-dimensional heat flux, and consequently one dimensional charring, the edges of the

beam specimens were protected by a layer of 20 mm thick pieces of wood and a second layer of 15 mm thick pieces of gypsum plasterboard type F, all of them fixed with nails. These layers were discontinuous in order to prevent composite action. Where the CLT beams were protected, 150 mm long pieces of gypsum plasterboard type F were screwed to the bottom face of the beams with 1 mm gaps between the pieces.

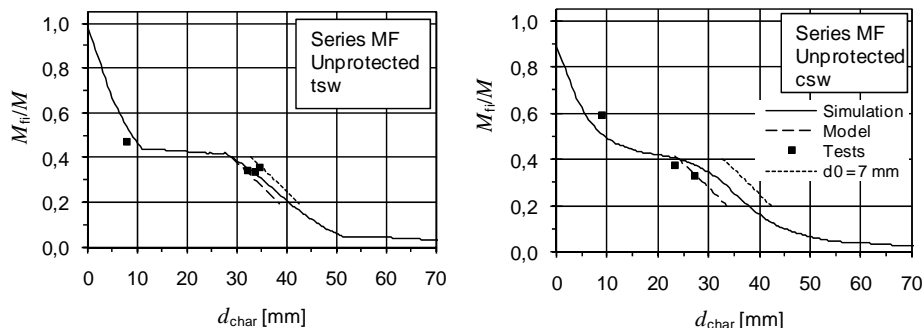
The supports of the specimens were located on the furnace walls outside the heated zone of one meter. The loads could be applied in upward or downward direction; a measuring device was placed on top of the specimens for measuring the deflection. The load was applied prior to the fire test, then the furnace was started and the load was kept constant until failure. Unlike the failure modes observed during the ambient reference tests, failure in fire was preceded by extensive deflections.

At bending failure or when the load could not be held constant, the burners were turned off, the specimen removed from the furnace and the fire in the wood extinguished with water. The time elapsed from turning off the burners to extinguishing the fire was normally from 1 to 1,5 minutes.

TEST RESULTS

From each of the test specimens, at five locations, the residual cross-sections were used to record the borderline of the shape. From these data, the area, second moment of area and the section modulus were determined. Since the charring depth was not equal over the width of the beams, the area was used for the calculation of the mean charring depth for a cross-section. For the determination of the second moment of area, only load-bearing layers (with the grain in longitudinal direction) were considered.

Comparisons of test results with the simulations using the dimensions of the test beams are shown in Fig. 5 with relationships of the bending resistance ratio versus charring depth. For each test, the bending moment resistance was predicted using the results from the reference tests at ambient temperature. The graphs also show the relative bending resistance obtained using the simplified model for the zero-strength layer, and the value that would be obtained applying a zero-strength layer of $d_0 = 7\text{ mm}$ as given in EN 1995-1-2 [1]. Since the model was fitted to give best results in the range of a relative bending resistances between 0,2 and 0,4, the values are only shown for this interval.



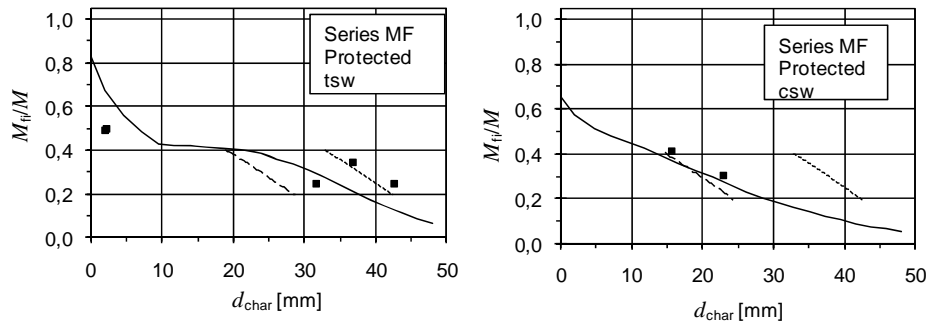


Figure 5: Comparison of Test results with simulation and simplified design model for series MF, unprotected and protected, with the fire-exposed side in tension "tsw" (left) and in compression "csw" (right).

In general, the test results agree fairly well with the simulations. Some deviations are, however, noticeable. A more in-depth analysis of the specimens after fire tests showed that some specimens exhibited local deficiencies of charring depth, caused by char ablation or other. This may have caused lower bending resistances of some tests. Since such local deficiencies are more effective in narrow beams, it can be argued that CLT of sizes used in practice are less vulnerable to local defects.

The simplified model for the zero-strength layer normally gives conservative results compared with the simulations, except for protected CLT. Non-conservative deviations are due to the assumption that the cladding would fall off after some time; during the fire tests, however, the protective cladding remained in place during the fire tests. The assumption of a zero-strength layer equal 7 mm gives unsafe results, especially when the fire-exposed side is in compression.

CONCLUSIONS

It has been shown that the complex performance of CLT exposed to fire can be described by advanced computer simulations, using the thermal and thermo-mechanical properties of wood given by EN 1995-1-2 [1] and that the simulation results are verified by test results from fire tests. In order to present a user-friendly easy-to-use design model for members in bending, the concept of the reduced cross-section method given in [1] was adopted and zero-strength layers determined for consideration of the reduced strength and stiffness properties at elevated temperatures. The simplified model gives reliable results, while the adoption of the zero-strength layer equal to 7 mm, as given in [1] for beams and columns, normally gives non-conservative results.

ACKNOWLEDGEMENT

The research described here was conducted at SP Trätekt, Stockholm, as a part of the FireInTimber project within the European Wood-Wisdom-Net framework. It is supported by industry through the European Initiative Building With Wood and public funding organisations. The test specimens were produced and delivered by Martinsons Trä (Sweden) and Stora Enso Austria.

REFERENCES

1. EN 1995-1-2, “Eurocode 5: Design of timber structures—Part 1-2: General—Structural fire design”, *European Standard*, European Committee for Standardization, Brussels, 2004.
2. König, J, Schmid, J., “Bonded timber deck plates in fire”, *Proceedings of CIB W18, Meeting 40*, Bled, Slovenia. Lehrstuhl für Ingenieurholzbau, University of Karlsruhe, Karlsruhe, Germany, 2007.
3. Franssen, J.M, Kodur, V.K.R., Mason, J., “User’s manual for SAFIR 2007—A computer program for analysis of structures subjected to fire”, University of Liege, Department Structures du Génie Civil – Service Ponts et Charpentes. Liege, Belgium, 2005.
4. Källsner, B. and König, J., “Thermal and mechanical properties of timber and some other materials used in light timber frame construction”, *Proceedings of CIB W18, Meeting 33, Delft*, Lehrstuhl für Ingenieurbau, University Karlsruhe, Karlsruhe, Germany, 2000.
5. Schmid, J, König, J., “Cross-laminated timber in fire. Research report SP”, in preparation, to be published 2010.
6. EN 338:2003, “Structural timber—Strength classes”, *European Standard*, European Committee for Standardization, Brussels, 2003.
7. Thunell, B., ”Hållfasthetsegenskaper hos svenskt furuvirke utan kvistar och defekter”, *Royal Swedish Institute for Engineering Research, Proceedings No. 161*, Stockholm, 1941.
8. Blass, H, Görlacher, R, “Brettsperrholz—Grundlagen. *Holzbau-Kalender* 2. 2003 (2002) S. 580-598.
9. EN 789:2004, “Timber structures—Test methods—Determination of mechanical properties of wood based panels”, *European Standard*, European Committee for Standardization, Brussels, 2004.
10. König, J, Norén, J, Sterley, M, “Effect of adhesives on finger joint performance in fire”, *CIB W18, Meeting 41*, St. Andrews, Canada. Lehrstuhl für Ingenieurholzbau, University of Karlsruhe, Karlsruhe, Germany, 2008.
11. Steiger, R, Köhler, J., “Analysis of censored data—examples in timber engineering research”, *Proceedings of CIB W18, Meeting 38*, Karlsruhe, Lehrstuhl für Ingenieurbau, University Karlsruhe, Karlsruhe, Germany, 2005.

Failure Mechanisms of Structural Insulated Panel (SIP) Systems Under Natural Fire Conditions

D. HOPKIN, T. LENNON, J. EL-RIMAWI and V. SILBERSCHMIDT

ABSTRACT

Structural Insulated Panels (SIPs) are formed from the lamination of two oriented strand board (OSB) facing plates and a highly insulated polymer based foam, such as expanded polystyrene (EPS) or polyurethane (PUR). The resulting lightweight panels are then used as primary load bearing compression elements for buildings such as domestic dwellings, apartment blocks, schools and hotels.

The regulatory fire performance of SIPs, like many systems, is assessed via a standard fire test. However, it is widely accepted that this is merely a comparative method for determining one product's performance relative to another and hence gives little indication of a component's likely behaviour in a real fire. With this in mind BRE Global, with support from the UK Government, have undertaken a research programme to determine the fire performance of SIPs. The project comprised a programme of laboratory testing on single panels, numerical modelling and four full scale fire tests on two storey SIP structures incorporating engineered joist floors. This paper presents the findings of the large scale experiments. A companion paper discusses the laboratory work undertaken [1].

The aim of this paper is to present the findings of the large scale fire experiments. In summary, it has been found that SIPs systems may be able to meet the performance requirements of the UK Building Regulations. However, combustion of floor joists may lead to excessive deflection accompanied with a large rate of deflection as collapse is approached.

D. Hopkin & T. Lennon, BRE Global, Garston, Herts, WD25 9XX, UK (HopkinD@bre.co.uk)
J. El-Rimawi, Dept. of civil and building engineering, Loughborough University, UK.
V. Silberschmidt, Wolfson school of mechanical engineering, Loughborough University, UK.

INTRODUCTION

The fire performance of SIP structures was identified as a major concern of key stakeholders including mortgage lenders, insurers, regulators and the fire and rescue service in a previous scoping study undertaken for the UK Government on Innovative Construction Products and Techniques [2]. As a result the overall aim of the project was to undertake an experimental programme to determine the resistance of a typical Structural Insulated Panel (SIP) system to a realistic fire scenario and to compare the results to the outcome from standard fire tests. Four experiments were completed in BRE's large scale test facility. The experimental work aimed to simulate realistic fires in single (houses) and multi-occupancy (apartment block) dwellings and, as such, were loaded appropriately using sand bags. The programme comprised two experiments on expanded polystyrene (EPS) SIP structures, one with a 30 minute fire resistant plasterboard lining and one with a 60 minute fire resistant plasterboard lining. In addition two experiments were conducted on structures formed from SIPs with polyurethane (PUR) cores, again with 30 and 60 minute fire resistant plasterboard linings respectively.

THE TEST PROGRAMME

Four large scale fire tests have been undertaken on structures built from SIP systems and protected from the effects of fire by fire resistant plasterboard linings. The order and configuration of the tests is as shown in Table I. The two most common types of insulation material used by the UK SIPS industry (EPS and PUR) have been tested. The test parameters are discussed in greater detail in the sections that follow.

Description of the test compartments

In total four experimental compartments/buildings were constructed by specialist contractors experienced in SIP installations. The buildings were constructed and tested in series of two (EPS then PUR) inside BRE's large scale test facility in Middlesbrough, UK. The structures were essentially two storey high compartments measuring 4x3m on plan and 4.8m in height (floor to first floor ceiling). The specification for the structures is summarised in Table II.

TABLE I. EXPERIMENTAL PROGRAMME.

Test	Design fire resistance period (min)	Core material	Height to underside of floor (m)	Floor area (m)	1 st floor loading (kN/m ²)	2 nd floor loading (kN/m ²)
F1	60	EPS	2.4	4 x 3	0.75	2.25
F2	30	EPS	2.4	4 x 3	0.75	0.75
F3	60	PUR	2.4	4 x 3	0.75	2.25
F4	30	PUR	2.4	4 x 3	0.75	0.75

TABLE II. TEST BUILDING SPECIFICATION.

	F1	F2	F3	F4
Wall lining	30mm type F plasterboard	15mm type F plasterboard	30mm type F plasterboard	15mm type F plasterboard
Party wall	See specification for 60 minute wall linings.			
Ceiling lining	30mm type F plasterboard	15mm type F plasterboard	30mm type F plasterboard	15mm type F plasterboard
SIP construction	11mm OSB either side of 89mm EPS core apart from the two load-bearing walls which have a 140mm core due to the increased load level.	11mm OSB either side of 89mm EPS core.	15mm OSB either side of 114mm PUR core.	
First floor timber	220mm x 58mm engineered floor joists (I section) @ 600mm centres – span in long direction.		245mm x 45mm engineered floor joists (I section) @ 600mm centres – span in long direction.	
Second floor timber	220mm x 89mm engineered floor joists (I section) @ 400mm centres – span in long direction.	220mm x 58mm engineered floor joists (I section) @ 600mm centres – span in long direction.	245mm x 45mm engineered floor joists (I section) @ 400mm centres – span in short direction.	

Fire load, imposed loading and test initiation

The purpose of the experiments was to evaluate the response of the SIP systems to a “realistic” fire scenario such as may occur in a room within a modern apartment building or dwelling. The dimensions and ventilation condition within the room of origin were consistent with a fire within the living area of an apartment building or house where the door is closed. They are also consistent with previous research into the performance of timber frame structures in fire [3]. In terms of the fire loading, it was determined that, based on the compartment geometry and available ventilation, a fire load density of 450 MJ/m² was required to achieve a fire of 60 minutes ISO834 equivalent. The equivalent severity was calculated using the time equivalence method of BSEN 1991-1-2 [4] taking into account the number and size

of openings and floor area. In addition the predicted compartment time-temperature response was calculated according to the parametric approach detailed in annex A of BS EN 1991-1-2 [4]. The design fire load was provided by twelve cribs each with 25 kg of solid timber, giving a total fire load of 5400 MJ for each experiment.

The 30 minute solution (F2 and F4) effectively modelled a two- storey domestic dwelling. The resulting applied load on the floor under test was 0.75 kN/m² per floor. The load was applied by sandbags weighing 25kg per bag resulting in 37 bags per floor.

The 60 minute solution (F1 and F3) modelled a four-storey building and the loading in the lower wall panels needed to reflect this. The second floor was loaded to a value of $3 \times 0.75 \times 4 \times 3 = 27\text{kN}$ or 2752kg made up from 110 sandbags (equivalent of 3 levels of imposed load). The design and spacing of the floor joists for the second floor reflected this increased load. The first floor was loaded in an identical manner to the 30 minute case.

The fire load was composed of 12 timber cribs spread uniformly over the floor area each consisting of 50 sticks of 50mm x 50mm x 500mm long softwood. Each crib was connected to the adjacent crib by means of a porous fibre strip. Prior to ignition approximately 1 litre of paraffin was poured over the fibre strips. The fire was ignited by setting light to each of the fibre strips.

RESULTS

Experiments F1 and F3 were terminated once the fire was around half way into its cooling phase. Experiments F2 and F4 were terminated at the peak of the compartment temperature development due to imminent collapse of the floor system. Termination times are summarised with other relevant information in Table III. In the inspection of the results discussed below Figure 1 should be referenced.

Fire development

The average measured compartment time-temperature curves for the four tests are shown in Figure 2. The figure also includes the standard fire curve and the predicted response according to the Eurocode parametric approach [4]. Generally the agreement between the measured and parametric prediction of the compartment temperature is very good. However the parametric approach is a little un-conservative in the prediction of peak compartment temperatures. It also under predicts the duration of the heating phase of the fire where the experiments have been allowed to enter the cooling phase.

TABLE III- SUMMARY OF RESULTS.

Experiment	Termination time (min)	Peak floor temp (°C)	Peak floor deflection (mm)
F1	75	200	10
F2	50	897	203
F3	87	237	16
F4	52	664	121

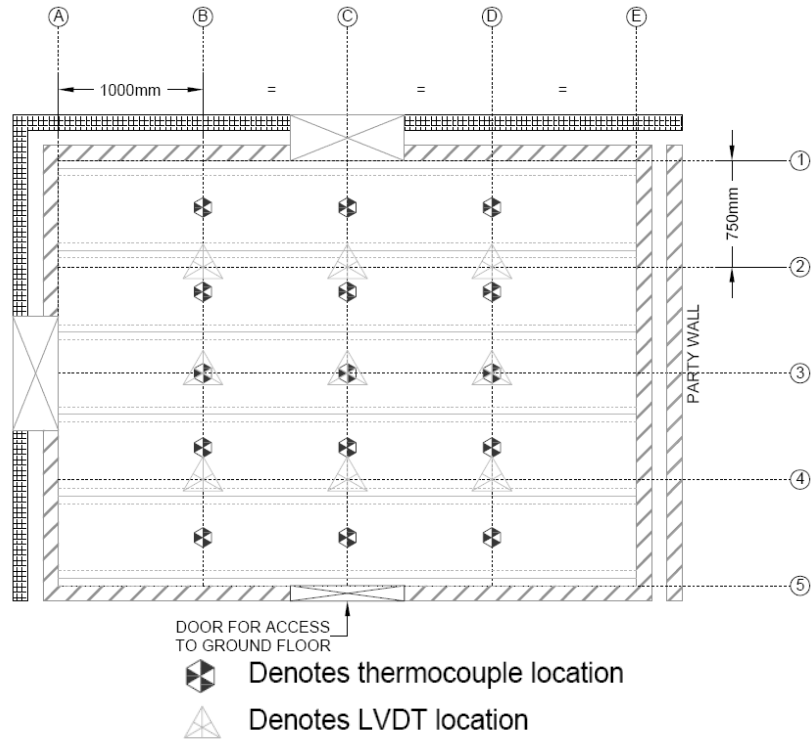


Figure 1. instrumentation locations.

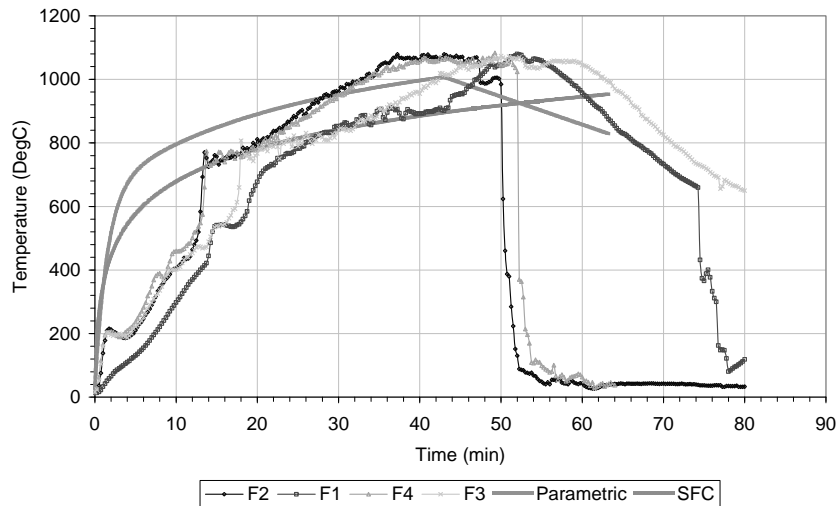


Figure 2. Average compartment temperatures with design parametric and standard fire curves.

Structural performance

The mid-span deflection of the joists spanning above the fire compartment for each experiment are shown in Figure 3. Quarter point deflections for experiments F1 and F3 were also measured (Grid lines B and D) however these have been omitted for clarity. The clear difference between floors protected with 15mm type F plasterboard (F2 & F4) and 30mm type F plasterboard (F1 and F3) is apparent in

Figure 3. The displacements in the former tests are an order of magnitude larger than the systems protected with 30mm plasterboard. The additional deflection associated with experiments F2 and F4 can be attributed to the high temperatures noted in the floor space, as shown in Figures 4 and 5.

POST TEST OBSERVATIONS

The test results and observations have highlighted a number of important issues in relation to the inherent fire resistance of the structural system:

SIP systems are capable of achieving the requirements of the performance criteria in Approved Document B to the UK Building Regulations [5] in relation to B2 internal fire spread (linings) and B3 internal fire spread (structure).

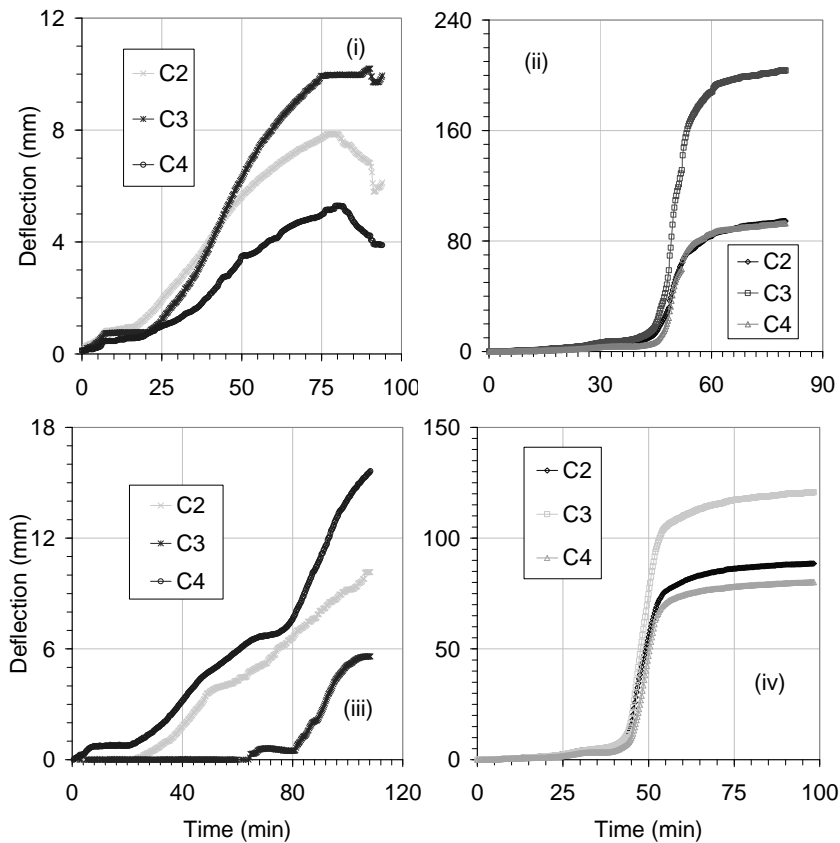


Figure 3. Floor deflections along grid line C for (i) F1, (ii) F2, (iii) F3 & (iv) F4.

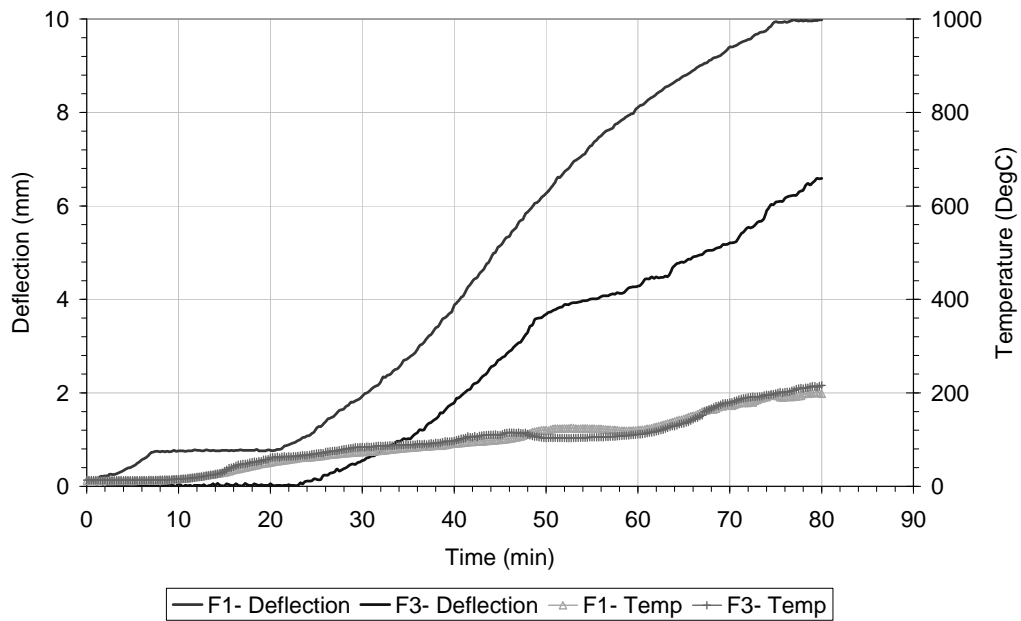


Figure 4. Displacement versus temperature for floor void- 60 minute buildings.

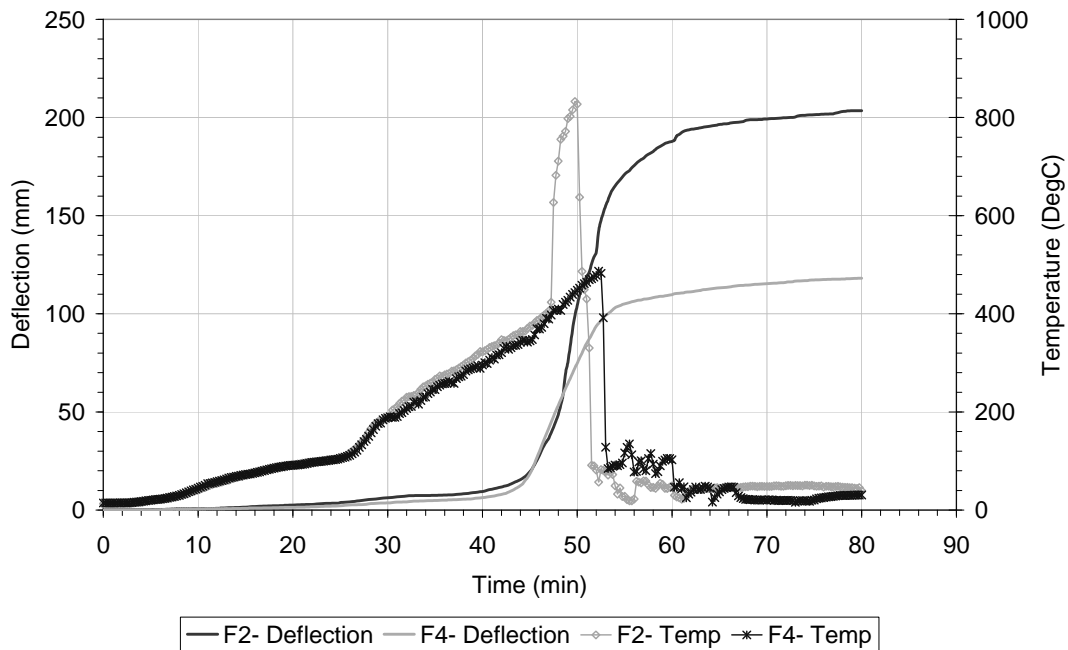


Figure 5. Displacement-temperature for floor void – 30 minute buildings.

The mode of failure of the system is excessive deflection of the first floor caused by ignition and rapid combustion of the engineered floor joists. The rate of deflection increases very rapidly as the floor system approaches collapse. This behaviour is not influenced by the performance of the SIP system and

would be the same for other panellised systems, traditionally built timber frame or joists supported on masonry walls [6].

There was no collapse of the floor in any of the tests despite the significant (>200mm or span/20) deflections. The chipboard flooring appears to have contributed to the stability of the floor at large deflections. Inevitably, in the instance of both the PUR 30 and EPS 30 compartments, the floors would have collapsed had the fire and rescue service not intervened. There was no collapse of the wall panels in any of the tests. There was also no obvious deflection or deformation of the wall members.

There was no integrity failure of either the wall panels or the floor system.

At the end of the tests, the composite action assumed in design can no longer be relied on due to either degradation of the inner layer of OSB and melting of the core (EPS) or degradation of the OSB and combustion of the core (PUR). As there was no collapse of the buildings, it is clear that an alternative load path was mobilised at the fire limit state. Load carrying capacity was maintained through the solid timber ring beams at first floor level and the presence of intermediate timber in the panels either at junctions between panels or around openings and the presence of timber studs in the corner.

There was no significant damage to the ring beam in any of the tests.

There was no evidence of any failures in the connections between the engineered floor joists and the timber ring beams.

ACKNOWLEDGMENTS

The authors would like to acknowledge CLG for funding this programme of work. The work reported herein was carried out under a contract placed by CLG and any views expressed are not necessarily those of CLG. The authors also acknowledge the contribution of the UK SIPs Association. Mr. Hopkin would like to thank EPSRC for continuing to fund his research work with Loughborough University. Finally, the authors would like to thank La Farge for their support with the experimental programme.

REFERENCES

1. Hopkin, D., Lennon, T., El-Rimawi, J., and Silberschmidt, V., 2010. A laboratory study into the fire resistance performance of structural insulated panels. Proceedings of the sixth international conference on structures in fire, Michigan 2-4th June 2010.
2. Communities and Local Government, Innovative Construction Products and Techniques BD 2503, Communities and Local Government, London, January 2008.
3. Lennon T, bullock M J and Enjily V, 2000. The fire resistance of medium rise timber frame buildings, Proceedings of the World Conference of Timber Engineering, Whistler, Canada.
4. British Standards Institution., 2002. Eurocode 1: Actions on structures – Part 1-2: General actions – Actions on structures exposed to fire, , BS EN 1991-1-2, BSI, London.
5. Communities and Local Government, 2007. The Building Regulations 2000, Fire Safety, Approved Document B, 2006 edition, NBS, London.
6. Lennon, T., Hopkin, D., El-Rimawi, J., and Silberschmidt, V., 2010. Large scale natural fire tests on protected engineered timber floor systems, Fire Safety J (2010), doi:10.1016/j.firesaf.2010.02.006 (in print).

Fire Resistance of Connections in Timber Structures

P. J. MOSS, T. M. NILSEN, M. FRAGIACOMO and A. H. BUCHANAN

ABSTRACT

This paper describes a series of experiments to obtain the embedment strength of wood at elevated temperatures. The results will be used in Johansen's yield equations to predict the fire resistance of nailed, screwed, and bolted timber connections. Johansen's yield equations are used in Europe and USA to predict the ultimate strength of bolted or dowelled connections in timber members, but only at ambient temperatures. Recently, several researchers have begun to investigate the embedment strength of bolted or dowelled connections at elevated temperatures applicable to fire conditions. Embedment strength varies with temperature. Recent studies have proposed a tri-linear relationship for bolted connections in LVL, following embedding tests carried out at high temperatures in accordance with the ISO standard. This research extends the investigation to determine if the model is accurate for other types of connections such as screws and nails.

All connection specimens had exposed steel side plates. Bolts, nails and screws were tested by loading in shear. Temperatures ranged from ambient to 250°C. The programme was divided into two different heating regimes. In Part 1, screwed connections were tested in tension parallel to grain, using a constant temperature furnace with 2 hours pre-heating time. In Part 2, compression tests were performed on nailed, bolted and screwed connections both perpendicular and parallel to grain, after several hours of heating for long enough to obtain a constant temperature throughout the wood.

The results from short-term heating tests (Part 1) and longer-term heating tests (Part 2) show very different answers. The two hour heating tests showed a tri-linear decline of the embedment strength, as found by earlier experiments, while the longer-term oven tests shows a more linear decline. The difference is attributed to different moisture profiles in the wood. The paper shows how this information can be used in design of timber fasteners for fire resistance.

Peter Moss, University of Canterbury, Christchurch, New Zealand
Trygve Nilsen, University of Trondheim, Trondheim, Norway
Massimo Fragiaco, University of Sassari, Alghero, Italy
Andrew Buchanan, University of Canterbury, Christchurch, New Zealand

INTRODUCTION

In recent years, a number of papers have been published on the performance of joints in timber members when subjected to fire temperatures [e.g. 1-8].

Over the last five years, research at the University of Canterbury has investigated the fire performance of a range of connections. This research focused initially on the fire resistance of nailed, screwed, bolted and self-drilling doweled connections in laminated veneer lumber (LVL) members. This was later extended to research the embedment strength of LVL timber product exposed to elevated temperatures up to 250°C, using bolted connections. More recently, a range of tests have been carried out on bolted Wood-Steel-Wood (WSW) connections and limited number of tests on screwed Steel-Wood-Steel (SWS) connections. A summary of the research on the fire performance of connections in LVL can be found in a number of papers [e.g. 9-12].

Looking at this previous research it becomes clear that little research has been carried out into the performance of screwed connections loaded parallel to grain in heated and fire conditions. Screws could show unexpected performance due to the increase in capacity caused by the withdrawal strength of the threaded part. There is also a need for testing of all types of connections loaded in compression perpendicular to the grain in heated and fire conditions. This paper looks at the embedment strength of nailed, screwed, and bolted connections in 36 and/or 63 mm thick laminated veneer lumber (LVL) made of New Zealand radiata pine both parallel and perpendicular to the grain, as well as the fire performance of screwed connections.

TEST PROGRAMME

The programme was carried out in three parts though only the first two are reported herein. All connection specimens had steel side plates to connect the LVL members. In Part 1, screwed connections were tested parallel to the grain after being heated in a constant temperature furnace for two hours. In Part 2, tests were performed on nailed, screwed, and bolted connections both parallel and perpendicular to the grain, after several hours of heating in an oven to obtain a constant temperature throughout the wood.

a. Part 1—Two hour heated tests on screwed connections (temperature gradient)

The connection tested is shown in Figure 1 with three screws per side in a triangular pattern. The LVL was 63 mm thick and 150 mm wide. The screws were 4.4 mm diameter and 65 mm long. The steel side plates were 6 mm thick. Thermocouples were inserted into the centre of each LVL member and between the steel side plate and the LVL member. Tests were carried out in a custom-made furnace with loading rig after two hours heating at constant temperatures ranging from ambient to 280°C with loading carried out as set out in ISO 10984-2 [13].

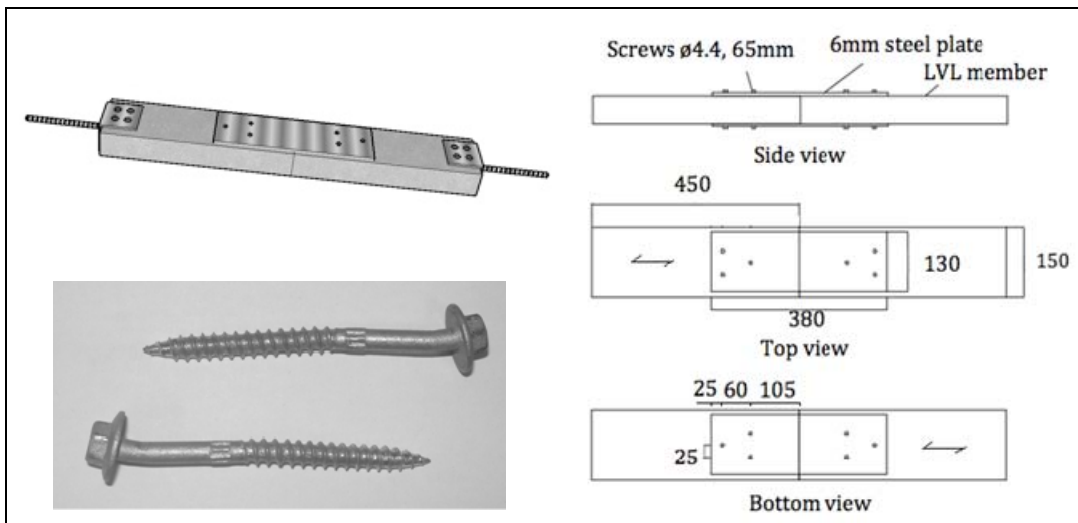


Figure 1. 3D view of screwed LVL connection specimens for tension tests, photo of the screws after the test, and dimensions (mm) for the heated tests.

b. Part 2—Long duration heated tests on nails, screws, and bolts (uniform temperature)

The connections used nails, screws, or bolts, to connect a 75 mm wide, 250 mm length of LVL to two 6 mm thick steel side plates. The tests were carried out using 63 mm thick LVL and the bolted tests were later repeated using 36 mm thick LVL to ensure that the bolts remained straight during the tests. The connections were preheated in an oven for between three and sixteen hours so that all of the wood was at uniform temperature and all the wood was dry.

For the nailed connections, two 60 mm long nails, one from each side with a spacing of 20 mm, with a diameter of 4.2 mm were used, as shown in Figure 2. The nail holes were predrilled to prevent splitting of the wood.

In the case of the screwed connections, two screws, one from each side with a spacing of 20 mm, with a diameter of 4.4 mm were used, in the same arrangement as for the nailed connection (Figure 2).

The bolted connection used a single 20 mm diameter bolt as shown in Figure 2.

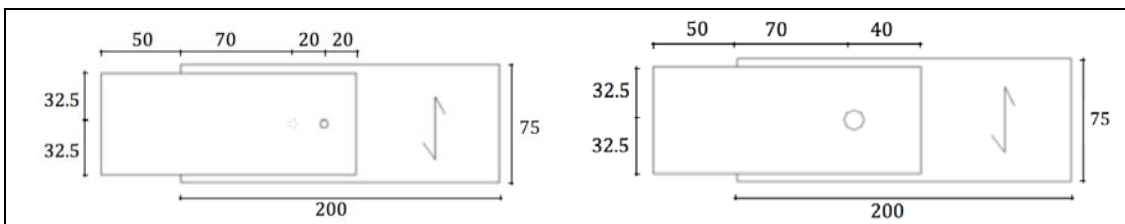


Figure 2. Dimensions (mm) of nailed and screwed connections with LVL loaded perpendicular to grain (left) and of bolted connections with LVL loaded perpendicular to grain (right).

RESULTS

a. Part 1—Two hour heated tests on screwed connections

The load-deformation curves for the screwed connections tested are shown in Figure 3. In all the tests, the screws remained relatively straight on one side of the connection, while on the other side the screws were bent with the formation of two plastic hinges along the screws as shown in Figure 1, and in some cases there was eventual fracture of the screw heads brought about by restraint from the steel side plates. The formation of two plastic hinges along the screws corresponds to a mode d failure according to Eurocode 5 [14]. In order to calculate the embedment strength, $f_{h,l,k}$, for the screws, it is necessary to determine the withdrawal strength $F_{ax,rk}$. The withdrawal strength for the screws used in these tests was based on tests by Gaunt and Penellum [15], modified to allow for differences in screw diameters and lengths. This gives a withdrawal strength per screw, $F_{ax,a}$, of approximately 5.7 kN, which corresponds to an addition by rope effect of 1.4 kN per screw ($\frac{1}{4}$ of $F_{ax,a}$) at ambient conditions. 1.4 kN equals 39% of the Johansen part in the ambient tests performed on the screwed connection and is less than the 100% limit permitted by EC5 [14]. The change of withdrawal strength at elevated temperature is unknown and a 39% constant rope effect is therefore assumed at any temperature. The resulting embedment strength as a function of temperature is given in Figure 3.

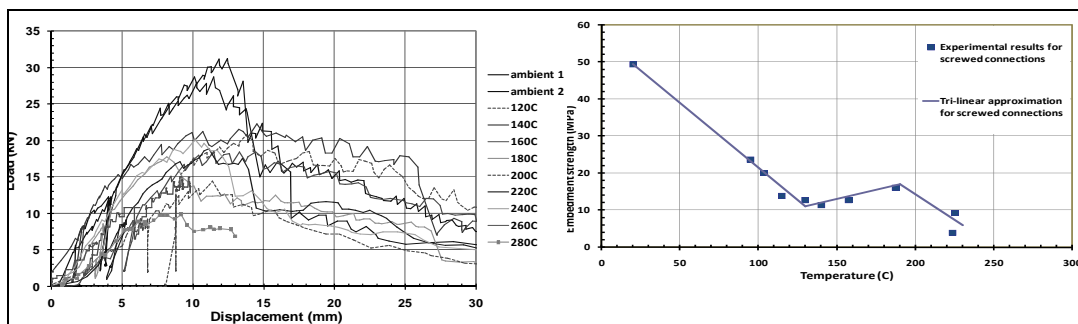


Figure 3. Load-slip curves for the screwed connections tested in tension at different temperatures (left) and embedment strength variation of screwed connection failing by mode d, Johansen equations (right).

b. Part 2—Long duration heated tests on nails, screws, and bolts

The load-displacement curves for some of the connections tested are shown in Figure 4. The individual curves are less important than the overall trends that can be observed. The results for the screwed connections were similar to those for the nailed connections, while the results for the bolted connections in 36 mm LVL were similar to those shown for the 63 mm LVL.

The load-deflection curves for the nailed and screwed connections show similar results for both the parallel and perpendicular to grain tests. All the nailed connections show increasing load capacity as the displacement increased beyond 5 mm, except for the 150°C tests, which failed after only 3-4 mm displacement. The screwed connections also showed similar results for both the parallel and

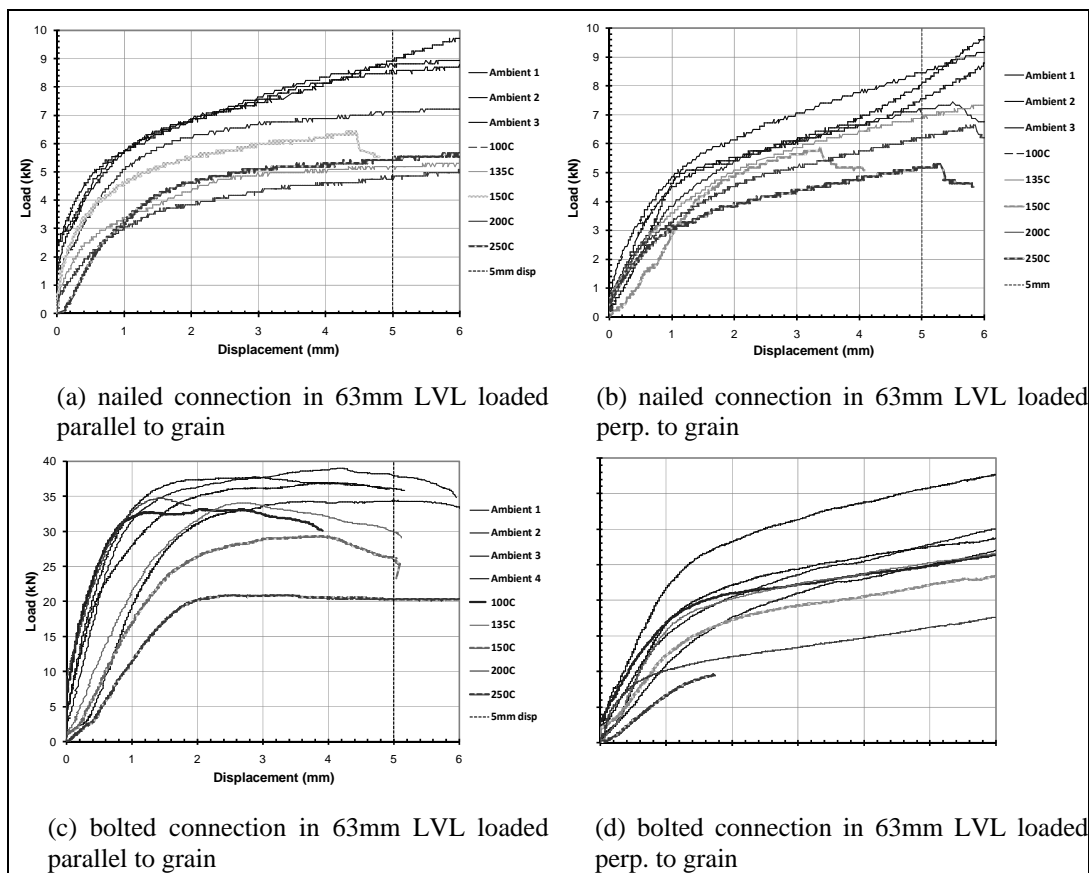


Figure 4. Load-displacement curves for the nailed and bolted connections in the Part 2 tests.

perpendicular load cases, and increasing strength up to failure at 5–7 mm displacement. The failure mode for both the nailed and screwed connections was the same as in the Part 1 tests on screwed connections with two plastic hinges formed along the fasteners and eventually followed by fracture.

The bolted connections failed at larger displacements and larger loads. In both the parallel and perpendicular load to the grain tests, the bolt holes elongated and the wood eventually split in the direction of the grain. In the perpendicular to grain tests, the connections resisted increasing load as the displacements increased and failed at displacements greater than 5 mm. The parallel to grain tests generally reached the maximum load at less than 5 mm displacement (i.e. about 2-3 mm). The tests using 63 mm LVL reached loads in the range of 1.5 to 2.5 of those for tests using 36 mm LVL. For the parallel to grain tests using 63 mm LVL, the 100°C and 200°C tests failed at low displacements, but after the maximum loads were reached. The bolts in the bolted connections remained straight at failure and this was a failure by crushing of the wood in mode j according to Johansen’s equations [14].

The maximum loads obtained are summarized in Table I. These maximum loads are used when calculating the embedment strength. Maximum load was either that found at 5 mm displacement or the maximum value if that occurred earlier. As expected the parallel to grain bolted connections achieved higher maximum loads than the perpendicular ones. For the nailed and screwed connections, there is little difference between the parallel and perpendicular to grain results. Screwed

connections could withstand higher loads than nails due to the extra withdrawal strength of the screws. It can be seen that there is not much drop off until a temperature of 150°C or 200°C is reached, as indicated in Table I.

TABLE I MAXIMUM EXPERIMENTAL LOADS (kN), PART 2.

		Temp (°C)	20*	100	135	150	200	250
Connection	Grain							
Bolt 36mm LVL	Par.		19.8	17.0	19.0	13.0	12.8	15.5
Bolt 36mm LVL	Perp.		14.4	13.6	15.5	10.6	8.8	4.7
Bolt 63mm LVL	Par.		37.1	33.0	34.0	30.2	35.0	21.0
Bolt 63mm LVL	Perp.		30.5	25.0	25.3	22.2	16.2	12.1
Nail	Par.		8.7	7.1	5.2	6.4	4.8	5.4
Nail	Perp.		8.1	7.2	7.0	6.0	6.2	5.2
Screw	Par.		11.8	9.9	9.7	12.1	7.1	10.4
Screw	Perp.		11.9	10.4	8.2	12.6	6.8	7.0

* average of three tests

EMBEDMENT STRENGTH

The embedment strength is found by back calculating the Johansen's equation that corresponds to the failure mode. For the nailed and screwed connections, this requires that the rope effect is known. The rope effect was estimated as follows. The withdrawal strength of a nail was based on that from the report by Gaunt and Penellum [15] modified for the different diameters and lengths which gives a withdrawal strength of 1.60 kN per nail. The rope effect is, according to EC, ¼ of the withdrawal strength, which equals 0.40 kN per nail. This is the same as 8.3% of the experimental Johansen term for ambient temperature and is less than the 15% allowed in EC5 [14]. The change of withdrawal strength at elevated temperature is unknown and 8.3% constant rope effect is therefore assumed at any temperature. A yield moment of 9.3 kNmm was used with a linear decay after 215°C.

EC5 [14] states that small screws can be expected to behave like nails. Since the nails and screws all failed with the formation of two plastic hinges along the screws corresponding to a mode d failure, the embedment strength for both the nails and screws could be determined as in Part 1. The bolts in the bolted connections remained straight for the parallel and perpendicular to the grain tests on both thicknesses of LVL tested. Since the 6mm steel side plates are seen as thin, only j and k failure modes are applicable to the specimens tested herein. Thus the failure mode for all the bolted tests was in mode j/l.

Figure 5 shows the embedment strength determined from the experimental results, a best fit linear variation, and the tri-linear approximation based on that of Moss et al. [11, 12]. It can be seen that the tri-linear approximation derived from short duration heated tests is not a good fit to the data from the tests on dry LVL. The grain direction does not appear to be important. This agrees with provisions of EC5, which provides empirical formulas for the embedment strength independent of the grain direction for nails and screws of less than 6 mm diameter, as opposed to bolts where there is a dependency upon the grain direction for any diameter. When

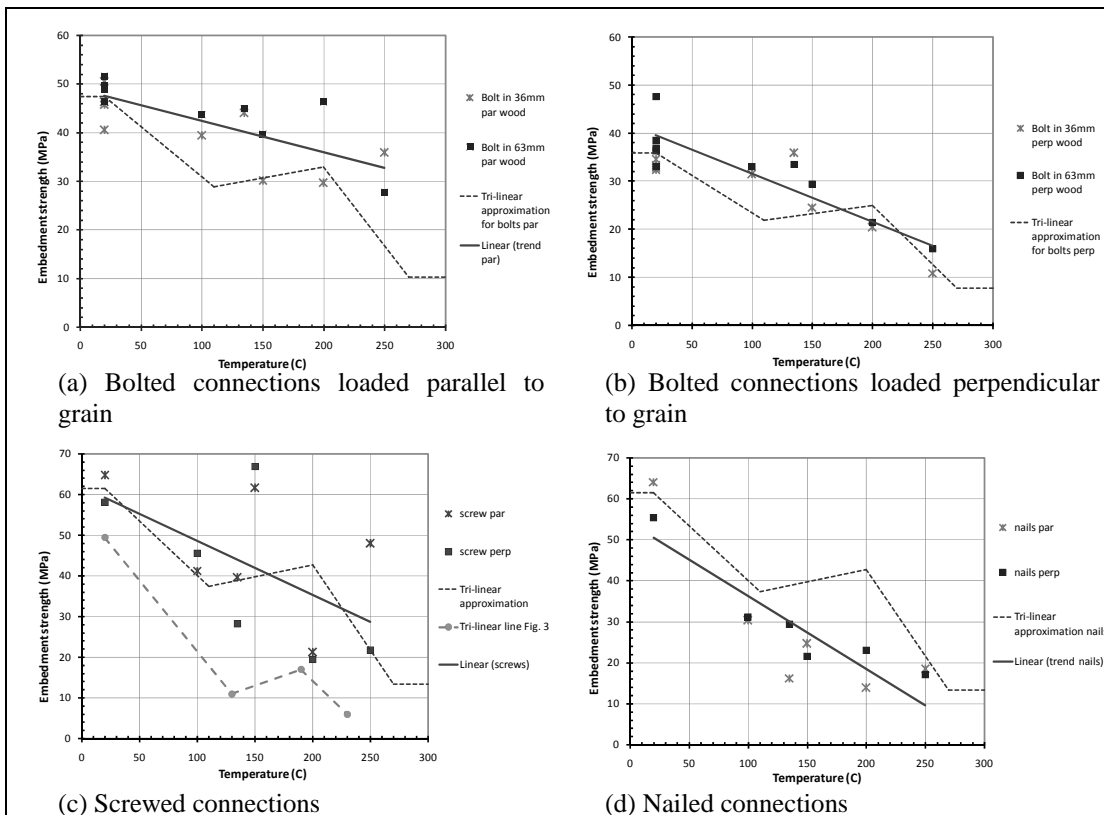


Figure 5. Embedment strength variation with temperature for the connections tested in Part 2.

using the Excel trend function, a linear variation seemed to be the best fit for both screws and nails.

DISCUSSION

When the surface timber heats up, moisture will move inward and the moisture content at the centre will rise, so that the 63mm thick wood in the two hour heated exposure is not fully dried at the time of testing. In the long duration heated tests, both the temperature and moisture content were uniform throughout the member. As a result, these tests showed much higher and more linear embedment strength than in the case where the LVL members were heated for only two hours.

CONCLUSIONS

The nailed and screwed connections generally showed an increasing load-displacement curve up to and beyond 5 mm displacement, for temperatures up to 250°C, with no dependency on grain direction.

The failure of bolts is more predictable and more dependent on grain direction than nailed or screwed connections.

Bolted connections loaded parallel to grain are stronger than bolted connections loaded perpendicular to grain, but reached their ultimate load at 2–3 mm

displacement whereas in the perpendicular to grain case, the ultimate load was reached at greater than 5 mm displacement.

Strength of all fasteners is dependent on moisture content.

A linear trend of embedment strength versus temperature was found for oven dry wood, different from the previous tri-linear trend determined from short duration heating and a moisture gradient.

REFERENCES

1. Norén J. 1996. *Load-bearing capacity of nailed joints exposed to fire*, Swedish Institute for wood Technology Research, Sweden.
2. König, J. and Fontana, M. 2001. *The performance of timber connections in fire- test results and rules of Eurocode 5*, Paper presented at International Rilem Symposium “Joints in Timber Structures”. University of Stuttgart, 12–14 September 2001.
3. Frangi, A. and Mischler, A. 2004. *Fire Tests on Timber Connections with Dowel type Fasteners*, Proc. International Council for Research and Innovation in Building and Construction, Working Commission W18 – Timber Structures, Meeting 37, Edinburgh, U.K.
4. Erchinger C., Frangi A., and Mischler A. 2005. *Fire behaviour of multiple shear steel-to-timber connections with dowels*, Proc. Intern. Council for Research and Innovation in Building and Constr. – Working Commission W18 – Timber Structure, Meeting 38, Karlsruhe, Germany.
5. Erchinger C., Frangi A., and Mischler A. 2006. *Thermal investigations on multiple shear steel-to-timber connections*, Proc. World Conf. on Timber Engineering, Portland, Oregon, USA.
6. Erchinger C., Frangi A., and Fontana M. (2010), *Fire design of steel-to-timber dowelled connections*, Engineering Structures, 32(2):580–589.
7. Racher P., Laplanche K., and Dhima D. 2006. *Thermo-mechanical modelling of the timber connection behaviour under fire*, Proc. 4th Intern. Workshop on Str. in Fire (SiF’06), 899-908.
8. Schabl S., and Turk G., (2006), *Coupled heat and moisture transfer in timber beams exposed to fire*, Proc. World Conference on Timber Engineering, Portland, Oregon, USA.
9. Lau, P.H., Moss, P.J., Buchanan, A.H. and Chuo, T.C.B. 2006. *Fire performance connections in laminated veneer lumber*. Proc. 9th World Conf. on Timber Engin., Portland, Oregon, USA.
10. Fragiaco, M., Buchanan, A.H., Carshalton, D., Moss, P.J., and Austruy, C. 2007. *Predicting the strength of bolted connections when subjected to fire conditions*. Proc. Intern. Council for Research and Innovation in Building and Constr.—Working Commission W18—Timber Structure, Meeting 40, Bled, Slovenia, paper 40-7-1.
11. Moss, P.J., Buchanan, A.H. and Fragiaco, M. 2008. *Predicting the behaviour of timber connections subjected to fire*. In T. Aravinthan, W. Karunasena and H. Wang (eds.), Progress in Mechanics of Structures and Materials, Taylor & Francis, pp. 857-863.
12. Moss, P.J., Buchanan, A.H., Fragiaco, M., Lau, P.H. and Chuo, T.C.B. 2009. *Fire performance of bolted connections in LVL*. Fire and Materials, 33(5):223–243.
13. ISO 10984-2 (1999), *Timber structures- Dowel-type fasteners- Part 2: Determination of Embedding Strength and foundation values*, International Standards Organization.
14. Eurocode 5, Part 1-1 2004. *Design of timber structures*, EN 1995-1-1:2004(E) Part 1-1: General- Common rules and rules for buildings, CEN/TC250
15. Gaunt, D. and Penellum, B. 2007. *Joint testing for Hyspan, Tryform, & Hycord laminated veneer lumber for Carter Holt Harvey Ltd*, Report No TE06-057.

Design of Timber-Concrete Composite Floors for Fire Resistance

J. O'NEILL, D. M. CARRADINE, P. J. MOSS, M. FRAGIACOMO
and A. H. BUCHANAN

ABSTRACT

This research investigated the fire performance and failure behaviour of timber-concrete composite floor systems currently under development in New Zealand, resulting in a calculation method for evaluating the fire resistance of these floors. Furnace tests were performed on two full-size floor specimens at the Building Research Association of New Zealand (BRANZ). Both floor specimens were 4m long and 3m wide, consisting of 65mm concrete topping on plywood formwork, connected to double LVL floor joists. They were tested over a 4m span, subjected to a nominal design live load of 2.5 kPa. Both floors were subjected to the ISO 834 test fire for over 60 minutes. Two separate connection types were tested; concrete notches cut into the timber beams with an incorporated shear key, and metal toothed plates pressed between the double beams.

It was found that the reduction in section size of the timber beams due to the fire governed the failure mode of the floors. The test data and visual observations aided in the development of an analytical model for evaluating the fire resistance of the floors. This was developed into a spreadsheet that is able to predict the expected fire resistance of these floors, taking into account some major time dependent variable properties that can have an effect on the overall performance. Load-span tables have been produced to give the estimated fire resistance of floors with differing floor dimensions, span lengths and applied loads.

James O'Neill, Graduate Student, Department of Civil and Natural Resources Engineering, University of Canterbury, Christchurch 8140, New Zealand

David M Carradine, Ph.D., Department of Civil and Natural Resources Engineering, University of Canterbury, Christchurch 8140, New Zealand

Peter J Moss, Associate Professor, Department of Civil and Natural Resources Engineering, University of Canterbury, Christchurch 8140, New Zealand

Massimo Fragiaco, Associate Professor, Department of Architecture, Design and Urban Planning, University of Sassari, Piazza Duomo 6, 07041 Alghero, Italy

Andrew H Buchanan, Professor of Timber Design, Department of Civil and Natural Resources Engineering, University of Canterbury, Christchurch 8140, New Zealand

INTRODUCTION

Timber-concrete composite floors are a combination of timber joists and concrete topping, creating a flooring system to best utilise the advantages each material has to offer. Laminated timber is used as the main tensile load bearing material due to its high strength-to-weight ratio, while concrete is used in floor slabs for its advantages in stiffness and acoustic separation. The strength of the system is dependent on the connection between timber and concrete, thus the connection must be strong, stiff, and economical to manufacture, to ensure that the flooring system is economically viable. The benefits in aesthetics, sustainability and economical savings due to fast erection time will undoubtedly be a significant factor to their widespread use in the future.

Timber-concrete composite structures arose in Europe in the early twentieth century as a means of strengthening existing timber floors by the addition of a concrete slab. Due to the many advantages they possess over traditional timber floors, they are now being used in new construction [1-2]. This is currently under investigation in many parts of the world such as Sweden [1-2], the United States [3], Germany [4, 5], Switzerland [6] and New Zealand [7-9]. There are many different types of composite flooring design, the main two categories being either solid timber slab type designs [4] or beam type designs. Several types of connection systems are available on the market, a number of which have been investigated by Ceccotti [10], Lukaszewska et al. [2] and Yeoh et al. [9].

The type of composite floor under study was a semi-prefabricated beam type system comprising of "M" panels that were built with laminated veneer lumber beams over-laid with plywood as permanent formwork for the concrete. The plywood had holes cut to accommodate the shear connections between the beams and the concrete slab. Both notched connections and toothed metal plates were used in this research. The panels can be prefabricated off-site then transported to site and craned into position, allowing the concrete slab to be cast in-situ (see Figure 1).

With the development of any new structural system, it is important to assess the fire safety to ensure that it can be used safely for its intended purpose. The fire performance of many different types of timber-concrete composite floors have been researched in the past, for example Frangi and Fontana [6, 11] have tested both beam and slab type composite floors. However the differing types of composite systems mean that different parts of these systems will govern failure in fires. It is therefore important to perform full-scale fire tests on any new composite systems.

TESTING DETAILS

The specimen construction and testing was carried out at the Building Research Association of New Zealand (BRANZ), located in Porirua, New Zealand. The full-scale testing involved two floor units tested under scaled loads, the dimensions of each floor unit being identical, apart from the beam depth and design load. A 300mm deep LVL beam floor was designed with a span of 5 m, and a 400mm deep LVL beam floor was designed with a span of 7.0m. A large range of beam sizes and floor spans are possible, however the floor designs tested were restricted by the loading capabilities of the full scale furnace at BRANZ. A modification on the

number of connections also had to be made to accommodate the 4m span of the furnace, having only four notches or eight plates per beam, as opposed to the usual six notches or twelve plates. The general design of the timber-concrete composite floors used in the testing was based on the semi-prefabricated system under development at the University of Canterbury, primarily developed by Yeoh [8, 12].

Each floor unit consisted of two 4.6m long double Laminated Veneer Lumber (LVL) beams (four beams in total) spaced 1200mm apart and fixed together with type 17 self-drilling screws. Two different connection types were used in each test specimen. The first connection type tested was the result of previous short and long term testing by Yeoh et al. [8] and O'Neill [13], and was a 50mm deep by 300mm long rectangular notch cut into each beam, with a 16mm coach screw installed in the centre of this notch. The other type of connection tested was toothed steel plates, which were pressed between the double beams, protruding into the concrete slab, tied to the steel reinforcement.

A 17mm thick plywood sheet was nailed to the top of the beams providing permanent formwork for the concrete topping. The plywood had no other structural purpose. A 65mm thick layer of 30 MPa concrete topping was cast on the plywood, filling the notched connections and the holes in the steel plate connections. For testing purposes the two slabs in each loading frame were separated at 1200mm centres with small plywood strips. This was to ensure that each set of beams and corresponding tributary slabs would act independently after the plywood formwork had burned through in the test.

During the construction of the floors thermocouples were placed in critical areas to allow for temperature data to be recorded. These areas included the mid-span of the double beams, in the concrete, the connections, the various composite interfaces and on the steel mesh. Six potentiometers were fixed to the loading rig and drawn down to the slab surface to measure the vertical displacement of the floors, approximately in line with the centrelines of the beams and spaced evenly at three points along the floor length.

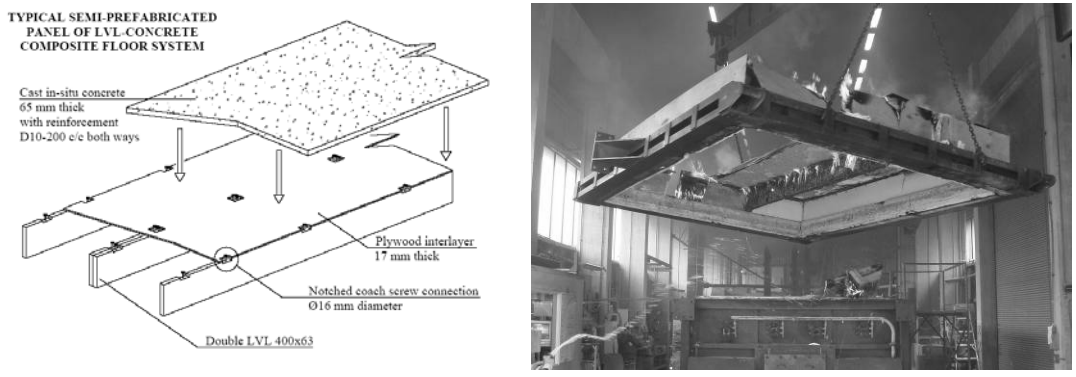


Figure 1. Sketch of the composite panel tested (left) and the 300mm floor being lifted off the furnace after testing (right).

FURNACE TESTING

General Observations

The main objective of the full scale testing was to investigate the failure behaviour of timber-concrete composite floors when exposed to fire, which encompassed a wide range of information that was required to be collected from different parts of the floor system. Specifically, the failure mode of the floors would identify the critical component of the floor that governed the design for fire safety, either a failure in the beams, the concrete slab or the connections between the two. Other areas of interest were the charring behaviour of the timber beams, spalling behaviour of the concrete, the level of fire damage near the connections and insulation to the concrete slab provided by the plywood sheathing. The test fire was the ISO 834 standard test fire [14].

As fire conditions cannot easily be scaled in the conventional manner, attempting to simulate the likely fire performance of a large structural system can be difficult. Due to their combustibility, timber beams cannot be scaled down in size as their fire behaviour is dependent on the actual cross-section present. This required that the loads on the floor units be scaled up in such a way that similar stresses were induced in the load bearing members of the floor and the same bending moment at the mid-span of the floors was obtained. The design loads of the test specimens were based primarily on a live load of 2.5 kPa and a dead load of the self weight of the floor only with no additional superimposed dead load. The first floor specimen tested was the 300mm beam floor, which was tested to destruction. Failure occurred at 75 minutes, and the floor is shown in Figure 1 directly after testing. The side with notched connections failed first, when the testing was terminated. The second floor was the 400mm beam floor, which was stopped shortly after 60 minutes to assess the damage at that time and to provide insight into how the beams were charring before complete destruction.

Timber Charring Effects

The initial and residual beam section sizes are shown in Table I. Measurements in the table were taken from intermediate regions in the beams as the char depth in the beams was observed, after testing, to be very uniform along the beams. The calculated average charring rates for each floor are shown in Table II.

TABLE I. RESIDUAL BEAM SIZES BEFORE AND AFTER FURNACE TESTING.

Test Specimen	Size before furnace testing		Size after furnace testing		Burning time (min)
	Width (mm)	Depth (mm)	Width (mm)	Depth (mm)	
300 mm	126	300	44	130	75
400 mm	126	400	52	255	60

TABLE II. CALCULATED BEAM CHARRING RATES.

Test Specimen	Charring rate (mm/min)		
	Side	Bottom	Average
300 mm	0.55	2.27	1.12
400 mm	0.62	2.42	1.22
Average of both floors	0.58	2.35	1.17

The average charring rates for the 400mm floor beams were slightly higher than the 300mm floor beams from both directions, and this was due to a shorter overall burning duration. The deeper layer of char on the 300mm beams provided better insulation from the fire in the latter stages of burning, thus reducing the average overall charring rates. The overall charring rate calculated in the table is for three-sided exposure, taking into account the timber surfaces exposed to the fire. The charring rate on the sides of the LVL beams was found to be 0.58 mm/min on average, lower than reported values of 0.72 mm/min based on research conducted by Lane [15] on similar LVL at the BRANZ facilities. This was most likely due to the double-tee configuration of the floor beams such that convection of flames and hot gases throughout the space was slightly impeded, and the beams were spaced far enough apart that re-radiation off the adjacent beam surface was not significant.

The charring rate on the underside of the beams was very high, being on average four times the charring rate from either side of the beams. The majority of this rapid charring occurred because the double beams splayed apart after significant burning, so that each beam (originally 126mm wide) became two much narrower beams, with both of these exposed to charring on three sides. This separation of the beams was primarily caused by the uneven drying of the timber beams during the fire, with the moisture gradient across the beams creating differential shrinkage. There was also loss of integrity around the few screws holding the beams together. The deeper floor beams exhibited greater beam separation than the smaller beams, hence a slightly greater rate of charring from the bottom.

Vertical Floor Displacement

The average vertical displacements on the top of the slab can be seen in Figure 2. From these measurements it is clear the 300mm floor sections sagged for the first 23 minutes of testing due to the applied load and reduction in timber beam cross section. However, it can be seen for both sides of the floor that the vertical displacement begins to decrease back towards the initial rest position after about 25 minutes. This time is concurrent with the almost complete burning through of the plywood sheathing, hence fire exposure of the underside of the concrete slab, causing a temperature rise in the concrete. A temperature rise in the concrete would have caused thermal expansion, but this expansion was restrained by the LVL beam due to the connections and resulting composite action, therefore a thermal bowing action was induced in the whole assembly that tended to hog the entire floor. This thermal bowing aided in resisting the gravity loads imposed on the floors, and was similar to the thrust force that can be developed via axial restraint [16]. This behaviour was more apparent in the side of the floor with plated connections, as the reduction in slip modulus due to fire exposure was less than for the notched

connections as the plates were well insulated from the fire and therefore the effect of the slab elongation was more significant, with less vertical floor displacement.

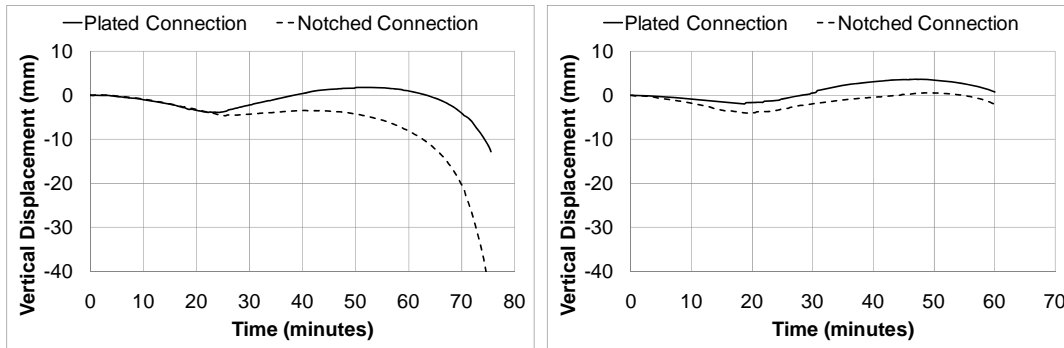


Figure 2. Vertical displacement of the 300mm (left) and 400mm (right) floors.

It can be seen for both floors tested, that the displacement up to structural failure was less than 1/20 of the span (200 mm) and the rate of increase of displacement was also low. Typical fire testing requirements specify deflections of less than 1/20 of the span or a limiting rate of deflection when deflection is 1/30 of the span [16], and on comparison the test floors were within these ranges.

SPREADSHEET DESIGN TOOL

The spreadsheet design tool has been developed to aid in the understanding of how certain timber-concrete composite systems can perform in fires, and to provide a fast method of estimating the expected fire resistance time of a floor under user-defined load conditions and floor geometries. The design equations were based on the calculation method in Chapter 25 of the Timber Design Guide [7] for simply supported beams.

To incorporate the effects of fire conditions into the spreadsheet the major portion of the calculations are run in a quasi steady state analysis. That is, the mechanical properties of the floor are evaluated iteratively over a number of equal time intervals (in this case each minute) during which time the effects of the fire reduce the residual beam size based on the charring rate, which may change during the fire. This relationship was derived from the charring recorded during the full scale testing.

The spreadsheet requires the input of floor geometry, material properties, loading conditions and corresponding safety factors, and outputs an expected fire resistance time for the floor to reach structural failure. The spreadsheet was used to derive a number of resistance span tables for varying spans of these timber-concrete composite floor systems, with different section sizes, and different combinations of live loads (Q) and superimposed dead loads (SDL). An example is shown in Table III, calculated up to a maximum fire resistance time of 120 minutes (120+). All beam sizes in the left column denote a double beam, and the results presented were calculated using a notch type connection.

TABLE III. FIRE RESISTANCE SPAN TABLE.

Fire Resistance Time (min) [SDL = 0.5 kPa, Q = 1.5 kPa]									
Beam Dimensions (mm)	Span (m)								
	4	5	6	7	8	9	10	11	12
200x45x2	40	38	-	-	-	-	-	-	-
240x45x2	44	42	-	-	-	-	-	-	-
300x45x2	49	47	41	-	-	-	-	-	-
360x45x2	-	51	45	41	-	-	-	-	-
400x45x2	-	-	48	44	40	36	-	-	-
450x45x2	-	-	-	47	43	40	37	-	-
600x45x2	-	-	-	-	53	49	46	44	41
200x63x2	71	69	64	-	-	-	-	-	-
240x63x2	75	73	67	-	-	-	-	-	-
300x63x2	80	78	72	67	-	-	-	-	-
360x63x2	-	83	77	72	68	-	-	-	-
400x63x2	-	-	80	75	71	68	-	-	-
450x63x2	-	-	-	79	75	71	68	-	-
600x63x2	-	-	-	-	84	81	78	75	72
200x90x2	117	115	110	-	-	-	-	-	-
240x90x2	120+	119	114	-	-	-	-	-	-
300x90x2	120+	120+	119	114	110	-	-	-	-
360x90x2	-	120+	120+	119	115	111	-	-	-
400x90x2	-	-	120+	120+	118	115	111	-	-
450x90x2	-	-	-	120+	120+	118	115	112	-
600x90x2	-	-	-	-	120+	120+	120+	120+	120+

CONCLUSIONS

Two full-scale timber-concrete composite floor systems with different types of connections were fire tested in a full-scale furnace.

Failure of the floors was governed by the reduction in section size of the timber beams due to charring. All the floor units were able to withstand prolonged exposure to the test fire, well exceeding one hour.

A simple analytical model has been developed to predict the expected fire resistance of these floors, taking into account time dependent variable properties, loading conditions, material properties and floor geometries.

A critical and unexpected test observation was excessive bottom charring due to lateral distortion of the double LVL beams during fire exposure, caused by a moisture gradient across the beams creating differential shrinkage. Further research to investigate this is in progress.

Further means of fire protection such as passive protection (fire rated suspended ceilings, gypsum plasterboard encasement) or active protection (sprinkler systems) can further increase the fire resistance of these floors.

REFERENCES

1. Lukaszewska, E., Johnsson, H., and Fragiaco, M. (2008) "Performance of Connections for Prefabricated Timber-Concrete Composite Floors." *Materials and Structures*, RILEM, Vol. 41, Issue 9, pp. 1533–1550.
2. Lukaszewska, E., Fragiaco, M., and Johnsson, H. (2010) "Laboratory Tests and Numerical Analyses of Prefabricated Timber-Concrete Composite Floors." *ASCE J. of Struct. Engrg.*, Vol. 136, Issue 1, pp. 46–55.
3. Fragiaco, M., Gutkowski, R.M., Balogh, J., Fast, R.S. (2007) "Long-Term Behavior of Wood-Concrete Composite Floor/Deck Systems with Shear Key Connection Detail." *ASCE Journal of Struct. Engrg.*, Vol. 133, Issue 9, pp. 1307–1315.
4. Kuhlmann, U., Michelfelder, B. (2006) "Optimized Design of Grooves in Timber-Concrete Composite Slabs." *Proc. The 9th World Conference on Timber Engineering WCTE 2006*, Portland, Oregon, USA, CD.
5. Bathon, L., Bletz, O., Schmidt, J. (2006) "Hurricane Proof Buildings-An Innovative Solution using Prefabricated Modular Wood-Concrete-Composite Elements." *Proc. 9th World Conference on Timber Engineering*, Portland, Oregon, USA.
6. Frangi, A., Knobloch, M., and Fontana, M. (2009) "Fire Design of Timber-Concrete Composite Slabs with Screwed Connections." *ASCE Journal of Struct. Engrg.*, Vol. 136, Issue 2, pp. 219–228.
7. Buchanan, A.H. (2007) "Timber Design Guide." Third Edition. New Zealand Timber Industry Federation Inc., Wellington, New Zealand.
8. Yeoh, D., Fragiaco, M., Buchanan, A., and Gerber, C. (2009) "A semi-prefabricated LVL-concrete composite floor system for the Australasian market." *Australian Journal of Struct. Engrg.*, Vol. 9, Issue 3, pp. 225–240.
9. Yeoh, D., Fragiaco, M., De Franceschi, M., and Buchanan, A. (2010) "Experimental tests of notched and plate connectors for LVL-concrete composite beams." Submitted on *ASCE Journal of Struct. Engrg.*
10. Ceccotti, A. (2002) "Composite Concrete-Timber Structures." *Prog. Struct. Engng Mater.* 2002; 4:264–275.
11. Frangi, A., Fontana, M. (1998) "Fire Behaviour of Timber-Concrete Composite Slabs." *Proc. The 5th World Conference on Timber Engineering*, Montreux, Switzerland, August 17–20, 1998.
12. Yeoh, D. (2009) "Behaviour and Design of Timber-Concrete Composite Floors under Short and Long-Term Loading." Doctorate Thesis in Civil Engineering, University of Canterbury, Christchurch, New Zealand.
13. O'Neill, J.W. (2007) "A Study of the Connections in Timber-Concrete Composite Systems." Project Report in Civil Engineering, University of Canterbury, Christchurch, New Zealand.
14. ISO (1975) "Fire Resistance Tests—Elements of Building Construction." ISO 834: 1975, International Organisation for Standardisation.
15. Lane, W.P. (2005) "Ignition, Charring and Structural Performance of Laminated Veneer Lumber." Fire Engineering Research Report 05/3, School of Engineering, University of Canterbury.
16. Buchanan, A.H. (2001) "Structural Design for Fire Safety." John Wiley & Sons Ltd., West Sussex, England.

Fire Performance of Epoxied Connections in Heavy Timber Structures

R. B. GERARD, D. M. CARRADINE, P. J. MOSS
and A. H. BUCHANAN

ABSTRACT

This paper describes an investigation into the fire performance of epoxied connections between steel rods and laminated veneer lumber (LVL) made from radiata pine.

To determine connection performance, a four-phase experimental investigation was carried out on the axial tensile strength of a connection that utilised a threaded steel rod bonded into the LVL using three different epoxy resins. The timber members had dimensions of 150 x 63 mm while the 16 mm diameter threaded steel rods were glued into an 18 mm diameter drilled hole. Laboratory experimentation included cold testing to establish the likely maximum strength of the connections at ambient temperature; oven heating to a constant elevated temperature to evaluate heating effects on steel to wood connections; heating to a constant temperature followed by cooling to ambient temperature to determine the residual strength of connections in minor fires; and finally, furnace testing under constant load to generate fire resistance design and analysis equations to be utilized for steel to wood connections.

The three epoxy resins used gave different connection strengths at ambient temperatures and showed different strength losses at elevated temperatures. When heated to a constant temperature and then cooled to ambient temperature, the three epoxy resins showed little strength loss compared to their ambient strength. The furnace tests were carried out at three levels of loading and showed a variation in the times to failure for the different load levels and the three epoxy types. The times to failure were in the range of 15 to 20 minutes in general. The average charring rates were found to be slightly greater than the values previously found in furnace testing at the University of Canterbury.

In addition to the 150 x 63 mm specimens, larger 150 x 150 specimens were also furnace tested at one level of loading. One type of epoxy connection lasted 45 to 65 minutes while the other two epoxy connections failed after 30 to 45 minutes. Design recommendations are given in the paper.

Robert B Gerard, ARUP Fire, San Francisco, USA
David M Carradine, Peter J Moss and Andrew H Buchanan, Department of Civil Engineering,
University of Canterbury, Christchurch 8140, New Zealand

INTRODUCTION

Over recent years, a number of papers have been published on the performance of joints in timber members when subjected to fire [i.e. 1-6].

During the last few years, connection research at the University of Canterbury has investigated the performance of nails, screws, bolts, and self-drilling dowels. A summary of this research on the fire performance of connections in LVL can be found in a number of papers [e.g. 7-10]. Other connection work has investigated the performance of epoxy bonded steel rod connections in glulam and LVL members in both ambient [11-15] and fire conditions [16, 17]. Research on the temperature effects on all-purpose epoxy was carried out by Barber [16], demonstrating significant strength loss with increasing temperature, suggesting that all-purpose epoxy reaches a strength plateau and has no significant strength beyond 100°C. One solution to this strength loss at elevated temperatures is the use of high temperature epoxy. Previous high temperature epoxies required curing at elevated temperatures [17, 18]. Current high temperature epoxies, however, cure at ambient temperatures, making their use in construction more viable and practical.

EPOXY ADHESIVES

Three epoxy adhesives were selected for testing. These were the Fischer 'FIS V 360 S' Injection Mortar [19], JB Weld 'Industro Weld' [20], and West 'Z206' Epoxy Hardener [21]. Each product has been designated as a high temperature epoxy adhesive and designed to maintain strength at elevated temperatures.

Fischer 'FIS V 360 S' Injection Mortar [19]

The Fischer 'FIS V 360 S' epoxy adhesive was designed as an injection mortar for gluing steel threaded rods into reinforced concrete. The Fischer Injection Mortar consists of a two part mixture containing styrene-free vinylester resin with quartz sand and hardener. After the two parts are mixed, the epoxy adhesive has a working time of five minutes and a cure time at ambient temperature of 24 hours before full strength is achieved. The Fischer epoxy adhesive used with steel threaded rods and reinforced concrete has been classified to resist design loads under fire conditions for up to 120 minutes. Technical data for use of the Injection Mortar prescribes a minimum 125mm embedment and an 18mm diameter hole in reinforced concrete when used to glue a 16mm diameter steel threaded rod.

JB Weld 'Industro Weld' [20]

The JB Weld 'Industro Weld' is described as an all-purpose cold-weld compound, allowing for curing at ambient temperature. Consisting of a two part system, an epoxy-resin and a hardener, the 'Industro Weld' requires thorough hand mixing after which, the product was injected using an empty cartridge and caulking gun. JB Weld epoxy had a working time of up to 30 minutes and a cure time of 24 hours. Product information claims 'Industro Weld' is resistant to temperatures up to 260°C, retaining strength far beyond the 100°C limit evidenced by Barber's previous testing [16].

West System ‘Z206’ Epoxy Hardener and Adhesive Technologies ‘ADR 310’ Epoxy Resin [21]

The West ‘Z206’ Epoxy Hardener was designed as a stud bonding adhesive intended for connecting timber, composite, concrete and other similar materials. Combined with the Adhesive Technologies ‘ADR 310’ Epoxy Resin, the ‘Z206’-‘ADR310’ combination of epoxy adhesives was developed as a high temperature post-cured carbon laminate to produce stronger and stiffer laminates with longer working times and a reliable cure time. The two-part epoxy adhesive requires thorough hand mixing prior to use. When combined this mixture provides a 20 minute working time and cures at ambient temperature to maximum strength in 24 to 48 hours.

COLD TESTING

A schematic drawing for epoxy test specimen used for the cold (i.e. ambient) testing can be seen in Figure 1. In all the tests, 16 mm diameter steel rods were glued into 150 mm long, 18 mm diameter holes.

Failure methods for all steel to wood connections were identified as brittle failures. Connections failed in sudden, abrupt methods resulting in significant loss of strength. Results for ultimate loads and failure modes established through cold testing can be found in Table I.

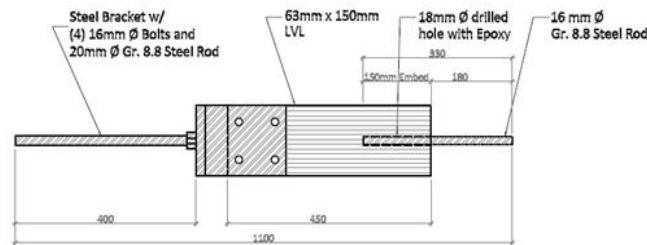


Figure 1. Epoxy Cold Test Specimen Schematic Drawing.

Failure in mode 1 occurs when the LVL splits perpendicular to the veneers and represents a confinement failure in the LVL. Failure mode 3 occurred when the epoxy grouted steel rod and a significant amount of timber pulled out from the test specimen. The mode 4 failure occurs as a result of a failure at the epoxy-LVL interface and represents an epoxy failure.

TABLE I. COLD AND OVEN TEST ULTIMATE STRENGTH RESULTS (kN).

Temperature	Fischer	JB Weld	West	Failure mode
20°C	60.3	66.8	74.1	1, 3
50°C	46.2	41.2	44.9	1
100°C	34.6	25.9	13.2	4
150°C	27.9	23.1	9.4	4
200°C	22.8	21.1	12.5	4

OVEN TESTING

Tensile testing of epoxy bonded steel to wood connections was performed at temperatures ranging from 50°C to 200°C. Both ultimate strength and failure modes were compared with the results from ambient testing to determine the heating effects on the connections. The specimens tested were similar to those used in the ambient testing shown in Figure 1. The specimens were heated overnight in an oven. After removal from the oven, the specimens were wrapped in a blanket to keep them from losing heat while the steel bracket was being attached to the test specimens.

Results for the ultimate strengths and failure modes are given in Table I. All three epoxies showed the same failure mode at each temperature. High temperature epoxy resins displayed a considerable decrease in ultimate strength with increasing temperature as can be seen in Table I.

COOLED TESTING

Tensile testing of cooled test specimens was performed to evaluate the residual strength after heating and allowed to cool to ambient temperature, simulating a minor fire event. Epoxy test specimens were heated in the oven overnight to ensure consistent heating throughout the entire specimen.

Results for the ultimate strengths and failure modes are given in Table II. All three epoxies showed the same failure mode at each temperature.

DISCUSSION OF AMBIENT, OVEN, & COOLED TEST RESULTS

All these tests were carried out on the same size of specimen. The results from the ambient, oven, and cooled tests are compared in Figure 2. The oven test results are shown by the solid lines in the bottom half of the figure. The results for the cooled

TABLE II. COOLED TEST ULTIMATE STRENGTH RESULTS (kN).

Temperature	Fischer	JB Weld	West	Failure mode
50°C	63.1	66.4	71.5	1
100°C	60.5	72.9	70.1	3
150°C	65.7	64.0	74.6	3
200°C	59.8	63.7	65.1	3

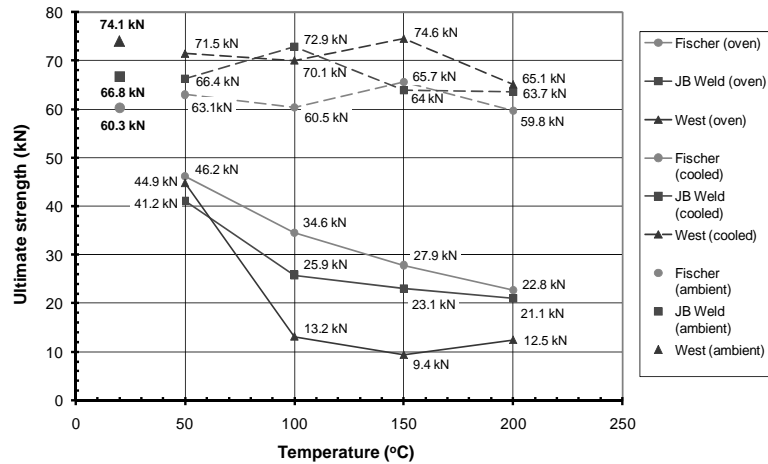


Figure 2. Comparison of Ambient, Oven and Cooled Test Results for the Fischer, JB Weld and West epoxy adhesives.

tests are given by the dashed lines at the top, with the ambient test results are the individual results at the left. While the oven tests show considerable reduction in strength with temperature increase, the cooled results show no significant difference from the ambient test values.

FURNACE TESTING

Furnace test specimens were similar to cold test specimens, except they were constructed with 650mm long LVL to match the furnace dimensions. Efforts were made to ensure heat transfer occurred through the LVL and not the exposed steel connections. Kaowool insulation was wrapped around the exposed portion of the steel threaded rod to prevent heat transfer by conduction.

All the small test specimens failed in Mode 1 with splitting on one side of the member as a result of confinement failure. Larger 150 x 153 mm LVL specimens were also tested in the furnace. A thermocouple was embedded in the epoxy adhesive close to the exposed end of the specimen and also at the mid-length of the steel rod. A number of the 150 x 63 mm test specimens were also instrumented in this way.

Each of the epoxy adhesives was tested in the furnace under three different loads of 10, 15, and 20 kN. The 20 kN load was approximately one third of the ambient strength of the test specimens, and the lower loads were used to check whether the load level showed any effect on the time to failure in the furnace. Figure 3 shows the failure times for the 150x63 mm specimens, all of which failed in splitting across the veneers. Also shown, are the results for the 150x153 mm specimens which failed by pulling out of the steel rod caused by a glueline failure. It can be seen that there is also considerable scatter.

DISCUSSION OF FURNACE TEST RESULTS

Figure 4(a) shows the temperatures reached in the glue-line near the end of the LVL and mid-way along the steel rod. It can be seen that in general, the glue-line temperatures for the 150x63 mm specimens had only reached about 100°C at the end of the member when the LVL split perpendicular to the grain. It can be seen that the temperature gradient along the steel rods reduced as the LVL charred and the cover to the rods reduced. For the larger 150x153 LVL members, Figure 4(b) shows that there is a temperature gradient along the steel rods that persists right up to failure. This shows that the protection of the steel rod was inadequate. Failure in these members seems to be a function of the glue-line temperature near the ends of the LVL, although the glue-line temperatures are considerably less than the fire temperature.

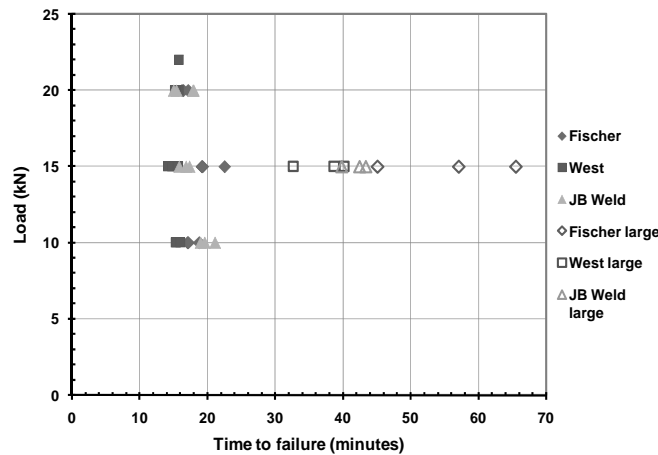


Figure 3. Failure times for all specimens in the furnace tests.

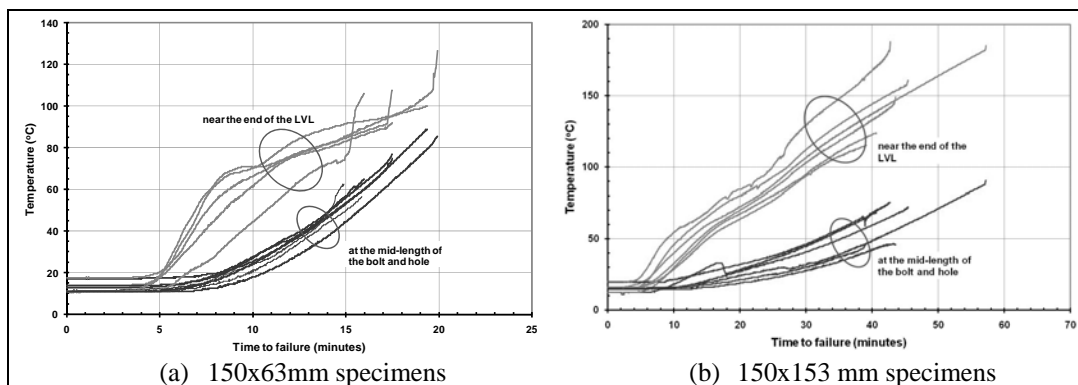


Figure 4. Typical time-temperature plots.

Table III gives a summary of the test results and fire resistance. The latter was determined by comparing the heat input from the furnace using the measured temperatures with the heat input that would occur if the furnace temperatures had matched the ISO 834 [22] requirements.

TABLE III. FURNACE TEST RESULTS.

Specimen	Thick-ness (mm)	Charring depth (mm)		Residual thickness (mm)		Time to failure (min)		Fire resistance (min)
		Range	Ave.	Range	Ave.	Range	Ave.	
Fischer	63	15-17.5	16	28-33	31	16.2-22.5	21.6	21.2
JB Weld	63	13.5-18	15.5	27-36	31	15.0-21.1	15.4	20.0
West	63	13.5-15.5	14.5	32-36	34	14.2-16.0	17.5	17.3
Fischer	150	33-42	38	69-87	77	45.0-65.5	55.9	47.1
JB Weld	150	29.5-32	31	90-94	92	39.8-43.4	41.9	39.4
West	150	24.5-31.5	28.5	90-104	96	32.7-40.2	37.2	38.2

DESIGN RECOMMENDATIONS

While high temperature epoxy provides greater fire resistance than all-purpose epoxy for steel to wood connections, testing results show that the most effective method of providing additional fire resistance is to increase the timber cover to the epoxied steel rod. Additional cover provides greater insulation for preventing heat transfer to the core connection.

CONCLUSIONS

1. Epoxy behaviour (Fig. 3)

All of the tested high temperature epoxies had less strength loss than standard epoxy at elevated temperatures. Of the three tested, Fischer was best, followed by JB Weld and West. All three had full strength recovery back to their cold strength after cooling from elevated temperatures up to 200°C.

2. Fire resistance

In the tests, the smaller specimens failed due to splitting of the wood after the cover was reduced below a critical level due to charring. There was not much difference in temperature at failure; hence there was no performance difference between the three epoxies.

The larger specimens failed when the glue-line temperature reached a critical value. Failure is very dependent on temperature, and hence on the type of epoxy and the thermal protection.

Fire resistance can be increased by providing an extra wood layer on the outside of the timber member, to give more protection against charring.

It is very important to provide fire protection to the ends of the steel rods where they come out of the end of the timber.

REFERENCES

1. König, J. and Fontana, M. 2001. "The performance of timber connections in fire- test results and rules of Eurocode 5", Paper presented at International Rilem Symposium *Joints in Timber Structures*. University of Stuttgart, 12/14 September 2001
2. Erchinger C., Frangi A., and Mischler A. 2005. "Fire behaviour of multiple shear steel-to-timber connections with dowels", *Proc. CIB—Working Commission W1—Timber Structure*, Meeting 38, Karlsruhe, Germany.
3. Erchinger C., Frangi A., and Mischler A. 2006. "Thermal investigations on multiple shear steel-to-timber connections", *Proc. World Conference on Timber Engineering*, Portland, Oregon, USA.
4. Erchinger C., Frangi A., and Fontana M. 2010. "Fire design of steel-to-timber dowelled connections", *Engineering Structures*, 32(2):580–589.
5. Racher P., Laplanche K., and Dhima D., 2006. "Thermo-mechanical modelling of the timber connection behaviour under fire", *Proc. 4th International Workshop on Structures in Fire (SiF'06)*, pp. 899–908.
6. Schabl S., and Turk G. 2006. "Coupled heat and moisture transfer in timber beams exposed to fire", *Proc. World Conference on Timber Engineering*, Portland, Oregon, USA.
7. Lau, P.H., Moss, P.J., Buchanan, A.H. and Chuo, T.C.B. 2006. "Fire performance connections in laminated veneer lumber", *Proc. 9th World conference in Timber Engineering*, Portland, Oregon, USA.
8. Fragiaco, M., Buchanan, A.H., Carshalton, D., Moss, P.J., and Austruy, C. 2007. "Predicting the strength of bolted connections when subjected to fire conditions". *Proc. CIB-W18, Meeting 40*, Bled, Slovenia, paper 40-7-1.
9. Moss, P.J., Buchanan, A.H. and Fragiaco, M. 2008. "Predicting the behaviour of timber connections subjected to fire", In T. Aravinthan, W. Karunasena and H. Wang (eds.), *Progress in Mechanics of Structures and Materials*, Taylor & Francis, pp. 857–863.
10. Moss, P.J., Buchanan, A.H., Fragiaco, M., Lau, P.H. and Chuo, T.C.B. 2009. "Fire performance of bolted connections in laminated veneer lumber", *Fire and Materials*, 33(5):223–243.
11. Deng, J. X. 1997. "Strength of Epoxy Bonded Steel Connections in Glue Laminated Timber". Doctoral Thesis in Civil Engineering. University of Canterbury, New Zealand.
12. Buchanan, A. and Deng X.J. 1996. "Strength of Epoxied Steel Rods in Glulam Timber". *International Wood Engineering Conference*, New Orleans, USA.
13. Buchanan, A. and Moss, P.J. 1999. "Design of Epoxied Steel Rods in Glulam Timber", *Proc. Pacific Timber Engineering Conference*, Rotorua, New Zealand.
14. Korin, U., Buchanan, A. and Moss, P.J. 1999. "Effect of Bar Arrangement on Tensile Strength of Epoxied End Bolts in Glulam". *Proc. Pacific Timber Engineering Conference*, Rotorua, New Zealand, Volume 2.
15. van Houtte, A. 2003. "Innovative Connections in Laminated Veneer Lumber Using Epoxied Steel Rods". Master's Thesis in Civil Engineering. University of Canterbury, New Zealand.
16. Barber, D. 1994. "Fire Resistance of Epoxied Steel Rods in Glulam Timber". Master's Thesis in Civil Engineering. University of Canterbury, New Zealand.
17. Harris, S. 2004. "Fire Resistance of Epoxy-grouted Steel Rod Connections in Laminated Veneer Lumber (LVL)". Master's Thesis in Civil Engineering. University of Canterbury, New Zealand." Fire performance of Laminated Veneer Lumber (LVL) with Glued-in Steel Rod Connections", *Proc. 3rd Int. Workshop on Structures in Fire (SiF'04)*, held in Ottawa, ON, Canada, 10-11 May 2004, pp 411–424.
18. FIS V 360 S Product Catalogue. 2006. "Fischer Fixing Systems". www.Fischer.de/en. Accessed March, 2009.
19. JB Weld Product Description. 2009. "Original J-B Weld". www.JBWeld.net. Accessed March, 2009.
20. Adhesive Technologies. 2009. "ADR Series Overview". www.AdhesiveTechnologies.co.nz. Accessed March, 2009.
21. ISO 834. 1975. *Principles of structural fire-engineering design with special regard to the connection between real fire exposure and the heating conditions of the standard fire-resistance test*, International Organization for Standardization.

Fire Resistance of Wood-Steel-Wood Bolted Timber Connections

L. PENG, G. HADJISOPHOCLEOUS, J. MEHAFFEY
and M. MOHAMMAD

ABSTRACT

This paper presents the results of a series of fire-resistance tests conducted in compliance with CAN/ULC-S101 on wood-steel-wood (WSW) bolted timber connections. The effects of wood side member thickness, fastener diameter, number of fasteners, edge distance, load level and protection were studied. During each test, a tensile load was applied at a constant level until the specimen failed. Results showed that the fire-resistance ratings of all tested connections with no protection were less than 45 minutes. Specimens with thicker wood side members were found to exhibit better fire resistances. Decreasing the load ratio increases the fire resistance. The results of tests on two protected specimens showed that the protection provided by a single-layer of 15.9 mm type X gypsum board increased the fire resistance rating by 37 min, whereas a double-layer of 12.7 mm Douglas fir plywood increased the fire resistance rating by 15 min. Finally, the test data were used to develop a correlation for the calculation of the fire resistance of bolted WSW connections. Comparison with test results showed good agreement between measured and predicted fire-resistance ratings using the correlation for unprotected bolted WSW connections.

INTRODUCTION

In heavy timber construction, timber connections are usually required to have the same fire resistance as main members such as timber beams and columns, when fire resistance is required. However, timber connections are the weakest link in timber buildings under fire attack. The metal fasteners and connectors of a timber connection heat up quickly in fire, transfer heat into the wood members and cause the wood to char faster. In recent years, a number of research efforts have been

Lei Peng and George Hadjisophocleous, Department of Civil & Environmental Engineering, Carleton University, Ottawa, Canada

Jim Mehaffey, FPIInnovations - Forintek Division, Ottawa, Canada

Mohammad Mohammad, FPIInnovations - Forintek Division, Quebec City, Canada

devoted to investigating the fire performance of timber connections and developing design rules for timber connections exposed to fire [1-9]. However, due to the complexity of timber connections, i.e.

connection type, wood member geometries, fastener diameter, fastener arrangements, load level and protection, more work is needed to study the influence of the various parameters governing the fire performance of timber connections [10].

This research aims at investigating the fire performance of wood-steel-wood (WSW) connections using bolts as fasteners. This type of connection is fabricated using a steel plate as the central member and two wood pieces as the side members, fastened with bolts. In France, a number of fire-resistance tests have been carried out for bolted WSW connections [2, 3] using ISO 834 fire exposure [11]. However, the tested wood side member thicknesses were only 50 mm and 60 mm. In New Zealand, researchers tested bolted WSW connections using LVL (laminated veneer lumber) in a small electrically-heated furnace, but parametric effects of the wood thickness and load level were not taken into account [6-8].

In Canada, the fire performance of timber connections is an area that has received little attention by researchers. The research reported herein entails a comprehensive experimental program on the inherent fire resistance of bolted WSW connections exposed to the CAN/ULC-S101 fire curve [12]. All specimens satisfied the Canadian standard CAN/CSA-O86-09 [13]. The effects of wood side member thickness, fastener diameter, number of fasteners, edge distance, load level and protection were studied. Test results in combination with previous experimental test data were then used to develop an empirical calculation method. Moreover, the data generated from this research will be used to validate and verify a numerical heat transfer and structural model in a future study.

EXPERIMENTAL PROGRAM

Test Specimens

A bolted WSW connection was fabricated with either two wood members sandwiching a steel plate or one wood member with a concealed steel plate. A typical bolted wood-steel-wood connection is shown in Figure 1.

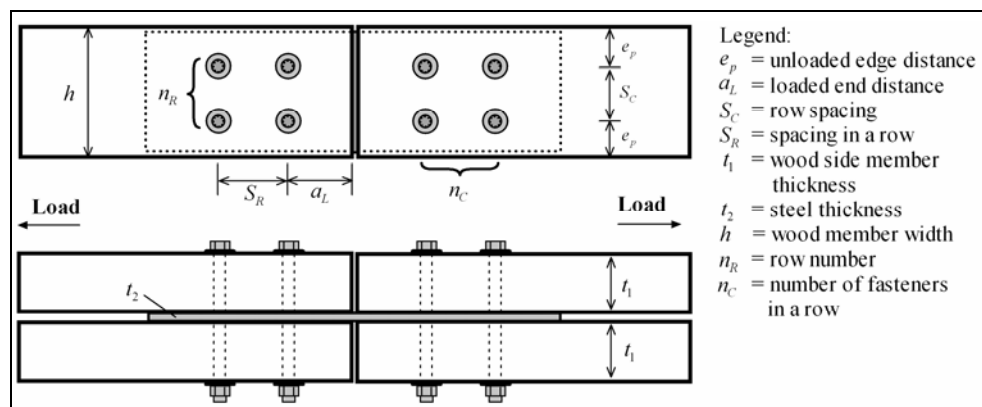


Figure 1. Bolted wood-steel-wood connection.

Wood members used in connections were either Canadian spruce-pine-fir (SPF) sawn lumber or spruce-pine grade 20f-EX glulam with a side thickness of 38 mm, 60 mm or 80 mm. All wood members had been conditioned at about 20°C and 60% RH, and the moisture content and density were measured prior to tests. The average moisture content was found to be about 11% and the wood density varied between 416 and 503 kg/m³. Steel plates (grade 300W) were 9.5 mm thick.

ASTM A307 bolts had diameter of 12.7 mm or 19.1 mm. Specimen configurations are summarized in TABLE I for all the 5 tested groups.

TABLE I. TEST SEPCIMEN CONFIGURATIONS AND LOAD RATIOS.

Test #	Bolt Diameter d (mm)	Wood Grade & Species	Wood Side Member Thickness t_1 (mm)	Wood Member Width h (mm)	Steel Thickness t_2 (mm)	Number of Rows n_R	Number of Bolts per row n_C	Loaded End Distance a_L (mm)	Bolt Spacing S_R (mm)	Row Spacing S_C (mm)	Load Capacity (kN)		Load Ratio
											Code	Ultimate	
1.1	12.7	No.2 SPF Lumber	38	140	9.5	1	2	$10d$	$10d$	Na	15	58	10%
1.2													10%
1.3													29%
1.4													30%
2.1	12.7	20f-EX SP Glulam	60	190	9.5	2	2	$10d$	$10d$	$5d$	50	115	11%
2.2													18%
2.3													29%
3.1	19.1	20f-EX SP Glulam	60	190	9.5	1	1	$10d$	Na	Na	22	65	11%
3.2													32%
4.1	19.1	20f-EX SP Glulam	60	190	9.5	2	2	$10d$	$10d$	$5d$	87	227	10%
4.2													30%
4.3 [†]													30%
5.1	19.1	20f-EX SP Glulam	80	190	9.5	2	2	$10d$	$10d$	$5d$	105	243	10%
5.2*													10%
5.3													29%
5.4 [‡]													29%

[†]: This specimen was protected by a single-layer of 15.9 mm Type X gypsum board.

[‡]: This specimen was protected by a double-layer of 12.7 mm Douglas fir plywood.

*: This specimen was designed to investigate the effect of edge distance.

Load ratio is defined as the applied load divided by the ultimate load-carrying capacity. The ultimate load-carrying capacity is the tested tensile strength of a connection at ambient temperatures. The ultimate load-carrying capacities presented in TABLE I were either from tensile tests conducted by the authors in accordance with ASTM Standard D1761-88 [14], or obtained from the literature reported by Mohammad [15]. The code design capacity given in TABLE I for each group was calculated based on the Canadian wood design standard CAN/CSA-O86-09 [13]. This code capacity (if multiplied by 1.25 for short-durations) is comparable to the 5th percentile value of the ultimate load-bearing capacity. It was found that the ratio of the Canadian code capacity to the mean ultimate capacity at ambient conditions is about 0.31 for bolted WSW connections (based on the average of 22 tested groups) [15]. Therefore, a load ratio of approximate 30% was applied to all groups, as shown in TABLE I. In addition, reduced load ratios of, about 10% and 20%, were also chosen to investigate the effect of load ratio on the fire performance of bolted WSW connections.

As seen in TABLE I, two protected specimens were tested. A single-layer of 15.9 mm thick Type X gypsum board and a double-layer of 12.7mm thick Douglas fir plywood were used as the protective membranes for Test #4.3 and Test #5.4, respectively. Only the connection zone was covered by protection membranes, not the entire specimen along the longitudinal direction.

Test #5.2 was designed to test the effect of edge distance. One layer of 19.1 mm plywood was installed on each lateral side of the specimen. This modification increased the width of the specimen from 190 mm to 228 mm.

Test Facilities

The fire-resistance tests were carried out in a medium-sized furnace at the Full-scale Fire Research Facilities of Carleton University. The interior dimensions of the furnace are $2.7 \times 2.7 \times 2.2$ m (B \times L \times H). Six shielded thermocouples and two plate thermometers were installed in the furnace. The furnace temperatures followed CAN/ULC-S101 standard curve during all tests.

For each test, the specimen was pre-loaded to the designated load level for over 20 minutes and the tensile load was sustained during the fire test until failure. Failure was assumed to occur when the specimen could not withstand the applied load, or the load dropped with no recovery. After failure, burners were shut down immediately and charring was stopped by spraying water onto the specimen. In each test, furnace temperature, load, specimen displacement, specimen temperature, failure time, failure mode and charring rate were measured or recorded.

Test Results

Typical furnace temperature curves are plotted in Figure 2 (left) for Test #5.1, as an example. The TC temperature curve, averaged from 6 shielded thermocouples, follows the standard curve quite well. The PT curve, averaged from 2 plate thermometers, shows slightly higher values than the TC curve throughout the test, due to the fast response of plate thermometers.

The load and displacement curves are plotted in Figure 2 (right) for Test #5.1, as an example. At the failure time, 36.5 min, the load curve drops rapidly without recovery while the displacement curve increases quickly. A plateau of the displacement after failure observed in the curve is because the hydraulic pump was stopped after the specimen failed.

The measured specimen temperature histories for Test #4.1 are shown in Figure 3 as an example. Thermocouples T1-T3 were placed on a bolt located in the top section of the specimen and B1-B3 were located on a bolt located in the bottom section. The temperature gradient along the bolt shank was measured for the two bolts, as seen in Figure 3 (left). The temperature measured in the top bolt was found to be slightly higher than the temperature measured in the bottom bolt at the same distance from the exposed surface. This is probably because the top section received more heat from the flames in the furnace. However, the difference, maximum about 20-30°C, is not significant.

Figure 3 (right) shows the wood temperatures for Test #4.1. Thermocouples T4-T7 and B4-B7 were placed in the top and bottom section of the specimen, respectively. T6/B6 and T7/B7 measured higher temperatures compared to T4/B4 and T5/B5. This is because T6/B6 and T7/B7 were more affected by the two-dimensional heat transfer due to the presence of the steel plate in the center and also because the thickness-wise surfaces (130 mm) were facing the burners. Again, the wood temperature measured in the top section was found to be slightly higher than the wood temperature measured in the bottom section, but the difference is not significant.

The measured failure times are given in TABLE II. It is found that all the unprotected specimens have a fire resistance-rating less than 45 min. Test results in Group #1 show that the failure times for the replicates are very close (i.e., Test #1.1 vs. #1.2, and #1.3 vs. #1.4).

The most common failure mode is the elongation of the holes in the wood members. The hole-elongation might result in a complete cutting-through to the end of wood member, or it could be combined with splitting in the side members as the final failure. Similar failures were also reported before [2-4, 6-8]. Another observed failure mode was edge material tear-out, shown in Figure 4. It occurred when the edge distance of wood members was insufficient to resist shear after charring. In addition, a few bolts showed slight deformation but in only 2 or 3 tests.

The charring rate in the exposed solid wood part was found to be about 0.7 mm/min and the charring rate in the connection was about 0.8 mm/min. This is due to the steel plates enhanced conductive heat transfer and increased charring rates.

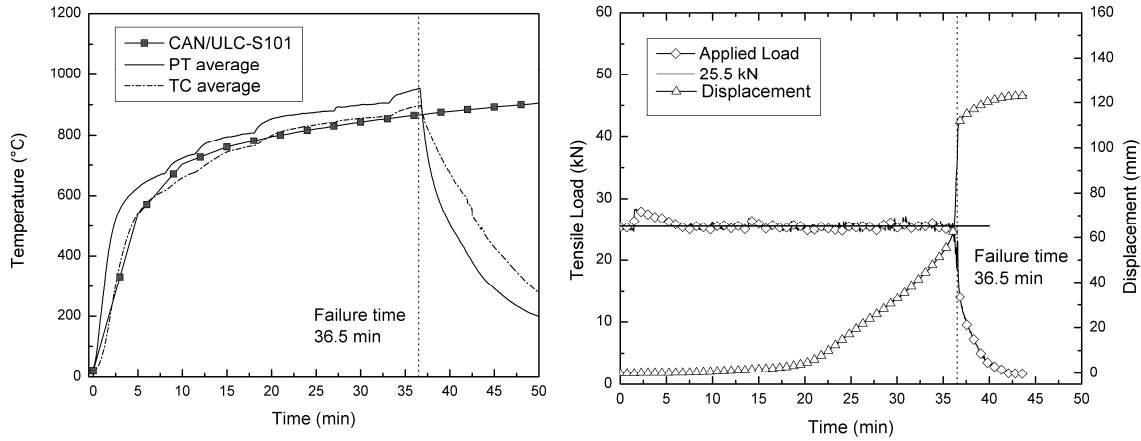


Figure 2. Measured furnace temperatures (left), load and displacement (right), for Test #5.1.

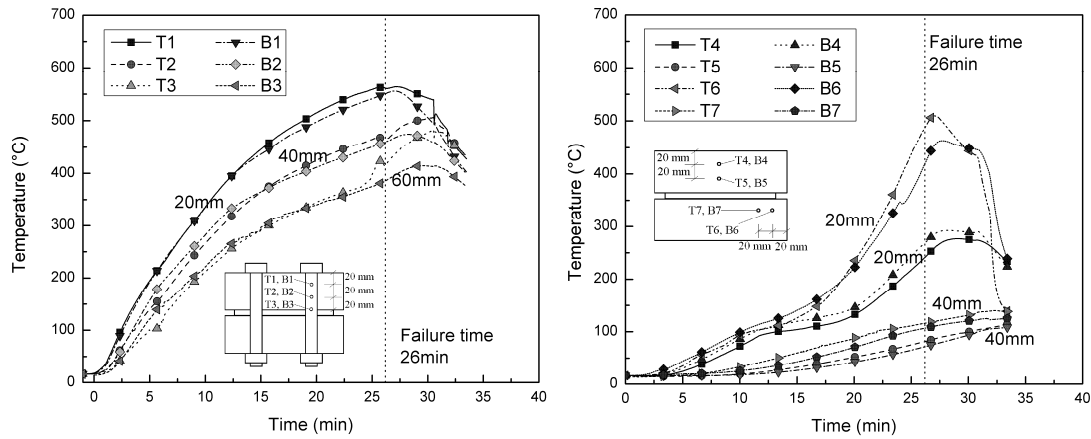


Figure 3. Measured bolt temperatures (left) and wood temperatures (right), for Test #4.1.

TABLE II. FAILURE TIMES AND FAILURE MODES.

Test #	1.1	1.2	1.3	1.4	2.1	2.2	2.3	3.1	3.2	4.1	4.2	4.3 [†]	5.1	5.2	5.3	5.4 [‡]
Specimen Information	SPF-L: 2@38×140 Bolt: 2×12.7				SP-G: 130×190 Bolt: 2×12.7			SP-G: 130×190 Bolt: 4×19.1		SP-G: 130×190 Bolt: 4×19.1			SP-G: 2@80×190 Bolt: 4×19.1			
Load Ratio	10%	10%	29%	30%	11%	18%	29%	11%	32%	10%	30%	30%	10%	10%	29%	29%
Failure Time (min)	14.5	15	8	8.5	28	22.5	17.5	27	15	26	14	51	36.5	43	19	34

[†]: The specimen was protected by a single-layer of 15.9 mm Type X gypsum board.

[‡]: The specimen was protected by a double-layer of 12.7 mm Douglas fir plywood.

DISCUSSION



Figure 4. Failure due to the edge material tear-out.

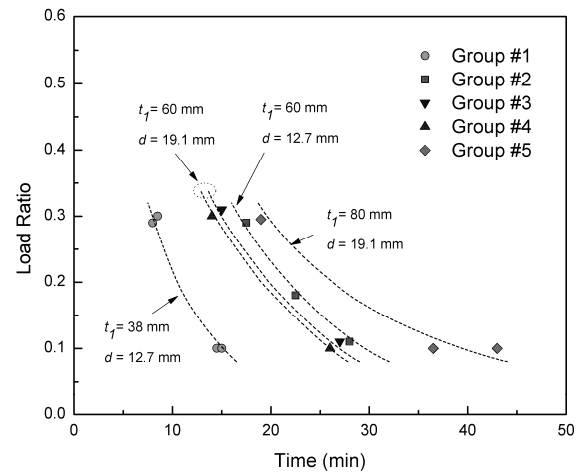


Figure 5. Load ratio versus failure time.

Figure 5 shows the relationship between load ratios and failure times for all 5 groups. Symbols are test results and dash lines are possible regression lines for the groups. It can be clearly seen that the specimens loaded at 10% have a better fire performance than the specimens loaded at 30%. Reducing the load ratio from 30% to 10% leads to a considerable increase of the fire-resistance rating for all groups.

The bolt diameter also plays a role on the fire resistance of timber connections. As seen in Figure 5, the difference of the fire-resistance rating at the same load ratio between Group #2 and #4 was found to be about 1-3 min. It is not significant. However, since the ultimate load capacities are greatly different between Group #2 and Group #4, increasing the bolt diameter directly reduces the load ratio and this improves the fire performance. The influence of the number of bolts is insignificant as seen from Group #3 and #4 (difference within 1 min).

Test #5.1 and Test #5.2 were designed to study the effect of the initial edge distance of wood. The initial edge distance was 47.5 mm (2.5d) for specimen #5.1, and 66.5 mm (3.5d) for specimen #5.2. The test results show that with the extra edge distance, the fire resistance increased from 36.5 min to 43 min. This means that the initial edge distance should be considered in order to satisfy a specified fire resistance. Otherwise, the edge distance is reduced due to wood charring in fire and the connection will fail pre-maturely because there is not sufficient edge material to carry the load.

Test #4.3 incorporated protection with a single-layer of 15.9 mm Type X gypsum board and the fire-resistance rating was improved by about 37 min, compared with Test #4.2. Test #5.4 showed that a double-layer of 12.7 mm DF plywood membranes improved the fire-resistance rating by about 15 min, compared with Test #5.3.

White [16] reported a series of fire-resistance tests on wood beams loaded in tension and protected with either 15.9 mm Type X gypsum boards or 12.7 mm plywood boards. As a comparison, it was found that, the fire-resistance rating improvement, the 140/180°C finish rating [17] and the time for 300°C behind the protection are very similar for both timber connections and timber beams, if the same protective membranes are used.

CORRELATION

A power law equation is proposed by the authors to estimate the fire-resistance rating of timber connections, shown in a non-dimensional equation:

$$t^* = 1 - (\eta)^M (d^*)^N \quad (1)$$

where non-dimensional factors: $t^* = t_f / (t_1 / \beta)$, $\eta = R_{fi} / R_0$ and $d^* = d / t_1$; t_f (min) is the fire-resistance rating, t_1 (mm) is the wood side member thickness, β (mm/min) is the charring rate, R_{fi} (kN) is the applied load, R_0 (kN) is the ultimate load and d (mm) is the fastener diameter; M and N are exponents to be determined.

Rewriting Equation (1) in a linear relationship by taking its logarithm gives:

$$\ln(1 - t^*) = M \ln(\eta) + N \ln(d^*) \quad (2)$$

M and N can be determined from the fire-resistance test data using a best-fitting by the method of least-squares. The charring rate β used in the correlation is approximated as 0.8 mm/min. Experimental test data used in the correlation were collected from this research and the literature [3]. Figure 6 shows the analysis result. It is found that $M = 0.15736$, $N = 0.06004$ and $R^2 = 0.82908$.

Rearranging Equation (2) to the dimensional form yields the following equation:

$$t_f = (t_1 / \beta) \left(1 - \eta^M (d / t_1)^N \right) \quad (3)$$

Equation (3) can be used to calculate the fire-resistance ratings of unprotected WSW bolted connections when $M = 0.15736$, $N = 0.06004$ and $\beta = 0.8$ mm/min. Figure 7 shows the calculated fire-resistance ratings using the equation vs. the tested fire-resistance ratings. It can be seen that the predicted fire-resistance ratings are almost within the $\pm 15\%$ envelope.

CONCLUSIONS

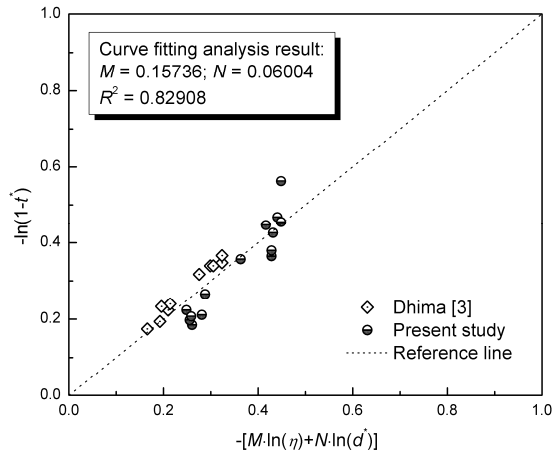


Figure 6. Curve fitting analysis result.

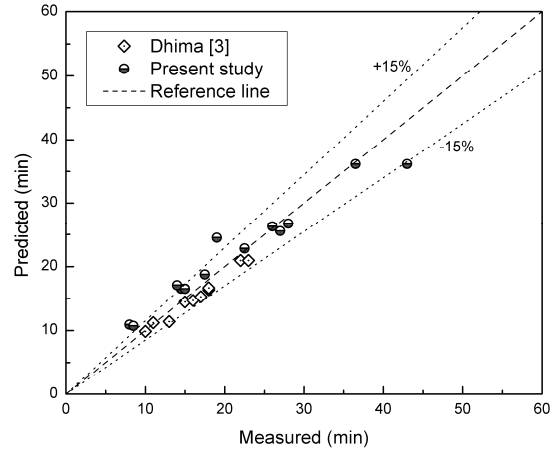


Figure 7. Comparison between predicted and measured fire-resistances.

In total, 16 specimens, belonging to 5 groups, were tested under exposure to the CAN/ULC-S101 standard fires. Particular attention was given to investigating the effects of different factors, i.e. wood side member thickness, load ratio, fastener diameter, edge distance and protection, on the fire performance of bolted WSW connections.

All the tested connection specimens with no protection were found to have a fire-resistance rating of less than 45 min, a target rating for code compliance. A reduction of the load ratio increases the fire-resistance rating significantly. Increasing the thickness of the wood side member leads to a considerable increase in the fire resistance. The bolt diameter does not play an

important role on the fire performance, but increasing the bolt diameter reduces the load ratio considerably, and as a result, it will improve the fire resistance. The protection provided by a single-layer of 15.9 mm type X gypsum board and a double-layer of 12.7 mm Douglas fir plywood improved the fire-resistance rating by 37 min and 15 min, respectively. These improvements for timber connections were found to be close to the improvements for timber beams, when the same protective membranes were used.

The test data from this research and the literature were used to develop a correlation proposed by the authors. It was found that the predicted fire-resistance ratings are almost within the $\pm 15\%$ envelope of the measured fire-resistance ratings.

ACKNOWLEDGMENTS

The authors would like to acknowledge the financial support from NSERC and FPIInnovations—Forintek Division. Thanks also go to Mr. Ba Lam-Thien and Mr. Osama Salem for their laboratory support.

REFERENCES

1. Noren, J. (1996) Load-bearing capacity of nailed joints exposed to fire. *Fire and Materials*, 20: pp 133–143.
2. Kruppa, J., Lamadon, T. and Rachet, P. (2000) Fire Resistance Test of Timber Connections. CTICM Ref. INC-00/187-JK/NB, CTICM, Paris, France.
3. Dhima, D. (1999) Vérification expérimentale de la résistance au feu des assemblages d'éléments en bios. CTICM Ref. INC-99/399-DD/NB, CTICM, Paris, France.
4. Ayme, N. (2003) Assemblages bois-métal en double cisaillement. Rapport Du Comportement Au Feu D'Assemblages Bois, CTICM Ref. SR21-03/121-NA/PB, CTICM, Paris, France.
5. Laplanche, K. and Dhima, D. (2003) Comportement au feu des assemblages bois, Assemblages bois/ bois et bois/métal en double cisaillement. CSTB research report, France.
6. Lau, P.H. (2006) Fire resistance of connections in laminated veneer lumber. Fire Engineering Research Report 06/3, Dept. of Civil Engineering, University of Canterbury, New Zealand.
7. Chuo, T.C.B. (2007) Fire performance of connections in LVL structures. Fire Engineering Research Report 07/4, Dept. of Civil Engineering, University of Canterbury, New Zealand.
8. Moss, P.J., Buchanan, A. H., Fragiocomo, M., Lau, P.H., Chuo, T. (2009) Fire performance of bolted connections in laminated veneer lumber. *Fire and Materials*, 33(5): pp 223–243.
9. Frangi, Andrea, Erchinger, Carsten and Fontana, Mario (2009) Experimental fire analysis of steel-to-timber connections using dowels and nails. *Fire and Materials*, 34(1): pp 1–19.
10. Konig, J. and Fontana, M. (2001) The performance of timber connections in fire test results and rules of Eurocode 5. in Proceedings of International Rilem Symposium 'Joints in Timber Structures', University of Stuttgart: Rilem Publications s.a.r.l., Cachan, France.
11. ISO 834 (1999) Fire resistance tests - Elements of building construction, Part 1: General requirements. International Organization for Standardization, Switzerland.
12. CAN/ULC-S101 (2007) Standard methods of fire endurance tests of building construction and materials. Underwriter's Laboratories of Canada, Scarborough, Canada.
13. CSA (2009) Engineering Design in Wood CAN/CSA-O86-09. Canadian Standards Association, Rexdale, ON, Canada.
14. ASTM D1761-88 (2000) Standard Test Methods for Mechanical Fasteners in Wood. American Society for Testing and Materials, Washington, DC, USA.
15. Mohammad, M. and Quenneville, J.H.P. (2001) Bolted wood-steel and wood-steel-wood connections: verification of a new design approach. *Can J Civil Eng*, 28: pp 254–263.
16. White, R.H. (2009) Fire resistance of wood members with directly applied protection. in Fire and materials 2009: 11th International Conference and Exhibition, Fisherman's Wharf, San Francisco, USA.
17. UL (1993) Fire Resistance Directory, Vol. 1. Underwriters Laboratories.

Fire Performance of Engineered Versus Traditional Lumber

R. BACKSTROM, M. TABADDOR and P. D. GANDHI

ABSTRACT

There has been a concern in the fire service that recent trend of replacing dimensional lumber with engineered lumber components in floor assemblies tend to increase the chances of catastrophic failures in a fire event. To address this concern, fire performance data from several wood-floor assemblies were generated and analyzed to provide insight into relative fire safety performance of traditional and lightweight wood constructions typical in residential homes. The floor assemblies used in this investigation consisted of unprotected floor assemblies as well as assemblies protected with gypsum wall board or lath and plaster, to prevent direct fire exposure to the assembly components. The floor assemblies were exposed to the standard time temperature curve, as defined in ASTM E119, in a large-scale floor furnace. Asymmetric loadings were applied to the floor along with some additional concentrated loads simulating the presence of fully equipped firefighters. The experimental data shows that the unprotected engineered lumber supported floor would perform at a substantially lower level than the unprotected traditional lumber supported floor. Observations from the test indicate that the thin webs typical of engineered lumber I-joists would quickly burn through, disengaging the lower chord, and therefore, leading to significant weakening and collapse.

INTRODUCTION

For several decades, wood 'I' beams and 2 x 4 inch wood trusses commonly known as lightweight wood construction have been replacing former traditional constructions consisting of mostly 2 x 10 inch solid lumber beams. According to a 2007 Engineered Wood Association newsletter, pre-fabricated joists comprise 50% of new wood-frame construction [1]. The main driver for the introduction of these products is the relatively higher stiffness to weight ratio as compared to traditional lumber. The economic benefits from using lightweight constructions and efficiencies in installation have lead to a preference for these types of wood-based products, whether for new residential constructions or renovations, typically of basements.

Robert Backstrom, Mahmood Tabaddor, and Pravinray D. Gandhi—Underwriters Laboratories Inc., 333 Pvingsten road, Northbrook, Illinois, 48309, USA.

However, over the years, residential fire incidents involving fatalities and injuries have led to concerns typified by firefighters falling through fire-weakened manufactured wood floors [2]. Though lightweight constructions have superior structural performance under ‘normal use’ conditions, this trend may reverse in a fire environment. In 1992, the National Fire Protection Research Foundation released a report citing 60 articles related to the fire performance of lightweight wood constructions between 1970 and 1990 [3]. The report highlighted the need for fire performance data and the need for focused training. A more recent review [4] details the work carried out on testing and modeling of lightweight wood framed assemblies. The cited tests consisted of mostly gypsum board protected wood assemblies.

As one example of papers in this area, a large set of fire tests [9] was carried out on a range of solid timber, wood I-joists, and different style of wood floor trusses but all for protected assemblies. There was little quantitative data presented and it was stated that ‘because those [gypsum board protected] ceilings had fallen from the assemblies before failure of the structural members occurred, the way in which the structure members failed would be no different from those for floor assemblies without ceilings’. Only one paper [10]¹ was found that examined the relative structural performance of unprotected wood floor assemblies, and found that ‘structural failure for the wood I-joist, steel C-joist, metal plate and metal web wood truss assemblies were 35-60% shorter than that for the solid wood joist assembly.’

Though only a brief synopsis of the literature review has been presented, the needs for baseline fire performance data for lightweight wood framed assemblies and possible effect on firefighter tactics are still mostly unmet. The objective of this work was to develop the data that would demonstrate the relative performance of the different wood constructions along with improvements in tactical methods for firefighting.

TEST PLAN

In this paper, the results of fire testing of 7 different floor constructions are described [6]. All assemblies were intended to represent a sampling of typical residential constructions (TABLE I). Of the 7 assemblies, 2 were unprotected. The 7 fire tests were subjected to the standard time-temperature curve - as prescribed by ASTM E119 [5] - in a large-scale floor furnace but with a non-traditional applied mechanical loading. The ASTM E119 standard dictates a uniform load on the floor to stress the supporting structural members, which is generally higher than the minimum design load of 40 lb/ft², specified by the building code for residential construction. However, for these tests, the load placed on the samples was intended to represent typical loading conditions in residential fire. 40 lb/ft² concrete blocks were placed along two of the four edges of the floor assemblies to represent the expected asymmetric loading of residences. In addition, on each floor sample, two 300-pound mannequins were placed near the center of the sample. Each mannequin was designed to apply the loading of a fully equipped firefighter (Figure 1).

¹ Release date of this paper was after completion of tests described herein.

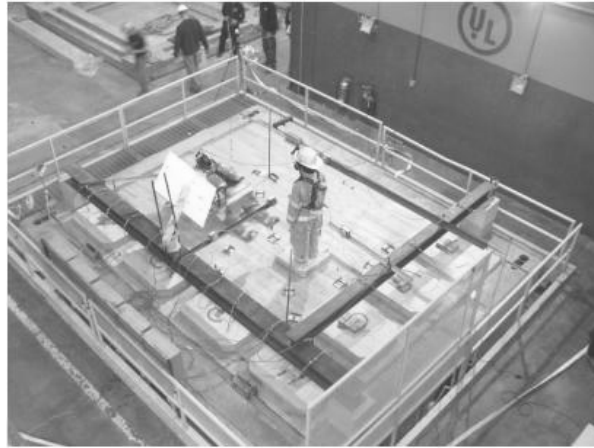


Figure 1. Photograph of test setup.

TABLE I. SUMMARY OF WOOD FLOOR CONSTRUCTION TEST SPECIMENS.

Test Assembly No.	Supports	Ceiling	Floor
1	2 by 10s @ 16 inch centers	None	1 by 6 subfloor & 1 by 4 finish floor
2	12 inch deep "I" joist @ 24 inch centers	None	23/32 inch OSB subfloor, carpet padding & carpet
3	2 by 10s @ 16 inch centers	1/2 inch regular gypsum wallboard	1 by 6 subfloor & 1 by 4 finish floor
4	12 inch deep "I" joist @ 24 inch centers	1/2 inch regular gypsum wallboard	23/32 inch OSB subfloor, carpet padding & carpet
5	Parallel chord truss with steel gusset plate connections, 14 inch deep @ 24 inch centers	1/2 inch regular gypsum wallboard	23/32 inch OSB subfloor, carpet padding & carpet
6	Parallel chord truss with glued connections, 14 inch deep @ 24 inch centers	1/2 inch regular gypsum wallboard	23/32 inch OSB subfloor, carpet padding & carpet
7	2 by 10s @ 16 inch centers	3/4 inch plaster	1 by 6 subfloor & 1 by 4 finish floor

Instrumentation

The furnace chamber temperatures were measured by 16 thermocouples placed approximately 12 inches below the surface of the exposed floor assembly. Additional thermocouples—over 50 thermocouples depending upon the test setup—were placed along interstitial spaces, the support beams, under the exposed surface of the sub-floor, on top of the unexposed surface of the floor and along interfaces between the sub-floor and floor (Figure 2).

The deflection of each assembly was measured with five electronic contacting transducers. In addition, there were eight camera views captured during the fire exposure period. One camera was positioned in the furnace recording the exposed surface of the assembly. Five other cameras recorded separate angles of the unexposed surface of the assembly and one infrared camera recorded the unexposed surface temperatures.

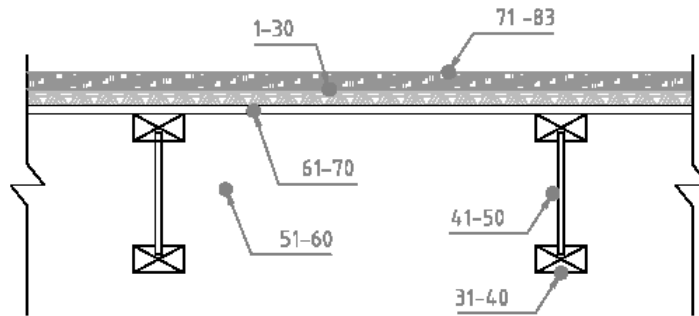


Figure 2. Thermocouple numbering scheme and placement for assembly 2.

RESULTS

The results of standard fire testing such as ASTM E119 fire tests are expressed as hours or some fraction thereof such as 1/2 hour, 1 hour or 2 hour rated assemblies. These time ratings are not intended to convey the actual time a specific structure will withstand a fire. All fires are different as actual outcomes are dependent on numerous parameters including compartment size, characteristics of combustible content and ventilation conditions. The ASTM E119 test method is more appropriately interpreted as providing a benchmark that enables a comparison of fire performance between test samples.

For unrestrained floor-ceiling assemblies such as the tested samples, ASTM E119 describes the following acceptance criteria: (i) the sample shall support the applied load without developing conditions that would result in flaming of cotton waste placed on the floor or roof surface, and (ii) any temperature measured on the surface of the floor or roof shall not increase more than 325 °F and the average temperature measured on the surface of the floor or roof shall not increase more than 250 °F. TABLE II shows the resulting fire resistance rating for the test samples along with some other milestones.

TABLE II. SUMMARY OF TEST RESULTS.

Test Assembly No.	Time of 250°F avg. temperature rise on surface of floor (min:sec)	Time of 325°F max. temperature rise on surface of floor (min:sec)	Flame passage through floor (min:sec)	Collapse (min:sec)	Fire resistance rating (min)
1	*	*	18:30	18:45	19
2	*	*	06:00	06:03	6
3	*	*	44:15	44:45	44
4	*	*	*	26:45	27
5	*	29:15	28:40	29:15	29
6	*	24:15	26:00	26:45	24
7	*	*	*	79:45	51**

Notes:

* - This condition was not achieved during the fire test.

** - Plaster ceiling in contact with furnace thermocouples at 51 minutes. The test method requires that the junction of the thermocouples in the furnace be placed 12 inches away from the ceiling surface at the beginning of the test and shall not touch the sample as a result of deflection.

Comparing the two unprotected floor assemblies, assembly 1 and assembly 2, the difference between the time to collapse for the engineered lumber and the traditional lumber is quite dramatic. In these tests, the engineered lumber floor only lasted about 6 minutes while the traditional lumber failed by collapse of loadings after 18 minutes. Though the actual performance of these constructions in field fire conditions is not predicted by these test data, the difference is sufficiently large to strongly suggest that engineered lumber, without protection typical of a Gypsum board type ceiling, will display much lower fire resistance performance as compared to traditional lumber, also unprotected.

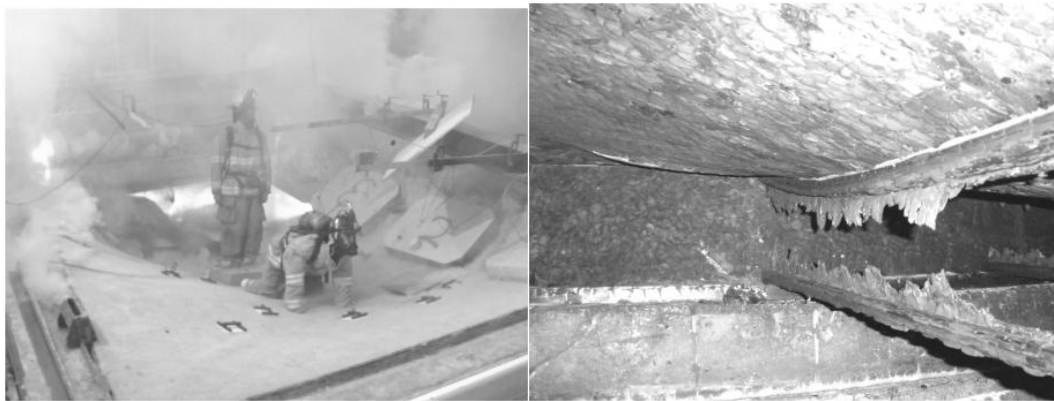


Figure 3. Photograph of assembly 2: (left) top view during test (right) view of exposed side of floor assembly after test.

Pictures from the assembly after the test provide some clues to the degraded performance of assembly 2. Looking at Figure 3, the right picture reveals that the web of the I-joist was burned completely. For an I-joist, the removal of the web will degrade the stiffness very quickly as the lower chord is also no longer

available. Some long sections of the lower chord were observed sitting at the bottom of the furnace at the end of the test. In contrast, the burning of a solid piece of lumber, the support for assembly 1, will be more uniform along the 3 exposed sides. The high stiffness to weight ratio of the engineered lumber, an advantage during normal conditions, will result in a structure with lower fire resistance. This holds true as the charring rates of the different wood samples was not found to vary significantly [8].

In addition to the fire resistance rating determined by the Conditions of Acceptance in ASTM E119, a finish rating is typically published for fire resistive assemblies with combustible supports such as the tested as samples. The finished rating is defined as the time when the first occurrence of either: (i) a temperature measured on the face of the combustible supports nearest to the fire increases more than 325 °F or (ii) the average temperature measured on the face of the combustible supports nearest the fire increases more than 250 °F.

Several fire test standards similar to ASTM E119 such as ISO 834:1 [7] provide additional guidelines on assigning the initiation of failure. For instance, the ISO 834:1 defines load bearing capacity as the elapsed time that a test sample is able to maintain its ability to support the applied load during the fire test. The ability to support the applied load is determined when both:

1. Deflection exceeds $L^2/400d$ (mm)
2. Deflection exceeds $L/30$, and the Rate of Deflection exceeds $L/9000d$ (mm/min)

where L is the clear span measured in millimeters and d is the distance from the extreme fiber of the design compression zone to the extreme fiber of the design tensile zone of the structural element as measured in millimeters. Other significant data obtained during the fire tests included observation of the conditions of the ceiling and floor surfaces, temperatures in the concealed space above the ceiling membrane and deflections of the floor surfaces, though due to space constraints, these are not included in this report but can be found in [6]. TABLE III provides a summary of some of this data for the wood floor assemblies. TABLE IV lists the milestones as it might relate to understanding the risks to firefighters and occupants.

TABLE III. SUMMARY OF OTHER KEY FIRE RESISTANCE MEASURES.

Test Assembly No.	Initial falling of ceiling material (More than 1 ft ²) (min:sec)	Average temperature on unexposed surface of ceiling at initial falling (°F)	Finish rating (min:sec)	Load bearing capacity (min)
1	No ceiling	No ceiling	00:45	18
2	No ceiling	No ceiling	00:30	4
3	23:30	605	15:30	45
4	17:15	531	7:45	25
5	16:30	519	10:45	24
6	16:00	559	12:15	25
7	74:00**	1109	74:00**	80

Notes:

** - plaster ceiling in contact with furnace thermocouples at 51 minutes

TABLE IV. FIRE PERFORMANCE MILESTONES.

Assembly	Structural Element	Type	Ceiling	Protective Membrane Breach	Allowable Deflection L/240 = 3/4" (min : sec)	Fire Fighter Breach (min : sec)
1	2x10 Joist Floor	Legacy	None	0:00	3:30	18:35
2	Wood I Joist Floor	Lightweight	None	0:00	3:15	6:00
8	2x10 Joist Floor	Legacy	Lath and plaster	74 ¹	75:45	79*
3	2x10 Joist Floor	Legacy	Regular gypsum wallboard	23:30	35:30	44:40
4	Wood I Joist Floor	Lightweight	Regular gypsum wallboard	17:45	3:30	26:43
5	Metal Gusset Truss Floor	Lightweight	Regular gypsum wallboard	16:30	20:45	29*
6	Finger Joint Truss Floor	Lightweight	Regular gypsum wallboard	16:00	24:00	26:30

* - Denotes approximate time
 1 - Denotes total failure of ceiling - plaster & lath had deflected down to & was supported by TC's prior to event
 2 - Kneeling fire fighter fell over & flaming impacting on
 3 - Denotes not applicable to roof structures

SUMMARY

The data presented in this research provides insight into the fire performance lightweight wood constructions relative to traditional lumber. The prevalence of these products has been driven by economic gains. However, there have been concerns that the fire performance of these products may be inferior to traditional lumber supports. For the lightweight constructions, the main concern is for unprotected floors, typical of basement/first floor constructions, whether in new homes or renovated homes. Incidents of firefighter injuries and deaths from the collapse of lightweight wood floors have highlighted the need for data and training methods to deal with these new wood products. Though research has been carried out on the fire performance of lightweight structures, most of these have not examined the unprotected designs.

The data from this research study, supported by the Assistance to Firefighters Grant, shows that for unprotected wood floor assemblies, the fire performance of an engineered wood I-joist is significantly lower than the traditional lumber. Though the actual numbers from the test cannot be extended to predicting actual outcomes of residential fires, the dramatic differences are likely to be present. Observations from the testing revealed that the likely culprit for this inferior fire performance of the engineered lumber is simply that thinner sections (with similar charring behavior as traditional lumber) will burn away much quicker. For an I-joist support, this means that the web will be burned away and

subsequently degrade the load carrying capacity of the floor assembly very suddenly as the lower chord is now detached.

The next step is the interpretation and translation of these results into policy and tactical changes as it relates to fire safety to help avoid and minimize injuries and deaths. UL in partnership with the Chicago Fire Department has developed a training program geared towards firefighters to educate them on the hazards associated with lightweight constructions gained from this research. In addition, recommendations for codes changes would include the requirement for protection floor (and roofing) systems utilizing engineered wood products, the protection of any truss girders within assembly within the assembly with a minimum of one-hour fire rating, requirements for current draft stopping to limit concealed spaces to no more than 500 feet, and elimination of the current exemption for ‘no usable space above or below the assembly’.

ACKNOWLEDGMENTS

This work was supported by a 2006 DHS grant EMW-2006-FP-01437. The authors would like to express their deep gratitude to the Chicago Fire Department, a partner in this project, especially to Chief Richard Edgeworth and Research Coordinator James M. Dalton.

REFERENCES

1. Technical Topics, Form TT-015 C, APA Engineered Wood Association, November 2007.
2. Kirsh, J., ‘Silent Floors, Silent Killers?’, *Fire Engineering*, April 2007.
3. Grundahl, K., National Engineered Lightweight Construction Fire Research Report, National Fire Protection Research Foundation, 1992.
4. Benichou, N., and Sultan, M., Fire Resistance Performance of Lightweight Wood-Framed Assemblies, *Fire Technology*, 36, 2000, pp. 184-219.
5. ASTM E119, Standard Test Methods for Fire Tests of Building Construction and Materials, ASTM Subcommittee E05.11, 2008.
6. Structural Stability of Engineered Lumber in Fire Conditions, UL Report, September 30, 2008.
7. ISO 834-1, Fire-resistance tests—Elements of building construction—Part 1: General requirements, International Organization for Standardization, First Edition, 1999.
8. Kodur, V., Pakala, P., and Tabaddor, M., High-Temperature Properties of Wood for Fire Resistance Modeling of Wood Floor Assemblies, *Journal of Fire and Materials*, *to be submitted*.
9. Richardson, L., Failure of Floor Assemblies Constructed with Timber Joists, Wood Trusses, or I-Joists During Fire Resistance Tests, *interflam 2004*.
10. Su, J.Z., Benichou, N., et al., Fire Performance of Houses, Phase I, Study of Unprotected Floor Assemblies in Basement Fire Scenarios, National Research Council Canada, 2008.
11. Underwriters Laboratories Inc, and Chicago Fire Department, Research and Development Grantees Midyear Meeting, Department of Homeland Security, December 2008.

Fire Resistance of Traditional Timber Post and Beam Construction—An Experimental and Modeling Study

A. NAKAJIMA^{*1}, Y. HASEMI^{*1}, N. YASUI^{*1}, A. SUZUKI^{*1},
D. HIRAKURI^{*1}, Y. SAWANO^{*2}, K. WATANABE^{*2}, H. HIRAI^{*2},
A. OGAWA^{*2}, M. S. SEKI^{*2}, M. KOSHIHARA^{*3}, M. MURAKAMI^{*4},
T. KIMURA^{*5} and Y. TAMURA^{*6}

1. ABSTRACT

Asia has long history and tradition of timber-based post and beam construction. However, in the Japanese building regulation, application of traditional construction has been limited to small buildings mostly for dwellings. This unvalued recognition of traditional construction is attributed to the lack of engineering research in its structural fire safety, especially on load-bearing assemblies such as wall timber frames and beam-floor complexes. For the application of such construction to large public buildings, it is necessary to make the load-bearing assemblies sustainable during a fire and rated as *Quasi-fireproof construction* in the Japanese building regulation^{*1}. Also, because of the openness typical in the planning of Japanese traditional buildings, it is necessary to verify the fire resistance of load-bearing interior walls exposed to both-sides fire heating. Such study is needed also for the fire protection of historic heritage timber buildings widely distributed in Asia. This work intends to develop predictive and design method for the principal structural members of traditional timber construction. The present report is a summary of a comprehensive study, and includes the following studies:

1. Modeling of char layer formation and fields of temperature and Young's modulus within column and beam due to fire exposure based on a series of small scale unloaded fire tests
2. Development of predictive method for the mechanical performance, especially the buckling criteria, of the load-bearing assemblies based on the char and temperature field modeling
3. Validation of the predictive method against full-scale loaded fire tests

Finally guideline is proposed for the achievement of the Japanese *Quasi-fireproof construction* based on the traditional timber construction.

2. INTRODUCTION

General Japanese traditional constructions are built with bare timber soil wall construction. Fire safety performance of timber wall demands mechanical performance, thermal insulation performance and flame insulation performance. They are determined by the buckling of the post, soil thickness, and the boundary conditions of the posts and walls. Among these three elements of the fire safety performance of load bearing walls, the greatest difficulty for the Japanese traditional bare timber walls¹⁾ is the improvement of the mechanical fire resistance. The timber posts can be directly exposed to a fire, because Japanese wood/soil wall construction has bare timber soil walls. Although soil covers part of a timber post from fire and restrains the temperature rise of the post, decrease of the cross-section of a post due to charring may make the post buckle and reduce the whole fire resistance.

^{*1} Waseda University, 3-4-1 Okubo, Shinjuku, Tokyo, 169-8555, JAPAN

^{*2} formerly graduate school, Waseda University, ^{*3} Institute of Industrial Science, Tokyo University, ^{*4} Kinki University, ^{*5} Kyoto Construction Industry Union, ^{*6} Kansai Association for Research in Traditional Housings

In the Japanese building regulation, fire safety performance of load-bearing walls is evaluated by standard heating under the loading of allowable unit stress for long sustained loading of the load-bearing part of the height for one-story of buildings. It has been considered that the evaluation of mechanical fire resistance of wood based construction can be tested only with full scale specimen. However, due to the low availability of large fire furnaces in most of local districts and cost effectiveness, we propose a *Prediction of the Fire Resistance of bare-timber soil walls* by post compression tests and a *Predictive Expression of Critical Load*.

3. PREDICTION OF THE FIRE RESISTANCE OF BARE-TIMBER SOIL WALL

In this paper, we propose a Prediction of the Fire Resistance without using large scale and loaded fire resistance test. Heated bare-timber walls have potentiality to reduce load-bearing-capacity due to three factors. First is deficit of cross-section by charring. Second is reduction of the Young's modulus due to the rise of inner temperature of post²⁾. Third is reduction of the geometrical moment of inertia by deficit of cross-section by holes for horizontal bars(*Nuki*). In consideration for these factors, Fig1 shows procedure of fire resistance design of a bare timber wall by predicting the post's mechanical performance after heating.

3.1. PREDICTIVE EQUATION OF CRITICAL LOAD

Generally, the maximum load under which the post deforms and collapses can be expressed by Euler's buckling load formula($P_k = k^2 \pi^2 EI / L^2 \dots Eq(1)$), where P_k , L_k , E , I and k are the buckling load, the buckling length, Young's modulus, the geometrical moment of inertia, and the boundary-coefficient respectively. Among these variables, L_k is equivalent to the overall post length and k depends on the post-wall configuration and the heating conditions. Because of the above, it is considered that buckling load is governed by E and I . In addition, the boundary-coefficient of Wood/Soil wall's post can be determined from a series of compression tests by taking correlation between P_k and EI/L^2 .



PHOTO.1 Japanese traditional construction of Fire Protective construction

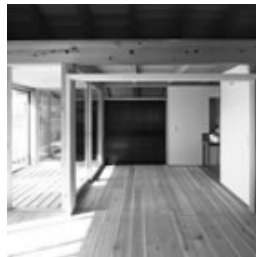


PHOTO.2 Ceiling of Bare-Beam



PHOTO.3 Japanese traditional construction of Quasi Fireproof construction using concrete for wall

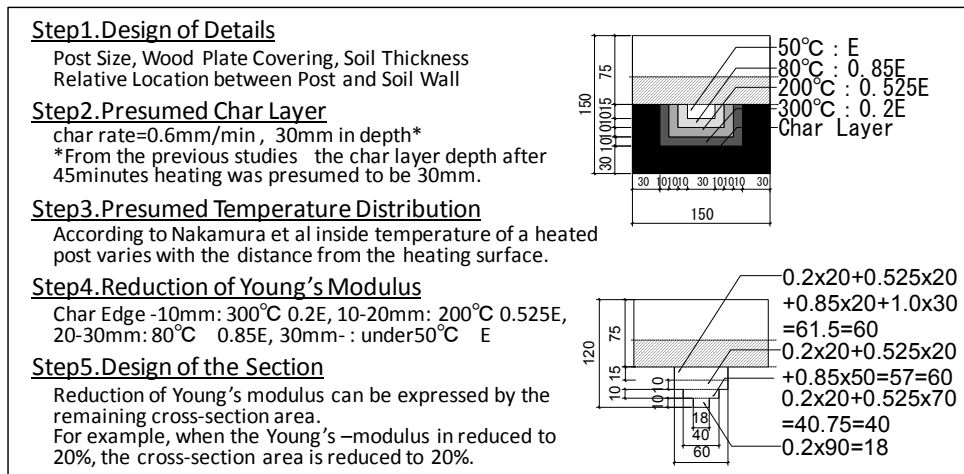


Figure.1. PROCEDURE TO PREDICT MECHANICAL FIRE RESISTANCE OF TIMBER MEMBER.

3.2. WOOD POST COMPRESSION TESTS

The purpose of this test is inspecting validity of the prediction method and quantifying “k” from critical load. If this method is verified, the mechanical fire resistance of a bare-timber soil walls becomes predictable without large testing.

Specifications of all the 41 specimens are shown in Table1. Each specimen has three holes (15mm width x 105mm high or 30mm width x 120mm high) in a parallel direction with wall surface for joining soil wall foundation with horizontal bars. The specimen’s cross-section after 45minutes heating was designed in the *Predictive Method for the Mechanical Resistance* (Fig.1.). All specimens were set up as shown in Fig3. The specimen was loaded vertically on the center with a hydraulic jack. While the horizontal displacement grows in correspondence with the growth of char layer, at some point the horizontal displacement begins developing without increase of the load. The load at this point is defined as critical load P_k . The test is stopped after the critical load is achieved.

3.2.1. RESULT AND DISCUSSION

Table1 shows the results. Graph1 shows a relation between the correction load “ P_k ”, and the value multiplied the geometrical moment of inertia “ I ” and Young’s modulus “ E ” can be represented as *Equations(2) and (3)*(Graph1).

$$\text{for - eccentricity - post}_{50\%} P_k = (0.83)^2 \pi^2 EI / l^2 \cdot \{Eq.2\}$$

$$\text{for - non - eccentricity - post}_{50\%} P_k = (1.22)^2 \pi^2 EI / l^2 \cdot \{Eq.3\}$$

TABLE.1. SPECIMENS AND RESULTS OF POST COMPRESSION TEST

ID	Post ¹⁾ (mm)	Wood Plate Covering (mm)	Soil Chicknes (mm)	Horizontal Bar		Gap ²⁾ (mm)	I ³⁾ (10 ⁶ mm ⁴)	E ⁴⁾ (t/cm ²)	Moisture Content (%)	Pk ⁵⁾ (kN)				
				Location of Penetration	W×H mm									
1	105sq	Covered in Both directions	20	center	15×105	13	4.7	50	7.9	27.4				
2	120sq					14	0.7	50	8.9	24.5				
3	120sq					16	8.7	70	8.9	44.3				
4	120sq					17	8.7	50	14	51.0				
5	105sq					15	4.4	50	8.4	27.6				
6	120sq					15	7.0	50	8.9	21.6				
7	120sq					20	14	7.9	88	12	61.7			
8	120sq					20	14	7.9	84	14	25.5			
9	120sq					25	14	8.6	71	13	42.1			
10	120sq					25	14	8.6	86	18	53.9			
11	105sq	Covered in One directions	20	center	15×105	25	1.9	50	9.8	5.8				
12	120sq					25	4.3	70	11	18.6				
13	135sq					25	8.2	70	12	42.0				
14	150sq					25	14.0	70	12	60.8				
15	165sq					26	21.8	90	13	100.9				
16	165sq					24	24.1	70	22	111.7				
17	180sq					27	32.8	70	15	157.8				
18	120×150					23	11.3	70	9	60.7				
19	135sq					-	-	-	-	21	9.0	65	11.6	62.6
20	150sq									22	15.5	65	12.4	102.6
21	135sq	Internal Side	15×105	24	8.5					65	11.7	64.7		
22	135sq			24	8.5					65	12.1	61.9		
23	135sq			25	8.4					65	11	54.1		
24	135sq	30×120	-	25	8.4					65	13.1	64.5		
25	150sq			24	14.9					65	11.8	106.5		
26	135sq			center	15×105					26	7.8	65	12.8	52.4
27	135sq	30×120	32							6.2	65	13.2	47.5	
28	150sq	30×120	30							12.2	65	11.4	80.5	
29	135sq	External Side	-	-	-	27	7.1	65	12.8	52.8				
30	135sq					27	7.1	65	12.6	51.9				
31	135sq					15×105	-	32	4.4	65	12.6	37.9		
32	135sq							30×120	32	4.4	65	11.9	33.5	
33	150sq								30×120	33	8.8	65	10.8	73
34	140sq					-	-	-	-	4.5	70	8	40.0	
35	165sq	8.5	50	11	65.0									
36	165sq	3.3	90	8	67.7									
37	165sq	12.8	90	9	70									
38	165sq	12.8	73	12	151.0									
39	180sq	6.4	70	9	84.0									
40	195sq	11.4	70	11	71.0									
41	180sq	center	15×105	9.0	50					25	74.0			

¹⁾ Post Length:3000mm/First class Japanese cedar ³⁾ Geometrical moment of inertia
²⁾The Gap of the loading point and the center of gravity of posts ⁴⁾Young's modulus ⁵⁾ Critical Load

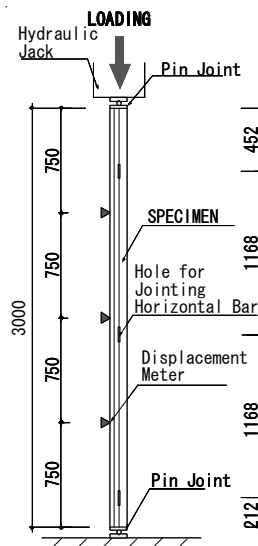


Figure.3. EXPERIMENTAL SET UP

UPSIDE: HEATING SIDE
wood plate covering

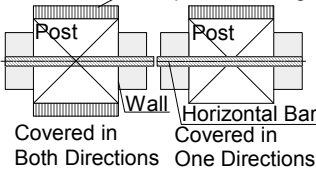
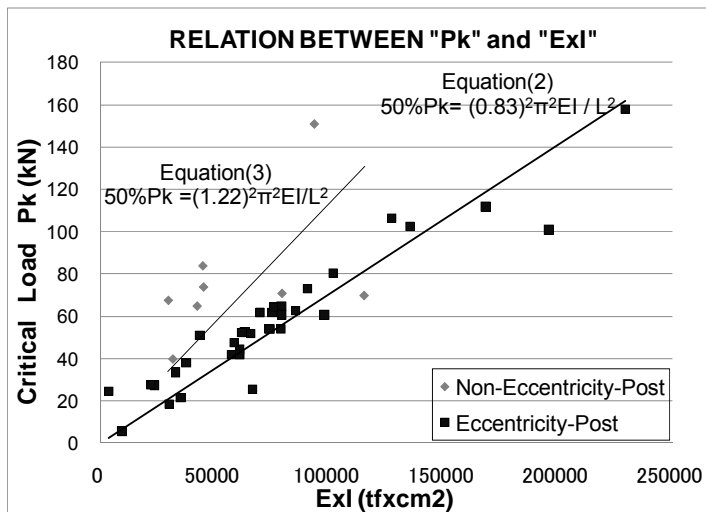


Figure.4. SPECIMENS DETAIL OF No.1~10



Photo.4. CROSS SECTION



GRAPH.1. RELATION BETWEEN CRITICAL-LOAD "Pk" and "ExI"

Photo.5. POST COMPRESSION TEST

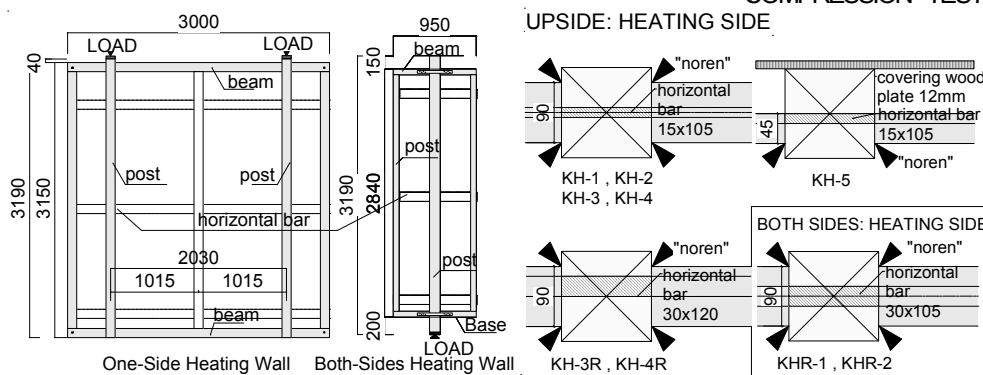


Figure.5. OUTLINE AND CROSS-SECTION OF TEST SPECIMENS.

3.3. LARGE SCALE LOADED FIRE RESISTANCE TESTS

With a Large Scale Loaded Fire resistance tests, we inspected validity of *the predictive method for mechanical fire resistance and the predictive equation of critical load* (Equations(2) and (3)).

Specifications and results are shown in Table2. Specimen outline is shown in Fig5. The specimens were designed to achieve 45minutes fire resistance and loaded *the predicted-critical-load* calculated from the predictive method. The calculation is made using Equ(2) for the one side heating(external walls) and Equ(3) for the both-sides-heating(interior walls). As KHR-1's horizontal-bar is in the center and the posts are heated from both-side, so we anticipated that the posts of KHR-1 are never eccentrically loaded and falling of the fire performance is not significant. By this reason, predicted critical load of KHR-1 was calculated without considering the reduction of the geometrical moment of inertia caused by horizontal bar's position and size.

Heating was controlled according to ISO834 Standard Time-Temperature curve, and was stopped when deformation of posts and soil wall panels became significant. A large-scale wall furnace was used for one-side-heating tests, and both-sides-heating tests were conducted using specimens with wing-like walls on both sides of a column(Fig4, middle) spreading diagonally in a column furnace. Vertical loading was applied on top of each post of specimens with a hydraulic jack. Measurements were made on the axial contraction, horizontal displacement, temperatures within the specimen, temperatures of wall back-surface, furnace temperature, and the char-layer depth of the post. Fire resistance time of *Quasi-Fireproof Construction* is determined by penetration, judged either by the temperature rise on the back surface (not higher than 140K) or the penetration of flame, or by the vertical deformation (not larger than h/100 where h is the furnace height), whichever reaches the critical condition earlier.

TABLE.2. SPECIMENS AND RESULTS OF LARGE SCALE LOADED TEST.

ID	Post Section (mm)	Predicted Critical Load (kN)	Load (kN/post)	Heating Time (min' sec")	Thermal Insulation			Flame Insulation	Mechanical Fire Resistance		Char Depth	
					Wall Backsurface Temperature(°C)			Flame Penetration	Maximum Horizontal Displacement (mm)	Maximum Velocity of Shrinkage (mm/min)	Front (mm)	Diagonal (mm)
					start	average	max					
ONE SIDE HEATING												
KH-1	120x150	166.71	176.5	55'00"	10	84.1 (55min)	90 (55min)	No	9.1	2.2	35	50
KH-2	180x180	43.7	40.8	38'00"	14	73.5 (38min)	78 (38min)	No	11.9	6.2	23	45
KH-3	135x135	77.2	65.6	64'00"	7	79 (64min)	85 (64min)	No	13.2	2.4	42	61
KH-4	150x150	44.4	40.8	67'00"	11	84 (67min)	89 (67min)	No	3.7	1	40	60
KH-5	135x135	19.5	19.5	41'00"	9	161 (45min)	191 (41min)	No	11.3	3.9	26	52
KH-3R	135x135	39.3	39.6	80'00"	23	96	164	No	3.66	0.32	49.2	0.59
KH-4R	150x150	72.9	67.8	76'30"	17	89	163	No	14.45	7	45.8	0.46
BOTH SIDES HEATING												
KHR-1	120x190	54.7	67.8	37'30"	-	-	-	-	43.7	19.8	40.9	-
KHR-2	165x165	48.9	37.2	53'30"	-	-	-	No	73.2	119	38.1	-

Post Length=3190mm/Japanese First Class Japanese Cedar
 Young's module "E" =70 tf/cm2 KH-1,KH-2), the others are 65tf/cm2

3.3.1. RESULT AND DISCUSSION -THE VALIDITY OF THE PREDICTIVE METHOD-

Table2 show specifications and result. Six large soil wall specimens, KH-1, KH-3, KH-4, KH-3R, KH-4R, KHR-2, loaded with each *predicted-critical-load (Equ.(2))* satisfied more than 45minutes fire-resistance without buckling. On the other hand, KHR-1 buckled under the *predicted-critical-load (Equ(3))* calculated without considering the reduction of the geometrical-moment of inertia caused by horizontal bar's position and size. KH-2 also buckled under the load greater than *predicted-critical-load (Equ(2))*. The test for KH-5 was terminated for the backsurface-temperature exceeding the regulatory requirement. It is attributed to its cedar plate covering not enough thick to delay the thermal penetration. These should indicate that the predictive method for fire resistance is effective to predict the buckling load of the post after heating on some conservative side.

4. FIRE RESISTANCE OF TIMBER BEAM AND FLOOR ASSEMBLIES

There had been virtually no research on the fire resistance of the Japanese traditional timber beam or floor assembly because traditional construction has been designated only for small housing buildings with which the Japanese *Building Standard Law* never require fire resistance of internal load bearing assemblies. However, we are challenging improvement of the applicability of traditional construction for larger buildings and wider range of occupations. This essentially needs higher fire resistive performance of internal assemblies including beam and floor assemblies.

Traditional wooden floor generally appears above beams. In this case, destruction and deflection of floor-board which keep a fire in a lower floor from the upper floor may receive two influences. First is the deformation of beam. Second is the combustion of the slab layers and joist which support the floor directly. Thermal insulation and mechanical sustainability are the two requirements for a floor of *Quasi-Fireproof construction*. Because the thermal penetration through a floor slab is uniform, the thermal insulation in fire could be assessed with small scale specimens. On the other hand, size is essential for the deformation of a beam and large scale loaded test is important to assess the mechanical fire performance of the beam.

In this chapter, we first study thermal insulation performance by small scale

non-loaded fire resistance test and grasp post-heating, char-depth and internal temperature which influence upon mechanical performance by small scale fire resistance test. Then, we propose design of the beam having the fireproof resistance of *Quasi-fireproof construction* for 45minutes.

4.1. SMALL SCALE NON-LOADED FIRE RESISTANCE TESTS

TABLE3 and Figure6 show the outline of specimens. They have two specifications, bare-beam type and ceiling with panel finishing type. This reflects the typical design of ceilings in Japanese traditional buildings; finishing with very fine wood panel is common when the room is designed as a main room(“*Zashiki*”) and bare-beam without panel finishing is normally used for shops, lobby or kitchen. The specimens were heated according to the ISO834 Standard-Time-Temperature-Curve for 45 minutes in a horizontal furnace without loading. Measurements were conducted on the temperature of the interior and surfaces of the specimens and char depth of the wooden assemblies.

TABLE3 shows the result. Thermal insulation performance as as 45 minutes *Quasi-Fireproof construction* was verified for all specifications. The charring rate of thin wood such as ceiling board was found to be large, say about 0.8mm/min. In addition, a total thickness of the ceiling board and the floor board, 60mm, was found to maintain the thermal insulation performance of 45 minutes. Figure7 and Figure8 are the time history of inner temperature of specimens. The char depth of the facing board is 9mm (testB) and 15mm (testD). And the time when lower part of facing-board-temperature became 260°C(an ignition temperature of the wood) is 37.5minutes (testB) and 41.5minutes (testD). These results indicate that the floor constitution including the joist is superior in thermal insulation performance. It is thought that the space between a facing and the lining caused by existence of joist functioned as thermal resistance.

Although total char depth of a facing and lining board of specification A, B, D is 38~45mm, total char depth of specification F which has ceiling remains in

TABLE.3 SPECIMENS AND RESULTS

ID	SPECIFICATIONS*1			Char Depth (mm)	max T*3 (°C)
	part	materials*2	size (mm)		
A	Facing	cedar	15	0	61
	Joist	cedar	45x45 @303	0	
	Lining	cedar	45	38	
	Facing	cedar	30	9	
B	Joist	cedar	21x45 @303	front:3 diagonal:12 destruction	54
	Lining	cedar	30		
C	-	Laminated cedar	60	36	57
D	Facing	cedar	30	15	57
	Lining	cedar	30	destruction	
E	Facing	cedar	30	7	61
	-	Hardened PB*	15	-	
F	Facing	cedar	15	0	54
	Lining	cedar	30	24	
	-	cedar	15	destruction	

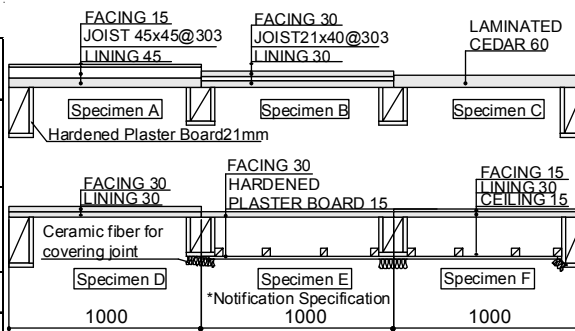


Figure.6 OUTLINE OF SPECIMENS

Heating Time=45min, Flame Penetration of all the specimens is nothing
 *1) Specimen Size: 1000x1000
 *2) First Class Japanese Cedar, Moistur
 *3) maxT means Wall Back surface maximum temperature Content is ≒ 15%

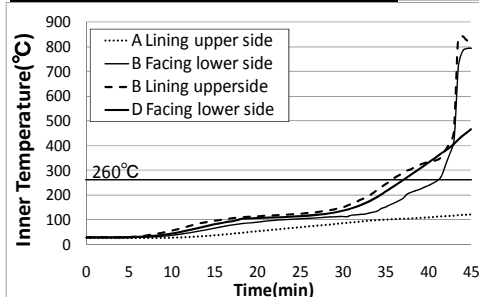


Figure.7. RELATION BETWEEN JOIST AND TEMPERATURE.

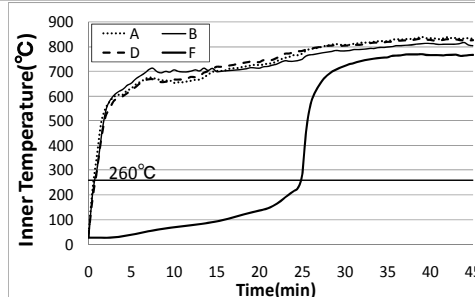


Figure.8. TEMPERATURE OF LOWER SIDE OF LINING BOARD.

24mm. It is thought that the ceiling can relax the direct heating of the floor board till the ceiling-board is destructed.

4.2. LOADED FIRE TESTS WITH LARGE SCALE SPECIMEN

Although the destruction of the beam is essentially controlled by bending stress, measurement of the bending stress in experiments is difficult and by this reason the present test protocol judges the mechanical fire resistance of a beam according to its deflection. However, if the span of a timber beam is increased, the allowable deflection may exceed the mechanical limit of timber. Therefore, we first ran loaded fire tests with 4m long floor-beam assemblies to verify the prediction of the deflection and its application to the fire safety design of short beams, and then ran another series of tests to verify fire safety design of longer floors based on the prediction of the post-heating bending stress of timber beam.

The specimens are summarized in Table 4 and Figure 9, where WF-1 and WF-2 were designed according to the prediction of the deflection(Deflection Method) and WF-3, 4, 5 were designed according to the prediction of the bending stress(Bending-stress Method). In the predictive method, we assumed the charring rate of beam as 0.8mm/min, the *deflection* given as $\delta = 5WL^4/384EI$ and the *allowable bending stress* as $22.5N/mm^2$ (*Japanese Building Standard*). Heating was controlled according to ISO834 Standard Time Temperature curve for 45 minutes, and was stopped when deformation of beams became significant. A large-scale horizontal furnace was used for test and vertical loading was applied on two points of beams with a plate-weight. The loading condition was decided basically according to the Japanese structural requirement for dwelling (bare beam, $1800N/m^2$) and for public meeting place(ceiling panel covering, $2900N/m^2$). Fire resistance time was evaluated according to the protocol for the *Quasi-Fireproof Construction*, which is determined by penetration, judged either by temperature rise on the back surface

TABLE.4. SPECIMENS AND RESULTS.

ID	Detail	Beam		Length WxH (mm)	Predicted		LOAD (N/m ²)	Heating Time (min' sec'')	Thermal Insulation			Mechanical Fire Resistance	
		Cross-Section MoistureContent Young's modulus	Span (mm)		Predicted char rate (mm/min)	Predicted Deflection (mm)			Wall Backsurface Temperature(°C)			Max Deflection (mm)	Limit Deflection (mm)
				start			average	max					
Use DEFLECTION as a standard and design the specimens by the prediction method													
WF-1	Bare-Beam	150x270 (11.6%) (E=65tf/cm ²)	1000	4105 x 2240	0.6 0.8	9.5 16.4	1800	50'00"	19	65.3 (50min)	86 (50min)	4.5	≤140.5
WF-2	Ceiling-Beam	120x270 (11.1%) (E=65tf/cm ²)	1000	4105 x 2240	0.6 0.8	13.8 23.9	2900	45'00"	23	51.5 (45min)	53 (45min)	13.6	≤140.5
Use BENDING STRESS as a standard and design the specimens by the prediction method													
WF-3	Bare-Beam	150x300 (11.6%) (E=99tf/cm ²) (Fb=22.5N/mm ²)	1000	6210 x 2320	0.6 0.7 0.8	49.8 60.5 74.5	2900	53'00"	20	60.5 (53min)	78 (53min)	47.2	≤300
WF-4	Ceiling-Beam	-	2000	2000 x 2195	0.8	131	2989	45'00"	17	52.0 (45min)	57.0 (45min)	30.2	≤222
WF-5	Bare-Beam	-	2000	2000 x 2195	0.8	59	2107	45'00"	17	40.0 (45min)	43.0 (45min)	7	≤222

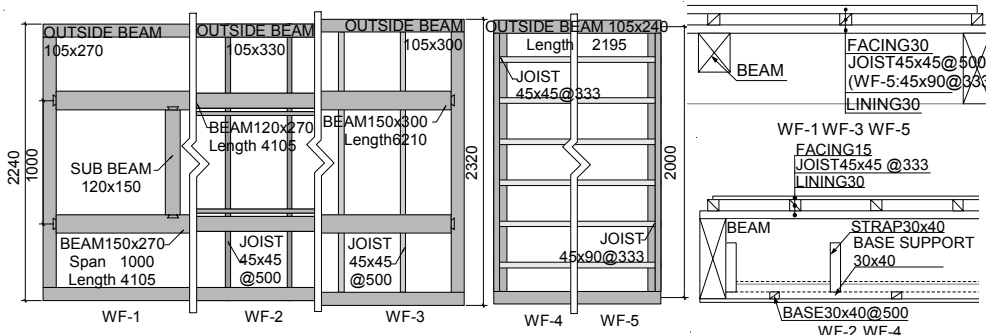


Figure.9. OUTLINE OF SPECIMENS.

(not higher than 140K) or the penetration of flame, or by the vertical deformation (not larger $L^2/400d$ where L is the length between fulcrums), whichever reaches the critical condition earlier.

Table4 shows the results. 45 minutes fire resistance was verified for all specifications. It is noteworthy that the Bending-stress Method(WF-3) results in the closer prediction of deflection than the Deflection Method(WF-1). The designed beam height of WF-3 was increased by only 30mm from WF-1 although the beam span was increased by 50% and the load was increased to 2900N/mm² from 1800N/mm².

6. CONCLUSIONS

Prediction of the post-heating mechanical response of columns and beams of Japanese traditional bare-timber construction has resulted in reasonable agreement with large-scale loaded fire tests and has been proven to provide a basis for the fire safety design of such construction. The proposed method could help attempts to resolve the difficulty in developing code-compliant design for wooden walls and beams for the limited availability of fire test furnaces. The Ref.4 further delivers a still more comprehensive methodology to predict mechanical fire resistance of bare-timber wall even without the column compression tests.

ACKNOWLEDGMENTS

This research was conducted mainly under the support of Japan Society for the Promotion of Science(JSPS) fund. The authors wish to thank General Building Research Corporation of Japan for the arrangements of the furnaces for the experiment. More detail of the analysis is seen in Refs. 3) – 7).

*1 *Quasi-Fireproof construction* in the Japanese regulation is to sustain the long-term load until the end of the designated time of fire exposure, but might collapse after the fire. *Fireproof construction* is on the other hand to survive a fire exposure of the designated fire resistance time.

REFERENCES

- 1) Hasemi, Y., Yasui, N., Kinoshita, K., Akizuki, M., Yoshida, M., Yamamoto, K., Tamura, Y., Takeda, M. Fire Safety Performance of Japanese Traditional Wood /Soil Walls and Implications for the Restoration of Historic Buildings in Urban Districts, Fire Technology, Vol.38, Issue 4, p391- 402, 2002.
- 2) Nakamura, K., Miyabayashi, M., Fire Resistance of Heavy Timber Construction, “*Mokuzaikogyo*”(Wood Industry), Vol.40-12, p3-7, 1985(*in Japanese*).
- 3) Shimizu, M., Hasemi, Y., Yasui, N., Murakami, M., Kimura, T., Prediction of Fire Resistance of Japanese Bare Timber Walls, Proceedings of Fire and Materials Conference, San Francisco, 2005.
- 4) Shimizu, M., Hasemi, Y., Murakami, M., Yasui, N., Prediction of the Fire Resistance of Japanese Bare Timber Walls, J. Struct. Constr. Engineering, AIJ, 611, p165-170, 2007(*in Japanese*)
- 5) Sawano, Y., Hasemi, Y., Yasui, N., Fire Resistance of Japanese Traditional Timber-frame Soil Internal Walls Exposed to Both-sides Heating, J. Environ. Eng., AIJ, 635, p1-7, 2009(*in Japanese*)
- 6) Hirai, N., Hasemi, Y., Yasui, N., Fire Resistance of Wooden Floor-Beam Assemblies of Japanese Traditional Post and Beam Construction. J. Struct. Constr. Eng., AIJ, 625, p480-495, 2008(*in Japanese*).
- 7) Yasui, N., Hasemi, Y., Hirai, N., Watanabe, K., Koshihara, M., Sawano, Y., Ogawa, A., Kimura, T., Yamamoto, K., Fire Resistance Design of Japanese Traditional Floor- Beam Assemblies Based on the Prediction of Bending Stress in the Timber Beam—An Experimental Study. J. Struct. Constr. Eng., AIJ, 642, p1523-1529, 2009(*in Japanese*).

Timber Bolted Joints Subjected to High Temperatures

N. D. CORREIA, J. P. C. RODRIGUES and P. D. MORAES

ABSTRACT.

The current standards have a gap in the design of timber bolted joints for temperatures between 20 and 300°C. In order to analyze this problem, an experimental study about the influence of temperature and moisture content on the strength of timber bolted joints was carried out. Mechanical tests at high temperatures to determine the load-bearing capacity of one- and three-bolt joints were performed. The timber embedment strength at high temperatures was also determined. The experimental study has revealed a reduction in the joint strength as the temperature increases.

INTRODUCTION

The behavior of timber joints subjected to fire is still a complex and not completely known subject. The assessment of the joint failure time, the influence of the typology and existence of metallic elements inside the joint in its thermal field and the modes of failure, require more research. In order to clarify these and other issues several experimental, numerical and analytical studies on timber joints at high temperatures have been carried out.

Fornather et al. carried out several fire resistance tests at reduced scale on timber joints with built-in steel plates and different types of bolts [1]. The results revealed that the embedment deformation of the timber, the thickness of the steel plates, the diameter of the bolts and the time of fire exposure, are very important parameters in the fire design of the joints.

König and Fontana carried out a study that resulted in a proposal of new design methods for EN 1995-1-2 [2, 3]. The new proposed methods took into account the influence of several parameters on the behavior of the joint subjected to fire, such as the typology of the connector, the geometry of the joint, the failure modes, the thermal conductivity of the steel, the type of timber and the thickness of the charred layer.

Moraes studied the behavior of dowel timber joints of *Pinus sylvestris* subjected to fire [4]. This research was divided in three parts. The first part was about the verification of the influence of the temperature on the embedment

Nadia D. Correia and João Paulo C. Rodrigues (jpaulocr@dec.uc.pt), Faculty of Sciences and Technology of University of Coimbra, Portugal.
Poliana Dias de Moraes, Federal University of Santa Catarina, Florianópolis, Brazil.

strength and module of elasticity of the timber. In the second part, the behavior of dowel joints at high temperatures was experimentally studied. The last part was devoted to the numerical simulations. The results led to the conclusion that the load-bearing capacity of the joints decreases with the increasing of temperature associated to a decreasing of the elasticity and embedment strength of the timber.

Laplanche et al. performed fire resistance tests at full scale on joints of timber laminated elements, GL28h, connected along two rows of connectors parallel to grain (each row was constituted by 3 nails and a bolt) [5]. The joints were first subjected to load cycles of charge and discharge with maximum amplitude of 40% of the joint ultimate strength at room temperature. Then, a tension force corresponding to 10, 20 or to 30% of the tensile resistance of the joint at room temperature, was applied. Maintaining the loading constant, fire resistance test was conducted following the ISO 834 fire curve. The fire resistance of this type of joints determined experimentally was between 30 and 60 minutes. The numerical simulations led to the conclusion that the thermal and mechanical properties proposed by Fredlund [6] in the literature of the area are the ones that give better results.

Moss et al have presented the results of an experimental and analytical study to validate the theory of Johansen and predict the failure strength of timber bolted joints subjected to fire [7]. One-bolt joints of three types were tested (type 1 - side steel plates and central wood plate, type 2 - side wood plates and central steel plate and type 3 - side and central wood plates). The joints have been heated at constant temperature (range of tested temperatures from 20 and 300°C) for several hours and the embedment strength determined. The temperature dependent embedment strengths have been used in an analytical study with the Johansen's yield equations. The result of this research was the proposal of a new method to estimate the fire resistance of timber bolted joints that included a temperature dependent model for the embedment strength.

In spite of the several experimental tests performed until the present, there is still a lack of knowledge about the behavior of timber bolted joints for temperatures between 20 and 300°C. Thus, the authors of the paper has performed mechanical tests on one- and three-bolt timber joints under high temperatures at the Laboratory of Testing Structures of the Federal University of Santa Catarina, in Brazil [8].

EXPERIMENTAL ANALYSIS

Mechanical tests to determine the load-bearing capacity of one- and three-bolt timber joints were carried out. The embedment strength of the timber was also experimentally assessed.

Specimens

The experimental analysis was carried out using 3 sets of 42 *Pinus taeda* specimens with a specific weight between 427 to 524 kg.m⁻³ and moisture content of around 12%. Each set was divided in 6 samples of 7 specimens with statistically homogeneous densities (table 1). The homogeneity was verified by variance analysis for a reliability threshold equal or superior to 95%. The timber elements, from where the specimens were cut, were visually classified in order to avoid timber defects. The timber originated from planted forests of the State of Santa Catarina, in Brazil.

Table 1. Test programme.

Samples	Density at 20 °C (kg.m ⁻³)	Number of specimens at temperature level					
		20°C	50°C	100°C	150°C	200°C	230°C
Embedment	449 to 519	7	7	7	7	7	7
One-bolt	429 to 490	7	7	7	7	7	7
Three-bolt	427 to 524	7	7	7	7	7	7

The specimens for the embedment strength tests were built according to NF EN 383 [9] and the ones for the assessment of the load-bearing capacity tests of one- and three-bolt timber joints were built according to EN1995-1-1 [10] (fig. 1).

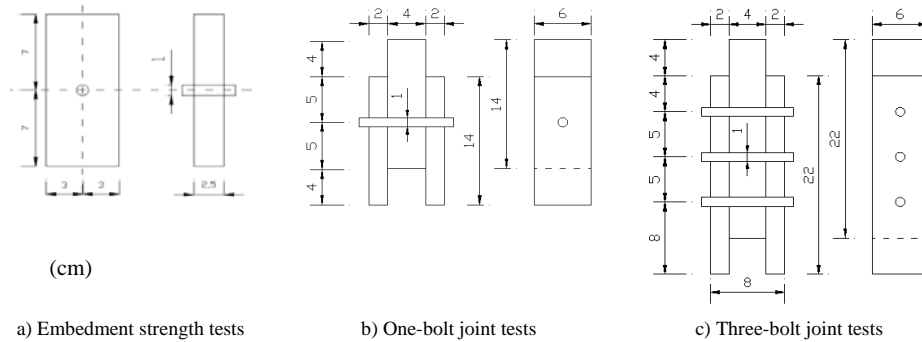


Figure 1. Specimens.

The mechanical fasteners used in the specimens were partially threaded steel bolts, class 8.8, and 10 mm in diameter. The unthreaded part of the bolts was located inside the timber in the specimens.

Mechanical tests

The mechanical tests were carried out in a universal testing machine provided with a heating chamber of internal dimensions 370mm × 500mm × 520mm (fig. 2).

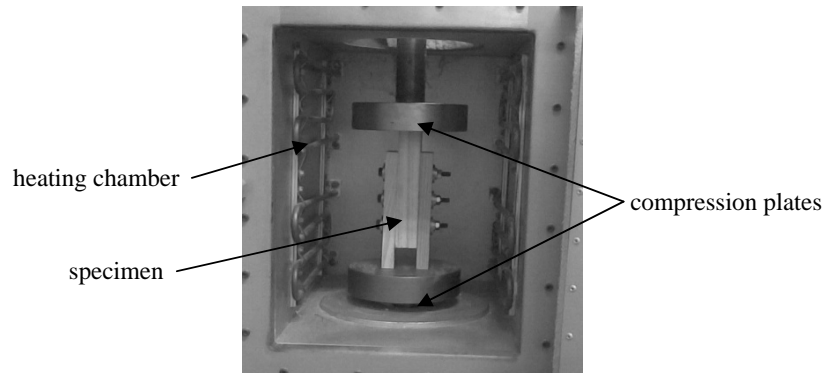


Figure 2. Testing system for the three-bolt joint tests.

For each test, the specimen was initially heated for 150 minutes in an oven previously heated for the test temperature. After a conditioning period, the specimen was placed between the compression plates of a universal testing machine, inside a heating chamber that was programmed for the test temperature. The test temperatures were: 20, 50, 100, 150, 200 and 230°C. The time necessary to stabilize the temperature inside the specimen, in the oven and

the heating chamber, was preliminary determined in heating tests on specimens with thermocouples.

For the embedment strength tests, the loading was applied in displacement control with a rate of 1.9 mm/min, in order to reach the maximum force within 300 ± 120 seconds, as established in NF EN 383 [9].

For the load-bearing capacity tests on one- and three-bolt joints, the load was also applied in displacement control at a rate of 1.5 mm/min and 1.3 mm/min, respectively. These load application rates were adapted from the values proposed in NF EN 383 [9].

The collapse of the specimens occurred when the displacement of the crosshead of the testing machine equalled the bolt diameter, 10 mm (rupture by embedment), or the specimen split.

The embedment strength, as defined in NF EN 383 [9], was determined by the rate between the ultimate force and the embedment area of the dowel in the timber surface in the direction of the force.

RESULTS AND DISCUSSION

The results of the experimental tests and the analytical simulations on timber bolted joints subjected to high temperatures are presented, compared and discussed in this section. Variance analysis tests were carried out in order to check statistically significant differences, with 95% of reliability, between the mechanical values at certain temperatures and those at room temperature.

Moisture content at the end of the tests

Figure 3 shows the moisture content of the specimens after the embedment strength tests in function of the test temperature.

The moisture content decreases linearly with the increasing of the test temperature up to nearly 150°C. At 150°C, the specimens are almost anhydrous. Above 150°C the timber loses mass with the realising of the bond water.

The same results were observed on the specimens of the load-bearing capacity of one- and three-bolt timber joint tests.

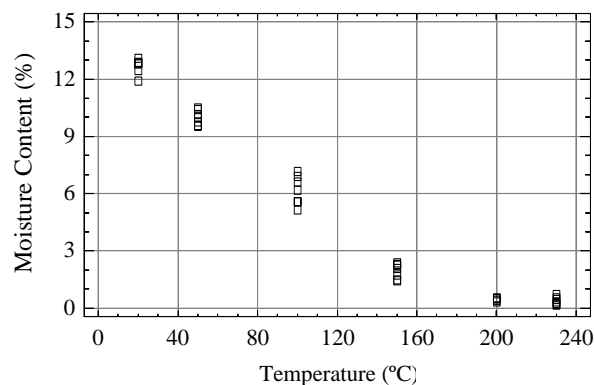


Figure 3. Moisture content in specimens after the embedment strength tests.

Embedment strength

Figure 4 presents the embedment strength parallel to the timber grain. The average value of the embedment strength at room temperature is 43.3 MPa. The embedment strength decreases with the increasing of the test temperature. However, this reduction is not monotonous with a relative minimum at 100°C.

This point corresponds to a reduction of 30.6% of the embedment strength at room temperature. At 230°C this reduction is 35.6%.

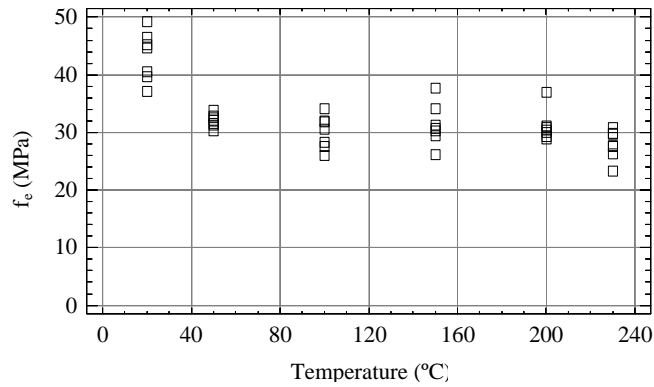


Figure 4. Embedment strength parallel to the grain.

Load-bearing capacity

Experimental tests

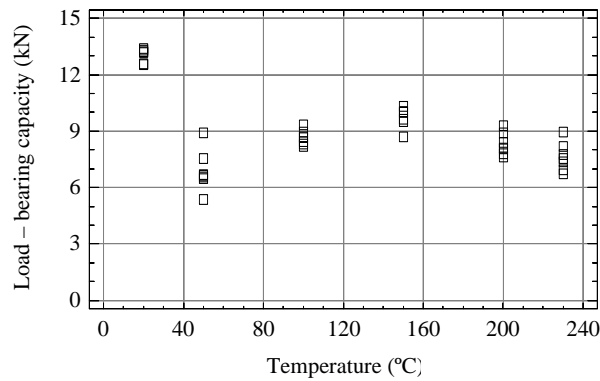


Figure 5. Load-bearing capacity of one-bolt timber joints.

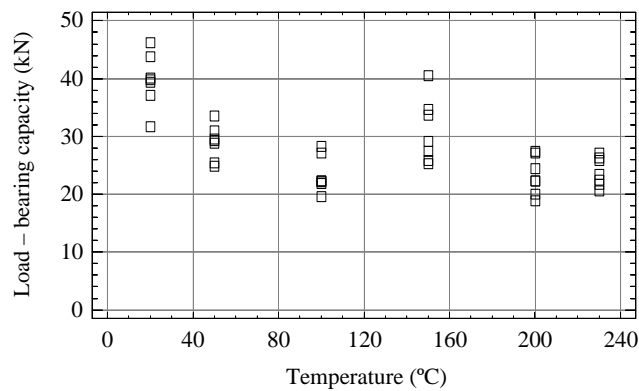


Figure 6. Load-bearing capacity of three-bolt timber joints.

Figures 5 and 6 illustrate the load-bearing capacity for the one- and three-bolt timber joints in function of the test temperature. At 20 °C, the average value is 13 kN for the one-bolt joints and 40 kN for the three-bolt joints. It is verified for the different test temperatures, except at 50°C, that the load-bearing capacity for the three-bolt joints is three times the one for the one-bolt joints, showing a

difference lower than 10%. At 50°C, this difference is more significant in the order of 28%.

Figures 5 and 6 illustrate a non-monotonous reduction of the load-bearing capacity with the temperature with the presence of a relative minimum of 6.9 kN at 50°C, for the one-bolt joints, and 23.4 kN at 100°C for three-bolt joints, corresponding to resistance reductions of 47.2% and 41.2% in relation to those at room temperature, respectively. It was verified, for the one- and three-bolt joints, for all levels of temperature, a similar reduction of the resistance in function of the temperature. This shows a pattern in the reduction of the load-bearing capacity of the timber joints in function of the temperature.

Colour change in the specimens

Timber colour changes occurred in the specimens used in the one- and three-bolt timber joints tests due to the high temperatures that were submitted. In figure 7, as an example, are presented three specimens for each tested batch illustrating the phenomenon. The colour change occurred for temperatures higher than 100 °C, being more pronounced for temperatures over 150 °C. These changes resulted from the thermal degradation of the timber.

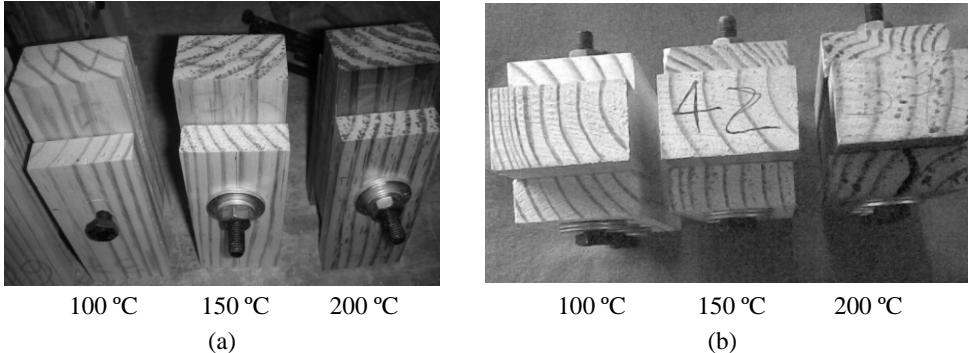


Figure 7. Timber colour change in the one-bolt (a) and three-bolt (b) specimens.

Failure Modes

Two modes of rupture were observed in the specimens, rupture by timber embedding and splitting.

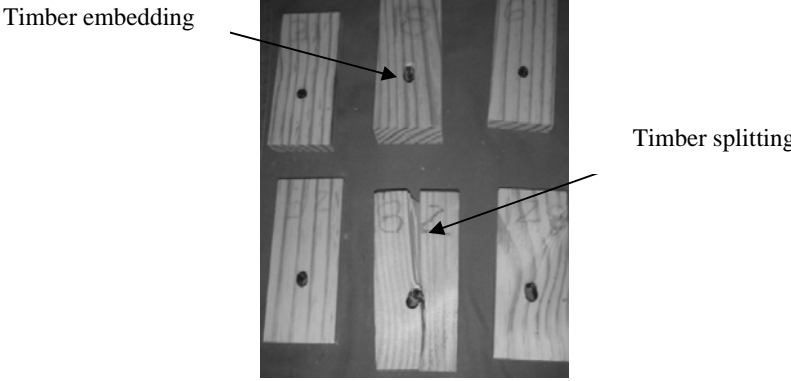


Figure 8. Failure modes in the one-bolt joints.

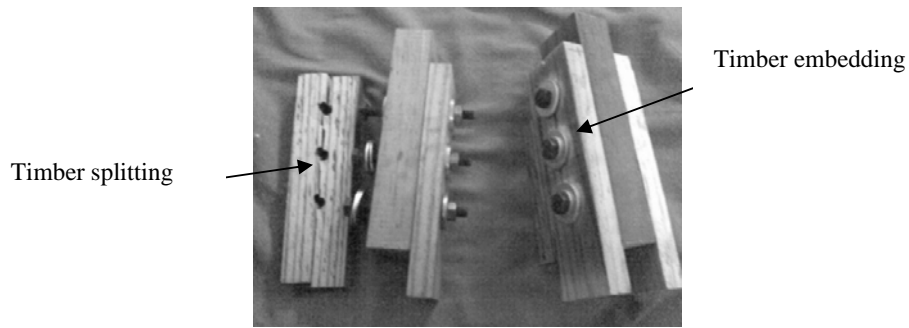


Figure 9. Failure modes in the three-bolt joints.

Table 2 presents the number of specimens failed by splitting in the one- and three-bolt load-bearing capacity tests.

Table 2. Number of ruptures by splitting for the one- and three-bolt timber joint specimens.

	Temperature (°C)					
	23	50	100	150	200	230
One-bolt joints	1	1	0	3	4	2
Three-bolt joints	4	4	1	7	7	7

The major part of the ruptures by splitting occurred for the three-bolt timber joints and for temperatures higher than 150°C.

CONCLUSIONS

In this study the influence of the temperature on the embedment strength and load-bearing capacity of one- and three-bolt timber joints of *Pinus taeda* was assessed. The results obtained lead to the following conclusions:

- the moisture content of the timber present a linear decrease up to 150°C;
- the load-bearing capacity of the one-bolt timber joints decrease to a minimum at 50°C, then present an increase up to 150°C, followed by a decrease up to 240°C;
- the load-bearing capacity of the three-bolt timber joints decrease to a minimum at 100°C, then present an increase up to 150°C, followed by a decrease up to 240°C;
- the temperature increase leads to a non-monotonous decrease of the timber embedment strength parallel to grain.
- the thermal degradation of the timber leads to changes in the colour, moisture content, modes of rupture and to losses of mass.
- for temperatures between 50 and 100°C, the failure modes were mainly by timber embedding due to the plastic behaviour of the *Pinus taeda* for this range of temperatures.

ACKNOWLEDGEMENTS

The authors thank Manuel Manriquez Figueroa, Ph.D. student at the Federal University of Santa Catarina, Brazil, for his help in the preparation of specimens and realization of tests.

REFERENCES

1. Fornather, J., Bergmeister, K. and Hartl, H., 2001. "Fire behavior of steel fasteners in wood composites—experimental analyses". *Proceedings of the RILEM Congress on Joints in Timber Structures*, Stuttgart, Germany.
2. König, J. and Fontana, M., 2001. "The performance of timber connections in fire – tests results and rules of Eurocode 5". *Proceedings of the RILEM Congress on Joints in Timber Structures*, Stuttgart, Germany.
3. CEN, 2004. "Eurocode 5: Design of timber structures—part 1-2: General—Structural fire design". Brussels.
4. Moraes, P. D., 2003. *Influence de la température sur les assemblages en bois*. PhD Thesis, Université Henri Poincaré, Nancy, France, (in French).
5. Laplanche, K., Dhima, D. and Racher, P., 2004. "Predicting the behavior of dowelled connections in fire: Fire tests results and heat transfer modeling". *Proceedings of the World Conference of Timber Engineering*, vol. 2, Berlin, Germany: 335–340.
6. Fredlund, B., 1993. "Modeling of heat and mass transfer in wood structures during fire". *Fire Safety Journal*, vol. 20: 39–69.
7. Moss, P., Buchanan, A., Fragiacomio, M. and Austruy C., 2008. "On the design of timber bolt connections subjected to fire" *SIF'08—Proceedings of the Fifth International Workshop Structures in Fire*, Singapore: 632–642.
8. Correia, N. D. F., 2009. *Behavior of timber joints subjected to high temperatures*. MSc Thesis in Structures, University of Coimbra, Portugal, (in Portuguese).
9. CEN, 2004. "Eurocode 5: Design of timber structures—part 1-1: General common rules and rules for buildings," Brussels.
10. Norme Française, 1993. "NF EN383 -Détermination de caractéristiques de fondation et de la portance locale d'éléments d'assemblages de type broche".

Post Protection Behaviour of Wooden Wall and Floor Structures Completely Filled with Glass Wool

A. JUST

ABSTRACT

The use of glass wool insulation in timber frame houses is popular because of its elasticity, sound and thermal insulation properties. Since fire design is an important part of the design procedure EN 1995-1-2 [1] gives rules for timber design in fire. Based on experiences of fire tests design rules are different for stone wool and glass wool even if differences are not specified in standards for mineral wool. Annex C of EN 1995-1-2:2004 gives design rules for walls and floors insulated by mineral wool. While for stone wool insulated construction a post protection phase is considered, constructions filled with glass wool are counted to fail directly after the failure of the cladding. There exists a design method for wall and floor assemblies with void cavities for this post protection phase.

This paper presents a design method for post protection behavior of timber frame assemblies insulated by glass wool insulation. It is based on non-load bearing small-scale tests at SP Träteck and full scale tests at TÜV Estonia at standard fire exposure according to EN 1363-1 [2]. Considering start of charring at 300 °C recession of glass wool insulation was measured during tests as a basic parameter for the presented method. Frangi et al [3] introduced a post protection study of floors with void cavities to complete the calculation model in EN 1995-1-2:2004 [1].

According to the method of this paper fire resistance of glass wool insulated walls and floors should be calculated similarly to stone wool insulated constructions according to existing rules during the protected phase. The proposed design model takes into account 3 phases: protected phase, recession phase and finally post protection phase similarly to design of timber frame assemblies with void cavities.

In the future this method is imaginable for other recessible insulations for example cellulose fibers, wood wool and -fiber and other natural insulation products where the recession rate can be defined by fire tests.

Alar Just, Resand Ltd., Tuglase 6, 63308 Põlva, Estonia

INTRODUCTION

Timber frame assemblies are normally built up of the timber frame (floor joists or wall studs) and a cladding attached to each side of the timber. The cavities may be void or partially or completely filled with insulation. Since the timber frame is sensitive to fire exposure, it must be effectively protected against fire. The greatest contribution to fire resistance is obtained from the membrane (layer) on the fire-exposed side first directly exposed to the fire, both with respect to insulation and failure (fall-off) of the membrane. In general, it is difficult to compensate for poor fire protection performance of the first membrane by improved fire protection performance of the following layers.

In small-sized timber frame members, e.g. floor joists or wall studs in assemblies with void cavities, increased charring takes place after failure of the cladding. However, the timber member will normally collapse before reaching the consolidation phase with a char depth of 25 mm. Such conditions are described in Annex D of EN 1995-1-2 [1].

For small-sized timber frame members in assemblies with cavity insulation, charring mainly takes place on the narrow, fire-exposed side. Since there is a considerable heat flux through the insulation to the sides of the member during the stage after failure of the lining (provided that the cavity insulation remains in place), the effect of increasing arris rounding becomes dominant and no consolidation of the charring rate is possible.

For the stage before failure of the cladding (protection phase $t \leq t_f$), both stone wool and glass wool insulation perform approximately equally. However, once the cladding has fallen off and the insulation is directly exposed to the fire (post-protection phase $t \geq t_f$), glass wool insulation will undergo decomposition, gradually losing its protecting effect for the timber member by surface recession. Stone wool insulation will continue to protect the sides of the timber member facing the cavity. It is assumed that insulation remains in place.

Immediate failure of the assembly with glass wool by EN 1995-1-2:2004 [1] is a conservative assumption. From full-scale wall tests it is known that it will take some time until the glass wool insulation has completely recessed once it has been directly exposed to the fire.

The aim of the article is to give design rules for post protection phase of wooden floor and wall assemblies insulated with traditional glass wool.

GLASS WOOL

Glass wool is a mineral wool manufactured predominantly from natural sand or molten glass [4].

After the fusion of different raw mineral materials at 1450°C, the liquid glass produced is converted into wool (mixture of fibers). Stable dimensions, cohesion and mechanical strength of the product is obtained by the addition of a binder. Most of the fiber intersections are “blocked” by a drop of binder. This wool is then heated above 200°C to polymerize the binder. During that stage, the wool is calendared to give it strength and stability. The final stage involves cutting the wool and packing it in rolls or panels (with or without compression) before palletizing the finished product in order to facilitate transport and storage. Densities of glass wool insulations, used in timber structures, are usually 14 to 20 kg/m³.

Traditional glass wool is sensitive for high temperatures standard fire. When temperature rises over more than 500°C, there will be a fast recession of traditional glass wool insulation. This will occur usually after the cladding failure.

CHARRING OF WALL AND FLOOR STUDS

Rules for fire design of wall and floor assemblies insulated by mineral wool are given in annex C of EN 1995-1-2:2004 [1], see Figure 1.

For larger cross-sections the time limit t_a exists. After that the charring rate is similar to charring of unprotected timber because of protective properties of char layer. For smaller floor and wall studs the protective char layer cannot be developed because of too small dimensions and two dimensional heat flux subsequently. Thus the time limit t_a cannot be used and high charring rate is valid until the end.

For timber members protected by claddings on the fire-exposed side, the notional charring rate is calculated as (equations (C.1) and (C.2) at [1]):

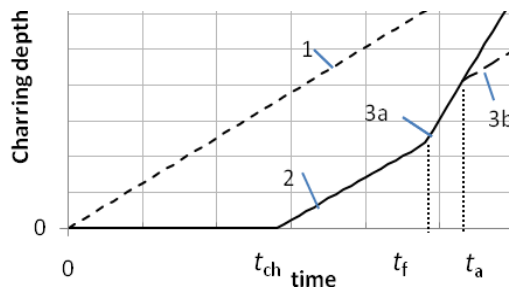
$$\dot{\rho}_x = k_n k_s k_2 k_3 \dot{\rho}_0 \quad \text{for } t_{ch} \leq t \leq t_f \quad (1)$$

$$\dot{\rho}_x = k_n k_s k_3 \dot{\rho}_0 \quad \text{for } t > t_f \quad (2)$$

where conversion factor $k_n = 1,5$

The cross-section factor is $k_s = 1,1..1,4$, depending on width of cross-section of stud. Factors k_2 and k_3 represent the reduced and decreased charring rates at protection phases 2 and 3.

At the protected phase 2 on Figure 1 the behavior of wall studs in stone wool and glass wool insulated walls and floors is similar. The behavior of structures with void cavities is different. Where the cavity insulation is made of glass wool, failure of the member should be assumed to take place at the time t_f . (Subclause C.2.1 (6) in [1])



- | | |
|------|---|
| 1- | Unprotected members |
| 2,3- | Initially protected members |
| 2- | Charring starts at t_{ch} at a reduced rate when protection is still in place |
| 3a- | After protection has fallen off, charring starts at increased rate |
| 3b- | Char layer acts as a protection and charring rate decreases |

Figure 1. Charring of timber studs with and without protection.

Method by EN 1995-1-2:2004 for Void Cavities

Charring of timber members at the protected stage is slower in the case of void cavities compare to the insulated cavities sine no local heat increase occurs. At the protection stage 2 the notional charring of narrow side of timber member is taken into account by notional charring rate $\dot{\rho}_n$ and factor k_2 .

When the cladding has fallen off there will be charring from 3 sides of timber studs. For the stage after failure of the protection the post protection factor $k_3 = 2$.

Method by ETH for Wall and Floor Assemblies with Void Cavities

Frangi et al [3] made a post protection study of floors with void cavities to complete the calculation model in EN 1995-1-2:2004. Increased charring rates compared to [1] were proposed. The reason for very fast charring is the missing protective char layer after cladding failure to protect from high temperatures.

The model in [3] is created for cross-section's width of 60 mm and larger. The method introduces also a phase 2c (resp 3b on Figure 1) to take into account the protective char layer created within 5 minutes. Using the notional charring rate \dot{c}_n instead of \dot{c}_0 is recommended for cross sections less than 60 mm wide.

INVESTIGATION OF POST PROTECTION EFFECT BY TESTS

Series of small-scale tests at SP Träteknik [5,6] and large scale tests at TÜV Estonia [7] were made to study the post protection effect of glass wool insulation. All of them were tested as non-load bearing structures in standard fire conditions (EN 1363-1, ISO 834) [2]. Studs with typical Scandinavian cross-section of 45x145 mm² were used.

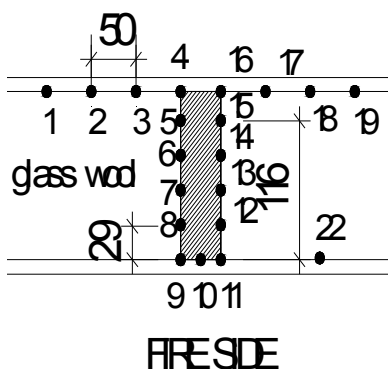


Figure 2. Test set-up for floor structures.

Table I. Recession of glass wool insulation in tests.

Test	Cladding	t_f	Delay of start of charring (from 29 to 116 mm height) [min.sec]	Recession speed [mm/min]
		[min.sec]		
Floor test A (5)	GtA 12,5	19.50	5.50	15
			4.00	22
Floor test B (6)	GtA 12,5	16.15	3.50	27
			3.10	28
Wall test 2.1 (7)	GtA 12,5	26.30	5.15	16
Wall test 2.5 (7)	GtF 15,4	48.30	1.15	28

Test floors were covered by one layer of gypsum plasterboard, type A on the fire exposed side. Test walls had gypsum board, type A and type F on fire exposed side. Charring spread was measured by thermocouples, placed on sides of timber studs with 29 mm distance.

Start of charring was counted to occur at temperature of 300°C. Table I describes the start of charring times (in minutes) of glass wool insulated studs. t_f shows the fall-off time of cladding.

Conclusions from Test Results

Tests show that decreasing of volume of glass wool insulation is fast after the claddings fall off. The post protective behavior of ordinary glass wool insulation is not comparable with stone wool insulation. Although the glass wool insulation provides some small protection after cladding failure compared to structures with void cavities. This effect can be noticeable for bigger cross-section height.

As it is shown in examples on Table I, start of charring spread within 4 ..5 minutes from down to top of cross-section of timber stud. Floor and wall tests showed similar effect of charring due to recession of glass wool insulation and are comparable.

Based on the test results [5, 6, 7] recession of glass wool insulation is proposed to design with 30 mm/min with sufficient safety margin. The shapes of charred cross-sections are close to trapezoid because the charring starts later on unexposed side of cross-section height when insulation recesses. The phase 3b (see Figure 1) is not used in this paper because of no ability to create the protective char layer on 45 mm wide cross-sections. Rapid heat transfer begins from the sides of studs before char layer will be built.

When the glass wool insulation is completely recessed, timber frame burns similarly to the structure with void cavities; the method of [3] should be used.

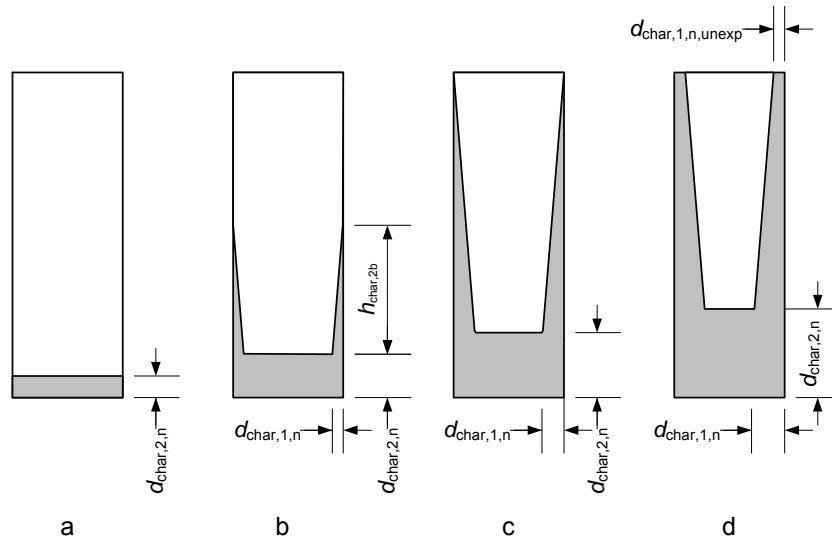
DESIGN METHOD FOR TIMBER WALL AND FLOOR STUDS PROTECTED BY GLASS WOOL

Based on test results and the method by ETH [3] for floors with void cavities the following design procedure is proposed.

For the time before failure of the cladding, charring takes place. The design model in annex C in [1] for phase 2 is valid for this case. See Figure 3 a. Once the cladding has fallen off at time $t = t_f$, surface recession of the glass wool insulation takes place due to thermal decomposition, so that the wide sides of the timber member are increasingly exposed to the fire and start to char, see Figure 3 b.

When surface recession of the glass wool insulation has reached the unexposed side of the insulation at $t = t_{f,ins}$, (Figure 3 c), charring on the wide sides of the timber member will take place over the whole depth of the cross-section (Figure 3 d).

In the following, it is either assumed that the cladding remains in place after the start of charring of the timber member, i.e. , $t_{ch} \leq t_f$, or that the cladding falls off at the time of start of charring, i.e. $t_{ch} = t_f$.



- a. Charring on narrow fire-exposed side before cladding has fallen off ($t_{ch} \leq t \leq t_f$)
- b. Charring on narrow side and wide sides during surface recession of glass wool insulation ($t_f \leq t \leq t_{f,ins}$)
- c. Recession of glass wool completed ($t = t_{f,ins}$)
- d. Charring on three sides after failure of glass wool insulation ($t \geq t_{f,ins}$)

Figure 3. Illustration of charring phases.

Failure time of the insulation is counted as

$$t_{f,ins} = t_f + \frac{h}{v_{rec,ins}} \quad (3)$$

where h is the cross-section height and the surface recession rate for glass wool is

$$v_{rec,ins} = 30 \text{ mm/min}$$

Charring depth on different stages is calculated as

$$1) \quad t_{ch} \leq t \leq t_f \text{ (Figure 3a)} \quad \text{Phase 2.} \quad (4)$$

$$d_{char,2,n} = k_2 k_s k_n \beta_0 (t_f - t_{ch})$$

$$2) \quad t_f \leq t \leq t_{f,ins} \text{ (Figure 3b):} \quad \text{Phase 3. } t_f \quad (5)$$

$$d_{char,1,n} = k_3 \beta_0 (t - t_f) \quad (6)$$

$$d_{char,2,n} = k_2 k_s k_n \beta_0 (t_f - t_{ch}) + k_3 \beta_n (t - t_f) \quad (7)$$

$$h_{char,3} = v_{rec,ins} (t - t_f)$$

$$d_{char,2,n} = k_2 k_s k_n \beta_0 (t_f - t_{ch}) + k_3 \beta_n (t - t_f)$$

This stage is relatively short and could be replaced by linear interpolation of section modulus between times t_f and $t_{f,ins}$.

$$3) \quad \geq t_{f,ins} \text{ (Figure 3d):} \quad \text{Phase 3. } t \quad (8)$$

$$d_{char,1,unexp,n} = k_3 \beta_0 (t - t_{f,ins}) \quad (10)$$

where

k_2 is the insulation factor of the cladding from [1] expressions (C.3) or (C.4).

k_3 is the post-protection factor, given as

$$k_{3a} = 1 + \frac{8}{75} t_f \quad \text{for } 0 \leq t_f \leq 15 \text{ min} \quad (9)$$

$$k_{3a} = 1,9 + \frac{7}{150} t_f \quad \text{for } 15 \text{ min} \leq t_f \leq 60 \text{ min} \quad (11)$$

If there is a risk of insulation to fall down before completely recessed, the time

$$t_{f,ins} = t_f$$

A further simplified model for calculations is a model using rectangular cross-sections. Compared to the trapezoidal model it is not universal for bending members and compression members. For that reason two different rectangular models should be used for two basic cases based on either the reduction of section modulus or cross-section area respectively. For more information see [8].

Strength and Stiffness Properties

The reduced cross-section method is recommended to use for calculating strength and stiffness. For $t_{ch} \leq t \leq t_f$ the method of [9] for counting zero-strength layer should be used for structural design. For the time period $t > t_f$ the zero strength layer should be taken as $d_o = 7$ mm from three side of cross-section.

Examples

Examples of charred cross-section are shown on the next diagrams for different studs and protection. The charring in corners is taken into account with using β_n on the narrow side of cross-section. Charring on the wide side could be calculated using one-dimensional charring rate β_o . Alternatively the curve with charring rate β_n on wide side is shown in Figure 5. Test results show that β_o gives the realistic approach.

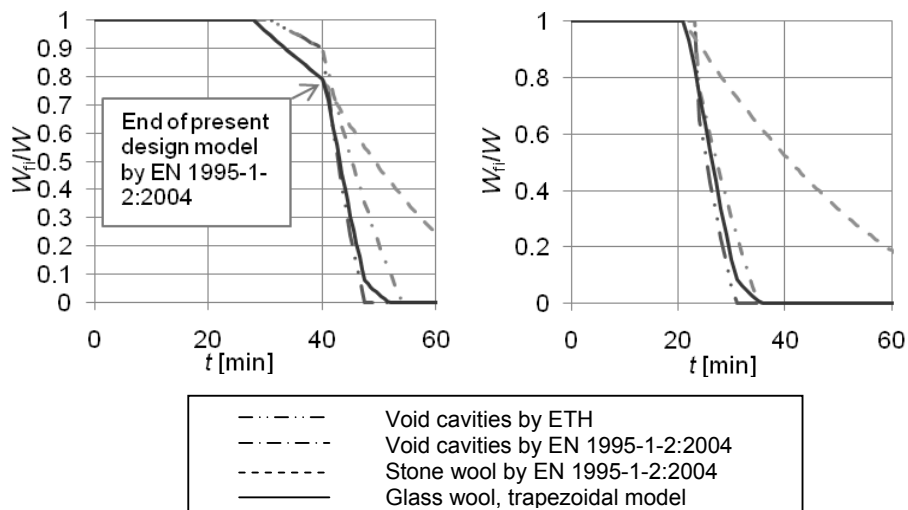


Figure 4. Example of existing and new design models for timber frame assembly with gypsum plasterboard type A (left) and type F (right) with timber studs 45x145 mm².

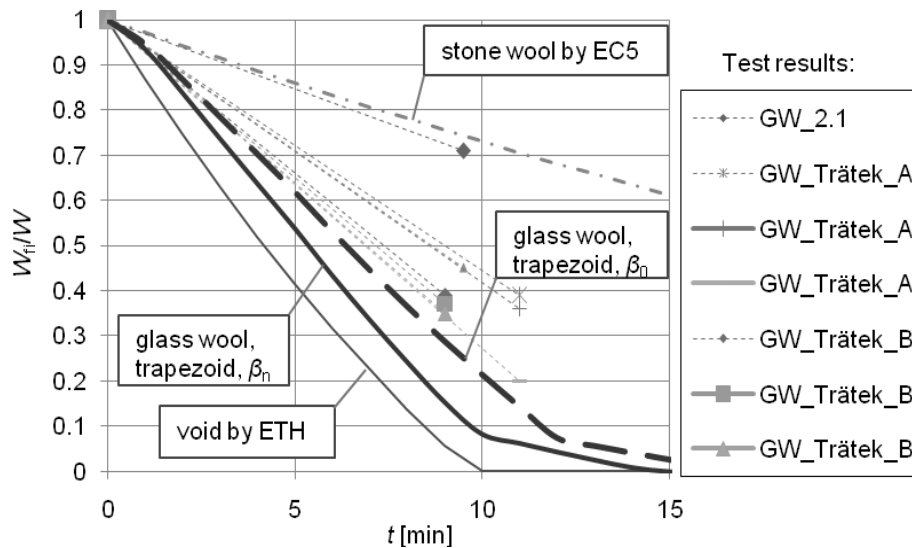


Figure 5. Comparison of calculation method with the test results.

CONCLUSIONS

Fire resistance of glass wool insulated walls and floors should be calculated similarly to stone wool insulated walls and floors when protected from direct fire by claddings (protection phase 2 according to EN 1995-1-2:2004). Post protection phase 3a begins with delay of start of charring on wide side of studs cross-section caused by recession of glass wool. After the delay the method by A.Frangi et al [3], created for timber frame floors with void cavities, should be used for phase 3a. Residual cross-section may be counted as trapezoid.

Recession of glass wool insulation with densities from 14 kg/m³ could be counted as 30 mm/min respectively to the insulation thickness. Post protection phase 3b should only be used for cross-sections wider than 60 mm. Reduced properties method [1] or reduced cross-section method [9] should be used for structural design.

REFERENCES

1. EN 1995-1-2:2004. "Eurocode 5: Design of timber structures - Part 1-2: General rules-structural fire design", European Committee of Standardization, Brussels, 2004.
2. EN 1363-1. "Fire resistance tests. General requirements", European Committee of Standardization, Brussels, 1999.
3. Frangi A., Erchinger C., Fontana M., "Charring model for timber frame floor assemblies with void cavities", *Fire Safety Journal*, 43, Elsevier Ltd, 2008.
4. prEN ISO 9229 "Thermal insulation - Definitions of terms", CEN/TC88, 2006.
5. Test report P705487A, SP Trätekt, Stockholm, 2009.
6. Test report P705487B, SP Trätekt, Stockholm, 2009.
7. Just A., "Full scale wall tests of timber frame assemblies", Test report, Tallinn University of Technology, 2009.
8. Just A., "Post protection behaviour of wooden wall and floor structures completely filled with glass wool". SP Trätekt, Stockholm, 2010.
9. König J., "The effective cross-section method for light timber frame construction with solid timber members", SP Trätekt, Stockholm, 2010.

Failure Times of Gypsum Boards

A. JUST, J. SCHMID and J. KÖNIG

ABSTRACT

EN 1995-1-2 gives rules how to calculate fire resistance (R, E, I) for timber framed walls and floors. For the design of load bearing capacity (R) the residual cross section is a decisive factor. Charring rates of wooden studs are significantly different before and after the failure of protective cladding. The failure time of boards is therefore an important parameter for the design of timber frame construction.

Gypsum boards are widely used for wall and floor assemblies but very little information is given for the failure of gypsum based boards in EN 1995-1-2 and standards for gypsum based boards do not give more information on this important parameter. However this parameter has to be used in the design process following EN 1995-1-2.

Since fall-off is a failure which can't be calculated using finite element programs due to the complex failure mechanism, easy-to-use rules are presented in this paper developed as a result of an extensive evaluation of available test data. Further more different build-ups and fixings were taken into account since failure is not only a question of the cladding itself.

To create necessary design procedures for structures with gypsum boards a database was created at SP Trätekt. The database consists more than 340 full scale test results from different institutes all over the world, mainly from Europe.

Alar Just, Resand Ltd., Tuglase 6, 63308 Põlva, Estonia
Joachim Schmid, SP Trätekt, Drottning Kristinas väg 67, 11428 Stockholm, Sweden
Jürgen König, SP Trätekt, Drottning Kristinas väg 67, 11428 Stockholm, Sweden

INTRODUCTION

Timber frame assemblies are normally built up of the timber frame (floor joists or wall studs) and a cladding attached to each side of the timber frame (the cladding may be a lining or, in the case of floors, the decking or a sub-floor and additional layers). The cavities may be void or partially or completely filled with insulation. Since the timber frame is sensitive to fire exposure, it must be effectively protected against fire.

In the design and optimisation of a timber frame assembly with respect to maximising fire resistance, there exists a hierarchy of contribution to fire resistance of various layers of the assembly. The greatest contribution to fire resistance is obtained from the membrane (layer) on the fire-exposed side first directly exposed to the fire, both with respect to insulation and failure (fall-off) of the membrane. In general, it is difficult to compensate for poor fire protection performance of the first membrane by improved fire protection performance of the following layers.

Charring of protected wooden members can start before the failure of cladding. Charring rate of wood is much slower in this stage compared to charring of unprotected wood. After the claddings fall off the charring increases to much higher rate than the charring rate of initially unprotected wood. Therefore the failure time of gypsum boards is an important property of cladding in design of wooden structures in fire.

The failure times for claddings made of gypsum plasterboard depend on two types of failures: thermal degradation of the cladding and pull-out failure of fasteners due to insufficient penetration length into unburnt wood.

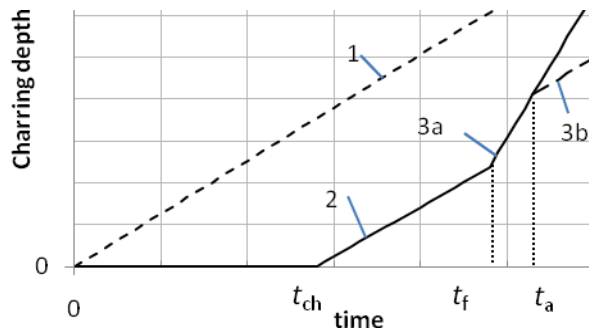
Existing design rules give simplified solution for calculation of pull-out failure. Failure times caused by thermal degradation are generally missing. According to EN 1995-1-2 [1] this data should be determined by tests which are time and cost consuming. Literature as well as national annexes of EN 1995-1-2 gives some rules but knowledge is restricted and rules are dubious.

The aim of the article is to present conservative design rules for failure times of gypsum plasterboards. The rules are intended to be open for new product developments and should fit to a high range of products where the producers can declare protection time of specific products to extend the protection phase given here and in EN 1995-1-2 [1] respectively.

TIMBER FRAME ASSEMBLIES

Rules for fire design of wall and floor assemblies insulated by mineral wool are given in annex C of EN 1995-1-2:2004 [1], see Figure 1. In the design and optimisation of a timber frame assembly with respect to maximising fire resistance, there exists a hierarchy of contribution to fire resistance of various layers of the assembly.

The greatest contribution to fire resistance is obtained from the membrane (layer) on the fire-exposed side first directly exposed to the fire, both with respect to insulation and failure (fall-off) of the membrane. In general, it is difficult to compensate for poor fire protection performance of the first membrane by improved fire protection performance of the following layers.



- | | |
|-------|---|
| 1- | Unprotected members |
| 2,3 - | Initially protected members |
| 2 - | Charring starts at t_{ch} at a reduced rate when protection is still in place |
| 3a - | After protection has fallen off, charring starts at increased rate |
| 3b - | Char layer acts as a protection and charring rate decreases |

Figure 1. Charring of timber studs with and without protection.

Figure 1 describes charring of unprotected and initially protected timber members. Note that charring in phase 3a is significantly higher than in phase 2. Therefore the failure time of gypsum boards is an important property of cladding in design of wooden structures in fire.

The thermo-mechanical properties of gypsum plasterboard Type F are not part of the classification given in EN 520 [2]. Failure times of different batches may vary considerably. No generic failure times for gypsum plasterboard are given nor required thus it is expected that the producer should declare failure times determined on the basis of tests, including information on spacing of joists, studs, battens etc. and edge distances and spacing of fasteners, see [1].

There are design methods in EN 1995-1-2:2004 [1] and according to ETH [3] to calculate the start of charring time and failure time of gypsum plasterboards, type A. No possibilities to calculate failure times of gypsum plasterboards, type F.

GYPSUM BOARDS

Raw materials for gypsum plasterboards are gypsum, paper and additives. Thermal behavior of gypsum boards is based on dehydration reaction which is an endothermic decomposition reaction occurring between 100°C and 120°C. Gypsum plaster also contains about 3% of free water, depending on the ambient temperature and relative humidity. Significant energy is required to evaporate the free water in the fire conditions and enforce the chemical change which releases the water in the crystal structure. The gypsum core consists of natural gypsum, industrial gypsum and recycled plasterboards, which may affect the properties in fire. Use of natural or industrial gypsum for producing boards is not declared by the producer of gypsum boards but may have influence to the properties in fire.

Types of Gypsum Boards

EN 520 [2] specifies different types of gypsum plasterboards with thickness from 9 to 30 mm.

Gypsum plasterboard type A (GtA)—common board with porous gypsum core and no reinforcement except the paper laminated surface.

Gypsum plasterboard, type F (GtF)—fire protection board with improved core cohesion at high temperatures. This type of boards contain glass fibres which control shrinkage, causing a maze of fine cracks rather than a single large crack which can initiate premature failure of regular board. One of the most critical aspects of fire-resisting gypsum board is the extent to which the glass fibre reinforcing can hold the board together after gypsum has dehydrated, to prevent the board pulling away from nailed or screwed connections when the board shrinks. Shrinkage can be reduced with various additives such as vermiculite [4]. Fire rated gypsum boards are to be tested according to EN 520 [2] but this test is not relevant to qualify thermo-mechanical properties such as fall-off times.

In North America gypsum boards, type X are commonly used as fire protection and are similar to the European GtF boards. In this study the test results with GtX boards are handled as GtF boards.

According to [2] there is also other types of gypsum plasterboards classified. For example type D with density over 800 kg/m^3 , type H with water resistance properties etc.

Gypsum fibreboards (GF) are the boards with cellulose reinforcement, made according to EN 15283-2:2008 [5]. Gypsum fibreboard is a high-performance building board, which can be used as an alternative to plasterboard or for flooring.

Behaviour of Gypsum Boards in Fire

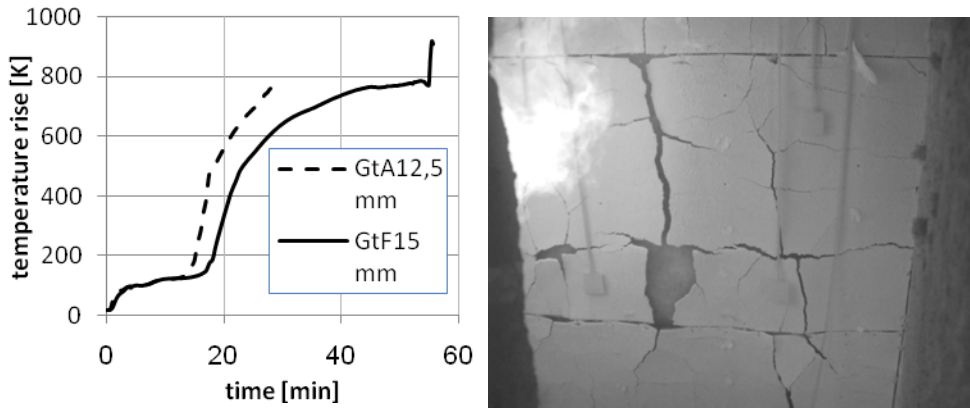
Gypsum is a non-combustible material and gives no contribution to fire. Its high water content provides up to 90% of the fire-resistance protection of gypsum boards. The calcination process is for the most part complete when the gypsum board reaches a temperature of 125°C . This process consumes much energy and time.

In Figure 2 the comparison of temperature rise behind 12,5 mm thick gypsum plasterboard, type A and 15 mm thick gypsum plasterboard, type F is shown. The phase of calcination can be seen clearly. First the temperature rise until 100°C is reached behind the board. Water starts to evaporate and a plateau can be observed in temperature curve, see Figure 2. Evaporation time is basically depending on the thickness. After the evaporation process the temperature raises again.

Failure Time

Start of charring time and failure time are the important times for design, see Figure 1. Present report deals with failure times.

Since there is no standard definition for failure time, the *failure time* or *fall-off time* of cladding is defined as the time from test start when at least 1 % of the board area has fallen down in this article.



Left – Temperature rise behind the board
 Right – Fall-off of the board

Figure 2. Gypsum plasterboards in standard fire (typical example).

Regular gypsum board falls off a wall or ceiling as soon as the gypsum plaster has dehydrated, at about the same time as charring of the timber studs begins. Boards with glass fibre reinforcing and closely spaced fixings will not fall off until the glass fibres melt, when the entire board reaches a temperature of about 600 to 800°C [4].

Sultan et al [6] have found that the temperature of gypsum board at the first piece fall-off is not an appropriate criterion for gypsum board failure, as it varies too extensively from assembly to assembly with no identifiable correlation to assembly parameters. There is nearly no information about failure of last piece in standard full-scale test reports in this study. The fall-off of first piece is counted as failure of the whole board. Figure 2 (right) shows an example of a wall test where the piece with more than 1% area of board has fallen off. Falling off of a whole board occurred in a short time. From that time the inside of structure is opened for fire.

DATABASE OF GYPSUM BOARDS

To create necessary design procedures for structures with gypsum boards a database was created at SP Trätekt [7]. There are 342 full-scale test results from the following countries collected to the database. The consistent of database by structures and by origin of testing laboratories is expressed on Table I and Figure 3. Parameters recorded in the database are following:

1. General test data—date, report number, fire exposition sides, loading.
2. Frame structure—height, span, stud material and cross-section, distance, noggings structure.
3. Insulation—type, density, thickness.
4. Cladding—producer, type, orientation, thickness, density, edge shape, fastener parameters, resilient channels.
5. Observations—failure time, thermocouple readings.

Table I. Numbers of full scale testS by country.

Austria	22	Netherlands	2
Canada	62	New Zealand	6
Denmark	13	Norway	5
Germany	22	Sweden	136
Estonia	6	Slovenia	2
Finland	3	UK	32
France	42		



Figure 3. Content of database by structure and cladding type.

Analysis of Database

The database shows that gypsum plasterboards of same types have large scatter of performance properties in fire.

As an important result it can be showed that the start of charring behind gypsum boards occurs often earlier than stated in present EN 1995-1-2:2004 [1] thus [1] gives non-conservative values. The explanation for this may be the optimizing process of the production, components etc to achieve compatible price for the product. Conservative minimal values as a result of this study provide data for design for the cases if the producer is unknown or if producer gives no necessary data for design. The rules based on the database take into account the worst cases.

The equations given in this report are a conservative approach to the problem. The producers must give a data which confirms better performance of their product and gives better values for design compared to the rules according to database. Failure times of gypsum boards of floors are smaller compared to walls because of negative effect of self weight.

The reason of failure is not always clearly understood in test reports. Some of the test results of failure times presented here may be caused by pull-out of fasteners. Designer has to calculate both, the failure time according to proposed rules in this study as well as the failure time according to pull-out of fasteners by [1]. The minimum should be selected.

There exists a difference in failure times of gypsum plasterboards backed by insulation or void cavity. In the worst case approach in present study the difference could be neglected. Also the distance between floor beams or resilient channels can be neglected when creating worst case equations. Solid timber as a backing material is not considered in this study.

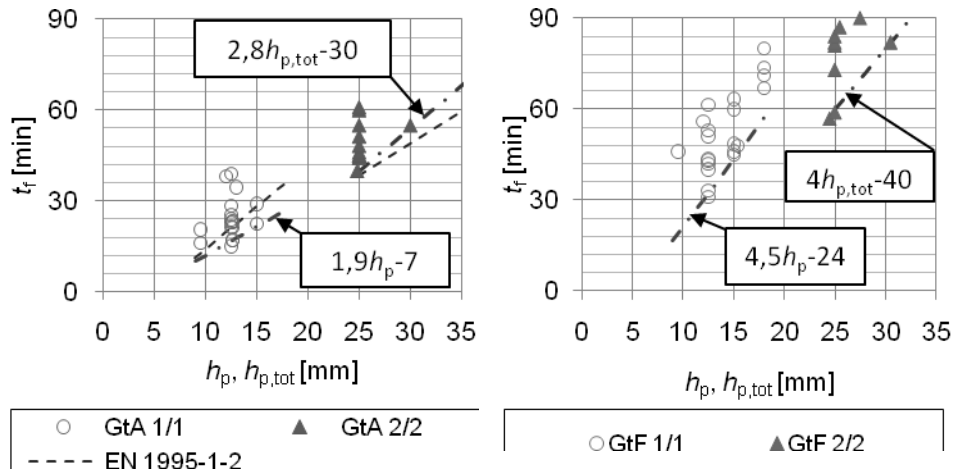


Figure 4. Failure times of wall claddings of gypsum plasterboards type A (left) and type F (right).

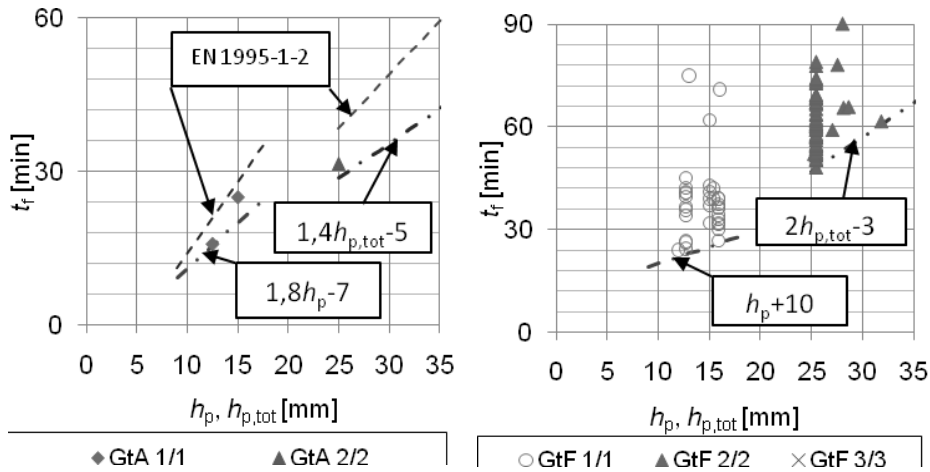


Figure 5. Failure times of floor claddings of gypsum plasterboards type A (left) and type F (right).

Database contains of wall tests with timber studs and steel studs. No differences could be seen on behavior of cladding in fire.

Failure times of gypsum boards, type A show a tendency that the values in EN 1995-1-2:2004 are non-conservative. Full scale tests in database show that failure of gypsum board type A occurs often earlier compared to design values according to EN 1995-1-2:2004 [1].

The test data of walls and floors with two-layer claddings with gypsum plasterboard type F on fire exposed side backed by gypsum plasterboard type A showed failure of two layers at the same time. There is no sufficient data for failure times of claddings for floors, consisting two or three layers of gypsum plasterboards, type A.

Table II. Design equations for failure time t_f

Cladding	Walls		Floors	
Type F, one layer	$4,5 h_p - 24$	$9 \text{ mm} \leq h_p \leq 18 \text{ mm}$	$h_p + 10$	$12,5 \text{ mm} \leq h_p \leq 16 \text{ mm}$
	57	$h_p > 18 \text{ mm}$	26	$h_p > 16 \text{ mm}$
Type F, two layers	$4,5 h_{p,\text{tot}} - 40$	$25 \text{ mm} \leq h_{p,\text{tot}} \leq 31 \text{ mm}$	$2 h_{p,\text{tot}} - 3$	$25 \text{ mm} \leq h_{p,\text{tot}} \leq 31 \text{ mm}$
	100	$h_{p,\text{tot}} \geq 31 \text{ mm}$	59	$h_{p,\text{tot}} \geq 31 \text{ mm}$
Type F + Type A ^a	81	$h_p \geq 15 \text{ mm}^b$	50	$h_p \geq 15 \text{ mm}^b$
Type A, one layer	$1,9 h_p - 7$	$9 \text{ mm} \leq h_p \leq 15 \text{ mm}$	$1,8 h_p - 7$	$12,5 \text{ mm} \leq h_p \leq 15 \text{ mm}$
	21,5	$h_p > 15 \text{ mm}$	20	$h_p > 15 \text{ mm}$
Type A, two layers	$2,8 h_{p,\text{tot}} - 30$	$25 \text{ mm} \leq h_{p,\text{tot}} \leq 30 \text{ mm}$	n.a.	
	49	$h_{p,\text{tot}} \geq 30 \text{ mm}$		
Type A, three layers	55	$h_{p,\text{tot}} \geq 37,5 \text{ mm}$	n.a.	
GF, one layer	$4,5 h_p - 24$	$10 \text{ mm} \leq h_p \leq 12,5 \text{ mm}$	n.a.	
^a Outer layer Type F, inner layer type A		^b Thickness of first layer (Type F)		

According to the analysis of available data the conservative design equations with the limitations of use are shown in

Table II. Design equations for failure time t_f ; given limitations result from available test data.

CONCLUSIONS

The work with database is an ongoing process. Variety of properties inflecting fire protection ability of different products of gypsum plasterboards is large. Classification according to EN 520 [2] does not give necessary information for fire safety design. The aim of design equations presented in this report is to give the information for design of timber frame assemblies according to EN 1995-1-2:2004 [1]. Producers should give failure times of their specific products. There is a need for common procedure for that. No significant influence of stud material and insulation has been found relevant regarding to minimum failure times.

REFERENCES

1. EN 1995-1-2:2004. "Eurocode 5: Design of timber structures - Part 1-2: General rules-structural fire design", European Committee of Standardization, Brussels, 2004.
2. EN 520:2004. "Gypsum plasterboards. Definitions, requirements and test methods", European Committee of Standardization, Brussels, 2004.
3. Schleifer V., "Zum Verhalten von raumabschliessenden mehrschichtigen Holzbauteilen im Brandfall" PhD Thesis No.18516. ETH, Zürich, 2009.
4. Buchanan A., "Structural Design for Fire Safety". Canterbury, 2001.
5. EN 15283-2:2008."Gypsum boards with fibrous reinforcement - definitions, requirements and test methods", European Committee of Standardization, Brussels, 2008
6. Sultan M., Roy-Poirier A., "Gypsum board fall-off temperature in floor assemblies exposed to standard fires". *NRCC-49240*, 2007
7. Just A., Schmid J., König J., "Gypsum plasterboards used as fire protective protection - a database", *Royal Swedish Institute for Engineering Research*, Stockholm, 2010.

Using Artificial Neural Networks for Predicting Temperatures in Timber

P. CACHIM

ABSTRACT

Neural networks are a powerful tool used to model properties and behaviour of materials in many areas of civil engineering applications. A neural network is basically a large number of highly interconnected idealized neurons that receives input from the neurons to which it is connected, computes an activation level, and transmits that activation to other processing neurons. In a feed forward neural network, as used in this work, the artificial neurons are grouped in layers. In each layer, all the neurons are connected to all the neurons in the next layer. No connection exists between neurons of the same layer or the neurons which are not in successive layers. In the present paper, the models in artificial neural networks for predicting the temperatures in timber under fire loading have been developed. For building these models, training and testing using the available numerical results obtained using design methods of Eurocode 5 have been used. The data used in the multilayer feed forward neural network models are arranged in a format of three input parameters that cover the density of timber, the time of fire exposure and the distance from exposed side. With these input parameter used in the multilayer feed forward neural network models the temperatures in timber are predicted. The training and testing results in the neural network model have shown that neural networks can accurately calculate the temperature in timber members subjected to fire.

1. INTRODUCTION

In recent years artificial neural networks (ANN) have become a very popular technique and have been used in many types of problems to which they are applied in also an extensively and varied forms that range from classification and prediction to data visualization and compression. ANN have been used in many fields such as

LABEST & Department of Civil Engineering, University of Aveiro, 3810-193 Aveiro Portugal.

finance, economics, medicine, engineering, etc., and the number of neuro-like models and schemas as well as procedures to implement ANN models is permanently increasing. Within the field of construction industry, ANN have mostly been used for estimating an extended range of concrete properties such as strength [1-4], slump [5-6] or modulus of elasticity [7].

An artificial neural network is basically a large number of highly interconnected idealized neurons that receives input from the neurons to which it is connected, computes an activation level, and transmits that activation to other processing neurons. Activation is the core of neural network computations. Each input neuron activates one or several additional neurons with different levels of efficiency. Subsequently these activated neurons will activate other neurons until an output has been reached. The final result, the output, of the network is strongly influenced by the interconnection between neurons, i.e., the strength and layout of the connections. In order to produce significant results an artificial neural network must learn and need to be trained. The learning process could be performed with known available data and could be continuously improved with new available results, meaning that the network is continuously adapting itself for the new data. After the learning process, the network is ready to perform computations.

Within the field of structural fire analysis the use of artificial neural network can greatly simplify some calculation models. For example, if an ANN could be trained to calculate the thermal field within a timber member as a function of timber density, time of fire exposition, cross section dimension and location of the point within a cross section, the parameters defining the network can be saved and used to calculate the temperature of any point within a timber section with very simple calculations without the need to perform a finite element thermal analysis of the section. The aim of this article is to describe the applicability of artificial neural networks for the prediction of temperatures in timber under fire loading.

2. ARTIFICIAL NEURAL NETWORKS

One of the most common type of ANN are feed forward neural network. Feed forward neural networks, as used in this work, are a type of ANN where the neurons are grouped in layers. This type of network has at least three layers: (i) the input layer, where each neuron represents one parameter necessary for the calculations (for example timber density, time, location, etc.); (ii) an output layer, where the neurons each neuron represents the calculated result (for example the temperature); and (iii) one hidden layer with a specified number of neurons. In more complex networks there can be more hidden layers. In each layer, all the neurons are connected to all the neurons in the next layer (see Figure 1). No connection exists between neurons of the same layer neither with neurons which are not in successive layers. Each connection between artificial neurons is characterized by a weight value. Each neuron of the input layer receives information (data from experiments or analysis) that will be the output of this layer and passes it to the neurons of the following layer weighted by the weight of the connection layer (see Figure 1). In all of the subsequent layers, each neuron computes the weighting sum of all the n neurons of the precedent layer, s_j , according to equation (1). At this stage a bias, b_j , can be introduced that is added to the weighted outputs.

$$s_j = b_j + \sum_{i=1}^n w_{ij} o_i \quad (1)$$

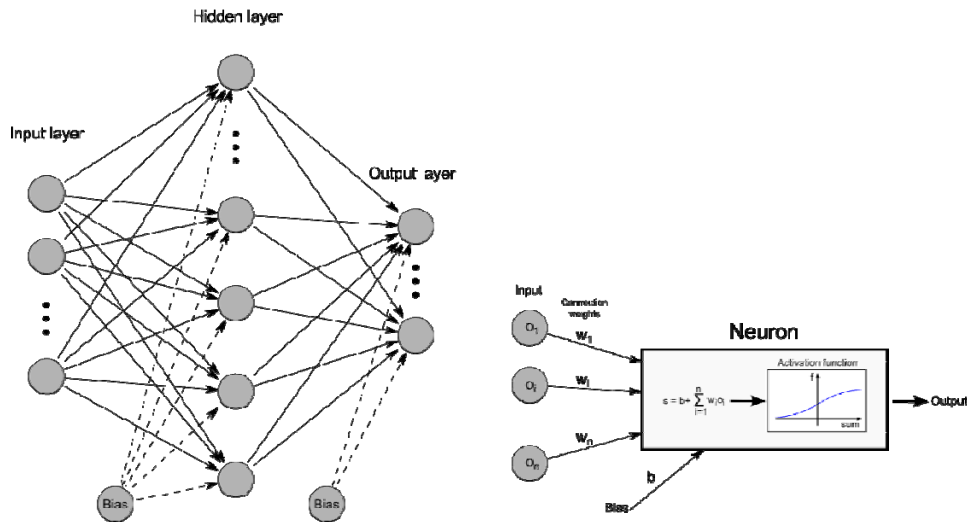


Figure 1. Scheme of a feed forward ANN (left) and individual neuron calculation scheme (right).

The weighted sum of the neurons of the precedent layer represents the input of each neuron and this input activates an output, o_j , by using a so-called activation function, f . One of the most used activation functions is the sigmoid function, see equation (2). The rate of changing of the sigmoid can be controlled by the parameter. Increasing parameter sharpens the shape of the function. In a feed forward network, the inputs and output variables are normalized to be in the range $[0, 1]$. For practical purposes, however, and to avoid gentle variations of the sigmoid, the applicable range is usually $[0.1, 0.9]$. Input and output values must subsequently be normalized.

$$o_j = f(s_j) = \frac{1}{1 + \exp(-\alpha s_j)} \quad (2)$$

Because there is no reliable method for choosing the number of neurons required for a particular problem, the choice of the number of hidden layers and of neurons in each layer must be based on experience and a few number of trials is usually necessary to determine the best configuration of the network.

The learning algorithm used is back propagation that is one of the most well-known training algorithms for the multilayer perceptron. It is a gradient descent technique to minimize the error for a particular training pattern in which it adjusts the weights by a small amount at a time. The network error is passed backwards from the output layer to the input layer, and the weights are adjusted based on some learning strategies so as to reduce the network error.

After the training process, outputs can be calculated from inputs following the pseudo-code presented in Figure 2. Layers are numbered 0 to $nlayer$, with layer 0 being the input layer and layer $nlayer$ the output layer. The outputs of layer 0 are

the input values, and are stored in the vector $output[0]$. The outputs are stored in vector $output[nlayer]$.

```

for  $ilayer=1$  to  $nlayer$ 
  for  $in=1$  to  $nneuron[ilayer]$ 
    // calculate activation weight
     $sum[in] = bias[ilayer][in]$ 
    for  $jn=1$  to  $nneuron[ilayer-1]$ 
       $sum[in] += weight[ilayer][in][jn]*output[ilayer-1][jn]$ 
    next  $jn$ 
    // calculate output using activation function
     $output[ilayer][in] = ActivationFunction( sum[in] )$ 
  next  $in$ 
next  $ilayer$ 

```

Figure 2. Pseudo-code for calculation of outputs of an ANN.

3. CALCULATION OF TIMBER TEMPERATURES UNDER FIRE LOADING USING EC5 THERMAL PROPERTIES

In this work, the temperature evolution within a timber member under fire loading was calculated using the conductive model presented in Eurocode 5, Part 1-2 (EC5) [8]. The conductive model presented in EC5 is based on the calculation of the two- or three-dimensional, transient, heat transfer differential equation, incorporating thermal properties that vary with temperature. Effects such as mass transfer within the structure, reaction energy released inside the wood due to pyrolysis or degradation of material, cracking of charcoal, which increases the heat transfer of the char layer are not accounted for. Thus, EC5 proposes properties that are equivalent properties taking these effects into account.

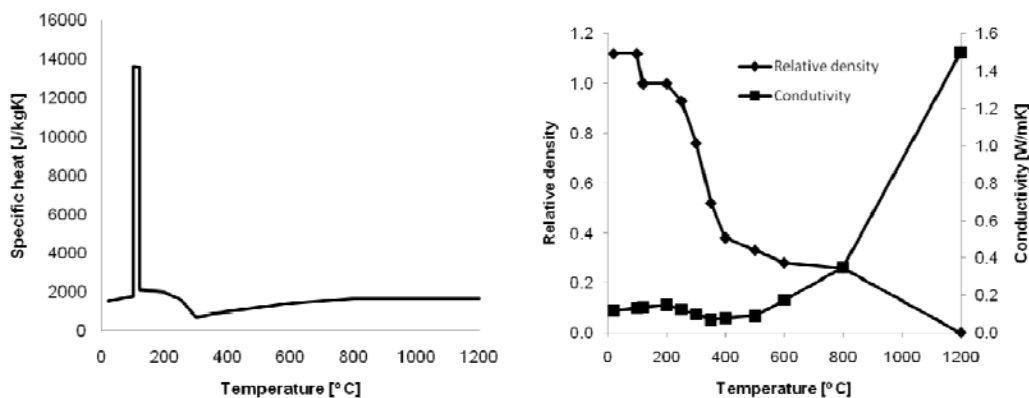


Figure 3. Specific heat in timber (left) and relative density and conductivity (right) [8].

The coefficient of heat transfer by convection on unexposed surfaces was considered $9 \text{ W/m}^2\text{K}$ and on heated surfaces with standard temperature-time curves $25 \text{ W/m}^2\text{K}$, as defined in Eurocode 1, Part 1-2 [8]. The surface emissivity of wood used in calculations was 0.8 [9]. Thermal conductivity, specific heat capacity and density ratio were used with values defined in EC5 (Figure 3). Moisture content of wood was considered equal to 0.12.

4. PREDICTION OF TEMPERATURES IN TIMBER USING ARTIFICIAL NEURAL NETWORKS

4.1. Numerical calculation of temperatures in timber

In this study results of numerical finite element simulations were used as data for the network. Numerical finite element calculations were carried out using the finite element code SAFIR [10], which is a special purpose finite element code, developed at University of Liege for studying structures subjected to fire.

The calculation of temperatures in timber was performed by using a finite element mesh with square elements (side is 5 mm); this will allow an adequate characterization of the thermal field within timber. Timber densities used in this study were 290, 380, 450, 600, 800 and 1000 kg/m^3 . Temperatures were stored every 60 seconds up to 1 hour.

4.2. Artificial neural network error assessment

Basic parameters of the model were selected and used as input neurons while the results, temperatures in timber, are used as outputs. For each case, a random number of available points were selected to serve as data for neural network training while the remaining results were used to test and validate the model. Details specific for each networks are given below, depending on the analyzed problem. The error occurred during the training and testing of the network was expressed as a root mean squared error (RMSE) and as a mean absolute error (MAE) that can be calculated by equations (3) and (4), where t_i is the desired output (numerical results), o_i is the predicted output (calculated by the network) and p is the number of points where the temperatures have been calculated.

$$RMSE = \sqrt{\frac{1}{p} \sum_{i=1}^p (t_i - o_i)^2} \quad (3)$$

$$MAE = \frac{1}{p} \sum_{i=1}^p |t_i - o_i| \quad (4)$$

In addition, accuracy of the network predictions were also assessed by the coefficient of distribution (R^2) and by the mean absolute percentage error (MAPE) calculated according to equations (5) and (6), respectively. In equation (5), \bar{t} represents the average of desired outputs.

$$R^2 = 1 - \frac{\sum_{i=1}^p (t_i - o_i)^2}{\sum_{i=1}^p (t_i - \bar{t})^2} \quad (3)$$

$$MAPE = \frac{1}{p} \sum_{i=1}^p \left| \frac{t_i - o_i}{t_i} \right| \quad (4)$$

4.3. Prediction of temperatures in timber using ANN

The input neurons were timber density, time after fire start, and distance from exposed side. There is only one output neuron that is the temperature. A total of 14760 results were available, from which 3000 (approximately 20%) were randomly chosen to train the network. After some trials a network with 2 hidden layers and 5 neurons in the first hidden layer and 7 neurons in the second layer was selected. Comparison of the training process results are shown in Figure 4, together with the error results. Network efficiency was assessed with the remainder points not used for network training. As for the training process, comparison of the testing process results is shown in Figure 5, with respective error results.



Figure 4. Comparison of the training process results.



Figure 5. Comparison of the testing process results.

Temperature profiles are plotted in Figure 6 where the predicted and calculated temperatures are compared. It can be seen that an excellent agreement was obtained between calculated and predicted temperatures.

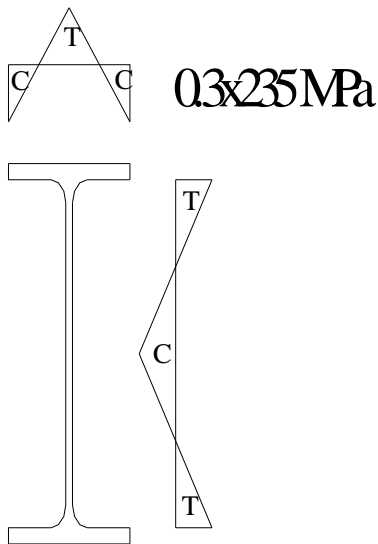


Figure 6. Comparison of temperature profiles for 30 and 60 minutes for timber with 450 kg/m³.

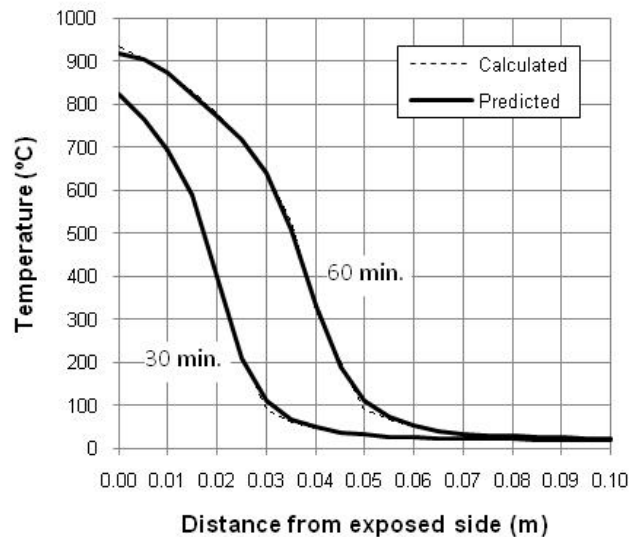


Figure 7. Comparison of temperature profiles for 30 and 60 minutes for timber with 800 kg/m^3 .

5. CONCLUSIONS

Because artificial neural networks can learn and generalize from examples and experiences they are a powerful tool for solving some of the complex civil engineering problems. In this study, artificial neural networks were used in order to predict the temperatures in timber under fire loading for different timber densities and time of exposure.

A feed forward neural network with two hidden layers with 5 and 7 neurons was used. From the obtained results it can be seen that very good agreement between the predicted values of the network and those calculated with finite element models.

The use of artificial neural networks allow designers to easily calculate the temperatures in a timber member at any time and to use these results into structural analysis and design without the need to use a thermal and mechanical model.

Although not specifically addressed in this work the results obtained so far indicate that ANN could be also used to predict temperatures in other materials such as steel or concrete.

6. ACKNOWLEDGEMENTS

Funding provided by the Portuguese Foundation for Science and Technology to the Research Unit LABEST—Laboratory for the Concrete Technology and Structural Behavior is gratefully acknowledged.

7. REFERENCES

1. Prasad, B.K.R., H. Eskandari, and B.V.V. Reddy, *Prediction of compressive strength of SCC and HPC with high volume fly ash using ANN*. Construction and Building Materials, 2009. 23(1): p. 117–128.
2. Topçu, I.B., C. Karakurt, and M. Sarıdemir, *Predicting the strength development of cements produced with different pozzolans by neural network and fuzzy logic*. Materials & Design, 2008. 29(10): p. 1986–1991.

3. Sarıdemir, M., *Prediction of compressive strength of concretes containing metakaolin and silica fume by artificial neural networks*. Advances in Engineering Software, 2009. 40(5): p. 350–355.
4. Öztas, A., et al., *Predicting the compressive strength and slump of high strength concrete using neural network*. Construction and Building Materials, 2006. 20(9): p. 769–775.
5. Ashu, J., J. Sanjeev Kumar, and M. Sudhir, *Modeling and Analysis of Concrete Slump Using Artificial Neural Networks*. Journal of Materials in Civil Engineering, 2008. 20(9): p. 628–633.
6. Bai, J., et al., *Using neural networks to predict workability of concrete incorporating metakaolin and fly ash*. Advances in Engineering Software, 2003. 34(11-12): p. 663-669.
7. Demir, F., *Prediction of elastic modulus of normal and high strength concrete by artificial neural networks*. Construction and Building Materials, 2008. 22(7): p. 1428–1435.
8. CEN, *EN 1995-1-2:2004: Eurocode 5: Design of timber structures - Part 1-2: General - Structural fire design*, CEN, Editor. 2004: Brussels, Belgium.
9. CEN, *EN 1991-1-2:2002. Eurocode 1: Actions on structures - Part 1-2: General actions - Actions on structures exposed to fire*, CEN, Editor. 2002: Brussels, Belgium.
10. Franssen, J.-M., *SAFIR. A Thermal/Structural Program Modelling Structures under Fire*. Engineering Journal, 2005. 42(3): p. 143–158.

A Laboratory Study into the Fire Resistance Performance of Structural Insulated Panels (SIPs)

D. HOPKIN, T. LENNON, V. SILBERSCHMIDT and J. EL-RIMAWI

ABSTRACT

In a process aimed at increasing knowledge in the area of the fire performance of emerging technologies, the UK Department for Communities and Local Government (CLG) have funded a research programme looking into the fire performance of SIPs. The project comprised a programme of laboratory testing on single panels, numerical modelling and four full scale fire tests on two-storey SIP structures incorporating engineered joist floors. This paper presents the findings of the laboratory programme. A companion paper provides details of the large scale fire tests undertaken [1].

The laboratory programme comprised a number of different tests on single panels with EPS and PUR cores, all protected with gypsum plasterboard. These included ambient ultimate load tests to determine appropriate loading levels for fire testing, heat transfer experiments on panels exposed to the ISO834 [2] heating curve and finally experiments on panels subject to combined heating and axial compression.

The experiments indicated that the fire resistance of a panel is entirely reliant on the performance of the lining material. However this was shown to be capable of protecting the panels for 30 and 60 minute furnace exposure times.

INTRODUCTION

Structural Insulated Panels (SIPs) are an emerging framing technology that offer excellent thermal performance and are manufactured from readily available sustainably sourced materials.

D.Hopkin & T. Lennon, BRE Global, Garston, Herts, WD25 9XX, UK (HopkinD@bre.co.uk)
V. Silberschmidt, Wolfson school of mechanical engineering, Loughborough University, UK.
J. El- Rimawi, Dept. of civil and building engineering, Loughborough University, UK.

SIPs are formed from the lamination of two oriented strand board (OSB) facing plates and a polymer-based foam, such as expanded polystyrene (EPS) or polyurethane (PUR). The resulting lightweight panels are then used as primary load bearing compression (wall) elements for buildings such as domestic dwellings, apartment blocks, schools and hotels.

To date, with the exception of standard fire tests commissioned by manufacturers, little testing or research has been undertaken to investigate the fire performance of SIPs. To this end, with a clear knowledge gap and the growing adoption of SIPs, CLG commissioned BRE Global to undertake a research project into the fire performance of SIPs.

LABORATORY TESTING PROGRAMME

In total 30 experiments were performed on single SIPs of overall dimensions 1200 mm x 1800 mm x 150 mm in BRE's structures laboratory, 24 of which are reported herein. In all instances the panels had two 15 mm thick OSB skins. These experiments were split into three distinct categories: uni-axial compression, heat transfer and combined heat and uni-axial compressive loading. The full experimental programme is summarised in Table I with corresponding test references which will be used in the identification of test samples below.

Uni-axial ambient compression tests

Three ambient temperature compression tests were performed on panels, two of which had PUR cores and the other had an EPS core. The experiments were conducted to establish (i) failure of the panels at ambient temperature due to a purely compressive load and (ii) an appropriate level of loading, which should be applied to the combined heat and loading tests later in the programme.

All samples were placed in BRE's 500 tonne compression machine and were tested to failure. In both PUR panels failure was initiated by a sudden brittle crack which propagated through the thickness and width of the OSB facings. Some micro-buckling and kinking was apparent in adjacent local areas in the OSB strands. In addition, some de-lamination occurred close to the crack site, separating the OSB and polymer insulation.

The results of the three compression experiments performed on SIPs are summarised in Table II (Δx and Δz denote lateral and vertical deflections, respectively). It should be noted that the abnormally high level of loading achieved in the EPS panel is due to the presence of solid timber edge studs, which framed the test sample. These are a common form of joining panels and can introduce high levels of redundancy into the structural system. They did however give a false indication of the panel's true ultimate load-bearing capacity and, as a result, only the PUR panels ultimate loads were used to derive loading levels for subsequent furnace tests.

TABLE I. SUMMARY OF LAB PROGRAMME.

Test No	Test	Test reference	PFP	Lining connection
1-2	UL	PUR_L1/L2	None	N/A
3	UL	EPS_L1	None	N/A
4-6	HT	PUR_301-303	15mm PB (Type F)	Battens
7-9	HT	EPS_301-303	15mm PB (Type F)	Battens
10-12	HT	PUR_601-603	30mm PB (Type F)	Battens
13-15	HT	EPS_601-603	30mm PB (Type F)	Battens
16-18	HL	PUR_301-303 HL	15mm PB (Type F)	Battens
19-21	HL	PUR_601-603 HL	30mm PB (Type F)	Battens
22-23	HL	EPS_301-302 HL	15mm PB (Type F)	Battens
24	HL	EPS_601HL	30mm PB (Type F)	Battens
PFP- Passive fire protection; UL- Ultimate load; HT- Heat transfer; HL- Heat and load; PB- Plasterboard				

Heat transfer experiments

A total of 18 furnace tests (12 of which are reported) were performed on unloaded SIPs protected with gypsum (type F) plasterboard, fixed via 25 mm x 50 mm vertical battens at 600 mm centres.

The experiments performed were relatively simple and comprised a SIP pressed up against BRE's barrel furnace. All of the gaps were sealed using ceramic fibre blanket. The gas furnace was then ignited and manually controlled to follow the ISO fire curve [2] by monitoring a plate thermocouple inside the furnace. Furnace temperatures were logged using 15 thermocouples. Temperatures within the SIP panel were monitored and logged at the centre line of the panel at three different heights corresponding to the third (X & Z) and mid-height (Y) levels. The placement of thermocouples through the panel depth is shown in Figure 1. At each height thermocouples measured the back of plasterboard (A), back of front OSB skin (B), mid-core (C), back of rear OSB skin (D) and unexposed face (E) temperatures.

Sample measurements of OSB and timber batten moisture content were measured using a moisture meter. The mean moisture content of the OSB veneers was 9.2% and the corresponding value for the timber battens was 11.7%.

RESULTS- 30 & 60 MINUTE (15 mm & 30 mm type F) EXPERIMENTS

The first 6 tests of the heat transfer programme exposed PUR and EPS panels protected with 15 mm (type F) plasterboard to 30 minutes of the ISO834 [2] fire curve using BRE's gas furnace. All samples survived the duration of the experiment without a need to terminate, and there was no indication of combustion below the plasterboard lining during the experiments. The resulting back of plasterboard temperatures (Location A) are shown in Figure 2(i). Mean temperatures for PUR and EPS panels are also shown; they are derived as the average of all PUR and EPS data sets, respectively.

TABLE II. SUMMARY OF AMBIENT AXIAL LOAD EXPERIMENTS.

Ref.	Ultimate load (kN)	Peak Δx (mm)	Peak Δz (mm)
EPS_L1	647	2.7	10.8
PUR_L1	331	2.4	16.4
PUR_L2	293	8.9	28.7

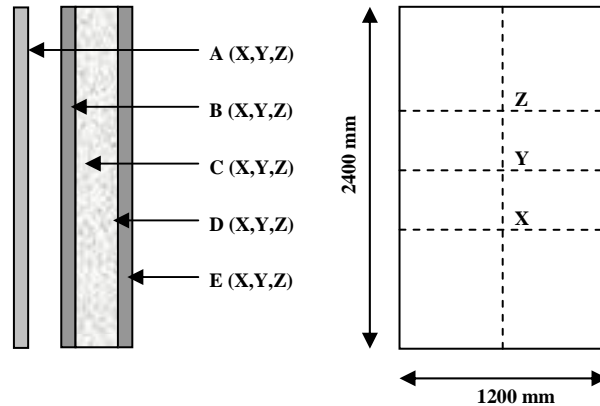


Figure 1. Placement of thermocouples through depth and height of panel.

Similarly, the back-of-OSB (Location B) temperatures are shown in Figure 2(ii), again with averages for each core material as noted previously.

A further six tests exposed PUR and EPS panels protected with 30 mm of type F gypsum plasterboard to 60 minutes of the ISO834 fire curve [2]. In all instances the panels survived the duration of the experiment with no indication of combustion internally within the panel. The back of plasterboard temperatures (Location A) are shown in Figure 3(i). These curves reflect the temperatures behind two layers of 15 mm type F plasterboard. An average temperature for each core material is shown for completeness. The corresponding rear-of-OSB temperatures are shown in Figure 3(ii) with the arithmetic mean for both core material types.

Combined heat and loading experiments

Nine combined heat and loading tests were completed in total as part of the laboratory programme. Each panel was first loaded in uni-axial compression to a load corresponding to 50% of the mean ultimate load achieved by the PUR test samples at ambient temperature. That equated to a target load of 130 kN or 108.3 kN/m. Once loaded the furnace was ignited and one side of the panels were exposed to either 30 or 60 minutes of the ISO834 fire curve, depending on the plasterboard lining specification (15 or 30 mm type F plasterboard). Six PUR samples were studied each with either 15 mm or 30 mm of type F plasterboard. Three EPS samples were tested, similarly with 15 mm or 30 mm of plasterboard lining. The instrumentation specification essentially merged the requirements of the heat transfer and ultimate loading elements of the research programme. The thermocouple placement and specification corresponded with that of Figure 1, whilst displacement transducers measured the mid-height lateral (out of plane) and rig cross head (vertical) deflections. The applied loading was logged using a load cell in the compression machine.

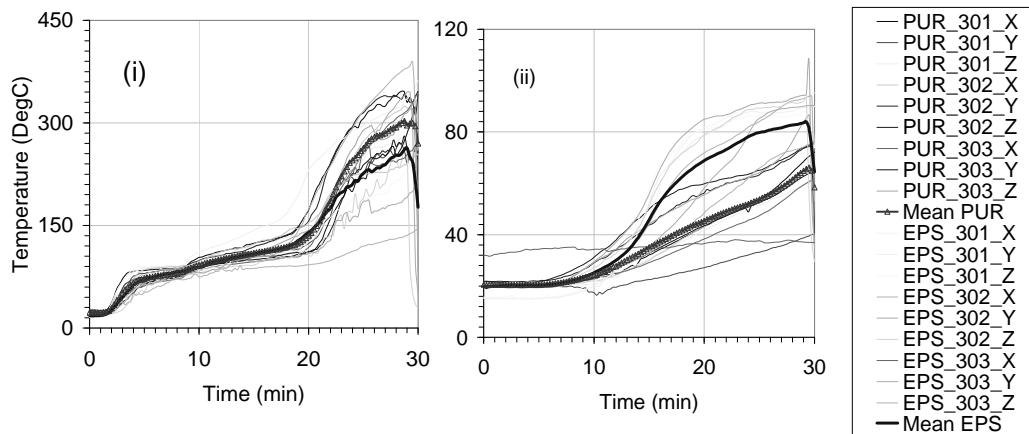


Figure 2. (i) Back of plasterboard (Location A) and (ii) back of OSB temperatures (Location B) for 30 minute PUR and EPS experiments.

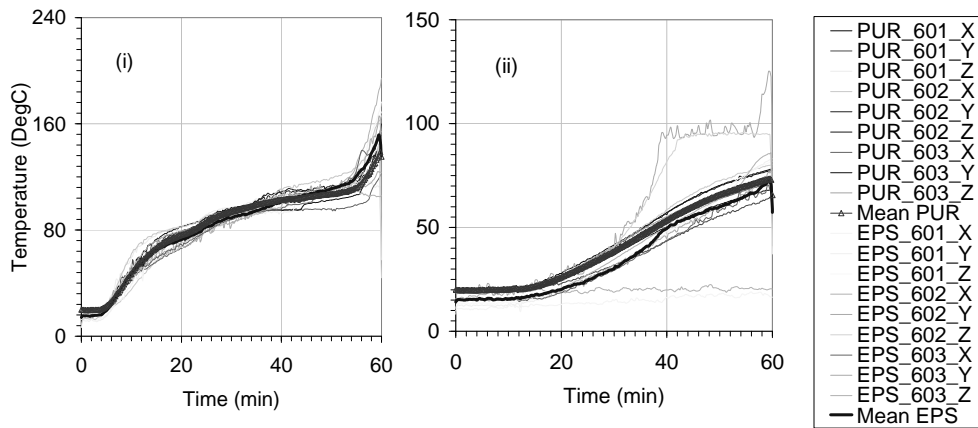


Figure 3. (i) Back of plasterboard (Location A) and (ii) back of OSB temperatures (Location B) for 60 minute PUR and EPS experiments.

RESULTS- 30 & 60 MINUTE (15 mm & 30 mm type F) EXPERIMENTS

The temperatures measured within the 30 minute loaded panels were very similar to those reported above for un-loaded specimens; as a result, they will not be discussed further. Sample mid-height lateral and vertical deflections are plotted versus mean furnace temperature for experiments PUR_303HL and EPS_302HL in Figure 4(i). The other experiments performed demonstrated similar results. In the graph positive deflection denotes movement downwards and away from the furnace for vertical and lateral deflections, respectively. The mean loading for experiments PUR_303HL and EPS_302_HL throughout the 30 minute duration were 127 kN and 126.5 kN, respectively, against a target load of 130 kN.

Similar to the 30 minute tests all temperatures measured within the 60 minute samples were in agreement with those measured previously on unloaded

samples. For this reason the results are not discussed further. The three PUR panels tested all survived 60 minutes exposure to the ISO834 curve [2] without loss of load-bearing capacity under mean loads of 125.5 kN, 124.2 kN and 124.7 kN, respectively. Experiment EPS_601HL was terminated after 34.5 minutes due to ignition of the insulation core. This, however, was a failure that arose as a result of the test setup and cannot be considered as a true failure of the panel. Hot gases issuing from poorly sealed gaps around the furnace edges ignited the exposed insulation edges (which would not be present in a real building) thus bypassing the passive fire protection. Sample deflection plots versus mean furnace temperature are shown in Figure 4(ii) for tests PUR_601HL and PUR_602HL. All experiments performed under 60 minute heat and loading conditions were generally in good agreement. However, due to the early termination of experiment EPS_601HL, no appreciable deformation developed due to the proportionally lower temperatures in the panel. The mean loading during the experiment was 82.5 kN. This was due to the almost instantaneous crushing of the timber spreader beam placed between the SIP and the compression machines loading platen. The damage to the spreader beam occurred on initial loading prior to the ignition of the furnace and as a result a consistent load of 82.5 kN was achieved with few fluctuations during the experiment duration (34.5 minutes).

DISCUSSION

Heat transfer experiments

A set of temperature profiles have been determined for SIPs protected with a number of different specifications of gypsum plasterboard. The study indicated that, in all instances, the specification of type F plasterboard of thickness 15 mm or 30 mm is sufficient to achieve the UK fire resistance periods of 30 and 60 minutes, respectively. The specification of 15 mm (type F) plasterboard for 30 minute fire resistant applications has been shown to prevent the ignition of the insulation core (regardless of material used) whilst also keeping the OSB temperatures sufficiently low to prevent structural integrity issues.

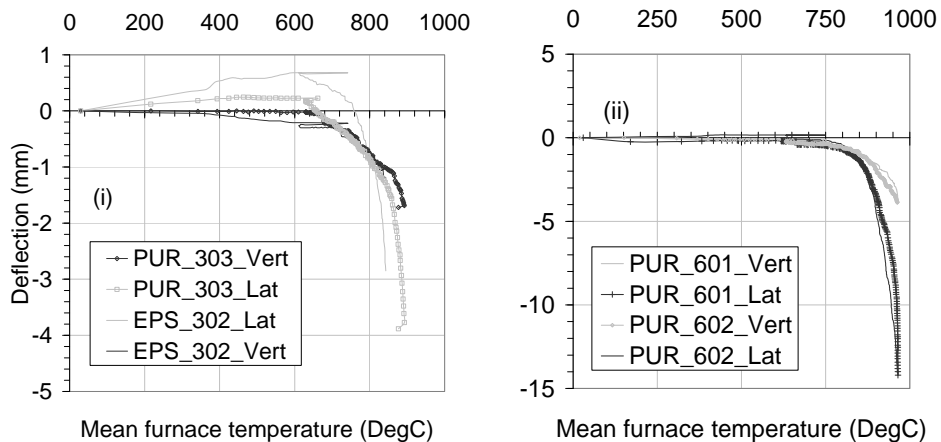


Figure 4. Mean furnace temperature versus vertical and lateral deflections for (i) PUR_303HL & EPS_302HL and (ii) PUR_601HL & PUR_602HL.

For the 30 minute experiments it was shown that there was little or no appreciable difference in the temperature development through the depth of the panel for PUR or EPS insulation. Any difference noted was largely due to the migration of steam through the more permeable EPS insulation.

Where steam, due to chemically bound water present in plasterboard, is allowed to permeate into the insulation core some local damage can occur in EPS panels due to the low glass temperature of polystyrene. This damage manifests itself as de-lamination between the core and 'fire-side' OSB veneer.

Although no combustion was apparent during the duration of any of the 30 minute heat transfer experiments some flaming was noted once the samples were removed from the furnace. Due to the severe temperature gradient, indicated previously in figure 2, the 'fire-side' OSB veneer reaches sufficiently high temperatures (in excess of 300°C) to ignite. However, while protected by the plasterboard, there is insufficient oxygen for this to occur. On removal of the samples from the furnace portions of the cracked gypsum plasterboard were removed, resulting in instantaneous combustion of the underlying pre-heated OSB face, due to the sudden availability of air.

The specification of 30 mm of type F plasterboard was shown to be more than sufficient for 60 minute fire resistance applications. The rear of plasterboard temperatures have been shown to be generally less than 150°C. This resulted in back-of-OSB temperatures, which did not exceed 100°C regardless of insulation type. There appears to be no appreciable difference in the temperature profiles, which develop in PUR or EPS insulated SIPs after 60 minutes furnace exposure. Any differences were again largely due to steam migration through the more permeable EPS core. Steam due to moisture in the plasterboard lining entered the core as a result of penetrations drilled for the placement of thermocouples. No combustion was apparent in any 60 minute test samples either during or post experiment after removal of the dry lining.

Combined heat and loading experiments

In all experiments there were no instances where load-bearing failures occurred, however, experiment EPS_601HL was terminated due to premature ignition of the polystyrene core. The loading levels imposed were far in excess of those typically allowable in SIP structures as these are limited by the levels achievable in the standard test procedure (typically, 30-100 kN/m). Deflections in all panels were relatively small and were typically characterised by a gradual creep with time. Fairly sizeable lateral deflections can develop in fire-exposed panels (10-15 mm); however these did not result in additional cracking in the plasterboard lining or any cracking in the OSB skins of the SIP. As a result, the temperatures observed in loaded specimens were essentially the same as those in the un-loaded experiments.

For SIPs adopted in 30 minute fire resistant applications (15 mm type F plasterboard) no clear difference was apparent in the load-bearing performance of PUR and EPS variants. Both developed approximately 3 mm lateral deflection and 1-2 mm vertical deflection. Due to the increased susceptibility of polystyrene to ignition it was not possible to adequately compare the fire resistance performance of such panels with those adopting PUR as an insulant for 60 minute applications.

CONCLUSIONS

The work undertaken is the first of its kind in the UK and has investigated the fire resistance performance of PUR and EPS variants of SIPs with variations in plasterboard specification. The data collected is valuable for developing numerical models aimed at simulating the fire performance of SIPs. BRE have been successful in developing such a tool and this will continue to be developed as an element of further work. A number of important conclusions can be derived from the project:

1. The specification of 15 or 30 mm type F plasterboard for applications where 30 or 60 minutes fire resistance is required has been shown to prevent damage to SIPs exposed to either 30 or 60 minutes ISO834 furnace exposure;
2. Due to the degree of redundancy inherent in panels, load levels (up to 108 kN/m) do not appear to play a significant role in the fire resistance of SIPs under furnace conditions;
3. The introduction of solid timber splining members significantly increases a SIPs load bearing capacity. The redundancy afforded by such studs in real buildings is likely to improve fire performance by allowing the redistribution of load should panels become damaged.

ACKNOWLEDGMENTS

The authors would like to acknowledge CLG for funding this programme of work. The work reported herein was carried out under a contract placed by CLG and any views expressed are not necessarily those of CLG. The authors also acknowledge the contribution of the UK SIPs Association. Mr. Hopkin would like to thank EPSRC for continuing to fund his research work with Loughborough University.

REFERENCES

1. Hopkin, D., Lennon, T., El-Rimawi, J., and Silberschmidt, V., 2010. Failure mechanisms of SIP systems under natural fire conditions. *Proceedings of the sixth international conference on structures in fire, Michigan 2-4th June 2010*.
2. International Organisation for Standardisation, 1999. *Fire-resistance tests -Elements of building construction -Part 1: General requirements*. ISO 834-1:1999. Geneva: ISO.

CONNECTIONS

Improved Details for Fire-Induced Steel Single Plate Shear Connections

S. SELAMET and M. E. M. GARLOCK

ABSTRACT

The objective of this paper is to identify cost-effective improved modification details for single plate (i.e., shear tab or fin plate) shear connections in a fire. Using ABAQUS, we developed a finite element model of a single plate connection that was tested full scale in Cardington. We modified several connection details to find modifications that led to increased strength and/or ductility, where an increase in either one also meant an increase in fire resistance time. The results illustrate some simple modifications to the connection design that improve the connection's fire performance.

INTRODUCTION

Simple shear connections are vulnerable to large compressive and tensile forces as well as imposed rotations induced by a natural fire during both heating and cooling phase. Recent fire events and full-scale experiments of steel buildings [2, 8, 11] have demonstrated that (1) the load and rotation capacity of the connections generally govern the behavior of floor systems in a building under fire and (2) shear connections are especially vulnerable during the cooling phase of the fire when large tensile force develop. Such results have been investigated and confirmed by numerical methods finite element software ABAQUS [5, 9].

We previously developed a finite element model of a single plate shear connection in a subassembly from a Cardington building full-scale fire test [5]. The model, which used a simplified method to structurally and thermally include the effect of the concrete slab, accurately captured the beam web and flange buckling and the failure modes like bolt shear and bolt bearing.

Serdar Selamet, Graduate Student, Department of Civil and Environmental Engineering, Princeton University, Princeton, NJ 08544 U.S.A.; sselamet@princeton.edu
Maria Garlock, Assistant Professor, Department of Civil and Environmental Engineering, Princeton University, Princeton, NJ 08544 U.S.A.; mgarlock@princeton.edu

Using that validated model, our objective in this paper is to investigate the following modifications to single plate connection details to evaluate if they can lead to improved performance under fire: bolt grade, bolt holes type, adding a doubler plate on the beam web, the thickness of the connection plate, bolt pretensioning, the gap distance between the beam and beam support, and the distance between the bolt hole and the edge of the plate, and the relationship between this distance and the bolt design. A more detailed discussion of this study will shortly be published elsewhere [10]. In this paper, we highlight some of the significant observations.

FINITE ELEMENT MODEL

A finite element model is developed based on a portion of a floor system from a full-scale building experiment performed in Cardington as shown in Figure 1 [11]. Figure 2 shows the floor subassembly and connection finite element model. The FE model details are given by Garlock and Selamet [5].

Ambient temperature material properties of different components of the subassembly are taken directly from Cardington experiment measurements [2]. Eurocode reduction factors [4] were used to reduce the stress-strain material properties at elevated temperatures of the connection members except the bolts. For the bolts, Kirby's suggested reduction factors were used [7].

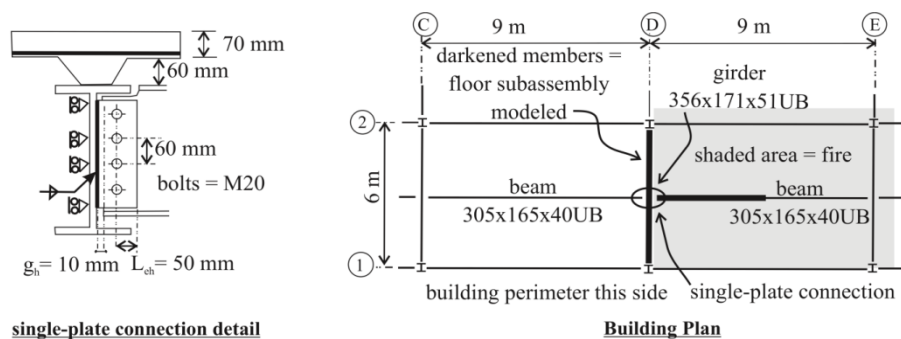


Figure 1. Structural design of the 2003 Cardington building tests [11].

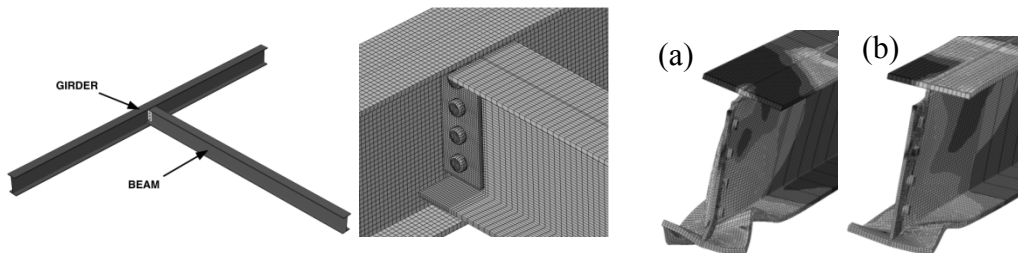


Figure 2. Finite element model of the (left) subassembly, (right) connection detail.

Figure 3. Buckling deformations at the maximum rotation (60 min) of (a) STD bolt (Test 0) and (b) SSLP bolt (Test 3).

ABAQUS implicit solver is employed for the finite element (FE) analyses. FE contact mechanics algorithm software simulated a realistic interaction between the connection parts (i.e. contact pressure and friction). To represent the slab, simple spring elements that only have vertical stiffness are used and calibrated with

experimental data. The FE model was validated with the Cardington test data as described by Garlock and Selamet [5].

RESULTS OF CARDINGTON FE MODEL

During the entire heating period, the beam was in compression and during the cooling period it was in tension. The FE results indicate that such tension lead to connection failure by bolt bearing on the beam web holes. “Failure” in our model is defined as the point where the field equations stop converging due to excessive plastic strains (larger than 20% strain) in the connection. The connection in the actual experiment had large bearing deformation on the beam web holes but no failure.

During the fire growth, the web and bottom flange sections bear almost all the compressive axial force in the connection region until they buckle. During the fire decay, the beam goes into tension and the web section carries almost all the tensile axial force. The results suggest that both compression and tension in the beam near the connection region is carried by an area less than the full beam cross section.

CONNECTION DETAIL MODIFICATIONS

This section describes the modifications to the connection details of the Cardington design to evaluate their effects on the fire performance of the floor system. The fire demand (time-gas temperature history) of all studies was the same as the one measured in the Cardington. Table I shows the parameters and results for the eight different studies (tests) that were based on modifications to the “Original” Cardington connection detail described in [5] and Figure 1, which we define as Test 0. The modifications are shown in bold font.

Bolt Grade (Test 1)

The effect of bolt strength is examined by reducing the ultimate strength of bolts by 40%, that is, by changing the grade from 8.8 to 5.6. The ambient temperature ‘measured’ [8, 11] yield and ultimate strength of Grade 8.8 are 695 MPa and 869 MPa, respectively. The ambient temperature ‘nominal’ yield and ultimate strength of Grade 5.6 are 300 MPa and 500 MPa, respectively.

Results show that the reduction of bolt strength does not affect the beam axial force and moment in the beam during heating phase; however Test 1 with Grade 5.6 bolts fails by bolt shear at 192 kN of axial force in tension. The Cardington connection model (Test 0) with Grade 8.8 bolts fails due to web bolt bearing at 359 kN of axial force in tension (see Table I). Both failures happen during the cooling phase.

TABLE I. TESTS WITH VARIOUS MODIFICATIONS (IN BOLD) TO THE SINGLE PLATE CONNECTION. TEST IS THE ORIGINAL CARDINGTON CONNECTION DESIGN.

TESTS		0	1	2	3	4	5	6	7	8	
PARAMETERS	Bolt grade	8.8	5.6	8.8	8.8	8.8	8.8	8.8	8.8	8.8	
	Bolt-hole size (mm) ¹	20	20	24	22x26	20	20	20	20	20	
	Shear plate thick. (mm)	10	10	10	10	10	6	10	10	10	
	Doubler Plate thick. (mm)	-	-	-	-	4	-	-	-	-	
	Bolt pretension (kN)	-	-	-	-	-	-	142	-	-	
	Gap g _h (mm)	10	10	10	10	10	10	10	19	19	
	L _{eh} (mm)	40	40	40	40	40	40	40	40	70	
RESULTS	Limit State ²		WB	BS	WB	WB	NF	PB/WB	WB	WB	NF
	Time of Events (min)	@ contact ³	14	14	15	15	15	14	14	20	22
		@ P _{max} (Comp.)	20	20	20	20	20	20	20	20	26
		@ end ⁴	123	101	126	140	202	178	165	165	202
	Rotation (mrad)	@ contact	43	41	34	34	46	46	45	84	89
		@ P _{max} (Comp.)	53	46	35	36	52	49	52	98	96
		max. rotation	97	96	78	74	81	83	108	136	127
	P(kN)	P _{max} (Comp.) ⁵	718	720	720	732	712	703	716	549	565
		P _{max} (Tension) ⁵	359	192	357	369	622	348	401	407	433
		P _{c max} (Tension) ⁶	316	157	323	358	555	286	352	368	396
T (°C) ⁷	@ P _{max} (Comp.)	260	260	260	261	260	260	260	431	431	
	@ P _{max} (Tension)	256	391	295	311	128	112	240	248	251	
Δ (mm) ⁸	max. deflection	344	349	350	366	368	325	336	349	354	

¹ STD, OVS and SSLP bolt hole sizes

² Limit States: WB=web bearing, PB=plate bearing, BS=bolt shear, NF=no failure

³ contact is when the beam bottom flange contacts the girder

⁴ end of analysis when convergence cannot be reached or when analysis is completed at 202 min (e.g. Test 4 and 8)

⁵ P_{max} is the maximum beam axial force

⁶ P_{c max} is the maximum tensile force in the beam coped web section (does not include the upper or lower flange)

⁷ T is the average beam temperature at midspan

⁸ Δ is the deflection at beam midspan

Bolt-hole Type (Test 2 and Test 3)

Three different bolt types are tested: standard bolt-hole type (STD) with equal bolt and hole diameter (20 mm), oversized bolt-hole type (OVS) with larger hole diameter (24 mm) and short slotted bolt-hole type (SSLP) with slightly elliptical hole shape (22x26 mm). These cases represent Tests 0, 2 and 3, respectively. A larger bolt-hole size allows the beam to rotate and expand more independently from the connection and this modification affects both buckling of the web and the lower flange (Fig. 3). It is seen that after 60 minutes of the fire, the beam of the STD design (Test 0) deforms much more than the SSLP design (Test 3) as well as the OVS design (although not shown).

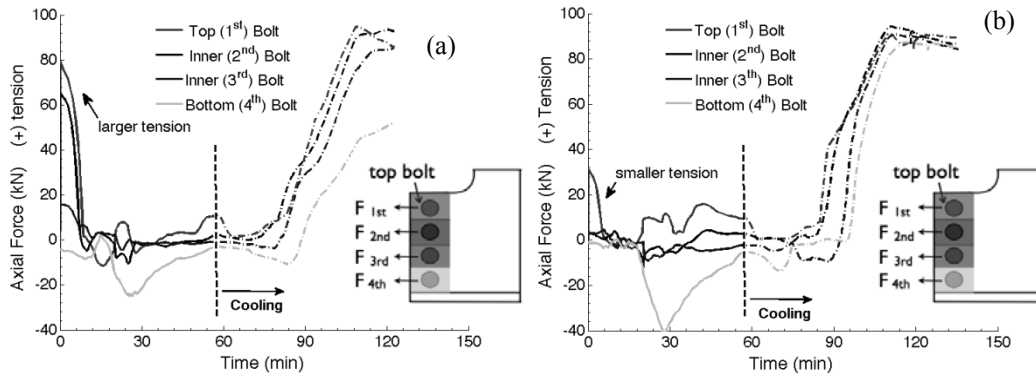


Figure 4. Bolt regions in the coped beam web and regional axial forces for (a) Test 0 and (b) Test 3.

When the tensile failure in bolt bearing (beam web or single plate) is considered as a design criterion at ambient temperature, uniform forces are assumed to act on all the bolt regions. The tensile capacity of the connection is found by multiplying the capacity of a single bolt by the number of bolts. This methodology is valid if the connection is not significantly deformed. However, due to the extent of lower flange buckling, as seen in Figure 3a, the bottom bolt in Test 0 is significantly bent out-of-plane at the end of the analysis, whereas such distortion is far less in Test 3. Figure 4a and 4b plot the four bolt section (internal) forces for the STD design (Test 0) and for the SSLP design (Test 3), respectively. In the STD design, the last bolt region (F_{4th}) takes lesser load during fire decay compared to other three bolt regions above it. Such behavior is due to significant plate distortion near the last (bottom) bolt. The SSLP design carried nearly equal tension in all four bolt regions since there was less distortion near the last bolt. The OVR design (not shown) performance in the last bolt region was between STD design and SSLP design as expected. Selamat and Garlock [10] propose an equation for bolt bearing capacity that is modified for reduced capacity due to such distortions.

Doubler Plate (Test 4)

In Test 4, 4 mm thick doubler plates (web stiffeners) were added to the original connection (Test 0). Since the web is 6 mm thick, adding 4 mm makes the combined thickness equal to the shear tab that is 10 mm thick. The FE results (Table I) indicate that adding a doubler plate to the beam web improves the connection performance: the buckling develops more gradually, the connection tensile strength increases by nearly 73% to 622 kN, and the subassembly survives the fire until gas temperature cools down to 70 °C (after 3 hours) with less visible plastic deformation in the connection region.

Thickness of the Single Plate (Test 5)

In Test 5, we reduced the thickness of the shear tab from 10 mm to 6 mm to match the beam web thickness which still satisfies the flexural buckling strength design of a shear tab according to Jaspart [6]. Significant deformation in both the shear tab and the beam web are observed (Test 5). The original design (Test 0) develops minimal deformations of the shear tab whereas the beam web develops excessive deformations. Since in Test 5, both the shear tab and the beam web are

deforming, the connection is more ductile and failure happens one hour later than the design with the thicker shear tab (Test 0). The connection strength (maximum P in tension) stays almost the same in both tests since it is controlled by beam web bearing and the beam web was not modified.

Pre-tensioned Bolts (Test 6)

In Test 6, we pretension the bolts to allow frictional forces to develop against slip of the components and hence prevent excessive rotation. According to LRFD provisions [1], 142 kN is applied to each bolt, which is equivalent to 0.7 times the nominal tensile bolt strength for M20 bolts.

The FE study indicates that the region where normal forces act on the contact surface is relatively small around the bolts and the entire plate surface is not engaged in friction. The fire induced forces and moments between the components overcome the frictional resistance forces. However, larger contact shear (tangential) forces between the beam and plate around the bolt-holes are observed in Test 6 (pretension) compared to Test 0 (no pretension). Such forces act against the bearing deformation of the bolt-holes during the fire decay when large beam tensile axial force is observed. Therefore, the maximum beam tensile strength at midspan of Test 6 is about 10% larger (401 kN) than that of Test 0 (359 kN). This additional strength adds about 40 minutes to the survival of the connection during cooling.

Gap Distance (Test 7 and Test 8)

Changing the gap distance (see Fig. 5) will change rotation at which the bottom flange contacts the girder (g_h). Test 0 had $g_h = 10$ mm, and the distance from the bolt center line to the edge of the beam (L_{eh}) equal to $2d_b = 40$ mm. In Tests 7 and 8, we increase g_h to 19 mm, and additionally for Test 8, we increase L_{eh} to $3.5d_b = 70$ mm. The Steel Construction Manual (SCM) [1] defines the value $a = g_h + L_{eh}$ and it limits $a \leq 89$ mm ($3 \frac{1}{2}$ "). Figure 5 shows a sketch of the 3 connection designs (Tests 0, 7 and 8) and the values of g_h and L_{eh} . All 3 designs meet the SCM's limit of the parameter a .

Figure 8b plots the axial force in the beam near the connection region. It is seen that the web and flange buckling is delayed slightly for Test 7 and Test 8 compared to Test 0 due to a larger gap distance g_h . Also, the peak compressive axial force in Tests 7 and 8 is about 20% less than that for Test 0. Furthermore, Figure 8b confirms that Tests 7 and 8 have more ductility where the connection is able to withstand the force for about 40 more minutes than Test 0. In these tests, the beam is permitted to rotate more before contact between girder and beam flange is established. Therefore, more of the thermal elongation is developed in the beam bending curvature compared to Test 0, which contacts the girder sooner and is therefore more axially restrained from elongating, leading to a larger compressive force in the beam (see Table I).

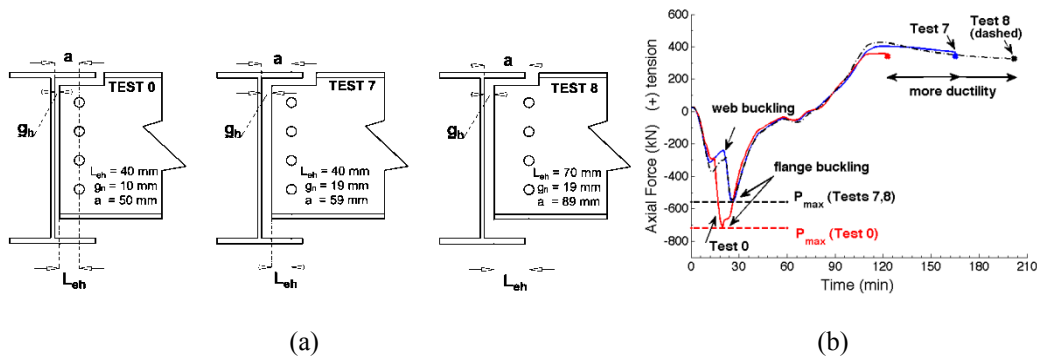


Figure 5. (a) Geometric details of connections with different L_{eh} and g_h (b) axial force near connection (0.1m from support) with different gap distances.

SUMMARY AND CONCLUSIONS

A finite element model of the single plate shear connection used in the full-scale experiments (Cardington) indicates that beam web bearing failure of the bolt holes was the limit state reached at the end of the analysis. The experiments show large bearing deformations but no failure. FE analysis indicated that near the connection region, the axial forces (tension and compression) are carried by an area that is less than the full cross-section. After the bottom flange contacted the supporting member, only the web and bottom flange carried the compressive force. The tensile forces that develop later are carried only by the web.

The modifications studied and the conclusions are the following:

Bolt Grade: A larger bolt grade (e.g. A490 or G8.8) is recommended for increased capacity.

Larger bolt holes: Using OVR or SSLP bolt holes in the beam web reduces buckling deformations of the beam near the connection allowing evenly distributed forces in the bolts. However, the overall global performance of the connection was only slightly affected by these larger hole sizes because they were not large enough. The oversized hole added only an extra 2 mm movement in each direction and the short slotted added only 3 mm in each horizontal direction.

Adding web doubler plate: Adding a plate to the beam web near the connection so that the combined beam web thickness (6 mm) plus doubler plate thickness (4 mm) equals the shear tab thickness (10 mm) increases the connection strength considerably. In fact, the analysis terminated without failure of the connection.

Matching the single plate (shear tab) thickness to the web thickness: When the shear tab thickness is reduced to 6 mm to match the web thickness, the overall connection strength (controlled by bearing) stays the same (as expected). However, the ductility in the connection is increased because bearing deformations develop in the shear tab in addition to the beam web, which results in additional axial flexibility and an increased fire resistance of nearly one hour.

Pretensioning the bolts: Adding pretensioned bolts to the single plate connection does not engage the entire plate and beam web surface into friction, however the tangential contact between these components around the bolt hole region creates

larger contact shear forces which resist the bearing deformation of the beam web bolt holes and thus slightly increase the tensile capacity of the connection and increase the time to failure.

Increased gap distance: The distance between the end of the beam and the supporting girder face was increased from 10 mm to 19 mm. This delayed the contact between the beam bottom flange and the supporting girder, which resulted in the following: (1) larger tensile strength since the flange buckling deformations were smaller and the tensile forces were therefore more evenly distributed between the bolt holes, (2) smaller maximum compression since there is less axial restraint from thermal elongation and (3) about 40 minutes of added fire resistance before bearing connection failure.

Increased distance from bolt hole centerline to the end of the beam (L_{eh}): The bearing capacity of the connection depends on the thickness of the beam web (t) and L_{eh} . In Test 8, the L_{eh} is increased from $2d_b$ to $3.5d_b$ and a significantly larger connection tensile capacity is achieved; the model survived the fire without failure. Increasing L_{eh} or t will increase the bearing capacity of the connection; however, one must consider that the limit state may change to bolt shear.

ACKNOWLEDGEMENTS

This research is supported by the National Science Foundation (NSF) under grant number CMMI-0756488. All opinions, findings and conclusions expressed in this paper are the authors' and do not necessarily reflect the policies and views of NSF.

REFERENCES

1. AISC. 2005. Manual of Steel Construction, Load and Resistance Factor Design.
2. Bailey, C.G., T. Lennon, D.B. Moore. 1999. "The behavior of full-scale steel-framed buildings subjected to compartment fires," *The Structural Engineer*, 77(8):15–21.
3. European Committee for Standardization. 2002. "Eurocode 1: Actions on structures Part 1-2: General actions on structures exposed to fire EN 1991-1-2:2002," Brussels, Belgium.
4. European Committee for Standardization. 2001. "Eurocode 3: Design of steel structures Part 1.2: General rules structural fire design ENV 1993-1-2:2001," Brussels, Belgium.
5. Garlock, M. and S. Selamet. 2010. "Modeling and behavior of steel plate connections subject to various fire scenarios," accepted to *Journal of Structural Engineering ASCE*
6. Jaspert, J.P. 2003. "European design recommendations for simple joints in steel structures," University of Liege.
7. Kirby, B.R. 1995. "The behavior of high-strength grade 8.8 bolts in fire," *Journal of Constructional Steel Research*, 33:3-38.
8. Lennon, T. and D. Moore. 2003. "Client Report: Results and observations from full-scale fire test at BRE Cardington," British Research Establishment, Client report number 215–741.
9. Sarraj, M., I.W. Burgess, J. Davison, R.J. Plank. 2007. "Finite element modelling of steel fin plate connections in fire," *Fire Safety Journal*, 42:408–415.
10. Selamet, S. and M. Garlock. 2010. "Robust Fire Design of Single Plate Shear Connections," tentatively accepted for publication in *Engineering Structures*.
11. Wald, F., L. Simes da Silva, D.B. Moore, T. Lennon, M. Chadn, A. Santiago, M. Benes, L. Borges. 2006. "Experimental behaviour of steel structures under natural fire," *Fire Safety Journal*, 41(7):509–522.

Fire Performance of External Semi-Rigid Composite Joints

P. SCHAUMANN¹, B. ZHAO², O. BAHR³ and C. RENAUD⁴

ABSTRACT

This contribution deals with the fire performance of external semi-rigid composite joints. First, the design principles of two newly developed joints are explained. Four fire tests were carried out to investigate the fire performance of the new joints. To study local phenomena in the joint, a three-dimensional numerical model was established with the Finite Element code Abaqus for one joint type. The data obtained from the fire tests were used to validate the model. It is shown that the model is suitable to predict the fire performance of the chosen external semi-rigid composite joint. Thus, parametric studies were conducted to extend the parameter set of the fire tests. Based on the results of the numerical studies, the paper concludes with recommendations for the design of the developed composite joints.

1. INTRODUCTION

Current Eurocodes for the fire design are limited to braced structures. However, a large market is seen for unbraced composite frames with three storeys at most and fire resistance classes up to R60. The frames could be used for instance in office, industrial, and school buildings. Thus, the ongoing European project 'Unbraced Composite Structures in Fire' addresses this topic [1]. The numerical investigations performed within the scope of this project showed that the joint behaviour is crucial for the overall fire performance of the frames. Exemplary numerical simulations of a fire-exposed unbraced composite frame at failure stage can be found [2].

However, even in composite constructions the connections between perimeter columns and beams are mostly pure steel connections. Therefore the authors investigated the fire performance of external composite joints experimentally and numerically. Two different types of composite joints were considered. As presented in Figure 1, the first type of composite joint is a full composite solution without any additional fire protection. The second type of joint is more conventional with reinforced concrete-filled steel tubes and normal composite beams. Four fire tests on composite joints were carried out by CTICM. The joints were designed to achieve a fire rating of 60 min. The Institute for Steel Construction established advanced calculation models of the joints in the non-linear software Safir and Abaqus. For the former, please refer to [2]. The latter is presented in this contribution and in [3].

¹Professor, Leibniz University Hannover, Institute for Steel Construction, Hannover, Germany

²Dr., Head of the Fire Research Section, CTICM, 91193 Saint-Aubin, France

³Research Assistant, Leibniz University Hannover, Institute for Steel Construction, Hannover, Germany

⁴Dr., CTICM, 91193 Saint-Aubin, France, email: chrenaud@cticm.com

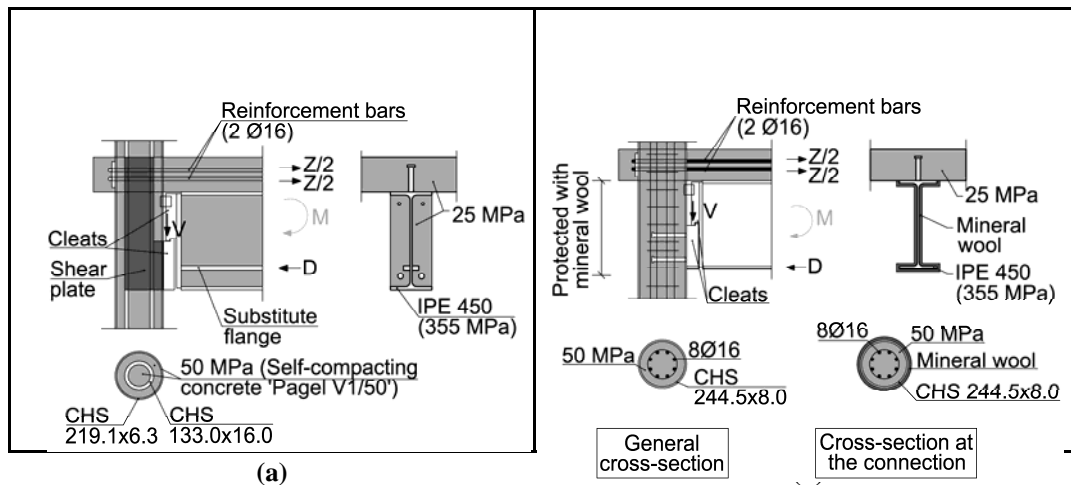


Figure 1. Design drawing of composite joint with concrete-filled double skin steel tubular (CFDST) columns (a) and of protected composite joint with concrete-filled steel tubular (CFST) columns (b).

2. DESIGN PRINCIPLES OF THE DEVELOPED JOINTS

As presented in Figure 1(a), the first type of composite joint is a full composite solution without any additional fire protection. This solution consists of concrete-filled double skin steel tubular (CFDST) columns combined with partially concrete encased composite beams. A shear plate that is welded to the inner tube transfers the load from the beam into the inner tube. Under fire condition, the inner tube progressively bears the loads due to the quick heating of the outer tube. In this context, it is referred to the extensive research on CFDST columns conducted by Zhao and Han [4].

The second type of joint is more conventional with reinforced concrete-filled steel tubular (CFST) columns and normal fire-protected composite beams. In consequence, the fire protection applied to the beams is extended to the joint zone, as it is shown in Figure 1(b). With cleats and additional studs penetrating the concrete core, this allows for transferring the high local forces into the column that result from the bending moment of the beam. Further details of the design of the joints are given in [3].

3. FIRE TESTS

3.1 Aim of the tests

Four isolated full-scale joint tests were carried out to study the fire performance of the new composite joints and to validate the established numerical models. For each joint type, two tests were conducted in the fire laboratory of Efectis France under the coordination of its parent company CTICM [5].

The tests were designed to study both global and local failure of the joints. The former clarified the performance of the joints in unbraced composite frames, whereas the last focused on their load-bearing and rotational capacity. Finally, the tests should ensure the theoretical design of the joints for a fire rating of at least 60 min to ISO standard fire.

3.2 Test specimens

The dimensions of the test specimens were chosen such that the test specimens could be integrated in the furnace. Furthermore, realistic cross-sections were taken from the design of a one-bay three-storey unbraced composite frame with span of 12 m (see [2], Figure 1). Table I gives the key test parameters.

Steel tensile coupon tests and concrete compression tests were carried out to determine the actual mechanical material properties at ambient temperature. For the steel specimens, Table I shows the average proof limit $R_{p0.2}$, which is the stress at 0.2% residual strain.

The CFDST columns of the composite joints (specimens 'C1' and 'C2' in Table I) were concreted with self-compacting concrete type 'V1/50' from the German company 'Pagel Spezial-Beton' of strength class C50/55. For the CFST columns (specimens 'P1' and 'P2'), normal-weight of strength class C50/55 was used. The beam was protected by one layer of mineral wool 'Insulfrax S' with a thickness of 25 mm. The protection was extended around the column and covered the connection over the full height of the beam. As shown in Figure 1, an IPE450 beam with a concrete slab of 160 mm height was used in all four tests. The slab and concrete between the flanges had nominal strength class of C25/30.

3.3 Test set-up

The base of the columns was fully restrained. Accompanying numerical studies in [2] showed that a fixed base support is crucial for the fire performance of the unbraced frames. In the fire tests, the pinned joint at the top of the column enforces the contraflexure that occurs at each storey level of realistic multi-storey frames. In longitudinal direction, the columns were free to move. To prevent out-of-plane bending of the joints, two additional profiles braced the column head. Some space was given to ensure that there was no initial contact between the column and the bracing.

3.4 Instrumentation and loading

As indicated in Figure 2(a), wire sensors were placed at the beginning and near the end of the beams. Additional sensors on the columns measured the axial deformation. Furthermore, the inclinations were measured by angular sensors. About eighty thermocouples were installed on each test specimen in different sections of the joint, beam, and column to record temperatures. Furthermore, sixteen plate thermometers captured temperatures inside the furnace. A special high temperature video camera was put inside the furnace to record visually the specimen deformations versus time.

Table I. Material properties.

Test	Steel strength $R_{p0.2}$ (MPa)		Reinforcement (MPa)		Concrete strength (MPa)	
	Outer tube	Inner tube	Beam Flange/Web	Slab	Column	Beam and slab
C1	369	422	374/397	659	74.0	33.5
C2	371	375	374/397	659	86.5	33.5
P1	368	./.	374/397	659	86.5	33.5
P2	379	./.	374/397	659	86.5	33.5

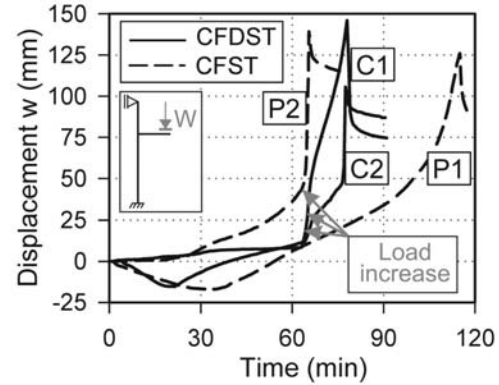
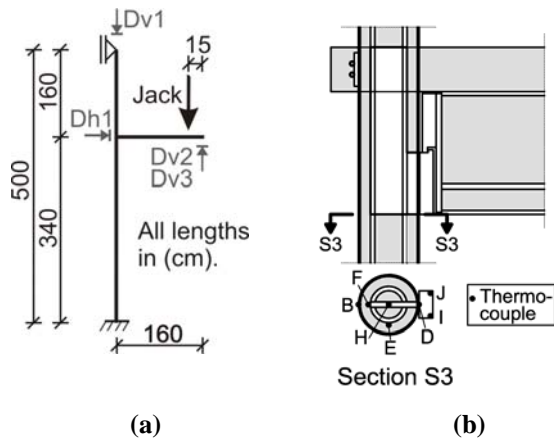


Figure 2. Static system of the fire tests (a); section for the temperature measurements (b).

Figure 3. Displacement at the beam end for the different joint tests.

A loading device was developed allowing the jack to follow the sway of the test specimens. Therefore the jack was fixed to a movable beam on a crane trolley. All specimens were exposed to ISO standard fire for at least 60 min. Before fire exposure, the load was applied manually with help of a hydraulic jack at the end of the beam as shown in Figure 2(a). The load was continuously monitored and manually regulated during the fire test. During the first 60 minutes of the test, the applied moment at the joint M remained in three of four tests well below the nominal moment. This was to ensure that sufficient thermal data could be gained for the validation of the established numerical model. After 60 min, the load was increased within three tests as reported in Table II. The tests had to be stopped when either the deformations became too large or when the inclination of the jack was exceeded. Table II also shows the nominal load ratio for the different joint tests, which is defined as the ratio of the resulting moment into the joint during the fire test to the nominal moment resistance of the joint at room temperature. To induce the global failure mode described in section 3.1, the total length of the circular CFST and CFDST columns in the furnace was exposed to ISO standard fire (see Figure 4). In contrast to this, for the local failure mode only the upper 750 mm of the column in the furnace were exposed to heating (see Figure 5). The rest of the column was protected with a layer of 25 mm mineral wool. After failure, the load was removed. All tests were continued to the next fire rating time to collect thermal data for the numerical validation.

3.5 Results

Figure 3 shows the evolution of the deflection 'w' at the end of the slab. In the first twenty minutes, thermal expansion of the columns was observed. The expansion was less concise for the specimens where local failure was induced since their heated length was only 750 mm. Overall, all joints failed with the expected global or local failure mode according to Figures 4 and 5.

Table II. Summary of test parameters.

Test	Outer tube	Inner tube	Applied load (kN)	Load ratio in the joint section (%)	Failure time (min)
C1	CHS 219.1×6.3	CHS 133.0 × 16.0	100 (140)*	83 (117)	78
C2	RHS 260×180×6.3	RHS 160×90×10.0	130 (200)**	109 (168)	78
P1	CHS 244.5×8.0	No inner tube.	75	63	115
P2	RHS 260×180×6.3	No inner tube.	100 (125)***	83 (105)	66

CHS denotes Circular Hollow Section and RHS denotes Rectangular Hollow Section. Load was increased between * 63-78 min, ** 63-68 min, and *** 63-66 min, respectively.

In addition, the joints showed sufficient ductility between $\theta = 80$ mrad (test C2) and $\theta = 100$ mrad (test C1). Thus, the joints are appropriate to allow for the large rotations that occur into the joints of fire-exposed unbraced composite frames.

Furthermore, the tests confirmed that both joint types with CFDST and CFST columns are suitable for fire ratings of at least 60 min, which is even true for the tests with load ratios higher than the nominal load-bearing capacity. For the last, their high load-bearing capacity can be attributed to the overstrength of the reinforcement bars bent around the column (see Table I).

4. THREE-DIMENSIONAL FINITE ELEMENT MODEL

4.1 General description of the model, Finite Element type, and mesh

A three-dimensional Finite Element model of the circular external composite joint was established in Abaqus/Explicit to conduct parametric studies. Most of the mesh consists of six-node linear triangular prism elements C3D6 with an element size of about 30 mm. The more complex geometry near the column was meshed with four-node linear tetrahedron elements C3D4 with an element size around 20 mm.

4.2 Boundary conditions, load application, and interactions

Rigid bodies represent the lower and upper support, where end plates with thickness of 40 mm and 20 mm were used in the test, respectively. Same as in the fire tests, the lower support is constrained against all degrees of freedom, whereas the upper support allows for rotation and axial movement of the column. The load was applied at a distance of 150 mm from the end of the cantilever, corresponding to the load configuration in the fire test. In the test, a circular knuckle was installed between the head of the jack and the slab. In the model, a rectangular pressure of same area was applied to simplify the mesh. The applied load in the model strictly followed the recorded load history of the test. Full contact was assumed between all steel and concrete elements.

4.3 Material modeling

For the steel and reinforcement bars, constitutive laws from Eurocode 4-1-2 [6] were used. The concrete damaged plastic model was adopted to simulate the concrete [7-9]. It describes the inelastic behaviour of concrete with concepts of isotropic damage combined with isotropic tensile and compressive plasticity. Real stress-strain relationships were used for all materials.

4.4 Validation of the model

Cross-sectional temperatures were recorded from thermocouples placed at six different sections during the fire tests. In general, the established numerical model accurately predicts the temperatures obtained in the fire tests. In this contribution, section S3 in Figure 2(b) was chosen. Figure 6(a) shows that the numerical model predicts reasonably the evolution of cross-sectional temperatures.

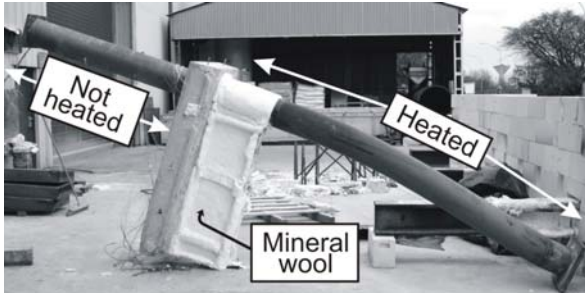


Figure 4. Specimen P1 after the fire test (global failure mode).

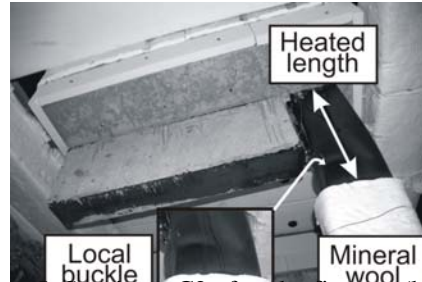


Figure 5. Specimen C2 after the fire test (local failure mode).

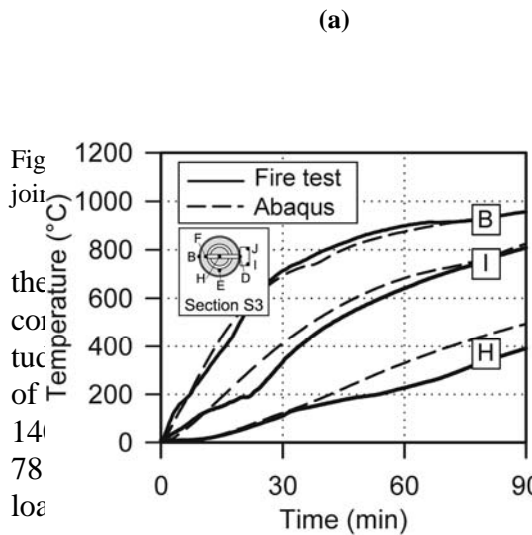


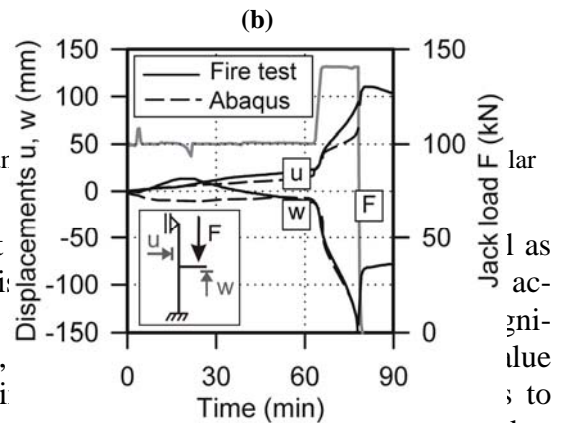
Fig 1200
join
the
co
tuc
of
14
78
loa

temperatures (a) ar
sults.

of the slab at
where the di
jack load 'F'
can be seen,
e load was li

calculation resulted in // min failure time compared to

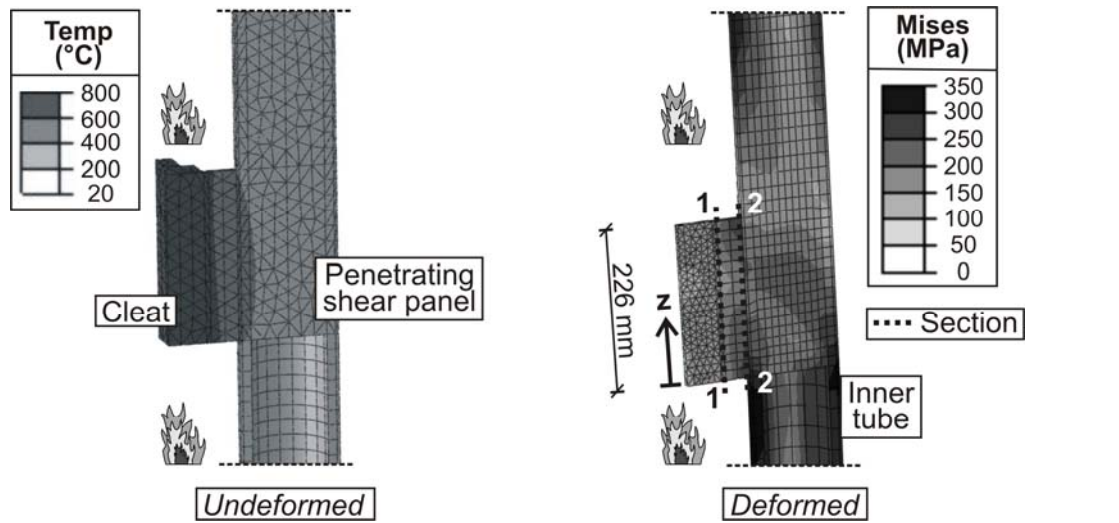
was a sharp increase of deformations when the applied
in Figure 6(b), the numerical results for the horizontal
movement 'u' of the column and the displacement 'w' at the end of the slab are close to the results obtained from the fire test. For a detailed discussion of the validation, it is referred to [3].



5. INFLUENCE OF THE LOCATION OF THE FIRE

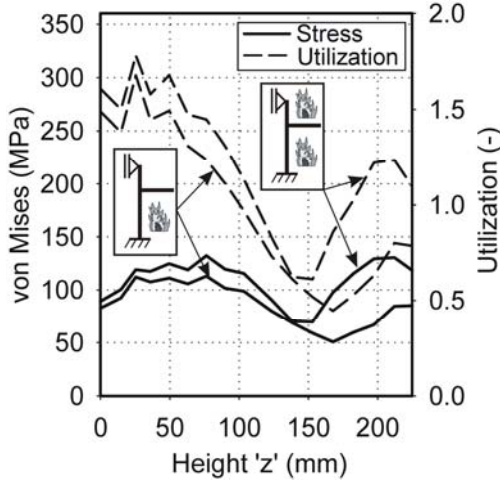
Numerical studies were conducted to investigate the effect of the location of the fire on the fire performance of the circular external composite joint. The fire performance of the joint was evaluated in terms of the global deformations and local stresses in the shear panel. The latter was chosen since it plays a crucial for the fire performance of the joint [3]. Figure 7(a) depicts the temperature field of the inner tube, shear panel, and cleat after 60 min exposure to ISO stan-

standard fire in the ground and first storey. The investigation showed that the cross-sectional temperatures in the penetrating shear panel are governed by the fire in the ground storey, whereas the influence of thermal action in the upper storey is negligible.

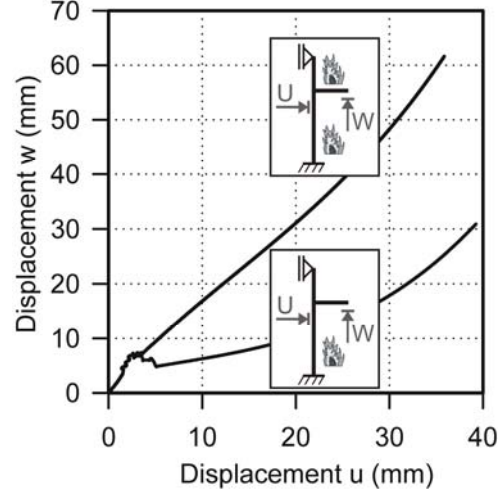


(a) Temperature distribution in the shear panel for fire in both storeys (concrete not shown).

(b) Von Mises stresses in the shear panel for fire in both storeys (concrete not shown).



(c) Stress and utilization in section 1-1 of the shear panel depending on position 'z'.



(d) Displacement w of the beam plotted versus sway u of the column.

Figure 7. Numerical results for the influence of the location of the fire.

In addition, Figure 7(b) shows the two deformed sections '1-1' and '2-2', where von Mises stresses were evaluated after 60 min fire exposure. The study showed that because of its higher cross-sectional temperatures section '1-1' at the cleat was more critical than section '2-2' at the thermally protected inner tube. The heating reduces the effective yield stress f_y . For this reason, Figure 7(c) shows the von Mises yield stress σ_v for multiaxial loading conditions for the critical section '1-1' and for both regarded fire scenarios. The stresses are plotted over the height 'z' of the shear panel, which is depicted in Figure 7(b). Furthermore, the utilization is given in Figure 7(c), which was defined as the ratio of the von Mises stress and the effective uniaxial yield

stress f_y , of the fire-exposed steel with nominal strength of 355 MPa. Results for section 2-2 are not shown because the maximum utilization was 74% and hence not critical.

From the utilization, it may be concluded that the shear panel that is exposed to fire only from the ground storey offers more residual load-bearing capacity in its upper part. Contrary, for fire in both storeys the panel was close to yielding and hence local failure of the joint. This conclusion is underlined by Figure 7(d) plotting the deflection 'w' of the beam versus the sway 'u' of the column. Accordingly, the deflection 'w' for fire in both storeys was significantly higher than for fire in the ground storey only. Besides the higher utilization of the shear panel, one reason is that the continuous column provides less moment resistance for fire in both storeys.

6. SUMMARY AND OUTLOOK

Based on the information presented, the following conclusions may be drawn:

It has been shown that the established numerical modeling predicts the fire performance of the investigated composite joints with a good accuracy. Altogether, the investigations showed that the developed semi-rigid joints may provide a promising alternative to common joints for perimeter columns.

The two developed external semi-rigid composite joints are suitable for fire ratings of at least 60 min exposure to ISO standard fire, which was confirmed by four full-scale fire tests.

Fire in both storeys is more critical than in one storey since it induces failure by yielding of the penetrating shear panel.

ACKNOWLEDGEMENTS

The work presented here has been carried out with a financial grant from the Research Fund for Coal and Steel (RFCS) of the European Community. The authors gratefully acknowledge the financial support and appreciate the intensive cooperation among the project partners. Furthermore, the authors would like to thank the company 'Pagel Spezial-Beton' for the supply of material and concreting of the test specimens in France and Germany.

REFERENCES

1. European Commission. 2007-2010. Research project 'Unbraced Composite Structures in Fire' (UCoSiF). Research Fund for Coal and Steel, Contract N°RFSR-CT-2007-00044, Brussels.
2. Schaumann, P. and Bahr, O., "A numerical model for unbraced composite frames in fire", Structures in Fire 2010, Michigan, USA, 2010 (*accepted for publication*).
3. Schaumann, P. and Bahr, O., "Fire design of external semi-rigid composite joints", ISTS13, Hong Kong, 2010 (*accepted for publication*).
4. Zhao, X.-L. and Han, L.-H., "Double skin composite construction", *Progress in Structural Engineering and Materials*, Volume , pp. 93-102, 2004.
5. Efectis France, "Fire test on composite external semi-rigid composite joints", Test reports 09-U-538, 09-U-543, 09-U-554, and 09-U-559, 2009.
6. European Committee for Standardization, EN 1994-1-2, "Design of composite steel and concrete structures, Part 1-2: General rules - Structural fire design", 2006.

7. Hillerborg, A., Modeer, M. and Petersson, P. E., "Analysis of crack formation and crack growth in concrete by means of fracture mechanics and Finite Elements", *Cement and Concrete Research*, Volume 6, Issue 6, pp. 773-782, 1976.
8. Lee, J. and Fenves, G. L., "Plastic-damage model for cyclic loading of concrete structures", *Journal of Engineering Mechanics*, Volume 124, Issue 8, pp. 892-900, 1998.
9. Lubliner, J., Oliver, S., Oller, S. and Oñate, E., "A plastic-damage model for concrete", *International Journal of Solids and Structures*, Volume 25, Issue 3, pp. 229-326, 1989.

Experimental Investigations and Analytical Model for the Behavior of Grade 8.8 Bolts and Butt Welds Under Heating and Subsequent Cooling

F. HANUS, G. ZILLI and J.-M. FRANSSSEN

ABSTRACT

Up to now, the mechanical behaviour of bolts and welds has been assumed as reversible during the cooling phase of a fire. The behaviour of bolts and welds submitted to cooling curves is a key issue in the evaluation of the fire resistance of steel structures under natural fires. The present article describes the experimental tests undertaken on bolts and welds at the Centro Sviluppo Materiali during heating or subsequent cooling, presents a model for the stress-strain diagram of bolts during a natural fire that integrates the influence of the temperature history, and gives values of strength reduction factors for the cooling phase.

INTRODUCTION

Recent full-scale experimental tests performed on steel and composite structures have demonstrated that the development of tensile forces in axially-restrained beams during the cooling phase of a natural fire can lead to the failure of bolts situated in the joint zone. In order to understand this phenomenon and to design structures that are not prone to such a failure mode, it is essential to have a deep knowledge of the material behaviour of all components, including bolts and welds, during both the heating and cooling phases.

Up to now, mechanical models of bolts and welds have been proposed essentially for elevated temperatures, without consideration of a cooling phase. Eurocode 3 Part 1-2 proposes strength reduction factors as a function of temperature for the design of bolts and welds under fire conditions. These factors have been determined on the basis of the experimental work carried out by Kirby and Latham at temperatures up to 800°C. However, the residual resistance of bolts and welds after a heating-cooling cycle has not been investigated yet (see Figure 1).

François Hanus (corresponding author), Research Engineer, Structural Engineering, University of Liège, Belgium.

Giuliana Zilli, Research Engineer, Centro Sviluppo Materiali, Rome, Italy.

Jean-Marc Franssen, Professor, Structural Engineering, University of Liège, Belgium.

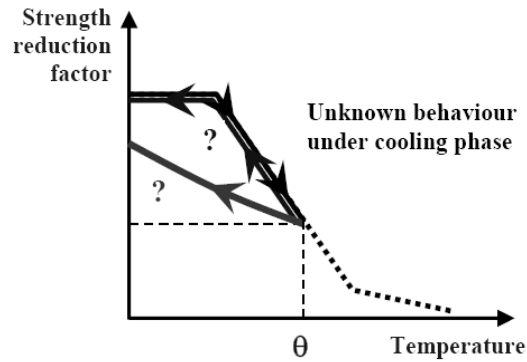


Figure 1. Objective of the tests performed on bolts and welds.

The behavior of carbon steel is usually assumed as reversible in usual fire design applications, see for example [1]. Due to the manufacturing process of bolts, the mechanical behaviors of bolts and carbon steel differ noticeably at elevated temperatures. Up to now, investigations about the mechanical properties of bolts and welds have essentially been founded on the results of isothermal tests performed on specimens heated up to different temperatures.

The first series of tests performed on bolts were displacement-controlled tests realized by Riaux at temperatures between 20°C and 700°C, showing the existence of a descending branch in the force-displacement diagram before the full breaking of bolts [2]. The strength reduction factors mentioned in EN 1993-1-2 [3] have been determined on the basis of the experimental work carried out at British Steel on Grade 8.8 M20 bolts at temperatures up to 800°C [4]. Tests in tension have highlighted that problems of premature failure by thread stripping are caused by the lack of fit between the nut and the bolt rather than the insufficient capacity of one component. The measured reductions of resistance showed similar patterns in tension and shear. In recent researches, tests performed on Grade 10.9 bolts have underlined the significant effect of creep on the behavior of bolt material at high temperatures [5].

To the knowledge of the authors, the unique available data about the evolution of welds resistance at elevated temperatures is the series of tests performed by British Steel [6] that lead to the reduction factors defined in EN 1993-1-2.

TEST METHODOLOGY

The experimental programme undertaken on bolts and welds at the Centro Sviluppo Materiali includes three different types of isothermal tests:

- Room temperature tests performed in order to get the reference strengths
- Steady-state tests performed at elevated temperatures in order to obtain the strength evolution of bolts/welds during the heating phase (see Figure 2a)
- Steady-state tests performed at various failure temperatures T_f after heating to temperature T_u , in order to investigate the strength behavior of bolts and welds during the cooling phase (see Figure 2b).

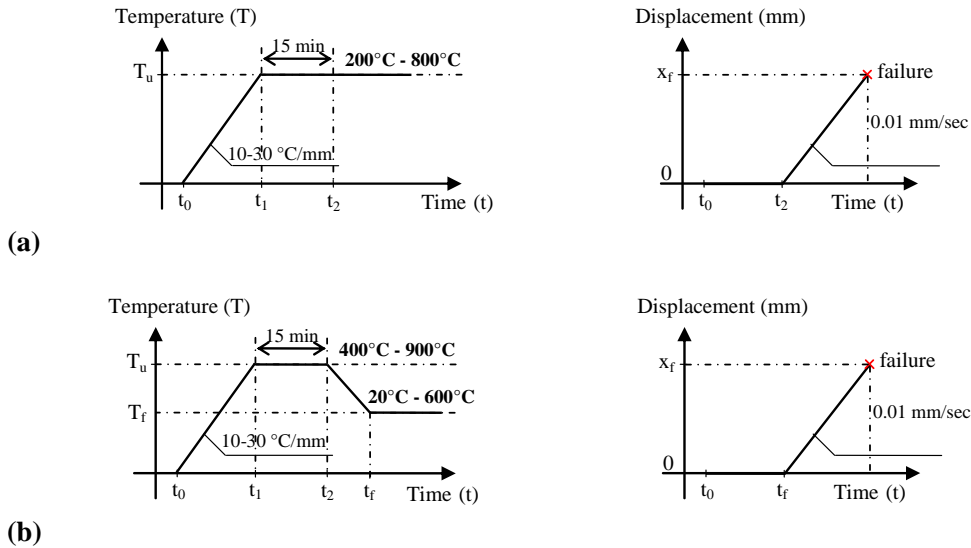


Figure 2. Test processes for bolt experiments after heating (a) or heating and subsequent cooling (b).

In all the tests performed at elevated temperatures, the tested specimens were heated and cooled down at a speed of 10-30°C/min. Temperature has been stabilized during 15 minutes after reaching the temperature T_u and the failure temperature T_f .

EXPERIMENTAL TESTS PERFORMED ON GRADE 8.8 BOLTS

The resistance of bolts in tension and shear are evaluated separately in the design codes. Consequently, two different test set-ups have been designed to investigate separately the mechanical behavior of bolts in tension and shear (see Figure 3). Due to the limited loading capacity of test equipment, size M12 bolts have been tested. Clamps for both tensile and shear tests have been fabricated using the NIMONIC 115 heat resistant alloy so that their behavior remains elastic during the complete test and prying actions due to clamps deformations are limited.

All the tensile tests have been characterised by a ductile yielding of the threaded shank and no nut stripping failure occurred (Figure 4).

The correlation between the results obtained from tests performed at the up temperature $T_u = T_f$ and the Eurocode recommendations demonstrated that the diameter has a limited influence on the reduction of bolt resistance (Figure 5). The reduction factors k_b obtained experimentally for $T_u = 400^\circ\text{C}$, 600°C and 800°C are plotted on Figure 6.

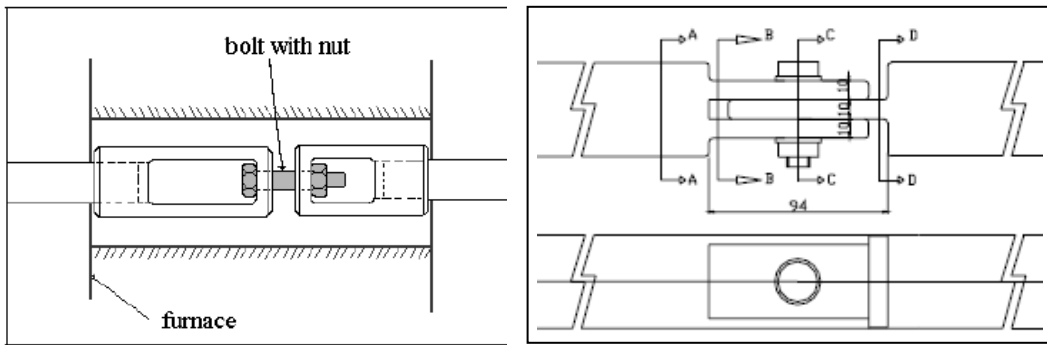


Figure 3. Test set-ups for tensile and shear tests performed on bolts.



Figure 4. Bolts tested in tension ($T_u = 600^\circ\text{C}$).

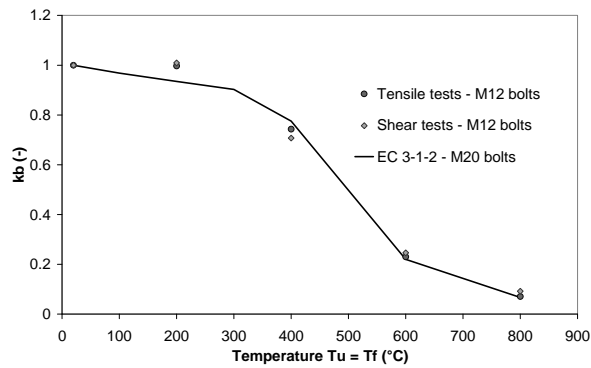


Figure 5. Comparison of the strength reduction factor for M12 and M20 bolts.

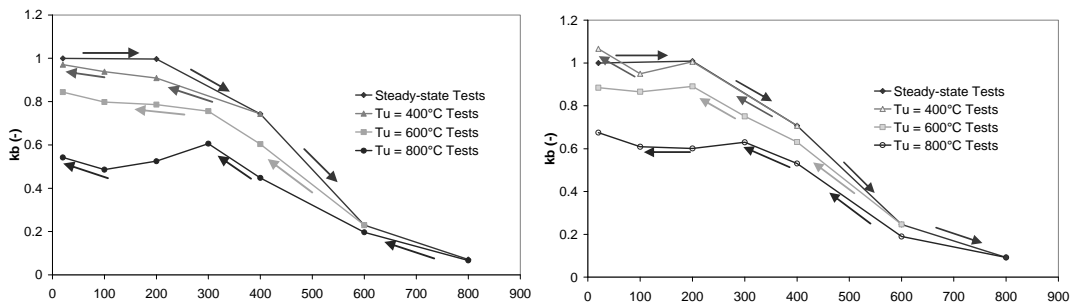


Figure 6. Reduction factor for bolt strength k_b in tension (left) and shear (right).

STRESS-STRAIN LAW FOR GRADE 8.8 BOLTS UNDER NATURAL FIRE

The ultimate bolt strength f_{ub,T_f,T_u} at a temperature T_f after the temperature has reached T_u at the end of the heating phase is given by Eq. 1, where k_b is the reduction factor for bolt strength during the heating phase (from EN 1993-1-2) and k_{nr} is a parameter accounting for the non-reversible behavior of bolts during the cooling phase (Eq. 2). The latter coefficient is equal to 1 if T_u is lower than 500°C and equal to 0.6 for T_u higher than 800°C ; a linear interpolation is proposed between these two values. The analytical and experimental values of the reduction factor k_b are plotted on Figure 7.

$$f_{ub}(T_f, T_u) = k_b(T_f) \cdot k_{nr,b}(T_f; T_u) \cdot f_{ub,20^\circ\text{C}} \quad (1)$$

$$k_{nr,b}(T_f; T_u) = \min\left(1; 1 - \frac{0.4}{300}(T_u - \max(T_f; 500^\circ\text{C}))\right) \quad (2)$$

The general shape of the stress-strain diagram proposed for bolts is given on Figure 8 and is composed of an elastic branch, an elliptic branch and a bilinear descending branch. The parameters f_p , f_t , ρ , ρ_u , ρ_t , and ρ_0 are defined in Eqs 3 to 7. The Young modulus E_{Tf} is supposed to be the same as the one of carbon steel at the temperature T_f and the coefficient k_p is given in Table 1. The analytical method is compared to experimental results on Figure 9.

$$f_{pb}(T_f, T_u) = k_p(T_u) \cdot f_{ub,20^\circ\text{C}} \quad (3)$$

$$f_{tb} = \max(f_{ub}; 500 \text{ MPa}) \quad (4)$$

$$\varepsilon_{pb} = f_{pb} / E_{Tf} \quad (5)$$

$$\varepsilon_{yb} = 0.02 \quad (6)$$

$$\varepsilon_{0b} = 0.15 + \max\left(0; 0.1 \cdot \frac{(\max(T_u; 800^\circ\text{C}) - 600^\circ\text{C})}{200^\circ\text{C}}\right) \quad (7)$$

T_u ($^\circ\text{C}$)	$k_{p,\theta}$ (-)
20	0.9
200	0.8
400	0.75
600	0.75
800	0.6
900	0.6

Table 1. Values of the factor k_p as a function of T_u

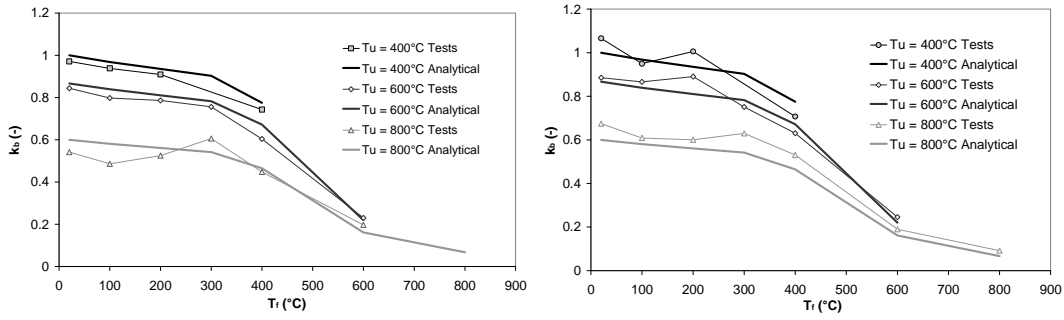


Figure 7. Reduction factor for bolt strength k_b in tension (left) and shear (right).

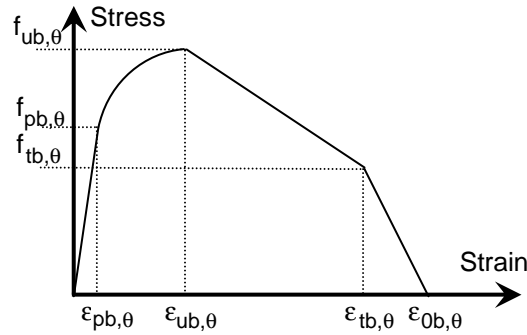


Figure 8. General shape of the stress-strain diagram for bolts.

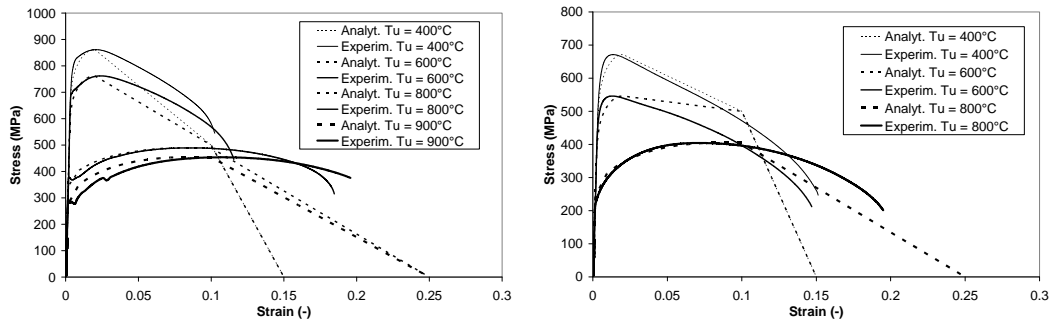


Figure 9. Comparison between analytical and experimental stress-strain curves: $T_f = 20^\circ\text{C}$ (left) and $T_f = 400^\circ\text{C}$ (right).

EXPERIMENTAL TESTS PERFORMED ON BUTT WELDS.

Tests have been performed on butt welds joints subjected to transversal tensile forces in order to characterize the evolution of welds resistance during a natural fire (Figure 10). For temperatures T_u lower than or equal to 600°C , welds recover their initial strength f_{uw} (Figure 11). When T_u is equal to 800°C or 900°C , the reduction of the ultimate strength after a complete heating-cooling cycle is around 20% of the initial ultimate strength. The ultimate strength of welds $f_{u,welds}$ during the cooling phase is expressed by Eq. 8, where the coefficient for the non-reversible behavior of welds $k_{nr,welds}$ is given by Eq. 9. The analytical values of the reduction factor for

welds k_w and the factor accounting for the non-reversible behavior of welds $k_{nr,welds}$ are compared to experimental results on Figures 11 and 12.

$$f_{u,welds}(T_f, T_u) = k_w(T_f) \cdot k_{nr,welds}(T_f, T_u) \cdot f_{u,welds}(20^\circ C) \quad (8)$$

$$\begin{cases} T_u \leq 600^\circ C \rightarrow k_{nr,welds} = 1 \\ 600^\circ C < T_u \leq 800^\circ C \rightarrow k_{nr,welds} = 1 - 0.2 \times (T_u - \max(T_f; 600)) \\ 800^\circ C < T_u \leq 900^\circ C \rightarrow k_{nr,welds} = 1 - 0.2 \times (800 - \max(T_f; 600)) \end{cases} \quad (9)$$



Figure 10. Specimen submitted to transversal tensile forces during weld tests.

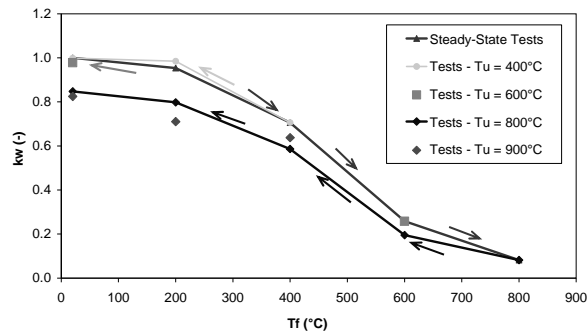


Figure 11. Experimental value of the reduction factor k_w during both the heating and cooling phases.

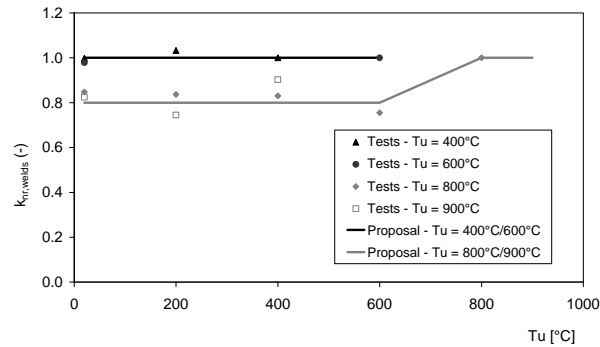


Figure 12. Comparison between the coefficients for non-reversible behavior of welds $k_{nr,welds}$ obtained experimentally and analytically.

CONCLUSIONS

Tensile and shear tests performed on bolts have demonstrated that a heating-cooling cycle implies two major modifications in the mechanical behavior of bolts. Firstly, the ultimate strength of bolts starts to reduce in a non-reversible manner when the temperature of bolts has reached 500°C. This reduction can be 40% of the initial bolt strength when the temperature has reached 800°C during the heating phase. Secondly, the ductility of bolts under tensile forces is significantly increased when the temperature T_u goes from 600°C to 800°C.

Tests on welds have also shown a reduction in strength but the reduction of ultimate strength of welds after a complete heating-cooling cycle is limited to 20% of the initial ultimate strength.

ACKNOWLEDGEMENTS

The article describes a part of the output of the COSSFIRE Research Project. The Research Fund for Coal and Steel is gratefully acknowledged for its financial support. Dr Bin Zhao from CTICM (France), Dr George Koutlas (UK) and Arnoud Breunese from Efectis Netherlands (NL) are also thanked for their active collaboration in the work presented by this article.

REFERENCES

1. Lapwood D.G. "The Effect of Fire Damage on the Mechanical Properties of Structural Steels Assessed Using Laboratory Heat Treatment Simulations", British Steel Report No T/RS/1189/8/80/C (1980).
2. Riaux H. "Comportement à l'incendie des assemblages simples boulonnés" (in French), Ph.D. Thesis, INSA Rennes, France (1980).
3. EN 1993-1-2 – Eurocode 3 "Design of steel structures—Part 1-2: Structural fire design", European Committee for Standardization, CEN, Brussels (2004).
4. Kirby, B.R. "Behaviour of High-Strength Grade 8.8 Bolts in Fire", Journal of Constructional Steel Research, Vol. 33, pp. 3-38 (1995).
5. Gonzalez F., Lange J. "Material Behaviour of High Strength Grade 10.9 Bolts under Fire Conditions", Fifth Conference on Steel and Composite, Graz, Austria (2008).
6. Latham D.J., Kirby B.R. "Elevated Temperature Behavior of Welded Joints in Structural Steelwork", Contract ECSC 7210 SA 824 (1993).

Investigations on the Behavior of Steel Single Plate Beam End Framing Connections in Fire

G. HU, E. SCHELL and M. D. ENGELHARDT

ABSTRACT

This paper summarizes the results of on-going computational and experimental investigations on the behavior of steel simple beam end framing connections subjected to fire. Connections are critical elements in maintaining the integrity of a structure during a fire. Fire can cause large force and deformation demands on connections during both the heating and cooling stages of a fire, while reducing connection strength and stiffness.

In the US, one of the most common types of simple beam end framing connections is the single plate connection. In order to better understand the behavior of this type of connection in fire, an extensive series of computational and experimental investigations are underway by the authors. The computational studies are investigating the typical behavior of the connection during heating and cooling phase of fires as well as the connection force and deformation demands. Experimental studies are also underway on connections at elevated temperatures to validate predictions of connection capacity developed by computational and design models as well as providing knowledge of failure modes. This paper will present key results from this study to date.

Guanyu Hu (Corresponding author), Graduate Student, Ferguson Structural Engineering Laboratory, University of Texas at Austin, Austin, TX 78758

Eric Schell, Electronics Engineer, Ferguson Structural Engineering Laboratory, University of Texas at Austin, Austin, TX 78758

Michael D. Engelhardt, Professor, Ferguson Structural Engineering Laboratory, University of Texas at Austin, Austin, TX 78758

INTRODUCTION

In fire, large axial forces can be generated in steel beams and beam end connections. These forces are initially compressive, while later on with temperature increasing, can become tensile due to catenary action. In addition, in the cooling stage of a fire, thermal shrinkage of the beam can generate large tensile forces in the beam and beam end framing connections. Both the compression and tension forces developed during a fire are not usually considered in the beam end framing connection design process and thus can lead to connection failure (Figure 1). This, in turn, can lead to collapse of the beam and potentially to buckling of a column resulting from the loss of bracing from the beam [1]. In US building construction practice for structural steel buildings, the most widely used steel simple beam end framing connection is the single plate connection (also referred to as a “shear tab” or “fin plate” connection). Normally designed to take shear force only, single plate connection can be vulnerable to failure under large axial loads and rotation demands resulting from a fire. Fire induced single plate connection failures have been observed in the Cardington Fire Test in UK [2] and World Trade Center Building 5 [3] which was subjected to large fire in the event of 9/11 (Figure 2). Connection failure was also believed to play a key role in the collapse of the 47-story World Trade Center 7 Building on 9/11 [1]. Therefore, a good understanding of the performance of beam end connections in fire becomes essential.

In recent years, some research work has focused on the behavior of simple beam connections in fire. Although some progress has been made in understanding the overall response of connections subject to fire, large gaps still exist. Specifically, force and deformation demands on single plate connections, as well as connection strength and deformation capacities during a fire are not well understood, particularly from a design perspective. In addition, failure modes of these connections under axial forces at elevated temperatures are not adequately understood. In this paper, the finite element method is used to characterize force and deformation demands on the connections in fire. Further, real scale single plate connection tests at elevated temperatures were conducted to characterize connection strength and deformation capacity at elevated temperatures. Finite element analysis was also used to simulate the experiments and to compare with the test results.



Figure 1. Failure of single plate connection in Cardington tests. [2].

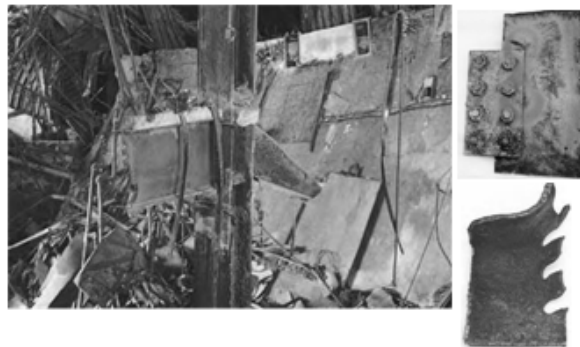


Figure 2. Failure of shear connections in fire of WTC 5. [3].

FINITE ELEMENT ANALYSIS

Finite Element Model

In this study, the ABAQUS (Version 6.7-4) finite element (FE) program was used to conduct all the analyses. A three-dimensional brick element was employed in all the connection components. The FE model details are given by the authors in another paper [4]. Limited validation of the finite element models was done by comparison with existing experimental data of connection tests under ambient and high temperatures.

As an example of the type of analyses undertaken to study connection force and deformation demands, a 30 feet (9.14 m) long W16x36 steel floor beam with three bolt single plate connections at its ends was simulated in fire conditions. Temperature was assumed to be uniform in the beam and beam end connections. A325 bolts were used in the model, and the strengths at elevated temperatures reported in tests by Yu [5] were used in the FE analysis. The steel beam was assumed to be made of ASTM A992 structural steel, which is the most common grade of structural steel currently used for wide flange shapes in the US. The properties of A992 steel at elevated temperatures tested by Hu *et al* [6] were employed in the FE model. Uniformly distributed loads were applied on the top of the beam with a constant load ratio of 1/2. Transient-state analysis was performed, meaning that in the analysis, the load applied on the beam was held constant, while temperature was changing. In this study, the temperature was increased to 650 °C and then cooled back down to 20 °C.

Connection Forces and Beam Deflection

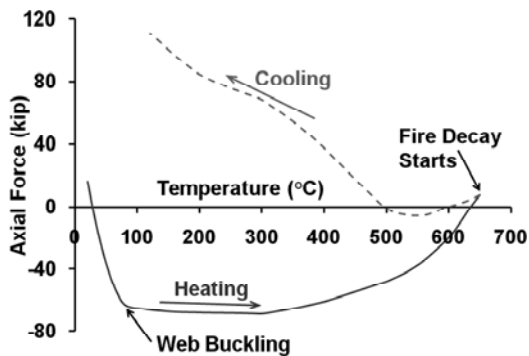


Figure 3. Connection axial force - temperature response in fire.

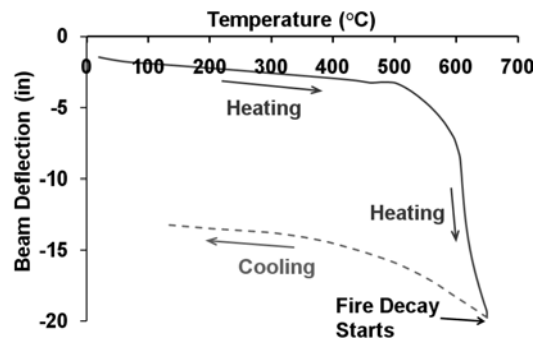


Figure 4. Beam mid span deflection - temperature response.

Figures 3 and 4 plot connection axial force and beam mid span deflection versus temperature during the heating and cooling phases of the fire. From Figure 3, it can be noted that during a fire, large axial compression and tension forces can be produced at the beam end connections. In Figure 4, it can be seen that large connection rotations and beam deflections can occur during a fire. Further, if the

beam has already entered the “run away” stage and experienced large deformations during heating, the deflection can only be partially recovered in the cooling phase, resulting in the beam with a large permanent residual deflection after the fire. In this analysis, the connection failed in the cooling stage of the fire due to large tension, which indicates that connections can be vulnerable to failure during the decay phase of a fire.

Resultant Shear Forces in Bolts

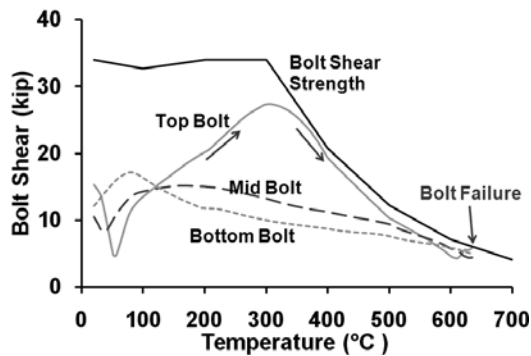


Figure 5. Bolt shear forces during heating.

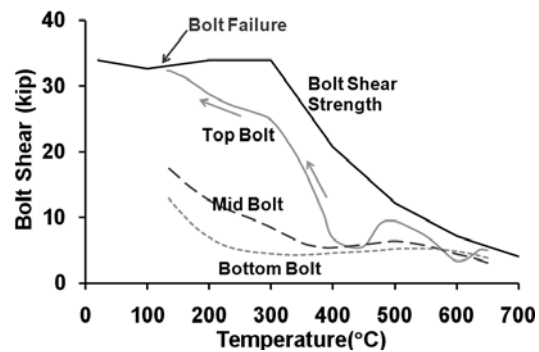


Figure 6. Bolt shear forces during cooling.

Figures 5 and 6 show the resultant shear forces in the three bolts during heating and cooling stage, respectively. Also plotted on these figures is the variation of bolt shear strength with temperature. In the heating stage, the top bolt experienced a larger shear force than the other two for most of the temperature range. For this analysis, the largest shear force in the top bolt occurred at temperatures in the range of 300°C to 400°C, when the beam was still expanding outward and the connection was under compression. However, bolt shear failure did not occur, as the bolt shear strength is still relatively high at these temperatures. With further increases in temperature, bolt shear force decreased significantly due to large connection rotations caused by the degradation of material strength and stiffness in the steel beam. After the temperature reaches 600°C the bolt shear force increased again slightly when axial tension starts to develop at the connection due to catenary action in the beam. The increasing bolt shear force may cause connection failure if the temperature keeps increasing and larger catenary forces develop. If the fire stops before failure of the connection and the cooling phase starts, shear forces in all bolts will significantly increase with temperature decrease, as shown in Figure 6. However, bolt shear strength also increases as temperature decreases. In the fire cooling phase, under this large tension, the top bolt still experienced the largest shear force among the three bolts. Also, as illustrated in Figures 5 and 6, predicting bolt shear failure in a fire is complex since both the bolt shear force and bolt shear strength vary with temperature. Consequently, bolt shear failure does not necessarily occur when the bolt shear forces are at their highest. Similarly, bolt shear failure may not occur when the bolt shear strength is at its lowest. Ultimately,

in this analysis, the top bolt failed in the cooling stage of the fire. It is noted that, for the analysis in cooling phase, bolt shear strengths were assumed to be same with those in heating phase. However, Yu [5] observed that if the bolts are exposed to a temperature higher than the manufacturing tempering temperature, the post fire residual strengths of bolts will be reduced from their original value. Therefore, the connections can be even more vulnerable in cooling than the analysis showed.

CONNECTION TESTS AT ELEVATED TEMPERATURES

Observations from major building fire events and the Cardington fire test showed that common failure modes seen in single plate connections subjected to fire are plate bearing failure and bolt shear failure. Based on the finite element analyses described above, these connection failures are mainly caused by large axial forces during heating and cooling phases of a fire. Therefore, the load and deformation capacities of the connections under axial load become key factors that influence performance in fire. In this section, a series of connection tests under axial tension at elevated temperatures are carried out to further investigate connection performance.

Test Setup

A 550 kip capacity MTS test frame (Figure 7) was used to conduct these connection tests. Specimens were heated using an Applied Test Systems, Inc. split box furnace with a 54 in. x 27 in. x 17 in. heated enclosure. The furnace uses electrical heating elements with a 1000 °C heating capacity.

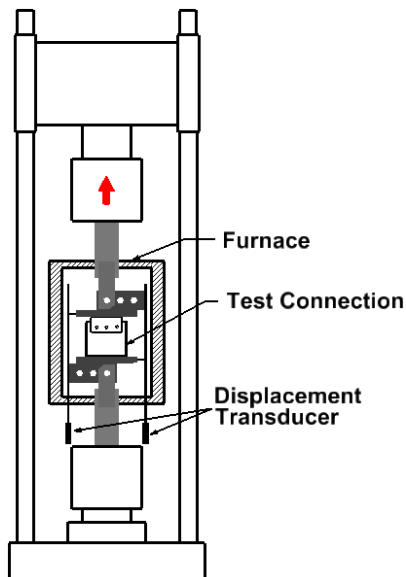


Figure 7. Test setup.

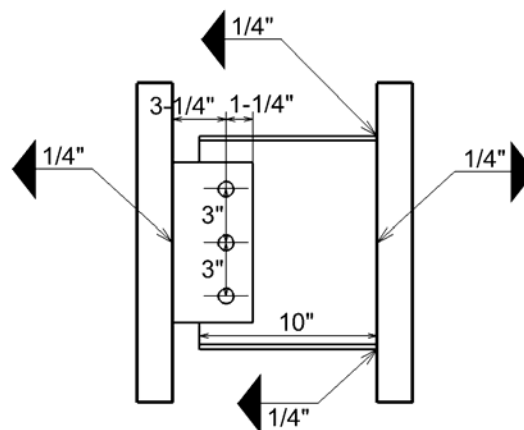


Figure 8. Test specimen dimensions

In the five tests conducted to date, two specimens were cut from a W12x40 wide flange shape and three from a W12x26. Both shapes were made from Grade 50 (minimum specified $F_y = 50$ ksi) structural steel. Beam sections were connected to 3/8 in (9.525 mm) single plates which were made from A36 structural steel with three hand tightened 3/4 in (19.05 mm) diameter A325 structural bolts. Threads were excluded from the shear plane of the bolts. Single plates and beam sections were welded to two loading plates by 1/4" (6.35 mm) fillet welds. Connection dimensions follow the standard dimension requirements of the AISC Specification [7] (Figure 8). Material properties of connection parts at ambient temperature were determined by experiments.

Thermocouples were attached to beam web, single plate and bolts to measure the surface temperature of the specimens at different locations. All tests were thermal steady state tests, in which the specimens were heated up to a target temperature and then loaded to failure while maintaining the same temperature. During the heating process, the load was maintained at zero to allow free expansion of the specimen. Besides being thermal steady state, all tests were displacement-controlled, in which a crosshead displacement rate of 0.05 in/min (1.27 mm/min) were maintained at a constant value throughout a test. The W12x26 specimens were tested at temperatures of 20 °C, 400 °C and 700 °C. Ambient temperature and 600 °C tests were conducted on the W12x40 specimens. The load on the test specimens were measured using the load cell in the MTS test frame. Displacements were measured by displacement transducers attached on two stainless steel rods extending outside of the furnace (Figure 7).



Figure 9. W12x26 connections after testing at 20°C, 400°C, 700°C (left to right).

Test Results

A summary of the test results is given in Table I. Figure 9 shows the W12x26 connections after testing. At ambient temperature, bearing failure at bolt holes of the beam web was the major failure mode, with little shear deformation observed in the bolts. At 400°C, the connection still failed due to tear out of beam web, but some amount of bolt shear deformation can be observed. Further, at higher

temperatures (600°C and 700°C) little permanent deformation of the bolt holes was observed after the tests, and connections failed by shear fracture of the bolts. This phenomenon implies that structure bolts have a larger strength reduction rates than structural steel of beams and plates with temperature increase. This is consistent with the strength reduction factors of bolts and carbon steel in Eurocode 3 [8]. Figure 10 shows the load-displacement relationships of the W12x26 specimens. As the temperature increased from 20°C to 400°C, the connection failure mode remained the same (bearing failure) but connection deformation capacity was smaller. This is consistent with test results on A992 structural steel at elevated temperatures [6], which show reduced material ductility at 400°C

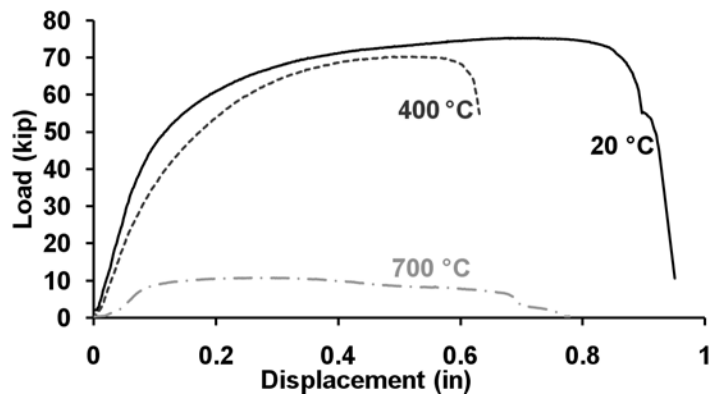


Figure 10. Load displacement responses of W12x26 connections.

Comparison with Finite Element Connection Model

To compare FE predictions with the test results, measured material properties at ambient temperature were employed in the FE model. For elevated temperatures, reduction factors for ASTM A992 steel reported by Hu et al [6] and reduction factors for A325 bolts reported by Yu [5] were used in the analysis. The comparisons of peak load obtained from FE analysis with test results are also shown in Table I. In general, the peak loads predicted by the FE analysis compared well with the tests.

Table I. TEST RESULTS.

Specimen	Temperature (°C)	Test Peak Load (kip)	FE Peak Load (kip)	Failure Mode
W12x40	23	109.4	110.8	Bearing/Fracture
W12x40	608	20.6	22.0	Bolt Shear
W12x26	23	75.3	81	Bearing
W12x26	405	70.1	67.4	Bearing
W12x26	702	10.8	12.1	Bolt Shear

CONCLUSIONS

This paper has presented highlights of on-going research on the behavior of steel single plate beam end connections in fire. A three-dimensional finite element model incorporating contact, geometric and material nonlinearity was used to study the connection behavior in fire. Tests on single plate connections subject to tension at elevated temperatures were also conducted to obtain further data and insights into connection behavior. Connection strengths at elevated temperatures were also evaluated using finite element analyses, and reasonable agreements were obtained between test results and FE model predictions. The research work presented in this paper is on-going. More connections with various loading parameters and connection details will be tested at elevated temperatures to provide further understanding of the behavior and controlling failure modes of the connections, and to provide further data for validation of modeling techniques.

ACKNOWLEDGEMENTS

This research is supported by the National Science Foundation (NSF Award 0700682). Elevated temperature tests were conducted using equipment procured through an NSF Major Research Instrumentation Grant (NSF Award No. CMS-0521086—*Acquisition of a High-Temperature Testing Facility for Structural Components and Materials*). The support of the National Science Foundation and of NSF Program Directors M.P. Singh and Douglas Foutch are gratefully acknowledged.

REFERENCES

1. NIST, "Final Report on the Collapse of World Trade Center Building 7," Report NIST NCSTAR 1A, National Institute of Standards and Technology, Gaithersburg, MD, November 2008.
2. Cardington Fire Test Report. "The Behavior of Multi-storey Steel Framed Building Subject to Fire Attack," Experimental Data, British Steel, Swinden Technology Center (1998).
3. FEMA, "World Trade Center Building Performance Study: Data Collection, Preliminary Observations, and Recommendations," FEMA 403, Federal Emergency Management Agency, Washington, DC (2002).
4. Hu, G. and Engelhardt, M.D., "Studies on the Behavior of Steel Single Plate Connections in Fire," *Proceedings, the Second International Workshop on Performance, Protection & Strengthening of Structures under Extreme Loading*, Hayama, Japan, August. 19-21, 2009.
5. Yu, L., "Behavior of Bolted Connections During and After a Fire," *Ph.D. Dissertation*, Department of Civil, Architectural and Environmental Engineering, University of Texas at Austin (2006).
6. Hu, G., Morovat, M.A., Lee, J., Schell, E. and Engelhardt, M.D., "Elevated Temperature Properties of ASTM A992 Steel," *Proceedings of ASCE Structure Congress 09*, April.30-May.2, Austin, TX, USA (2009).
7. AISC, "Specification for Structural Steel Buildings, Standard ANSI/AISC 360-05," American Institute of Steel Construction, Inc, Chicago, IL (2005).
8. EN 1993-1-2 European Committee for Standardisation. CEN, Eurocode 3: Design of steel structures. Part 1-2: General rules. Structural fire design (2005).
9. Yu, H., Burgess, I.W., Davison, J.B., Plank, R.J., "Experimental Investigation of the Behavior of Fin Plate Connections in Fire," *Journal of Constructional Steel Research*, 65(3): 723-746 (2009).
10. ABAQUS Version 6.7 User's Manual. Hibbit, Karlsson, & Sorensen, Inc., Pawtucket, RI, 2007.

A Simplified Model for Modelling End-Plate Connections in Fire

Z. HUANG

ABSTRACT

In this paper a robust 2-noded connection element has been developed for modelling the bolted end-plate connection between steel beam and column at elevated temperatures. In this model the connection failure due to bending, axial tension and compression, and vertical shear are considered. Also the influence of the axial force of the connected beam on the connection is taken into account. A total of 18 fire tests were employed to validate the model, 8 of which are presented in this paper. It is evident that the current model is robust and has a capability to predict the behaviour of bolted end-plate connection in fire with reasonable accuracy. The idea described in this paper can also easily be applied to develop other kind of connections.

INTRODUCTION

Structural engineers and architects have a responsibility for incorporating fire safety into their building designs in order to minimize loss of life and property. One aspect of this is to ensure that structural stability is maintained if a fire develops. It is well known that robustness of steel connection is vital important to the fire resistance of steel-framed composite buildings. In recent years, a large amount of research has been conducted on the behaviour of steel connections at elevated temperatures [1-5]. Currently, there have mainly three approaches which can be adopted for modelling the behaviour of connections:

- 1) to represent the moment-rotation characteristics of a connection by mathematical expression (in the form of curve-fitting equations) [2];
- 2) to use component-based (also known as spring-stiffness) models for predicting the connection's behaviour [3];
- 3) to model the connection as assembly of 3D finite shell, brick and contact elements [5].

It is obvious that the first method is very simple, however test data is

Zhaohui Huang (corresponding author), Lecturer, Department of Civil & Structural Engineering, University of Sheffield, Sheffield, S1 3JD, UK

needed for individual connections, and the influence of the axial force of beam on the connection is ignored. The component-based model is now becoming popular to be used for modelling the responses of connections subject to fire attack. Due to the complexity of the connection's behaviour in fire it is not an easy task to precisely determine the characteristic of spring for each component. The third method can be attempted using general commercial software, such as ABAQUS or ANSYS. However, because of the computational cost it is difficult to use this approach for analysis of global structures or sub-structures.

The main objective of this paper is to present the new development of a robust 2-noded connection element for modelling the bolted end-plate connection between steel beam and column at elevated temperatures. The model developed here has the advantages of both simple and component-based models.

DEVELOPMENT OF THE CONNECTION ELEMENT

As shown in Fig. 1 the bolted end-plate connection element is a specialized two-noded element of zero length, which has three translational degrees of freedom u , v , w and three rotational degrees of freedom θ_x , θ_y , θ_z at each node, where x , y , z are local coordinates of steel beam element in which x is the direction of longitudinal axis of the beam element. When modelling composite construction it is common practice to position the nodes of the slab and the beam elements at the reference plane, which is normally located at the middle of the slab element. Therefore, the nodes of the connection element have to be placed at the reference plane. In order to do this the connection element should have the same offset as the beam element.

In this research, for simplicity, it is assumed that there is no coupling of effects due to different degrees of freedom for the connection element, hence in the local co-ordinates the nodal force increment vector, $\Delta \mathbf{F}$ of the element can be related to its nodal displacement increment vector $\Delta \mathbf{u}$ as:

$$\begin{Bmatrix} \Delta F_{x,1} \\ \Delta F_{y,1} \\ \Delta F_{z,1} \\ \Delta M_{x,1} \\ \Delta M_{y,1} \\ \Delta M_{z,1} \\ \Delta F_{x,2} \\ \Delta F_{y,2} \\ \Delta F_{z,2} \\ \Delta M_{x,2} \\ \Delta M_{y,2} \\ \Delta M_{z,2} \end{Bmatrix} = \begin{bmatrix} k_{11} & 0 & 0 & 0 & -k_{11}\ell & 0 & -k_{11} & 0 & 0 & 0 & k_{11}\ell & 0 \\ 0 & k_{22} & 0 & 0 & 0 & 0 & 0 & -k_{22} & 0 & 0 & 0 & 0 \\ 0 & 0 & k_{33} & 0 & 0 & 0 & 0 & 0 & -k_{33} & 0 & 0 & 0 \\ 0 & 0 & 0 & k_{44} & 0 & 0 & 0 & 0 & 0 & -k_{44} & 0 & 0 \\ -k_{11}\ell & 0 & 0 & 0 & (k_{55} + k_{11}\ell^2) & 0 & k_{11}\ell & 0 & 0 & 0 & -(k_{55} + k_{11}\ell^2) & 0 \\ 0 & 0 & 0 & 0 & 0 & k_{66} & 0 & 0 & 0 & 0 & 0 & -k_{66} \\ -k_{11} & 0 & 0 & 0 & k_{11}\ell & 0 & k_{11} & 0 & 0 & 0 & -k_{11}\ell & 0 \\ 0 & -k_{22} & 0 & 0 & 0 & 0 & 0 & k_{22} & 0 & 0 & 0 & 0 \\ 0 & 0 & -k_{33} & 0 & 0 & 0 & 0 & 0 & k_{33} & 0 & 0 & 0 \\ 0 & 0 & 0 & -k_{44} & 0 & 0 & 0 & 0 & 0 & k_{44} & 0 & 0 \\ k_{11}\ell & 0 & 0 & 0 & -(k_{55} + k_{11}\ell^2) & 0 & -k_{11}\ell & 0 & 0 & 0 & (k_{55} + k_{11}\ell^2) & 0 \\ 0 & 0 & 0 & 0 & 0 & -k_{66} & 0 & 0 & 0 & 0 & 0 & k_{66} \end{bmatrix} \begin{Bmatrix} \Delta u_1 \\ \Delta v_1 \\ \Delta w_1 \\ \Delta \theta_{x,1} \\ \Delta \theta_{y,1} \\ \Delta \theta_{z,1} \\ \Delta u_2 \\ \Delta v_2 \\ \Delta w_2 \\ \Delta \theta_{x,2} \\ \Delta \theta_{y,2} \\ \Delta \theta_{z,2} \end{Bmatrix} \quad (1)$$

In this model only the in plane (x - z plane) behaviour of the connection is considered. It is therefore reasonable to assume that the stiffness coefficients of k_{22} , k_{44} , k_{66} in Eq. (1) have infinite magnitude (10^9 kN/mm). In current model a very simplified approach was used to determine the axial stiffness of connection element, k_{11} . That is, before the connection failure k_{11} has infinite magnitude (10^9

kN/mm) and when the connection fails due to tension or vertical shear $k_{11} = 0$. However, when the connection failed by compression it is assumed that $k_{11} = 10^9 kN/mm$. The same principal was used for determination of vertical stiffness of the connection, k_{33} . It is assumed that before the connection failure due to vertical shear k_{33} has infinite magnitude ($10^9 kN/mm$) and after the connection fails by vertical shear, $k_{33} = 0$.

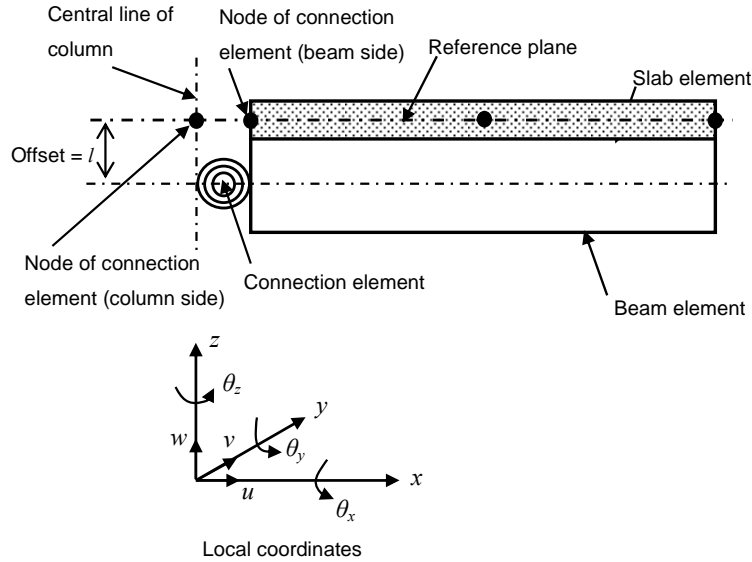


Figure 1. Two-noded connection element configuration.

The detail of the bolted end-plate connection between steel column and beam is shown in Fig. 2. The rotational stiffness of a connection should be determined from the flexibilities of its basic components, each represented by an elastic stiffness coefficient k_i . A typical moment-rotation characteristic for a connection can be represented as curve OABC (solid line as shown in Fig.3). In the figure Φ_{Xd} is the rotation at which the bending moment applied to a connection $M_{j,Ed}$ first reaches the moment resistance $M_{j,Rd}$. Φ_{Cd} is the rotation capacity of a connection, which is equal to the maximum rotation of the moment-rotation characteristic. In this model, it is a conservative assumption to use tri-linear O-A-B-C (broken line as shown in Fig. 3) to represent the moment-rotation characteristic for a connection.

Therefore, the moment-rotation characteristic of an end-plate connection can be expressed as (see Fig. 3): for line OA ($\phi \leq \phi_{Id}$):

$$M_j = k_{55} \phi = S_{j,ini} \phi \quad (2)$$

where, $k_{55} = S_{j,ini}$. For line AB ($\phi_{Id} < \phi \leq \phi_{Xd}$):

$$M_j = k_{55} (\phi - \phi_{Id}) + \frac{2}{3} M_{j,Rd} \quad (3)$$

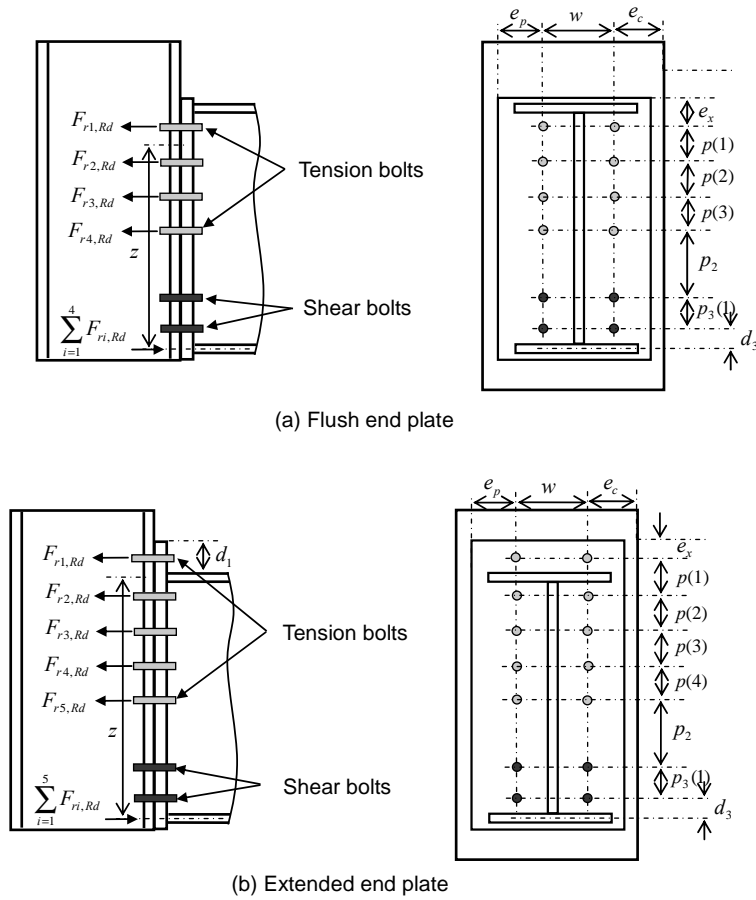


Figure 2. The detail of bolted end-plate connection between steel column and beam.

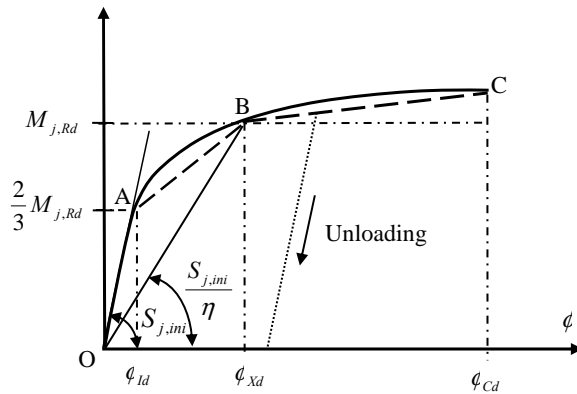


Figure 3. Tri-linear moment-rotation characteristic used for the connection element.

where, $k_{55} = \frac{M_{j,Rd}}{3(\phi_{Xd} - \phi_{1d})}$. For line BC ($\phi_{Xd} < \phi \leq \phi_{Cd}$):

$$M_j = k_{55} (\phi - \phi_{Xd}) + M_{j,Rd} \quad (4)$$

where, $k_{55} = 0.065 S_{j,ini}$. If $\Phi > \Phi_{Cd}$ the connection is assumed to be broken, hence $M_j = 0$ and $k_{55} = 0$.

In order to consider the influence of co-existing axial force $N_{j,Ed}$ in the

connected member on the moment resistance of a connection $M'_{j,Rd}$ the following equation is proposed:

$$M'_{j,Rd} = \left(1.0 - \left(\frac{N_{j,Ed}}{N_{j,Rd}} \right)^B \right) M_{j,Rd} \quad (5)$$

where $N_{j,Rd}$ is axial tension resistance of the connection, assuming no applied moment; $B = f_{y,T} / f_{y,20}$ in which $f_{y,T}$ and $f_{y,20}$ are the yield strength of steel at elevated temperatures and ambient temperature, respectively.

In the model developed above, the calculations of the moment resistance $M_{j,Rd}$, initial stiffness $S_{j,ini}$, compression, tension and vertical shear resistance of the end-plate connection was mainly based on the ambient temperature formulations proposed in Eurocode 3 Part 1.8 [6] and the model is extended into fire conditions by relating all material properties, such as yield strength; ultimate tensile strength and Young's module to the temperature. It is assumed that the material degradation of bolt at elevated temperatures is the same for the beam, column and end plate and the model specified in Eurocode 3 Part 1.2 [7] is adopted in this research.

VALIDATIONS

In order to validate the model developed, a series of validations were conducted. In this section, the results of 8 fire tests were presented to demonstrate the robustness and accuracy of the model.

Connections Tested without Axial Force

Leston-Jones [1] conducted a total of four cruciform fire test on flush end-plate connection with three bolt rows (M16-8.8) connecting beam (254x102x22UB) and column (152x152x23UC). In those tests different load levels were applied to the connection for individual tests. The load levels applied to Test 1, Test 2, Test 3 and Test 4 were 5 kNm, 10 kNm, 15 kNm and 20 kNm, respectively. In the current model the temperature distribution within the connection are considered and the end-plate connection is divided into several regions. For the modelling the tested temperature distribution within the connection was used as input data for individual tests. In this research all four tests were modelled and the comparisons of the predicted connection rotation (which is referenced to ambient temperature) with the test results for Tests 1 and 3 are shown in Fig. 4 together with the predictions by Block et al [3] which considered bolt rows as a group. It is evident that results predicted by the current model agree reasonably well with the test results and the component model's predictions.

Connections Tested with Axial Force

A total of 12 tests on the flush end-plate connection with three bolt rows (M20-8.8) connecting beam (305x165x40UB) and column (254x254x89UC) at elevated temperatures were conducted at the University of Sheffield during 2007

and 2008. A force (P) with inclined angle (θ) to the axis of connected beam was applied at a distance of 630mm away from the axis of column to generate axial, vertical forces and moment on the connection tested. Three angles, $\theta = 35^\circ, 45^\circ$ and 55° , were employed and three temperatures, $450^\circ\text{C}, 550^\circ\text{C}$ and 650°C , were used. The detail information of the tests can be freely downloaded from the Sheffield Research Group web site.

In this research all 12 tests were modelled to validate the model developed. Due to the space limit only 4 tests, at temperatures, $450^\circ\text{C}, 550^\circ\text{C}$ and 650°C , and the applied load P angles, $\theta = 35^\circ, 45^\circ$ and 55° , are presented in Figs 5 and 6. It is clear that axial force has a significant affect on the connection behaviour, especially at high temperatures. A good agreement was achieved between the tested results and current model's predictions.

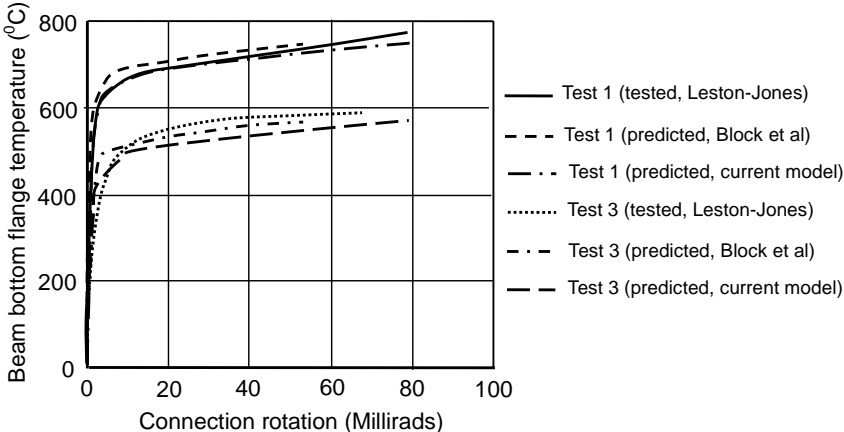


Figure 4. Comparison of predicted and measured connection rotations at elevated temperatures for Test 1 and Test 3 [1].

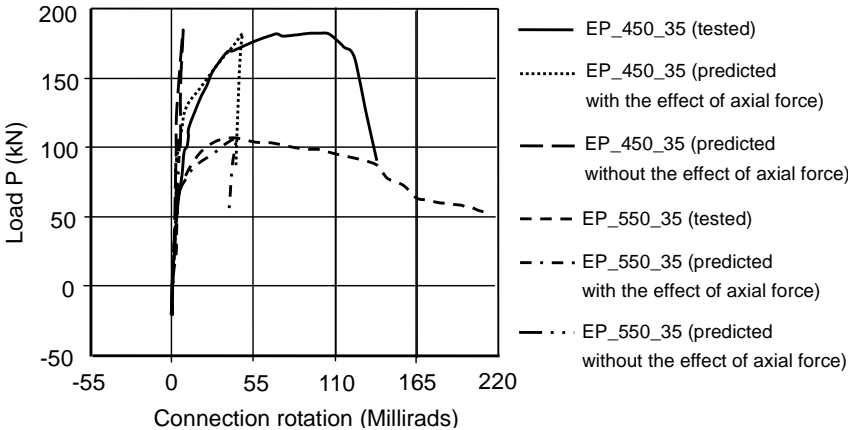


Figure 5. Comparison of predicted and measured connection rotations for Tests EP_450_35 and EP_550_35 (Sheffield tests).

Fire Tests on a Beam-to-Column Substructure

A series of fire tests on a steel sub-frames composed by two thermally insulated HEA300 cross-section columns and an unprotected IPE300 cross-section beam with 5.70 m free span was conducted at the University of

Coimbra [4]. A natural fire which includes heating and cooling phases was used in the tests. In this study two tests, EJ01 and FJ03 were modelled. EJ01 is the extended end-plate connection with three bolt rows (M20-8.8) and FJ03 is the

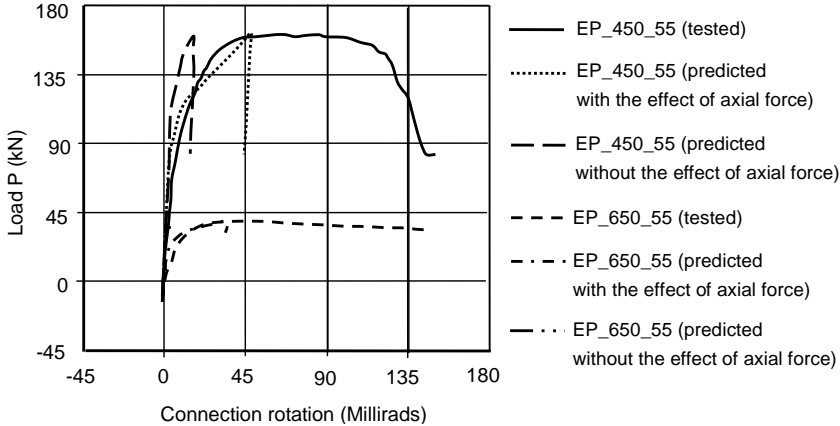


Figure 6. Comparison of predicted and measured connection rotations for Tests EP_450_55 and EP_650_55 (Sheffield tests).

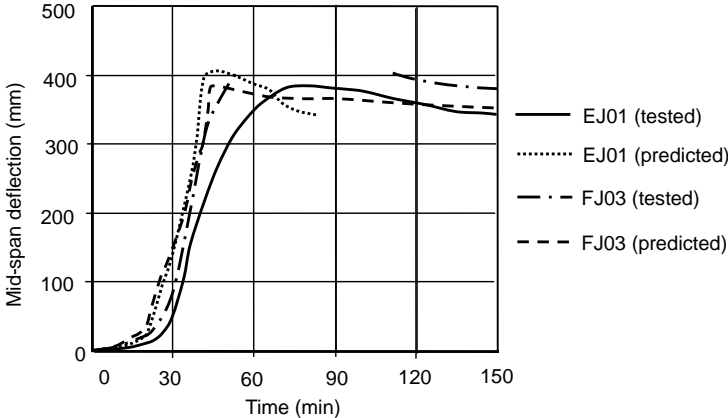


Figure 7. Comparison of predicted and measured beam's mid-span deflections for Tests EJ01 and FJ03 [4].

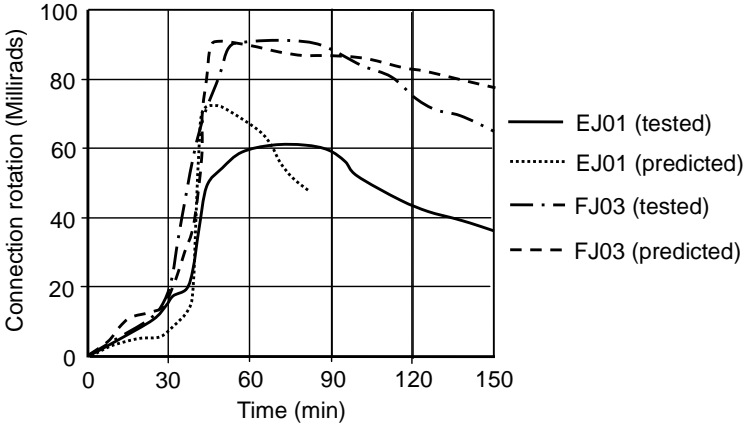


Figure 8. Comparison of predicted and measured connection rotations for Tests EJ01, FJ03 [4].

flush end-plate connection with two bolt rows (M20-8.8). All tested material properties and temperatures were used as input for the modelling. For EJ01 the maximum beam temperature of 898⁰C was reached at about 50 min then cooled down to about 180⁰C at 150 min. For FJ03 the maximum beam temperature of 900⁰C was reached at about 40 min and kept almost constant until 50 min then cooled down to about 200⁰C at 150 min. Fig. 7 shows the comparison of predicted and measured beam's mid-span deflections for both tests. The comparison of predicted and measured connection rotations of the tests is shown in Fig. 8. The predictions of current model were in reasonable agreement with test results. It is difficult to precisely use all tested temperatures for the structure modelled, especially for the connections.

CONCLUSIONS

In this paper a robust 2-noded connection element has been presented for modelling the bolted end-plate connection at elevated temperatures. The model has the advantages of both simple and component-based models. In this model the connection failure due to bending, axial tension and compression, and vertical shear are considered. Also the influence of axial force of the connected beam on the connection is taken into account. The current model also allows for a non-uniform temperature distribution within the connection. In this research a total of 18 fire tests were used to validate the model in which 8 tests were presented in this paper. It is evident that the current model is robust and has a capability to predict the behaviour of bolted end-plate connection in fire with reasonable accuracy. Also the connection element developed allows the element nodes to be placed at reference axis with offset. Hence, the model can be used for structural fire engineering design on steel-framed composite buildings. The idea described in this paper can also easily be applied to develop other kind of connections.

REFERENCES

1. Leston-Jones, L.C., "The influence of semi-rigid connections on the performance of steel framed structures in fire", Ph.D. Thesis, University of Sheffield, Sheffield, (1997).
2. Al-Jabri, K.S., et al, "Moment-rotation-temperature curves for semi-rigid joints", *Journal of Constructional Steel Research*, 61, (2005), pp. 281-303.
3. Block, F.M., et al, "The development of a component-based connection element for endplate connections in fire", *Fire Safety Journal*, 42, (2007), pp. 498-506.
4. Santiago, A., "Behaviour of beam-to-column steel joints under natural fire", Ph.D. Thesis, University of Coimbra, (2008).
5. Qian, Z. H., et al "Numerical and analytical investigations of steel beam-to-column joints at elevated temperatures", *Journal of Constructional Steel Research*, 65, (2009), pp. 1043-1054.
6. Commission of the European Communities, "Design of steel structures, Part 1.8: Design of joints" *Eurocode 3*, Brussels, (2005).
7. Commission of the European Communities, "Design of steel structures, Part 1.2: General rules – structural fire design" *Eurocode 3*, Brussels, (2005).

Testing of Composite Top-and-Seat-and-Web Angle Joints at Ambient and Elevated Temperature

Y. ZHEN, T. K. HAI and T. S. KIONG

ABSTRACT

The paper presents the experimental results of six ambient tests and eight elevated temperature tests on composite top-and-seat-and-web (TSW) angle joints under monotonic loading. The main aim is to ascertain the moment-rotation characteristics of the composite TSW angle joints at both ambient and elevated temperatures, which could provide validation of the authors' proposed mechanical model. The experimental work is the first test programme to investigate the behaviour of composite TSW angle joints at elevated-temperatures. A comparison study with the test results shows that the authors' mechanical model is capable of giving close and consistent predictions of the joint behaviour. The knowledge gained from both experimental and analytical works would give deeper insight into the moment-rotation characteristics of composite TSW angle joints at elevated temperatures.

1. INTRODUCTION

In this area of composite steel construction, many research works have focused on the beam-to-column joints design because it is a critical design issue affecting structural performance and construction cost. In practice a typical composite joint is designed as either perfectly pinned or completely fixed. However, the actual joint behaviour falls in-between these two extreme cases and is conventionally classified as "semi-rigid" or "semi-continuous".

Composite top-and-seat-and-web (TSW) angle joints are commonly used in some seismic zones (USA, Japan) due to its high strength and ductility characteristics, large rotation range and good energy absorption capacity. However, there are limited test results on this type of joint at

School of Civil and Environmental Engineering, Nanyang Technological University, 50 Nanyang Avenue, Singapore

ambient condition, and under elevated temperature condition (if at all). Many experimental works had been conducted on composite joint behaviour since the 1970s (Zandonini [1]). Among them, most of the tests were conducted on limited types of steel joint, viz. flush or extended end plate joints, web-cleat, and top-and-seat angle joints. Moreover, most of the tests were conducted at ambient temperature; only a few full-scale joint tests on steel and composite flush/extended end plate joints were conducted under fire conditions (Leston-Jones [2], Al-Jabri [3]). To the authors' best knowledge, no elevated-temperature test has been conducted on composite TSW angle joints.

Hence, the objective of this paper is to present the test results of fourteen composite TSW angle joints: six ambient tests and eight elevated-temperature tests. It is to shed light on the behaviour of these joints at ambient and elevated temperatures. The test results were also used to validate the proposed mechanical model.

2. EXPERIMENTAL PROGRAMME

The test programme was included in Table I. In total, fourteen composite TSW angle joints were tested as "cruciform" assemblies under monotonic loading. Six of them were tested at ambient temperature and eight of them at elevated temperature between 400°C and 700°C to study the full-scale joint behaviour in fire.

The fourteen joint specimens were fabricated in two batches because of constraint of time and laboratory storage space. The cruciform specimens were designed to fit within existing electrical furnace at the fire laboratory at Nanyang Technological University, as shown in Fig. 1. All the steel beams supported the 130mm thick profiled steel decking with reinforced concrete slab. The concrete slab was connected to the steel beam with six 19mm x 95mm shear studs.

Parameters investigated included steel beam depth, different temperatures and failure mechanisms. Each series had two joint specimens fabricated to identical design details and tested at the ambient temperature. The purpose was to minimise the systematic errors of control specimens so that they could serve as reference points for ensuing elevated-temperature tests.

2.1 Test Setup

During the test, the cruciform specimen was inverted inside the furnace and loaded centrally to the column stub, due to load frame set-up (Yuan [4]). It should be noted that for ease of readers, the steel beam flange in contact with the profile decking slab will be referred to as the top flange in the ensuing discussions. The specimen was also laterally restrained to prevent out-of-plane deflection under the loading.

2.2 Material and Geometrical Properties

The geometrical properties were obtained by measuring the dimensions

Table I. Test programme.

Ambient Test Programme				
Specimen No.	Beam	Column	Production Batch	Furnace Air Temperature (°C)
C1-A1	UB 254x146x31 kg/m	UC 254x254x89 kg/m	1	26 (ambient)
C1-A2				
C2-A1	UB 305x165x54 kg/m		2	
C2-A2				
C3-A1	UB 356x171x67 kg/m			
C3-A2				
Elevated Temperature Test Programme				
Specimen No.	Beam	Column	Production Batch	Furnace Air Temperature (°C)
C1-T1	UB 254x146x31 kg/m	UC 254x254x89 kg/m	1	600
C1-T2				750
C2-T1	UB 305x165x54 kg/m		2	830
C2-T2				890
C2-T3	UB 356x171x67 kg/m		700	
C3-T1			915	
C3-T2		845		
C3-T3		690		

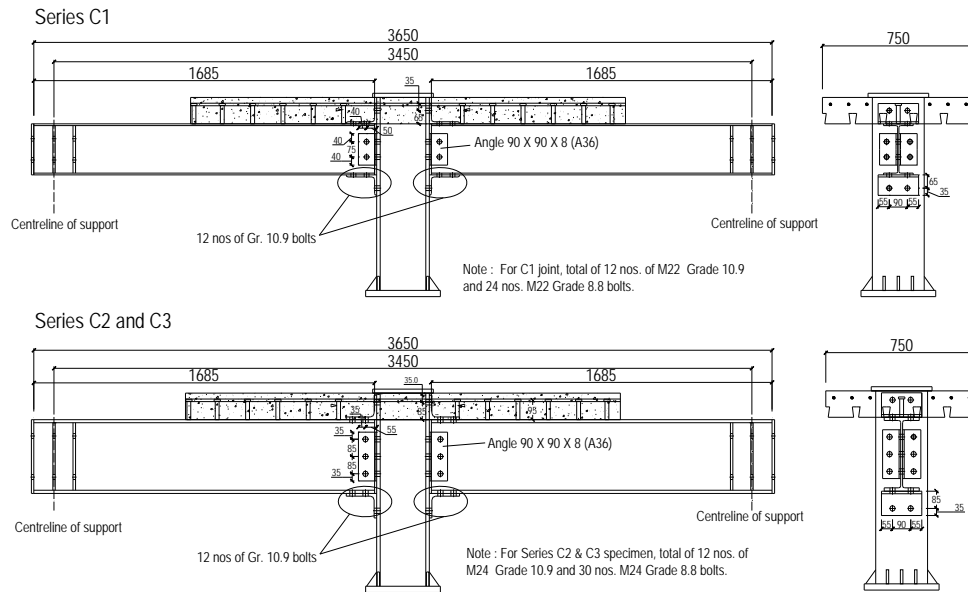


Figure 1. Details of composite top-and-seat and web angle joint Joints.

of steel beams, columns, angles, reinforcement bars and concrete slab. The material properties were obtained by conducting various material tests at ambient temperature, as summarised in Table II.

Two push-out tests of shear stud connectors were conducted to obtain its load-slip characteristics, following EC4 Part 1.1 [5] provisions. The average maximum shear capacity was 128.5 kN per connector.

The slab reinforcement consisted of standard 13 and 10 rebars for primary and secondary reinforcement, respectively. The average yield stress and ultimate stress were 510 and 612MPa, respectively. The average elastic modulus of 13 rebar was determined as 191GPa.

2.3 Instrumentation and Thermal Proofing

The instrumentation system included readings from load cells, thermocouple measurements, vertical and rotational deflections measured by LVDTs. The layout of LVDTs is as shown in Fig. 2.

The temperatures across the joint depth were measured by Type K thermocouples. Up to forty of them were used to measure each joint section.

Table II. Material Properties.

Ambient Test Sample																
Joint Specimen	Concrete		Structural Steel												Main Rebar	
	f_c	f_t	f_y (N/mm ²)						f_u (N/mm ²)						f_y (N/mm ²)	f_u (N/mm ²)
	(N/mm ²)	(N/mm ²)	Beam Flange	Beam Web	Column Flange	Column Web	Top/ Seat Angle	Web Angle	Beam Flange	Beam Web	Column Flange	Column Web	Top/ Seat Angle	Web Angle		
C1-A1	33.4	2.60	394	403	397	416	345	241	543	541	509	530	566	394	524	610
C1-A2	31.4	2.53	404	415	398	425	304	380	558	565	503	539	469	526	507	610
C2-A1	44.3	3.23	384	570	398	425	412	304	570	571	503	539	565	469	510	612
C2-A2	46.3	3.66	384	570	398	425	412	304	570	571	503	539	565	469	510	612
C3-A1	45.2	3.62	397	415	398	425	412	304	503	522	503	539	565	469	510	612
C3-A2	42.9	3.58	397	415	398	425	412	304	503	522	503	539	565	469	510	612
Elevated Temperature Test Sample																
Joint Specimen	Concrete		Steel												Main Rebar	
	f_c	f_t	f_y (N/mm ²)						f_u (N/mm ²)						f_y (N/mm ²)	f_u (N/mm ²)
	(N/mm ²)	(N/mm ²)	Beam Flange	Beam Web	Column Flange	Column Web	Top/ Seat Angle	Web Angle	Beam Flange	Beam Web	Column Flange	Column Web	Top/ Seat Angle	Web Angle		
C1-T1	42.4	3.00	394	403	397	416	345	241	543	541	509	530	566	394	524	610
C1-T2	42.7	3.12	404	415	398	425	304	380	558	565	503	539	469	526	507	610
C2-T1	45.2	3.28	384	570	398	425	412	304	570	571	503	539	565	469	510	612
C2-T2	43.6	3.23	384	570	398	425	412	304	570	571	503	539	565	469	510	612
C2-T3	45.1	3.56	384	570	398	425	412	304	570	571	503	539	565	469	510	612
C3-T1	44.8	3.44	397	415	398	425	412	304	503	522	503	539	565	469	510	612
C3-T2	46.5	3.49	397	415	398	425	412	304	503	522	503	539	565	469	510	612
C3-T3	47.6	3.45	397	415	398	425	412	304	503	522	503	539	565	469	510	612

* f_c = compressive strength; f_t = tensile strength; f_y = yield strength; f_u = ultimate strength

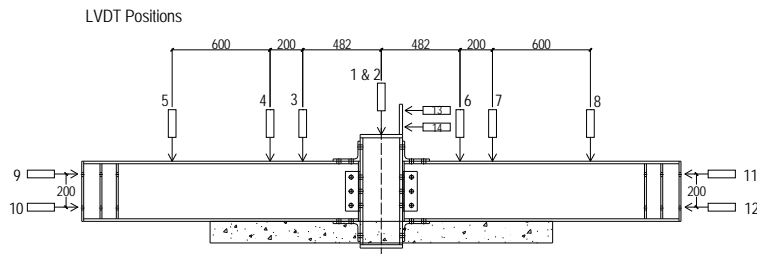


Figure 2. LVDT Positions.

Temperatures of beams, columns, angles and bolts were recorded accordingly. Another nine thermocouples were used to measure the temperatures of reinforcement bars (4 nos.), concrete slab (3 nos.) and shear studs (2 nos.). Furnace air temperature was also measured. The specimen was protected from heating by wrapping it with a fibre-glass blanket at both ends of the beams. The only exposed region was the 400 mm beam length from the centreline of column on both sides (Yuan [4]) of the cruciform assemblies.

2.4 Test Procedure

The ambient test was conducted by increasing the load at centre position until the specimen failed. The elevated temperature test was conducted in two stages, namely, (1) heating up the joint specimen to the desired

temperature and (2) applying load until the specimen failed. From a few trial tests, a temperature increase rate of 10°C/min was chosen for the furnace temperature, which is within a practical heating rate range for steel sections described by BS5950 Part 8 [6] from 5 to 20 °C/min.

3. THE PROPOSED MECHANICAL MODEL

For advanced analysis of steel frame structures, the accurate prediction of full-range moment-rotation behaviour is indispensable for a successful prediction of overall structural behaviour. Based on the research work on bare steel TSW angle joints by Faella et al. [7], the authors have proposed a mechanical model for predicting the moment-rotation response of composite TSW angle joints (Yuan Zhen et al., [8]) shown in Fig. 3. The general concept is to superimpose the moment-rotation relationship of each row of components to get the overall moment-rotation behaviour of the joint.

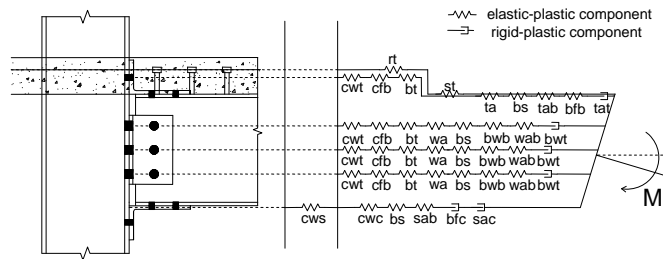


Figure 3. The proposed mechanical model for composite top-and-seat-and-web angle connection.

The full-range tension-displacement response of a new component, namely, reinforced concrete slab was also proposed by the authors, which was developed from the analytical model of reinforced concrete in tension by Maekawa et al. [9]. With the incorporation of elevated-temperature material (EC3 Part 1.2 [10] and EC4 Part 1.2 [11]) and component properties, this mechanical model can be used for predicting the behaviour of these joints at elevated temperature.

4. TEST RESULTS

A summary of six ambient and eight elevated-temperature tests is presented in Table III. The predicted ultimate moment values $M_{u,pred}$ was compared with the joint maximum moment in the test, $M_{max,exp}$. Joint rotation was taken as the average of two joint rotations on each side of a cruciform specimen. From Table III, it is seen that the authors' mechanical model could satisfactorily predict the actual failure modes. The ratio of $M_{max,exp}/M_{u,pred}$ is fairly consistent ranging from 0.91 to 1.16 with a small standard deviation of 0.075. For initial rotational stiffness, the predicted values could also predict reasonably well as compared with the test values.

Table IV summarises the ultimate component strength of some key elements, which are critical in determining the joint failure mode. The

weakest element would determine the joint failure mode. For example, although C1 series had two joint specimens fabricated to the identical design details, the failure modes of two C1 series joints (C1-A1 and C1-A2) are different, due to differences in the capacity of longitudinal shear transfer of profile decking slab.

Table V summarises the joint temperature profile at the time of maximum moment. The ratios are obtained by dividing the temperature of measured points by the temperature of the beam bottom flange.

Table III. Summary of test results.

Ambient Temperature Test									
Specimens	BFC Temperature (°C)	$M_{max,exp}$ (kNm)	$M_{u,pred}$ (kNm)	$M_{max,exp} / M_{u,pred}$	Failure Mode		$K_{i,exp}$ (kNm/rad)	$K_{i,pred}$ (kNm/rad)	$K_{i,exp} / K_{i,pred}$
					Test	Predicted			
C1-A1	26	215	221	0.973	a	a	60544	41648	1.454
C1-A2		154	133	1.155	b	b	40372	41648	0.969
C2-A1		269	245	1.098	b	b	104600	64494	1.622
C2-A2		279	245	1.139	b	b	61646	64494	0.956
C3-A1		286	273	1.048	b	b	81970	84025	0.976
C3-A2		278	273	1.018	b	b	65450	84025	0.779
Elevated Temperature Test									
C1-T1		434	201	207	1.030	a	a	40063	99380
C1-T2	569	138	126	0.913	c	c	32946	37073	1.125
C2-T1	633	165	161	0.976	c	c	57470	58877	1.024
C2-T2	616	150	146	0.973	c	c	45073	58089	1.289
C2-T3	491	211	199	0.943	c	c	61664	58801	0.954
C3-T1	651	207	205	0.991	d	d	56064	71108	1.268
C3-T2	551	278	303	1.091	d	d	42056	37888	0.901
C3-T3	424	338	323	0.957	b	b	67452	78729	1.167
				Average			1.022		
				Std. Dev.			0.075		
						Average			1.212
						Std. Dev.			0.432

a = yielding of longitudinal reinforcement; b = longitudinal shear split of RC slab; c = longitudinal concrete slab split; d=buckling of column web in compression; BFC = beam flange in compression

Table IV. The ultimate component strength for some key elements.

Ambient temperature tests							
Specimen	Ultimate capacity of key elements (kN)					Failure Mode	
	Longitudinal Shear Capacity of RC Slab	BFC	CWC	Main Rebar	Shear Stud	Predicted	Test
C1-A1	636	604	853	417	690	a	a
C1-A2	236	646	828	404	690	b	b
C2-A1	340	1070	858	406	690	b	b
C2-A2	341	1070	858	406	690	b	b
C3-A1	337	1329	858	406	690	b	b
C3-A2	333	1329	858	406	690	b	b
Elevated temperature tests							
C1-T1	642	573	853	417	690	b	a
C1-T2	241	419	576	404	690	c	c
C2-T1	248	421	397	406	690	c	c
C2-T2	220	497	351	406	690	c	c
C2-T3	283	956	642	406	690	c	c
C3-T1	500	631	335	406	690	d	d
C3-T2	581	883	496	406	690	d	d
C3-T3	561	1287	782	406	690	b	b & c

a = yielding of longitudinal reinforcement; b = longitudinal shear split of RC slab; c = longitudinal concrete slab split; d=buckling of column web in compression; BFC = beam flange in compression; CWC = beam flange in compression

Table V. Joint temperature profile at maximum moment.

Thermocouple Location	C1-T1	C1-T2	C2-T1	C2-T2	C2-T3	C3-T1	C3-T2	C3-T3	Average
Beam upper flange	0.70	0.80	0.83	0.87	0.79	0.88	0.90	0.83	0.83
Beam mid-height web	0.97	0.99	0.99	0.98	0.97	0.98	0.98	0.96	0.98
Beam bottom flange	1.00	1.00	1.00	1.00	1.00	1.00	1.00	1.00	1.00
Central web angle	0.84	0.95	0.97	1.01	0.98	1.01	1.03	1.04	0.98
Seat angle	0.99	1.00	0.96	1.04	1.01	0.98	0.98	1.02	1.00
Top angle	0.70	0.81	0.79	0.82	0.71	0.77	0.76	0.70	0.76
Column Flange (near seat angle)	0.88	0.93	0.95	1.01	1.00	0.97	1.01	1.06	0.98
Column Flange (near top angle)	0.79	0.84	0.91	0.95	0.99	0.93	0.97	1.04	0.93
Column web in compression at seat angle	0.82	0.94	0.96	1.01	1.03	0.97	1.02	1.04	0.97
Reinforcement bar	0.27	0.21	0.27	0.31	0.25	0.17	0.27	0.26	0.25
Shear stud	0.41	0.57	0.52	0.52	0.44	0.43	0.48	0.43	0.48
Concrete slab at directly above top flange	0.47	0.52	0.49	0.63	0.58	0.49	0.44	0.42	0.50
Concrete slab at 50mm above top flange	0.34	0.33	0.31	0.38	0.35	0.29	0.23	0.25	0.31
Concrete slab at 100 mm above top flange	0.31	0.21	0.24	0.31	0.24	0.21	0.21	0.24	0.25
Furnace temperature	1.38	1.32	1.30	1.22	1.43	1.41	1.54	1.63	1.40

Fig. 4(a) and 4(b) plots the predicted moment-rotation curves versus the experimental curves for joints C1-A1 and C3-T3. It can be observed that the authors' mechanical model could produce consistent and good predictions of the actual moment-rotation curves. To account for the effect of bolt slip, an additional rotation (equal to the bolt clearance divided by the beam depth) was superimposed onto the predicted moment-rotation curves.

Compared with the ambient test, the joint behaviour at elevated temperature is more non-linear and weaker due to deteriorating strength and stiffness of concrete and steel, and plastic shearing of bolt at seat angle at elevated temperatures.

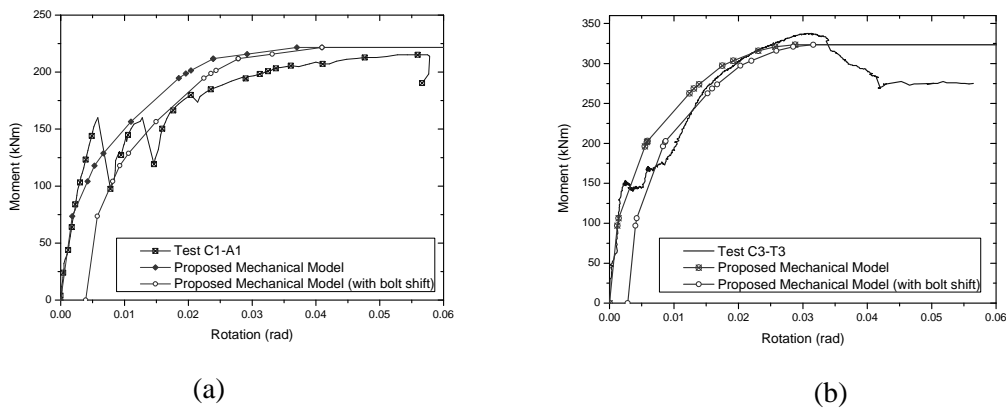


Figure 4. The predicted moment-rotation curves versus the experimental curves.

5. DISCUSSIONS

For composite TSW angle joints, its characteristic moment-rotation response at ambient temperature showed two times of abrupt reduction in moment due to sudden slip of bolts (two 'spikes'). However, at elevated temperature, the bolt shanks expanded and the clamping forces in the bolts were reduced, so the phenomena of 'spikes' are not so obvious.

Moreover, the ultimate moment capacity at ambient condition was greater than at elevated temperature. The steel strength weakens with increasing temperature. In EC3 Part 1.2, from 400°C onwards the ultimate

strength is assumed to be the same as the decreasing yield strength at 0.02 strain with a truncation for purpose of simplification. The strain hardening behaviour is also neglected at temperature above 400°C.

Furthermore, the longitudinal splitting strength of profile decking slab could significantly affect the joint ultimate moment capacity. This effect could be illustrated qualitatively by comparing the experimental maximum moment of joints C1-T1 and C1-T2, as shown in Table III.

Lastly, the steel beam depth would significantly influence the initial rotational stiffness and moment capacity of composite joints. This effect is illustrated by comparing the experimental maximum moment of joints C1-T2 and C2-T1 as in Table III. The weakest element (longitudinal splitting strength of slab) is of almost identical strength and the failure modes are the same. Hence, the joint moment capacity is determined by the beam depth. Therefore, joint C2-T1 with a larger beam depth has a greater moment capacity.

6. CONCLUSIONS

A total of fourteen of composite TSW angle joints were tested at ambient and elevated temperature. Experimental moment-rotation characteristics of the joints were obtained. The effects of temperature longitudinal shear strength of RC slab, steel beam depth, bolt behaviour at seat angle were studied. The test results also validated the authors' 'component-based' mechanical model for composite TSW angle joint.

REFERENCES

1. Zandonini R. 1989, Semi-rigid Composite Joints. In *Structural Connections : Stability and Strength*. Narayanan R, editor. Elsevier, London. pp. 63–120.
2. Leston-Jones, L.C. 1997. *The influence of semi-rigid connections on the performance of steel framed structures in fire*. PhD thesis. Department of civil and structural engineering. University of Sheffield.
3. Al-Jabri, K.S. 1999. *The behaviour of steel and composite beam-to-column connections in fire*. PhD thesis. Department of civil and structural engineering. University of Sheffield.
4. Yuan Zhen, Tan Kang Hai and Ting Seng Kiong. 2010. Testing of composite top-and-seat-and-web-angle joints at elevated temperatures, *Engineering Structures*, in submission.
5. European Committee for Standardization (CEN) 2004, "Eurocode 4: Design of Composite Steel and Concrete Structures, Part 1.1: General Rules and Rules for Buildings", EN1994-1-1:2004, Brussels, Belgium.
6. British Standards Institution (BSI) 2003, "BS5950 : Structural use of steelwork in building, Part 8 : Code of practice for fire resistance design". BS 5950-8:2003, London, UK.
7. Faella, C., Piluso, V. & Rizzano, G. 2000. *Structural steel semirigid connections : theory, design and software*. Florida, CRC press LLC.
8. Yuan Zhen, Ting Seng Kiong and Tan Kang Hai. 2007. Development of a component mechanical model for composite top-and-seat-and-web angle connection, in *The Third International Conference on Steel and Composite Structures*, 30 July–1 August 2007, Manchester, UK.
9. Maekawa, K., Pimanmas, A. & Okumura, H. 2003. *Nonlinear mechanics of reinforced concrete*, Chapter 2, 8 and 9, New York, Spon Press.

10. European Committee for Standardization (CEN) 2005, “Eurocode 3: Design of Steel Structures, Part 1.2: General Rules—Structural Fire Design”, EN1993-1-2:2005, Brussels, Belgium.
11. European Committee for Standardization (CEN) 2005, “Eurocode 4: Design of Composite Steel and Concrete Structures, Part 1.2: General Rules—Structural Fire Design”, EN1994-1-2:2005, Brussels, Belgium.

Numerical Modelling of HSS Endplate Connections at Elevated Temperatures

X. QIANG, F. BIJLAARD, H. KOLSTEIN and L. TWILT

ABSTRACT

In order to investigate the behaviour of high strength steel (HSS) endplate connections in fire conditions, a numerical modelling is conducted and compared with that of mild steel. Validation against test results shows that the proposed model can reproduce the behaviour of mild steel endplate connections at elevated temperatures with reasonable accuracy. Using HSS instead of mild steel as endplate material, this model is also able to predict the performance of HSS endplate connections. By a parametric study on the effects of endplate thicknesses, it is found that a thinner HSS endplate possesses more ductility than mild steel endplate connection at elevated temperatures, and their load bearing capacities are almost the same. This finding is positive and beneficial for further investigation of improving the robustness of endplate connections in fire conditions.

INTRODUCTION

In Europe, endplate connections are typical for low-rise steel buildings erected using welding at workshops and bolting in situ. The simplicity and economy associated to their fabrication, make the connections popular in steel structures.

Xuhong Qiang, Ph.D. Student, Faculty of Civil Engineering and Geosciences, Delft University of Technology, 2600GA Delft, Netherlands

Frans Bijlaard, Professor, Faculty of Civil Engineering and Geosciences, Delft University of Technology, 2600GA Delft, Netherlands

Henk Kolstein, Associate Professor, Faculty of Civil Engineering and Geosciences, Delft University of Technology, 2600GA Delft, Netherlands

Leen Twilt, Ir., Formerly: Center for fire research of Institute TNO for Building and Construction Research, Delft, Netherlands

Rules for prediction of strength and stiffness of this connection configuration at ambient temperature have been included in design codes, such as Eurocode3 Part1-8 [1], but they are mainly based on mild steel connections. Ana M. Girao Coelho et al. [2] have found that the HSS S690 endplate connections satisfy the design provisions for resistance and achieve reasonable rotation demands at ambient temperature. However, no quantitative guidance for HSS endplate connections in fire is available.

Recently, in a bolted connection project it has been found that bolts failure becomes critical at elevated temperatures, although design for ambient temperatures assumes more ductile failure [3-5]. It means that mild steel bolted connections' failure modes are relatively brittle at elevated temperatures. So, making these connections more ductile at elevated temperatures is a significant mission for structural engineers.

In order to enhance fire safety of endplate connections, a research is being conducted at Delft University of Technology, using HSS endplate instead of mild steel endplate. In this paper, numerical modelling of HSS endplate connections is compared with that of mild steel endplate connections, to gain essential understanding and quantification of how HSS endplate connections behave at elevated temperatures. The accuracy of this numerical model is validated against the results of Yu et al.'s tests conducted on mild steel flush endplate connections at elevated temperatures [3, 5]. Moreover, a parametric study on the effects of endplate thicknesses is conducted, and an achievement is obtained for improving the ductility of endplate connections at elevated temperatures.

EXPERIMENTAL TESTS

The tests were performed in an electrical furnace under steady-state conditions. See Figure 1. Four kinds of connections were subjected to a combination of tension and shear forces [3, 5]. Only the tests on flush endplate connections are used in this paper. Figure 2 shows the details of the flush endplate connection. In all cases, UC254×89 made of S355 was used for the column; the UB305×165×40 beam specimens were made of S275.

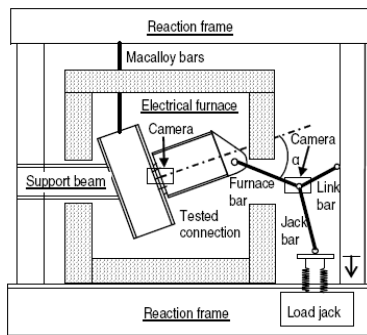


Figure 1. Test setup.

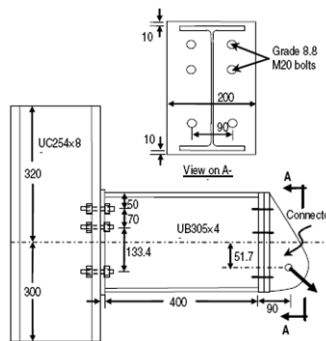


Figure 2. Typical flush endplate connection specimen.

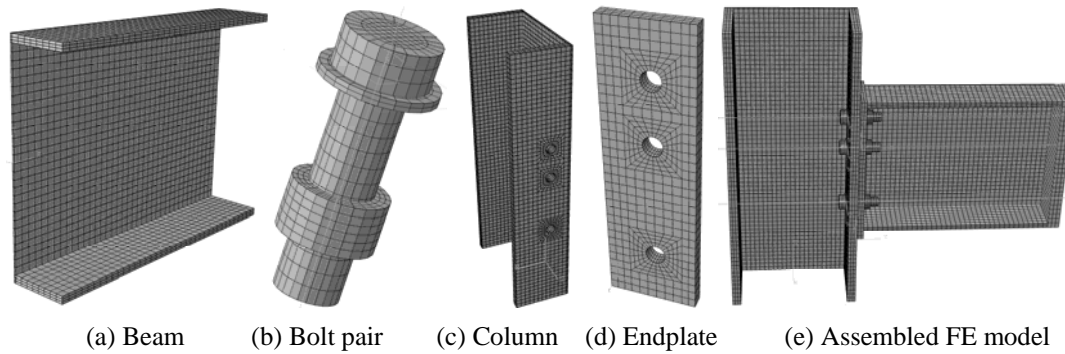


Figure 3. FE model and its mesh generation.

FINITE ELEMENT ANALYSIS METHOD

The commercial finite element software ABAQUS is used to simulate the behaviour of endplate connections at elevated temperatures.

Geometric Details of Connections

The details of all connections' components used in FEM are exactly the same as those of the test specimens. Because the geometric details, load, temperature distribution and boundary conditions are symmetric, half of the endplate connection is modelled, to save computer costs and shorten computing time. The components of this FE model are shown in Figure 3, including bolt shank, nut, washer, endplate, beam and column. The boltholes are modelled 2mm larger than the bolt shank diameter, and the hexagon bolt heads are modelled as cylinders for simplicity.

Mesh Generation and Element Type

There are 13 surface-to-surface contact interactions and 14 tie interactions in this model, and the materials are endowed with non-linear properties. These make this analysis sensitive to mesh, so the mesh should be fine. To capture accurate stress distribution in the region around boltholes where likely failures would initiate, an intensive mesh is created in the vicinity of boltholes, shown in Figure 3.

The whole connection is modelled using C3D8I element, because of its excellence in simulating contact interactions, non-linear material properties and stress concentrations.

Contact Interaction

An effective analysis method is used, to handle the contact interaction problem in ABAQUS/Standard. The whole analysis process comprises 6 analysis steps. In the first step, bolts, washers and the endplate are restrained of all direction freedoms temporarily, and then a very small pretension is applied to every bolt for restraining the bolt pairs temporarily. The temperature field for all components is 20°C. In the second step, the bolts, washers and the endplate are freed of any temporary

restraint. In the third step, the actual magnitude of pretension is applied to every bolt. In the fourth step, the length of every bolt is fixed. In the fifth step, the temperature field for all components is modified to a preselected elevated temperature. In the sixth step, an equivalent surface traction converted from the actual inclined force with its preselected initial load angle is applied to the end of the beam. The first four steps help contact interactions to be established smoothly, which is effective to decrease calculation time and eliminate errors.

Surface-to-surface contact, with a small sliding option, is used for all contact surfaces to fully transfer the load. The contact pairs in the endplate connection comprise the washers-to-column flange, column flange-to-endplate, endplate-to-nuts. The washer is tied to bolt head in each bolt pair for simplicity and the nuts are tied to the corresponding bolt shanks.

Material Properties

In this FE modelling, the material properties of mild steels (including S275 and S355) and bolt pairs are the same as those reported by the University of Sheffield [6-8]. The material properties of S690 at elevated temperatures reported by Chen and Young [9] are used for HSS.

Loads

At the other end of the beam, an additional endplate is modelled just for applying surface traction, shown in Figure 3(e). The initial load angles used in tests are also taken into consideration when applying the surface traction. The pretension for bolts is simulated using the bolt load function in ABAQUS/Standard. The magnitude of pretension for each bolt is 224kN, to agree with the average value in the experimental investigation [3, 4].

Welds Treatment

Because ABAQUS/Standard is not capable of simulating fracture failure, the welds between endplate and beam are modelled by tie restraint instead of solid modelling, in order to simplify the model. But this will result in an overestimation of the robustness of the connections.

VALIDATION AGAINST EXPERIMENTAL RESULTS

A validation of the numerical modelling is performed against Yu et al.'s experimental data on mild steel endplate connections at elevated temperatures under steady-state conditions, to check the accuracy of the proposed numerical model.

Comparison of Results

In the fire tests, the connection specimens (10mm S275 endplate connections) have been heated to three preselected elevated temperatures (450°C, 550°C and 650°C) and then loaded till failure occurred. For each elevated temperature level, the specimens were tested with three initial load angles (35 degree, 45 degree and 55degree). The corresponding numerical modellings are based on the above-mentioned FE analysis method.

The force-rotation capacities of 10mmS275 endplate connections at elevated temperatures obtained by FEM are compared with test results, as shown in Figure 4-6. The following remarks can be drawn. The FE model cannot simulate the descending branch of force-rotation curves obtained in tests. For the first two stages of the semi-trilinear curves obtained by FEM simulations, they are in good agreement with Yu et al.'s test results at 450°C and 550°C. But at 650°C the strength of the connections obtained from FEM are much higher than test data. This is because in tests the specimens are heated very slowly (i.e. the specimens are loaded till failure in about 120 min), but there are no material properties of S275 corresponding to such very slow steady-state conditions available. So the material used in FEM can not exactly reflect the actual behaviour in tests, especially at very high temperatures, such as 650°C. Moreover, at very high temperatures, creep effects will have a significant influence, especially when the specimens are heated very slowly. However, in the FE analysis creep has not been taken into account, leading to an overestimation of the strength and stiffness of the connections. For these reasons the tests at 650°C will be excluded from the FE analysis.

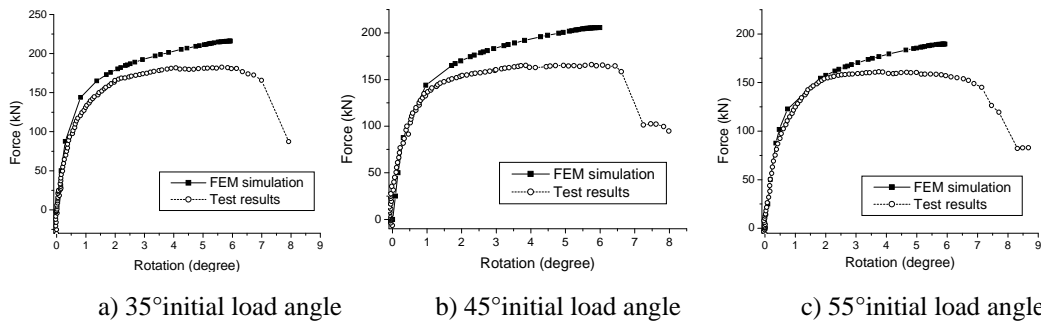


Figure 4. Force-rotation comparisons of 10mmS275 at 450°C

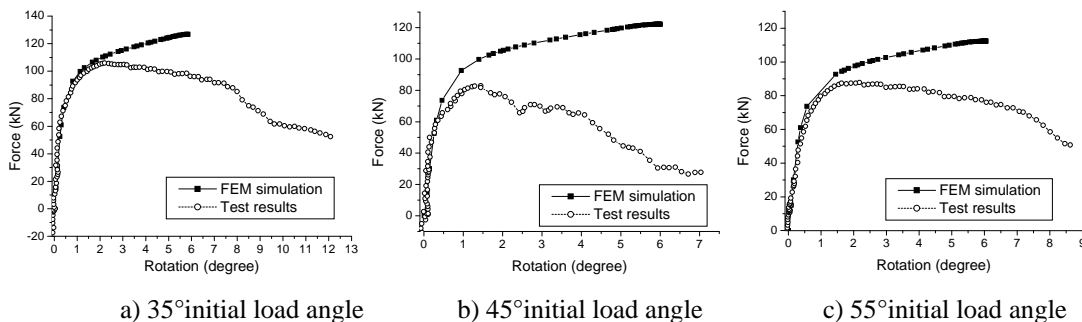


Figure 5. Force-rotation comparisons of 10mmS275 at 550°C.

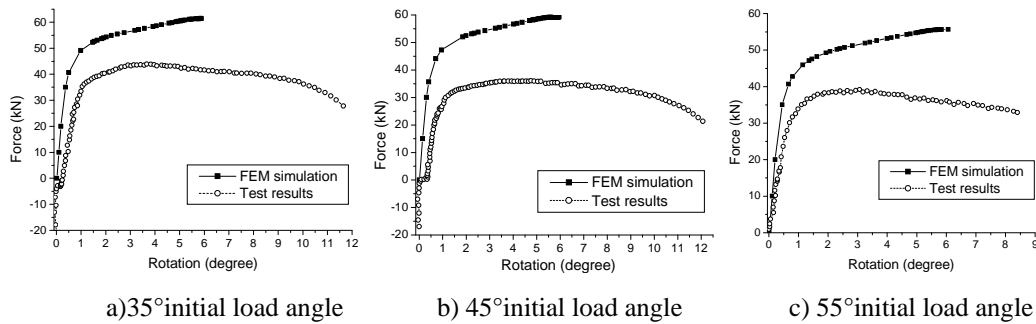


Figure 6. Force-rotation comparisons of 10mmS275 at 650°C.

Discussion of Discrepancies

For 450°C and 550°C, the discrepancies between numerical results and test results need some discussion. Firstly, the stress-strain relationships for structural steels and high strength bolts used in the FEM are of an elastic-plastic nature, including strain-hardening. The material properties are obtained from tests, in which the strain rates are faster than that of the current connection tests. This may result in discrepancies between test and numerical results. Secondly, the welds between endplate and beam are not solidly modelled but treated with tie restraint. Consequently, the fracture of welds can not be reflected. So, the overestimation of the third stage of semi-trilinear performance is attributable to this welds treatment. This means that solid modelling of welds is necessary to improve the accuracy of numerical simulation. Thirdly, the value of the applied pretension for each bolt is determined by the average value given in Yu et al.'s tests. In conducting actual tests it is very difficult to induce accurately a bolt force by pretension techniques. As a result, this may also be a reason for discrepancies between the FEM simulation and the test results.

NUMERICAL COMPARISON AND PARAMETRIC STUDY

Comparison of Ductility and Strength for the Same Endplate Thickness

For the same endplate thickness, the force-rotation capacity of HSS endplate connections at elevated temperatures obtained in the numerical simulation is compared with that of mild steel ones, as presented in Figure 7. The results for 10mm endplate with initial load angle of 55 degree at two elevated temperature levels are shown.

It is found that at elevated temperatures the load-bearing capacities of HSS endplate connections are stronger than mild steel endplate connections with the same endplate thickness, but the ductility of the former is worse. It is obvious that using the same thickness of HSS endplate instead of mild steel endplate in connections is not effective to improve the ductility of the endplate connections.

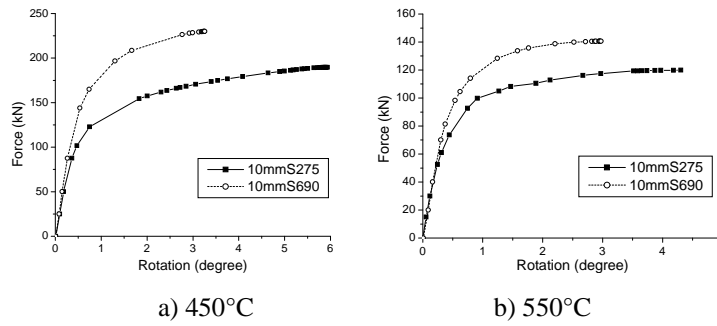


Figure 7. Comparisons of HSS endplate connections and mild steel endplate connections.

Parametric Study on Endplate Thickness Effects

In order to analyze the endplate thickness effects on strength and ductility of the whole connection, a parametric study is conducted using the proposed FE model. At the same elevated temperature, the simulated force-rotation capacities of various thicknesses of HSS endplate connections are compared with that of mild steel endplate connections, as shown in Figure 8. A comprehensive conclusion can be drawn from Figure 8: at elevated temperatures, a thinner HSS endplate can provide the same load-bearing capacity as that for a mild steel endplate connection, but enhance the ductility of the connection. This quantitative achievement is very positive for improving the design of endplate connections at elevated temperatures.

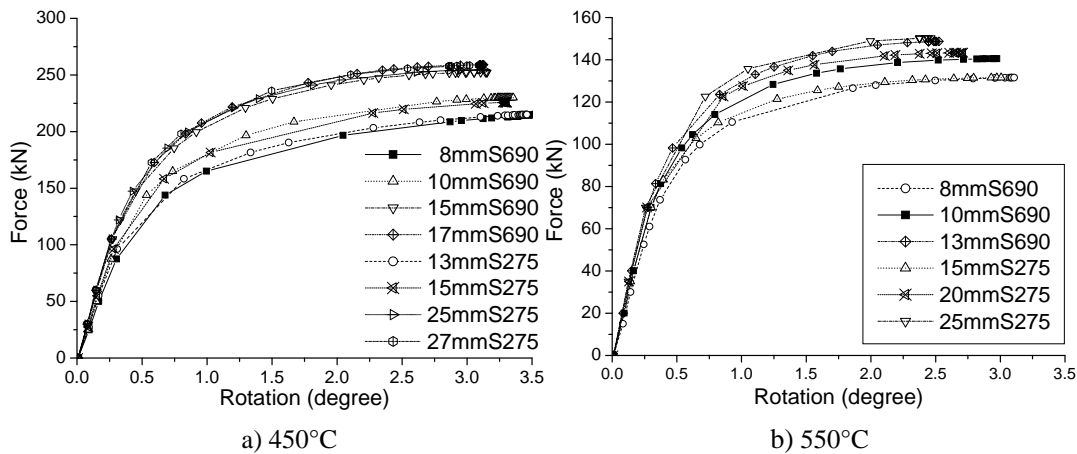


Figure 8. Force-rotation comparisons of various thicknesses of endplate connections.

CONCLUSION

The big challenge of modelling contact interactions is solved successfully by FEM, considering material and geometric non-linear effects. The proposed FE modelling is verified appropriate to simulate mild steel endplate connections at elevated temperatures with reasonable accuracy. Based on this, a further numerical comparison is conducted between the behaviour of HSS and mild steel endplate connections at elevated temperatures. By a comprehensive parametric study, it is

found that a thinner HSS endplate can enhance ductility of the connection at elevated temperatures, and simultaneously achieve the same load-bearing capacity as a mild steel endplate connection. This finding can be used for further investigation into the behaviour of HSS endplate connections in fire conditions.

By the present modelling method, the critical locations of endplate connections can be identified, but the occurrence of component failure cannot be predicted. To improve the capability of this numerical simulation, solid modelling of welds taking into account fracture features is necessary. Since ABAQUS/Standard is not capable of simulating fracture or failure because of excessive plastic deformations, ABAQUS/Explicit should be considered for further numerical investigation.

REFERENCE

1. European Committee for Standardization (CEN) 2005. BS EN 1993-1-8, Eurocode3: Design of steel structures, Part 1-8: Design of joints. British Standards Institution.
2. Gir`ao Coelho AM and Bijlaard FSK 2007. Experimental behaviour of high strength steel end-plate connections. *Journal of Constructional Steel Research* 63:1228–1240.
3. Yu, H.X., Burgess, I.W. Davison, J.B., and Plank, R.J. 2008. Experimental Investigation of the Behaviour of Flush Endplate Connections in Fire. *Proc. Structures in Fire Workshop, Singapore*: 150-157.
4. Yu, H.X., Burgess, I.W. Davison, J.B., and Plank, R.J.2009. Tying Capacity of Web Cleat Connections in Fire. Part 1: Test and Finite Element Simulation. *Engineering Structures* 31 (3): 651-663.
5. Burgess I.W. 2009. The Robustness of Steel Connections in Fire. *Proc. ASCCS 2009, Leeds*: 103-114.
6. Hu Ying, Burgess Ian, Davison Buick, Plank Roger 2008. Modelling of flexible endplate connections in fire using cohesive elements. *Proc. Structures in Fire Workshop, Singapore*.
7. Yu, H.X., Burgess, I.W., Davison, J.B. and Plank, R.J. 2009. Development of a Yield-Line Model for Endplate Connections in Fire. *J. Construct. Steel Research* 65 (6): 1279-1289.
8. Renner A 2005. The effect of strain-rate on the elevated-temperature behavior of structural steel. Research dissertation. UK: University of Sheffield; 2005.
9. Ju Chen and Ben Young 2006. Behaviour of High Strength Structural Steel at Elevated Temperatures. *Journal of Structural Engineering*: 1948-1954.

Experimental Study of Mechanical Properties of High-Strength Bolts After Fire

G.-B. LOU, S. YU and R. WANG

ABSTRACT

Fire is one of the greatest and most common threats to steel structures of buildings. In the past 100 years, there were many cases that steel structures collapsed in fire. However, steel structures were not fatally destroyed in the most cases of fire. These damaged steel structures may be reused after structural inspection, safety appraisal and necessary repair by means of reinforcement and strengthening. Effects of heating and cooling of steel in fire are similar to tempering and annealing, thus mechanical properties of steel after fire will be different from the initial properties. High-strength bolts which are widely used in steel structural connections are more temperature-sensitive than hot finished steel because the manufacturing process of high-strength bolts consists of cold drawing, annealing, cold forging and heat treatment. A number of experiments have been carried out on mechanical properties of high-strength bolts at elevated temperatures, however very limited studies focused on mechanical properties of high-strength bolts after fire. To obtain the mechanical properties of high-strength bolts after fire including stress-strain curves, strength and elasticity modulus, a series of experiments on 10.9s bolts and 8.8s bolts were carried out in this study. In order to simulate the real situations in event of fire, both natural cooling and water cooling were employed in this experimental study. The results show that heating and cooling has a great effect on the mechanical properties of high-strength bolts after fire, and the effect of natural cooling is very different from that of water cooling.

Guo-Biao LOU (corresponding author), Ph.D., State Key Laboratory for Disaster Reduction in Civil Engineering, Department of Structural Engineering, Tongji University, Siping Road 1239, Shanghai 200092, China

Shan YU, Graduate Student, Department of Structural Engineering, Tongji University, Siping Road 1239, Shanghai 200092, China

Rui Wang, Student, Department of Structural Engineering, Tongji University, Siping Road 1239, Shanghai 200092, China

INDUCTION

Fire is one of the greatest and most common threats to steel structures of buildings. In the past 100 years, there were many cases that steel structures collapsed in fire. However, steel structures were not fatally destroyed in the most cases of fire. These damaged steel structures may be reused after structural inspection, safety appraisal and necessary repair by means of reinforcement and strengthening. Effects of heating and cooling of steel in fire are similar to tempering and annealing, thus mechanical properties of steel after fire will be different from the initial properties. High-strength bolts which are widely used in steel structural connections are of great importance to fire resistance of the structure. However, limited studies focused on mechanical properties of high-strength bolts after fire has been carried out.

It is necessary to obtain mechanical properties of steel after fire for evaluating the post-fire load bearing capacity and structural behavior of steel structure. The effect of fire is similar to temper, which will offset the effects of heat treating and cold working during the manufacturing process of steel, thus it has a greater effect on high-strength steel than hot finished steel. Tovey[1] and Min[2] carried out a number of experiments to study mechanical properties of hot finished rebars after fire, meanwhile Kirby [3], Outinen [4] and Cao [5] conducted a similar investigation into hot finished steel. As shown in the experiments, the mechanical properties of hot finished rebars and structural steel are not significantly affected until they have achieved temperatures well in excess of 600°C. The strength loss of them is approximately 10% on cooling from temperature 725°C and significantly increases after being heated to temperatures in excess of 725°C. Hu [6], Zheng [7] and Fan [8] conducted a series of systematic experiments respectively on prestressing wires with strength of 1570N/mm² and steel cables with strength of 1770N/mm² and 1860N/mm² to study their mechanical properties after fire. It was concluded from these experiments that the strength properties of prestressing wires and steel cables reduced significantly after being heated to 300°C and the strength loss was nearly 50% after being heated to 600°C.

The studies on mechanical properties of high-strength bolts were mainly focused on them at normal temperature and elevated temperatures while little have been carried out on the mechanical properties of high-strength bolts after fire [9~12]. Li [13] carried out tensile experiments on the 8.8s high-strength bolts fastened to two steel beams which buckled significantly after a building fire. The results indicated obvious necking in the bolts and a maximum decrease of the ultimate tensile strength up to 33%. As a result, for the purposes of this paper a series of systematic experiments on the mechanical properties of high-strength bolts have been performed.

TEST PROGRAMME

Test Objectives

To obtain the mechanical properties of high-strength bolts after fire including stress-strain curves, strength and elasticity modulus, uniaxial tension experiments were carried out on 10.9s bolts and 8.8s bolts. By comparing the results to the case of normal temperature, the effects of fire exposure on high-strength bolts were obtained. In this way, the stress-strain curves, the strength reduction factor and the reduction factor of elasticity modulus of high-strength bolts after fire were attained which may be used to analyze the post-fire load bearing capacity of connections.

In order to simulate the real situations in event of fire, both natural cooling and water cooling were employed in this experimental study. The results show that heating and cooling has a great effect on the mechanical properties of high-strength bolts after fire, and the effect of natural cooling is very different from that of water cooling.

Test Procedure

The following procedure has been adopted in this study: (1) Heat the specimens up to the desired temperature and maintain the temperature for 60 minutes; (2) Cool the specimens to the ambient temperature using either natural cooling method which relies on the air only or water cooling method which puts the specimens in the water to provide forced cooling; (3) Conduct uniaxial tension tests on the cooled specimens until failure occurs. The rate of loading is kept at 1200N/s; (4) Obtain the stress-strain curve, strength and elasticity modulus using the methods given in GB/T228-2002.

Totally 11 temperature points have been chosen which are 100°C, 200°C, 300°C, 400°C, 500°C, 600°C, 700°C, 750°C, 800°C, 850°C and 900°C. Three specimens were tested at each temperature point. The high-strength bolts which have not exposed to fire were also tested for comparison.

Test Specimen

The manufacturing process of high-strength bolts is as following: hot finished rod—cold drawing—soft annealing—mechanical descaling—acid cleaning—cold drawing—cold forging—thread machining—heat treating—check, in which the heat treating process consists of feeding, cleaning, heating, quenching, cleaning, tempering and coloring up etc. After this manufacturing process, the mechanical properties of bolts are very different from the raw steel material. Thus it is necessary to use finished bolts for the proposed tests. In this paper both 10.9s and 8.9s bolts have been tested. The mechanical properties of the bolts at normal temperature were presented in Table I.

TABLE I. MECHANICAL PROPERTIES OF HIGH-STRENGTH BOLTS AND RAW MATERIALS.

grade and size of bolts	raw material	surface color	mechanical properties of raw material				mechanical properties of bolts	
			tensile strength σ_b (MPa)	yield strength $\sigma_{0.2}$ (MPa)	elongation ϵ_5 (%)	shrinkage Ψ (%)	capacity (kN)	elongation ϵ_5 (%)
10.9s,M20×120	20MnTiB	Black	1190	990	13.0	58.0	281.5	
8.8s,M20×120	45# steel	Black	655	385	24.0	46.0	≥ 203	≥ 12

TEST RESULTS

Test Phenomenon

Table II details the visual observations of the tested bolts after failure. The failure mode of some bolts is presented in Figures 1 to 4.

Stress-Strain Relationship of High-Strength Bolts after fire

Stress-strain curves of 8.8s and 10.9s bolts after fire were shown in Figures 5 and 6 respectively.

TABLE II. VISUAL OBSERVATION OF TESTED BOLTS AFTER FAILURE.

attained temp. (°C)	color of screw surface		color of fracture face		failure mode of 8.8s bolts		failure mode of 10.9s bolts			
	natural cooling	water cooling	natural cooling	water cooling	natural cooling	Water cooling	Natural cooling	Water cooling		
ambient	black	black	grey	grey	fractured at 45° with slight necking	fractured at 45° with slight necking	fractured at 45° without necking	fractured at 45° without necking		
100	black	black	grey	grey	fractured at 45° with more obvious necking	fractured at 45° with more obvious necking	fractured at 45° with increased necking but not obvious	fractured at 45° with slight necking 2 bolts failed with thread stripping		
200										
300	light black							fractured at 45° with slight necking		
400	blue grey	gradually become	grey white	grey white	fractured at 45° with less obvious necking	fractured at 45° with less obvious necking	fractured at 45° without necking	fractured at 45° without necking		
500	blue grey				fractured at a smaller angle with increased necking	fractured at a smaller angle with increased necking	fractured at 45° with increased necking but not obvious	fractured at 45° with increased necking		
600	light blue									
700										
750	light blue	grey matt	grey white	white	fractured irregularly with necking	fractured almost along cross section without necking	fractured at 45° with increased obvious necking	fractured almost along cross section without necking		
800	grey matt				fractured almost along cross section with slight necking					
850					fractured almost along cross section with more obvious necking					
900					fractured at 45° with obvious necking					



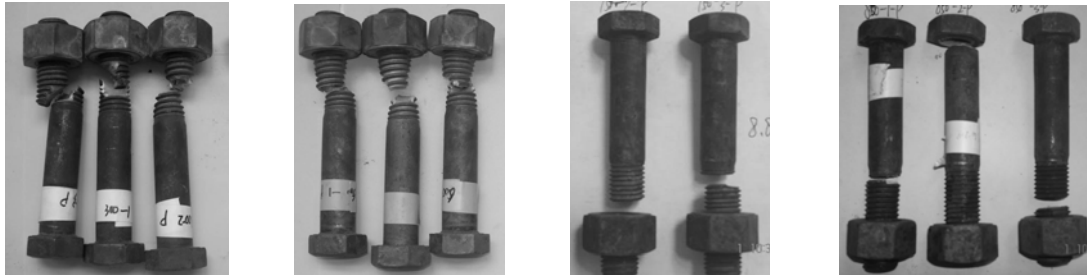
a) attained temp.300°C b) attained temp.700°C c) attained temp.750°C d) attained temp.900°C
Figure 1. Failure of 10.9s high-strength bolts: Natural cooling.



a) attained temp.200°C b) attained temp.300°C c) attained temp.750°C d) attained temp. 900°C
Figure 2. Failure of 10.9s high-strength bolts: Water cooling.



a) no fire exposure b) attained temp.400°C c) attained temp.700°C d) attained temp.800°C
 Figure 3. Failure of 8.8s high-strength bolts: Natural cooling.



a) attained temp.300°C b) attained temp.600°C c) attained temp.750°C d) attained temp.800°C
 Figure 4. Failure of 8.8s high-strength bolts: Water cooling.

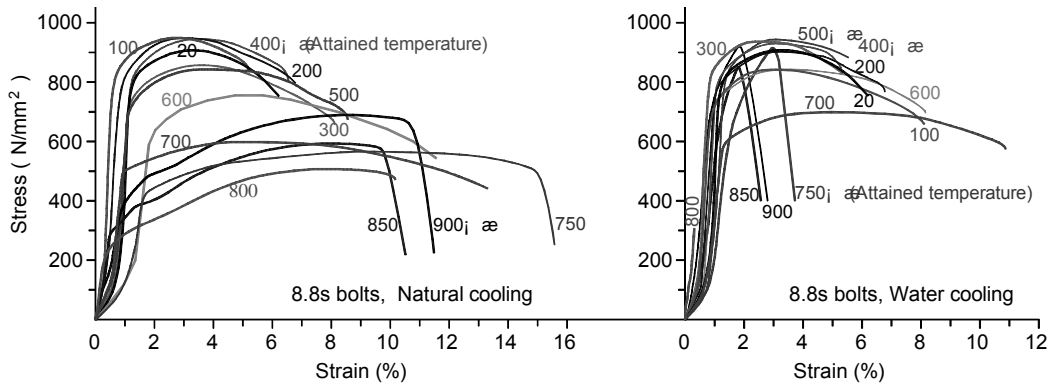


Figure 5. Stress-strain curves of 8.8s high-strength bolts after fire.

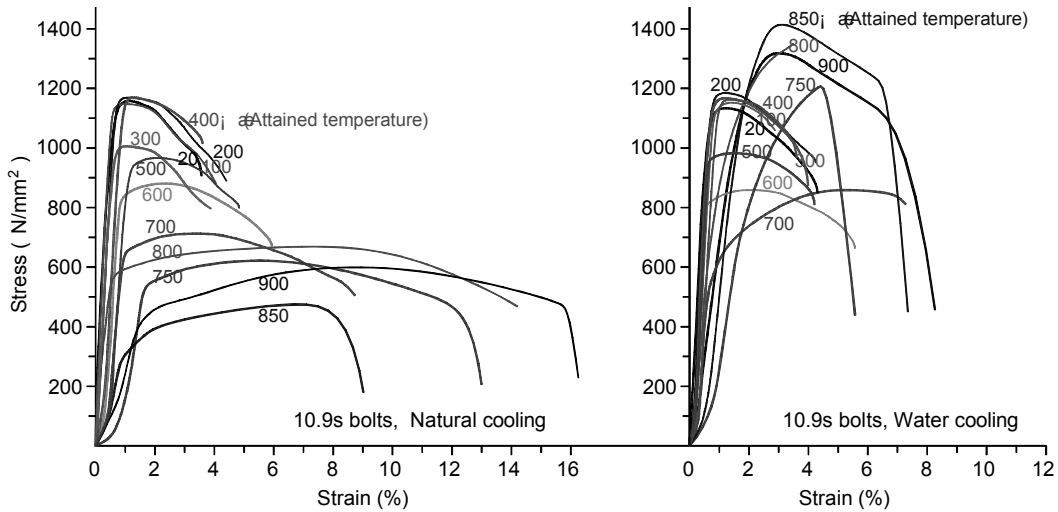


Figure 6. Stress-strain curves of 10.9s high-strength bolts after fire.

Strength and Elasticity Modulus of High-Strength Bolts after fire

The reduction factors of strength and elasticity modulus for 8.8s and 10.9s high-strength bolts after exposed to different temperatures are given in Table III and Table IV respectively (also refer to Figure 7 and Figure 8).

TABLE III. REDUCTION FACTORS OF STRENGTH AND ELASTICITY MODULUS OF 8.8s BOLTS AFTER FIRE.

Attained temp. T_m (°C)	Yield strength $\sigma_{0.2, T_m}$ (N/mm ²)		Tensile strength σ_{b, T_m} (N/mm ²)		Reduction factor of yield strength $\sigma_{0.2, T_m}/\sigma_{0.2}$		Reduction factor of tensile strength $\sigma_{b, T_m}/\sigma_b$		Reduction factor of elasticity modulus E_{T_m}/E	
	Natural cooling	Water cooling	Natural cooling	Water cooling	Natural cooling	Water cooling	Natural cooling	Water cooling	Natural cooling	Water cooling
	20	837.0	837.0	910.5	910.5	1.00	1.00	1.00	1.00	1.00
100	812.0	781.5	913.3	901.0	0.97	0.93	1.00	0.99	0.97	0.94
200	821.5	794.7	925.5	900.7	0.98	0.95	1.02	0.99	—	0.95
300	805.0	844.5	903.0	952.5	0.96	1.01	0.99	1.05	0.94	1.06
400	843.5	831.0	951.0	936.0	1.01	0.99	1.04	1.03	0.86	0.71
500	824.0	843.7	930.0	951.7	0.98	1.01	1.02	1.05	0.93	0.78
600	731.5	761.0	836.0	860.5	0.87	0.91	0.92	0.95	0.53	0.88
700	530.0	620.5	634.0	704.5	0.63	0.74	0.70	0.77	0.50	0.51
750	447.0	720.0	594.5	849.0	0.53	0.86	0.65	0.93	0.32	0.74
800	258.7	257.5	513.0	257.5	0.31	0.31	0.56	0.28	0.38	0.34
850	312.5	785.5	598.5	928.5	0.37	0.94	0.66	1.02	0.38	0.57
900	425.5	790.0	697.5	948.5	0.51	0.94	0.77	1.04	0.26	0.72

TABLE IV. REDUCTION FACTORS OF STRENGTH AND ELASTICITY MODULUS OF 10.9s BOLTS AFTER FIRE.

Attained temp. T_m (°C)	Yield strength $\sigma_{0.2, T_m}$ (N/mm ²)		Tensile strength σ_{b, T_m} (N/mm ²)		Reduction factor of yield strength $\sigma_{0.2, T_m}/\sigma_{0.2}$		Reduction factor of tensile strength $\sigma_{b, T_m}/\sigma_b$		Reduction factor of elasticity modulus E_{T_m}/E	
	Natural cooling	Water cooling	Natural cooling	Water cooling	Natural cooling	Water cooling	Natural cooling	Water cooling	Natural cooling	Water cooling
	20	1129.5	1122.5	1152.0	1152.0	1.00	1.00	1.00	1.00	1.00
100	1136.5	1136.5	1157.5	1157.5	1.02	1.01	1.00	1.00	1.00	0.92
200	1162.7	1115.0	1183.0	1191.0	1.03	0.99	1.03	1.03	1.03	0.86
300	999.0	1088.0	1016.5	1171.0	0.88	0.97	0.88	1.02	0.88	1.02
400	1163.0	1096.0	1175.0	1168.0	1.03	0.98	1.02	1.01	1.02	0.80
500	943.0	953.0	979.5	1004.5	0.83	0.85	0.85	0.87	0.85	1.00
600	850.0	812.0	886.5	866.0	0.75	0.72	0.77	0.75	0.77	0.92
700	659.0	647.3	722.0	800.3	0.58	0.58	0.63	0.69	0.63	0.67
750	539.5	869.5	621.0	1233.5	0.48	0.77	0.54	1.07	0.54	0.28
800	564.0	972.0	664.5	1372.0	0.50	0.87	0.58	1.19	0.58	0.51
850	332.0	1235.5	499.0	1409.0	0.29	1.10	0.43	1.22	0.43	0.39
900	425.0	1120.3	605.0	1330.0	0.38	1.00	0.53	1.15	0.53	0.38

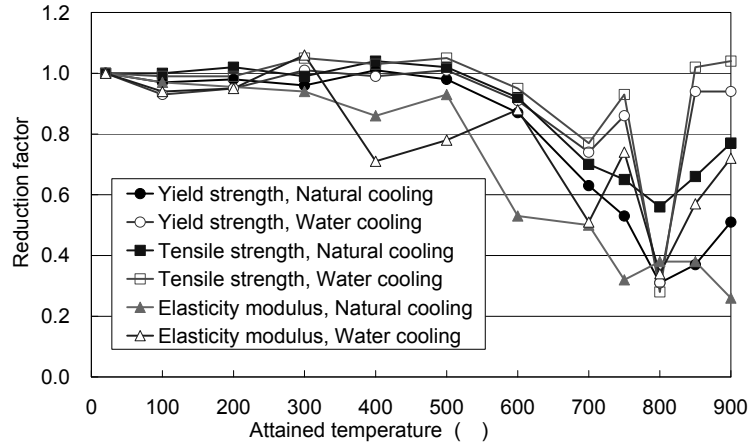


Figure 7. Reduction factors of strength and elasticity modulus of 8.8s high-strength bolts after fire.

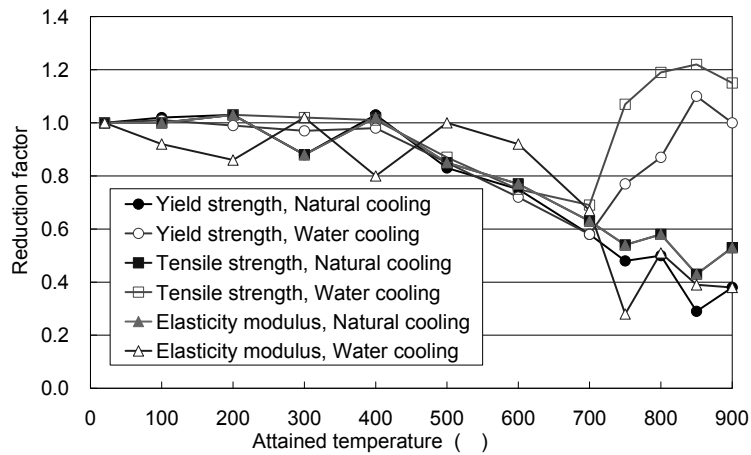


Figure 8. Reduction factors of strength and elasticity modulus of 10.9s high-strength bolts after fire.

CONCLUSIONS

This paper presents a series of experiments on the mechanical properties of high-strength bolts after fire. In order to simulate the real situations in event of fire, both natural cooling and water cooling were employed in the tests. The main conclusions that can be drawn from this study are given below:

(1) When high-strength bolts have achieved temperatures in no excess of 400°C, the mechanical properties of the bolts cooling after fire are not significantly affected regardless of the cooling method. Almost 100% strength of the bolts is regained and the ductility of them is changed slightly.

(2) When the temperature of high-strength bolts attained is between 400°C to 700°C, the stress-strain curves become more relaxed with increased ductility. With the attained temperature increasing, the strength and elastic modulus of the bolts cooling after fire reduce significantly. Furthermore, the different effects of natural cooling and water cooling on mechanical properties of high-strength bolts begin to appear, especially on the post-yield stress-strain curves at the attained temperature of 700°C.

(3) When the temperature of high-strength bolts attained is above 700°C, the cooling method

appears to have a great effect on the mechanical properties of high-strength bolts after fire. After natural cooling, the stress-strain curve becomes more relaxed with increased ductility, and the strength is regained slightly. After water cooling, the ductility reduces significantly which results in the disappearance of the yielding platform in the stress-strain curve, and with the attained temperature increasing the elasticity modulus remains decreasing with reduced rate, whereas the strength is regained to a great extent. For 8.8s high-strength bolts subjected to water cooling, the post-fire strength recovers to almost the same as the normal strength (but the post-fire strength decreases sharply at the attained temperature of 800°C), while for 10.9s high-strength bolts subjected to water cooling the post-fire strength even exceeds the normal strength approximately 20% when the attained temperature is in excess of 800°C.

(4) 400°C and 700°C are the key attained temperatures to the mechanical properties of high-strength bolts after fire.

(5) After heating and cooling the surface color of the bolts differs from the original color and is affected by the attained temperature and cooling method. This phenomena may be used during the post-fire inspection to determine the highest temperature attained in the bolts.

ACKNOWLEDGEMENTS

The research project was financially supported by National Natural Science Foundation of China (No.50308019) and the State Key Laboratory for Disaster Reduction in Civil Engineering (No.SLDRCE08-C-01). The financial support is highly appreciated.

REFERENCES

1. Tovey A K. Assessment and repair of fire-damaged concrete structures—an update. Evaluation and Repair of Fire Damage to Concrete, Publication SP-92, Harmathy T Z (Ed.), American Concrete Institute, Detroit MI., 1986.
2. Min M B, Li Y H. Assessment and repair of fire-damaged building structures. Jiangsu Science and Technology Press, 1994. (in Chinese)
3. Kirby B, Lapwood D, Thomson G. Reinstatement of fire damaged steel and iron framed structures. British Steel Corporation, Swinden Laboratories, UK, 1986.
4. Outinen J, Kaitila O, Mäkeläinen P. High-temperature testing of structural steel and modeling of structures at fire temperatures. Lab. of steel structures publications, TKK-TER-23, Espoo, 2001.
5. Cao W X. Structural behavior of steel frame with cumulative damage in fire. PhD. Thesis, Tongji University, 1998.
6. Hu Q. Experimental research on the mechanical properties of prestressing steel wire and stress-strain relationship in fire. PhD. Thesis, Harbin Institute of Technology, 2005. (in Chinese)
7. Zheng W Z, Hu Q & Zhang H Y. Experimental research on the mechanical properties of prestressing steel wire at and after high temperature. *Journal of Building Structures*, 2006, 27(2): 120–128. (in Chinese)
8. Fan J, Lü Z T. Experimental study on materials properties of prestressed steel wire post high temperatures. *Industrial Construction*, 2002, 32(9): 30–31. (in Chinese)
9. Kirby B R. The behavior of high-strength grade 8.8 bolts in fire. *Journal of Constructional Steel Research*, 1995, 33(1): 3–38.
10. Kokubo I, Tanaka A, Furumura F. Mechanical properties of high strength bolt under high temperatures : Part 1 The primary creep test. *Transactions of the Architectural Institute of Japan*, 1980, 309: 21–28. (in Japanese)
11. Kokubo I, Tanaka A, Furumura, Abe T. Mechanical properties of high strength bolt under high temperatures : Part 2 The relaxation test. *Transactions of the Architectural Institute of Japan*, 1982, 320: 56–63. (in Japanese)
12. Li G Q, Li M F, Yin Y Z. Experimental studies on the behavior of high-strength bolts made of 20mntib steel at elevated temperatures. *China Civil Engineering Journal*, 2001, 34(5): 100–104. (in Chinese)
13. Li X, Gu X L, Zhang W P etc. Safety assessment on a mill building with steel structure after fire. *Industrial Construction*, 2005, 35(z1): 376–379. (in Chinese)
14. GB/T228-2002 Metallic materials—Tensile testing at ambient temperature. (in Chinese)

Finite Element Analyses of Flexible End-Plate Connections Between Steel Beams and Columns at Elevated Temperatures

K. AL-JABRI and F. AL-JAHWARI

ABSTRACT

This paper presents a finite element analysis procedure developed to study the behavior of a flexible end-plate connection between steel beams and a column at elevated temperatures and generates temperature-rotation diagrams that describe the behavior of the connection. The analysis used a highly detailed three dimensional finite element model that is created using the commercial ABAQUS software. The steel connection properties are selected in a way that reflects commonly used connections in steel framed buildings.

The results of the finite element model are calibrated and compared to the results of experimental fire tests conducted on similar connections. The results show that the predicted behavior of the joints is in a good agreement with actual behavior of the joints. A regression model is developed to describe the behavior of flexible end-plate joints in fire.

Khalifa Al-Jabri (corresponding author), Ph.D., Department of Civil and Architectural Engineering, College of Engineering, Sultan Qaboos University, P.O. Box 33, Al-Khod, Post Code 123, Oman
Farooq Al-Jahwari, Lecturer, Department of Mechanical and Industrial Engineering, College of Engineering, Sultan Qaboos University, P.O. Box 33, Al-Khod, Post Code 123, Oman

INTRODUCTION

The behavior of structural steel connections is a complex phenomenon that had been investigated thoroughly by many researchers as such connections play an important role in overall structural stability. The behavior of those connections is even more complex under fire condition because of the material softening as well as the complex nature of the interaction between various members within the structural frame configuration.

Experimental investigation of those connections at elevated temperatures is very expensive both financially and from time aspect. However, a thorough understanding of the response of such connections under fire is a vital part in today designs of buildings from safety point of view. And hence, a finite element model that can reasonably predict the behavior of steel connection under fire will be a great aid for nowadays design engineers.

In recent years there has been an increased interest in the use of FE models in studying the behavior of beam-to-column semi-rigid joints in fire. The additional merit of using FE models over other numerical modeling techniques is that the behavior of the joint can be inspected visually in which the failure mechanism of the joint as well as the deformation of different components can be observed. Al-Jabri et al. [1] reviewed the available FE models that have been developed by various authors to predict the response of different joints at elevated temperature taking into account geometrical and materials non-linearity. They observed that there are little FE codes that were developed to predict the elevated temperature behavior of joints while ABAQUS and ANSYS are the most widely used general purpose FE programs which were used to model different types of bare-steel joint configurations at both ambient- and elevated-temperature. Both programs have demonstrated ability to predict the behavior of joints accurately.

GEOMETRY OF THE JOINT

An 8-mm thick flexible end-plates (FLB3) connecting a pair of 356 x 171UB51 beams to a 254 x 254UC89 column with eight M20 Grade 8.8 bolts was considered for this study based on experimental tests conducted by Al-Jabri et al. [2] as shown in Fig. 1. The test specimen consisted of a symmetric cruciform arrangement of a single column 2.7 m high with two cantilever beams of 1.9 m long connected either side to the column flanges. The beams connected to the column flanges with mild steel end-plates of Grade S275 and the bolts were tightened to 160 N.m torque. Tests were performed in a gas-fired portable furnace lined with ceramic fiber specially designed for testing connections. The instrumentation included clinometers for measuring rotations, displacement transducers, load cells and thermometers. Both analog and digital output devices were monitored through and Orion data logger.

The commercial finite element software ABAQUS [3] was used to develop a three dimensional finite element model for the analysis of the connection response under fire as shown in Fig. 2. A quarter model had been considered because of geometrical, material and boundary conditions symmetry. The extreme right end of the beam was restrained against lateral movement while allowing axial expansion. The bottom of column was fixed from all degrees of freedom while the top was allowed to have axial expansion. Symmetry boundary conditions have been assigned at appropriate directions at each sliced plane of the overall geometry. A concentrated force applied at distance 1500 mm from the centre of the column. A linear temperature gradient achieving 900°C have been assigned at the connection vicinity at an approximate coverage distance of 100 mm.

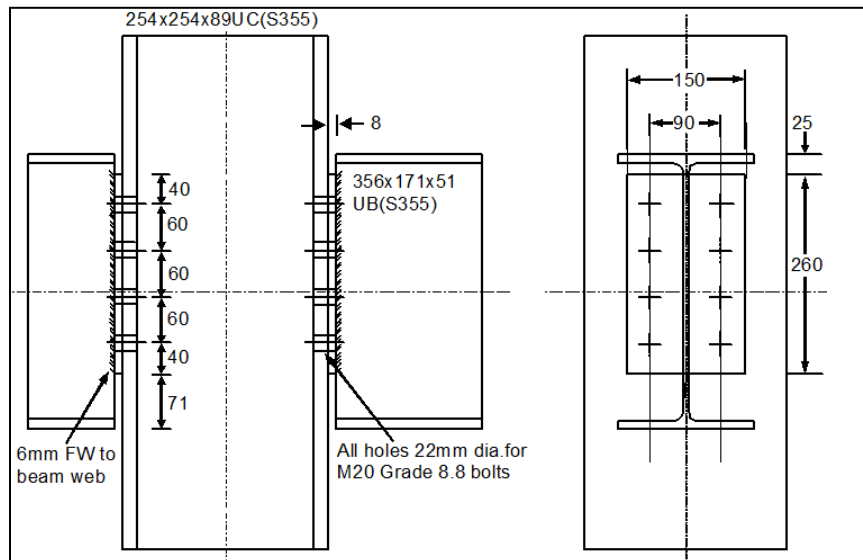


Figure 1. FLB3 flexible end-plate joint details.

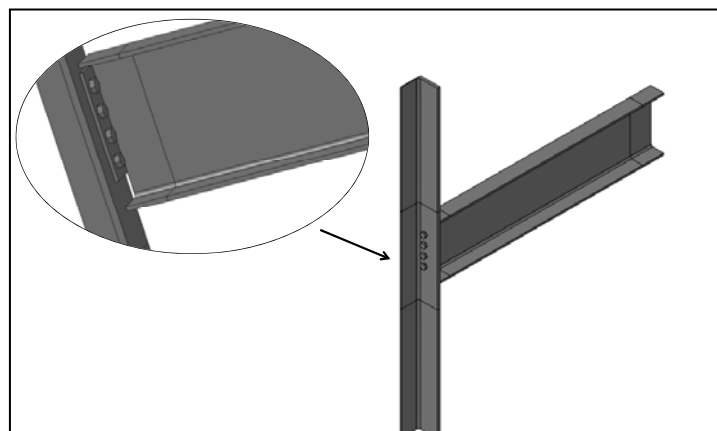


Figure 2. Three dimensional geometry of FLB connection.

An 8-node thermally coupled brick, trilinear displacement and temperature element was used with a 29582 total number of elements. The mesh density was aimed to be more at the connection vicinity at which the load severity is going to be present as shown in Fig. 3. The advanced front meshing routine was used to guarantee a reasonable aspect ratio for the elements and hence accurate prediction for the localized response. A 64-bit machine with parallel processing was used to tackle the computational efforts resulted from that large number of elements. The contact between different components was modeled using classical Coulomb friction model with a frictional coefficient of 0.1. The following equation was used for the calculations of connection rotation as the direct output is disabled in ABAQUS Coupled-Temperature-Displacement analysis step.

$$\varphi = \tan^{-1} \left(\frac{w}{L} \right) \quad (1)$$

where u is the vertical deflection of the point along the beam, and L is distance from the connection centerline to the point where deflection is taken.

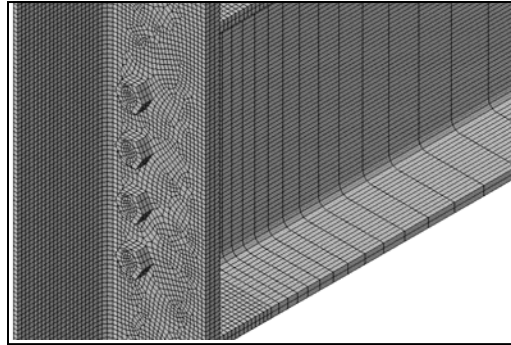


Figure 3. The mesh with more density at the connection vicinity.

The thermal and mechanical properties of steel at elevated temperatures were used as per EC3-1.2 [4]. The reduction factors for both the effective yield strength and modulus of elasticity at different temperatures that reflect the degradation of steel properties as it gets heat up were taken as per the above mentioned standard. The basic properties considered at ambient temperature are shown in Table 1.

Table 1. Material properties of steel at ambient temperature.

Mechanical Properties			Other Properties	
	σ_y (N/mm ²)	E (kN/mm ²)	Poisson's Ratio	0.3
Grade 355	412	195	Density (kg/mm ³)	7.85×10^{-6}
Bolts Grade 8.8	480	195	Thermal Expansion (1/°C)	1.2×10^{-5}
			Thermal Conductivity (W/mm.°C)	6.05×10^{-2}
			Specific Heat (J/Kg.°C)	434

RESULTS AND DISCUSSION

The rotations at different temperatures obtained from finite element analysis (FEA) were compared to those obtained experimentally. FEA results are in a good agreement with experimental findings as shown in Figs. 4 and 5. Fig. 4 shows the runs that were made for 10%, 20%, and 50% of the calculated moment capacity, namely, 8 kNm, 16 kNm, and 40 kNm. The deformation mode compared between the experimental observation and FEA is shown in Figs. 5a and 5b, respectively. The FEA is very much predicting the deformation mode as enough mesh density was provided at the connection vicinity where the critical loading effect is present and severe contact condition predominant there. Fig. 5c shows the Von Mises stress distribution of a

deflected beam where the maximum stress localized around the bolts at which the bending effect is pulling off the bolts and stressing the column area that comes in contact with the beam-flange at which the moment-rotation profile takes a higher slope values as shown in Fig. 6.

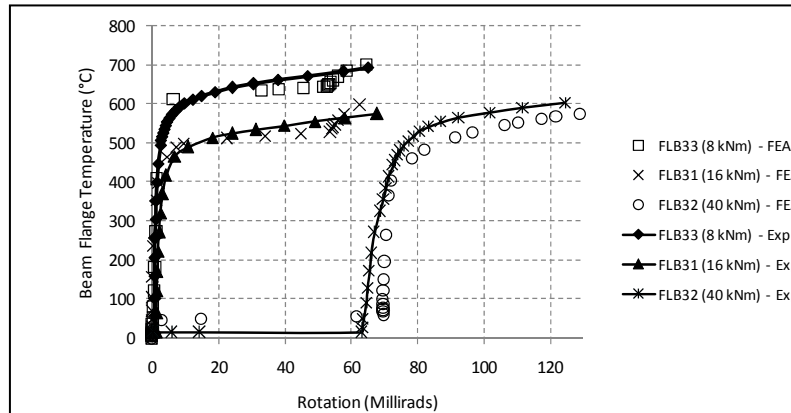


Figure 4. Temperature- rotation response of FLB3 tests.

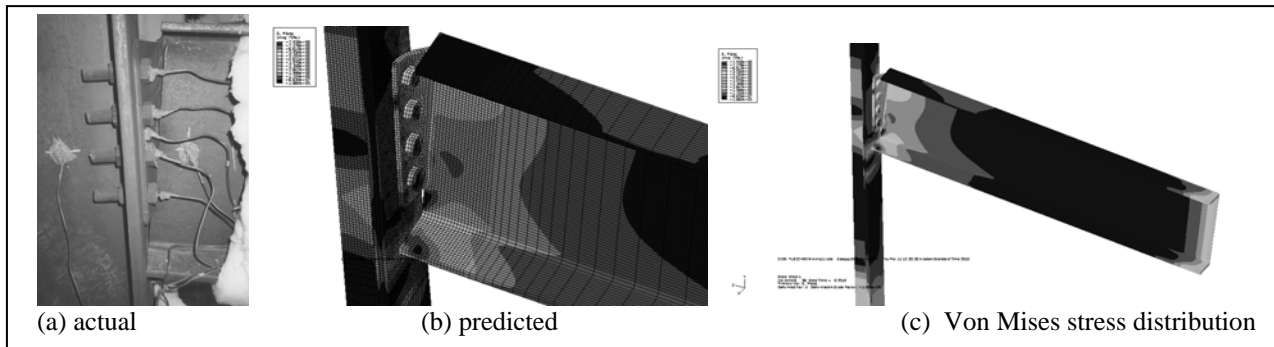


Figure 5. Comparing the FEM deformation mode to the experimental observed deformation and the Von Mises stress distribution over the deflected beam.

Simplified mathematical expressions based on a modified Ramberg-Osgood expression [5] were developed using FEA results after verifying them against experimental observations. Such expressions will help in describing the connection behavior over the entire range of rotation up to failure which provides designers with the right tool for safe designs. SPSS software was used to perform a nonlinear regression analysis to find out the best-fit parameters of the equations 2 and 3. Those finalized parameters are shown in Table 2.

$$\phi = \frac{M}{A} + 0.01 \left(\frac{M}{E} \right)^n \quad (2)$$

$$\phi = \phi_1 + \frac{(M - M_1)}{A_1} + 0.01 \left[\frac{(M - M_1)}{E_1} \right]^{n_1} \quad (3)$$

Fig. 6 shows the good agreement between FEA and experimental findings for the entire range of rotation including the two stages before and after the contact between the beam-flange and the column. As observed, a rapid rotation initially occur at low values of the bending moment while requiring higher values of moment for even smaller rotations once that contact initiated. The

nonlinear regression model developed in this paper providing an accurate approximation for the moment-rotation curve for both stages as clearly presented by Fig. 7.

Table 2. Nonlinear regression parameters of modified Ramberg-Osgood expression.

Temperature (°C)	A	B	n	A ₁	B ₁	n ₁	θ_1 (Millirads)	M ₁ kNm
100 - 400	15.490	7.220	8.432	1.985	2.135	2.73	56.47	20.79
600	-0.509	0.314	2.540	0.613	0.655	2.330		11.74

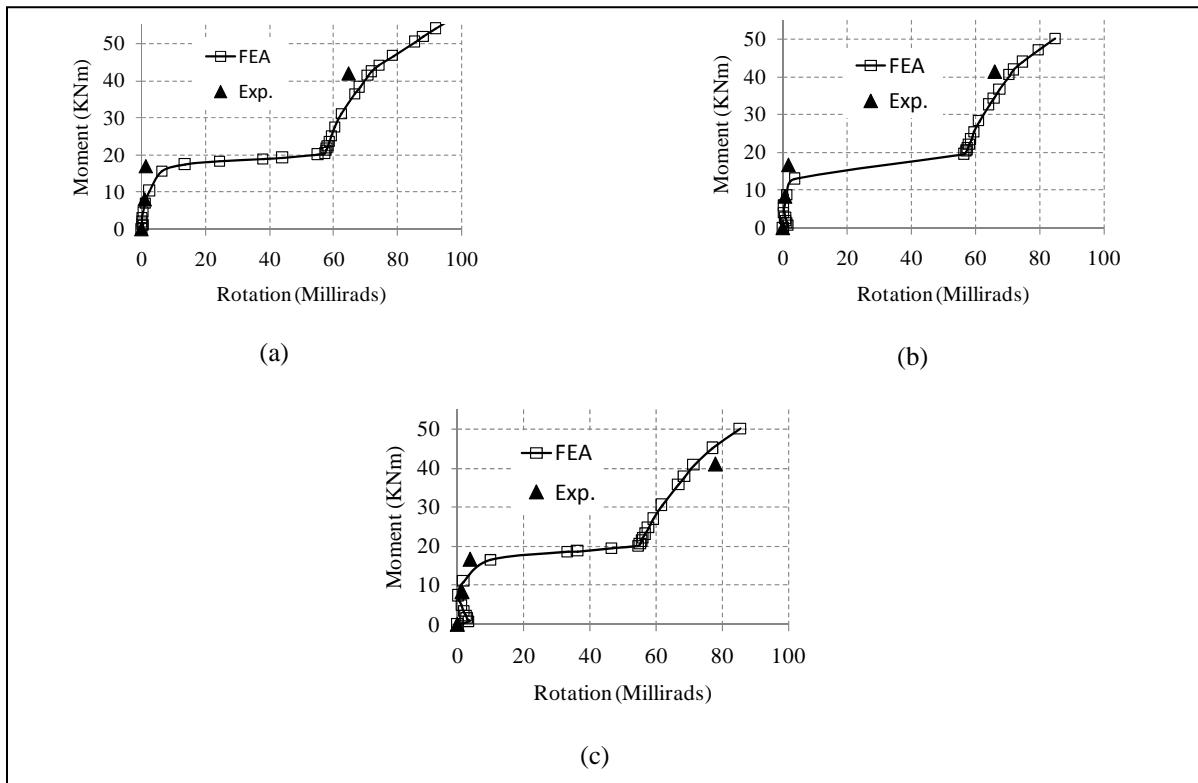


Figure 6. Moment- rotation curves for temperature of; (a) 100°C, (b) 200°C and (c) 400°C.

CONCLUSIONS

This paper presented a finite element analysis procedure developed to study the behavior of a flexible end-plate connection between steel beams and a column at elevated temperatures and generates temperature-rotation diagrams that describe the behavior of the connection. The analysis used a highly detailed three dimensional finite element model that was created using the commercial ABAQUS software. The results of the finite element model were calibrated and compared to the results of experimental fire tests conducted on similar connections. The results showed that the predicted behavior of the joints is in a good agreement with actual behavior of the joints. A

regression model was developed to describe the rotational behavior of flexible end-plate joints in fire providing an accurate approximation for the moment-rotation-temperature response for both stages.

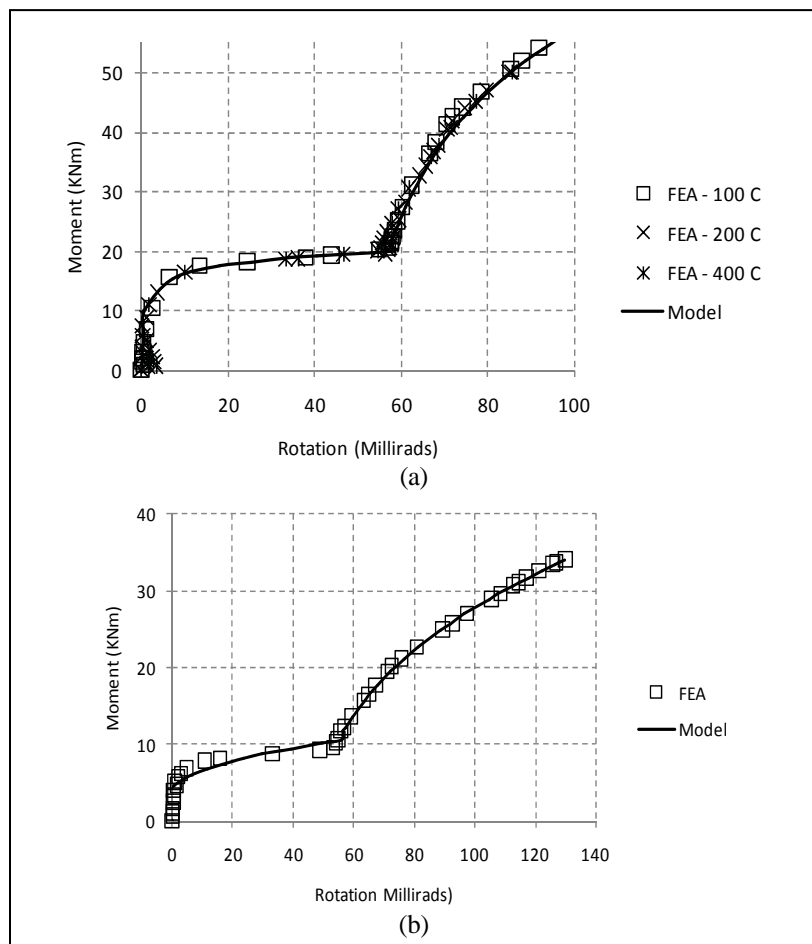


Figure 7. Nonlinear Regression model for (a) 100-400°C, (b) 600°C.

REFERENCES

1. Al-Jabri K.S., Davison, J.B. and Burgess I.W. "Performance of beam-to-column joints in fire - a review", *Fire Safety Journal*. 43(2008), p. 50–62.
2. Al-Jabri K.S., Burgess I.W., Lennon T. and Plank R.J. "Moment-rotation-temperature curves for semi-rigid joints", *Journal of Constructional Steel Research*, 61(2005), p. 281–303.
3. ABAQUS. *Abaqus/Standard User's Manual*. V6.9. 1, Hibbit, Karlsson and Soresen, Inc., USA, 2009.
4. EC3. *Design of steel structures—Part 1.2: general rules—structural fire design*. European Committee for Standardization, DD ENV 1993-1-2:2001, CEN, Brussels.
5. Ramberg W., and Osgood W.R. *Description of stress-strain curves by 3 parameters*. Technical Report 902, National Advisory Committee for Aeronautics; 1943.

How Connections Affect Global Response

K. ANDERSON and M. GILLIE

ABSTRACT

Recent research into the behaviour of steel connections in fire has focused on the testing of isolated connections with the aim of establishing moment-rotation-shear-axial behaviour. Experiments have typically been conducted on unprotected connections without an adjacent concrete slab. Numerical research, meanwhile, has focused on the characterisation of connection response given specific loading (thermal and mechanical) conditions. While these research areas are invaluable for structural understanding, it is important to consider how interaction with the surrounding structure can affect connection response.

In this paper, a numerical study has been conducted to examine the effect of connection type on structural response. The structure considered is a 16 bay single storey steel-concrete composite structure where one bay is subject to heating and then cooling during a parametric fire curve. The beam-to-beam and beam-to-column connections are varied from fully-fixed in rotation to partially-fixed to pinned. It is demonstrated that the magnitude of forces, deflections and rotations in the connections and beams are not significantly affected by the connection behaviour. However, the moments in the structural columns are found to be affected by varying the connection stiffness.

INTRODUCTION

The subject of connection behaviour in fire has recently been at the forefront of many researchers' activities. Studies have ranged from experimental isolated joint testing [1-5] to finite element modelling [6-8] and the development of the

BRE Centre for Fire Safety Engineering, School of Engineering and Electronics, The University of Edinburgh, King's Buildings, Mayfield Rd, Edinburgh EH9 3JL

component method for the design of connections in fire [9-11]. Experiments have typically been conducted on unprotected connections without an adjacent concrete slab. Meanwhile, numerical modelling has focused on the characterisation of connection response given specific loading (thermal and mechanical) conditions. While these research areas are invaluable for structural understanding, it is important to also consider how interaction with the surrounding structure can affect connection response and, as the design of structures moves towards a performance-based approach, an understanding of this interaction becomes essential. During the design process, it is often assumed that the steel-steel connection rotational capacity in steel-framed composite structures is unlikely to affect response of a structure. This paper explores the validity of this assumption.

Another important consideration is the interaction between the slab and beams. In numerical modelling, complete composite action is often assumed and to model this composite action, the slab will be tied completely to the beams. However, in practice there will be no shear tie in the direct vicinity of the columns. Use of this modelling technique will be validated here.

The final design assumption considered in this paper is that internal columns will not be subject to large bending moments and are therefore designed as such. This is appropriate for ambient temperature but a fire may increase these moments to a degree which should be accounted for in design.

This paper initially discusses how varying connection rotational behaviour, from fully fixed to partially fixed to pinned, affects structural response. It then examines how varying the extent of shear connection between the slab and the beams changes structural behaviour. Finally, the bending moments along the length of the column at various temperatures are investigated.

For these purposes, steel-framed composite building was modelled numerically. The building has 16 bays of 9m by 6m with compartment walls assumed to be located every 9m in the x -direction and every 12m, or at every second column, in the z -direction, see Fig. 1. Beams and columns were sized according to the structural Eurocodes and a 2.5kN/m^2 load, the design load for an office [12], was imposed on the floor slab. Temperature dependant material properties were used also according to the Eurocodes.

MODELLING TECHNIQUE

One storey of a structure was modelled using the finite element program Abaqus with the layout as shown Fig. 1. To provide a basic representation of a multi-storey structure, two storey columns have been included where the bases of the columns are fully fixed and the tops are free to translate in the vertical direction.

During the analysis, one 12m by 9m compartment (shaded in figs 1 and 2) was first heated then cooled whilst the other areas remained at ambient temperature throughout. A gas phase temperature-time curve was calculated according to a parametric fire curve [13]. The heating phase of the fire lasted 70 minutes and the

cooling phase 80 minutes. Heat transfer calculations were carried out to calculate the steel temperatures (assumed to be constant through beam and column cross-sections), and the slab temperatures at 5 points through the depth. Temperatures in the structure were calculated for a period of 80 minutes beyond the point at which peak gas temperatures were reached.

Initially, composite action between the beams and slab was assumed in all locations apart from the 300mm adjacent to all columns. This was modelled by tying each beam node to an adjacent slab node. At each beam-to-beam and beam-to-column location, a connector element was included. The stiffness of this element was varied from fully fixed to partially fixed to pinned. Where partial fixity was specified, the rotational stiffness was based on a percentage of the stiffness of the columns e.g. 25% fixity was defined as 25% of the column stiffness varying with temperature.

Each model was run for 160 minutes. The first 10 minutes represent the loading stage where the whole structure is at ambient. For the next 70 minutes, an area of the structure, as indicated with dark grey shading in fig. 1, is heated and for the remaining 80 minutes the structure cools back to ambient.

RESULTS

Rotational Stiffness

In order to evaluate the effect of connection rotational stiffness on structural behaviour, beam mid-span deflection and axial force in the beam adjacent to the connection were considered.

Figures 3 and 4 show the axial force for the fixed and pinned models in two locations: A—the heated beam located next to the beam-to-column connection where the column is assumed to be protected, and B—the heated beam next to the beam-to-beam connection where the primary beam is assumed to be protected. Whilst there is an observable difference in the axial force at A in the later cooling stage, the overall trend of axial forces at both locations is very similar for the models using fixed or pinned connections. Only the pinned and fixed situations are shown as the partially fixed results fall between these two results.

Similarly, the vertical deflections observed at C and D in the fixed and pinned models predict almost identical deflection trends. These two results suggest that the rotational capacity of a connection will affect neither the deformed shape of a structure nor the axial force experienced in the connection.

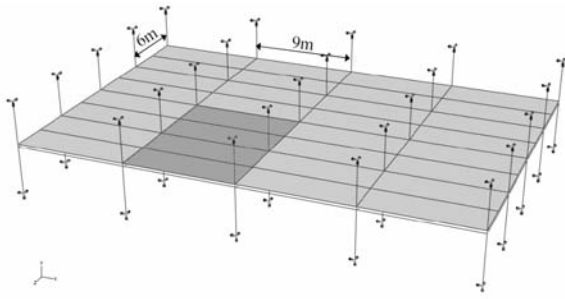


Figure 1. General Layout.

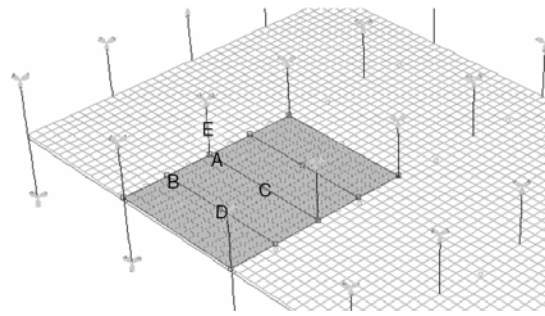


Figure 2. Locations of Interest.

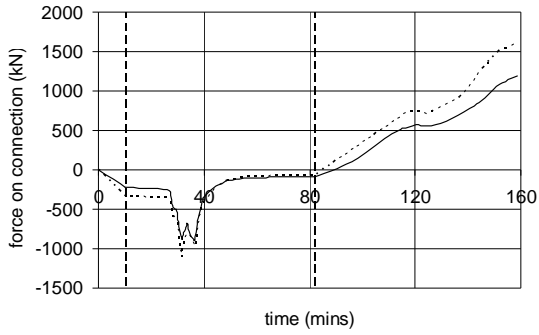


Figure 3. Axial Force at A.

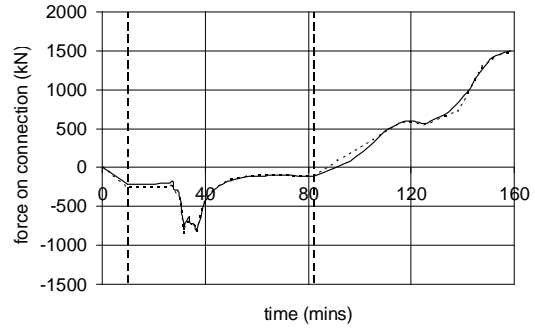


Figure 4. Axial Force at B.

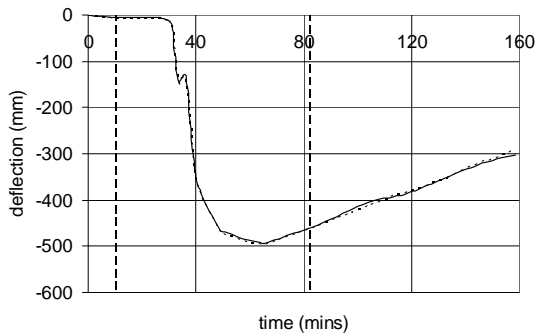


Figure 5. Vertical Deflection at C.

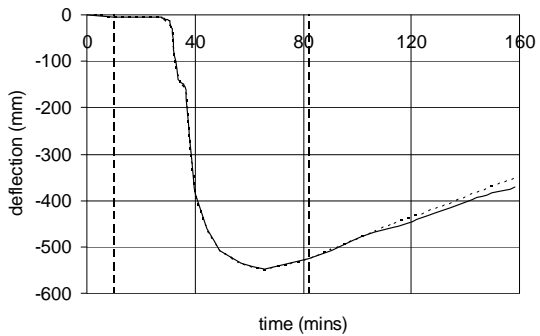


Figure 6. Vertical Deflection at D.

..... Pinned Model
 — Fixed Model

..... Pinned Model
 — Fixed Model

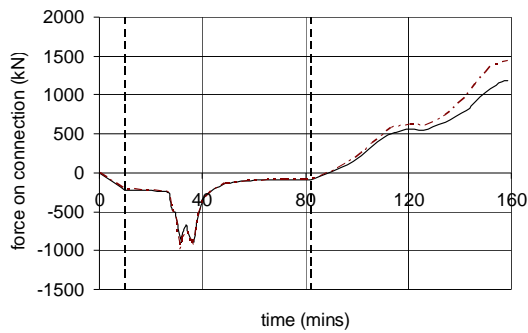


Figure 7. Change in Axial force with change in slab restraint at location A.

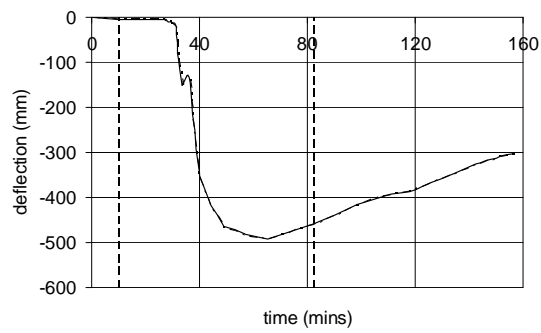


Figure 8. Change in vertical deflection with change in slab restraint at location B.

— Normal Restraint
 ---- Increased Restraint

NB: The starts of the heating and cooling stages are indicated by vertical dashed lines at 10 minutes and 80 minutes into the analyses.

Shear Tie

Figures 7 and 8 show the axial force and beam deflection for fixed connection models where in the normal restraint condition, which has been used in the rest of the analyses, each beam node is tied to the slab directly above apart for at the node nearest the column. This results in 300mm of slab in all directions around the column not being tied to the beams. This is more representative of common construction practice in the UK. For the increased restraint condition the slab is completely tied to all beam nodes including those adjacent to the columns. This interaction model is common in numerical modelling of this type. It can be seen in Figs. 8 and 9 that changing this restraint has a minimal effect on beam axial forces and also that there is no noticeable difference in the predicted beam mid-span deflection.

Column Bending Moments

The bending moments in column E, Fig. 2, are shown in Figs. 9–12 at a number of temperatures throughout the analysis and for 4 different connection assumptions: pinned, 25% fixed, 50% fixed and fully fixed where the percentages indicate the percentage of column stiffness the connection is assumed to possess rotationally. These figures show that the assumption of minimal moment at ambient is valid however as the structure heats and deforms, large moments occur in the columns: moments at 200°C are around 20 times larger than those at ambient. As the temperature increases and the materials begin to degrade, the moments reduce by up to 60% but still remain significantly larger than at ambient temperature.

The connection rotational stiffness appears to have a more significant effect on column bending moments than on either the beam axial forces or deflections. The

maximum moment at 200°C is around 200kNm for the pinned and partially fixed connections but 225kNm for the fixed. A more apparent difference is at high temperature where the maximum moment at 800°C is about 100kNm for the fixed and partially fixed models however this reduces to 60kNm in the pinned model.

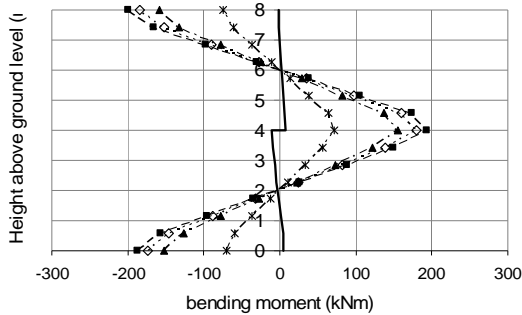


Figure 9. Column bending moments, pinned connections.

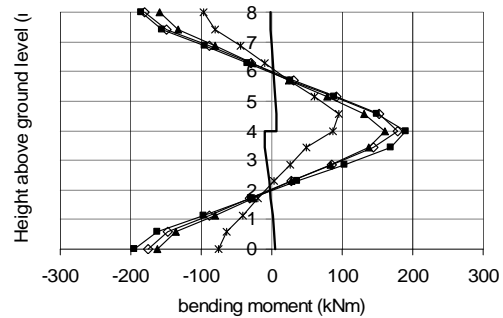


Figure 10. Column bending moments, 25% fixed connections.

— 20°C
 - - - 200°C
 ···· 400°C
 - · - · 800°C

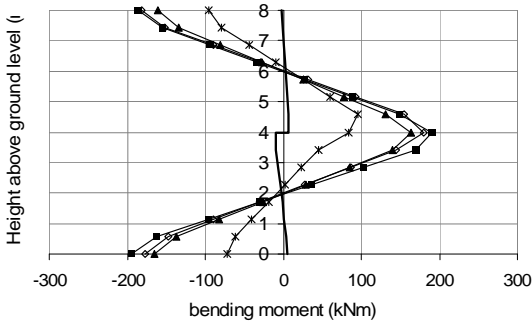


Figure 11. Column bending moments, 50% fixed connections.

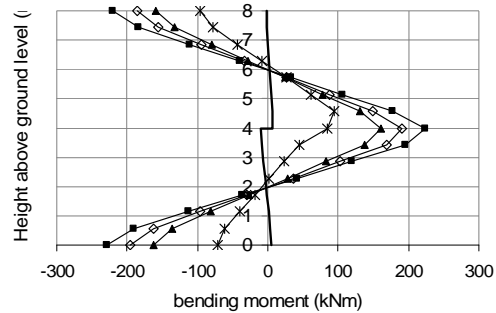


Figure 12. Column bending moments, fully fixed connections.

CONCLUSIONS

During fire, connection rotational stiffness has been found to have negligible effect on the deflected shape of a structure and the axial forces of the beams near the connections.

The extent of the shear tie between the slab and beams in this situation showed no significant differences in axial force of deflections.

Upon heating, the bending moments in the columns become significant.

The third conclusion here is of interest because it implies that care should be given to modelling connection behaviour realistically in structural-fire calculations if accurate estimates of column moments are to be obtained. In this modelling the

columns were assumed to be cold (due to fire protection) in line with common design practice. It is noteworthy that fire protected members may be subject to loads for which they are not designed due to the response of non-fire protected members elsewhere in the structure.

The shear tie between the slab and beams is assumed here, and in many numerical models, to be sustained for the length of a fire. It has however been shown experimentally that this will not always be the case [14] Further work must be carried out where the degradation of this interaction is included.

ACKNOWLEDGEMENTS

The financial support of the Arup Fire and EPSRC that allowed this work to be undertaken is gratefully acknowledged.

REFERENCES

1. Yu, H., et al., *Experimental investigation of the behaviour of fin plate connections in fire*. Journal of Constructional Steel Research, 2009. 65(3): p. 723–736.
2. Yang, K.-C., S.-J. Chen, and M.-C. Ho, *Behavior of beam-to-column moment connections under fire load*. Journal of Constructional Steel Research, 2009. 65(7): p. 1520–1527.
3. Al-Jabri, K.S., et al., *Behaviour of steel and composite beam-column connections in fire*. Journal of Constructional Steel Research. 46(1-3): p. 308–309.
4. Al-Jabri, K.S., et al., *Moment-rotation-temperature curves for semi-rigid joints*. Journal of Constructional Steel Research, 2005. 61(3): p. 281–303.
5. Saedi Daryan, A. and M. Yahyai, *Behaviour of welded top-seat angle connections exposed to fire*. Fire Safety Journal, 2009. 44(4): p. 603–611.
6. Al-Jabri, K.S., A. Seibi, and A. Karrech, *Modelling of unstiffened flush end-plate bolted connections in fire*. Journal of Constructional Steel Research, 2006. 62(1-2): p. 151–159.
7. Sarraj, M., et al., *Finite element modelling of steel fin plate connections in fire*. Fire Safety Journal, 2007. 42(6-7): p. 408–415.
8. Selamat, S. and M.E.M. Garlock, *Behavior of Steel Plate Connections Subject to Various Fire Scenarios*, in *Structures in Fire 2008*: Singapore. p. fad.
9. CEN, *Eurocode 3: Design of steel structures part 1-8: Design of Joints*. 2005, British Standards Institute.
10. Simões da Silva, L., A. Santiago, and P. Vila-Real, *A component model for the behaviour of steel joints at elevated temperatures*. Journal of Constructional Steel Research, 2001. 57(11): p. 1169–1196.
11. Block, F.M., et al., *The development of a component-based connection element for endplate connections in fire*. Fire Safety Journal, 2007. 42(6-7): p. 498–506.
12. CEN, *Eurocode 1: Actions on Structures part 1-1: General actions—Densities, self-weight, imposed loads for buildings*. 2002, British Standards Institute.
13. CEN, *Eurocode 1: Actions on structures part 1-2: General actions—Actions on structures exposed to fire*. 2002, British Standards Institute.
14. Lim, L., *Membrane Action in Fire Exposed Concrete Floor Systems*, in *Department of Civil Engineering*. 2003, University of Canterbury: Canterbury.

MATERIAL BEHAVIOUR

Constitutive Equations and Empirical Creep Law of Structural Steel S460 at High Temperatures

R. SCHNEIDER and J. LANGE

ABSTRACT

The knowledge of the stress-strain relationships of structural steel at elevated temperatures is essential for the assessment of the load-carrying capacity of steel structures in case of fire. In the Eurocode 3 Part 1-2 [1], constitutive equations are given for temperatures up to 1200°C. They are uniform for steel grades from S235 to S460 and are based on numerous test results predominantly obtained on steel grade S235. For the high strength fine-grained structural steel S460 only very few and widespread test results exist. Especially the short time creep behaviour at high temperatures has not been analysed yet for this steel type. A current research project comprises transient tests for numerous commercial fine-grained S460 steels and allows therefore a more precise determination of the stress-strain relationships at high temperatures. Especially the influences of the delivery condition (normalized rolled or thermomechanical rolled) and the chemical composition focussing on certain alloying elements are investigated. A second main work package concentrates on the analysis of creep. For this purpose, transient tests at different heating rates are carried out for the quantification of creep strain, and an empirical creep law, based on the concept of temperature-compensated time, is derived. As a result, the constitutive equations can be expressed taking account of the heating rate. Differences between the high temperature load-carrying capacity of steel structures made of S460 according to the research results and under the terms of [1] are pointed out.

1 STATE OF THE ART

Figure 1 shows the temperature dependent yield strength given in [1] for fine-grained structural S460 steel ($f_y = 460 \text{ N/mm}^2$) in comparison with documented research results; see Ruge and Winkelmann 1980 [2], ARBED-Recherches 1991 [3], Winter 1998 [4], Outinen et al. 2001 [5] and Lange and Wohlfeil 2007 [6]. These few existing research results for S460 have a wide scatter range and deviate noticeably from the normative standard. This puts the validity of the constitutive equations given in [1] into question for this steel type. One possible reason for the diverging high temperature performance of S460 is the grain-boundary strengthening that is mainly responsible for the elevated strength of S460 at room temperature, but it is assessed to be ineffective or even disadvantageous at elevated temperatures.

Dipl.-Ing. Regine Schneider and Prof. Dr.-Ing. Jörg Lange, Institute for Steel Structures and Material Mechanics, TU Darmstadt, Petersenstrasse 12, 64287 Darmstadt, Germany

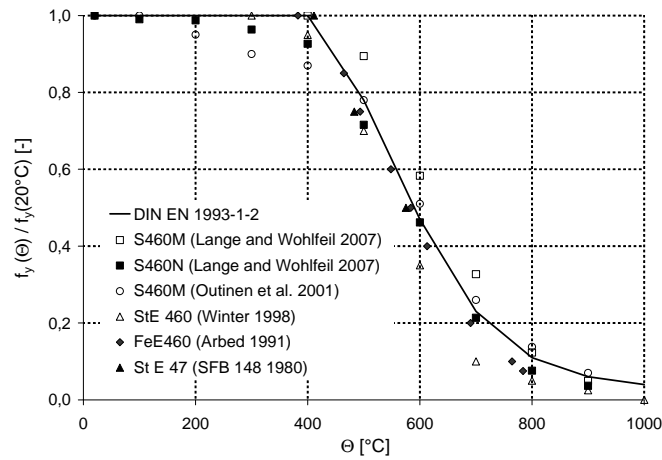


Figure 1. Temperature-depending yield strength reduction ($R_{2,0}$) for S460.

Lange and Wohlfeil [6] did research on the high temperature behaviour of S460 quite recently at the Institute for Steel Structures and Material Mechanics. In the performed transient tests, the tested S460M showed a very good high temperature performance, see Fig. 1. According to [6], the reason for that lies in the very special rolling process, leading to a fine grain microstructure, and in the niobium and titanium segregations retarding the creep process. The tested S460N showed, by contrast, a material behaviour which lay considerably below the standards given in [1]. With the objective of a larger data base, extensive experimental tests are currently carried out with numerous commercial high strength fine-grained structural S460 steels. This paper describes the test programme of the present research project and the obtained results and compares them to the actual state of the art. Furthermore, an innovative way of dealing with time-depending strain components is pointed out. While in the past, creep strain was either taken into account implicitly by performing transient tests or was determined explicitly in steady state tests, in this paper creep is explicitly expressed on the basis of transient test results.

2 HIGH TEMPERATURE TESTS OF S460 SPECIMENS

2.1 Test Method and Experimental Set-up

Stress-strain relationships at elevated temperatures can either be obtained in steady state or transient tests. Transient tests which are characterized by a constant load in combination with a defined heating process deliver more realistic results concerning the material behaviour in case of fire, and therefore for the current tests the transient test method was chosen. Carrying out several tests at different load levels, the result of the transient tests is a set of temperature-strain curves. After elimination of the thermal strain ϵ_{th} , stress-strain relationships can be derived from these curves. Strictly speaking, the obtained stress-strain relationships are only valid for the particular heating rate chosen for the testing procedure. Furthermore, the time-independent, load-dependent strain ϵ_{pl} and the creep strain ϵ_c can no longer be separated from each other without further ado. Figures 2 and 3 show the experimental set-up and the shape of the standard test specimen. The dimensions were chosen in accordance with DIN EN 10002 Part 5 [7]. The tests were carried out at the Institute for Physical Metallurgy, Department of Materials Science, TUD, in a furnace which was equipped with three separately controlled heating zones. The gauge length of the extensometer was 15 mm. The temperature of the test specimen was determined by an additional thermocouple attached to the specimen surface.

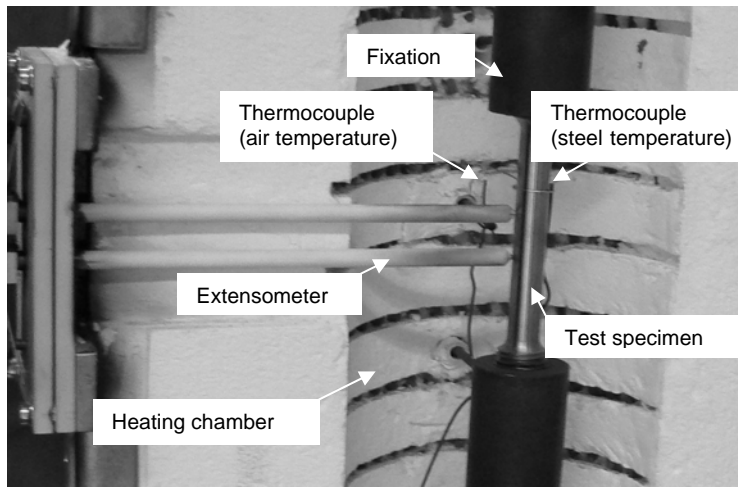


Figure 2. Testing device.

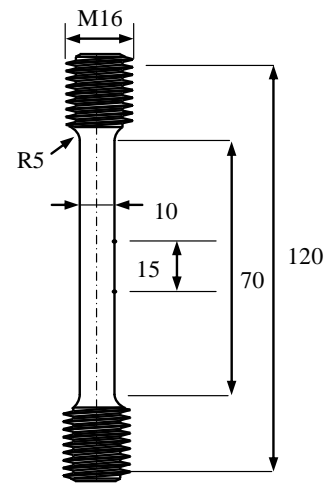


Figure 3. Test specimen [mm].

2.2

2.3 Tested Materials and Test Programme

The investigated weldable fine grain structural S460 steels are standardized in DIN EN 10025 Parts 3 and 4 ([8], [9]) and differ in their delivery conditions (normalized - N - or thermomechanical - M - rolled) as well as in their chemical composition. To assess the influence of these differences on the high temperature performance of S460, a total of 8 common materials was tested, see Table 1. Material “PM” is a thermomechanical rolled steel for pressure purposes according to DIN EN 10028 Part 5 [10]. All materials were tested under transient test conditions at a constant heating rate of 10 K/min and at 10 different load levels between 25 and 500 N/mm². In general, two tests were carried out on each load level. In addition, two quasi-unstressed tests were carried out for each material to determine the thermal expansion. Materials M1 and M2 were additionally tested in transient tests at constant heating rates of 3, 6, 20 and 30 K/min and at different load levels.

TABLE I. CHEMICAL COMPOSITION IN % (MANUFACTURER’S MELTING ANALYSIS) AND STRENGTH VALUES (IN ROLLING DIRECTION, OWN TESTS).

Steel grade	S460M				P420M	S460N		
Shortcut	M1	M2	M3	M4	PM	N1	N2	N3
Fabrication	ACC	ACC	ACC	QST				
Type of product	Plate 25 mm	Plate 25 mm	Plate 58 mm	HEA 320	Plate 60 mm	Plate 60 mm	Plate 35 mm	IPE 550
C	0.090	0.130	0.084	0.070	0.060	0.161	0.170	0.100
Si	0.280	0.300	0.366	0.210	0.257	0.423	0.320	0.220
Mn	1.610	1.520	1.640	1.030	1.260	1.610	1.550	1.660
Nb	0.049	0.038	0.022	0.039	0.020	0.003	0.002	0.030
V	0.004	0.060	0.000	0.010	0.000	0.156	0.163	0.110
Al	0.036	0.028	0.032	0.003	0.034	0.011	0.022	0.026
Ti	0.020	0.015	0.003	0.001	0.002	0.001	0.002	0.000
Cr	0.030	0.060	0.208	0.170	0.047	0.034	0.030	0.050
Mo	0.003		0.009	0.030	0.361	0.035	0.002	0.010
Ni	0.040	0.030	0.034	0.140	0.038	0.131	0.640	0.050
Cu	0.060	0.030	0.026	0.350	0.022	0.015	0.030	0.040
CEV	0.372	0.411	0.405	0.316	0.356	0.484	0.512	0.417
R _{eH} [N/mm ²]	525	558	521	509	444	507	489	479
R _m [N/mm ²]	598	666	589	584	529	640	644	584

3 TEST RESULTS

3.1 Transient Tests with 10 K/min Heating Rate

Figures 4 and 5 show the yield strength ($R_{t2,0}$) reduction factor in dependence of the temperature for all tested materials, separately for the delivery conditions M and N, compared to [1]. Figures 6 and 7 show the stress-strain relationships for 500 °C as constructed from the temperature-strain curves of the transient tests. It can be seen clearly that the thermomechanical rolled steels show a better high temperature performance than the normalized ones. However, nearly none of the tested materials reaches the specifications of [1]. This applies to the whole tested temperature range up to 800 °C. Comparing just the S460M steels, material M2 performs best. Compared to M1, M3 and M4, it has the highest total content of niobium, vanadium und titanium. These elements are important for the development of the fine grain microstructure. This shows that a high content of certain alloying elements has, in combination with the thermomechanical rolling process, a positive influence on the high temperature performance of structural S460 steel. Remarkable are the very favourable results for the tested steel “PM” due to a high content of molybdenum (0.36 %, see Table 1) that increases the creep resistance by solid solution strengthening.

Based on the weakest thermomechanical and normalized rolled steel, the test results were described for both delivery conditions by mathematical functions. The stress-strain relationships can be described by an elliptical curve and straight lines as in [1], by a power function according to Ramberg and Osgood 1943 [11] or by an equation proposed by Richard and Abbott 1975 [12], as shown by Poh 1997 [13]. Figures 8 and 9 show the test results approximated by an elliptical curve and straight lines. It is obvious that the stress-strain relations according to [1] considerably overestimate the high temperature performance of S460 shown in the tests. The consequence is an overestimation of the bearing capacity of structural members made of S460 steel in fire design according to [1], see Chapter 4.

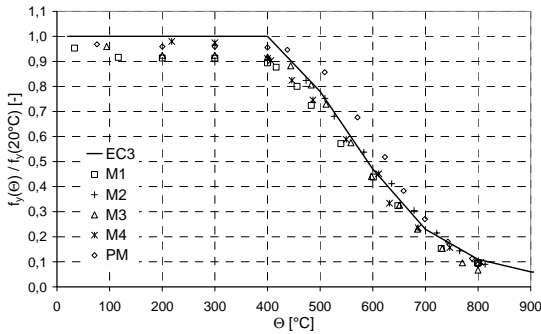


Figure 4. Yield strength reduction factor (M).

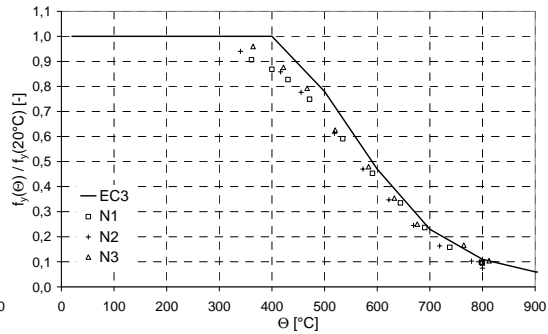


Figure 5. Yield strength reduction factor (N).

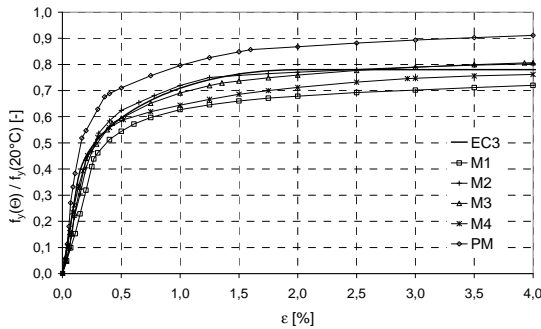


Figure 6. - -relationships at 500 °C (M).

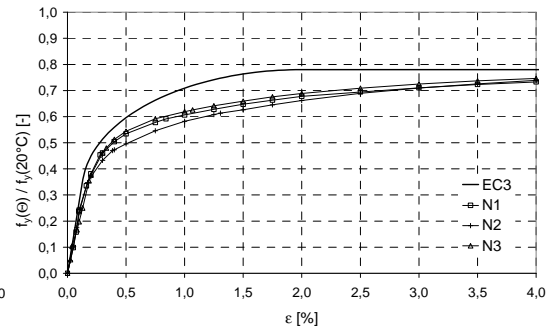


Figure 7. - -relationships at 500 °C (N).

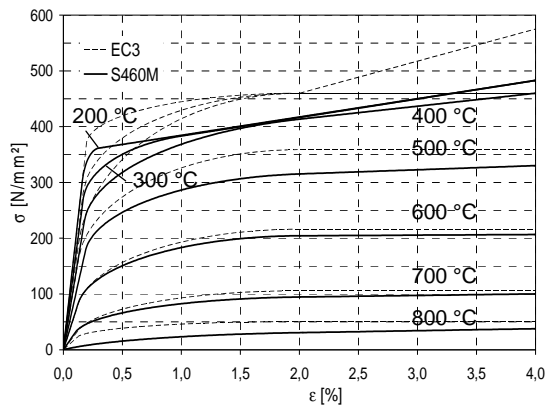


Figure 8. - -relationships 200 - 800 °C (M).

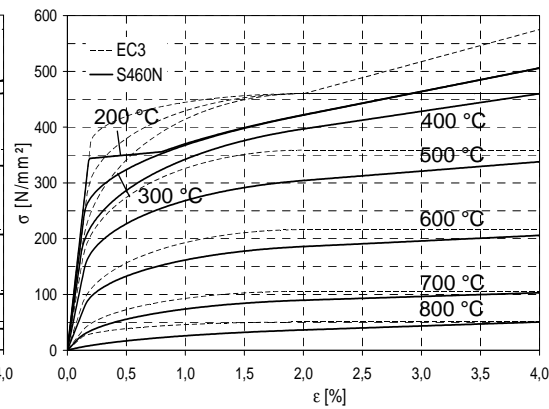


Figure 9. - -relationships 200 - 800 °C (N).

3.2 Transient Tests with Different Heating Rates

Figure 10 shows the results of transient tests at a uniform load level of 170 N/mm², but at different heating rates. With increasing heating rates, smaller strain values and higher failure temperatures can be observed because of the smaller amount of creep included in the test results. Regarding a certain temperature, the differences between the measured strain values of the various curves are only due to different amounts of creep strain ϵ_c . Hence creep behaviour of the material can be described by analysing the strain differences between the curves measured at different heating rates. The evaluation of the test results was carried out using the concept of temperature-compensated time θ , see Dorn 1954 [14], Harmathy 1967 [15] and Skowronski 2004 [16], because it allows for taking into account continuously varying temperatures during the creep process without the application of laborious superposition rules, e.g. the strain hardening rule.

The objective was the quantification and analytical description of the creep strain as a function of time, stress and temperature. This approach offers for the first time the possibility of taking the creep strains explicitly into account by performing exclusively transient tests. The temperature-compensated time θ is defined as:

$$\theta = \int_0^t e^{-\frac{\Delta H}{RT}} dt \quad (1)$$

- H Activation energy of creep [J/mol]
- R Gas constant [J/mol K]
- t Time [h]
- T Temperature [K]

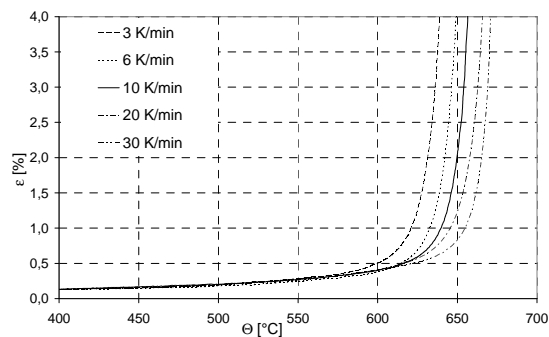


Figure 10. Temperature-strain curves, $\sigma = 170 \text{ N/mm}^2$, material M1.

The creep strain ε_c can be described by the following expression, where $B(\sigma)$ is a function only depending on the stress σ :

$$\varepsilon_c = f(\sigma, \theta) = B(\sigma) \cdot \theta^n \quad (2)$$

By means of a two-step regression procedure, the exponent n and the stress-dependent function B were determined. Analyses of the test data showed that a constant value of $n = 1/3$ as proposed by Skowronski [16] is not suitable for a proper description of the measured strain differences between the various temperature-strain curves, because it does not comprise the ultimate creep stage before rupture (tertiary creep stage). Already Cho and Findley 1984 [17] indicated a dependence of n on the temperature. In excess of a pure temperature dependency, in the current research project n was defined as a function of σ . The creep law finally derived for material M1 is given in Equation (3). For material M2 slightly deviant values for the constants were obtained.

$$\varepsilon_c = B(\sigma) \cdot \theta^{a(\sigma) \cdot \theta + \frac{1}{3}} \quad (3)$$

$$B(\sigma) = \begin{cases} 803 \cdot \sigma & \text{if } \sigma < 0,08 f_{yk} \\ 15300 \cdot e^{0,01789 \cdot \sigma} & \text{if } \sigma \geq 0,08 f_{yk} \end{cases}$$

$$a(\sigma) = \begin{cases} -2,48 \cdot 10^6 \cdot \sigma^{4,586} & \text{if } \sigma < 0,4 f_{yk} \\ -1,8 \cdot 10^{13} \cdot e^{0,0442 \cdot \sigma} & \text{if } \sigma \geq 0,4 f_{yk} \end{cases}$$

The resulting ε_c - θ -relationship describes all states of creep including the tertiary creep stage. It is shown in Fig. 11 for materials M1 and M2 in comparison to the shape of a creep law obtained with $n = 1/3$.

For a defined heating process, leading to a certain maximum temperature, the expression θ has a constant value because it does not depend on stress. This means that the formula for the creep strain occurring during this heating process is transformed into a function only depending on stress. This permits the elimination of the time-dependent strain proportions from the stress-strain relationships obtained in the transient tests. Furthermore, the stress-strain relations can be adapted to any heating process that a structural member might be subjected to in the course of a fire. The influence of creep on the stress-strain-relationships for S460M derived from the transient tests with a heating rate of 10 K/min is shown in Figure 12 for heating rates from 2 to 50 K/min.

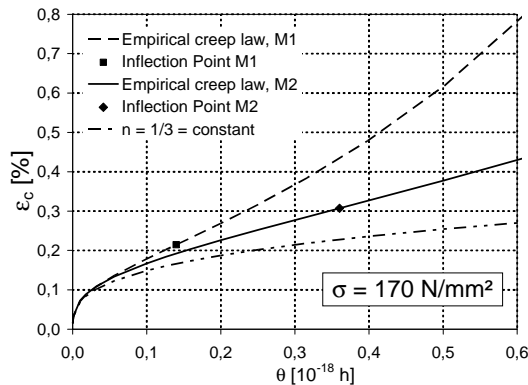


Figure 11. Empirical creep laws for M1 and M2, compared to creep law with $n = 1/3$.

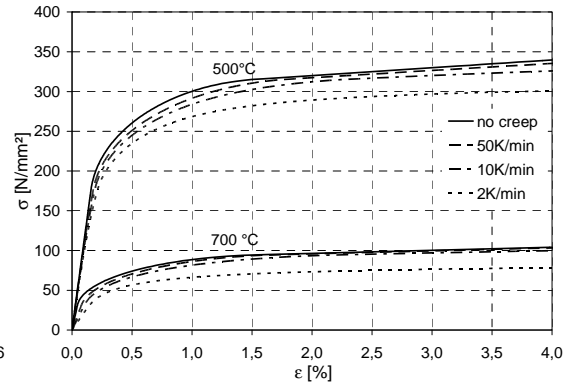


Figure 12. Influence of creep on stress-strain relationships of S460M.

4 LOAD-CARRYING CAPACITY OF STRUCTURAL MEMBERS

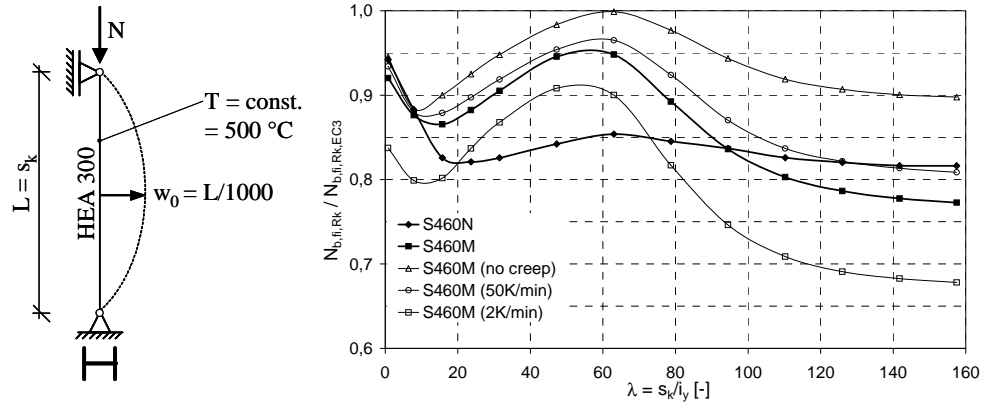
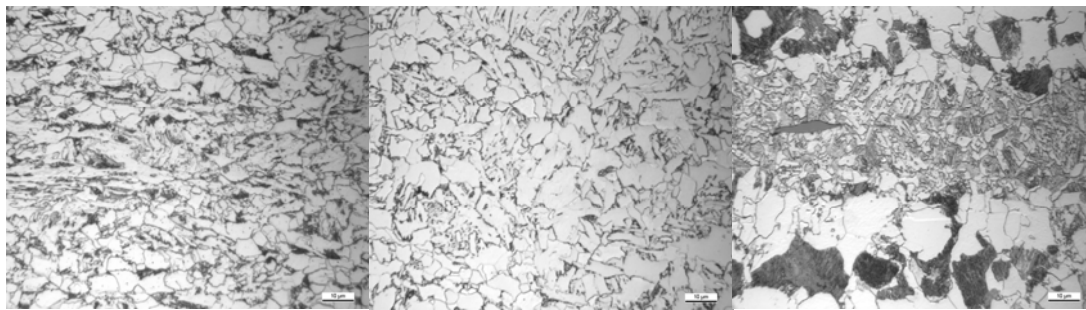


Figure 13. Ultimate loads of a column at 500 °C according to the test results compared to [1].

The influence of the differences in the stress-strain relationships on the load-carrying capacity of structural members was investigated by nonlinear limit load calculations. The results for a column with varying slenderness under central axial compression and initial bow imperfection at 500 °C are shown exemplarily in Fig. 13. The limit load $N_{b,fi,Rk}$ was calculated with the derived stress-strain relationships for S460M and S460N and related to the limit load $N_{b,fi,RkEC3}$ according to [1]. Additionally, the influence of creep according to the creep law given in Equation (3) was examined for S460M. It can be seen that the load bearing capacity compared to [1] is remarkably reduced for both delivery conditions and that the influence of creep is not negligible. For the slowest heating rate taken into account, the ultimate load can drop below 70 % of the value according to [1]. The observed undulation of the curves is due to the fact that, depending on λ , different parts of the constitutive equations are relevant for failure (slender column: $E_{0,T}$, compact column: $R_{t2,0}$).

5 METALLOGRAPHY

The current work concentrates on the determination of the influence of the chemical composition and the delivery condition on the high temperature performance of S460 by means of metallographic investigations. Figure 14 shows that there are remarkable differences in the initial microstructure of different S460 steels, even from the same delivery condition, caused by differences in the rolling process and the alloying concept. Various further micrographs have been taken from specimens tested under transient conditions to visualize the occurring structural changes.



a) M2 – Bainite/Ferrite b) M3 – Ferrite/Cementite c) N2 – Bainite/Ferrite/Pearlite

Figure 14. Micrographs: Initial microstructure of three S460 steels (before testing).

6 SUMMARY AND OUTLOOK

The transient tests carried out at seven commercial high strength fine-grained structural S460 steels show that the thermomechanical rolled steels have a better high temperature performance than the normalized rolled ones. Nevertheless, nearly all tested materials do not reach the specifications of EC3-1-2 [1]. It was shown by nonlinear limit load calculations that this can lead to a considerable overestimation of the bearing capacity of structural members made of S460 steel if fire design is done using the constitutive equations given in [1]. The evaluation of the transient tests with different heating rates allows for the derivation of an empirical creep law based on the concept of compensated time which permits the explicit consideration of the creep strain arising from any arbitrary heating process in the stress-strain relationships. Further examination is necessary to establish recommendations concerning suitable alloying elements and quantities as well as fabrication processes to improve the high temperature performance. For this purpose, metallographic investigations are actually carried out at selected specimens that were subjected to certain combinations of thermal and mechanical loading during the testing procedure. They shall relate the differences in the initial microstructure of the tested steels to the observed differences in their high temperature performance.

REFERENCES

1. DIN EN 1993-1-2, EC 3-1-2: *Bemessung und Konstruktion von Stahlbauten, Teil 1-2: Allgemeine Regeln - Tragwerksbemessung für den Brandfall*. 2006. Berlin: Beuth Verlag.
2. Ruge, J. and O. Winkelmann. 1980. "Verformungsverhalten von Bau-, Beton- und Spannstählen bei hohen Temperaturen," Special research field 148 – Fire behaviour of structural elements – Sub-project B4, Work report for the period 1978-1980, Part II. Braunschweig.
3. C.E.C. Agreement No 7210-SA/505. 1991. "Practical design tools for unprotected steel columns submitted to ISO-Fire – Refao III, Final Report, Parts I-II-III," RPS Report No 11/91, ARBED-Recherches, Luxemburg.
4. Winter, S. 1998. "Untersuchungen zum Tragverhalten von Profilverbundstützen aus hochfestem Feinkornbaustahl StE 460 bei Normaltemperatur und im Brandfall," Dissertation, Technische Universität Darmstadt.
5. Outinen, J. et al. 2001. "High-Temperature Testing of Structural Steel and Modelling of Structures at Fire Temperatures," Report TKK-TER-23, Helsinki University of Technology.
6. Lange, J. and Wohlfeil, N. Oct. 2007. "Untersuchungen zum Werkstoffverhalten des Feinkornbaustahls S460 unter erhöhten Temperaturen," *Bautechnik*, 84(10):711-720.
7. DIN EN 10002: *Metallische Werkstoffe – Zugversuch, Teil 5: Prüfverfahren bei erhöhter Temperatur*. 1992. Berlin: Beuth Verlag.
8. DIN EN 10025: *Warmgewalzte Erzeugnisse aus Baustählen, Teil 3: Technische Lieferbedingungen für normalgeglühte / normalisierend gewalzte schweißgeeignete Feinkornbaustähle*. 2005. Berlin: Beuth Verlag.
9. DIN EN 10025: *Warmgewalzte Erzeugnisse aus Baustählen, Teil 4: Technische Lieferbedingungen für thermomechanisch gewalzte schweißgeeignete Feinkornbaustähle*. 2005. Berlin: Beuth Verlag.
10. DIN EN 10028: *Flacherzeugnisse aus Druckbehälterstählen, Teil 5: Schweißgeeignete Feinkornbaustähle, thermomechanisch gewalzt*. 2003. Berlin: Beuth Verlag.
11. Ramberg, W. and W. R. Osgood. 1943. "Description of stress-strain-curves by three parameters," Technical Note No. 902, National Advisory Committee for Aeronautics, Washington.
12. Richard, R. M. and B. J. Abbott. August 1975. "Versatile Elastic-Plastic Stress-Strain Formula," *Journal of the Engineering Mechanics Division*, 101(4):511-515.
13. Poh, K. W. Nov. 1997. "General Stress-Strain Equation," *J. of Mat. Civil Eng.*, 9(4):214-217.
14. Dorn, J. E. January 1955. "Some Fundamental Experiments on High Temperature Creep," *Journal of the Mechanics and Physics of Solids*, 3(2):85-116.
15. Harmathy, T. Z. Sept. 1967. "A Comprehensive Creep Model," *J. of Basic Eng.*, 89:496-502.
16. Skowronski, W. 2004. *Fire Safety of Metal Structures*. Polish Scientific Publishers PWN.
17. Cho, U. W. and W. N. Findley. December 1984. "Creep and Creep Recovery of 2618-T61 Aluminium Under Variable Temperature," *Journal of Applied Mechanics*, 51:816-820.

Experimental Study of the Mechanical Properties of Prestressed Steel Wire at Elevated Temperatures

Y. WANG, Z. SHEN and Y. LI

ABSTRACT

This paper presents the experimental investigation on the mechanical properties of prestressed steel wire at elevated temperatures. Prestressed steel structures have been used extensively in China. Fire safety design of the structures has, therefore, become more important. However, current design standards for fire resistance of steel structures are mainly based on the investigation of hot-rolled carbon steel with normal strength. A search of the literature on performance of prestressed steel wire at elevated temperatures reveals little evidence. Therefore steady tensile coupon tests were conducted at temperatures in the range of 10 to 600°C to investigate the mechanical properties of prestressed steel wire which are widely used in applications in China. In this research, a new experimental set-up is developed for the special specimens to determine the elastic modulus, yield strength and the stress-strain curves. The test results obtained from this research are plotted and compared with the the test results predicted by other researchers, and also compared with prestressed reinforcement and hot-rolled carbon steel with normal strength from the British, European and Chinese standards predictions. It is shown that the important mechanical properties (yield strength and elastic modulus) of prestressed steel wire is deteriorated more significantly at elevated temperatures than other lower strength structural steel, so currently available reduction factors cannot be used safely for prestressed steel structures.

Yehua Wang, Ph.D.student. Department of Building Engineering, Tongji University, 1239 Siping Road, Shanghai, 200092, P.R.China

Zuyan Shen, Professor, Academician of Chinese Academy of Engineering. Department of Building Engineering, Tongji University, 1239 Siping Road, Shanghai, 200092, P.R.China

Yuanqi Li, Professor, Department of Building Engineering, Tongji University, 1239 Siping Road, Shanghai, 200092, P.R.China

INTRODUCTION

In recent times, prestressed steel structures have been increasingly used in architectural and structural application because of their aesthetic appearance, high strength to weight ratio compared with hot-rolled steel structures, as well as cost-effective. Mechanical properties of structural steel at elevated temperatures are important for fire resistant design of steel structures. However, current design standards for fire resistance of steel structures are mainly based on the investigation of hot-rolled carbon steel with normal strength. Limited data is available for the mechanical properties of prestressed steel wire at elevated temperatures. Hence, an experimental program has been carried out to conduct to derive accurate reduction factors of mechanical properties of prestressed steel wire at elevated temperatures.

EXPERIMENTAL INVESTIGATION

Jin Fan et al.[1]and Yi-jie Hua[2]undertook a series of tensile coupon tests to determine the mechanical properties of prestressed steel wire at elevated temperatures. However, it is found that the strain measuring methods and devices they adopted in the experiments were not accurate. Therefore improved test methods and device were used in this research to determine the mechanical properties at elevated temperatures accurately.

Testing Device

A hydraulic testing machine was used, and the electrically heated furnace simulated fire tests in this research. The prestressed steel wire specimen crossed the furnace and was heated partly. The extension in the heated part of the specimen is the essential characteristics, and the accurate evaluation of it is highly important. Fig.1 shows the special device which was developed by this research. By specially using two pairs of heat-resistant gripping holders and other methods, this device can firmly prevent slippage within the strain-measuring set-up as the cross-sectional area of the small diameter wire (5mm) reduced. A carefully selected extensometer was used to measure the strain of the heated part. The gauge length of the extensometer was 20mm, so a complete strain of the heated part of the coupon specimen could be obtained.

Test Specimens

The prestressed steel wire specimens have the nominal tensile strength of 1670MPa and the measured ultimate strength of 1880MPa at normal room temperature 10°C, the nominal diameter of every specimen is 5mm, and the length of every specimen is 1000mm with a uniformly heated segment of 150mm, as shown in Fig.1. Temperature was varied as follows:10, 200, 300, 400, 500 and 600°C for elevated temperatures. The tests were repeated two or three

times at every temperature point, so a total of 15 tests were conducted in this research.

Test Procedure

In this research, the steady-state test method was used to determine the mechanical properties of prestressed steel wire due to its simplicity and accurate data acquisition. In the steady-state test, the specimen was heated up to a specified temperature. After the temperature inside the furnace was stabilized for 15min, the tensile load was applied to the specimen. The heating rate of the electric furnace was 10°C/min, and there were three thermocouples used to measure the inside temperature of the furnace. In the steady-state test, strain control was used in the tensile testing machine. The constant strain rate obtained from the extensometer was 0.005/min, which is with the range 0.005 ± 0.002 /min as specified by the ASTM Standard E21-05[3].

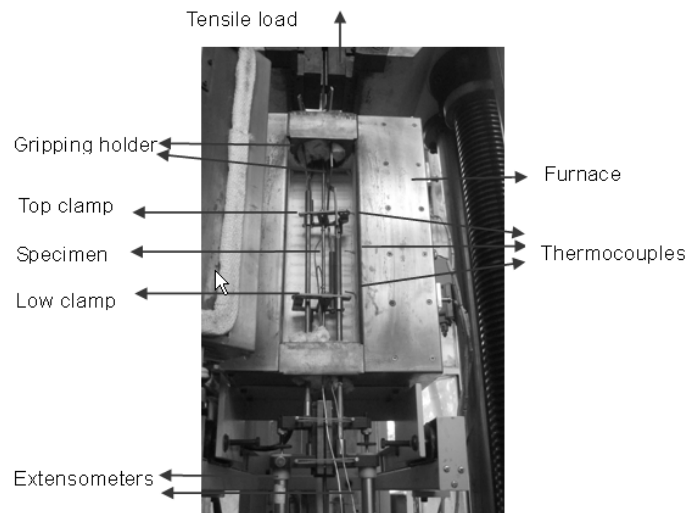


Fig. 1 Testing device.

DETERMINATION OF MECHANICAL PROPERTIES

Yield Strength

Normally at ambient temperature the yield strengths at strain level of 0.2% was used to determine the yield strength of steel. While at elevated temperatures the yield strengths at strain levels of 0.2%, 0.5%, 1.5% and 2% are widely accepted. The 0.2% yield strength ($f_{0.2}$) is the intersection point of the stress-strain curve and the proportional line off-set by 0.2% strain level. Meanwhile the yield strengths at the strain levels of 0.5%, 1.5% and 2.0%, ($f_{0.5}$, $f_{1.5}$, f_2) respectively, are the intersection points of the stress-strain curve and the non-proportional vertical line specified at given strain values.

The reduction factors at different elevated temperature ($f_{y,T}/f_{y,10}$) were determined from the ratio of yield strengths at elevated temperature ($f_{y,T}$) to yield strengths at normal room temperature ($f_{y,10}$). They were calculated based on four strain levels of 0.2%, 0.5%, 1.5% and 2%. While TABLE I presents the reduction factors of yield strength at these special strain levels.

Based on the results at strain level of 0.2% obtained from the tensile coupon tests at various temperatures, Equation (1) were derived to determined the reduction factors for prestressed steel wire. Fig.2 shows the experimental results and the predictions of Equation (1). It can be seen that there is very good agreement between the test results and predicted values from Equation (1).

$$\frac{f_{0.2,T}}{f_{0.2,10}} = 1.013 - 1.3 \times 10^{-3} \times T + 6.179 \times 10^{-6} \times T^2 - 2.468 \times 10^{-8} \times T^3 + 2.279 \times 10^{-11} \times T^4 \quad 10^\circ\text{C} \leq T \leq 600^\circ\text{C} \quad (1)$$

Where T is the temperature in degrees Celsius($^\circ\text{C}$), $f_{0.2,T}$ and $f_{0.2,10}$ are the normal yield strength at strain level of 0.2% at elevated and normal room temperatures respectively, and the values of $f_{0.2,10}$ is 1710N/mm² in this research.

TABLE I . REDUCTION FACTORS OF YIELD STRENGTH.

Temperature($^\circ\text{C}$)	10	200	300	400	500	600
$f_{0.2,T}/f_{0.2,10}$	1	0.845	0.684	0.502	0.240	0.083
$f_{0.5,T}/f_{0.5,10}$	1	0.950	0.763	0.635	0.316	0.121
$f_{1.5,T}/f_{1.5,10}$	1	0.925	0.772	0.566	0.250	0.088
$f_{2,T}/f_{2,10}$	1	0.970	0.795	0.580	0.250	0.089

Elastic Modulus

Elastic modulus is an important factor determining the fire resistance of prestressed steel structures and it also deteriorates with the temperature as yield strength. It was determined from the stress-strain curve based on the tangent modulus of the initial elastic linear curve.

The elastic modulus reduction factors were measured at different elevated temperatures. The reduction factor (E_T/E_{10}) was determined as the ratio of the elastic modulus at elevated temperature (E_T) to that at room temperature (E_{10}). The results are presented in Fig.3. Proposed equation to predict the elastic modulus reduction factors (E_T/E_{10}) is

$$\frac{E_T}{E_{10}} = \frac{1}{1.043 + 9.266 \times 10^{-17} \times T^{6.04}} \quad 10^\circ\text{C} \leq T \leq 600^\circ\text{C} \quad (2)$$

Where T is the temperature in degrees Celsius($^\circ\text{C}$), E_T and E_{10} are the elastic modulus at elevated and room temperatures, respectively, and the value of E_{10} is $2.05 \times 10^5 \text{N/mm}^2$ in this research.

The calculated values from Equation (2) are also presented in Fig.3. It is clear that the predicted values agree well with the test results.

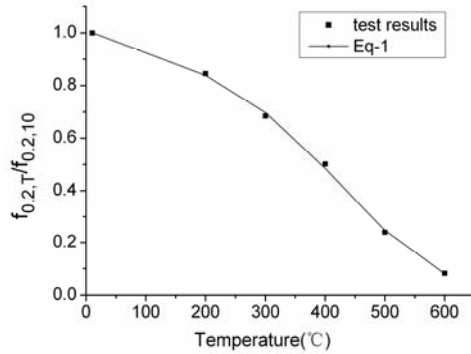


Fig.2 Yield Strength reduction factors versus temperature for prestressed steel wire.

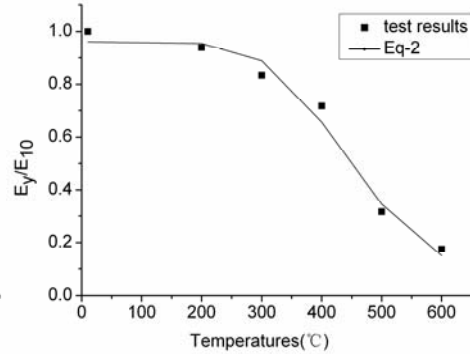


Figure.3 Elastic modulus reduction factors versus temperature for prestressed steel wire.

DISCUSSION OF TEST RESULTS

Comparison of Reduction Factors with Available Research Results

Yin Fan[1] carried out high temperature tests to obtain the mechanical properties of prestressed steel wire (measured ultimate strength is 1728N/mm^2 , diameter is 5mm, low relaxation of prestress) and provide reduction factors for yield strength and elastic modulus. Yijie Hua[2] provided reduction factors for both yield strength and elastic modulus by undertaking tests on prestressed steel wire (measured ultimate strength is 1720N/mm^2 , diameter is 5mm, low relaxation of prestress). Wenzhong Zheng [4] also investigated the behavior of prestressed steel wire (measured ultimate strength is 1800N/mm^2 , diameter is 5mm, low relaxation of prestress) at elevated temperatures throughout experiment. All of their values were compared with the reduction factors obtained from this research.

Fig.4 compares the yield strength reduction factors obtained from this research and other's results. It can be seen that the results obtained from this study are generally close to the results conducted by Wenzhong Zheng [4]. Yin Fan[1] and Yijie Hua[2] unconservatively predicted the yield strength reduction factors. Fig.5 shows the elastic modulus reduction factors presented by this research and other's results. The comparison shows that:(1) from 10 to 300°C , elastic modulus decreases slightly and all the values are similar;(2) but from 300

to 600°C, elastic modulus decreases rapidly and the values are discrete.

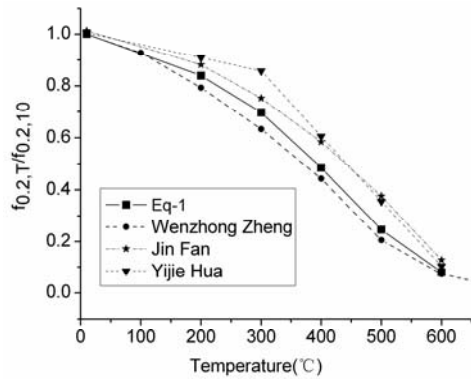


Figure.4 Comparison of yield strength reduction factors by Eq-1 and other's results.

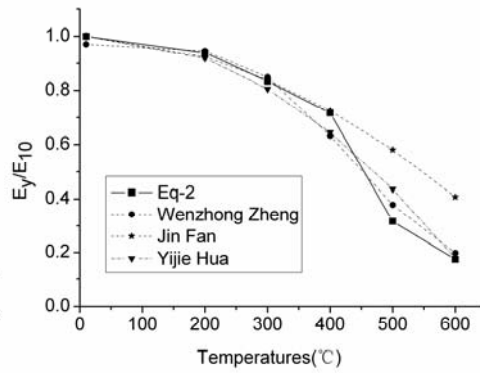


Figure.5 Comparison of elastic modulus reduction factors by Eq-2 and other's results.

Comparison of Reduction Factors with some design standards

Current design standards for fire resistance of steel structures are mainly based on the investigation of hot-rolled carbon steel with normal strength. The performance of prestressed steel wire at elevated temperatures is unknown. But EC4 [5], BS8110 [6] include the performance of prestressed reinforcement at elevated temperatures. Consequently this research was compared with these predictions.

Fig.6 shows yield strength reduction factors for prestressed steel wire and prestressed reinforcement from this research, EC4 [5] and BS8110[6]. It can be seen that yield strength reduction factors of prestressed reinforcement is higher than that of prestressed steel wire. Fig.7 shows elastic modulus reduction factor from this research and EC4. It can be seen that 460°C or so is the turning point of elastic modulus reduction factors of prestressed steel wire and prestressed reinforcement.

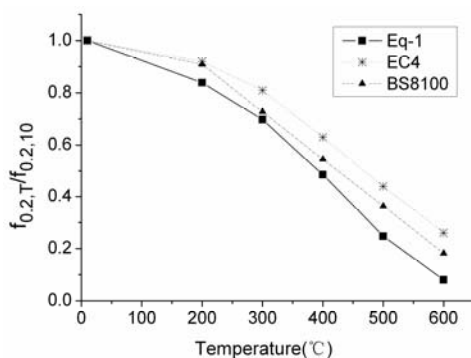


Figure.6 Comparison of yield strength reduction factors by Eq-1, EC4, and BS8110.

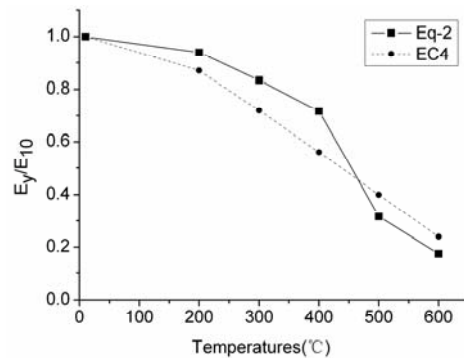


Figure.7 Comparison of elastic modulus reduction factors by Eq-2 and EC4.

Comparison of Reduction Factors for Prestressed Steel and Hot-rolled Steels

The reduction factors of 0.2% yield strengths obtained from the tests were compared with hot-rolled steel with normal strength from the Chinese Standard CECS200:2006 predictions [7], the European Standard ECCS [8] and EC3[9] predictions.

As shown in Fig.8, there are difference in yield strength reduction factors of hot-rolled steels in various standards and ECCS[8] is generally conservative for yield strength. While the comparison indicates that yield strength reduction factors of prestressed steel wire is less than that of hot-rolled steels from ECCS[8] and is about 10% at 300°C, 30% at 400°C, 50% at 500°C and 70% at 600°C. In Fig.9 the comparison of elastic modulus reduction factor indicates that the result of prestressed steel decreases more rapidly than that of hot-rolled steel, ecstastically in the range of 400 to 600°C.

Therefore it is clear that the reduction factor obtained from hot-rolled steel cannot used to design the prestressed steel structures under fire conditions.

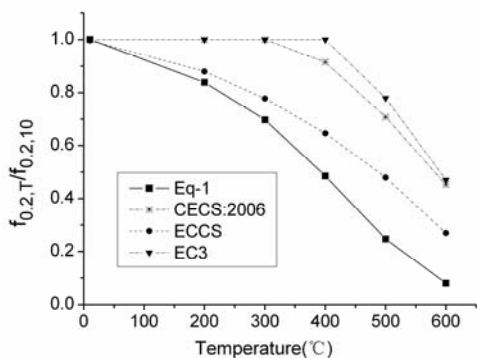


Figure.8 Comparison of yield strength reduction factors by Eq-1,CECS200:2006,EC3 and ECCS.

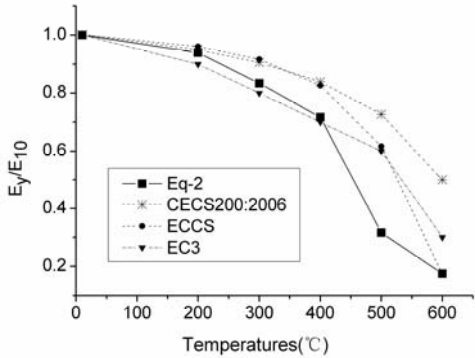


Figure.9 Comparison of elastic modulus reduction factors by Eq-2, CECS200:2006, EC3 and ECCS.

CONCLUSION

A experimental program on the mechanical properties of prestressed steel wire at elevated temperatures has been presented. A new testing device was developed to determine the important mechanical properties at different temperatures in the steady-state tests. Proposed equations to determine the yield strength and elastic modulus for temperature ranging from 10°C to 600°C has been proposed in this paper. The results obtained from this research were compared with available research results, prestressed reinforcement and hot-rolled steel with normal strength from some design standards. It is shown that the mechanical properties of prestressed steel wire reduce significantly with increasing temperatures and are quite different from those of hot-roll steel and prestressed reinforcement. The reduction factor of yield strength of prestressed

steel wire is less than that of prestressed reinforcement and hot-rolled steel with normal strength in the temperature range of 10 to 600°C. While the reduction factor of elastic modulus of prestressed steel wire is less than that of hot-rolled steel with normal strength in the temperature range of 10 to 600°C, but greater than that of prestressed reinforcement for temperature ranging from 10 to 460°C or so, and less than that of prestressed reinforcement for temperature ranging from 460 or so to 600°C.

ACKNOWLEDGMENT

This research funded by Key Program of Chinese National Natural Science (No.50638050) is gratefully acknowledged.

REFERENCES

- 1 Jin Fan, Zhitao Lv. 2002. "Experimental on mechanical property of prestressed steel wire at high temperature," *Building Structure.*, 32(3):50–51.
- 2 Yijie Hua. 2000. "Fire response and fire-resistance of prestressed concrete structures," *Doctoral Dissertation*. Tongji University, Shanghai.
- 3 ASTM. 2005. "E21-05. Standard test methods for elevated temperature tension tests of metallic materials," *Annual book of ASTM standards*, Vol. 03.01: *Metals-mechanical testing; elevated and low-temperature tests; metallography.*, West Conshohochken, Pa.
- 4 Wenzhong Zheng. "Experimental research on the mechanical properties of prestressing steel wire at and after high temperature," *Journal of Building Structures.*, 27(2):120–128.
5. European code 4(EC4).1994. *Eurocode 4: Design of composite and concrete structures, Part 1.2: structural fire design*, European Committee for Standardization, DD ENV 1994-1-2, CEN, Brussels.
6. British Standards Institution (BSI). 1985. *BS8110: Structural Use of Concrete*, British Standards Institution, UK.
7. China Association for Engineering Construction Standardization (CECS).2006.*CECS 200:2006-Technical code for fire safety of steel structure in buildings*, China Planning Press, Beijing.
8. European code 3(EC3). 1993. *Eurocode 3: Design of steel structures, Part 1.2: structural fire design*, European Committee for standardization, DD ENV 1993-1-2, CEN, Brussels.
9. European convention for constructional steel work(ECCS). 1985. "Technical committee 3-fire safety of steel structures," *Design manual on the European recommendations for the fire safety of steel structures*, Elsevier Scientific Publishing Company, Amsterdam.

Influence of Polypropylene Fibres on the Thermal Strain of High Strength Concrete at High Temperatures

S. HUISMANN, F. WEISE, B. MENG and U. SCHNEIDER

ABSTRACT

This paper presents the results of an experimental study on the influence of polypropylene (PP) fibres on the thermal strain of high strength concrete (HSC) at temperatures up to 750°C. Concerning this topic only few results can be found in the literature and systematic investigations are missing. However, basal knowledge is necessary for the understanding of the internal damage processes as well as for the structural design.

To explain the differences in the thermal strain of HSC with and without addition of PP fibres the internal damage processes were investigated with acoustic emission (AE) analysis and ultrasound (US). Furthermore the weight loss was measured continuously during heating to monitor the drying of the specimen. This novel approach by combining these different methods with strain measurements at high temperatures allows the integral description of the internal damage processes.

The results reveal significant differences in the thermal strain of HSC when PP fibres are added. Between 200°C and 250°C the thermal strain of HSC with PP fibres is superimposed by shrinkage caused by accelerated drying. Above 250°C it is lower than that of plain HSC without PP fibres. It is supposed that it is caused by a more homogeneous distribution of micro cracks whereby the fibre beds acting as defects in the concrete.

Hence this paper gives a contribution to the general understanding of the impact of PP fibres in HSC at high temperatures and points out the influence of the fibres on the thermal strain of HSC.

Sven Huismann (corresponding author), Ph.D. candidate, BAM Federal Institute for Materials Research and Testing, Unter den Eichen 87, 12205 Berlin, Germany.

Frank Weise, Ph.D., BAM Federal Institute for Materials Research and Testing, Unter den Eichen 87, 12205 Berlin, Germany.

Birgit Meng, Professor, BAM Federal Institute for Materials Research and Testing, Unter den Eichen 87, 12205 Berlin, Germany.

Ulrich Schneider, Professor, University of Technology Vienna, Research Centre of Building Materials, Material Technology and Fire Safety, Karlsplatz 13/E206, 1040 Vienna, Austria.

1. INTRODUCTION

The application of PP fibres is an effective way to prevent explosive spalling of HSC in case of fire. They are added to the fresh concrete during mixing. However, only few results can be found in the literature concerning the influence of PP fibres on the thermal strain of HSC [3, 5]. Systematic investigations are missing completely, although they are very important for the general understanding of the impact of PP fibres in concrete and elucidation of basic mechanisms.

In the frame of a research project [4] the influence of PP fibres on the thermal strain of HSC up to 750°C was studied systematically. The strain measurements were performed on HSC with and without addition of PP fibres according to RILEM recommendations [7]. Some specimens were pre-dried at 105°C before testing to remove the free and physically bound water. Moreover, for a better understanding of the mechanisms, weight loss, AE and US were measured continuously during heating and microscopic analysis was performed on polished sections after the heating tests.

2. EXPERIMENTAL PROGRAM

2.1 Test set-up

The experiments were performed with a special test setup (Figure 1). The servo hydraulic testing machine has a load capacity of 1600 kN. The loading rams as well as the calotte consist of a nickel based alloy. Axial deformations were measured with an extensometer consisting of two displacement transducers placed outside the furnace. The transducers were connected to the measuring points on the specimen with thin bars of quartz glass. The furnace has three zones to create a homogenous temperature field. The temperature is controlled by three cromel-alumel thermocouples located on the surface of the specimen.

- | | |
|-------------------|------------------------|
| ① Testing machine | ④ Device for AE and US |
| ② Extensometer | ⑤ Specimen |
| ③ Furnace | |

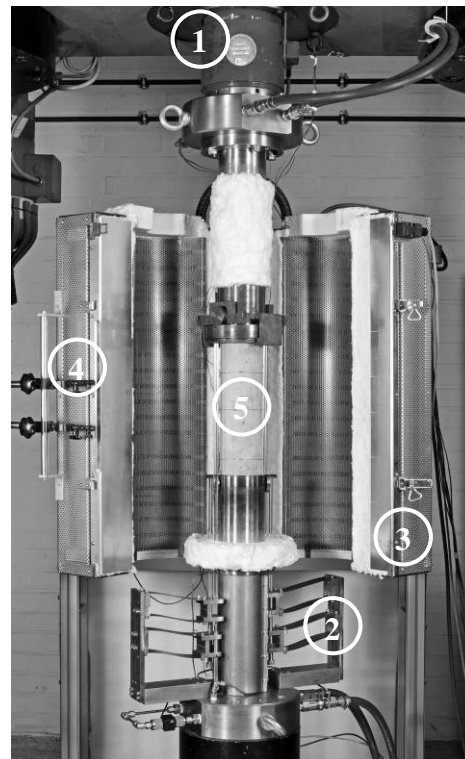


Figure 1: Test setup.

For the weight loss measurements the specimen was placed on a fibre brick inside the furnace. It has the same position as in the strain measurements. The whole system was placed on a balance.

Internal damage processes were monitored using AE analysis in combination with US measurements. AE is an indirect and passive non destructive test (NDT) method and enables the acquisition of elastic waves which are caused due to crack formation or friction. The analysis of the results allows the assessment of the internal damage process in the microstructure. US is an indirect and active NDT method which enables the integral acquisition of changes in the microstructure by the variation in the US time-of-flight in the specimen. The formation of cracks is increasing the time-of-flight since the cracks impede the propagation of the US pulse.

The AE as well as the US measurements were performed with a commercial AE system (Valen AMSY-5). Due to the high temperature the acoustic sensors (resonance frequency 150 kHz) couldn't be fixed directly to the specimen inside the furnace. Therefore they were located outside the furnace and connected to the surface of the specimen with 2 mm thick waveguides according to [2] and [8] (Figure 2). The system facilitates the measurements of US with calibration pulses. The time-of-flight of these pulses between two opposite sensors was measured. After subtraction of the time-of-flight in the waveguides the time-of-flight in the specimen was obtained.

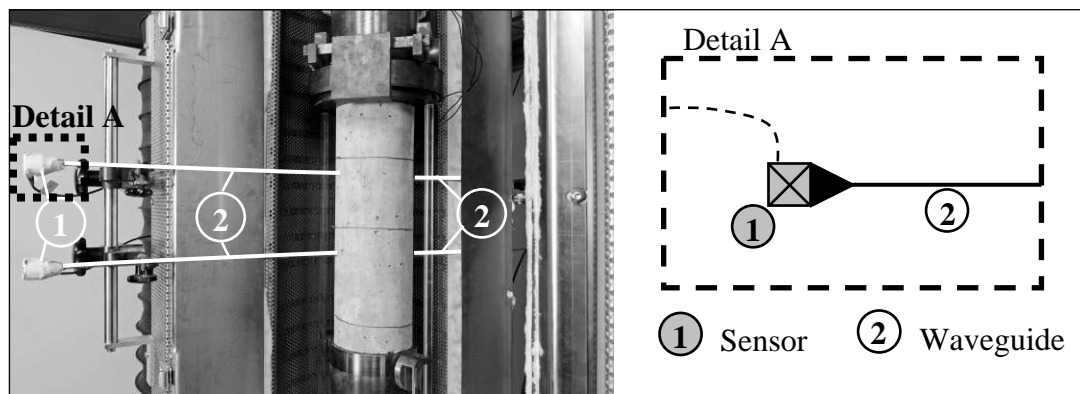


Figure 2. Connection of the acoustic sensors to the specimen via waveguides.

2.2 Specimens

The compositions for the two HSC mixes are given in Table 1. They differed only in the presence of PP fibres. The cylindrical specimens had a diameter of 100 mm and a height of 300 mm. They were demoulded after one day of hardening. Afterwards they were stored for six days in water and in the following at 23 °C and 50 % relative humidity until testing (for at least 160 days).

Table 1. Concrete mixture.

Materials	[kg/m ³]	
Concrete - Series	HSC-PP	HSC
Cement CEM I 42.5 R	580	
Water (w/c = 0.32)	173	
Aggregates (siliceous)	0 – 2 mm	769
	2 – 4 mm	231
	4 – 8 mm	538
Silica fume	63.8	
Superplasticizer	17.4	
PP fibres	2	-
	2372.2	

The compressive strength at the time of the high temperature tests was 110 MPa with and 113 MPa without PP fibres respectively. Both concretes had a moisture content of 4.4 M.-%.

2.3 Test procedure

The tests for the strain measurements have been carried out according to the RILEM recommendations Part 6 [7]. The corresponding temperature regime is described in Figure 3. The heating rate was 1 K/min related to the specimen surface temperature which was taken as reference temperature in all tests. For each temperature level at least two specimens were tested.

The pre-conditioning of selected specimens before testing was done at 105°C until no changes in mass are observed.

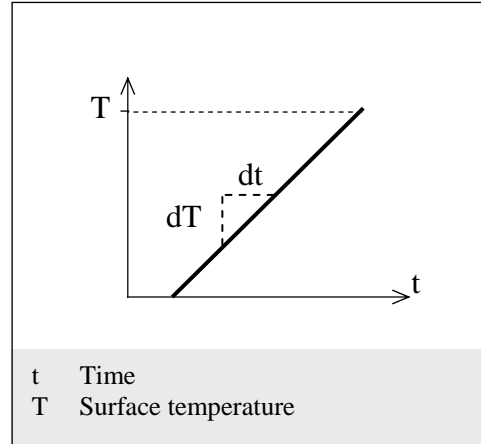


Figure 3. Temperature regime.

3. RESULTS AND DISCUSSION

The results of all measurements are summarized in Figure 4. On the left (I) the HSC mixes with and without PP fibres are compared. On the right (II) the HSC mix with PP fibres is compared for different preconditioning.

The results of the thermal strain measurements (Figure 4-Ia) show two distinctive temperature ranges. In the first from 200°C to 250°C the thermal strain stagnates if the HSC contains PP fibres. At higher temperatures the thermal strain of the HSC with PP fibres is significant lower than that of the HSC without PP fibres. Both observations are discussed one after another as follows.

For understanding the mechanisms which cause the stagnation in the thermal strain between 200°C and 250°C some specimens with PP fibres were pre-dried at 105 °C. In this case the free and physically bound water was removed before testing. During the tests these specimens didn't show the stagnation in the thermal strain (Figure 4-IIa). It is therefore assumed that this anomalous strain behaviour is related to an evaporation process. This assumption is supported by the results of the weight loss measurements in Figure 4-Ib. In the temperature range from 200 °C to 270°C the weight loss of the HSC with PP fibres was faster than that of the HSC without PP fibres. Since faster weight loss is associated with accelerated evaporation it is supposed that the apparent stagnation in the thermal strain is caused by additional shrinkage that is acting in opposite direction of the thermal strain. When the specimens were preheated less moisture was present (Figure 4-IIb) and shrinkage due to accelerated evaporation was not as significant as to counteract visible the thermal strain.

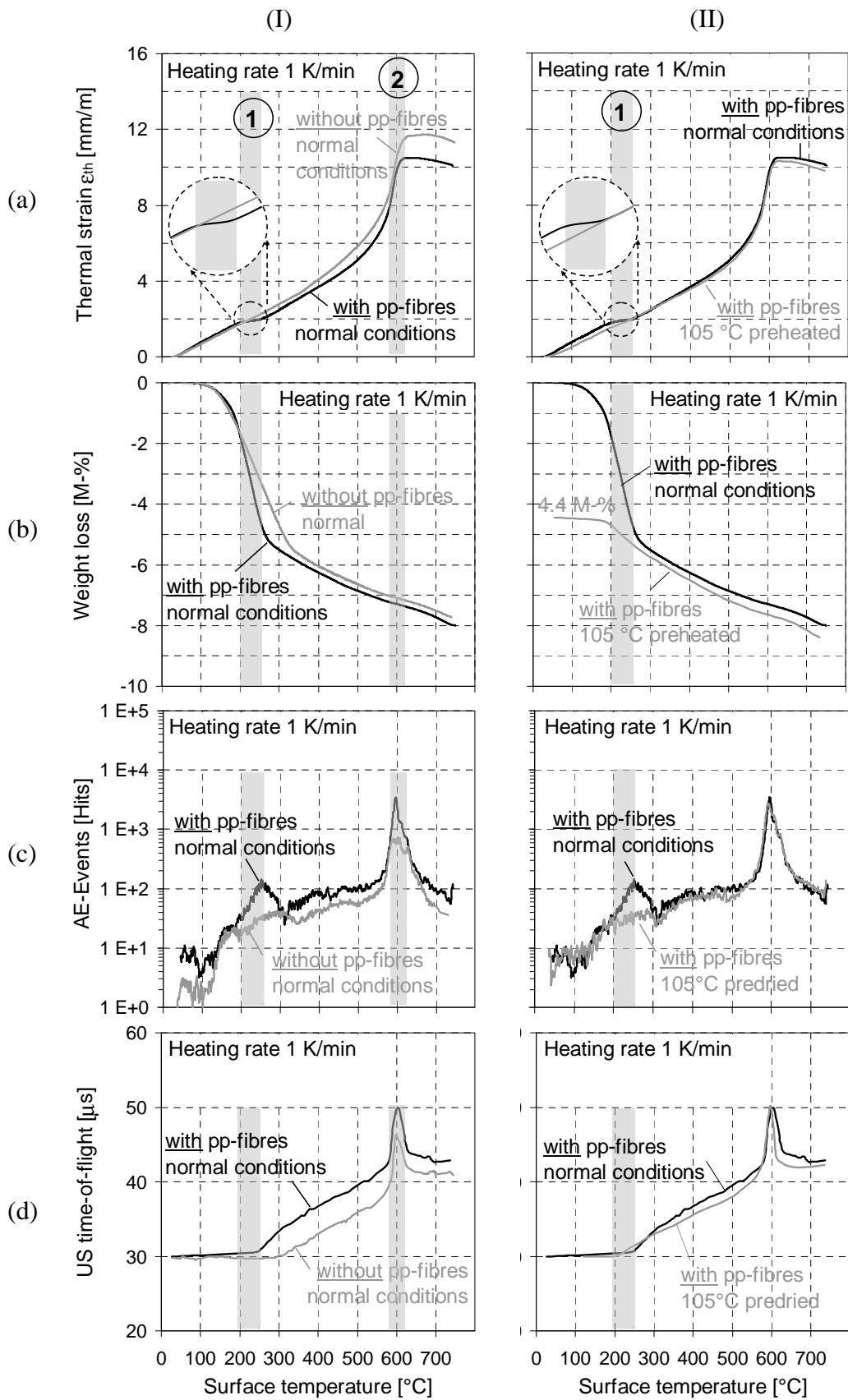


Figure 4. Overview of the results.

The accelerated evaporation is obviously caused by the impact of the PP fibres which increases the permeability of the HSC significantly [9] when the fibres are melting at 160°C. The physical mechanism of the process of increasing permeability is up to now not sufficiently understood [1]. It is assumed that micro cracking is an important factor.

The results of the AE analysis for the HSC with and without PP fibres are presented in Figure 4-Ic. Significant increase of AE-Events was observed at temperatures above 120°C which correlates roughly with the time when the weight loss increased. In the temperature range from 200°C to 300°C the HSC with PP fibres exhibited a higher number of AE-Events than the HSC without PP fibres with a peak at 250°C. In general there are two possible reasons to explain these observations:

1. Friction of the flowing water or water vapour at the inner concrete surfaces
2. Micro cracking starting from the fibres beds

Friction of the flowing water or water vapour at the inner concrete surfaces is a reasonable explanation because the weight loss measurements indicate an accelerated evaporation (i.e. moisture flow) in the HSC with PP fibres particularly in the temperature range where the number of AE-Events is increased. This is supported by the absence of such an increase in AE-Events when the specimens were preheated and moisture was removed before testing (Figure 4-IIc).

On the other hand a higher moisture flow requires higher pressure differences or a higher permeability. However, it is known from [9] that the PP fibres increase the permeability of HSC significantly above the melting temperature of the fibres. This might be caused by micro cracking. The mechanisms leading to this micro cracking are still unidentified and part of future investigations. However, it is evident that there are different kinds of stresses which could be responsible for the cracking. They can be caused by vapour pressure or different thermal dilatation of the concrete components. Another possibility is the high volume dilatation of the melting PP fibres. Thereby the fibre beds are acting as defects in the concrete and favour the formation of micro cracks.

The results of the US measurements on the HSC with PP fibres revealed no significant increase of the time-of-flight below 250 °C (Figure 4-Id). If we consider that the free water was not yet removed completely from the specimen we may assume that the water inside the cracks initially compensated the increase in the US time-of-flight. At the temperature at which the weight loss reached the amount of the free and physically bound water (4.4 M. % in Figure 4-Id) the US time-of-flight started to increase. Similar results were obtained with the HSC without addition of PP fibres. The US time-of-flight started to increase at 300°C when the weight loss was approximately 4.4 M.-%. The assumption of the compensated US time-of-flight is supposed by the results obtained with the pre-dried specimens (Figure 4-IIId). Since the free and physically bound water was already removed before testing, the increase in the US time-of-flight increased earlier at 200°C.

Micro cracking as well as friction of the flowing water or water vapour at the inner concrete surfaces are both reasonable explanations for the high amount of AE-

Events between 200°C and 300°C. It is supposed that both mechanisms are partly superimposed. The differentiation has to be part of future investigations.

Above 300°C the thermal strain of the HSC is lesser with addition of PP fibres than without (Figure 4-Ia). The difference is significant above 600°C when the quartz transformation of the aggregates at 573°C has occurred.

The fibres turned into vapour at 341°C [6] but the fibre beds are still existent. They are defects in the concrete which help the nucleation and favour the distribution of micro cracking. The stronger internal damage progress follows from the results of the US measurements because the US time-of-flight was larger with addition of PP fibres than without (Figure 4-Ic). Furthermore the number of AE-Events around 600°C was higher in the HSC with PP fibres (Figure 4-Id) which confirms a stronger internal damage progress.

To verify the differences which were observed in the results of the NDT measurements polished sections were prepared from HSC specimens with and without PP fibres heated to 600°C. Microscopic analysis revealed significantly different crack patterns (Figure 5). Without addition of PP fibres the HSC generally exhibited larger cracks. The smaller cracks in the HSC with PP fibres were higher in number and well distributed. Similar results were reported in [6] with PP fibre reinforced HSC heated to 400°C.

On the basis of these observations it is hypothesized that the well distribution of the micro cracks reduced the thermal elongation of the HSC if PP fibres were added to the mix.

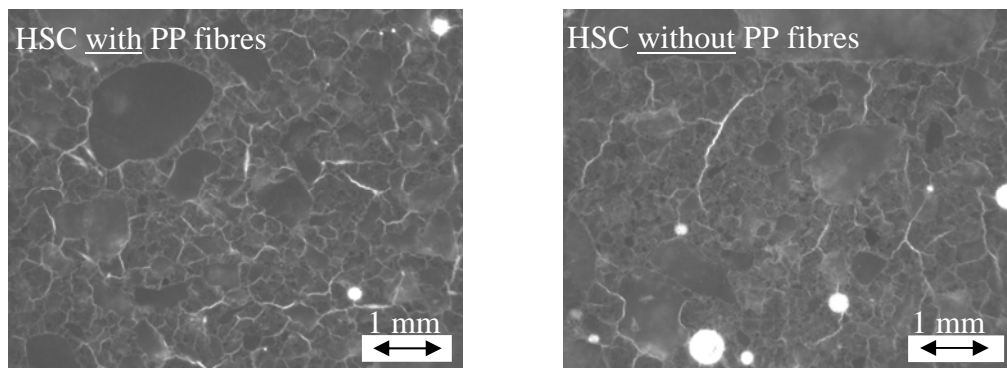


Figure 5. Polished sections of HSC with (left) and without (right) PP fibres heated to 600°C.

4. SUMMARY AND CONCLUSION

In the presented study the influence of PP fibres on the thermal strain was investigated. Therefore a unique test set up was used which allows the investigation of the internal damage process with AE and US.

Two distinct temperature ranges were observed in which the PP fibres influence the thermal strain of the HSC significantly. In the first one between 200°C and 250°C the thermal strain of the HSC containing PP fibres stagnated. In the second temperature range above 300°C the thermal strain of the HSC was lower when PP fibres were added. With the results of the combined application of weight loss, AE

and US measurements some reasonable assumptions on the basic mechanisms could be made.

The stagnation in the thermal strain between 200°C and 250°C is attributed to an elevated shrinkage due to an accelerated moisture loss. It is caused by the fibre impact which increases the permeability of the HSC. It is assumed that the fibre beds are acting as defects in the cement paste matrix and favour the nucleation of micro cracks whereby the permeability is increased.

The increased number of AE-Events detected in this temperature range might be induced due to these micro cracks. But it is possible that at the same time it is superimposed with the friction of the flowing water or water vapour at the inner concrete surfaces. Future investigations are necessary to enable the separation of AE signals from different sources.

Above 300°C the thermal strain of HSC was slightly higher when PP fibres were not added to the mix. The difference becomes more significant at 600°C when the quartz transformation has occurred and the aggregates have the maximum thermal dilatation. On the basis of AE, US and microscopic analysis this observation might be explained with the different kind of micro cracking. Thereby it is hypothesized that the homogeneous distribution of the cracks induced by the fibre beds results in a lower thermal strain.

REFERENCES

1. 1st International workshop on concrete spalling due to fire exposure, Leipzig, 2009.
2. DGZfP SE 2: Richtlinie zur Charakterisierung der Aufnehmer und ihrer Ankopplung im Labor, Deutsche Gesellschaft für Zerstörungsfreie Prüfung, Berlin, 1992.
3. Diederichs, U.; Mertzsch, O.: Behaviour of Ultra High Strength Concrete at High Temperatures, Second International Symposium on Ultra High Performance Concrete Vol. 1, Kassel, S. 347–354, 2008.
4. Huisman, S.: Materialverhalten von hochfestem Beton unter thermomechanischer Beanspruchung, Dissertation, Technische Universität Wien, 2010. (in preparation)
5. Jansson, R.; Boström, L.: Experimental study of the influence of polypropylene fibres on material properties and fire spalling of concrete, Fire design of concrete structures—From materials modelling to structural performance, Coimbra, S. 177-188, 2007.
6. Kalifa, P.; Chene, G.; Galle, C.: High-temperature behaviour of HPC with polypropylene fibres from spalling to microstructure, Cement and Concrete Research, Vol. 31 (10), S. 1487–1499, 2001.
7. RILEM TC 129 MHT: Test methods for mechanical properties of concrete at high temperatures: Part 6: Thermal strain, Materials and Structures, Vol. 30 (196), S. 17–21, 1997.
8. Schneider, U.; Rosenberger, W.; Diederichs, U.: Untersuchung der Rißkinetik in Beton durch Schallemissionsanalyse, Mitteilungsblatt für die amtliche Materialprüfung in Niedersachsen, Vol. 20/21, S. 44–51, 1980.
9. Zeiml, M.: Concrete subjected to fire loading—From experimental investigation of spalling and mass-transport properties to structural safety assessment of tunnel linings under fire, Dissertation, Technische Universität Wien, 2008.

Fire Induced Transient Creep Causing Stress Relaxation and Tendon Rupture in Unbonded Post-Tensioned Structures: Experiments and Modeling

J. GALES, L. BISBY and C. MACDOUGALL

ABSTRACT

Unbonded post-tensioned (UPT) flat plate concrete structures are widely used in multi-storey construction. They have numerous benefits, including reductions in slab thickness and excellent deflection control over large spans; their inherent fire resistance is also widely considered a key benefit compared to competing floor systems. The fire resistant design of UPT structures is typically assured largely on the basis of results from unrealistic standard fire resistance tests performed prior to 1983. However, much remains unknown about the true behavior of continuous multiple bay UPT slabs in real fires. Relatively little data exist on the effects of localized exposure to elevated temperature on cold drawn prestressing steel under realistic sustained service stress levels, and the potential consequences of the resulting thermally induced stress relaxation and/or tendon rupture remain unexamined. To aid in the fire-safe design and post-fire evaluation of real, multiple-bay, continuous UPT structures, large-scale tests and computational modeling have been performed to assess high temperature stress relaxation in unbonded prestressing steel tendons subjected to localized heating, as would be the case in a real building fire. A series of novel high temperature experiments and computational modeling on locally-heated, stressed and restrained prestressing tendons with realistic configurations is presented to shed light on the transient response of the tendons at high temperature. Reasonable agreement is achieved between observed and predicted stress variation during heating, although minor refinement of the predictive model's creep parameters appears to be required. Both the experiments and the modeling show that inherent inclusion of high temperature creep, as assumed in essentially all available fire design guidance documents and software packages globally, is unable to represent the true response of UPT tendons in realistic UPT concrete slabs. This may lead to unconservative design against, and assessment of, fire damage to UPT slabs in both full floor-plate and localized fires.

J Gales, Doctoral Student, University of Edinburgh, UK. j.gales@ed.ac.uk

L Bisby, Reader & Ove Arup Foundation/Royal Academy of Engineering Senior Research Fellow in Structures in Fire, University of Edinburgh, UK. luke.bisby@ed.ac.uk

C MacDougall, Associate Professor, Queen's University, Canada. colin@civil.queensu.ca

INTRODUCTION

Unbonded post-tensioned (UPT) concrete slabs are flooring systems which are prestressed internally with cold-drawn steel tendons that are free to move longitudinally within a duct. These systems have several advantages over non-prestressed reinforced concrete, most notably larger span-to-depth ratios, more efficient and sustainable construction, and excellent deflection control. Unrealistic and outdated structural fire resistance tests performed several decades ago, on single span UPT elements, are routinely invoked to demonstrate UPT slabs' adequate performance in fire; current design of UPT slabs for fire safety is based largely on such tests. In recent years additional testing has led to debate [1, 2] regarding the fire safety of these structures. The more recent tests have clearly shown that much remains unknown about the true response of UPT concrete structures in fire. In particular, localized tendon damage in one bay of a UPT structure can have consequences across the entire floor plate since UPT tendons are continuous across many bays. Loss of prestress (caused by thermally induced stress relaxation or tendon rupture during fire) can thus decrease a UPT structure's ability to resist flexural and shear effects over several bays [3].

No fire tests have ever been performed on realistic, continuous UPT flat plate slabs. In the absence of such tests, computational models are being used to study the response of UPT buildings in fire [4]. It is crucial however that these models show a proven capability to simulate all relevant structural behaviors, including tendon stress relaxation due to creep and strength degradation during (and after) heating and cooling. This paper presents novel experiments and computational modeling [5] on the effects of transient localized heating and cooling on a restrained UPT tendon.

BACKGROUND & RESEARCH SIGNIFGANCE

The strength and modulus of a UPT tendon are reduced at elevated temperature. For a longitudinally restrained but unbonded tendon, high temperatures can cause thermal and creep deformations which result in irrecoverable prestress relaxation [6]. This relaxation reduces the ability of the structure to resist flexural and shear forces. Localized heating of stressed tendons can also cause the tendons to rupture if the prestress exceeds the tendons' tensile strength. A complex strength-stress-temperature-time interdependency exists in UPT structures which can influence structural response and which must be properly considered to build defensible computational models to simulate full-structure response.

An explicit computational creep model (coded in FORTRAN) was previously developed and validated by the authors [5] to predict stress relaxation for a restrained tendon under various heating and cooling scenarios. The model considers the reduction of tendon stress due to reversible restrained thermal expansion [7] and (depending on the current stress level, temperature, and duration of heating) irreversible transient creep (essentially based on the Harmathy creep model [8, 9]). The model is capable of treating any transient heating and cooling regime for any tendon length, heated length, tendon profile, and initial prestress level (see [5, 10] for full details of model development and validation). The authors' model *explicitly* accounts for transient creep deformation in computing the prestress relaxation on

heating. Conversely, available structural fire design parameters and procedures purport to *implicitly* include creep at elevated temperature by using stress-strain curves developed from stress relaxation tests performed under (and strictly valid only for) prescribed heating rates. Such an *implicit* approach was apparently used, for instance, in determining the strength and modulus reduction factors for steel that are specified in the Eurocodes [7].

EXPERIMENTAL PROCEDURE

Creep of prestressing tendons is negligible for most UPT structures under ambient conditions. However, at temperatures above 250°C [6], irrecoverable creep can accelerate and cause relaxation of prestress. In a localized heating scenario (e.g. an isolated fire, localized cover spalling, or variable cover due to parabolic tendon profile) UPT tendons may rupture due to a combination of accelerating creep strains and loss of tensile strength. To investigate the strength-stress-temperature-time dependency of locally heated, stressed, unbonded and restrained tendons of realistic length and parabolic tendon profile, eleven transient high temperature stress relaxation tests were conducted using a bespoke “strongback” testing frame.

Tendons with a length of 18.3m were stressed against the strongback frame (Figure 1). The strongback frame was specifically designed to simulate the tendon conditions found in typical UPT concrete slabs. A custom fabricated tube furnace was installed in the strongback to locally heat the tendon at mid-length. The tendon was mounted in a guide channel which was attached to parabolic profile plates welded to the top flange of the strongback beam. Bearing plates were added at both ends to accommodate end anchorages, load cells, and jacking of the tendon.

Individual seven-wire 12.7mm Ø Grade 1860 low relaxation prestressing tendons were stressed to $0.5f_{pu} \sim 0.6f_{pu}$ along the strongback frame (a typical stress for a UPT structure after time dependent prestress losses have accumulated [11]). The tendons were then locally heated with a 3% heated length ratio following a prescribed heating and cooling regime (see Table 1 for testing details).

Each test comprised three phases: (1) an increasing temperature ramp at 10°C/min to a predefined temperature set point between 200°C and 700°C (the ramp rate was chosen to be consistent with previous experimentation by MacLean [5, 12]); (2) a soak time of 90mins at constant temperature (selected to be representative of typical North American fire resistance ratings for restrained UPT floor systems with 20mm of concrete cover); this allowed observation of the steady-state temperature dependency of creep deformation; and (3) slow cooling to ambient temperature, which enabled investigation of residual prestress after heating. These experiments were similar to those performed previously by MacLean [5, 12] although they used a more realistic (longer) total tendon length and (smaller) heated length ratio. MacLean’s tests had an 11% heated length ratio and a total tendon length of only 5.4m. These two sets of data with different heated length ratios allow a better understanding of the effects of localized heating on prestress relaxation. Heated length ratios in available furnace tests of isolated UPT flexural elements range from 70% to 85% [2, 13, 14]. This may not be representative of real fires, particularly in open plan UPT buildings with travelling or localized fires [15].

In reality, thermal deformations (elongation of the slab, thermal bowing), continuity, restraint, and membrane action (both compressive and tensile) may influence the response of continuous multiple-bay UPT structures in fire [9]. Future research will attempt to address these additional issues.

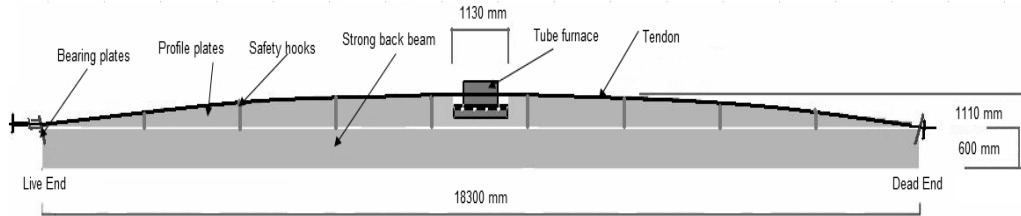


Figure 1. Strongback frame and custom tube furnace configuration.

TABLE I. TEST PROGRAMME, TEST DATA, AND MODEL PREDICTIONS.

Test #	Test set up				Experimental		% Difference	
	Initial stress (MPa)	Soak temp (°C)*	Soak time (mins)	Ramp rate (°C/min)	Hot stress (MPa)	Residual stress (MPa)	Soak period (%)	Residual period (%)
1	974	200	90	10	961	972	<1	<1
2	971	300	90	10	941	948	<1	1
3	973	400	90	10	808	831	17	17
4	1009	400	90	10	807	831	18	17
5	600	400	90	10	549	569	3	2
6	997	400	5	10	882	897	8	6
7	1015	400	45	10	815	824	15	13
8	1007	400	90	2	805	814	20	18
9	1015	400	90	30	769	786	19	17
10	983	700	0	10	Rupture	Rupture	Rupture	Rupture
11	997	500	2	10	477	Rupture	21	Rupture

* Note: the prescribed soak temperature indicates the specified set point, actual temperature for Test 10 was 524°C and for Test 11 was 501°C.

EXPERIMENTAL RESULTS

Several testing regimes were used to assess the tendon's performance during heating and cooling; these are summarized in Table 1. Tests 1 to 4, 10, and 11 considered different target set point temperatures (200°C to 700°C) but were otherwise identical. This allowed experimental investigation of the effect of creep/relaxation at different temperatures and also provided a comparison against MacLean's tests [5, 12]. It should be noted that Tests 10 and 11 both resulted in tendon rupture either at or before the target soak temperature was reached.

Available creep parameters that are used in the authors' predictive creep model are extrapolated beyond the stress range for which they were originally generated (up to 690MPa) and may therefore require updating [5]. Test 5 therefore considered a lower initial prestress level which lay within the limits of available high temperature creep data. Tests 6 and 7 varied the soak phase duration (5min and 45min) and Tests 8 and 9 explored the effect of different heating ramp rates (2°C/min and 30°C/min).

Figure 2 shows the predicted and observed stress versus time plots for Tests 1 to 3, with a heated length ratio of 3%, along with otherwise identical tests performed

by MacLean [12] with an 11% heated length ratio. Upon cooling from a soak temperature of 200°C (Test 1) a small amount of irrecoverable tendon stress loss (about 2MPa) was observed. After cooling from soak temperatures of 300°C or more, greater irrecoverable losses were observed; 23MPa for Test 2 at 300°C and 142MPa for Test 3 at 400°C. This clearly illustrates the irrecoverable stress relaxation that occurs due to transient creep at high temperatures.

The residual prestress levels for Tests 3 and 4 (both at 400°C) differ by less than 1MPa, indicating good test repeatability. Figure 2 compares Tests 1 through 3 to MacLean’s tests with a larger heated length ratio [12]. The larger heated length ratio is seen to result in more prestress loss on heating and the smaller heated length ratio shows proportionally less prestress recovery on cooling. Both of these observations are due to the proportionally greater recoverable effects of thermal expansion for the larger heated length ratio. The shorter heated length ratio maintains a higher overall stress level, which leads to greater irrecoverable creep losses in the heated region for the same soak time.

Tendon failure was observed in Tests 10 and 11 between 500°C and 525°C. However, tendon failure was not observed in any of MacLean’s tests [12], in some cases up to 700°C. This highlights the complex interplay between stress, time, and temperature for the tendon.

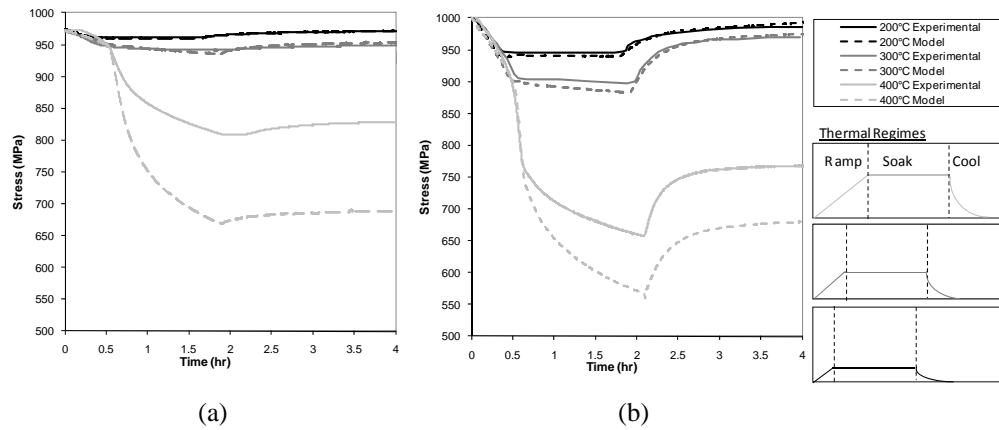


Figure 2. Stress versus time for (a) 11% heated length ratio and (b) 3% heated length ratio.

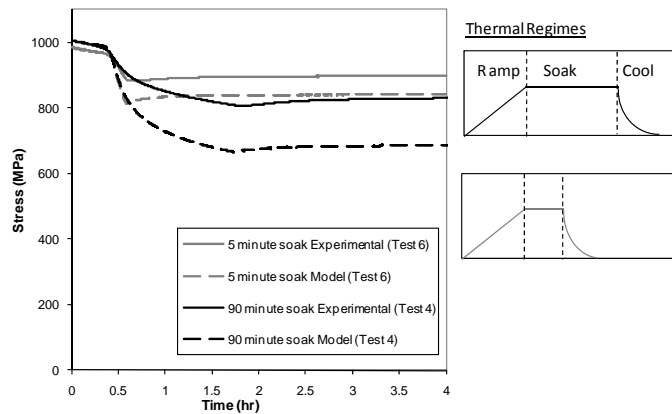


Figure 3. Effects of varying soak time.

Predictions were made for each of the tests using a computational explicit creep model developed previously [5]. The model used temperature input values from

actual thermocouple readings collected on the tendons during the strongback tests, and imposed the actual initial prestress levels recorded by the load cells. The predictions are given in Figure 2 and Table 1. For the strongback tests, the model shows reasonable agreement at 200°C and 300°C (a maximum difference of less than 1%). At 400°C the error is considerably larger at about 18%. This is expected since the model is known to calculate creep in a conservative manner [5]. It should also be reiterated that the creep parameters used in the model are based on steady-state creep tests up to stress levels of only 690MPa, whereas the initial prestress levels in the current experiments were about 1000MPa.

For Test 5, which had a lower initial prestress of 600MPa, the computational model predicts slightly more prestress loss than observed in the experiment, with differences of only 3% (16 MPa) during the soak phase and 2% (13 MPa) on cooling. This is in comparison to Test 3 (initial prestress of 1000MPa but otherwise identical) where the difference was 18%. This confirms that the creep is modeled more accurately at lower stress levels using the available creep parameters.

Tests 6 and 7 had soak times of 5mins and 45mins and were compared against Test 3 with a soak time of 90 minutes, all at a soak temperature of 400°C. As expected, Figure 3 shows that the amount of creep after a 5min soak at 400°C (115 MPa) is less than after a 90mins soak at the same temperature (202 MPa). The accuracy of the model increases with shorter soak times since creep is a function of time and thus lower creep losses occur with smaller soak periods. As already noted, the model conservatively over-predicts the amount of creep so that longer soak times lead to greater errors in prediction.

To the knowledge of the authors no information is available on the effects of varying heating rates on the mechanical response of prestressing steel. Different heating rates can be considered akin to tendons placed with different depths of concrete cover in a real UPT structure; a parabolic tendon in a real UPT slab will always experience different heating rates at different locations along its length. Figure 4 shows the effect of heating rate on the response of the tendons used in the strongback tests with a temperature set point of 400°C (Tests 4, 8, and 9).

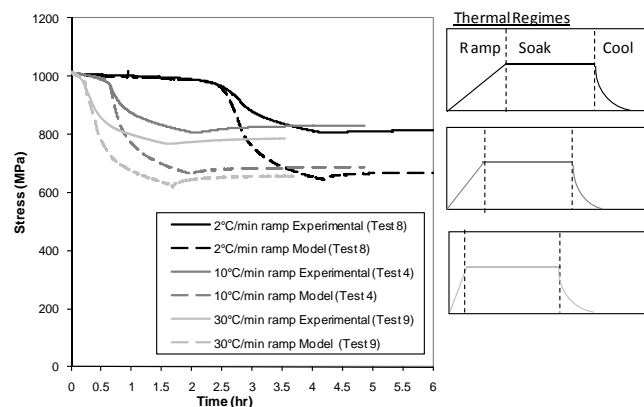


Figure 4. Varied Heating rates.

Tests 4, 8, and 9 all tend toward the same residual prestress level (within about 50 MPa of each other). Test 4 (10°C/min) displayed less residual prestress loss (178 MPa) than either Test 8 (2°C/min, 193 MPa) or Test 9 (30°C/min, 229 MPa), indicating no significant trend due to heating rate. The model predicted the experimentally observed trends but differed by up to 30MPa between the three tests.

DISCUSSION

With various countries currently in the process of adopting performance based structural fire design codes, it is a necessity to better understand various aspects of the real behavior of UPT concrete flat plates (and other types of structures) when subjected to elevated temperatures. A rational first step in this direction for UPT slabs involves accurately evaluating the response of the cold-drawn steel prestressing tendons under transient high temperature conditions. It is clear that available high temperature mechanical property reduction models for prestressing steel which *implicitly* account for creep cannot possibly capture the time-dependency of creep under transient heating conditions as would occur in a real fire. The consequences of this inability for computational structural modeling in support of performance based structural fire engineering remain unknown.

The interactions between strength, stress, time, and temperature at high temperatures in prestressing tendons of realistic length with localized heating have, until now, gone largely unexamined. Creep data currently do not exist for realistic in-service tendon stress levels; such data are needed as inputs for computational models and are currently being elucidated by the authors.

CONCLUSIONS AND RECOMMENDATIONS

A series of eleven transient high temperature stress relaxation tests on locally heated prestressing tendons have been performed and are compared herein to a previously developed [5] explicit creep model. Soak temperature, initial prestress level, soak duration, and heating ramp rate were all studied, both experimentally and computationally, leading to the following conclusions:

Irrecoverable (pre)stress losses resulting from transient creep deformations increased with higher soak temperatures periods and became noticeable above 300°C.

Small heated length ratios (3%) resulted in tendon rupture at soak temperatures above 500°C, confirming that localized heating of a tendon, which is reasonably likely for a real fire in a UPT building, may result in tendon rupture. No ruptures were observed up to 700°C for a larger heated length ratio of 11%.

The authors' explicit creep model [5] predicts the correct trends in tendon response subject to transient localized heating, although in general it over-predicts creep relaxation. This is thought to be due to the fact that the creep parameters used in the model are based on tests performed at stress levels below 690MPa. Additional testing is needed to develop creep parameters appropriate for realistic in-service stress levels of 1000MPa or more.

An important time dependency for creep relaxation was observed at elevated temperatures below the critical temperatures commonly assumed for prestressing steel [16]. Thus, thermal exposures in the range of minutes may become important for structural response at these tendon temperatures.

Stress relaxation was observed to be unaffected by different heating ramp rates between 2°C/min and 30°C/min up to a soak temperature of 400°C.

The consequences of prestress relaxation and tendon rupture for the global

structural performance of UPT concrete structures in fire should be evaluated, both through detailed finite element modeling of full-structure response to fire, and through large scale non-standard fire tests on UPT multi-bay model structures.

The authors' creep model is currently limited to consider only the behavior of the prestressing tendon. A more complete understanding of the performance of a UPT slab in fire can be made by studying the tendon's interaction with concrete and associated structural actions in fire such as thermal bowing, global thermal expansion, restraint, in-service concrete stresses, and compressive or tensile membrane action. Consideration must also be given to spalling during fire, since this would obviously cause localized heating of the tendons and is likely to occur in a real structure. These factors should be considered in future studies to arrive at a more rational treatment of the structural fire safety of UPT members and structural systems in modern concrete buildings.

ACKNOWLEDGEMENTS

We gratefully acknowledge the support of NSERC, Queen's University, Dr TI Campbell, the Ove Arup Foundation, and the Royal Academy of Engineering.

REFERENCES

1. Kelly, F. & Purkiss, J. 2008. "Reinf. Conc. Struct. in Fire," *The Struct. Eng.*, 86(19): 33–39.
2. Bailey, C. & Ellobody, E. 2009. "Comparison of Unbonded and Bonded PT Concrete Slabs under Fire Conditions," *The Struct. Eng.*, 87(19): 23–31.
3. Post, N. & Korman, R. 2000. "Implosion Spares Foundations," *ENR*, June 12: 12–13.
4. Ellobody, E. & Bailey, C. 2009. "Modelling of UPT Concrete Slabs under Fire Conditions," *Fire Safety J.*, 44: 159–167.
5. Gales, J., Bisby, L., MacDougall, C. & MacLean, K. 2009. "Transient High-Temperature Stress Relaxation of Prestressing Tendons in Unbonded Construction," *Fire Safety J.*, 44: 570–579.
6. Anderberg, Y. 2008. "The impact of various material models on structural fire behavior prediction," in *5th Int. Conf. on Structures in Fire*, Singapore, 13 pp.
7. CEN, 2004. *Eurocode 2: Design of concrete structures, Parts 1-2: General rules- Structural fire design, ENV 1992-1-2*. European Committee for standardization, Brussels.
8. Harmathy, T.Z. & Stanzak, W. 1970. *Elevated-Temperature Tensile and Creep Properties of Some Structural and Prestressing Steels*, National Research Council of Canada, Ottawa.
9. Purkiss, J.A. 2007. *Fire Safety Engineering: Design of Structures*. BH, London, UK.
10. Gales, J. 2009. "Transient high-temp. prestress relaxation of unbonded prestressing tendons for use in concrete slabs," *M.A.Sc. thesis*, Dept of Civil Eng., Queen's Univ., Kingston, Canada.
11. PTL, *Post-Tensioning Manual-Fifth Edition*. Post-Tensioning Institute, Phoenix, AZ, (1990).
12. MacLean, K. Bisby, L. & MacDougall, C. 2008. "Post-fire assessment of unbonded post-tensioned slabs: Strand deterioration and prestress loss," *ACI-SP255: Designing Concrete Structures for Fire Safety*, American Concrete Institute, Detroit, 10 pp.
13. Underwriters Laboratories. 1968. "Report on Unbonded Post-tensioned Prestress Reinforced Flat Plate Floor with Expanded Shale Aggregate," *PCI Journal*, pp. 45–56.
14. Van Herberghen, P. & Van Damme, M. 1983. "Fire Resistance of Post-Tensioned Continuous Flat Floor Slabs with Unbonded Tendons," *FIP Notes*, pp. 3–11.
15. Stern-Gottfried, J., Rein, G. & Torero, J. 2009. "Travel guide: A newly developed methodology, based on concept of 'travelling fires' in large enclosures," *Fire Risk Mgmt*, Nov., pp. 12–16.
16. ASCE 1992. *Manuals and reports on engineering Practice. no.78: Structural Fire Protection*. American Society of Civil Engineers, NY.

Experimental Study of Aging Effects on Insulative Properties of Intumescent Coating for Steel Elements

L. WANG, Y. C. WANG and G. Q. LI

ABSTRACT

Intumescent coating for steel elements suffers from ageing problems when exposed to complicated natural environments because most of its components are organic. Although research studies on durability of intumescent coating have been carried out in the last few years, the results of these research studies can only offer a criterion based on which one intumescent coating may be differentiated from the other. They cannot provide the residual fire protection properties of an intumescent coating after aging. In order to understand the ageing mechanism and how the thermal properties of intumescent coating changes with time in certain environment, accelerated ageing and fire tests have been carried out on 36 intumescent coating protected steel specimens, of which 18 specimens were applied with intumescent coating of 1mm thick and the other 18 with 2mm thick coating. This paper presents the experimental results with particular focus on the effects of the various cycles of accelerated aging on the effective thermal conductivity of the coating and on the temperature of the protected steel plate. It has been concluded that the intumescent coating thickness has little influence on the accelerated aging test results. Compared to the specimens without accelerated aging, the specimens that went through 2 and 4 cycles of accelerated aging experienced little degradation of thermal protection performance. However, the specimens after 21 and 42 cycles of accelerated aging experienced considerable degradation in their fire protection performance, with much higher effective thermal conductivity and protected steel temperatures, the effective thermal conductivity being about 30% and the steel temperatures about 100°C higher respectively. Furthermore, the fire protection properties of the intumescent coating after 21 and 42 cycles of accelerated ageing test were similar, indicating the intumescent coating had become stable after a long period of being exposed to environmental condition.

G Q Li, L L Wang, 1239 Siping Road Shanghai China
Y C Wang Sackville Street Machester M601QD UK

1 INTRODUCTION

Light-weight thin filmed intumescent coating is becoming more widely used as the fire protection material to steel structures because it has many advantages such as convenient construction, lightweight, and attractive architectural appearance. When exposed to heat, the chemical components in intumescent coating react to cause the coating to swell many times its original thickness so that the effective thermal conductivity (with reference to the initial thickness) of the expanded foam reduces to a fraction of the original value, thereby forming a lightweight flame-retardant char to protect the steel substrate from heat effectively. In addition, when the catalyst and blowing agents in the intumescent coating decompose under heat, water is evaporated, which absorbs some heat thus further reducing the steel temperature.

When specifying intumescent coating fire protection for steel structure, the following assumptions are made: the type and thickness of fire protection are correctly specified; the intumescent coating is correctly applied and its performance meets the fire protection needs without degradation in time. However, since most of the chemical components of intumescent coating are organic, it should be expected that the fire protection function of intumescent coating over time would not be as reliable as when freshly applied. Clearly, there is a need to understand the durability of intumescent coating.

Research studies on durability of intumescent coating have been carried out in the last few years. Two deficiencies still exist: first, the aging mechanism of intumescent coating was not analyzed theoretically; second, the results of these research studies can only offer a criterion based on which one intumescent coating may be differentiated from the other. To ensure sufficient fire resistance of intumescent coating protected steel structure, it is necessary to conduct research studies to investigate how aging affects the fire protection properties of intumescent coating.

This paper investigates the ageing mechanism of intumescent coating and provides some quantitative data on how the effective thermal conductivity of one type of intumescent coating changes with time and the extent to which the steel temperatures may increase after accelerated aging tests.

2 EXPERIMENTAL INVESTIGATIONS

2.1 Specimen Preparations

In total, accelerated aging and fire tests were conducted on 36 specimens, 18 of which were applied with 1mm coating and the other 18 with 2mm coating. For each coating thickness, three replicate tests were performed for each of the following 6 cycles of accelerated aging: 0 (no aging), 2 (simulating 1 year in service), 4 (2 years), 11 (5 years), 21 (10 years) and 42 (20 years). The steel substrate measured 200mm by 270mm by 16mm thick. Intumescent coating was applied to six sides of the steel plate. A primer was applied to the steel surface first to act as an aid to the adhesion to the reactive coating; this was then followed by different layers of intumescent coating (product type: unitherm

interior 38091), each layer having a dry film thickness of 0.2~0.3mm and with a time interval of at least 12 hours between different layers. Before the accelerated ageing test, the specimen was cured for 17 days under environmental condition of (23±3) °C, (50±5)% RH. Specimen labels were listed in table 1.

2.2 Accelerated Ageing Test

Aging is an extremely complicated process of physical and chemical interactions between the chemical components of the intumescent coating and the external environment. Whilst it would be ideal to carry out real time aging test, this process would be extremely long, running into many tens of years. An alternative is to conduct accelerated aging test, in which a real environmental condition over a long period of time is represented by short cyclic exposure of the intumescent coating to a concentrated dosage of the environment. During any accelerated aging test, it is necessary to determine the environmental conditions that the product (intumescent coating) will be exposed to, the length of time of the exposure and the performance criterion based on which the effect of aging is assessed.

According to the European Code ETAG 018 Part 2, four types of environmental exposure should be considered for reactive coating systems: (a) type X for all conditions; (b) type Y for internal and semi-exposed conditions; (c) type Z1 for internal conditions which have above zero temperatures but high humidity; and (d) type Z2 for internal conditions that have above zero temperatures but humidity conditions that are not in class Z1. The accelerated aging tests reported in this paper adopted exposure condition type Z2 because it simulates the exposure condition in most areas in China, each cycle of exposure is as follows:

- 4 h at (23 ± 3) °C and (80 ± 5) %RH
- 16 h at (40 ± 3) °C and (50 ± 5) %RH
- 4 h at (5 ± 3) °C and (50 ± 5) %RH

2.3 Fire Tests

After the specimens were subjected to accelerated aging as described in the previous section, they were placed in a furnace and exposed to fire. The furnace

Table I SPECIMEN LABELS

coating thickness(mm)	cycles of accelerated aging tests	specimen labels
1(2)	0	UI1(2)00- <i>i</i> (<i>i</i> =1, 2, 3)
	2	UI1(2)02- <i>i</i> (<i>i</i> =1, 2, 3)
	4	UI1(2)04- <i>i</i> (<i>i</i> =1, 2, 3)
	11	UI1(2)11- <i>i</i> (<i>i</i> =1, 2, 3)
	21	UI1(2)21- <i>i</i> (<i>i</i> =1, 2, 3)
	42	UI1(2)42- <i>i</i> (<i>i</i> =1, 2, 3)

temperature was measured by four thermocouples and the average furnace temperature followed the ISO 834 standard temperature—time relationship^[2]. Figure 1 shows the four specimens inside the furnace in each test. The steel temperature was measured by two to three thermocouples embedded in the steel plate and recording was made every minute continuously. The test was continued until the steel temperature reached 700°C.

3 TEST RESULTS AND DISCUSSION

3.1 Experimental Phenomena

The observed phenomena for specimens with both 1mm and 2mm coating were generally similar.

The following stages were experienced by specimens with 0, 2 and 4 cycles of accelerated aging:

- The intumescent coating began to melt and blacken 2 to 4 minutes after ignition, shown in figure 1(a); H₂O was also seen evaporating;
- Bubbles began to appear on the black intumescent coating surface 8 to 10 minutes after ignition; bubbling became more and more intense with increasing time, as shown in figure 1(b);
- The intumescent coating kept swelling and the thickness of the intumescent coating experienced great expansion with increasing bubble production; A lightweight spongy flame-retardant char finally formed on the surface of the steel substrate as shown in figure 1(c).

Specimens after 11, 21 and 42 cycles of accelerated aging experienced the same stages of behaviour as those with 0, 2 and 4 cycles of accelerated aging. However, the bubble production stage for specimens after 11 cycles of accelerated aging decreased greatly (shown in figure 1(d)) and the bubble production stage was almost non-existent for specimens with 21 and 42 cycles of accelerated aging. In addition, the final intumescent char after 0, 2 and 4 cycles of accelerated aging was much more compact and uniform than that with 11, 21 and 42 cycles of accelerated aging. The difference in char structures is shown in figure 1(e) and figure 1(f).

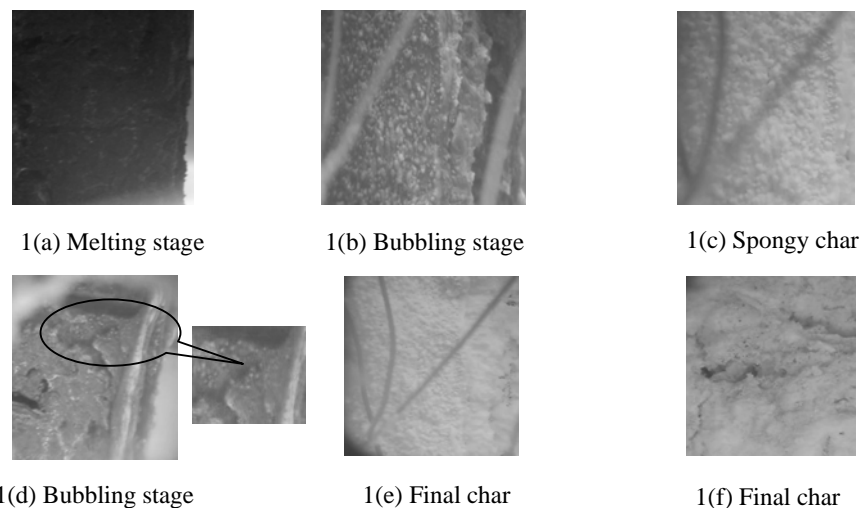


Figure 1. Changes in intumescent coating during different stages of fire tests.

3.2 Effective Thermal Conductivities

The effective thermal conductivity is associated with the original, rather than the expanded, thickness of the coating. In the European standard ENV 13381-4:2002 [4], the calculation equation for the effective thermal conductivity of fire protection to steel is:

$$\lambda_{p,t}(t) = \left[d_p \times \frac{V}{A_p} \times c_a \rho_a \times (1 + \phi/3) \times \frac{1}{(\theta_t - \theta_{a,t}) \Delta t} \right] \times \left[\Delta \theta_{a,t} + (e^{\phi/10} - 1) \Delta \theta_t \right] \quad (1)$$

In theory, the temperature dependent specific heat and density of intumescent coating should be used when calculating the effective thermal conductivity of intumescent coating using equation (1). However, since the amount of heat stored inside the intumescent coating is very small and may be considered to be negligible compared to that in the steel substrate, equation (1) may be simplified to equation (2) below:

$$\lambda_{p,t}(t) = \left[d_p \times \frac{V}{A_p} \times c_a \rho_a \times \frac{1}{(\theta_t - \theta_{a,t}) \Delta t} \right] \times \Delta \theta_{a,t} \quad (2)$$

For each specimen and for each time interval, the intumescent coating temperature θ_p may be taken as the mean of the steel and fire temperature so that

$$\theta_p = \frac{\theta_t + \theta_a}{2} \quad (3)$$

where

$\Delta \theta_{a,t}$ - increase of steel temperature during the time interval t ; $\lambda_{p,t}$ - effective thermal conductivity of intumescent coating during the time interval t ; d_p - initial thickness of intumescent coating; c_a - specific heat of steel; ρ_a - density of steel; θ_t - furnace temperature at time t ; $\theta_{a,t}$ - steel temperature at time t ; $\Delta \theta_t$ - increase of furnace temperature during the time interval t ; $\Delta t \leq 30s$

$$\phi = \frac{c_p \rho_p d_p A_p}{c_a \rho_a V} \frac{A_p}{V} \text{ - section factor of the protected steel section}$$

Figure 7 presents the results for the two different coating thicknesses.

It can be seen from figure 7 that compared to specimens without aging, the effective thermal conductivities of specimens with 2 or 4 cycles of accelerated aging change very little. Specimens with 11 cycles of accelerated aging have noticeably higher effective thermal conductivity. Specimens with 21 and 42 cycles of accelerated aging show a step increase in their effective thermal conductivity compared to the specimens without aging.

The observed changes in effective thermal conductivity of intumescent coating after different cycles of accelerated aging may be explained by the mechanisms of flame retardancy and aging. A conventional intumescent coating consists of flame-retardant system, acrylic resin and fillers. The flame-retardant system of unitherm 38091 is APP-MEL-DPE mainly, aided with zinc borate. Without aging effect, shortly after being exposed to heat, the coating turns to

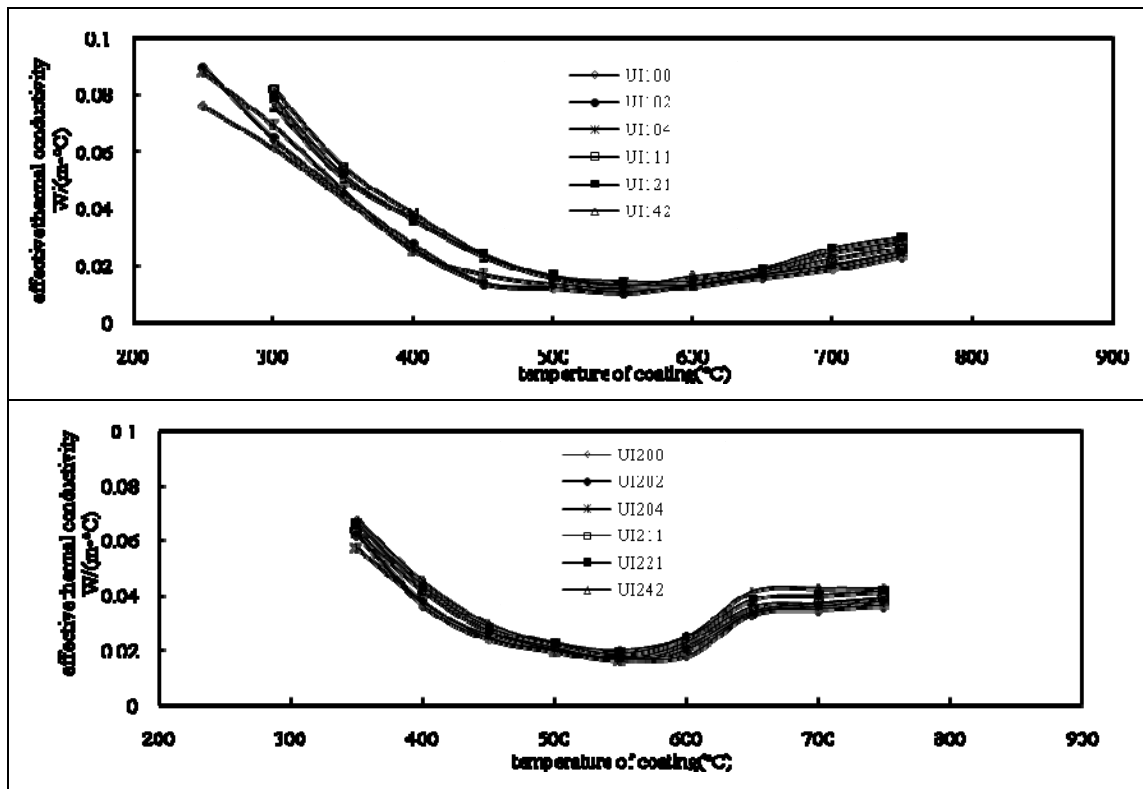


Figure 7. Effects of aging on effective thermal conductivity of intumescent coating.

melted state from dry film, and water of crystallization in the coating is decomposed. A porous structure is formed because the steam of water cannot be released freely from the highly viscous melted coating. With increasing temperature, APP as a catalytic agent begins to decompose and the mineral acid liberated from decomposition of APP causes DPE to dehydrate and carbonize. At the same time, a large quantity of H₂O and CO₂ released from the decomposition of APP, together with the nonflammable gases of CO₂ and NH₃ released from MEL cause the coating to swell and form a porous protective char. The reason for the value of effective thermal conductivities of the intumescent coating to drop initially with increasing temperature is owing to expansion of the coating and chemical reactions at 200°C ~400°C, such as char formation and release of nonflammable gases, which are endothermic reactions. The effective thermal conductivity of the intumescent coating keeps decreasing in the temperature range of 400°C -550°C as a result of multicellular char forming and further expansion when the zinc borate system begins to react. After reaching final expansion, the effective thermal conductivity of the intumescent coating rises with increasing temperature due to increased radiation within the voids and thermal degradation of the intumescent char.

Under the accelerated aging regime used in this study, the hydrophilic components APP, MEL and DPER move to the surface of the coating and mix with the moisture, which can destroy the intended chemical reactions of these components to form an effective intumescent char. With low number of cycles (2,4) of accelerated aging, the time is short so it is hard for APP, MEL and

DPER to move out and for the moisture to permeate into the coating, thus maintaining the effectiveness of the APP, MEL and DPER components and ultimately the fire protection effectiveness of the intumescent coating. As a result, the effective thermal conductivities of specimens with 2 or 4 cycles of accelerated aging are almost equal to those of the specimens without aging. In fact, the expanded thickness and inner structure of the expanded intumescent char are almost the same as those of the specimens without exposure to accelerated aging.

With increasing cycles and duration of accelerated aging exposure, the hydrophilic components of APP, MEL and DPER are gradually lost. Figures 3(e) and 3(f) indicate that after 21 and 42 cycles of accelerated aging exposure, the intumescent coating could not form a fine and closed honeycomb-like texture as specimens after 0, 2 or 4 cycles of exposure. The final expanded thickness was also lower. Consequently, the effective thermal conductivity of the coating experienced an increase. Since the intumescent coating system appeared to have reached chemical equilibrium after 21 cycles of exposure, the intumescent coating did not change much in its behaviour and the resulting effective thermal conductivity values were almost the same after 21 and 42 cycles of accelerated aging exposure.

In order to provide better pictorial comparison of the effects of aging on the effective thermal conductivity of intumescent coating, the arithmetical mean value of $\bar{\lambda}$ for each specimen over different temperature ranges were calculated and are listed in table II.

TABLE II. AVERAGE VALUE OF EFFECTIVE THERMAL CONDUCTIVITIES DURING DIFFERENT TEMPERATURE RANGE.

average value of $\bar{\lambda}$ specimen	400-450	500-550	600-650	700-750
UI10	0.022417	0.012057	0.016119	0.023416
UI12	0.02256	0.012392	0.016131	0.024492
UI14	0.02285	0.013462	0.016167	0.024507
UI111	0.029468	0.015177	0.017075	0.0273
UI121	0.029673	0.01528	0.01805	0.029892
UI142	0.029692	0.015597	0.01872	0.031812
UI20	0.028283	0.017335	0.027092	0.034283
UI22	0.029715	0.017432	0.027967	0.03615
UI24	0.031233	0.017496	0.02865	0.03775
UI211	0.035385	0.018999	0.030569	0.038499
UI221	0.035455	0.0198	0.035683	0.041679
UI242	0.035565	0.020332	0.03585	0.044668

Conclusions

This paper has presented the results of fire tests on intumescent coating protected steel plates after the intumescent coating has been exposed to different cycles of accelerated aging according to exposure condition Z2 in Eurocode ETAG 018 Part 2 ^[1]. The numbers of cycles were 0, 2, 4, 11, 21, and 42, corresponding to 0, 1, 2, 5, 10 and 20 years of nominal service. The results have been presented in terms of the steel substrate temperature and the effective thermal conductivity of the coating. The following conclusions may be drawn:

- (1) The values of effective thermal conductivity of the tested intumescent coating, which reflect the fire protection effectiveness of the coating, would change only slightly in the early years (2 years corresponding to 4 cycles) of service;
- (2) The gradual loss of hydrophilic components with increasing exposure time causes the intumescent coating to lose some effectiveness, as evidenced by reduced final expansion thickness and inferior inner texture of the intumescent char, resulting in increased coating effective thermal conductivity and steel substrate temperature. After ten years of service (corresponding to 21 cycles of exposure), the expansion thickness reduces significantly and the intumescent coating may not be able to form a fine and closed honeycomb-like structure texture, with the result being significant increase in the effective thermal conductivity of the coating;
- (3) The intumescent coating system would reach physical and chemical equilibrium with the adopted exposure condition after ten years of service (>21 cycles);
- (4) The increase in steel substrate temperature after 21 (10 years) and 42 (20 years) cycles of accelerated aging ranged from 50-100°C.

ACKNOWLEDGEMENTS

Funding for this research was provided by the Natural Science Foundation of China (NSFC) through an overseas research collaboration grant (50728805). The authors would like to thank professor G J Wang from Tongji University for conducting the accelerated aging and fire tests.

REFERENCES

1. European Organization for Technical Approvals, ETAG018, Guideline for European Technical Approval of Fire Protective Products, Part2: Reactive Coatings for Fire Protection Of Steel Elements,2006.
2. ISO-834 Fire resistance tests-elements of building construction. International Standard ISO 834, Geneva; 1975.
3. ENV 13381-4 Test methods for determining the contribution to the fire resistance of structural members-part 4: Applied protection to steel members, Brussels: European Committee for Standardization, 2002.
4. EN 1993-1-2 Eurocode 3: Design of steel structures, Part1-2: General rules - structural fire design European Committee for Standardization, 2005.

Bond Strength Degradation for Prestressed Steel and Carbon FRP Bars in High-Performance Self-Consolidating Concrete at Elevated Temperatures and in Fire

C. MALUK, L. BISBY, G. TERRASI and E. HUGI

ABSTRACT

Novel structures are emerging utilizing high performance, self-consolidating, fibre-reinforced concrete (HPSCC) reinforced with high-strength, lightweight, and non-corroding prestressed reinforcement. One example of this is a new type of precast carbon fibre reinforced polymer (CFRP) pretensioned HPSCC panel intended as load-bearing panels for building envelopes. As for all load-bearing structural members in building applications, the performance of these members in fire must be understood before they can be used with confidence. In particular, the bond performance of CFRP prestressing reinforcement at elevated temperatures is not well known. This paper examines the fire performance of these new types of structural elements, placing particular emphasis on the bond performance of CFRP and steel wire prestressing reinforcement at elevated temperatures. The results of large-scale fire tests and transient high temperature tensile and bond-pullout tests on CFRP and steel prestressing bars embedded in HPSCC cylinders are presented and discussed to shed light on the fire performance of these structural elements.

INTRODUCTION

Current trends in construction are forcing the development of more durable and sustainable concrete structures. Careful selection, design, and optimization of both the concrete mixes and the reinforcing materials used are now commonplace. One result of this has been the emergence of structural elements incorporating optimized, high-performance, self-consolidating, fibre-reinforced concrete (HPSCC) and novel reinforcing and prestressing materials such as carbon fibre reinforced polymer (CFRP) tendons, which are high-strength, creep resistant, lightweight, non-corroding, and magnetically invisible. One example of such an element is precast CFRP pretensioned HPSCC members used as load-bearing panels for building envelopes (Figure 1). However, the performance of these HPSCC precast members in fire is not well known and must be understood before

C Maluk, Pontificia Universidad Católica de Chile, Santiago, Chile.

L Bisby, BRE Centre for Fire Safety Engineering, University of Edinburgh, UK.

G Terrasi & E Hugi, EMPA Dübendorf, Zurich, Switzerland.

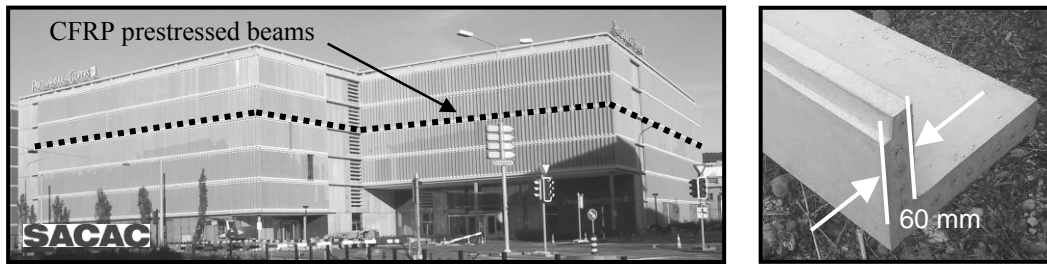


Figure 1. Use of precast CFRP pretensioned HPSCC members in a building envelope [3].

they can be used with confidence. The bond between both steel and FRP reinforcing bars (prestressed and non-prestressed) and concrete deteriorates at elevated temperature. Indeed, for FRP reinforcement, bond strength reductions are thought to be a limiting factor for the fire-safety of FRP reinforced or prestressed concrete [1], although the precise magnitude of bond strength reductions and their impacts on the load-bearing capacity of heated reinforced (or prestressed) concrete structures have not been studied and remain unknown. The tensile strength of steel & CFRP is also reduced by exposure to elevated temperatures; the reductions are well known for steel tendons [2] but remain largely unknown for CFRP tendons.

To address all of the above issues, an ongoing study is underway which includes: (1) large-scale furnace tests on CFRP prestressed HPSCC panels, (2) transient tensile strength tests on CFRP prestressing tendons, (3) transient bond pullout tests on CFRP tendons and steel prestressing wires, and (4) micro-mechanical characterization of the CFRP tendons. The goal in all cases is to better understand the response of CFRP prestressed HPSCC panels and to determine the factors that should be considered in their fire-safe design and application.

LARGE SCALE FIRE TESTS

Seven large scale fire tests were performed on CFRP prestressed HPSCC slabs in a floor furnace at EMPA (ISO 834 Fire). Figure 2 shows schematics of the specimens and test setup, and Table I provides details of the experimental program.

Initial scoping tests (not presented) performed on small scale slabs [4] indicated that loss of bond between the FRP tendons and the concrete was a governing factor in determining the fire resistance of the CFRP prestressed slabs. Bond failure occurred at bond line temperatures near the glass transition temperature of the CFRP's epoxy matrix ($T_g = 121^\circ\text{C}$ for these CFRP tendons). Thus, the testing programme included slabs with unheated overhangs (of varying length) at each end to provide a cold anchorage region during fire testing. The smallest anchorage

TABLE I. FIRE TEST PROGRAMME AND SELECTED RESULTS (REFER TO FIGURE 2).

No.	Age (mths)	Tendon type	Prestress (MPa)	Cover c (mm)	Thickness t (mm)	Overhang (mm)	Failure time	Failure mode
4	9.3	CFRP	1200	19.8	45	160	26'12"	spalling → crushing
7	8.8	CFRP	1200	20.3	46	280	34'36"	spalling → crushing
8	8.4	CFRP	1200	28.3	62	280	24'12"	spalling → crushing
5	8.4	CFRP	1200	27.8	61	160	47'00"	spalling → crushing
9	9.3	CFRP	1200	34.8	75	280	1h00'24"	spalling → crushing
6	9.3	CFRP	1200	34.8	75	160	1h31'36"	spalling → crushing
40	1.0	Steel	1200	34.8	75	160	29'00"	spalling → crushing

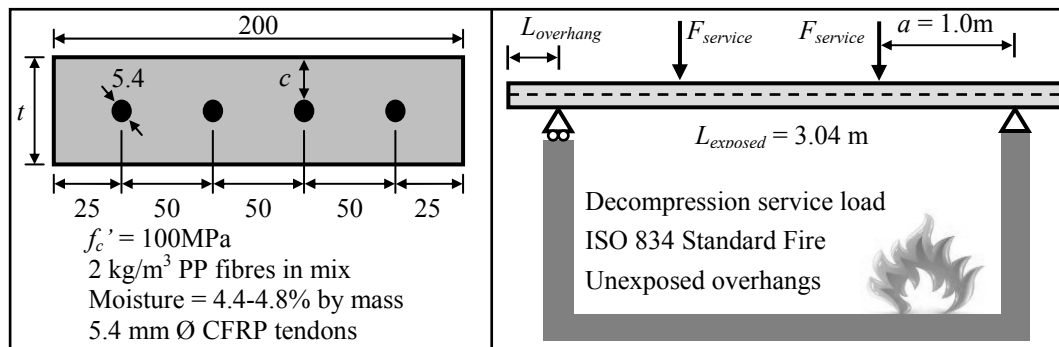


Figure 2. Details of fire test specimens and fire test setup.

length (160mm) represented the room temperature prestress development length for a tendon stress of 1200MPa, as determined from previous testing. The slab thickness, and hence the cover to the reinforcement, varied between 45mm and 75mm. The 100MPa concrete incorporated 2kg/m³ of short polypropylene (PP) fibers and had a high moisture content at the time of testing (4.4-4.8%). The load in the central span corresponded to a typical service load condition [3]. One slab used 6mm Ø cold-drawn steel prestressing wire stressed to 1200MPa.

The fire resistance of the slabs varied between 24min and 91min, with the thicker slabs generally achieving higher fire endurances. The notable exception was the steel prestressed slab, which suffered severe spalling early in the test (likely due to its very young age at the time of testing). This test is being repeated in May 2010 to properly account for the differences in slabs' age at the time of testing. Despite including PP fibers in the mix, the dominant failure mode was sudden collapse due to accumulated HSPCC spalling, which reduced the slabs' cross-sections until they failed in bending due to crushing of the remaining concrete under the service load. Spalling was first localized in the shear and bending span (i.e. near the supports where the bending moment is low and the exposed face of the slab is most precompressed). It is widely known that concrete's propensity for spalling is increased by compressive stress, so the location of first spalling is unsurprising.

Longitudinal splitting cracks were observed on the exposed and unexposed surface prior to failure for both 45mm thick slabs and, to a smaller extent, for the 60mm slabs. These were possibly caused by thermal incompatibility between the CFRP tendons and the HPSCC. Most 75mm slabs displayed single longitudinal cracks. Significantly, tendon slip versus time measurements showed no evidence of slip increases during the tests, indicating that the anchorage length of 160mm was sufficient to prevent bond failure. Tendon temperatures recorded in the fire exposed spans during these tests indicated that the tensile strength of the CFRP was maintained at temperatures above 330°C. Full details of these tests will be presented elsewhere [4]. Nevertheless, it appears that a fire resistance of 30min is achievable for these slabs when a concrete cover of 35 mm or more is used and a 160mm cold anchorage is provided.

TENSILE & BOND STRENGTH AT ELEVATED TEMPERATURE

The tensile strength of both steel and CFRP prestressing tendons can be expected to be reduced at elevated temperatures. For cold-drawn steel prestressing

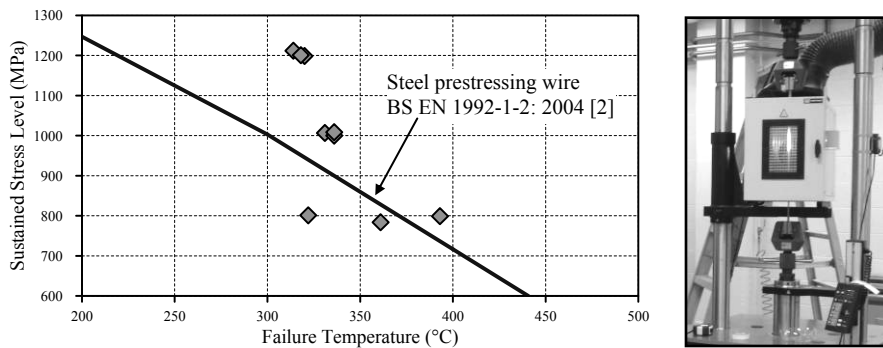


Figure 3. Results of transient tensile tests on CFRP tendons at high temperature.

tendons the relationship between temperature and tensile strength is relatively well established and is available, for example, in the Eurocodes [2]. The effects of elevated temperature on the specific strength of the CFRP tendons used in the current study are not known. Thus, a series of nine transient high temperature tensile tests was performed on the CFRP tendons at sustained stress levels between 800MPa and 1200MPa (a realistic stress range for prestensioning applications). The tendons were stressed to sustained loads of approximately 800, 1000, or 1200MPa and then heated, at 10°C/min, to failure. The anchorages were protected from high temperature. The results of these tests are given in Figure 3, along with the yield stress reduction curve recommended by the Eurocode [2] for Class A cold-drawn prestressing steel. It is evident that the performance of the CFRP tendons is similar to steel prestressing in terms of retention of tensile strength at elevated temperature, and that CFRP tendons stressed to 1000MPa can be expected to fail at about 330°C.

Past research on the bond performance of FRP and steel reinforcing bars at high temperatures has often been performed by heating a pullout sample without any load applied and then loading it to failure once a target temperature is reached [5, 6]. This is not representative of conditions in a prestressed concrete structure in a real fire, where materials are heated under sustained load (hence the transient procedure used for the tensile tests described above). Furthermore, in prestensioned prestressed elements there is considerable bond strength demand throughout the structure's lifetime needed to develop and maintain the required prestressing forces. It seems likely that sustained stresses are likely to be much more important than short terms loads for CFRP tendons at elevated temperature, since the tendon's epoxy matrix may undergo considerable creep deformation under sustained load at elevated temperature. Thus, in the current research bond pullout testing has been performed by applying a sustained load to a predefined bonded length and then heating the bond line at a prescribed rate until failure occurs; this is more representative of the state of stress within a real FRP prestressed structural element during a fire. Although the stress conditions in a reinforced concrete element differ greatly from those produced in a pullout test [7], this type of test has been widely adopted in the assessment of bond performance of steel reinforcing bars in concrete. The pullout test setup adopted in the current study is shown in Figure 4.

A total of 18 pullout specimens were tested, nine with CFRP tendons and nine with steel prestressing wire. Round, sand-coated unidirectional CFRP tendons supplied by SACAC, Switzerland were used in the pullout tests (identical to those used in the large scale tests described previously). The tendons' design ultimate

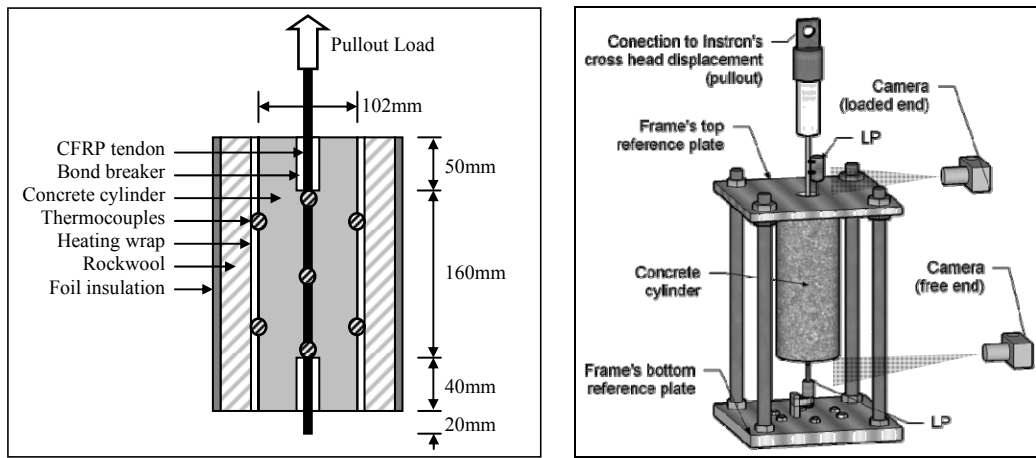


Figure 4. Schematic of pullout test specimens and experimental setup for pullout tests.

tensile strength is 2000MPa, with an elastic modulus of 150GPa, a linear-elastic tensile stress-strain response to failure, and an ultimate strain of 1.33%. The maximum prestress level for the CFRP tendons is governed by anchorage issues during stressing and is currently 1200MPa. To compare the bond performance of the CFRP tendons against conventional steel prestressing wire, 6mm \varnothing steel wire produced by NEDRI Spanstaal BV, specifically for prestressing applications, was also studied (identical to that used in Slab 40 in Table I). The wire's design yield strength is 1592MPa (0.2% offset) and its modulus is 210GPa.

The relatively high cost of CFRP tendons necessitates a correspondingly high quality of concrete. A high performance self-consolidating concrete (HPSCC) was designed for a strength of 90-100MPa at 28 days. 2kg/m³ of short PP fibres were included in the concrete to simulate the concrete mix used in the fire tests.

The pullout samples were 102mm \varnothing concrete cylinders with total length of 250mm. The moulds were designed in such way that the tendons/wires were placed vertically and axisymmetrically. The tendons/wires were debonded over a portion of their embedded length at the top and bottom of the cylinders to: (1) allow for the bonded length to be equal to the prestress transfer length of the CFRP prestressing tendons (160mm); (2) prevent localized artificial confinement of the bonded length due to compressive load on the concrete at the loaded end; and (3) promote an axisymmetric heat transfer condition along the bonded length and assure a uniform bond line temperature. Special consideration was given to the accuracy of the measurements of bar slip at both the loaded and free ends of the specimens. A unique digital image correlation analysis was used to measure slip [8] (Figure 4).

The behaviour of the specimens during heating turned out to be far more complex than expected, resulting in three distinct types of bond tests:

1. Regular pullout test (RPOT): Specimens were loaded at room temperature under displacement control until pullout failure occurred.
2. Regular prestress and heated pullout test (Regular PHPOT): Specimens were loaded at room temperature to a prescribed load under load control and then heated under sustained load until pullout occurred.
3. Extended PHPOT: Identical to regular PHPOTs except that bond stress was insufficient to produce failure of the bond interface on heating. After 230mins at steady state temperature the load was increased until failure.

The prescribed sustained loads were taken as increasing percentages of the average strength of RPOT tests: for CFRP tendons these were 15, 30, 38, 45, 53, 60 and 68% and for steel prestressing wires they were 37, 46 and 55%.

Steel Pullout Test Results

A summary of the test results for all of the pullout tests is presented in Table II. Steel RPOT samples failed by tensile rupture of the steel wire at the loaded end (i.e. the bond failure capacity was greater than the tensile failure capacity of the wire). The average RPOT failure load of $\tau_{ave, s} = 16.6\text{MPa}$ was used to define subsequent test loads.

Extended PHPOTs executed on steel pullout samples were stressed to 37% and 46% of $\tau_{ave, s}$. Under $0.37\tau_{ave, s}$ the samples were heated to a bond line temperature of about 162°C and were then loaded to failure of the bond interface, which occurred at an average bond stress of 12.6MPa . Under $0.46\tau_{ave, s}$ the samples were heated to about 166°C and were then loaded to failure of the bond interface, which occurred at an average bond stress of 13.2MPa .

Regular PHPOTs on steel tendons were at a sustained stress of $0.55\tau_{ave, s}$. In these cases failure occurred by transverse splitting failure of the concrete cylinder in less than six minutes of heating when the average bond stress was being maintained at 9.1MPa and the bond line temperature had not yet increased. Failure of these tests was likely the result of the concrete's tensile strength being exceeded due to the summation of the mechanical stresses produced by the pullout conditions and the thermal stresses produced by the steep thermal gradient in the concrete.

The results show that the bond performance of steel prestressing wire in concrete is influenced by a number of parameters, notably including transverse splitting cracking of the concrete. However, on the basis of the current results it appears that the bond between the steel wires and the concrete was reduced by up to 30% at a temperature of 166°C . Considerable additional research is needed before meaningful conclusions can be drawn. Such research appears to be warranted.

TABLE II. PULLOUT TEST PROGRAMME AND SELECTED RESULTS.

Test	Prestressing Condition			Failure Condition					Residual bond strength (MPa)
	Bond stress (MPa)	Tensile stress (MPa)	Pullout load (kN)	Bond stress (MPa)	Tensile stress (MPa)	Pullout load (kN)	Temperature Bar ($^{\circ}\text{C}$)	Temperature Blanket ($^{\circ}\text{C}$)	
CFRP RPOT	-	-	-	5.3	633	14.5	21	24	4.1
CFRP RPOT	-	-	-	4.4	524	12.0	20	24	2.9
CFRP 15%	0.7	87	2.0	3.9	461	10.6	166	182	2.3
CFRP 30%	1.5	175	4.0	5.1	601	13.8	166	182	2.2
CFRP 38%	1.8	218	5.0	4.3	513	11.8	164	185	2.3
CFRP 45%	2.2	262	6.0	-	-	-	109	169	0.65
CFRP 53%	2.6	306	7.0	-	-	-	102	155	0.89
CFRP 60%	3.0	349	8.0	-	-	-	95	148	0.92
CFRP 68%	3.3	393	9.0	-	-	-	21	76	-
Steel RPOT	-	-	-	16.6	1774	50.2	22	24	-
Steel RPOT	-	-	-	16.6	1772	50.1	21	24	-
Steel 37%	6.1	648	18.3	11.8	1257	35.5	164	184	-
Steel 37%	6.1	648	18.3	13.5	1434	40.6	160	178	-
Steel 46%	7.6	810	22.9	12.8	1365	38.6	170	192	-
Steel 46%	7.6	810	22.9	13.7	1460	41.3	162	179	-
Steel 55%	9.1	972	27.5	-	-	-	31	155	-
Steel 55%	9.1	972	27.5	-	-	-	25	118	-
Steel 55%	9.1	972	27.5	-	-	-	25	105	-

CFRP Pullout Test Results

CFRP RPOT samples failed by slipping at the bond interface between the sand coating on the CFRP tendons and the tendon. After failure occurred, pullout continued at a constant slip rate and a residual bond strength capacity of 66-77% of the peak load was measured. The average RPOT failure load was $\tau_{ave, f} = 4.9\text{MPa}$.

Extended CFRP PHPOT samples were prestressed to 15, 30 and 38% of $\tau_{ave, f}$. In all cases the samples were heated to a bond line temperature of about 170°C and were then loaded to failure, which occurred at an average bond stress of about 4.4MPa . Again, after failure occurred pullout continued and a residual bond strength of 44-58% was measured. The residual bond strengths observed in Extended PHPOTs on CFRP were consistently larger than the bond stresses at which the bond interface failed *during* heating in Regular PHPOTs at higher stress levels. This suggests a time dependency of bond strength related to the duration of loading at a given stress level, likely related to the time-temperature-stress dependent creep properties of the polymer coating at the surface of the CFRP tendons.

Regular PHPOTs on CFRP were prestressed to 45, 53, and 60% of $\tau_{ave, f}$. These samples failed during heating with decreasing failure temperatures observed as the sustained bond stress level increased. Figure 5 shows a plot of loaded end slip versus bond line temperature for these three tests, where the correlation between bond stress, temperature, and slip initiation is clear. For regular PHPOTs, pullout continued after the initial bond failure as the loading frame attempted to maintain the load, and a residual strength of about 29-35% of the bond stress at which the tendons were prestressed was observed. The Regular PHPOTs on CFRP at 68% of $\tau_{ave, f}$ failed soon after heating began. This was likely initiated by a small slip produced by longitudinal thermal expansion of the concrete during initial heating.

On the basis of the pullout tests on CFRP tendons, it appears that the bond between CFRP tendons and concrete is damaged by exposure to temperatures in the range of $90\text{-}120^\circ\text{C}$. Significantly, the glass transition temperature (T_g) for the epoxy matrix used in the fabrication of these tendons was measured at EMPA by DMTA as 125°C (as T_g -onset, the temperature above which the polymer softens and suffers a reduction in strength and stiffness of several orders of magnitude). This idea is supported by previous research studying the bond strength of Glass FRP bars used as non prestressed reinforcement for concrete structures [1]. However, considerable additional testing is needed to fully understand the complex interactions between time, stress, temperature, and strength that eventually lead to bond failure.

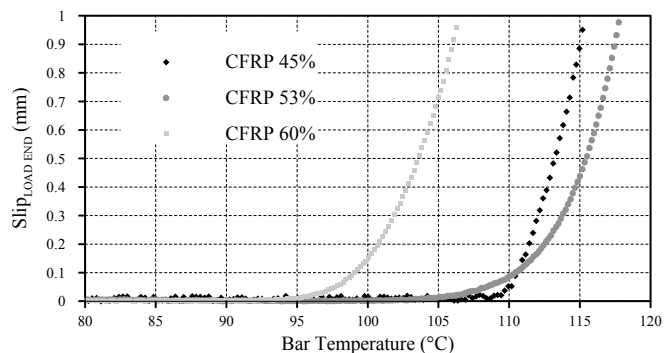


Figure 5. Loaded end slip versus bar temperature for Regular PHPOTs on CFRP tendons.

SUMMARY & CONCLUSIONS

Several conclusions can be drawn on the basis of the data presented herein:

The HPSCC concrete used in these elements experienced considerable spalling, which eventually led to structural failure during large scale furnace tests. This was despite the concrete containing 2kg/m^3 of short PP fibres. Additional research to mitigate spalling is badly needed. When CFRP anchorage is maintained, CFRP prestressed concrete can perform as well or better than steel prestressed concrete in fire, achieving fire resistances of 30mins or more.

Loss of bond (anchorage) is potentially a governing factor for CFRP prestressing tendons in concrete at elevated temperatures. It appears that temperatures in range of the T_g of the tendon's epoxy matrix (used also for the bond enhancing sand coating) are critical for maintaining anchorage.

For the CFRP tendons used in the current study, greater than 50% of the design ultimate tensile strength was maintained at temperatures exceeding 330°C . This is similar to values widely quoted for cold-drawn steel prestressing but can only be relied on if a cold anchorage zone is provided.

Many aspects of bond performance at elevated temperature (for both FRP tendons and steel prestressing wires) remain poorly understood and require additional investigation.

ACKNOWLEDGEMENTS

We gratefully acknowledge the support of SACAC and EMPA (Switzerland), Prof M Green at Queen's Univ. (Canada), the BRE Centre for Fire Safety Engineering, the Ove Arup Foundation, and the Royal Academy of Engineering (UK).

REFERENCES

1. L.A. Bisby, M.F. Green, V.K.R. Kodur. 2005. "Response to fire of concrete structures that incorporate FRP," *Prog. Struct. Engng Mater.*, 7: 136–149.
2. BS EN 1992-1-2. 2004. *Eurocode 2: Design of concrete structures—Part 1-2: General rules—Structural fire design*. Brussels: European Committee for Standardization.
3. G.P. Terrasi. 2007. "Prefabricated Thin-walled Structural Elements made from HPC Prestressed with Pultruded Carbon Wires," *8th Int. Symp. on FRPs for Reinf. Concrete Struct.*, Univ. of Patras, Greece, 10 pp., Jul. 2007.
4. G.P. Terrasi, A. Stutz, M. Barbezat, L. Bisby. 2010. "Fire behaviour of CFRP prestressed high strength concrete slabs," in *5th Int. Conf. on FRP Comps in Civ. Eng.*, Sept., Beijing, China.
5. É. Lubl6y, G.L. Bal6zs, A. Borosny6i, S.G. Nehme. 2005. "Bond of CFRP wires under elevated temperature," in *Int. Symp on Bond of FRP in Struct.*, The Hong Kong Polytechnic University, China, 163-168, Dec. 2005.
6. A.F. Bing6l, R. G6l. 2009. "Residual bond strength between steel bars and concrete after elevated temperatures," *Fire Safety Journal*, 44: 854–859.
7. ACI 408R-03. 2003. *Bond and Development of Straight Reinforcing Bars in Tension*. Detroit, USA: American Concrete Institute.
8. D.J. White, W.A. Take. "GeoPIV: Particle Image Velocimetry (PIV) software for use in geotechnical testing," *Cambridge Uni. Eng. Tech. Report CUED/D-SOILS/TR322*, Oct. 2002.

Strain Development of Traditional and Self-Compacting Concrete During Fire

E. ANNEREL and L. TAERWE

ABSTRACT

In this paper a complete strain model is derived that describes the strains developed during fire (till 400°C) and is based on the model of Anderberg, published in 1976. This model describes the total measured deformation as a superposition of 4 strain types: free thermal strain, instantaneous stress-related strain, creep strain and transient strain. The strains are derived from experimental loading tests on cylinders with dimensions Ø106x320mm, submitted to load ratios of 0, 20 and 30% of the initial strength before heating. The instantaneous stress-related strain should be derived from a loading test till failure at high temperature. However, to avoid damage to the furnace, this strain is assumed to be in the same order of magnitude as for cylinders tested for Young's modulus immediately after cooling. The parameter k_2 used to model the transient strain according to Anderberg is in this paper found to have a non-linear relationship with temperature, instead of linear as originally proposed by Anderberg. All tests occurred at a heating rate of 5°C/min and the specimens were pre-dried to avoid explosive spalling. The investigated concretes are a traditional and self-compacting concrete with a testing age of about 30 months. Only small differences between both types are found for the transient strain.

INTRODUCTION

The development of strains which occur during heating of concrete has been studied extensively in the past [1, 2], from which different constitutive models were derived. This paper uses the Anderberg model [1] as a basis.

Annerel E. & prof. Taerwe L., Ghent University, Magnel Laboratory for Concrete Research, Department of Structural Engineering, Technologiepark Zwijnaarde, 904, B-9052 Ghent, Belgium, email: Emmanuel.Annerel@UGent.be - Phone: +32 9 264 55 19 - Fax: +32 9 264 58 45

The total strain of heated concrete as function of the temperature and the load level can be formulated as a superposition of several strains. Equation 1 presents the total strain ε_{tot} as the sum of the free thermal strain ε_{th} , the instantaneous stress-related strain ε_{σ} , the classical creep strain ε_{cr} and an additional type of strain introduced by first time heating under load, namely the transient strain ε_{tr} .

$$\varepsilon_{tot}(c, T, t) = \varepsilon_{th}(T) + \varepsilon_{\sigma}(c, T) + \varepsilon_{cr}(c, T, t) + \varepsilon_{tr}(c, T) \quad (1)$$

The latter strain was added by [1, 2], since the total deformations under load could not be explained by only considering the creep and stress-related strains. The equation is generally accepted and is also mentioned in EN 1992-1-2 [3]. The different strain components are a function of temperature T , the corresponding stress σ and time t .

In [4], the transitional behaviour of concrete is called Load Induced Thermal Strain, abbreviated as LITS. This strain consists of three terms: the transient strain, basic creep and the change in elastic strain. Transient strain occurs in drying (unsealed) concrete and is by far the largest component of LITS. The term must not be confused with transitional thermal creep which only exists in non-drying (sealed) concrete and forms together with drying creep the transient strain. LITS is obtained from the difference in strain between the thermal strain of an unloaded concrete specimen (ε_{th}) and the strain measured under constant load prior to heating and maintained during heating (ε_{tot}), and after subtracting the initial elastic strain ($\varepsilon_{e,20^{\circ}\text{C}}$) [4].

Transitional thermal creep (ttc) results in relaxation and redistribution of thermal stresses during first heating under load to a given temperature. The thermal incompatibility between aggregates and cement paste due to differences in thermal expansion coefficients is compensated to a large extent. These incompatibilities are particularly manifest above 100°C, when unsealed cement paste experiences considerable shrinkage and the aggregates continue to expand [5]. Transient creep is irrecoverable on cooling and/ or unloading. However, it may reappear if a long period elapses between first and second heating [4]. Also, when heating to a higher temperature than a previous heating phase, the concrete specimen will first follow the free thermal strain curve and secondly, the transient creep will proceed when the temperature is above initial heating. During cooling, excessive tensile stresses can arise because of the absence of this transitional thermal creep, resulting in cracking and serious weakening of the material [5]. Transient creep develops rapidly above 100°C and is assumed to be temperature-dependent and not time-dependent. In practical terms this assumption can be made in fire applications which last only a limited number of hours [4]. This is the reason why some authors prefer the term transient strain above transient creep.

TEST PROGRAMME

A traditional vibrated concrete (TC) and a self-compacting concrete (SCC) are considered in this paper. Both concretes are made with OPC and siliceous aggregates. According to RILEM recommendation [6], cylinders with a 1/3 diameter/height ratio, namely a diameter of 106 mm and a height of 320 mm are

cast. These specimens are cured for 28 days at $20\pm 1^\circ\text{C}$ and $>90\%$ R.H., followed by storage at 60% R.H. and $20\pm 1^\circ\text{C}$ until heating. The testing age of SCC and TC is about 30 months. This long storage period results in a drop of the moisture content of the concretes to about 2.5% and a stabilization of the compressive strength development. The concrete composition and the initial mechanical properties are given in Table I.

TABLE I. CONCRETE MIX AND INITIAL MECHANICAL PROPERTIES.

	<i>SCC</i> <i>siliceous</i>	<i>TC</i> <i>siliceous</i>
sand [kg/m ³]	782	640
gravel 2-8 mm [kg/m ³]	300	525
gravel 8-16 mm [kg/m ³]	340	700
Portland cement I 52.5 [kg/m ³]	400	350
water [kg/m ³]	192	165
limestone powder [kg/m ³]	300	-
superplasticizer [l/m ³]	2.90	-
W/C [-]	0.48	0.47
density at 28 days [kg/m ³]	2343.8	2373.8
$f_{ccub150,28d}$ [N/mm ²]	65.0	55.9
$f_{ccil106x320,900d}$ [N/mm ²]	63.3	46.0
$E_{ccil106x320,900d}$ [N/mm ²]	38500	37500

Preliminary tests showed a high spalling risk for both TC and SCC samples. In order to avoid damage to the test setup, the TC specimens are pre-dried for 1 day (1.5% remaining moisture content), while the SCC samples are pre-dried for 1 week (constant mass). This drying procedure is allowable, since in [1] only a small difference was found between the measured strains on samples pre-dried for 1 day and without drying. Further, LITS and transient strain occur for transient heating only beyond 100°C [5,7]. During the heating tests, the heating rate is $5^\circ\text{C}/\text{min}$ which corresponds to the RILEM recommendation [6] and was also used in [1]. The target temperature is held constant for about 750 minutes, resulting in a uniform temperature distribution inside the concrete specimens.

In order to obtain a model that describes the transient strain, two types of tests are executed. Firstly, the specimens are heated to different target temperatures ($\pm 175^\circ\text{C}$, $\pm 300^\circ\text{C}$, $\pm 500^\circ\text{C}$) under external load ratios of 0, 20 and 30% of the initial strength. Secondly, creep tests are performed by loading to the same load ratios ($\alpha = 0.2$, $\alpha = 0.3$) after first reaching the target temperature (>180 minutes at maximum oven temperature).

Figure 1 illustrates the test setup, consisting of an electrical split oven, a loading system (pump, hydraulic jack, loading frame, accumulator), a specially designed displacement device and a PC unit (Vishay S5000 data acquisition system). Once the required pressure is reached in the hydraulic jack, the pump is disconnected. From then on, the pressure is maintained by means of the accumulator, which is filled with oil to about half of its volume and the other half with nitrogen gas. The displacements of the concrete cylinder are measured by means of two LVDT's,

consisting of a quartz tube that is glued to the core of an LVDT which slides in a coil. The test setup is provided by two such LVDT's, one on top of the concrete cylinder and one at the bottom. The tube used at the bottom of the concrete is pressed against the test specimen by means of a spring. The strain development of the concrete cylinder is then the difference between both displacements, divided by the 320 mm height of the cylinder.

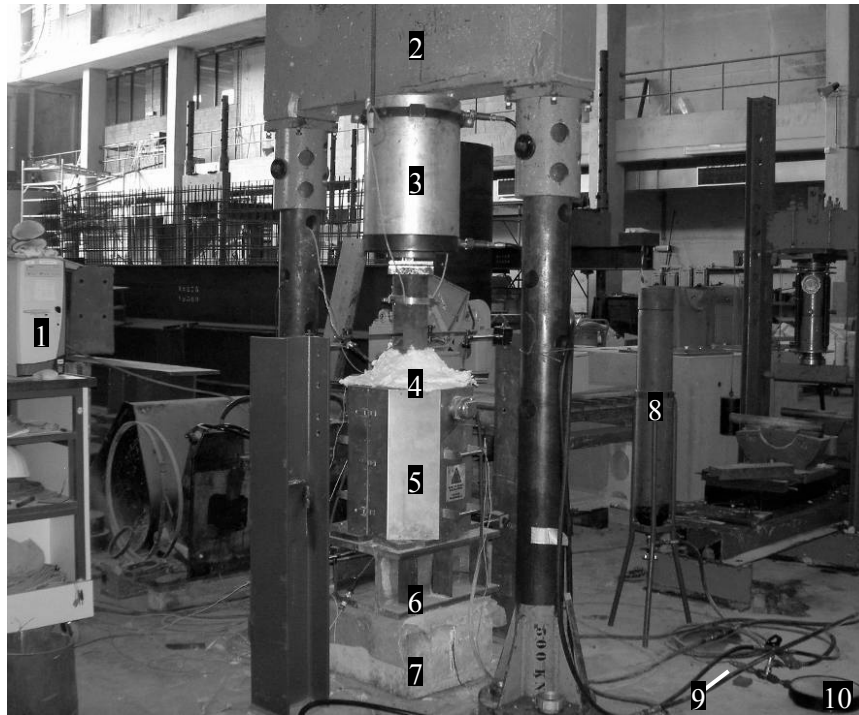


Figure 1. Test setup: 1. PC unit, 2. loading frame, 3. hydraulic jack, 4. glass fibre insulation, 5. oven, 6. HE 200 M profiles, 7. concrete block, 8. accumulator, 9. pressure sensor, 10. pressure gauge.

THERMAL STRAINS

Figure 2 shows the recorded thermal strains during heating of respectively TC and SCC concrete cylinders under different load ratios ($\alpha = 0.0$, $\alpha = 0.2$ and $\alpha = 0.3$). The free thermal strain ($\alpha = 0.0$) is generally directly measured during a heating test without external loads. In this graph, the initial elastic deformation due to application of the load before heating is already subtracted from the measured total strains corresponding to load ratios $\alpha = 0.2$ and $\alpha = 0.3$. The results of TC are comparable to those found in [2]. Only small differences are found between the curves belonging to TC and SCC. Notice that SCC yields the highest values, which is in contrast with the expected lower expansion due to the larger part of cement matrix. Till about 100°C , the thermal strains under a load ratio of 20 and 30% are close to the free thermal expansion. For both TC and SCC, the free thermal expansion as given in EN 1992-1-2 [3] is an upper limit.

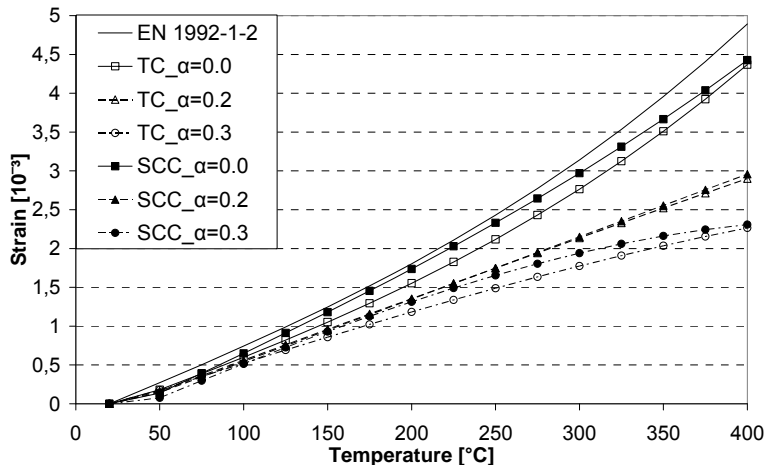


Figure 2. Thermal strain models of TC and SCC.

INSTANTANEOUS STRESS-RELATED STRAIN

The instantaneous stress-related strain (ϵ_{σ}) should be measured from a loading test till failure at high temperature. Such a test is not executed to avoid damage to the oven. Instead, this strain is assumed to be in the same order of magnitude as for the samples tested for Young's modulus (displacement controlled test, according to B15203-1990: 0.002 mm/s) immediately after cooling. This assumption seems to be acceptable, since the further strength losses upon post-cooling storage are then not introduced yet and will only occur about 7-14 days after cooling [8]. Figure 3 illustrates the instantaneous stress-related strain at high temperatures, corresponding to a load level of 20% and 30% of the initial strength. For comparison, the strain ($\epsilon_{c1,T}$) belonging to the compressive strength is also depicted as a function of temperature.

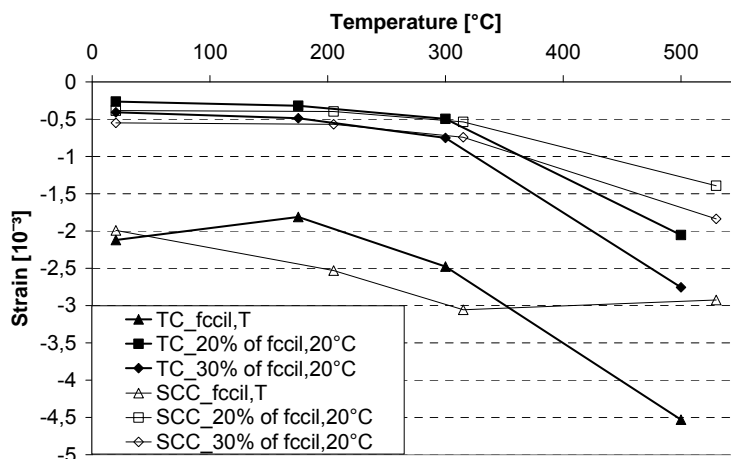


Figure 3. Instantaneous stress-related strain of TC and SCC, belonging to load levels of 20 and 30% of the initial strength.

CREEP STRAIN

The creep strain is small compared to for instance the thermal expansion. In [1] it is stated that only above 400°C creep may have some significance. This observation is confirmed by Hu (mentioned in [9]) who concludes that creep strains may be neglected during heating. Figure 4 shows the creep strain (ϵ_{cr}) of SCC, recorded for 400 minutes and belonging to different target temperatures and load ratios of 20% and 30% of the initial strength. The creep strains for TC have a similar curve, but with lower values. After 400 minutes creep, the TC values reach -0.30 ($\alpha=0.2$) & -0.40 ($\alpha=0.3$) at 175°C, -0.49 ($\alpha=0.2$) & -0.75 ($\alpha=0.3$) at 300°C and -1.23 ($\alpha=0.2$) & -1.85 ($\alpha=0.3$) at 400°C. Thus, the creep strains of SCC reach about twice the values found for TC, which must be attributed to the larger part of cement matrix. Notice that the strain values are in the neighbourhood of the instantaneous stress-related strains (Fig. 3).

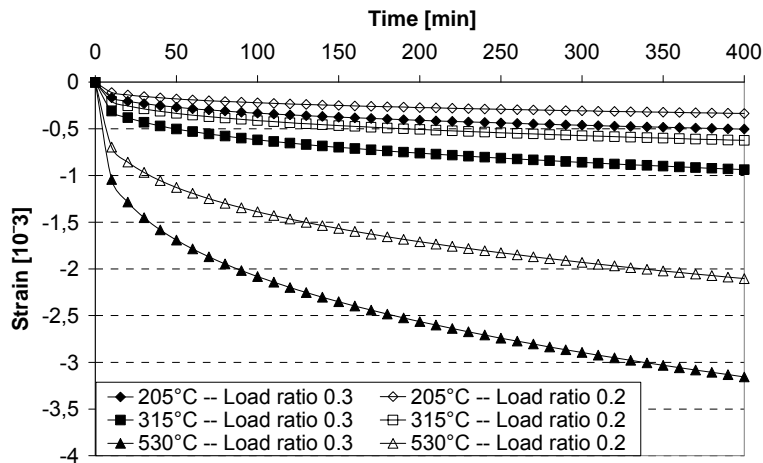


Figure 4. Creep strain of SCC measured for load ratios of 0.2 and 0.3.

TRANSIENT STRAIN

As discussed above, the transient strain can not directly be measured, but should be derived from the superposition of strains given in Equation 1. The model of Anderberg [1] gives a linear relationship between the transient strain, the load factor and the free thermal strain till 500°C (Table II). The parameter k_2 is a dimensionless constant that varies from 1.8 to 2.35 for quartzite aggregate concrete, based on published tests. Recently, new tests were performed by several authors [10, 11] to study the variation of the k_2 parameter for different concrete types. The results derived from the tests presented in this paper are also included in Table II. A non linear relationship is found between the transient strain and the temperature, which is also stated in [9]. As a consequence, as basis for a model for the transient strain, the model by Tao (2008) is chosen (Table II).

Figure 5 depicts the transient strain values for TC and SCC. Only small differences are found between TC and SCC, whereas TC yields the largest values

for the transient strain. Since the transitional behaviour is determined by the aggregate content by volume [4], larger differences were expected. Looking at the superposition of strains of Equation 1, it is clear that the influences of the larger creep strain values for SCC are compensated by the higher Young's modulus of SCC.

TABLE II. TRANSIENT STRAIN COMPONENT BASED ON ANDERBERG.

<i>Function</i>		<i>Reference</i>
$T \leq 500^\circ\text{C}$	$\varepsilon_{tr} = -k_2 \cdot \frac{c}{f_{c,20^\circ\text{C}}} \cdot \varepsilon_{th}$	Anderberg (1976) [1]
Quartzite (OPC) NSC:	$k_2 = 2.35$ (Anderberg) $k_2 = 2$ (Weigler and Fischer) $k_2 = 1.8$ (Schneider)	Anderberg (1976) [1]
Limestone (OPC) NSC:	$k_2 = 1.3$	Tokoyoda (2007) [10]
Siliceous (OPC) HSC:	$k_2 = 4.03$	Hirashima (2007) [11]
$\varepsilon_{tr} = c \cdot \frac{c}{f_{c,20^\circ\text{C}}} \cdot A_T$ $A_T = \begin{pmatrix} -2.6413 \cdot 10^{-13} \cdot T^4 + 2.9306 \cdot 10^{-10} \cdot T^3 \\ -9.4554 \cdot 10^{-8} \cdot T^2 - 5.7862 \cdot 10^{-6} \cdot T + 2.7 \cdot 10^{-4} \end{pmatrix}$		Tao (2008) [9]
Limestone (OPC) NS SCC:	$c = 1$	
Limestone (OPC) HS SCC:	$c = 1.55$	
$T \leq 400^\circ\text{C}$	$\varepsilon_{tr} = c \cdot \frac{c}{f_{c,20^\circ\text{C}}} \cdot A_T$ $A_T = \begin{pmatrix} -1.11 \cdot 10^{-10} \cdot T^4 - 1.82 \cdot 10^{-7} \cdot T^3 + 3.45 \cdot 10^{-5} \cdot T^2 \\ -1.3 \cdot 10^{-2} \cdot T + 0.202 \end{pmatrix}$	Annerel (2010)
TC (OPC, siliceous – Table I):	$c = 1.06$	
SCC (OPC, siliceous – Table I):	$c = 0.94$	

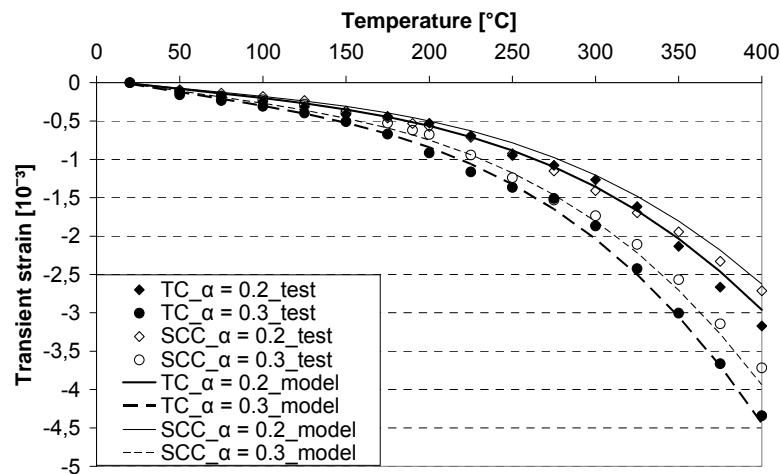


Figure 5. Transient strain of TC and SCC.

CONCLUSIONS

- The creep strain values found for SCC are twice those reached by TC
- A non-linear relationship is found between the transient strain and the load ratio and the temperature
- Small differences are found between SCC and TC for the transient strain, since SCC is also a stiffer material

REFERENCES

1. Anderberg, Y., Thelandersson, S. 1976. "Stress and deformation characteristics of concrete at high temperatures: 2. experimental investigation and material behaviour model, Bulletin 54," Lund Institute of Technology, Lund.
2. Schneider, U. 1976. "Behaviour of concrete under thermal steady state and non-steady state conditions," *Fire and Materials*, 1:103–115.
3. 2004. EN 1992-1-1: 2004 – Eurocode 2: Design of concrete structures—Part 1-1: General rules and rules for buildings. CEN, Brussels.
4. Khoury, G.A., Anderberg, Y., Both, K., Fellingner, J., Høj, N.P., Majorana, C. 2007. fib bulletin 38: Fire Design of Concrete Structures – Materials, Structures and Modelling, State-of-the art Report. International Federation for Structural Concrete (fib TG 4.3.1), Lausanne.
5. Khoury, G.A., Grainger, B.N., Sullivan, P.J.E. 1985. "Transient thermal strain of concrete: literature review, conditions within specimen and behaviour of individual constituents," *Magazine of Concrete Research*, 37 (132):131–144.
6. Schneider, U. Felicetti, R., Debicki, G., Diederichs, U., Franssen, J.-M., Jumppanen, U.-M., Khoury, G.A., Leonovich, S., Millard, A., Morris, W.A., Phan, L.T., Pimienta, P., Rodrigues, J.P.C., Schlangen, E., Schwesinger, P., Zaytsev, Y., 1998. "Recommendation of RILEM TC 200-HTC: mechanical concrete properties at high temperature—modelling and applications. Part 7: Transient creep for service and accident conditions", *Materials and Structures*, 31 (209):290–295.
7. Mindeguia, J.-C., Pimienta, P., Beurotte, A., La Borderie, C., Carré, H. 2007. "Experimental study of mechanical behaviour of high performance concrete at high temperature," in *Proceedings of the international workshop: fire design of concrete structures, from materials modelling to structural performance*, J.P.C., Rodrigues, G.A., Khoury, N.P., Høj, eds. Coimbra: University of Coimbra, pp. 25–37.
8. Annerel, E., Taerwe, L. 2007. "Approaches for the Assessment of the Residual Strength of Concrete Exposed to Fire," in *Proceedings of the international workshop: fire design of concrete structures, from materials modelling to structural performance*, J.P.C., Rodrigues, G.A., Khoury, N.P., Høj, eds. Coimbra: University of Coimbra, pp. 489–500.
9. Tao, J. 2008. Mechanical performance and thermal-mechanical constitutive model of self-compacting concrete at high temperature. Ghent University, Tongji University, PhD.
10. Tokoyoda, M., Yamashita, H., Toyoda, K., Hirashima, T., Uesugi, H. 2007. "An experimental study of transient strain for a concrete with limestone aggregate," in *Proceedings of the international workshop: fire design of concrete structures, from materials modelling to structural performance*, J.P.C., Rodrigues, G.A., Khoury, N.P., Høj, eds. Coimbra: University of Coimbra, pp. 105–114.
11. Hirashima, T., Toyoda, K., Yamashita, H., Tokoyoda, M., Uesugi, H. 2007. "Compression of high-strength concrete cylinders at elevated temperature," in *Proceedings of the international workshop: fire design of concrete structures, from materials modelling to structural performance*, J.P.C., Rodrigues, G.A., Khoury, N.P., Høj, eds. Coimbra: University of Coimbra, pp. 47–58.

Behaviour at High Temperature of Concretes Prepared with Flint, Quartzite or Limestone Aggregates

Z. XING, A.-L. BEAUCOUR, R. HEBERT, A. NOUMOWE
and B. LEDESERT

ABSTRACT

This paper presents the results of an experimental study carried out on concrete mixes made with three different types of aggregates: alluvial silico-calcareous gravels with 70% of flint, crushed calcareous aggregates consisting mainly of pure calcium carbonate and rolled siliceous aggregates made of quartzite (90%). The objective of this study is to better understand the influence of the chemical and mineralogical nature of aggregates on the thermomechanical behavior of concrete.

The aggregates underwent heating-cooling cycle from room temperature to 5 different temperatures at a heating rate of 1°C/min. Experimental results showed that aggregates with a same chemical nature (SiO₂) can present different thermal behaviours. Calcareous aggregates showed significant deterioration due to the decarbonation of calcium carbonate after 600°C.

For each aggregate type, two concrete mixes were studied: a normal concrete (W/C:0,6) and a high performance concrete (W/C:0,3). They were subjected to a heating-cooling cycle similar to the one undergone by aggregates. The evolutions of the residual mechanical and physical properties of the concretes were analyzed. The study shows that residual mechanical properties vary depending on the aggregate type.

Zhi XING, Ph.D. Student, Laboratoire de Mécanique et Matériaux du Génie Civil (L2MGC), Université de Cergy-Pontoise (UCP), 95000 Cergy-Pontoise Cedex France.

Anne-Lise BEAUCOUR, Associate Professor, L2MGC, UCP, France.

Ronan HEBERT, Lecturer, Laboratoire Géosciences et Environnement Cergy (GEC), UCP, France.

Albert NOUMOWE, Professor, L2MGC, UCP, France.

Béatrice LEDESERT, Professor, GEC, UCP, France.

INTRODUCTION

Numerous studies have improved the understanding of the physico-chemical and microstructural evolution of the binding phase of concrete [5],[6],[7]. According to recent studies [4],[7],[11], aggregates only play a minor role. However, the aggregates occupy an important part of concrete (70%) and their thermomechanical behaviour must have an impact on the thermal stability of concrete. The behaviour of aggregates in the face of temperature varies depending on their chemical composition and their mineralogy. Several studies have shown the worst behaviour of concrete made of siliceous aggregate in comparison to calcareous aggregate concrete [3],[8],[9]. This is generally attributed to the higher thermal dilation of siliceous aggregates and expansion of volume of quartz at the moment of phase change at 573°C. At contrary, Robert [15] showed that concretes prepared with some siliceous aggregates can have better thermal behaviour than those with calcareous aggregates. The scope of this work is to provide experimental data on the thermomechanical behaviour of concretes prepared with different nature of aggregate to provide a better understanding of the influence of the chemical composition and mineralogy of aggregates.

EXPERIMENTAL CAMPAIGN

AGGREGATES

Three different types of aggregates are used in this study: alluvial silico-calcareous aggregates (6,3/20mm and 0/4mm), crushed calcareous aggregates (6,3/14mm, 14/20mm and 0/4mm) and rolled siliceous aggregates (2/14mm, 14/20mm and 0/2mm). The densities of these three types of aggregates are 2480, 2670 and 2590 kg/m³, respectively.

Calcareous aggregates consist of nearly pure carbonate (99,5%), forming a homogeneous population. Silico-calcareous aggregates present a large petrographic variety. They are mainly composed of flint (70%), carbonate (24%) and a large variety of rocks (sandstone, quartzite, microconglomerat, etc...). Siliceous aggregates contain quartzite (91%), sandstone (7%) and other rock types (2%).

COMPOSITIONS OF CONCRETES

For each of the three types of aggregate, two types of formulation are studied, a normal concrete (NC) with a water to cement ratio of 0.6 and a high-performance concrete (HPC) with a water to cement ratio of 0.3. Compositions of concretes are listed in Table I. Portland cement (CEMI 52.5) is used. The dosage of superplasticizer (modified polycarboxylate) is adjusted to maintain a constant workability, very plastic (S4) for all the compositions. Cylindrical specimens (16*32 cm and 11*22 cm) are prepared. After seven days, the specimens are demoulded and placed into sealed plastic bags at ambient temperature for 90 days in accordance with the RILEM TC-129 recommendations.

TABLE I. MIXTURE PROPORTIONS, COMPRESSIVE STRENGTH, ELASTIC MODULUS OF TESTED CONCRETES.

	NC-SC	NC-C	NC-S	HPC-SC	HPC-C	HPC-S
Mineralogical nature	<i>Silico-calcareous</i>	<i>Calcareous</i>	<i>Siliceous</i>	<i>Silico-calcareous</i>	<i>Calcareous</i>	<i>Siliceous</i>
Cement CEM I 52.5 [kg/m ³]	362	362	362	500	500	500
Coarse Aggregate [kg/m ³]	956	447	396	987	459	411
Fine Aggregate [kg/m ³]		625	740		646	764
Sand [kg/m ³]	692	714	585	715	738	604
Water [kg/m ³]	217	217	217	150	150	150
Superplasticizer [kg/m ³]				1.65	2.15	1.5
[% by mass of cement]				0.33%	0.43%	0.30%
W/C	0.6	0.6	0.6	0.3	0.3	0.3
Vol. Mass [kg/m ³]	2227	2365	2300	2354	2495	2431
Compressive Strength (Mpa) before heating	35,9	38,1	38,8	81,2	76,3	72,8
Tensile Strength (Mpa) before heating	3,7	3,2	4	5,2	4,6	5,9
Young's Modulus (Gpa) before heating	35,6	31,5	36,6	45,2	43,4	44,2

HEATING/COOLING CYCLES

Aggregates and concrete specimens are subjected to five heating/cooling cycles whose maximum temperatures are fixed at 150°C, 300°C, 450°C, 600°C and 750°C. Each cycle consists of 3 phases: heating-up, stabilization at constant temperature during one hour and finally decrease of the temperature level until the ambient temperature. Heating and cooling occur at a rate of 1°C/min. In order to investigate the influence of initial moisture content, aggregates are tested saturated and oven-dried before heating. For saturated state, aggregates are immersed in water for 24 hours. For dry state, aggregates are dried at 105°C in the oven until weights of individual grain varied no more than a few centigrams on succeeding days. Their cooling takes place in the desiccator after exit from the oven.

RESULTS AND DISCUSSION

DESCRIPTION OF THERMAL DAMAGE OF AGGREGATES

Calcareous aggregates: be they initially saturated or dried before heating, calcareous aggregates remain intact up to 600°C. At 600°C, only some aggregates become gradually more reddish. At 750°C, they are cracked and the grain surface has whitened. This is due to the decarbonation; a proportion of calcite (CaCO₃) is converted to lime CaO releasing CO₂. About three days after leaving the sample at room temperature, aggregates disintegrate. After cooling, the free CaO reacts with atmospheric relative humidity and is transformed into Ca(OH)₂ (portlandite) by multiplying its volume ratio by 2.5 [10].

Silico-calcareous aggregates (Figure 1): *In the case of saturated gravel*, some black flints have burst between 150 and 300°C. At 450°C, aggregates flints, for the most part and whatever their color, have exploded. All of the flints showed cracks. Color of brown flints has changed into red at 300°C. The core of all the flints began to bleach from 600°C. At 750°C, the bleaching has reached the overall of the flint grain, with the exception of brown flints which retain their red color. *In the case of*

dry gravel, the major part of flint aggregates have exploded between 450 and 600°C, whatever their color, and all samples were cracked. The core of all the flints began to bleach from 600°C too. Carbonates of silico-calcareous aggregates appear intact up to 600°C but cracked at 750°C. The quartzites are intact up to 750°C with the only slight and gradual reddening of color that is observed at 600°C. Sandstone, granite and rhyolite remain intact up to 750°C.

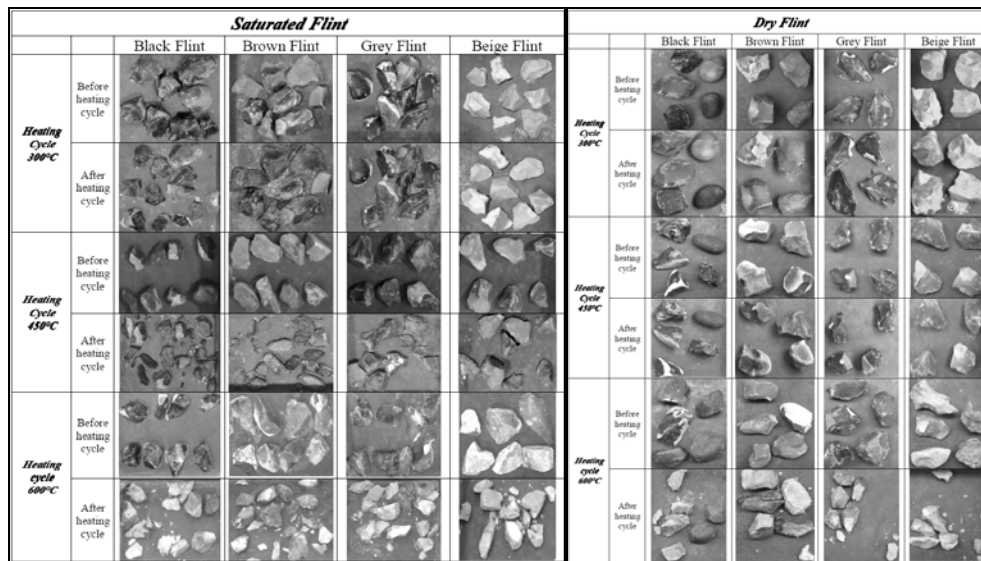


Figure 1. Comparison of different types of flint before and after heating at 300°C, 450°C and 600°C.

Siliceous aggregates: The quartzites and the sandstones remain intact up to 750°C. Slight and gradual reddening appears from 600°C.

The initial moisture condition seems to have a major influence on the thermal stability of flints. Permeability of flints would be insufficient for allowing water vapour to be evacuated. The vapor pressure in pores increases with the temperature and causes the explosive spalling of saturated flints between 150°C and 450°C. The explosive behaviour of initially dried flints between 450°C and 600°C could be also explained by an excessive pressure of water vapour. Flint can contain hydrated silica: water molecules in micropores or silanols groups ($\text{SiO}_{5/2}\text{H}$) [16]. The amount of this trapped water is estimated at about 1%. During the heating, the silanols groups are condensed to give loose water [2] [18]. Other authors assumed that the presence of calcite or iron oxides into the flints could explain their thermal damage [1] [13] [14].

DESCRIPTION OF THERMAL DAMAGE OF CONCRETES

For all concretes, the first cracks are visible after the heating/cooling cycle of 300°C. The highest rate of cracking is noted in silico-calcareous (SC) concrete. The figure 2 shows cracking and aggregate surface spalling of HPC-SC and NC-SC specimen after heating at 600°C.

Explosive spalling occurred on some specimens of HPC made of siliceous (S) aggregate (in the proportion of 1/7) and made of SC aggregate (in the proportion of 2/9) at 600°C and 750°C. Calcareous (C) aggregate concretes heated at 750°C are disintegrated several days after cooling due to the hydration of CaO in $\text{Ca}(\text{OH})_2$ in

the mortar and in the aggregates. The formation of portlandite is associated to a volume increase and leads to specimen disintegration. Same phenomena are also observed on NC-SC, NC-S, HPC-SC and HPC-S after the heating/cooling cycle at 750°C. But they are much slower and of smaller extent than on C-concrete.

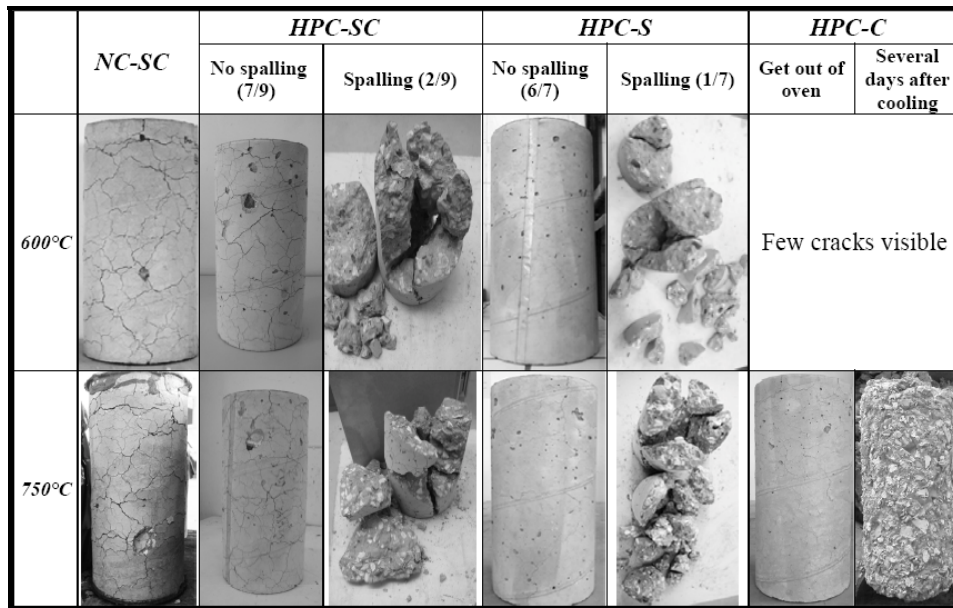
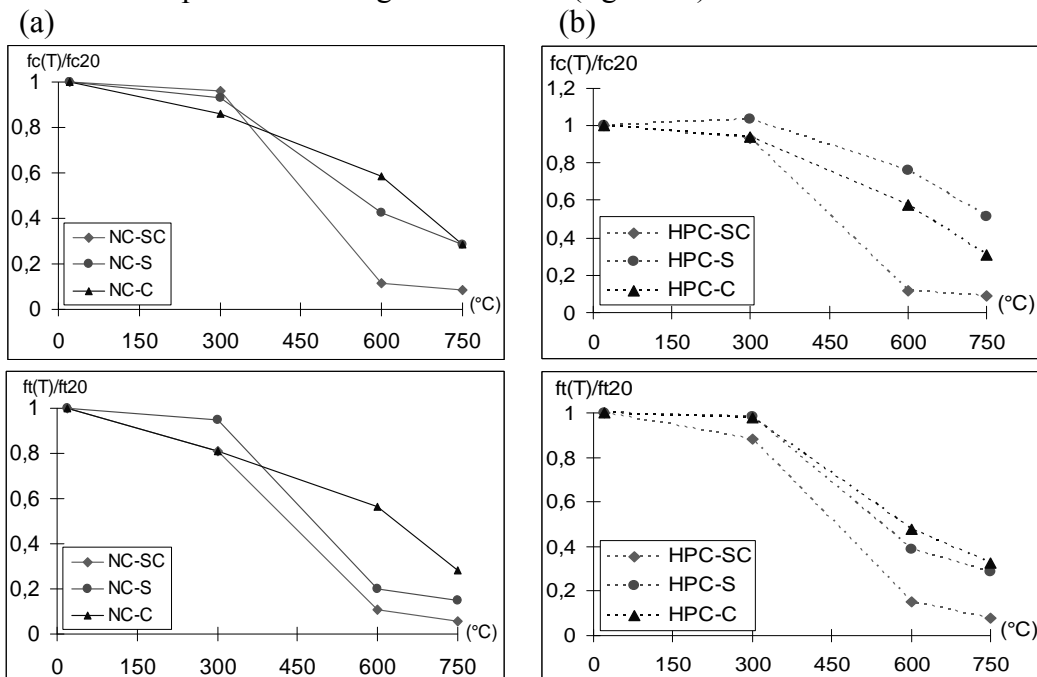


Figure 2. Specimens 16*32 after heating/cooling cycles 600° and 750°C.

RESIDUAL MECHANICAL PROPERTIES OF NORMAL CONCRETES

At 20°C, concretes with SC, C and S aggregates have very similar mechanical characteristics (Table I). After heating and cooling, the relative residual mechanical properties of NC-C are higher than those of NC-S and NC-SC. At 600°C, NC-SC shows a loss in performance higher than 90% (figure 3a).



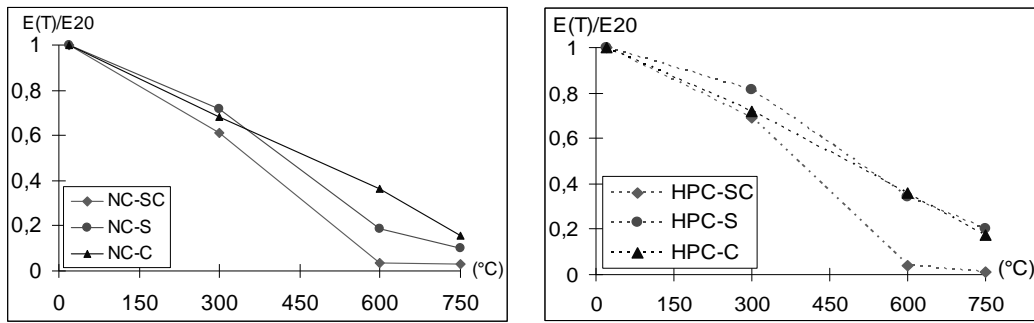


Figure 3. The residual mechanical performances of concretes as a function of heating temperature, (a) Normal concretes. (b) High-performance concretes.

The evolution of residual compressive strength is similar for the three concretes up to 300°C. In fact, most of the damage at this step comes from the elimination of free water (150°C) and from the dehydration of CSH in concrete (300°C). Beyond 300°C, the aggregates nature affects the degradation of the concrete, strength loss becoming more important for the NC-SC. The use of C aggregates compared with SC aggregates can reduce about 47% the compressive strength loss at 600°C and the use of S aggregates compared with SC aggregates can reduce about 32% the compressive strength loss at 600°C. However, above 600°C, the strength loss of NC-C and NC-S continues contrary to NC-SC; the residual compressive strength gain decreases from 32 to 21% for NC-S and from 47% to 20% for NC-C. Mechanical tests were realised immediately after the cooling. The residual performances after heating at 750°C would have been lower for C-concretes if specimens had been tested several hours after. Indeed, the hydration of CaO in $\text{Ca}(\text{OH})_2$ is associated to a volume increase and leads to specimen disintegration.

As for residual tensile strength and residual Young's modulus, the behaviour of NC-C is significantly better than that of NC-SC and of NC-S after heating at 600°C. The C-concrete has the best residual tensile strength. After heating at 600°C, its residual strength is 56,3% of original strength instead of 20% and 10,8% for NC-S and NC-SC. The loss of tensile strength of NC-S is higher than its loss of compressive strength. It can be explained by microcracking at the paste-aggregate interface. The better performance of NC-C compared to NC-S in tension is probably due to better bonding of C aggregates to the paste. Quartzite aggregates are round and have a smooth surface conversely to calcareous aggregates which are crushed and have a rough texture. In addition, there are chemical reactions between C aggregates and the paste which improve adhesion strength [12]. Beyond 600°C, the loss of tensile strength of NC-C becomes more important because of the dissociation of calcium carbonate.

The residual Young's moduli of normal concretes after exposure to high temperatures show the same conclusions. The ascending order of residual performances is NC-SC, NC-S and NC-C. Differences between the three concretes are less significant than for compressive or tensile strength.

Differences in residual mechanical performances are particularly sensitive between 300 and 600°C. The paste properties and volume are the same for all three concretes and the differences in residual mechanical performance are related to differences in mineralogical and chemical composition of aggregates. Due to decarbonation, mechanical strength of calcareous aggregates decreases after 600°C.

For the same chemical nature (SiO_2) the quartzites aggregates show greater thermal stability than the flints aggregates [17].

RESIDUAL MECHANICAL PROPERTIES OF HIGH PERFORMANCE CONCRETES

The figure 3b shows the evolution of residual mechanical characteristics of high-performance concretes made with SC aggregates (70% of flint), S aggregates (quartzite) and calcareous aggregates.

For the compressive strength, the HPC-S has better residual behavior than the HPC-SC and the HPC-C. The loss strength difference between HPC-S and HPC-C is 18% at 600°C and 20% at 750°C. The loss strength difference between HPC-S and HPC-SC is 65% at 600°C and 42% at 750°C. In comparison to normal concretes, the loss of compressive strength of HPC-S is moderate up to 600°C and accelerates beyond. The better compressive and tensile behavior of HPC-S compared with NC-S can be explained by higher bond strength at the paste-aggregate interface. The lower water-to-cement ratio of the paste leads to a decrease of the porosity of the interfacial transition zone. It can be noted that the increase of quartzite aggregate volume due to quartz alpha to quartz beta transformation which occurs at 573°C doesn't lead to poorer performances of S-concretes compared with C-concretes. The compressive strength loss of HPC-SC between 300 and 600°C is due to spalling of flints.

For the tensile strength, the performance loss of C-concretes is lower than that of quartzite aggregate concrete and that of SC-aggregates. For the Young's modulus, the performance loss is almost the same for HPC-C and HPC-S concretes.

CONCLUSION

This study presents a comparative analysis of mechanical and physical properties of six concretes exposed to heating/cooling cycles at 300°C, 600°C and 750°C at a heating rate of 1°C/min. Two types of paste matrix were tested, normal and high performance one.

The study on the thermal behaviour of aggregates showed the importance of the initial moisture state of flints aggregates. Explosive spalling occurred between 150°C and 450°C for saturated ones. Oven-dry flints aggregates showed important damages after 450°C (cracks, bursting into fragments). Though they have the same siliceous nature, quartzite and flints have a completely different behaviour. The crystallization and microstructure of quartz may play an important role in the thermal stability of siliceous aggregates.

Concretes with the same paste volume and composition were made with the three different types of aggregates. The residual mechanical behaviour varies depending on the type of aggregate. The SC-concrete presents severe cracking, and significant mechanical strength loss between 300 and 600°C. For example, residual compressive strength of NC-SC at 600°C is 4,2MPa and 3-5 times lower than that of NC-S and NC-C, respectively. The thermal instability of flints contained into SC aggregates explains the higher damage of SC-concretes with the temperature increase. For C-concrete, lime coming from the decarbonation of calcite (between 600°C and 750°C) reacts with ambient humidity and forms $\text{Ca}(\text{OH})_2$ (Portlandite)

by multiplying its volume by 2.5. This increase of volume leads to concrete disintegration. The residual mechanical characteristics are measured shortly after the cooling. Values after the heating at 750°C would be lower for C-concrete several hours after the cooling.

The influence of the aggregate is also dependent on the paste composition; C-concrete has the best residual compressive strength for normal matrix concrete while it's the S-concrete which behaves the best when using a high-strength matrix. With a lower W/C ratio, the porosity of the paste-aggregate interface zone decreases, and bond strength between paste and aggregate is improved. The increase of quartzite aggregate volume due to alpha-beta quartz transformation which occurs at 573°C causes cracking at the paste-aggregate interface. A better tensile strength at the interface delays the occurrence of cracks.

5. REFERENCES

1. Domanski M., Webb J, Robert Glaisher, Jan Gurba, Jerzy Libera and Anna Zakościelna. 2009. "Heat treatment of Polish flints," *Journal of Archaeological Science*, 36(7): 1400–1408.
2. Ek S. 2001. "Determination of the hydroxyl group content in silica by thermogravimetry and a comparison with 1H MAS NMR results," *Thermochimica Acta*, 379: 201–212.
3. Eurocode 2. 2004. "Design of Concrete Structures," Comité Européen de Normalisation, CEN, Brussels, Belgium, EN 1991-1.2.
4. FELICETTI, R., GAMBAROVA, P.G. 1995. "Effets of High Temperature on the Residual Compressive Strength of High-Strength Siliceous Concretes," *ACI materials Journal*, 95(4).
5. Georgali B., Tsakiridis P.E. 2005. "Microstructure of fire-damaged concrete-A case study," *Cement and Concrete Composites*, 27: 255–259.
6. Kalifa Pierre, François-Dominique Menneteau and Daniel Quenard. 2000. "Spalling and pore pressure in HPC at high temperatures," *Cement and Concrete Research*, 30(12): 1915-1927.
7. Kanéma-Tshimanga M., Influence des paramètres de formulation sur le comportement à haute température des bétons, Thèse de doctorat de l'Université de Cergy-Pontoise, 2007.
8. Khoury G.A., Anderberg Y., Both K., Fellingner J., Hoj N.P., Majorana C. 2007. "Fire design of concrete structures-materials, structures and modelling," *Fib Bulletin* 38, State-of-art report.
9. Kodur, V.K.R., et Sultan, M.A. 1998. "Structural behaviour of high strength concrete columns exposed to fire," *Symposium international sur les bétons à haute performance et de poudres réactives*, Sherbrooke, pp.217–232.
10. Matesova Dita, Bonen David, Shah, Surendra P. 2006. "Factors affecting the resistance of cementitious materials at high temperatures and medium heating rates," *Materials and Structures*, 39(4): 455–469.
11. Mindeguia J.-C., Pierre Pimienta, Albert Noumowé, Mulumba Kanema. 2010. "Temperature, pore pressure and mass variation of concrete subjected to high temperature," *Cement and Concrete Research*, 40(3): 477–487.
12. Neville a.M. 1993. "Properties of concrete," UK Longman House, 3rd edition.
13. Patterson L.W. 1995. "Thermal damage of chert," *Lithic Technology*, 20: 72–80.
14. Purdy B.A. 1974. "Investigations concerning the thermal alteration of silica materials: an archaeological approach," *Tebiwa*, 17(1): 37–66.
15. Robert F. 2009. "The influence of aggregates on the mechanical characteristics of concrete exposed to fire," *Magazine of Concrete Research*, 61(5): 311–321.
16. Vansant E.F., Van Der Voort P., Vrancken K.C. 1995. "Characterization and chemical modification of silica surface," Elsevier, Amsterdam, Chapitre 1–6.
17. Xing Z., Beaucour A-L., Hébert R., Noumowé A., Ledésert B. 2009. "Influence de la nature minéralogique des granulats sur le comportement à haute température des bétons," 27èmes AUGC.
18. Zhuravlev L.T. 1989. "Structurally bound water and surface characterization of amorphous silica," *Pure & Appl.Chem.*, 61(11): 1969–1976.

How the Steel Fibres Improve the Residual Properties of Concrete Subjected to High Temperature

P. PLIYA, A.-L. BEAUCOUR and A. NOUMOWÉ

ABSTRACT

Concrete structures in buildings or other constructions can be subjected to accidental conditions such as fire. Among many parameters, the safety of the structures depends on the thermal stability and the residual mechanical properties of the concrete. The aim of this study is to investigate the effect of steel fibres on the behaviour of concrete subjected to high temperature. Steel fibres were added to the studied concrete mixes in order to improve the concrete residual mechanical properties. Two groups of concrete with and without steel fibres were studied. Two water/cement ratios 0.45 and 0.30 were defined for each group of concrete. Steel fibres were used in mass proportions of 20, 30 and 40 kg/m³. The specimens resulting from these compositions were kept and tested at room temperature and after heating. Specimens were subjected to heating-cooling cycles from the room temperature to 150°C, 300°C, 450°C and 600°C at a heating rate of 1°C/min. The various properties studied were the porosity, the compressive strength, the flexural strength and the modulus of elasticity. The interesting results underlined that steel fibres have improved the concrete residual mechanical properties. The improvement of residual strength was more important in flexural tests. The residual flexural strength improved with increasing amount of fibre. The paste matrix quality (normal or high performance) didn't have a significant effect on the mechanical contribution of steel fibres.

Prosper PLIYA, PhD Student, L2MGC, University of Cergy-Pontoise, F-95000, France.
Anne-Lise Beaucour, PhD, Prof, L2MGC, University of Cergy-Pontoise, F-95000, France.
Albert Noumowé, PhD, Prof, L2MGC, University of Cergy-Pontoise, F-95000, France.

INTRODUCTION

The risk of thermal instability of concrete caused by fire was shown by several previous studies. This instability is related to the matrix compactness, the moisture content and the aggregates. The addition of polypropylene fibres in concrete mix improves its thermal stability. To improve the mechanical properties of heated concretes, steel fibres were added to concrete mixes [1-6]. The advantage of steel fibres compared to polypropylene fibres is that steel fibres do not melt at over 1200°C.

Some authors as [1, 2] observed thermal instabilities with concretes containing steel fibres. Peng et al. [1] observed thermal instabilities with concretes containing 100 kg/m³ of steel fibres for a heating at a temperature lower than 200°C. Chen and Liu [2] showed that the presence of steel fibres or carbon can delay the phenomenon of spalling. Concretes specimens containing steel fibres spalled at the temperature of 800°C. Lau and Anson [3] noted a good mechanical contribution of steel fibres for temperature lower than 1000°C. Beyond this temperature, there is no more difference between concrete with and without steel fibres. The tests were carried out for an amount of 100 kg/m³ of steel fibres.

The aim of this study is to investigate the effect of steel fibres on the behaviour of concretes subjected to high temperature. Different concrete mixes and amounts of steel fibres were used. The mechanical properties, before and after the different heating-cooling cycles, were studied. The evolution of concrete porosity was also investigated.

EXPERIMENTAL SCHEDULE

Materials

The cement used was CEM I 52.5 N CE CP2 NF. The aggregates were alluvial gravels composed of silica (70–75%), calcareous (20–25%) and feldspaths (5%). The fraction was 0/4 (sand) and 4/22.4 or 6.3/20 (gravel). The superplasticizer (Sup) used was a high water reducer containing modified polycarboxylate. The steel fibres (S-F) used were high carbon filaments of wire with hooked ends. It was Dramix® RC-80/30-BP. They were cylindrical of 30 mm length with a diameter of 0.38 mm.

Cure condition

Specimens were kept in their mould at 20°C ± 2°C and covered in order to avoid any water evaporation from the day of mixing until the seventh day. They were then demoulded and kept in plastic bags until the day of the tests. The specimens were cured up to at least 90 days in order to make sure that the pozzolanic reactions were stabilized and also to have less interstitial water in the concrete.

Tests

Heating-cooling cycles: four heating-cooling cycles were carried out in an electric furnace from the ambient temperature up to 150°C, 300°C, 450°C or 600°C. The cycles included a phase of rise in temperature, a phase of temperature dwell (one hour) and a phase of cooling. The heating rate was 1°C.mn⁻¹ and the specimens were then free to cool down to room temperature in the furnace. The heating and cooling rates were chosen in accordance with the RILEM TC-129 [7] recommendations.

Compressive strength (fc): tests were carried out on four cylindrical specimens Ø 160 x 320 mm in accordance with NF EN 12390-3 [8] standard.

Flexural strength (ft): tests were carried out on three prismatic specimens 100 x 100 x 400 mm in accordance with NF EN 12390-5 [9] standard.

Modulus of elasticity (E): tests were carried out on three cylindrical specimens Ø 160 x 320 mm in accordance with [10] procedures.

Water porosity (P): it was obtained on samples removed from specimens after the mechanical tests. The samples were oven dried at 60°C until constant weight and immersed in water until complete saturation. The test method is slightly different from the AFREM procedures [11].

CONCRETE MIXES

Two groups of concrete mixes were studied: one group of concrete mixes without fibres and one group of concrete mixes with steel fibres (S-F). For all the concretes, two water/cement (W/C) ratios were investigated, 0.45 (C2) and 0.30 (C3). All the mixes have the same paste volume. The consistency class obtained was S4 (16 cm < slump < 20 cm). The percentage of superplasticizer was adjusted in order to keep workability constant. The volumes of fibres in concrete were 0.25%, 0.38% or 0.50% which were equivalent to 20, 30 and 40 kg/m³. S-F reinforced concretes are defined as CS (CS2-30: C2 concrete with 30 kg/m³ of S-F). Table I summarizes the composition of the studied concretes.

One part of the specimens was tested without thermal load (20°C) and the second part was subjected to heating-cooling cycles before the mechanical load.

RESULTS AND DISCUSSION

The results obtained on the various concretes at ambient temperature are gathered in the table II. Porosity, compressive strength, flexural strength and modulus of elasticity were studied as a function of the heating temperature (T). Figures (1–3, 5) show relative residual mechanical properties or relative porosity obtained on heated specimens. The relative residual strength (modulus) or porosity

was calculated by dividing the residual strength (modulus) or porosity after heating-cooling cycles (f_T , E_T , P_T) by the strength (modulus) or porosity of the unheated concrete (f_{20} , E_{20} , P_{60}).

TABLE I. MIXTURES PROPORTION.

Comp. (kg/m ³)	C2	CS2-20	CS2-30	CS2-40	C3	CS3-20	CS3-30	CS3-40
Cement	400	400	400	400	500	500	500	500
Water	181	181	181	181	150	150	151	151
Sand 0/4	668	670	669	667	667	668	656	652
Gravel 4/22.4	1105	1095	1093	1091	1102	1091	-	-
Gravel 6.3/20	-	-	-	-	-	-	1072	1072
Steel -Fibres	-	20	30	40	-	20	30	40
Sup (dry extract)	0.64	0.6	0.58	0.60	1.55	1.52	1.28	1.42
Density	2355	2367	2374	2380	2421	2430	2410	2416

TABLE II. INITIAL CONCRETES CHARACTERISTICS.

T (°C)	Unit	C2	CS2-20	CS2-30	CS2-40	C3	CS3-20	CS3-30	CS3-40
P ₆₀	(%)	13.9	13.4	14.2	15.3	10.7	10.1	11.2	12.2
F _{C20}	(MPa)	46.0	57.9	57.7	55.9	70.2	69.7	74.7	77.9
F _{t20}	(MPa)	5.2	5.1	6.4	5.8	7.3	7.2	6.7	7.2
E ₂₀	(GPa)	37.7	39.7	39.2	37.6	44.1	43.7	45.3	44.9

Porosity

Figure 1 illustrates the evolution of the relative porosity of C2 (a) and C3 (b) concretes with and without S-F.

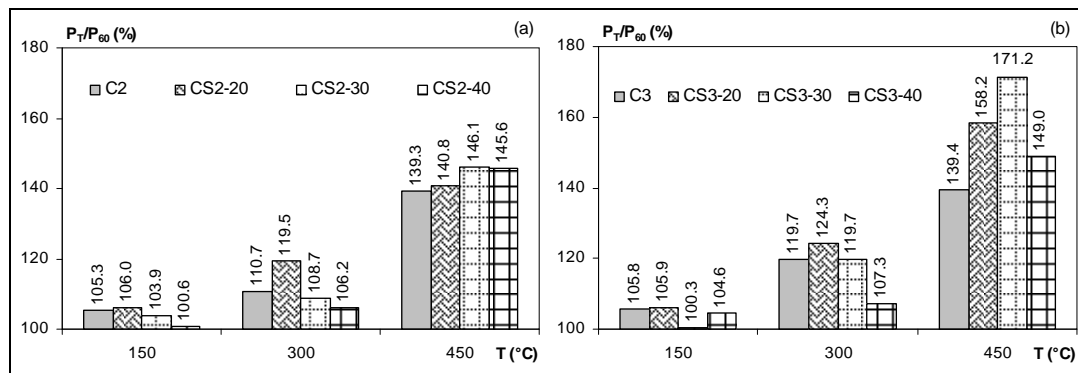


Figure 1. Relative porosity of C2 (a) and C3 (b) concretes with and without S-F as a function of the heating temperature.

Concretes porosity increases with the heating temperature. Up to 300°C, the steel fibres have no significant influence on the porosity evolution of normal (C2) and high strength concrete (C3). After the heating at 450°C, the porosity of S-F reinforced concretes increases more than that of concretes without fibres. Relative porosities of CS2-30 and CS3-30 concretes were 146.1% (C2: 139.3%) and 171.2% (C3: 139.4%), respectively.

The additional porosity of the S-F reinforced concretes at this temperature can be explained by a loss of adherence between the cement paste and the fibres. Indeed, the differential thermal expansion between steel fibres and the paste may cause stresses around the fibres which can lead to cracks and interface debonding. The porosity increase rate is more important for high strength concrete (CS3) than for normal concrete (CS2). But it should be noted that the porosity (P_T) of CS2 concretes remains higher than that of CS3 concretes. After the heating at 450°C, the porosity of CS2-40 and CS3-40 concretes was 22.3% and 18.2%, respectively.

Compressive strength

Figure 2 shows the evolution of the relative residual compressive strength as a function of the heating temperature. The relative compressive strength drops with the temperature increase.

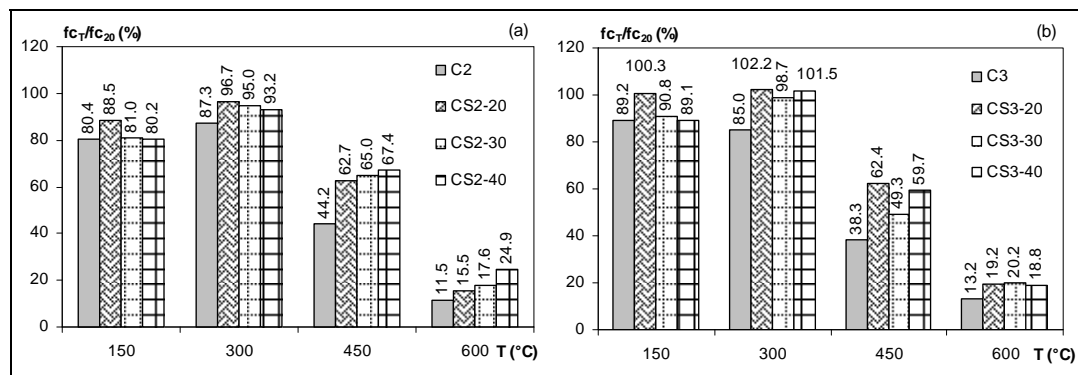


Figure 2. Relative residual compressive strength of C2 (a) and C3 (b) concretes with and without S-F as a function of the heating temperature.

With the addition of S-F, the strength improvement was noted from the room temperature until the temperature of 600°C for the two series of concrete. After the heating at 450°C, the average relative residual strength of CS2 concretes was 65% and that of CS3 concretes was 57.1% (C2: 44.2% and C3: 38.3%). The improvement of compressive strength was almost the same for the two series of concretes: 21% for C2 and 18% for C3. An improvement of residual compressive strength of concretes reinforced with S-F was also noticed by other authors [2-5].

After the heating at 150°C, CS2 concretes containing 0.25% (20 kg/m³) and 0.50% (40 kg/m³) of S-F have a relative compressive strength of 88.5% and 80.2%, respectively. The equivalent compressive strength loss was 11.5% and 19.8%, respectively. For the same proportions of S-F, the variation of compressive strength

loss with fibres volume was noticed by [6]. The loss strength varied from 6% to 12% for a volume of fibres of 0.25% and 0.50% at a temperature of 200°C.

Up to 300°C, the amount of fibre 20 kg/m³ (volume fraction of 0.25%) leads to better relative residual compressive strength. When the percentage of fibre increases, residual strength improvement decreases. Beyond 300°C, the reverse trend is observed for C2 concretes (Fig. 2 (a)). The results of C3 concretes do not show a significant influence of S-F volume (Fig. 2 (b)) after 300°C.

Flexural strength

Figure 3 shows the evolution of the relative residual flexural strength of CS2 (a) and CS3 (b) concretes compared to that of C2 and C3 concretes as a function of the heating temperature.

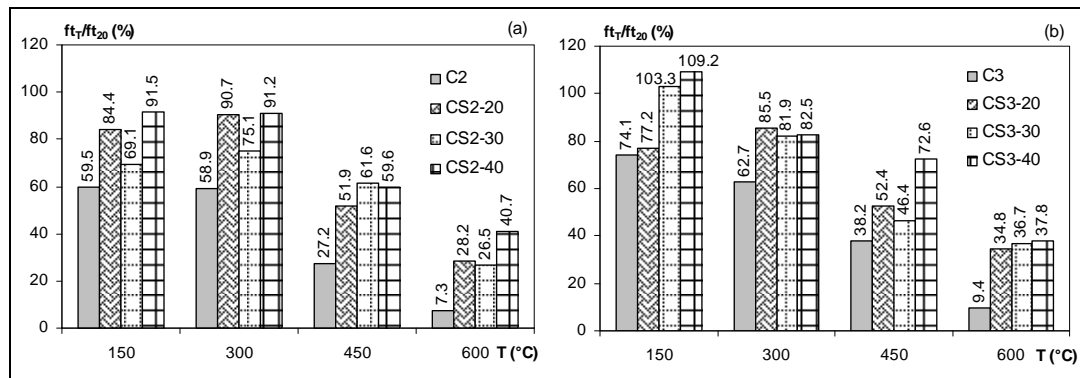


Figure 3. Relative residual flexural strength of C2 (a) and C3 (b) concretes with and without S-F as a function of the heating temperature.

An improvement of relative flexural strength was noticed for the two concretes containing S-F until 600°C. The improvement varies with the amount of S-F. The relative flexural strength of CS2-20 and CS2-40 concretes heated at 600°C was 28.2% and 40.7%, respectively. The improvement of relative flexural strength is better than that of compressive strength. At 600°C, the average flexural strength of CS2 and CS3 concretes are 31.8% and 36.4% while that of compressive strength is 19.3% and 19.4%, respectively. For high strength concretes (C3), the influence of fibre volume on the strength improvement at 600°C is not so important compared with C2 concretes.

Steel fibres induce an improvement of residual flexural behaviour from 150°C in this study. Works of [3] and [6] did not show significant improvement below 400°C. The improvement at 450°C ranges between 8 and 35% according to the concretes and the volume of fibres. These results corroborate those of [2] and [3]. At 600°C, the improvement is about 25% on the whole of the tested concretes. Addition of S-F in concretes improves the residual flexural strength. The improvement depends on the amount of fibres.

Figure 4 shows the influence of fibres on the post-cracking behaviour during flexural tests. When fibres are introduced in concrete the shape of the load-

displacement curve is changed. Concretes containing fibres show flattened descending path in the curves and an increase in the displacement at the peak-load. Up to 600°C, the ductile behaviour is retained. The brittle failure mode of the high-strength concrete is not observed any more for CS3 concretes.

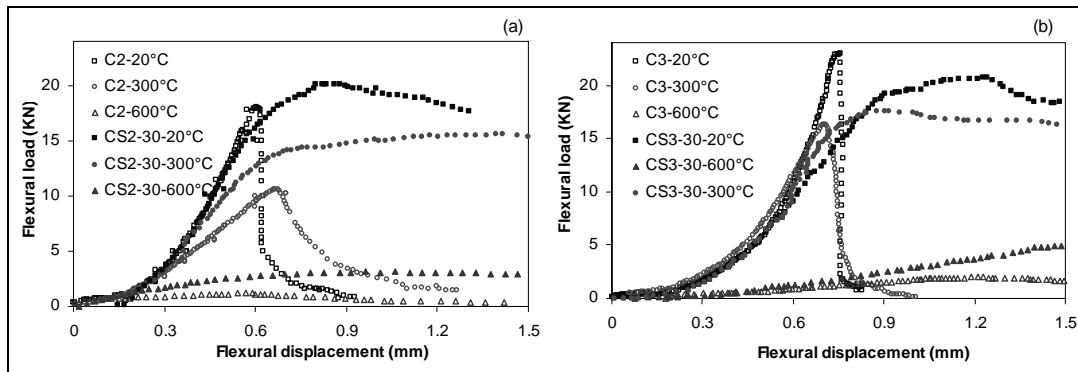


Figure 4. Flexural load of concretes with and without S-F as a function of displacement.

Modulus of elasticity

The evolution of the relative residual modulus of elasticity as a function of the heating temperature is shown by figure 5. For the heating-cooling cycles of 150°C, 300°C and 450°C, minor improvements of the modulus of elasticity are achieved by the addition of S-F. These results corroborate those of [4, 6].

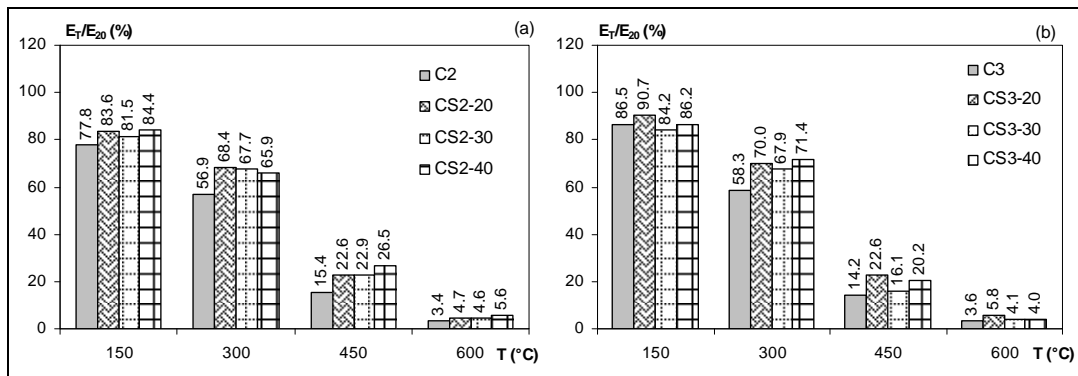


Figure 5. Relative residual modulus of elasticity of C2 (a) and C3 (b) concretes with and without S-F as a function of the heating temperature.

The average improvement of relative residual modulus of elasticity is approximately 11% for CS2 and CS3 concretes at 300°C. At 450°C, this improvement varies with the W/C ratio. The average gain of CS3 concretes is 5% while that of CS2 concretes is 9%. The average relative modulus of elasticity of CS2 concretes is 24% and that of CS3 concretes is 19.6%. CS3 concretes are more damaged than CS2 concretes as shown by porosity results.

At 600°C, there is very low difference between the concretes with and without S-F, whatever the amount of S-F.

CONCLUSION

In this investigation, normal (C2) and high (C3) strength concretes with and without S-F were made and subjected to different heating-cooling cycles. Concretes porosity and residual mechanical properties were studied. Some conclusions could be drawn from the experimental results:

- Porosity results of the heated S-F concretes show minor variation until the temperature of 300°C. The porosity of the two series of concrete increases very quickly beyond the temperature of 300°C. The rate of porosity increase is higher for CS3 concretes than for CS2 concretes. However, the porosity of CS2 (W/C=0.45) concretes remains higher than that of CS3 (W/C=0.30) concretes. The evolution of porosity depends on the amount of S-F.

- S-F in concrete involves an improvement of its mechanical properties at room temperature and also after heating. The improvement of flexural strength is better than that of compressive strength. The influence of fibres on the residual behaviour of the S-F concretes depends on the W/C ratio and the volume of fibres. The relative flexural strength of CS2-20, CS2-40, CS3-20 and CS3-40 concretes, after the heating at 600°C, were 28.2%, 40.7%, 36.7% and 37.8%, respectively. The residual ductility of the S-F concretes is kept for the various heating-cooling cycles.

REFERENCES

1. Peng G-F., Yang W-W., Zhao J., Liu Y-F., Bian S-H., Zhao L-H. 2006. "Explosive spalling and residual mechanical properties of fiber-toughened high-performance concrete subjected to high temperatures". *Cement and Concrete Research*, Vol. 36, pp. 723–727.
2. Chen B., Liu J. 2004. "Residual strength of hybrid-fiber reinforced high strength concrete after exposure to high temperature". *Cement and Concrete Research*, Vol. 34, p. 1065–1069.
3. Lau A., Anson M. 2006. "Effect of high temperatures on high performance steel fiber reinforced concrete". *Cement and Concrete Research*, Vol. 36, pp. 1698–1707.
4. Cheng F-P., Kodur V.K.R., Wang T-C. 2004. "Stress-strain for high strength concrete at elevated temperatures". *Journal of Materials in Civil Engineering*, Vol. 16, pp. 84–90.
5. Poon C.S., Shui Z.H., Lam L. 2004. "Compressive behavior of fiber reinforced high-performance concrete subjected to elevated temperatures". *Cement and Concrete Research*, Vol. 34, pp. 2215–2222.
6. Suhaendi S.L., Takashi H. 2006. "Effect of short fibers on residual permeability and mechanical properties of hybrid fibre reinforced high strength concrete after heat exposition". *Cement and Concrete Research*, Vol. 36, pp. 1672–1678.
7. Rilem Technical Committee 129-MHT. 1995. "Test methods for mechanical properties of concrete at high temperatures, Part 1: Introduction, Part 2: Stress-strain relation, Part 3: Compressive strength for service and accident conditions", *Materials and Structures*, Vol. 28-181, pp. 410–414.
8. NF EN 12390-3, AFNOR. 2003. Essai pour béton durci – Partie 3: Résistance à la compression des éprouvettes, Indice de classement: P 18–455.
9. NF EN 12390-5 AFNOR. 2001. Essai pour béton durci – Partie 5: Résistance à la flexion des éprouvettes, Indice de classement: P 18–433.
10. Torrenti J.M., Dantec P., Boulay C., Semblat J.F. 1999. Projet de processus d'essai pour la détermination du module de déformation longitudinale du béton, notes techniques. *Bulletin Des Laboratoires Des Ponts et Chaussées*, 220 NT 4263, pp. 79–81.
11. AFPC-AFREM, sur la durabilité des bétons, Méthodes recommandées pour la mesure des grandeurs associées à la durabilité des bétons, INSA-LMDC, Toulouse, Dec. 1997.

Experimental Study on Fire Performance and Protection of Building Seismic Rubber Bearings

B. WU, L. HAN, F. ZHOU and C. SHEN

ABSTRACT

This paper presents an experimental study to determine the fire resistance of seismic rubber bearings subjected to different durations of fire exposure and vertical loads. Besides, a simple yet effective fire protection method for seismic rubber bearings is proposed and its effectiveness is also investigated in fire test.

In the first experiment, four lead rubber bearings and two natural rubber bearings with the diameters of 600mm were tested subjected to different vertical loads and fire durations in furnace under the ISO834 standard heating process. The failure modes of rubber bearings were observed and experimental results reveal a) the fire resistance of rubber bearings fails to exceed 1.5 hours without protection; b) the duration of fire exposure has significant influence on the degree of the rubber bearings' mechanical properties degradation after fire; and c) there is an absence of evident link between vertical loads, to which rubber bearings are subjected during the fire, and their residual mechanical properties after fire.

In the second experiment, two seismic rubber bearings protected by thick type Fire Retardant Coating (FRC) were tested under ISO834 standard heating process, and then a comparison between the mechanical properties of the specimens after fire and those before fire was conducted. Test results indicate that a) after 3 hours of fire exposure, the specimens insulated with 50 mm thick FRC do not show visible changes in their appearance; and b) the degradation of their fundamental mechanical properties does not exceed 8%. Conclusion can be drawn that proposed insulation measure serve as a feasible fire protection for seismic rubber bearings.

Bo WU, Professor, State Key Laboratory of Subtropical Building Science, South China Univ. of Technology, Guangzhou, PRC, 510640

Liwei HAN, Graduate Student, State Key Laboratory of Subtropical Building Science, South China Univ. of Technology, Guangzhou, PRC, 510640

Fulin ZHOU, Professor, Earthquake Engineering Research & Test Center, Guangzhou Univ., Guangzhou, PRC, 510405

Chaoyong SHEN, Associate Professor, Earthquake Engineering Research & Test Center, Guangzhou Univ., Guangzhou, PRC, 510405

1. INTRODUCTION

Rubber bearings are formed of alternating thin rubber layers and steel plates chemically bonded together. Although rubber material is extremely low in thermal conductivity, degradation occurs to its material properties and chemical bonds to steel in high temperature [1]. Directly subjected to the exposure of potential fire hazards, bearings used in storey seismic isolation are the bottleneck of the structure's fire safety, posing significant menace to the safety of the entire building structure. In comparison with the behaviors of seismic rubber bearings which have been studied extensively, such as their mechanical properties and seismic capacity, their fire resistance, however, has not been sufficiently reported to the author's best knowledge.

Previous studies on fire resistance of seismic rubber bearings have been concentrated on a number of isolated fire tests [2, 3], fire protection methods [1, 4-12], and combustibility evaluation [13]. Much is still left to unknown and further works of research are needed as a) there is an absence of study on post-fire performances of rubber bearings after different durations of fire exposure; and b) the possible influence of loads, to which rubber bearings are subjected during the fire, on their performances after fire needs to be considered.

Regarding to aforementioned issues, the paper outline an experimental study and presents experimental results of fire tests of four Lead Rubber Bearings (LRB) and two Natural Rubber Bearings (NRB) in dimensions commonly used in China's engineering practice. The objective of this study is to investigate the fire resistance, failure mode, and residual mechanical properties of rubber bearings and the influences the duration of fire and working loads have on them.

This paper also proposes a fire protection method for building seismic rubber bearings using Fire Retardant Coating (FRC) as the thermal insulation of isolators. In comparison with existing fire protection methods of building seismic rubber bearings, which fail to gain popularity in China due to their high cost and complexity, FRC features remarkable fire resistance, fast construction ability, low cost, and high adaptability to the shape of specimens. Its effectiveness was tested in the study.

2. EXPERIMENTAL STUDY ON FIRE RESISTANCE

2.1 Test specimens

This experiment involves four Lead Rubber bearings (LRBs) and two Natural Rubber Bearings (NRBs) with diameters of 600 mm. Table I shows the detailed parameters of specimens. The influences of fire duration and vertical loading are considered in the experiment (as listed in Table II).

TABLE I. PARAMETERS OF SPECIMENS.

Specimen No.	Diameter (mm)	Height (mm)	T_r (mm)	d (mm)	S_1	S_2	E (N/mm ²)
GZY600-1, 2, 3, 4	600	192	5×22=110	120	30	5.45	0.392
GZP600-5, 6	600	192	5×22=110	—	28.5	5.45	0.392

Where S_1 , S_2 , E denote the total thickness of rubber layers, diameter of lead core, the first shape factor, the second shape factor, and elastic modulus of rubber, respectively.

TABLE II. SUMMARY OF FIRE TESTS.

Parameters	GZY600-1	GZY600-2	GZY600-3	GZY600-4	GZP600-5	GZP600-6
Vertical compressive stress (MPa)	10	10	10	15	10	10
Fire duration (h)	0.5	1	1.5	0.5	0.5	1



Figure1. Test apparatus.

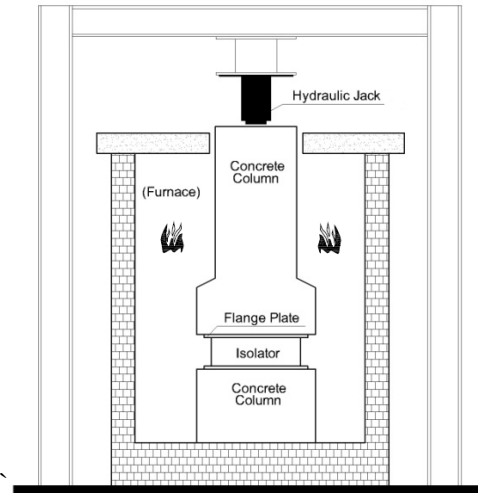


Figure 2. Schematic diagram of test apparatus.

2.2 Test Set-up

The fire resistance tests of rubber bearings were conducted at South China University of Technology. As Figs.1 and 2 show, the isolators were mounted between two concrete columns, which were connected to the isolators on their internal steel mounting plates using steel flange plates. The behavior of concrete columns was not investigated in the fire test as they are designed for the mere purpose of exerting vertical loads and simulating isolators' thermal condition. Ceramic fiber layers are blinded to the surfaces of concrete columns to protect the columns in the fire tests. Vertical load was applied and maintained on the top of columns through hydraulic jack during the fire tests, which was controlled and recorded manually to maintain constant load. A reaction frame constructed outside the furnace and fixed to ground was used to apply the vertical loads. The average temperature inside the furnace is recorded by 8 thermocouples and automatically controlled by computers to follow the standard ISO834 curve. Test records show that the actual heating process met the requirement of GB/T 9978-1999 [14] and were in good agreement with the designated heating process.

2.3 Failure Mode

Fig.3 shows the visible damage features of isolators after fire, it can be seen as follows:

- After 0.5 hours of fire exposure, 10 mm thick surface rubber of Specimens GZY600-1, GZY600-4 and GZP600-5 have been charred into carbonized layers composed of loose particles.
- The visible damage features of Specimens GZY600-1 and GZY600-4, which were subjected to different vertical loads but the same durations of fire, are similar.

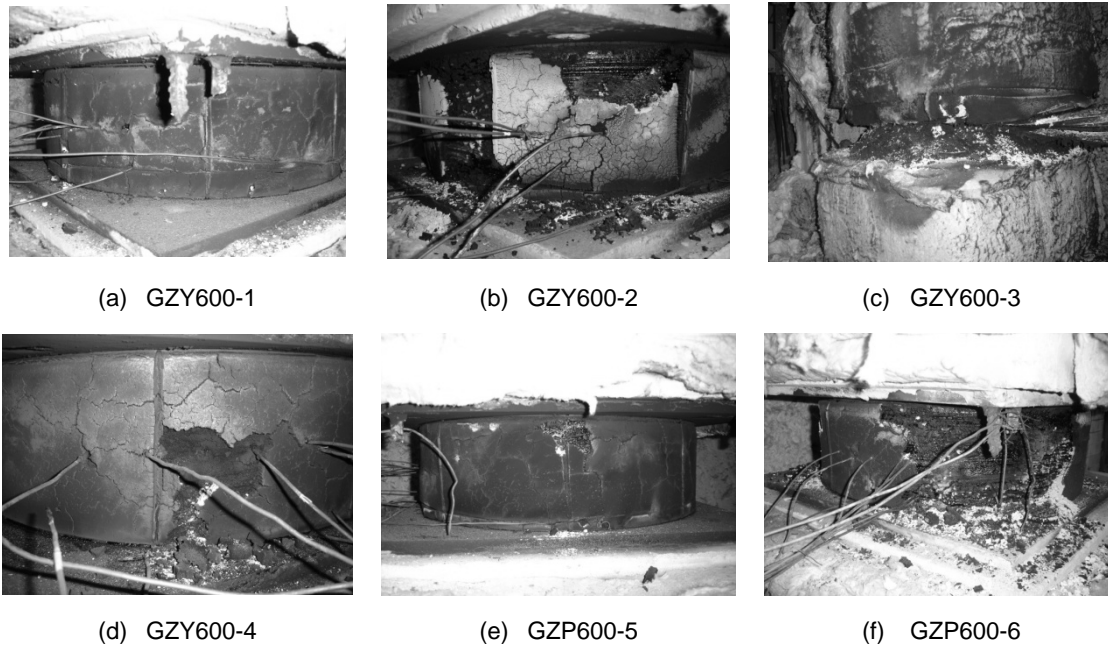


Figure 3. Failure mode of seismic rubber bearings after fire.

- After one hour of fire exposure, Specimens GZY600-2 and GZP600-6's surface rubber have been completely charred and fallen off to a fair degree. Evident decomposition of exposed brims of rubber layers was observed and brims of steel plates were rendered protruded from the rubber for approximate 5 mm.
- Specimen GZY600-3, which was supposed to endure 1.5 hours of fire exposure, collapsed 1 hour and 28 minutes after the ignition, when the vertical load applied on the top of the concrete column during the fire test failed to maintain and dropped rapidly. Fire test was terminated instantly. After the cooling process, it was observed that the integrity of the isolator had been destroyed. The rubber part of the isolator was completely incinerated, white ashes and carbonized particles spread around the isolator. Lead plug was melt. Inner steel plates slid laterally without regularity. The isolator lost the loading capacity and the upper concrete column sank into the debris of isolator.

2.4 Mechanical Properties

Mechanical properties tests of isolators are conducted in an electrohydraulic servo compressive-shear system. After over 72 hours of cooling succeeding to the fire tests, fundamental mechanical properties of Specimens GZY600-1, GZY600-2, GZY600-4, GZP600-5 and GZP600-6 were measured according to GB50011-2001 [15]. A summary of fundamental mechanical properties tests was shown in Table III. In comparison to the performance after fire, the same tests were conducted prior to the fire exposure. Table IX and Table X show the comparison of fundamental mechanical properties of LRBs and NRBs before and after fire tests, respectively. It can be seen from Tables IX and X that:

- After 0.5 hour of fire exposure, the vertical stiffness, yielding strength, and energy dissipation of the LRB were reduced by approximately 5%~10%. However, the variation of its yielding stiffness, lateral equivalent stiffness, and equivalent damping ratio were around 2%,

which is even lower than its natural performance fluctuation at room temperature. After 1 hour of fire exposure, the reduction of the LRB's vertical stiffness, yielding strength, and energy dissipation were similar to those after 0.5 hour of fire exposure. However, the yielding stiffness of isolator decreased by as high as 36% after fire. Consequently, its lateral equivalent stiffness and equivalent damping ratio decreased by 20% and increased by 20%, respectively.

- After 0.5 hour of fire exposure, the degradations of the NRB's vertical stiffness and lateral stiffness were minor. However, after 1 hour of fire exposure, the degradations of the NRB's vertical stiffness and lateral stiffness were, respectively, as high as 27% and 62%, which are significantly greater than those of the LRB after one hour of fire exposure.

- After the same duration of fire exposure, no evident discrepancy of the degradations of the fundamental properties of isolators under different vertical loads (GZY600-1 and GZY600-4) was observed. Therefore, the vertical load, to which the isolators subjected during the fire, might have little influence on the mechanical properties of the isolators after fire.

TABLE III. SUMMARY FOR FUNDAMENTAL MECHANICAL PROPERTIES TESTS.

Parameter	Vertical load (kN)	Vertical compressive stress (MPa)	Lateral displacement (mm)	Shear strain (%)	Frequency (Hz)
Compression test	2827	10	0.0	0	0.02
Shear test	2827	10	±110	±100	0.01

TABLE IV. COMPARISON OF FUNDAMENTAL MECHANICAL PROPERTIES OF LRB BEFORE AND AFTER FIRE.

Specimen Parameter	GZY600-1			GZY600-2			GZY600-4		
	Before fire	After fire	Rate of change	Before fire	After fire	Rate of change	Before fire	After fire	Rate of change
Vertical stiffness (kN/mm)	2901	2727	-6.00%	2846	2557	-10.2%	3086	2789	-9.63%
Yielding strength (kN)	86.46	81.56	-5.67%	84.35	80.88	-4.11%	84.03	81.13	-3.45%
Yielding stiffness (kN/mm)	1.127	1.148	1.86%	1.064	0.682	-35.9%	1.096	1.116	1.82%
Energy dissipation (kJ)	389.1	361.3	-7.11%	379.2	350.1	-9.23%	373.9	345.9	-7.49%
Lateral equivalent stiffness (kN/mm)	1.796	1.756	-2.23%	1.689	1.353	-19.9%	1.703	1.662	-2.41%
Damping ratio (%)	28.9	28.3	-2.08%	29.6	35.6	20.3%	28.4	28.5	0.35%

TABLE V. COMPARISON OF FUNDAMENTAL MECHANICAL PROPERTIES OF NRB BEFORE AND AFTER FIRE.

Specimen Parameter	GZP600-5			GZP600-6		
	Before fire	After fire	Rate of change	Before fire	After fire	Rate of change
Vertical stiffness (kN/mm)	2597	2578	-0.72%	2616	1903	-27.2%
Lateral stiffness (kN/mm)	1.033	1.008	-2.42%	1.079	0.408	-62.4%

3. EXPERIMENTAL STUDY ON FIRE PROTECTION

3.1 Test Specimens

This experiment involves one LRB (GZY600-8) and one NRB (GZP600-7) with the same

detailed parameters as those of LRBs and NRBs listed in Table I, respectively. The vertical load, to which isolators are subjected in engineering practice, is limited (e.g., typically under 10 MPa), and the aforementioned study indicates that vertical loads, to which rubber bearings are subjected during fire, have little influence on their residual mechanical properties after fire. Thus vertical load was not taken into account in this experimental study.

3.2 Test Set-up and Fire Resistant Protection

Similar to the first experiment, isolators were mounted between two concrete columns, which were connected to the isolators using steel flange plates. However, no axial load was exerted to the top of the upper column. In this study, thick type Fire Retardant Coating (FRC) was applied for the protection of rubber bearings in fire. 50 mm thick FRC was painted on the rubber surface of isolators. To avoid the hot bridge effect of the steel flange plates and their neighboring concrete, the same thickness of FRC was also painted on them within a vertical distance of 200 mm from the isolators. Fig.4 shows the setup of an insulated specimen. The durations of fire exposure of both specimens are 3 hours. Test records show that the actual heating processes of the two specimens met the requirement of GB/T 9978-1999 [14] and were in good agreement with the designated ISO834 standard heating process.

3.3 Failure Mode

Fig.5 shows a picture of one insulated specimen after fire. The FRC painted on the specimen spalled in the manner of being layered. This is due to the weak planes existing within the insulation arising from the way they were layered-painted. After scraping the insulation, it can be seen from Fig.6 that the isolator basically maintains its original appearance after fire, no obvious change occurred on its surface.

3.4 Mechanical Properties

After exceeding 72 hours of cooling succeeding to the fire tests, fundamental properties of Specimens GZP600-7 and GZY600-8 were measured according to GB/T20688.1-2007^[15]. In comparison to the performances after fire, the same tests were conducted prior to the fire exposure. The comparison of fundamental mechanical properties and hysteresis loops before and after the fire tests are shown in Table VI, Table VII, from which it can be seen that:



Figure 4. Insulated specimen before fire.



Figure 5. Insulated specimen after fire.



Figure 6. Seismic rubber bearings after fire.

TABLE VI. COMPARISON OF FUNDAMENTAL MECHANICAL PROPERTIES OF GZP600-7 BEFORE AND AFTER FIRE.

Parameter	Before fire	After fire	Rate of change
Vertical stiffness (kN/mm)	2112.0	2046.3	-3.11%
Lateral stiffness (kN/mm)	0.982	0.954	-2.85%

TABLE VII. COMPARISON OF FUNDAMENTAL MECHANICAL PROPERTIES OF GZY600-8 BEFORE AND AFTER FIRE.

Parameter	Before fire	After fire	Rate of change
Vertical stiffness (kN/mm)	2661.0	2542.0	-4.47%
Yielding strength (kN)	91.1	95.8	+5.16%
Yielding stiffness (kN/mm)	0.869	0.807	-7.13%
Lateral equivalent stiffness (kN/mm)	1.647	1.566	-4.91%
Energy dissipation (kJ)	368.3	366.7	-0.43%
Equivalent damping ratio	0.306	0.324	+5.88%

- The vertical stiffness and lateral stiffness of GZP600-7 have slight degradation after fire, which did not surpass 4%.
- The vertical stiffness, yielding stiffness, lateral equivalent stiffness, and energy dissipation of GZY600-8 decreased to various degrees after the fire, whereas the equivalent damping ratio increased because of the degradation of lateral equivalent stiffness. The increase of yielding strength was also observed (the reason needs further investigation). However, the range of all its mechanical properties variation did not exceed 8%.

4. CONCLUSIONS

- After approximate 1.5 hours of fire exposure, the isolator was completely destroyed, and its integrity and loading capacity was lost; after 1 hour of fire exposure, the inner rubber layers and steel plates of the isolator were damaged to a fair degree, but the integrity of the isolator was maintained; after 0.5 hour of fire exposure, there was no evident damage on exposed inner rubber layers and steel plates.
- After 0.5 hour of fire exposure, the degradations of mechanical properties of LRBs and NRBs were under 10%, and vertical loads, to which isolators were subjected in fire, have little influence on the isolators' mechanical properties after fire.
- After 1 hour of fire exposure, the degradations of LRB's vertical stiffness, yielding strength and energy dissipation, were similar to those after 0.5 hour of fire exposure, but its yielding stiffness and lateral equivalent stiffness decreased by 36% and 20%, respectively. Meanwhile its equivalent damping ration rose by 20%. After 1 hour of fire exposure, the vertical stiffness and lateral stiffness of the NRB were reduced by 27% and 62%, respectively, which are significantly greater than those of the LRB.
- Using the fire protection proposed in this study, no visible changes are observed in the appearances of the rubber bearings after 3 hours of fire exposure. Degradations of their mechanical properties do not exceed 8%.

ACKNOWLEDGEMENTS

The authors want to express their gratitude to the financial support of National Natural Science Foundation of China (No.90815027), and Key Research Project of State Key Laboratory of Subtropical Building Science of China (No.2008ZA10).

REFERENCES

1. Derham, C. J., and A. P. Plunkett. 1976. "Fire Resistance of Steel-Laminated Natural Rubber Bearings," *NR Technology*, 7(2): 29–37.
2. Liu, W. G., F. L. Zhou, F. Sun, D. Huo, and W. M. Yan. 2001. "Product Specification and Mechanical Properties of Chinese Rubber Bearings," *Transactions of the 16th International Conference on Structural Mechanics in Reactor Technology*, Washington, D.C.
3. Kato, A., M. Oba, S. Michikoshi, and T. Minami. 1999. "Study on Structural Design for Seismic Isolated FBR : Part 28. Fire Test Results of Rubber Bearings," *Summaries of technical papers of Annual Meeting Architectural Institute of Japan. B-2, Structures II, Structural dynamics nuclear power plants*, Chugoku, Japan, pp. 1215–1216. (in Japanese)
4. Miyazaki, M., F. Arima, Y. Mitsusaka, M. Ikennaga, and Y. Hosono. 1988. "Study on Fire Resistance of Steel-Laminated Rubber Bearings: (Part 1) Performance Tests of a Fire-Protected Lead Rubber Bearing," *Summaries of technical papers of Annual Meeting Architectural Institute of Japan. B, Structures I*, Kanto, Japan, pp.389–390. (in Japanese)
5. Mitsusaka Y., M. Miyazaki, and F. Arima. 1989. "Study on Fire Resistance of Steel-Laminated Rubber Bearings: (Part 2) Fire Tests of Protected and Unprotected Rubber Bearing," *Summaries of technical papers of Annual Meeting Architectural Institute of Japan. B, Structures I*, Kyushu, Japan, pp.493–494. (in Japanese)
6. Aoki, K., H. Masuda, M. Sudou, Y. Asano, I. Nishikawa, and K. Shimizu. 1991. "Fire Resistance of Laminated Rubber Bearings," *Summaries of technical papers of Annual Meeting Architectural Institute of Japan. B, Structures I*, Touhoku, Japan, pp.623–624. (in Japanese)
7. Takahashi, K., N. Hori, and A. Teramura. 1999. "Study on Fireproof Cover System of Rubber Bearing for Base Isolation," *Summaries of technical papers of Annual Meeting Architectural Institute of Japan. A-2, Fire safety, off-shore engineering and architecture, information systems technology*, Chugoku, Japan, pp.7-10. (in Japanese)
8. Tkakahashi, I., M. Sawaguchi, and K. Tanaka. 2007. "Research and development of fireproof construction methods for seismic isolators," *Summaries of technical papers of Annual Meeting Architectural Institute of Japan. A-2, Fire safety, off-shore engineering and architecture, information systems technology*, Kyushu, Japan, pp.45–48. (in Japanese).
9. Miyamoto, K., H. Satoh, and T. Ohuchi. 1990. "Fire resistance test of laminated rubber bearings", *Summaries of technical papers of Annual Meeting Architectural Institute of Japan. A, Materials and construction, fire safety, off-shore engineering and architecture, information systems technology*. Chugoku, Japan, pp.1049-1050. (in Japanese)
10. Takayama, K., T. Katoh, M. Yamanaka, A. Hazawa, and I. Nishikawa. 1997. "Practical Study on Natural Rubber Bearings with Fire Protection," *Summaries of technical papers of Annual Meeting Architectural Institute of Japan. B-2, Structures II, Structural dynamics nuclear power plants*, Kanto, Japan, pp.513–514. (in Japanese)
11. Koyama, M., O. Hasegawa, and R. Yokoyama. 1998. "Fire Resistance Test of Fire-protected Laminated Rubber Bearings," *Summaries of technical papers of Annual Meeting Architectural Institute of Japan. B-2, Structures II, Structural dynamics nuclear power plants*, Kyushu, Japan, pp.573–574. (in Japanese)
12. Onishi, Y., K. Izawa, O. Tanaka, M. Fuji, K. Kawai, and Y. Miyauchi. 1998. "Experimental study of multi-layer fire resistive covering for rubber bearing," *Summaries of technical papers of Annual Meeting Architectural Institute of Japan. B-2, Structures II, Structural dynamics nuclear power plants*, Kyushu, Japan, September, pp.575–578. (in Japanese)
13. Hori, N., K. Takahashi, K. Muraoka, K. Umeki, and A. Kato. 1997. "Study on Structural Design for Seismic Isolated FBR Plant: Part16. Combustible Evaluation of rubbers using Cone Calorimeter Method", *Summaries of technical papers of Annual Meeting Architectural Institute of Japan. B-2, Structures II, Structural dynamics nuclear power plants*, Kanto, Japan, pp.1047-1048. (in Japanese)

14. GB/T 9978-1999: Fire-resistance tests - Elements of building construction, Beijing, 1999 (in Chinese)
15. GB/T20688.1-2007: Rubber Bearings - Part 1: Seismic-Protection isolators test methods, Beijing, 2007 (in Chinese)
16. G118-2000: Rubber Isolation Bearings for Buildings, Beijing, 2000 (in Chinese)

Consideration of Transient Creep in the Eurocode Constitutive Model for Concrete in the Fire Situation

T. GERNAY and J.-M. FRANSSSEN

ABSTRACT

This paper presents a new formulation of the generic Eurocode 2 concrete model that contains an explicit term for consideration of the transient creep. The simplicity and generic characteristics of the Eurocode model are preserved and the new explicit formulation is calibrated to give the same results as the implicit formulation that is proposed in the Eurocode when the material is heated under constant load. However, the improvements allow taking into account with more accuracy the phenomenon of transient creep in concrete under more complex situations such as, for example, the cooling phase of a fire. The differences between the two formulations are highlighted for a simple structure. A comparison is given between experimental and calculated results on a centrally loaded concrete column submitted to heating-cooling sequence.

DEFINITIONS

The total strain can be divided into its components as follows:

$$\varepsilon_{tot} = \varepsilon_{th} + \varepsilon_m \quad (1a)$$

$$\varepsilon_{tot} = \varepsilon_{th} + \varepsilon_\sigma + \varepsilon_{tr} \quad (1b)$$

where ε_{tot} is the total strain, ε_{th} the thermal strain, ε_m the mechanical strain, ε_σ the instantaneous stress-related strain and ε_{tr} the transient creep strain. The instantaneous stress-related strain can in turn be divided in elastic and plastic

Thomas Gernay, Research Fellow F.R.S.-FNRS, University of Liege, Structural Engineering, Chemin des Chevreuils 1, 4000, Liege, Belgium
Jean-Marc Franssen, Professor, University of Liege, Structural Engineering, Chemin des Chevreuils 1, 4000, Liege, Belgium

strains. Basic creep, defined as the additional strain that develops when only time is changing with all other conditions such as stress and temperature being constant, could also be added as another component of the total strain, but this term is generally omitted for the structural calculation of building structures in the fire situation. Eq (1a) is used in implicit models where the transient creep is implicitly included in the mechanical strain whereas, in Eq. (1b), the transient creep is considered explicitly.

Physically, the transient creep strain is the additional strain that develops irrecoverably during first-time heating of concrete under load [1]. Even though several models have been proposed in the literature [1 and 2], the transient creep has been incorporated into the Eurocode model [3] in an implicit manner, leading to some approximations in the representation of this effect. The aim of this paper is to present a new formulation of the Eurocode 2 (EC2) model which contains an explicit term for the transient creep strain.

LIMITATIONS OF THE IMPLICIT MODEL OF THE EUROCODE

The EC2 model is commonly used for structural calculations. The advantages of this model are its simplicity and its relative reliability established by a widespread use for many years, at least under ISO fire conditions. Nevertheless, some limitations remain due to the implicit consideration of transient creep. For instance, no distinction is made in the model between heating under stress and loading at elevated temperature. Moreover, the transient creep that is implicitly considered is treated as reversible because, at a given temperature, the elastic modulus used for unloading is taken as the initial tangent to the constitutive curve in terms of $(\varepsilon_m ; \sigma)$ instead of $(\varepsilon_\sigma ; \sigma)$ [4].

The necessity to use an explicit transient creep model has been questioned [5], based on the fact that sufficiently accurate results have been obtained in numerous occasions when modeling reinforced concrete or composite steel-concrete elements with the implicit model of EC2. This opinion was yet based on simulations considering only the heating phase of the fire. However, the structural behavior during the cooling phase may not be so accurately represented by an implicit model because of its inherent limitations.

EXPLICIT TRANSIENT CREEP FORMULATION OF THE MODEL

Assumptions

1) For developing the new formulation, it was assumed that the stress-strain relationship of concrete at high temperature from EC2 implicitly includes transient creep. Accordingly, for first-time heating under constant stress, the new formulation was calibrated to yield the same mechanical strain as the EC2 model. From Eq. (1a) and (1b), this leads to:

$$\varepsilon_m^{\text{implicit}} = \varepsilon_\sigma^{\text{explicit}} + \varepsilon_{tr}^{\text{explicit}} \quad (2)$$

2) The actual elastic modulus of the material is the initial tangent of the instantaneous stress-strain relationship curve $(\varepsilon_\sigma; \sigma)$. In the ENV version of Eurocode 2 [6], the $(\varepsilon_m; \sigma)$ relationship based on the minimum value of the peak stress strain $\varepsilon_{c1,min}$ does not include transient creep strain, as shown for example by Schneider [7], see Figure 1. Therefore the elastic modulus from $(\varepsilon_m; \sigma)$ of ENV can be seen as a good estimation of the actual elastic modulus of $(\varepsilon_\sigma; \sigma)$ for an explicit formulation. It can in fact be noted that relationships for the evolution of the elastic modulus with temperature presented by Schneider et al. [2] as well as Nechnech [8] are in line with the values given by ENV.

3) Transient creep models have been developed by several authors in literature and, generally, transient creep is proportional to the applied stress [1 and 2]. Adopting the same assumption, the formulation was developed as follows:

$$\varepsilon_{tr} = \phi(T) \times \sigma \quad (3)$$

Development of the Model

Let $E_{EC2}^{implicit}(T)$ be the Young modulus of concrete considered in the EC2 implicit model, i.e. the initial tangent to the EC2 $(\varepsilon_m; \sigma)$ curve:

$$\frac{E_{EC2}^{implicit}(T)}{f_c(T)} = \frac{3}{2\varepsilon_{c1,EC2}(T)} \quad (4)$$

with $\varepsilon_{c1,EC2}$ the peak stress strain and f_c the compressive strength [3]. Similarly, $E_{ENV}(T)$ is the modulus of concrete considered in the ENV constitutive relationship with the minimum value of the peak stress strain $\varepsilon_{c1,min}$.

The transient creep is assumed to be, on one hand, a linear function of the applied stress and, on the other hand, the difference between the mechanical strain and the instantaneous stress-related strain. In the elastic part of the constitutive law,

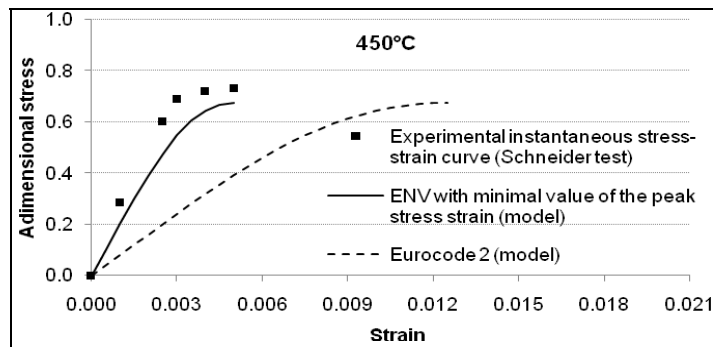


Figure 1. Comparison of EC2 and ENV models with experimental data of the instantaneous stress-strain relationship at 450°C [7].

i.e. for a stress level $\sigma^* / f_{c,T} \ll 1$, the instantaneous stress-related strain ε_σ and the elastic strain ε_{el} coincide. Therefore, considering the modulus from ENV as the actual elastic modulus of concrete, relationship (5) can be written.

$$\varepsilon_\sigma = \sigma^* / E_{ENV} \quad (5)$$

For the same stress level, the mechanical strain according to the EC2 relationship is related to the stress by the apparent modulus as expressed by Eq. (6).

$$\varepsilon_m = \sigma^* / E_{EC2}^{implicit} \quad (6)$$

Transient creep strain has been defined as the difference between mechanical and instantaneous stress-related strains. Since it has been assumed proportional to the applied stress, Eq. (7) is valid whatever the stress level.

$$\varepsilon_{tr}(T) = \left[\left(\frac{1}{E_{EC2}^{implicit} / f_c} \right) - \left(\frac{1}{E_{ENV} / f_c} \right) \right] \frac{\sigma}{f_c} = \frac{2}{3} (\varepsilon_{c1,EC2} - \varepsilon_{c1,min}) \frac{\sigma}{f_c} = \phi'(T) \frac{\sigma}{f_c} \quad (7)$$

The Young modulus is calculated taking into account the fact that transient creep is not recovered during the cooling phase:

$$\frac{E(T)}{f_c(T)} = \frac{1}{\left(\frac{2 \cdot \varepsilon_{c1,EC2}(T)}{3} - \phi'(T_{max}) \right)} \quad (8)$$

where $\phi'(T_{max})$ is given by Eq. (7) with the maximum value of temperature reached in the material during its history.

Figure 2 compares the transient creep of the model presented here with experimental data and models given in the literature [7]. In this example, the test specimen was subjected to a constant uniaxial compressive load equal to $0.33 f_c$ and immediately afterwards heated at a constant rate to a pre-specified temperature.

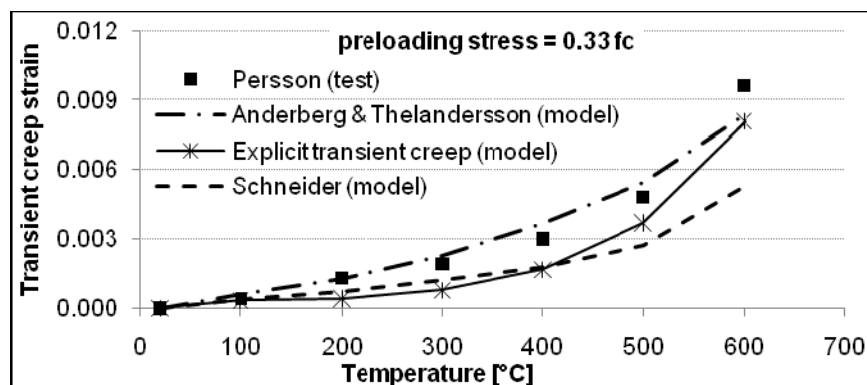


Figure 2. Comparison between different models of transient creep and experimental data.

Introduction of Transient Creep into an Existing Code

The transient creep term is calculated during the step-by-step analysis of the structure using the incremental form of equation (7). At each step, the path followed by the material in the stress-temperature space is considered in order to determine whether the transient creep term has to be incremented or not. Knowledge of the transient creep term allows deriving the instantaneous stress-related strain from the mechanical strain as follows:

$$\varepsilon_{\sigma}^{\text{explicit}} = \varepsilon_m - \varepsilon_{ir}^{\text{explicit}} = \varepsilon_{tot} - \varepsilon_{th}^{\text{explicit}} - \varepsilon_{ir}^{\text{explicit}} \quad (9)$$

In the explicit transient creep formulation (ETC) of the model, the aim is to express the constitutive relationship in terms of the instantaneous stress-related strain, in order to treat the transient creep effects separately from the elastic and plastic effects.

The constitutive relationship of the implicit model of EC2 is given by Eq. (10) (for the ascending branch).

$$\frac{\sigma}{f_c(T)} = \frac{3 \varepsilon_m^{\text{implicit}}}{\varepsilon_{c1,EC2}(T) \left(2 + \left(\varepsilon_m^{\text{implicit}} / \varepsilon_{c1,EC2}(T) \right)^3 \right)} \quad (10)$$

According to the first assumption, Eq. (2) has to be satisfied for first-time heating under constant stress. In this case, the transient creep that develops is directly given by Eq. (7) (no incremental calculation) because the stress is constant. After replacing Eq. (7) into Eq. (2), the first assumption gives Eq. (11). In this equation, $\phi'(T_{\max})$ is calculated with the maximum temperature reached in the material during its history to generalize the theory when it is not a first heating.

$$\varepsilon_m^{\text{implicit}} = \varepsilon_{\sigma}^{\text{explicit}} + \phi'(T_{\max}) (\sigma / f_c) \quad (11)$$

When replacing Eq. (11) into Eq. (10), the relationship between the stress and the instantaneous stress-related strain is obtained:

$$\frac{\sigma}{f_c(T)} = \frac{3 \left(\varepsilon_{\sigma}^{\text{explicit}} + \phi'(T_{\max}) (\sigma / f_c) \right)}{\varepsilon_{c1,EC2}(T) \left(2 + \left(\frac{\varepsilon_{\sigma}^{\text{explicit}} + \phi'(T_{\max}) (\sigma / f_c)}{\varepsilon_{c1,EC2}(T)} \right)^3 \right)} \quad (12)$$

At a given step, knowledge of the instantaneous stress-related strain can theoretically give the stress from Eq. (12). However, it is not easy to extract σ from Eq. (12). Two methods can be applied: a direct relationship $\sigma = f(\varepsilon_{\sigma}^{\text{explicit}})$ can be derived that approximates Eq. (12) or an algorithmic strategy can be implemented to solve Eq. (12). The first method should probably be preferred in order to allow an easier generalization of the ETC model in three dimensions.

It is noteworthy that the instantaneous stress-related strain, as calculated by Eq. (9), is stress-dependent because of the transient creep term. However, a possible method is to increment the transient creep term at the beginning of the time step, considering the stress at the previous converged step. This allows decoupling the calculation of the transient creep strain from the integration of the constitutive law of the material.

The Young modulus is calculated according to equation (8). The distinction between the Young modulus and the initial tangent modulus to the constitutive curve in terms of (ϵ_m, σ) allows including the transient creep as permanent strain.

RESTRAINED ELEMENT SUBMITTED TO HEATING-COOLING SEQUENCE

Law and Gillie have demonstrated the significant difference between the apparent and the actual elastic modulus of a model [4] and its implication for structural behavior. The explicit calculation of transient creep strain developed in this paper allows distinguishing between both moduli. The influence is demonstrated on the simple case presented by Law and Gillie [4] and analyzed here with the finite element software SAFIR [9]. The specimen is an axially restrained concrete cylinder (Figure 3). The temperature was raised uniformly to 500°C and then cooled down to 20°C. The implicit formulation of the Eurocode model was compared with the explicit transient creep formulation (ETC). The resulting stress during the heating and cooling regimes was plotted against the temperature (Figure 3).

During heating, thermal expansion caused compressive stresses to build up in the column due to its fixed ends. During this heating phase, the response of both models was the same, which confirms that the new model gives the same results as the EC2 model in the cases where transient creep fully develops.

Though both models followed the same path through heating, the transient creep explicitly calculated in the new model was accounted as irreversible, while the

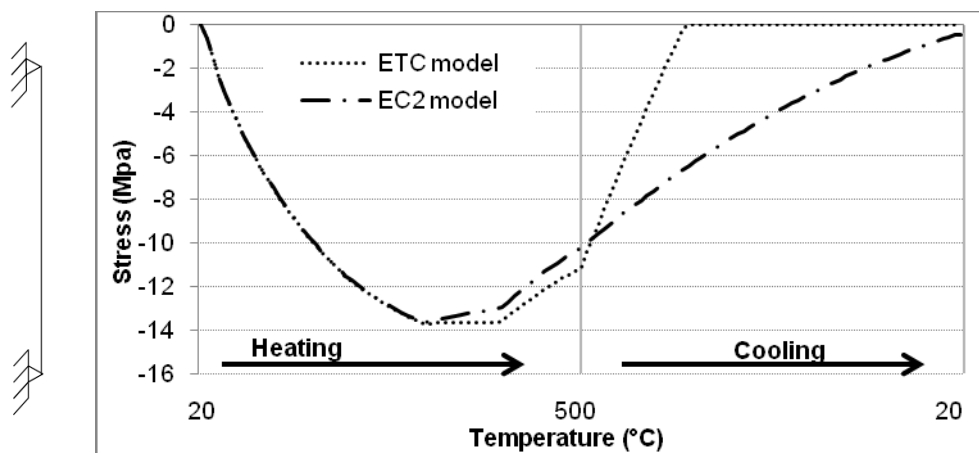


Figure 3. Stress response to heating and cooling regime.

implicit model considered transient creep as elastic. The difference is notable during the cooling phase, where the implicit formulation released the stresses slowly while, in the new model, the strains developed were unable to recover and the stress rapidly decreased. This highlights the importance of considering the irreversibility of transient creep when studying the cooling phase of a fire.

COMPARISON WITH EXPERIMENTAL DATA

In order to validate the model on a structural member, an experimental fire test made in Japan on centrally loaded concrete columns was simulated [10]. A comparison between the numerical results considering different concrete models and the experimental data was performed. The column is 300 by 300 mm² in cross section with a centre hole of 100 mm diameter. The concrete compressive strength is 55 MPa. Four 16 mm longitudinal rebars are present with a cover of 40 mm. The column, submitted to a load of 677 kN, was exposed to Japanese standard fire temperature-time curve during 180 minutes. Then, the element was allowed to cool down. The deformation behavior can be observed on Figure 4.

The ENV model with recommended value of the peak stress strain [6] leads to too large elongations, because of a highly underestimated transient creep strain. This model had been found to be by far too stiff and has been removed when transforming the Eurocode from an ENV to an EN.

The ETC model leads to results comparable with the EC2 model during approximately the first 140 minutes of heating. Beyond 140 minutes, the behavior predicted by the ETC model tends to differ from the behavior predicted by the EC2 model, i.e. the effect of the explicit consideration of transient creep on the structural behavior becomes notable. The ETC model matches better than the EC2 model the actual behavior of the structure.

The difference between the behaviors predicted by the ETC and the EC2 models is particularly significant during the cooling phase. Measured data showed a very important decrease of the elongation, due to a progressive decrease of

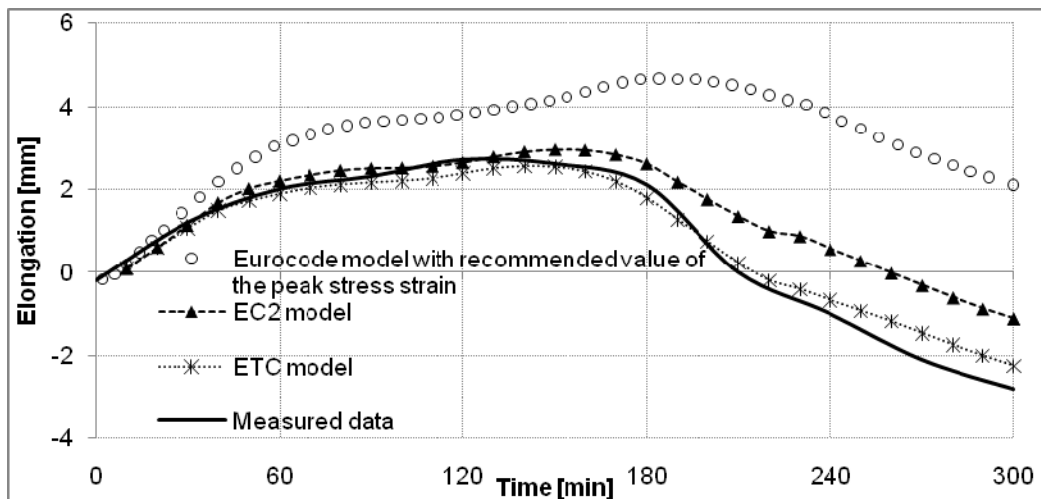


Figure 4. Comparison between numerical simulations and experimental test.

thermal strain coupled with a very limited recovery of mechanical strain. Indeed, mechanical strain is mostly composed of permanent strain. This behavior is well represented with the ETC model owing to the explicit consideration of transient creep. However, the EC2 model implicitly recovered the transient creep leading to an underestimated final shortening of the column.

CONCLUSION

The implicit consideration of transient creep in the current model of the Eurocode leads to some approximations in the representation of the transient creep strain, especially when modeling the behavior of concrete structures during the cooling phase of a fire. The new formulation of the generic Eurocode 2 concrete model that contains an explicit term for consideration of the transient creep (ETC) brings a supplementary accuracy without removing the generic characteristic of the EC2 model. The model implementation in finite-element software can be performed by an adaptation of the current EC2 model. The improvement is significant as it has been showed by modeling an experimental test. The ETC model is particularly useful when modeling the cooling phase of the fire because the irreversibility of transient creep is considered.

REFERENCES

1. Anderberg, Y. 1976. "Fire-exposed hyperstatic concrete structures – an experimental and theoretical study", University of Lund, Sweden.
2. Schneider, U.; Schneider, M.; Franssen, J.-M. 2008. "Consideration of nonlinear creep strain of siliceous concrete on calculation of mechanical strain under transient temperatures as a function of load history". Proceedings of the Fifth International Conference—Structures in Fire SIF 08 Singapore, pp. 463–476.
3. Eurocode 2. 2004. "Design of concrete structures—Part 1–2: General rules—Structural fire design".
4. Law, A. and M. Gillie. 2008. "Load induced thermal strain: implications for structural behavior". Proceedings of the Fifth International Conference—Structures in Fire SIF 2008 Singapore, pp. 488–496.
5. Franssen, J.-M. 2005. "Plastic analysis of concrete structures subjected to fire". Proceedings of the Workshop "Fire Design of Concrete Structures: What now? What next?", pp. 133–145.
6. Eurocode 2. 1995. "Design of concrete structures—Part 1–2: General rules—Structural fire design", European Prestandard.
7. Youssef, M.A., M. Moftah. 2007. "General stress-strain relationship for concrete at elevated temperatures", *Engineering structures*, 29, pp. 2618–2634.
8. Nechnech, W. 2000. "Contribution à l'étude numérique du comportement du béton et des structures en béton armé soumises à des sollicitations thermiques et mécaniques couplées : Une approche thermo-élasto-plastique endommageable", Thèse, INSA Lyon.
9. Franssen, J.-M. 2005. "SAFIR. A thermal/Structural Program for Modeling Structures under Fire", *Engineering Journal, A.I.S.C.*, Vol 42, No. 3, pp. 143–158.
10. Schneider, U.; Morita, T.; Franssen, J.-M. 1994. "A concrete model considering the load history applied to centrally loaded columns under fire attack". Fourth International Symposium on Fire Safety Science, Ottawa, pp. 1101–1112.

Deformation of Concrete Due to Mechanical and Fire Loads

E. JENSEN, J. VAN HORN and M. JOSHI

ABSTRACT

The deformation of axially loaded concrete prisms subjected to fire is the focus of this paper. An experimental investigation was conducted to determine the total deformation during axial loading, heating and subsequent cooling. The deformations considered are the total free expansion as well as the total deformation, comprised of thermal and transient strain, of loaded concrete. The testing variables are 1) strength ratio defined by the applied axial stress and the cold compressive strength of the concrete; and 2) maximum core temperature when cooling is induced. The strength ratios are 0, 17, 33 and 50% and the maximum core temperatures are 200, 400, 600 and 800 °C. The experiments were performed in a large scale fire/load test chamber. Overall, the measured axial elongation follows similar trends as reported in the literature. This is a significant observation as the data reported in the literature was obtained using different specimen types and sizes and performed in electrical furnaces.

1 INTRODUCTION*

Many countries are moving towards performance based design as it allows engineers to quantify the behavior of a structural system exposed to the entire fire, and not only at the point of failure. While the performance based design method provides detailed information about the structural performance during the fire, it also requires adequate and accurate material models, analysis tools and detailed information about the model input parameters. Such predictions are warranted for large framing or critical structures where members are highly stressed during the fire, and building codes require high fire resistance ratings.

Dr. Elin Jensen, Jacob Van Horn, and Meenakshi Joshi, Lawrence Tech University, 21000 W Ten Mile Rd, Southfield, MI 48075, U.S.A.

Like other materials the mechanical and physical properties of concrete change with increasing temperature. The total deformation or strain of concrete is considered the sum of four components; which are, thermal strain, stress related strain, creep strain and transient strain. The thermal strain, ϵ_{th} , causes thermal expansion and is a function of the temperature (T). The stress related strain, ϵ_{σ} , is a function of stress (σ) and the temperature (T). Transient strain, ϵ_{tr} , is a function of both stress (σ) and temperature (T) and is only observed in the first heating cycle. The creep strain, ϵ_{cr} , is a function of the time (t), stress (σ) and temperature (T). Creep strain is typically insignificant in concrete below 600 °C and due to computational difficulties it is often ignored in the constitutive models [1]. The total strain is:

$$\epsilon = \epsilon_{th}(T) + \epsilon_{\sigma}(\sigma, T) + \epsilon_{cr}(\sigma, T, t) + \epsilon_{tr}(\sigma, T) \quad (1)$$

Work reported by researchers such as Schneider [2, 3], Anderberg and Thelandersson [4] and Khoury [5] provide a fundamental understanding of the mechanisms associated with concrete deformation at high temperatures. As an example the data reported by Schneider was obtained on concrete cylinders with a diameter of 8 cm, length of 30 cm, and the concrete had a water-to-cement (w/c) ratio of 0.54.

The objective of this study is to determine if the thermal strains and the total strains due to combined heating and loading, in general, are significantly influenced by specimen size, concrete proportioning and source of heat. The results obtained in this study are compared with existing data or models denoted as:

Schneider's Model [2, 3].

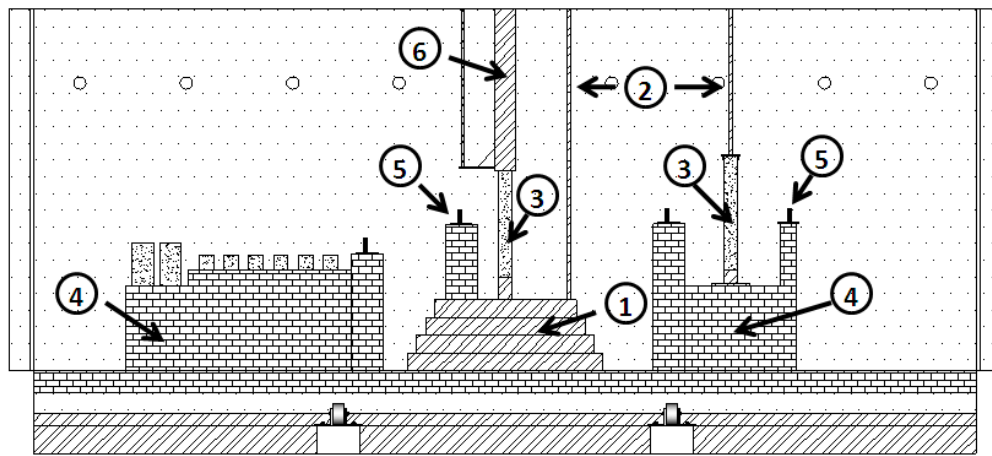
Anderberg & Thelandersson's Model [4].

Li & Purkiss Model [5, 6, 7].

The strain versus temperature curves for these models were obtained either by using the proposed equations by the researchers (for Li & Purkiss [5, 6, 7] and Schneider [2]), or were interpreted from their data (for Anderberg's [4] & Schneider's model [3]).

2 METHODOLOGY AND EXPERIMENTAL SET-UP

The experimental tests were carried out to evaluate the total deformation of concrete prisms' subjected to fire and axial compressive loads. The project specific experimental test-setup was developed at Lawrence Tech. Extensive resources were allocated to the development of the test method including determination of the adequate combination of chamber heating rate, net concrete heating rate, and concrete moisture conditions. A profile view of the test set-up is shown in Figure 1. The specimen on the right is equipped with thermocouples measuring the thermal gradient of the specimen. It is only subjected to thermal loading and therefore the free thermal expansion of the concrete is obtained from this specimen. The specimen on the left is subjected to compressive axial load and thermal load simultaneously. The deformation characteristics are obtained from measuring the displacement of the actuator, ram, and base.



1. Base 2.Ceramic Tubes 3.Concrete Specimen 4.Fire Brick Support Stands 5.Plate Thermocouple 6.Ram

Figure 1. Front view of fire chamber set-up for axial elongation test.

Ceramic tubes, with close to zero coefficient of thermal expansion, extend from the reference surface. The ceramic tubes are connected to a displacement sensor test bracket installed on the external roof beams. The axial load was applied before heating was initiated. The axial load was held constant throughout the test. The environmental fire temperature was measured using plate thermocouples.

The following axial deformation characteristics were obtained: thermal strains (free expansion) and total strain (thermal + strain due to sustained load). Tests were performed with different axial load levels of 0, 90, 180 and 270 kN. These load levels corresponds to about 0, 15, 30 and 50 % of the concrete 'cold' compressive strength. The specimens were heated to a maximum core temperature before cooling. The maximum temperatures were 200, 400, 600, and 800 °C. The heating rate was 1.5 °C/min for the first three test series, and it was 2.0 °C/min for the 800 °C test series. The internal relative humidity was 84% or below before testing to avoid extreme spalling. The 50 MPa concrete mix contained limestone (calcareous) aggregates, cement content of 312 kg/m³ and had a water/cement ratio of 0.41. The concrete prism was 10.2 cm by 10.2 cm and 91.4 cm long.

TABLE I. TESTING MATRIX FOR SPECIMENS SUBJECTED TO FIRE AND LOAD.

Temperature °C	Axial Load			
	0 kN	90 kN	180 kN	270 kN
Strength ratio α	0	0.167	0.33	0.5
200C	X	X	X	X
400C	X	X	X	X
600C	X	X	X	
800C	X	X		

(*X denotes completed testing)

The test matrix, shown in Table 1, outlines the successful experiments to date. Each of the loaded specimens was tested with an accompanying unloaded specimen to capture the free expansion and the concrete temperatures.

3 RESULTS AND DISCUSSION

As the core temperature increases the specimen will undergo a length change which causes each component of the system to deform. Representative examples of the measured deformations and associated temperatures are presented below. At the end of this section, the development of total axial strains with temperature for different load levels are presented and compared with existing models.

3.1 Temperature vs. Time

An example of the development of environmental, as well as surface and core temperature with time, is shown in Figure 2. The example represents a specimen heated to 600° C at the rate of 1.5° C/min and subjected to a load of 180 kN.

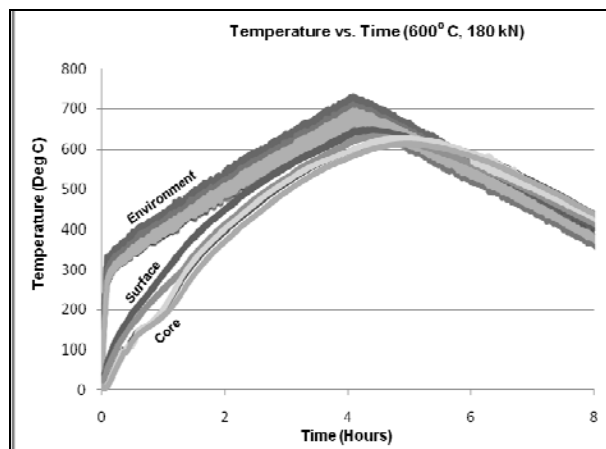


Figure 2. Temperature vs. Time.

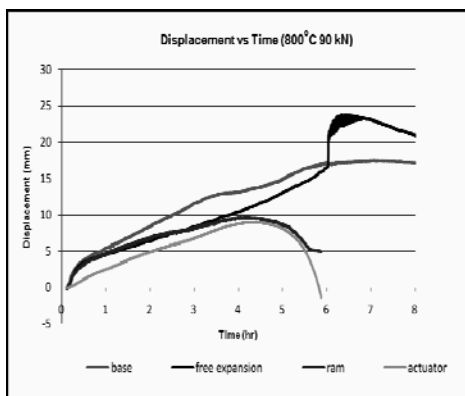


Figure 3. Displacement vs. Time.

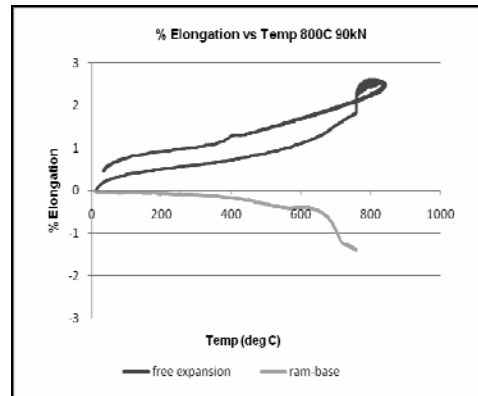


Figure 4. % Elongation vs. Temperature.

3.2 Deformation vs. Temperature

Displacements were recorded at base, ram and actuator levels as well as the top surface of the unloaded specimens. An example of the measured deformation with time is shown in Figure 3 for the specimen heated to 800° C and subjected to an axial compressive load of 90 kN. The percent axial strain for the specimen, restrained with applied axial load, is calculated from the displacements recorded at the base and ram level. These restrained and free expansion strains are then represented as a function of the concrete core temperature (Figure 4).

3.3 Comparison of Experimental Results with Existing Models

The data shows expected trends of total strains due to combined heating and loading. All of the data for different stress-to-strength ratios (α) for all temperature ranges are combined to obtain a single representative trend of axial strains versus temperature for heating. Following are the fourth order polynomial expressions for total percentage strain versus temperature for the different α values considered in this study. The results are shown in Figure 5:

$$\alpha=0: \quad \varepsilon_t = 7.6 \cdot 10^{-12} T^4 - 5.06 \cdot 10^{-9} T^3 - 4.3 \cdot 10^{-7} T^2 + 0.00241 T \quad (2)$$

$$\alpha=0.167: \quad \varepsilon_t = -4 \cdot 10^{-11} T^4 + 4 \cdot 10^{-8} T^3 - 1 \cdot 10^{-5} T^2 + 0.0011 T \quad (3)$$

$$\alpha=0.33: \quad \varepsilon_t = -5 \cdot 10^{-11} T^4 + 3 \cdot 10^{-8} T^3 - 4 \cdot 10^{-6} T^2 - 0.0004 T \quad (4)$$

$$\alpha=0.50: \quad \varepsilon_t = 1 \cdot 10^{-11} T^4 - 7 \cdot 10^{-8} T^3 + 1 \cdot 10^{-5} T^2 - 0.0011 T \quad (5)$$

It is observed that for free thermal expansion the strains were tensile up to failure. As the strength ratio increases, the strains start shifting towards compressive, from tensile. Larger compressive strains are observed for larger stress ratios.

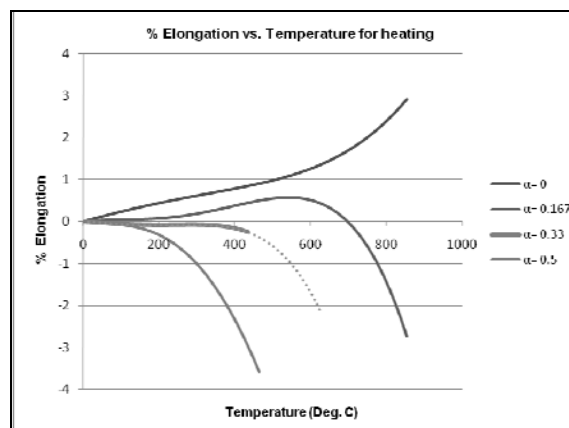


Figure 5. Percentage Strain versus Temperature: Experimental. (For $\alpha = 0.33$, the specimen failed at about 450 deg C, Dotted portion of the curve shows the extrapolated data points).

3.3.1 Comparison with Anderberg's Model

The strain-temperature relationships obtained in this experimental study are compared with those proposed by Anderberg's model (see Figure 6). The free thermal strains from normal conditions to 800 °C were an order of magnitude higher for Anderberg's siliceous concrete model as compared to the data from this study for calcareous concrete. While it is expected that concrete containing siliceous aggregate exhibits larger thermal expansion than concrete containing calcareous aggregate, such a large difference was not expected. For the different values, there is an improved agreement between the results.

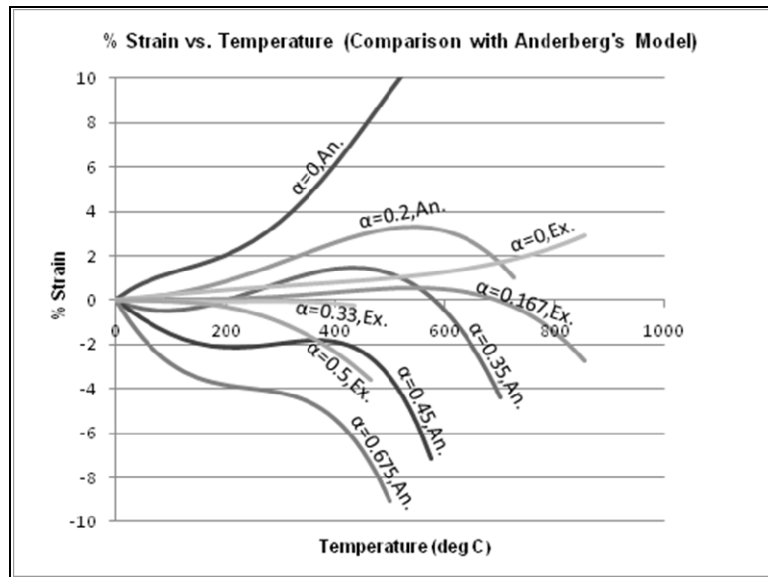


Figure. 6. Percentage Strain versus Temperature :Comparison with Anderberg's Model[4].

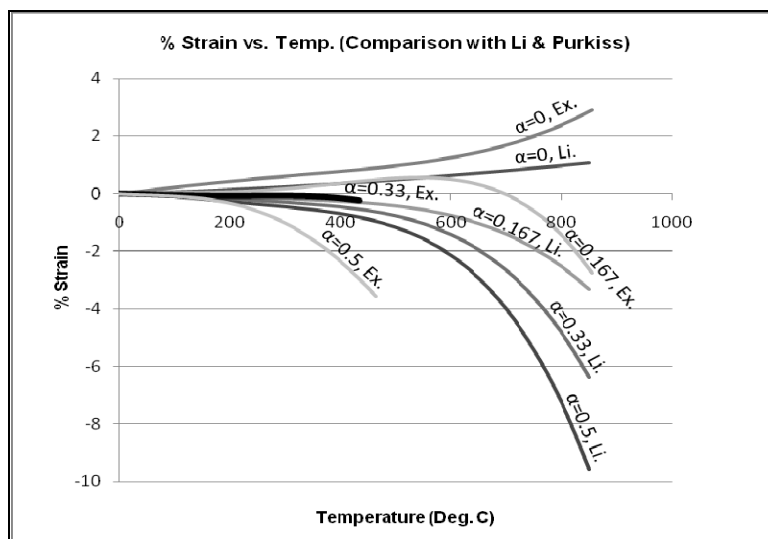


Figure. 7. Percentage Strain versus Temperature :Comparison with Li & Purkiss.

3.3.2 Comparison with Li & Purkiss's Model

The strain-temperature relationship for calcereous concrete denoted here as the Li & Purkiss model is extracted from other work [5,6,7]. There is close agreement between the results from the Li & Purkiss model and the experimental results from this study (Figure 7). In general, the Li and Purkiss model predicts a lower expansion and contraction irrespective of load level. For the mid range stress-to-strength ratios ($\alpha=0.167$ & 0.33) there is the best agreement between the models. It is also noted that the strains predicted by the Li & Purkiss model for $\alpha > 0$ are in contraction only, while this study showed expansion for $\alpha = 0.167$, before going into contraction and failure.

3.3.3 Comparison of Free Expansion Data with Schneider's and Anderberg's Model

The free expansion versus temperature is shown in Figure 8 for the data from this study, and those predicted with the existing models. The free expansion obtained from this study follows similar trends as predicted by Schneider's model for calcereous concrete [3] and siliceous concrete [4] with little deviation. The strains obtained from the Anderberg model are not comparable with the data obtained in this study. This could in part be due to differences in concrete proportioning, specimen size, different heating rates, different fire chambers (electrical vs. gas powered), etc. The reasons for the differences are not currently quantified.

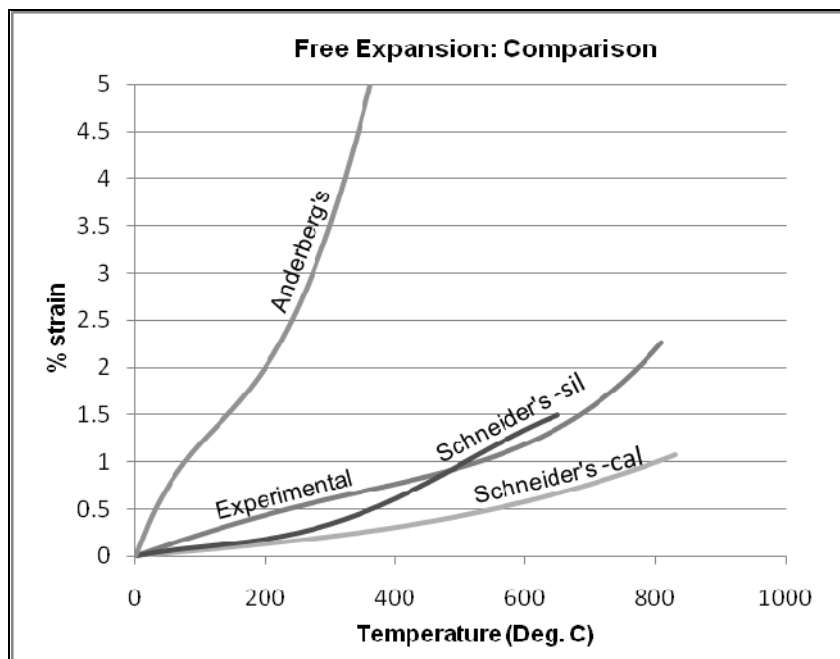


Figure 8. Percentage Strain vs. Temperature for Free Expansion: Comparison with Anderberg's & Schneider's Model.

SUMMARY

New data on free thermal expansion and total deformation during combined heating and loading was successfully obtained on concrete prisms (10.2cm x 10.2cm x 91.4cm). The tests were performed in a large scale structural fire chamber and the heating source was natural gas. The following observations were made:

The free expansion of concrete as obtained in this study shows close agreement with Schneider's model for concrete containing quartzite (siliceous) aggregates [3] and Schneider's model for concrete containing calcareous aggregates [2].

The deformation results for the specimens subjected to both thermal and mechanical loading, are similar to the deformations predicted using the Li & Purkiss model. Similarities are also found between the experimental data from this study and those predicted by the Anderberg & Thelandersson's model [4]. While not included in this paper, the data from this study shows higher contraction under loading than that of the study reported by Schneider [3]. This indicates that there could be an effect of specimen length. Additional testing is underway to further evaluate this phenomenon.

For low stress-to-strength ratios (), the thermal strains govern the behavior, hence specimens undergo an initial thermal expansion. For higher values the concrete undergoes contraction immediately as a result of heating. In general, at low temperatures the thermal strains govern the concrete deformation behavior, and with increasing temperature the effect of the sustained load dominates the concrete deformation behavior.

REFERENCES

1. Buchanan, Andrew H. *Structural Design for Fire Safety*. 2006. John Wiley and Sons. ISBN 0-471-89060-X, 2006.
2. Schneider, U. (1986a) "Properties of Materials at High Temperatures—Concrete" (Second Edition), RILEM Report, Gesamthochschule Kassel, Germany. (Referenced by Purkiss J.A.).
3. Schneider, U. (1988) "Concrete at High Temperatures – A General Review", *Fire Safety Journal*, 13, pp. 55–68.
4. Anderberg, Y. and Thelandersson, S. (1976) "Stress and Deformation Characteristics of Concrete", 2—Experimental Investigation and Material Behaviour Model, Bulletin 54, University of Lund, Sweden. (Referenced by Purkiss J.A., 2007).
5. Khoury, G.A., "Strain Components of Nuclear-Reactor-Type Concretes during First Heat Cycle" *Nuclear Engineering Design* 1995; 156(1/2) pp. 313–332.
6. Li, L.Y. and Purkiss, J.A. (2005) "Stress-strain constitutive equations of concrete material at elevated temperatures" *Fire Safety Journal*, 40, pp. 669–686.
7. Terro MJ. "Numerical modeling of thermal and structural responses of reinforced concrete structures in fire". PhD thesis, Department of Civil Engineering, Imperial College, 1991. (referenced by Li and Purkiss, 2005)
8. Purkiss, J.A. 2007. *Fire Safety Engineering*, Elsevier, ISBN-13: 978-0-7506-6443-1

Acknowledgement

This work was made possible with funding from NSF Award #0747775, and support from the Center for Innovative Materials Research (CIMR) at Lawrence Tech. The authors wish to thank the undergraduate student research team including Cody Telgheder, Andrew Hermiz, Daniel Ziemba, and Dustin Franklin.

Physical Properties and Behaviour of High-Performance Concrete at High Temperatures

U. SCHNEIDER, M. C. ALONSO, P. PIMIANTA and R. JANSSON

ABSTRACT

The following report gives an overview of the TC program and some preliminary results.

1. INTRODUCTION

The Technical Committee TC 227 HPB was established by the RILEM Council in 2007. The first committee meeting took place in Coimbra, Portugal in November 2007. The program of the new TC was prepared by members of the former TC 200 HTC “Mechanical Concrete Properties—Modelling and Applications”.

The objectives of the new TC comprise the characteristic behaviour, physical properties and modelling of different types of high performance concrete (HPC) at temperatures of up to 1000°C including the effects of the exposure of concrete structures to fire. The behaviour of five types of HPC is under the main focus of the TC (see fig. 1). Among these are high strength concrete (HSC), ultra high performance concrete (UHPC), self compacting concrete (SCC), special temperature resistant concrete (STRC) and special aggregate concrete (SAC), please see fig. 1. The topic of high strength concrete is of major interest for the TC.

The TC HPB started its work program with 18 members and now has 28 members. The increase in membership shows the great international interest in the field of HPB research and application.

U. Schneider, Vienna University of Technology, Karlsplatz 13, 1040 Vienna, Austria

M. C. Alonso, IETcc, Serrano Galvanche 4, 28033 Madrid, Spain

P. Pimienta, CSTB, Departement Securite, Structures et Feu, 84, avenue Jean Jaures, F-77447 Marne la Vallee, Cedex 02, France

R. Jansson, SP Technical Research Institute of Sweden, Fire Technology—Fire Resistance, Brinellgatan 4, Box 857, SE-501 15 Boras, Sweden

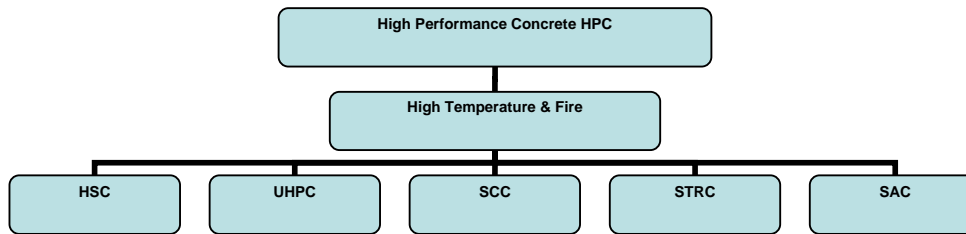


Figure 1. Concretes investigated within the work program of the proposed TC.

2. PROGRAM AND WORK GROUPS

The work program of the TC is divided into the following tasks:

Task 1: State of Art Report on HPC Properties

Task 2: Technical Report on Spalling of HPC

Task 3: Technical Report on Pore Pressure Measurements

Task 4: State of Art Report on Modelling

Task 5: Experimental Methods and Data

Sub-Task 5.1: Fracture Energy Methods

Sub-Task 5.2: Thermal Property Methods

Sub-Task 5.3: Permeability Methods and Properties

Sub-Task 5.4: Temperature Measurements

Sub-Task 5.5: Weight Loss Measurements

For the different task programs individual Work Groups (WG) have been set up. Now there are six work groups which work in the areas 1 to 4, 5.1 and 5.3.

3. STAR ON PROPERTIES AND BEHAVIOR OF HIGH-PERFORMANCE CONCRETE

3.1 Introduction

3.2 Degradation reactions in HPB at high temperatures in relation with conventional concrete

When portland cement concrete is subjected to heat, a number of transformations and reactions of different kinds occurs even at a moderate rise in temperatures. These phenomena comprise the so-called degradation reactions, which bring about a progressive breakdown in the micro structure of the concrete. They occur particularly in the hardened cement paste, but may also occur in the aggregate. The thermal analyses clearly reveal the reactions in cement paste, caused by temperature effects like a) water expulsion at about 100°C; b) breakdown of CSH gel (first stage of dehydration) at 180°C; c) decomposition of portlandite at 500°C; d) transformation of quartz at 570°C; e) decarbonation of limestone from 800°C onwards; f) start of melting from 1150°C–1200°C onwards, as figure 2 left shows.

The structure of CSH gel initiates alterations at temperatures above 100°C, as shown in figure 2 right. The initial CSH structure is considered to be formed by chains of silica-tetrahydrate, indicated by peak of (Q¹) in figure, associated to tetrahydrate at the extreme of the chain and by (Q²) tetrahydrate in the middle of the chain. The binding water is located in between the CSH chains. This water is progressively lost during heating as water vapor, that constitutes the well

identified dehydration processes of CSH cement paste, by thermal analysis as indicated in figure 1 (left), and further to the built up of pore pressures.

However the chain structure of the CSH also suffers transformation due to heating, which can be identified with ^{29}Si MAS-NMR, as shows figure 2 (right). After temperatures above 200°C the (Q^1/Q^2) ratio increases indicating that silicon chains initiate breaking and at 400°C the CSH structure has been completely destroyed. Simultaneously to these transformations in CSH, a new nesosilicate phase of monomers of silicon tetrahedrate is formed (Q^0) having a similar but less crystalline structure than the anhydrous cement grains of larnite. The CSH degradation with temperature contributes to mechanical strength losses.

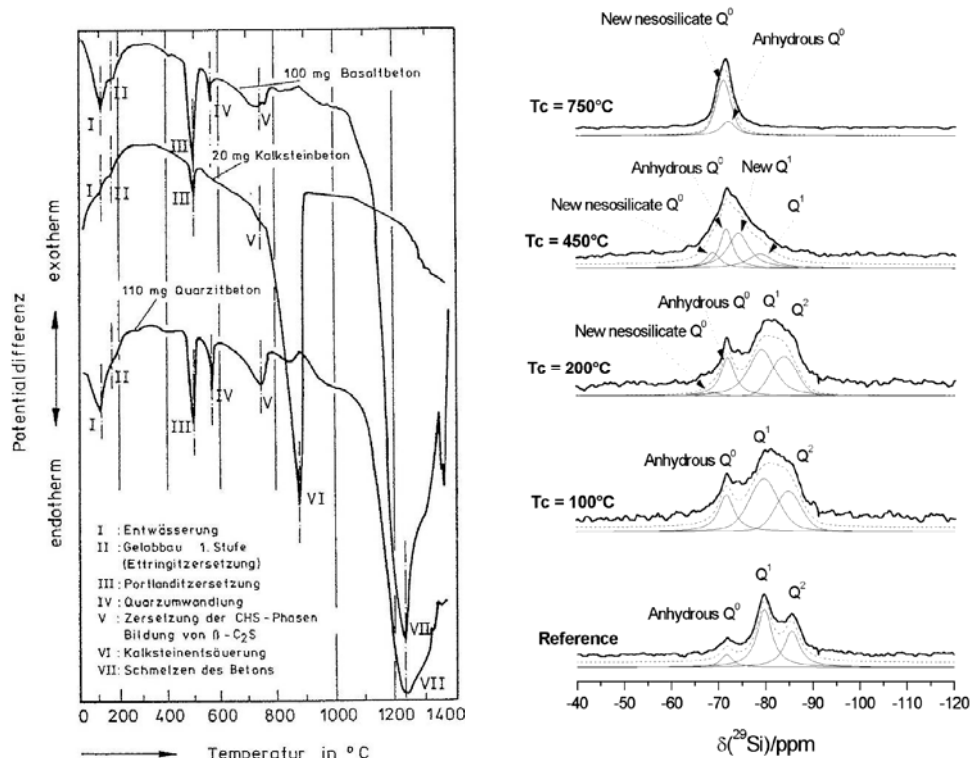


Figure 2. Left- Differential thermal analysis of various normal weight concretes, Right- CSH transformations with temperature as shown with ^{29}Si MAS-NMR spectra (C. Alonso).

In the case of High Performance Concretes (HPC) or Self Compacting Concrete (SCC), the thermograms follow a similar evolution with temperature, as figure 3 shows. The changes in portlandite $\text{Ca}(\text{OH})_2$ also takes place at similar temperatures. Although the thermal transformation of this component occurs abruptly but not a progressive dehydration as follows the CSH transformations with increasing temperature. The high contents of mineral additions, many times employed in the production of HPC, diminishes or even eliminates completely the region of transformation of portlandite at 450°C due to its lower content, that certainly changes the processes occurring at high temperature in the cement paste.

Other differences are in the type of aggregate used, usually of smaller size, figure 2 (left). If gabbro and quartzite are used, do no suffer mass loss but the use of lime as aggregate decomposition occurs above 750°C, however the clear difference in the amount of mass loss is detected in SCC due to lime transformation coming from not only the aggregate but also from the calcareous

filler, typically employed for production of SCC, figure 2 (right). At 1200°C all the concrete components have dehydrated completely and melting initiates, similarly to conventional concrete. In fact in conventional concrete, the liquefaction of the concrete commences with the melting of the matrix of hardened cement paste that begins to melt at about 1200° C and that melting of the aggregates takes place only after this.

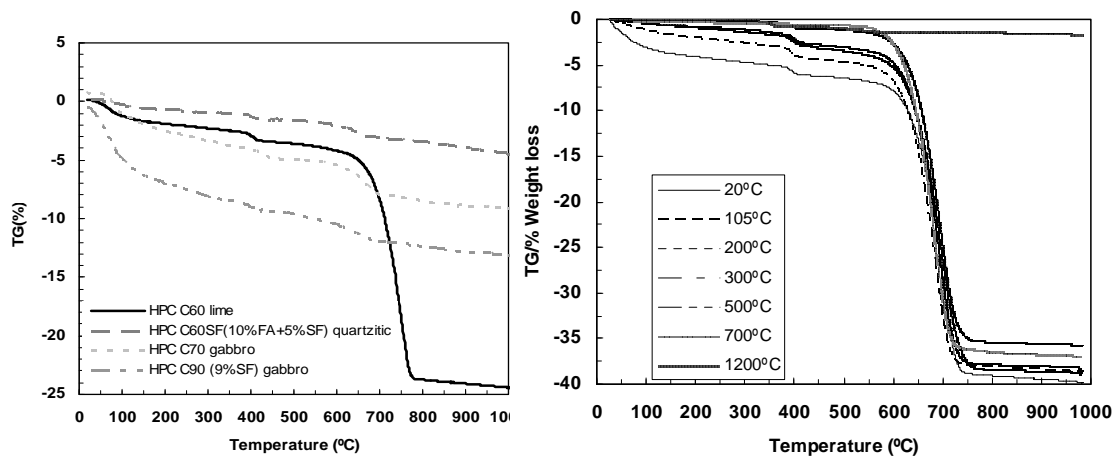


Figure 3. Differential thermal analysis of various concretes. Left: TG for HPC and Right: TG for SCC (C. Alonso, L. Fernandez)

3.3 Mechanical properties of concrete at high temperatures

In this field a PhD thesis has been submitted by S. Huismann (G) at the Vienna University of Technology. Parts of the thesis are presented in this conference.

4. REPORT ON SPALLING OF HPC

4.1 Introduction

The Work Group 2 for Spalling has made great progress in the past two years and an international workshop was organized by TC members F. Dehn and E. Koenders in Germany in 2009. In total, the workshop has written 51 reports on 548 pages. The following provides a short introduction into spalling of HCP under ISO fire conditions and in microwave tests.

4.2 Test method and results for spalling

The spalling of concrete during heating up is well known since several decades. Generally it is assumed that spalling is caused by the thermo-hydraulic effects due to vaporization of capillary and gel water, by the chemical phase changes during heating and by the thermo-physical effects due to thermal stresses. Those effects may occur in the hardened cement paste (HCP) and as well in aggregates used in concrete. From fire tests it is known that the spalling of concrete is mainly caused by vapor pressure in capillary and gel pores being filled with residual parts of mixing water after the hydration. Up to now the connection between pore pressure and spalling of concrete is not clear. It is neither known how the chemical water in concrete influences the spalling effect. From HPC and UHPC it is known that those types of concrete may explode

heavily under fire attack, respectively, even if they do not contain nearly any capillary water and are generally produced at very low water/cement ratios.

In the following a few preliminary results concerning investigations with respects to principal parameters influencing spalling of concretes are given. The reference concrete is an ordinary concrete (B40), which has been used for the construction of a tunnel in France. B60 concrete has been fabricated by only varying the W/C ratio (by increasing cement content and reducing water content) and by fixing the aggregates quantity constant. Exactly the same material has been used to fabricate the 2 concretes. The compressive strength of B60 is higher than 60 MPa. This concrete is considered an HPC.

Figure 4 presents pictures taken on several slabs after ISO fire tests and moderate heating rate. After the tests the volume of spalled concrete layers was determined by mapping. Thanks to these mappings, maximal depth and volume of concrete that had been ejected during heating were assessed.

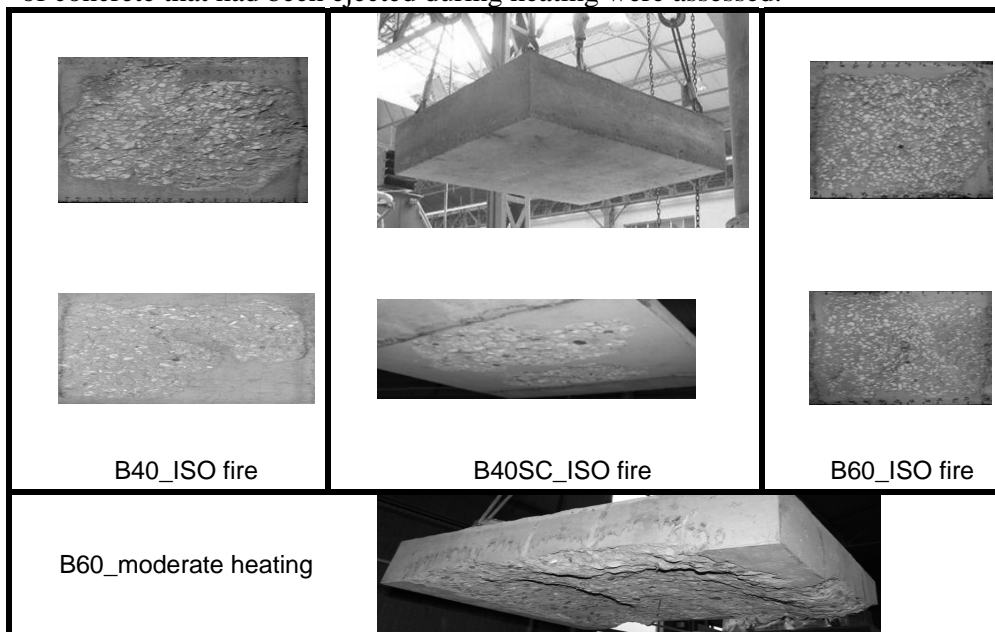


Figure 4.1. Views of the exposed surface of slabs after one hour of ISO fire (spalling between the 10th and the 20th minute of the test accord. to Pimienta).

From the mapping results, the following observations were obtained:

The dense concrete (HPC) ejected more concrete and larger damage (i.e. deeper and greater damaged zone),

Only one of the B40SC slabs showed little surface spalling. The spalling induced damage for this slab is weak like similar concretes which are fabricated only with calcareous aggregates.

The result underlines the important influence of aggregate type on the risk level of concrete thermal instability and its characteristics,

During moderate heating (i.e. for very slower heating than ISO fire) on B40 slabs, no spalling was observed whereas spalling of B60 has been observed in that case. Under ISO fire conditions the B60 lost a 6 cm thick concrete layer by spalling.

From these measurements it appears that no clear link exists between the built-up of vapour pressure and concrete spalling potential. This result is not in accordance with classical interpretations that state that concrete spalling is dependent on the vapour pressure level. We also note that this pressure level is

very low compared to concrete tensile strength. Some special test configurations (slow heating on cylindrical sample and moderate heating on slabs) led to high vapour pressures but without any concrete spalling. Based on these results it is assumed that vapour pressure is not the only physical origin for concrete spalling.

Contrary to these results microwave experiments show that spalling is mainly caused by the input of thermal energy, i.e. local increase of pressure in the pore system of the specimen so that the explosive spalling is a common appearance regardless of the type of cement, w/c-ratio, curing and test age etc. The reason of the local spalling is a result of structural defects of the specimen which appear in the specimen during the compacting and hydration (build-up of nano (gel) pores), but it cannot be excluded that local shrinkage cracks or differences in strength occur (see fig. 4.2 and 4.3 according to Schneider).

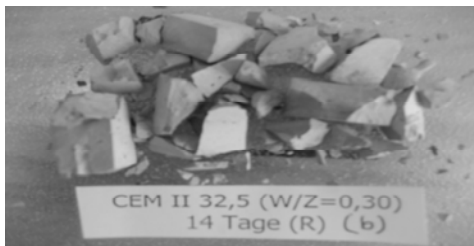


Figure 4.2. Explosive Spalling of HPC-Paste.

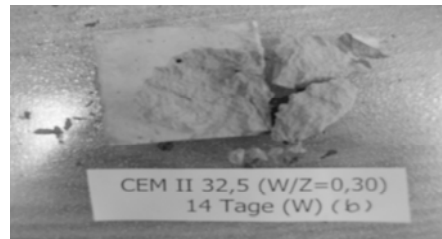


Figure 4.3. Local Spalling of HPC-Paste.

The spalling of specimen occurred mainly after 2-3 minutes of MW-heating. The observed temperatures of spalling range from 100 °C to 250 °C. The larger specimen and specimen with higher strength or longer curing time needed more energy until spalling. The mass specific energy absorption was determined ranging from 300 J/g to 600 J/g for all specimen of the 86 series tested.

5. WG 3 PORE PRESSURE MEASUREMENT

Measurement of the pore pressure in concrete can be done with either embedded or external measurement gauges. Embedded gauges means that the measurement is performed in the high temperature zone. With external gauges the pressure is transferred from the measurement point to a gauge outside the specimen by a pipe from inside the specimen. When measuring the pressure development in concrete the corresponding temperature is important. In some systems the temperature is measured in the pressure measurement devices and in some experimental setups the temperature is measured externally. The most common different pressure measurement setups shown in figure 5.1 include:

- A. Embedded pipe, which transforms the pressure to an external pressure gauge. In this and other similar applications (B-D) the pipe exits the specimen away from the heat source (Jansson).
- B. Embedded pipe with internal rod, which transforms the pressure to an external pressure gauge. The internal rod is used to reduce the volume in the pipe. A cavity is created around the measurement point (Schneider).
- C. Embedded pipe with clamped sintered material in contact with the concrete, which transforms the pressure to an external pressure gauge. A thermocouple is included in this method to monitor temperature. The thermocouple can be introduced either as a volume reducer in the pipe (Kalifa) as shown in Figure 1, or externally to the pipe (Phari).

- D. Embedded pressure gauge (Consolazio).
- E. Embedded pipe, which transforms the pressure to an external pressure gauge. In this application the pipe parallel to the heated surface.

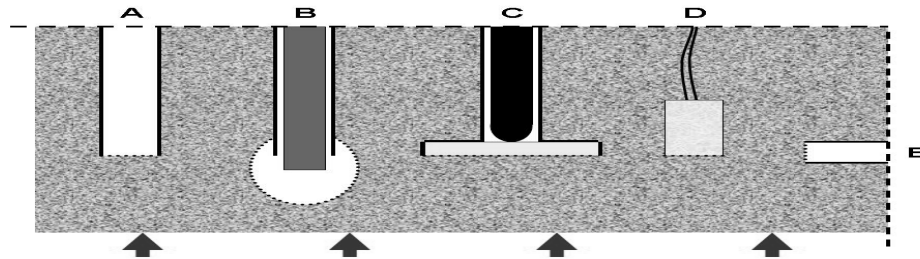


Figure 5.1. Different pressure measurement setups according to Jansson. Heating heated from below.

In measurement setup types A, B, C, D and E the pressure is transformed to the outside of the concrete using a medium in the pipe. In different applications of these methods the following media have been used: a) air, b) water, c) oil, d) mercury.

A direct comparison of the results from different methods is not possible. Therefore some general potential sources of error may be discussed. Cracks around the sensor which could lead to depressurisation of the measurement point are of major concern. All systems could potentially suffer from this problem to a lesser or greater degree. Ultimately a type D setup with a very small pressure gauge and the electrical wires exiting the specimen along the isotherms (horizontally in figure 1) would be preferable. The type E setup with a pipe exiting along the isotherms is promising but if this system contains oil a careful analysis of the influence of oil expansion must be made. Similar analysis for an oil filled pipe exiting away from the hot zone, i.e. type A, shows that oil expansion during rapid heating in this configuration is not a problem. In the case of a Type C arrangement a possible error might be that compared with the surrounding concrete an extra portion of liquid moisture might be trapped in the sintered material giving rise to a potential error. Despite the above mentioned potential errors, pressure measurement studies to date have shown that:

The pore pressure development in heated high strength concrete is higher than in normal concrete (Schneider, Kalifa, Phan, Mindeguia).

Higher initial moisture content leads to higher pore pressure (Phan).

Slow heating generally leads to higher pressure than faster heating (standard fire), probably due to induced thermal damage during fast heating (Mindeguia, Phan).

An addition of polypropylene fibre reduces the pressure in concrete that does not spall (Schneider, Phan, Mindeguia).

The direct connection between fire spalling and pore pressure is weak during fire exposure of large externally loaded specimens, i.e. concrete with the addition of polypropylene fibres that does not spall typically exhibits higher pressure than a concrete without polypropylene fibres that spalls (Jansson, Boström, Consolazio).

6. STAR ON MODELLING

6.1 Introduction

6.2 Chapters and writers

More than ten TC members are involved in the work of modelling. Several parts of the chapters have been drafted and a few of the writers participate in this conference. Therefore no specific details of preliminary results are presented in this report. Further information may be obtained from the chairman of the Work Group 4, A. Millard, CEA, France and F. Pesavento, Univ. of Padova, Italy.

7. FRACTURE PROPERTIES OF HPC AT HIGH TEMPERATURES

7.1 Introduction

7.2. Test methods and results

Within the WG 5.1 a new test method for $K_{I, E}$ and $K_{II, C}$ and G_f measurements at high temperatures has been developed. A joint research program in which OPC and HPC specimens were tested at temperatures up to 700°C has been carried out at the Belarus State University of Technology and at the Vienna University of Technology. The tests were carried out by means of concrete cubes 5 or 10 cm in length. Fig. 7.1 and 7.2 show the test set-up for this type of fracture tests with cubes at high temperatures.

Figure 7.1. Fracture test method for K_{IC} values of HPC (Schneider).

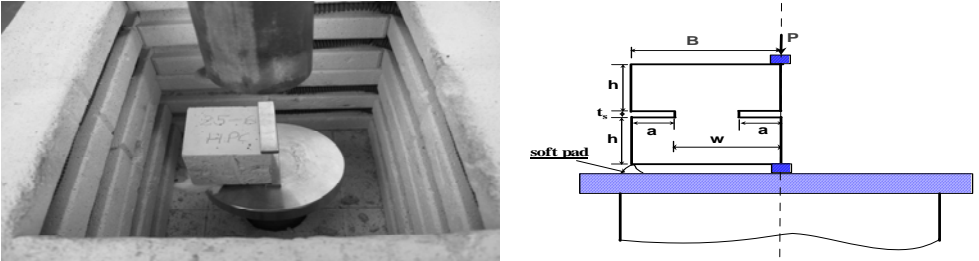
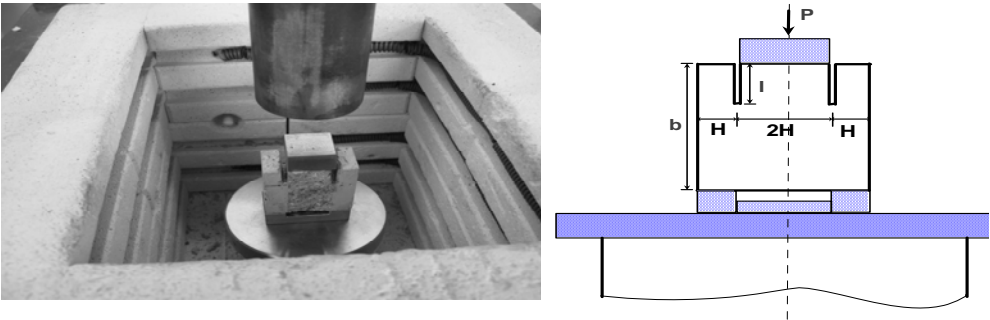


Figure 7.2. Fracture test method for K_{IIC} values of HPC (Schneider).



The latest test results for K_{IC} and K_{IIC} which were derived from 10 cm cube tests of HPC with a strength of 86 N/mm² and after 28 days of curing are given in table 7.1.

Table 7.1. Results of measures K_{IC} and K_{IIC} values and concrete strength at high temperatures according to Leonovich (Minsk).

Temperature (°C)	$f_{c,28}$ (MPa)		K_{IC} (MN/m ^{3/2})		K_{IIC} (MN/m ^{3/2})	
	I	II	I	II	I	II
20	85,7	87,5	0,89	0,82	5,82	4,62
100	83,6	-	0,88	0,85	4,45	5,03
200	83,6	-	0,88	1,00	3,45	6,32
300	99,5	100,4	0,72	0,83	3,61	5,90
400	102,2	110,6	0,35	0,76	3,33	4,77
500	88,7	92,1	0,32	0,37	2,09	3,76
600	81,0	-	0,27	0,24	1,25	3,43
700	76,3	-	0,26	0,19	1,46	1,20

Similar results were obtained for K_{IC} -values derived from 5 cm cubes with a strength of 84 N/mm² after curing. The test results are given in fig. 7.3. Each test value is the average of at least 3 measurements. The values of K_{IC} for specimen after 90 days of curing at 300°C are unexpectedly low compared to the 120 day data. In principal the measurements are in agreement with the data given in table 7.1.

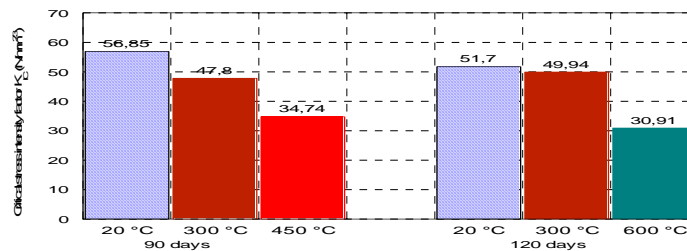


Figure 7.3. K_{IC} -values of HPC after 90 and 120 days of curing according to Schneider.

8. STAR ON PERMEABILITY OF HPC AT HIGH TEMPERATURES

There are two TC members working in the field of permeability measurement: G. Debicki, INSA Lyon (France) and U. Schneider, Vienna University of Technology (Austria). The theoretical background has recently been completed and two test methods for measurements have in the meantime been developed. As part of the conference new test results will be presented in a separate paper by the Vienna University of Technology.

9. FINAL REMARKS

The TC 227 HPB has a life-span of 5 to 6 years and reaches its first period of 3 years in September 2010. It is very likely that several STARs and reports will be finalized during the second period and we look forward to getting inputs from experts from all over the world.

Permeability of High Performance Concrete at Elevated Temperatures

U. SCHNEIDER

ABSTRACT

High performance concrete is a heterogeneous system comprising solid, liquid and gas phases at ambient temperatures which determine its mechanical, physical and chemical behaviour under ambient environmental conditions in a complex manner. Under high temperature the solid skeleton of HPC changes its surface due to dehydration and internal growth. Permeability is a material property which is used to quantify the structural changes and is described in this report.

1. MICROSTRUCTURE AND PORES OF HPC

The structural changes of HPC are closely related to the liquid and gas phases in the concrete pores which occupy round about 15 % of the total volume. Therefore concrete may be defined as a system of a solid skeleton which is crossed over by a fluid skeleton of liquid (water) and gas (air). The space of the fluid skeleton includes pores of different types and sizes which are known as gel pores, capillary pores, air pores, inkbottle pores, shrinkage pores and coarse pores (compaction pores). It is practical to classify the pore sizes according to their different diameters and to measure the pore size distribution of the solid concrete.

Table I. Pore classifications of concrete.

Pore diameter d [μm]		Name of pores	
[1]	[2]	[2]	[2]
< 0,01		gel pores	
> 0,01	< 0,1	capillary pores	micro pores
	> 0,1		meso pores
< 5	< 0,63	capillary pores	
	< 0,125		macro pores
> 5	not defined	coarse pores (shrinkage, air and compaction pores)	not defined

Ulrich Schneider, University of Technology Vienna, Research Centre of Building Materials, Material Technology and Fire Safety, Karlsplatz 13/E206, 1040 Vienna, Austria.

At the time being there is no international accepted system defined which describes the classification of pores in concrete. Two different classification systems for pores which are practically used are shown in the table I.

2. TEMPERATURE EFFECTS IN HPC DURING FIRST HEATING

During heating up of HPC different degradation processes occur which are accompanied by the loss of capillary water (about 100°C), gel water (about 180°C) and chemical water from hydration products of cement (about 200°C to 700°C), whereby a mass flow of water, air and vapour across the pore system along the pore tubes and cracks via the free concrete surfaces takes place.

- The flow is mainly driven by forces from temperature and pressure gradients according to the rules of irreversible thermodynamics. If the temperature is constant and dehydration is completed at that point only pressure gradients may exist inside the material, i.e. a mass flow is still possible.
- If one puts up an external pressure gradient against two surfaces of a concrete specimen which are parallel and opposite to each other a mass flow gets going. After the flow reaches steady state conditions at each point in the flow the flow rate is constant. These conditions are generally used for permeability measurements at high temperatures.

3. FLOW OF COMPRESSIBLE FLUIDS IN POROUS SOLIDS

The flow rate for compressible fluids in porous solids is derived under the assumption that at any point of the flow regime the specific mass flow G (kg/m²s) is constant and therefore may be described by equ. (1).

$$G = \rho \cdot v = -\frac{K}{\eta} \cdot \rho \cdot \frac{dp}{dx} \quad \text{equ. (1)}$$

with: ρ : density of the fluid in (kg/m³)

Under the assumption of an isotherm flow along a distance L between the flow inlet ($x = 0$) and the flow outlet (point $x = L$) one receives from equ. (1) for the flow rate v_2 at the outlet:

$$v_2 = \frac{K_v}{\eta} \cdot \frac{(p_1^2 - p_2^2)}{p_2 \cdot 2L} \quad \text{equ. (2)}$$

The equ. (2) is valid if η is independent of the pressure p which is for air practical the case in the range of flow pressures from 0.1 to 5.0 bar. The intrinsic coefficient of permeability K_v does not depend on the type of fluid according to Darcy's law. From this definition it is clear that the permeability K_v according to equ. (2) has lost its intrinsic character and must be evaluated as apparent permeability because the property depends on the applied pressure. Therefore we define:

$$v_2 = \frac{K_{app}}{\eta} \cdot \frac{(p_1^2 - p_2^2)}{p_2 \cdot 2L} \quad \text{equ. (3)}$$

The concept of apparent permeability is suitable for the determination of viscous flows in high performance concrete at elevated temperatures [1.1].

4. SLIP-FLOW OF GAS FLOW IN POROUS SYSTEMS

More than a century ago Kundt and Warburg (1875)—cited by Bamforth (1987) [3] – observed that the gas flow in materials with very small pores may be larger than the observed results according to equ. (3). The effect was originally attributed to the so-called slip-flow theory developed by Klingenberg (1941) [4]. According to this the flow of gases in porous systems may be determined after equ. (4) as follows:

$$G = \frac{K_{app}}{\eta} \cdot \frac{(P_1^2 - P_2^2)}{P_2 \cdot 2L} \rho_2 \quad \text{equ. (4)}$$

The permeability K_{app} in equ. (5) is obtained by the following approximation:

$$K_{app} = K_{intr} \left(1 + \frac{b}{P_m} \right) \quad \text{equ. (5)}$$

with: $P_m = (P_1 + P_2)/2$ and b to be measured.

If K_{app} is being measured at different P_m the value of K_{app} is related to the parameter $1/P_m$. Generally the measuring points follow a straight line, i.e. the increase of K_{app} with $1/P_m$ is determined by the constant parameter b . In the case $P_m \rightarrow \infty$ one gets $1/P_m = 0$ and after equ. (5) $K_{app} = K_{intr}$, i.e. the permeability is only determined by a viscous flow. K_{intr} is called intrinsic permeability.

5. MOLECULE FLOW IN POROUS SYSTEMS

The slip-flow theory after Klingenberg [4] is based on the observation of flow rates observed in porous media with very small pores, i.e. pores which may be attributed to the group of gel pores mentioned above. As the slip-flow is independent of the viscosity of the type of gas (Carman 1956) [5] it suggests itself that the observed phenomena is actually based on molecule flow in porous media which are dominated by gel pores (nano pores). This type of mass flow in pore systems occurs if the free path length of gas molecules dominates the flow in the pores. The flow is called Knudsen diffusion and is independent of the viscosity.

The Knudsen transport is proportional to P and the transport equation may be transformed using the ideal gas equation into:

$$G_k = -D_k \cdot \frac{M}{RT} \cdot \frac{dP}{dx} \quad \text{equ. (6)}$$

Using the coefficient of diffusion for hot gases the Knudsen flow may be derived from equ. (6) and rewritten as follows:

$$G_k = \frac{\epsilon_p}{\tau_p} \cdot \frac{4}{3} r \cdot v_s \cdot \frac{M}{RT} \cdot \frac{\Delta P}{\Delta L} \quad \text{equ. (7)}$$

with: $\Delta P = P_1 - P_2$ and $\Delta L = L_2 - L_1$

At the exit of the pore system the following equation for Knudsen diffusion is obtained:

$$\frac{v_2 \cdot P_2 \cdot L}{\Delta P} = \frac{4}{3} K_K \cdot v_g \quad \text{equ. (8)}$$

The flow parameter K_K in m for the diffusion flow is defined as follows:

$$K_K = \frac{\varepsilon_p}{\tau_p} \cdot r \quad \text{equ. (9)}$$

In analogy to equ. (7) one may get from equ. (3) the governing equation for the viscous flow:

$$\frac{v_2 \cdot P_2 \cdot L}{\Delta P} = \frac{K_v}{\eta} \cdot P_m \quad \text{equ. (10)}$$

with: $\Delta P = P_1 - P_2$ $P_m = (P_1 + P_2)/2$ v_2 : flow velocity

The summation of the right hand sides of equ. (8) and (10) leads to an equation describing the total flow of gas in a porous system:

$$\frac{v_2 \cdot P_2 \cdot L}{\Delta P} = \frac{K_v}{\eta} \cdot P_m + \frac{4}{3} K_K \cdot v_g \quad \text{equ. (11)}$$

The equation is applicable for all types of porous materials and fluids (Carman 1956) [5] and is therefore of general interest. It may be noted that the equ. (11) comprises two different types of gas flow regimes. One regime is influenced by the viscosity of the gas and the other one is a non-viscous flow. It is therefore of general interest to determine both parts in the flow separately and the percentage of their contributions. The differentiation may be achieved by special permeability measurements in porous materials as ordinary concrete and HPC.

The proposed theory by Carman (1956) [5] allows to determine K_{app} and K_{intr} directly from flow measurements. From the measurement of the gas flow in concrete one obtains easily the total mass flow per unit area:

$$G = \rho_2 \cdot v_2 = \frac{P_2 \cdot M}{R \cdot T} \cdot v_2 \quad \text{equ. (12)}$$

Further we assume that the total flow is determined by two different effects which were discussed above. Therefore we define

$$G = G_v + G_k \quad \text{equ. (13)}$$

and normalize this equation by the parameter $L/\Delta P$. From this we receive:

$$\frac{G \cdot L}{\Delta P} = G_v \cdot \frac{L}{\Delta P} + \frac{L}{\Delta P} \cdot G_k \quad \text{equ. (14)}$$

Carman (1956) has proposed the following equation to be applied:

$$\frac{G \cdot L}{\Delta P} = a \cdot P_m + b_k \quad \text{equ. (15)}$$

The parameters a and b_k are to be determined by experiments with concrete at defined temperatures and for different mean pressures P_m . The results of $(G \cdot L)/\Delta P$ are determined for different P_m values. From three or four measure points at different test pressures a linear regression may be applied to determine the parameters a and b_k according to equ.(15). For $P_m = 0$ the equ. (15) gives the value of b_k therefore identical dimensions must be used for all parameters in use. The parameter b_k determines directly the flow of the non viscous type described above.

6. PERMEABILITY TEST APPARATUS

For the high temperature measurements a special test apparatus was developed (see Figure 1). Slightly conical concrete specimen of 100 mm diameter and 45 mm thickness were used for casting. The fresh concrete was filled, compacted and cured in rings made of heat resistant steel. For testing the ring was installed in an electric furnace (see Pos. 7 and Pos. 15). The steel ring was loaded by an external steel frame with a hydraulic pressure system as to ensure the gas tightness according to the gas pressure difference on the concrete surfaces. The steel frame is shown on Figure 1.

The pressure difference between inflow and outlet of the gas (dry air or nitrogen) was measured. After the outlet the gas was cooled to nearly ambient temperatures. Before cooling the pressure difference between the inlet and outlet was recorded. The gas pressure was controlled at the gas inlet (Pos. 3) and the flow rate at the gas outlet (Pos. 13). The flow meters covered a range of 5 decades of gas flow. Leakage tests were performed before and after the tests. The maximum gas pressure is 5 bar and temperatures up to 500°C were applied.

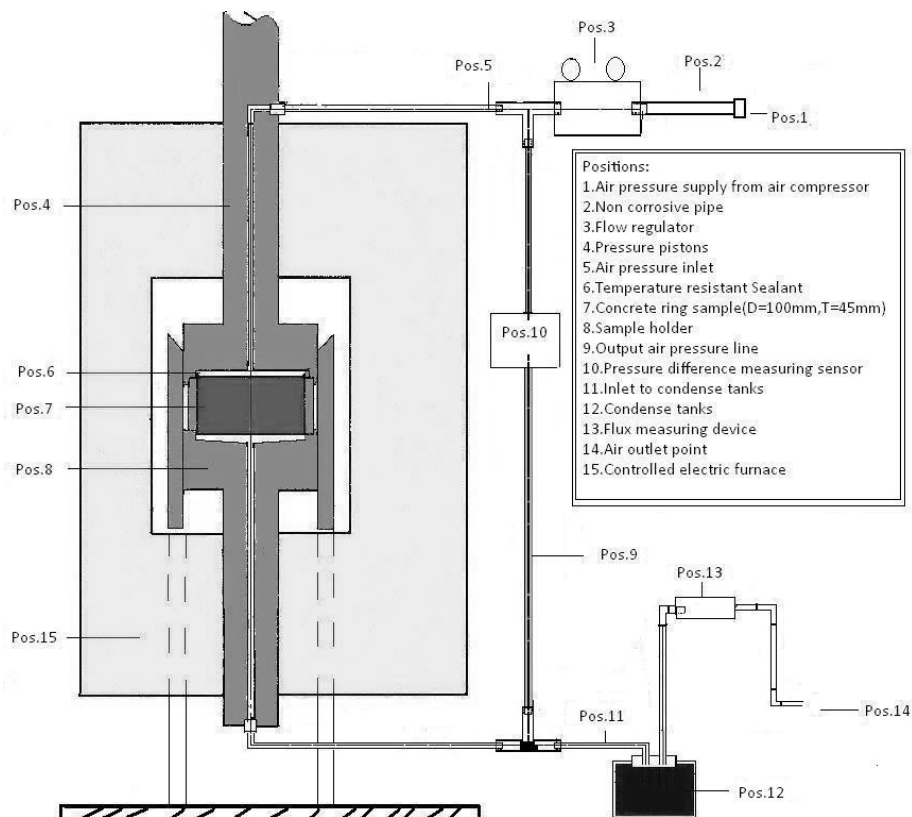


Figure 1. Test apparatus for permeability measurements at high temperatures.

7. PERMEABILITY TEST AT HPC

Two types of HPC were investigated. The concrete mix 1 reached after 28 day of curing a compressive strength of 95 N/mm² and a density of 2.270 kg/m³ and concrete mix 2 a compressive strength of 77 N/mm² and a density of 2.190 kg/m³. Mix 2 was similar to mix 1 but 1% by weight of PP fibers were used in this

concrete. In both cases cement class CEM II was used. The data of mix 1 and 2 are given in Table II. About 455 kg of cement and 111 kg of silica fume were used in both mixes for 1 m³ fresh concrete.

Table II. Data of HPC concrete mixes 1 and 2.

data	mix 1	mix 2
w/c ratio	0,4	0,4
w/a ratio	0,09	0,09
sand/cement	3,56	3,56
fiber/cement	0,0	0,01
superpl./cement	0,035	0,0035
fresh concrete [kg/m ³]	2.327	2.227
f _{c,28} [N/mm ²]	95,0	76,6

8. TEST PROGRAM AND RESULTS FOR HPC WITHOUT FIBERS

The tests comprised the following test temperatures for heating and cooling:
 Heating: 20, 95, 105, 200, 300, 400°C
 Cooling: 400, 300, 20°C

The inlet pressures p₁ were chosen as follows:
 Absolute pressure: 5, 4, 3 and 2 bar

The outlet pressures p₂ varied according to the temperature effects on the permeability. The lowest band of the pressure difference is about 0,5 bar. Typical test results with gas pressure p₁ of 5 bar and 3 bar are given on Figure 2 and 3. The permeability covers a range from 10⁻¹⁵ m² (20°C) to 10⁻¹² m² at 400°C. The residual permeability after heating to 400°C and cooling to 20°C is about 0,5 · 10⁻¹³ m² lower than the high temperature value of the permeability.

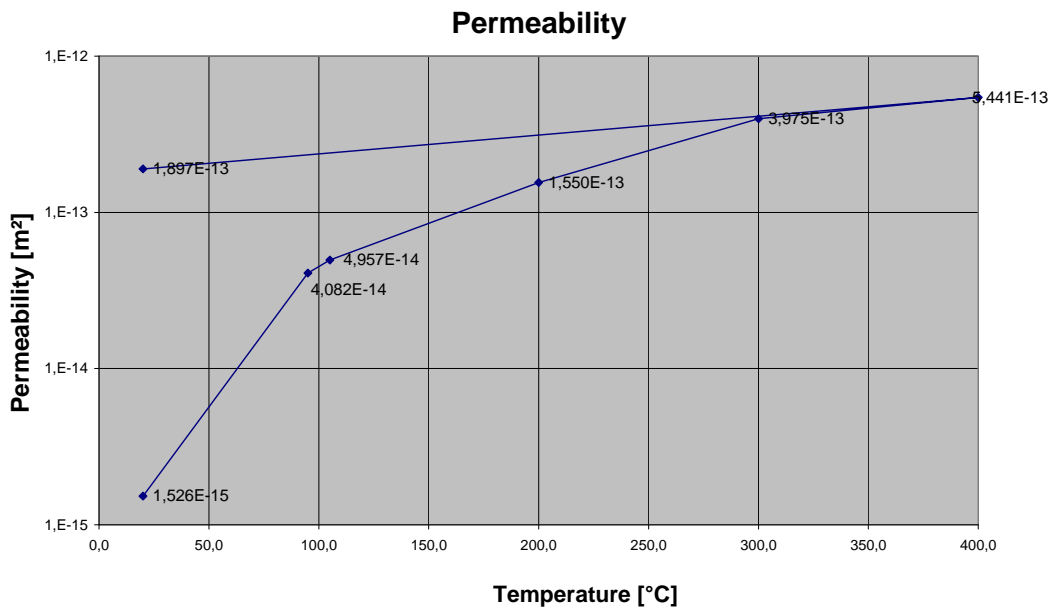


Figure 2. Permeability of HPC 95 during heating and cooling (p₁ = 5 bar).

All measurements were performed under conditions of nearly thermal and hygroscopic equilibrium in the concrete. In the range of 95°C to 105°C the drying at 105 °C was two days, at higher temperatures the heating and hold time for each temperature level comprised in the other cases one day.

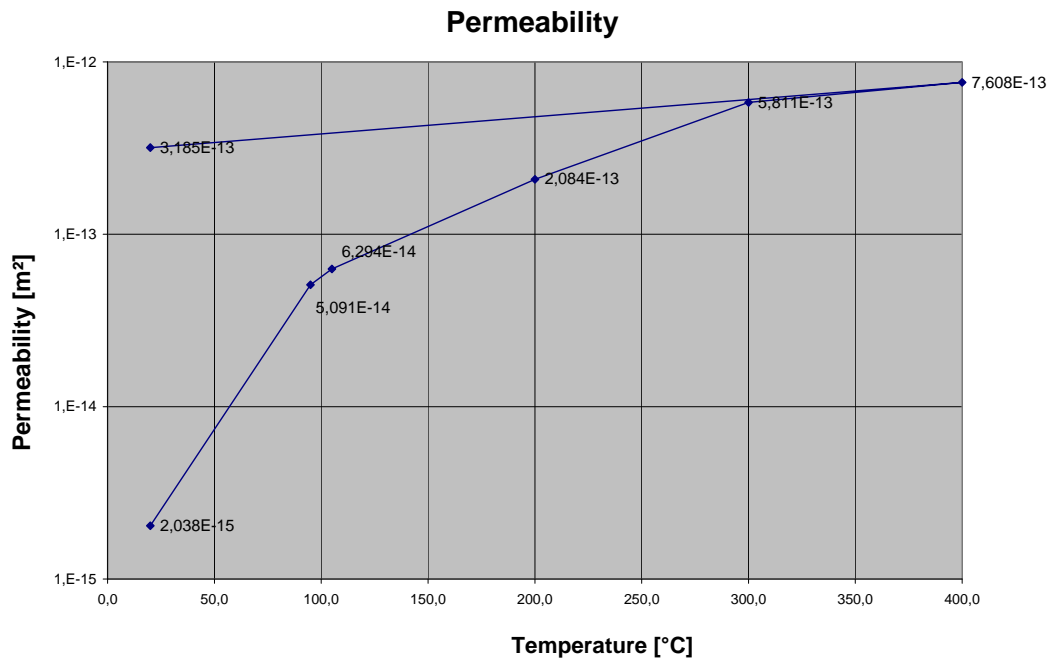


Figure 3. Permeability of HPC 95 during heating and cooling ($p_1 = 3$ bar).

9. EXTENDED EVALUATION OF TEST RESULTS

The measured permeabilities were evaluated to the theories given before. Table III shows the data derived after the theories of Klingenberg and Carman with respect to test temperatures on the intrinsic permeability K_{intr} of HPC.

Table III. Intrinsic permeabilities after Klingenberg and Carman for HPC at high temperatures.

Klinkenberg results			Carman results		
T	K_{intr}	b-constant	K_{intr}	a-constant	b_k -constant
20	7E-16	4,00E+05	1,54E-15	1E-15	2E-11
95	3,00E-14	6,00E+04	6,93E-14	3,00E-14	2,00E-11
105	3,00E-14	2,30E+05	7,18E-14	3,00E-14	1,00E-10
200	9,00E-14	3,30E+05	1,41E-13	4,00E-14	3,00E-09
300	2,00E-13	5,00E+05	4,42E-13	9,00E-14	5,00E-09
400	3,00E-13	3,00E+05	6,44E-13	1,00E-13	3,00E-09
20	3,00E-14	2,30E+06	1,39E-13	9,00E-14	1,00E-08

Concerning the results of Klingenberg there is a scatter of the slip-flow constant b at 20°C. Above 105°C the value of b is in the order of $5 \cdot 10^5$ bar. K_{intr} at 20°C is of the order $7 \cdot 10^{-16} \text{ m}^2$ and reaches at 400°C $3 \cdot 10^{-13} \text{ m}^2$, after cooling $K_{intr} = 3 \cdot 10^{-14} \text{ m}^2$.

The k_{intr} values of Carman seem to be a little higher than the Klingenberg values, but altogether the differences are comparatively small and from the technical standpoint of view acceptable. It should be mentioned that the evaluation of K_{intr} was derived from 3 measured P_m -values in all cases and it is proposed to use more than 3 measured points for the extrapolations in the direction $P_m = 0$. Figure 4 shows an example for the derivation of K_{intr} after Carman at 300°C. It is obvious that a higher amount of measurements would improve the extrapolation results, but from the experimental standpoint of view measurements with pressures higher than 8 bar are not easy to handle, the same holds for P_m less than 2 bar.

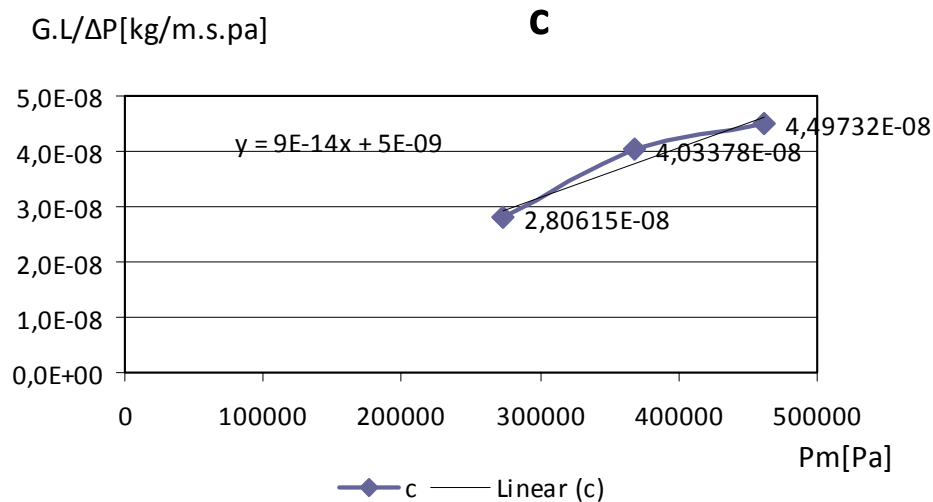


Figure 4. Evaluation of K_{intr} for HPC at 300°C after Carman.

10. CONCLUSIONS

A test method for permeability measurements at high temperatures was developed and successfully applied on HPC up to 400°C and the values for K_{app} and K_{intr} were determined applying two different permeability theories. The apparatus allows the determination of permeability for one specimen at different temperature levels. The duration of tests up to 400°C and cooling to ambient temperature comprises about 10 days for 8 permeability values.

11. REFERENCES

1. Billard, Y.: Contribution à l'étude des transferts de fluides au sein d'une paroi en béton. Ecole Doctorale des Sciences de l'Ingénieur de Lyon, INSA, Lyon, 2003.
2. Schneider, U.: Wiener Baustofflehre Blätter—Grundlagen. Institut für Hochbau und Technologie, Forschungsbereich für Baustofflehre, Werkstofftechnik und Brandschutz, 19. Auflage, Techn. Univ. Wien, Wien, 2009.
3. Bamforth, P.B.: The relationship between permeability coefficients for concrete obtained using liquid and gas. Magazine of Concrete Research, Vol. 39, No. 138 pp 3–11, 1987.
4. Klingenberg, L.J.: The permeability of porous media to liquids and gases. American Petroleum Institute; Drilling Production Practice, pages 200–213, 1941.
5. Carman, P.C.: Flow of gases through porous media. Butterworths Scientific Publications, London, 1956.

Uni-Axial Behaviour of Confined Fiber Reinforced High Strength Concrete Exposed to Elevated Temperatures

K. A. ZAIDI, U. K. SHARMA, P. BHARGAVA and N. M. BHANDARI

ABSTRACT

The concept of using a combination of suitable randomly distributed discrete fibers with nominal amount of lateral steel has been discussed in the literature to ease the requirement of high amount of confinement in the plastic hinge regions of high strength concrete (HSC) columns. However, the effect of high temperatures such as during fire, on the effectiveness of confinement, remains to be investigated. The objective of this study is to gain the knowledge of the strength and deformability of confined fiber reinforced high strength concrete after exposure to a thermal cycle at high temperature. Twenty one unconfined and sixty three confined cylindrical specimens of 150 mm in diameter and 450 mm in height and reinforced with 6 bars of 8mm Φ as longitudinal reinforcement and 6mm Φ hoops equally distributed along the height, were casted under this program. After exposing to the desired elevated temperatures ranging from room temperature to 800⁰ C, the concrete specimens were allowed to cool down naturally in the furnace before testing them under axial compression the next day. The variables considered in this experimental study included different exposure temperatures, equally spaced lateral hoops and addition of steel and polypropylene fibers. The effects of temperature on confined fiber reinforced high strength concrete were studied and quantified with respect to strength and ductility gains. The test results show that the confined concrete performed better as compared to unconfined concrete both at room temperature as well as at elevated temperatures. Further, the residual strength and strain capacities of fiber concrete were better than the comparable non-fiber concrete.

Kaleem A Zaidi, Research Scholar, Department of Civil Engineering, Indian Institute of Technology Roorkee –247 667 (India)

Umesh K Sharma, Assistant professor, Department of Civil Engineering, Indian Institute of Technology Roorkee – 247 667 (India).

Pardeep Bhargava, Professor, Department of Civil Engineering, Indian Institute of Technology Roorkee – 247 667 (India).

N M Bhandari, Professor, Department of Civil Engineering, Indian Institute of Technology Roorkee – 247 667 (India).

INTRODUCTION

In the present day practice, the reinforced concrete structures are designed to behave in a ductile manner to resist natural and man-made hazards like earthquake, fire and blast loading. Thus inelastic deformability of reinforced concrete elements is essential for overall stability of structures in order to sustain these hazards. Deformability of reinforced concrete structural components is generally achieved through proper confinement of the core concrete. The gradual development of concrete technology has promoted the use of high strength concrete (HSC) in construction industry owing to its wide range of advantages over normal strength concrete. But the HSC when subjected to short term or sustained loads tends to be brittle when loaded to failure, lacking the plastic deformation typical of normal strength concrete. The behavior of HSC confined by well-detailed lateral confinement reinforcement is well-documented now at ambient conditions [1], [2], and [3]. However, the studies undertaken in the past to investigate the confinement of reinforced concrete columns at ambient conditions have indicated that a higher degree of confinement is required in columns with higher concrete strength than in columns with lower concrete strength to achieve the desired ductility [4], [5] and [6]. The earlier studies indicate that the use of fibers in the concrete mix can improve the strength and ductility of concrete and can ease the requirement of high amount of transverse confining reinforcement in the potential hinge regions of HSC columns [7], [8] and [9].

Although most of the concrete structures are subjected to a range of heat no more severe than that caused by the weather, there are important cases in which structures are exposed to much higher temperatures. Examples include building fires and some industrial applications where reinforced concrete structural elements are close to furnaces and reactors. Such fires or elevated temperatures result, in most cases, in considerable damage to structures [10], [11], [12], [13] and [14]. Therefore, it becomes important to evaluate the effectiveness of confinement devices in confining core concrete after exposure to elevated temperatures, especially in seismic resistant structures. Thus the main aim of the present investigation is to provide experimental data on the residual behaviour of confined fiber reinforced high strength concrete subjected to high temperature.

EXPERIMENTAL PROGRAM

A total of 84 high strength concrete short column specimens were cast and tested under this investigation. They included 63 numbers of hoop confined specimens and 21 unconfined specimens. All the specimens were of cylindrical shape with a size of 150 mm x 450 mm. The details of all the confined specimens are illustrated in Table I. The unconfined specimens (Table II) were of the same size and shape as confined specimens but without reinforcement. The specimens were cast and tested in triplicate in order to get the average of three results. The two different types of fibers i.e. steel fibers and polypropylene fibers were used in the study. The confined and unconfined concrete specimens were cast in four different series (A, B, C, and D). The steel fibers used were crimped fibers with a length of 25mm and an aspect ratio of 20. The dimension of fibrillated polypropylene fibers

were 18 micron in diameter and length of 12mm. The standard plain concrete cylinders (100 x 200 mm) were also cast and tested to determine the nominal strength of concrete on the day of testing of test specimens. The specimens were cast in PVC moulds in the laboratory. After 24 hours, the specimens were removed from the moulds and submerged in a water tank for curing. The water curing period lasted for 28 days after which the specimens were kept in the laboratory at ambient temperature and humidity conditions for another 62 days until they reached equilibrium moisture content. After 90 days of ageing, the specimens were exposed to various heating regimes. Subsequent to a single heating and cooling cycle, the specimens were tested under monotonic compression.

TABLE I. PROPERTIES OF CONFINED CONCRETE COLUMN.

Specimens	f_c (MPa)	Longitudinal steel			Transverse steel				Fibers Volume fractions Vf(%)	
		Number & Diameter (mm)	ρ_l (%)	f_y (MPa)	Diameter (mm)	Spacing (mm)	ρ_s (%)	f_y (MPa)	Steel fibers	PP fibers
CBH CB2H CB3H CB4H CB5H CB6H CB8H	71.36	6Nos 8	1.70	650	6	42	2.26	510	-	-
CCHF CC2HF CC3HF CC4HF CC5HF CC6HF CC8HF	71.92	6Nos 8	1.70	650	6	42	2.26	510	1%	-
CDHF CD2HF CD3HF CD4HF CD5HF CD6HF CD8HF	71.83	6Nos 8	1.70	650	6	42	2.26	510	-	0.1%

A programmable electrical furnace designed for a maximum temperature of 1200⁰C was used to heat the specimens. The temperature inside the furnace was measured and recorded with specially installed thermocouples. The thermocouples were also fixed during casting at mid height of the specimens at three different locations inside the cylinder i.e. at the surface, at cover core interface and at the centre of the specimen to record temperature histories. At an age of 90 days the specimens were heated in the furnace to different target temperatures ranging from ambient temperature to 800⁰C. Heating rate was set at 5⁰C /min and the each target temperature was maintained for 4.5 hrs to achieve a thermal steady state. After

reaching the maximum desired temperature the furnace was switched off, and samples were left in the furnace to allow natural cooling. The rate of cooling was not controlled but was measured during complete test. The data from thermocouples were recorded in a PC by data logger.

The mechanical testing of specimens was carried out after a complete cycle of heating and cooling. The test specimens were loaded using 2500 kN capacity (INSTRON) UTM with displacement controlled capabilities. The monotonic concentric compression was applied at a very slow rate (0.1mm/min) to capture the complete post peak behavior of the measured load deformation curve. The axial contraction of the cylindrical specimens was monitored by the average of the data of two linear variable displacement transducers (LVDT) placed on the circumferential opposite to each other of the specimens. The mean axial displacement of the central zone of the specimens (gauge length 200mm) was measured and converted into an average strain over the measured base of the LVDTs. Loads were recorded through a load cell inbuilt in the UTM. The recorded data from the LVDTs and load cell were fed into a data acquisition system and stored on a computer.

OBSERVATIONS

The confined non-fiber and fiber reinforced concrete cylinders did not show any distinct sign of cracking when heated up to a temperature of 600⁰C. However beyond this temperature, cracks were noticed on the heated surface along the confined specimens heated at 800⁰C. No observable symptoms of spalling were noticed during heating and cooling cycle in confined concrete specimens, however, unconfined concrete specimens exposed to 600⁰C and 800⁰C temperatures did show spalling tendencies. The temperature histories as recoded by the various thermocouples were closely monitored during the testing. The target temperatures could not be achieved in the specimens exposed to 200⁰C and 300⁰C temperatures. Therefore, a true steady state condition could not be achieved in these specimens. However, the target temperatures and a steady state condition were obtained in the specimens subjected to higher temperatures.

The residual compressive behavior of unconfined concrete cylinders exposed to temperatures ranging from room temperature to 500⁰C exhibited brittle longitudinal splitting. No mechanical testing could be undertaken for unconfined specimens exposed to 600⁰C and 800⁰C temperatures due to their spalling during thermal exposure. The failure of non-fiber confined concrete specimens of CBH series under compressive loads was observed to be of shear type for temperatures up to 400⁰ C. Above 500⁰C, the failure of confined concrete specimens was marked by significant lateral dilation of concrete and softening of strain mainly at their mid height. The failure of confined concrete specimens in the presence of fibers was observed to be considerably more ductile compared to non-fiber confined concrete specimens, especially in specimens constructed with steel fibers. This gradually led to the fracture of hoops and bucking of longitudinal steel in many cases.

TABLE II. PROPERTIES AND RESULTS OF UNCONFINED SPECIMENS.

Specimens	Temperature of exposure (°C)	f'_c (MPa)	f'_{co} (MPa)	ϵ_{co}	ϵ_{c50o}
CAH	Ambient	71.68	70.09	0.00208	*
CA2H	200	71.68	70.51	0.00209	*
CA3H	300	71.68	74.96	0.00262	*
CA4H	400	71.68	72.42	0.00367	*
CA5H	500	71.68	42.75	0.00347	*
CA6H	600	71.68	Spalling	*	*
CA8H	800	71.68	Spalling	*	*

* could not be measured

TABLE III. RESULTS OF CONFINED CONCRETE SPECIMENS.

Specimen	Exposure Temperature (°C)	P_{max}	P_{max}/P_o	ϵ'	$\epsilon' / \epsilon_{co}$	ϵ'_{80}	$\epsilon'_{80} / \epsilon_{co}$	ϵ'_{50}	$\epsilon'_{50} / \epsilon_{co}$
CBH	AMBIENT	1348	1.07	0.00316	1.52	0.0064	3.08	0.0092	4.423
CB2H	200	1358	1.08	0.00371	1.79	0.0069	3.32	0.0109	5.240
CB3H	300	1449	1.15	0.00377	1.81	0.0074	3.56	0.0135	6.490
CB4H	400	1385	1.10	0.00798	3.84	0.011	5.29	0.0140	6.731
CB5H	500	1214	0.97	0.01030	4.95	0.0161	7.74	0.0183	8.798
CB6H	600	952	0.76	0.01402	6.74	0.0218	10.48	0.0246	11.827
CB8H	800	590	0.45	0.0200	9.62	0.0310	14.90	0.0366	17.596
CCHF	AMBIENT	1508	1.19	0.00354	1.70	0.0125	6.01	0.0240	11.538
CC2HF	200	1513	1.2	0.00251	1.21	0.00878	4.22	0.0192	9.134
CC3HF	300	1546	1.22	0.00433	2.08	0.00945	4.54	0.0210	9.615
CC4HF	400	1459	1.15	0.00682	3.28	0.0129	6.20	0.0222	10.576
CC5HF	500	1351	1.07	0.00932	4.48	0.0167	8.03	0.0272	12.980
CC6HF	600	1120	0.88	0.0184	8.85	0.0235	11.30	0.0288	13.461
CC8HF	800	619	0.495	0.0200	9.62	0.0338	16.25	0.0431	20.673
CDHF	AMBIENT	1517	1.2	0.00252	1.21	0.00502	2.41	0.0124	5.961
CD2HF	200	1544	1.22	0.00305	1.47	0.00561	2.70	0.0125	6.009
CD3HF	300	1444	1.14	0.00360	1.73	0.00643	3.09	0.0136	6.538
CD4HF	400	1374	1.09	0.00903	4.34	0.0134	6.44	0.0192	9.230
CD5HF	500	1201	0.955	0.0103	4.95	0.0149	7.16	0.0201	9.615
CD6HF	600	980	0.779	0.0188	9.04	0.0244	11.73	0.0300	14.423
CD8HF	800	559	0.444	0.0191	9.18	0.0261	12.55	0.0391	18.75

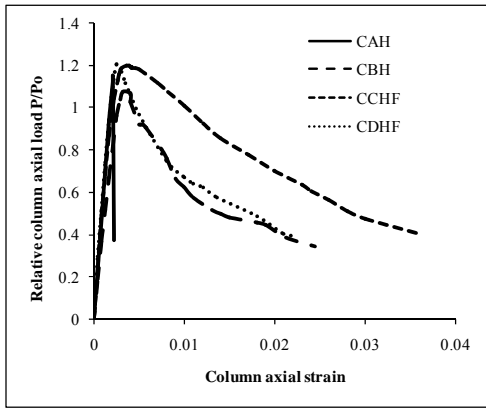
TEST RESULTS

The test results are given in Table II for unconfined specimens and in Table III for confined concrete specimens. Figs. 1 (a) to (g) illustrate measured axial load-deformation curves for the various specimens tested under this program. The load-strain responses of unconfined concrete specimens are also shown for comparison purpose. Each result in Tables II and III represents the average result of three specimens. To facilitate the comparison of behavior of different confined concrete specimens, the maximum observed load, P_{max} , has been nondimensionalized with respect to the concentric theoretical capacity of specimens, P_o , at ambient

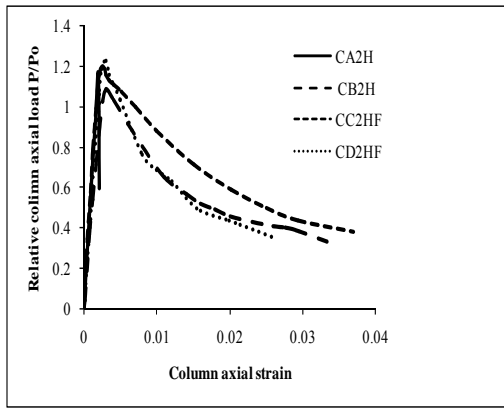
temperature. Similarly, the strain corresponding to the peak load, ϵ' , and the post-peak strains, ϵ'_{80} (axial strain at which the load drops to 80% of the peak load) and ϵ'_{50} (axial strain at which the load drops to 50% of the peak load) have been normalized with respect to the peak strain of the corresponding unconfined concrete, ϵ_{co} , at ambient temperature.

The residual load ratio P_{max}/P_o ranges from a maximum value of 1.22 at ambient temperature to a minimum value of 0.444 at 800°C temperatures for the confined concrete specimens tested under this program. It can be observed that the residual peak load of confined specimens does not get affected in the temperature range of 100 to 400°C. In fact, the peak load and hence the load ratio P_{max}/P_o increases slightly up to a temperature of 300°C in most of the specimens. Similar trends were noticed in unconfined specimens as well. In the temperature range of 500°C to 800°C, the peak load in each case drops markedly. However, the results indicate that the peak load of confined specimens drops only to 71 to 95% of the theoretical concentric capacity up to a temperature of 600°C. It is only beyond 600°C temperatures i.e. at 800°C temperature that the carrying capacity of confined concrete specimens falls to 40 to 49% of the theoretical capacity. The addition of fibers seemed to further help in retaining the load capacity at higher temperatures. However in unconfined concrete specimens, the residual maximum load drops sharply even after 400°C. It can be observed that the strain ratio ϵ'/ϵ_{co} increases from a minimum value of 1.21 at ambient temperature to a maximum value of 9.62 at 800°C temperature in the confined concrete specimens. The strain ratio $\epsilon'_{80}/\epsilon_{co}$, $\epsilon'_{50}/\epsilon_{co}$ ranges from a minimum value of 2.41 at ambient temperature to a maximum value of 16.25 at 800°C temperature. Both these strains and hence the corresponding strain ratios do not vary significantly within the temperature range of 100 to 400°C. However, in the temperature range of 500°C to 800°C, both peak and post-peak strains increase considerably.

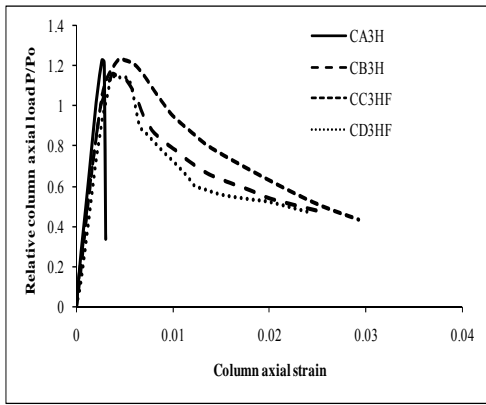
The results indicate that the addition of 1% steel fibers result into more ductile behavior irrespective of the temperature of exposure. It can be observed that incorporating the steel fibers in the confined high strength concrete leads to more limited thermally induced losses in terms of load carrying capacity, especially in the temperature range of 500°C to 800°C. However, on the contrary the behavior of polypropylene fiber reinforced concrete specimens indicate that an addition of polypropylene fibers in confined high strength concrete did not render any benefit in terms of residual post-peak deformability. The post peak curves of the polypropylene fiber concrete specimens are distinctly steeper indicating a faster rate of strength decay as compared to the steel fiber concrete specimens. A considerably higher peak (ϵ') and post-peak strains (ϵ'_{80}), (ϵ'_{50}) were noticed in steel fiber reinforced concrete specimens compared to polypropylene fiber reinforced concrete specimens at all the temperatures of exposure. Enhancement in the load carrying capacity P_{max}/P_o , was also observed to be more in the specimens constructed with steel fiber reinforced concrete compared to polypropylene fiber reinforced concrete specimens both at room temperature and at high temperatures.



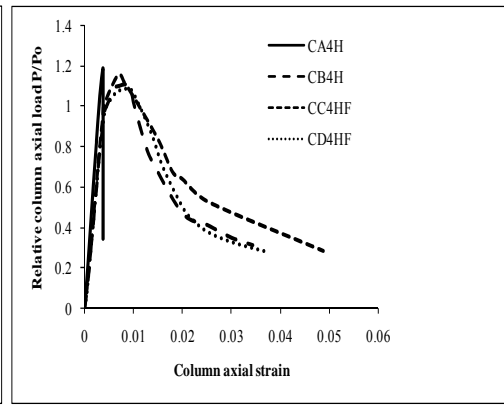
(a) Load vs strain at ambient temperature



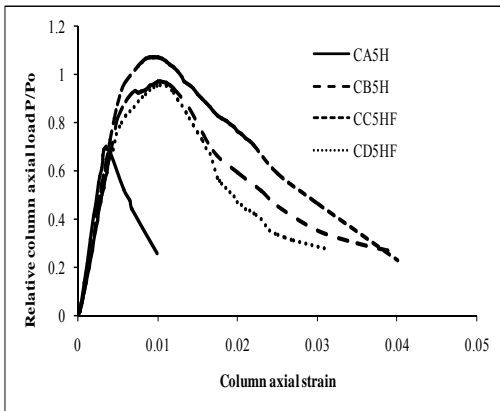
(b) Load vs strain at 200°C



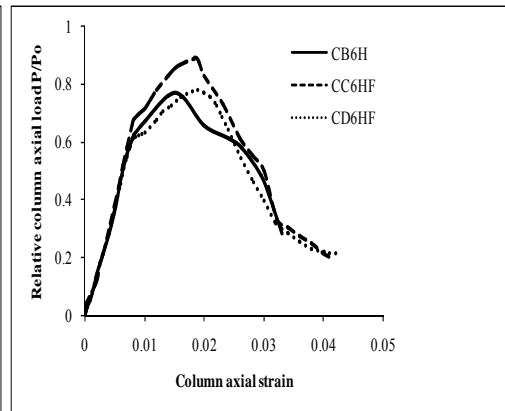
(c) Load vs strain at 300 °C



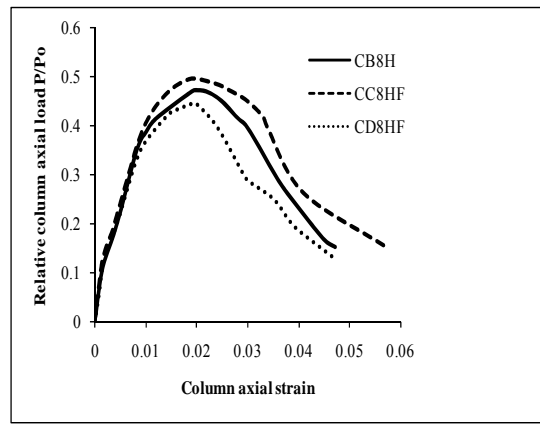
(d) Load vs strain at 400 °C



(e) Load vs strain at 500 °C



(f) Load vs strain at 600 °C



(g) Load vs strain at 800 °C

Figure 1(a) to (g). Load Vs Strain Curves for Various Confined HSC Specimens at Different Elevated Temperatures.

CONCLUSIONS

Within the scope of the present investigation, the following conclusions may be drawn:

- 1 The provision of transverse reinforcement confinement and addition of fibers in the mix are beneficial for reducing the spalling tendency of high strength concrete at high temperatures.
- 2 The influence of temperature on residual behavior of fibrous and non-fibrous confined concrete does not matter much up to a temperature of 400°C. Further, the load carrying capacity of confined concrete specimens drops only to 76 to 88% of the corresponding ambient temperature theoretical concentric capacity up to a temperature exposure of 600°C. Nevertheless, this nominal drop in load carrying capacity of confined concrete specimens up to 600°C is associated with a considerable enhancement in deformability.
- 3 The residual strength and ductility of confined high strength concrete increased with the addition of steel fibers in the concrete; the strength enhancement being less sensitive than ductility. However, polypropylene fibers did not significantly influence the residual load-deformation behavior of confined concrete at elevated temperatures.

NOTATIONS

f'_c = cylinder compressive strength of concrete

f_y = yield strength of steel

P_{co} = unconfined strength of concrete specimen

P_{max} = maximum load capacity of the confined specimen

P_o = theoretical concentric capacity of specimen

ϵ_{co} = strain at peak load of unconfined concrete specimen

ϵ' = axial strain corresponding to the peak load of confined concrete specimen

ε'_{80} = axial strain at which the load drops to 80% of the peak load
 ε'_{50} = axial strain at which the load drops to 50% of the peak load
 ρ_s = volumetric ratio of hoops
 ρ_t = ratio of longitudinal reinforcement
 V_f = Fibers Volume fractions

REFERENCES

1. Yong YK, Nour MG, Nawy EG.1988 "Behavior of laterally confined high-strength concrete under axial loads". J. Struct. Engineering., ASCE;114(2):333–51.
2. Sheikh, S.A.and Uzumeri, S. M. 1980. "Strength and ductility of tied concrete columns. Journal of Structural Division, ASCE, 106 (5): 1079–1102.
3. Razvi, S., and Saaticioglu, M., 1994. "Strength and deformability of confined high strength concrete columns," ACI Structural Journal, 91(6):678–687.
4. Cusson ,D and Paultre. P.1994. "High Strength concrete columns confined by rectangular ties"Journal of Structural Division, ASCE, 120 (3): 783–804.
5. Sharma, U., Bhargava, P. and Kaushik, S.K., 2005. "Behavior of Confined High Strength Concrete Columns under Axial Compression", International Journal of Advanced Concrete Technology, Japan Concrete Institute, 3 (2): 267–281.
6. Hong, K. N. Han, S. H. Tac-Yi, S. 2006 .“High strength concrete column confined by low volumetric ratio lateral ties”, Engineering Structure 28: 1346–1353.
7. Ezeldin,A.S and Balagru ,P.N 1992 Normal and high strength fibre reinforced concrete under compression. ASCE journal of structural Engineering , 121 (3):468–477.
8. Foster, S.J.and Attard, M.M.2001. "Strength and ductility of fibre reinforced high strength concrete columns. Journal of Structural Division, ASCE, 127 (1): 281–289.
9. Sharma, U., Bhargava, P. and Sheikh.S.A, 2007. "Tie Confined fiber reinforced High Strength Concrete short Columns", Magazine of Concrete Research 59 (10) :757–769.
10. Chan , Y.N Luo, X. and W .Sun 2000. "Compressive strength and pore structure of high performance concrete after exposure to high temperature up to 800°C," Cement and concrete Research 30:247–251.
11. Phan, L. T., Lawson, J. R., and Davis, F. L., 2001. "Effects of Elevated Temperature Exposure on Heating Characteristics, Spalling, and Residual Properties of High Performance Concrete," Materials and Structures, (34): 83–91.
12. Kodur V.K.R and Grath R Mc 2006. "Effect of silica fume and lateral confinement on fire endurance of high strength concrete columns," Canadian journal Civil Engineering 33:93–102.
13. Kodur V.K.R, Fu Ping Cheng, Tien-Chih wang and MA Sultan. 2003, "Effect of strength and fibre reinforcement on fire resistance of High strength concrete columns," journal of structural Engineering February: 253–259.
14. Sideris A.,Halit ,Y and Bulent ,B 2009. "Performance of thermally damaged fiber reinforced concrete," Construction and Building Materials 23:1232–1239.

Effect of Heating Method on the Physical Properties of Hybrid Fibre Reinforced High Strength Concrete at High Temperature

K. WATANABE and T. HORIGUCHI

ABSTRACT

Recent fire disasters in tunnels have clearly become a matter of public interest due to greater risks involved in tunnels exposed to higher temperature condition. It is really important to gain an understanding of the behaviour of concrete under high temperature condition. Moreover, only a limited number of studies have been conducted on the bending behaviour of High-Strength Concrete (HSC) during heating exposure.

In this research, the effect of different heating conditions on the physical properties of HSC and Hybrid-Fibre-Reinforced High-Strength Concrete (HFRHSC) was evaluated in order to understand the bending behaviour of concrete at high temperature using two kinds of heating conditions. Physical characteristics of HSC and HFRHSC (i.e. bending strength and fracture energy) were carried out.

The different heating experimental results show a significant effect on physical properties of HSC and HFRHSC. Bending strength and fracture energy test results show a clear difference between residual test and hot test. Comparing two heating conditions, hot test was observed to be the severest on all series at maximum heating temperature resulting in the lowest fracture energy.

Kazuo Watanabe, Ph.D. Course Student, Graduate School of Engineering, Hokkaido University, Kita-13, Nishi-8, Kita-ku, Sapporo, Hokkaido, Japan

Takashi Horiguchi, Associate Professor, Hokkaido University, Graduate School of Engineering, Hokkaido University, Kita-13, Nishi-8, Kita-ku, Sapporo, Hokkaido, Japan

1. Introduction

High-Strength Concrete (HSC) has been greatly utilized in civil engineering structures like road-tunnels across the world, due to its increased performance. HSC provides better properties such as increased strength and durability that exceed those of Normal-Strength Concrete (NSC). In terms of design, with its higher load bearing capacity, HSC allows smaller size segments to be utilized in more durable construction leaving more space to be utilized.

However, several investigations have clearly shown that property deficiencies of HSC occur under high temperature condition. In some cases, HSC fails in a catastrophic manner during exposure to fire characterized by explosive spalling of the concrete surface [1], [2]. With this trend increasing, improvement in the fire resistance of HSC is required. Unfortunately, research that deals with fracture behaviour of HSC under high temperature condition is still scanty compared with NSC. Therefore, detailed investigation regarding fire resistance of HSC is required worldwide as quickly as possible.

In this research, an investigation on the effectiveness of the hybrid fibre was done by incorporating steel fibres together with polypropylene fibres inside the concrete mixture, and the physical properties of HSC and Hybrid-Fibre Reinforced High-Strength Concrete (HFRHSC) during and after exposure to high temperatures were investigated to comprehend the effect heating temperature up to 600 °C. Experimental tests in the mentioned literature were usually performed on HSC and NSC with emphasis on the comparison of fracture properties after exposure (residual test)[3]. Polypropylene fibres were utilized to prevent explosive spalling [4], while steel fibres maintained the residual strength of the concrete even after fire exposure [5]. This experimental study compares fire resistance of two types of HFRHSC that utilized various fibres volume contents inside HSC mixture during and after exposure to high temperatures. Evaluation of fracture energy is back-calculated using the poly-liner approximation method [6].

2. Experimental programme

2.1 Materials, fibres and specimens

The mixture proportions of the concrete are shown in Table I. All series of concrete were cast using Ordinary Portland Cement, river sand, and crushed hornblende andesite. The specific gravity of the river sand and crushed hornblende andesite were 2.68 and 2.65, respectively (maximum nominal size of crushed hornblende andesite is 13 mm).

Some parameters of mixture proportion were kept constant: W/C = 0.3, sand to aggregate ratio (s/a) = 50 %, unit cement content = 567 kg/m³, and water content = 170 kg/m³. A polycarboxylate-based super-plasticizer air-entrained agent was used to attain the desired workability and air content of fresh concrete. Specimens were mixed using an Omni mixer. All specimens were prisms of 100 × 100 × 400 mm.

Polypropylene fibres and two types of steel fibres having 18, 160 and 600-micron effective diameter, respectively, were used in this experimental study. Properties of the fibres are shown in Table II.

The specimens were demoulded 24 hours after casting, and then cured under lime-saturated water at a temperature of 20 ± 2 °C for 91 days. The notch with a thickness of 4 mm and a depth of 30 mm was cut in the center section of all specimens using a concrete cutter according to the test method in a JCI (Japan Concrete Institute) Test method JCI-S-002-2003: Method of test for load displacement curve of fibre reinforced concrete by use of notched beam [7].

TABLE I. MIXTURE PROPORTIONS OF HSC AND HFRHSC.

Series	W/C (%)	Air (%)	s/a (%)	Fibre volume (%)			W (kg/m ³)	C (kg/m ³)	SP*1 (%×C)	f _c -20°C (MPa)
				Polypropylene	Steel (S30)	Steel (S13)				
Plain				-	-	-				73
HY1	30	6.0	50	0.1	0.5	-	170	567	0.9	83
HY2					0.4	0.1				84

*1SP: super plasticizer

TABLE II. PROPERTIES OF FIBRES.

	Polypropylene	Steel (S30)	Steel (S13)
Diameter (mm)	0.018	0.6	0.16
Length (mm)	6	30	13
Shape	Filament	Indent	Straight
Density (gr/cm ³)	0.9	7.8	7.8
T _{melt} (°C)	160-170	1370	1370
T _{vaporize} (°C)	341	-	-

2.2 Heating conditions

A lateral furnace was designed to allow the bending under both the residual test and the hot test. Diagrammatic illustrations are shown in Figure 1.

The heating rate of the device was set at 20°C/min for the lateral furnace, with the maximum temperature kept at 200, 400, and 600°C for 2 hours. The surface temperature of the specimen was controlled at the center of the beam.

In the case of residual tests, heated specimen was left to cool inside the furnace until their temperature coincided with room temperature to prevent micro cracks induced upon cooling. In the hot test, by contrast, specimen was continuously heated during the loading until it failed (i.e. Plain concrete) or until the loading machine cross-head reached its deflection limit (i.e. Hybrid series).

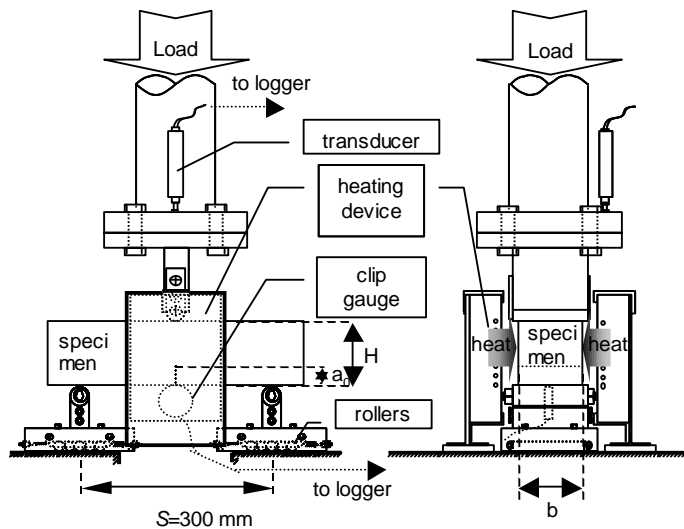


Figure 1. Fracture Energy Test Set-up (with Heating Device of Hot Test).

2.3 Fracture energy measurement

With a designated loading span of 300 mm, the fracture energy test was executed under load control using a servo hydraulic testing machine. The beam specimen was arranged on roller supports under both fulcrums in order to allow it to move freely in the horizontal direction.

In the case of the fracture energy tests, the loading rate was set at 0.1 mm/min. The fracture energy test was conducted in accordance with JCI-S-002-2003 [7].

During the fracture energy test, load (P), Crack-Mouth Opening Displacement (CMOD), and Load-Point Displacement (LPD) were measured. The loading device and measurement points are shown in Figure 1.

The fracture energy of each specimen was calculated as follows:

$$\begin{aligned} G_F &= (0.75W_0 + W_1) / A_{lig} \\ W_1 &= 0.75(S/L \cdot m_1 + 2m_2)g \cdot CMOD_c \end{aligned} \quad (1)$$

where,

G_F : Fracture Energy (N/mm), W_0 : Area under Load-CMOD Curve before Specimen Breaking (N·mm), W_1 : Weight of the Specimen and the Work from Loading Jig Forms (N·mm), A_{lig} : Area of Ligament (mm²), m_1 : Weight of Specimen (kg), S : Loading Span (mm), m_2 : Weight of Jig Appearing in a Specimen (kg), $CMOD_c$: Crack-Mouth Opening Displacement (mm)

The modulus of elasticity test in bending by considering the self-weight of the notched beam specimens was calculated based on Equation (2). In order to keep the modulus of elasticity value in bending (E_b) to within serviceability limit range, calculation of this parameter will be based on CMOD of 0.05 mm.

$$E_b = \frac{[P_u + 0.5mg(L/S)(2 - L/S)]}{4B(H - a_0)^3 D} \quad (2)$$

where,

P_u : Maximum Load at Peak (kN), L : Full Length of the Beam (mm), H : Specimen Depth (mm), B : Width of the Beam (mm), a_0 : Initial Notch Depth (mm), D : Deflection at the Center of the Beam (mm)

3 Results and discussion

3.1 Bending strength

As shown in Figure 2, the bending strength of under residual test and under hot test decreases with respect to increasing heating temperature. This phenomenon may be explained the fact that dried concrete specimens yield at a higher strength that counters the negative effect of micro-cracks after heat exposure of the specimen. However, the reduction is significant in Figure 2 under hot test because the hybrid series were not able to even maintain the bending strength.

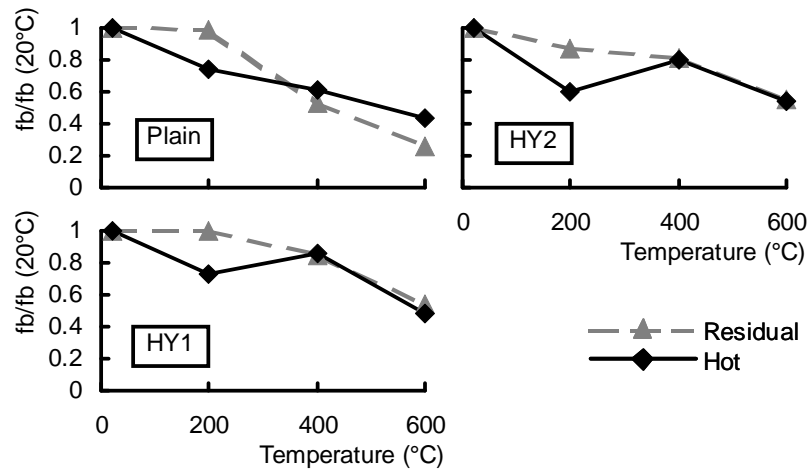


Figure 2. Bending Strength Ratio with Heating Temperature.

3.2 Modulus of elasticity in bending

Modulus of elasticity in bending is illustrated in Figure 3. In general, the modulus of elasticity gradually decreases with respect to increasing heating temperature. The reduction of under hot test is the highest among all series. In the case of Plain concrete, the reduction under hot test reaches up to about 40 % at 200 °C and then less than 10 % at 600 °C. However, the hybrid series maintain higher modulus of elasticity compared with Plain concrete at any particular heating temperature, and even at 600 °C. Hybrid reinforcement cannot mitigate a decrease in modulus of elasticity.

3.3 Fracture toughness

The relationships between fracture energy and heating temperatures are shown in Figures 4. As shown in these figures, a large difference in fracture energy of Plain mixture in relation to HY mixtures was observed. For the HY mixture, it was observed that the fracture energy decreased with increase in heating temperature, especially for HY2 mixture that is observed to have the highest fracture energy of all HY mixtures at all of the set heating temperatures

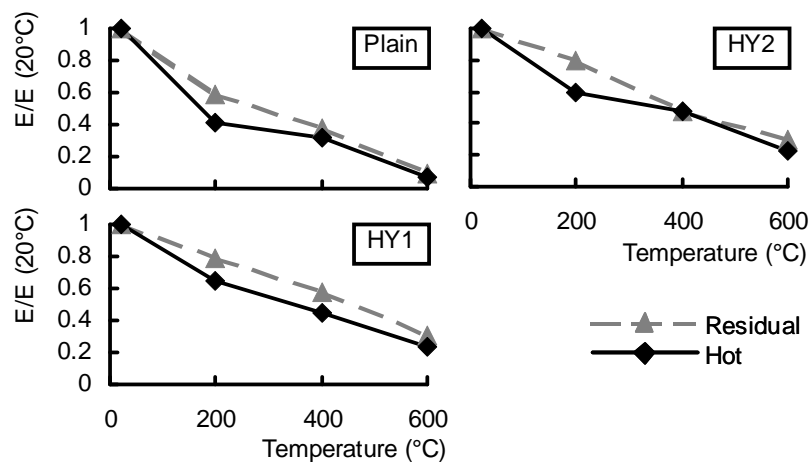


Figure 3. Modulus of Elasticity in Bending with Heating Temperature.

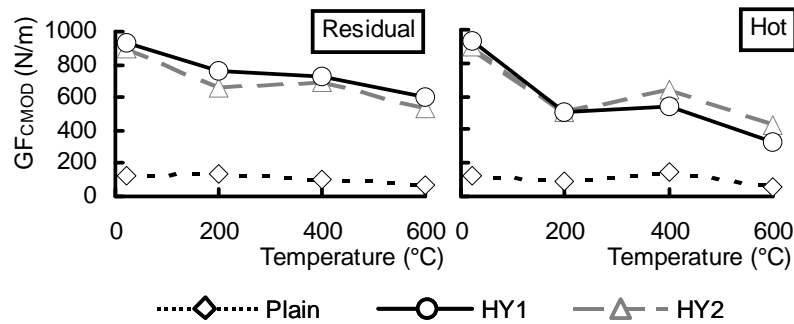


Figure 4. Fracture Energy with Heating Temperature.

under the residual condition. Furthermore, when HY mixtures were exposed to high temperatures above 200 °C under hot condition, the fracture energy of the concrete decreased suddenly and failed in a brittle manner. This phenomenon is thought to be influenced by the tensile stresses arising in concrete during heating due to the expansion of aggregates which leads to the reduction in bending strength during the hot test.

For both residual and hot tests, it was observed that the fracture energy of concrete with steel fibres exceeded that of Plain mixtures at any heating temperature. This is consistent with the previous studies [8]. In general, HY2 shows higher performance under residual condition, while, HY1 shows higher performance beyond 400°C. Addition of short steel fibres (S13) in HY2 increases the number of fibres per unit of volume compared with HY1. Which shows better performance under residual test condition, as shown in Figure 4. However, it was observed that it is not so effective under hot test condition.

Conclusions

1. The bending strength of specimen in lateral furnace is decreasing. Hybrid fibre reinforced concrete maintains higher bending strength.
2. In general, it was observed that modulus of elasticity in bending is decreasing with increasing heating temperature. This does not depend on heating methods.
3. It was confirmed that fracture energy test under hot test was the severest test method among all series, due to rapid decrease of fracture energy at 200 °C.
4. It is necessary to think that the fracture energy of concrete is one of the main factors influencing mechanical properties of HSC.

References

1. Phan, L. 2007. "Spalling and Mechanical Properties of High Strength Concrete at High Temperature," Fifth International Conference on Concrete under Severe Conditions, Environment and Loading, CONSEC'07 Tours, France, June 4-6, pp. 1595–1608.
2. Castillo, C. and A. J. Durrani. 1990, "Effect of Transient High Temperature on High-Strength Concrete," Technical Paper, ACI Materials Journal, V. 87, No. 1, January-February 1990, pp. 47–53.
3. Nielsen, C.V. and Bicanic, N. 2003, "Residual fracture energy of high-performance and normal concrete subject to high temperatures," Materials and Structures, RILEM, Vol. 36, October 2003, pp. 515–521
4. Suhaendi, S.L. Suto, M. and Horiguchi, T. 2006. "Optimization of Polypropylene Fibres for High Strength Concrete under High Temperature Condition," Proceedings of the 10th East Asia Pacific Conference on Structural Engineering and Construction, Vol. 6, 467–472.
5. Suhaendi, S.L, Shimura, K. and Horiguchi, T. 2006. "Non-Destructive Test of Heated

- Fibre Reinforced High Strength Concrete,” Proceedings of the Japan Concrete Institute, JCI, Vol. 28, No. 1, 407–412.
6. Kitsutaka, Y. 1997. “Fracture Parameters by Poly-Linear Tension Softening Analysis,” Journal of Engineering Mechanics, ASCE, Vol.123, No.5, 444–450.
 7. Japan Concrete Institute Research Committees. 2003. “Method of test for load displacement curve of fibre reinforced concrete by use of notched beam,” JCI-S-002-2003, Japan Concrete Institute.
 8. Felicetti, R. et al. 1996. “Residual Mechanical Properties of High-Strength Concrete Subjected to High-Temperature Cycles,” Proceedings, 4th International Symposium on Utilization of High Strength/High Performance Concrete, Paris, France, pp. 578–588.

Pore Pressure Measurement Inside Hybrid Fibre-Reinforced High Strength Concrete Under High Temperature Condition

M. R. BANGI and T. HORIGUCHI

ABSTRACT

Pore pressure development inside high strength concrete when exposed to fire plays a key role in the thermal instability of concrete. Addition of organic fibres to high strength concrete has been widely used as an effective measure for mitigating explosive spalling of concrete. However, pore pressure development in relation to the severity of fire in high strength concrete is not clearly understood.

In this paper, we investigate the pore pressure development in a series of concretes containing Polypropylene (PP) fibres, Steel Fibres (SF) and Hybrid Fibres (HF) with all fibre-reinforced concretes containing 0.1 % (0.9 kg/m^3) by volume of PP fibres. Three different rates of heating have been studied and the pore pressures at various depths inside concrete have been measured.

The experimental results show that addition of PP fibres is very effective in mitigating of explosive spalling of high strength concrete. However, it is observed that in the deeper regions of concrete, a dosage 0.1% (0.9 kg/m^3) by volume of PP fibres is not sufficient for pore pressure reduction under a fast heating rate but is adequate for slow and moderate heating rates. Furthermore, it is observed that increasing the heating rate leads to an increase in the pore pressure which is in agreement with classical theoretical considerations and that during a fast heating rate, Hybrid Fibres is more effective in pore pressure reduction in the deeper regions of concrete compared to PP fibres.

Mugume Rodgers Bangi, Graduate Student, Laboratory of Environmental Material Engineering, Graduate School of Engineering, Hokkaido University, Japan.

Takashi HORIGUCHI, Associate Professor, Laboratory of Environmental Material Engineering, Graduate School of Engineering, Hokkaido University, Japan.

1. INTRODUCTION

Concrete should perform well under high temperature condition compared to other construction materials such as wood and steel due to its high incombustibility, good insulation and low thermal diffusivity which decreases with increase in temperature. However, many studies have shown that concrete has a high occurrence of thermal instability in form of spalling which leads to breaking off of layers or pieces of concrete from the thermally exposed surface which greatly compromises the structural integrity of the concrete structures [1, 2]. In particular High strength concrete is susceptible due to its low water cement-ratio which produces a dense and almost impervious microstructure [3], which keeps the moisture vapour from escaping in a high temperature environment resulting in build-up of pore pressure in the cement paste and hence spalling. Thus the material behavior of High Strength concrete under fire exposition needs to be clearly understood since it greatly impacts on structural integrity and load—bearing capacity of structural elements.

Two main theories have been presented to explain the occurrence of spalling in concrete. Moisture clog spalling theory was presented by Harmathy [4] which explained spalling as a moisture phenomenon while thermal stress spalling has been presented which relates to thermal expansion gradients of concrete [5].

Moisture clog spalling theory (also called thermal-hydral process) has been studied by many researchers by measuring the build—up of pore pressure inside concrete exposed to high temperature environment [6, 7]. However, findings by some researchers [8, 9] are not in agreement with classical theoretical considerations of the effect of heating rate on pore pressure development in concrete. The purpose of this experimental study is to measure the build—up of pore pressure at different depths inside concrete as well as the effect of heating rate on pore pressure development.

The study involves the analysis of the thermal—hydral process of different series of concretes at 10, 30 and 50 mm depth using three heating rates of slow, moderate and fast heating.

2. EXPERIMENTAL DETAILS

2.1 Materials and Mix Proportions

Six series of concretes were prepared using OPC (Ordinary Portland Cement) and crushed stone with the maximum nominal size of 13 mm. Some parameters of the mix proportion were kept constant for all series: W/C of 30 %, water content of 170 kg/m³ and sand to aggregate ratio (s/a) of 50%. Addition of polypropylene (PP) fibres, steel fibres and a combination of polypropylene and steel fibres was the main differentiation of the series. Two types of steel fibres were used in this experimental study and the fibre properties are as shown in Table I. A polycarboxylate ether hysplasticizer was used at a dosage of 0.9 % of cement content to achieve the desired workability (slump of 150-175 mm). Concrete mix proportions of all series cast are shown in Table II.

TABLE I. CHARACTERISTICS OF FIBRES.

	Polypropylene	Steel (S13)	Steel (S30)
Diameter (mm)	0.018	0.16	0.6
Length (mm)	6	13	30
Shape	Filament	Straight	Indent
Density (gr/cm ³)	0.9	7.8	7.8
T _{melt} (°C)	160-170	1370	1370
T _{vaporize} (°C)	341	-	-

TABLE II. MIXTURE PROPORTIONS.

Series	W/C (%)	s/a (%)	Fiber vol. (%)			W	C	S	G	SPAE*1 (%×c)
			PP	(S30)	(S13)					
Plain	30	50	-	-	-	170	567	796	781	0.9
PP			0.1	-	-			795	780	
HY1				0.3	-			790	776	
HY2				0.5	-			788	773	
HY3				0.2	0.1			790	776	
HY4				0.4				788	773	

SPAE*1: Super plasticizer and air entraining agent

Specimens in form of 100×200 mm and 175×100 mm were cast for strength and pore pressure tests respectively. After casting, the specimens were covered with wet burlap under polyvinyl sheet. After 24 hours, the specimens were remolded and cured under lime-saturated water at temperature of $20 \pm 2^\circ\text{C}$ for 28 days and 3 months for strength and pore pressure tests respectively.

2.2 Experimental Procedures

All specimens tested during pore pressure measurement experiment were 175 mm in diameter and 100 mm in height. Thermal load was applied on one face of the concrete specimen by means of a computer-controlled radiant heater of power 500 watts placed 10 mm above the specimens. Ceramic fibre was used to heat-insulate the lateral faces of the specimens to ensure quasi-undirectional thermal load upon it.

Three heating patterns were applied in the experiment. The first pattern, a slow heating rate ($5^\circ\text{C}/\text{min}$), where the temperature is increased gradually at a rate of $5^\circ\text{C}/\text{min}$ until it reaches the maximum temperature of 600°C . Then this maximum temperature is maintained for a few hours. The second pattern, a moderate heating rate ($10^\circ\text{C}/\text{min}$), is applied in the same manner as the slow rate but at a rate of $10^\circ\text{C}/\text{min}$. The third pattern, a fast heating rate was conducted by thermally shocking the specimen after the heating device has reached the designated maximum temperature of 800°C . The specimen was exposed to the maximum temperature of 800°C lasting for a few hours. The three heating patterns and ISO 834 pattern are shown in Figure 1.

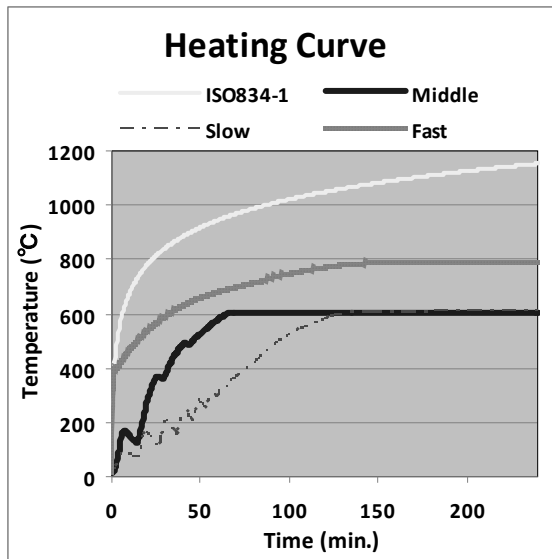


Figure 1. Heating patterns for pore Pressure measurement test and ISO 834.

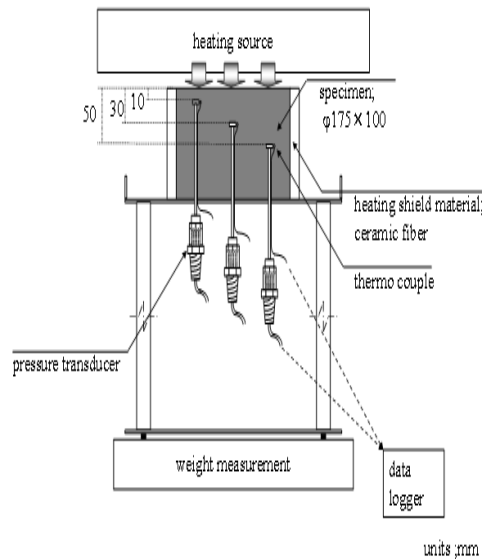


Figure 2. Experimental test set-up.

All specimens were instrumented with pressure gauges that allow pore pressure measurements. The gauges were made of a disk of porous sintered metal ($\varnothing 12 \text{ mm} \times 4 \text{ mm}$) encapsulated into a metal cup that was brazed to a metal tube with inner diameter of 1.5 mm. The free end of the tube then stuck out at the rear face of the specimen. Three gauges were placed within the central zone of the specimen at 10, 30 and 50 mm respectively, from the heated face. Thermocouples were attached on the sides of the gauges which were used to measure the temperature inside the heated specimens. The set up of the experimental test is shown in Figure 2.

After casting, specimens were cured inside lime-saturated curing tank for at least 3 months in order for a homogenous moisture state to be achieved. Prior to heating, all gauges were filled with silicon oil.

3. RESULTS AND DISCUSSIONS

3.1 Specimens' Properties

There was no significant difference observed in the properties of concrete specimens for all series as shown in Table III. Compressive strength increase of 25 % and 15% was observed for PP and Hybrid concrete respectively, compared with plain concrete.

3.2 Thermal Instability

For all concrete series tested, explosive spalling was only observed in plain concrete during a slow heating rate at 10 mm depth with a maximum pore pressure of 4.009 MPa as shown in figure 3(a). This can be seen as a sudden drop in pressure from 3.8 MPa to 0 at a depth of 10 mm caused by the breaking-off of pieces of

TABLE III. FRESH AND HARDENED PROPERTIES OF CONCRETE.

Series	FRESH PROPERTIES		HARDENED PROPERTIES		
	Slump (mm)	Air content (%)	Density (g/cm ³)	fc (MPa)	E (GPa)
Plain	215	3.5	2.42	84.1	40.4
PP	208	2.1	2.47	105.0	35.7
HY1	145	3.0	2.47	96.3	43.3
HY2	178	3.3	2.46	94.6	37.4
HY3	195	3.2	2.46	96.2	35.5
HY4	193	1.6	2.50	95.4	37.7

concrete from the heated surface which resulted in moisture vapour rapidly escaping to the atmosphere and hence an abrupt drop in pore pressure. For all other specimens which did not spall, bell—shape pressure curves were observed which are explained by the moisture clog spalling theory [4] which describes the hydra—thermal behavior of concrete when exposed to fire as a formation of fully saturated layer during moisture migration towards deeper colder regions which prevent further migration of moisture vapour leading it to move towards the exposed side of concrete. This causes the region of concrete between the moisture clog and exposed side to dry and dehydrate and when the rate of vapour escaping from the pores exceeds that filling the pores, the pressure starts to drop hence the bell—shaped pressure curves.

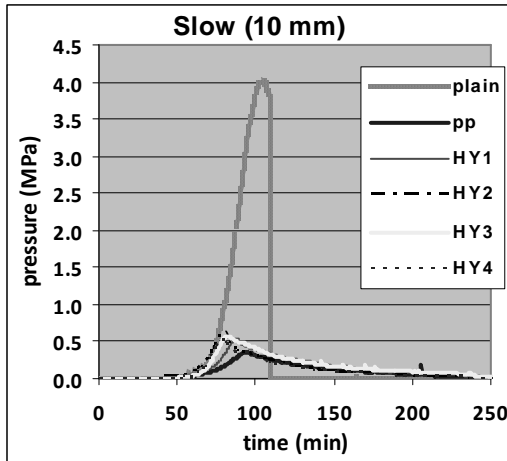
3.3 Build – up Pore Pressure

Figure 3 shows the evolution of pore pressure measured during slow and fast heating rates at different depths for different concrete series. It can be clearly observed that the maximum pressure in plain concrete for all heating rates at all depths is higher than that of PP and HY concrete series. This clearly shows the effectiveness of PP fibres in mitigating the build – up pore pressure in concrete and thus addition of PP fibres plays a significant role in the mitigation of explosive spalling of concrete under exposure to a high temperature environment.

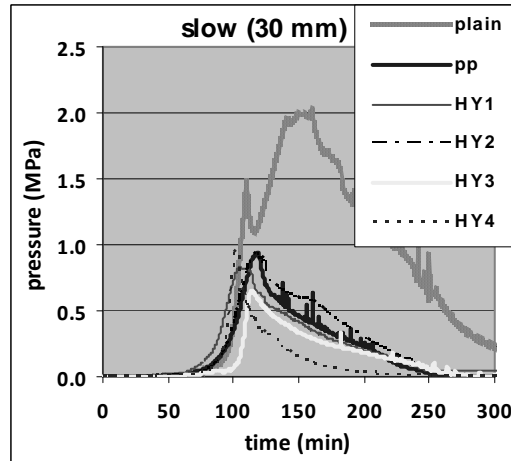
Furthermore, it can be observed in figure 3 (b) and (c) that pore pressure in plain concrete at 50 mm depth of 2.17 MPa after 234 minutes is slightly higher than that at 30 mm depth of 2 MPa after 160 minutes. This shows that even after the initial spalling, if concrete continues to be exposed to high temperature, pore pressure will again build – up with time in the deeper undamaged regions which will lead multiple spalling of layers of concrete occurring.

3.4 Effect of Heating Rate

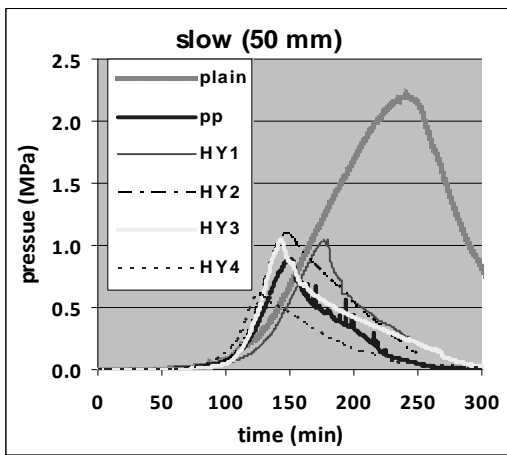
In PP concrete series as shown in figure 4, it was observed that pore pressure near the surface of concrete (10 mm depth) is nearly the same for both slow and fast heating rates at 0.3 and 0.35 MPa respectively. However, it was observed that in deeper regions of concrete (50 mm depth), a fast heating rate leads to a much higher



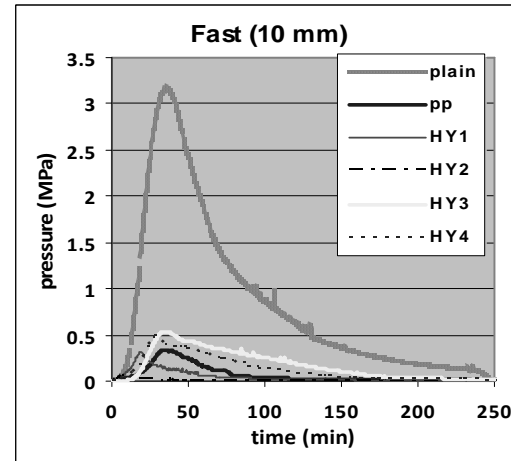
(a) Slow heating rate at 10 mm depth



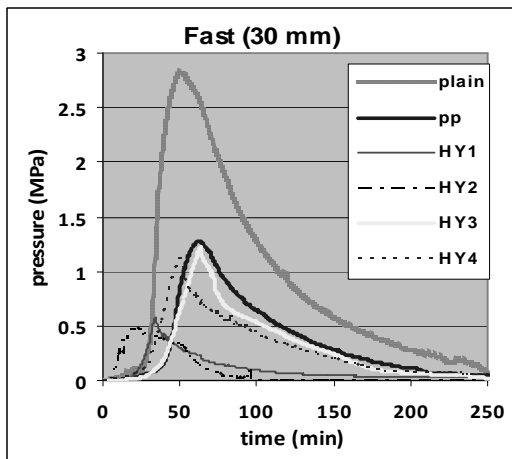
(b) Slow heating rate at 30 mm depth



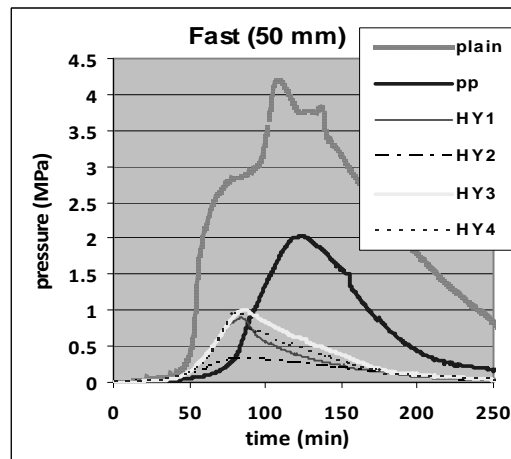
(c) Slow heating rate at 50 mm depth



(d) Fast heating rate at 10 mm depth



(e) Fast heating rate at 30 mm depth



(f) Fast heating rate at 50 mm depth

Figure 3. Build – up of pore pressure with time for slow and fast heating rate at different depths of concrete.

pore pressure of 2 MPa which is more than twice that of a slow heating rate at 0.9 MPa. This clearly shows that a fast heating rate leads to higher pore pressure in the deeper regions of concrete compared to a slow heating rate. Pore pressure near the surface being nearly the same for both heating rates is because of surface cracking of concrete which was observed on concrete specimens exposed to a fast heating rate which resulted in water vapour escaping and thus a low build-up in pore pressure near the surface compared to deeper regions of concrete under a fast heating rate. Otherwise if there was no surface cracking during a fast heating rate, it is expected that pore pressure would increase with increasing heating rate for all regions of concrete. Thus pore pressure development in concrete is highly dependent on the severity of the fire which affects the rate and the amount of vapour migrating to the inner regions of concrete and thus surface cracking is a very important aspect of the fire severity. It can also be observed that this fire severity dependent degradation of concrete is limited to a relatively thin layer of concrete near the heated surface but will increase slowly with increasing time of exposure to fire.

Furthermore, it was observed that 0.1 % (0.9 kg/m³) dosage of only PP fibres is not sufficient in pore pressure reduction for a fast heating rate since a high pore pressure of 2 MPa was measured in PP concrete series. Thus there is need to increase the optimum PP fibre volume in relation with increasing severity of fire if only PP fibres are added to concrete.

3.5 Role of Steel Fibres in Pressure Reduction

Comparing PP and Hybrid concrete series under a fast heating rate as shown in figure 3 (f) , it was observed that in deeper regions (50 mm depth) the pore pressure in Hybrid concrete series with a maximum pore pressure of 1.0 MPa reduces to at least half(½) that in PP concrete at 2 MPa. This clearly shows that addition of steel fibres plays some role in pore pressure reduction in deeper regions of concrete under a fast heating rate. According to figure 3 (c) and (f), HY2 and HY4 series

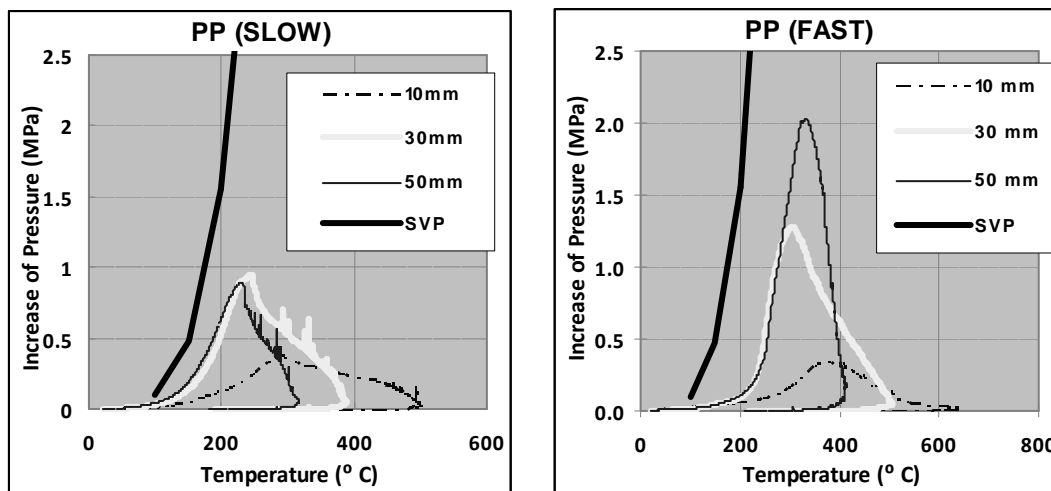


Figure 4. Build – up of pore pressure with temperature in PP concrete for slow and fast heating rate at different depths of concrete.

shows the lowest pore pressure of 0.3 and 0.6 MPa for a fast and slow heating rate respectively in the deeper regions of concrete. This means that higher volume of steel fibres of 0.5 % is more effective in pore pressure reduction than that of 0.3 %.

4. CONCLUSIONS

The experimental results showed that PP fibres are very effective in mitigating the build-up of pore pressure inside concrete. Steel fibres were found to contribute to pore pressure reduction in the deeper regions of concrete during exposure to a fast heating rate with a higher volume of 0.5 % of steel fibres being more effective compared to a lower volume of 0.3 %.

Pore pressure development inside concrete is highly influenced by the severity of fire with pore pressures increasing with increasing heating rate specifically for deeper regions of concrete. Also increased heating rate greatly leads to degradation of concrete through surface cracking which in turn affects the amount of pore pressures measured near the surface of concrete under a fast heating rate. This is the reason why pore pressures are often observed to be higher during lower heating rates compared to higher heating rates [9]. However, the surface cracking degradation is limited to a relatively thin layer of concrete.

Multiple spalling of layers of concrete will occur if concrete continues to be exposed to high temperature with time even after the initial spalling has already occurred.

REFERENCES

1. Suhaendi S.L. and Horiguchi T., “Explosive spalling mitigation mechanism of fiber reinforced high strength concrete under high temperature condition”, Proceedings of the International fib Workshop on Fire Design of concrete structure (2008), p. 189–197.
2. Suhaendi S.L. and Horiguchi T., “Effect of short fibers on residual permeability and mechanical properties of hybrid fibre reinforced high strength concrete after heat exposition”, Cement and Concrete Research, vol.36, Issue 9 (2006), p. 1672–1678.
3. Komen J., Vesa P., “effects of high temperature on the pore structure and strength of plain and polypropylene fiber reinforced cement pastes, fire technology, 39, 2003.
4. Harmathy T.Z., “Effect of moisture on the structural endurance of building materials”, Moisture in Materials in Relation to Fire Tests, ASTM special Technical Publication No. 385, p. 74–75 , 1965.
5. Bazant Z.P., “Concrete at High Temperature and its interactions with Fracture” Recent progress”, Concreep-7 Conference: Creep, shrinkage and durability of Concrete and concrete structures, p. 449–460, 2005.
6. Phan T.L., “High – strength Concrete at High Temperature—An Overview” Utilization of High Strength/High performance Concrete, 6th International symposium. Proceedings. Volume 1. June 2002, Leipzig, Germany.
7. Kalifa P., Menneteau F.D., Quenard D., “Spalling and Pore Pressure in HPC at high temperatures” Cement and Concrete Research 30 (2000), p. 1915–1927.
8. Jansson R., “Material properties related to fire spalling of concrete”, Report TVBM – 3143 (Lund 2008).
9. Mindeguia J.C., Pimienta P., La Borderie C. and Carre H., “Experimental study of fiber behavior of different concretes – thermo – hydal and spalling analysis”, fib Task 4.3 workshop “Fire Design of Concrete Structures— From Materials Modelling to Structural Performance” (University of Coimbra, Portugal, November 2007), p. 225–236.

The Application of RGB Histogram Analysis of Colour Images as a Method of Assessing the Condition of Concrete in Structures after Fire

I. HAGER

ABSTRACT

A new method was developed using image analysis to estimate the temperature and residual compressive strength of concrete in structures subjected to fire. The method is based on an observed property of concrete which changes colour under the influence of heat. The colour change is primarily a result of a gradual dehydration of the cement paste, but also of transformations occurring within the aggregate.

During testing, concrete was observed to change colour upon heating and the change was measured using Scion Image v. 4.0.3, an image analysis software package (Scion Corporation ©, USA). In the proposed method the digital image is split into three RGB colour components: red, green and blue, which are then presented as a histogram using counts of pixel intensity. The histogram results show colour distributions in unheated concrete and in concrete heated across a temperature range from 100 to 1000 °C. Histograms from laboratory heated concrete provide a scale, which is then used to determine the temperature actually reached by concrete in a structure by comparing the scale images with images of cored samples taken from the structure.

The method offers a simple and inexpensive way of identifying the areas affected by different temperatures. When the information obtained on temperature is compared to the relationships established between the residual compressive strength of concrete and temperature, the method can efficiently diagnose the condition of a concrete structure affected by fire. The paper presents the results of a preliminary test carried out on high performance concrete (HPC) with natural river-bed aggregates which illustrates the methodology of testing.

Izabela Hager, Ph.D., Institute of Building Materials and Structures, Cracow University of Technology, ul. Warszawska 24, 31-155 Cracow, Poland, e-mail: ihager@pk.edu.pl

INTRODUCTION

The diagnosis of damage to concrete in a structure normally begins with a general check of the concrete for the presence of flaking, cracking, or colour change caused by heating [1, 2, 3, 4]. A detailed assessment of the colour change in concrete can be a sufficiently precise tool to estimate the temperature that the material was exposed to during a fire [5,6,7,8]. The assessment also allows the identification of the extent of damage on the surface (surface colour analysis) and in depth (core colour analysis).

The existing technique of rough estimation of the temperature to which concrete was subjected involves an inherently subjective visual colour analysis. It is generally agreed [8], that when heated up to between 300 and 600°C concrete will turn red, between 600 and 900°C it will turn whitish-grey, and heating to between 900°C and 1000°C gives the concrete a buff colour. The red colouration in the temperature range of 300 and 600°C is caused by the oxidation of mineral components with iron compounds (oxides or hydroxides, etc.).

Two different approaches can be used when assessing the condition of concrete after a fire using image analysis:

a) a surface analysis is performed which involves the external layer of the concrete element (cement paste). By looking at the surface colour change one can assess the extent of the temperature impact. This method is not feasible if the surface is affected by smoke or covered with soot.

b) a surface with the signs of spalling or core surface. The observation involves surfaces with aggregate grains exposed or a cut surface produced as a result of boring. The cutting of the concrete reveals grains of aggregate that also change colour during heating and some aggregates change into more intense colours than the does the cement paste.

Colour changes observed in concrete during heating are mainly caused by dehydration and chemical reactions in the mineral components of the aggregate and the cement paste. The most intense colour change is observed in components containing minerals including iron (jarosyte, goethite). As temperature rises aggregates and components containing calcium carbonate CaCO_3 go through the process of calcination and their colour is dominated by pale shades of white and grey.

Colour changes caused by temperature within construction concrete are easy to identify by visual comparison with details unaffected by high temperature. However, costly measurement equipment and/or colour analysis computer software is often necessary to perform precision measurements. Various authors who analysed the change of heated concrete to assess its condition used tools such as a spectrophotometer applied directly to the concrete surface [5] or a polarising microscope equipped with a colour analysing software package [8]. Other authors [6, 7] took digital images of the surface of the concrete sample and analysed them with computer programmes. The latter method, however, requires consistent lighting, which is difficult to achieve and the white balance of the camera has to be adjusted. [6].

Colour change is not directly related to the change of mechanical and physical properties of concrete, but provides an indicator of the temperature achieved by the concrete sample. Temperature data can, however, be used for a quantitative estimation of properties such as the compressive strength or modulus of elasticity.

MATERIALS AND METHODS

The testing was performed on high performance concrete (HPC). It consisted of the cement type CEM II/A-V 42.5R (478 kg/m³), water 129 kg/m³ and natural river-bed aggregates: sand 0-2 mm

(623 kg/m³), gravel 2-8 mm (660 kg/m³) and gravel 8-16 mm (550 kg/m³). A plasticiser admixture allowed to produce a concrete with w/c=0.27.

The colour change observation was performed on the concrete sample surface (cement paste) and on a surface with the aggregate visible (cut surface). The samples were heated at a constant rate of 1°C/min. to reach subsequent temperatures of 100, 200, 300, 400, 500, 600, 700, 800, 900 and 1000°C.

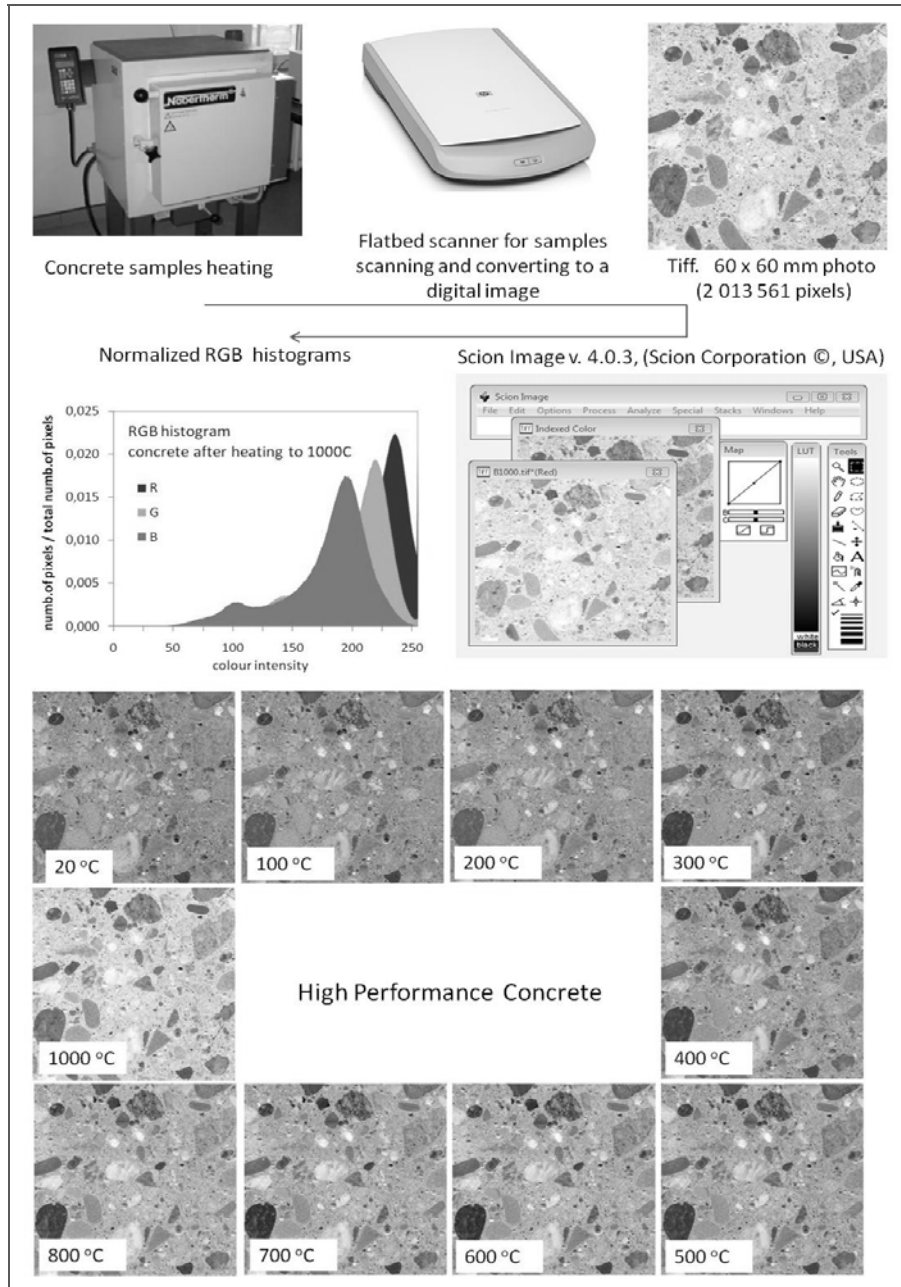


Figure 1. Testing procedure.

After cooling digital images were taken from the sample surfaces. To achieve consistent lighting conditions the sample surfaces were scanned with a general purpose scanner (HP Scanjet G2410). The pictures were taken at 600ppi. The images were then exported in .tiff raster files into the Scion

Image package v. 4.0.3, (Scion Corporation ©, USA). The package is a freeware tool created for medical purposes and facilitating digital image analysis. It features an option to export the results in a text file for further processing. The testing was based on the RGB (Red, Green, and Blue) colour model because of its widespread use in digital equipment (scanners and computer screens). The model is of the additive type, where colours are produced by adding the RGB components.

The digital image was decomposed into the RGB components using Scion Image. The frequencies of occurrence of red, green and blue pixel components were presented as frequency histograms. The RGB model assumes intensity levels ranging from 0 to 255 that are shown on the horizontal axis. On the vertical axis the numbers of pixels of a certain intensity in an image are presented. The testing procedure is presented in details on Fig. 1.

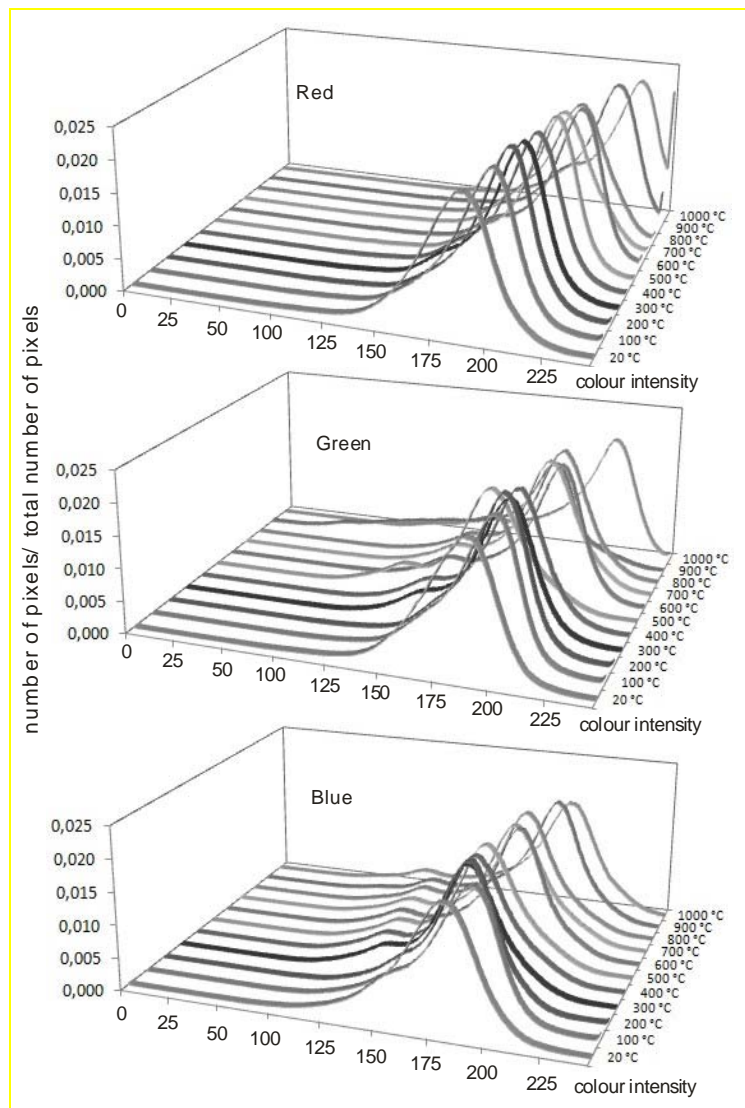


Figure 2. Normalised histograms of the Red, Green and Blue components from images of unheated concrete samples (20oC) and samples heated to temperatures ranging from 100 to 1000°C.

The testing involved a normalisation process where the values corresponding to the number of pixels with a specified intensity were divided by the total number of pixels in a given image. Histogram normalisation makes comparison of images with different pixel counts easier. Additionally the process produces functions that have properties of the probability density function. Histograms can be used to generate a number of parameters defining the properties of this function, including the maximum and standard deviation values, curtosis, etc.). Differences between these parameters reflect different properties of the image histogram and allow comparisons. In this case the comparisons are between concrete samples damaged during a fire and a test sample produced in a laboratory.

The results of the testing of the impact of heating temperature on the colour change in concrete are presented in normalised histograms of the RGB components (Fig. 2). For each of these function graphs, maximum and standard deviation values were determined for each of the tested temperatures. The values were shown as a function of temperature on graphs (Fig. 3a and 3b). The graph shows a comparison of maximum and standard deviation value profiles from the analysis of images of three samples. Individual sets of the three curves suggest a high degree of uniformity in the properties determined.

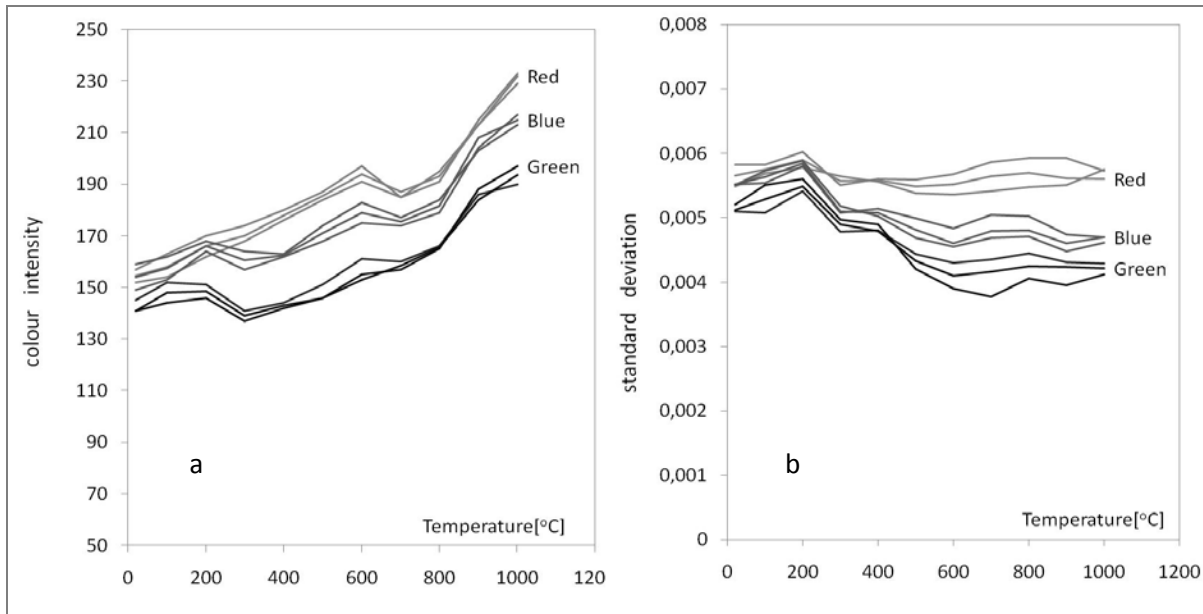


Figure 3. A comparison of change profiles of a) maximum value of intensity and b) standard deviation values obtained in the test of three concrete samples in the range of temperatures from 20 to 1000°C.

The samples were tested in compression in order to determine a relationship between the changes in colour and changes in the strength parameters of the material concerned. To this end samples in the form of a 15 cm cube were heated at a rate of 1°C/min. to reach the target temperatures of 200, 400, 600 and 800°C. Once the temperature was reached the samples were heated for five more hours to stabilise the temperature across the section. The samples were then cooled down to 20°C and tested in compression. The chart on Fig. 4. shows the average residual compressive strength of tested HPC concrete (each value is a average of two results) .

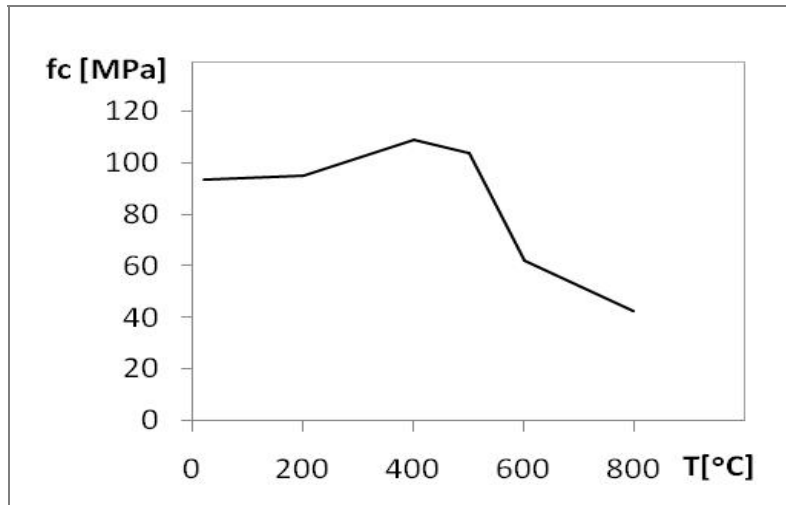


Figure 4. Residual compressive strength of concrete as a function of temperature.

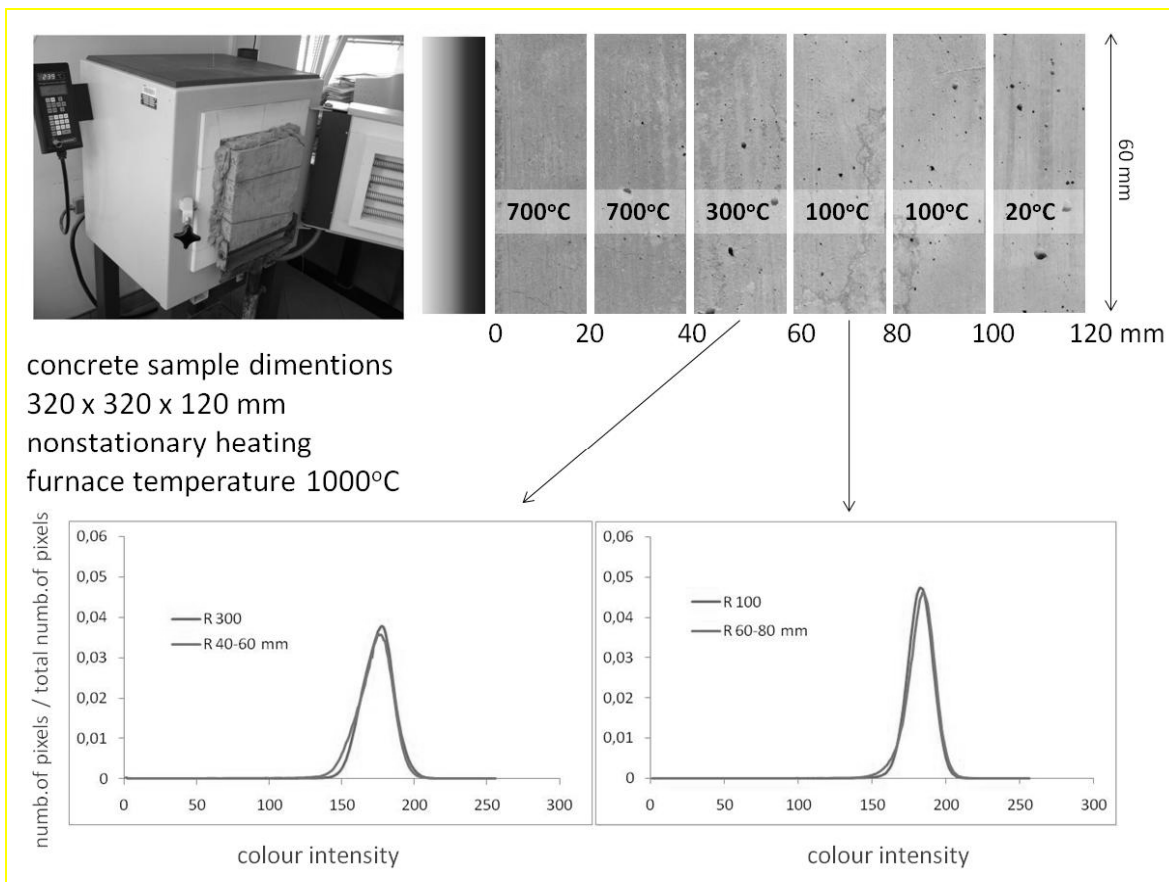


Figure 5. Concrete block heating procedure, images of its individual layers and estimated temperatures of the layers, as determined by a comparison of the normalised histograms of the model sample and the red (R) colour histograms in each layer.

APPLICABILITY OF THE TEST RESULTS TO THE ESTIMATION OF THE TEMPERATURE TO WHICH CONCRETE HAS BEEN EXPOSED

During a real fire, temperatures within a concrete section do not generally reach equilibrium values. A thermal gradient is established with the temperature of the outside layers being drastically increased, while the temperatures of the inner concrete may be low. Preliminary testing was performed to verify the applicability of the technique in the assessment of the condition of concrete exposed to fire. A concrete block was heated in transient heating conditions to develop a temperature gradient inside. The block side surface was then scanned (HP Scanjet G2410) producing an image.

The image was divided into strips sized 20 mm by 60 mm representing layers. RGB component histograms were obtained and normalised using the image analysis procedure described above. The result was compared with a scale. The scale had been prepared for a sample surface heated across the 100°C to 1000°C. temperature range. The comparison yielded values allowed to reveal the temperature to which the concrete block had been heated in each 20 mm strip. Fig. 5 presents the way the concrete block was heated, its images and the estimated temperatures of the layers by using developed technique.

CONCLUSIONS

The results described in the paper confirm the usefulness of the proposed method of estimating the condition of concrete using an analysis of a colour image of a sample heated to a high temperature.

A scanner is also a useful and simple tool to make digital images of the samples/cores with guaranteed consistent lighting conditions and it requires no special preparation of the samples. A similar degree of usefulness and simplicity was established with regard to the colour analysis using the RGB model and the readily available software package Scion Image.

A calibration scale was produced by taking images of concrete samples heated to temperatures across the 100–1000°C range. The scale can be used to estimate the exposition temperature of concrete in structures subjected to a real fire.

REFERENCES

1. “Présentation des techniques de diagnostic de l'état d'un béton soumis à un incendie, n°62, Laboratoire Central des Ponts et Chaussées“, Paris, France, 2005, p. 114.
2. “Assessment, Design and Repair of Fire-Damaged Concrete Structures“, *Technical Report No.68*, The Concrete Society, London, United Kingdom, 2008, p.80.
3. “Fire design of concrete structures—structural behavior and assessment“. *State-of-art report prepared by Task Group 4.3, “Fire design of concrete structures“*, FIB - Federation International du Béton, 2008, p. 209.
4. Hager, I., “Methods for assessing the state of concrete in fire damaged structures“, *Cement Lime Concrete*, July / August 2009, nr 4, p. 167–178.
5. Annerel E., Taerwe L., “Reveling the temperature history in concrete after fire exposure by microscopic analysis“, *Cement and Concrete Research* 39 (2009).
6. Felicetti, R. “Digital camera colorimetry for the assessment of fire-damaged concrete“, in: P.G. Gambarova, R. Felicetti, A. Meda, P. Riva, *Proceedings of the Workshop: Fire Design of Concrete Structures: What now? What next? fib Task Group 4.3 ‘Fire Design of Concrete Structures’*, Milan, 2004, pp. 211–220.
7. Luo H. L., Lin D.F. “Study the surface color sewage sludge mortar at high temperature“, *Construction and Building Materials* 21 (2007), p 90–97.
8. Short N. R., Purkiss J. A., Guise S. E., Assessment of fire damaged concrete using color image analysis, *Construction and Building Materials*, Vol. 15 (2001) p. 9–15.

On High-Temperature Properties of Structural Shotcrete Containing Different Accelerating Agents

P. BAMONTE, P. G. GAMBAROVA and A. NAFARIEH

ABSTRACT

Shotcrete has been increasingly used in the past years as a structural material for the construction of the final lining in blasted tunnels, and a number of subway, pilot and service tunnels demonstrates the reliability of this technique. To consider shotcrete as a true structural material, however, its fire resistance should be ascertained, something not adequately done so far. In this project, three mixes (C1 containing an accelerating agent based on sodium-silicates, and C2F/C2 with/without steel fibers containing sulpho-aluminates) are thermally and mechanically characterized after being exposed to high temperature. The results show that (a) the alkali-based mix is more temperature-sensitive than the alkali-free mixes; (b) alkali-free mixes are less porous, but steel fibers increase their porosity; (c) the thermal diffusivity decreases with the introduction of the fibers and with the use of alkali-based agents; and (d) there are no major differences between the high-temperature mechanical behaviors of ordinary vibrated concrete and alkali-free shotcretes.

INTRODUCTION

Shotcrete is often considered a minor offshoot of structural concrete, since it is often used in provisional structures or to fill intentional/unintentional gaps in R/C structures or even to insulate fire-sensitive members. However, in a number of countries—like U.K., Austria, Germany and Switzerland—shotcrete is increasingly used as a structural material, in the construction of the final lining in road and railway tunnels, as well as in pilot and service tunnels.

Since in road tunnels fire is certainly the most dangerous load condition, knowing shotcrete thermal and mechanical properties during and after a fire is preliminary to any safe use of this material, something that has never been done to date, at least in a systematic way, in spite of the many studies devoted so far to shotcrete (see – for instance – [1-6]).

The limited knowledge of shotcrete behavior at high temperature is also detrimental to the structural analysis of shotcrete linings, since the first layer sprayed on the rock surface and incorporating—in many cases—steel ribs, the intermediate sprayed-on water-polymeric membrane and the second shotcrete layer lead to a “composite” structure, whose thermal behavior raises a number of issues [7].

Patrick Bamonte, Pietro G. Gambarova, Alireza Nafarieh; Dept. of Structural Engineering, Politecnico di Milano, Piazza Leonardo da Vinci 32, 20133 Milan, Italy

Being a cementitious material, shotcrete is likely to have a high-temperature thermo-mechanical behavior similar to that of ordinary vibrated concrete, but the larger amount of cement and fine aggregates generally found in shotcrete, as well as the relatively-high content of accelerating agents, may alter its behavior at high temperature and in fire.

Within this context, the thermal and mechanical properties at high temperature of three shotcrete mixes are investigated in this research project ($T = 20-750^{\circ}\text{C}$), following two preliminary studies [8,9]. The first mix refers to a low-strength concrete (Mix C1, C24/30, actual core strength $f_c = 20$ MPa) containing an accelerating agent based on sodium-silicates, while the two remaining mixes refer to high-quality concretes (Mixes C2 and C2F, C36/45, actual core strength $f_c = 45-50$ MPa), whose accelerating agent is based on sulpho-aluminates (*alkali-free* agent). The mix designs of Mixes C2 and C2F are the same, but the latter contains steel hooked fibers (Table I). All shotcretes were sprayed according to the wet process.

Beside the compressive strength, the elastic modulus, and the stress-strain curves in compression (all in residual conditions, i.e. past cooling), the density, the thermal diffusivity and the porosity were evaluated on concrete cores extracted from shotcrete slabs.

SPECIMENS

Mix-design and expected compressive strength of the virgin materials

The shotcretes considered in this project are used in the construction of the first-phase lining of the main tunnel of Turin Automatic Subway (Mix C1) and of the service tunnels of the soon-to-be excavated Railway Brenner Base Tunnel (Mixes C2 and C2F), through the Alps, between Italy and Austria.

In the latter case, the service tunnels are bored by rock blasting, to connect the building sites to the pilot tunnel (now under construction).

With reference to Mix C1, the mean compressive strength expected at 28 days was close to 20 MPa, but decreased to 12, 7 and 6 MPa at 44, 94 and 154 days, something not unusual in shotcretes containing sodium-silicates.

Concrete	C1	C2	C2F
Cement Portland "c" [kg/m^3]	450	450	450
Sand (0-4) [kg/m^3] *	1500	1324	1314
Aggregate (4-8) [kg/m^3] *		336 [^]	336 [^]
Added water [kg/m^3] (w/c)	230 (0.51)	198 (0.44)	198 (0.44)
Superflux [kg/m^3] (sp/c)	0	4 (0.9%)	4 (0.9%)
Sulpho-Aluminates [kg/m^3] (sa/c)	0	29 (6.4%)	29 (6.4%)
Sodium-Silicates [kg/m^3] (ss/c)	45 (10%)	0	0
Fibers [kg/m^3] (v_f)	0	0	30 (0.4%)
Nominal/actual mass [kg/m^3]	2225/2109'	2341/2222''	2361/2226''
Expected strength f_c at 28 days	20 MPa	40 MPa	40 MPa
Actual strength at the beginning of the tests	12 MPa'	50 MPa''	45 MPa''

TABLE I. Mix designs. (*) Dry-surface conditions with 2.0-2.2% of water by mass; (^) mixed natural aggregates; (^^) crushed granite; (') at 44 days; (') at 60 days.

As for Mixes C2 and C2F, the equivalent cylindrical strength at 28 days measured by testing cubes was 38/41 MPa, while the compressive strength measured in Milan at 60 days on slender cores extracted from special slabs made of the same shotcrete used in the building site was 50/45. The cubic strength of the base concrete measured in Milan after 90 days (51/53 MPa) confirmed the cylindrical strengths of the shotcrete at 60 days (50/45 MPa) and at 28 days (38/41 MPa), which means that there are no significant differences between the base concrete and the shotcrete on condition that the accelerating agent be alkali-free.

Casting of the specimens

The material for the specimens was collected directly in the building sites (automatic subway of Turin for Mix C1, and inside the Maults Nord Service Tunnel close to Bozen, Italy, for C2 and C2F). Shotcrete casting was performed according to typical on-site procedures.

The ready-mix concrete (base concrete) coming from an agitator truck was mixed with the accelerating agent, pumped through a pipeline and sprayed through a nozzle into wooden moulds, to produce the slabs (size: 40 × 40 × 20 cm).

During shotcreting, the moulds were oriented at about 45° to the horizontal. The spraying direction was approximately perpendicular to the bottom panel of the moulds. The spraying process continued until the thickness of each slab was a bit larger than the depth of the moulds; all the shotcrete in excess was scraped off.

The moulds filled with shotcrete were then brought to the laboratory of the Department of Structural Engineering in Milan, and a few days later the formwork was removed. The slabs were cured in moist conditions for 30 days ($T = 20^{\circ}\text{C}$; Relative Humidity $\text{RH} = 90\%$) and then were cored. The cores were kept in the same conditions for 30/45 days, and then were thermally cycled and tested.

The final diameter and length of the cores are 80 and 160 mm, respectively ($h/d = 2$). The extremities were ground and polished to guarantee both parallelism and planarity, according to ASTM C39-81 Standard.

For each mix, from 14 to 20 cores were extracted, as required by the temperature levels (four for Mix C1: 20, 200, 400 and 600°C; six for Mixes C2 and C2F: 20, 105, 200, 400, 600 and 750°C, Fig.1a) and by test repeatability (three cores per temperature). Six cores were set aside for measuring the thermal diffusivity.

In general, 8-9 cores were extracted from each slab. After being ground and polished, each core was weighed and visually inspected, and a few cores were discarded for want of homogeneity (large voids, lack of fine aggregates, partially-filled moulds...). However, the overall quality of the cores was very good.

It is worth noting that the mass per unit volume measured on the cores (*actual mass* in Table I) is slightly smaller (roughly -5/6%) than the theoretical mass resulting from the mix design. The difference is mostly due to the spraying process, since some water is expelled during shotcreting and porosity increases.

TEST PROGRAM AND RESULTS

Thermal cycles and mass loss

Prior to the mechanical tests, the specimens were subjected to a thermal cycle, in order to induce various levels of mechanical damage. Each cycle was carried out

in an electric furnace ($T_{\max} = 1000^{\circ}\text{C}$; size of the chamber 300 500 600 mm), and consisted of a heating phase at $+1^{\circ}\text{C}/\text{min}$, followed by a rest of 2 hours at the maximum temperature (“reference” temperature) and by a cooling phase at $-0.25^{\circ}\text{C}/\text{min}$ (Figure 1a). In this way no “structural” phenomena - such as self-stresses and spalling - occurred [10,11].

During the heating process, each specimen was weighed immediately before and after the thermal cycle to measure the mass loss (Figure 1b).

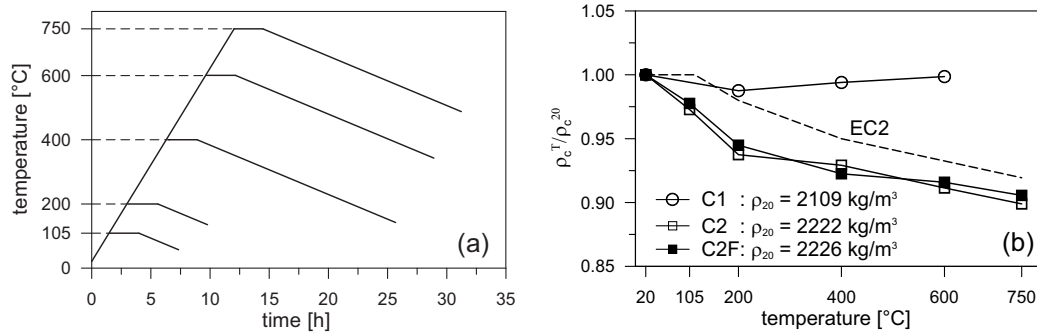


Figure 1. (a) Thermal cycles and reference temperatures (Mixes C2 and C2F); and (b) mass loss of the cores subjected to the thermal cycles (dashed curve = EC-2).

Test set-up

The displacement-controlled residual tests in compression were carried out by means of an electromechanical press (INSTRON, capacity 100 kN for Mix C1; SHENK, capacity 1000 kN for Mixes C2 and C2F). All tests were displacement-controlled and the control signal was provided by the LVDT located in the press.

The shortening of the specimen was monitored via 3 LVDTs connected by means of an elastic ring and placed at 120° astride the mid-height section (base length = 50 mm, Figure 2a).

The displacement rate of the press platens was 0.005 mm/s for both the loading and unloading processes; hence, in each test the mean loading rate up to the peak load was roughly 0.6 MPa/s (virgin specimens).

Stress-strain curves in compression

For each mix and for each reference temperature, three specimens were tested. In most cases the three tests exhibited a limited scattering, but in a few cases one test had to be discarded or further tests had to be run, because of the early failure of the specimen (loss of control right after the peak load, formation of diagonal bands) or for the blockage of the press during the loading process. One example of the repeatability of the tests is shown in Figure 2b (all other curves were less scattered). The mean curves (Figures 3a-c) were obtained by normalizing each single curve ($\epsilon_{c,\max}$ and ϵ_{c1}), by working out the mean normalized curve and by reconstructing the stress/strain curve on the basis of the mean values of both $\epsilon_{c,\max}$ and ϵ_{c1} .

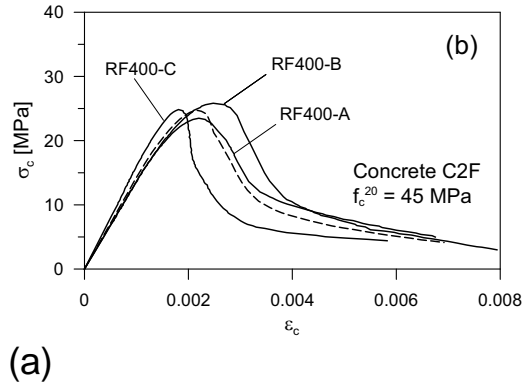
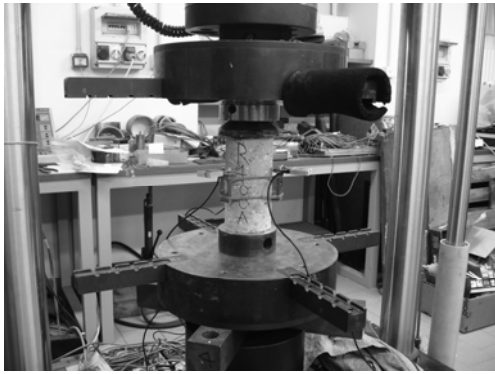


Figure 2. (a) Specimen placed under the press during a displacement-controlled compression test (Mix C1, INSTRON press, capacity = 100 kN); and (b) example of test repeatability after a cycle at 400°C (Mix C2F); the dashed curve is the mean curve.

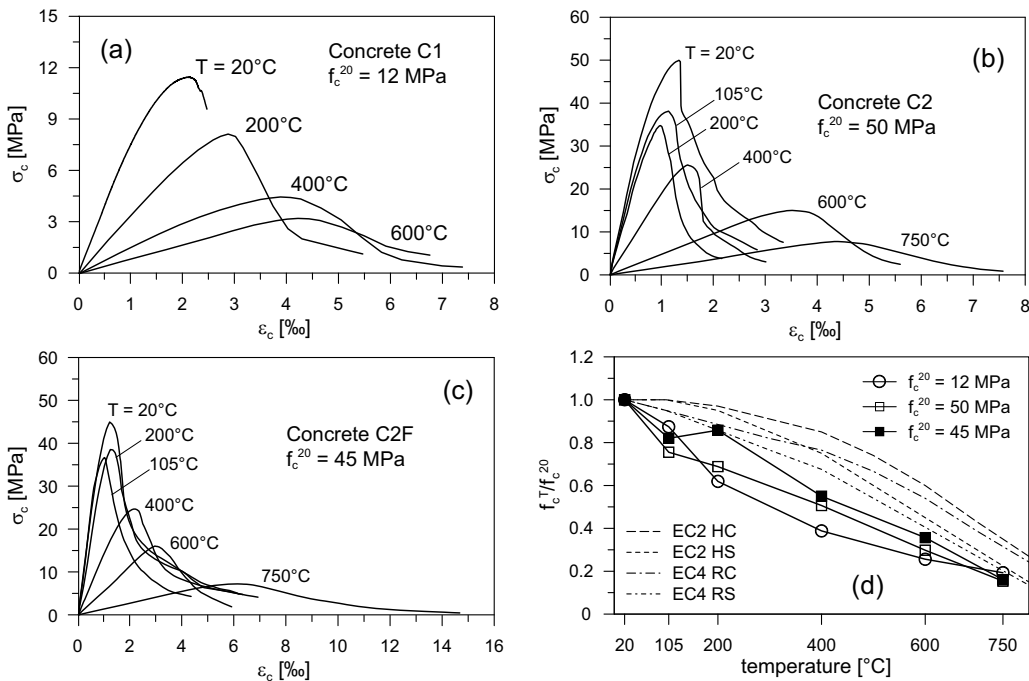


Figure 3. Mean stress-strain curves: (a) Mix C1; (b) Mix C2; (c) Mix C2F; and (d) normalized compressive strength; in (d): HC/HS = Hot Calcareous/Siliceous, EC2; RC/RS = Residual Calcareous/Siliceous, EC4.

Compressive strength and strain at the peak stress

The normalized compressive strength and the normalized strain at the peak stress are plotted in Figures 3d and 4a, respectively, as a function of the temperature. The dotted and dashed curves in Figure 3d are provided by EC-2/EC-4 for high temperature (dashed curves) and after cooling (dash-dotted curves). The top and bottom curves refer to calcareous and siliceous concretes, respectively. In both figures, the mean values pertaining to the virgin material ($T = 20^\circ\text{C}$) are indicated at the head or in the caption.

Elastic modulus

The plots of the actual and normalized elastic moduli are shown in Fig. 4b. In all specimens the elastic modulus was evaluated from each stress-strain curve, as the secant modulus between 30% and 50% of the peak stress. In this way, the first part of the loading branch (that tends to have an upward concavity) does not affect the evaluation of the modulus. As a matter of fact, the damaged material has to “adjust itself” to the increasing load, such being the reason of the upward concavity, barely noticeable in the tests reported here. (In the treatment of the results, the branches with an upward concavity have been always neglected).

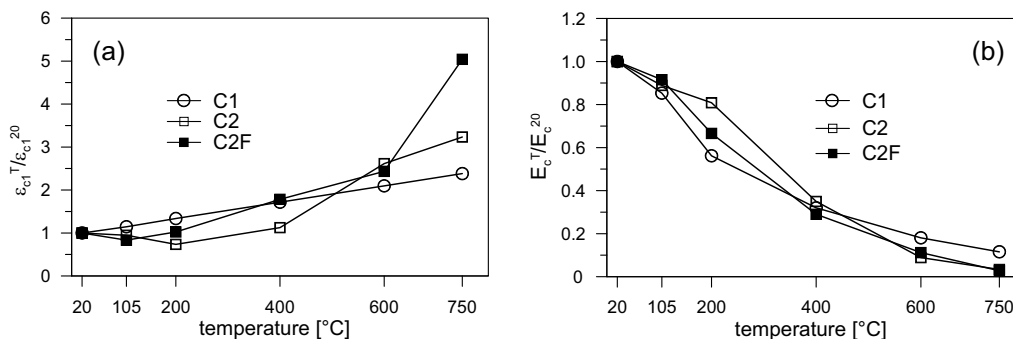


Figure 4. Plots of the normalized strain at the peak stress (a); and of the normalized elastic modulus (b); C1/C2/C2F: $\epsilon_{c1}^{20} = 2.00/1.20/1.30$ ‰; $E_c^{20} = 4.6/54/50$ GPa.

Thermal diffusivity

The thermal diffusivity D (Fig. 5a) was measured in accordance with the theoretical solution of slowly-heated long cylinders subjected to a constant heating rate v_h :

$$T = v_h R^2 / (4D) \quad ; \quad D = v_h R^2 / (4 T) \quad (1)$$

where R and T are the distance and the differential temperature between the two thermocouples embedded in each cylinder. (The first was placed close to the heated surface and the second along the axis).

In the range 200-600°C all shotcretes have a rather low diffusivity ($2.5-3 \times 10^{-7}$ m²/s, compared to $6-4 \times 10^{-7}$ m²/s for ordinary concretes, Figure 5a). A possible explanation may be found in the larger porosity ensuing from the spraying process.

Porosity

The porosity (Figure 5b) was evaluated by means of the traditional technique based on mercury intrusion, that allows to measure the capillary porosity. In virgin conditions ($T = 20^\circ\text{C}$) Mix C2 appears to have a porosity close to that indicated in the literature (9-11% by volume for $w/c = 0.55-0.75$ [12]), while Mixes C2F and C1 are 25% and 33-50% more porous, respectively.

In all mixes the residual porosity increases markedly within the range 20-750°C, from +50% (Mixes C1 and C2F) to +60% (Mix C2).

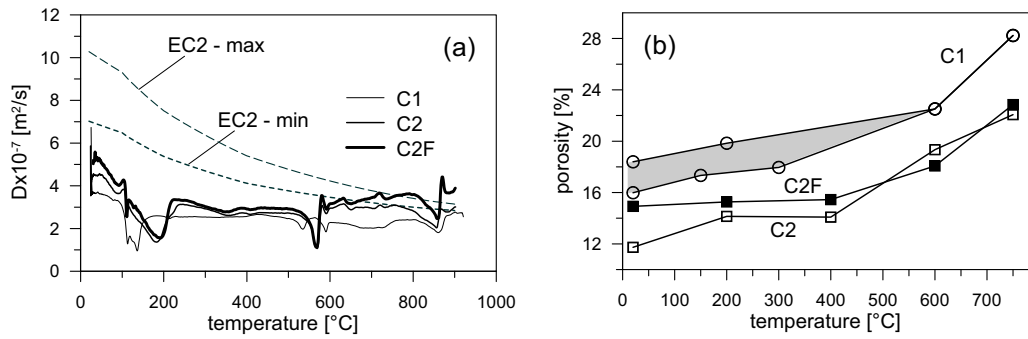


Figure 5. (a) Plots of the thermal diffusivity; and (b) plots of the residual porosity.

COMMENTS AND CONCLUSIONS

Temperature-induced mass loss (Fig. 1b): the mass loss is practically the same for both C2 and C2F mixes, and marginally larger than that indicated by EC-2 for ordinary concrete; the behavior of Mix C1 is rather different, since there is practically no mass loss, unless reference is made to the nominal mix design.

Stress-strain curves (Figs. 3a-c): all mixes seem to be affected by high temperature in the same way; at all temperatures, the loading branches are markedly linear and the softening branches exhibit a rather limited toughness.

Residual compressive strength (Fig. 3d): the marked decrease with the temperature is very close to that measured in ordinary concretes for Mixes C2 and C2F (at 400/600°C, $f_c^T/f_c^{20} = 50/35\%$); on the contrary, Mix C1 is more temperature-sensitive (at 400/600°C, $f_c^T/f_c^{20} = 40/30\%$).

Strain at the peak stress (Fig. 4a): as usually observed in ordinary concretes, the strain at the peak remains rather constant up to 200°C, and then start increasing; at 600°C, the normalized strain $\epsilon_{c1}^T/\epsilon_{c1}^{20}$ is close to 2.5. At 750°C, the normalized strain may be as large as 5.

Elastic modulus (Fig. 4b): the elastic modulus is markedly affected by the temperature, more in Mixes C1 and C2F than in Mix C2; in spite of the large scattering of the results, at 600-750°C Mix C1 seems less affected than Mixes C2/C2F.

Thermal diffusivity (Fig.5a): all shotcrete mixes exhibit good insulation properties, as demonstrated by the values of the diffusivity from 50 to 60% lower than in ordinary concretes. In the range 200-600°C, the mean values are close to 2.5, 2.75 and 3.0 m²/s for the Mixes C1, C2 and C2F, respectively.

Porosity (Fig.5b): the residual capillary porosity increases with the temperature (+50-60% between 20 and 750°C); however, Mixes C2F and C1 tend to be more porous even in virgin conditions (+25 and +33-50% compared to Mix C2, that is very close to ordinary concrete in virgin conditions).

Summing up, the residual mechanical properties of the two alkali-free shotcretes examined in this project are similar to those well known for ordinary concrete, while the alkali-based shotcrete is more heat-sensitive. In all cases, the thermal dif-

fusivity is definitely lower. The conclusions on the mechanical properties may look obvious, since shotcretes are still cementitious composites and should behave as such. However, the rather small aggregates and the nature of the accelerating agent may in principle significantly affect shotcrete behavior at high temperature, something not found in this project with reference to alkali-free shotcretes, and only partially found in the single alkali-based shotcrete.

ACKNOWLEDGEMENTS

This project was financially supported by the Italian Ministry of Higher Education and Research within the National Project–PRIN 2006 (2007-08) “Optimization of Construction Methods and Materials in Tunnel Linings”. Subproject “SCCs and Shotcretes”.

The firm in charge of the construction of Turin Automatic Subway (Turin, Italy), and the Society BBT of the Brenner Base Tunnel should be thanked for the preparation of the shotcrete slabs necessary for extracting the cores.

REFERENCES

1. Hamilton, C.H., Pardoen, G.C., Navalpakkam, S. and Kanzañjy, R.P. 2004. “Reinforced Concrete Bridge Column Performance Enhancement Through Shotcrete Jacketing”, *ACI Structural Journal*, V.101, No.3, pp.332–340.
2. Schliessler, O. and Peter, C. 2004. “Spritzbeton für komplexe, innerstädtische Tunnelbauarbeiten”, *Beton und Stahlbetonbau*, V.99, No.2, pp.128–133.
3. Leung, C. K. Y., Lai, R. and Lee, A.Y.F. 2005. “Properties of wet-mixed fiber reinforced shotcrete with similar composition”, *Cement and Concrete Research*, V.35, pp.788–795.
4. Ansell, A. 2007. “Dynamic Finite Element Analysis of Young Shotcrete in Rock Tunnels”, *ACI Structural Journal*, Vol.104, No.1, pp.84–92.
5. Yang, C.Y., Xu, M.X. and Chen, W.F. 2007. “Reliability Analysis of Shotcrete Lining during Tunnel Construction”, *ASCE Journal of Construction Engineering and Management*, V.133, No.12, pp.975–981.
6. Thomas A.H. 2009. *Sprayed-Concrete Lined Tunnels*. Pub. by Taylor and Francis, London.
7. Collotta T., Barbieri G. and Mapelli M. 2010. “Shotcrete Tunnel Linings with Steel Ribs: Stress Redistribution due to Creep and Shrinkage Effects”, *Proc. 3rd Int. Conf. on Engineering Developments in Shotcrete*. Queenstown (New Zealand), March 15-17, in press.
8. Bamonte P., Marazzi M. and Rinaldi A. 2009. “Mechanical Properties of Shotcrete Exposed to High Temperature – Preliminary Results”, *Proc. 4th International Conference on Construction Materials “ConMat’09”*, Nagoya (Japan), August 24-26, V. 2, pp.959–964.
9. Bamonte P., Gambarova P.G., Marazzi M., Nafarieh A. and Rinaldi A. 2010. “On the Residual Behavior of Shotcrete Exposed to High Temperature”, *Proc. 6th Int. Conf. on Concrete under Severe Conditions— CONSEC’10*, Merida (Mexico), June 7–9, in press.
10. Felicetti R. and Gambarova P.G. 1998. “Effects of High Temperature on the Residual Compressive Strength of Siliceous HSCs”, *ACI Materials Journal*, V.95, No.4, pp. 395–406.
11. Felicetti R. and Gambarova P.G. 2008. “Fire Design of Concrete Structures: Structural Behaviour and Assessment”, State-of-Art Report, Chapter 6, fib Bulletin No. 46, pp. 63–114.
12. Neville A.M., and Brooks J.J. 1999. *Concrete Technology*. Pub. by Longman, Edinburgh Gate, Harlow (Essex, U.K.).

Proposal for the Model and the Mechanical Properties at High Temperature for High Strength Concrete Mixed with Fiber Cocktail

K.-H. PARK, H.-Y. KIM, H.-J. KIM, H. K. JEON and K. S. YOUM

ABSTRACT

This research is to propose the model and characteristics about compressive strength and modulus of elasticity for high strength concrete up to 100 MPa in order to set the prospective model for mechanical properties at high temperature depending on the existence of fiber cocktail.

We have simulated various temperatures (100 to 800°C) using the heating furnace and the method of installing a thermocouple.

As the result, both permanent strength loss and permanent loss of modulus of elasticity are shown over 300°C. After over 600, the structural stability is lost and the physical characteristics keep the changed. And, in this research, the model for compressive strength and modulus of elasticity about the high strength concrete up to 100 MPa depending on existence of fiber cocktail are suggested.

Kyung-Hoon Park, Researcher, Fire Safety Research division, Department of Construction Quality Policy Department, Korea Institute of Construction Technology, Republic of Korea
Heung-Youl Kim, Ph. D, Research Fellow, Fire Safety Research division, Department of Construction Quality, Policy Department, Korea Institute of Construction Technology, Republic of Korea
Hyung-Jun Kim, Researcher, Fire Safety Research division, Department of Construction Quality Policy, Department, Korea Institute of Construction Technology, Republic of Korea
Hyun-Kyu Jeon, Ph. D, Senior Researcher, GS E&C Research Institute, Republic of Korea
Kwang-Soo Youm, Ph. D, Senior Researcher, GS E&C Research Institute, Republic of Korea

INTRODUCTION

At the ambient temperature, the strength and the elasticity of concrete with ordinary strength are generally considered to be decreased as the inner temperature of concrete increases, showing further decreasing rate in the high temperature range above 600 °C, and the stress-strain curves has been reported to show inordinate changes as it is exposed to high temperature heat[1]. Especially, the sharp performance decrease of a high strength concrete structure is anticipated in severer degree than the ordinary concrete in case of fire due to the low water-concrete ratio, the decreased sectional size, the increase of pore pressure interiorly, and the exposure of steel bars due to spalling. Therefore, the evaluation of material's physical properties, including the compressive strength reduction factor, the reduction factor of modulus of elasticity, the stress-strain curve, and creep strain, need to be examined in order to evaluate the functional decrease of high strength concrete structure in terms of thermal characteristic changes while the structure is exposed to fire[2], [3], [4], [5].

The evaluation can be utilized as an important database for the heat behavior interpretation along with the interior temperature increase in concrete with such identical conditions of actual fire as heat temperature and load. The study performed a fire resistance test for high strength concrete up to 100 MPa, which was mixed with the fiber cocktail blended steel and polypropylene fibers for the spalling reduction, and the evaluation of mechanical properties and a model of high strength concrete exposed to high temperature are to be proposed.

EXPERIMENTAL PROGRAM

To compare and analyze factors and different conditions that influence the characteristic changes at high temperature for the 40 to 100 MPa high strength concrete, the mechanical properties for the compressive strength and the modulus of elasticity were evaluated as the interior concrete temperature reaches the target ranges (20, 100, 200, 300, 400, 600, and 800 °C). Also, a temperature increase model is to be proposed on the basis of the test results as evaluation data for the thermal behavior interpretation of the high strength concrete structural material

The water-cement ratio for the concrete of the 40, 50, 60, 80, and 100 MPa which are utilized in actual construction sites, was determined to be 18 to 35 % and the unit quantity as of 145 to 163 kg/m³. The fly ash was set as 0, 10, and 15 %, and the silica fume and the high range water reducing admixture were applied in appropriate quantities according to the mixture design and the pre-tests as seen at Table 1. The fiber cocktail for the spalling reduction was used for the test specimen production employing 0 or 0.5 % steel fiber per volume and three different concentrations of the polypropylene fiber as 0, 0.5, and 1.0 kg/m³.

Three 100 × 200 mm cylinders were cast from each mix and three thermocouple extension wires for the interior temperature measurement were placed at designated positions before the initial set, and the specimens were removed after 24 hours followed by the submerged curing for 27 days in a water that maintained continuous temperature of 23±2 °C.

Since most existing furnace fixtures for concrete heating were hard to be moved and transported, their utilization for the thermal characteristics of concrete has been confined in the residual property evaluation of cooled down concrete at ambient temperature after heating it up, not appropriate for the thermal characteristic evaluation during exposure to fire.

Fig. 1 shows small size movable furnace, which is attachable to other test equipments for the compressive strength and the modulus of elasticity measurements, was prepared and utilized during the test. As a metal heater with electrical heating method, the furnace was designed to transmit heat to the test specimen through a set of heating panels located on both sides of the furnace, and thermocouples were inserted at the lower portion of the specimen to measure interior temperature of the concrete according to the changes of applied heat in a interval of 1 minute during the test.

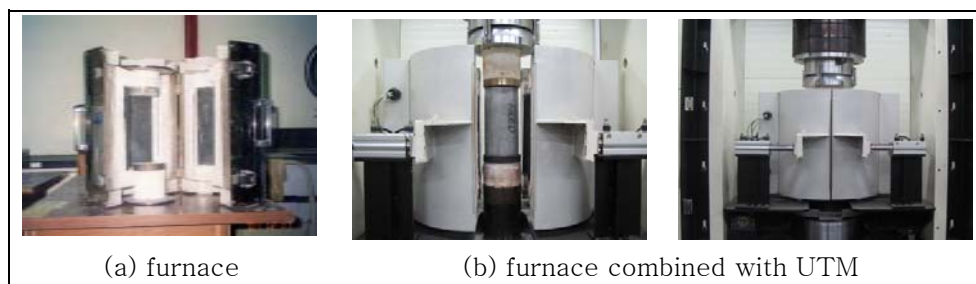


Figure 1. Furnace for residual properties evaluation

TEST RESULTS

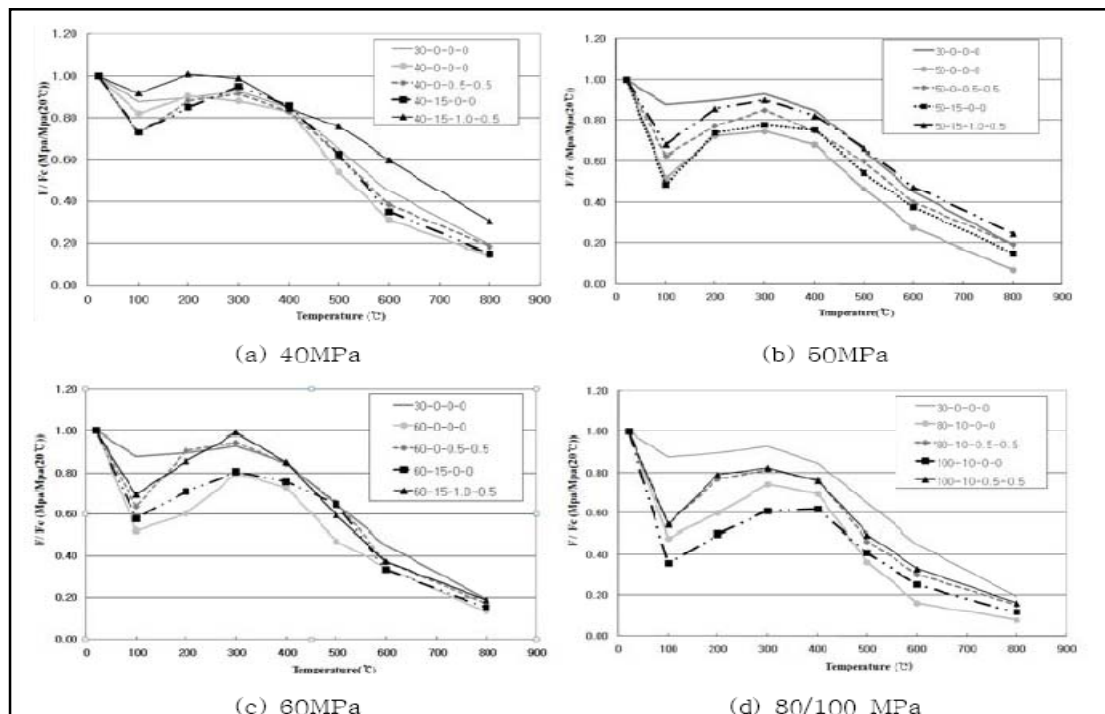


Figure 2. Ratio of residual compressive strength to original compressive strength for the 40 to 100 MPa

The temperature-compressive strength reduction factors for the 40 ~ 100 MPa high strength concrete are shown in Fig. 2 .

For the 40 MPa high strength concrete, the mixture with 15 % fly ash, 1.0 % polypropylene, and 0.5 % steel fiber showed the highest value, and the value at 400 °C as 0.845 MPa/MPa(20 °C) turned to be similar with other cases. Also, a tendency of reduction was observed from 300 °C as the starting point. In the specimen of the mixture with the fly ash, the polypropylene fiber and the steel fiber, the value corresponding the temperature range from the ambient to 100 °C was measured 0.098 MPa/MPa (20 °C) higher than concrete with no mixture. The values of the specimens with only polypropylene and steel fibers and with only fly ash were measured to have insignificant 0.005 MPa/MPa (20 °C) difference. At 300 °C, the value was 0.034 MPa/MPa (20 °C) higher than the specimen prepared with polypropylene and steel fibers and increased until the high temperature but decreased thereafter. For the 50 MPa high strength concrete, the value was sharply decreased at 100 °C but recovered up to 300 °C, showing a sharp decrease above 300 °C again. In case of specimen with no mixture, it showed the similar increasing pattern up to 200 °C, but the value of the specimen with only fly ash exhibited 0.775 MPa/MPa(20 °C), the 0.033 MPa/MPa (20 °C) higher value, and decreased thereafter at 300 °C.

For the 40 MPa high strength concrete, the specimen with no mixture showed the highest value, and the values of the specimens with fly ash an polypropylene and steel fibers and with only polypropylene and steel fibers were measured to have insignificant difference. However, the specimen with only polypropylene and steel fibers showed 0.636 MPa/MPa (20 °C), a 0.059 MPa/MPa (20 °C) lower value, at 100 °C and 0.906 MPa/MPa (20 °C) at 200 °C, a 0.048 MPa/MPa (20 °C) higher value. The overall temperature changes exhibited a drastic decrease at 100 °C, a sharp increase at 300 °C, and sudden drops at the high temperature range.

For 80 MPa and 100 MPa concrete, the specimen with the fly ash and polypropylene and steel fibers showed a similar tendency throughout entire temperature ranges while the specimen with only fly ash turned to be lower than that of the specimen with the fly ash and polypropylene and steel fibers. The 80 MPa concrete specimen with only fly ash was measured to be 0.482 MPa/MPa(20 °C) at 100 °C that is about 0.127 MPa/MPa(20 °C) higher than that of 100 MPa concrete specimen while the value of 100 MPa concrete specimen is higher at 400 °C.

Consequently, the temperature effects on both the ordinary and the high strength concrete showed a similar tendency above 400 °C but significant differences between 100 °C and 400 °C. More, noticeable differences were observed along with the mix-proportioning of the fly ash and polypropylene and steel fibers. The cement hydrates seems to lose its chemical bonds under the effect of high temperature, and the degradation and expansion of calcium and the interior pore pressure increase changes the physical properties of the high strength concrete.

Fig. 3 shows the reduction factors of elasticity for the ordinary 30 MPa and the high strength 40 to 100 MPa concrete are as follows. For the 40 MPa high strength concrete from the ambient temperature to 100 °C, the specimen with only 15% fly ash and the specimen with 15 % polypropylene and steel fibers showed the similar results, 0.956 MPa/MPa (20 °C) and 0.955 MPa/MPa (20 °C) respectively. Also, they exhibited a similar pattern up to 500 °C. However, the

specimen with polypropylene and steel fibers showed higher value of 0.829 MPa/MPa (20°C) at 800 °C, a 0.013 MPa/MPa (20°C) higher value. In case of specimen with no mixture, the value decreased from 300 °C and drastically decreased at 400 °C. The value 0.813 MPa/MPa (20°C) at 800 °C was similar to that of the specimen with only fly ash.

For the 50 MPa concrete, the specimens with no mixture and only with the fly ash showed similar 91.6 to 96.0 % decrease at 100 and 200 °C. The specimen with the fly ash and fiber cocktail showed the highest value throughout the entire temperature ranges, showing decrease after 300 °C. At 800 °C, the specimen with polypropylene and steel fibers showed a 0.015 MPa/MPa (20°C) higher value than that of the specimen with only fly ash.

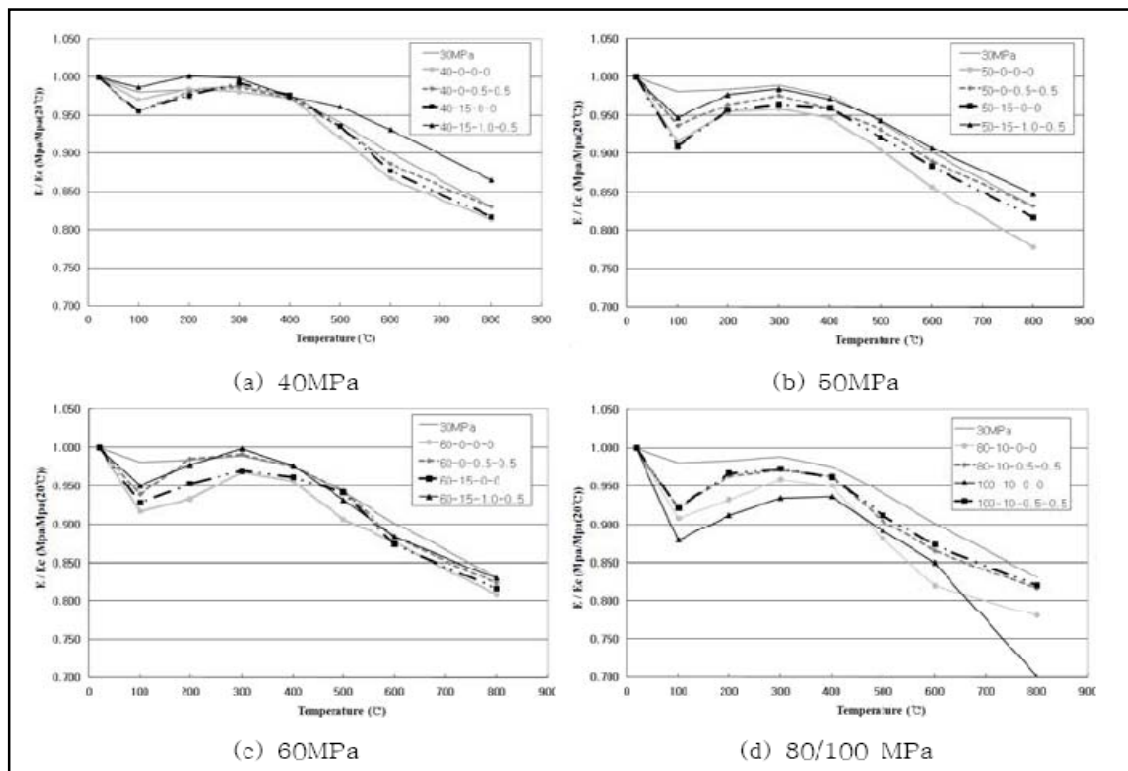


Figure 3. Ratio of residual modulus of elasticity to original modulus of elasticity for the 40 to 100 MPa

For the 60 MPa high strength concrete, the specimen with the fly ash and polypropylene and steel fibers showed the highest value of 0.950 MPa/MPa (20°C) while the specimen with no mixture showed the lowest value of 0.917 MPa/MPa (20°C). The specimen with the polypropylene and steel fibers was measured to be 0.939 MPa/MPa (20°C), a 0.011 MPa/MPa (20°C) higher value than that of the specimen with only fly ash. Though there was a noticeable difference, the fiber cocktail specimens with the fly ash and the specimens without fly ash showed a similar pattern generally up to 300 °C, but they showed a general decrease after 300 °C. Moreover, the specimen with fiber cocktail turned to have higher value than that of the specimen with only fly ash from 100 to 400 °C, about 0.022 MPa/MPa (20°C) difference at 300 °C.

In case of 80 and 100 MPa high strength concrete, specimens with fly ash, polypropylene and steel fibers showed nearly identical tendency, decreasing 92 % at 100 °C. The 80 MPa concrete specimen with only fly ash mixing was measured to be 0.908 MPa/MPa (20°C), a 90 % decreased value, and 100 MPa specimen as the lowest 0.879 MPa/MPa (20°C). In addition, the 100 MPa concrete specimen with only fly ash increased up to 500 °C but decreased sharply after 800 °C, which was 0.08 MPa/MPa (20°C) lower than that of 80 MPa.

Though there was a little bit of differences about the elasticity reduction factors, a sharp decrease and gradual increase were watched between 100 to 300 °C while another sharp decrease was observed after 300 °C. More, specimens according to mix-proportioning of fly ash, polypropylene and steel fibers showed a big differences between 100 to 400 °C, and the difference was also affected greatly by the mix-proportioning of polypropylene and steel fibers.

PROPOSAL FOR THE MODEL

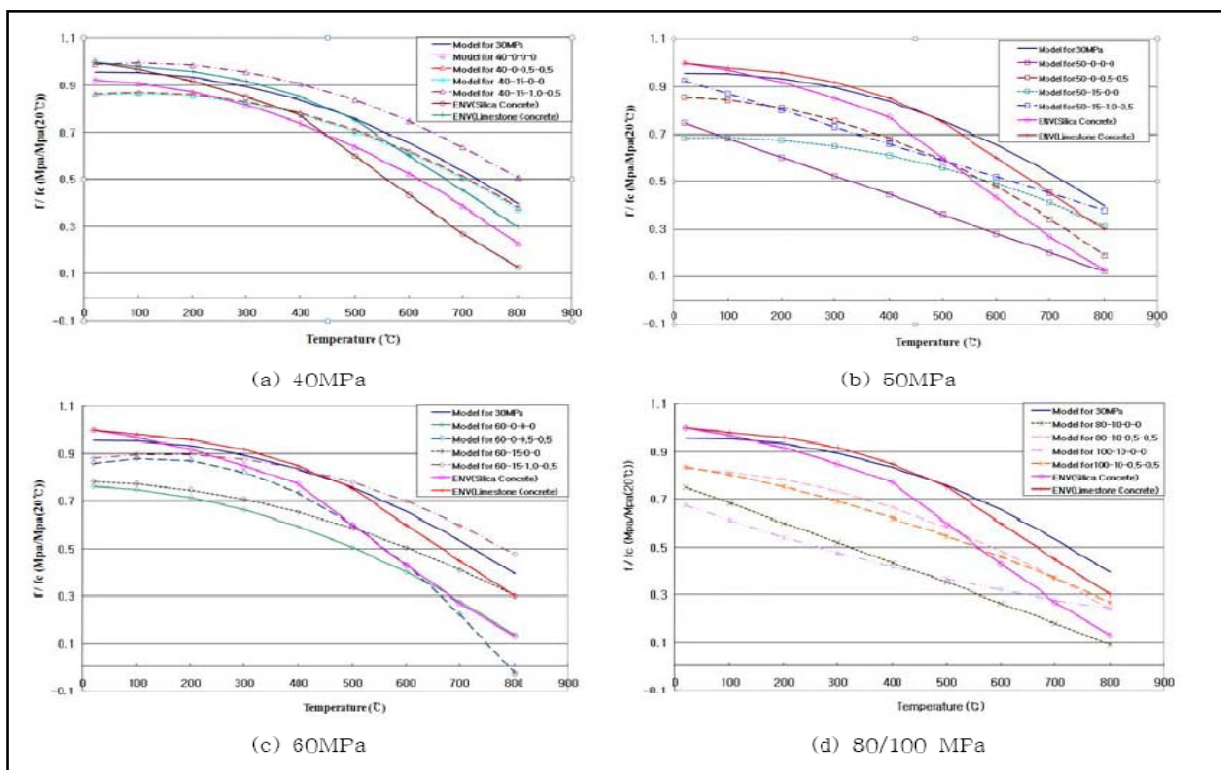


Figure 4 . Compressive strength of proposal for the model exposed to high temperature

Fig. 4 shows the compressive pressure reduction factor model of the ordinary and the high strength concrete as well as the compressive pressure reduction factor model proposed by ENV. As shown in figures, the compressive strength reduction factor model drawn by the study and the ENV model exhibit a similar pattern despite of minor differences.

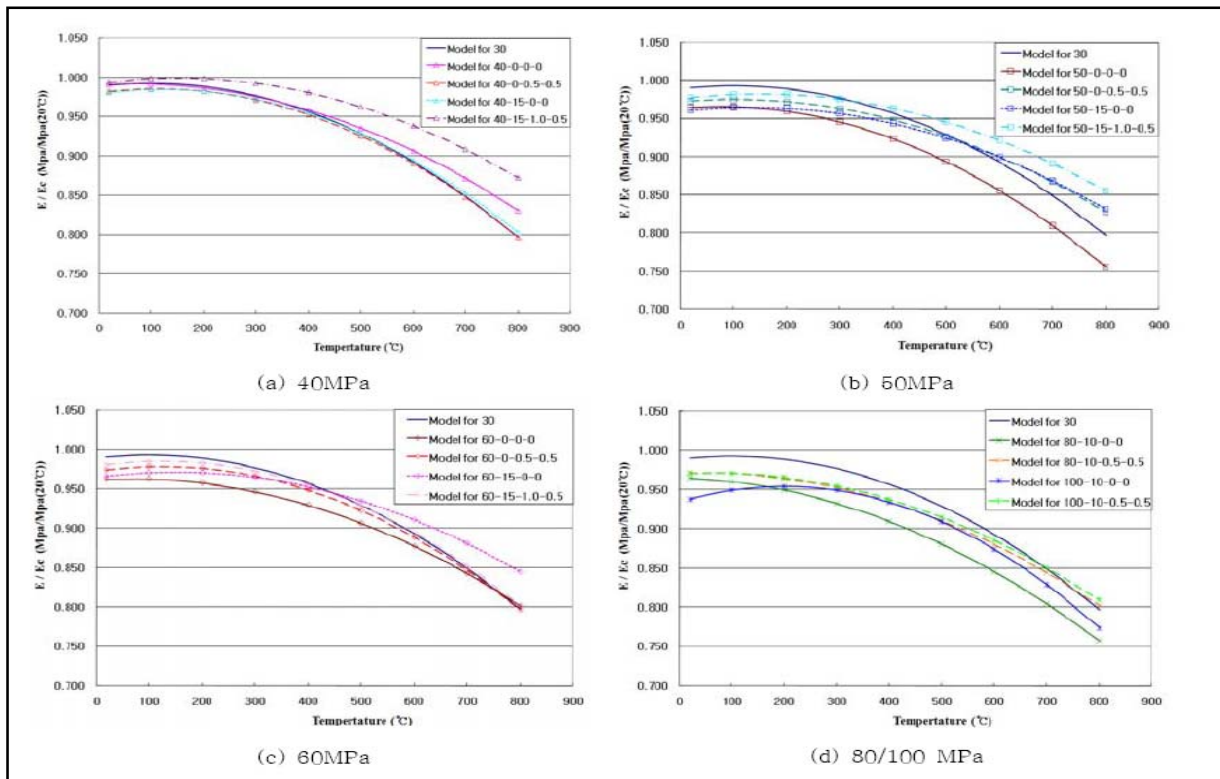


Figure 5 . Modulus of elasticity of proposal for the model exposed to high temperature

Fig. 5 shows the model of the modulus of elasticity for the ordinary and the high strength concrete is postulated as follows on the basis of the test results that the high strength concrete showed the more sharp decrease of elasticity in the low temperature region than that of the ordinary concrete as well as higher results in the high temperature region; the modulus of elasticity becomes lower as the strength of concrete is getting higher.

CONCLUSIONS

Following conclusions were drawn after the study of the mechanical properties and the model proposal for 40 to 100 MPa high strength concrete exposed to fire.

1. As of the 40 MPa strength concrete, the compressive strength reduction factor showed the initial strength loss between the ambient temperature to 100 °C, the strength gain and stabilization phase between 100 to 300 °C, and the permanent strength loss after 300 °C.
2. The pattern was similar to the level of 40 MPa regardless of the fiber cocktail mixture, but the higher strength concrete above 50 MPa with the fiber cocktail exhibited 10 to 20 % lower reduction rate.

3. The 40, 50, and 60 MPa high strength concrete with fiber cocktail mixture showed the similar pattern with the ordinary concrete, but the concrete above 80 MPa turned to have 20 to 30 % higher strength reduction.
4. The elasticity loss phase was observed in both the ordinary and high strength concrete at the ambient temperature and at 100 °C temperature range.
5. The increase and stabilization phases for elasticity of both the ordinary and the high strength concrete were identified between 100 to 300 °C, and the permanent elasticity loss for both the ordinary and the high strength concrete was observed after 300 °C.

ACKNOWLEDGMENTS

Korea Institute of Construction Technology carried out this study regarding the subject of “(10 Basic) Analysis of Fire Behavior and Study on relevant Design Technology based on Structural Performance” supported by the Ministry of Science and Technology. We would like to thank all those who took part in it.

REFERENCES

1. Castillo, C., “Effect of transient high temperature on high-strength concrete”, *ACI Materials Journal (American Concrete Institute)*, vol. 87 no.1(1990), p. 47-53
2. Comites Euro - *International Du Beton, Fire Design of Concrete Structures* - in accordance with CEB/FIP Model Code 90(Final Draft), CEB Bulletin D'Information No 208, Switzerland,(1991)
3. Comité, Européen de Normalisation(CEN), Eurocode 4 : Design of Composite Steel and Concrete Structures, Part 1-2 : General Rules - *Structural Fire Design*, CEN ENV(1994)
4. G.A. Khoury, Compressive strength of concrete at high temperatures: A reassessment. *Mag. Concrete and Cement research* 44 (1992), pp. 291–309.
5. Mehmet Sait Culfik., "Effect of elevated temperatures on the residual mechanical properties of high-performance mortar", *Concrete and Cement research* 32 (2002), p. 809-816.

High-Strength Concrete Reinforced Jute Fiber and Water-Soluble PVA Fiber Under High Temperature

M. OZAWA and H. MORIMOTO

ABSTRACT

Fire poses one of the most serious risks to concrete buildings and other concrete structures because it often results in explosive concrete spalling. The addition of organic fibres to high-strength concrete (HSC) is widely used as an effective measure to prevent explosive spalling. However, few studies have investigated the effectiveness of adding natural fibres to HSC in preventing spalling under high temperature.

In this study, we examined the relationship between the spalling behaviour and the internal vapour pressure of HSC reinforced with natural fibre and organic fibre and subjected to heating. The concrete specimens had a water cement ratio of 0.30 ($f_c \approx 70$ MPa). The fibres used were jute (natural) fibre and water-soluble poly-vinyl alcohol (PVA:organic) fibre. The length of jute and PVA fibres were 12 mm and 4 mm, with addition rates of 0.075% and 0.15%, by volume, respectively. HSC specimens were subjected to high temperature and their internal temperature and vapour pressure were measured.

Mitsuo Ozawa, Dr, Eng., Assistant professor Concrete Laboratory, Department of Civil Engineering, Gifu University, Gifu City, Yanagido, 1-1, Japan

Hiroaki Morimoto Dreg., Professor Concrete Laboratory, Department of Civil Engineering, Gifu University, Gifu City, Yanagido, 1-1, Japan

INTRODUCTION

Fire poses one of the most serious risks to concrete buildings and other concrete structures because it often results in explosive concrete spalling. The spalling of concrete from exposure to fire is a result of two phenomena. The first phenomenon is restrained thermal dilation, resulting in biaxial compressive stress states parallel to the heated surface, which then leads to the development of tensile stress in the perpendicular direction. The second phenomenon is the build-up of concrete pore pressure as a consequence of the vaporization of the physically/chemically bound water, resulting in tensile loading of the microstructure of the heated concrete. The addition of organic fibres to high-strength concrete (HSC) is widely used as an effective measure to prevent explosive spalling [1-5]. However, few studies have investigated the effectiveness of adding natural fibres and other organic fibres [6] to HSC for preventing spalling under high temperature. In this study, we examined the relationship between spalling behaviour and the internal vapour pressure of HSC reinforced with natural fibre and, especially, water-soluble poly-vinyl alcohol (PVA) fibre and subjected to heating.

OUTLINE OF EXPERIMENT

The experiment consisted of fire endurance tests on three different types of concrete specimens. One is Control specimen without fibre, and the two others are Jute fibre specimen and PVA fibre specimen. Numbers of replicate are two for each type specimen.

Concrete

Tables I show the mixture proportions of the HSC. A water-cement ratio of 0.3 and ordinary Portland cement (density: 3.15 g/cm^3) were used in this study. Crushed stone with a maximum size of 20 mm was used as coarse aggregate. The main component of the super-plasticizer (SP) was polymeric acid. After casting, the concrete specimens were left in the formwork for one day. The specimens were then wet cured at $20 \pm 2 \text{ }^\circ\text{C}$ for 14 days. Heating test of all specimens were done from 14 days to 28 days. Table II presents the fresh concrete properties of the specimens, and their average compressive strength and elastic modulus tested.

Fibres

Table III shows the properties of Jute [7] and PVA [8] fibres, which were used as natural and organic fibres, respectively, with fibre addition rates of 0.075% and 0.15% (by volume) and lengths of 12 mm and 4 mm, respectively. Photos 1 and 2 show Jute fibre and PVA fibre. Straw-like structures in Jute fibre was observed on the photograph obtained by a scanning electron microscope (SEM). The PVA fibre, which has low melting and low dissolving points, are also used for explosion prevention in concrete. PVA fiber has a lower dissolving point than the other fibers and has been used in Japan for more than 30 years. The mechanism of explosion prevention by adding fibers is not fully elucidated yet, however organic fibers are considered to improve the permeability of concrete by dissolving/melting and vaporization [8].

Table I. Mixture proportion.

Water cement ratio	Unit weight (kg/m ³)				
	Water	Cement	Fine aggregate	Coarse aggregate	Admixture
0.3	170	567	763	913	6.237

Table II. Fresh concrete properties and mechanical Properties.

	Slump flow	Air	Temperature	Compressive strength	Elastic modulus
specimen	cm	%	°C	MPa	GPa
Control	75.8	1.3	15.2	66.8 ^{*)}	32.9 ^{*)}
Jute	63.5	1.6	17.1	73.7 ^{#)}	32.6 ^{#)}
PVA	50.5	1.9	16.8	76.8 ^{#)}	31.5 ^{#)}

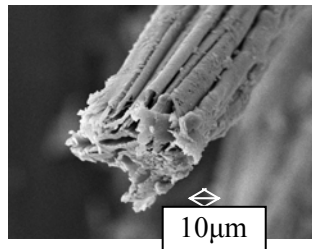
*) :at 14days, #): at 28days

Table III. Properties of Jute and PVA.

Type of fibers	Length	Diameter	Melting point	Density	Other property
	mm	μ m	°C	g/cm ³	
Jute	12	10-30	-	1.3-1.45	Carbonation
PVA	4	12	220-240	1.30	Water dissolving



a) Appearance

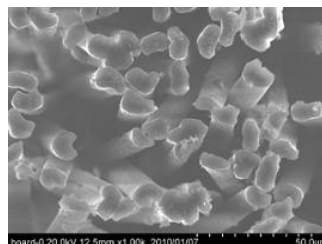


b) SEM

Photograph 1. Jute fiber.



a) Appearance



b) SEM

Photograph 2. PVA fiber.

Specimen dimensions and heating system

The configuration and dimensions of the specimens are shown in Fig.1. The specimens had dimensions of 400 × 400 × 100 mm. Two pairs of steel pipes (inner diameter: 2 mm; length: 200 mm) were placed in the concrete at distances of 10 and 20 mm from the heated face, and set parallel to the heated face. Five Type-K thermocouples were placed in the central zone of the specimen at 10, 20, 30, 40, and 50 mm from the heated face. Before testing, a steel pipe that extended out from

the specimen was connected to a miniature pressure transducer, located outside the furnace. The miniature pressure transducer had a pressure range of 0–10 MPa. The entire pore pressure assembly (steel pipe and transducer) was filled with hydraulic jack oil. Fig.2 shows the typical instrumentation scheme. An electric furnace (power voltage: 200 V, maximum current: 280 A, heating element: 9 nichrome wires) was used for heating the specimen. The pressure transducer and thermocouples were connected to the data acquisition system to record pressure and temperature. In the heating tests, the temperature was first increased to 1200 °C from 0 to 10 minutes, and was then kept constant at 1200 °C from 10 to 25 minutes. The heating curve is illustrated in Fig. 3.

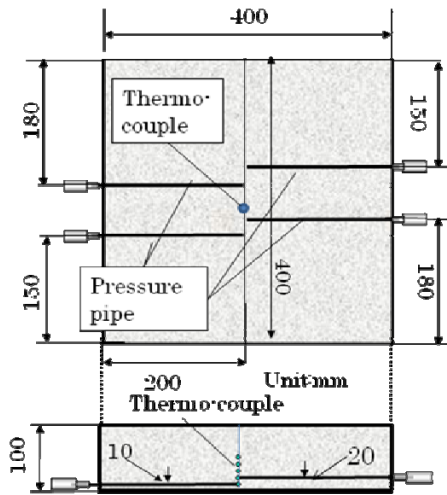


Figure 1. Specimen.

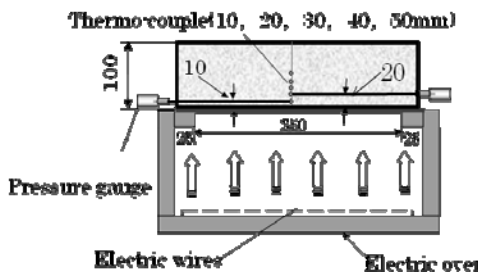


Figure 2. Heating system.

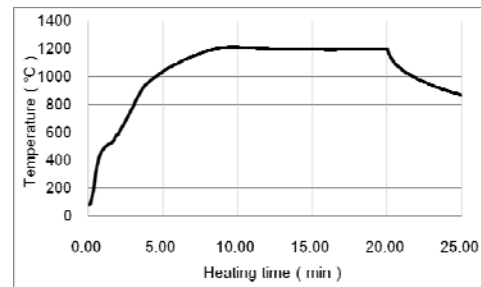


Figure 3. Heating Curve.

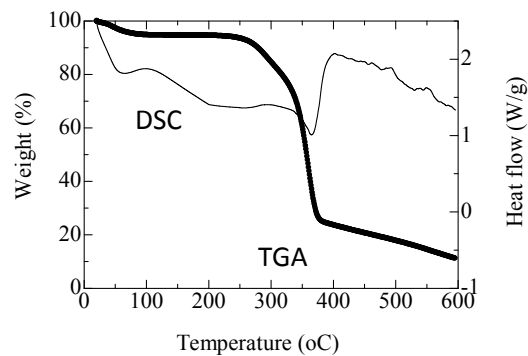


Figure 4. DSC-TGA results (Jute).

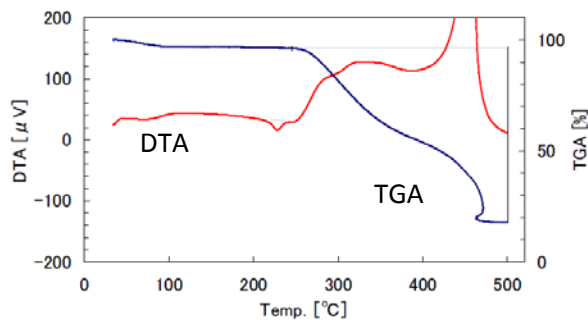


Figure 5. DSC-TGA results (PVA).

RESULTS AND DISCUSSION

Thermal analysis results of Jute and PVA fibres

Fig.4 shows the results of the thermal analysis of the jute fibre concrete specimen using differential scanning calorimetry (DSC) and thermo-gravimetric analysis (TGA). The exothermic peak (which represents heat released from the concrete sample) of the DSC curve in the case of jute fibre was observed at a maximum temperature of 360°C. The TGA curve of the jute fibre specimen initially indicated

a slight decrease in weight below 100°C due to a loss of moisture. After that, the two curves showed an onset of decomposition at 265 and 340°C, respectively. The decomposition temperature of the jute fibre specimen at 80% weight loss was at 390°C. Fig.5 shows the DTA and TGA results in the case of PVA fibre. The melting, vapour, and burning points of this fibre were 227°C, 246°C, and 470°C, respectively.

Internal temperature and vapour pressure

Fig.6 shows the variations in internal temperature (at 10, 20, 30, 40, and 50 mm from the heated face) and vapour pressure (at 10 and 20 mm from the heated face) in the case of the control specimen. The internal temperature at 10 mm from the heated face reached 130°C after 5 minutes of heating. Explosive spalling began to occur at temperatures higher than 130°C. The vapour pressure started to increase at 100°C, reaching 2.83 MPa at 252°C. The internal temperature at 20 mm from the heated face reached 67°C after 5 minutes of heating. The vapour pressure started to increase at 100°C, reaching 4.7 MPa at 275°C. Explosive spalling occurred several times after 5 min of heating. Fig.7 shows the variations in internal temperature (at 10, 20, 30, 40, and 50 mm from the heated face) and the vapour pressure (at 10 and 20 mm from the heated face) in the case of a Jute specimen. The internal temperature at 10 mm from the heated face reached 125°C after 5 min of heating. Explosive spalling did not occur. The vapour pressure started to increase at 100°C, reaching 2.5 MPa at 268°C. The internal temperature at 20 mm from the heated face reached 100°C after 6.7 minutes of heating. The vapour pressure started to increase at 100°C, reaching 2.0 MPa at 197°C. Jute specimen was effective at preventing explosive spalling in this study. Fig.8 shows the variations in internal temperature (at 10, 20, 30, 40, and 50 mm from the heated face) and the vapour pressure (at 10 and 20 mm from the heated face) in the case of the PVA specimen. The internal temperature at 10 mm from the heated face reached 116°C after 5 minutes of heating. Explosive spalling did not occur. The vapour pressure started to increase at 100°C, reaching 1.3 MPa at 255°C. The internal temperature at 20 mm from the heated face reached 39 °C after 5 minutes of heating. The vapour pressure started to increase at 100°C, reaching 1.45 MPa at 168°C. The PVA specimen was effective at preventing explosive spalling in this study.

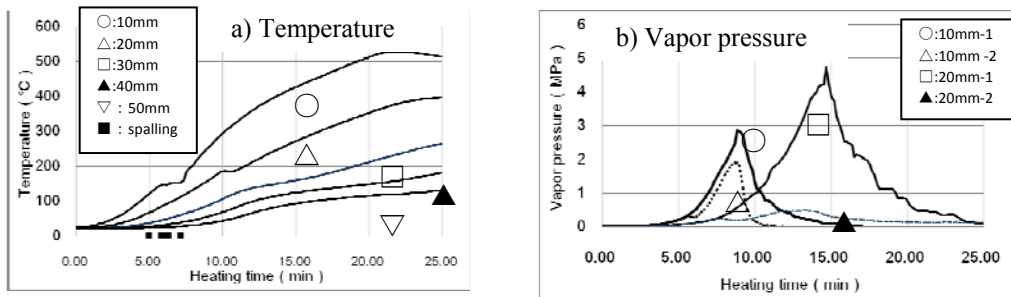


Figure 6. Temperature and vapour pressure (Control).

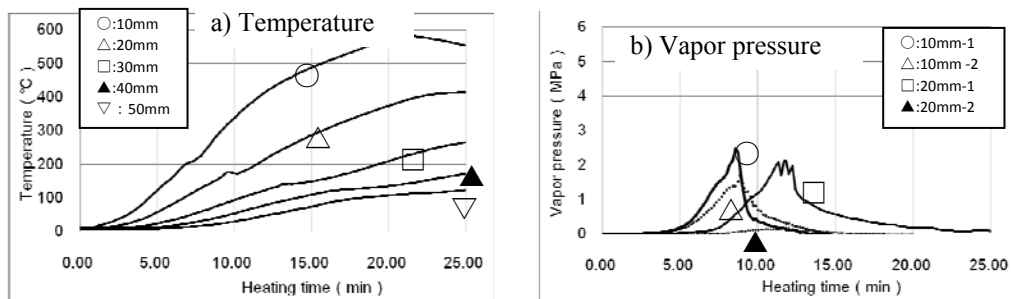


Figure 7. Temperature and vapour pressure (Jute)

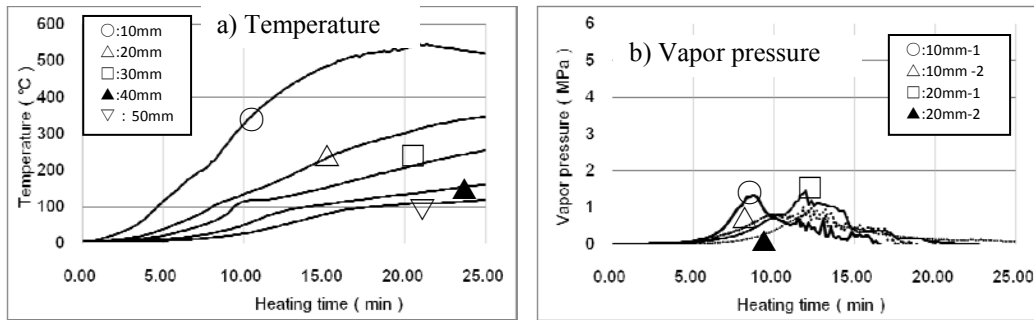
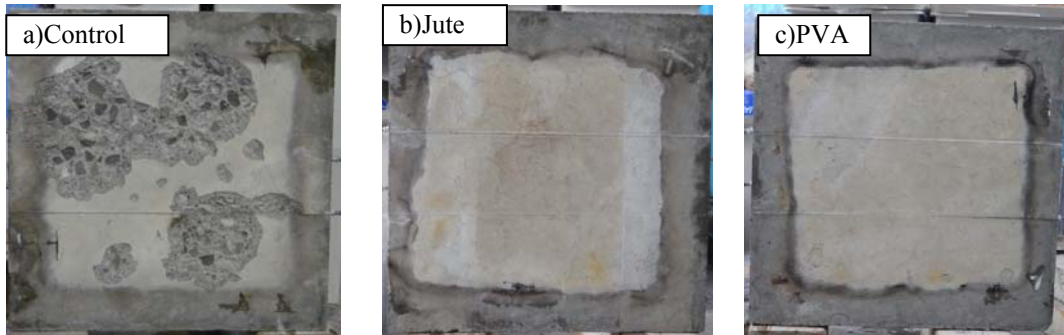
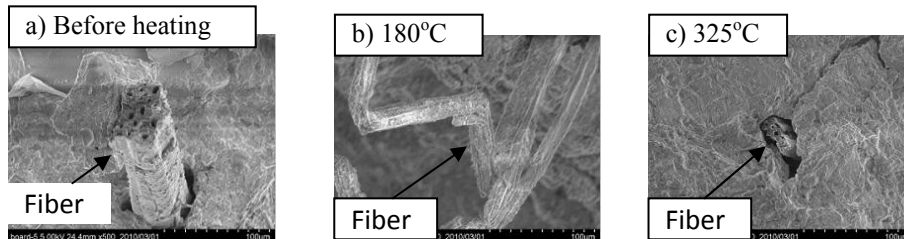


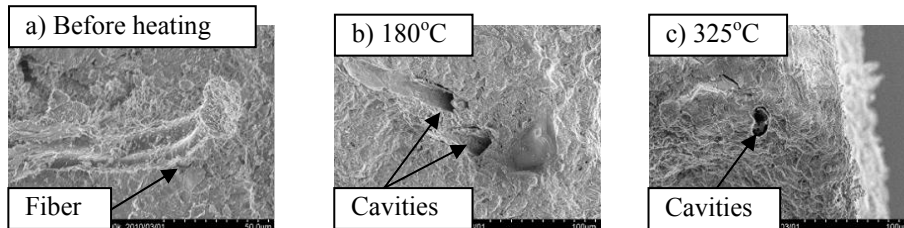
Figure 8. Temperature and vapour pressure (PVA).



Photograph 3. Specimens after the heating tests.



Photograph 4. Fiber in concrete at heating (Jute).



Photograph 5. Fiber in concrete at heating (PVA).

Effects of heating on the specimen surfaces

Photo 3 shows images of the specimens after the heating tests. The control specimen was severely damaged; it had a maximum spalling depth of 7 mm. The Jute specimen and PVA specimen did not undergo explosive spalling.

Microstructure and fiber–concrete interactions

In order to study the behavior of fibers after heating, observations with a scanning electron microscope were done. New specimens were exposed to a temperature ranging between 180°C and 325°C for 1 hour. Photo 4 shows Jute

specimens before and after the heating treatment. These images show that the jute fiber is still visible in their initial location. Despite the heating at 325°C, jute fiber still displays straw-like structures in concrete. Photo 5 shows PVA specimens before and after the heating treatment. After the heat treatment at 180°C, it is difficult to confirm the existence of PVA fiber; only the voids left by the fibers can be observed. After the heat treatment at 325°C, only the voids left by the melted fibers were visible. These images showed that, as soon as temperature exceeds the fiber dissolving point (50–90°C), the fibers are not visible anymore in their initial bed.

Effect of Jute fibre and PVA fibre on spalling

Table IV shows the results of the heating tests for all the specimens in terms of: a) occurrence or non-occurrence of explosive spalling, b) crack pattern, c) vapour pressure at first spalling, d) internal temperature at first spalling, e) maximum value of vapour pressure, and f) maximum spalling depth. In the case of the control specimen, the maximum vapour pressure was measured at 4.7 MPa. Peaks of vapour pressure over 1.4 MPa were recorded for all the specimens. It appears that the addition of jute fibre (natural fibre) with a fibre dosage rate of 0.075% by volume (0.975 kg/m³) and a fibre length close to 12 mm to HSC is effective in preventing spalling. It is hypothesized that the straw structure of jute prevented the development of significant vapour pressure in concrete. Additionally, it is considered that jute fibre is carbonized during heating, which created the so-called pressure-induced tangential space (PITS) at the fiber–concrete interface, as suggested by Khoury [3]. This space can transport vapour from concrete to outside. It can be therefore assumed that the degree of adhesion between the fibre and concrete is poor at best. In which case, the role of the fibre–concrete interface as a channel for moisture transfer under pressure cannot be ignored. It also appears that the addition of water-soluble PVA fibre with a fibre dosage rate of 0.15% by volume (1.95 kg/m³) and a fibre length close to 4 mm to HSC is also effective in preventing spalling. Peaks of vapour pressure were reduced by using PVA fibres. It may be assumed that PVA fibre can develop PITS [3] at the fibre–concrete interface when solid PVA itself became increasingly more flexible in the dissolving temperature range of 50–90 °C.

Table IV. Results of the heating tests.

Inspection parameter	unit	Control	Jute	PVA
a) Explosive spalling (Yes or No)		Yes	No	No
b) Properties of heating surface (crack)		Spalling	Hexagonal pattern	Hexagonal pattern
c) Vapor pressure (Beginning explosive spalling)	MPa	0.19	-	-
d) Internal temperature (Beginning explosive spalling)	°C	122	-	-
e) Maximum vapor pressure	MPa	4.7	2.4	1.45
d) Maximum spalling depth	mm	7	-	-

CONCLUSIONS

From the above experimental study, the following conclusions can be drawn:

- 1) After heating to 325°C, jute fiber was still visible in its initial bed, with an observed straw-like structure in the concrete specimen.
- 2) After a heat treatment at 180°C, it is difficult to confirm the existence of PVA fiber in concrete; voids left by the melted fiber could be seen. After a heat

treatment at 325°C, only voids left by the melted fiber could be seen. These observations revealed that, as soon as temperature exceeds the fiber dissolving point (50-90°C), the fiber is not visible anymore in its initial bed.

- 3) The addition of jute fibre (natural fibre) with a dosage rate of 0.975 kg/m³ and a fibre length close to 12 mm to HSC is effective at preventing spalling. It is hypothesized that the straw-like structure of jute prevented the development of significant vapour pressure in concrete. Additionally, it is considered that carbonizing of jute occurs during heating, which created the so-called pressure-induced tangential space (PITS) at the fiber–concrete interface. This space can transport vapour from concrete to outside.
- 4) The addition of PVA fibre (organic fibre) with a dosage rate of 1.95 kg/m³ and a fibre length close to 4 mm to HSC is effective at preventing spalling. It may be assumed that PVA fiber can create PITS at the fiber–concrete interface when solid PVA itself became increasingly more flexible in the dissolving temperature range of 50–90°C.
- 5) Peaks of vapour pressure were reduced considerably by using natural and organic fibres.

ACKNOWLEDGEMENTS

We wish to thank JAPAN INSULATION Co., Ltd. for supporting this study. Also, we also extend our thanks to TESAC Co., Ltd. for graciously providing the jute fibre and KURARAY Co., Ltd. for grateful providing the PVA fibre. This experiment was supported by SHOWA CONCRETE INDUSTRY. Co., Ltd. We also acknowledge the contribution of The National Research Council of Canada (NRC-IRC) where the DSC and TGA tests had been conducted.

REFERENCES

1. Phan,L.T. 2008. “Pore pressure and explosive spalling in concrete”, *Material and Structres*.**41**(10) 1623–1632.
2. Khoury,G.A. 2008.”Polypropylene fibers in heated concrete Part 2: Pressure relief mechanisms and modeling criteria”, *Magazine of Concrete Research*, **60**(3)189–204.
3. Kalifa,P.,Chene,G. and Galle,C. 2001.”High-temperature behavior of HPC with polypropylene fibers from spalling to microstructure”,*Cement and Concrete Research*, **31**, 1487–1499.
4. Suhaendi,S.L., Horiguchi,T. 2006.”Effect of short fibers on residual permeability and mechanical properties of hybrid fibre reinforced high strength concrete after heat exposition”, *Cement and Concrete Research*, **36**.1672–1678.
5. Bilodeau,A., Kodur, V.K.R. and Hoff,G.C. 2004.”Optimization of the type and amount of polypropylene fibers for preventing the spalling of lightweight concrete subjected to hydrocarbon fire,” *Cement & Concrete Composites*, **26**.163–174.
6. Heo,Y.H., Sanjayan,J.G. and Han,C.G., Han,M.C.2009.”Effect of Fiber type, Length and Numbers of Fibers Per Unit Volume on Spalling Protection of High Strength Concrete,” in *1st International workshop on Concrete Spalling due to Fire Exposure*,Germany,Lipzig, F.Dehn, E.A.B.Koender(Ed.), RILEM. pp.211–220.
7. Ozawa,M., Iizuka,T. and Rokugo,K.,Morimoto,H. 2009.”Relationship between spalling behavior and internal vapor pressure of high-strength concrete reinforced with natural fiber under high temperature,” in *1st International Workshop on Concrete Spalling due to Fire Exposure*, Germany,Lipzig, F.Dehn, E.A.B.Koender(Ed.), RILEM,pp.140–149.
8. Kobayashi,T.,Nakashima,M.2009.”Optimization of the PVA Fiber for Explosion Control of Refractory Castables,”No.127 in *conference on UNITECR*,CD-ROM.

A Theoretical Approach for Estimating Mechanical and Electric Properties of Polymers and Polymer-Concrete Mixtures at Elevated Temperatures

I. E. SHKOLNIK and H. R. HIZIROGLU

ABSTRACT

Structural fire safety depends on the high-temperature properties of industrial materials. Strength and modulus of elasticity at elevated temperatures are critical properties assessing structural elements constructed of concrete, polymers, metals.

In this paper the fundamental concepts of thermal behavior of concrete, polymers and concrete-polymer mixtures are addressed. Theoretical models are discussed to present the relationships between the mechanical and electrical properties of materials and their structures, interatomic interactions, thermal pressures and stress rates at elevated temperatures. Using the proposed approach, calculated strength ratios of concrete at elevated temperatures are found to be in good agreement with experimental results, data obtained using numerical models and presented in standards.

INTRODUCTION

Classical approach in estimating different properties of solids explains and illustrates the trend of thermal and mechanical properties of a solid body as a function of temperature [1]. In general, existing experimental data indicate that the thermal conductivity, strength and modulus of elasticity decrease with temperature [2, 3].

Because of their excellent dielectric properties solid polymeric and concrete-polymeric materials have found a wide variety of applications as electrical insulation. Since the failure of the insulating material in an electrical equipment or system is absolutely undesired due to very expensive ramifications, one has to pay the utmost attention in selecting the insulating material. The ultimate failure of polymers is often due to the combination of such multifactor effects as electrical,

Iosif E. Shkolnik, Huseyin R. Hizirolu, Department of Electrical & Computer Engineering, Kettering University, Flint, MI 48504

thermal and mechanical. Consequently, electrical breakdown strength is one of the most important criteria [4, 5] along with mechanical and thermal properties in selecting a polymeric material for an application as electrical insulation.

Additionally, the polymeric material could possibly be subjected to elevated temperatures depending on its operating conditions, which may lead to the rapid aging of the material. Although it appears to be simpler to determine the strength of an industrial material according to the standards at room temperature, direct experimental determination of the strength of such an industrial material at elevated temperatures requires the usage of a set of complex special equipment. Therefore, it is the objective of this study to propose and assess a theoretical approach based on fundamental principles [6] to estimate the mechanical and electrical properties of polymers, concrete-filled polymers and concrete at elevated temperatures.

FUNDAMENTAL PROPERTIES OF A SOLID BODY

The thermal and mechanical properties of a solid body can be obtained using its diatomic model. Indeed, it is well known [1] that the nonlinear approximation of the potential energy, $U(\varepsilon)$, of two atoms as a function of their relative displacement, ε , adds an additional third-order term to the quadratic relationship as,

$$U(\varepsilon) \approx (1/2) E_o \varepsilon^2 - (1/3) g \varepsilon^3 \quad (1a)$$

where E_o is the modulus of elasticity and g is the nonlinear (anharmonic) coefficient in N/m^2 . By differentiating Eq. (1a), the relationship between the stress (σ) and the strain (ε) can be obtained as

$$\sigma = E_o \varepsilon - g \varepsilon^2 \quad (1b)$$

If g in Eq. (1a) is negligible, the potential energy can be described only by the quadratic term at different temperatures leading to the values of energy at negative and positive displacements to be the same. The original distance (R_o) does not change between atoms at increasing energy (temperature). However, when g exists due to material nonlinearity, approximation in Eq. (1a) leads to an asymmetric curve where potential energy becomes flatter with positive displacements and steeper with negative displacements than the case with $g = 0$. It means that the average displacement increases between atoms with temperature causing the thermal expansion of a solid body [1] as given by

$$\alpha = gk/E_o^2 R_o^3 \quad (2)$$

where α is the coefficient of thermal expansion, $k = 1.38 \cdot 10^{-23}$ J/K is Boltzmann's constant. The nonlinear (anharmonic) approach also yields the trend of the dependency between thermal conductivity, χ , and temperature T of non-metals [1] as

$$\chi \sim C_v c_o / g^2 \sim \text{constant} / T \quad (3)$$

where C_v is the volumetric heat capacity measured in $\text{J/m}^3\cdot\text{K}$, c_o is the velocity of sound in m/s and g is the anharmonic coefficient in N/m^2 . The existing data for different concretes indicate that the thermal conductivity decreases with increasing temperature consistent with Eq. (3) [2]. The reduction in energy with positive displacements [Eq.(1a)] testifies the softening of mechanical properties of a material at increasing temperature thus explaining the dependence between modulus of elasticity and temperature [1].

Based on the nonlinear approximation the relationship between strength, F , and thermal properties of a material is given by [3] as,

$$F \sim E_o^2 / g \sim \rho^2 (c_o)^4 (\chi / C_v c_o)^{1/2} \quad (4)$$

where ρ is the density in kg/m^3 . Eq. (4), in whole, illustrates that the strength of a solid body is dependent on density, sound velocity, thermal conductivity, heat capacity and should decrease with temperature.

Thermal fluctuations of energy, exceeding the average energy of atoms, depend on time of test, have an essential influence on the structure of real materials and predetermine their behavior under loading. However, the diatomic model [Eqs. (2-4)] does not take into account the influence of impurities, different defects of structure, physicochemical instability, and the time-rate of change of loading of industrial materials. Different flaws in structure (dislocations, micropores, and microcrevices) have a significant influence and predetermine the behavior of the material under mechanical loading and/or electrical stress at elevated temperatures [7-9]. Consequently, in accordance with kinetic nature of strength [6], it means that the fracture of a solid body does not occur as a critical event. It is rather the result of a process of nucleation, accumulation, and development of damage elements, *i.e.* a time dependent phenomenon.

For a mechanical loading, it was shown that the strength of different materials, σ_r , depends on the temperature and the rate of the loading [7, 11] as shown in Eq. (5),

$$\sigma_r (T, \dot{\epsilon}) = U_o / \gamma - (kT / \gamma) \ln(kT / \tau_o \gamma) + (kT / \gamma) \ln \dot{\epsilon} , \quad (5)$$

where U_o is the initial dissociation energy of the interatomic bonds and γ is structurally a sensitive coefficient which determines the slope for the relation $\sigma_r(\ln \dot{\epsilon})$ at constant temperature, $\tau_o \sim 10^{-13}$ s is the period of interatomic vibration and $\dot{\epsilon}$ is the rate of stress of the loading.

An analogy can be established between the mechanical strength and dielectric strength in such a way that the mathematical model in Eq. (5) can be rewritten as

$$E (T, \dot{E}) = U_i / \beta - (kT / \beta) \ln(kT / \tau_o \beta) + (kT / \beta) \ln \dot{E} \quad (6)$$

in order to predict the dielectric withstand of an insulating material [12]. In Eq. (6), E is the dielectric strength in V/m , U_i is the energy that corresponds to the initial barrier of electrical destruction, \dot{E} is the rate of the change of electric field intensity in $\text{V/m}\cdot\text{s}$, β is a structurally sensitive coefficient in $\text{C}\cdot\text{m}$ that determines the slope

between dielectric strength, E (T, \dot{E}) and \dot{E} at a constant temperature T .

Here, it is also important to indicate that equations that are mathematically similar to Eq. (1a) describe the various physical processes mentioned above in such materials with industrial importance as concrete, polymers, wood and stone under mechanical loading, are valid in a wide range of strain (10^{-4} - 10^{-6}) [13], and lead to the nonlinear 'stress-strain' relationship which deviates from Hook's law. For parabolic stress-strain relationship it was shown [7, 8] that

$$\gamma \sim W_a dE/d\sigma, \quad (7)$$

where W_a , in general, is the volume of vacancies or voids in a solid body or a porous structure; $dE/d\sigma$ is the nonlinear parameter, *i.e.* change of modulus of elasticity with stress. In dielectric materials, on the other hand, different processes may lead also to a non-linear relationship between the electric field and current density with a deviation from Ohm's law. For instance, the nonlinear dependence between electrical field and current density was found in samples of polyimide irradiated by high ion energy [14].

The fundamental relationships presented above are used further for the evaluation of the mechanical and electrical properties of concretes and polymers under mechanical loading and electrical stress when subjected to high temperatures.

RESULTS AND DISCUSSIONS

Let us assume that the mechanical strength σ_r of a concrete cylinder in Eq. (5) is represented by a function f_{ct} at a certain temperature. When normalized with respect to the maximum strength $\sigma_{max} = U_o/\gamma = f_{ck}$, Eq. (5) can be rewritten as

$$f_{ct}/f_{ck} = 1 - (kT/\gamma f_{ck}) [\ln(kT/\tau_o \gamma \dot{c})] \quad (8)$$

From Eq. (5), it also follows that at constant temperature the strength is a linear function of the stress rate of loading. Therefore, it is important to indicate that data obtained by various researches in the various countries for different concretes under compressive loading in the range of stress rate about ten orders of magnitude (decimal) at room temperature yield the average value of γ , namely $\gamma \sim 3$ kJ/mol·MPa, for normal weight concretes (NWC) [7, 9, 10, 11]. Thus, the relative slope, $d(f_{ct}/f_{ck})/dT$, of the relationship in Eq. (8), "normalized-strength vs. temperature", can be obtained as,

$$d(f_{ct}/f_{ck})/dT = -(k/\gamma f_{ck}) [\ln(kT/\tau_o \gamma \dot{c}) + 1] = -0.088(\text{MPa}/f_{ck} \cdot ^\circ\text{C}) \quad (9)$$

where k and τ_o are the aforementioned physical constants, and $\gamma = 3$ kJ/(mol·MPa) and stress-rate of loading $\dot{c} = 0.24$ MPa/s are the testing parameters. For different strengths of high strength concrete (HSC) the average value of the relative slope

($-0.088 \text{ MPa}/f_{ck}\cdot^{\circ}\text{C}$) is about $-0.001/^{\circ}\text{C}$. Taking into account the average value of the relative slope as $-0.001/^{\circ}\text{C}$, and the melting points of different aggregates, for example, 1060°C as the lower limit of all types of rocks, it is possible now to estimate and compare the predicted data of strength ratio with corresponding data for HSC in the range of temperature between 20°C and 1000°C) from

$$f_{ct}/f_{ck} = 1 - 0.001(T - T_c) \quad (10)$$

where T_c is the reference (room) temperature. It is important to note that the standard deviations (STDEV), standard errors (SE) for calculated results from Eq. (10) and existing ratios of strength [15] are highly close to each other as evident from Fig. 1. Numerical models [16-18] also confirm the linear relationship between strength and temperature. Linear relative strength-temperature relationship for HSC at the temperature above 350°C is proposed in NIST [19].

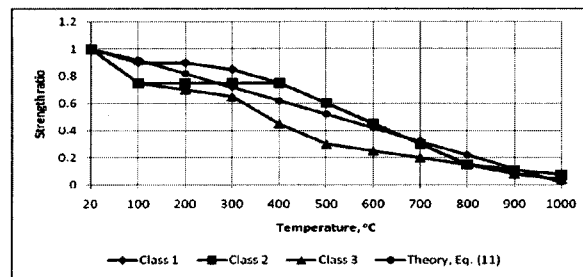


Figure 1. Comparison of predicted strength ratios from Equation (10) with the existing data [15] for HSC.

Equation (7) explains also the influence of initial porosity, permeability (*i.e.* $\sim W_a$) of concrete specimens on the strength at elevated temperatures. Because the initial porosity, permeability of lightweight concrete (LWC) is greater than for NWC and HSC, the rate of loss of strength is less for LWC concrete than for NWC, and for NWC is less than for HSC, respectively [20]. Consequently, “the spalling was quite significant in the HSC columns as compared to NSC columns”. Similar effect of silica fume on concrete strength leads to decreasing of the fire endurance of columns with silica fume content about 15% [20].

Further continuing with the analogy, when Eq. (6) is normalized with respect to the dielectric strength of the insulating material at room temperature the following equation can be obtained,

$$E(T, \dot{E}')/E_r = 1 - (kT/\beta E_r) \ln(kT/\beta \tau_o \dot{E}') \quad (11)$$

where $E(T, \dot{E}')$ is the dielectric strength of the insulating material in V/m at a certain temperature in $^{\circ}\text{C}$, $E_r = U/\beta$ is the dielectric strength at room temperature and finally \dot{E}' is the rate of the change of the electric field strength in V/m-s (ASTM D 149-97a). From these equations it follows that at constant temperature dielectric strength increases as the logarithm of strength ramp rate. At constant value of \dot{E}' the dielectric strength is a linear function of the temperature (the logarithmic dependence on T is small in comparison with linear dependency), *i.e.* the dielectric

strength decreases with temperature. These conclusions are in agreement in general with existing experimental data for different insulators. For comparison with experimental data we can use the slope of Eq. (11),

$$d[E(T, \dot{E})/E_r]/dT = - (k/\beta E_r)[\ln(kT/\beta\tau_0\dot{E}) + 1] \quad (12)$$

where k and τ_0 are physical constants mentioned above. For a polymer, if the order of magnitudes are, $E_r \sim 4 \times 10^8$ V/m, $\dot{E} \sim 5 \times 10^6$ V/m·s, $\beta \sim 1.4 \times 10^{-28}$ C·m [12], then Eq. (12) yields the following approximate value of relative slope at ambient temperature as $-0.008 / ^\circ\text{C}$. Thus, it is possible to predict the dependence between dielectric strength and temperature by Eq. (11).

In addition the analysis indicates that the developed approach is promising for polymer concrete insulators which provide combination of mechanical as well as dielectric strength. Fig. 2 illustrates that again the relationship “strength – temperature” is essentially linear (the proximity of the correlation coefficient to negative one in corresponding ranges of temperature) which is in agreement with kinetic theory of strength.

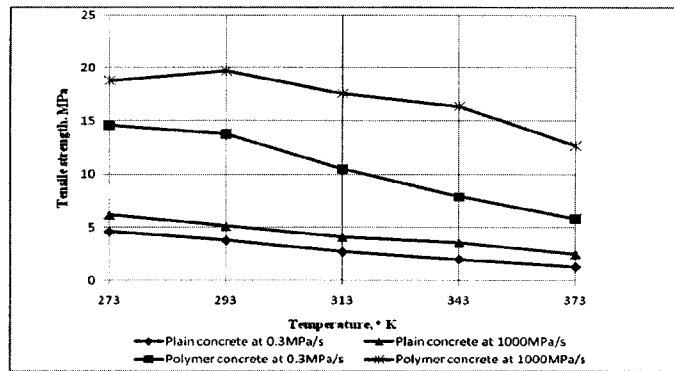


Figure 2. The “strength-temperature” relationship for plain and polymer concretes.

From the practical point of view, it is important to find the nonlinear parameter of concrete in the field. Therefore, two nondestructive methods were developed based on the measurement on resonant frequency shift and phase shift [7, 8, 21]. The obtained data proved that ultrasound pulse velocity (dynamic modulus of elasticity) and nonlinear parameters are independent characteristics, and the nonlinear parameters are more sensitive to the structure of concrete than ultrasound pulse velocities (linear parameters).

CONCLUSIONS

Using the theoretical Eq. (5, 7, 11, 12), estimations of the mechanical and dielectric strengths of concrete and polymers at elevated temperatures were evaluated and compared with respect to the published experimental results and data available in standards. These relationships indicate how mechanical properties of concrete affect its structure, interatomic interaction, the thermal pressure, and the rate of mechanical loading at elevated temperatures. Also, the relationship in Eq.(11) indicated that the dielectric strength of a polymer at a specific temperature was

influenced by the time-rate of the applied electric field. Calculated results of mechanical and dielectric strength ratios, Eqs.(10, 11), are in good agreement with the data presented in standards, numerical models, and published experimental results. Obtained data shows that developed nondestructive method can be used to estimate strength of concrete with equal modulus of elasticity. Although additional tests are needed for better statistical representation, the developed approach would be a valuable alternative to the traditional time-consuming and expensive experimental data.

REFERENCES

1. Frenkel J., "Introduction to the theory of metals. Publications of technical-theoretical literature", Moscow- Leningrad, 1948 (in Russian).
2. Kodur VKR., Dwaikat MMS, and Dwaikat MB, "High-Temperature Properties of Concrete for Fire Resistance Modeling of Structures", ACE Materials Journal, V. 105, No. 5, September-October 2008, pp. 517-525.
3. Krilov NA, Kalashnikov VA, Polischuk AM. Radiotechnical methods of quality testing of ferroconcrete. Stroyisdat, Moscow-Leningrad, 1966 (in Russian).
4. Dincer M.S., Hiziroglu H.R., and Bektas S., "The Behavior of N₂ + SF₆ Gas Mixtures Subjected to Orthogonal Electric and Magnetic Fields", IEEE Transactions on Dielectrics and Electrical Insulation, Vol.13, No.2; April 2006, pp. 257-263.
5. Hiziroglu H.R. and Ersoy A., "Electrical Breakdown of Polyurethane-Based Nanocomposites", accepted for publication in the Proceedings of International Conference on Solid Dielectrics, July 2010.
6. Regel VR., Slutzker AI, Tomashevsky EE., Kinetic Nature of Solids Strength, Nauka: Moscow, 1974 (in Russian).
7. Shkolnik IE. Effect of nonlinear response of concrete on its elastic modulus and strength. Cement and Concrete Composites, 27 (2005), pp.747-757.
8. Shkolnik IE. Evaluation of Dynamic Strength of Concrete from Results of Static Tests. J. Eng. Mech., v. 122, No. 12, 1996, pp. 1133-8.
9. Shkolnik IE. Diagnostics of concrete quality: new aspects. Technoproect. Moscow, 1993 (in Russian).
10. Betekhtin VI, Kuksenko VS, Slutzker AI, Shkolnik IE. Fracture kinetics and the dynamic strength of concrete. Phys Solid State, American Institute of Physics. 1994: 1416-21.
11. Shkolnik IE. Influence of high strain rates on stress-strain relationship, strength and modulus of elasticity of concrete. Cement and Concrete Composites, 30 (2008), pp.1000-1012.
12. Slutzker AI, Polikarpov YuI, Gilarov VL On Elementary Events in the Electrical Failure Kinetics of Polymers, ISSN 1063-7842. Technical Physics, Vol 51, No.12, pp. 1591-1595.
13. Bell, J. F., Mechanics of Solids: The experimental foundations of solid mechanics, Springer-Verlag, New York, 1983.
14. Garg M, Quamara JK, Electrical conduction behavior of high energy ionirradiated Kapton-H polyimide film. Nuclear Instruments and Methods in Physics Research B 179 (2001), pp.389-396.
15. British Standards Institution (2005) Eurocode 2: Design of Concrete Structures- Part1.2: General Rules Structural Fire Design. BSI, London, BS EN 1992-1-2.
16. Committee Euro-International Du Beton, Fire Design of Concrete Structures – in accordance with CEB/FIP Model Code 90 (Final Draft), CEB Bulletin D'Information No. 208, July 1991, Lausanne, Switzerland.
17. ASCE, Structural Fire Protection, Manual No. 78, ASCE Committee on Fire Protection, Structure Division, American Society of Civil Engineers, New York, 1992.
18. Kodur VKR, Wang TC., and Cheng FP. Predicting the Fire Resistance Behavior of High Strength Concrete Columns, Cement and Concrete Composites, V. 26, No. 2, 2004, pp.141-153.
19. Phan LT and Carino NJ. Code provisions for high strength concrete strength temperature relationships at elevated temperatures. Materials and structures. V. 36, Issue 256, 2003, pp. 91-98.

20. Kodur V.K.R. , Phan L., Critical factors governing the fire performance of high strength concrete systems, *Fire Safety Journal* 42(2007), pp.482–488.
21. Shkolnik IE, Krasilnikov VA, Zarembo LK On structural nonlinear diagnostics of solids and determination of their strength. *Frontiers of Nonlinear Acoustics; Proceedings of 12th ISNA* edited by M.F. Hamilton and D.T. Blackstock. Elsevier Science Publishers Ltd, London, 1990, pp.589–594.

Fire Behaviour of High Performance Concrete—An Experimental Investigation on Spalling Risk

P. PIMIENTA, D. PARDON and J.-C. MINDEGUIA

ABSTRACT

The results presented in this paper were obtained within the framework of the French National Project "BHP 2000". The aim of this project, which was completed in 2005, was to study the behavior and the characteristics of High Performances Concretes according to various fields: mix design, durability, association with high performance reinforcing bars and fire behavior.

HPC fire behavior was analyzed as well in an experimental way (assessment of high temperature mechanical properties, evolution with temperature of permeability, porosity and thermal properties, measurement of vapour pressure, fire behavior) as numerical (development of a coupled THM model).

We present in this paper some experimental results concerning the fire behavior of a HPC ($R_c > 100$ MPa). After a preliminary study done on small columns, three different samples geometries were tested under the ISO fire curve: beams, columns and walls. All these elements were loaded during fire.

As suggested by the European regulation Eurocode 2, fire spalling of concrete can be prevented with solutions such as the introduction of polypropylene fibres on concrete or by the installation of a thin steel mesh between the exposed surface and the reinforcement. The influence of these parameters on concrete spalling was analyzed and their respective efficiency was then considered. At last, the results of these fire tests allow us analyzing the most probable mechanisms that could be responsible for concrete spalling.

Pierre Pimienta, PhD, CSTB, Paris-Est University, Department of Mechanical tests and studies, 77447 Marne la Vallée, France.

Dominique Pardon, Eng., CSTB, Paris-Est University, Department of Fire tests and studies, 77447 Marne la Vallée, France.

Jean-Christophe Mindeguia, PhD, Pau University, LaSAGeC², 64600 Anglet, France.

INTRODUCTION

The behavior of certain High Performance Concretes in fire conditions can constitute a limitation in their use and development for the tunnels and the buildings. Indeed, under certain thermal and mechanical conditions, they can suffer from a high risk of spalling [1-8]. Spalling can take several aspects but always leads to the loss of a part of the structure and the loss of the mechanical resistance for the remaining concrete [9].

Numbers of researches concerning the fire behavior of different HPC structures were experimentally performed [10-11] or by mathematical modelling [12-13]. Meanwhile, the exact mechanisms controlling the behaviour of concrete, and especially the spalling risk, in fast fire conditions are still not well known. This is due to the complexity of parameters playing a role in this phenomenon. As a consequence, experimentation is still the only reliable way of assessing the fire resistance of a concrete structure.

Between the hypotheses on the process leading to spalling, two hypotheses are largely considered today: the thermo-mechanical one that is essentially based on the differential dimensional constraints developed during exposure to high temperature [14-15], and the thermo-hygral one that considers the pores water vapour pressures developed when the structure is exposed to a fast firing as responsible for the physical destruction of the concrete [16-17]. This latter is often used to explain the higher spalling risk that exists for HPC due to their weak permeability. More recent studies have shown that none of these two hypotheses can be directly linked with concrete spalling [18]. A new explanation for concrete spalling is linked with the creation of a saturated zone close to the exposed surface [19].

In parallel to these research works, technological solutions have been developed to predict risky configurations. Among them, the addition of polypropylene fibers in fresh concrete is now recognized to be effective regarding spalling risk [20]. Thermal protection boards have been also recognized as efficient, even in the case of a fast fire (e.g. HCM curve) [21]. Both solutions (polypropylene fibers and thermal protection) are retained by the Eurocode 2 as means to limit the spalling risk HPC. This standard document also proposes the use of a thin steel mesh, placed between the surfaces that are potentially exposed to fire and the reinforcement.

The purpose of this paper is to study the effectiveness of polypropylene fibers and of a thin steel mesh end regarding the spalling risk of HPC. The reference concrete has been studied in detail under the French national project "BHP2000"; we study here the influence of the addition of polypropylene fibers on its ISO fire behavior. We also analyze the effectiveness of a steel mesh placed at specific locations (in some corners of small columns and at the surface of a wall). To this end, a preliminary study was carried out on small columns, highlighting the positive role of polypropylene fibers. In a second step, we present the results of ISO fire tests performed on samples that are representative of structural elements (beams, columns and walls).

CONCRETE MIXTURES

More of the tests have been carried out on a high performance concrete with a compressive strength of about 100 MPa. This concrete, which is called M100C, has been largely studied in the framework of the French national project "BHP 2000". Large amount of results relative to their properties at high temperature have been published. They mainly concern their mechanical properties [22–25] and their pore pressure which were determined by Kalifa and al. [11, 26].

The gravels used for this concrete are purely calcareous (limestone rocks).

Polypropylene fibres have been added to this concrete mixture in order to study their influence on fire behavior. These 19 mm long fibrillated fibres have a square cross section of $50 \times 150 \mu\text{m}^2$ and they start melting at 171°C . It must be emphasized that these fibers have been chosen in the beginning of the French national Project at the end of the 90's. Today, fibers designed to prevent spalling are generally monofilament and their diameter is lower to $35 \mu\text{m}$. Their section are then from 10 to 50 times lower than the ones we have used in this study. It has been shown [27] that polypropylene fibres are more effective when their slenderness is important (between 300 and 600 for most of the monofilament fibres). Different fibres contents have been studied: 0.9 and 1.75 kg/m^3 (the concretes made with these fibres are respectively called M100C_f=0.9 and M100C_f=1.75). In order to guaranty a good workability for these fibred concretes, cement paste volume and superplasticizer content have been increased. A fourth type of HPC has been studied: the B80 is a concrete that has been used for a real French construction.

All the concrete mixtures and the 28 days compressive strength are given in the Table I.

TABLE I. CONCRETE MIXTURES.

(kg/m^3)	M100C	M100C_f=0.9	M100C_f=1.75	B80
CPA CEM I 52,5 PM CP2 Cement	377	415	415	450
0/5 Sand	439	439	439	
0/4 Sand	432	432	432	731
5/12,5 Calcareous gravel	488	488	488	1060
12,5/20 Calcareous gravel	561	561	561	
Silica fume	37.8	41.6	41.6	40
Superplasticizer	10.7	11.5	11.5	9
Water	124	139	139	150
Water/(cement + SF) ratio	0.30	0.30	0.30	0.30
19 mm polypropylene fibres	0	0.9	1.75	0
28 days compressive strength	111.6	105.0	102.6	89.4

EXPERIMENTAL CONTENT

The experimental study is divided in two stages. First, a preliminary study has been carried out on small unloaded columns. Thanks to simple fire tests, this pre-study allowed analyzing the influence of polypropylene fibres on concrete spalling. Moreover, the influence of a thin steel mesh has been studied. The second part of the study focused on the fire behavior of big structure elements: beams, columns and walls. To be representative of a real structure, all these elements were loaded during fire tests. Parameters such as polypropylene fibres and steel mesh were analyzed.

Commonly, all the fire tests were done under the ISO 834 fire curve.

Preliminary study on small columns

Small columns of cross section $30 \times 30 \text{ cm}^2$ and with a height of 1 m are suspended in a horizontal furnace with a dynamometer that is placed outside of the furnace (Figure 1). This system allows following the evolution of the column mass during the heating. The mass loss is dependent with the water departure (drying and dehydration of concrete) and with the fall of scales due to concrete spalling.

The small columns are reinforced in a way which varies along the length of the sample: a half is representative of a column reinforcement, the other one is representative of a beam reinforcement. Moreover, 2 contiguous sides are provided with a steel mesh (5 cm mesh) that is placed in contact with the reinforcements (Figure 1). The using of such a mesh is one of the solutions proposed by the Eurocode 2 to reduce the fire spalling of the concrete. 2 small columns per concrete composition (M100C, M100C_f=0.9 and M100C_f=1.75) were tested.

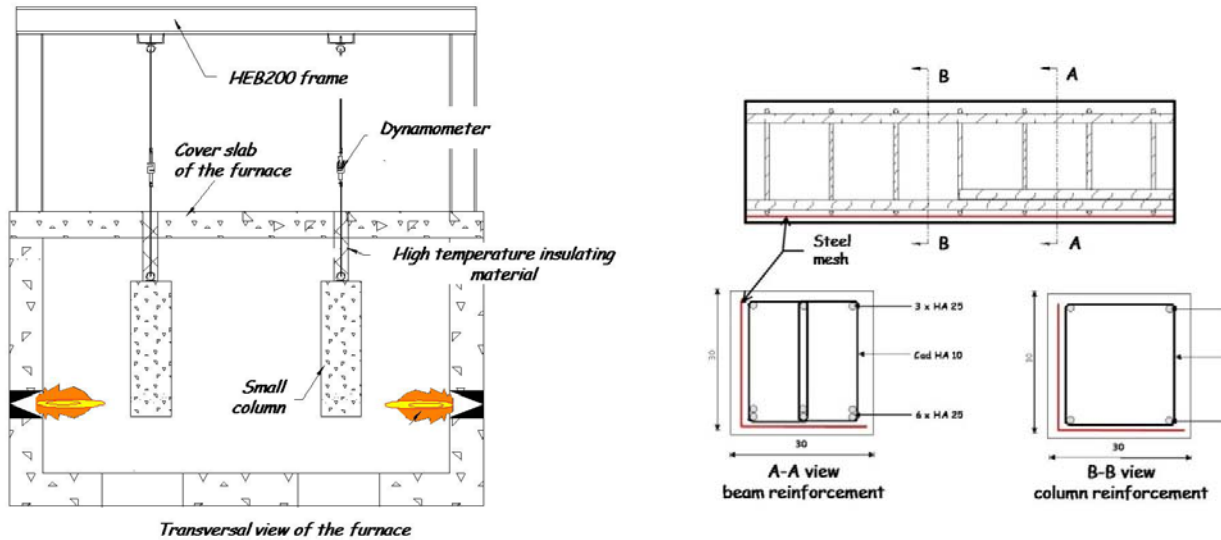


Figure 1. Fire test on small columns. Experimental set-up (left) and reinforcement (right).

Study on structure elements

In this part of the study, big elements have been tested (Figure 2). All of them were loaded in order to be as representative as possible of a real structure. All the concrete elements are reinforced according to standard documents (Eurocode 2).

- **Beams:** rectangular cross section of 60 x 25 cm², total length of 4.60 m and a mechanical span of 4.30 m. The exposed part of the beam is 4.00 m long. A beam is exposed to fire on the three sides of its cross section. A 4 points bending load is applied: 2 jacks applies 210 kN to the superior bed of the beam (distance between each jack and the beam support = 1.20 m).

- **Columns:** 60 cm diameter circular cross section and a total length of 2.60 m. The exposed part of the column is 2.0 m long. The columns have been horizontally tested in the furnace. Columns are loaded thanks to 4 prestressing steel bars (Mac Alloy bars) that are placed inside the column before the concrete casting. Each bar allows applying a force of 1314 kN, which finally results in a compressive stress of 18.5 MPa in the column.

- **Walls:** their surface is 2.80 x 2.80 m² for a thickness of 15 cm. The entire surface is exposed to fire. During fire test, walls are loaded in one direction with a distributed force of 2620 kN. Concerning the concrete walls without polypropylene fibres, a steel mesh (5 cm mesh) has been placed in contact with the reinforcement, in half of the exposed surface.

Experimental program

The final experimental program is summarized in the Table II.

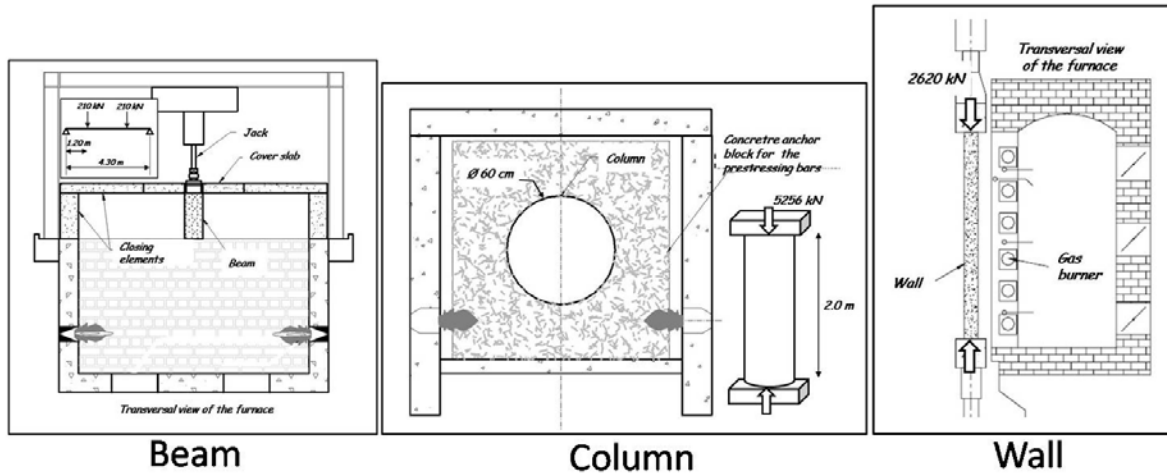


Figure 2. Experimental principles of fire test on structure elements.

TABLE II. EXPERIMENTAL PROGRAM.

Number of tests		M100C	M100C _{f=0.9}	M100C _{f=1.75}	B80
Type of samples	Loading				
Small columns	-	2	2	2	-
Beams	4 points bending (2 jacks of 210 kN)	1	-	1	-
Columns	Compressive loading (5256 kN - prestressing bars)	-	-	1	1
Walls	Distributed compressive loading (2620 kN)	1	-	1	-

RESULTS

Preliminary study on small columns

The tests on small columns showed a very clear difference in behavior between the concrete without fibres (M100C) and the concretes with polypropylene fibres (M100C_{f=0.9} and M100C_{f=1.75}): the concrete without fibres presents a relatively important spalling between the 7th and the 20th minute. This result have been clearly shown by the mass loss curves (results not presented in this paper). Pictures in

Figure 1 show that the small columns without fibres lost scales of mean size $15 \times 15 \times 5 \text{ mm}^3$. Spalling took place mainly in the angles of the small columns, causing the direct exposure to fire for the reinforcement. On the other hand, the degradation of the fibred concretes was very limited: some concrete detachments in the angles (Figure 1). We note that for the conditions of this test, a fibre content of 0.9 kg/m^3 seems as effective regarding spalling than a content of 1.75 kg/m^3 .

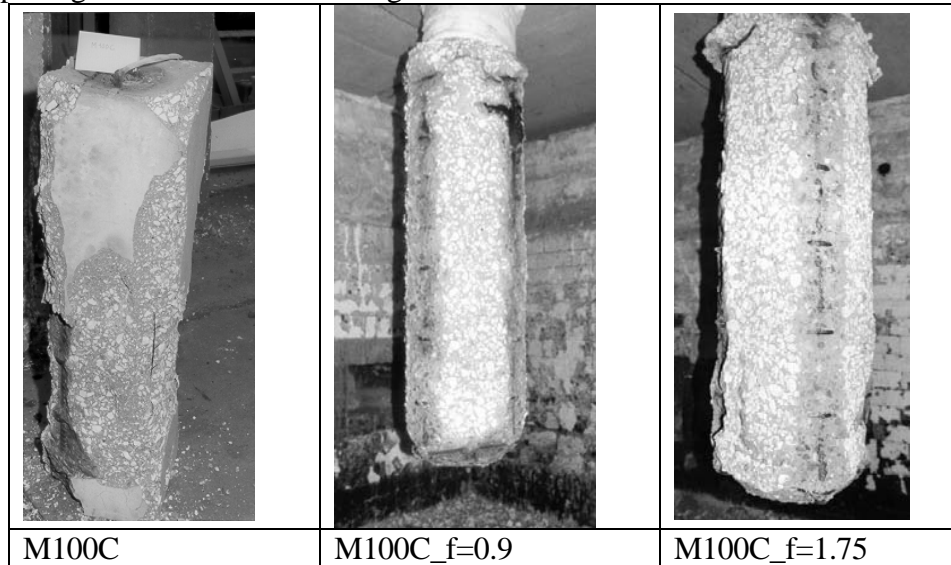


Figure 1. Fire test on small columns. Post-fire view of the samples: comparison between concrete with (M100C_f=0.9 & _f=1.75) and without polypropylene fibres (M100C).

Concerning the concrete without fibres, we note that the faces and the angles which were provided with the steel mesh present a very reduced damage (Figure 2). We think however that the mesh does not directly reduce spalling of the concrete; on the other hand this one makes it possible to retain in its meshes the concrete scales that are ejected during fire. This is a positive effect for the reinforcement to preserve an insulating barrier to fire. This was particularly visible from temperature measurements. Reinforcement temperature were lower close to the faces that were provided with the steel mesh (results not presented in this paper).

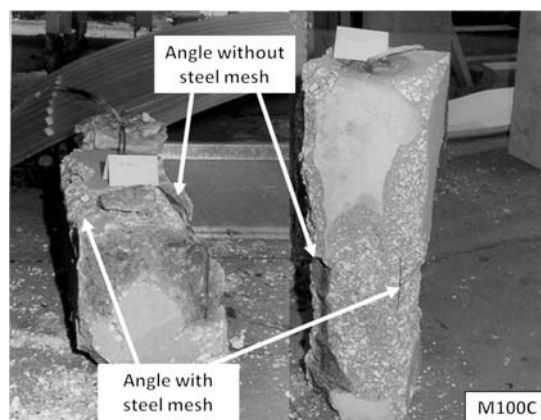


Figure 2. Fire test on small columns. Post-fire view of the sample without polypropylene fibres (M100C): comparison between the angles with and without steel mesh.

Study on structure elements

- **Beams:** after 3 hours of ISO fire, none of the two beams (concrete with and without fibres) have collapsed. However, the fibres had an influence on concrete spalling (Figure 3):

For the beam without fibres, spalling of the concrete began as soon as the 9th minute of the test and continued until the 50th minute. Spalling was limited to the side faces of the cross section and especially related to the high part (compressed part) of the beam. On the contrary, the lower part of the beam (tensioned part) showed no spalling.

For the fibred beam, concrete spalling was minor and was localized in the superior part of the beam, just below the application points of the forces.

The analyze of these tests clearly shows a dependence of concrete spalling to the mechanical stress field. It seems indeed that the compressed zones are the most sensitive to spalling risk. On the contrary, in the tensioned zones spalling risk seems limited.

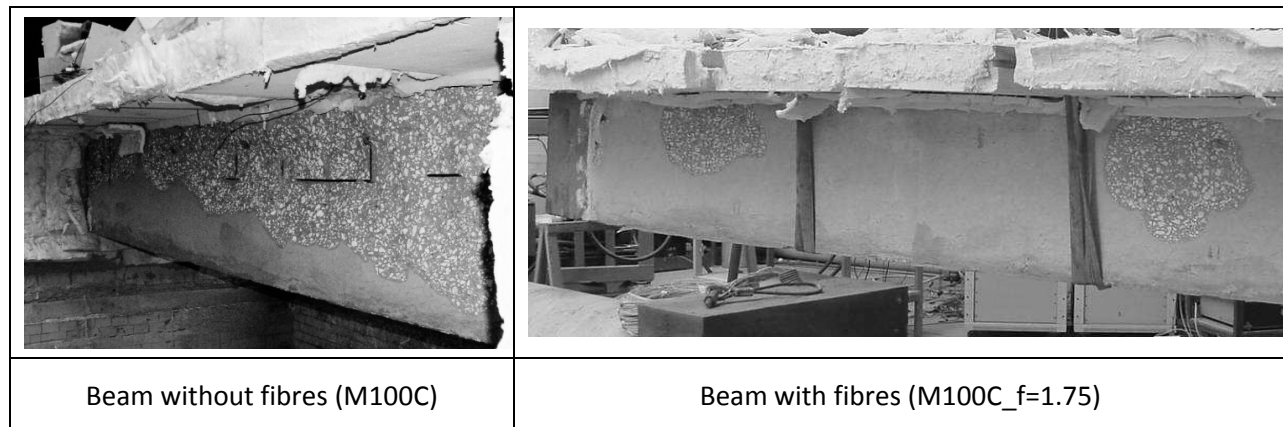


Figure 3. Fire test on structure elements. Post-fire view of the beam with (M100C_f=1.75) and without polypropylene fibres (M100C).

- **Columns:** it is important to note that at the end of the fire tests, the force applied to the column (thanks to the prestressing bars) was lower in comparison with the initial force (5256 kN). The following observations were done (Figure 4):

For the columns without fibres, the spalling of the concrete (B80) took place as soon as the first minute of the test. Very quickly, hooping reinforcement and then the longitudinal reinforcement were directly exposed to fire. Concrete spalling continued until the 50th minute of the test in the form of a progressive chipping of the section.

For the fibred column, concrete spalling was strongly limited (some small scales observed around the 30th minute of the test). The reinforcement was not directly exposed to fire. Reinforcements are visible in the bottom part of the picture. However, it must be noted that this is due to the drop of the heated concrete after and not during the fire test.

Spalling of the concrete without fibres took place as soon as the first minute of the test. In parallel, at the same time of test, the fibred concrete did not show any spalling. At this early moment of the heating, the polypropylene fibres are not melting, and thus do not allow an evacuation of vapour pressure from the concrete pores. Then it seems that vapour pressures are not directly

responsible for the spalling risk of concrete. In the same way, the effectiveness of the polypropylene fibres does not seem to rest on the limitation of vapour pressures.

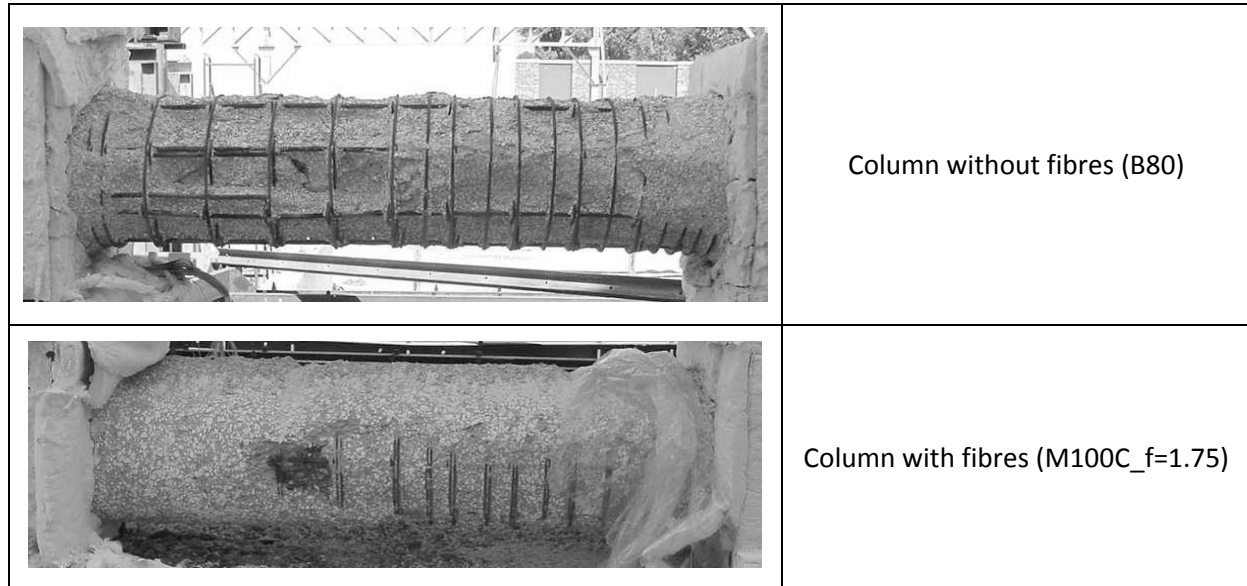


Figure 4. Fire test on structure elements. Post-fire view of the beam with (M100C_f=1.75) and without polypropylene fibres (B80).

- **Walls:** the behavior of the walls was the least good among the three tested elements. The load applied to the walls has being reduced during the test in order not to cause their collapse. For safety reasons, the tests could not last more than two hours. The observations were as following (Figure 5):

For the wall without fibres, concrete spalling took place as soon as the 4th minute of the test in the shape of very small scales (\varnothing 2.5 cm, 5 mm thick) and was continuous until the end of the test (01h45min). The reinforcement was directly exposed to fire and the spalling depth could reach 8 cm (at the central part of the wall). We point out that on half of the surface exposed to fire, a steel mesh was placed onto the reinforcement. Contrary to the tests done on small columns, the mesh did not allow to retain the concrete scales because of the verticality of the wall and the small dimensions of the scales.

For the fibred wall, the fibres did not allow to limit the concrete spalling. They simply made it possible to delay spalling (it began 6 minutes later compared to the wall fibre). The reinforcement was directly exposed to fire.

The main teaching of the tests on walls is that under particular conditions (HPC, element loaded in its plan and exposed to fire on only one face), the concrete spalling can be very severe and can occur even if polypropylene fibres are used. It must be however emphasized that section of the fibres that have been used in this research are larger than the actual most common ones which are more effective [27]. Tests are currently carried out at the CSTB in order to better study these severe conditions (development of a biaxial loading device for small ISO fire-exposed slabs).

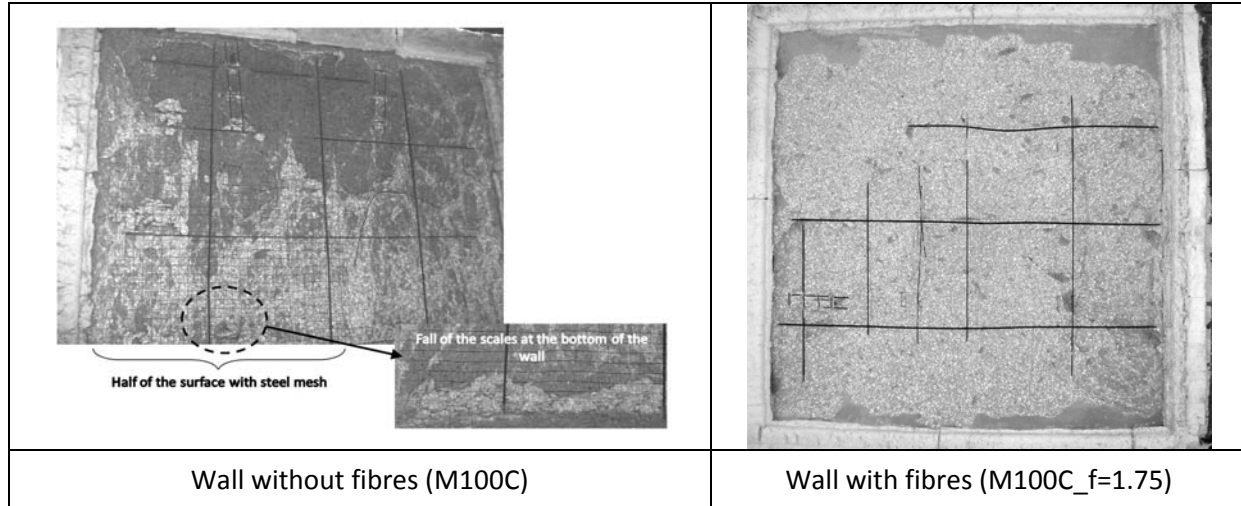


Figure 5. Fire test on structure elements. Post-fire view of the wall with (M100C_f=1.75) and without polypropylene fibres (M100C).

CONCLUSIONS

The aim of this paper was to analyze the ISO fire behavior of a HPC. The influence of parameters such as the addition of polypropylene fibres and the presence of a thin steel mesh was studied. Thanks to a simple preliminary study, the positive role of polypropylene fibres regarding to the spalling risk of concrete has been highlighted. As a consequence, for concretes with fibres, the reinforcement remains protected during the fire by concrete, involving a longer fire resistance of the structure. This positive effect has been also observed during ISO fire tests done on loaded structure elements, at least concerning the beam and the column. An interesting point of the study is that the polypropylene fibres had almost no influence on the concrete spalling in the case of a loaded wall. This seems that under certain boundaries (element loaded in its axis and/or one-side exposure to fire), the fibres can be not efficient anymore. It must be highlighted that fibers used in this research were fibrillated with a section larger than the common actual ones. A study is running at this time at the CSTB in order to better study spalling under severe conditions. In this study, we also highlighted that concrete spalling seems to be dependent on the mechanical stress field of the fired element: no spalling occurred in the tensioned zones of the beam and it occurred very soon for the column without fibre. At last, the efficiency of a steel mesh is dependent on the scales dimensions: if the scales are big enough (e.g. in the corner of a column), the thermal protection of the reinforcement is remained whereas if the scales are very thin (in the case of our wall), they are not retained by the mesh and the reinforcement can be directly exposed to fire.

REFERENCES

1. Castillo C. and Durani A.J., "Effect of transient high temperature on high-strength concrete" ACI Materials Journal, Jan-Feb, pp 47–53, (1990).
2. Hertz K.D., "Danish investigations on silica fume concretes at elevated temperatures." ACI Materials Journal 89(4): 345–347, (1992).

3. Sanjayan, G. and Stocks L.J., "Spalling of High-Strength Silica Fume Concrete in Fire." *ACI Materials Journal* 90(2): 170–173, (1993).
4. Diederichs U., Jumppanen U.-M., and Schneider U., *High Temperature Properties and Spalling Behaviour of High Strength Concrete. High Performance Concrete: Materials and Properties.* Aedification-Verlag, Freiburg, (1995).
5. Aldea, C. M., Franssen J.M., and Dotreppe J.C., *Fire test on normal and high-strength reinforced concrete columns. International workshop on fire performance of high-strength concrete.* Gaithersburg, USA, (1997).
6. Chan, S. Y. N., G. F. Peng, and Anson M., "Fire behaviour of high-performance concrete made with silica fume at various moisture contents." *ACI Materials Journal* 96(3): 405–411, (1999).
7. Ali, F. A., D. O'Connor, and Abu-Tair A, "Explosive spalling of high-strength concrete columns in fire." *Magazine of Concrete Research* 53(3): 197-204, (2001).
8. Phan L.T. *High-Strength Concrete at High Temperature: An Overview. Utilization of High Strength/High Performance Concrete, 6th International Symposium.* Leipzig, Germany, (2002).
9. Khoury G.A. and Anderberg Y. *Concrete spalling - Review, Fire Safety Design,* (2000).
10. Jansson R. and Bostrom L. *Experimental study on the influence of polypropylene fibres on material properties and fire spalling of concrete. fib task group 4.3 workshop "Fire design o concrete structures - from materials modelling to structural performance".* Coimbra, Portugal, (2007).
11. Kalifa, P., G. Chéné, and Gallé C. "High-temperature behaviour of HPC with polypropylene fibres: From spalling to microstructure." *Cement and Concrete Research* 31(10): 1487-1499, (2001).
12. Schrefler, B. A., G. A. Khoury, Gawin D. and Majorana C.E. "Thermo-hydro-mechanical modelling of high performance concrete at high temperatures." *Engineering Computations* 19(7-8): 787-819, (2002).
13. Ulm, F.-J., P. Acker, and Levy M. "The ``Chunnel" Fire. II: Analysis of Concrete Damage." *Journal of Engineering Mechanics* 125(3): 283-289, (1999).
14. Bazant, Z. P., G. Cusatis, and Cedolin L. "Temperature Effect on Concrete Creep Modelled by Microprestress-Solidification Theory." *Journal of Engineering Mechanics* 130(6): 691-699, (2004).
15. Sercombe, J., C. Galle, Durand S.F., and Bouniol P. *On the importance of thermal gradients in the spalling of high-strength concrete 14th Engineering Mechanics Conference Austin, USA,* (2000).
16. Harmathy, T. Z. *Effect of moisture on the fire endurance of building elements. Research paper 270.* Ottawa, Division of Building Research, (1965).
17. Phan L.T. *High-Strength Concrete at High Temperature: An Overview. Utilization of High Strength/High Performance Concrete, 6th International Symposium.* Leipzig, Germany, (2002).
18. Mindeguia J.C., "Contribution expérimentale à la compréhension du risqué d'instabilité thermique des bétons", PhD thesis, University of Pau, France, (2009).
19. Jansson R. and Bostrom L., *The influence of pressure in the pore system on fire spalling of concrete. 5th International conference on Structures in Fire (SIF'08).* Singapore, (2008).
20. Jansson R. and Bostrom L. *Experimental study on the influence of polypropylene fibres on material properties and fire spalling of concrete. fib task group 4.3 workshop, "Fire design of concrete structures - from materials modelling to structural performance".* Coimbra, Portugal, (2007).
21. Pimienta P., Anton O., Mindeguia J.C., Avenel R., Cuyper H., Cesmat E., *Fire protection of concrete structures exposed to fast fires. 4th International symposium on Tunnel Safety and Security (ISTSS), Frankfurt, Germany, 17th-18th March* (2010).
22. Pimienta P., Hager I, *Mechanical behaviour of HPC at high temperature. 6th International Symposium on Utilisation of High Strength/high Performance Concrete.* Leipzig, Germany, 16-20 June (2002).
23. Hager I, Pimienta P., *Transient thermal strains of High Performance Concretes. Key note for Concreep7, International conference on creep, shrinkage and durability of concrete and concrete structures. Nantes, France, 12 pages, 12-14 September* (2005).
24. Hager I, Pimienta P., *Impact of the polypropylene fibers on the mechanical properties of HPC concrete, BEFIB , Proceedings of the 6th International RILEM Symposium. Editor Di Prisco et al. Varenna, Itale, 20 – 22 septembre* (2004).
25. HAGER, I, *Comportement à haute température des bétons à haute performance - évolution des principales propriétés mécaniques, Thèse de Doctorat de l'Ecole Nationale des Ponts et Chaussées* (2004)
26. Kalifa P., Menneteau F.D., Quenard D., *Spalling and pore pressure in HPC at high temperatures, Cement and Concrete Research, pp 1915-1927, August* (2000).
27. Heo Y.S., Sanjayan J.G., Han C.G. and Han M.C., *Effect of fiber type, length and numbers of fibers per unit volume on spalling protection of high strength concrete, 1st International Workshop on Concrete Spalling due to Fire Exposure, Leipzig, Germany, 3-5 September* 2009.

Stress-Strain Curves of Steel and Aluminum Exposed to Natural Fires

J. MALJAARS

ABSTRACT

The temperature-dependent reduction factors on the yield stress in codes for steel structures, k_y , are derived using a constant heating rate and a constant stress, where the influence of creep is implicitly taken into account. This paper considers the material properties of steel and aluminium on the basis of a Natural Fire Safety Concept, where heating rates and stresses are possibly non-constant in time and the influence of creep may be different. The paper shows that a non-constant heating rate and stress in time significantly influences the critical temperature in some cases.

INTRODUCTION

Stress-strain curves for fire exposed steel and aluminium provided in standards for fire design [1], [2] are based on uniaxial tensile tests. Creep strains are implicitly taken into account in these stress-strain curves. The conditions for which these curves are derived are:

- heating by the standard temperature-time curve (STTC);
- a constant stress in time.

The temperature history in case of the Natural Fire Safety Concept (NFSC) may deviate significantly from the standard temperature-time curve. Besides, restrained thermal expansion and a changing force distribution during fire exposure result in stresses that are not constant in time. The creep strain—and therefore stress-strain curves—depend on the temperature and stress history and may be different for the NFSC compared to STTC. This paper investigates whether or not the stress strain curves in the standards are representative for the NFSC.

A modified constitutive model—originally developed by Dorn and Harmathy—is used to simulate stress-strain curves at various temperature and stress histories. This model takes creep strains explicitly into account. The model is calibrated with creep tests and validated with transient state tests.

STRESS-STRAIN RELATIONSHIPS IN THE EUROCODES

2 % proof stress of steel

EN 1993-1-2 [1] provides reduction factors for the 2% proof stress of steel as a function of temperature, k_y . These factors are derived from an extensive test programme carried out at British Steel in 1980's on carbon steel grades 43A (appr. S275) and 50B (appr. S355) (Kirby and Preston, 2). The test programme consisted of uniaxial transient state tests at heating rates $d\theta/dt$ between 5 and 20°C/min (Fig. 1a) and various stress levels σ . The stress level in each test was constant in time. Each test gave a strain-time curve (Fig. 1b). These can be plotted as a function of temperature (Fig. 1c). Combining the stress-strain points at the same temperature and heating rate leads to a stress-strain curve (Fig. 1d) in which creep strains are implicitly taken into account. The 2% proof stress was distracted from the stress strain curve. Repeating this for several temperatures generates the reduction of the 2% proof stress as a function of the temperature. The reduction factors for the 2% proof stress are thus valid for a constant stress in time and for heating rates between 5 and 20°C/min.

0.2 % proof stress of aluminium alloys

Instead of the 2% proof stress, EN 1999-1-2 [2] provides reduction factors for the 0.2% proof stress. Due to lack of transient state test results on aluminium alloys, the data in EN 1999-1-2 [2] are based on steady state tests. These tests are carried out with strain rates of appr. 0.005/min and after 30 minutes of exposure to a constant elevated temperature.

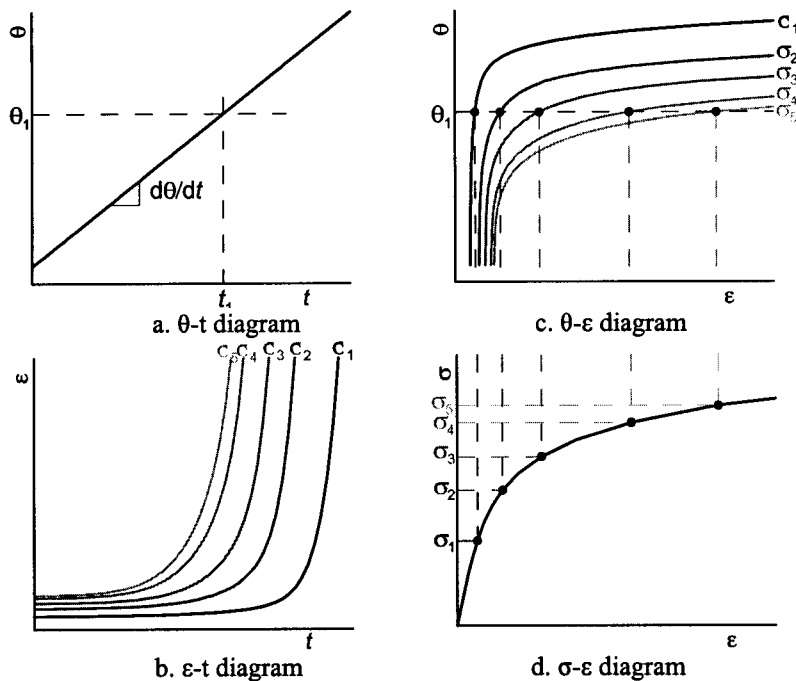


Figure 1. Derivation of stress-strain curves based on transient state tests.

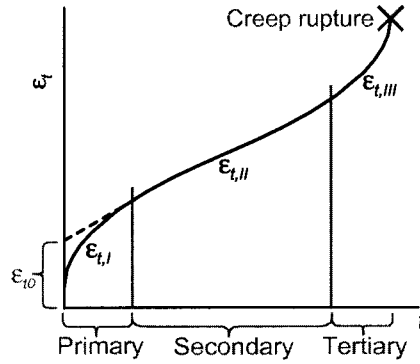


Figure 2. Strain development in a creep test.

MODIFIED DORN-HARMATHY MODEL

Description of the model

Fig. 2 shows the strain development in time ε_t in a creep test (i.e. a test at constant stress σ and constant elevated temperature T). The creep process is normally divided into three stages, i.e. a primary stage $\varepsilon_{t,I}$ with a decreasing strain rate in time, a secondary stage $\varepsilon_{t,II}$ with constant strain rate (the minimum strain rate) and a tertiary stage $\varepsilon_{t,III}$ with increasing strain rate. At the end of the tertiary creep stage, creep rupture occurs. The strain rate increases at increasing temperature and/or stress.

An analytical model is available with which the primary and secondary creep strain, $\varepsilon_{t,I+II}$, can be determined as a function of time, temperature and stress. The model is known as the Dorn-Harmathy model. The basis of the model is an equation by Dorn 4 for secondary creep $\varepsilon_{t,II}$ (Eq. 1). In Eq. (1), $Z(\sigma)$ is the Zener-Holloman parameter (Zener and Holloman 5), describing the influence of stress on the secondary strain rate. Dorn proposed Eq. (2) for $Z(\sigma)$. Alternatively Eq. (3) is proposed for Z in McQueen and Jonas 6. Harmathy 7 extended the model to incorporate primary creep $\varepsilon_{t,I}$ (Eq. 4). Parameter ε_{t0} is the projection back to zero time of the secondary strain curve (Fig 2). Eq. (5) is proposed for this parameter.

$$\dot{\varepsilon}_{t,II}(\sigma, T) = Z(\sigma) \cdot e^{\frac{-Q/R}{T}} \quad (1)$$

$$Z(\sigma) = \begin{cases} C_1 \cdot \sigma^{C_2} & \text{if } \sigma \leq \sigma_r \\ C_3 \cdot \exp(\sigma \cdot C_4) & \text{if } \sigma > \sigma_r \end{cases} \quad (2)$$

$$Z(\sigma) = C_5 \cdot (\sinh(C_6 \cdot \sigma))^{C_7} \quad (3)$$

$$\dot{\varepsilon}_{t,I+II}(\sigma, T) = \dot{\varepsilon}_{t,II}(\sigma, T) \cdot \coth^2 \left(\frac{\varepsilon_{t,I+II}}{\varepsilon_{t0}(\sigma)} \right) \quad (4)$$

$$\varepsilon_{t0}(\sigma) = C_8 \cdot (\sigma)^{C_9} \quad (5)$$

For some aluminium alloys the tertiary creep stage starts at a relatively low total creep strain. This makes it necessary to incorporate the tertiary creep stage in the

model. The strain at the start of the tertiary stage appeared to be approximately homogeneous, i.e. tertiary creep starts before necking. Maljaars et al. 8 proposed Eq. 6 to incorporate the first—homogeneous—part of the tertiary creep stage for aluminium alloys.

$$\dot{\varepsilon}_{t,I+II+III}(\sigma, T) = \begin{cases} \dot{\varepsilon}_{t,I+II}(\sigma, T) & \text{if } \varepsilon_{t,I+II+III} \leq \varepsilon_{t,\text{lim}} \\ \dot{\varepsilon}_{t,I+II}(\sigma, T) \cdot \frac{\varepsilon_{t,I+II+III}}{\varepsilon_{t,\text{lim}}} & \text{if } \varepsilon_{t,I+II+III} > \varepsilon_{t,\text{lim}} \end{cases} \quad (6)$$

In equations (1) to (6), Q , σ_r , ε_{lim} and C_1 - C_9 are material-dependent parameters that have to be determined with creep tests (Section 3.2). R is the universal gas constant. Dorn 4 pointed out that the model can also be applied in case of a varying temperature in time. This makes the model suited for application in fire conditions. Harmathy 7 showed that the model can be applied with reasonable accuracy for non-constant stress in time, provided $d\sigma / dt$ is not too large. Equation (4) is an implicit equation, where the creep strain rate depends on the creep strain already developed. A numerical procedure is used to determine the creep strain at the end of each timestep i based on the creep strain of the previous timestep $i-1$ and the creep strain increment. Eq. (7) gives the procedure for steel, i.e. without the extension for tertiary creep. Finally the entire strain at elevated temperature is considered to consist of thermal strain, elastic strain and creep strain, Eq. (8) (Harmathy 7 and Thor 9). The elastic strain and creep strain together form the mechanical strain.

$$\varepsilon_{t,I+II}^i(\sigma, T, t) = \varepsilon_{t,I+II}^{i-1} + Z(\sigma) \cdot \exp\left(\frac{Q/R}{T}\right) \cdot \coth^2\left(\frac{\varepsilon_{t,I+II}^{i-1}}{\varepsilon_{t0}(\sigma)}\right) \cdot \Delta t \quad (7)$$

$$\varepsilon(c, T, t) = \varepsilon_{th}(T) - \varepsilon_{el}(c, T) - \varepsilon_{t,I+II(+III)}(c, T, t) \quad (8)$$

Model parameters for steel and aluminium - calibration of the model

Harmathy 7, Thor 9 and Anderberg 10 carried out individual creep tests in order to determine the material-dependent parameters of the Dorn-Harmathy model for various steel qualities. Series of tests with the same stress level but with different temperatures are used to determine parameter Q . Series of tests with the same temperature but with different stress levels are used to determine parameters σ_r , C_1 - C_4 and C_8 - C_9 . The parameter values are summarised in Table I (for σ in $[\text{N}/\text{mm}^2]$ and T in $[\text{K}]$). Maljaars et al. used a similar procedure to determine parameters Q , ε_{lim} and C_5 - C_9 for two aluminium alloys (Table II).

Table I. Model parameters for carbon steel (Sources: Harmathy 7, Thor 9, Anderberg 10).

Steel quality	$f_{y,20^\circ\text{C}}$ [N/mm ²]	Q/R [K]	σ_r [N/mm ²]	C_1 [1/min]	C_2 [-]	C_3 [1/min]	C_4 [-]	C_8 [-]	C_9 [-]
1312 (1)	254	$5.58 \cdot 10^4$	108	$6.10 \cdot 10^9$	7.81	$1.38 \cdot 10^{23}$	$5.78 \cdot 10^{-2}$	$5.56 \cdot 10^{-6}$	1.72
1312 (2)	263	$5.39 \cdot 10^4$	108	$8.98 \cdot 10^8$	7.64	$5.00 \cdot 10^{12}$	$6.02 \cdot 10^{-2}$	$2.66 \cdot 10^{-7}$	2.25
1411 ¹	340	$6.60 \cdot 10^4$	118	$8.37 \cdot 10^{12}$	8.49	$2.42 \cdot 10^{27}$	$6.04 \cdot 10^{-2}$	$3.53 \cdot 10^{-7}$	2.08
A36-66	304	$3.89 \cdot 10^4$	103	$6.23 \cdot 10^6$	4.70	$2.00 \cdot 10^{14}$	$4.34 \cdot 10^{-2}$	$4.07 \cdot 10^{-6}$	1.75

¹ Some parameter values differ between Thor and Anderberg for steel quality 1411. The listed values are according to Thor because these are more consistent.

Table II. Model parameters for aluminium (Source: Maljaars et al. 8).

Aluminium alloy	$f_{0.2,20^\circ\text{C}}$ [N/mm ²]	Q/R [K]	C_5 [1/min]	C_6 [-]	C_7 [-]	C_8 [-]	C_9 [-]	ϵ_{lim} [-]
5083-O/H111	150	$1.83 \cdot 10^4$	$6.7 \cdot 10^{10}$	$2.5 \cdot 10^{-2}$	3.0	$4.0 \cdot 10^{-10}$	3.4	$> 4 \cdot 10^{-2}$
6060-T66	200	$2.35 \cdot 10^4$	$7.0 \cdot 10^{12}$	$4.0 \cdot 10^{-2}$	3.0	$2.0 \cdot 10^{-18}$	7.45	$2.0 \cdot 10^{-3}$

Validation of the model

In order to check the outcome of the model, a comparison is made between the reduction factors k_y , according to EN 1993-1-2 [1] and the results of simulations with the model. To arrive at the simulated reduction factors k_y , the same procedure has been followed as described in Fig. 1 but then using the Dorn-Harmathy model. The constant heating rates applied in the simulations are such that the temperature considered is reached after 30 minutes, i.e. a heating rate of 13°C/min for k_y at 400°C and 26°C/min for k_y at 800°C. The results of the simulations for carbon steels are provided in Fig. 3 together with the data in EN 1993-1-2 [1]. A good agreement exists between k_y based on the model and k_y in EN 1993-1-2 [1], where the latter are based on tests.

Transient state tests are carried out on the aluminium alloys 5083-O/H111 and 6060-T66 and these tests are simulated with the Dorn-Harmathy model in Maljaars et al. 8. As an example, Fig. 4a presents the strain as a function of temperature in a test on alloy 5083-O/H111, with a constant stress in time and Fig. 4b presents the strain as a function of temperature in a test on alloy 6060-T66, carried out with an increasing stress in time. In total, 27 transient state tests care carried out and simulated. For all cases, the temperature was determined at which the plastic strain was equal to 0.02%. The difference in this temperature between the tests and the simulations was on average 1°C and the standard deviation was 5°C. Thus, the model is well-able to simulate the transient state stress-strain curves of metals at elevated temperatures.

It should be noted that the (modified) Dorn-Harmathy model describes the diffusional creep process. This process dominates the behaviour at high-enough temperatures. At moderately elevated temperatures, other degradation processes are relevant. Consequently the model is valid for temperatures higher than appr. 400°C for carbon steel and higher than appr. 175°C for aluminium alloys.

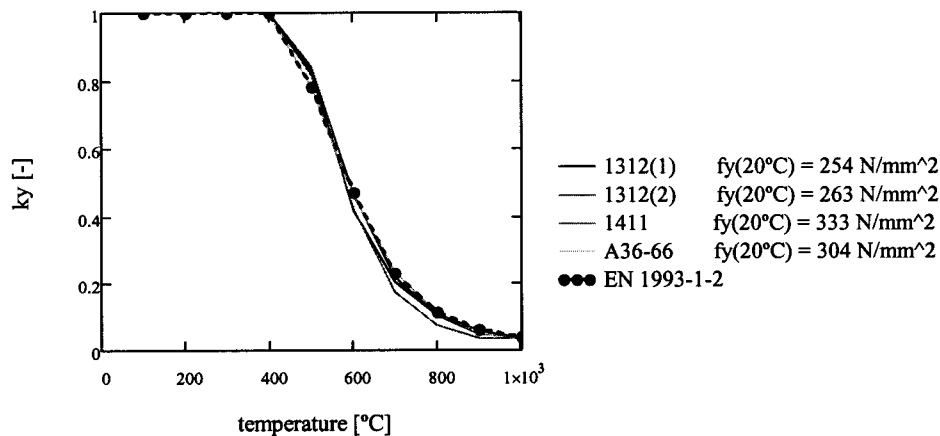
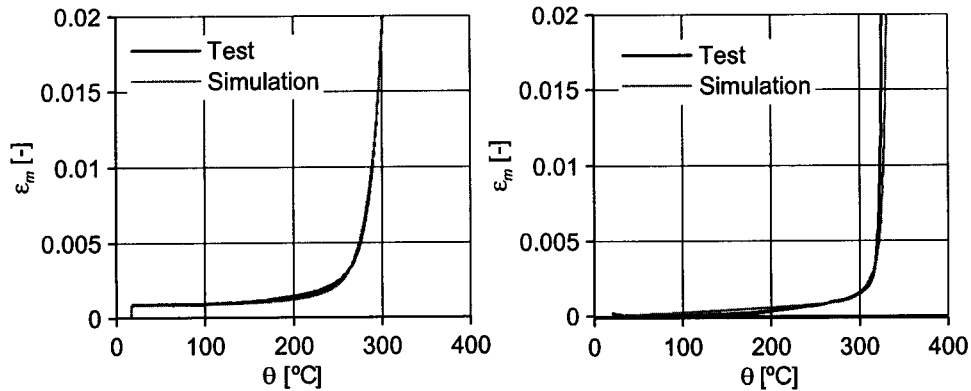


Figure 3. Yield strength reduction at elevated temperatures for carbon steels.



a. Alloy 5083-O/H111

b. Alloy 6060-T66

$$d\theta / dt = 10^{\circ}\text{C}/\text{min}, \sigma = 60 \text{ N}/\text{mm}^2 \quad d\theta / dt = 10^{\circ}\text{C}/\text{min}, d\sigma / dt = 1.67 \text{ N}/\text{mm}^2/\text{min}$$

Figure 4. Simulations of uniaxial transient state tensile tests on aluminium alloys.

STRESS-STRAIN CURVES FOR NATURAL FIRE CONDITIONS

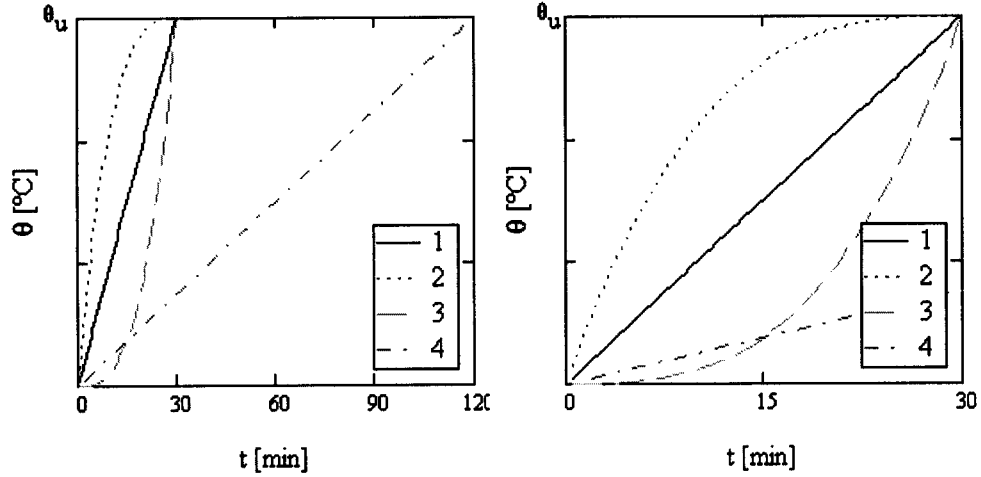
Strain development for various heating curves

In this study the heating curves according to Fig. 5 are considered. These heating curves – numbered 1 to 4 – are artificial curves with the same maximum temperature θ_u . Most heating curves of insulated or uninsulated members exposed to realistic fires are expected to fall in between curves 2 and 3, when neglecting the pre-flash-over phase of the fire. The maximum temperature θ_u is selected as 600°C for steel members and 300°C for aluminium members. (These member temperatures are to be achieved by applying appropriate insulation). For all cases the stress is considered as constant in time.

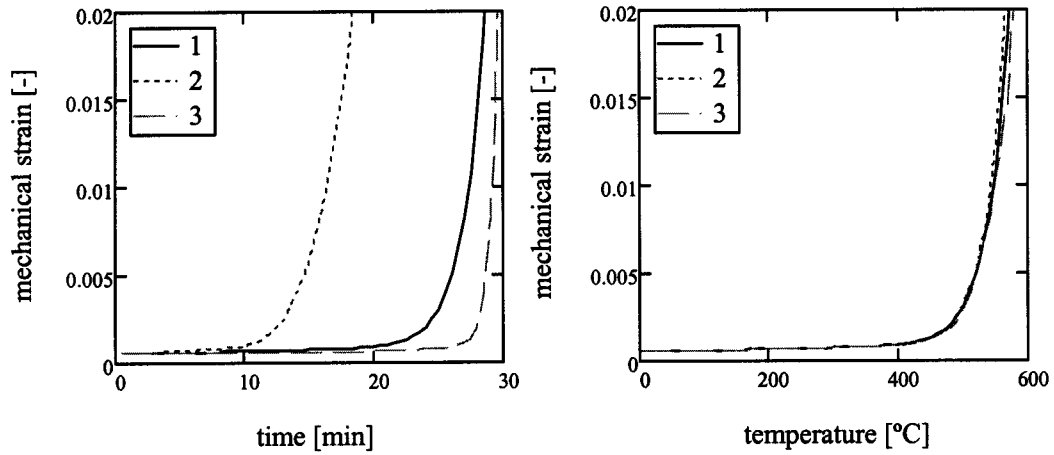
Eq. (8) is used to determine the strain development for the heating curves 1-3 of Fig. 5. Fig. 6 presents the mechanical strain as a function of time (Fig. 6a) or temperature (Fig. 6b) for steel 1312 with $\theta_u = 600^{\circ}\text{C}$ and $\sigma = 127 \text{ N}/\text{mm}^2$ ($= \frac{1}{2} f_{y,20^{\circ}\text{C}}$). Fig. 6a shows that the time at the attainment of 2 % mechanical strain for heating curve 2 is considerably lower than for heating curves 1 and 3, even though the maximum temperature of the three curves is equal. Fig. 6b shows that the strain development as a function of temperature is almost equal for the three curves. Thus, it appears that not only the maximum temperature, but also the heating curve has an important influence on the fire resistance. This should be considered in the safety margins in a natural fire safety concept.

Fig. 7 presents stress-strain curves of steel 1312 at $\theta_u = 600^{\circ}\text{C}$ (Fig. 7a) and aluminium alloy 5083-H111 at $\theta_u = 300^{\circ}\text{C}$ for the heating curves of Fig. 5. These curves are generated in the way described in Fig. 1. The figure indicates that the influence of the heating curve on the stress-strain curves is larger for the aluminium alloy than for steel. This more significant influence was found for both aluminium alloys. Fig. 8 presents the reduction of the proof stress as a function of θ_u for various heating curves. Following the definitions in EN1993-1-2 and EN1999-1-2, the 2% proof stress is plotted for steel while the 0,2 % proof stress is plotted for aluminium. The figure indicates that the reduction as a function of temperature is similar for all heating curves considered. However in the interpretation of these

figures it should be considered that the heating curves have an important influence on the fire resistance, as shown in Fig. 6a.

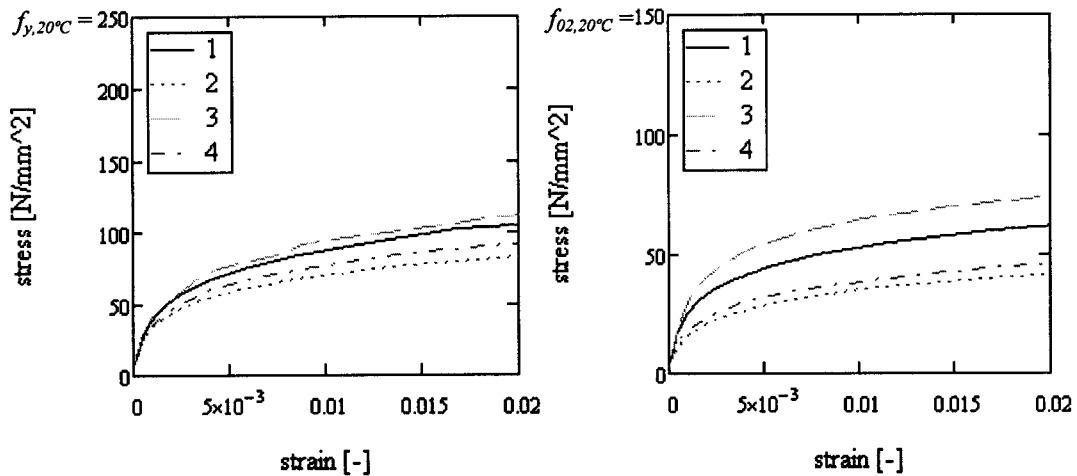


The 2nd graph gives the same heating curves but focuses on the first 30 min.
Figure 5. Member temperature – time curves considered.



a. mechanical strain as a function of time b. mechanical strain as a function of temp.

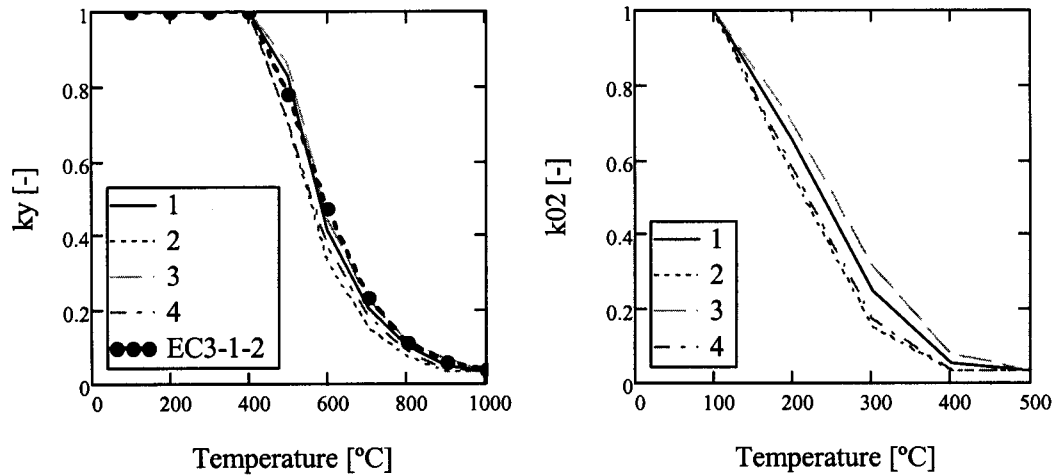
Figure 6. Strain development for steel, heating curves 1,2 and 3, $\theta_u = 600^\circ\text{C}$ and $\sigma = \frac{1}{2} f_{y,20^\circ\text{C}}$



a. Steel 1312 at $\theta_u = 600^\circ\text{C}$

b. Alu 5083-H111 at $\theta_u = 300^\circ\text{C}$

Figure 7. Stress-strain curves of steel and aluminium for various heating curves.



a. Steel 1312 at $\theta_u = 600^\circ\text{C}$ b. Alu 5083-H111 at $\theta_u = 300^\circ\text{C}$
 Figure 8. Reduction of the proof stress as a function of temperature for various heating curves.

Strain development for various stress curves

Four different stress-time relationships are considered in the study. These are indicated in Fig. 9. Curve represents a constant stress in time, curve b an increasing stress in time (e.g. due to restrained thermal expansion), curve c a decreasing stress in time (e.g. due to weakening) and curve d represents an increasing stress followed by a decreasing stress (first thermal expansion followed by weakening). The stress after 30 minutes of fire exposure is the same for all curves and is equal to 0.5 times the yield stress at room temperature. The same heating curve was considered for all stress-time relationships. This heating curve is curve 1 in Fig. 5 (constant heating rate) with $\theta_u = 600^\circ\text{C}$ for steel and $\theta_u = 300^\circ\text{C}$ for aluminium.

Eq. (8) is used to determine the strain development for the stress-time relationships a-d. Fig. 10 presents the mechanical strain as a function of time (Fig. 10a) or temperature (Fig. 10b) for steel 1312 with $\theta_u = 600^\circ\text{C}$. Fig. 11 gives the same results but for aluminium alloy 5083-O/H111 with $\theta_u = 300^\circ\text{C}$. The figures show that the stress rate influences the fire resistance. Again the influence in case of aluminium is larger as compared to steel.

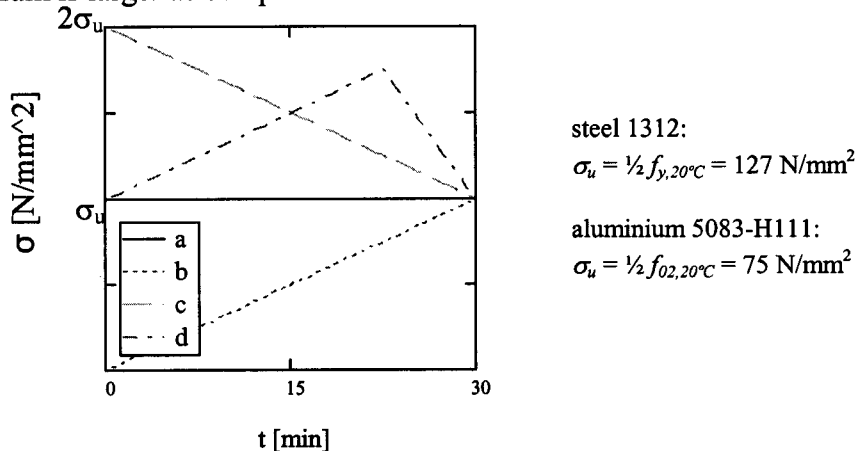


Figure 9. Stress-time relationships considered.

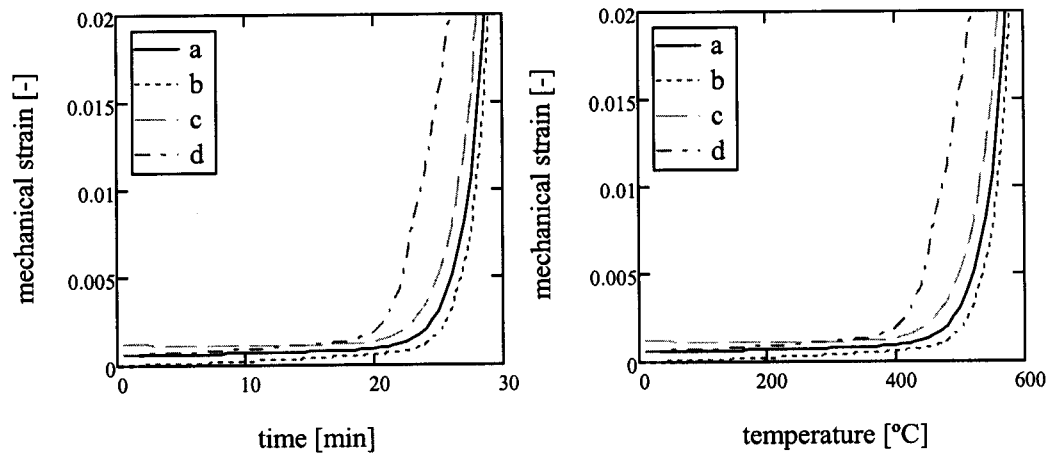


Figure 10. Strain development for steel 1312, stress rates a-d, $\theta_u = 600^\circ\text{C}$ and $\sigma = \frac{1}{2} f_{y,20^\circ\text{C}}$

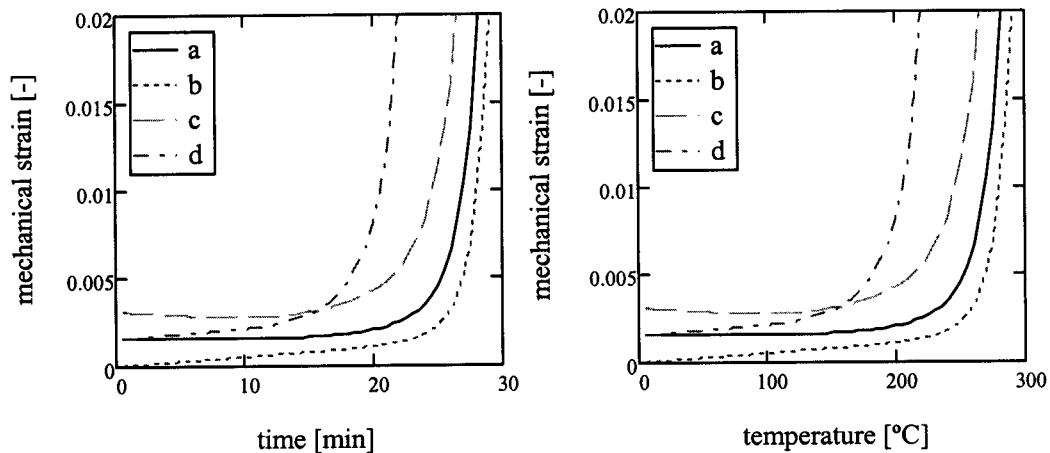


Figure 11. Strain development for alu 5083-O/H111, stress rates a-d, $\theta_u = 300^\circ\text{C}$, $\sigma = \frac{1}{2} f_{02,20^\circ\text{C}}$

CONCLUSIONS

- The mechanical strain for metals exposed to fire exposed metals is dominated by creep.
- The Dorn-Harmathy creep model provides an excellent basis to simulate the material properties of metals exposed to fire. The agreement with transient state tests is very good.
- The fire resistance not only depends on the stress and the maximum temperature, but also on the stress history and temperature history (i.e. heating curve). This is especially relevant for natural fire safety concepts, where a large range of stress and temperature histories are possible.
- Applying the reduction of the yield stress according to codes such as EN1993-1-2 [1] in natural fire safety concepts might be unsafe in cases where the heating rate near the maximum temperature is low and / or when the stress rate near the maximum temperature is high. This should be considered in the safety margins. Alternatively the Dorn Harmathy model can be used as a basis to determine the fire resistance.

- The influence of the stress rate and the heating rate is more important for aluminium alloys than for carbon steels.

REFERENCES

1. EN 1993-1-2, Eurocode 3 (2007) Design of steel structures—Part 1-2: General Rules—Structural fire design.
2. EN 1999-1-2, Eurocode 9 (2007) Design of aluminium structures—Part 1-2: General Rules—Structural fire design.
3. Kirby, B.R. and Preston, R.R. (1988). 'High temperatures properties of hot-rolled structural steels for use in fire engineering design studies.' *Fire Safety J.*, 13, pp 27–37.
4. Dorn, J.E. (1954) Some fundamental experiments on high temperature creep, *J. Mech. Phys. Solids*, 3, pp. 85-116.
5. Zener, C. and Holloman, H.H. (1944) Effect of strain rate on the plastic flow of steel, *J. Applied Phys.* 15, p. 22.
6. McQueen, H.J. and Jonas, J.J. (1971) in *Metal Forming, Interrelation between Theory and Practice*, Ed. A.L. Hoffmann, Plenum Publ. Corp., New York, pp. 393-428.
7. Harmathy, T.Z. (1967) A comprehensive creep model, *J. Basic Engineering*, 89, pp. 496-502.
8. Maljaars, J. Soetens, F. and Katgerman, L. (2008) Constitutive model for aluminium alloys exposed to fire conditions, *Metall. mat. trans. A*, 39, pp. 778-789.
9. Thor, J. (1973) Deformations and critical loads of steel beams under fire exposure conditions, *National Swedisch Building Research D* 16.
10. Anderberg Y. (1988) Modelling Steel Behaviour, *Fire Safety Journal*, 13, pp. 17-26.

Tangent Modulus of ASTM A992 Steel at Elevated Temperatures

M. A. MOROVAT, J. LEE, G. HU and M. D. ENGELHARDT

ABSTRACT

Predicting the response of steel structures to fire requires a thorough characterization and understanding of steel material properties at elevated temperatures. A key material property of interest is the tangent modulus of the uniaxial stress-strain curve. Tangent modulus is a critical property for predicting stability controlled limit states of steel members, such as column buckling, beam lateral-torsional buckling, and local buckling. In this paper, the authors propose a methodology for calculating the tangent modulus of steel at elevated temperatures based on a Ramberg-Osgood formulation for true stress versus true strain. This methodology is applied to elevated-temperature stress-strain data for ASTM A992 steel developed by the authors and is compared to tangent modulus predictions from Eurocode 3. The proposed approach is intended to provide a simpler and more accurate prediction of tangent modulus for stability predictions at elevated temperatures.

Mohammed Ali Morovat (corresponding author), Graduate Research Assistant, Ferguson Structural Engineering Laboratory, The University of Texas at Austin, Austin, Texas 78758
Jinwoo Lee, Graduate Research Assistant, Ferguson Structural Engineering Laboratory, The University of Texas at Austin, Austin, Texas 78758
Guanyu Hu, Graduate Research Assistant, Ferguson Structural Engineering Laboratory, The University of Texas at Austin, Austin, Texas 78758
Michael D. Engelhardt, Professor, Ferguson Structural Engineering Laboratory, The University of Texas at Austin, Austin, Texas 78758

INTRODUCTION

The tangent modulus of the uniaxial stress-strain curve of steel is a key material property for predicting stability controlled limit states of steel members at both ambient temperature and at elevated temperatures. Stability limit states of interest include flexural buckling of columns, lateral torsional buckling of beams, plate buckling, and others. At high temperatures, the shape of the stress-strain curve of steel is fundamentally different from that at ambient temperature. At high temperatures, steel does not exhibit a well-defined yield plateau and becomes highly nonlinear at low levels of stress. Consequently, the variation of tangent modulus with stress is highly temperature dependent, and accurate prediction of this relationship is crucial for predicting instability of steel members for structural fire engineering applications.

Analytical expressions have been proposed to model the stress-strain behavior of metals in general and structural steel in particular at both ambient and elevated temperatures. These models can be grouped into three major categories: multi-linear [10], combination of linear and smooth curves [3, 6, 17, and 18], and power-law forms [1, 7, 8, 11, 12, 13, 16, 17, and 19]. Owing to the fact that stress-strain behavior is highly nonlinear at high temperatures, multi-linear models are usually not very accurate to model such nonlinear behaviors, especially in the “knee” region of the stress-strain curve. Ludwick [11], is among the first to introduce the power-law form of stress-strain behavior in order to predict strain-hardening characteristics of metals.

It should also be added that most of the models noted above express stress as a function of strain. Nadai [16] attempted at developing stress-strain relationships, in which strain is expressed as a function of stress. Such representations of the stress-strain curve can be more suitable for buckling studies [13, 16]. Later on, Ramberg and Osgood [13, 16] modified Nadai’s formulation and came up with simpler form in which only three parameters were used to describe stress-strain curves.

In this paper, a methodology for computing the tangent modulus of steel at elevated temperatures is proposed. This methodology is based on using a Ramberg-Osgood formulation for describing the true stress versus true strain response of steel at elevated temperatures, and then using this relationship to derive expressions for tangent modulus. Results of the proposed methodology are compared with experimental data and with predictions derived from Eurocode 3 [5, 18].

METHODOLOGY FOR TANGENT MODULUS CALCULATIONS

It can be shown that if expressed in true values and plotted on a logarithmic scale, stress-strain behavior of steel in the inelastic range is linear [4]. In other words, the log of true stress varies linearly with the log of true strain in the inelastic range. This suggests that there exists a power-law relationship between true-stress and true-strain for inelastic strains, which simplifies description of the strain-hardening characteristics of metals. The most simplified power-law equation is the one suggested by Hollomon [8] as,

$$\sigma = K\varepsilon_p^n \quad \text{or} \quad \sigma = K\left(\varepsilon - \frac{\sigma}{E}\right)^n \quad (1)$$

where, σ is true stress, ε_p is true plastic strain, ε is total true strain, E is the Young's modulus, K is the strength coefficient, and n is the strain-hardening exponent. Ludwick [11], Voce [19], Swift [17], and several other researchers [1, 12] made some adjustments to this equation to get better fits to experimental data on metals at different plastic-strain ranges. Looking more closely at different variations of Equation (1) proposed in the literature, one can see that a common strategy has been to replace σ on the right-hand side of the equation with yield stress and to add some factors inside parentheses, apparently to avoid complications of having σ on both sides of the equation in the fitting process. Yet, another strategy that seems reasonable is just to move all the stress terms to one side of the equation by a simple algebraic manipulation, which leads to,

$$\varepsilon = \frac{\sigma}{E} + \left(\frac{\sigma}{K}\right)^{1/n} \quad (2)$$

which is similar to the Ramberg-Osgood equation for stress-strain behavior [13, 16]. One of the main advantages of the stress-strain law in the form of Ramberg-Osgood to the one by Hollomon is the ability to relate stress and strain using just one single continuous equation. In other words, using the differential form of Equation (2) and considering the tangent to be the slope of stress-strain curve ($d\sigma/d\varepsilon$), a mathematical expression relating tangent modulus to stress can be derived as follows,

$$E_T = \frac{E}{1 + \frac{E}{n\sigma} \left(\frac{\sigma}{K}\right)^{1/n}} \quad (3)$$

in which, E_T is the tangent modulus.

Since the main goal here is to develop equations to predict the tangent modulus, the smoothness of the proposed stress-strain law is important, since the tangent modulus is the derivative of the stress-strain curve. The fact that the Ramberg-Osgood form of the stress-strain curve expresses strain explicitly in terms of stress in a single continuous curve describing both the elastic and inelastic ranges of behavior makes it a suitable candidate for tangent modulus calculations. The application of Equation (3) to predict tangent modulus of ASTM A992 steel at elevated temperatures will be discussed in the following section.

As a final note in this section, it should be recalled that the following equations [4] can be used to estimate true stress and true strain in terms of engineering stress and engineering strain,

$$\varepsilon = \ln(1 + \varepsilon_{eng}) \quad \text{and} \quad \sigma = \sigma_{eng}(1 + \varepsilon_{eng}) \quad (4)$$

where, σ_{eng} and ε_{eng} denote engineering stress and strain respectively. These formulas are valid up to the formation of necking for which the assumption of

uniform distribution of strain over the gauge length of a tension coupon is approximately valid.

APPLICATION OF THE PROPOSED METHODOLOGY

In this section, the application of Equations (2) and (3) in predicting stress-strain and tangent modulus-stress behaviors of ASTM A992 steel [6] at elevated temperatures is presented. The application involves fitting Equation (2) to an experimental data on ASTM A992 steel [9] and comparing the estimations with the corresponding ones from Eurocode 3. Strain-hardening parameters, K and n , evaluated throughout the process of fitting Equation (2) to data, are then used along with the Equation (3) to calculate tangent modulus.

The experimental data on ASTM A992 steel used as a basis for curve-fitting is reported by Hu, et al [9], wherein tension coupon tests were conducted at temperatures from 20°C to 900°C. Further, tests were conducted at two different crosshead displacement rates of 0.01 in/min and 0.1 in/min to examine strain rate effects. The results of fitting Equation (2) to this test data at 400°C for two different crosshead displacement rates are shown in Figure 1. The corresponding predictions of Eurocode 3 are also presented. It should be pointed out that the predictions using Equation (2) are considered valid only up to the onset of significant necking, since this is the limit of validity of the equations that convert true and engineering values of stress and strain. The limit of applicability of the predicted stress-strain response using Equation (2) is indicated by the end of the solid curves in Figure 1. Since the intent of these predictions is to develop tangent modulus expressions for stability calculations, the pre-necking behavior is of interest.

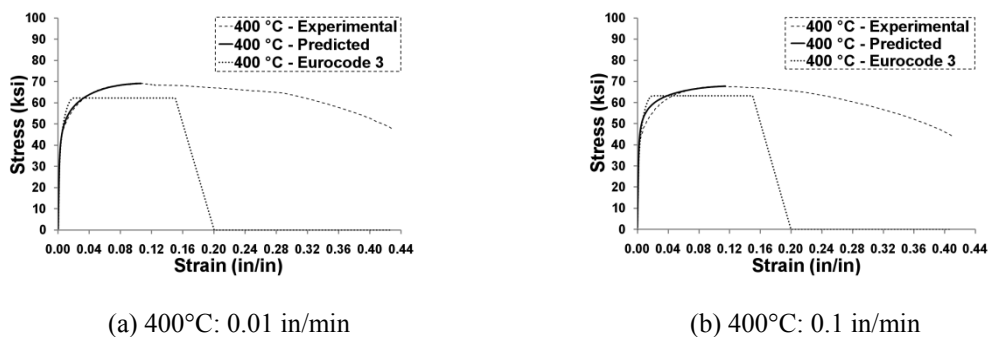


Figure 1. Stress-strain predictions at 400 °C at two different displacement rates.

Normalized stress-strain curves with respect to the room temperature values are shown in Figure 2. The solid lines in this figure are the stress-strain curves predicted using Equation (2). The dotted lines are the stress-strain curves predicted by Eurocode 3. In general, there is reasonable agreement between the two predictions. There is somewhat better agreement for the low displacement-rate data, especially at higher temperatures.

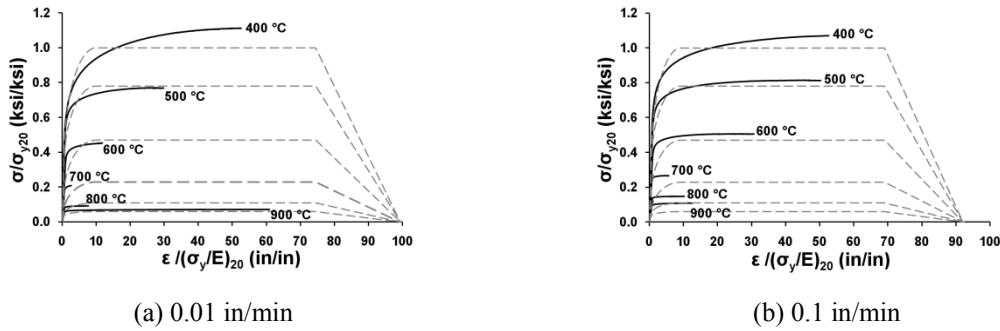


Figure 2. Normalized stress-strain predictions at elevated temperatures—a comparison with Eurocode 3.

The direct outcomes of the fitting process using Equation (2) are strain-hardening parameters, K and n . Figure 3 shows the variation of K and n values with respect to temperature and displacement rates. The general trend is that both K and n are decreasing with increasing temperature, as expected. Another point to be taken from Figure 3 is that for the most part, K has higher values for the high displacement-rate tests. This is in accord with the observation that strength is rate-dependent and generally has higher values at higher rates. Figure 3 also clearly shows that at 800°C, n has the lowest value of all, suggesting the least strain-hardening at this temperature.

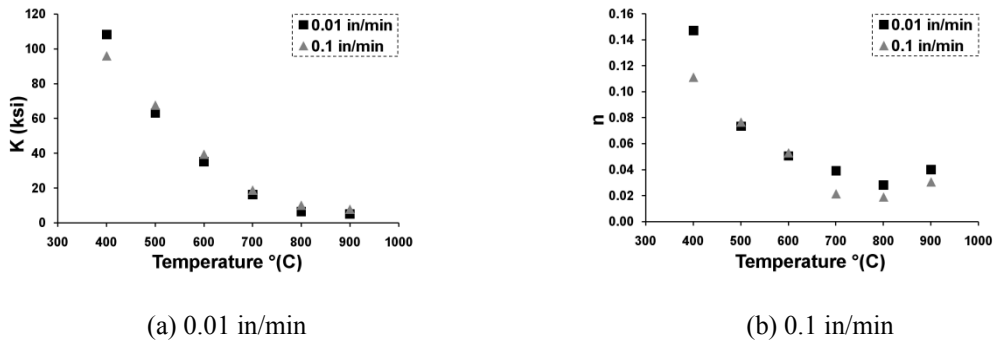


Figure 3. Strain hardening parameters, K and n as functions of temperature and displacement rates.

In Figure 4, a comparison has been made between tangent modulus predictions using Equation (3) and using Eurocode 3 with the tangent modulus derived directly from the experimental data at 700°C and a crosshead displacement rate of 0.01 in/min. A good agreement can be seen between predictions and test data. Such agreement has been also observed for tangent modulus calculations at other temperatures and displacement rates.

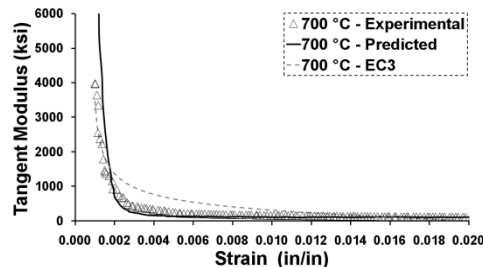


Figure 4. Tangent modulus-strain relationship.

Figure 5 presents normalized tangent moduli from Equation (3) with respect to Young's modulus at various temperatures as a function of stress. Such a representation of tangent modulus clearly shows that at higher temperatures, the tangent modulus drops to zero at a very low level of stress. Figure 6 also shows the same concept with actual values of tangent moduli instead of normalized ones.

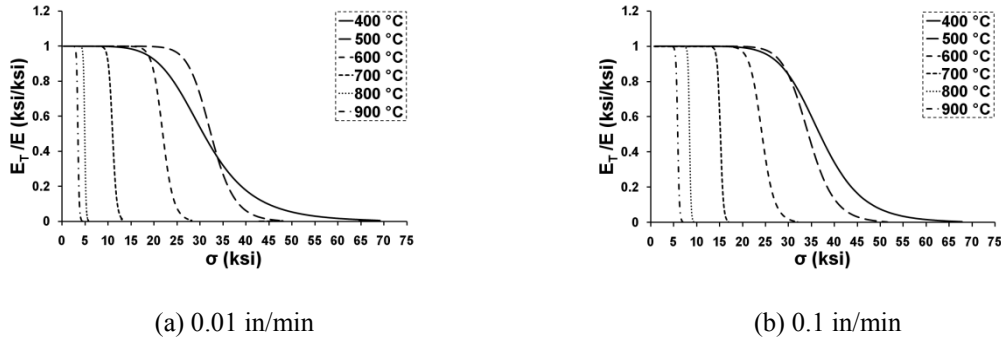


Figure 5. Normalized tangent modulus-stress relationship at elevated temperatures.

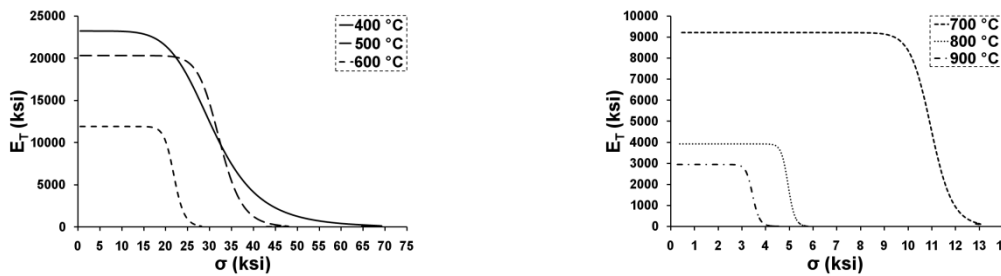


Figure 6. Tangent modulus-stress relationship at elevated temperatures for 0.01 in/min data.

Although implementing the proposed methodology results in tangent modulus as a function of stress, it is also useful to study the variation of tangent modulus with respect to strain. This is especially helpful for the purpose of comparison with predictions by the Eurocode 3. The variation of tangent modulus predicted by Equation (3) with strain is plotted in Figures 7 and 8, in normalized and non-normalized forms.

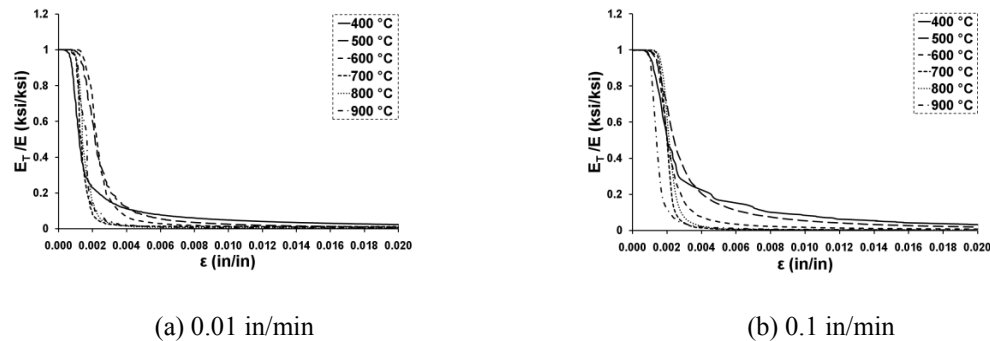


Figure 7. Normalized tangent modulus-strain relationship at elevated temperatures.

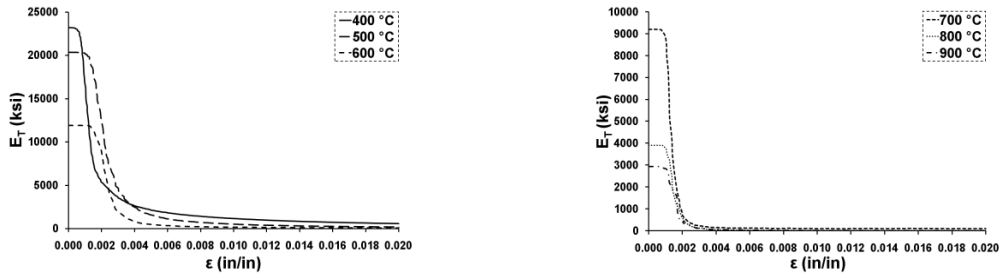


Figure 8. Tangent modulus-strain relationship at elevated temperatures.

For the purpose of comparison, the tangent modulus prediction from the proposed methodology has been plotted along with the corresponding one from Eurocode 3 for the 700 °C, 0.01 in/min displacement-rate test. As can be seen from Figure 9 there are significant differences between the two approaches, and these differences can have a large impact on stability predictions.

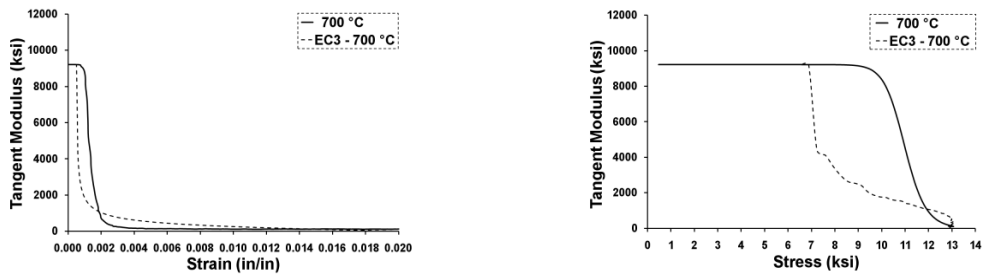


Figure 9. Tangent modulus as a function of both stress and strain compared with Eurocode 3 predictions 700°C.

CONCLUSION

Empirical formulas in the form of Ramberg-Osgood have been proposed to predict the tangent modulus for ASTM A992 steel at elevated temperatures. The Ramberg-Osgood form has been utilized mainly due to its ability to simply express strain explicitly in terms of stress in a single continuous curve that covers both the elastic and inelastic ranges of behavior, up to the onset of significant necking. This approach can lead to simpler and more accurate predictions of tangent modulus for use in stability predictions of steel members at elevated temperatures.

ACKNOWLEDGEMENT

The research reported herein was conducted as part of a research project on *Creep Buckling of Steel Columns Subjected to Fire* supported by the National Science Foundation (NSF Award 0927819). Elevated temperature material tests were conducted using equipment procured through an NSF Major Research Instrumentation Grant (NSF Award No. CMS-0521086—*Acquisition of a High-Temperature Testing Facility for Structural Components and Materials*). The

support of the National Science Foundation and of NSF Program Director M.P. Singh is gratefully acknowledged.

REFERENCES

1. Adams, C. and Beese, J.G. 1974. "Empirical Equations for Describing the Strain-Hardening Characteristics of Metals Subjected to Moderate Strains," *Journal of Engineering Materials and Technology*, 96(4):123–126.
2. Aitchison, C.S., and Miller, J.A. 1942. *Tensile and Pack Compressive Tests of Some Sheets of Aluminum Alloy, 1025 Carbon Steel, and Chromium-Nickel Steel*, NACA Technical Note No. 840, February 1942.
3. Anderberg, Y. 1988. "Modelling Steel Behaviour", *Fire Safety Journal*, 13(1):17–26.
4. Dieter, G.E. 1986. *Mechanical Metallurgy*, 3rd edition, McGraw-Hill, New York.
5. Eurocode 3 2003. *Design of steel structures. Part 1-2: General rules*. Structural fire design, EN 1993-1-2 European Committee for Standardization. CEN.
6. Gayle, F.W., Fields, R.J., Luecke, W.E., Banovic, S.W., Foecke, T., McCowan, C.N., McColskey, J.D. and Siewert, T.A. 2005. "Federal Building and Fire Safety Investigation of the World Trade Center Disaster - Mechanical and Metallurgical Analysis of Structural Steel (Draft)," *Report NCSTAR 1-3*, National Institute of Standards and Technology, Gaithersburg, MD.
7. Hill, H.N. 1944. *Determination of Stress-Strain Relations from "Offset" Yield Strength Values*, NACA Technical Note No. 927, February 1944.
8. Hollomon, J.H. 1945. "Tensile deformation," *Transactions of Metallurgical Society, AIME*, 162:268–290.
9. Hu, G., Morovat, M.A., Lee, J., Schell, E., and Engelhardt, M.D. 2009. "Elevated Temperature Properties of ASTM A992 Steel," *Proceedings, Structures Congress*, ASCE, Austin, April 2009.
10. Lie, T.T. (ed.) 1992. *Structural Fire Protection*, ASCE Manuals and Reports on Engineering Practice No. 78, New York, NY.
11. Ludwick, P. 1909. *Elemente der Technologischen Mechanik*, 3rd edition, Springer, Berlin.
12. Morrison, W. 1966. "The Effect of Grain Size on the Stress-Strain Relationship in Low-Carbon Steel," *Transactions of the ASM*, 59:824–846.
13. Osgood, W.R. 1932. "Column Curves and Stress-Strain Diagrams," *National Bureau of Standards Journal of Research*, 9:571–582.
14. Poh, K.W. 1997. "General Stress-Strain Equation," *Journal of Materials in Civil Engineering*, ASCE, 9(4):214–217.
15. Poh, K.W. 2001. "Stress-Strain-Temperature Relationship for Structural Steel," *Journal of Materials in Civil Engineering*, ASCE, 13(5):371–379.
16. Ramberg, W., and Osgood, W.R. 1943. *Description of Stress-Strain Curves by Three Parameters*, NACA Technical Note No. 902, July 1943.
17. Swift, H.W. 1946. "Plastic Strain in Isotropic-Hardening Material," *Engineering*, 162: 381–384.
18. Twilt, L., Both, C. 1991. "Stress-strain Relationships of Structural Steel at Elevated Temperatures: Analysis of Various Options and European Proposal," *TNO-Rep. BI-91-015*, TNO Building and Construction Research, Delft, The Netherlands.
19. Voce, E. 1948. "The relationship between stress and strain for homogeneous deformation," *Journal of the Institute of Metals*, 74: 537

Behaviour of Galvanized High Strength Grade 10.9 Bolts Under Fire Conditions

F. GONZÁLEZ and J. LANGE

ABSTRACT

In the last decades structural fire design has changed essentially. In the past the structural integrity of single elements was mostly proven by load tables which were based on fire tests. The introduction of the “hot” Eurocodes (Parts 1-2) offers the possibility to assess the resistance even of complex structural systems under fire conditions. For this purpose a calculation can be made according to the Eurocodes taking into account the relevant material behaviour which is mainly known for structural steel and concrete elements. The material behaviour is defined in the ECs by stress—strain curves, depending on the temperature. Even for connections design rules are given in the Eurocodes. The resistance of bolts and welding seams under fire conditions can easily be calculated using global reduction factors which depend on the element temperature. The global reduction factors for bolts are currently valid for all grades. The experience shows that either differing alloying materials or varying treatment methods can lead to a relevant change in the ultimate strength. These two points have an important influence on the production process of galvanized high strength grade 10.9 bolts. Due to this tension tests on specimens and galvanized bolt assemblies have been carried out in order to evaluate the behaviour under fire conditions. The results will give on one hand the possibility to verify the reduction factors for grade 10.9 bolts given in the Eurocode and on the other hand a more precise understanding of high strength bolt behaviour under fire conditions. The paper will describe the state of the art, the elaborated tests in more depth and present results.

1 STATE OF THE ART

The joint behaviour under fire exposure has currently moved into the focus of researchers. The global aim of forecasting the behaviour of complete structures under fire conditions can only be achieved by merging the knowledge of all single structural elements. The behaviour of the joint area is very complex and still not fully predictable in the hot stage. On that background various publications have

Dipl.-Ing. Fernando González and Prof. Dr.-Ing. Jörg Lange, Institute for Steel Structures and Material Mechanics, TU Darmstadt, Petersenstraße 12, 64287 Darmstadt, Germany

been published in recent years dealing with the behaviour of bolted connections like fin plate or endplate connections ([1], [2]). Research concerning the behaviour of pure bolt assemblies is rare. In [3] and [4] series of tests have been realized using grade 8.8 bolts, analysing the pure material and the bolt assembly behaviour. Experiences respectively test series for galvanized grade 10.9 bolts ($f_y = 900 \text{ N/mm}^2$; $f_u = 1000 \text{ N/mm}^2$) are not existent. The reason for that is, that from the international point of view the galvanized grade 10.9 bolts are rarely used and therefore not in the focus of investigations. In Germany by contrast galvanized grade 10.9 bolt assemblies are very common for endplate connections. Globally very little knowledge exists in this area. In [5] high-strength fire resistant (FR) bolts have been tested, showing similar properties at room temperature compared to grade 10.9 bolts. But due to some differences concerning alloy and fabrication the test results at high temperatures are not comparable.

Eurocode 3 Part 1-2 Annex D [6] proposes for the connection area a design concept which is based on strength reduction factors for bolts and welding seams. The value of the reduction factor depends finally on the affecting temperature and is basically valid for all bolt grades. The local element temperature can be estimated using a method given in Annex D. It has to be stated that the handling is quite opaque and leads to very rough solutions.

2 HIGH TEMPERATURE TEST OF SPECIMENS AND GALVANIZED GRADE 10.9 BOLT ASSEMBLIES

2.1 General Procedure

Due to the obvious lack of knowledge concerning the behaviour of galvanized grade 10.9 bolt assemblies under fire conditions a large test series was planned and executed in order to fill up the gaps. This paper will focus on the pure material and bolt assembly tension test results.

As described in numerous publications, the high temperature test procedure itself has an enormous impact on the outcome and can lead to clearly differing results. Therefore the specification of the test procedure is fundamental for the outcome. In [7] different high temperature test methods are listed and described. In the present work steady state tests, transient state tests as well as creep tests have been performed in order to enable a comparison between the single results. At first glance a direct comparison between the steady state and the transient state test results seems not to be possible. The measured strain of the transient state test is composed of thermal strain, stress related strain and creep strain, where thermal strain can easily be eliminated measuring the thermal elongation of an unstressed specimen. In comparison to the steady state test results the strain is mainly composed of the stress related strain. Creep effects are negligible because of the short duration of the test. Due to the creep test results a comparison between steady state and transient state tests is definitely possible.

Galvanized bolt assemblies have only been tested under steady state conditions. The performance of a transient state test is from the author's point of view very difficult to realize. The failure load of bolt assemblies is in comparison to those of small material specimens very high. Due to the necessary testing loads (app. 270 kN at room temperature) massive brackets are needed to stress the bolt until rupture. As a consequence the bolt assembly is not able to heat up in accordance with the chosen heating rate in the test setup. The steady state test results of the specimens and of the bolts are basically comparable. Therefore a Finite Element calculation of the bolt has to be performed using the temperature dependent stress- strain curves of the steady state tests. A good correspondence between the single results allows

further determination of transient failure loads using the transient material parameters.

2.2 Test Arrangement and Test Method

The round milled test specimens were made from galvanized high strength grade 10.9 bolts with a diameter of 16 mm. The bolts were manufactured by cold forging followed by a quench and temper heat treatment in order to achieve the required minimum mechanical properties given in DIN EN ISO 898-1. The dimensions of the specimens are in accordance with DIN EN 10002 Part 5 [8] and are shown in Figure 2. The gauge length was 30 mm. The extensometer which was fixed on the specimen was able to measure a maximum extension of 3 mm. The furnace in which the specimen was situated is equipped with three separate controlled resistor elements and three thermocouples (Figure 1). For the steady state test the specimens were heated to a given temperature, held for approximately half an hour and then tested. The tension test was performed using a strain rate of 0,001/min to provide proof stress values up to 2 %, after that the strain rate was raised to 0,025/min and maintained constant until rupture. The strain rates used correspond to the values given in [8]. The test results can finally be shown in a stress strain curve. Three specimens were tested under steady state conditions at ten different temperatures. For the transient state test the specimens were located accordingly in the testing device and stressed with a constant load. The steel temperature was measured by a K-Type thermocouple which was directly fixed on the surface of the specimen. The test was performed using a constant heating rate of 10 K/min. The results can be shown in a temperature strain curve. It has to be kept in mind that under these testing conditions the thermal expansion is included in the results which can be eliminated easily as explained before. For the transient state tests two specimens were tested at various stress levels. The performed creep tests require a constant loading and a constant temperature. Due to this the specimens were heated up to a certain temperature and loaded subsequently. After applying the load the occurring strain was recorded constantly.

The bolt assemblies have been tested in a device with a maximum traction load of 1000 kN. The load transfer into the bolt assemblies was realized by a bracket made of Nimonic 80A which has been designed to fit with all the constraints like furnace and bolt dimensions. The bracket is shown in Figure 3. The opening on the

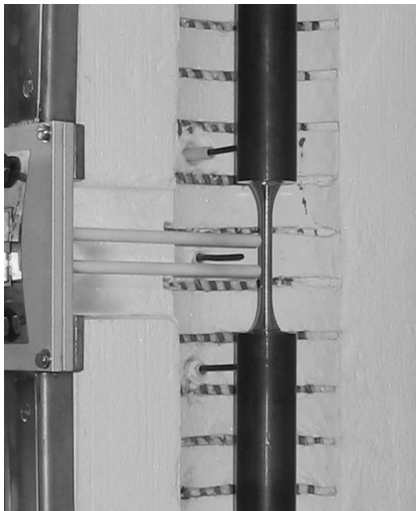


Figure 1.
Testing device with specimen.

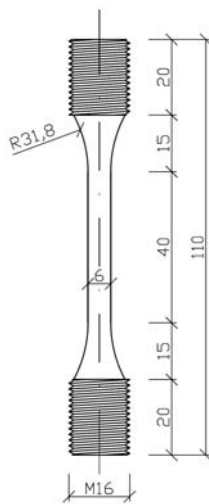


Figure 2.
Dimensions of
specimen in mm.



Figure 3.
Testing device with brackets and bolt.

front of the bracket is necessary to put the bolt assembly in place. An additional fitting was used to realize a rotation symmetric load transfer into the bolt. The bolt temperature was constantly measured by two K-type thermocouples which were fixed on the nut and on the shank of the bolt. Due to the big mass of the brackets the duration of the heating phase was extremely long and a small temperature gradient between shank and nut was not avoidable. The temperature gradient was about $\pm 5^{\circ}\text{C}$. The target temperature was held constant for about half an hour before starting the test. The tension test of the bolts was performed using a constant displacement rate of the traverse which was equivalent to a strain rate of 0,001/min in the elastic range of the thread. The initiation of plastification in the thread area leads to a considerable strain rate acceleration to approx. 0,025/min. A code for tension tests of bolt assemblies is not existent. Due to this the test procedure follows closely DIN EN 10002 Part 5 [8].

2.3 Test Results

The results of the high temperature tests on round milled specimens are shown in Figure 4. The indicated continuous curves show the stress- strain relationship up to 2% strain and are based on steady state tests. From 300°C onwards the strength reduction is significant and clearly visible, see also Figure 5. At 700°C respectively 800°C the strength is only about 5% in comparison to the strength at room temperature. As indicated before the strain rate was increased after an extension of 2% in order to obtain the tensile strength. The strain rate acceleration leads to a considerable hardening of the material. Comparing the 2% strain ratio at 600°C with the tensile strength ratio at the same temperature a hardening of about 70% occurs (comp. Figure 5). In [3] the strain rate was held constant until an expansion of 5% was reached. The maximum stress was obtained within this range, so that a significant hardening effect was not noticeable. During a transient state test the strain rate increases constantly. The performance of a steady state test using only very slow strain rates leads to a significant smaller ultimate strength in comparison to the transient state test results. The tensile strength ratios fit well with the reduction factors given in the Eurocode 3 Part 1-2 Annex D. By contrast the tension test results of galvanized bolt assemblies are only until 450°C similar to the reduction factors given in the Eurocode. From that point onwards the bolt

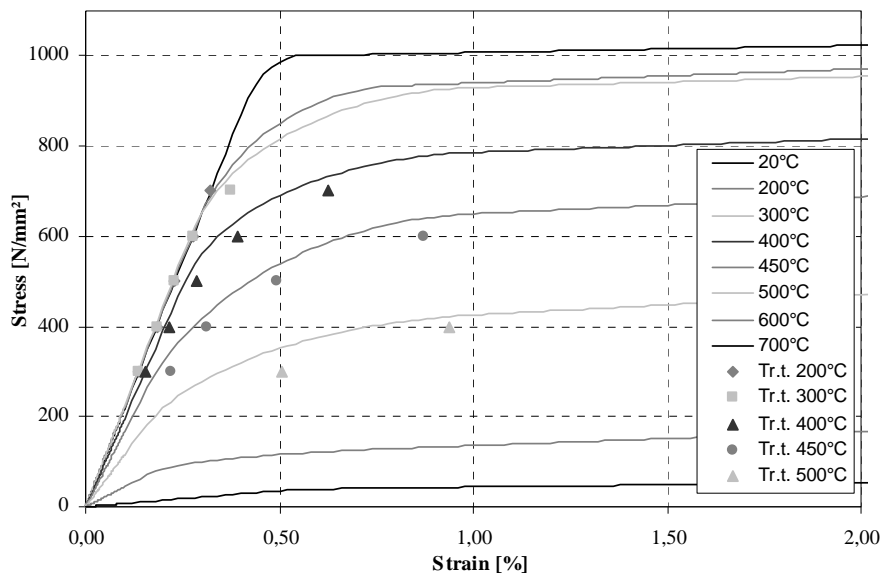


Figure 4. Stress-Strain Curve.

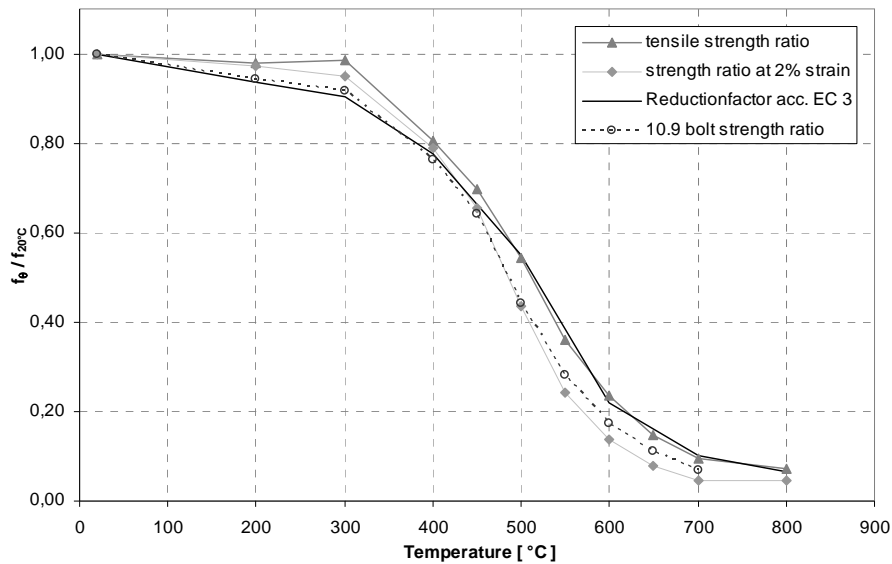


Figure 5. Reduction factors.

assemblies shows a significant loss of strength in comparison to the Eurocode values. This is interesting due to the fact that the bolt assembly was expected to behave like the specimens did. One of the main reasons for this discrepancy will be explained in course of the paper.

In Figure 4 the values resulting of the transient tests are indicated by dots. The values belonging to a temperature of 200°C (Transient test Tr.t. 200°C) are following quite well the curve obtained by a steady state test. This is understandable comparing it with the results of the creep tests. At low temperatures none or just negligible creep deformation occurs, so that the transient tests results fully correspond with the results of the steady state tests. For higher temperatures the transient state test values are quite beneath the corresponding steady state test results, due to the fact that from 300°C onwards a creep effect is visible and not further negligible. The horizontal distance in Figure 4 between the transient state test values and the steady state curve is approximately the creep deformation measured in the corresponding tests.

3 FAILURE MECHANISM

Figure 6 shows longitudinal sections of the thread area for the tested bolts in a temperature range from 20°C to 700°C. The section reveals the failure mechanism at the ultimate limit state. The tensile test of the bolt assembly was generally stopped after reaching the maximum traction load. This allows the examination of the thread deformation just after reaching the maximum tension load. An axial loaded bolt assembly fails in a temperature range from 20°C to 420°C by thread stripping and in some cases by ductile necking. The enlargement of Figure 6(a) shows a large plastic deformation in the thread of the bolt. The thread of the nut is nearly not deformed. The final thread stripping is shown in Figure 6(b). From 420°C onwards the failure mechanism changes from thread stripping to cracking. Figure 6 (e) to (f) reveals a multitude of small cracks in the thread area while at higher temperatures (e.g. 600°C) only one macroscopic crack occurs. The crack runs perpendicular to the trajectories of tension and leads to a brittle fracture of the bolt. At 650°C two failure mechanisms have been observed. Some bolts showed a

brittle fracture while others failed by stripping. At high temperatures ($T > 650^{\circ}\text{C}$) the bolt assembly fails only by stripping, see Figure 6(j). It can be observed that the failure mechanism of the bolt assemblies changes in a certain temperature range. The reason for the brittle bolt failure in a temperature range from 420°C to 650°C has to be analysed in more depth. A scan along the cracks with a SEM (scanning electron microscope) reveals the cause of the failure. Figure 7 shows some SEM-pictures where an intergranular failure can be recognized. This is quite typical for a stress corrosion cracking (SCC). An additional EDX- analysis (energy dispersive X-ray spectroscopy) revealed that zinc (melting temperature $\sim 420^{\circ}\text{C}$) atoms covers the crack surface right down to the very fine crack tip. This is the final evidence for the failure mode which is called “liquid metal assisted cracking” (LMAC). In the late nineteen eighties a similar failure mechanism was detected at high strength grade 10.9 bolts but in a different context. At that time LMAC was detected at bolt just after the galvanising process; see Hasselmann [10]. The present test series show that there is a direct connection between LMAC in galvanized bolts and fire. This understanding is not existent in the current literature and has necessarily to be taken into account if galvanized bolts are used under fire exposure. The strength ratio for bolts shown in Figure 5 lies due to this understandably underneath the tensile strength ratios of the specimens.

The harming effect of liquid metals on solid steels is known for about 125 years. Rädiker [9] gives in his work a good overview of the causes for LMAC. The crack initiation occurs in presence of a tensile stress and a corrosive liquid metal (in the present case zinc). Furthermore, the element temperature has to lie in a critical

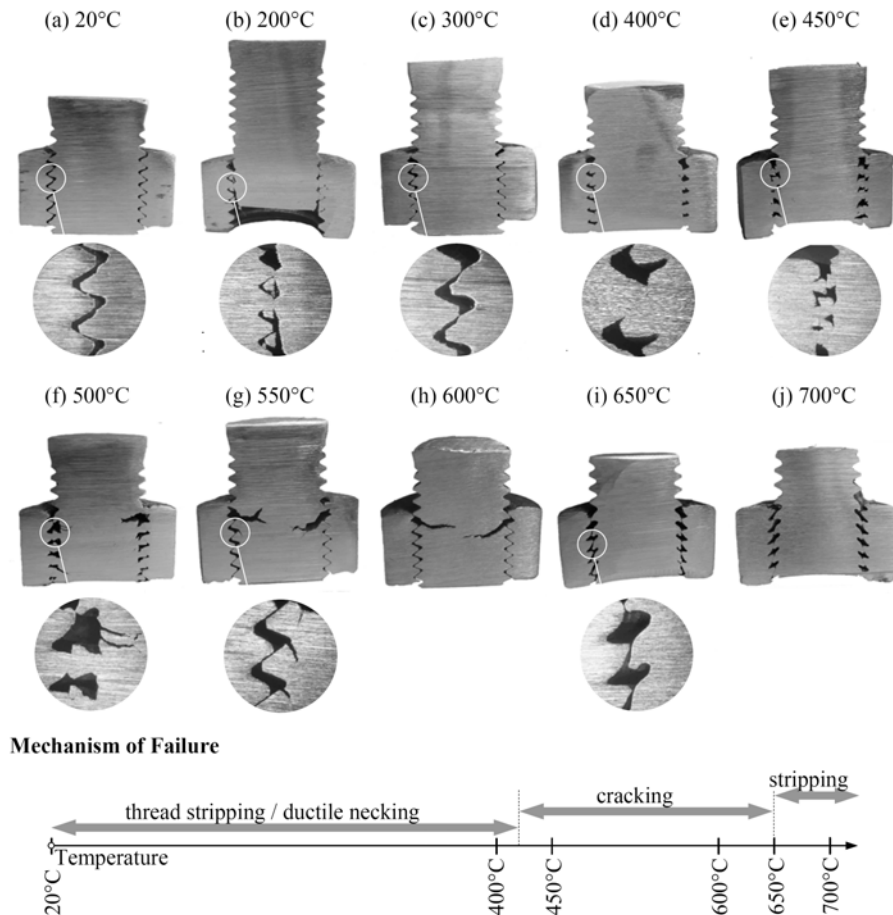


Figure 6. Failure mechanism.

temperature range. The real failure mechanism is even today not fully known. Gordon [11] proposed in his work a concept for the explanation of the failure mechanism. During the incubation process the brittle atoms penetrate by stress aided diffusion a short distance into grain boundaries of the steel. In the penetration zones the presence of the embrittler atoms lowers the crack resistance and increases the difficulty of slip. After reaching a sufficient concentration of embrittler atoms up to a critical depth a crack initiation takes place. Probably the crack is initiated at the head of already existing dislocation pileups where the stress becomes critical for the lowered resistance. The concept proposed may explain the reason for the cracks but it gives no overview how the single influences have to be combined. For very low stress levels no LMAC occurs even if the molten metal is in contact with the steel and the temperature is in a critical region. Even the alloying materials of the steel can have an effect on the LMAC risk. It has to be stated that the knowledge concerning the LMAC crack risk is very limited. Spähn [12] showed in his work that by reaching a certain recovery temperature the ductility of the solid metal recuperates to a normal level. This effect can be observed having a look on the present test results. From $\sim 650^{\circ}\text{C}$ onwards no further cracking was detected.

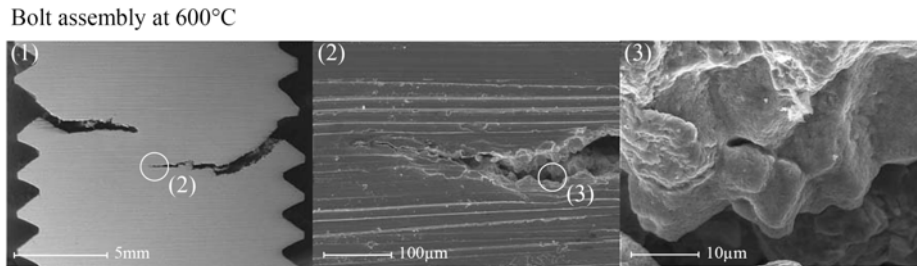


Figure 7. Scan of a crack (SEM).

4 CALCULATION OF A BOLT ASSEMBLY USING THE FE- METHOD

Due to the fact that the execution of transient state tests is not possible for bolt assemblies, the intention is to calculate the ultimate bolt strength by the Finite Element Method using the transient state material parameters. First of all it has to

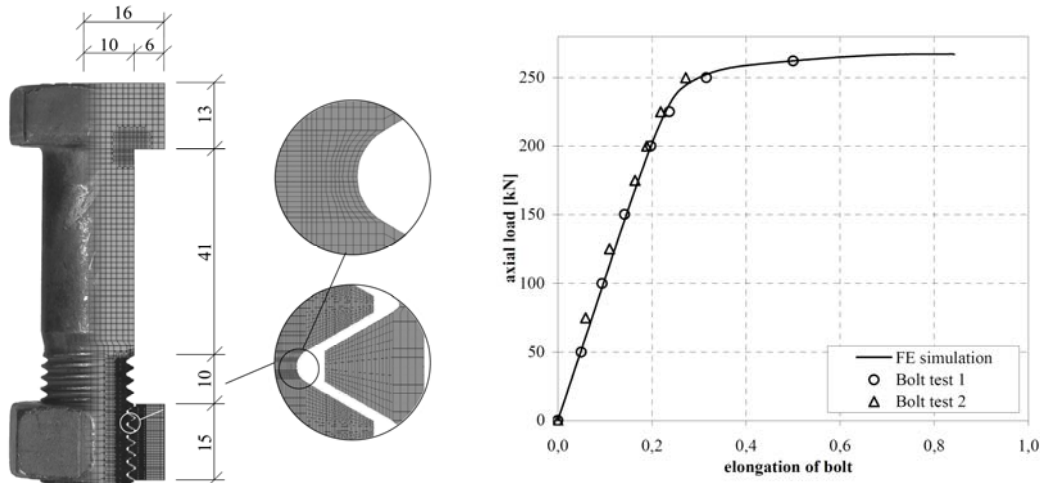


Figure 8. FE Simulation of an axial loaded bolt for room temperature (M20x80).

be checked that this procedure is able to generate the steady state ultimate strengths, using the accompanying material parameters. For the calculation of the bolt assemblies the FE- program ANSYS[®] was used. The FE-model is shown in Figure 8. The PLANE42 element is able to develop an axial symmetric calculation algorithm so that a three dimensional modelling of the bolt assembly is unnecessary. The result of the steady state FE calculation at room temperature is shown in Figure 8 and reveals a good correspondence between the calculation and the test results. Based on this it can be stated that a simulation of a bolt using the transient state material parameters delivers a realistic ultimate failure load. The crack initiation due to LMAC can not be simulated. As a consequence only black bolts and galvanized bolts outside the critical temperature range can be simulated.

REFERENCES

1. Heddrich, Rolf, „Untersuchungen zum Trag- und Verformungsverhalten von Schraubenverbindungen bei feuerwiderstandsfähigen Verbundprofil-Konstruktionen unter Brandeinwirkung“, Doctoral thesis D17, *Konstruktiver Ingenieurbau der Technischen Universität Darmstadt*, 1990.
2. Hongxia Yu, I.W. Burgess & J.B. Davison, “Experimental investigation of the behaviour of fin plate connections in fire”, Proceedings of the 3rd International Conference on Steel and Composite Structures (ICSCS07) Manchester, *Taylor and Francis*, 2007.
3. Kirby, B.R., “The behaviour of high-strength grade 8.8 bolts in fire”, J. Construct. Steel Research 33, *Elsevier Science Limited*, 1995.
4. Hu Y, J.B. Davison & I.W. Burgess, “Comparative study of the behaviour of BS 4190 and BS EN ISO 4014 bolts in fire”, Proceedings of the 3rd international conference on steel and composite structures (ICSCS07) Manchester, *Taylor and Francis*, 2007.
5. Sakumoto Y., “Test of fire resistant bolts and joints”, Journal of Structural Engineering Vol. 119 No. 11, *ASCE Publication*, 1993.
6. DIN EN 1993-1-2, “Eurocode 3: Design of Steel Structures - Part 1-2 General Rules - Structural Fire Design”, *Beuth Verlag*, 2006.
7. Anderberg, Yngve, “Modelling Steel Behaviour”, Report LUTCDG/(TVBB-3028), *Lund Institute of Technology*, 1986.
8. DIN EN 10002-5, “Metallische Werkstoffe Zugversuch Teil 5: Prüfverfahren bei erhöhter Temperatur”, *Beuth Verlag*, 1992.
9. Rädiker W., „Der interkristalline Angriff von Metallschmelzen auf Stahl“ *Werkstoffe und Korrosion* 24, 1973, p. 851–859.
10. Hasselmann U., „Flüssigmetallinduzierte Rissbildung bei der Feuerverzinkung hochfester HV-Schrauben großer Abmessungen infolge thermisch bedingter Zugeigenspannungen“ *Shaker Verlag*, 1998.
11. Gordon P.; Henry H.; “The Mechanisms of Crack Initiation and Crack Propagation in Metal-Induced Embrittlement of Metals” *Metallurgical Transactions A*, 13 ; 1982, p. 457–472.
12. Spähn H.; „Einwirkung von flüssigen oder festen Metallen auf andere Metalle“ E. Kunze (Hrsg.): *Korrosion und Korrosionsschutz*; Weinheim : WILEY-VCH Verlag GmbH, 2001, S. 506–541.

FIRE SAFETY ENGINEERING AND PRACTICE

Using OpenSees for Structures in Fire

A. USMANI, J. ZHANG, J. JIANG, Y. JIANG, P. KOTSOVINOS,
J. ZHANG and I. MAY

ABSTRACT

OpenSees is an open source object oriented software framework developed at UC Berkeley and currently supported by PEER and Nees. OpenSees has so far been focussed on providing an advanced computational tool for analysing the non-linear response of structural frames subjected to seismic excitations. Given that OpenSees is open source (available for free download at opensees.berkeley.edu) and has been available for best part of this decade it has spawned a rapidly growing community of users as well as developers who have added to it's capabilities over this period. For instance it has significant geotechnical modelling capabilities developed by this community so that the seismic response analyses can include full soil structure interaction if required. It also has a structural reliability and sensitivity analysis capability offering many reliability calculation tools. Furthermore it has an HPC or parallel version for solving large problems on high-performance computing hardware. In addition to it's availability as an analysis tool OpenSees is also the software platform of choice for the US NEES network that enables earthquake engineers to organise and share data, participate in remote experiments, and perform hybrid simulations. It therefore represents the largest community of this kind in structural engineering and has the potential to bring together the best structural engineering computational modeling capabilities under one platform accessible to all facilitating new collaborations across geographical boundaries to solve ever more challenging problems.

Asif Usmani (corresponding author), Professor, School of Engineering, The University of Edinburgh, Edinburgh EH9 3JF, United Kingdom

Jian Zhang, PhD student, School of Built Environment, Heriot-Watt University, Edinburgh EH14 4AS, United Kingdom

Jian Jiang, PhD student, School of Engineering, The University of Edinburgh, Edinburgh EH9 3JF, United Kingdom

Yaqiang Jiang, PhD student, School of Engineering, The University of Edinburgh, Edinburgh EH9 3JF, United Kingdom

Panagiotis Kotsovinos, PhD student, School of Engineering, The University of Edinburgh, Edinburgh EH9 3JF, United Kingdom

Johnson Zhang, Lecturer, School of Engineering and the Built Environment, Edinburgh Napier University, Edinburgh EH10 5DT, United Kingdom

Ian May, Professor, School of Built Environment, Heriot-Watt University, Edinburgh EH14 4AS, United Kingdom

The work being introduced in this paper is aimed at solving fire induced structural problems by developing new methods within the OpenSees framework. It is considered vital that the existing merits of this framework, such as flexibility and extensibility and computational efficiency, should be inherited during the development.

INTRODUCTION

The decades since the 60s saw explosive growth in computing power and its affordability leading to the kind of ubiquity where access to network computing is now seen as practically at par with services such as the electricity grid or the water and sewerage networks. Structural Engineers were one of the earliest exploiters of the opportunity offered by digital computers driven very much by the need of solving larger and larger systems of linear equations to analyse their structures. This led to a great deal of legacy code being written, primarily developed in Fortran. This activity however peaked in the 80s and much of the development found its way into the many currently available commercial codes such as SAP, ANSYS, ABAQUS etc. Much of the billions of lines of special purpose research codes written in this period (representing thousands of man-years of effort) are now very likely unusable not just because of the dramatic changes in operating systems, interface software, storage media etc. but the change in the whole working environment brought about by information technology. The potential offered by this explosion in information technology is immense for structural engineers (as it is for all other type of engineers) however so far there is a relative lack of imagination from our profession in taking on this challenge. Structural engineers who were once the pioneers in exploiting the new digital computing technologies emerging in the 60s and 70s, now run the risk of being seen as dinosaurs, perhaps because of, rather than despite, that early success.

The picture is not however uniformly dismal as there have been a number of very forward looking developments starting incidentally from that most productive of places, California. Among the most imaginative examples of a structural engineering project is the Nees network [1], bringing together 15 earthquake engineering research labs in universities across the USA. The key vision of this network is to enable hybrid testing of structures, where one (or more) part(s) of a structure is constructed in a lab and the rest exists virtually as a computer model in a separate (geographically remote) location, perhaps on a high performance computing platform. The two are then made to interact in real time via sensors and actuators acting on the real model in the lab exchanging information with the virtual model over the internet or Grid. The Nees network recommends the use of the software framework OpenSees [2] for simulating virtual components of hybrid testing. OpenSees is another example of an excellent imaginative project that addresses some of the issues discussed earlier. It takes a different route to software development from the traditional research codes that routinely die and commercial packages which are by definition restricted access (both in terms of affordability and more importantly in terms of adding functionality for problems that can not be adequately dealt with by the package as it stands). The OpenSees route is not in itself new and the most ubiquitous and successful expression of it is the linux movement, *i.e.* an open source “community” code offering free access to all developers wishing to add new functionality to the core framework.

The structural engineering community is clearly considerably smaller than the linux community and it remains to be seen if OpenSees will be as successful, however the potential it

offers is arguably very attractive. The potential is that of a common community owned research code with a large and growing collection of modelling capability in many areas of structural engineering enabling researchers to collaborate freely across geographical boundaries and being secure in the knowledge that the fruits of their effort will continue to exist in a living code (until superseded by a better version). Other strengths of the OpenSees framework is the inclusion of a high performance computing (or parallel) version [3] and the adoption of the object oriented paradigm of software development using C++, which enforces a discipline on the developers and ensures that the framework will develop in a manner that is manageable and easy to maintain and most of the its components are “reusable” by other developers.

This paper will present an overview of the work currently underway at three universities in Edinburgh to add a “structures in fire” modelling capability in OpenSees which will be consistent with the ethos of the other components of OpenSees in terms of being object oriented and enabling the use of HPC hardware. Furthermore this work will also enable the modelling of earthquake damaged structural frames subjected to a subsequent fire. The development of this capability will involve work in the following areas:

Fire load modelling to provide a boundary condition for the structure

Modelling of heat transfer to structural components accounting for changes in heat transmission as a result of seismic damage

Implementing temperature dependent material properties for the main material models available in OpenSees

Implementing temperature dependent transient thermal strain or LITS (load induced thermal strain) type effects

Modification of beam and shell element classes available in OpenSees to develop new classes that include the temperature variable

This paper will provide a summary of the work carried out on each of the topics above and present a benchmark example problem solved using the new code developed within the OpenSees framework.

FIRE LOAD MODELLING

The aim of this part of the work is to allow a wide range of heterogeneous and homogeneous fire boundary conditions to be applied to the boundaries of the structural model. To this end, it is proposed that the following methods for simulating fire loading conditions will be developed in this work (see [4] for a good summary):

1. Post flashover standard compartment fires evolving according to time-temperature curves established in various codes and standards (such as ISO 834 and ASTM E119)
2. Post flashover natural compartment fires evolving according to various parametric time-temperature relationships recommended in the research literature and codes (such as EN1991-1-2)

3. In addition to the code based standard fires and parametric natural fires, simple energy balance laws can be used to create “zone models” to produce relatively more realistic representations of temperatures in a fire compartment.
4. Localised fires and travelling fires, such as in large compartments where whole compartment involvement (flashover) is unlikely to occur. EN1991-1-2 offers useful empirical approaches for dealing with small and large localised fires. There are no current guidelines for moving fires, however NIST investigation [5] of the collapse of the WTC 7 building on September 11, 2001 offers interesting insights (based on CFD modelling),
5. Fires impinging on the structure from external sources. Some guidelines for this are provided in EN1991-1-2 for flames emerging out of compartment windows. This however could be a common situation in the case of fires following an earthquake and façade fires for high rise buildings, for which there is no current guidance.

The first three types of fire loading produce spatially homogeneous compartment temperatures where a single temperature is supposed to represent the temperatures at all points in the compartment at a specific instant of time (in case of zone models this applies to one or more zones used to model the compartment). The last two types of loading conditions could produce both spatially and temporally non-uniform temperatures. All types of fire loading will be implemented by applying radiation and convective flux boundary conditions to the structure.

The most realistic heterogeneous temperature distributions in the compartment can be produced using a computational fluid dynamics (CFD) based model. Addition of a full CFD model to OpenSees is not feasible however an interface will be developed in OpenSees based on the work of Jowsey [6] which will enable a time dependent and non-uniform heat flux boundary condition to be derived from CFD computations, which can be applied to the structure.

MODELLING OF HEAT TRANSFER TO STRUCTURAL COMPONENTS

Once the fire boundary conditions have been determined, the heat transfer to the structural components must be computed to establish the time evolution temperatures within the structure. This will be done by adding a 3D conduction heat transfer modelling capability in OpenSees. It will be possible to reuse parts of existing OpenSees framework to create a new “main()” heat transfer function in C++, not least the virtual domain class, geometric meshing classes, brick element and the assembly and solver classes.

The heat transfer module will take advantage of the “fibre section” beam elements used in OpenSees. Heat transfer in building structures as a result of a fire typically has a character that naturally suits fibre type modelling of structural members because the greatest thermal gradients exist in the cross-section of the member rather than along its length. A finite element mesh that has the same character will therefore be best suited to heat transfer modelling. Figure 1 shows a schematic sketch of such a mesh of 3D brick elements with fine discretisation in the cross-section and coarse along the length of the member.

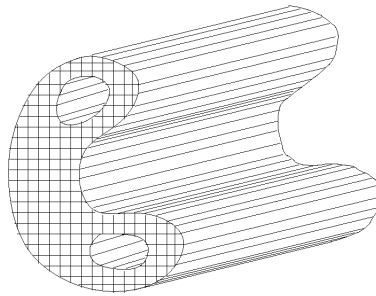


Figure 1. Schematic of a 3D brick element mesh for an arbitrary length of an arbitrary structural member.

In the cases where heat transfer along the longitudinal direction can be neglected, a 2D heat transfer modelling capability for the structural section will also be developed, which can save computational resources and offer additional flexibility to users.

The proposed modelling of fire and heat transfer as described above will enable the most general fire loading conditions to be modelled in a relatively straightforward manner. The temperature history from the heat transfer module could be stored or recorded for reproduction if only a heat transfer analysis is to be carried out. If a mechanical analysis is to follow, a temperature history file will automatically be generated for all fibres of beam-column (and slab) fibre elements if the fibre definitions are identical to the heat transfer discretisation, otherwise the temperatures will be mapped to the mechanical fibre definitions.

In traditional “structures in fire” analysis typically only a one-way coupling is assumed between the heat transfer and the thermo-mechanical analysis, *i.e.* there is no feedback to the heat transfer calculation from the mechanical analysis, thus the structural deformation is not considered in HT modelling [7]. This assumption is reasonable for the global structural behaviour modelling that is the aim of this work. Local detailed investigation of, for instance, concrete spalling behaviour typically requires a fully coupled thermo-mechanical analysis also including mass transport of multi-phase fluids in the concrete matrix, for example [8]. Though important, there is no plan so far to include this kind of analysis in this work. But as we are explicitly considering the modelling of earthquake damaged structures in fire in this work, some effect of mechanical damage must be included in the heat transfer model. Recently some experiments have been carried out [9] to investigate the influence of tensile cracking type damage (in a four point bending test on an RC beam) on the local diffusivity of heat, however the results are so far inconclusive. It is anticipated that local thermal conductivity could be made a function of the damage state in the structure. It seems reasonable that damage will create preferred directions of heat transfer (promoting heat transfer along the cracks and perhaps inhibiting it across cracks) as shown in Figure 2.

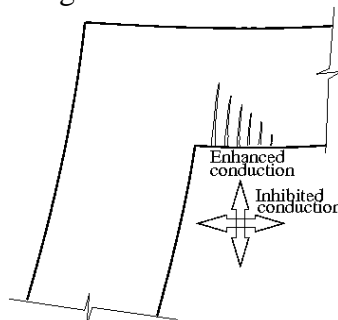


Figure 2. Thermal conductivity change depending on mechanical damage.

TEMPERATURE DEPENDENT MATERIAL PROPERTIES

There are many types of material models available in OpenSees for steel and concrete, defining their mechanical constitutive behaviour, however some of these need to be modified to include temperature dependent stress and strain including effects such as LITS. At this stage temperature dependence will only be added to the uniaxial concrete and steel models and this data is not reliably available for the multiaxial case. This also naturally suits the fibre beam and shell models where the section behaviour can be derived from integrating fibre stress, strain and temperature states. The uniaxial properties for steel and concrete will be primarily based on Eurocode stipulations. For concrete additional information from the literature, such as [10, 11], will be used to take into account LITS type effects.

A new set of material properties (also temperature dependent) will need to be added for the heat transfer model as well. These in the first instance will be based on Eurocode data for steel and concrete. As mentioned earlier, the thermal properties, particularly thermal conductivity will be related to a localised strain measure representing damage.

MODELLING OF THERMO-MECHANICAL BEHAVIOR

This work has started by creating new versions of existing OpenSees nonlinear beam-column elements. OpenSees has two main types of these elements, one based on the traditional total Lagrangian displacement formulation and the other seemingly more efficient set of elements based on flexibility or force formulation [12]. The work has been slower than anticipated because of a steep learning curve for the whole team in understanding C++ and object oriented programming concepts along with the structure of the OpenSees framework. The work done so far is as follows:

1. Modifying the 2D displacement beam-column element `DispBeamColumn2d` to enable thermal loading to be applied. The thermal loading is calculated by integrating fibre (or layer in 2D) thermal expansions over the depth of the section taking into account the temperature dependent properties of the fibre. The tangent stiffness matrix terms of the beams are also modified based on temperature dependent properties.
2. Temperature dependent properties have been added for a uniaxial steel and concrete models (`Steel02` and `Concrete02`), creating new temperature dependent versions of these materials (`SteelTemp02` and `ConcreteTemp02`).
3. New element load classes `Beam3dTempLoad` has been created to receive temperature loading inputs (`Beam2dTempLoad` was similarly modified).

EXAMPLE

The example chosen to illustrate the progress so far is the restrained beam test at Cardington [13]. Although this test was meant to test one of the secondary beams only, it offered considerable insights into the behaviour of steel frame composite structures in fire [14, 15]. The test showed true 3D behaviour and considerable interaction between the longitudinal section of the composite beam (as shown in Figure 3) and the transverse deck slab (in the direction of the

slab ribs). However as we are only testing a 2D element here, only the longitudinal section shown in Figure 3 will be modelled as a fully composite section to test the code added to OpenSees.

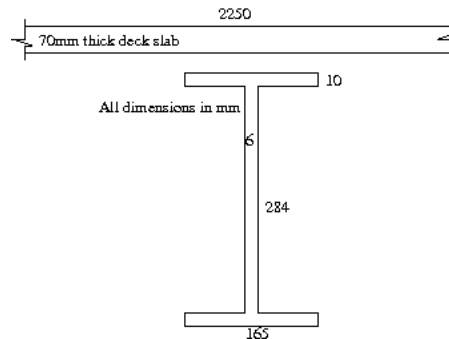


Figure 3. Example problem (derived from the restrained beam test at Cardington).

The two parts of the composite beam were modelled using 9 DispBeamColumn2d elements each (taking advantage of symmetry, so only half the beam length of 9m was modelled), and were connected together using the rigidlink beam type constraint condition in OpenSees (at all nodes except at the end supports). The two end nodes were restrained against all translation but were left free to rotate. Because of the composite nature of the beam, even with the end rotations free, the beam is able to generate resisting moments at the end, creating a full fixity like condition for the whole composite beam. The beam was first loaded using the gravity load used in Cardington. Both parts of the beam were divided into four fibres (or layers) each and the full temperature history at each fibre was applied in a number of thermal loading stages.

The result from the analysis is shown in Figure 4 against the actual test result. The model did not converge for the full temperature history, however the comparison for the converged part is compares reasonably well. Another discrepancy in the model seems to be the lack of the initial “plateau” seen in the experiment. Perhaps a rotationally fixed boundary condition will produce this behaviour. The work on modelling this problem is ongoing and will be presented at the conference in June.

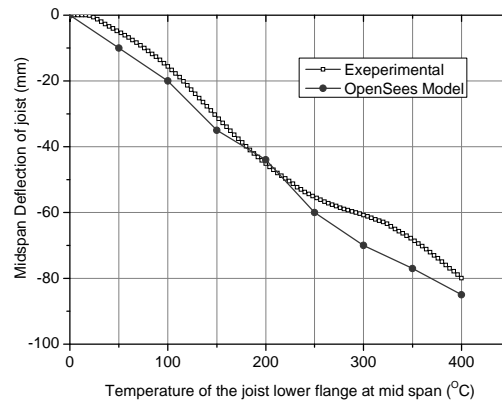


Figure 4. Comparison of OpenSees model against restrained beam test results.

CONCLUSIONS

It is still very early in the life of this work to make definite conclusions, however a good start has been made in developing an understanding of the OpenSees framework and comprehensive plan for developing all new modules has been developed. The code implemented so far has been restricted to mechanical behaviour and this mainly involves creating new classes out of existing OpenSees classes. Even this work is far from complete and early results were presented in the previous section. The work on fire loading and heat transfer will require the addition of an entirely new set of classes to the framework, and this must be done very carefully to remain consistent with OpenSees philosophy and existing structure.

ACKNOWLEDGMENTS

This work is made possible by co-funding of Mr Jian-Zhang by the BRE Centre for Fire Safety Engineering (University of Edinburgh) and by Heriot-Watt University. The collaboration between the three universities is organized under the umbrella of the Edinburgh Research Partnership. Thanks are also due to Dr Frank McKenna of UC Berkeley and PEER for his assistance in the developments so far.

REFERENCES

1. <https://www.nees.org/>
2. <http://opensees.berkeley.edu/>
3. McKenna, F. T., Object-Oriented Finite Element Programming: Frameworks for Analysis, Algorithms and Parallel Computing, PhD thesis, University of California, Berkeley (1997).
4. <http://www.mace.manchester.ac.uk/project/research/structures/structfire/>
5. <http://wtc.nist.gov/>
6. Jowsey, A., Fire Imposed Heat Fluxes for Structural Analysis, PhD thesis, University of Edinburgh (2006).
7. Welch, S., Miles, S. D., Kumar, S., Lemaire, T. and Chan, A., "FIRESTRUC - Integrating advanced three-dimensional modelling methodologies for predicting thermo-mechanical behaviour of steel and composite structures subjected to natural fires", *Fire Safety Science* 9, 1315-1326 (2009).
8. Gawin, D., Pesavento, F. and Schrefler, B. A., "Modelling of hygro-thermal behaviour of concrete at high temperature with thermo-chemical and mechanical material degradation", *Comput. Methods Appl. Mech. Engrg.*, 192, 1731-1771 (2003).
9. Irvine, A. A., "The effect of tensile cracking on thermal diffusivity", internal communication, University of Edinburgh (2009).
10. Khoury G. A., Grainger B. N. and Sullivan P. J. E., "Strain of concrete during first heating to 600°C under load", *Magazine of Concrete Research*, 37, 195-215 (1985).
11. Neilsen, C. V., Pearce, C. J. and Bicanic, N., "Theoretical model of high temperature effects on uniaxial concrete member under elastic restraint", *Magazine of Concrete Research*, 54, 239-249 (2002).
12. Neuenhofer, A. and Filippou, F. C., "Geometrically nonlinear flexibility-based frame finite element", *Journal of Structural Engineering*, ASCE, 124, 704-711 (1998).
13. O'Connor, M. A., Martin, D. M., "Behaviour of a multi-storey steel framed building subjected to fire attack" *Journal of Constructional Steel Research*, 46, 1-3 (1998).
14. Sanad, A. M., Rotter, J. M., Usmani, A. S. and O'Connor, M. A., "Composite beams in large buildings under fire numerical modelling and structural behaviour", *Fire Safety Journal*, 35, 165-88 (2000).
15. Usmani, A. S., "Understanding the Response of Composite Structures to Fire", *Engineering Journal*, AISC, 42, 83-98 (2005).

Significance of Common U.S. Construction Details on Fire Resilience of Structural Steel Floor Systems

N. ABBOUD, C. McARTHUR, C. BEYLER, T. FAY
and N. IWANKIW

ABSTRACT

To-date, the preponderance of instrumented large-scale testing of structural systems has been carried out in Europe and the United Kingdom. These tests have been a fountainhead of information for advancing the science of structures in fire worldwide, but in order for the gathered data to be leveraged in the design and assessment of buildings in the United States, the significance of predominant North American construction details must be considered.

This paper provides a case-study utilizing a finite element analysis model of a steel framed floor with concrete slab on metal deck to assess the impact of the variation of framing connection types and the amount of slab reinforcement on the structural system's ability to resist fire loads, under the standard ISO fire scenario. The baseline model replicates and is benchmarked against test data from the FRACOF fire test published in [1, 2] and the structural modeling approach using NLFlex[3], including treatment of slab and connections, is described. The secondary beam connection detail is modified from an all-bolted double-angle connection with 3 rows of bolts to a single finplate connection with 3 bolts, and the slab reinforcement is reduced to reflect details that are more consistent with traditional fire resistive construction in the United States. The effects of these modifications are shown to have minimal impact on the structural response in the FRACOF test configuration.

Najib Abboud, PE, PhD, Principal, Weidlinger Associates Inc., New York, NY
Chad McArthur, PE, MS, Project Engineer, Weidlinger Associates Inc., Albuquerque, NM
Craig Beyler, PhD, Technical Director, Hughes Associates Inc., Baltimore MD
Terry Fay, MS, Fire Protection Engineer, Hughes Associates, Inc. Baltimore MD
Nestor Iwankiw, PE, SE, PhD, Senior Engineer, Hughes Associates, Inc. Chicago, IL

INTRODUCTION

The Fire Resistance Assessment of partially protected Composite Floors (FRACOF) fire test [1, 2] forms the basis of this study. It is a 8.735m (~28.7 ft) by 6.66m (~21.8ft) structural steel frame with concrete slab cast compositely on metal deck which was fire tested with gas temperatures controlled to a standard ISO834 fire curve. This test offers the advantages of a full scale test of a complete structural assembly being well documented and well instrumented while remaining of convenient size for structural modeling and analysis purposes. These benefits make the test subject ideal for analytical study and benchmarking purposes which are, in-turn, well suited to conducting parametric, “what-if” studies to extrapolate the test results over a reasonable range of scenarios. This paper briefly presents an analytical model benchmarked against the FRACOF test. This model is then modified to reflect connection and slab-reinforcing details which may be more indicative of common US practice and the associated changes in performance of the modified model are evaluated.

NLFLEX STRUCTURAL BENCHMARK MODEL

The analytical model used for structural analysis in this study is constructed using NLFlex [3]. This is an explicit non-linear finite element analysis program that includes capabilities for assessing temperature dependent material properties and thermal expansion effects. The model is constructed using shell elements for the steel framing and the slab while beam elements are used for the bolts and non-linear spring elements account for the shear studs. Figure 1 provides a series of images illustrating the modeling approach and the degree of spatial discretization used for the benchmark model.

The steel floor framing consists of IPE300, grade S235 (W12, 34ksi) secondary steel beams framing to IPE400, grade S355 (W16, 51ksi) girders. These have been discretized using 4in elements and the steel constitutive model has been constructed with piecewise linear properties consistent with Eurocode 3 [4]. It is assumed that the HEB260 steel columns remain un-heated and are considered to respond with ordinary linear-elastic steel properties.

Analytical formulation of the slab is a more involved exercise. The prominent characteristics of the slab’s behavior is considered to be primarily driven by its’ heterogeneous, orthotropic properties. Analytically, this is accommodated using a layered, orthotropic shell model. Using this modeling approach, integration points through the thickness of the shell are assigned different properties according to the make-up of the slab. In these models, a 6-layered approach was adopted that utilizes orthotropic steel layers at the top and bottom of the deck and for the reinforcement while concrete material having different properties in tension and compression to represent the concrete that fill the troughs and covers the deck.

For the purposes of this study, shear studs were modeled using non-linear spring elements where the slip resistance properties were derived from [5] where, at ambient temperature, the studs develop a plastic capacity of 17kips over ¼” of slip.

The bolted double clips angle connections used to connect the secondary beams to primary girders and the bolted end plate connections used to connect primary girders to columns were modeled using a pragmatic approach; consisting of shell elements for the angles and beam webs, and beam elements for the bolts. This approach offers the benefits of computationally efficiency while replicating the connection rigidity and bolt failure mechanism. Note however, that the effects of bolts holes were not explicitly accounted for in this analysis so bolt-hole related failure mechanisms (e.g. block shear, hole bearing failure) are not represented in this model. Because these modes of failure were not observed in the test, this approach is reasonable for the purposes of benchmarking the analysis approach.

After [2], the boundary conditions of the model were treated with slab edge continuity only along one (short) edge of the model, while the base of the columns were supported in all three translational directions and in rotation about its' axis. For the purposes of benchmarking the modeling approach, steel and slab temperature time-histories were prescribed based on the test data reported in [1]. The test was conducted with furnace temperatures controlled to the ISO-834 fire curve; achieving gas temperatures in excess of 1000° C after 120minutes of heating. The two infill secondary beams were not fire protected; resulting in temperature histories that closely follow the ISO curve and achieving 1040° C after 120minutes uniformly through the depth of the section. Girders and the two secondary beams at the edge of the slab were fire protected and had reduced fire exposure at the edge of the furnace and achieved a peak temperature of 300° C at the bottom flange. Slab temperatures were recorded to range from 100° C at the unexposed surface, to 350° C at reinforcement depth and to nearly 800° C in the concrete within the troughs of the slab.

For analysis purposes, the slab heating was treated as uniform through the thickness of the slab; utilizing temperature data recorded at the height of the reinforcement mesh. Thermal expansion effects of the slab were included. Localized temperatures at the connections (bolts, angles, and connection plates) were taken to be the average of the two connected components (e.g. average of secondary beam web and primary girder web temperature time histories)

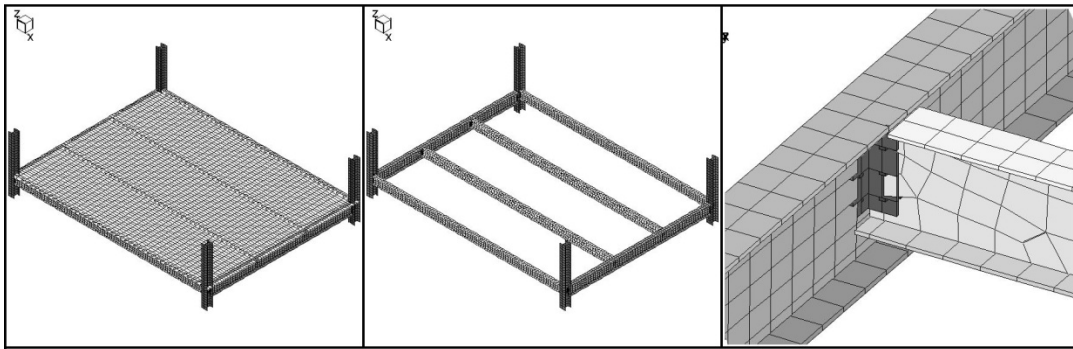


Figure 1. NLFlex model of FRACOF fire test article.

ANALYSIS BENCHMARK

Deflection time histories calculated in the analysis are compared against the test results below in Figure 2. The analysis results compare well against the recorded test data; achieving accurate calculation of the peak deformation response as well as the deformation history of the center of the slab and of the unprotected secondary beams.

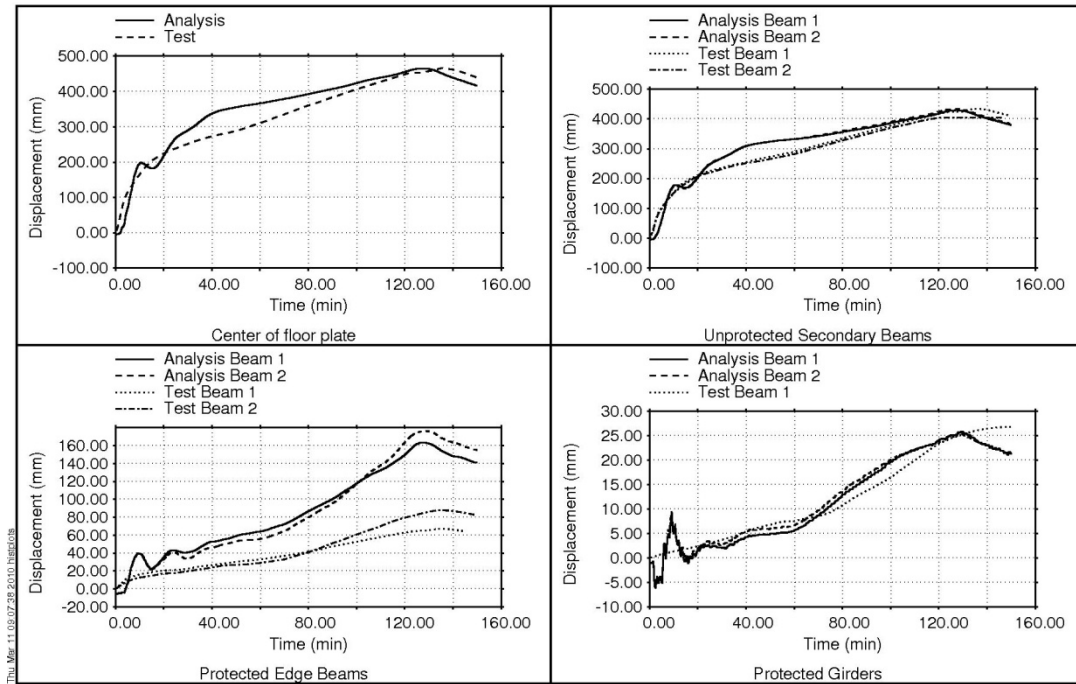


Figure 2. Deflection time histories- NLFlex analysis vs. FRACOF test data.

SIGNIFICANCE OF CONNECTION TYPE

Having benchmarked the modeling and analysis approach against the FRACOF test, the model was modified to reflect design and construction details that are more common in US practice. We identified two specific areas of interest for additional study: secondary beam connections, and slab reinforcement.

The self weight of the test article was estimated to be 3.1kN/m^2 (65psf) and, based on the FRACOF design loads supplied in [1], the floor plate was designed for 1.2kN/m^2 (25psf) superimposed dead load and 5kN/m^2 (105psf) live load. Applying the ACI 318 [8] load factors of 1.2 and 1.6 respectively along with the secondary beam spacing of 2.22m (~7.3ft) and span of 8.735m (~28.7ft), the secondary beam connection ultimate design forces were 128kN (28.7kips) vertical shear. Secondary beams in the FRACOF test were connected to primary girders using all-bolted double clip angles with 3rows of bolts. Depending on fabrication or erection

preferences within the US, a bolted finplate connection may also be utilized to satisfy the capacity requirements at these locations and the decision was made to select a connection of this type that meets the US requirements for further evaluation.

Consulting the single shear plate connection tables in [6], a suitable connection detail was selected with an ultimate capacity of 38.3kips and the following characteristics: 3 3/4" dia. ASTM A325-X bolts spaced 3" on center in a 1/4" A36 steel fin plate. Note that for the load case considered in the FRACOF test (1.0 DL + 0.5 LL), this connection provides a safety factor of 2.5 under ambient conditions.

This connection detail was modeled in a similar manner to that described for double clip angle connections used in the FRACOF test, except for the incorporation of temperature degradation properties of A325 bolts based on recent experimental research published in [7].

Considering the potential difficulties of the connection modeling approach's ability to resolve all potential failure mechanisms (i.e. bolt failure vs. bolt hole failure), the connection model used in the analysis was benchmarked against a more refined model of the connection that is well suited to resolving these failure mechanisms using small continuum elements for the beam web, angles, and bolts. This model was exercised in tension (considered the dominant failure mechanism in fire) in the temperature range of interest (between 500° C and 600° C). Comparison of the results of this benchmarking study is provided in Figure 3. The analysis shows that, in this temperature range, the connection failure in tension is governed by bolt failure, shown in Figure 4, and that the use of beam and shell elements to model the behavior of the finplate connections in the model of the floor plate provides an excellent representation of the strength and ductility of the connection at elevated temperatures. It should be noted that a tensile failure of the finplate connection under ambient conditions would have been governed by bolt hole tearing, as shown in Figure 5. Under elevated temperatures, the connection becomes not only weaker but also much more brittle as result of the failure localizing at the bolts rather than in the connection plates.

Re-analysis of the test article with the described finplate detail shows only a modest effect on the structural response when compared to the benchmark model in Figure 6. It shows that peak central deflections and secondary beam sagging is reduced by approximately 10%; a difference which is attributed to the slightly stiffer characteristics of the finplate.

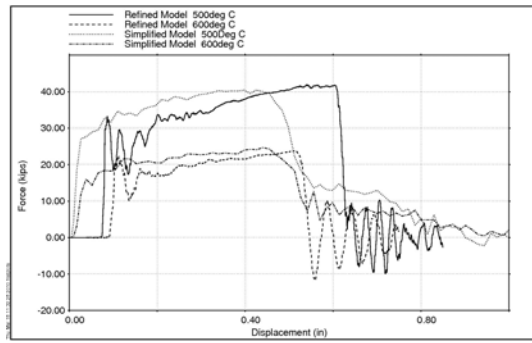


Figure 3. comparison of detailed and simplified modeling approaches at 500°C and 600°C temperatures.

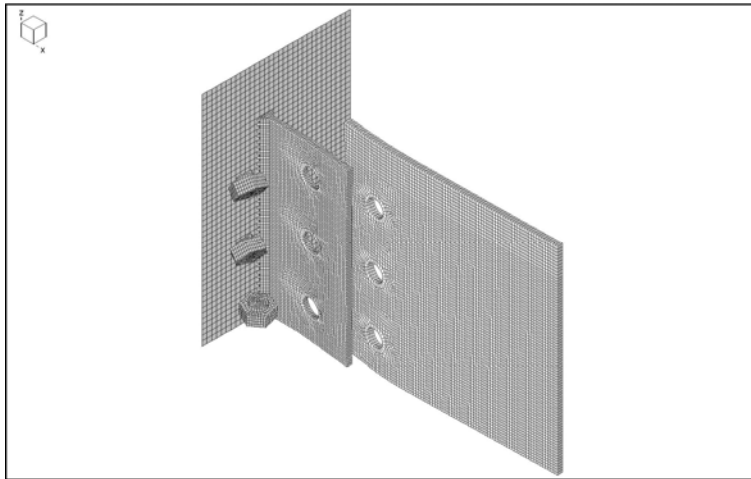


Figure 4. Detailed model of finplate failure at 500°C.

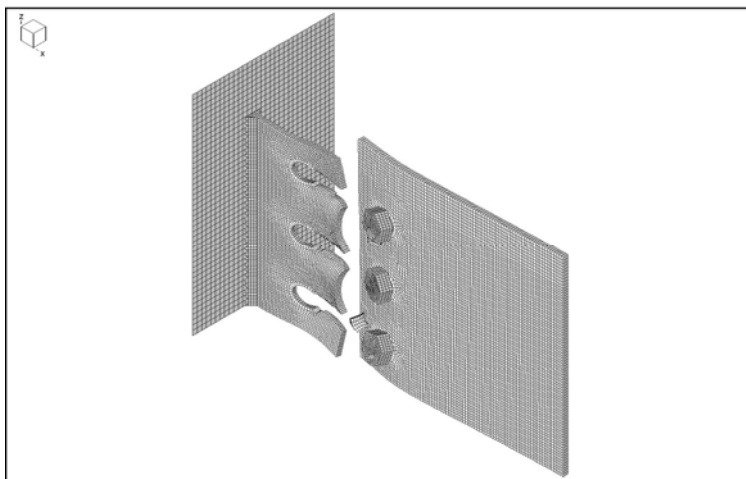


Figure 5. Detailed model of finplate tensile failure at ambient temperature.

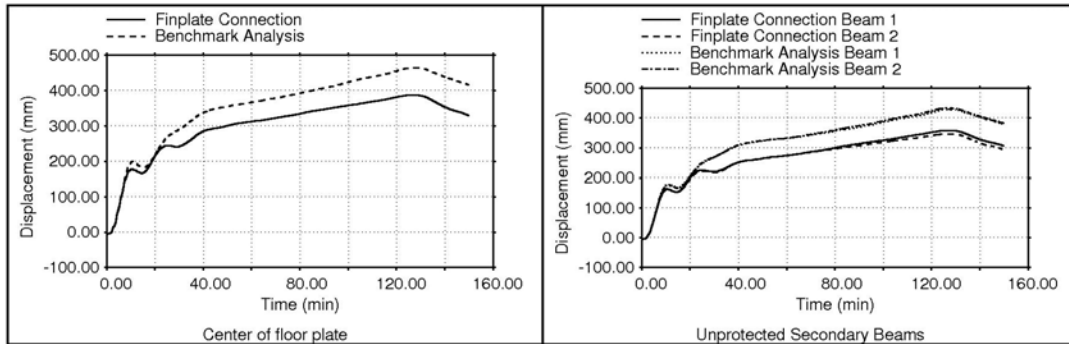


Figure 6. Analysis with finplate connection compared to benchmark model.

SIGNIFICANCE OF SLAB REINFORCEMENT

The FRACOF test used 7mm (0.275in) dia. Steel reinforcement bars placed at 150mm (6in) on center in both directions ($0.121\text{in}^2/\text{ft}$); whereas a US design for a comparable slab would call for $0.040\text{in}^2/\text{ft}$ (satisfied for this slab with 6x6-W2.0xW2.0 steel wire mesh) [8].

Re-analysis of the test article under ISO-834 exposure with the described reinforcement properties shows modest effect on the structural response when compared to the benchmark model in Figure 7. It is important to point out that the analysis results presented here include the net effect of both the finplate connections and the slab reinforcement sized to US standards.

These results suggest that, had a comparable test been conducted with these connection details and slab reinforcement ratios, the response of this structure might have been marginally more severe in terms of deflection when compared to the FRACOF test article. However, the magnitudes of the changes in deflection observed in these analyses do not appear to be dramatic and may well be within the ordinary variability of the test.

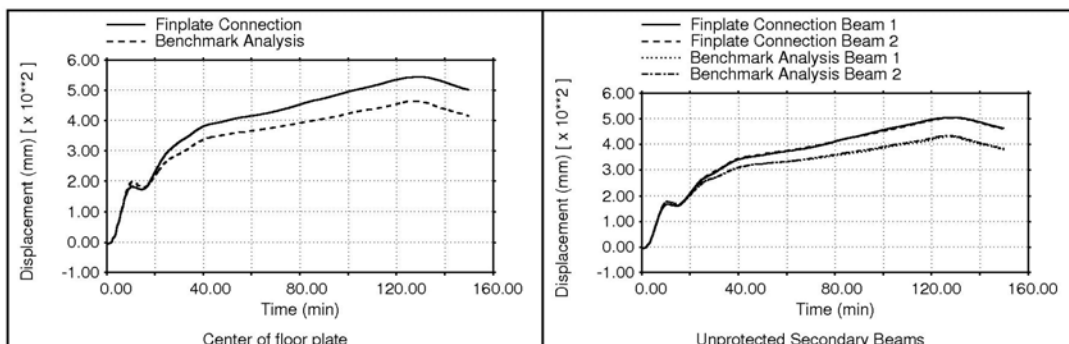


Figure 7. Comparison of analysis with combination of reduced slab reinforcement and finplate connection as compared to the benchmark model.

CONCLUSIONS

Based on the analysis results presented in this paper, the following conclusions have been drawn:

- 1) The modeling and analysis techniques used in this study compare well against data recorded in the FRACOF test.
- 2) Modification of the connection details and slab reinforcement, so as to reflect US practice described in the paper, only modestly affect the response of the test structure in a comparable exposure (same FRACOF elevated temperature fields).

REFERENCES

1. Zhao, B., Roosefid, M., and Vassart, O. 2008. "Full Scale Test of a Steel and Concrete Composite Floor Exposed to ISO Fire," Proceedings of the Fifth International Conference on Structures in Fire.
2. Abu, A., Block, F., Butterworth, N., and Burgess, I. 2009. "Structural Fire Engineering Assessments of the FRACOF and MOKRSKO Fire Tests, An Engineering Prediction" Application of Structural Fire Engineering, 19-20 February, 2009.
3. Vaughan, D. K., "FLEX User's Guide", Report UG8298, WA, Palo Alto, CA, May, 1983 plus updates through 2010.
4. Eurocode 3: Design of steel structures—Part1-2: General rules—Structural fire design. 2005
5. Huang, Z. Burgess, I., Plank, R. 1999. "The Influence of Shear Connectors on the Behavior of Composite Steel-Framed Buildings in Fire". J. Constr. Steel Rsrch. 51 (1999) pp. 219–237
6. American Institute of Steel Construction, *Steel Construction Design Manual, 13th Edition*.
7. Yu., L., *Behavior of Bolted Connection During and After a Fire*. 2006, The University of Texas at Austin.
8. American Concrete Institute, *building Code Requirements for Structural Concrete (ACI 318-05)*. 2005

Structural Response of Unprotected Floor Assemblies in Realistic Residential Fire Scenarios

N. BÉNICHOU, J. Z. SU, A. C. BWALYA, G. D. LOUGHEED,
B. C. TABER and P. LEROUX

ABSTRACT

This paper presents the results of a full-scale experimental program undertaken to study the impact of basement fire scenarios on the structural integrity of unprotected floor assemblies. The experiments utilized fast-growing fires to challenge the structural integrity of the unprotected floor system above the basement, which may provide an egress route for occupants. A range of floor assemblies were used in the experiments. The results show that the type of joist used and the ventilation conditions have the most impact on the time to structural failure of the floor assemblies. The results also helped in establishing the sequence of fire events and their impact on the ability of occupants to escape during a fire.

INTRODUCTION

With the advent of new materials and innovative products for use in the construction of houses, there is a need to understand their potential impacts on occupant life safety under fire conditions. To address this need, the National Research Council of Canada undertook a research study to understand the factors that affect the life safety of occupants in single-family house fires from the perspective of tenability for occupants and structural integrity of structural elements as egress routes. The research sought to establish the typical sequence of events, such as smoke alarm activation, onset of untenable conditions, and structural failure of floor assemblies using specific fire scenarios in a full-scale test facility. The experimental studies focused on basement fires and the unprotected floor assembly located over a basement. A range of floor systems, including solid wood joist, wood I-joist, steel C-joist, and wood truss assemblies were used in the experiments. This paper focuses on the structural response of the test floor assemblies and the time of loss of structural integrity of these assemblies.

N. Bénichou, J.Z. Su, A.C. Bwalya, G.D. Lougheed, B.C. Taber, and P. Leroux, National Research Council of Canada, Ottawa, Ontario, Canada, K1A 0R6

EXPERIMENTAL PROGRAM

Full-Scale Test Facility

A test facility was designed to represent a typical two-storey single-family house with a basement. The floor layout of the facility is shown in Figure 1. Each storey had a floor area of 95 m² and a ceiling height of 2.4 m. The basement was partitioned to create a fire room representing a 27.6 m² living area. An exterior window opening measuring 2.0 m wide by 0.5 m high and located 1.8 m above the floor was provided in the south wall of the fire room. A 0.91 m wide by 2.05 m high doorway opening located on the north wall of the fire room led into a stairwell enclosure. At the top of this stairwell, a 0.81 m wide by 2.05 m high doorway led into the first storey. The first storey had an open-plan layout. A floor assembly was constructed directly above the fire room. A 0.89 m wide by 2.07 m high doorway led to the exterior. The second storey had a corridor and two bedrooms.



Figure 1. Three-storey facility.

Fire scenarios

Bench-, medium- and full-scale fire tests were conducted in order to select a fuel package and fire scenarios for use in the experiments. A simple fuel package was developed to fuel a fire that simulated a basement living area fire [1]. The fuel package consisted of a mock-up sofa and wood cribs; see Figure 2. Full-scale fire scenario tests were conducted in the facility using the fuel package to investigate the effect of fuel quantity and ventilation on fire development [2]. The placement of the fuel package in the basement is illustrated in Figure 3. Two fire scenarios were selected for use in experiments with the unprotected floor assemblies: using a closed or open door to the basement from the first floor.



Figure 2. Fuel package.

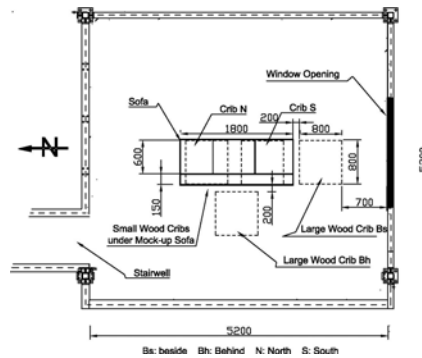


Figure 3. Layout of the fuel package.

Floor Assemblies and Instrumentation

A range of floor systems, including solid wood joist, wood I-joist, steel C-joist, metal plate wood truss and metal web wood truss assemblies were used in the full-scale fire experiments (see Table 1). For each experiment, a floor assembly was constructed on the first storey directly above the basement fire compartment. A single layer of 15.1-mm thick oriented strand board (OSB) was used for the subfloor of all assemblies. The span of the assemblies was chosen based on the load and the type of framing. An imposed load of 0.95 kPa (i.e., half of the imposed load of that prescribed by the National Building Code of Canada [3]) was applied on each floor assembly.

Various measurement devices were used in the experiments, including thermocouples to measure temperatures in the test facility and on the test floor assemblies, flame-sensing devices, floor deflection devices, smoke alarms, smoke density and gas measurement devices, and video cameras. Details of the design, construction and instrumentation are provided in a series of reports [4-9].

Table 1. Fire Tests with Unprotected Floor Assemblies.

Unprotected assemblies	Open door	Closed door
Solid wood joist (235 mm deep)	UF-01	UF-02
Wood I-joist A (302 mm deep)	UF-03	UF-09
Steel C-joist (203 mm deep)	UF-04	N/A
Metal-plate wood truss (305 mm deep)	UF-05	N/A
Wood I-joist B (302 mm deep)	UF-06/UF-06R/UF-06RR	N/A
Metal web wood truss (302 mm deep)	UF-07	UF-08

Test Procedure

The mock-up sofa was ignited.

The fire room's exterior window opening was opened when the temperature measured at the opening reached 300°C.

The exterior door on the first storey was opened at 180 s after ignition and left open, simulating a situation where some occupants escaped leaving the exterior door open.

The tests were terminated when excessive flames penetrated through the floor assembly and/or structural failure of any part of the floor assembly occurred.

EXPERIMENTAL RESULTS

Fire development

Figure 4 shows the temperature profiles measured at the centre of one quadrant of the basement fire room. The polyurethane foam used for the mock-up sofa dominated the initial fire growth. The fast development of the fire from ignition to attainment of the first temperature peak was consistent for all of the tests. Following this initial stage, the effects of ventilation became more pronounced and the fire became wood-crib-dominated and also involved the unprotected floor assemblies.

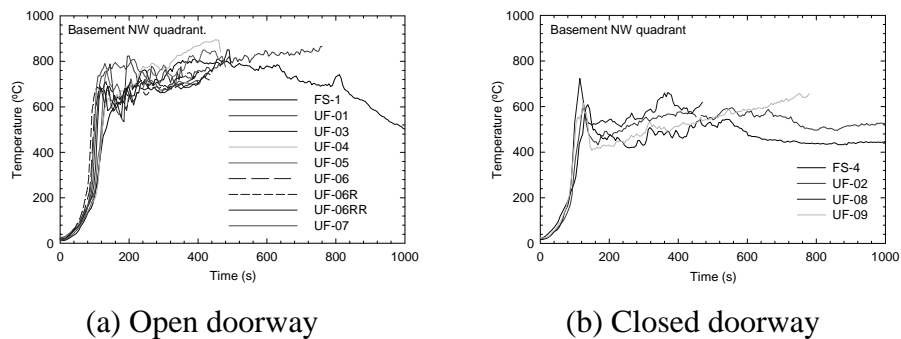


Figure 4. Temperature profiles in the fire compartment at 2.4 m height.

The temperatures at the 2.4 m height exceeded 600°C at approximately 120 s, indicating that the basement fire compartment reached flashover. Figure 4(a) indicates that under the full ventilation conditions (open basement doorway) the fire scenario provided a very reproducible fire exposure to the floor assemblies in all experiments. As shown in Figure 4(b), under the limited ventilation conditions (closed basement doorway), the fire scenario also provided a relatively severe and consistent fire exposure to the floor assemblies. The results from the fire scenario tests (FS-1 and FS-4) [2] in the fire room are also included in the figures for reference.

Flame Penetration

A floor system provides an egress route for occupants and its structural integrity directly impacts the safe evacuation of the occupants. Figure 5 shows exemplar data plots, which are representative of the results for tests with the engineered floor assemblies. The temperatures shown in Figure 5(a) are from measurements by nine

thermocouples (TC) under insulated pads on top of the OSB subfloor. A rapid increase in temperature indicates that the floor was being significantly breached. The subsequent rapid decrease in temperature was due to the termination of the experiment by extinguishing the fire with water. Under standard fire resistance testing, the temperature failure criterion is defined as a temperature rise of 140°C on average of the nine TCs or a temperature rise of 180°C at any single point [10].

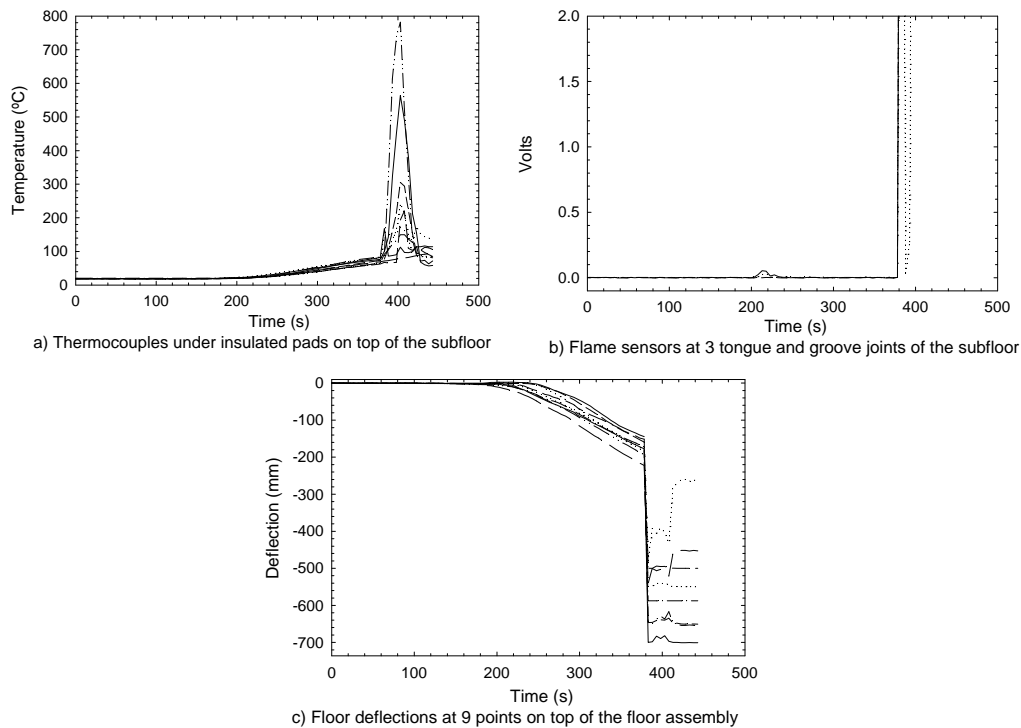


Figure 5. Exemplar plots of measurements for Test UF-06R.

Flame penetration through a floor assembly is considered to be an initial indicator of failure of the assembly, and is also a failure criterion in standard fire resistance testing [10]. Flame penetration could also impact the ability of occupants to evacuate. Flame-sensing devices were placed at joints on the unexposed side of the OSB subfloor to detect flame penetration through the floor. As shown in Figure 5(b), the flame-sensing devices produced noticeable voltage spikes, an indication that the devices are being struck by flames penetrating through the assembly.

Deflections

The floor deflection was measured at nine points in the central area of the test assembly. Figure 5(c) shows examples of the deflection measurements. The sharp increase in deflection is an indication that structural collapse had occurred.

Figure 6 shows a comparison of the floor deflection near the centre of all of the test assemblies prior to structural failure. The steel C-joist assembly produced the highest deflection rate, followed by metal-web wood trusses and metal-plate wood

trusses. The solid wood joist assemblies produced the lowest deflection rate. There were three distinct patterns of failure of the test floor assemblies. In UF-01 and UF-02, the subfloor failed, with most of the solid wood joists charred but still in place at the end of the tests. In UF-03, UF-05, UF-06R, UF-06RR, UF-07 and UF-08, the assemblies with wood I-joists or wood trusses structurally deflected and then broke at the mid-points and the floor assemblies collapsed in the form of a “V” shape. In UF-04, UF-06 and UF-09, the assemblies with steel C-joists and wood I-joists structurally deflected and then they completely collapsed into the basement.

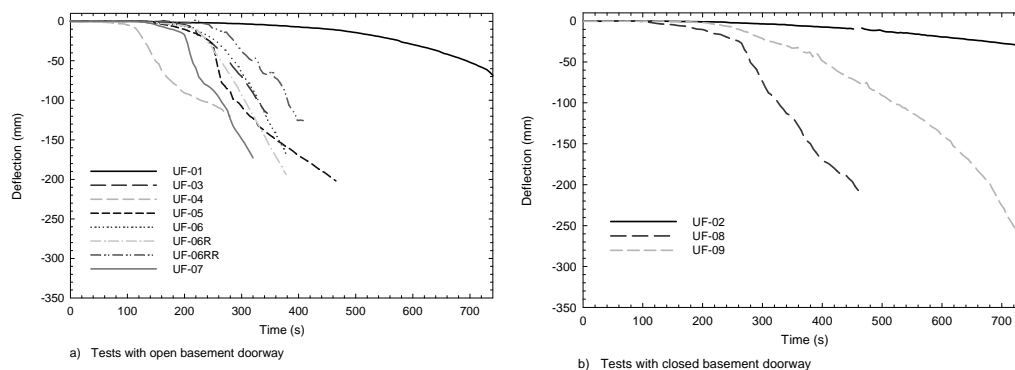


Figure 6. Floor deflection near the centre of assemblies prior to structural failure.

Failure times

Table 2 shows the times to failure for the assemblies based on temperature measurements, flame penetration and floor deflection, and confirmed by visual observations. The times to reach structural failure for the wood I-joist, steel C-joist, metal plate and metal web wood truss assemblies were 35–60% shorter than that for the solid wood joist assembly. As shown by the results from the three replicate tests with Type B wood I-joist assembly (Tests UF-06, UF-06R and UF-06RR), the times to structural failure were repeatable. Having a closed door to the basement limited the air available for combustion and delayed the time for the test assemblies to reach structural failure (50-60% longer than with the open basement doorway).

Table 2. Summary of Structural Failure Times of the Assemblies (in seconds).

UF-01	UF-02	UF-03	UF-04	UF-05	UF-06	UF-06R	UF-06RR	UF-07	UF-08	UF-09
740	1200	490	462	469	382	380	414	325	474	778
DO	DC	DO	DO	DO	DO	DO	DO	DO	DC	DC

DO: Door Open DC: Door Closed.

Sequence of events

The two scenarios (door open or closed) were designed to better understand how the structural integrity and tenability conditions would affect the ability of

occupants on the upper storeys to escape a single family house in the event of a basement fire. Reference [11] provides the chronological sequence of the fire events in the full-scale experiments—fire initiation, smoke alarm activation, onset of untenable conditions, and structural failure of the test floor assembly. For the experiments with the open basement doorway the untenable conditions generally occurred within 180 to 240 s after ignition and the structural failure of the test floor assemblies occurred after the untenable conditions were reached. With the presence of the closed door to the basement, the structural failure of the solid wood joist assembly (Test UF-02) and wood I-joist Type A assembly (Test UF-09) also occurred well after untenable conditions were reached. However, one case (UF-08, scenario with the closed door) showed that structural failure occurred concurrently with the onset of untenable conditions.

CONCLUSIONS

Two basement fire scenarios were used in the full-scale fire experiments to meet the objectives of the research. Overall, the fire scenario with the open basement doorway was more severe than the fire scenario with the closed basement doorway to the structural integrity of the unprotected floor assemblies and the life safety of occupants on upper storeys.

In all of the experiments, structural failure of the test floor assemblies occurred. The time to structural failure was characterized by an increase in floor deflection and was usually accompanied by considerable flame penetration through the assemblies and an increase in compartment temperature above the floor assemblies. The times to reach structural failure for the wood I-joist, steel C-joist, metal plate wood truss and metal web wood truss assemblies were 35-60% shorter than that for the solid wood joist assembly. It was also found that having a closed door to the basement limited the air available for combustion and delayed the times to structure failure for the assemblies (50–60% longer than with the open basement doorway).

There was structural deflection of all floor assemblies prior to their structural failure. The steel C-joist floor assembly produced the highest deflection rate, followed by metal-web and metal-plate wood trusses. The solid wood joist assemblies produced the lowest deflection rate. For all engineered floor assemblies, the structure failure occurred either in the form of complete collapse into the basement or in the form of a “V” shaped collapse due to joist or truss failure.

In general, untenable conditions occurred before structural failure of unprotected floor assemblies. However, the time gap between the onset of untenable conditions and the structural failure of the floor assembly was smaller for the engineered floor assemblies than it was for the solid wood joist assembly used in the experiments. There was one case where structural failure of the unprotected assemblies was concurrent with untenable conditions.

ACKNOWLEDGEMENTS

The following organizations provided valuable financial and technical support to the research as the project partners: Canada Mortgage and Housing Corporation, Canadian Automatic Sprinkler Association, Canadian Wood Council, Cement Association of Canada, City of Calgary, FPInnovations - Forintek Division, North American Insulation Manufacturers Association, Ontario Ministry of Community Safety and Correctional Services/Office of the Fire Marshal, Ontario Ministry of Municipal Affairs and Housing, Wood I-Joist Manufacturers Association.

The authors would like to acknowledge contributions of G. Proulx, A. Kashef, C. McCartney, J.R. Thomas, D. Carpenter, G. Crampton, E. Gibbs, C. McCartney, M. Ryan, M. Wright, J. Henrie, R. Monette and R. Rombough in the project.

REFERENCES

1. Bwalya, A.C., Lougheed, G.D., Su, J.Z., Taber, B.C., Bénichou, N., Kashef, A. (2007) Development of a fuel package for use in the fire performance of houses project. In: Fire and Materials Conference, San Francisco, CA, January 29, 2007.
2. Su, J.Z., Bwalya, A.C., Lougheed, G.D., Bénichou, N., Taber, B.C., Thomas, J.R. (2007) Fire Scenario Tests in Fire Performance of Houses Test Facility - Data Analysis, Research Report 210, National Research Council of Canada, Ottawa, ON
3. Canadian Commission on Building and Fire Codes (2005) National Building Code of Canada, National Research Council of Canada, Ottawa, ON.
4. Bénichou, N., Su, J.Z., Bwalya, A.C., Lougheed, G.D., Taber, B.C., Leroux, P., Kashef, A., McCartney, C., Thomas, J.R. (2009) Fire Performance of Houses, Phase I, Study of Unprotected Floor Assemblies in Basement Fire Scenarios, Part 1 - Results of Tests UF-01 and UF-02 (Solid Wood Joists), Research Report 246, National Research Council of Canada, Ottawa, ON.
5. Su, J.Z., Bénichou, N., Bwalya, A.C., Lougheed, G.D., Taber, B.C., Leroux, P., Kashef, A., Thomas, J.R. (2009) Fire Performance of Houses, Phase I, Study of Unprotected Floor Assemblies in Basement Fire Scenarios, Part 2 - Results of Tests UF-03 and UF-09 (Wood I-Joists A), Research Report 247, National Research Council of Canada, Ottawa, ON.
6. Bénichou, N., Su, J.Z., Bwalya, A.C., Lougheed, G.D., Taber, B.C., Leroux, P., Kashef, A., Thomas, J.R. (2009) Fire Performance of Houses, Phase I, Study of Unprotected Floor Assemblies in Basement Fire Scenarios, Part 3 - Results of Test UF-04 (Light-Gauge Steel C-Joists), Research Report 248, National Research Council of Canada, Ottawa, ON.
7. Su, J.Z., Bénichou, N., Bwalya, A.C., Lougheed, G.D., Taber, B.C., Leroux, P., Kashef, A., Thomas, J.R. (2009) Fire Performance of Houses, Phase I, Study of Unprotected Floor Assemblies in Basement Fire Scenarios, Part 4 - Results of Test UF-05 (Metal-Plate-Connected Wood Trusses), Research Report 249, National Research Council of Canada, Ottawa, ON.
8. Bénichou, N., Su, J.Z., Bwalya, A.C., Lougheed, G.D., Taber, B.C., Leroux, P., Thomas, J.R. (2009) Fire Performance of Houses, Phase I, Study of Unprotected Floor Assemblies in Basement Fire Scenarios, Part 5 - Results of Tests UF-06, UF-06R and UF-06RR (Wood I-Joists B), Research Report 250, National Research Council of Canada, Ottawa, ON.
9. Su, J.Z., Bénichou, N., Bwalya, A.C., Lougheed, G.D., Taber, B.C., Leroux, P., Thomas, J.R. (2009) Fire Performance of Houses, Phase I, Study of Unprotected Floor Assemblies in Basement Fire Scenarios, Part 6 - Results of Tests UF-07 and UF-08 (Metal-Web-Connected Wood Trusses), Research Report 251, National Research Council of Canada, Ottawa, ON.
10. Underwriters' Laboratories of Canada (2007) Standard Methods of Fire Endurance Tests of Building Construction and Materials, CAN/ULC-S101-07, Scarborough, ON
11. Su, J.Z., Bénichou, N., Bwalya, A.C., Lougheed, G.D., Taber, B.C., Leroux, P., Proulx, G., Kashef, A., McCartney, C., Thomas, J.R. (2008) Fire Performance of Houses, Phase I, Study of Unprotected Floor Assemblies in Basement Fire Scenarios, Summary Report, Research Report, National Research Council of Canada, Ottawa, ON.

Mitigation of Post-Earthquake Fire Risk to Building Structures

M. H. YASSIN, A. BAGCHI and V. K. R. KODUR

ABSTRACT

Fire following an earthquake can lead to damage to buildings and life-line structures. In performance-based design approach structural behavior under normal load and multi-hazard scenarios including ground-shaking, and the fire should be considered in high seismic zones. However, the current design codes and standards do not consider the post-earthquake fire and a design scenario, which leaves many buildings in high seismic areas vulnerable. Although there is a significant volume of analytical and experimental studies on structural behavior under fire and earthquakes are available, separately, there is a clear lack of research on their combined effect. The paper discusses these issues and outlines the methods of estimating and mitigating the risk associated with such events.

INTRODUCTION

The occurrence of fire following an earthquake is not very uncommon. It produces a disastrous effect, and the past records show that fire following earthquakes in Japan and North America has been a major factor for post-earthquake damage in the twentieth century [1]. The history shows that the lack of adequate attention to post-earthquake fires in both individual building design and urban design can result in a catastrophe. The main parameters that trigger post-earthquake fires, and strategies that are to be considered to minimize the impact of these events to buildings and built infrastructure are discussed here.

Risk by definition is the likelihood of injury or loss, while the hazard could be used to describe that loss and injury physically. According to the EERI report [2], seismic risk is defined as the probability of the social or economic consequences of earthquakes to equal or exceed specified values at a site, at several sites or in area,

Mohammad H. Yassin, Building, Civil and Env. Eng., Concordia University, Montreal, Canada
Ashutosh Bagchi, Building, Civil and Env. Eng., Concordia University, Montreal, Canada
Venkatesh K.R. Kodur, Civil and Env. Eng., Michigan State Univ, East Lansing, MI., USA

during a specified exposure time. Seismic hazard, on the other hand, is defined as any physical phenomenon associated with an earthquake (e.g. ground motion) that may produce adverse consequences to human activities. The seismic risk can be expressed in the following form [3]:

$$\text{Seismic Risk} = (\text{Seismic Hazard}) \times (\text{Vulnerability}) \times (\text{value}) < 1 \quad (1)$$

where, the term vulnerability represents the loss in percentage value of an item before the occurrence of the event. Knowing that the likelihood of PEF event is relatively high and by combining the seismic probability with the risk of damage due to fire following an earthquake we can estimate the PEF risk. PEF risk represents a conditional probability which can be expressed in the following form.

$$\text{PEF risk} = P(\text{Seismic Risk} \cap \text{Ignition Risk}) / \text{Seismic Risk} \quad (2)$$

Reducing the risk of fires following an earthquake is a complex task and it involves many interdisciplinary aspects. Information, opinions and statistical data would lead to risk reduction decisions and actions. A detailed discussion on seismic risk can be found in [2], based on which a simplified chart for PEF risk assessment and mitigation as shown in Figure 1 has been developed here to show the relationship between different groups of professionals and users involved.

Structural members are normally designed to satisfy the requirements of serviceability and safety limit states for various environmental conditions. According to [4], the following factors should be considered in structural fire safety design phase: (a) damage limits for structural elements; (b) provisions for preventing local collapse; (c) limits on the deformation of structural components to minimize the negative impact on non-structural components and fire protection systems; and (d) measures taken to prevent progressive collapse of buildings.

FACTORS INFLUENCING POST-EARTHQUAKE FIRES

The factors that influence fire hazard following an earthquake include the types of construction materials, building usage and amenities, loss of water supply for extinguishing fire, the response time of occupants and emergency crews that might be affected by obstructed access and insufficient resources, and architectural configuration including improper building separation. Post-earthquake fire may also be viewed as a course of events consisting of the followings [1]: (1) seismic event causes damage in structural and non-structural components and might result in falling down of items such as candles or overturning of cooking stoves; (2) ignition may be caused by breakage of utility lines such as gas line, or electrical short-circuiting; (3) discovering the existence of a fire may be difficult because of panic following an earthquake; (4) reporting a fire to the fire department is the next important step; (5) response of the fire department may be impeded by damage to the station itself or the transportation and communication networks; (6) failure of water distribution systems due to earthquake affects the fire-fighting effort; and (7) if the fire control measures fail, the fire could end up in a conflagration and fire spread, which will stop only when all the fuel is burnt up.

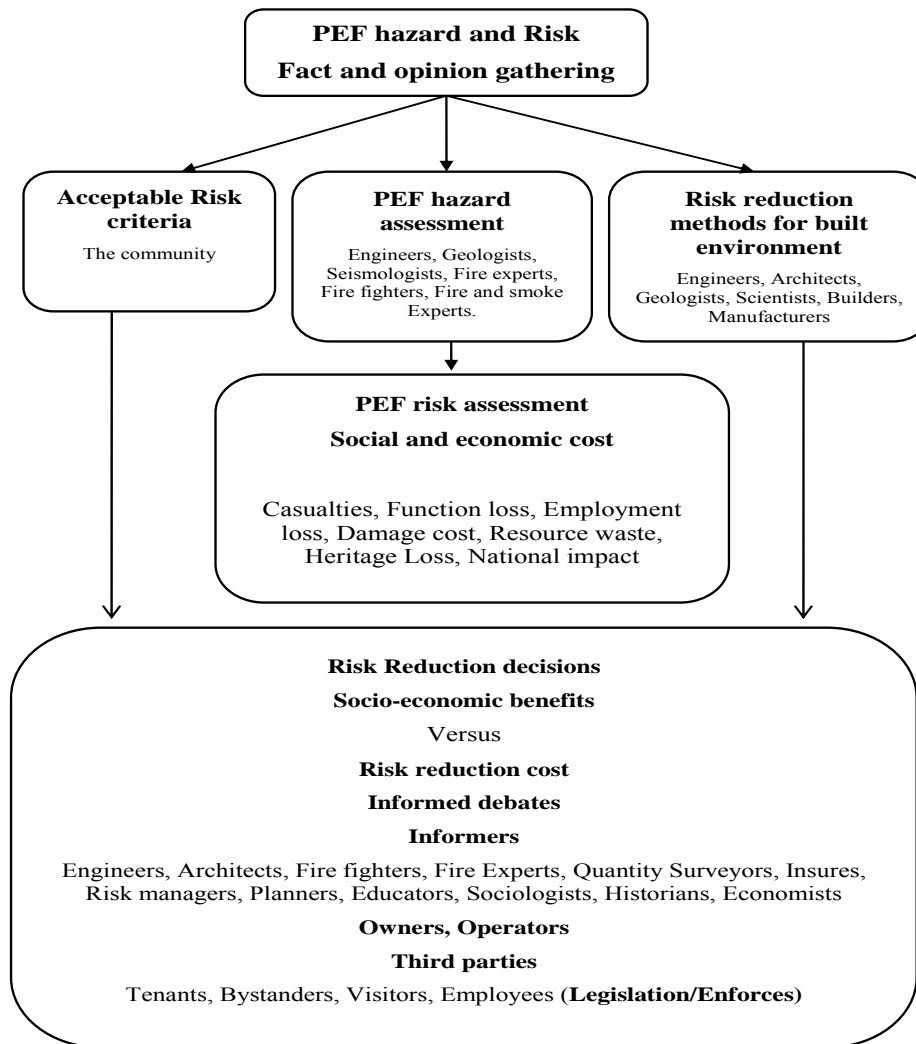


Figure 1. Flow chart showing the interaction of personnel involved in the PEF risk reduction process.

STRATEGIES FOR THE MITIGATION OF PEF HAZARD

Mitigation measures for post-earthquake fire can be achieved at the following two levels: (a) regional or area level, and (b) individual building level.

Mitigation at the Area Level:

At the area level, an approach based on Geographical Information System (GIS) can be effective in the analysis process [5,6]. In the regional level, there are several factors that need adequate attention and enhancement. Some of which are as follows [7]: (a) post-earthquake fire ignitions due to short circuit; (b) fire ignition due to the breakage of gas distribution system; (c) fire spread between buildings; (d) disruption of the water distribution network; (e) enhancing the water-based fire protection systems; and (f) life-line systems design for earthquake and subsequent fire. Water supply is an important factor in mitigating fire hazard. For an effective approach to mitigate post-earthquake fires in the area level, following actions have

been suggested in [8], (a) identifying major pipelines in the network, (b) provisions for redundant water supply for fire fighting, (c) mapping up the hazards on them and then determining alternatives for them including replacement and upgrade, and (d) constructing above-ground ultra large diameter hose pipe bypass.

Mitigation at the Individual Building Level:

At the individual building level four fundamental types of analyses are to be incorporated into the performance-based design approach. These steps are as follows [5]: (i) analysis of the hazard that provides input data like duration of earthquake and its intensity, fire load and resulting compartment temperatures; (ii) analyses of the structural and non structural components based on the prior estimation of hazards that include structural demand parameters like drift and acceleration experienced by the building, peak structural temperatures and deflections; (iii) damage analysis of the buildings including condition evaluation and required modifications; and (iv) loss analysis consisting of casualties, injuries, direct and indirect financial losses.

The performance of structural systems in post-earthquake fire scenarios is greatly dependent on the constituent materials (e.g., concrete, steel, wood etc.). All construction materials lose their strength and stiffness properties when subjected to high temperatures due to fire exposures [9]. In choosing the building materials or construction processes, it is necessary to consider the thermal properties (e.g., low thermal conductivity, high effective heat capacity etc.) of the materials that would help delay the rise of temperature in the structure.

Usually, the following two types of fire protection mechanisms, active and passive fire protection systems, are employed in buildings to minimize the impact of fire hazards. The active systems (non-structural protection schemes) include the fire and smoke detection and sprinkler systems, fire-proof doors, and fire extinguishing systems like hydrant and emergency exits. The passive systems, built into the structural members employ schemes like insulation, flame shielding and heat sinks. However, the high likelihood of the failure of both active and passive fire safety systems as observed in many earthquakes in the past, underscores the need for implementing redundant fire protection systems in a building.

EVALUATION OF THE PEF PERFORMANCE OF STRUCTURES

Evaluation of the post-earthquake fire performance of a structural system is a key to the performance-based design. A scheme for the evaluation of PEF performance of structural systems for buildings has been proposed in [10]. Prior to the occurrence of an earthquake, a building frame is primarily subjected to gravity loads, P due to dead and live loads. To evaluate the seismic damage in the structure, first the seismic hazard level is determined from the seismic hazard spectrum for the given site, followed by the selection of appropriate ground motion records and structural analysis. The lateral deformation, Δ in the damaged structure causes additional stresses in the frame due to the secondary moment caused by P - Δ effect. Structural members and joints are also weakened by the cyclic inelastic deformation causing stiffness and strength degradation. In addition, the fire proofing systems are also damaged. Once the earthquake induced damage in the structure is determined, the damaged structure is subjected to a post-earthquake fire scenario, which

involves fire hazard analysis to determine the time history of fire growth and spread, and stress and collapse analysis of the structure.

ANALYSIS AND SIMULATION TOOLS

Currently there are a few research and commercial level software tools available for the analysis of fire hazard, loss estimation and structural response. While software packages like SAFIR [11], and VULCAN [12] are capable of performing structural fire safety analysis to a certain degree of accuracy, they cannot be used for simulating the combined effects of earthquake and fire scenarios. Some commercial finite element analysis packages such as, ANSYS [13] and ABAQUS [14] are more sophisticated in terms for structural analysis under fire and earthquakes, separately. However, the combined analysis including seismic hazard and structural damage evaluation, subsequent fire hazard and corresponding thermo-structural analysis as envisioned in the previous section is not easy. A combination of SAFIR, FDS [15], ANSYS, and analytical methods has been used in the present study to evaluate the PEF performance of structural systems.

EXAMPLES

(1) PEF Analysis of A Wood Stud Wall

Timber structures are constructed widely in North America for housing. As wood is a combustible material careful attention must be given to their fire safety design. An analytical model is developed in [16] for determining the PEF fire resistance of stud walls considering the temperature dependent material properties and charring of wood elements, and composite action between stud and sheathing. It is found that the PEF resistance of a stud wall is reduced considerably even due to a moderate level of damage. One of the wood stud walls (F-19) tested by the National Research Council of Canada (NRC) [17] has been used here as a case study. The geometry of the wall is presented in Figure 3. The critical buckling load of the wall unit degrades with time during fire until it drops to the level of the applied load at which point the unit is deemed to have failed (Fig. 4). The present numerical model shows similar results to the NRC fire tests which reported a failure in the wall F-19 in 43-48 minutes [17]. Fire resistance in PEF is performed by modeling the damage due to earthquake assuming that the gypsum board is to be fully damaged due to ground shaking.

(2) PEF Analysis of A Steel Frame

Under high temperature the loss of strength and stiffness is considered to be the major weakness of steel structures exposed to fire. In a post-earthquake scenario, the building frame and its fire protection system may be significantly damaged and consequently resistance to subsequent fire is reduced. Here PEF analysis of a one-story moment resisting frame as shown in Figure 5 is presented to demonstrate the effect of lateral drift and associated damage on fire resistance. The heat transfer analysis is performed on the elements sections in 2D by using SAFIR, and the snapshots of temperature distribution in the column cross section are shown in

Figure 6. PEF analysis has been performed using ANSYS finite element software, and the sample results are presented in Figures. The comparison between the vertical displacement in the frame nodes in normal and post-earthquake fire as presented in Fig. 8 shows an earlier failure in the structure in the case of PEF.

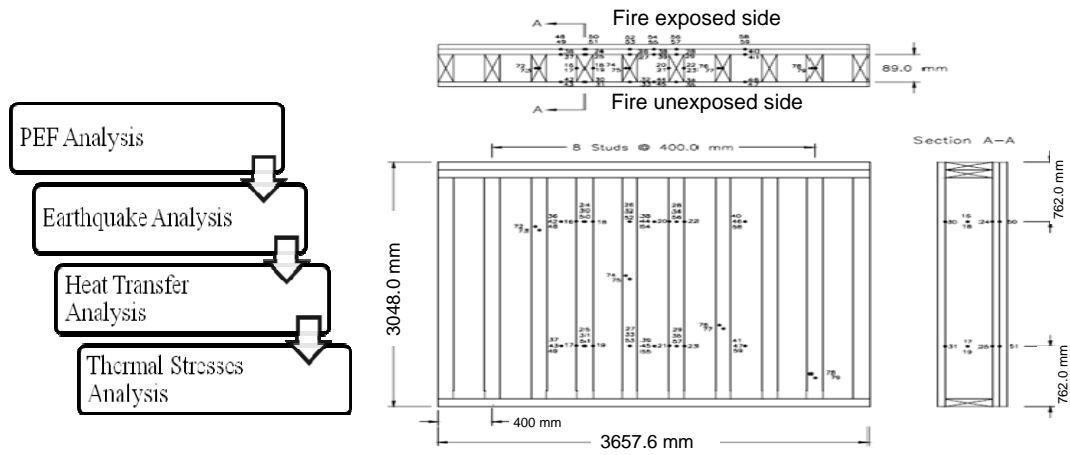


Figure 2. Scheme for PEF Performance estimate.

Figure 3. Wood stud assembly F-19, NRC fire test, Kodur and Sultan (1996).

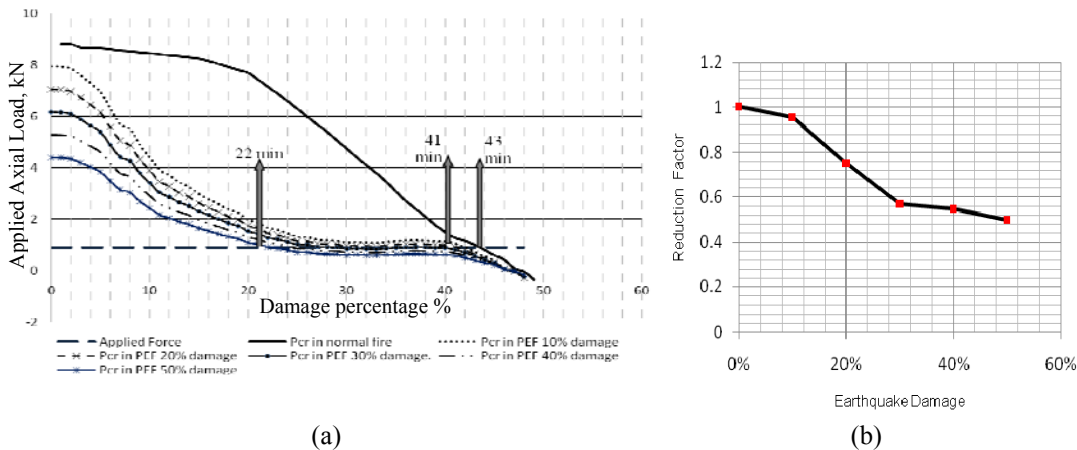


Figure 4. Results of the stability analysis of the stud-wall: (a) time history of buckling capacity, and (b) effect of seismic loads on fire resistance of the wall.

SUMMARY AND CONCLUSIONS

The main factors related to post-earthquake fire hazard are identified to be earthquake intensity and duration, fire scenarios, performance of active and passive fire protection systems, materials used in construction, and availability of emergency services (including water supply) following an earthquake.

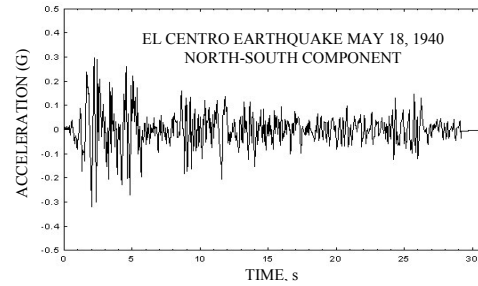
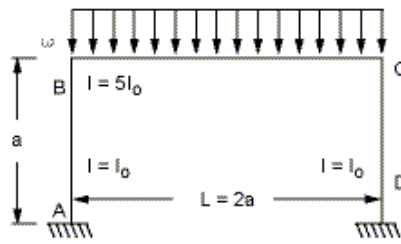


Figure 5. (a) geometry and properties of the frame ($w = -500$ lb/in, $a = 400$ in), (b) El Centro time history acceleration data [18].

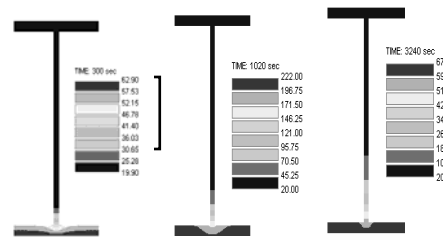
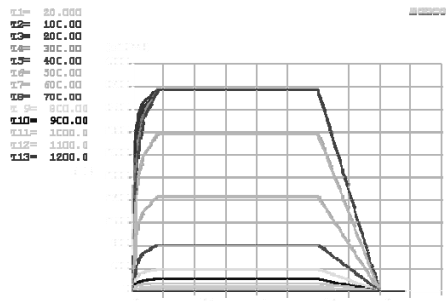


Figure 6: Thermal analysis of steel sections: (a) stress strain relationship for steel, (b) snapshots of temperature distribution in the cross section

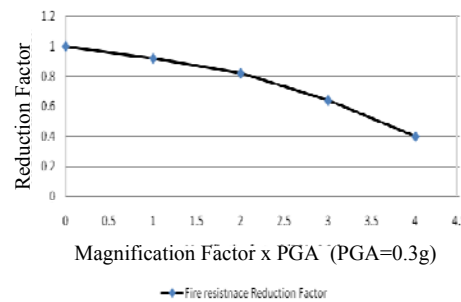
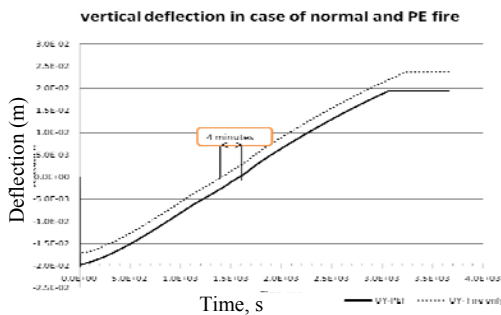


Figure 7. Sample results of the steel frame: (a) vertical deflection of the top right corner, (b) effect of ground acceleration on fire resistance.

Although post-earthquake fire hazard is not uncommon, the current design practices do not consider it for design of structures in the seismic areas. There is very little information for the assessment of the performance of buildings for this hazard and for addressing the performance-based design issues related to it. A strategy for the evaluation of post-earthquake fire performance of building structures along with a rational approach to design has been proposed here. Key research needs are identified as: need for developing guidelines for performance-based design of buildings for post-earthquake fire events; methods and tools for evaluating the structural performance under such scenarios; understanding the performance of high-performing materials such as high strength concrete and FRP

under post-earthquake fire; developing innovative schemes for structural health monitoring of structures under normal and post-earthquake fire events; and updating the risk models using the performance profile of structures under these events.

ACKNOWLEDGEMENT

The support of the Natural Sciences and Engineering Research Council (NSERC) of Canada is gratefully acknowledged.

REFERENCES

1. Scawthorn C., Eidinger J.M., and Schiff A.J., 2005. Fire following earthquake. Technical Council on Lifeline Earthquake Engineering, Monograph No. 26, American Society of Civil Engineers (ASCE), Reston, VA.
2. EERI Committee on Seismic Risk, 1984, "Glossary of Terms for Probabilistic Risk and Hazard Analysis", *Earthquake Spectra*, 1(1): 33-40.
3. Dowrick, D.L, 2003. *Earthquake Risk Reduction*, J. Wiley, NJ, USA.
4. Bernhart D., 2004. The Effect of Support Conditions on the Fire Resistance of a Reinforced Concrete Beam. Research project report, University of Canterbury, Christchurch, New Zealand
5. Chen S., Lee G.C., and Shinozuka M., 2004. Hazard Mitigation for Earthquake and Subsequent fire. ANCER Annual Meeting: Networking of Young Earthquake Engineering Researchers and Professionals, July, Honolulu, Hawaii, U.S.A.
6. Zhao S.J., Xiong L.Y., and Ren A.Z., 2006. A Spatial-Temporal Stochastic Simulation of Fire Outbreaks Following Earthquakes based on GIS. *Journal of Fire Sciences*, 24: 313–339.
7. Chung R.M., Jason N.H., Mohraz B., Mowrer F.W., and Walton W.D., 1995. Post-Earthquake Fire and Lifelines Workshop: Long Beach, California. National Institute of Standards and Technology, Gaithersburg, MD.
8. Eidinger J.M., 2004. Fire Following Earthquake- Flex Hose. 13th World Conference on Earthquake Engineering, Vancouver, B.C., Canada August 1–6, 2004, Paper No. 3268.
9. Anchor R.D., Malhotra H.L., and Purkiss J.A., 1986. Design of structures against fire. In Proceedings of the international conference on Design of Structures against Fire, held at Aston University, Birmingham, UK
10. Mousavi, S.; Bagchi, A.; Kodur, V., 2008. A review of Post-Earthquake Fire Hazard to Building Structures, *Canadian Journal of Civil Engineering*, 35: 689-698.
11. Franssen J.M., Kodur V.K.R., and Mason J. 2000. User's Manual for SAFIR 2002—A Computer Program for Analysis of Structures Submitted to Fire. Department Structures du Génie Civil, Service Ponts et Charpentes, University of Liège, Belgium
12. SUEL, 2010. Vulcan – A software for Structural Fire Engineering. Vulcan Solutions Ltd—a Company of Sheffield University Enterprises Limited, Sheffield, UK. Available from <http://www.shef.ac.uk/suel/companies/vulcan.html> [cited March, 2010]
13. ANSYS, 2010, ANSYS-CFX: <http://www.ansys.com/products/cfx.asp> [cited March, 2010].
14. ABAQUS, 2010, "ABAQUS FEA", http://www.simulia.com/products/abaqus_fea.html, [cited March, 2010], Dassault Systèmes, USA.
15. NIST, 2010, Fire Dynamics Simulator (FDS) and Smokeview, <http://www.fire.nist.gov/fds/> [cited March, 2010]
16. Yassin M.H., Bagchi A., Kodur, V., 2009. Numerical Model for Assessing the Post-Earthquake Fire Resistance of Wood-stud Wall, CSCE, Annual General Conference, St. John's, Newfoundland and Labrador
17. Bénichou, N.; Kodur, V.R.; Sultan, M.A.; (2002). Experimental study and numerical modelling of the fire resistance of wood-stud wall assemblies, 4th Specialty Conference of the Canadian Society for Civil Engineering, June 5-8, Montreal, Canada.
18. PEER, 2010, Pacific Earthquake Engineering Research Center Strong Motion Database, <http://peer.berkeley.edu/smcat/> [cited March, 2010], University of California, Berkeley, CA.

The Use of Adiabatic Surface Temperature to Design Structures for Fire

U. WICKSTRÖM, A. ROBBINS and G. BAKER

ABSTRACT

Ongoing international collaborative research clearly demonstrates that the concept of adiabatic surface temperature is a simple single parameter to describe the complex convective and radiative conditions to which the surface of a structural element is exposed during fire. This parameter is a convenient and simple interface between fire and thermal/structural models. This paper presents existing published and new unpublished research for fire/structural engineers so as to contribute to the advancement of the engineering practice of designing structures in fire.

INTRODUCTION

In recent years, the design of structures for fire exposure conditions has developed into a separate discipline of engineering. Momentum in this new field has only accelerated since the World Trade Centre (WTC) disaster in 2001. The subsequent investigation focused attention on a number of aspects relating to the practice of designing buildings to withstand fire events. One of the recommendations that resulted from the official WTC investigation was that the capability of computational models be enhanced so as to be able to study the effect of realistic fires on buildings, through to the burn-out, cooling and/or collapse stages [1]. In a number of countries there are insufficient requirements in building/fire codes to ensure that multi-storey buildings will withstand severe, long duration, post-flashover fire events. The issue is that little if any attention is paid to the fire-induced loadings that will be imposed on the structure of a building, often for periods well beyond those required for the safe evacuation of building occupants.

Ulf Wickström. SP Technical Research Institute of Sweden, Box 857, SE-501, Borås, SWEDEN.
Amanda Robbins, Greg Baker. BRANZ Ltd, Private Bag 50-908, Porirua 5240, NEW ZEALAND.

Traditionally, fire resistance testing is carried out to standard time-temperature curves contained in standards such as ASTM E 119, ISO 834-1, EN 1363-1 and AS 1530.4, and this testing is the basis for fire resistance design in buildings. This simple approach would appear to be effective, with structural collapse due to fire being a rare event, but a prescriptive time-temperature curve does not reflect what structural members will actually be exposed to during a severe post-flashover fire - this reinforces the need for “fire” to be accounted for as a discrete category of structural loading when a building is being designed [1]. In some regions this latter issue is addressed—EN 1991-1-2 is an example—but this is not universally the case.

Collaborative research, involving a number of the member research laboratories of the International Forum of Fire Research Directors (FORUM), is currently underway to investigate the use of the “adiabatic surface temperature” (AST) concept as a tool for modelling structures in fire. The research has shown that the AST is virtually equivalent to the temperature measured by a plate thermometer (PT) in the vicinity of a surface [1], and that the AST can therefore be used as a simple boundary condition input for finite element (FE) thermal/structural models. The research has also demonstrated that the PT can be used as a general radiation measuring device both in steady-state (furnace-like) environments, but also potentially under ambient (compartment fire) conditions.

PLATE THERMOMETERS, ADIABATIC SURFACE TEMPERATURE AND MODELLING

The PT, a temperature measuring device described in the fire resistance test standards ISO 834-1 and EN 1363-1, was originally developed as a reliable method of controlling the temperature of fire resistance test furnaces [2, 3].

Plate Thermometers and Heat Flux Meters

The PT consists of a 150 mm long by 100 mm wide by 0.7 mm thick nickel alloy sheet strip folded to give a 100 by 100 mm plate, with a type K thermocouple fixed at the centre of the back face, and including a 10 mm thick pad of inorganic insulation material. In its original application in fire resistance furnaces, the PT was considered to measure an effective temperature, having a similar convective heat transfer coefficient and emissivity as the test specimen [4, 3]. Further to its original function, the PT is starting to gain acceptance as a device suitable for measuring heat flux, as an alternative to water-cooled total heat flux meters (HFM).

Traditionally, HFM’s of the Gardon or Schmidt-Boelter (S-B) type have been used to measure total heat flux in fire tests, measuring total heat flux to a water-cooled surface [5]. However, errors can occur with these devices as the result of convective heating of the gauge and convective and radiation heat exchange with the ambient environment [6]. Away from controlled laboratory environments, the PT generally has a number of advantages over HFM’s in that they are inexpensive and robust, as well as being relatively easy to set up.

Fire and Thermal/Structural Model Interface

From a numerical modelling perspective, the AST is a very useful parameter because it is a convenient interface between a fire and thermal/structural computer model that overcomes

the inherent incompatibility between the two types of model. A typical fire “computational fluid dynamics” model, such as Fire Dynamics Simulator (FDS) [7], generates outputs that give a multi-variable description of the gas phase while the boundary heat transfer is simplistically modelled as 1-D heat conduction in an infinitely thick slab. Conversely, a FE thermal/structural model generally requires a single global gas temperature input that surrounds a detailed 2 or 3-D model of a structural element, or must be able to add mixed radiation and convection boundary conditions. AST combines the complexity of the fire model outputs into a single parameter that is suitable as an input variable for a thermal/model [3, 8].

Heat Transfer Theory

In a post-flashover fire compartment (e.g. the environment within a fire resistance furnace), AST is an effective boundary temperature that represents a combination of radiation and convection boundary conditions. In this context it is defined as the surface temperature of an ideal perfectly insulated surface exposed to the same thermal conditions as the real surface under consideration. The total net heat flux, \dot{q}_{tot}'' , at the real surface then becomes [3, 8]:

$$\dot{q}_{tot}'' = \varepsilon_s \sigma (T_{AST}^4 - T_s^4) + h_c (T_{AST} - T_s) \quad (1)$$

where ε_s is the emissivity of the real surface, σ is the Stefan-Boltzmann constant, T_{AST} is the AST, T_s is the surface temperature and h_c is the heat transfer coefficient.

Eqn. (1) resembles the formulation given in Eurocode 1 to calculate the heat transfer to fire-exposed structures, with T_{AST} simply being replaced by the time-dependent standard furnace temperature, T_f [3], i.e. $T_{AST} \approx T_f$. The PT temperature, T_{PT} , can also be used to derive an alternative approximation for the net heat transfer to a fire-exposed surface, which takes the same form as Eqn. (1) but where T_{PT} replaces T_{AST} , i.e. $T_{AST} \approx T_{PT}$.

CALCULATING INCIDENT RADIATION

The PT also has utility as a device for measuring incident radiation. In a post-flashover environment, the incident radiation, \dot{q}_{inc}'' , is defined as [3]:

$$\dot{q}_{inc}'' = \sigma T_{PT}^4 - h_{PT} (T_g - T_{PT}) / \varepsilon_{PT} \quad (2)$$

where h_{PT} is the convective heat transfer coefficient of the PT, T_g is the gas temperature and ε_{PT} is the emissivity of the PT. For this application the latter term in Eqn. (2) is relatively small and can be neglected. The same is not the case however when using the PT in ambient conditions, as would occur in the lower layer of a pre-flashover compartment fire, where greater accuracy is required to account for conduction and the thermal response time of the PT. In this application, the incident radiation measured by a PT is defined as [9]:

$$\dot{q}_{inc}'' = \sigma T_{PT}^4 + \frac{(K_{cond} - h_{PT})(T_{amb} - T_{PT})}{\varepsilon_{PT}} + \frac{\rho_{PT} c_{PT} \dot{\varepsilon}_{PT} (\Delta T_{PT} / \Delta t)}{\varepsilon_{PT}} \quad (3)$$

In Eqn. (3), K_{cond} is a conduction correction factor that allows for the combined heat lost as 2-D conduction away from the central measuring point in the plane of the PT as well as the heat lost through the insulating pad on the back face of the PT. Also, T_{amb} is the ambient gas

temperature, ρ_{PT} , c_{PT} and δ_{PT} are the density, specific heat capacity and plate thickness of the PT, while ΔT_{PT} is the PT temperature difference between consecutive temperature readings over a time step Δt - the combined term $\rho_{PT}c_{PT}\delta_{PT}(\Delta T_{PT}/\Delta t)$ represents the heat stored per unit area and time in the PT.

CALCULATING ADIABATIC SURFACE TEMPERATURE

Considering again the post-flashover environment, an iterative numerical procedure to calculate AST can be defined [10, 11] where the heat balance at a PT, neglecting conduction losses, is approximated in finite difference form as:

$$\rho_{PT}c_{PT}\delta_{PT}(T_{PT}^{i+1} - T_{PT}^i)/(t^{i+1} - t^i) = [\epsilon_{PT}\sigma(T_{AST}^4 - T_{PT}^4) + h_{PT}(T_{AST} - T_{PT})] \quad (4)$$

where t is the time and the superscripts i and $i+1$ represent sequential time increments and T_{AST} is the only unknown term in Eqn. (4). Now, defining the function $F(T_{AST})$ at time step i as:

$$F(T_{AST}) = [\epsilon_{PT}\sigma(T_{AST}^4 - T_{PT}^4) + h_{PT}(T_{AST} - T_{PT})] - \rho_{PT}c_{PT}\delta_{PT}(T_{PT}^{i+1} - T_{PT}^i)/(t^{i+1} - t^i) \quad (5)$$

then T_{AST} can be obtained at each time step for $F=0$. The iteration formula can be derived using the Newton-Raphson method as:

$$T_{AST}^{i+1} = T_{AST}^i - F(T_{AST}^i)/F'(T_{AST}^i) \quad (6)$$

where $F'(T_{AST}^i)$ is the derivative of $F(T_{AST}^i)$.

EXPERIMENTAL RESULTS

The use of PT's in furnace situations is well documented in the literature [2, 3]. This paper describes a series of experiments conducted by members of the FORUM, to provide additional substantiation for the use of PT measurements and the concept of AST for predicting heat transfer to fire-exposed structures. Firstly, a comparison was done between PT's and HFM's in ambient environments, i.e. conditions that deviate from the post-flashover conditions in a fire resistance test furnace, where convection is significant. Secondly, experiments were conducted using PT measurements to determine the AST for structural sections. Thirdly, AST values were used as input to a FE model to calculate surface temperatures and compared to actual temperature readings.

Experimental Comparison of Plate Thermometers and Heat Flux Meters

The initial step for experimental comparisons between PT's and HFM's was to expose PT's to steady-state radiation in a cone calorimeter, at varying levels of incident heat flux. The radiation levels in the cone calorimeter are set by a calibrated S-B HFM. At the point where the measured PT temperatures reached steady-state, the storage

term, $\frac{\rho_{PT} c_{PT} \dot{\epsilon}_{PT} (\Delta T_{PT} / \Delta t)}{\epsilon_{PT}}$, in Eqn. (3) can be ignored and an appropriate value for the conduction correction factor, K_{cond} , can be evaluated.

FREE-BURNING EXPERIMENTS

In a series of quasi steady-state fire experiments conducted by SP [12], a comparison is made between PT's and S-B HFM's. For these experiments, the storage term in Eqn. (3) became relevant, and its use gave a better match in the results between the two measuring devices. In a further series of transient fire experiments conducted by SP [13], the corresponding comparison is made between PT's and S-B HFM's for cellulosic fuel. To a more significant degree, the storage term in Eqn. (3) is relevant. In addition to the free-burning experiments conducted by SP, a complementary range of experiments were also conducted by BRANZ in a furniture calorimeter [14] with a standard gas burner and soft furnishing materials, in this case using PT's and Gardon HFM's.

COMPARTMENT FIRE EXPERIMENTS

Compartment fires represent a more complex heat transfer environment, when compared to free-burning situations. To investigate this particular application, BRANZ also conducted a number of tests [14] in an ISO 9705 Room enclosure, to compare incident radiation values calculated from Eqn. (3), derived from PT temperature measurements, with Gardon HFM results – a representative example of these results is shown Figure 1.

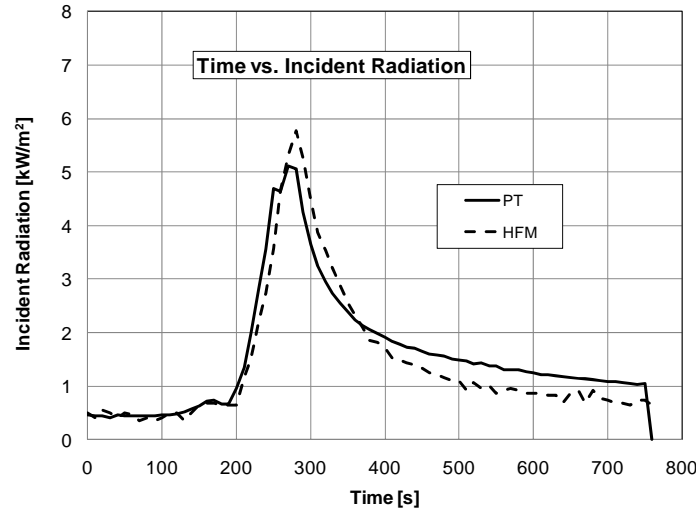


Figure 1. Comparison between PT and HFM.

For the example shown in Figure 1, a mattress was ignited at the far corner of the 3.6 x 2.4 x 2.4 m high compartment and reached a peak heat release rate (HRR) of approximately 800 kW at 300 s. The PT and HFM were located a radial distance of approximately 3.6 m from the centre of the mattress, near the door opening of the enclosure.

In associated experimental research conducted at BRANZ, further PT/Gardon comparisons in an ISO 9705 Room were made. This work is part of a joint BRANZ/University of Canterbury research project [15], the relevant portion of which compares experimental

radiation measurements with a sub model that calculates radiation in compartment fires. Figure 2 illustrates an example of this comparison.

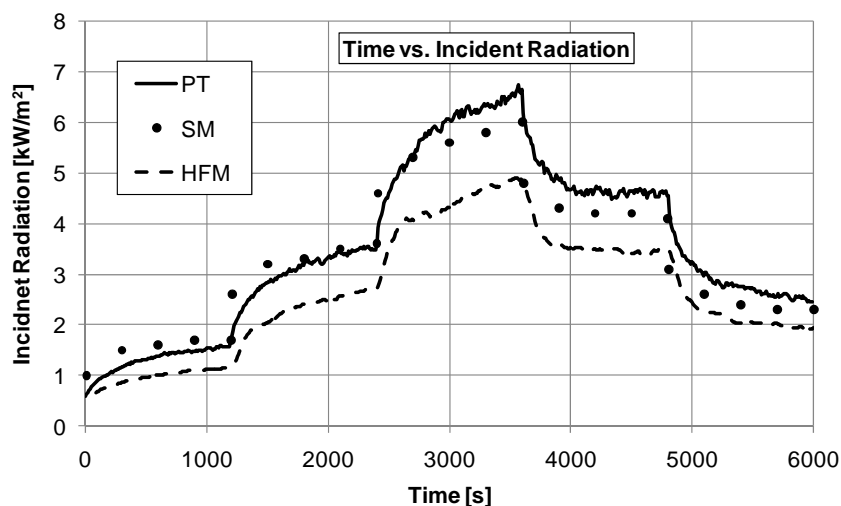


Figure 2. Comparison between PT, Gardon HFM and theoretical Sub Model.

For the example shown in Figure 2, a standard gas burner was located in the far corner of the enclosure, and radiation was measured at a location on the compartment transverse centreline and 0.6 m from the longitudinal wall opposite the burner, at a height 1.0 m above the enclosure floor level. The burner was operated at a HRR of 100, 200, 300, 200 and 100 kW for consecutive 1200 s time increments. For the results shown in Figures 1 and 2, the temperature of the water cooling the Gardon HFM's was approximated as being T_{amb} .

Heat Transfer Experiments and Finite Element Modelling

Having demonstrated the ability of PT's to act as radiation measuring devices, a series of heat transfer experiments were conducted at SP [10, 11]. The experiments involved both square tube and I-beam steel sections suspended 0.2 m below the ceiling of a standard ISO 9705 enclosure and a gas burner operating at a constant HRR of 450 kW. PT's were located on all four sides of the beams and these locations corresponded to thermocouple measurements being taken on the surface of the beams.

Making use of the PT measurements, AST's were calculated in accordance with the procedure associated with Eqn. (6), and then the results were used as input to the 2-D FE temperature calculation code TASEF [16]. Figure 3 shows an example of the temperatures that TASEF calculated in this manner, compared to the measured temperatures in the steel of the square tube section at three locations.

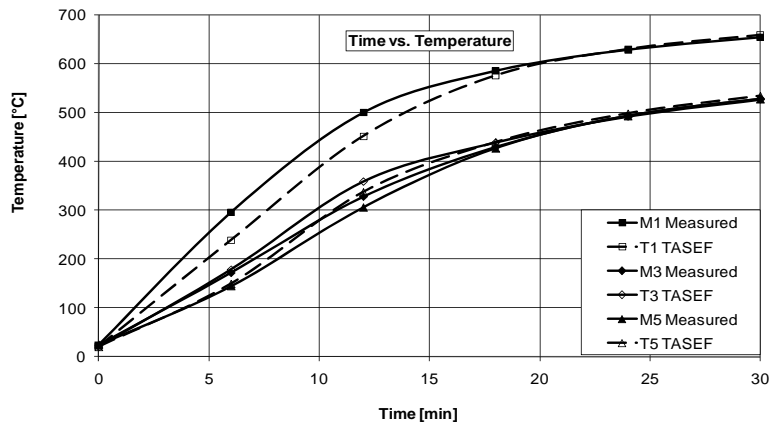


Figure 3. Comparison between temperature calculated with FE code TASEF and corresponding measured temperatures for a square tube.

As part of the National Institute of Standards and Technology (NIST) investigation of the WTC disaster, the AST interface for fire/structural models was also successfully trialled. A series of compartment fires experiments were carried out with insulated and un-insulated steel sections and hydrocarbon pan fires. The experiments were also modelled using FDS, producing AST values which were used as input boundary condition data for the FE thermal/structural model ANSYS [17]. Where the mesh of the FDS modelling did not match that required by ANSYS to define the structural sections, a simple interpolation procedure was used [8]. A full description of this work can be found in Hamins et al. [18].

DISCUSSION AND CONCLUSIONS

When using PT's and HFM's in mixed radiative-convective environments, consideration needs to be given to the limitations in the assumptions underlying the heat transfer theory presented. Recent research [19] indicates that Gardon HFM measurements were 8-18% less than the corresponding measurements for S-B HFM's when forced convection was present. A compartment fire is a dynamic, turbulent environment and under transient conditions the inherent response delay of a PT must be considered. Determining the K_{cond} value for PT's under the steady-state conditions of a Cone Calorimeter (with S-B HFM's), and h_{PT} being based on natural convection only, must also be borne in mind. In addition, at low incident radiation levels, convection becomes more significant and influences the PT and HFM measurements.

An apparent gap exists between the research and theory of designing structures exposed to fire, and industry practice. One key area that has restricted the transfer of theory to practice has been the efficiency and accuracy of the interface between fire and thermal/structural models. In this paper the theory and the successful practical application of the AST concept to modelling structures in fire has been demonstrated, based on a range of experiments and analysis in different research laboratories around the world. The AST concept therefore provides a valuable tool to help advance the practice of fire/structural engineering internationally. It is important that designing structures to withstand fire moves from a

reliance on the standard fire resistance testing approach to a more rational and scientific methodology that accounts for the likely thermal response of structures to fires.

REFERENCES

1. Duthinh, D., K. McGrattan, and A. Khaskia. 2008. "Recent advances in fire-structure analysis," *Fire Safety Journal*, 43(2):161–167
2. Wickström, U. 1994. "The plate thermometer—a simple instrument for reaching harmonized fire resistance tests," *Fire Technology*, 30(2):195–208
3. Wickström, U. 2008. "Adiabatic surface temperature and the plate thermometer for calculating heat transfer and controlling fire resistance furnaces," presented at the 9th Int. Symposium on Fire Safety Science, 21–26 Sept. 2008.
4. Wickström, U. 2004. "Short communication: Heat transfer by radiation and convection in fire testing," *Fire and Materials*, 28(5):411–415
5. Olsson, S. 1991. "Calibration of radiant heat flux meters – The development of a water cooled aperture for use in black body cavities—Nordtest project 873-90," SP Report 1991:58, SP Technical Research Institute of Sweden, Borås, Sweden.
6. Robertson, A.F., and T.J. Ohlemiller. 1995. "Low heat-flux measurements: Some precautions," *Fire Safety Journal*, 25(2):109–124
7. McGrattan, K.B., *et al.* 2005. "Fire Dynamics Simulator (version 5), technical reference guide, NIST SP 1018-5," NIST, Gaithersburg, MD., US.
8. Wickström, U., D. Duthinh, and K. McGrattan. 2007. "Adiabatic surface temperature for calculating heat transfer to fire exposed structures," presented at the 11th Int. Interflam Conference, 3–5 Sept., 2007.
9. Ingason, H., and U. Wickström, U. 2007. "Measuring incident radiant heat flux using the plate thermometer," *Fire Safety Journal*, 42(2):161–166.
10. Wickström, U. 2009. "Heat transfer and temperature calculations based on plate thermometer measurements," presented at the 11th Int. Fire and Materials Conference, 26-28 Jan., 2009.
11. Wickström, U., R. Jansson, and H. Tuovinen. 2009. "Validation fire tests on using the adiabatic surface temperature for predicting heat transfer," SP Report 2009:19, SP Technical Research Institute of Sweden, Borås, Sweden.
12. Arvidson, M., and H. Ingason. 2005. "Measurement of the efficiency of a water spray system against diesel oil pool and spray fires," SP Report 2005:33, SP Technical Research Institute of Sweden, Borås, Sweden.
13. Lönnermark, A., and H. Ingason. 2005. "Fire spread in large industrial premises and warehouses," SP Report 2005:21, SP Technical Research Institute of Sweden, Borås, Sweden.
14. Robbins, A.P., and P.C.R. Collier. 2009. "Heat flux measurements: Experiments and modelling," Study Report SR 206, BRANZ Ltd, Porirua, New Zealand.
15. Baker, G.B., and C.A. Wade. 2009. "Development of probabilistic design and analysis tools for performance-based fire safety engineering," presented at the 2009 Int. Symposium on Fire Science and Fire-Protection Engineering, 17-18 Oct., 2009.
16. Sterner, E., and U. Wickström. 1990. "TASEF—Temperature analysis of structures exposed to exposed to fire," SP Report 1990:05, SP Technical Research Institute of Sweden, Borås, Sweden.
17. ANSYS Inc., Canonsburg, Pennsylvania, US. (<http://www.ansys.com>).
18. Hamins, A., *et al.* 2005. "Experiments and modeling of structural steel elements exposed to fire," *Federal Building and Fire Safety Investigation of the World Trade Centre Disaster*, NIST NCSTAR 1-5B, NIST, Gaithersburg, MD., US.
19. Lam, C.S., and E.J. Weckman. 2009. "Steady-state heat flux measurements in radiative and mixed radiative-convective environments," *Fire and Materials*, 33(7):303–321.

Variability of Fire and Concrete Temperatures and the Associated Uncertainty in Structural Behavior

E. JENSEN, J. VAN HORN and C. D. EAMON

ABSTRACT

This paper presents new statistical data on environmental and concrete temperatures as obtained from three different types of fires. The fires are denoted as: high intensity-short duration, progressive burning and standard fire. Three concrete beams were subjected to the high intensity-short duration fire; two beams were subjected to the progressive burning fire, and two concrete slabs were subjected to a standard fire.

The coefficient of variation (COV) was evaluated at 30 minute increments throughout the fires. The COV of the environmental fire temperatures ranged from 5.3 and 6.8%. The COV of the concrete surface and internal temperature measurements were typically higher. The COV for a fire type of concrete internal temperatures ranged from 5.6 to 9.9% and the COV for surface temperatures ranged from 7.4 to 23.5%.

Data from this study can be used in the assessment of the reliability of structures subjected to fire. A simple example demonstrates the potential outcomes of 'prescriptive, deterministic and probabilistic analysis of a simply supported, transverse loaded, reinforced concrete beam subjected to a standard fire. The fire temperature, as obtained from this study, is considered as one of six random variables.

1. INTRODUCTION

In order to advance the technical area of performance based design for structural fire safety, information is needed that will allow the stakeholders to assess the probability of failure in the event of a fire. One goal of performance-based design is to reduce variability and arbitrariness in structural performance for structures designed to the same set of rules. It is well-known that significant performance variations result in traditional prescriptive fire load design methods [1, 2, 3, and 4].

Dr. Elin Jensen, Jacob Van Horn, and Dr. Christopher D. Eamon, Lawrence Tech University, 21000 W Ten Mile Rd, Southfield, MI 48075, U.S.A.

Fire resistance ratings of structural assemblies and members are commonly based on a small number of test specimens subjected to the standard fire endurance test [5]. In order to perform adequate risk analysis on a structure, statistical data describing the random variables that affect the structural performance throughout the fire are needed. The lack of such statistical data, for the event of fire, is a major obstacle in performing meaningful risk analysis and effectively implementing performance based design for structural fire safety. Many sources of uncertainty are inherent in structural design. However, design for fire has far more uncertainties than design for normal temperature conditions [6, 7, and 8]. These uncertainties are associated with structural geometries, mechanical and thermal properties of the construction materials, dead and live loads, as well as the thermal impact from fire. The objectives of this paper are to:

- Quantify the uncertainty in the ‘near specimen’ fire temperature as well as surface and internal concrete temperatures for different types of fire.
- Assess the structural performance of a simply supported reinforced concrete beam in terms of prescriptive and deterministic design for fire safety, and estimate the associated probability of failure.

2. EXPERIMENTAL METHOD AND DESIGN FIRES

The fire profiles are shown in Figure 1. Fire A represents a short duration-high intensity room fire with high fuel load, high ventilation and highly insulated linings, and Fire B represents temperatures during progressive burning in a deep room where oxygen depletion controls the delayed second temperature peak. These fires are not designed to follow a design fire. Fire A and Fire B in terms of accumulated temperature-time (C-h) are approximately equal to the standard fire at 2 hour.

The experiments were conducted at the Center for Innovative Material Research at Lawrence Tech. The fire chamber is capable of testing at controlled temperatures within the range of 100° to 1300°C. The furnace is fueled by natural gas. The internal workload dimensions of the fire chamber are 6.0 m x 1.5 m x 1.5 m. Data is recorded from up to 100 thermocouples (R or K-type) and 48 other multipurpose sensors such as load cells, strain gages and displacement gages.

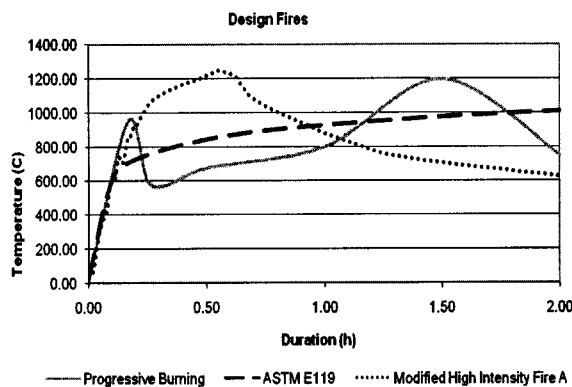


Figure 1. Fire profiles.

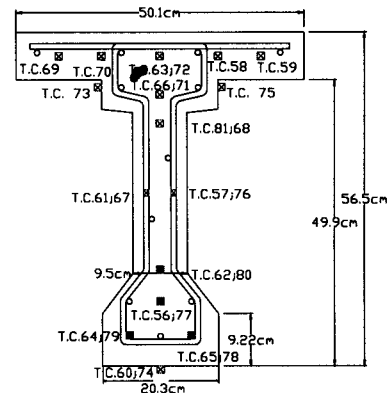


Figure 2. Thermocouple Placement.

2.1 Concrete Specimens and Instrumentation

Two specimen types were used in this study. The first is a 0.125 m thick concrete slab with dimensions 1.5 m by 1.5 m. A bottom reinforcement mesh was placed with a cover of 30 mm. The second is a 3.6 m long concrete T-beam with cross-section dimensions as shown in Figure 2. The specimens were placed inside the chamber exposing all free surfaces to hot gases. Thermocouples were installed in each concrete member at the surface, core and other locations throughout the cross-section (see Figure 2). K-type thermocouples were installed in surface holes.

The T-beams had at the time of testing reached moisture equilibrium with the air in the range of 85% RH at 25°C. The T-beams were constructed from a concrete containing carbonate aggregate which had a 48 MPa 28-day compressive strength. The concrete slab had at the time of testing reached moisture equilibrium with the air in the range of 72% RH at 25°C. The slabs were constructed from concrete containing carbonate aggregates and it had a 32 MPa compressive strength. The experiments do not represent fire endurance tests.

The temperature of the environment around the specimen shall be an average of all the environmental thermocouples placed symmetrically around the specimen at 150 to 300 mm away from the surface. Different environmental thermocouple designs were used during testing. The first type used was a 12.5 mm non-galvanized steel pipe cut to a desired length with K-type thermocouples fed through the length of the pipe. At the end of the pipe the bulb of the thermocouple was either placed inside densely packed ceramic fiber or inside a hole drilled into a small piece of steel to minimize fluctuation in temperature readings throughout the duration of each test. The second type used was a plate thermocouple [9] which can assess the total thermal impact transferred by radiation and convection to the surface of the specimen using a K-type thermocouple in direct contact with the Inconel 600™ steel and protected on its reverse side by 25.4 mm of thick ceramic fiber insulation.

3. COEFFICIENT OF VARIATION OF TEMPERATURES

New statistical data on environmental and concrete temperatures are presented for the three different types of fires presented above. Three concrete T-beams were subjected to the high intensity-short duration fire; two T-beams were subjected to the progressive burning fire, and two concrete slabs were subjected to the ASTM E119 standard fire curve.

The temperature data was sorted into groups by location and exposure such that each group represented data that theoretically should be the same. Table I denotes every data series for every test at each location separated only by fire type. This is the 'Total Adjusted' COV for each fire. The statistical data representing the group 'Total Adjusted' are to be used in further analysis. The COV in percent is defined by the standard deviation (σ) divided by the mean (μ) of the data series as:

$$\text{var}(\%) = \frac{\sigma}{\mu} * 100 \quad (1)$$

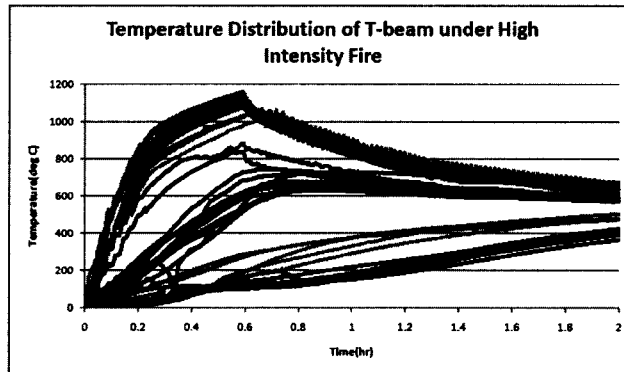


Figure 3. High Intensity Fire [Total (Adjusted)].

The temperature versus time relationships for the concrete T-beams subjected to the high intensity fire is shown in Figure 3. The upper series represents the thermocouples (TCs) measuring the 'near surface' temperature; the series below represents the TCs measuring the concrete surface temperature; the following two series are representing the core temperatures at the top and bottom of the T-beam, respectively.

In general, there is close agreement between the data obtained at each thermocouple location. The COV, as shown in Table I, is between 5.2 and 23.5 % for all of the T-beam and slab tests. The first two hours of both the high intensity and progressive burning fire profiles produce the highest COV in part due to changing temperature demands. When there is a change in demand, the burners will increase/decrease in intensity while the exhaust maintains a constant negative pressure in the chamber.

As expected, the surface thermocouples had the highest variability. This is due to the difficulty of post-construction installation of the thermocouples, as well as the shadowing effect of certain thermocouples from the flames. The shadowing effect occurs as the gas burners are placed just under the roof line above the T-beam section, and the surface thermocouples lie below the t-beam flange and below the bulb as seen in Figure 2. Also adding to the shadow effect is the fact that the chamber roof and walls are lined with ceramic fiber blankets and the floor is lined with fire bricks. The net effect has been quantified.

The shadow effect was significant during the tests with the concrete slabs which yielded higher COV between thermocouples above and below the specimen for the individual test. However, when the data was averaged, for the two tests, the total COV was 5 %. The two slab specimens were subjected to the fire curve defined by ASTM E119. Fewer thermocouples were measuring at the core and the surface in these tests because several thermocouples became faulty.

4. EXAMPLE - PRESCRIPTIVE, DETERMINISTIC AND PROBABILISTIC DESIGN OF RC BEAM

Structural reliability concepts are well established and many current design codes are based on probabilistic-based models of loads and resistance through the use of

Table I. Coefficient of Variation (COV) (%)
 The number inside the () gives the number of representative data in the series.

Time(hr)	Variance (%)									
	High Intensity Fire Total (adjusted)			Progressive Burn Total (adjusted)			ASTM E119 Total (adjusted)			
	Top Core(7)	Bottom Core(7)	Surface(12)	Environment (10)-steel; (7)-R-type; (4)-plate	Core(11)	Surface(10)	Environment (7)-steel; (3)-R-type; (4)-plate	Core(8)	Surface(10)	Environment (3)-steel; (9)-R-type
0	28.90	30.11	26.01	18.44	5.97	4.60	2.40	5.19	11.94	9.62
0.5	8.71	31.47	24.33	5.31	13.16	29.27	4.07	4.91	51.55	8.29
1	13.04	10.02	5.33	2.61	11.92	20.91	2.24	8.87	30.87	5.27
1.5	6.92	3.57	3.86	3.56	10.98	14.87	3.88	12.98	20.11	3.36
2	3.90	2.86	3.05	3.46	9.64	6.65	11.59	14.05	15.20	2.63
2.5	2.04	1.42	2.21	1.08	4.41	4.87	3.04	13.35	11.23	2.18
3	1.83	0.23	0.86	2.44	2.83	6.63	3.68			
3.5	1.78	0.16	1.22	3.22	2.25	7.41	4.42			
4	1.52	0.51	2.57	5.68	1.99	7.95	4.83			
4.5	1.51	0.77	5.62	10.31	1.87		7.11			
5	1.37	1.32	6.54	10.03	2.27		8.08			
5.5	1.10	1.73	7.19	10.93	2.33		8.37			
6	0.93	2.38	7.54	11.15	2.59		8.54			
Average	5.66	6.66	7.41	6.79	5.55	11.46	5.56	9.89	23.48	5.23

load factors and strength reduction factors, respectively [10]. This section provides an example of the application of structural reliability theory to design for fire safety of a structural member in a school building. The structure will be subjected to the design fire defined by ASTM E119.

Rectangular reinforced concrete beams are supporting a 0.125 m thick floor slab and they are placed 2 m center-on-center. The beams are simply supported and unrestrained. The beams are subjected to a 3-sided fire from below. The moment capacity at normal temperatures is determined according to ACI 318-05 [11]. The ultimate moment is according to ASCE 7-05 [12] using the controlling load combination of 1.2DL + 1.6LL. The live load for the classroom floor is 1.92 kN/m². The beams are 300 mm wide, 500 mm high and span 8.2 m. The beam is reinforced with three #29 reinforcing bars placed with 44 mm of concrete cover.

4.1 Prescriptive Design

The prescriptive design approach according to ASCE/SEI/SFPE 29-05 [13] calculates the fire resistance rating based on the thickness of the cover of concrete to the reinforcing bars. The controlling concrete cover value used for this example is half of the actual distance of the corner cover to reinforcing steel of the smaller dimension from the side or bottom. For a non-prestressed reinforced concrete beam that is unrestrained with a beam width of greater than 254 mm the fire resistance rating given is 3 hr with a corner cover value of 22 mm.

4.2 Deterministic Analysis

At normal temperatures, the beam is 'over designed' and the failure mode is tension-controlled. The structural capacity at elevated temperatures is determined from the reduced material strengths at high temperatures. Strength reduction factors are not applied. The structural superimposed load per ASTM E119 should simulate the maximum natural loads, which in this example was taken as a load factor of 1.0.

The moment capacity of the RC beam will be determined using the 500° C isotherm method. The location of the 500 °C isotherm and the temperatures at the rebar locations (x, y) were determined using Wickström's empirical method [6, 8]. The temperatures at the reinforcing steel at any time during the fire can be determined by [12]:

$$\Delta\theta_{xy} = (\eta_w(t_x - t_y - 2t_x t_y) - t_x t_y)\Delta\theta_f \quad (2)$$

Where $\Delta\theta_f$ is the ASTM E119 fire curve in degrees Celsius, and η_w is dependent on time and is given as [12]:

$$\eta_w = 1 - 0.0616t^{-0.88} \quad (3)$$

$\eta_{x,y}$ depends on time and the ratio of thermal diffusivity of the specimen, a_c , to a reference value of $a = 0.417 \cdot 10^6 \text{ m}^2/\text{s}$. The ratio of thermal diffusivity used in this example is 1.2, which means that are concrete specimen heats up slightly faster than Wickström's concrete. $\eta_{x,y}$ is given as [12]:

$$\eta_{x,y} = 0.18 \ln\left(\frac{a}{a_c} * \frac{t}{x^2}\right) - 0.81 \quad (4)$$

The strength of the reinforcing steel is adjusted using the factor $k_{y,T}$ which is the ratio of yield strength at elevated temperatures to the yield strength at normal conditions [6]:

$$k_{y,T} = (720 - T)/470 \quad (5)$$

The location of the 500° C isotherm is given by [12]:

$$x = \left[\frac{\frac{a}{0.417 * 10^{-6}} * t}{\exp\left(4.5 + \frac{\Delta\theta_x}{0.18\eta_w\Delta\theta_f}\right)} \right]^{0.5} \quad (6)$$

The residual strength of concrete at or above 500° C is assumed to be zero, thereby reducing the effective width of the beam to the 500° C isotherm locations. The residual strength in the concrete at temperatures below 500° C is assumed to be equal to the design strength at normal temperatures. Per this deterministic design method, the beam is able to resist the ultimate moment during fire for 127 minutes. This yields a confirmed 2-hour fire resistance rating.

4.3 Probabilistic Analysis

Based on the beam described above, a reliability analysis was performed using the random variables (RVs) presented in Table II. In the table, T is the fire

Table II. Random variables.

RV	bias factor	COV	Distribution
T	1	0.06	Normal
f_c	1	0.18	Lognormal
DL	1.05	0.1	Normal
LL	1	0.25	Extreme Type I
A_s	1	0.02	Normal
f_y	1.11	0.06	Normal
P	1	0.17	Normal

Table III. Failure Probability.

Case	Reliability Index	Approx. P_f
Cold	3.76	8.49E-05
1 hr	3.21	6.64E-04
1.5 hrs	2.38	8.66E-03
2 hrs	1.01	0.1563
2.5 hrs	-1.29	0.9015

temperature; f_c is the maximum concrete compressive strength at 28 days, DL is the total dead load; LL is the 50 year maximum total occupancy live load (sustained and extraordinary), A_s is the total area of tension steel, f_y is the steel yield stress, and P is the 'professional' or analysis factor. P was given a coefficient of variation (COV) higher than usual to account for sources of uncertainty not directly considered in the analysis (such as geometric variation in the concrete section and depth of rebar). The Bias factor is the ratio of the mean value to the nominal (i.e. theoretically calculated) value. RV statistics for the fire was obtained from this study and the remaining RV statistics were taken from the literature [14, 15, and 16]. Note that the statistics for the compressive strength are derived from the database used in [15]; considering all strength data obtained at temperatures below 500° C.

Based on these RV values, a Monte Carlo simulation was run using 1×10^6 simulations. Failure probability (P_f) results were converted to a reliability index and are reported in Table III. Notice between 2 and 2.5 hours, the reliability index becomes negative. This indicates that the failure probability is greater than 50%.

The probability of failure of the reinforced concrete beam designed according to the deterministic method is 0.1563, which is equivalent to 16 out of 100 beams that will fail before 2 hours. Similarly, the probability of failure of the concrete beam designed according to the prescriptive method is higher than 0.90.

Studies are underway assessing the uncertainties resulting from the predicted internal concrete temperatures based on simple empirical as well as transient heat analysis methods for different types of fires.

5. SUMMARY

Development of codified resistance models for structural design for fire safety requires that additional performance data be collected. This paper presents data on the observed COV of 'near surface' fire temperatures as well as concrete temperatures throughout the considered fires. The key observations made in this study are:

- The average COV for the 'near surface' fire temperatures is about 6%; for the internal temperatures the COV is about 6–10%; and for surface temperatures the COV values approach 25%.

- The application of structural reliability to assess the performance of a concrete beam subjected to fire demonstrated that the prescriptive as well as deterministic designs can be quantified in terms of probability of failure.

REFERENCES:

1. Bennetts, I.D. and Thomas, I.R. "Design of Steel Structures Under Fire Conditions." *Progress in Structural Engineering and Materials*, Vol. 4, No. 1, 2002, p 6–17.
2. Gewain, R.G. and Troup, E.W.J. "Restrained Fire Resistance Ratings in Structural Steel Buildings." *ASIC Engineering Journal*, Vol. 38, No. 2, 2001, p 78–89.
3. Kruppa, J. "Recent Developments in Fire Design." *Progress in Structural Engineering and Materials*, Vol. 2, No. 1, 2000, p 6–15.
4. Meacham, B.J. "An Introduction to Performance-Based Fire Safety Analysis and Design with Applications to Fire Safety." *Building to Last, Proc. Struct. Congress XV, American Society of Civil Engineers*, New Your, 1997, p. 529–533.
5. ASTM E119-05a. *Standard Test Methods for Fire Tests of Building Construction and Materials*.
6. Buchanan, A.H. 2006. *Structural Design for Fire Safety*. John Wiley & Sons, LTD. ISBN 0-471-89060-X.
7. Lange, D., Usmani, A., Torero, J. 2008. "The Reliability of Structures in Fire," *Proceedings of the Fifth International Conference on Structures in Fire 2008 ASCE*
8. Purkiss, J.A. 2007. *Fire Safety Engineering*, Elsevier, ISBN-13: 978-0-7506-6443-1
9. Wickstrom, Ulf. *Adiabatic Surface Temperature and the Plate Thermometer for calculating Heat Transfer and Controlling Fire Resistance Furnaces*. Conference proceedings from 9th IAFSS Symposium, Karlsruhe, Germany, 2008
10. Nowak, A.S. 2000. *Collins K.S. Reliability of Structures*. McGraw Hill. ISBN 0-07-048163-6
11. *ACI 318-05 Building Code Requirements for Structural Concrete and Commentary*.
12. *ASCE 7-05 Minimum Design Loads for Buildings and Other Structures*, American Society of Civil Engineers. ISBN: 0784408092
13. *ASCE/SEI/SFPE 29-05 Standard Calculation Methods for Structural Fire Protection*, American
14. Ellingwood, B. Galambos, T.V., MacGregor, J.C. and Cornell C.A. *Development of A Probability-Based Load Criteria for American National Standard A58*, NBS Special Publication No. 577, NBS, US. Dept. of Commerce, Washington, DC, 1980.
15. Knaack, A., Kurama, Y., Kirkner, D. 2009. "Stress-Strain Relationships for Concrete at Elevated Temperatures," *Structures 2009: Don't Mess with Structural Engineers*©2009 ASCE, p 660–669.
16. Melchers, R.E. "Structural Reliability Analysis and Prediction", 2nd Ed. Wiley, 1999.

ACKNOWLEDGEMENT

This work was made possible with funding from the NSF Award #0747775, support from the Center for Innovative Material Research (CIMR) at Lawrence Tech, and undamaged beam segments from US-DOT grant DTOS-59-06-G-00030 awarded to University Distinguished Professor Nabil Grace, Lawrence Tech. The authors wish to thank the undergraduate student research team: Cody Telgheder, Andrew Hermiz, Daniel Ziemba, and Dustin Franklin as well as graduate student Mishu Joshi.

Feedback and Knowledge Gaps from a Variety of Structural Fire Engineering Projects

F. M. BLOCK, N. A. BUTTERWORTH and M. G. GREEN

ABSTRACT

During the design process of structures in fire the engineer frequently reaches the boundaries of the available information in design codes and has to resort to published research papers or get in contact with the research community directly.

This gives the opportunity for state of the art research to be used in real building designs and requires a close collaboration between the engineer and the research community. Due to this close link researches should have this direct application in mind during the research and visa versa the engineer should provide feedback to the researchers and should highlight any gaps in the knowledge on structures in fire.

The intension of this paper is to share experiences from a variety of recent projects, to highlight knowledge gaps found during these projects and to encourage similar papers from other practising engineers. The paper discusses the following topics:

- Heat fluxes and temperatures at floor level of fire compartments,
- Long-span space-frame roof structures,
- Steel cable-net Roofs and
- External steelwork calculations of slender columns.

With this feedback to the research community it is hoped that the applicability of future research will be further enhanced and that the identified gaps will be closed.

Florian M. Block, PhD., Senior Structural Fire Engineer, Buro Happold Ltd, 2 Brewery Place, Brewery Wharf, Leeds LS10 1NE, United Kingdom

Neal A. Butterworth, Technical Director, Buro Happold Ltd, 2 Brewery Place, Brewery Wharf, Leeds LS10 1NE, United Kingdom

Mick G. Green, Discipline Director, Buro Happold Ltd, 2 Brewery Place, Brewery Wharf, Leeds LS10 1NE, United Kingdom

INTRODUCTION

In the United Kingdom and other parts of the world more and more structures are designed to resist fires rather than to rely on the prescriptive guidance to fire resistance. During this design process the engineer frequently reaches the boundaries of the available information in the design codes and has to resort to published research papers or get in contact with the research community directly.

This gives the opportunity for state of the art research to be used in real buildings but also requires a close collaboration between the engineers and the research community. Due to this close link, researches should have this direct application in mind during the research and visa versa the engineers should provide feedback to the researchers and should highlight any gaps in the knowledge on structures in fire.

The intension of this paper is to share experiences from a variety of recent projects, to highlight knowledge gaps found during these projects and to encourage similar papers from other practising engineers. With this feedback to the research community it is hoped that the applicability of future research will be further enhanced and that the identified gaps will be closed.

HEAT FLUXES AND TEMPERATURES AT FLOOR LEVEL OF FIRE COMPARTMENTS

An office building in London uses a relatively new form of construction of precast concrete vaults and upstand cellular beams as it can be seen in Figure 1. The advantage of this form of construction is that the exposed concrete soffit can be used as thermal mass in a low energy solution. The building services are distributed in the void underneath a raised access floor.

This form of construction is more likely to be susceptible to fire from above than more traditional forms of construction where the steelwork is protected from fires above by the floor slab itself. Therefore, despite the recommendation in the prescriptive guidance for fire safety in the UK that fire resistance for floors / beams only having to be assessed from a fire from below, it is considered prudent to conduct an assessment of the fire resistance from a fire above the beams.

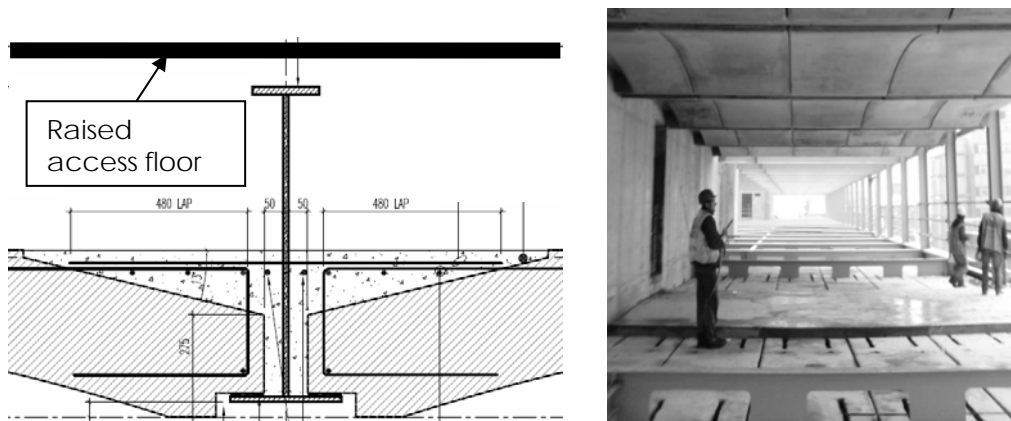


Figure 1. Typical floor construction using upstand beams and precast vaults.

However, to do this in a realistic manner the heat flux and the gas temperatures at the base of a fire compartment are needed to calculate the survival time of the raised access floor and then the temperatures of the upstand beams. A review of the commonly available experimental data of a number of fire tests has shown that the lowest thermocouples could be found in the Dalmarnok fire test [1] at a height of 500mm above the floor. The temperature readings showed a slight temperature reduction and it is expected that lower down a further reduction can be expected.

It is therefore recommended that more research on large compartment fires is conducted including measurements of temperatures and heat flux at the of the fire compartment to enable the realistic design new forms of construction.

LONG-SPAN SPACE-FRAME ROOF STRUCTURES

Another current project is a multi-purpose exhibition hall complex in Egypt for over 6000 people with clear spans between 120m and 200m as is can be seen in Figure 2. The roof structure follows a free-form geometry, which is only possible with a space-frame. The depth of the space-frame is 5m and the grid is set at 6m as can be seen in the inset of Figure 2. Due to the complex geometry an efficient design of the roof structure is only possible via a specifically written numerical optimisation process, which allows a relatively uniform and therefore economic utilisation of the very large number of individual roof members under an envelop of gravity, wind and earthquake loads.

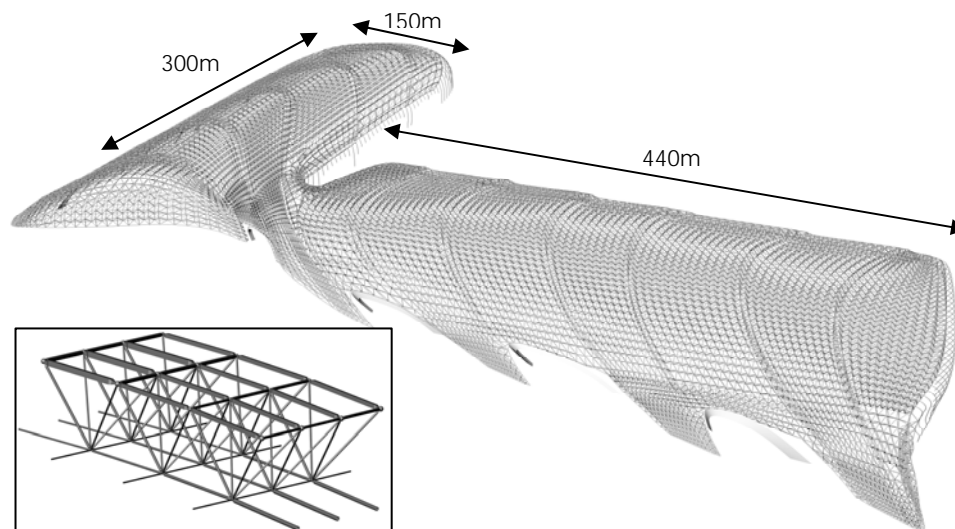


Figure 2. Free-form roof structure of the exhibition halls and detailed view of the space-frame (inset).

The fire resistance requirement of the roof structure is one hour in accordance with NFPA 5000 [2]. However, NFPA 5000 states that when every part of the roof is more than 6.1m above any floor directly below no fire resistance is required to the roof structure, which would be the case for the exhibition halls. However, this rule has been written with normal buildings in mind and it is therefore good practise to investigate the real fire behaviour of such a long-span and optimised space-frame structure further before the fire protection is omitted from the roof.

Space-frame structures are known to be sensitive to localised heating due to their large in-plane stiffness. Such localised heating can occur for relatively small in combination with the proposed smoke control systems, which splits the large halls into individual smoke reservoirs of about 60 x 60m to contain and extract the smoke locally above the fire. To ensure that the smoke layer remains at high level it is required to keep the smoke layer hot and average smoke layer temperatures of 200°C have been calculated in the smoke reservoirs.

To investigate the response of the space-frame to this localised heating redundancy analyses have been conducted in which the thermal loading in the smoke reservoir, as shown in Figure 3a, in combination with the Fire Limit State loading is applied and then iteratively the members which fail are removed until either a stable damaged structure is found or a progressive collapse occurred.

It was found that large parts of the highly optimised space-frame would fail as a result of temperature rise in the smoke reservoir well below 200°K. This is due to the very stiff support conditions, required for the seismic design, and the buckling of slender tension members, which are receiving compression forces due to restrained thermal expansion. The lighter coloured members in Figure 3b indicate the failed members for a T of 50°C. As temperatures of less than 200°C, the normal activation temperature of intumescent paint, can cause significant damage to the structure the only way of preventing an early collapse is to consider the localised heating cases during the structural optimisation.

This example shows that the understanding of large free-form space-frames in fire is still at early stages and research into the fires found in this type of buildings and the detailed response of the space frame to localised fires is needed.

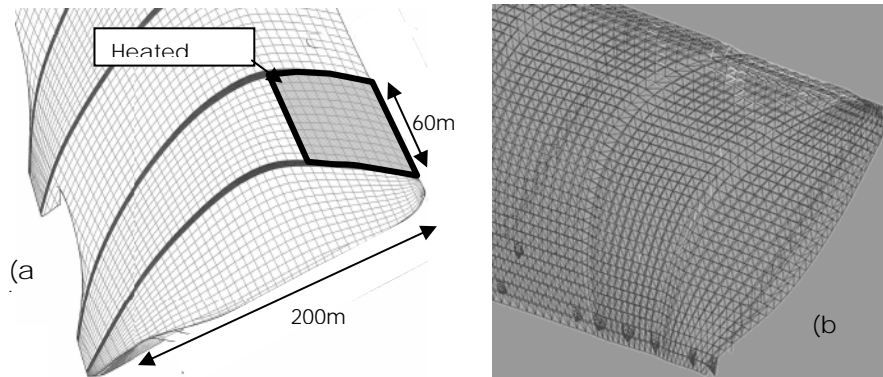


Figure 3. (a) Worst case smoke reservoir for heating and (b) failed roof members a heating of 50°K.

STEEL CABLE-NET ROOFS

Some sports stadia use a cable-net roof structure as an efficient form of covering the seating tiers. These structures are based on the principle of a bicycle wheel in which a compression ring around the out perimeter stabilises a tension ring suspended and pre-stressed by radial cables along the inner perimeter of the roof. The area between the two rings is filled with a fabric to provide the weather protection for the spectators. An example of such a roof structure taken from a current Buro Happold project is shown in Figure 4 below.

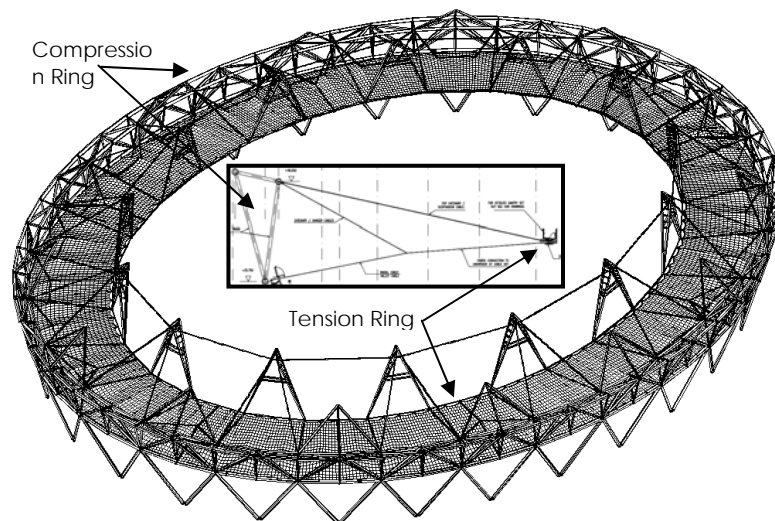


Figure 4. Typical cable net roof structure for a large athletics stadium.

One disadvantage of these roofs is that their entire stability relies on the tension ring. If the tension ring fails the roof will collapse. In order to minimise the risk of this occurring the tension ring in the current project consists of 10 individual 60mm thick spiral strand steel cables, which are only utilised to about 60% under accidental limit state load conditions. This means that 40% of the tension ring cables could fail in an extreme situation without causing a roof collapse.

However, a small fire in close proximity of the tension ring could heat up all 10 cables at the same time to temperatures high enough to cause a collapse of the cable-net. Such a fire could be caused by lighting equipment or loudspeakers frequently suspended from tension rings.

Furthermore, high strength steel cables have a yield stress of 1550 N/mm^2 or more, which is achieved by cold drawing of the individual wires of the cables. This means that high yield strength of cable will be reduced at lower temperatures than the one of mild steel commonly used in steel structures. Additionally, when a cable is heated, the hotter, outer wires expand at a faster rate than the cooler inner wires, which causes an uncoiling of the cable that can lead to an overstressing of the internal cooler wire and therefore to a further reduction in failure temperature.

Another important effect, which could be caused by a fire close to the tension ring at temperatures below the failure temperature of the cables, is the change in geometry and pre-stress due to the thermal elongation of the cables. This could lead to significant deformations of the cable-net and second order effects.

The research into the fire behaviour of structural steel cable is still very limited and for large spiral strand cable no publication could be found. The most appropriate temperature reduction factors for the steel cables could be found in EN 1992-1-2 Table 3.3 [3] for cold worked pre-stressing strand used in concrete constructions. The material and the manufacturing process for these pre-stressing strands are very similar to the ones used for structural spiral strand cables in the tension ring.

However, due to the uncertainties of the real behaviour of cables with much large diameters than what is used in pre-stressed concrete, it was decided to rather reduce the amount of combustible material directly underneath the tension ring to a

practical minimum and in the case of the loudspeakers treat the plywood of the casings with fire retardant. This reduces the risk of a fire occurring in the close proximity of the tension to a minimum.

Even so that the risk of a major collapse of a cable net roof could be eliminated there is still a significant gap in the knowledge about the fire behaviour of large structural steel cables and their connectors, which limits the application of this very efficient form of construction.

EXTERNAL STEELWORK CALCULATIONS OF SLENDER COLUMNS

EN1991-1-2 [4] and EN1993-1-2 [5] provide a method to design external steelwork for the fire case. However, the method averages the heat flux received by the different sides of the external steel element and assumes a uniform and average temperature of the element. This uniform temperature is then compared with the critical temperature of the structural element and if the critical temperature is higher than the average temperature the inherent fire resistance of the structural element is sufficient and no applied fire protection is required.

However, by calculating the average temperature of the structural elements the differential heating and the associated thermal bowing towards the fire is ignored. This becomes particularly relevant for slender columns, which are not engulfed in the flames of the fire. One good example of the consequences of ignoring the differential heat flux to the different sides was found in a current Buro Happold project in the US with a large number of external about 20m long steel columns. A typical section of the building can be seen in Figure 5.

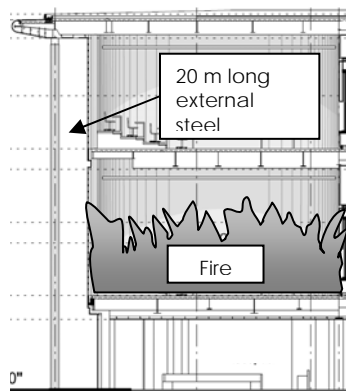


Figure 5. Design case for a slender external column.

The external columns have a slenderness of $\lambda = 127$ and an utilisation of up to 40% in the fire limit state. The floors in the building are compartment floors the worst position of a fire would be at mid height of the columns. Therefore, a fire with a constant heat flux from the middle storey was assumed to be heating the middle 5m of the columns. In order to investigate the effects of the non-uniform heating of such slender columns the temperature distribution in the column was calculated using TASEF [6]. A comparison of the FEM results and the average temperature calculation after the Eurocode can be seen in Figure 6a. The 2D temperature field after 60 minutes fire exposure is given in Figure 6b.

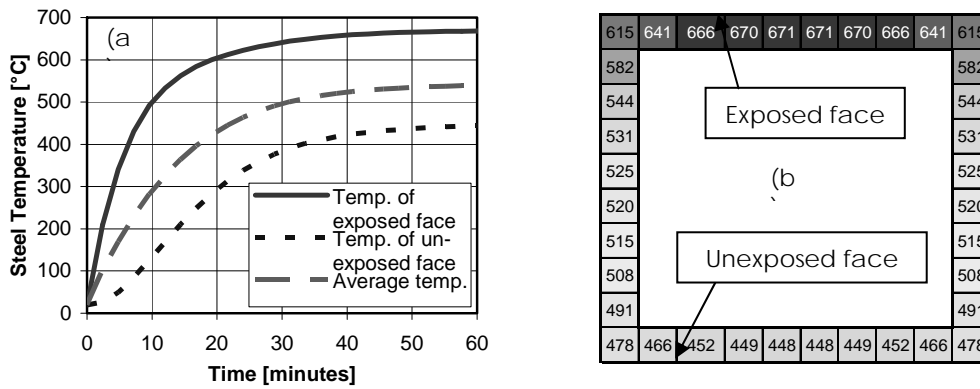


Figure 6. (a) Time-temperature curves for average and the non-uniform heating and (b) temperature field in the column section due to the non-uniform heating.

After the thermal analyses had been performed, the finite element software Vulcan [7] was used to predict the behaviour of the columns. The horizontal and the vertical displacement versus time plots for the average and the non-uniform heating are shown in Figure 7a and 7b respectively.

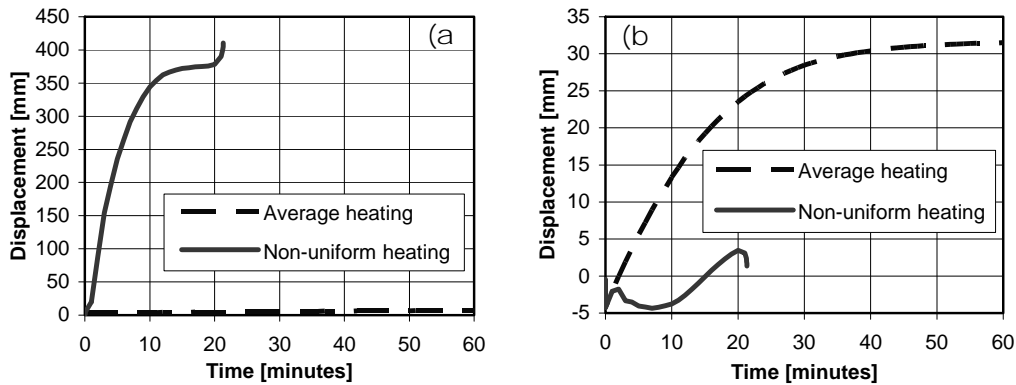


Figure 7. (a) Time-horizontal displacement curves at mid-span of the column and (b) time-vertical displacement curves at the top of the column.

One can see that the thermal bowing towards the fire (Figure 7a) of the non-uniform heating increases very rapidly in the first 10 minutes. During this phase of the fire the thermal differences between exposed and the unexposed face of the columns is largest. After just over 20 minutes the horizontal mid-span displacements of about 375mm and the increasing temperatures of the columns lead to stability failure of the column.

However, the column with a uniform temperature across the section, as it is suggested in the Eurocode approach, survives more than 60minutes of the fire exposure without a sign of stability failure. This means that if the design would have been entirely based on the EN 1991 Part 1.2 [4] and EN 1993 Part 1.2 [5] an un-conservative design would have been built. This is a clear indication that further work is required to establish if the problem is real, as a number of conservative assumptions have been made during the design, and to establish the boundaries of applicability for the design method for external steelwork in fire given in the Eurocodes or to extend it to included thermal bowing.

CONCLUSIONS

In this paper a variety of real structural fire engineering projects have been discussed and the main findings can be summarised as follows:

Heat flux and temperatures at the floor of a compartment fire are required to enable the proper fire design of upstand beams.

Optimised long-span space-frame roof structures are sensitive to localised heating to relatively low temperatures due to their large in-plane stiffness. A heating like this could occur in commonly used smoke control systems, which split large halls into individual smoke reservoirs to contain the smoke locally above the fire. As the temperature increase required to fail a significant number of elements is lower than the activation temperature of intumescent paint fire protecting the roof is unlikely to solve the problem.

Cable-net roof structures can be sensitive to localised fires if key elements like tension rings are in proximity of fire load due to the relative low failure temperatures of high strength cables and glued in cable connectors. The elevated temperature behaviour of spiral strand cable needs to be investigated.

The Eurocode 1 and 3 provide a method to design the external steelwork for the fire case. However, the method averages the heat flux received by the different sides of the external steel element and assumes a uniform temperature. This assumption ignores the effects of thermal bowing, which can be critical for slender column sections.

Due to the space limitations of this paper the following topics could not be discussed: fires in large compartments, integrity failure of floor slab and timber in natural and external fires. With this feedback to the research community it is hoped that the applicability of future research will be further enhanced and that the identified gaps will be closed.

REFERENCES

1. C. Abecassis-Empis, P. Reszka, T. Steinhaus, A. Cowlard, H. Biteau, S. Welch, G. Rein and JL. Torero, Characterisation of Dalmarnock fire Test One, *Experimental Thermal and Fluid Science* 32 (7), pp. 1334–1343, (2008).
2. NFPA 5000 Building Construction and Safety Code 2009 Edition.
3. European Committee for Standardisation, EN 1992-1-2: 2004, Eurocode 2: Design of Concrete Structures - Part 1-2: General Rules - Structural Fire Design.
4. European Committee for Standardisation, EN 1991-1-2: 2003, Eurocode 1—Basis of Design and Action on Structures - Part 1.2: Action on Structures Exposed to Fire.
5. European Committee for Standardisation, EN1993-1-2: 2005, Eurocode 3—Design of Steel Structures—Part 1-2: General Rule - Structural Fire Design.
6. Ulf Wickström, TASEF (Temperature Analysis of Structures Exposed to Fire), V. 3.0 PC, Computer Programme for the determination of fire resistance of structural elements with or without insulation. Swedish National Testing Institute.
7. www.vulcan-solutions.com

Prediction and Calibration of Fire Resistance of Standard Units

T. MOLKENS and L. PYL

ABSTRACT

A fire safety analysis of standard units is performed, the required time of the fire resistance is R 60. The thermal response of the structural elements exposed to the standard fire (ISO 834) as well as to the natural fire (case study) is calculated. The structural response is calculated using an elastic approach, a thermo-elastic approach and a plastic approach.

A verification in the temperature domain, using the critical temperature method for an ISO 834 fire, gives a fire resistance of 26 minutes. An infinite fire resistance results from a natural fire with 20 mm joint/unit openings, because the fire is at that moment ventilation controlled and the steel temperature stays below the critical temperature. In case of a total of 5,4 % openings, a fire resistance of about 50 minutes is obtained.

The material properties of the cement fibreboard, used as floor, are obtained from numerical simulations which are validated with test results. However, this approach requires an extrapolation to another thickness and therefore has to be validated by means of more tests. This is also the case for the joint behaviour where a transmission of tensile membrane forces at elevated temperatures will be needed.

The thermo-plastic analysis of the floor with cement fibreboard gives valuable results with deflections limited to $L/25$. These models have shown that R 60 under ISO 834 is not possible without additional measures (extra board needed). The natural fire causes a time delay in the temperature rise but the gain in fire resistance is limited. For the concrete flooring, additional reinforcement and insulation around the columns is sufficient.

1. DESCRIPTION OF SYSTEMS FOR TEMPORARY UNITS

1.1. Scope of the study

Standard units are widely used for the construction of temporary or almost permanent constructions such as site offices, schools and even hospitals. The aim of this study was to predict the behaviour of such constructions, with a specific case study located in Belgium, used as a restaurant at 0-level and with offices and meeting rooms at the 1st-level (Figure 1).

A fire resistance of 1 hour without progressive collapse is needed for the construction. Except for the roof where 30 minutes will be sufficient.

The conventional fire scenarios as nominal fires or natural (parametric) fire scenarios, including passive and/or active fire protection measures might be used. Passive fire measures (gypsum board 2x12,5 mm – R 60) are applied to the columns. The stability of the floor must in this case be assured by membrane effect of the floor and the plastic resistance of the primary beams at elevated temperature.

1.2. Structural properties

This type of structures is generally composed of a steel frame with four columns, one on each corner, connected with primary beams at floor and roof level. Secondary beams support the floor and roof. The panels (wood- or cement-based fibreboard) are fixed on cold formed steel profiles. The floor, the roof and the wall cladding are assumed to act as stiff walls capable of resisting the lateral forces. The walls are composed of metal sheeting (ext.), insulation 50mm+CFS vertical studs, OSB-board 12mm and gypsum plate of 12 mm (int.).

At this moment, two different types of floor systems are used on the Belgian market, as far as we know. Cement fibreboard floor panels (denoted as system 1 in this text) or concrete floors (denoted as system 2 in this text) apply. The roof can be out of wood based panels, steel cladding or sometimes the floor of the unit above (tailor made constructions). The types of elements which are used in both systems are summarized in TABLE I.

System 2 is, at this moment, mainly used if there is a special need to control the effect of induced vibrations by man, some equipment or coming from the environment.

TABLE I. Section types.

Construction element	System 1	System 2
Columns	RHS 150/100/5	SHS 100/100/6
Primary beams	RHS 200/100/5	UPN220
Secondary beams floor	CFS Z 200/60/2	IPE 120
Floor plate	Cement fibreboard (thickness 25 mm)	Concrete slab (thickness 100 mm) with mesh 150x150x6x6
Secondary beams roof	CFS U 200/40/4	CFS U 200/40/4
Roof slab	Fibreboard with resin	Fibreboard with resin

1.2. Material properties

The material properties for the steel members used for the primary and secondary beams correspond with EN 1993-1-2. Steel S235 with $f_y = 235 \text{ N/mm}^2$ is used. For wood based products there is an agreement [4] that the 5% characteristic value should not longer be used. Instead, the 20% characteristic value can be used $f_{20} = k_{fi} f_k$, with $k_{fi} = 1,15$. The characteristic value for the tensile stress $f_t = 4 \text{ N/mm}^2$, so $f_{t,20} = 4,60 \text{ N/mm}^2$.

The material properties of the cement fibreboard are summarized in TABLE II and may be assumed to be independent of the temperature according to EN 1994-1-2 for LC concrete.

TABLE II. Material properties of the cement fibreboard.

ρ [kg/m ³]	f_c [N/mm ²]	$f_{m,k}$ [N/mm ²]	f_t [N/mm ²]	E [N/mm ²]	ω [%]	$\Delta L/L$ [mm/mK]	λ [W/mK] at 20°C	[-]	c [J/kgK]	α_c [W/m ² K]	ϵ_m
1250	15,0	9,0	4,0	4500	9	0,011	0,35	0,2	840	25,0/4,0	0,80

Based on technical data sheets with results from a fire test of the Duripanel board, a product of Eternit, the material properties in TABLE II are adopted. The temperature as a function of time in a point on the upper layer of a 32 mm thick Duripanel board subjected to an ISO 834 fire curve underneath, is measured and compared with the results of a thermal analysis using SAFIR [10]. The updated density ρ_{test} and conductivity λ_{test} , summarized in TABLE III, are used then to obtain the temperature distribution as a function of time in the

upper part of the board for the Duripanel of 25 mm thickness assuming an ISO 834 curve and the natural fire, which will be explained below, underneath as shown in Figure .

TABLE III. Thermal properties of the cement fibreboard validated with test results.

test [kg/m ³]		20°C	50°C	300°C	500°C	700°C	≥ 900°C
2400	test [W/mK]	0,35	0,30	0,25	0,20	0,15	0,10

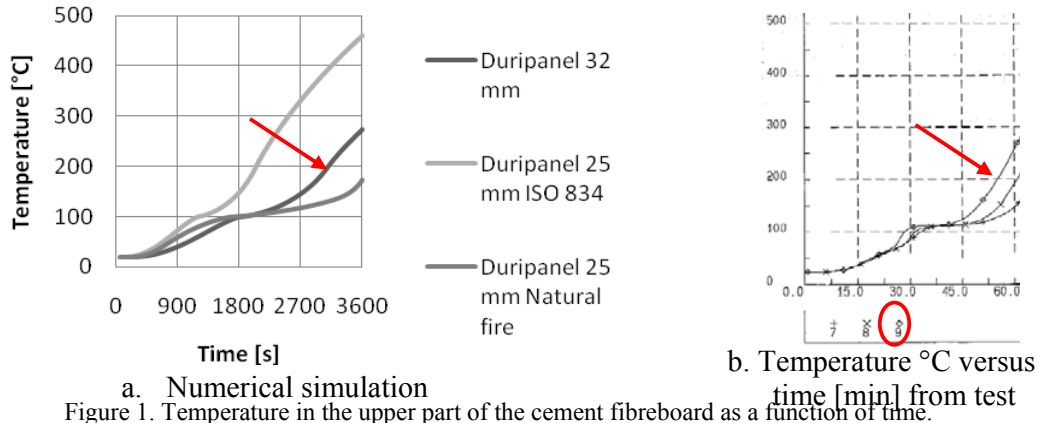


Figure 1. Temperature in the upper part of the cement fibreboard as a function of time.

2. LOAD ACTIONS

The mechanical behaviour of the structure is depending on thermal actions and their thermal effect on material properties and indirect mechanical actions. The analysis is based on the Eurocode standards with their National Annex [1], [2], [3], [4]. First, the mechanical actions are described. The thermal actions are discussed afterwards. The analysis is based on the fire resistance of the floor as this is the most critical.

The accidental actions from fire design comprises the permanent fixed action (self-weight of the beams, self-weight of the cement fibreboard $12,5 \times 0,025 = 0,31$ kN/m² and laminate flooring 0,10 kN/m²) and imposed loads on buildings arising from occupancy assuming category B of use (offices) (3 kN/m² with combination factors $\Psi_0=0,7$; $\Psi_1=0,5$ and $\Psi_2=0,3$).

The application of the standard fire (ISO 834) permits to ignore thermal loads according to limited thermal expansion, following Belgian regulations [2]. This is only valid if free axial thermal expansion can be guaranteed for materials with low massivity and good conduction. This is in a certain way the case due to possible movements in the connections in between the units.

To estimate the effect of a natural fire, the Ozone v 2.2.2 software is used [7]. The introduced materials are already mentioned above. Temperature dependent openings are used:

For each joint 20 mm in between the units with a linear variation in function of temperature (10% of total openings at 20°C, 50% at 400°C and 100% at 500°C).

Following the information obtained by AGC glass manufacturer [6], the inner skill of normal double glass is broken after 2 till 3 minutes of ISO 834. This means that a smoke temperature of 450 till 500 °C can be achieved. At a temperature of 400°C, windows and doors are completely open (safe approximation).

Detection is done by smoke $\delta_{n4} = 0,73$, an automatic alarm transmission to the fire brigade will be installed $\delta_{n5} = 0,87$, there is a reduction for an off site fire brigade $\delta_{n7} = 0,78$ and a fire risk area of 907 m² or $\delta_{q1} = 1,72$. The fire load is uniformly distributed and equal to 377 MJ/m², with a medium growth rate (RHR 250 kW/m²) & a rather low fire risk ($\delta_{q2} = 1,00$) [2].

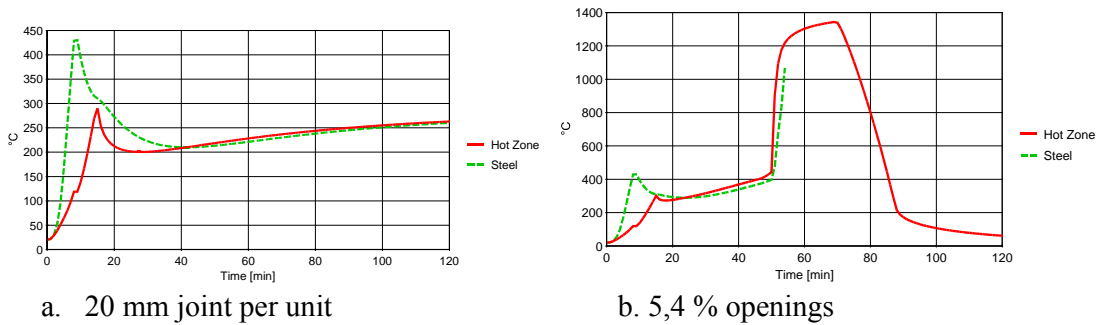


Figure 2. Gas and steel temperature (Section factor $A_m/V = 200 \text{ l/m}$ and $r = 0,70$) above fire axis.

From **Figure a** it can be observed that the critical steel temperature is not reached. The fire will be ventilation controlled under the conditions described above. The influence of the openings is investigated by replacing the 20 mm joint to 2 % of the length of the compartment times the height. At 500°C a total opening factor of 5,4 % is obtained. **Figure b** shows that after 45 min, a fully engulfed fire would occur.

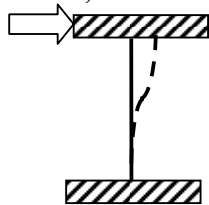
Furthermore, if only the 2% opening factor, corresponding to the joints, in the walls without the effect of glass falling out is considered, a time delay of the temperature rise of 10 minutes in comparison with the ISO 834 is obtained. First, the ISO 834 is investigated. The natural fire will be introduced afterwards. The advantage of this last one is that there is a rather big time delay which gives a smoother surface temperature as with the ISO 834. It is at this moment already clear that an additional board or insulation will be needed for the ISO 834 fire to fulfill the insulation criterion.

3. SIMPLIFIED APPROACH

In a first approach for system 1, a verification in the temperature domain is performed using the critical temperature method. The ISO 834 is considered. Temperature induced stability phenomena are neglected. The secondary beams supporting the plates are omitted. The degree of utilization μ_0 is equal to the load capacity in the quasi permanent situation. This approach allows the use of a simple calculation model at ambient temperature.

Unity check gives 0,15 except for columns (0,20 but protected). Using table 3.1 of EN 1993-1-2 [3], a critical steel temperature $t_{a,cr} = 767 \text{ °C}$ is obtained. For an ISO 834 fire, this temperature is reached after 26 minutes. With wood protection it stays 26 minutes, with a natural fire and 20 mm joint/unit there is no limit and with in total 5,4 % openings a fire resistance of about 50 minutes is obtained.

Another more scientific way to make a first estimation is with a so called thermo-elastic approach, which is also applied to system 1 with the cement fibreboard. By using such a model, the restraints become important.



To simulate the reaction or support of the adjacent units, a spring constant $F/\Delta = 12EI/L^3$ is introduced. Assuming a temperature equal to 500 °C, the Young's modulus is equal to $E = 126000 \text{ N/mm}^2$. An axial spring constant $K_{ax,s} = 444 \text{ kN/m}$ (for the strong axis) and $K_{ax,w} = 235 \text{ kN/m}$ (for the weak axis) is obtained. The half of the value for the top unit can be assumed.

The unity check go far over the elastic range so the results above have no physical value anymore, because the plastic behaviour of the material is not in this model.

4. FINAL DESIGN SITUATIONS

The fire behaviour of the units for system 1 was evaluated by using a two step analysis. First, the temperature distribution inside the structural members was predicted. In a second step, the response of the structure is predicted under the applied accidental loads and the thermal action for both an ISO 834 fire and the natural fire with 5,4% openings.

For the primary beams RHS 200/100/5, a two side exposure was adopted. A beam element IPE 80 ($7,64 \text{ cm}^2$, $A_m/V=509 \text{ m}^{-1}$ uniformly heated) is used to model the secondary beams as these CFS Z 200/60/2 ($A=6,36 \text{ cm}^2$, $A_m/V=719 \text{ m}^{-1}$ three sides exposed) would require a huge number of additional shell elements. The cement fibreboard (TABLE II) is represented using shell elements. **Figure** shows the temperature distribution in the elements.

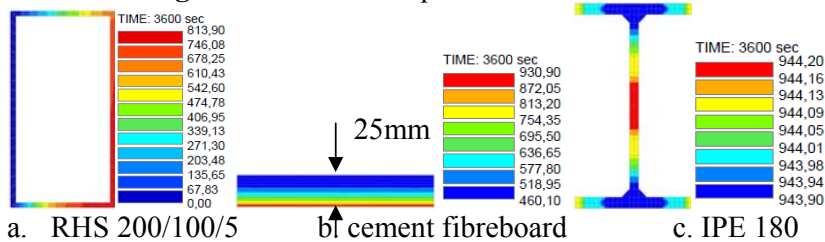


Figure 3. Temperature in the cross section after 60 minutes of ISO 834 fire.

Figure 4. shows the structural model. Only the cement fibreboard, supported by the beams is modelled (section properties TABLE I) as the protected columns stay cold during the fire. To be able to check easily the influence of neighboring units, a model with separated springs instead of a spatial frame is used. There is a transfer of vertical forces and moments from the primary beams to the columns. Furthermore horizontal displacements are limited by the moment stiffness of these columns. A short bar has to simulate the bending stiffness of the column and a long bar is used to simulate the axial stiffness.



The bending stiffness of a bar clamped at the base and with a unit moment on top is given by the ratio $3EI/L$. The column is a RHS 150/100/5 with height 2,7 m and moment of inertia $I_y=719,2 \text{ cm}^4$ and $I_z=384,0 \text{ cm}^4$. An IPE 160 ($I_y=869,3 \text{ cm}^4$) was chosen to model the stiffness around the strong axis ($K_{rot,s}$) and an IPE 120 ($I_y=317,9 \text{ cm}^4$) around the weak axis of the column ($K_{rot,w}$). So the adapted lengths become 3,264 m for the IPE 160 and 2,234 m for the IPE 120.

As already mentioned, the horizontal stiffness can be simulated using a spring constant of 444 kN/m in the strong direction ($K_{ax,s}$) and 235 kN/m in the weak direction ($K_{ax,w}$). The spring constant of a bar uniaxially loaded can be written as EA/L . Using the same bars as above, a bar length of 950,2 m for the IPE 160 and 1180,5 m for the IPE 120 is obtained. The torsion stiffness of the IPE 120 and IPE 160 is disregarded. TABLE IV summarizes the boundary conditions applied to the structural model.

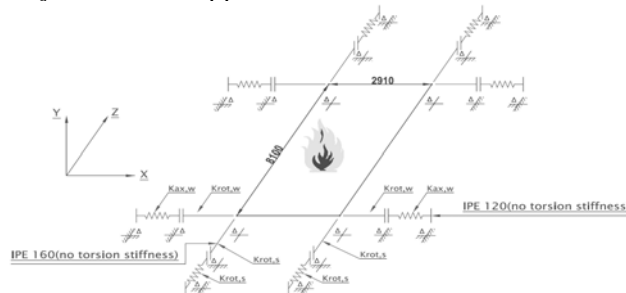


Figure 4. Structural model of the floor.

TABLE IV. Boundary conditions

	U_x	U_y	U_z	ϕ_x	ϕ_y	ϕ_z
Δ	FREE	BLOCKED	FREE	FREE	FREE	FREE
Δ / ϕ	FREE	BLOCKED	BLOCKED	FREE	FREE	FREE
Δ / ϕ'	BLOCKED	BLOCKED	BLOCKED	FREE	FREE	FREE
\vdash	---	---	---	BLOCKED	BLOCKED	BLOCKED

Figure shows the displacement as a function of time of the mid-point of the floor for both the ISO 834 and the natural fire underneath the floor. The deflection is limited to $L/25$.

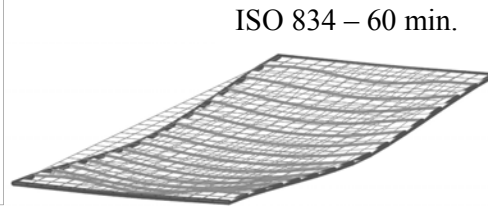
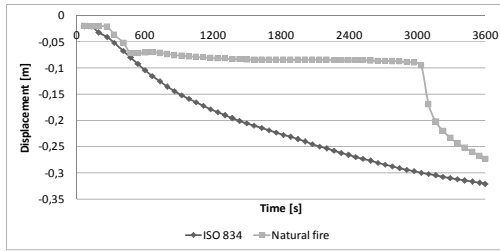
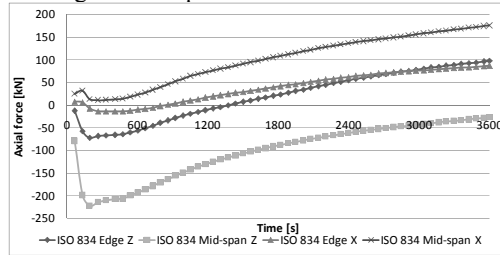
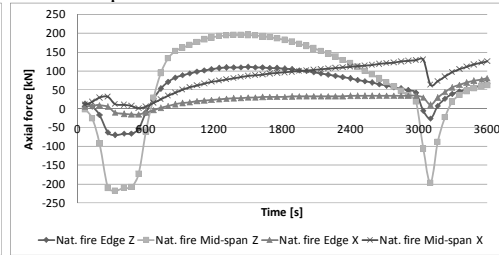


Figure 5. Displacement as a function of time of the mid-point of the floor and deformed floor.



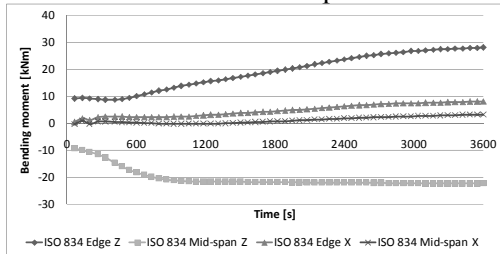
a. ISO 834 curve



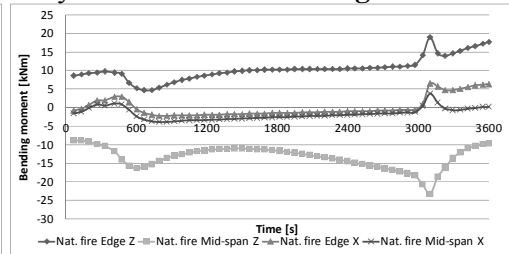
b. Natural fire curve

Figure 6. Axial force in the primary beams.

Figure shows the axial forces in the primary beams. The thermal elongation causes compression forces in the beams due to the end restraints ($K_{ax,s}$). At mid-span in the z-direction the RHS stays in compression (due to difference in $\Delta L/L$) whereas at the edges, tensile forces occur after 23 minutes. In the short direction of the floor, the edge beams are always in tension at mid-span. **Figure b** shows a less smooth axial force pattern as a function of time which follows the temperature-time history of the natural fire in **Figure**.



a. ISO 834 curve



b. Natural fire curve

Figure 7. Bending moment in the primary beams.

Figure shows the bending moments in the primary beams. The negative bending moment at mid-span of the beams in the z-direction (8,1 m) correspond to tensile stresses in the bottom part of the RHS, whereas the positive moment at the edge is due to the (semi-)rigid end restraints. As temperature rises, the bending moments increase in a ratio similar between a beam with rigid end restraints ($p^2/24$) or hinges ($p^2/8$). The bending moments in the short span (2,91 m) cause tensile stresses in the top part of the RHS. A less smooth bending moment pattern as a function of time is obtained in **Figure b** which follows the natural fire.

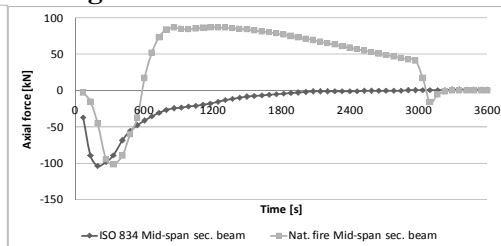
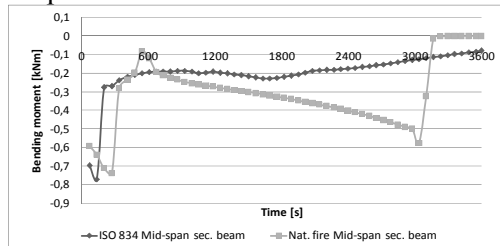


Figure 8. Axial force and bending moment in the secondary beams as a function of time.

Figure shows the axial force and bending moment in the secondary beams as a function of time. As the temperature rise of these profiles with low massivity is high, the thermal expansion of the beams causes compression. Under the ISO 834 fire, the axial force decreases

rapidly and the membrane effect of the cement fibreboard takes over the loading. When submitted to the natural fire, shown in **Figure b**, the temperature rise is less pronounced and after a loss of strength due to a local peak (after +/-10 minutes), the beam regains his strength in bending (with decrease of the axial force as logic consequence) just till the fast increase of temperature after about 50 minutes of fire.

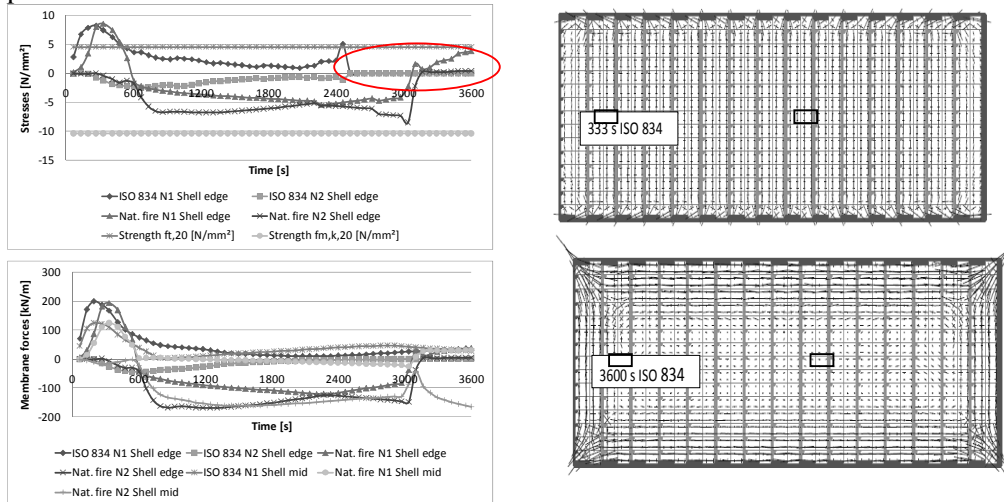


Figure 9. Stresses in the cement fibreboard due to membrane forces as a function of time and vector plot after 333 s and 3600 s of ISO 834 fire.

Figure shows the principal stresses in the cement fibreboard in the middle of the board and on the edge due to the membrane forces N_1 and N_2 as a function of time subjected to the ISO 834 and the natural fire. The 20 % fractile of the tensile strength property $f_{t,20} = 4,60$ N/mm² and the bending strength property $f_{m,k,20} = 10,35$ N/mm² (safe assumption as compression strength $f_{c,20} = 17,25$ N/mm²) at normal temperature are indicated in Figure . The principal tensile stresses in the middle of the floor are oriented in the direction of the long span of the floor. The principal compression stresses on the edge are oriented in the direction of the short span of the floor. Taking into account the charring depth, the maximum tensile strength is exceeded only in the first 5 minutes of the board subjected to an ISO 834 and the natural fire. The results of the tests do not confirm these results. The char-line should be taken as the position of the 300°C isotherm [4]. This is taken into account in Figure using a reduced thickness of the panel in the calculation of the stresses. However, after 2520s of ISO 834 fire, the temperature of the panel exceeds 300°C everywhere and the panel would fail.

Based on the maximum tensile membrane forces of approximately 200 kN/m after about 5' for both fires, a thickness of $(200/4,60 =) 44$ mm will be needed. Based on the maximum compression membrane forces of approximately 165 kN/m, which seems more realistic, a thickness of $(165/10,35 =) 16$ mm will be sufficient. The required total thickness then becomes equal to 32 (test result) + 16 (based on maximum compression membrane forces) = 48 mm for an ISO 834 fire (extra board of 24 mm) and only 14 mm (according to material model see Figure) + 16 mm in the case of a natural fire = 30 mm (extra board of 8 mm in case study).

The acting of membrane forces is only possible if there is a transfer of forces between adjacent boards. Therefore some models of the joint (2 mm) are made. **Figure** shows a kind of cooling phenomenon in the joint of a single board of 25 mm. With an extra board on top of it this phenomenon disappears completely and the situation is even reversed. It is rather difficult to make a confident study of this 3D problem, this can only be shown by tests.



Figure 10. Temperature profile at a joint with single or double board.

Previous research has shown that membrane effects can develop in plates which have the capacity to take also compression forces, like for system 2 (protected contour beams) [11].

Such a plate can act auto stable. The concrete slab with thickness 100 mm and mesh reinforcement 150x150x6x6 fulfills the insulation criteria after 60 minutes according to EN 1992-1-2. The UPN 220 contour profile is partially embedded in concrete so it will stay relatively cool. In this approximation, a Young's modulus in correspondence with the mean temperature of the profile after 60 minutes (454°C or $E = 135660 \text{ N/mm}^2$) is introduced. The mesh is sufficient in the short direction ($A_{s,req} = 186 \text{ mm}^2/\text{m}$) but the results in Figure 1 show that it must be reinforced by bars of 20 mm x 6000 mm each 110 mm in the long direction (total amount 392 kg). The deflection is limited to 18,7 mm.

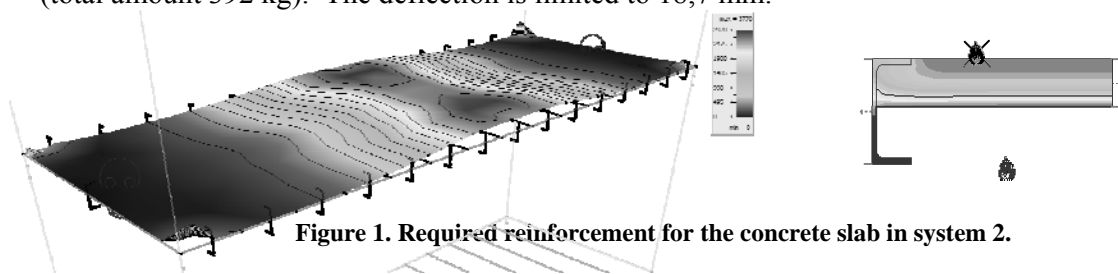


Figure 1. Required reinforcement for the concrete slab in system 2.

5. CONCLUSIONS

To ensure a “smooth” fire it is very important that all joints between units are well filled with a fire resistant material (foam, insulation) such that a fully developed fire can be avoided.

In order to fulfill the insulation criterion, and for membrane forces, an extra cement fibreboard will be needed for system 1. This adaptation can be carried out rather easily in practice. Only the door heights and the stair case must be slightly adapted.

Nevertheless, tests must confirm for system 1 the results of this study (temperature profile, joint behaviour, reduction of the original thickness by the charring depth and values of the tensile, compressive and bending strength in the fire situation. For system 2, additional reinforcement will be needed to guarantee REI 60 for the construction. This requires an extra cost, valued at 17 €/m², for the 392 kg reinforcement/floor in place of insulation.

REFERENCES

1. EN 1990:2002+Nationale Bijlage NBN EN 1990-ANB:2005, Eurocode 0: Grondslag voor het ontwerp, European Committee for Standardization CEN, 2002.
2. EN 1991-1-2:2002+Nationale Annex NBN EN 1991-1-2-ANB:2008, Eurocode 1: Actions on structures - Part 1-2: General actions - Actions on structures exposed to fire, European Committee for Standardization CEN.
3. EN 1993-1-2:2005+Nationale Bijlage prNBN EN 1993-1-2-ANB:2008, Eurocode 3: Design of steel structures - Part 1-2: General rules - Structural fire, European Committee for Standardization CEN, 2005.
4. EN 1995-1-2:2004+Nationale Bijlage prNBN EN 1995-1-2-ANB:2008, Eurocode 5: Design of timber structures - Part 1-2: General -Structural fire design, European Committee for Standardization CEN, 2004.
5. Technical data sheet Duripanel S3(B1).
6. AGC test report glass.
7. A tool to design steel elements submitted to compartment fires OZone V2. Part 1: pre- and post-flashover compartment fire model, Cadorin J.-F. & Franssen J.-M., Fire Safety Journal, Elsevier, 38 (2003), 395-427, <<http://hdl.handle.net/2268/29650>> <http://hdl.handle.net/2268/29650>.
8. A tool to design steel elements submitted to compartment fires OZone V2. Part 2: Methodology and application, Cadorin J.-F., Pintea D., Dotreppe J.-C. & Franssen J.-M., Fire Safety Journal, Elsevier, 38 (2003), 429-451, <<http://hdl.handle.net/2268/29651>> <http://hdl.handle.net/2268/29651>.
9. PowerFrame and Diamonds by BuildSoft.
10. SAFIR. A Thermal/Structural Program Modelling Structures under Fire, Franssen J.-M., Engineering Journal, A.I.S.C., Vol 42, No. 3 (2005), 143-158.
11. FRACOF - Méthode de dimensionnement de la résistance au feu des planchers mixtes partiellement protégés, CTICM (France), ArcelorMittal (France) et SCI (Royaume Uni), incendie@cticm.com.

A Simplified Approach for Evaluating Equivalent Fire Resistance Under Design Fire Exposures

P. PAKALA, V. KODUR and M. DWAIKAT

ABSTRACT

This paper presents an energy based approach for estimating equivalent fire resistance of structural members under design fire exposures. The approach is based on the principle of equivalent energy and estimates equivalent fire resistance by equating the total energy transferred from a design fire to that transferred by a standard fire exposure. The proposed approach is validated by comparing predictions from the proposed approach with those obtained from existing time equivalent methods, empirical formulae and non-linear finite element analysis. Based on the results, a correlation between equivalent fire resistance and maximum design fire temperature has been developed and is validated for RC beams. It is shown that the proposed method provides a reliable estimate of time equivalency and hence facilitates rational fire design.

INTRODUCTION

Provisions of fire safety is a key consideration in buildings and built infrastructure since fire represents one of the rare, yet detrimental, loading condition encountered by structures during their life time. Reinforced concrete (RC) construction is frequently used in buildings due to its high fire resistance properties. Fire resistance of RC members is generally evaluated based on standard fire tests or empirical calculation methods, wherein many of the critical factors that govern the

Purushotham Pakala, Ph.D Candidate, Dept. of Civil & Env. Engineering, Michigan State University, East Lansing, MI (pakalapu@msu.edu).

Venkatesh Kodur, Professor, Dept. of Civil & Env. Engineering, Michigan State University, East Lansing, MI. (kodur@egr.msu.edu.)

Monther Dwaikat, Assistant Professor, Dept. of Building Engineering, An-Najah National University, Nablus, West Bank (montherdw@gmail.com)

fire resistance of RC members are not accounted. Hence these prescriptive provisions may not be fully applicable for realistic fire performance assessment of RC members.

Rational fire design of RC members can be achieved through the use of performance based approach wherein the realistic fire resistance is evaluated under actual fire, loading and restraint conditions. The use of time equivalent approach, which relates the severity of design (realistic) fire to that of standard fire exposure, facilitates easy evaluation of fire resistance under realistic fire conditions. Hence it can be used as a tool in promoting the application of performance based design in practice.

Currently available time equivalent methods include equal area method, maximum temperature method, minimum load capacity method, maximum deflection method [1, 2]. Equal area method computes time equivalency by equating the areas under the time-temperature curve of design fire scenario to that under standard fire scenario. Maximum temperature method, minimum load capacity method and maximum deflection method utilizes temperature, strength and deflection criteria, respectively, between a design and standard fire scenario to estimate the time equivalency. Fire resistance obtained using temperature and strength criterions are generally greater than those obtained using deflection criteria. Although, failure in an RC beam occurs when the strength criteria is reached deflection criteria may play a crucial role as the integrity of the beam cannot be maintained if the beam undergoes excessive deflections. Thus the application of deflection criteria can give a better estimate of the time equivalent values. Furthermore, computation of time equivalent using maximum temperature method, minimum load capacity method requires significant amount of computational effort and hence they may not be applicable in practical design situations.

In addition to the above four methods, empirical formulae proposed by CIB, Law and Eurocode can also be used in computing time equivalency. Time equivalent values from these empirical formulae along with equal area method can be computed using basic spreadsheet calculations, thus making them an attractive choice for use in design situations. However currently available time equivalent methods and empirical formulae have a number of drawbacks and time equivalent predicted from these approaches show large variation under same design fire exposures [3,4]. Additionally, these approaches are validated for protected steel members only [1] and may not be applicable to RC members.

ENERGY BASED APPROACH

To provide a better estimate of equivalent fire resistance, in comparison to existing methods and empirical formulae, an energy based time equivalent approach is developed. The proposed approach is based on the principle of equivalent energy i.e., two different fire exposures will have same fire severity if they transfer the same amount of energy to a structural member. Energy transfer from fire to a structural member occurs by heat transfer mechanisms such as convection and radiation, from the fire exposed surfaces of the member. The convective and radiative heat flux on the surface of a structural member exposed to fire can be computed from the following formulae [1].

$$q_c = h_c(T_f - T_c) \quad (1)$$

$$q_r = \sigma \varepsilon (T_f^4 - T_c^4) \quad (2)$$

where q_c = convective heat flux (W/m^2), q_r = radiative heat flux (W/m^2), h_c = convective heat transfer coefficient ($\text{W}/\text{m}^2\text{K}$), T_f = temperature of fire ($^{\circ}\text{C}$ or $^{\circ}\text{K}$), T_c = temperature on the surface of boundary ($^{\circ}\text{C}$ or $^{\circ}\text{K}$), σ = Stefan-Boltzmann constant ($5.67 \times 10^{-8} \text{ W}/\text{m}^2\text{K}^4$) and ε = emissivity.

As the temperature on the fire exposed surface of the structural member (T_c) is almost equal to the fire temperature (T_f), the radiative heat flux can be approximated as follows:

$$\begin{aligned} q_r &= \sigma \varepsilon (T_f^4 - T_c^4) = \sigma \varepsilon (T_f^2 + T_c^2)(T_f^2 - T_c^2) = \sigma \varepsilon (T_f^2 + T_c^2)(T_f + T_c)(T_f - T_c) \\ &\approx \sigma \varepsilon (T_f^2 + T_f^2)(T_f + T_f)(T_f - T_c) \approx 4\sigma \varepsilon T_f^3 (T_f - T_c) \end{aligned} \quad (3)$$

Thus the total amount of heat flux transferred to a structural member can be written as:

$$q = q_c + q_r \approx h_c(T_f - T_c) + 4\sigma \varepsilon T_f^3 (T_f - T_c) \quad (4)$$

Further, if we can assume that the difference in the temperature on the surface of structural member and fire is proportional to fire temperature i.e., $T_f - T_c = \alpha T_f$, (where α is a constant), then the total heat flux can be expressed as follows:

$$q \approx \alpha (4\sigma \varepsilon T_f^4 + h_c T_f) \quad (5)$$

Using this value of heat flux, the amount of energy transferred to a structural member under fire exposure can be computed by integrating the area under the heat flux curve (Eq.(5)) as shown below:

$$E = \int q A dt \approx \int A \alpha (4\sigma \varepsilon T_f^4 + h_c T_f) dt = \alpha A \int (4\sigma \varepsilon T_f^4 + h_c T_f) dt$$

$$= \alpha A \times (\text{Area under heat flux curve } (\frac{q}{\alpha})) \quad (\text{as } A \text{ and } \alpha \text{ are constants}) \quad (6)$$

where A = area of boundary exposed to fire and E = total energy.

This E represents the total amount of energy transferred from the fire to structural member and is equal to the area under the time-heat flux curve for a particular fire exposure.

A comparison of time equivalent as computed by energy based method and equal area method is illustrated in Figure 1. Figure 1(a) shows a comparison of time-temperature (plotted on primary y-axis) and heat flux (plotted on secondary y-axis) curves for a design fire scenario and a standard (ASTM E119) fire scenario, while Figure 1(b) shows the time-temperature curves for a design fire scenario and a standard fire scenario. The design fire corresponds to FS5 (see Figure 4), which is discussed in later sections of the paper. It can be seen from Figures 1(a),1(b) that both the temperature and heat flux of standard fire increases continuously, whereas in a design fire there is a well defined decay phase (i.e., the fire temperatures eventually drops down due to burn out of combustibles or lack of ventilation). The presence of the decay phase can considerably influence of the behavior of RC beams wherein the concrete and reinforcing steel can regain a part of their original

strength. But the current approaches do not take into account the presence of decay phase in evaluating fire resistance of RC beams.

The procedure for evaluating time equivalent using the proposed energy method and equal area method is graphically illustrated in Figure 1(c) and Figure 1(d) respectively. To arrive at the time equivalent, the total energy (area under the heat flux curve) transferred from the design fire exposure (area B in Figure 1(c)) is computed first. Next, the area under heat flux curve of standard fire (area A in Figure 1(c)) is computed at various time steps. Time equivalent (t_e) is then defined as the time at which heat flux area A equals heat flux area B.

Figure 1(d) illustrates the equal area method which computes time equivalent by equating the areas of time-temperature curves under design and standard fire exposure. In this method, first the area under the time-temperature curve of a design fire scenario (area B in Figure 1(d)) is computed. Then the area under the time-temperature curve for standard fire exposure (area A in Figure 1(d)) is computed at different time intervals. Then time equivalent (t_e) is defined as the time at which both the areas are equal. It can be clearly seen that the energy based approach takes into account the total heat flux transferred from the fire exposure to the structural member in computing the time equivalent while equal area method considers only temperatures in evaluating time equivalent. Thus energy based method has a stronger technical basis than equal area method and hence the energy based method gives a better estimate of time equivalent values. Full details, including derivation of the approach from basic principles, is presented elsewhere [4].

DEVELOPMENT OF A SIMPLIFIED APPROACH

The above proposed energy based approach was used to evaluate the equivalent fire resistance of RC beams. Results obtained from the approach are used in developing a simplified approach for evaluating equivalent fire resistance of RC beams. In order to develop such an approach, substantial amount of data on RC beams subjected to design fire exposures is required. Data on the fire resistance of RC beams is developed by carrying out numerical simulations on RC beams subjected to different fire exposure conditions. These numerical simulations are conducted using a macroscopic finite element (MFE) based computer program as various fire scenarios and support conditions can be accounted for in evaluating the fire response of RC beams [5].

In this MFE program, the RC member is divided into a number of longitudinal segments and the mid-section of each segment is assumed to represent the behavior of the whole segment. The mid-section is further discretized into two dimensional mesh and the fire resistance analysis is carried out at various time steps till the beam fails. At each time step, the model establishes fire temperature for a specified fire exposure (design or standard). Then a heat transfer analysis is conducted to establish the temperature distribution across the cross-section of each segment. The cross-sectional temperatures of each segment are used to generate time dependent segmental moment-curvature relationships and these relationships are used to trace the response of RC beams in the entire range of loading up to collapse under fire conditions. More details about the macroscopic finite element model, including its validation, are presented elsewhere [5, 6].

ANALYSIS DETAILS

Macroscopic finite element model, described above, was used in analyzing RC beams with different support conditions (such as simply supported, axially restrained, rotationally restrained and axially and rotationally restrained) under seventeen design fire exposures and a standard fire (ASTM E119 [7]) exposure, producing 72 beam-fire combinations. All the beams used in the analysis were of rectangular cross-section (300mm x 500mm) spanning a length of 6m, made of concrete having a compressive strength of 30 MPa and reinforced with rebars of 400 MPa strength. Cross-sectional details of the rectangular beams with different support conditions used in the analysis are shown in Figure 2. Different support conditions were simulated by varying the value of axial restraint stiffness from zero to 20 kN/mm. A value of zero axial restraint stiffness represents simply supported conditions while 20 kN/mm simulates a fully restrained condition. Simply supported beams were analyzed with a load ratio of 40% (with an applied load of 14 kN/m) while the restrained beams were analyzed with a load ratio of 43% (with an applied load of 30 kN/m). Load ratio is defined as the ratio of applied load on the beam under fire conditions to the ambient temperature capacity of the beam.

Apart from rectangular cross-sections, T and I cross-sections were also analyzed using the FE model. Cross-section and elevation details of T and I beams are shown in Figure 3. These beams were analyzed by subjecting them to six randomly selected design fire scenarios (namely FS3, FS6, FS7, FS11, FS16, FS17 of Figure 4) under a load ratio of 50%.

Different design fire scenarios used in the analysis of rectangular, T and I beams are shown in Figure 4, where the time-temperature curves for seventeen design fire scenarios (FS1 through FS17) and a standard fire (ASTM E119) are plotted. It can be seen from the figure that the design fires have a well defined decay phase, whereas the temperatures in the standard fire increases continuously. The absence of decay phase in standard fire can have a significant influence on the fire resistance performance of structural members. Various fire scenarios shown in Figure 4 are selected to cover a wide variety of compartment characteristics, ventilation factors and fuel loads generally encountered in buildings. Values of compartment characteristics used in developing these design fire scenarios can be found elsewhere [3]. The parametric fire time-temperature curve [8] proposed in Eurocode1 [9] along with the recent modifications suggested by Feasey and Buchanan [10] are implemented to arrive at different design fire scenarios.

Results from analysis are utilized in computing time equivalency under design fires with respect to standard fire through maximum deflection method. In the maximum deflection method, time equivalency is computed by comparing the maximum deflection attained under design fire exposure to the corresponding deflection under standard fire exposure [1, 4].

CALIBRATION

Time equivalent values obtained from the energy approach are calibrated against those obtained from the FE program. FE analysis data obtained for

rectangular beams is randomly divided into two data sets and the first data set is used for calibrating the energy approach while the second set of data along with the data for T and I beams is used to validate the proposed approach. Comparison of time equivalents obtained from the first data set of FE analysis and the energy method indicate that there exists a correlation between the maximum temperature of design fire and the ratio of time equivalents ($t_{e(FE)}/t_{e(Energy)}$) [4]. Regression analysis has been conducted on the data generated from the proposed approach and non-linear finite element analysis and a correlation is established between the ratio of time equivalents predicted by these two methods and the maximum fire temperature as shown below:

$$\frac{t_{e(FE)}}{t_{e(Energy)}} = 1.6 - 0.00042 * T_{max} \quad (7)$$

where $t_{e(FE)}$ = time equivalent computed from FE analysis, $t_{e(Energy)}$ = time equivalent computed from energy method and T_{max} = maximum temperature of design fire.

Hence, the actual time equivalent of the design fire can be evaluated as follows:

$$t_{e(FE)} = (1.6 - 0.00042 * T_{max}) * t_{e(Energy)} \quad (8)$$

VALIDATION

Validity of the correlation (Eq.(8)) has been established by comparing the time equivalent values obtained from existing methods with those obtained FE analysis. Second data set obtained from the analysis of rectangular beams along with the FE analysis of T and I beams is used in validating the proposed approach. In order to further illustrate the applicability of the correlation to an independent set of data, four rectangular beams are selected from literature and are analyzed under six randomly selected design fire scenarios. Details about the properties of beams selected from literature can be found elsewhere [6].

Figure 5 shows a comparison of time equivalent values predicted by the proposed energy method with those obtained from equal area method, empirical formulae and FE analysis for rectangular, T and I beams along with conservative and unconservative regions. It can be seen from the figure that the time equivalent values predicted by energy method are on the conservative side and have less variation throughout the range of fire scenarios considered. In contrast, the time equivalent values predicted by equal area method and empirical formulae show a significant variation and the variation increases as the fire severity increases (as time equivalent value increases). Hence the energy based method can be used to arrive at a reliable estimate of time equivalent for design fire.

Figure 5(d) shows the comparison of time equivalents predicted by the energy method (Eq. (8)) and those obtained from FE analysis for the analysis of rectangular beams selected from the literature. As can be seen from the figure, the time equivalent values predicted by energy method are in good agreement with those obtained from FE analysis. A coefficient of determination value of 0.94 indicates that the proposed equation (Eq.(8)) predicts the time equivalents with an accuracy that is sufficient for design purposes in comparison with the FE analysis.

CONCLUSIONS

Current time equivalent methods and empirical formulae show large variation and are unconservative for evaluating time equivalent of RC beams subjected to design fires.

The proposed energy based approach gives a reliable estimate of time equivalent and the time equivalents are in good agreement with those obtained from a detailed finite element analysis.

Results obtained from the energy method provides a reliable estimate of time equivalent as it takes into account the total amount of energy transferred from the fire, in estimating the time equivalent.

Time equivalent values obtained from the energy based method have less variation in comparison to other methods and are conservative.

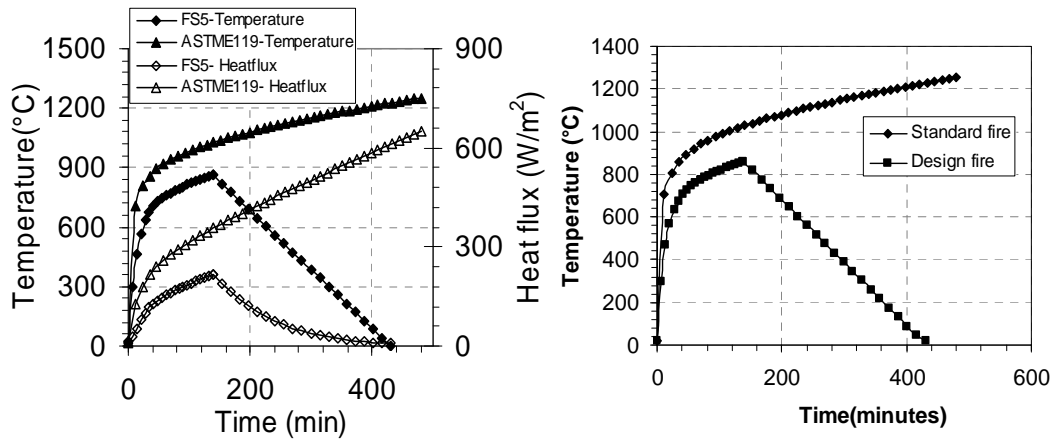
ACKNOWLEDGEMENTS

The authors wish to acknowledge the support of Michigan State University through the Strategic Partnership Grant Award (SPG 71-4434). Any opinions, findings, conclusions, or recommendations expressed in this paper are those of the authors and do not necessarily reflect the views of the sponsors.

REFERENCES

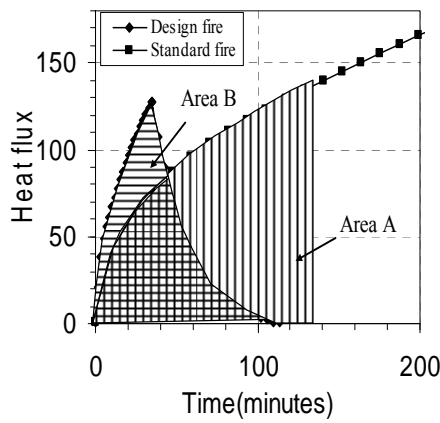
1. Buchanan, A.H. 2002. *Structural Design for Fire Safety*, John Wiley & Sons Ltd., Chichester, England.
2. Dwaikat, M.B. 2009. "Flexural response of reinforced concrete beams exposed to fire", PhD Dissertation, Michigan State University, East Lansing, Michigan, USA.
3. Kodur V.K.R., Pakala, P., and Dwaikat, M.B. 2009. "Energy based Time Equivalent Approach for evaluating Fire Resistance of Reinforced Concrete Beams", Submitted to *Fire Safety Journal*.
4. Pakala, P. 2009. "Energy Based Equivalent Approach for Evaluating Fire Resistance of Reinforced Concrete Beams", *MS Thesis*, Michigan State University, East Lansing, Michigan, USA.
5. Kodur, V.K.R., Dwaikat, M.B. 2008. "A numerical model for predicting the fire resistance of reinforced concrete beams", *Journal of Cement & Composites.*, 30:431-443.
6. Kodur V.K.R., Pakala, P. 2010. "Energy Based Time Equivalent Approach for Evaluating Fire Resistance under Design Fire Exposures", to be presented at 2010 Structures Congress, May 12-15, 2010.
7. ASTM 2008. "Standard Methods of Fire Test of building Construction and Materials", *Test Method E119a-08*, American Society for Testing and Materials, West Conshohocken, PA.
8. Magnusson, S.E., Thelandersson, S. 1970. "Temperature-time curves of complete process of fire development; Theoretical study of wood fuel fires in enclosed spaces", Civil engineering and building series 65, Acta, Polytechnica, Scandinavia.
9. EN1991-1-1. 2002. "Eurocode 1: Actions on structures. Part 1-2: General actions-actions on structures exposed to fire", Brussels: European committee for standardization, Germany.
10. Feasey, R., Buchanan, A.H. 2002. "Post-flashover fires for structural design", *Fire safety journal.*, 37(1):83-105.

FIGURES

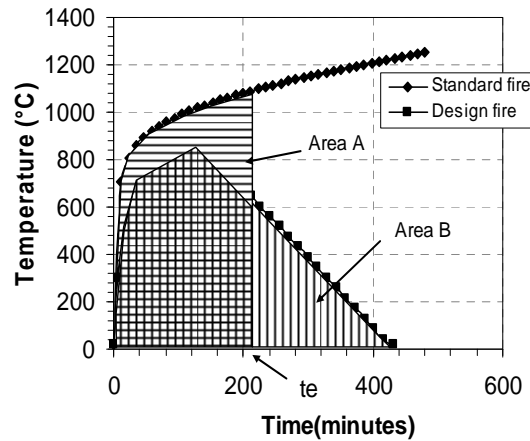


(a) Comparison of time-temperature, heat flux curves for a design and standard fire

(b) Time-temperature curves for a design and standard fire



(c) Energy based method



(d) Equal area method

Figure 1. Comparison of energy based approach and equal area method.

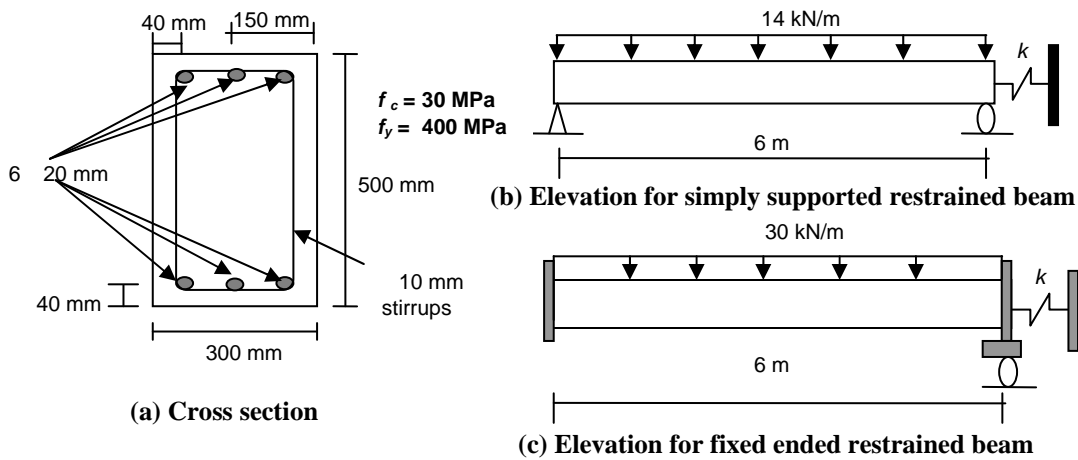


Figure 2. Cross-sectional details of RC beams used in the analysis.

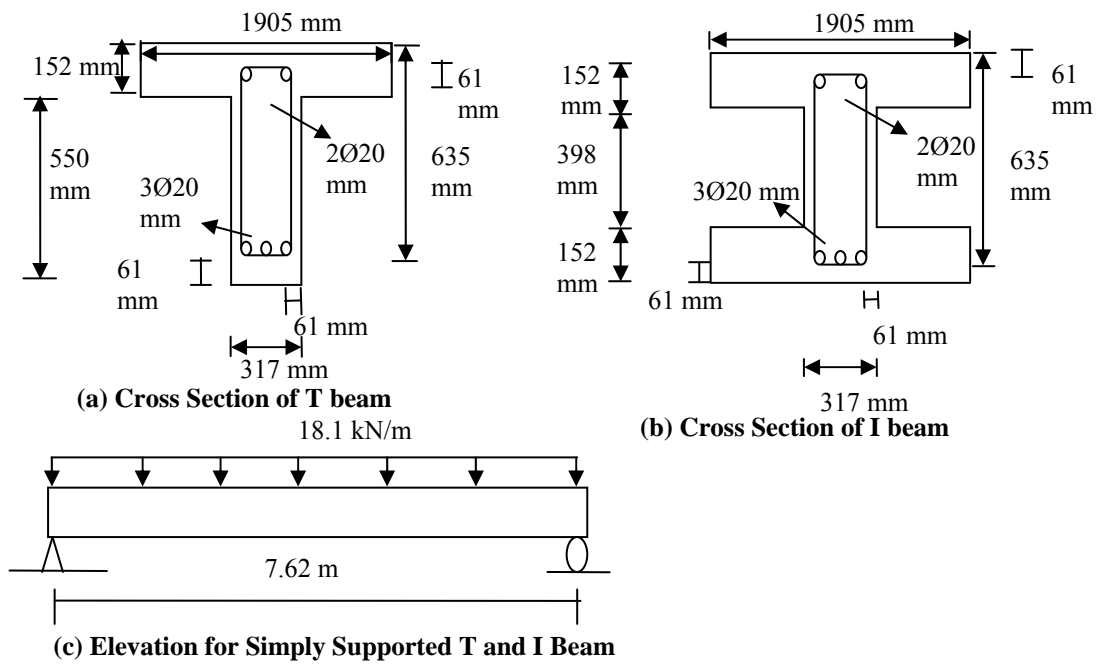


Figure 3. Cross-section and elevation of T and I beams used in the analysis.

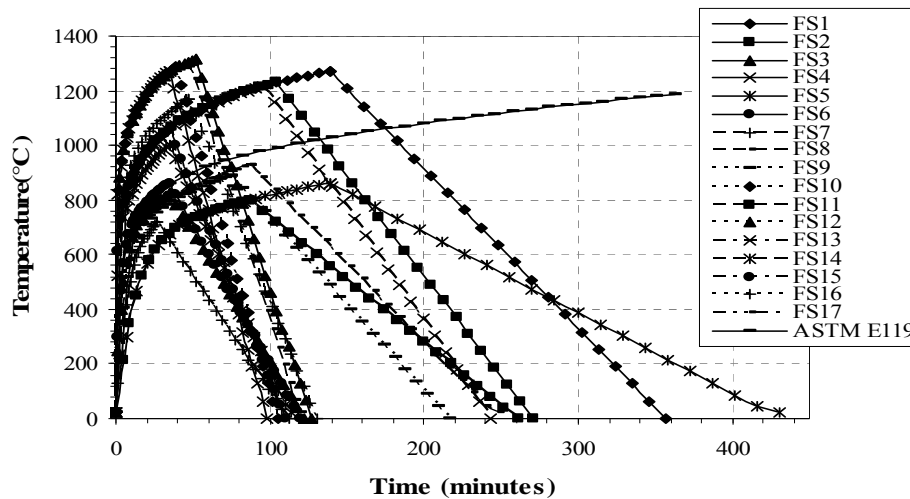
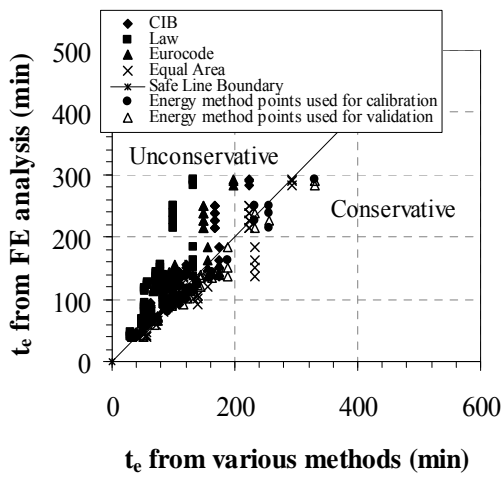
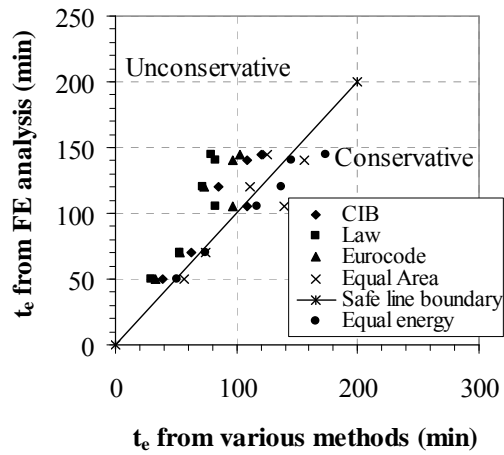


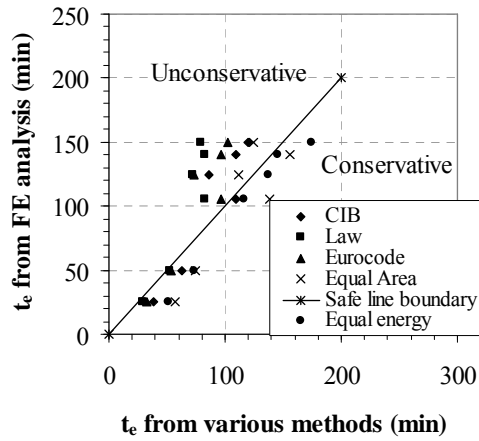
Figure 4. Time-temperature curves for design and standard fire exposures.



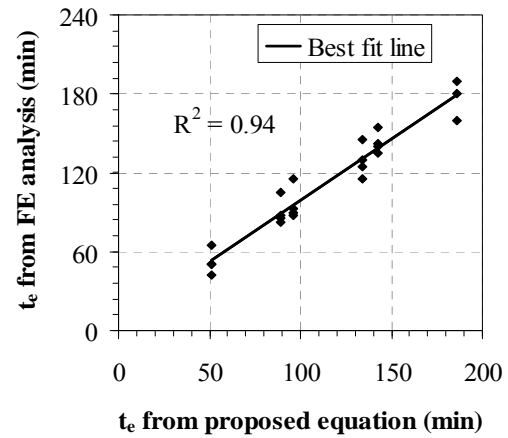
(a) Comparison of time equivalent values for rectangular beam



(b) Comparison of time equivalent values for T beam



(c) Comparison of time equivalent values for I beam



(d) Comparison of time equivalent from FE analysis and proposed equation

Figure 5. Comparison of time equivalent values predicted by various methods and FE analysis.

An Assessment of the Use of Structural Deformation as a Method of Determining Area of Fire Origin

A. T. TINSLEY and D. J. ICOVE

ABSTRACT

Current methodologies of origin investigation have yet to include the structural deformations seen in steel buildings as a viable indicator of the area of origin of a given fire. As many steel structures are of larger size, it is often difficult to determine the area of origin using the typical dig and sift methods advocated in NFPA 921, especially if the extent of the fire was large and there were no witnesses as to the origin of the fire. As has been investigated for years, the performance of steel is highly affected by the application of heat. The science of predicting the deformations of steel members is such that an investigator may be able to “reverse engineer” the fire to get an idea of its relative growth rate and length of combustion even if it is not possible to compute a heat release rate curve. The information derived from careful analysis of the deformations may also yield valuable input for use in computer fire modeling. Using several example cases, this paper will explore the methodology that can be applied in order to use the structural deformations as a viable tool to determine the point of origin of large, single story steel framed structures.

Andrew T. Tinsley, Eastern Kentucky University, Department of Fire and Safety Engineering Technology, 521 Lancaster Ave., 250 Stratton Building, Richmond, KY 40475

David J. Icové, University of Tennessee, Electrical Engineering and Computer Science, 301 Ferris Hall, 1508 Ferris Dr., Knoxville, TN 37996-2100

INTRODUCTION

NFPA 921 states that the basic methodology of fire investigation should rely on the use of a systematic approach and attention to all relevant details [1]. In order for a fire investigator to pay attention to all relevant details, it is imperative that they be able to recognize, record, and interpret all of the useful details of a scene. Typically, however, the scene is here today and may be gone tomorrow. Thus on scene documentation at the time of initial investigation is a necessity in order to properly determine the origin and cause of a fire. There are many indicators of a fire's growth and travel left behind at most scenes. These indicators, when interpreted correctly, will almost always lead the investigator to the true origin of a fire. The real question is: Are these traditional "dig and sift" methods practical or advisable in large loss fires?

Imagine a large warehouse fire, say 150 m by 150 m (500' by 500'). The warehouse is a total loss. After the initial investigation, it is evident that the fire had spread to over half of the warehouse prior to the first engine company's arrival. After a defensive fire attack was established the fire burned for over five hours and the fire became fuel controlled and basically self-extinguished. Prior to control of the fire, one of the sides of the building partially collapsed inward. There is 1 meter (3-4 feet) of debris on the floor of the warehouse and no witnesses as to the origin of the fire. Where would the investigation begin? Would it be possible or practical to "dig up" the entire half of the warehouse involved at the beginning of the fire? An investigator's first guess on where to start should be the immediate area around the collapsed portion of the building.

Why should the location of partial collapse be the first guess as to the origin of the fire? The method presented herein explains in detail the underlying principles and how they can be applied to the investigation of fires as described above along with almost any other fire encountered.

FIRE EFFECTS ON STEEL

While the effects of fire on steel have been long researched and documented, a more in-depth understanding of the exact engineering properties will be necessary to understand exactly what happens when a steel structure deforms to the point of collapse. An understanding of plastic theory and the method in which design engineers perform their analysis on buildings is also a necessity in order to understand this concept.

Steel is an elastoplastic material used in all types of construction. Steel can have varying properties which are dependent upon the amount of carbon and alloying agents used in the production process. Structural steel is generally produced to be ductile as opposed to having a high yield capacity. In steel production, ductility must be traded for strength and vice versa. Steel's behavior at room temperature as well as elevated temperatures is discussed in detail in the following sections.

Modulus of Elasticity and Poisson's Ratio

The elastic modulus, E , is the ratio of stress to the strain it produces. It represents the stress required to produce unit strain [2]. The elastic modulus of steel is typically assumed to be 200 GPa (29,000 ksi) at room temperature and is subject to variation with temperature increases. The typical point of degradation of strength of steel is approximately 150 C [2]. At this point, the strain increases under the action of a given stress. The variation of the modulus of elasticity (E) and the yield stress (F_y) of steel can be found in Figure 1 below.

Poisson's ratio (ν) is defined as the ratio of lateral strain to longitudinal strain. Poisson's ratio basically quantifies the reduction in cross sectional area as the member is placed into tension or vice versa. According to Cooke, it has been well documented that the Poisson's ratio of steel is negligibly affected by the temperature of the member [2]. Poisson's ratio for steel will be taken as 0.3 for all calculations in this paper and is the recommended value to use in the field.

Strain in Steel

Deformation of steel members is a function of the strain generated by the three components of strain [3]. The three components of strain that are of concern for analysis of deformations induced by fires are thermally induced strain, stress induced strain, and creep induced strain. In a typical structural analysis of a steel member, only stress induced strain is considered since the other two are generally small enough to be neglected. Strain, regardless of type, is defined as the change in length (δ) divided by the original length of the undeformed member (L). The typical maximum strain that structural steel can endure before failure is 20-30% at room temperature [2].

Stress related strain is induced by the deformations caused by the loads the member in question is designed to support (i.e. dead loads, live loads, wind loads, etc.). This form of strain is evident in all beams regardless of the thermal loading on the beam. The stress (σ) can be calculated by the accepted methods of structural analysis.

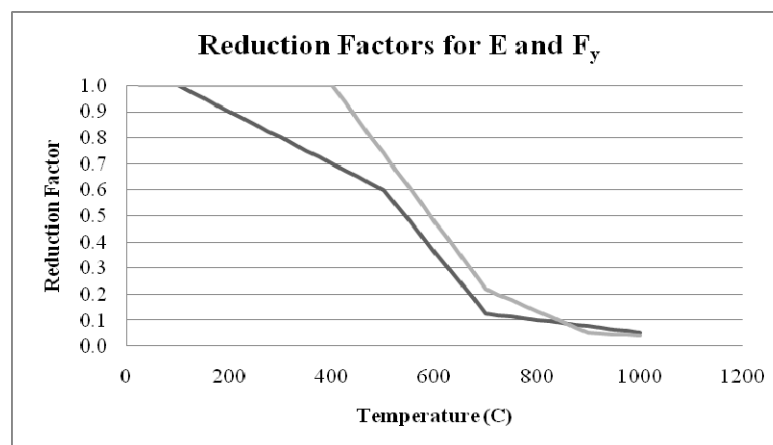


Figure 1. Reduction Factors.

Stress related strain can then be calculated as the stress divided by the modulus of elasticity (E) which varies with temperature. As noted earlier, E is generally taken as 200 GPa (29,000 ksi) at room temperature.

Thermally induced strain is of primary concern during the analysis of steel members during a fire. Almost all materials will expand when heated. The coefficient of thermal expansion dictates how much a certain material will expand when heated. The unrestrained length of a heated member can be found using $L_t=L_0(1+\alpha T)$, where L_0 is the original length, α is the coefficient of thermal expansion, and T is the change in temperature. The coefficient of thermal expansion is subject to minor variations at increasing temperatures and is typically taken as $14 \times 10^{-6}/C$ [2].

PORTAL FRAMING

According to Buchanan, portal framing systems are typical in large warehouses as well as in commercial establishments and are one of the more prevalent steel building types [3]. They are fairly simple to design and even easier to construct. They are widely adaptable since the bay lengths or clear spans can be adjusted with the use of larger structural members to suit the needs of the tenant. Portal frames were chosen for this analysis because of their frequency of use as well as their simplicity to analyze by non-engineering background individuals.

FIRE EFFECTS ON STRUCTURAL COLLAPSE

Due to the weakening of steel members in fire, a building that was well designed to accept the design loads will often undergo significant plastic deformations and possibly total structural failure. Engineers perform their design with a factor of safety in mind. A factor of safety is defined as the nominal resistance divided by the applied force. In structural design, it is possible to see factors of safety as high as 2-3. In other words, the building has a reserve capacity of 2-3 times the anticipated loading. Upon thermal degradation, the nominal resistance is decreased. When the nominal resistance is decreased enough to cause the factor of safety to fall below 1, failure of the structural member will occur.

Another factor that adds to a structure's likelihood of collapse during fire conditions is the addition of unexpected loadings such as firefighting personnel and water from extinguishment efforts. Water can be a large problem for buildings especially if the roof drains have been poorly maintained or the floors have deflected enough to allow the water to pool. All of these factors must be taken into consideration when attempting to use structural deformations to locate the origin of a fire.

Steel design intends to insure that the steel remains in the elastic behavior range under service loads. This is to say that the steel has yet to yield. When fire degrades the structural capacity of a member, the member can quickly enter into the plastic range on the elasticity curve. When this happens, the loading must be redistributed. In the case of a simple beam, this redistribution will not occur since it has no redundancy.

THEORETICAL EXAMPLES

Simple Beam Example

In the first example analysis, a simply supported steel beam is exposed to a linear time-temperature curve under a uniform load of 43.8 kN/m (3 kips/ft). This example assumes that the steel has no thermal gradients. In other words, the steel receives heat as one mass and is the same temperature throughout (i.e. instantaneous thermal equilibrium).

The steel will yield and suffer plastic deformations when the bending stress is equal to the yield stress. Beams are designed so that the loads placed on them are not sufficient to yield the steel. However, temperature increase is accompanied by a decrease in yield strength. Thus, the beam will fail when the yield stress is reduced to the point where it equals the bending stress.

The deflection of a simply supported beam can be simply found using elastic theory. The AISC Steel Construction Handbook states that the deflection of a simply supported beam with a uniformly distributed load can be calculated as follows [4]:

$$\Delta_{max} = \frac{5wL^4}{384EI} \quad (1)$$

Where, w=Distributed Load (N/m), l=Length of Beam (m) E=Modulus of Elasticity (MPa) I=Moment of Inertia (m⁴)

The deflection for a W14x53 section under a uniform load of 43.8 kN/m (3 kips/ft) equates to 17.5 mm (0.69 in). Also, according to the AISC Steel Manual, the unfactored nominal moment capacity is 270 kN-m (199 kip-ft) [4].

This simple equation was programmed into a spreadsheet in order to show the general deflection behavior under an increasing thermal loading with no increase in gravity loading. This calculation utilizes the yield stress and modulus of elasticity reduction factors shown in Figure 1. Deflection is mainly a function of the modulus of elasticity. Figure 3a shows the increase in deflection with temperature, and Figure 3b shows the decrease in nominal moment capacity with temperature.

The deflections stop at approximately 600 °C. At that point, this particular beam undergoes plastic deformation and for all practical purposes has failed. In other words, the deflection will increase greatly with no increase in loading since the steel has yielded. Therefore, it can no longer take any additional loading. As can be seen in these figures, the steel has lost its ability to retain the design moment at approximately 400 °C (750 °F). At this particular loading, the beam is expected to fail at approximately 600 °C (1000°F), or when the steel yields.

Finite Element Model

A simple finite element model can be constructed to show the deformations undergone by a building depending on the origin of the fire. Several modeling conflicts prevented a coupled analysis from being performed. The thermal portion of the model was performed to obtain the temperatures of the specific members in

the cross section of the portal frame. The degraded modulus of elasticity and yield stress were then imported into a structural model to get the general deflected shape. The member sizes and criteria are not important in this run of models as the purpose is to obtain general deflected shapes. ADINA was used for all finite element modeling. Figures 4 and 5 show the deflected shape with respect to the area of origin of the fire. Also note that the lowest area is not always the area with the most deflection. The largest deflection is the point on the frame that has translated from its original position the most.

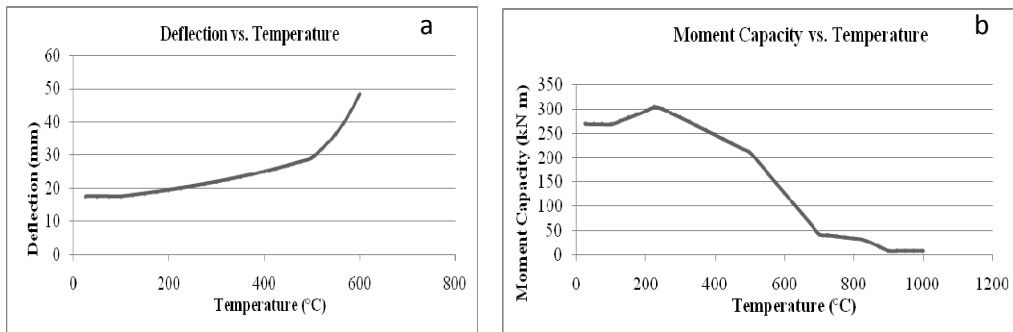


Figure 3. Simply supported beam deflection behavior under temperature loading.

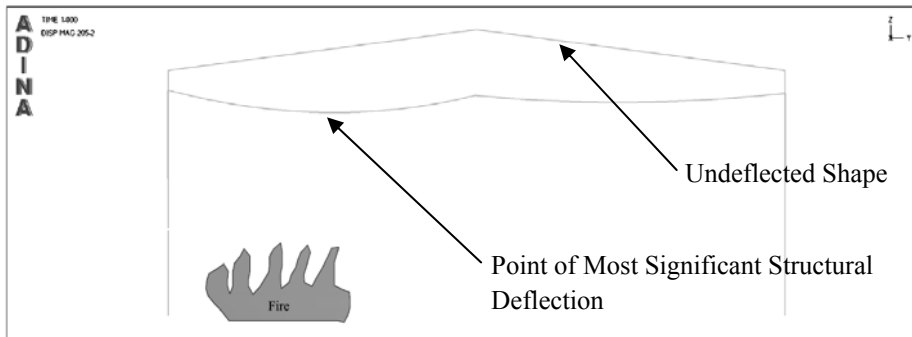


Figure 4. Fire on One Side of Building.

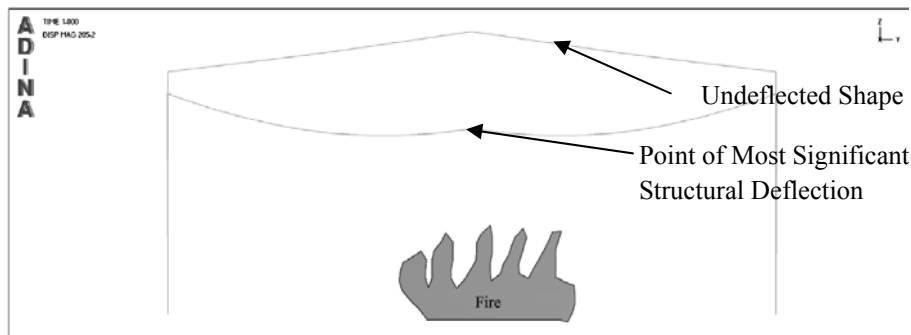


Figure 5. Fire Under Peak of Roof.

HISTORICAL EXAMPLES

There are several examples where the use of structural deformations would have significantly contributed to the investigation. While in most cases deformations are noted as a viable indicator, it is rarely used as evidence in an investigative report. The McCormick Place fire in Michigan as well as the Livonia Transmission Plant fire both consisted of a more complicated version of the portal frame design/construction method. Both fires consisted of total destruction of the buildings. Both had witnesses to confirm the area of origin of the fire, so validation of the use of the structural deformations was possible. Figures 8 and 9 show the deformed shapes of McCormick and Livonia, respectively, and their confirmed area of origin.

By starting at the areas of partial collapse and high deformation, the investigators would have been able to disregard a lot of the fire debris and had a much easier time finding the area of origin if there had not been witnesses to point them in the right direction. These two examples are extremely complicated, large loss fires. This method is highly applicable to steel buildings of any size and in almost any condition.

DISCUSSION

As a smoke plume reaches the ceiling, it begins to mushroom out over the area of the ceiling. This smoke plume will generate the most intense temperatures at the point directly over the origin of the fire. As time progresses, the remainder of the room heats up, but the area directly above the origin of the fire will sustain the highest intensity and longest duration of thermal degradation. This fact still holds true even if the room is allowed to reach flashover. It has been proven that the temperatures in a flashover situation will produce a fairly constant temperature throughout the upper layer of the fire plume. The members above the origin of the fire will have the same temperature application throughout the flashover even though the fire directly beneath this point may have run out of fuel.

The amount of exposure the steel has to elevated temperatures will determine the amount of strength lost. This would indicate that different members will have differing strengths. The loads will redistribute themselves as much as they can until failure finally occurs. If the fire is stopped prior to a total structural collapse, deflection patterns similar to the above figures should be encountered.

If a fire is allowed to burn long enough, it is possible that most structural members will receive similar heat fluxes and deflect in a similar manner, but this is not a reason to ignore this method. The structural deformations will still be a valid indicator for use in any forensic work to be done after the fire is completed. With the recent advancements in fire and structural modeling, it will be possible to reconstruct a fire and the structure which contained it to “reverse engineer” the scenario. This allows for timeline collaboration with witnesses, added fire load detection, and possibly even arson and/or suppression system sabotage.

With proper use, this method of investigation can yield much valuable information about the investigation at hand. This information can vary from significantly reducing the amount of time digging in the rubble of a fire to valuable

input for an advanced forensic model. The intricacies of this method should be left up to qualified structural engineers, but the entire scope of this method can be performed by virtually any investigator with a competent amount of knowledge about the behavior of structures.



Figure 6. McCormick Place Collapse and Confirmed Area of Origin [5].



Figure 7. Livonia Plant Partial Collapse and Confirmed Area of Origin [6].

REFERENCES

1. NFPA Technical Committee on Fire Investigation. NFPA 921: Guide for Fire and Explosion Investigation. 2004 edition.
2. Cooke, G.M.E., "An Introduction to the Mechanical Properties of Structural Steel at Elevated Temperatures." *Fire Safety Journal* 13, 1988. p.45-54.
3. Buchanan, Andrew H. Structural Design for Fire Safety. John Wiley and Sons, 2002.
4. American Institute of Steel Construction. Steel Construction Manual. 13th Edition. 2005.
5. American Iron and Steel Institute. "An Engineering Report on the January 16, 1967 McCormick Place Fire." New York, NY. May 1968.
6. The Factory Insurance Association. "General Motors Corporation Fire (Detroit Transmission and Ternstedt Division)." Hartford Connecticut. August 1953.

Structures Fire Safety: The Brazilian Research Project

C. CALIL, JR., V. P. E SILVA, A. L. MORENO, JR., and J. M. NETO

ABSTRACT

This research has the aim to join the groups of University of Sao Paulo (USP) and University of Campinas (UNICAMP) in order to develop a numerical and experimental research in Structures Fire Safety through a global project for steel, concrete and timber structures. The objective is provides safe and economic recommendations, adequate to Brazil, as well as aggregate researchers from different Universities. As a final contribution, to propose recommendations for the design and construction of fire safety structures.

INTRODUCCION

The resistance of structural elements is reduced under fire situation, due the burned area reduction (timber), spalling (concrete) or material strength reduction when exposed to high temperatures. Recently, in Brazil, were published Brazilian Standards for steel and concrete structures fire design (NBR 14323:1999[1]/NBR 15200:2004[2]), and looking forward timber structures under fire situations. In some States, specific codes are published also. The financial support and interest in research about structures in fire must be increased, because the aim of structures in fire is to prevent the collapse, allowing enough time for safe evacuation of building occupants, safe fire fighting operations and reductions in damage neighboring construction. This can be carried out by analyzing structural behaviors by numerical and experimental model, considering geometric and materials non-linearity about

Carlito Calil Jr, University of São Paulo, Av. Trabalhador Saocarlense 400, São Carlos, 13566590,SP, Brazil

Valdir Pignatta e Silva, University of Sao Paulo, Av. Prof. Almeida Prado, trav 2, n.271, CEP 05508-900 Sao Paulo, SP, Brazil

Armando Lopes Moreno Jr, Campinas University, Av. Albert Einstein, 951 - Caixa Postal: 6021 - CEP: 13083-852 - Campinas – SP - Brazil

Jorge Munaiar Neto, University of Sao Paulo, Av. Trabalhador Sao carlense 400, São Carlos, 13566490,SP, Brazil

building in fire context, in consequence of mechanical properties reductions in fire situation. The complexity of fire situations analysis need computers and specific software which provides mechanical, thermal and coupled analysis, in association with experimental procedures, looking forward a group work in Brazilian and worldwide context. Both University of Sao Paulo (USP) and University of Campinas (UNICAMP), with support of FAPESP and others, had been providing numerical and experimental studies. For this purpose master of science, doctoral and pos doctoral researches start to be developed using the funds of FAPESP to acquire software's for numerical analysis and with the purpose to make the experimental research of structural elements in fire a furnace was designed following the rules of the ASTM E119[3]. The furnace will be install in the Structure Laboratory(LE) of the Department of Structural Engineering of School of Engineering of Sao Carlos of the University of Sao Paulo. The furnace was constructed by the Brazilian Industry Master Fiber of Sao Paulo State. This work aims to give details of the theoretical, numerical and experimental research program

RESEARCHES IN DEVELOPMENT

MSc RESEARCH:

Behavior of the concrete slab and composite slab steel-concrete in fire: Mariele Gonçalves[4]

The objective of this topic is to analyze the behavior of the slab in fire, since the influence of the axial restraint against the thermal expansion until the membrane effects. The software Vulcan can be used in this research.

Concrete columns under symmetric fire: Paulo Henrique Lubas[5]

The aim of this theme is to elaborate software to build a interaction curves between bending moment vs normal force for concrete columns in a symmetric fire. Sensibility parametric analysis will be also made.

Numerical analysis of compressed steel columns considering the restraint axial displacement on fire condition - Jonas Benedett Dorr[6]

The aim is to present a numerical study of steel columns with of type I open section, whereas the compartment of the environment in fire. Using commercial code ANSYS, the numerical model considers temperature dependent properties, cross section temperature gradient, radiation emissivity 0.7, heat loss at opposite face and axial restraint.

DOCTORAL RESEARCH:

Temperature on external steelwork in fire: Macksuel Soares de Azevedo)[7]

The aim of this topic is to analyze the method proposed by Eurocode, to develop software based on it and compare it with results from numerical CFD software Smartfire and experimental tests. Practice tools will also be made.

Cold formed steel columns in fire - Igor Pierin[8]

This thesis aims the elaboration of software based on the method of finite strips, including geometric and material non linear analysis of the cold formed steel column. A preprocessor for thermal analysis is also included in this research.

Development and application of computational code for analysis of steel structures in fire situation- Ronaldo Rigobello[9]

The objective of this topic is the development and application of a computational code, with basis in the Finite Element Method (FEM) and the positional formulation, for thermo-mechanical analyses of steel frame structures when exposed to typical thermal actions of fire situations.

Numerical and experimental analysis of compressed cold-formed steel members submitted to high temperatures - Saulo José de Castro Almeida[10]

This project aims enhancing understanding of the behavior of cold-formed steel columns at elevated temperatures via experimental and numerical analysis in order to help to improve the Brazilian and international design codes procedures.

Structural behavior of cold-formed steel double-angle under fire condition: Érica Fernanda Aiko Kimura[11]

The present study aims to raise the main aspects related to the structural behavior and strength of such sections under fire condition. The future presented results will be important in order to review specific technical documents and therefore consider thermal effects in design of cold-formed steel structure.

Evaluation of the effectiveness of the process of heat treatment on the strength and durability of wood to forest planted in brazil – Marcio Rogério da Silva[12]

The aim of this topic is evaluation numerical and experimental of the performance of dowel-type shear connectors in composite timber-concrete test specimens, considering the thermal effects.

Spalling of fire exposed concrete – Adriana A. Ambrósio de Souza [13]

The intention of this topic is to identify some preconditions for spalling and some limits within which spalling may occur. For this purpose a test method to identify the probability of spalling have been proposed.

Fire Resistance of Axially Loaded Slender Concrete Filled Steel Tubular Columns – Geraldo Silveira Leite Junior[14]

This project aims enhancing understanding of the experimental behavior of concrete filled steel tubular columns in fire situation.

POS-DOCTORAL RESEARCH:

Steel connections of composed wood concrete deck in fire: Julio Cesar Molina[15]

The aim of this topic is evaluation numerical and experimental of the performance of dowel-type shear connectors in composite timber-concrete test specimens, considering the thermal effects.

THE NUMERICAL ANALYSIS

For the numerical analysis the group did the acquisition of the software Super Tempcalc. It is a two-dimensional, thermal, finite element program. The program solves the two-dimensional, non-linear, transient, heat transfer differential equation incorporating thermal properties which vary with temperature. Structures comprising of several materials can be analyzed. Heat transferred by convection and radiation at the boundaries can be modeled as a function of time. Super Tempcalc has been validated against a large number of fire tests since 1985 both in Sweden and abroad.

DESIGN AND CONSTRUCTION OF A FURNACE

With the purpose to make the experimental research of structural elements in fire a furnace was designed following the rules of the ASTM E119[15]. The furnace will be install in the Structure Laboratory(LE) of the Department of Structural Engineering of School of Engineering of Sao Carlos of the University of Sao Paulo. The Department of Structural Engineering began whose activities in 1955 named Department of Structures and Architecture, and together with other departments and research and support centers, is part of the University Of Sao Paulo Sao Carlos School Of Engineering (EESC-USP). The EESC, whose activities began in 1953, currently offers the following graduate courses: Civil Engineering, Mechanical Engineering, Electrical Engineering, Computer Engineering, Mechatronical Engineering, Mechanical Production Engineering, Aeronautical Engineering, Environmental Engineering, Architecture and Urbanism. The graduate programs began officially in 1970. Within the graduate ambit, the Department is responsible for the Structural Engineering Program, which is offered only *stricto sensu*. The Department also has experience in *lato sensu* programs. The Structural Engineering area today has 101 graduate students, 48 on master's level and 53 on doctoral level, most of them holders of grants from various research funding agencies. To date, SET has awarded 163 doctoral and 396 master's degrees

The furnace was constructed by the Brazilian Industry Master Fiber of Sao Paulo State.[16] The main characteristics of the furnace are:

- Size: 3.000 mm width, 1.500 mm deep and 4.000 mm length
- Bottom surface: aisled concrete of high strength and refractory bricks for maximum temperatures of work of 1260 ° C;
- Lateral walls and cover: fiber ceramic with 200 mm of thickness and 160 kg/m³ of density;
- Structure box made of SAE 1020 steel of 5 mm thick reinforced and welded to avoid deformations;
- Combustion 8 burners of high speed type Kromschröder, with total power of 3.600 kW (3.096.000 kcal/h);
- Combustion control: proportional with operation system of “ On-Off” (high /low flame);
- Temperature control: the temperature control furnace is made using PLC, install in the control panel working continuously with the medium of the values of nine points temperature readings;

- Graphics readings: to register, the reading values during the tests,
.Details of this furnace is presented in figures 2 and 3.

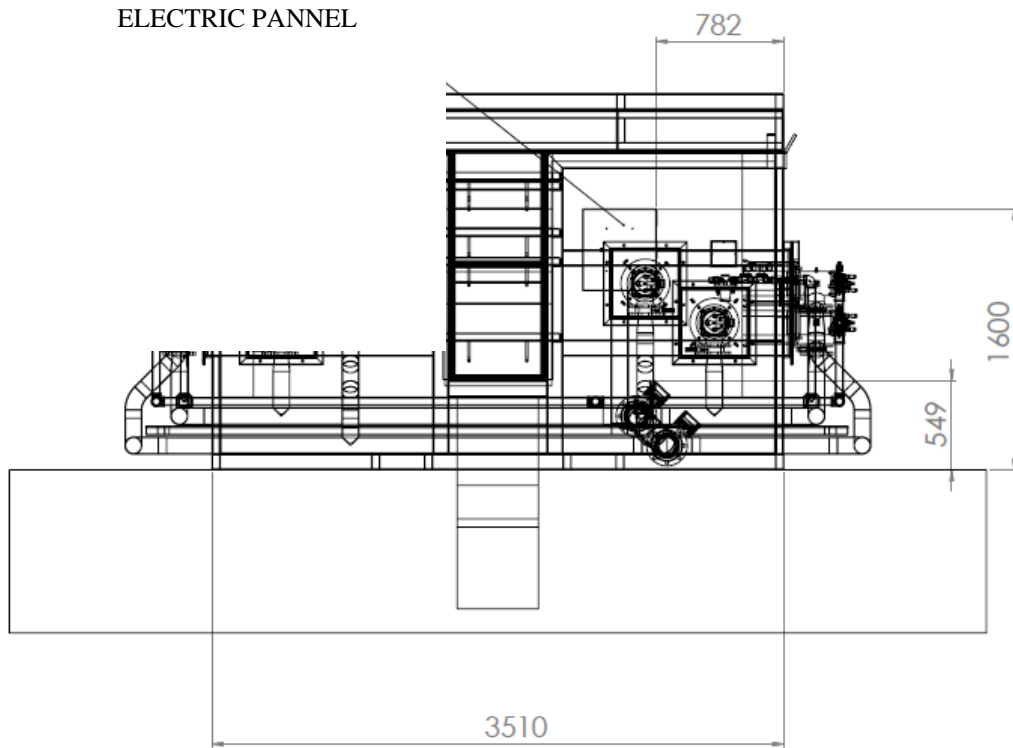


Figure 2. Furnace elevation drawing.

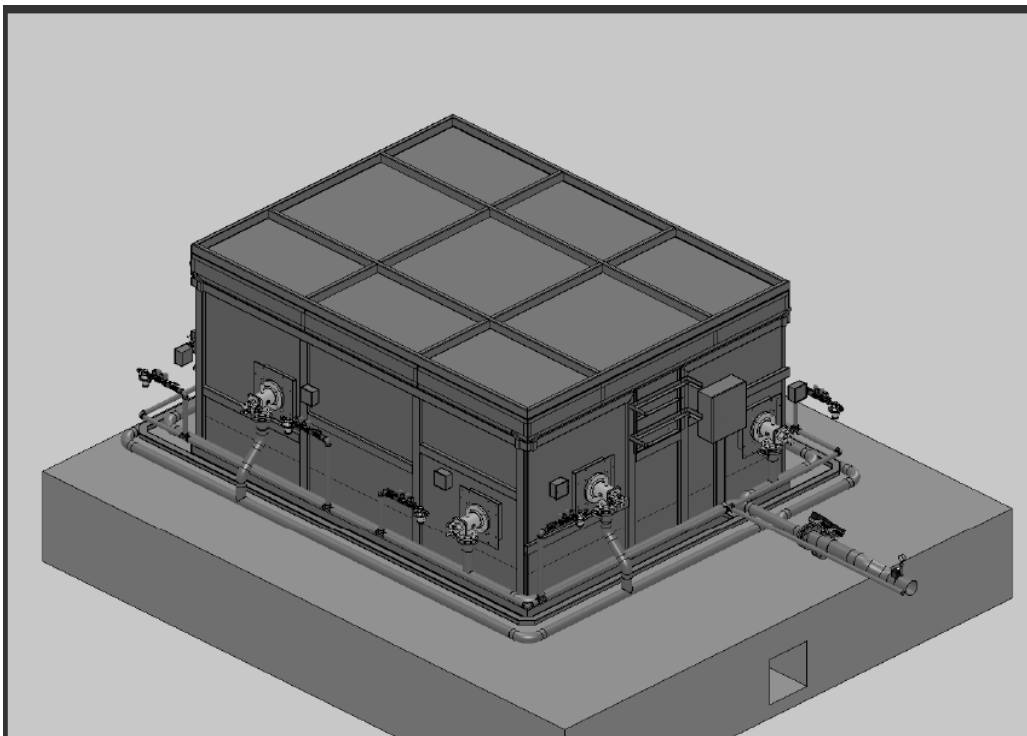


Figure 3. Furnace picture

PRELIMINARY PROGRAM FURNACE TESTS SCHEDULE FOR THE FAPESP RESEARCH PROJECT

The following program furnace tests are schedule for the FAPESP research project:

Concrete structures

- To propose recommendations for the design and construction of fire safety structures based on Brazilian Codes NBR 6118:2003[17], NBR 8681:2003[18] e NBR 15200:2004[2];
- Analysis of the behavior of ribbed slabs usually constructed in Brazil;
- Analysis of thermal deformations usually not considered in concrete;
- Tests of concrete beams and columns with load in fire situation.

Steel structures and composite concrete-steel structures

- To propose recommendations for design of these structures including cold formed steel, composite steel-concrete structural elements and connections, concrete and masonry and steel framing also analyzing the influence of thermal protections.:- Composite steel-concrete beam tests used in composite slab according ASTM E119 (2007), with the aim of determine the effect of beam dilatation;
- Tests in steel structural elements with fire protection in order to determine the thermal properties of these materials based in a simple test and theoretical analysis..

Timber structures and composite timber-concrete structures

- Charring rate properties determination of tropical and reforestation wood species of structural elements;
- Thermal structural anlysis of strutral timber elements;
- Tests in composite timber-concrete plates under load in fire situation.
- Experimental tests in shear connectors of the composite timber-concrete specimens and beams considering fire conditions.

REFERENCES

1. ASSOCIAÇÃO BRASILEIRA DE NORMAS TÉCNICAS . Exigências de resistência ao fogo de elementos construtivos de edificações - Procedimento. NBR 14432, 2000.
2. ASSOCIAÇÃO BRASILEIRA DE NORMAS TÉCNICAS Projeto de Estruturas de Concreto em situação de Incêndio. NBR15200, 2004.
3. AMERICAN SOCIETY FOR TESTING AND MATERIALS. ASTM E119 – fire tests of building construction and materials (CD ROM). Philadelphia. 2007
4. GONÇALVES, M. Behavior of the concrete slab and composite slab steel-concrete in fire. Dissertation for Master Degree to be presented to Polytechnic School of the University of Sao Paulo
5. LUBAS, P. H. Concrete columns under symmetric fire. Dissertation for Master Degree to be presented to Polytechnic School of the University of Sao Paulo
6. DORR, J. B., Numerical Analysis Of Steel Columns Considering The Restraint Axial Displacement On Fire Condition, (under construction), São Carlos-SP, Brazil, 2009

7. AZEVEDO, M. S. Temperature on external steelwork in fire 302 p. Thesis for Doctoral Degree presented to Polytechnic School of the University of Sao Paulo Sao Paulo, 2010.
8. PIERIN, I. Cold formed steel columns in fire. Thesis for Doctoral Degree to be presented to Polytechnic School of the University of Sao Paulo
9. RIGOBELLO, R. Development and application of computational code for analysis of steel structures in fire. Research Proposal Report, 158 p., São Carlos Sao Paulo, Brazil, 2009
10. ALMEIDA, J. C. A., Numerical and Experimental Analysis of Compressed Cold-Formed Steel Members Submitted to High Temperatures. Research Project: CNPQ, 25p., São Carlos → Sao Paulo, Brazil, 2009.
11. KIMURA, E. F. A., Structural Behavior of Cold Formed Steel Double Angle under Fire Condition. Research Project Report: CAPES, 32p., São Carlos Sao Paulo, Brazil, 2009.
12. MOLINA, J. C., Study of metallic connections of composite systems of wood-concrete in situation of fire – Partial scientific report: FAPESP, 59p., São Carlos-SP, Brazil, 2009.
13. MASTER FIBER Fornos Industriais Ltda. Tabuão da Serra, SP, Brazil.
14. ASSOCIAÇÃO BRASILEIRA DE NORMAS TÉCNICAS Projeto e execução de obras de concreto simples, armado e protendido – Procedimento. NBR 6118, 2001.
15. ASSOCIAÇÃO BRASILEIRA DE NORMAS TÉCNICAS Ações e segurança nas estruturas. Procedimento. NBR 8681, 1984.

ACKNOWLEDGMENTS

The authors thank the State of Sao Paulo Research Foundation (FAPESP) for the financial support for this research.

Overview of the AISC Specification Appendix 4—Structural Design for Fire Conditions

N. IWANKIW and B. R. ELLINGWOOD

ABSTRACT

The American Institute of Steel Construction (AISC) has historically taken a prominent leadership role in the development of structural steel design and steel fire protection in the United States. AISC issued a *Specification for Fireproofing Structural Steel Buildings* as early as 1927, which was based on the standard fire test method for construction developed by ASTM, and was published as part of the *AISC Steel Construction Manual* through its 4th Edition of the 1950's era.

Modern provisions for structural design for fire conditions were introduced for the first time in Appendix 4 of the 2005 edition of the *AISC Specification*, which now has been revised and updated for 2010.

This paper provides an overview of Appendix 4 of the AISC Specification, including the recent 2010 updates and what they could mean for advancing structural engineering for fire conditions in the US. These design criteria were developed by an AISC Specification Task Committee (TC8) and were approved by the full AISC Committee on Specifications through the ANSI voluntary consensus standard approval process, which enables their direct adoption by reference into the US building codes. Appendix 4 provisions address identification of fire scenarios and fire exposures, behavior of materials at elevated temperatures, and performance of structural elements and systems at elevated temperatures.

Nestor R. Iwankiw, Hughes Associates, Inc., 5953 N. Oconto Ave, Chicago, IL 60631, U.S.A.

Bruce Ellingwood, Georgia Institute of Technology, 790 Atlantic Drive, Atlanta, GA 30332-0355, U.S.A.

INTRODUCTION

The American Institute of Steel Construction (AISC) has long been the lead organization in the development of structural steel design and steel fire protection criteria in the United States. AISC issued a *Specification for Fireproofing Structural Steel Buildings* as early as 1927, which was based on the standard fire test method developed by ASTM, and was published as part of the AISC *Steel Construction Manual* through its 4th Edition. Modern provisions for structural steel design for fire conditions were introduced for the first time in Appendix 4 of the 2005 edition of the *ANSI/AISC Specification* [1] (see Figure 1), which now has been revised and updated for 2010. It permits project compliance to be accomplished either by performance-based structural fire engineering or by the traditional qualification testing.

ANSI/AISC 360-05
An American National Standard

Specification for Structural Steel Buildings

March 9, 2005

Supersedes the *Load and Resistance Factor Design Specification for Structural Steel Buildings* dated December 27, 1999, the *Specification for Structural Steel Buildings—Allowable Stress Design and Plastic Design* dated June 1, 1989, including Supplement No. 1, the *Specification for Allowable Stress Design of Single-Angle Members* dated June 1, 1989, the *Load and Resistance Factor Design Specification for Single-Angle Members* dated November 10, 2000, and the *Load and Resistance Factor Design Specification for the Design of Steel Hollow Structural Sections* dated November 10, 2000, and all previous versions of these specifications.

Approved by the AISC Committee on Specifications and issued by the
AISC Board of Directors



AMERICAN INSTITUTE OF STEEL CONSTRUCTION, INC.

One East Wacker Drive, Suite 700
Chicago, Illinois 60601-1802

Figure 1. 2005 AISC Specification—First To Include Modern Steel Fire Design Provisions

The worldwide move toward performance-based fire engineering has reinforced the need for such provisions in the US, and has provided invaluable research and information sources for fire-resistant structural design. The state-of-the-art knowledge in the field has advanced to the point where structural and fire protection engineers should be provided the opportunity to develop creative alternative and economical solutions for passive fire protection applications. In addition, there exist special, more critical, or unusual design conditions where performance-based fire engineering will provide the better, or only, option for achieving a reliable solution to mitigate fire-induced structural damage and potential for collapse.

This paper presents an overview of Appendix 4 of the AISC Specification, including the recent 2010 updates, and their advancement of structural engineering design options for fire conditions in the US. These criteria were developed by TC8 and were approved by ballot of the full AISC Committee on Specifications through the ANSI voluntary consensus standard approval process, which enables their direct adoption by reference into the US building codes. The Appendix 4 provisions deal with identification of fire scenarios and fire exposures, behavior of steel and concrete materials at elevated temperatures, and performance of structural elements and systems at elevated temperatures. The expected key role of related ancillary National Fire Protection Association (NFPA) and Society of Fire Protection Engineers (SFPE) documents (which are still under committee development) on fire loads, natural fire curves, and heat transfer will also be outlined.

This Appendix 4 of the *AISC Specification* is divided into the following three major sections:

- 4.1. General Provisions
- 4.2. Structural Design for Fire Conditions by Analysis
- 4.3. Design by Qualification Testing

Section 4.3 on qualification fire testing only recognizes use of the conventional prescriptive rating practices for fire resistance, as determined via the ASTM E119 [2] standard for building construction fire tests and specified by the governing building code. Demonstration of compliance with these requirements is also explicitly allowed through use of the simpler computational procedures for steel construction given in Section 5 of SEI/ASCE/SFPE Standard 29-05, *Standard Calculation Methods for Structural Fire Protection* [3].

The new criteria discussed further in this paper are contained within Sections 4.1 and 4.2 of AISC Appendix 4. An extensive Commentary supplements these design provisions with explanatory information, references, additional analytical/design data and guidance. This Commentary represents essential reading for all practitioners, but especially those unfamiliar with the subject. In the remainder of this paper, the formal distinctions between the mandatory Appendix 4 provisions and its advisory Commentary will not be made to simplify the overview.

GENERAL PROVISIONS

Section 4.1 on “General Provisions” provides a “road-map” in defining the performance objectives, engineering analysis and qualification testing alternatives, and load combination/required strength.

The underlying performance objective is one of life safety. The structural elements and framing must maintain their load-bearing function during the design-basis fire and satisfy other performance requirements, including deformation criteria, for the particular building occupancy. Explicitly included is the requirement that forces and deformations arising from the design-basis fire not cause a breach of its vertical or horizontal compartmentation.

The *required structural strength* for the design-basis fire is to be determined from the following gravity *load combination*, including any notional loads necessary for checking frame/member stability:

$$[0.9 \text{ or } 1.2] D + T + 0.5 L + 0.2 S \quad (1)$$

where

D = nominal dead load

L = nominal occupancy live load

S = nominal snow load

T = nominal forces and deformations due to the design-basis fire (or other extreme event)

This load combination is taken from Section 2.5.2.1 of *SEI/ASCE Standard 7-10* [4] governing general design under extreme events, characterized as low probability but potentially high-consequence occurrences, such as uncontrolled fires, explosions, sabotage, or vehicular impacts. The nominal D , L and S loads are defined as specified in *SEI/ASCE 7* or in the applicable building code. Only LFRD (limit states or strength) design procedures are permitted when using this load combination.

STRUCTURAL DESIGN FOR FIRE CONDITIONS BY ANALYSIS

Section 4.2 is the most comprehensive part of AISC Appendix 4 and has the most pertinent content for performance-based structural fire engineering applications. As stated in the opening paragraph of Appendix 4, the key characteristics to be analyzed in this design option are the heat input, thermal expansion, material property degradation at high temperatures, and the associated loss of strength and stiffness of the structural members and frame. Again, LFRD (limit states or strength) design procedures are required to be used exclusively in this regard because of the potentially highly non-linear nature of the structural fire response experienced during sustained exposures to elevated temperatures.

For the design-basis fire, the main characteristics and required variables (such as fuel load density, ventilation, duration, and pertinent spatial dimensions) of localized, compartment post-flashover, and exterior fire exposures are provided. These are only verbally described and without any given equations or quantitative data because it is expected that documents from NFPA and SFPE will become available to provide the necessary detailed information. Appropriate references for their detailed assessment and actual computations are given to the existing technical literature, most notably ECCS, 2001 [5] and the SFPE Handbook [6]. Consideration of active fire suppression system effects in the determination of the design-basis fire is allowed, but specific exposure factors not provided, aside from a

general Commentary reference to the potentially maximum 60% reduction in fuel loads allowed in the Eurocodes for automatic sprinkler installation.

Heat transfer analyses for the selected design-basis fire are stipulated in a general manner, with the features, limitations and possible complexity levels of different modeling approaches summarized. The iterative equations for solution of the simplest lumped mass, first-order heating of both unprotected and protected steel members are provided, together with the special case of an exterior fire exposure. The much broader two- and three-dimensional capabilities of advanced computer (numerical) methods are briefly outlined. The lumped mass approach can only predict a uniform material temperature within a given member, which could be gross approximation of the actual more complex thermal gradients that may occur in all three directions.

The remainder of Section 4.2 covers the more direct structural aspects of this design problem, including reduction of steel and concrete material mechanical properties at high temperatures, strength and deformation limits, and methods of analysis.

Elevated material properties, as derived from tests, are permitted for this type of analysis and design. If project-specific data are unavailable, the set of default values given in Section 4.2.3 are permitted. These tabulated material property retention ratios (value at elevated temperature to benchmark value at ambient) for steel are elastic modulus, proportional limit, yield and ultimate strength are adopted from ECCS, 2001 [5] and are consistent with those given in the Eurocodes. In similar format and from the same sources, design retention ratios for the compressive strength of concrete, its elastic modulus, and ultimate strain are also given, with property distinctions noted between normal and light weight concretes.

The all-important central performance requirement of Appendix 4, Section 4.2.4.1 for structural integrity states the following:

The structural frame shall be capable of providing adequate strength and deformation capacity to withstand, as a system, the structural actions developed during the fire within the prescribed limits of deformation. The structural system shall be designed to sustain local damage with the structural system as a whole remaining stable.

Continuous load paths shall be provided to transfer all forces from the exposed region to the final point of resistance. The foundation shall be designed to resist the forces and to accommodate the deformations developed during the design-basis fire.

Forces and deformations caused by the design fire are to be analyzed for their effects on individual structural members, their connections, and the entire framing system. In the advanced analysis method option, both thermal and mechanical effects must be included in conjunction with the temperature-dependent material properties. Two- or three-dimensional computer models and software with appropriate nonlinear capabilities will be necessary for this type of solution.

The other alternative offered in the AISC Appendix 4 is a simple analysis focused on individual structural members, whose support and thermal restraint conditions can be assumed to remain unchanged from those existing at ambient.

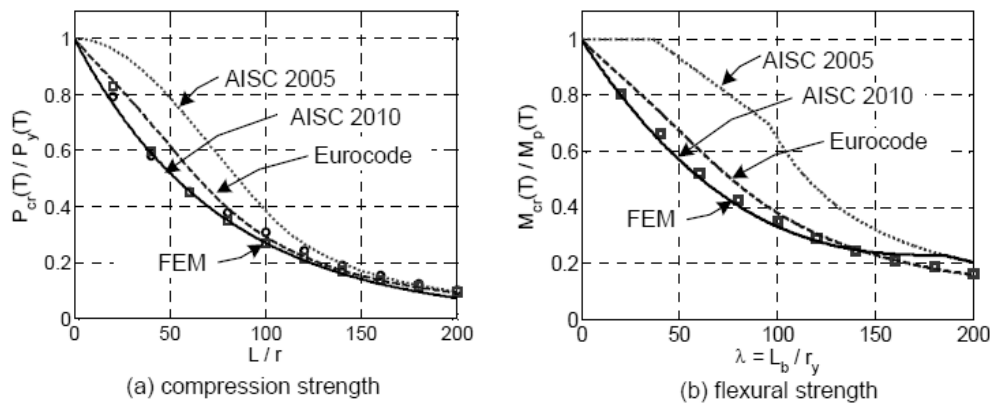


Figure 2. Comparisons of Compression and Flexural Strengths at 500°C [7].

Above 204 °C (400 °F) steel temperatures, the degradation effects in material properties must be included; otherwise, it may be omitted for lower temperatures. Thermally-induced strains must be incorporated in all cases. Some approximate and conservative temperature field assumptions are provided for steel tension, compression, and bending members to enable a much quicker design solution. A substantive change made in the recent 2010 criteria introduced new equations for column and beam stability at high temperatures [7], which more accurately represent their response at high temperatures. These equations now better represent the results of nonlinear finite element solutions and tests, and which correspond more closely to the Eurocode provisions, see Figure 2.

RELATED NEW DOCUMENTS in US

The more abstract, complex and less understood parts of this design problem, at least for most structural engineers and architects, as well as building officials, who are not familiar with the subject, are the actual determination of the natural (design-basis) fire exposure profile and analysis of the heat transfer that converts this particular load-demand into temperatures of the structural material(s). It is probable that collaboration with fire protection engineers will be necessary in many situations involving fire-resistant structural design. These initial steps of the problem definition are substantially different from the traditional prescriptive fire resistance ratings, wherein the standard ASTM E119 fire and its acceptance criteria for tested assemblies had served as a convenient surrogate for these types of real issues for nearly a century. Therefore, explicit design/analysis guidance is essential to further its applications in the US, as had been done in other countries.

Three new related draft standards are currently still under development by the Society of Fire Protection Engineers (SFPE) and National Fire Protection Association (NFPA):

1. SFPE – Fire Design Exposures
2. SFPE – Prediction of Thermo-mechanical Response of Fire Resistive Construction
3. NFPA 557 – Standard for Determination of Fire Load for Use in Structural Fire Protection Design

The two SFPE documents are intended to provide more extensive and rigorous analysis/design provisions for the calculation of a limited set of bounding natural time-temperature curves for compartment and local fires, together with further design aids and guidance in heat transfer computations for structural members. NFPA 557 will establish procedures and some default values for quantifying fuel design loads in different types of buildings and occupancies, which is a critical input variable in the characterization of the design-basis fire and its effects. These three draft documents remain works in progress, which have not undergone full review, approval, or public release. Their final completion and availability is not imminent and estimated to be on the order of 1-2 years away. Once these supplementary standards become officially released, they will be directly referenced in the AISC Appendix 4.

CONCLUSIONS

The design standards and code community in the US, including organizations such as AISC, SFPE, ASCE, NFPA, and ICC, is still in the process of developing design-oriented information, documents and references for use in this country. The 2005 ANSI/AISC 360-05 Specification and its successor 2010 edition now contains Appendix 4 on methods that enable engineered structural fire protection design of steel buildings. International sources have and continue to provide important cornerstones in these developments. Additional research in this area is also being identified and pursued.

Performance-based fire design is still an emerging design option in the US. Its use to date has been mainly confined to select notable large or special projects in which fire effects were considered particularly unique, critical or complicated in terms of life safety. While traditional fire protection methods have served the public well from a life safety standpoint, structural engineers should be provided the opportunity to add value to the building process through their professional services. The availability of more design information and guidelines in this regard is likely to lead to increased interest and applications.

REFERENCES

1. ANSI/AISC. 2005. *Specification for Structural Steel Buildings*. American Institute of Steel Construction (AISC), Chicago, IL. p. 360.
2. ASTM E119. *Standard Test Method for Fire Tests of Building Construction and Materials*. American Society for Testing and Materials (ASTM), West Conshohocken, PA.
3. ASCE/SFPE. 2005. *Standard Calculation Methods for Structural Fire Protection*. Structural Engineering Institute of the American Society of Civil Engineers, Reston, VA, p. 29.
4. SEI/ASCE. 2010. "Minimum Design Loads for Buildings and Other Structures," American Society of Civil Engineers (ASCE), Reston, VA, pp. 7–10.
5. ECCS. 2001. "Model Code on Fire Engineering," European Convention for Constructional Steelwork (ECCS), Technical Committee 3, First Edition, May, 2001, Brussels, Belgium, p. 111.
6. SFPE. 2008. *SFPE Handbook of Fire Protection Engineering*. Society of Fire Protection Engineers (SFPE), 4th Edition, Bethesda, MD.
7. Takagi, J. Deierlein, G.G. 2007. "Strength Design Criteria for Steel Members at Elevated Temperatures," *Journal of Constructional Steel Research*, 63:1036–1050.

Determining the Moment-Curvature Diagram of Aluminium Cross-Sections in Fire; A Numerical Code and Practical Examples

O. R. VAN DER MEULEN, J. MALJAARS, F. SOETENS and L. TWILT

ABSTRACT

The use of aluminium as a construction material has been increasing since its first invention. At present, limited knowledge of the behaviour of aluminium beams in fire gives rise to excessively high insulation demands, decreasing its competitiveness. To study the behaviour of (statically undetermined) bending members in fire, it is required to know the moment-curvature diagram. For aluminium and stainless steel at both room and elevated temperatures, and for steel at elevated temperatures, this curve cannot be calculated analytically, but needs to be obtained numerically. A versatile numerical code is presented, capable of calculating the moment-curvature diagram for arbitrary geometries along any axis with arbitrary temperature and initial strain distributions.

INTRODUCTION

Aluminium alloys are a class of construction materials with many favourable properties for the construction industry; its excellent corrosion resistance, generally not requiring a coating system; a low self weight, its density being only a third of that of steel; and the possibility to produce highly optimized cross-sections through extrusion, often integrating load carrying with other functions such as fastening systems. These advantages outweigh its higher material costs in many instances, and the usage of aluminium in the construction industry has therefore been constantly increasing [8]. At present, the industry accounts for nearly 15% of the North-American aluminium consumption [13].

A less favourable property of aluminium and its alloys is their relatively low melting points of approximately 550 to 600°C, and a decrease of load carrying potential at lower temperatures, as demonstrated in figure 1. This figure shows the majority of the reduction in strength to take place in a temperature range between 150 and 350°C,

O. R. van der Meulen, MSc, PhD student *,†,‡,(r.vandermeulen@m2i.nl)

J. Maljaars, MSc PhD, Senior researcher ‡

F. Soetens, Prof. MSc †,‡,

L. Twilt, MSc, Senior researcher (ret.)‡

* Materials innovation institute (M2i), Delft, the Netherlands

† Eindhoven University of Technology, the Netherlands

‡ TNO Built Environment and Geosciences, Delft, the Netherlands

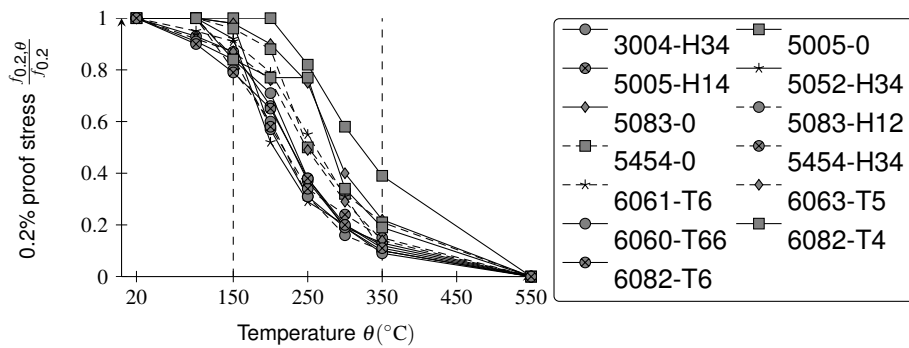


Figure 1. The reduction of 0.2% proof stress of common aluminium alloys at elevated temperatures. Its value at elevated temperatures ($f_{0.2,\theta}$) is normalized to the room temperature value ($f_{0.2}$). Source:[3], after: [7].

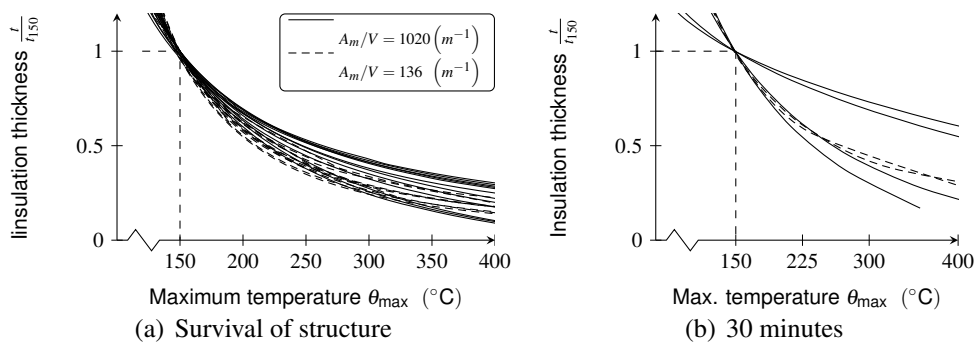


Figure 2. The required normalized, insulation thickness as a function of the maximum allowable temperature in the member. Two conditions are considered, the first (a) the structure surviving the fire, and the second (b) the structure withstanding the fire for at least 30 minutes. A dwelling with a fire load density of 948 MJ/m^2 and an area of 200 m^2 is assumed. The insulation thickness t is normalized to the thickness (t_{150}) for a maximum member temperature of 150°C . The opening conditions are varied between a partial opening in the 10 m short façade of the structure and two fully open, 20 m long façades. Two area-over-volume ratios A_m/V are considered as are three active measure factors ($\Pi\delta_n \in \{0.78, 0.50, 0.26\}$). The insulation material is a type of rockwool. It is noted that for an office of 800m^2 , the results are nearly identical. Source:[7], modified from: [5].

which is therefore the main temperature range of interest for fire design.

As the temperatures associated with fire easily exceed these values, insulation is generally required. The thickness of which decreases as the maximum allowable temperature is increased. Figure 2 shows the reduction in the required insulation thickness, for a fire according to the *natural fire safety concept* or NFSC [11], obtained from a study by Maljaars [7]. There is a 65 to 85% reduction in the required insulation thickness as the maximum allowable temperature in the member is increased from 150 to 350°C . An accurate knowledge of the behaviour of aluminium members and their maximum allowable temperature thus results in significant savings in insulation costs, even allowing unprotected members in certain low fire load density applications, such as transport facilities [7].

In the study of the behaviour of bending members, having knowledge of the moment-curvature curve is required. An example of such a study is given in [9], where the stabilizing effects of elevated temperatures in aluminium alloys for plastic design are examined. For aluminium and stainless steel at both room and elevated temperatures, and steel at elevated temperatures, obtaining moment-curvature diagrams for all but the simplest, idealized, cross-sections is analytically impossible. This is

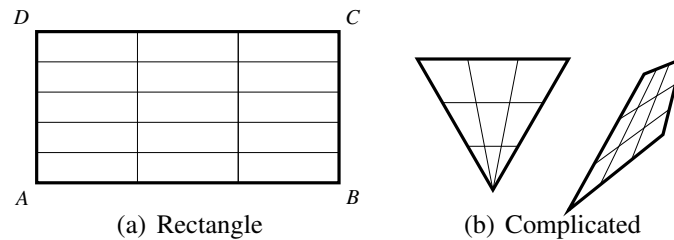


Figure 3. Shapes with their subdivision into elements. Shapes are defined by their four corner coordinates, but these may overlap, creating triangles. Complicated shapes are possible as long as the corner coordinates define a convex area.

because their stress-strain diagrams are inelastic and are described by a Ramberg-Osgood equation [10], which does not permit the stress to be calculated as a function of the strain explicitly. In fire design, the situation is further complicated by effects as varying material properties as a result of uneven temperature distributions, and thermal expansion. It is for these reasons, numerical approaches were developed, for example [2] which separates the cross-section into smaller parts with equal material properties and thermal expansions and sums up their contributions to the moment resulting from a certain induced curvature. In this paper a more generally applicable code is presented, which allows the calculation of the moment-curvature diagram of any conceivable cross-sections, consisting of one or multiple different materials, subjected to a combination of normal and bending loads along an arbitrary axis, while taking into account thermal- and initial-stresses as desired.

SPECIFYING PROPERTIES

Geometry

The cross-section of a beam, prismatic in the out of plane direction, is performed by building it up from *shapes*. These shapes are polygons which may in principle have an arbitrary number of nodes, but four noded shapes are used here for ease of meshing. An example is shown in subfigure 3a, where a rectangle is defined by the coordinates *ABCD*. The shape does not need to be rectangular, any convex shape is permissible and even overlapping corner nodes are possible, the only non-trivial application being the definition of triangles. These examples are shown in subfigure 3b. In figure 3, all shapes are already subdivided into smaller entities known as *elements*. It is these elements that are used in the calculation. Properties as temperature, area, centroid, inertia, rotated coordinates and temperature dependent material models are assigned in pre-processing and are constant throughout the element. Their response to applied loads is calculated in the main algorithm and summed over all elements to produce the cross-sectional response.

Material models

All the elements belonging to a single shape share a single, temperature dependent, material model. Different material models or material models with different temperature dependent properties, may thus be combined in a single cross-section by dividing it into multiple shapes. This is useful when studying the effects of degenerated material properties in the heat affected zones near welds for example. It is possible to use an arbitrary material model, but because of the intended application to fire design, the Ramberg-Osgood [10] model is used throughout the paper.

PRE-PROCESSING

Rotated coordinates

The curvature can be specified by the user to operate about any line as specified by the angle α . A value of 0 indicating a curvature about the vertical axis, leading to compressive strains at the left hand side of the cross-section. The rotated coordinates are calculated by:

$$\begin{bmatrix} \hat{x}_i \\ \hat{y}_i \end{bmatrix} = \begin{bmatrix} \cos(-\alpha) & -\sin(-\alpha) \\ \sin(-\alpha) & \cos(-\alpha) \end{bmatrix} \begin{bmatrix} x_i \\ y_i \end{bmatrix}. \quad (1)$$

Geometric properties

The area of a non-self intersecting polygon is given by the surveyor's formula.

$$A_i = \frac{1}{2} \left| \sum_{j=1}^N (x_j y_{j+1} - x_{j+1} y_j) \right|, \quad (2)$$

where i is the element number, and j number of the node along the perimeter of the polygon, the total number of which is N , equal to 4 in this case. $x_{N+1} = x_1$, and $y_{N+1} = y_1$. The coordinates of the centroid of the polygon are equal to

$$\begin{aligned} C_{x,i} &= \frac{1}{6A_i} \sum_{j=1}^N (x_j + x_{j+1}) (x_j y_{j+1} - x_{j+1} y_j), \\ C_{y,i} &= \frac{1}{6A_i} \sum_{j=1}^N (y_j + y_{j+1}) (x_j y_{j+1} - x_{j+1} y_j). \end{aligned} \quad (3)$$

The second moment of area (inertia) is dependent on the direction of loading and is thus a function of the rotated coordinates (\hat{x}, \hat{y}) . The expression was obtained from [12]

$$I_{x,i} = \frac{1}{12} \sum_{j=1}^N (\tilde{y}_j^2 + \tilde{y}_j \tilde{y}_{j+1} + \tilde{y}_{j+1}^2) d_j, \quad (4)$$

where \tilde{x} and \tilde{y} are the coordinates in the rotated axis system relative to the centroid of the element; $\tilde{x}_j = \hat{x}_j - \hat{C}_{x,i}$ and $\tilde{y}_j = \hat{y}_j - \hat{C}_{y,i}$. d_j is equal to $\tilde{x}_j \tilde{y}_{j+1} - \tilde{x}_{j+1} \tilde{y}_j$.

Thermal expansion and initial stresses/strains

The free thermal expansion of each of the elements is obtained by multiplying the temperature T_i above the initial temperature T_0 , with a coefficient of (temperature dependent) thermal expansion.

$$\varepsilon_{th,i} = \alpha_{th,i}(T_i)(T_i - T_0), \quad (5)$$

The normal component of the cross-sectional thermal expansion may be restrained or not depending on the support conditions. For the unrestrained case, the normal component does not contribute to the stress, and needs to be subtracted. Initial stresses can be implemented by expressing them as strains

$$\varepsilon_{0,i} = \frac{\sigma_{0,i}}{E_i}, \quad (6)$$

while taking care to make them self balancing, or subtracting a normal component afterwards.

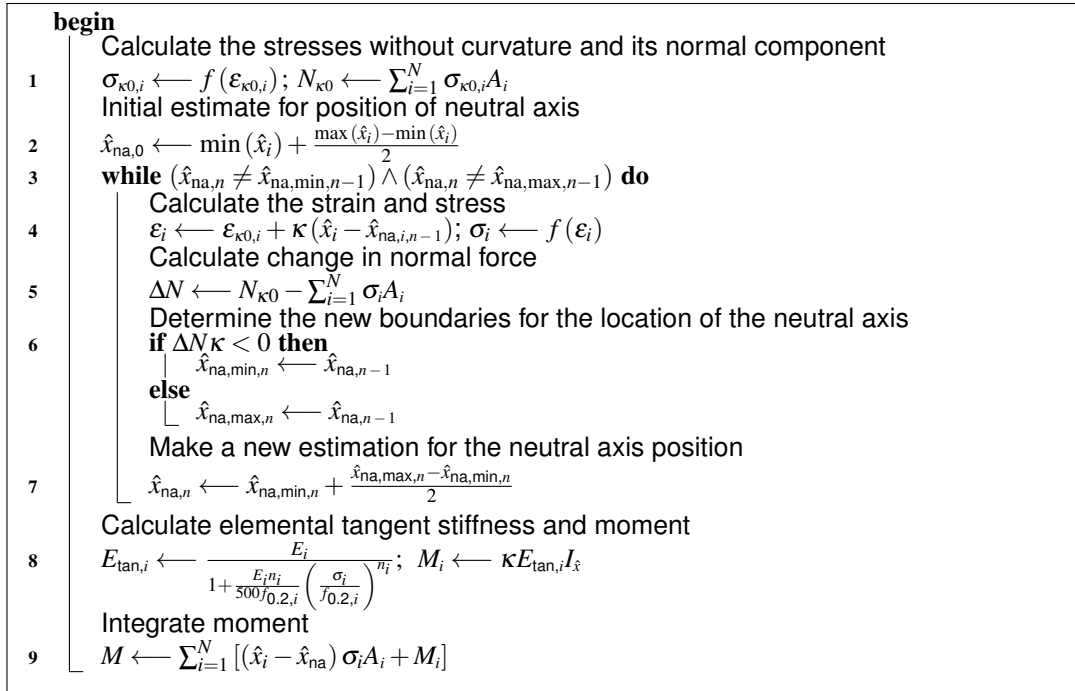


Figure 4. The main moment-curvature curve calculation algorithm.

THE MOMENT-CURVATURE CURVE CALCULATION ALGORITHM

The object of the algorithm is to find the strain and stress distribution in the cross-section for a number of independent calculation steps. Each calculation-step is characterized by a different curvature, all the calculation steps together forming a moment-curvature diagram. The algorithm is summarized in figure 4, the different steps are elaborated on hereafter, the number in the title corresponding to the number in the left hand margin of the algorithm.

1: Calculate stress without curvature The strain without curvature being is calculated by

$$\varepsilon_{\kappa 0,i} = -\varepsilon_{th} - \varepsilon_0 + \varepsilon_N. \quad (7)$$

The stress without the applied curvature ($\varepsilon_{\kappa 0,i}$), and its normal component, are then calculated and stored for efficiency. The implicit Ramberg-Osgood material model [10] is solved using a numerical, bi-section root finding algorithm [1].

2: Initial estimate for the position of the neutral axis The neutral axis at the current calculation step (n) is defined by the line $\hat{x}_{na,n} = \hat{x}$. The initial estimate $\hat{x}_{na,0}$ is determined by taking the average value of the minimum and maximum \hat{x} coordinate of all the centers of the elements in the cross-section.

3: Iterative procedure stop condition Finding the stress distribution in the cross-section is done in an iterative procedure because the location of the neutral axis is unknown a-priori. The procedure is using the bisection method, modified for floating point operations [1], and converges to the correct location of the neutral axis and corresponding stress-strain distribution until terminated by the stop condition.

4: Calculating stress and strains The stress is calculated by taking the strain without curvature $\varepsilon_{N,i}$ and adding the strain due to the curvature using the trial solution for the location of the neutral axis. The corresponding stress σ_i is then calculated.

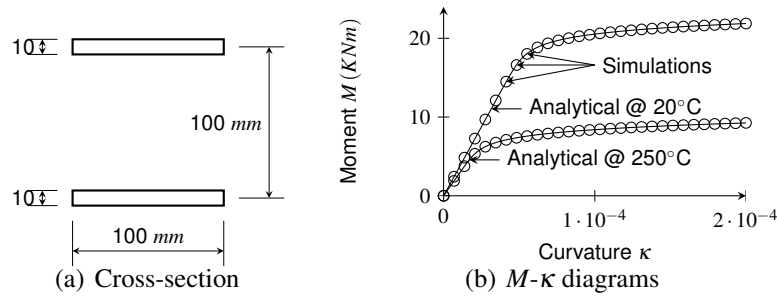


Figure 5. Verification case for the numerical code, a close to perfect bending member. The material used is AA6060-T66 with $f_{0.2} = 205$, $E = 7.0 \cdot 10^4$ and $n = 19$ at 20°C , and $n_\theta = 9$, $E_\theta = 5.46 \cdot 10^4$ and $f_{0.2,\theta} = 79$ at 250°C .

- 5: Checking the equilibrium** When the position of the neutral axis is chosen correctly, the applied curvature should not induce a change in normal force. This condition is verified here, and a deviation is expressed as ΔN .
- 6: Updating the bounds** Depending on the sign of the product of the applied curvature and ΔN , the bounds for the neutral axis position are adjusted.
- 7: Neutral axis position estimate** A new estimate is made for the position of the neutral axis. This is the mean value of the two bounds.
- 8: Tangent stiffness and in-element moment** because of the (small) bending stiffness of the elements themselves, a moment will be present in each element, which is denoted by M_i . To calculate the elemental moment, the tangent stiffness in the element ($E_{\text{tan},i}$) is calculated, and multiplied with the second moment of area as given in equation (4). By assuming a constant tangent moment throughout the element, a small error is introduced, as the real (tangent) stiffness is not constant.
- 9: Integrate moment** The moment is integrated across the cross-section and is used to derive a moment–curvature (M – κ) diagram. The contribution from the in-element stiffnesses M_i becomes very small as the number of elements is increased. For a mesh as shown in figure 6a, the term is completely irrelevant

VERIFICATION

To validate the numerical code, it is tested against analytical solutions for moment–curvature diagrams. As indicated before, such solutions are only obtainable for simple geometries. The case of a theoretical, perfect bending cross-sections with all mass in the outmost fibres, has its moment–curvature diagram expressed by

$$\kappa(M) = \frac{2}{h} \left[\frac{2M}{EA} + 0.002 \left(\frac{2M}{f_{0.2}A} \right)^n \right], \quad (8)$$

where A is the total area of the cross-section. Equation (8) is tested against the simulations for a cross-section as shown in figure 5a. The results of these simulations, and the analytically derived curves are presented together in figure 5b, demonstrating the proper functioning of the program.

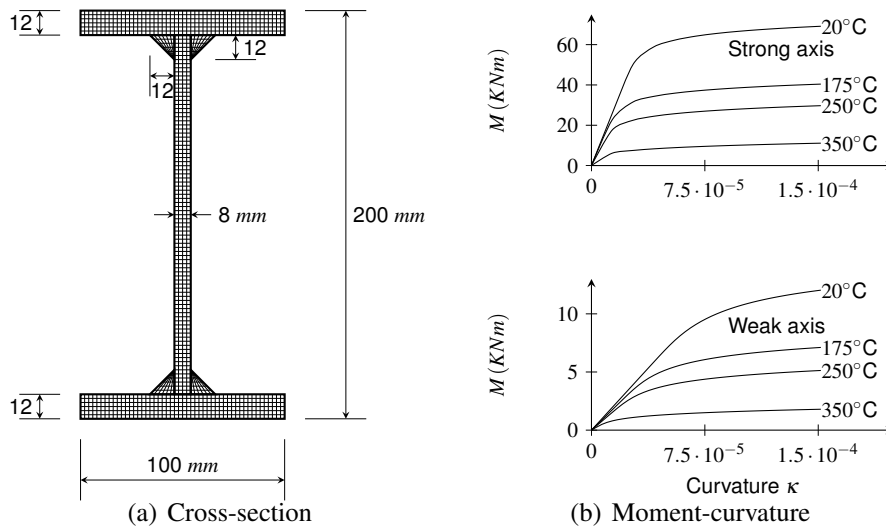


Figure 6. An I-section of AA6060-T66 subjected to a bending force along its weak and strong axis, at four different, constant temperatures. Material properties are taken from [6], thermal expansion is unrestrained.

PRACTICAL EXAMPLES

To illustrate the usability of the numerical code, an I-section with a geometry according to figure 6a is subjected to a bending force in its strong and weak direction for aluminium alloy 6060-T66 for a number of different temperatures. The resulting moment-curvature diagrams are given in figure 6b. At a curvature equal to $1.5 \cdot 10^{-4}$, the moment at 250°C is approximately 43% of the room temperature value for both bending directions. The value for the 0.2% proof stress at this temperature is only 38% of the room temperature proof stress [4], illustrating the potential savings of obtaining moment-curvature diagrams at elevated temperatures as opposed to scaling them by the 0.2% proof stress.

In a second example, the geometry as was given in figure 6a is subjected to a linear temperature gradient, ranging from the highest temperature at the lower flange of the cross-section, to the lowest temperature at the upper flange. This an arbitrary, but not unrealistic approximation of an insulated beam in fire conditions with a temperature drain such as a floor against its top flange. In figures 7a and 7b, we can see the moment-curvature curve for the beams subjected to a temperature gradient, compared to beams with a single, elevated temperature. From these figures it is clear that modeling a beam with a temperature gradient by a beam with a single temperature may be possible, but that taking the highest temperature in the gradient as the single temperature is over conservative. Taking a mean value for the temperature; 250°C gives reasonable results in the case of figure 7a, but is unconservative for the case of figure 7b. It is noted that this result is only applicable for situations where thermal expansion and instability effects do not play a role. No generally valid approximation can be given, underlining the need for a numerical calculation technique as the one offered in this paper.

CONCLUSIONS

For the economical design of aluminium structures, an accurate understanding of the behaviour of beams at elevated temperatures is required. To study the behaviour of such members, the moment-curvature diagram is required, which is generally unobtainable analytically. A numerical solution technique is presented, capable of

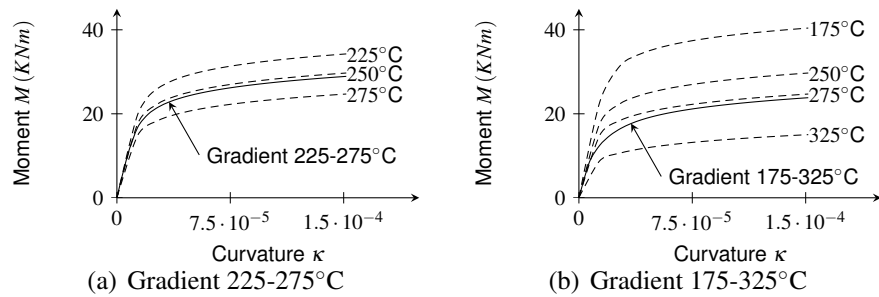


Figure 7. An I-section of AA6060-T66 subjected to a bending force along its strong axis with a temperature gradient along its height, the material properties are taken from [6], the thermal curvature is subtracted.

correctly calculating this curve for any cross-section, inelastic material, load direction and temperature distribution. The code was verified with the help of an analytical solution (which is available for certain idealized cross-sections) and shown to behave correctly. Practical examples are given for an I-section in bending, underlining the potential decrease in over-conservativeness as incurred by simpler approximations.

ACKNOWLEDGEMENT

This research was carried out under project number M81.1.108306 in the framework of the Research Program of the Materials innovation institute M2i (www.m2i.nl).

REFERENCES

- [1] Burden, R. L. and J. D. Faires (2004, December). *Numerical Analysis* (8 ed.). Brooks Cole.
- [2] Burgess, I. W., J. A. El-Rimawi, and R. J. Plank (1990). Analysis of beams with non-uniform temperature profile due to fire exposure. *Journal of Constructional Steel Research* 16(3), 169–192.
- [3] EN 1999-1-1 (2007, May). *Eurocode 9: Design of aluminium structures - Part 1-1: General structural rules*. Brussels, Belgium: European Committee for Standardization.
- [4] EN 1999-1-2 (2007, February). *Eurocode 9: Design of aluminium structures - Part 1-2: Structural fire design*. Brussels, Belgium: European Committee for Standardization.
- [5] Maljaars, J. (2008, March). *Local buckling of slender aluminium sections exposed to fire*. Ph. D. thesis, Eindhoven University of Technology.
- [6] Maljaars, J., F. Soetens, and H. H. Snijder (2010, January). Local buckling of fire-exposed aluminum members-a new design model. *Journal of Structural Engineering* 136(1), 66–75.
- [7] Maljaars, J., L. Twilt, and F. Soetens (2006, May). Heating of aluminium members exposed to natural fire conditions. In P. Vila Real, J.-M. Franssen, and N. Lopes (Eds.), *Proceedings of the Fourth International Workshop Structures in Fire (SIF'06)*, Volume 1, Aveiro, Portugal, pp. 75–88. Universidade de Aveiro. held at the University of Aveiro, Portugal, 10-12 May 2006.
- [8] Mazzolani, F. M. (2008). Design criteria for aluminium alloy structures. In *Proceedings: Eurocodes: Background and applications, "dissemination of information for training" workshop, 18-20 February 2008, Brussels, Belgium*. European Commission DG Enterprise and Industry, Joint Research Centre.
- [9] van der Meulen, O. R. (2010). Cross-sectional classification of aluminium beams subjected to fire. In *Proceedings of the 11th INALCO conference, Eindhoven June 23-25*, pp. [pages unknown].
- [10] Ramberg, W. and W. R. Osgood (1943, July). Description of stress-strain curves by three parameters. Technical Report NO. 902, National Advisory Committee for Aeronautics, Washington D.C., United States.
- [11] Schleich, J.-B., L.-G. Cajot, M. Pierre, D. Joyeux, G. Aurtenetxe, J. Unanua, S. Pustorino, F.-J. Heise, R. Salomon, L. Twilt, and J. van Oerle (2002). *Valorisation project, natural fire safety concept, final report*. Number EUR 20349 EN in technical steel research. Luxembourg: Office for Official Publications of the European Communities.
- [12] Soerjadi, R. (1968). On the computation of the moments of a polygon, with some applications. *Heron* 16(5), 43–58.
- [13] The Aluminum Association (2004). *Aluminum statistical review for 2003*. Arlington, VA, United States: The Aluminum Association.

Author Index

- Abboud, N., 927
Abu, A., 382
Adelzadeh, M., 149
Ahmed, A., 328
Ali, F., 98, 165
Al-Jabri, K., 687
Al-Jahwari, F., 687
Alonso, M. C., 800
Anderson, K., 694
Annerel, E., 751
Aurtenetxe, J., 91
- Baba, S., 157
Backstrom, R., 560
Bagchi, A., 286, 943
Bahr, O., 425, 629
Bai, Y., 458
Bailey, C. G., 349, 398
Baker, G., 951
Bamonte, P., 320, 848
Bangi, M. R., 833
Bao, X., 149
Beaucour, A.-L., 759, 767
Bednar, J., 484
Bénichou, N., 149, 935
Beyler, C., 927
Bhandari, N. M., 817
Bhargava, P., 231, 247, 817
Bihina, G., 349
Bijlaard, F., 671
Bisby, L., 149, 727, 743
Block, F. M., 967
Both, K., 141
Bratina, S., 466
Breunese, A., 141
Buchanan, A. H., 216, 528, 536, 544
- Burgess, I. W., 98, 366, 382
Butterworth, N. A., 967
Bwalya, A. C., 935
- Cachim, P., 602
Calil, C., Jr., 1001
Carradine, D. M., 536, 544
Cashell, K. A., 374
Chen, S.-W., 130
Choe, L., 3
Choi, S. M., 449
Choi, S., 98
Chu, J., 130
Chung, K. S., 449
Clifton, G. C., 492
Correia, A. M., 341
Correia, N. D., 576
Couto, C., 27
- da Silva, L. S., 67
de la Quintana, J., 91
Deeny, S., 270
Dhakal, R., 216
Doherty, P., 165
Dwaikat, M., 106, 983
- e Silva, V. P., 1001
Eamon, C. D., 959
Eedson, R., 149
Eguia, S., 91
El-Fitiany, S. F., 239
Elghazouli, A. Y., 374
Ellingwood, B. R., 1008
El-Rimawi, J., 520, 611
Engelhardt, M. D., 646, 900
Ervine, A., 224

- Falke, J., 114
Faria, R., 197, 262
Fay, T., 927
Fike, R., 417
Fontana, M., 19, 503
Fox, D., 278
Fragiacomo, M., 528, 536
Fragomeni, S., 301
Frangi, A., 503
Franssen, J.-M., 67, 349, 398, 474, 638, 784
- Gales, J., 727
Gambarova, P. G., 848
Gandhi, P. D., 560
Garlock, M. E. M., 11, 122, 621
Gasperi, A., 173
Gerard, R. B., 544
Gernay, T., 398, 784
Gernay, Th., 474
Ghoreishi, M., 286
Gijbers, J., 141
Gillie, M., 189, 224, 231, 694
Gillies, A. G., 492
Gomide, K. A., 433
González, F., 908
Green, M. F., 149
Green, M. G., 967
Guerrieri, M., 301
Gunalan, S., 43
- Hadjisophocleous, G., 552
Hager, I., 841
Hai, T. K., 662
Han, L., 775
Han, L.-H., 358
Hanus, F., 638
Harichandran, R. S., 75
Hasemi, Y., 568
Hawes, M., 349, 398
Hebert, R., 759
Hirai, H., 568
Hirakuri, D., 568
Hirashima, T., 157
Hiziroglu, H. R., 872
Hjiaj, M., 51
Hopkin, D., 520, 611
Horiguchi, T., 826, 833
Hozjan, T., 466
Hu, G., 646, 900
Huang, Z., 654
Hugi, E., 458, 503, 743
- Huisman, S., 312, 719
- Icove, D. J., 993
Iqbal, S., 75
Iwankiw, N., 927, 1008
Izzuddin, B. A., 374
- Jansson, R., 800
Jensen, E., 792, 959
Jeon, H. K., 856
Jiang, J., 919
Jiang, S.-C., 441
Jiang, Y., 919
Joshi, M., 792
Jung, S. K., 449
Just, A., 584, 593
- Keller, T., 458
Khalifa, T., 149
Kim, H.-J., 856
Kim, H.-Y., 856
Kim, S. H., 449
Kimura, T., 568
Kiong, T. S., 662
Knobloch, M., 19
Kodur, V. K. R., 106, 206, 328, 417, 943, 983
Köhler, J., 511
Kolsek, J., 466
Kolstein, H., 671
König, J., 511, 593
Korzen, M., 312, 341
Koshihara, M., 568
Kotsovinos, P., 919
Kowalski, R., 254
Krol, P., 254
Kumar, V., 247
- Lange, J., 703, 908
Law, A., 189
Le, Q-T., 51
Ledesert, B., 759
Lee, J., 900
Leite, G. S., Jr., 433
Lennon, T., 520, 611
Leroux, P., 935
Li, G-Q., 35, 130, 441, 735
Li, W., 149
Li, Y., 711
Lo Monte, F., 320
Lopes, N., 27, 67

- Lou, G.-B., 679
Lougheed, G. D., 935
Ludwig, C., 458
- MacDougall, C., 727
Mago, N., 492
Mahendran, M., 43
Maljaars, J., 141, 890, 1015
Maluk, C., 743
Manohar, C. S., 231
Marjanishvili, S. M., 59
Martins, A. M. B., 181
Maxia, D., 294
May, I., 231, 919
McArthur, C., 927
Mehaffey, J., 552
Meng, B., 719
Michikoshi, S., 157
Mim, J-K., 216
Mindeguia, J.-C., 880
Mohammad, M., 552
Molkens, T., 975
Moraes, P. D., 576
Moreno, A. L., Jr., 433, 1001
Morente, F., 91
Morimoto, H., 864
Morovat, M. A., 900
Moss, P. J., 216, 528, 536, 544
Murakami, M., 568
Mustafa, H. N., 114
- Nadjai, A., 98, 165, 349, 398
Nafarieh, A., 848
Naili, E., 98
Nakajima, A., 568
Neto, J. M., 1001
Nilsen, T. M., 528
Noordijk, L., 141
Noumowe, A., 759, 767
- O'Neill, J., 536
Ogawa, A., 568
Ozawa, M., 864
- Pakala, P., 417, 983
Pankaj, 224, 231
Pardon, D., 880
Park, K.-H., 856
Pauli, J., 19
Payá-Zaforteza, I., 11
Peigneux, C., 349
- Peng, L., 552
Phani Prasad, D. M. S., 247
Pimienta, P., 800, 880
Planinc, I., 466
Plank, R. J., 98, 366
Pliya, P., 767
Porcu, A., 294
Porcu, R., 294
Proe, D. J., 390
Pultar, M., 83
Pyl, L., 975
- Qiang, X., 671
Quiel, S. E., 59, 122
- Ramanitrarivo, V., 382
Raut, N., 206
Real, P. V., 27, 67, 197, 262
Rein, G., 189
Renaud, C., 629
Robbins, A., 951
Rodrigues, J. P. C., 27, 181, 341, 576
Roosefid, M., 407
- Saje, M., 466
Sakamoto, S., 157
Sawano, Y., 568
Schaumann, P., 425, 629
Schell, E., 646
Schleifer, V., 503
Schmid, J., 511, 593
Schneider, R., 703
Schneider, U., 312, 719, 800, 809
Seki, M. S., 568
Selamet, S., 621
Sharma, U. K., 231, 247, 817
Shen, C., 775
Shen, Z., 711
Shkolnik, I. E., 872
Silberschmidt, V., 520, 611
Silva, V. P., 433
Simms, W. I., 349
Simms, W. I., 398
Singh, B., 231
Singh, Y., 231
Soetens, F., 1015
Sokol, Z., 83
Somaini, D., 19
Song, H., 98
Srpcic, S., 466
Stern-Gottfried, J., 189

- Stratford, T., 270, 278
Stujberova, M., 484
Su, J. Z., 935
Sultan, M. A., 286
Suzuki, A., 568
- Tabaddor, M., 560
Taber, B. C., 935
Taerwe, L., 751
Tamura, Y., 568
Tattoni, S., 173, 294
Terrasi, G., 743
Thomas, I. R., 390
Tinsley, A. T., 993
Torero, J., 231
Twilt, L., 671, 1015
- Usmani, A., 231, 919
- van der Meulen, O. R., 1015
Van Horn, J., 792, 959
van Overbeek, T., 141
Varma, A. H., 3, 417
Vassart, O., 349, 398
Vulcu, C., 474
- Wald, F., 83, 484
Wang, L., 735
Wang, R., 679
Wang, W.-H., 358
- Wang, Y. C., 735
Wang, Y., 711
Watanabe, K., 568, 826
Weise, F., 719
Wellman, E., 417
Wickström, U., 951
Won, Y. A., 449
Wong, B., 98
Wong, V. Y. B., 366
Wu, B., 775
- Xavier, H. F., 197, 262
Xing, Z., 759
- Yassin, M. H., 943
Yasui, N., 568
Youn, K. S., 856
Youssef, M. A., 239
Yu, H.-X., 358
Yu, S., 679
- Zaharia, R., 474
Zaidi, K. A., 817
Zhang, C., 35, 441
Zhang, J., 919
Zhang, J., 919
Zhao, B., 51, 398, 407, 629
Zhen, Y., 662
Zhou, F., 775
Zilli, G., 638